A Wide-Area Perspective on Power System Operation and Dynamics

Robert Matthew Gardner

Dissertation submitted to the Faculty of Virginia Polytechnic Institute and State University in partial fulfillment of the requirements for the degree of

Doctor of Philosophy

in

Electrical Engineering

Committee Members:

Dr. Yilu Liu (Chair)

Dr. A. Lynn Abbott

Dr. Lamine M. Mili

Dr. David L. Russell

Dr. James S. Thorp

28 March 2008

Blacksburg, Virginia U.S.A.

Keywords: FNET, FDR, PMU, event location, wide-area power system monitoring

©2008 Robert Matthew Gardner

A Wide-Area Perspective on Power System Operation and Dynamics

Robert Matthew Gardner

Abstract

Classically, wide-area synchronized power system monitoring has been an expensive task requiring significant investment in utility communications infrastructures for the service of relatively few costly sensors. The purpose of this research is to demonstrate the viability of power system monitoring from very low voltage levels (120 V). Challenging the accepted norms in power system monitoring, the document will present the use of inexpensive GPS time synchronized sensors in mass numbers at the distribution level. In the past, such low level monitoring has been overlooked due to a perceived imbalance between the required investment and the usefulness of the resulting deluge of information. However, distribution level monitoring offers several advantages over bulk transmission system monitoring. First, practically everyone with access to electricity also has a measurement port into the electric power system. Second, internet access and GPS availability have become pedestrian commodities providing a communications and synchronization infrastructure for the transmission of low-voltage measurements. Third, these ubiquitous measurement points exist in an interconnected fashion irrespective of utility boundaries. This work offers insight into which parameters are meaningful to monitor at the distribution level and provides applications that add unprecedented value to the data extracted from this level. System models comprising the entire Eastern Interconnection are exploited in conjunction with a bounty of distribution level measurement data for the development of wide-area disturbance detection, classification, analysis, and location routines.

Acknowledgement

I am grateful in the utmost for financial support from the Via Foundation. As a Bradley Fellow in the Bradley Department of Electrical and Computer Engineering at Virginia Tech, I have been given the privilege of freedom in my research by means of generous funding from the Via Foundation for the whole of my doctoral studies.

My deepest personal gratitude is offered to Dr. Yilu Liu for her patient guidance and gracious provision throughout my greater than four year tenure under her advisement. I shall always regard Dr. Liu as more than a mentor. Indeed, she is a dear friend, staunch champion, and fond counselor. Never afraid to say what I did not want to hear nor to lead me where I dare not trod for my betterment, her wise leadership cannot be priced among the riches of this world.

To those who came before me and made the way plain, I am indebted. I am thankful for the foundational work done especially by Shu-Jen Tsai, Zhian Zhong, Jian Zuo, Tao Xia, and Jingyuan Dong.

I am yet further indebted to my closest circle of friends: Joshua K. Wang, Mark W. Baldwin, and Philip R. Hassell. Where would I be without them as my friends?

Special thanks go also to my family – my father, Robert C. Gardner, my mother, Cathy M. Gardner, and my ever-caring sister, Ashley G. Townsend. Their prayers and support have sustained me through the darkest of nights and ignited the sun making the brightest days. They truly are examples of character.

Finally, and above all, I offer thanks and praise to my personal Lord and Savior, Jesus Christ – for from Him and through Him and to Him are all things. To Him be the glory forever. Even so, come, Lord Jesus. Amen. (Romans 11:36 NASB, Revelation 22:20 KJV)

Table of Contents

Table of Figures

List of Tables

Chapter 1: Preliminaries

The past two decades have marked vast improvements in the field of wide-area power system monitoring. The science of wide-area monitoring has matured from its infancy, marked by the development of the first global positioning system (GPS) time-synchronized phasor measurement unit (PMU) at Virginia Tech in the early 1988. Since its invention under the leadership of Dr. Arun Phadke, the PMU has become a cornerstone of wide-area power system monitoring even to the point of defining the science [1]. To understand the importance of wide-area monitoring and any improvements made thereupon, we must first examine the topology of the electric grid from a broad perspective. Figure 1-1 presents a reduced schematic of the eastern portion of the U.S. electric grid. The figure includes some of the transmission lines identified from 345 kV and higher. The system model comprises 2,287 generators, 16,016 busses, 20,093 transmission lines, and 7,221 branches with transformers [2].[1] This model is presented here for the purpose of illustration. However, in subsequent chapters, we shall use the model extensively as a baseline for location of disturbance (LoD) studies.

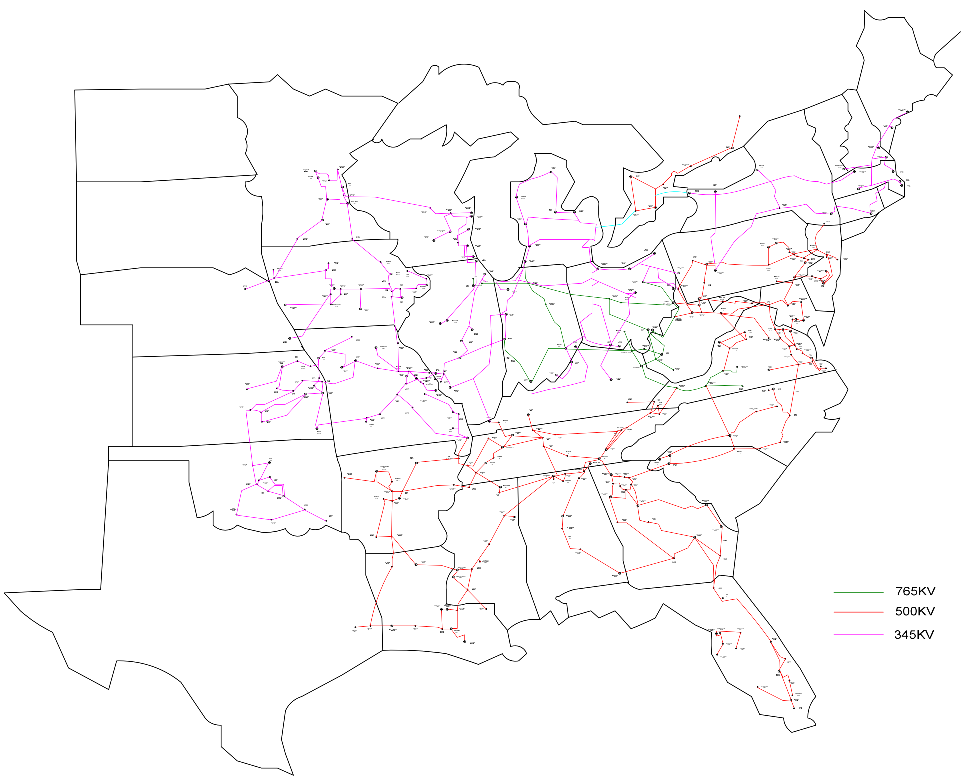

Figure 1-1: Schematic of Eastern Interconnection model.

[1] As of the time of this report, non-disclosure agreements with the provider of this model prohibit the dissemination of further model details.

Wide-area monitoring of such a large electrical circuit is accomplished with sensors and measurement devices, such as PMUs, that measure the complex quantities of system voltage, $\mathbf{E}_i$, and current, $\mathbf{I}_i$, at select nodes, i, throughout the network. These complex quantities of voltage and current are commonly referred to as "phasors." Since network conditions such as topology, loading, and generation, are continuously changing, and since voltage and current at each point in the grid are themselves functions of time, the phasors measured at separate and distinct points across the grid are only meaningful in the wide-area sense if said measurements are all made against a synchronized time reference. The requirement for synchronous measurements is fulfilled by these wide-area monitoring devices using globally synchronized timing pulses generated by satellites positioned in orbit around the globe as a part of the GPS network. Volumes have been written regarding the importance and usefulness of synchronized phasor measurements. However, we shall focus our discussion on the study of wide-area distribution-level voltage frequency monitoring.

Frequency Monitoring Using FNET

The Wide-Area Frequency Monitoring Network (FNET) developed at Virginia Tech consists of several Frequency Disturbance Recorders (FDRs) distributed across the United States and Canada as well as a central data collection server as shown in Figure 1-2.

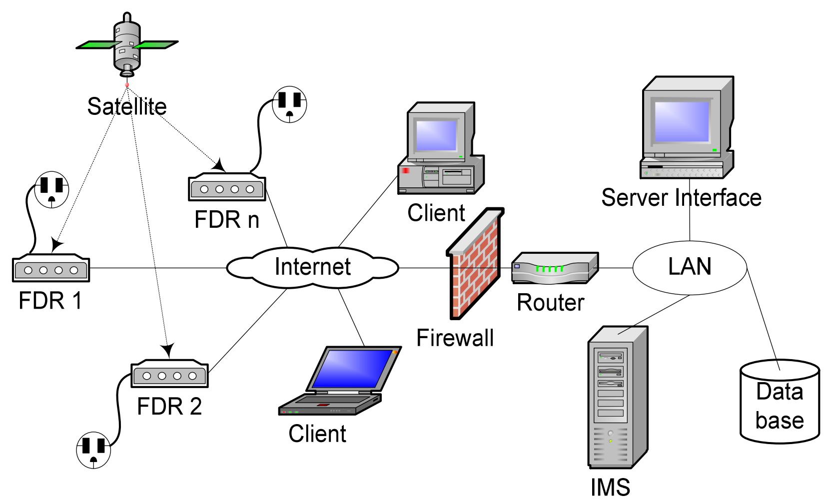

Figure 1-2: The structure of FNET

Each FDR in the network measures the voltage, phasor angle, and frequency of the 110 V outlet (220 V for sensors placed in Europe) into which it is connected. A GPS timestamp is then applied to the measured quantities and sent via the internet to an information management server (IMS) maintained in the FNET labs at Virginia Tech [3]. We can therefore relate to FDRs as limited capability PMUs installed at low, distribution level voltages. There are two important but subtle points that define the true worth of FNET. First, each FDR interfaces with the electric grid at low, easily-accessible, voltage levels. The installation costs for an FDR are non-existent. This feature gives FNET an extreme cost advantage over PMU technology which is designed to instrument high-voltage substations. Since installation and instrumentation costs increase almost exponentially with the voltage level at which a device must be installed, the installed cost of a single FDR is on the order of $1,000 whereas the installed cost of a single PMU can range upwards of $100,000 [4]. The tradeoffs for monitoring the electric grid at low voltage levels include losing the ability to measure three-phase quantities, increasing the amount of noise in the measured signal, risk of losing the ability to measure meaningful voltage magnitudes, and losing the ability to measure meaningful current flows. When current flows cannot be measured, one loses the ability to calculate meaningful power flows and power factors. One further set of disadvantages of distribution level monitoring is a matter of logistics. Given that 110 V access points (receptacles) are ubiquitous throughout North America, logistical questions as to how and where FDRs are placed arise. To date, the disbursement of FDRs as executed by the FNET research group has been driven by both convenience and a general desire to widely cover each of North America's major interconnections. A further logistical issue with distribution level monitoring results from an inherent dependence upon the sensor's host to consistently provide the three necessary elements to ensure uninterrupted power system parameter measurement: internet access for the reporting of measurements, GPS satellite visibility for the precise time stamping of said measurements, and electrical connectivity. After all of the technical disadvantages of measuring low-voltage quantities have been considered, one last very meaningful and observable quantity exists – frequency. Because the frequency of a voltage signal is invariant to the voltage level at which it is measured, wide-area frequency measurements can be made at voltage levels as low as 110V, a standard voltage accessible in homes and offices across North America. Logistical disadvantages can also be offset by widely redundant, nearly indiscriminant, placement of FDRs as allowed by the comparatively insignificant cost of establishing such a network.

A second subtle but important advantage of FNET is its ability to measure frequency with sub-second precision (10 samples per second). For many reasons, sub-second frequency measurements have typically been unavailable in the past [5-7]. Two main reasons are demand and cost. The time constants of conventional power system controls are typically large enough so as not to take full advantage of sub-second wide-area frequency measurements [8, 9]. Also, the cost of making such measurements historically has been notably high [3]. However, as we shall see later in this report, sub-second frequency measurements actually provide a wealth of knowledge regarding the health and dynamics of the electric grid. In fact, the frequency measured at any location in a synchronized grid is a special quantity insofar as it is directly related to the rotational speed of the synchronized generators supplying the system [10, 11]. Other quantities, especially those accessible at the distribution level such as voltage, are localized quantities. Perturbations or deviations (even those of a significant magnitude) in these localized quantities do not necessarily reflect the dynamics of the entire interconnection whereas perturbations in frequency measured at the distribution level usually reflect the dynamics caused by system-wide generation-load mismatch [12, 13]. Further, steady or stable voltage readings in one portion of an interconnection are not necessarily an indication of global voltage stability throughout the interconnection. However, by definition, the time-average of frequency is necessarily equal throughout a synchronized interconnection.

FNET in the Context of the North American Interconnections

The North American power system comprises four major electrical interconnections, the Eastern Interconnect (EI or EUS), the Western Electricity Coordinating Council (WECC), the Electric Reliability Council of Texas (ERCOT), and Hydro-Québec. The interconnections are connected only by DC tie lines and thus are isolated from each other in terms of frequency. We shall henceforth assume that frequency disturbances in any arbitrary interconnection shall not significantly affect either of the remaining grids. Figure 1-3 shows an approximate mapping of the four North American interconnections.

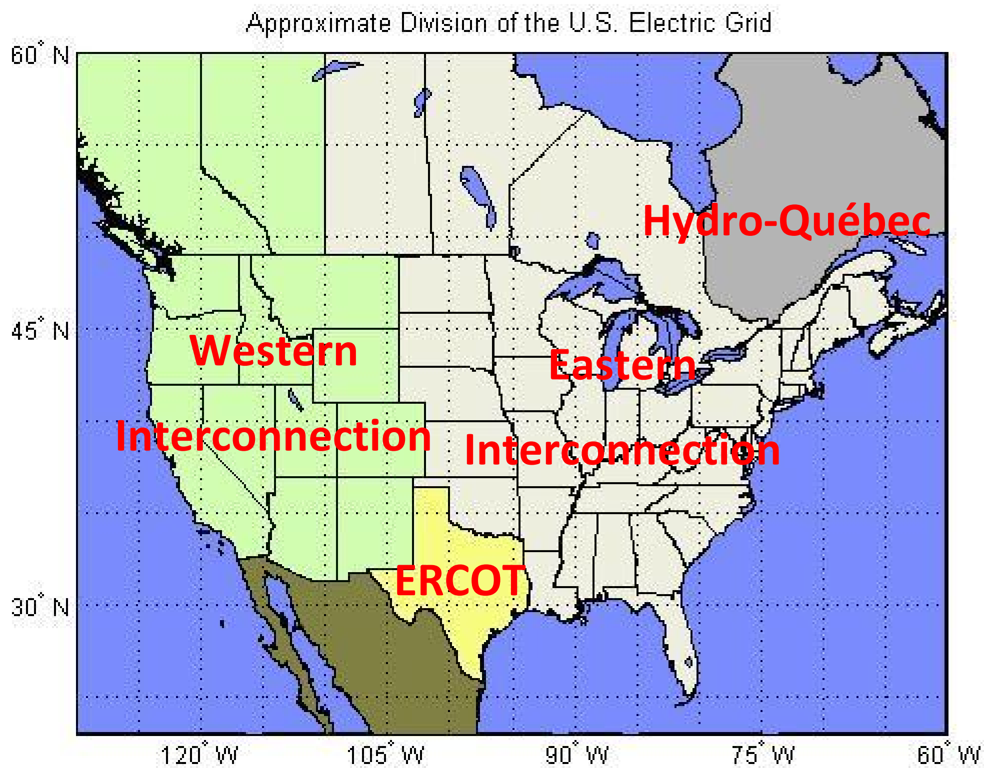

Figure 1-3: The division of the North American electric grid along its electrical borders.

Keeping in mind the overall configuration of the electric grid, we now introduce the location of the frequency sensors, or FDRs. Although the exact number of sensors is increasing almost weekly, Figure 1-4 gives a general idea of locations of current FDR placements. We note that the work reflected in this report is progressive and has been accomplished in phases since late 2005. Therefore, some phases of research have not been afforded the luxury of the dense sensor placement seen in Figure 1-4. The latest analysis performed yet struggles with the issue of sensor duty. An average network duty for FNET tends towards 50%. That is, at any instant in time, one might expect with some level of randomness, that 50% of the commissioned FDRs are actually online and functioning properly. Again, this duty issue is primarily a function of the above-mentioned logistical difficulties. It has been postulated that these duty issues might also be a function of internet latency and/or the data transmission protocols used by the FNET system. Cursory investigations indicate, however, that these issues are not significant. Henceforward, FDR data that is considered in this research is placed in the context of a subset of sensors corresponding to a subset of the locations shown below.

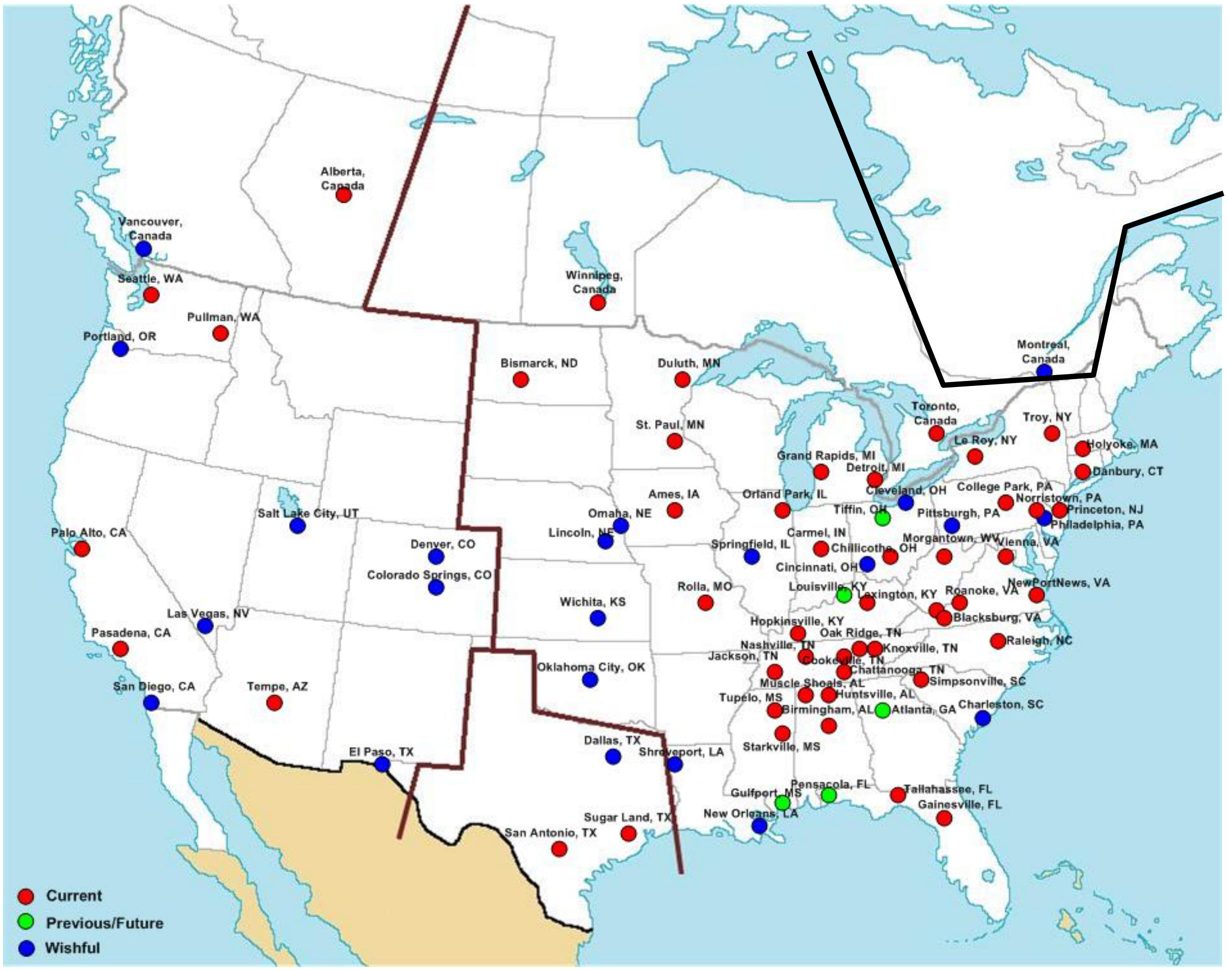

Figure 1-4: Current location of FDRs in North America.

Further Motivation for Wide-Area Frequency Monitoring

Frequency, as one of the power system's states, is an optimal parameter for the detection (and as will be discussed later, location) of events that affect the bulk electric power grid. The necessary uniformity (in the time-averaged sense) of frequency measurements, even at the distribution level, provides the advantage of detecting significant generation-load mismatch contingencies from any point in the grid. Conversely, large contingencies may not necessarily cause measureable deviations in other power system states such as voltage at any level (distribution or otherwise). Two examples follow that illustrate the preeminence of power system frequency amongst other power system states.

Motivational Example #1

We now broadly consider the abrupt tripping of the W. H. Zimmer generating station near Clermont, OH (1300± MW capacity). This particular contingency occurred at least three times in the

2007 calendar year. The following four figures present pre- and post-contingency profiles for two power system states, voltage and frequency, respectively, as simulated using PSS/E. At the instant of the generation trip, the interconnection suffered a significant mismatch between total electrical demand, P_e, and the total power injected by the sum of the generators remaining online, P_m. More concisely,

$$\Delta P_{\text{system}} = \sum_{\text{All Generation}} P_m - \sum_{\text{All Loads}} P_e \approx -1300 \text{ MW}$$

Notice how the voltage profile (rendered using voltage deviations from steady state per unit voltage values) remains largely unchanged between pre-contingency (Figure 1-5) and post-contingency levels (Figure 1-6). Alternatively, it is obvious that the frequency profile is universally perturbed as a result of the generation trip. This global affect is due to the grid-wide slowing of machine speeds to satisfy Newton's second law of motion. Compare Figure 1-7 with Figure 1-8. Throughout the report, it will become evident that the behavior in this scenario is representative of general power system behavior.

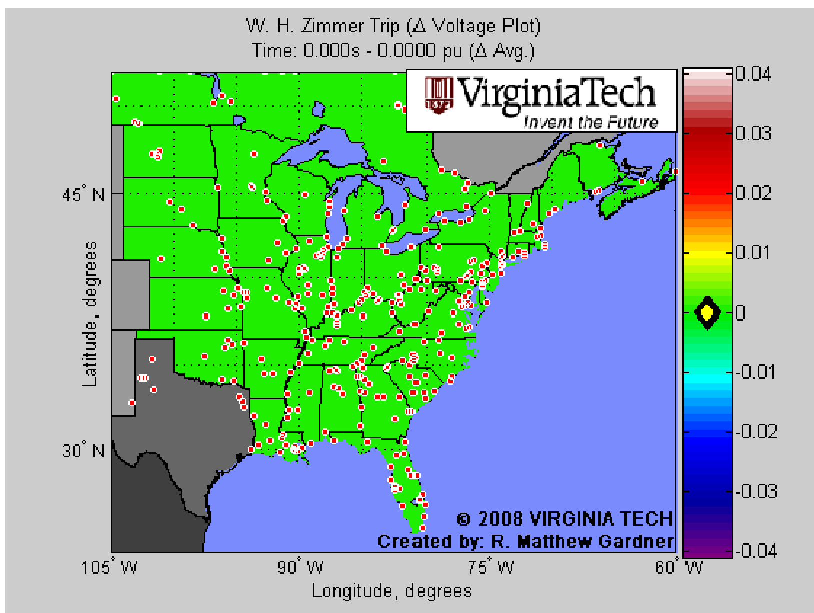

Figure 1-5: Voltage profile of the EI before trip of W.H. Zimmer plant.

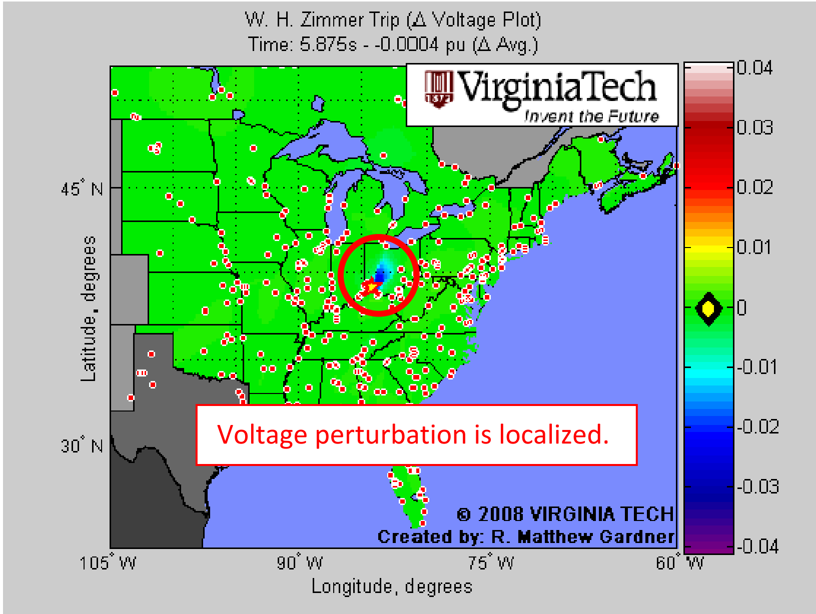

Figure 1-6: Voltage profile of EI 4.875s after trip of W.H. Zimmer plant.

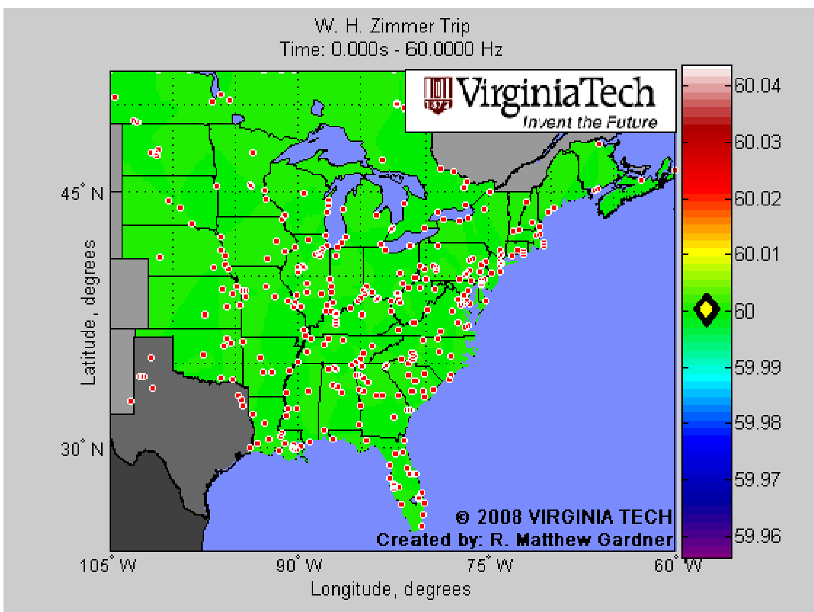

Figure 1-7: Frequency profile of EI before trip of W.H. Zimmer plant.

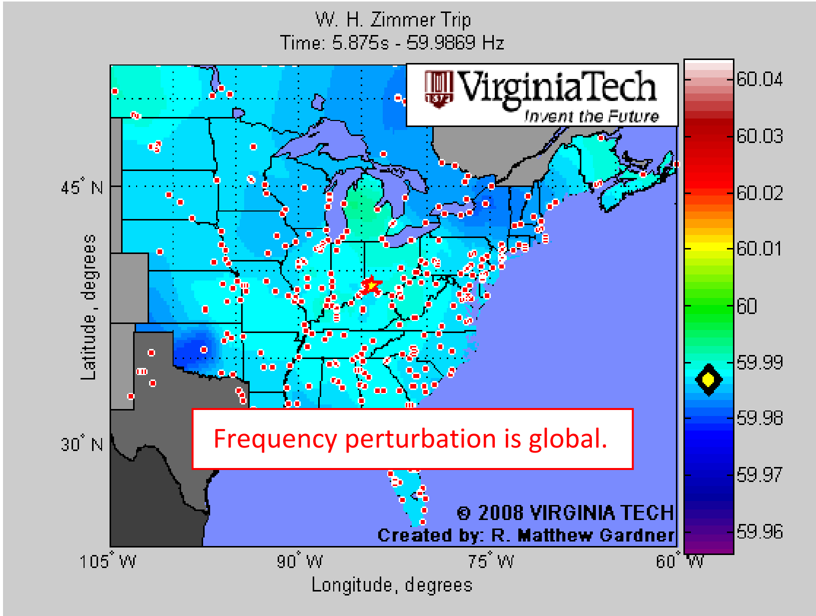

Figure 1-8: Frequency profile of EI 4.875s after trip of W.H. Zimmer plant.

The above so called voltage profiles are in fact plotted as voltage deviation profiles in terms of per unit voltage deviation. That is, the plots are displaying a voltage profile in terms of location parameters x, y, and time , t, according to the following function :

$$E_{\text{dev}}(x, y, t) = E(x, y, t) - E(x, y, t_0)$$

where E is a voltage dependant on both space and time. The reason for considering voltage deviation is rather simplistic. The time averages of voltages at any two points in a synchronous interconnection are by no means constrained to equal one another. However, by definition, for a synchronously interconnected power system the following relationship in frequency must hold:

$$\int_{t-\frac{T}{2}}^{t+\frac{T}{2}} f(x_i, y_i, \tau)\, d\tau = \int_{t-\frac{T}{2}}^{t+\frac{T}{2}} f\left(x_j, y_j, \tau\right) d\tau \tag{1.1}$$

for some T[2] at nodes located at any two arbitrary points (x_i, y_i) and $\left(x_j, y_j\right)$ within said interconnection. Figure 1-9 and Figure 1-10 illustrate an effectual inability to discern between pre- and post-contingency voltage profiles – the plots are practically the same. A similar argument can be made for nearly every other power system parameter available through wide-area measurements. Figure 1-11 and Figure 1-12 display true phase angle profiles for the EI to further illustrate the point.

[2] The parameter, T, is related to the coupling of each of the spinning machines within an interconnection. The parameter is affected by both the machine inertias and the reactances of the transmission network.

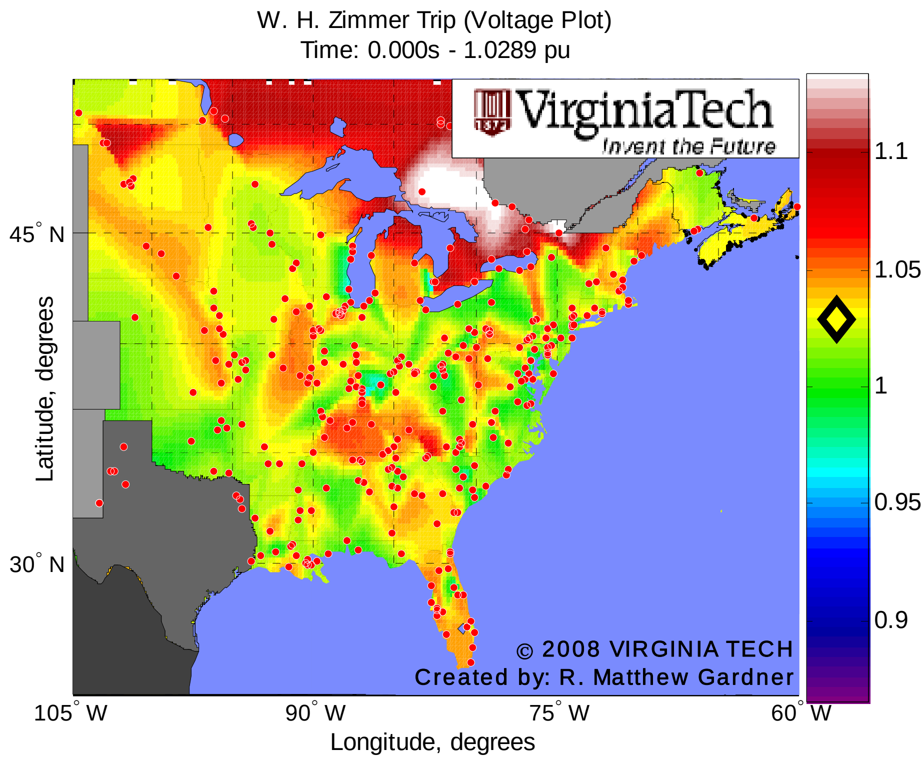

Figure 1-9: True voltage profile before trip of W. H. Zimmer plant.

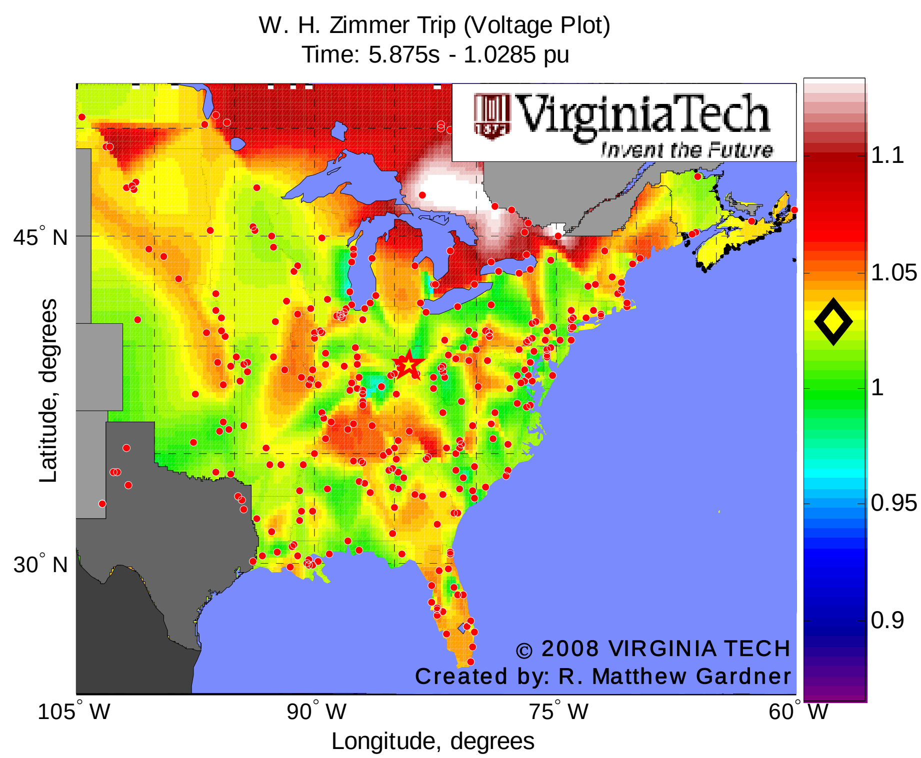

Figure 1-10: True voltage profile 4.875s after trip of W. H. Zimmer plant.

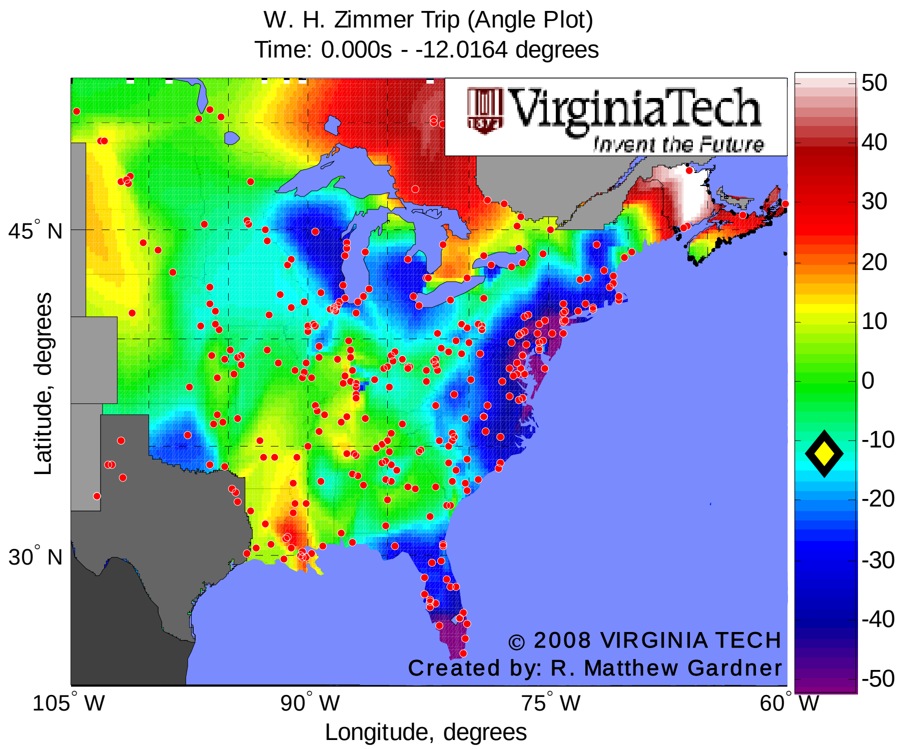

Figure 1-11: True phase angle profile before trip of W. H. Zimmer plant.

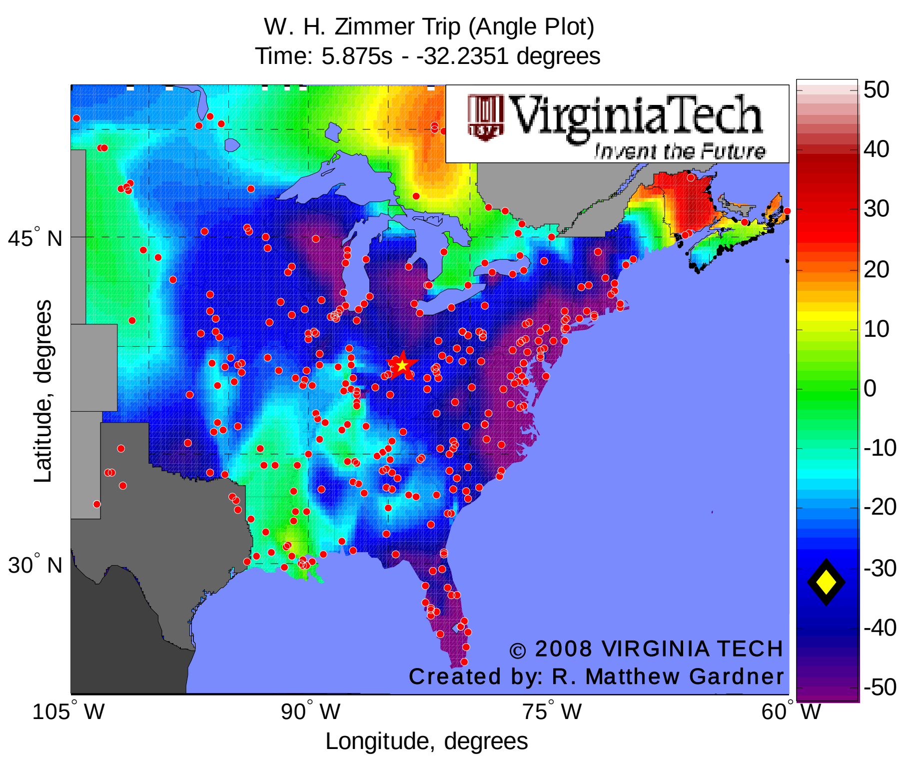

Figure 1-12: True phase angle profile 4.875s after trip of W.H. Zimmer plant.

The main point behind this example is to support the notion that voltage frequency is a quite convenient parameter to consider when studying large-scale power system disturbances. Frequency is often considered to be a good "health" indicator for electrical interconnections. Loosely speaking, when all is well, the frequency at all points in an interconnection will have instantaneous values close to one another and close to 60Hz as a whole. Again, it is worth noting that the time average of frequency across a single interconnection must be consistent per equation (1.1). However, instantaneous frequency values are by no means constrained to be constant throughout an interconnection. In fact, sub-second wide-area frequency measurements can reveal large volumes of information regarding the electromechanical dynamics of an interconnection [14].

Motivational Example #2

The first example utilized simulation data to demonstrate that power system frequency is a more suitable system parameter to examine than is voltage when attempting to detect large power system disturbances that involve significant generation-load mismatch. This example will focus on the practicality of examining frequency measurements at low-voltage distribution levels as opposed to other parameters such as voltage. To make such a comparison, we must rely on the availability of known power system events such as system-wide tests.

In September of 2005, the Western Electricity Coordinating Council (WECC) performed a battery of tests to both assess the dynamic response of the western interconnection (also referred to simply as "WECC" – see Figure 1-3) and validate the modeling of the interconnection [15]. Of the numerous tests, four in particular were monitored both by WECC PMUs and by Virginia Tech FDRs. These tests were monitored by the following FDRs:

Table 1-1: FDRs online for September 2005 WECC tests.

Unit Number:	Unit Name:	Unit Location:
5	Seattle	Seattle, WA
8	EPRI	Palo Alto, CA
14	Arizona State University	Tempe, AZ
16	Los Angeles	Pasadena, CA

Several WECC PMUs were also online during the four tests of interest:

Table 1-2: PMUs online for September 2005 WECC tests.

Unit Name:	Unit Location:	Voltage Level (kV):
GC50	Grand Coulee Dam	500
MALN	Malin Substation	500
SYLM	Sylmar PDCI Terminal	230
SCE1	Vincent Substation	500
COLS	Colstrip Generating Station	500
MPLV	Maple Valley Substation	230
BE23	Big Eddy Dam	230
BE50	Big Eddy Dam	500

The online FDRs and PMUs both measured quantities of voltage magnitude and frequency. By design, each FDR measured voltage at the distribution level, namely, 120 V. However, the PMUs are installed at both the 230 kV and 500 kV transmission levels. Hence, an important component of this example is to shed light on any differences that may exist between system response as measured at the distribution level and system response as seen from the transmission level. To add spatial context to the information in Table 1-1 and Table 1-2, examine Figure 1-13.

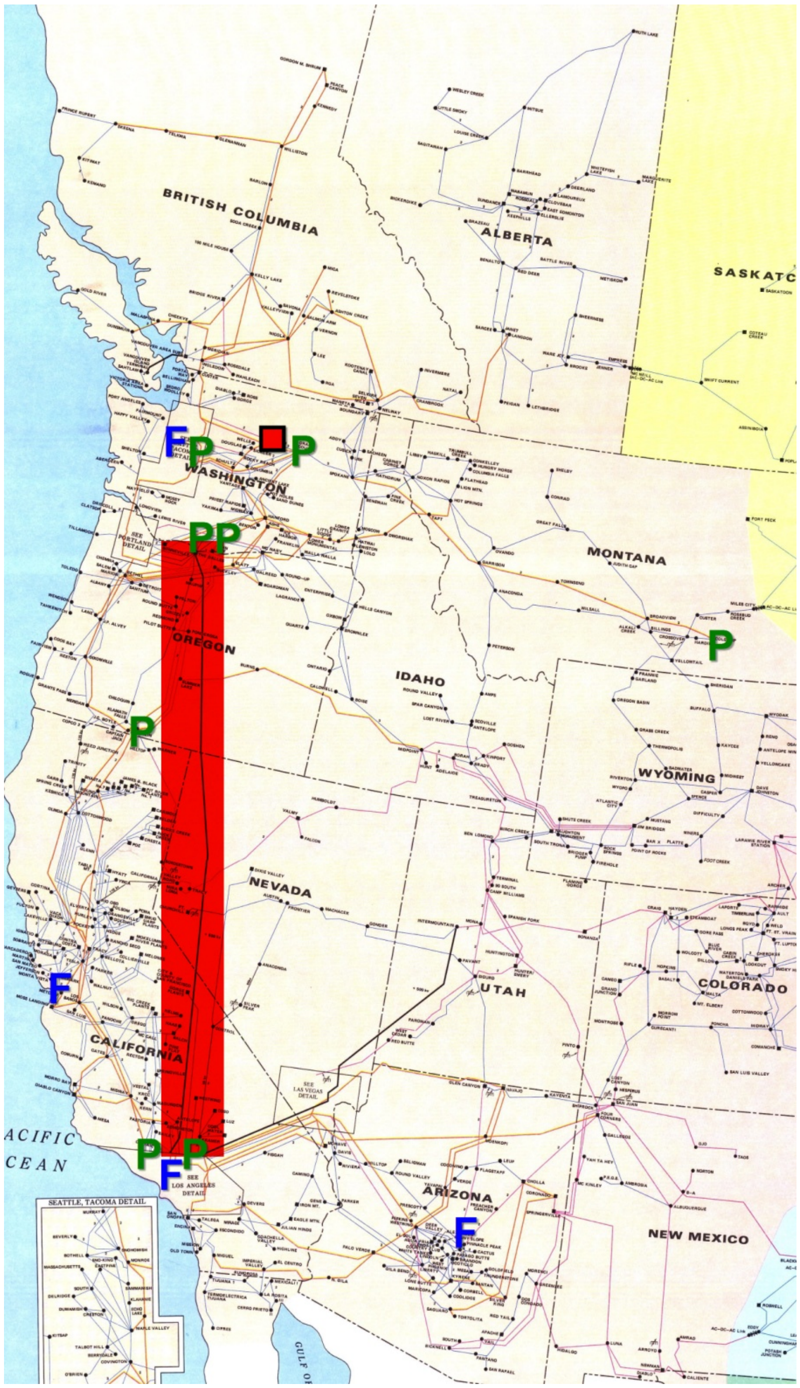

Figure 1-13: Location of FDRs and PMUs for 2005 WECC test battery.

In the above figure, the blue **F**s indicate the approximate locations of FDRs while the green **P**s indicate the approximate locations of PMUs. There are two further features on the map worth noting: the Pacific DC Intertie (PDCI) and the Chief Joseph Dynamic Brake. The PDCI is an extremely strong electrical connection between northern Oregon and southern California (highlighted red in Figure 1-13). The 1,000 kV DC line (positive and negative poles at ±500 kV) was originally constructed in 1965 as a joint effort between Asea Corporation (now ABB) and General Electric Company. The line, running between The Dalles, Oregon and Sylmar, California, serves as a crucial transmission path from the hydro-generation rich Pacific Northwest to the fossil generation rich areas of southern California and Arizona. With a capacity of 3,100 MW (approximately 2% of WECC peak capacity), the DC line benefits both regions though seasonal power exchanges. In the spring and summer, power flows from north to south serving the summer-peaking southern loads with large air conditioning demands. In the winter, the power flow reverses direction to serve the winter-peaking Pacific Northwest. In short, the PDCI has become perhaps the single most crucial element in the entire WECC [16, 17].

The second feature of note in Figure 1-13 is the Chief Joseph dynamic braking resistor installed near the Chief Joseph Dam in north central Washington (indicated by a red square). The large resistor was strategically placed in the Bonneville Power Administration (BPA) system in 1973 to essentially serve as a 1,400 MW load (at 230 kV) that can be energized almost instantaneously when needed. The large fast-acting brake was installed to ensure stability during severe faults near generation-rich areas of the BPA system. Therefore, the brake can allow for increased tie-line capacity (for transmission paths interfacing with the Pacific Northwest) without a loss of transient stability. Further information regarding the necessity, design, benefits, and control schemes associated with the brake can be found in [18]. The brake is only meant to be activated for relatively short periods of time (approximately 30 cycles or 0.5 seconds) due to the device's thermal limitations and operational effectiveness.[3]

The capacities of both the PDCI and dynamic brake are such that their influence extends throughout the WECC. On September 14, 2005, a battery of tests was performed using both of these devices. Specifically, we draw our attention to the tests listed in Table 1-3 as a part of Test Series D performed on the afternoon of the 14th.

Table 1-3: List and explanation of relevant 2005 WECC tests.

Test Series D		
Step:	**Time (EDT):**	**Test Procedure:**
D1	15:10	Insertion of Chief Joseph Dynamic Brake
D2	15:15	Insertion of Chief Joseph Dynamic Brake (second insertion)
D4	15:45	Modulation of PDCI power flow using square-type wave (0.25 Hz at ±125 MW)
D5	15:47	Modulation of PDCI power flow using sine wave (0.25 Hz at ±125 MW)

The following figures display the dynamic response of the WECC as observed by the constellation of measurement devices listed in both Table 1-1 and Table 1-2. Figure 1-14 contains

[3] Since the installation of the Chief Joseph brake, other technologies such as "fast-valving" have been introduced as solutions for the improvement of transient stability.

annotated plots of voltage measurements made at the 500 kV level by WECC PMUs. The effects of each test are clearly differentiable from the ambient noise in each signal. (Step D3 in the test battery occurred between Steps 2 and 4 but we omit discussion of this test for its lack of relevance to the context of this report.)

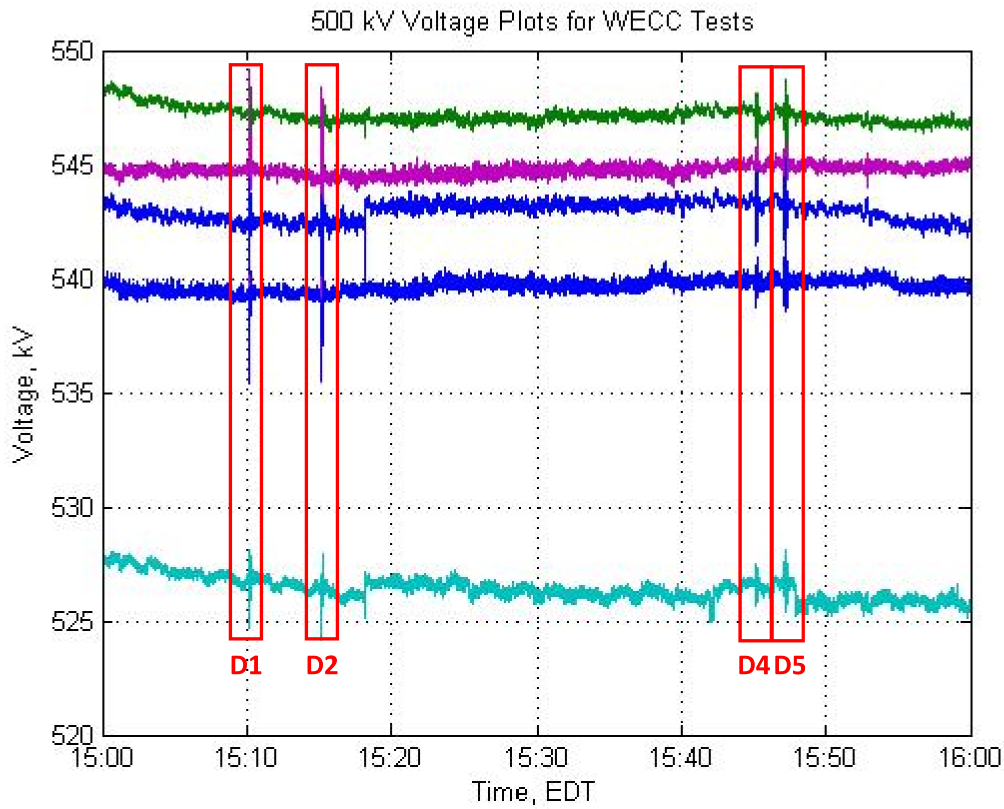

Figure 1-14: WECC response to testing as observed from five 500 kV PMU installations.

Conventionally, wide-area distribution level measurements have been considered to be of little or no value wholesale. This example, and in fact this entire report, is directed at not only proving the value and consistency of certain types of distribution level measurements but also further revealing which types of measurements are of value and which measurements are not. Since 2003, the FNET research group at Virginia Tech has been attempting to extract information about the operation and dynamics of the bulk electric grid directly from low-voltage measurements. In 2006, this effort was peer-justified by the publishing of results from an independent effort undertaken by O. Samuelsson at Lund University in Sweden [19]. These results showed agreement in wide-area measurements made at both the transmission and distribution levels (in this case 132 kV and 400 V, respectively). The agreement was clear in both voltage and frequency measurements. Hence, we use the WECC tests of 2005 to serve as a baseline for measurement comparison between transmission and distribution levels (in this case, 230 kV and 500 kV distribution level measurements and 120 V distribution level measurements). Figure 1-15 give results for the same tests at the same times as those shown in Figure 1-14 the only difference being the sensors used to observe the tests.

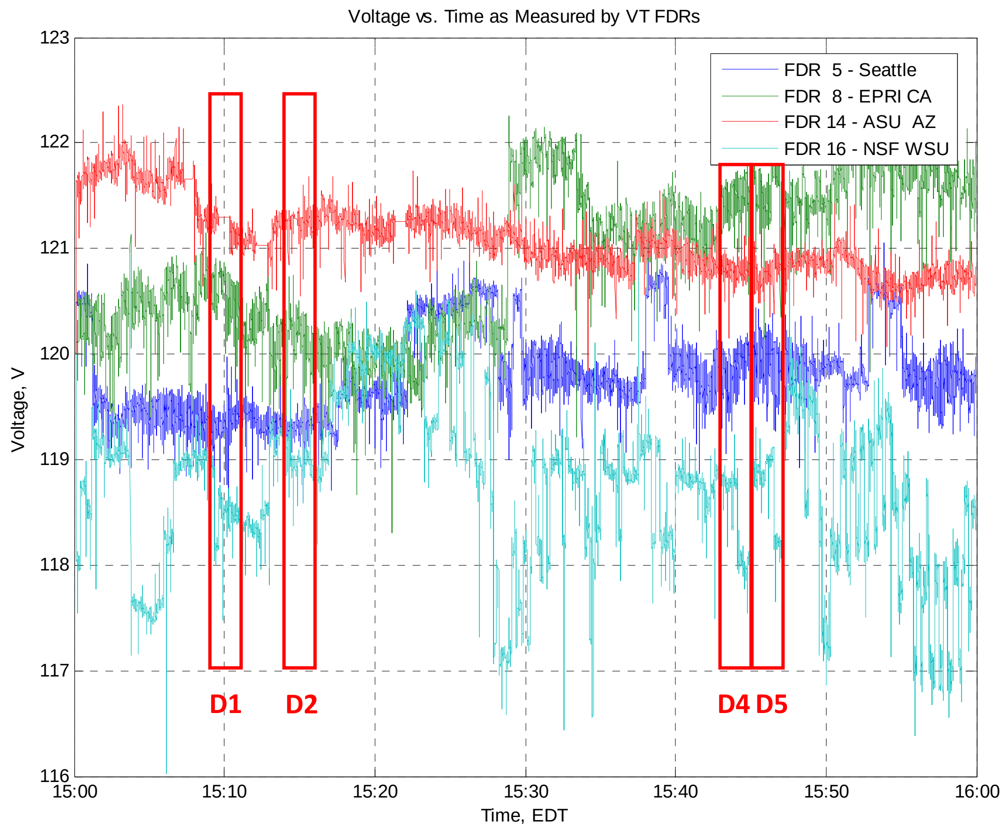

Figure 1-15: WECC response to testing as observed from four 120 V FDR installations.

The results shown in Figure 1-15 do not seem to be promising. Any effect of the tests on the 120 V measurement points seems to be buried in noise. In fact, far from discouraging, this finding is part of the motivation behind the use of low-voltage frequency measurements. Having demonstrated that perhaps voltage magnitude is perhaps a poor quantity to measure at the distribution level, we now turn our attention to frequency. Figure 1-16 shows the response of system frequency to the WECC tests as observed from both transmission and distribution levels. It is clearly noticeable that the low-voltage frequency measurements track the high-voltage frequency measurements quite well as expected. Higher measurement noise levels are noted but do not seem to wash out the trend variations caused by testing. For further insight in to the performance of the WECC, see Appendix II.

The main point of this example was to demonstrate the ability to discern significant grid disturbances using low-voltage frequency measurements even though little information is provided by voltage magnitude measurements at the same level. Samuelsson's work presented more promising results for voltage measurements taken at slightly higher voltage levels (400 V). However, as shown, local loads at 120 V seem to dominate voltage readings. Further analysis of the WECC tests will be performed in later chapters.

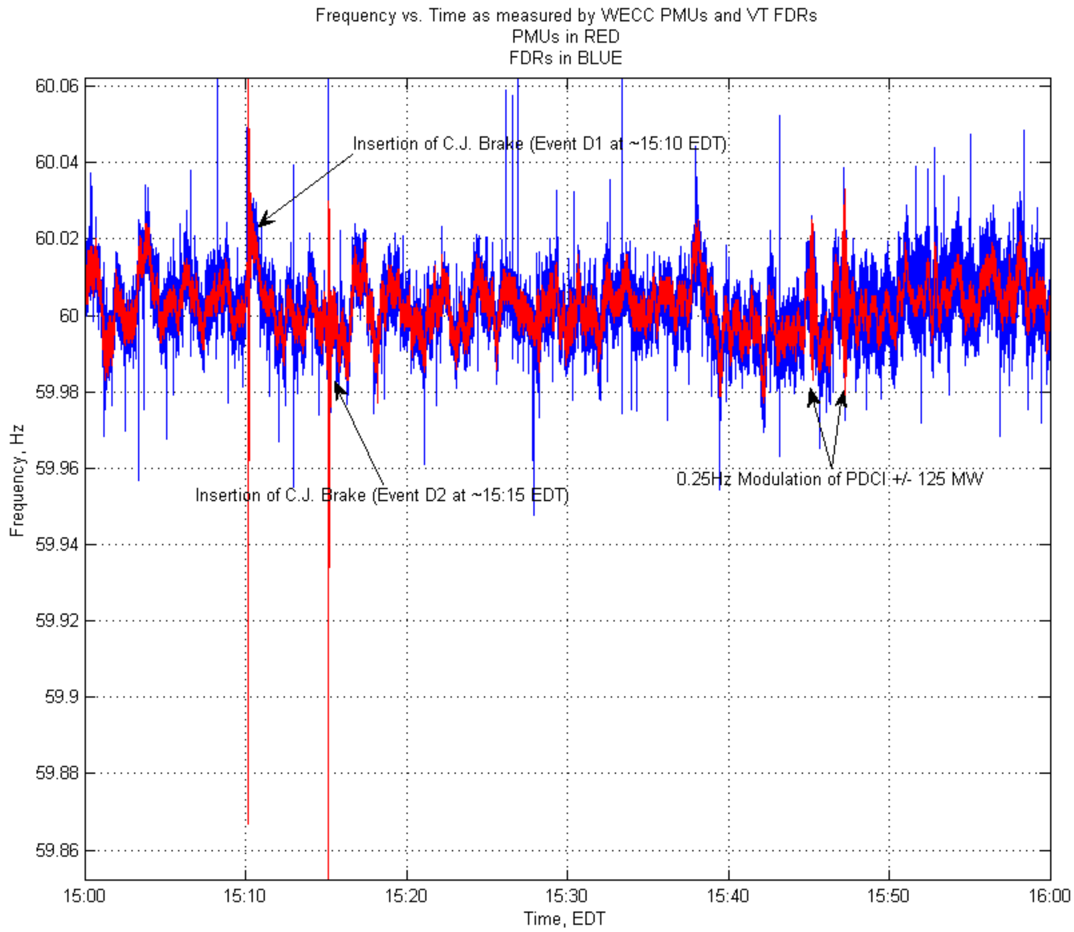

Figure 1-16: WECC system frequency response to testing.

The Nature of FNET Measurements

In order to use data collected from FNET, one must first attempt to understand its nature. The data is by nature riddled with noise and outliers. We do not consider these noisy FNET data to be mistake-ridden, but rather we consider these data to be error-ridden. If indeed the data were mistake-ridden, then we could make improvements by simply eliminating the source of mistakes and no statistical treatment would be necessary. However, according to the latest science available to the FNET research group, we consider this data to be mistake free. The frequency data is perhaps error-ridden, meaning that, in the data recorded by each FDR, there are measurements that depart from the true value of the frequency [20]. What is the source of the error that renders the FDR measurements so noisy? Aside from the inescapable experimental errors that arise from the ever-present although minuscule measurement error, each FDR is prone to measuring noise from the utility's distribution network. A key benefit of FNET is that it relies upon FDRs that are, in general, installed to take measurements of frequency at the distribution level. Furthermore, these units are not in any manner protected or buffered from other devices also connected to the distribution network that may cause disturbances in voltage signals or otherwise degrade local power quality. Many have researched and explained the power quality problems that appear at the distribution level [11, 21-23]. Although the FDRs read and measure the small disturbances at the distribution level, we do not wish to consider these relatively minute disturbances, that are not a true reflection of power system frequency, when analyzing large scale power system contingencies [24]. These local disturbances become to us as noise with possible outliers. The following figure is a prime example of a set of problematic data recorded by an older FDR running a previous, now updated and replaced, firmware version.

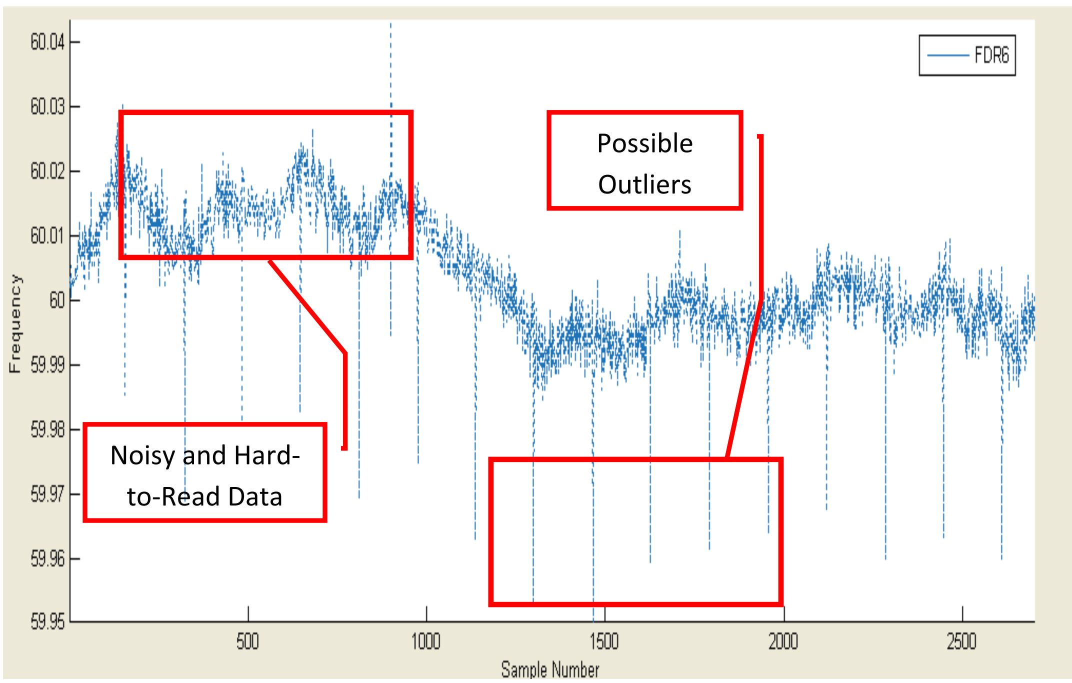

Figure 1-17: Problematic FDR data with signal quality issues highlighted.

From Figure 1-17, it is obvious that the frequency waveform as measured at the distribution level is quite noisy making discernment of the actual frequency values difficult. Appendix III discusses a few techniques used to estimate the true value of the frequency. These techniques draw ideas from the realms of conventional and robust statistics to deal with noisy data [25-29]. An effort is made to keep the complexity of data conditioning to a minimum for the purpose of computational efficiency.

We shall not consider wide-area frequency data as collected by FNET, a stochastic process in general, to be a strictly stationary process since the probability distribution of frequency data at one instant in time is not guaranteed to be the same for all times. Raw wide-area frequency data also does not meet the requirements for wide-sense stationarity. Although all machines on the electric grid are operated such that nominal system frequency is held at or very near 60 Hz, this scenario is not always realized. Therefore, the following condition of wide-sense stationarity is not met:

$$\mathbb{E}\{f(t)\} = \mu_f(t) = \mu_f(t+\tau) \ \forall \tau \in \mathbb{R}$$

where $f(t)$ is the interconnection frequency. Trend variations in interconnection frequency are often displayed in seasons of heavy loading such as mid-summer for the EI. In the late evening, typically between 10:00 pm and 12:00 am EDT, peak demand generation units (often called "peakers") ramp down as demand decreases and market prices fall. This process can result in "frequency slumps" as the remaining generation units adjust to accommodate the rapid grid-wide reductions of power injections. Although these so called slumps usually last for thirty minutes or less, the nominal frequency (trend) is significantly detracted from a nominal value of 60 Hz. The slumps are usually rectified within the next schedule change affected by the regional system operators. Nevertheless, such slumps can be quite dangerous should any large contingency occur during the slump. Figure 1-18 provides an example of the EI's occasional but severe trend deviations.

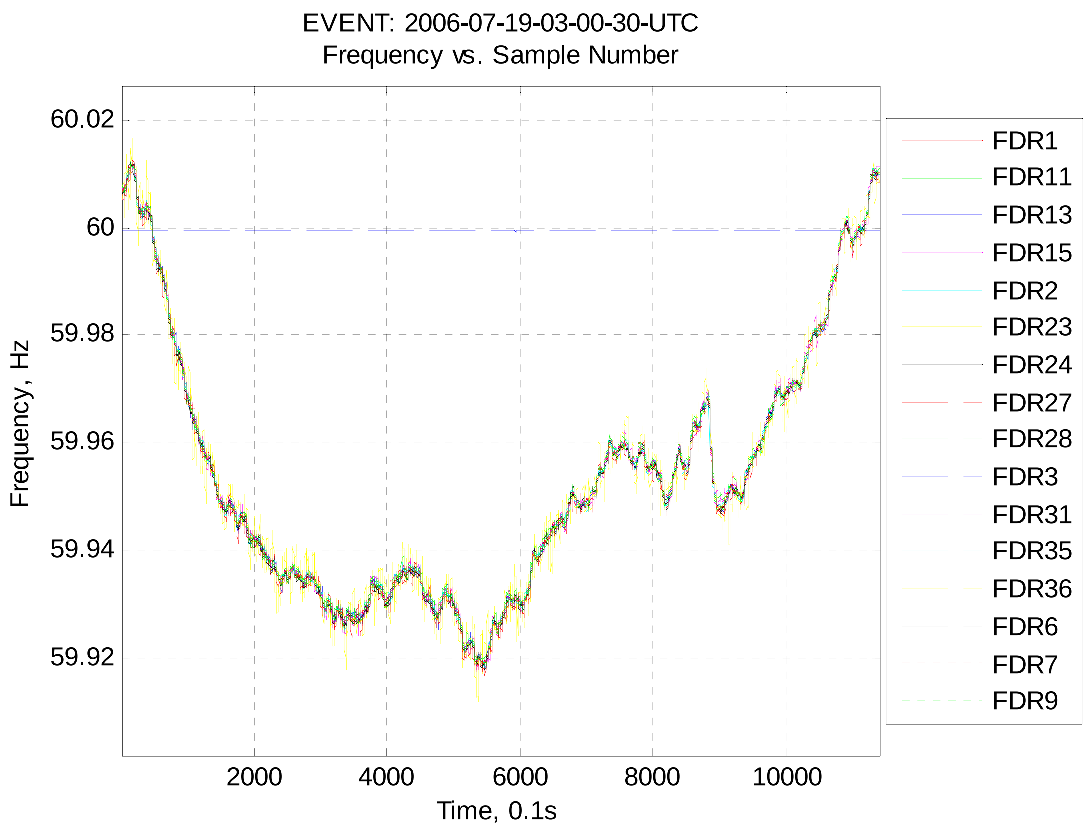

Figure 1-18: EI system frequency between 10:00 pm and 10:20 pm (EDT) on July 18, 2006.

To place the severity of this particular event in context, we examine the histogram of interconnection frequency during a normal peak season day (Figure 1-19). Notice the scarcity of data in bins near 59.94 Hz in Figure 1-19. Figure 1-18 shows an excess of 4,000 frequency records (more than six minutes) below 59.94 Hz.

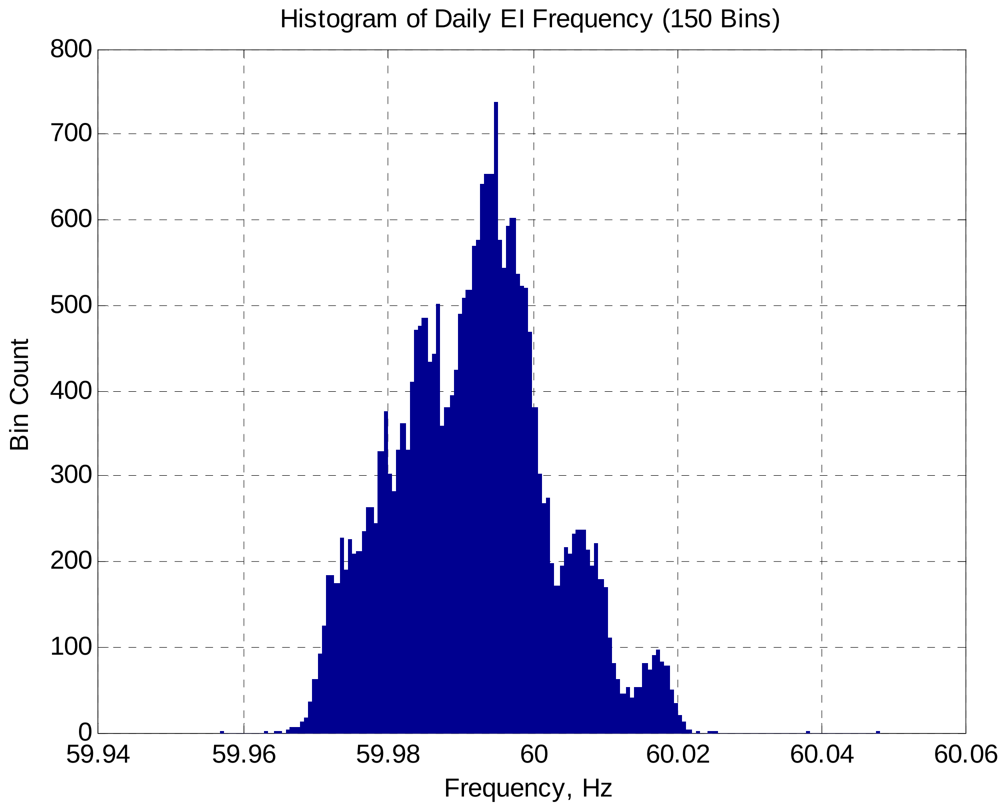

Figure 1-19: Histogram containing one day's frequency records (864,000 points) during peak season.

Frequency measurements from throughout an interconnection may also have different noise patterns. Let us consider measurements made from two arbitrary FDRs, labeled with indices i and j. These two sensors are placed at two different locations within a single (non-islanded) electrical interconnection at points $\mathbf{x}_i = (x_i, y_i)$ and $\mathbf{x}_j = (x_j, y_j)$, respectively. For the moment, let us assume that sensors in separate geographical locations within an interconnection are also located at topologically separate electrical nodes within the interconnection. Further, let us make the assumption that any two sensors geographically close are also electrically close and that any two sensors geographically distant are also electrically distant. We now decompose our frequency measurements as follows:

$$f(\mathbf{x}_i, t) = \mu_i(t) + s_i(t) + \eta_i(t)$$
$$f(\mathbf{x}_j, t) = \mu_j(t) + s_j(t) + \eta_j(t)$$

where $\mu_n(t)$ is some "slowly" varying trend component, $s_n(t)$ is a seasonal components, and $\eta_n(t)$ are the noise components of the signals. Having not yet identified seasonal trends in ambient frequency data we shall operate under the assumption regarding the seasonal components:

$$s_i(t) = s_j(t) = 0$$

Also, we recognize that, for two measurements made within a synchronous interconnection, the trend components are constrained to be equal as well (but in general not zero). Such that:

$$\mu_i(t) = \mu_j(t)$$

and under normal or near-normal operating conditions we should hope to see:

$$\mu_i(t) = \mu_j(t) \approx 60\,\mathrm{Hz}$$

We cannot, however, make any further generalizations about the model to constrain the noise components, $\eta_n(t)$, based upon empirical observations. In fact from past examinations, we have found the distributions of the noise components both stray from Gaussianity and differ between measurement units. The following Q-Q plots demonstrate these notions.

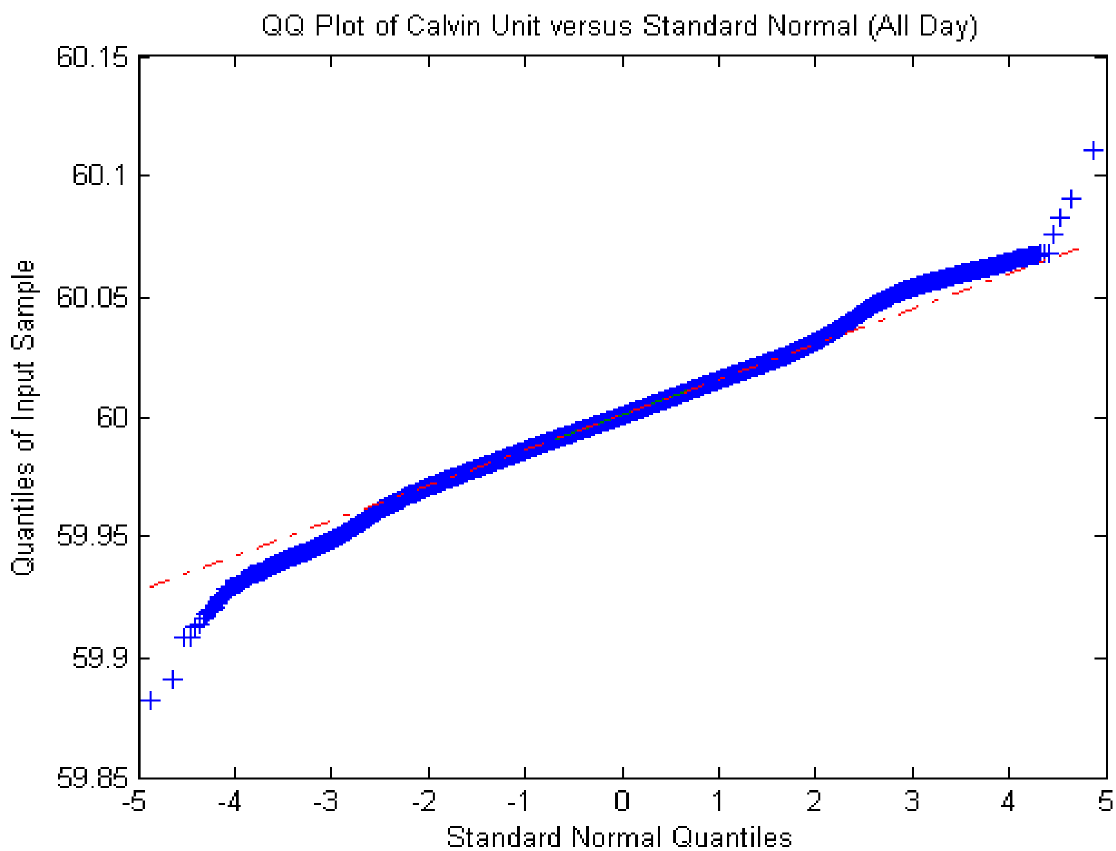

Figure 1-20: Q-Q Plot of daily frequency measurements versus the standard normal distribution.

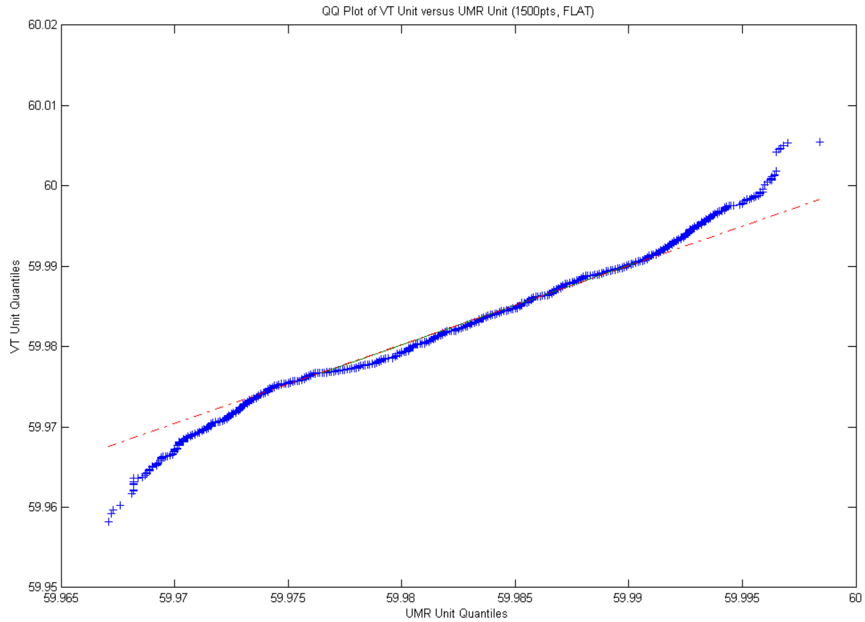

Figure 1-21: Q-Q plot of frequency measurements made concurrently by two separate FDRs approximately 750 miles apart.

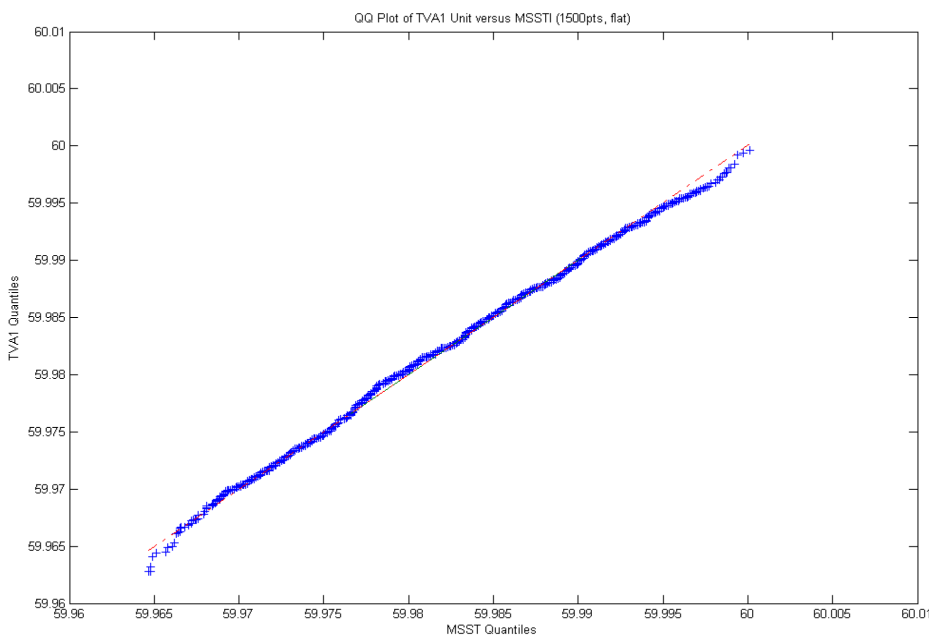

Figure 1-22: Q-Q plot of frequency measurements made concurrently by two separate FDRs approximately 500 miles apart.

From Figure 1-20, Figure 1-21, and Figure 1-22, it is possible to see slight variations in the probability distributions of the noise components. In summary, noise in data recorded by FDRs tends to be slightly heavy-tailed compared to the standard normal distribution. Further, comparisons between the noise components of different FDRs show that the noise distributions are not always consistent.

The nature of the wide-area frequency measurements made by FNET is mentioned so that, in subsequent chapters, we might understand the need for various filters used.

Scenario Information

In 2007, 67 generation trips have been detected, identified, and confirmed as a foundation for base cases used within this report. Each of these cases, or events, occurred in the EI. Appendix IV contains information regarding the scenario details. No guarantee is made that every generation trip of 2007 is listed in the appendix. This caveat is made for three reasons:

- Some events may have been overlooked due to equipment and or algorithm malfunctions.
- Some events have been detected but not confirmed and/or cross-validated.
- Some events were of such low magnitude that they are not considered relevant for the analysis in this report. In general, events resulting in a generation-load mismatch of less than 500 MW are considered insignificant to the analysis contained herein.

Of note is the fact that not all of the frequency data from every scenario are available due to server and/or sensor malfunctions. An attempt was made to identify the location of each of the triggered disturbances within the PSS/E model. The table in Appendix IV identifies which events have been found either in measured data or in the PSS/E model.

Model Information

Some sections of this report refer to simulated data and interconnection modeling. The simulations presented within this report were conducted using PSS/E. Of the 2,287 generators mentioned earlier in this chapter, 336 units with nameplate capacities greater than 500 MW have been identified in the system model. More than a trivial identification of large units, this identification process has located each of the machines listed in Appendix V geographically. The red points in Figure 1-5ff indicate the identified generators in the model.

Organization of Study

Chapter 2 will discuss the process by which generation-load mismatch events can be identified in near real-time (delays on the order of a few seconds). The chapter begins by presenting the basics of frequency behavior during disturbances. A method is then developed that takes advantage of the statistical distance measure, the Mahalanobis distance, to detect and trigger upon disturbances that impact the entire interconnection. The chapter closes with a discussion on event magnitude and its relation to the interconnections frequency response.

Chapter 3 focuses on the detection and analysis of oscillations that occur during both “clear-sky” conditions and events. The chapter opens with a discussion on the significance of power system oscillations and the ability of FNET to observe these oscillations. Both single-channel and multi-channel matrix pencil methods are discussed and applied to wide-area frequency data. The oscillation analysis is further verified by application to the WECC tests presented earlier in this introduction.

Chapter 4 treats power system event location in the context of distribution level frequency measurements. Several deterministic methods are presented and their disadvantages exposed. A discussion of electromechanical wave-front speed results in the development of rudimentary interconnection speed maps. Non-parametric event location methods are presented and applied to both measurement and simulation data. The notion of using voltage angle measurements is also introduced and applied to simulation data.

Chapter 5 draws Chapters 2 through Chapter 4 together and presents some practical aspects of power system event reporting.

Chapter 6 concludes the report and discusses both a proposal of future work and the contribution of the presented research.

Working Context

This report relies heavily on the presentation and examination of power system measurements, specifically wide-area frequency measurements. Since 2003, the FNET research team at Virginia Tech has been measuring, collecting, and archiving wide-area frequency data from across North America, Asia, Europe, and Africa. Access to similar data from utilities is rather limited if it exists. Hence, this report provides first access and first analysis to an entire realm of distributed power system monitoring. The 2007 EI case study material is unique and provides great insight into the behavior of the electrical grid for years to come. Having established the data intensive nature of this report, we commence into a discussion power system event detection and frequency response.

Chapter 2: Generation-Load Mismatch Detection and Analysis

In the demonstration of the utility of distribution level wide-area measurements, system frequency becomes of capital importance due to the ability to accurately estimate the parameter at virtually any voltage level in the interconnection. This chapter examines the meaning of changes in system frequency in a wide-area context. Classically, due to a general lack of high-resolution frequency data, "accurate measurement of system response is difficult unless the frequency deviation... is significant [30]." However, using the FNET system, we demonstrate the ability to detect power system disturbances, classify the disturbances, and estimate the magnitude of the disturbances.

Generation-Load Mismatch and System Frequency

Consider the generator depicted in Figure 2-1:

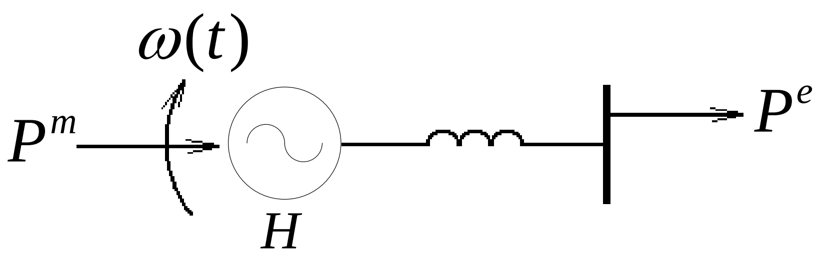

Figure 2-1: Single machine electromechanical diagram.

The dynamics of this system are governed by an extension of Newton's second law of motion applied to rotating masses, the *Swing Equation*:

$$\frac{2H}{\omega_0}\frac{d\omega(t)}{dt} = P^m - P^e \tag{2.1}$$

where P^m is the mechanical power injection in megawatts (MW) resulting from a torque applied by the machine's turbine onto the generator's shaft. The parameter, P^e, is the electrical power in megawatts (MW) withdrawn by an electrical load applied to the generator's terminal. The machine's inertia is represented by H with units of megajoule per megavoltampere (MJ/MVA or seconds) and its rotational velocity in radians per second is $\omega(t)$. Synchronous frequency of the electrical system is denoted by the parameter ω_0. In North America, we have $f_0 = 60\text{ Hz} \rightarrow \omega_0 = 2\cdot\pi\cdot 60\ \frac{\text{rads}}{\text{s}}$, whereas in Europe and other parts of the world: $f_0 = 50\text{ Hz} \rightarrow \omega_0 = 2\cdot\pi\cdot 50\ \frac{\text{rads}}{\text{s}}$. Given the simple system of Figure 2-1 and the Swing Equation (2.1), it becomes quite easy to determine the magnitude of any power mismatch experienced by the generator based upon frequency measurements assuming all system parameters are known. An interconnection, however, includes many machines and many loads. Therefore, we seek to extend the theory of single-machine single-load behavior to multiple machines connected through some network to multiple loads as shown in Figure 2-2.

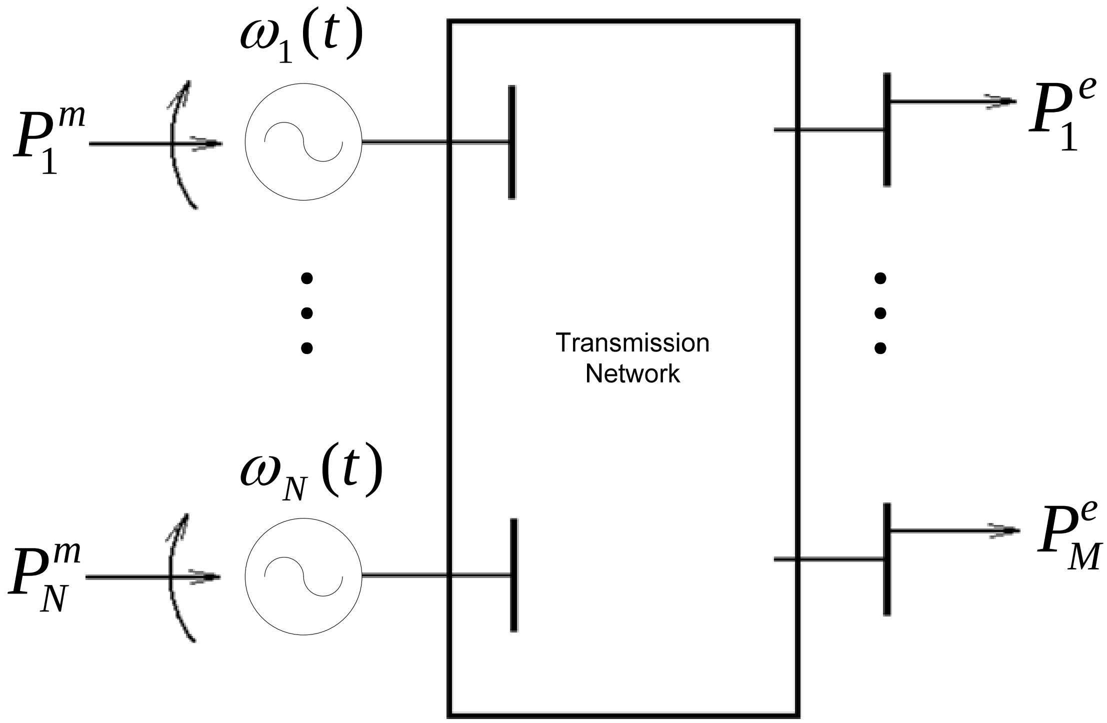

$$\int_{t-\frac{T}{2}}^{t+\frac{T}{2}} \omega_1(t)dt = \int_{t-\frac{T}{2}}^{t+\frac{T}{2}} \omega_2(t)dt = \cdots = \int_{t-\frac{T}{2}}^{t+\frac{T}{2}} \omega_N(t)dt$$

Figure 2-2: An arbitrary synchronous interconnection (*N* machines, *M* loads).

Stipulating that all system parameters follow the per-unit system on a common system MVA base, a familiar convention in the analysis of an electrical interconnection large or small, we can construct an aggregate model of the system through appropriate summations as follows:

$$H_{\text{system}} = \sum_{i=1}^{N} H_i$$

$$P_{\text{system}}^m = \sum_{i=1}^{N} P_i^m$$

$$P_{\text{system}}^e = \sum_{i=1}^{M} P_i^e$$

Thus we can write a swing equation for using our aggregate system parameters:

$$\frac{2H_{\text{system}}}{\omega_0}\frac{d\hat{\omega}(t)}{dt} = P^m_{\text{system}} - P^e_{\text{system}} \tag{2.2}$$

Notice that (2.2) uses an interconnection frequency estimate term, $\hat{\omega}(t)$. We have defined our understanding of frequency behavior within a synchronous interconnection based upon (1.1). Though instantaneous frequency values may vary from point to point within the transmission network, we know the time average of frequency as observed at each node in the network to be consistent. Therefore, we estimate the interconnection frequency as follows for p observation points:

$$\hat{\omega}(t) = \frac{1}{p}\sum_{i=1}^{p}\omega_i(t)$$

Equation (2.2) provides a method of describing an entire interconnection aggregated into a single machine as shown in Figure 2-3.

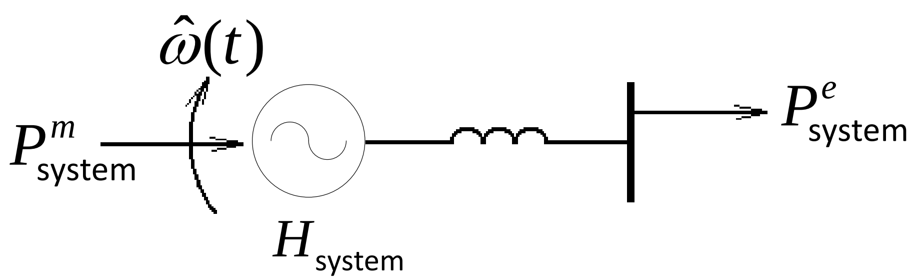

Figure 2-3: Aggregate representation of a synchronous electrical interconnection.

Individual machine and interconnection modeling is an entire area of study within the realm of power systems and has been well treated, including the basics covered in this report, by [8, 15, 31].

Under normal operation conditions, we should expect that generation and load are nearly matched for stable power system operation. Therefore:

$$P^m_{\text{system}} \approx P^e_{\text{system}}$$

When this situation is true, we have:

$$\frac{2H_{\text{system}}}{\omega_0}\frac{d\hat{\omega}(t)}{dt} \approx 0 \tag{2.3}$$

Further, the system inertia term in (2.3) is non-zero and, under normal circumstances, slowly varying. Therefore, the derivative of system frequency is close to zero under normal system operating conditions indicating that we expect system frequency to be flat. Let us now consider situations where generation and load are not nearly exactly matched. This situation can manifest itself in two fashions. First, load might exceed generation and thus:

$$P^m_{\text{system}} < P^e_{\text{system}}$$

Or, conversely, generation may exceed load:

$$P^m_{\text{system}} > P^e_{\text{system}}$$

From the aggregate swing equation, (2.3), it is clear that these situations result in system decelerations and accelerations, respectively. That is, with the understanding the interconnection frequency is, in fact, a rotational velocity. Two dramatic, yet frequent scenarios when such mismatches occur on the EI (and other interconnections) are generation trips and load shedding events. In the case of load shedding we have:

$$P^e_{\text{system}}(t^-) > P^e_{\text{system}}(t^+)$$
$$P^m_{\text{system}}(t^-) \approx P^m_{\text{system}}(t^+)$$

due to a discrete step decrease in load of amount $\Delta P^e_{\text{system}}$ such that:

$$P^e_{\text{system}}(t^-) = P^e_{\text{system}}(t^+) + \Delta P^e_{\text{system}}$$

The frequency of load shedding events, though often, is markedly lower than that of generation trip events within the North American interconnections. Load shedding typically occurs in one of two scenarios. First, because of some drastic chain of events causing an under-frequency situation, load is shed to save the interconnection from collapse. Or, secondly, and much more frequently, load is inadvertently shed when one or more pumped storage facilities trip offline. These tripping events typically occur in the early morning hours when many pumped storage facilities are operating to serve as a power sink for large generators that are not so easily cycled on and offline. The other generation-load mismatch scenario, which is much more frequent than load shedding, is generation tripping[4]. In this case we have:

$$P^m_{\text{system}}(t^-) > P^m_{\text{system}}(t^+)$$
$$P^e_{\text{system}}(t^-) \approx P^e_{\text{system}}(t^+)$$

due to a discrete step decrease in generation of amount $\Delta P^m_{\text{system}}$ such that:

$$P^m_{\text{system}}(t^-) = P^m_{\text{system}}(t^+) + \Delta P^m_{\text{system}}$$

[4] Generation trips occur on nearly a daily basis in the WECC whereas generation trips happen on about weekly in the EI.

Rather blatantly, in our discussion of the Swing Equation, we have ignored the effects of speed governors on the system. This oversight is justified for two reasons: First, and more strongly, the reaction times of speed governors due to generation-load mismatch take on values on the order of several seconds. This, compared to the immediate decline in frequency experienced by the interconnection, is quite large and worthy of oversight for our purposes. Second, especially in the case of the EI, governors on many machines have been observed to be minimally responsive [32].

In the wide-area sense, we now focus our attention on the effect of generation-load mismatch on system frequency response. In the case of a generator trip, which henceforward shall be our main focus, equation (2.3) no longer holds. There is an imbalance in power, $\Delta P^{m}_{\text{system}}$, yielding a negative slope in frequency representing the expenditure of rotating kinetic energy by the generators remaining online. Given that this imbalance is large enough, it must affect frequency throughout the electric grid[5]. In the context of Figure 2-2, however, our sensor locations are located demand-side. Also, we must consider the fact that most generators are distant from one another in remote locations. Therefore, due to the fact that the influence of such electromechanical disturbances travels throughout the electric grid exhibiting wave-like propagation behavior, the aforementioned decrease in frequency slope is typically not experienced *simultaneously* throughout a synchronous interconnection [33, 34].

Figure 2-4 through Figure 2-6 display the system frequency response of several generation trip events in each of the three major U.S. interconnections (as measured by FNET). Each figure contains a set of generator trips. The generation trips in each of the three figures are of comparable size to one another. It is therefore trivial to see that the behavior of each of the interconnections is relatively unique in the frequency recovery phase but definitely similar insofar as the generation-load mismatch causes a steep initial decline in frequency. The most predominant factor affecting frequency response of the various interconnections is the inertia of the systems. The inertia of the EI is approximately four times larger than that of the WECC and even larger than that of ERCOT [2, 35]. Therefore, we see lesser magnitude frequency excursions in the EI than in the WECC or ERCOT. Referencing the North American Electric Reliability Corporation's (NERC) frequency response standard (example given in Figure 2-7), differences in frequency recovery also manifest themselves amongst the three interconnections. For instance, the WECC and ERCOT appear to employ much more responsive governor actions [36]. Note the possible locations of the following points the figures that follow (see Figure 2-7):

- Point A: Interconnection frequency immediately before disturbance.
- Point B: Interconnection frequency at the point immediately after the frequency stabilizes due to governor action but before contingent control area takes action.
- Point C: Point of maximum frequency excursion due to the loss of rotating kinetic energy from the interconnection.
- Point D: Interconnection settling frequency 60 seconds after contingency.

[5] Empirically we have found "large enough" to be quantified by generation-load imbalances of greater than 500 MW ($\Delta P^{m}_{\text{system}} > 500$). This is not to say that smaller disturbances have no effect on system frequency. Rather, the effects of smaller imbalances become difficult to detect and discern from ambient noise and the normal undulating nature of electric power system frequency.

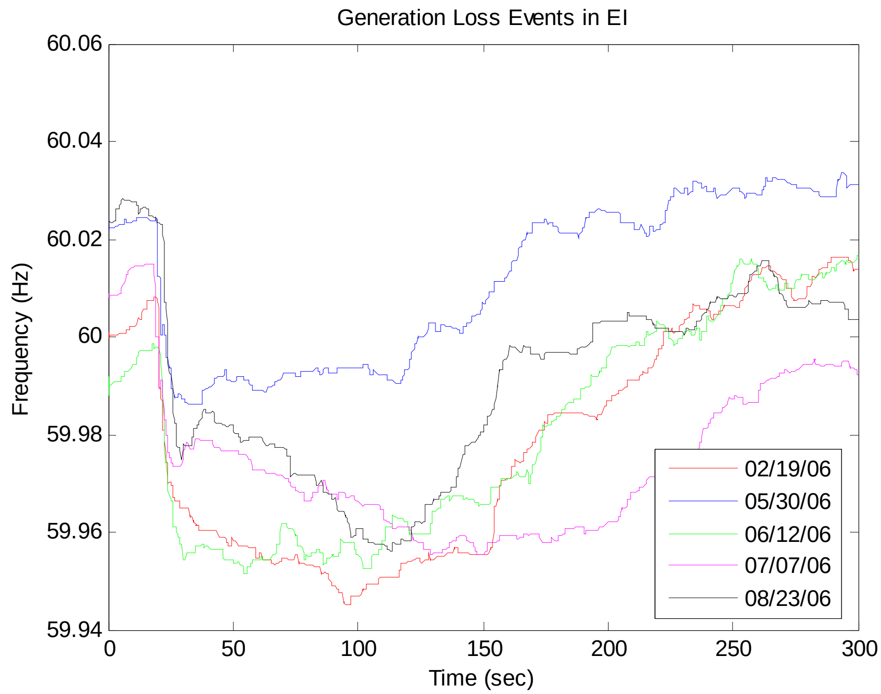

Figure 2-4: Generation Trips in the Eastern Interconnection (EI).

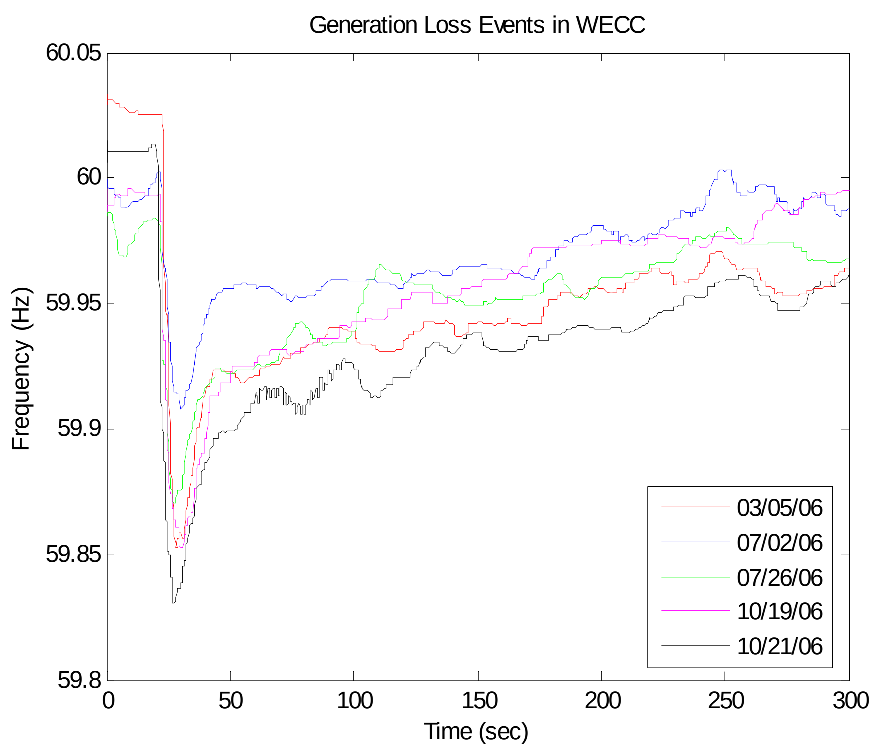

Figure 2-5: Generation Trip Events in the Western Interconnection (WECC).

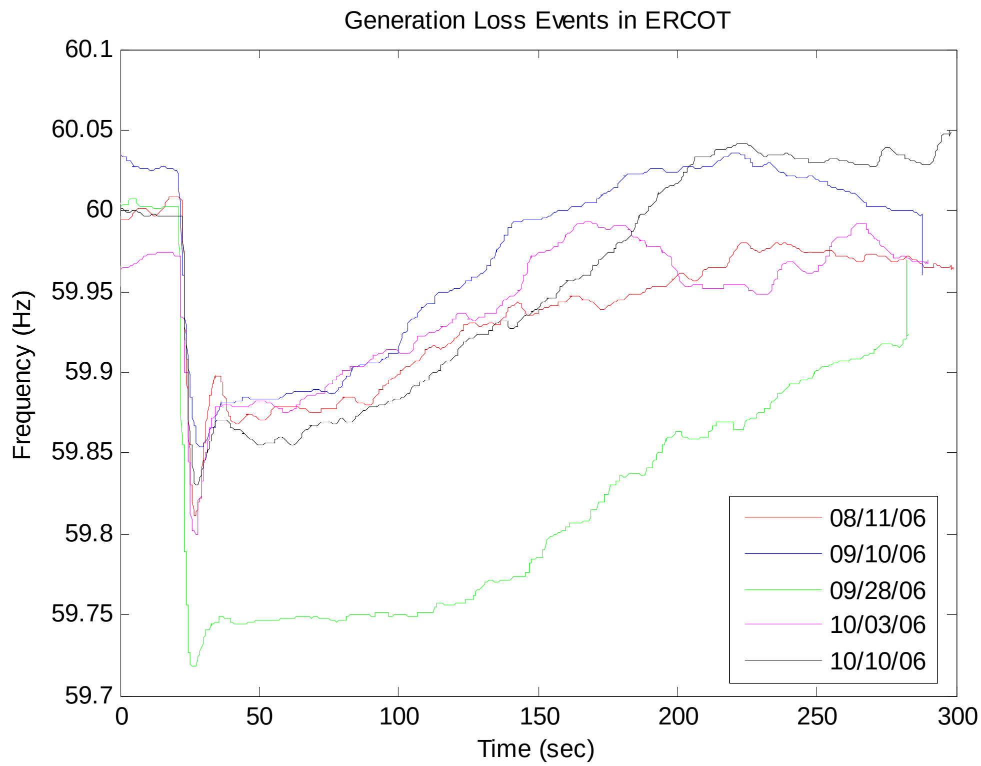

Figure 2-6: Generation Trip Events in the Texas Interconnection (ERCOT).

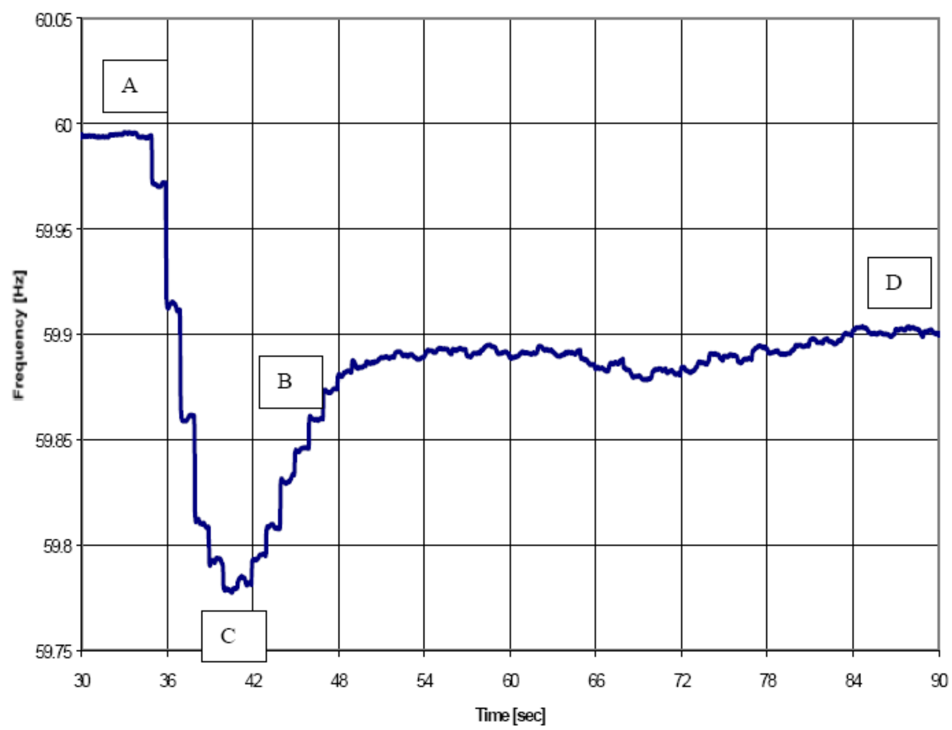

Figure 2-7: NERC frequency response standard definition of event points A, B, C, and D.

Large load shedding events also have an impact on the frequency of an interconnection. Load shedding, due to its rarity relative to generation trips and generally benign nature, is significantly less regulated by NERC. Figure 2-8 through Figure 2-10 display a collection of representative load shedding frequency signatures as measured by FNET. Similar remarks can be made about these data as were discussed above. The main point is that an overall system acceleration results from the reduction in system load.

We now consider a very unique but extremely rare situation – interconnection islanding. In the five years of FNET's operation, only one islanding event has occurred. We say that an islanding event occurs when a single synchronized interconnection divides into one or more asynchronous interconnections. The individual systems' frequency response due to islanding relies mainly on the generation-load balance in each of the islands before separation. If there is a near balance in both regions then the event may have a negligible effect on system frequency:

$$\sum_{\Re_i} P^m - P^e \approx 0 \rightarrow \frac{2H_{\Re_i}}{\omega_0}\frac{d\omega_{\Re_i}(t)}{dt} \approx 0 \quad \forall \text{Regions}, \Re_i$$

However, in the case of the 2007 EI separation, there was not a near generation-load balance before the islanding. The northwestern portion of the EI, say $\Re_1$, was supplying power to the rest of the interconnection, $\Re_2$, as shown in Figure 2-11. Cross reference Figure 2-11 with Figure 1-11 (obtained from simulation). Conventional wisdom tells us that power flows "downhill" in terms of phase angle.

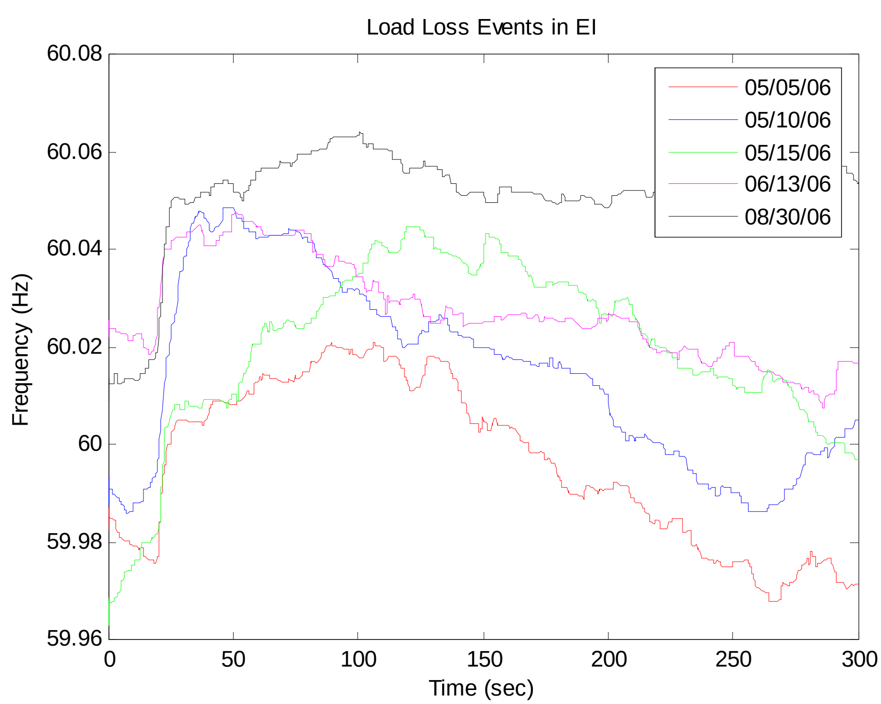

Figure 2-8: Load shedding events in the Eastern Interconnection (EI).

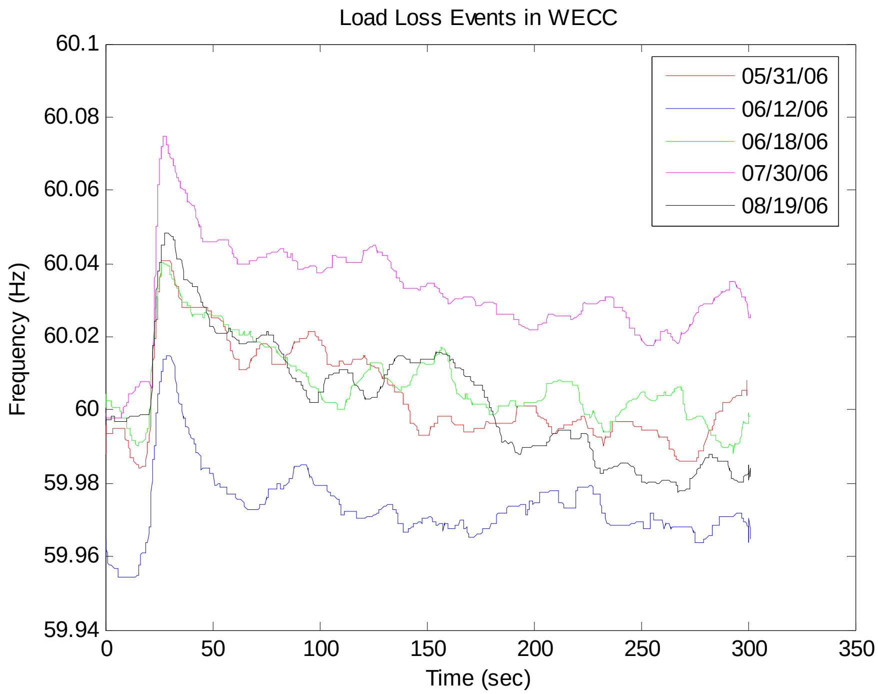

Figure 2-9: Load shedding events in the Western Interconnection (WECC).

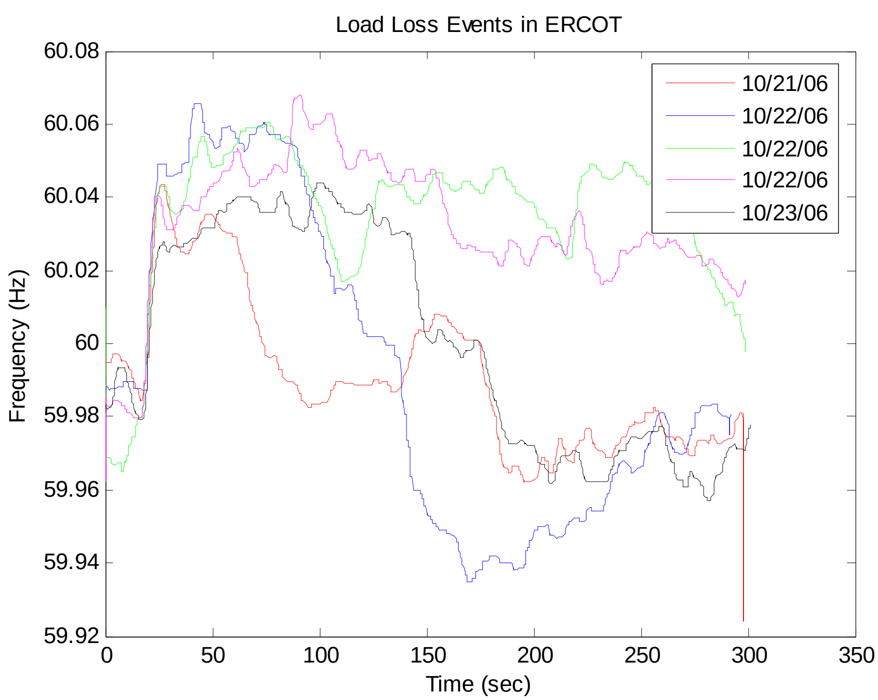

Figure 2-10: Load shedding events in the Texas Interconnection (ERCOT).

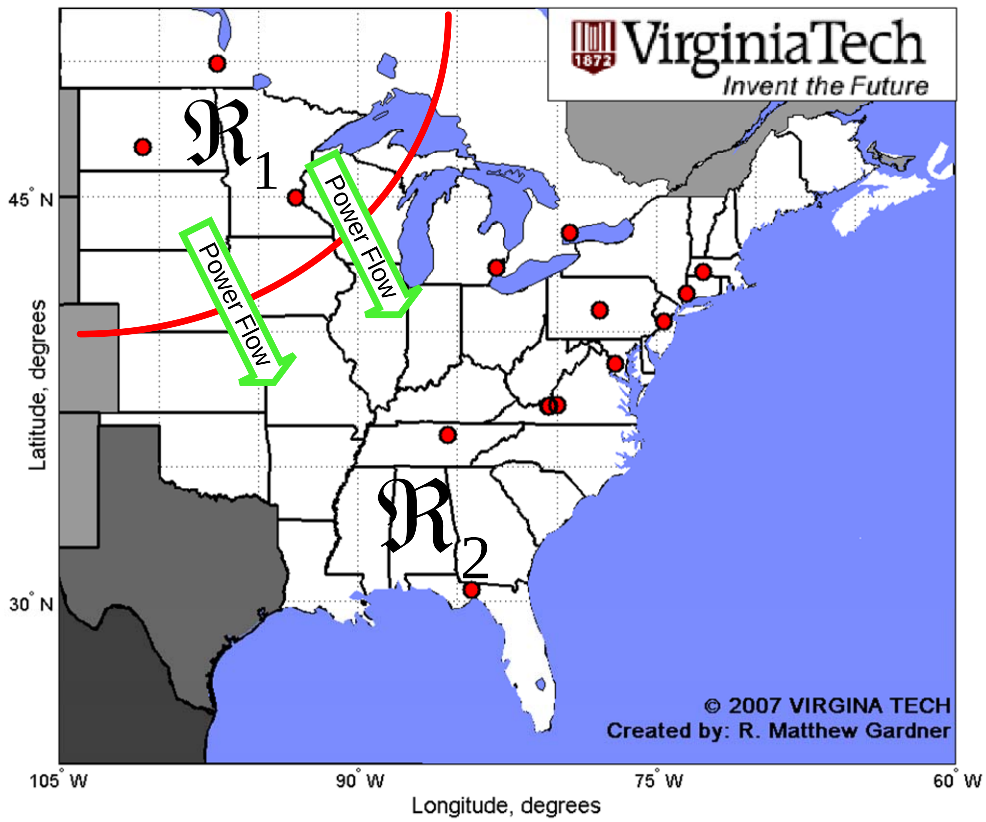

Figure 2-11: EI separation map.

In this case there is not a generation-load balance in both regions in fact we have:

$$\sum_{\Re_1} P^m - P^e > 0$$
$$\sum_{\Re_2} P^m - P^e < 0$$

Or, more concisely:

$$\sum_{\Re_1} P^m - P^e - P^t \approx 0$$
$$\sum_{\Re_2} P^m - P^e + P^t \approx 0$$

where P^t is the power transfer from $\Re_1$ to $\Re_2$ at the time of islanding. In this scenario, which exhibits significant power transfer from one region to another, when islanded, one island will accelerate while another will decelerate according to the magnitude of P^t respective to the magnitude of each interconnections islanded inertias, $H_{\Re_i}$. In context with our discussion about generation trips and load shedding, such an islanding scenario will behave like load shedding in the generation-rich island and like a generation trip in the loaded island.

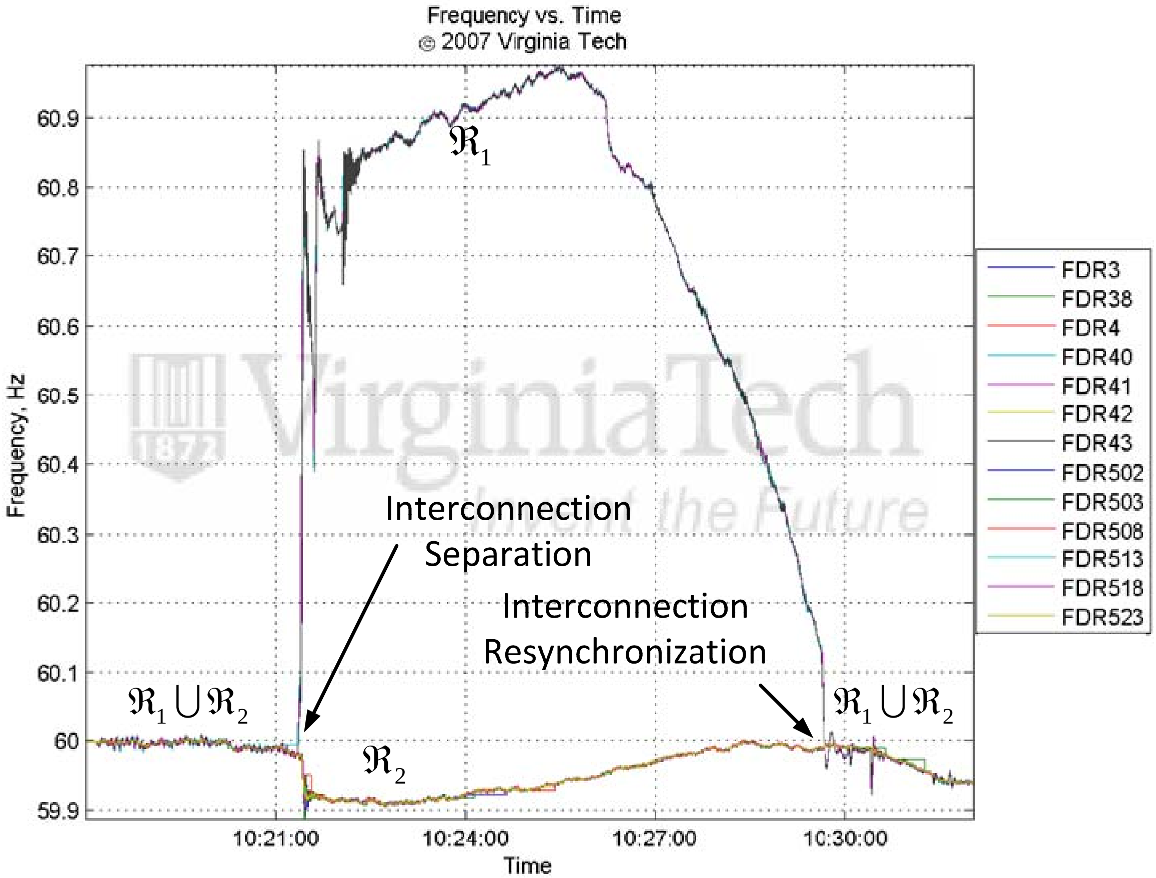

Figure 2-12: EI response to system islanding.

Detection of Generation Trips in Ambient Frequency Data

The last section discussed the basics of interconnection behavior due to generation-load mismatch. In this section we shall cover the details of how we can detect generation trips using wide-area frequency data. Based upon examination of the generation trips of Figure 2-4 or the islanding scenario of Figure 2-12, one might be tempted to trigger a detection algorithm based upon migration of system frequency outside of a predetermined dead band. In fact, previous methods used by the FNET team have included triggering off of the migration of the frequency signal outside of a set dead band or the derivative of the frequency signal. However, given that frequency is not necessarily stationary throughout the day (as discussed in Chapter 1) and since noise exists in the frequency signal, the use of these methods alone will result in false alarms. Furthermore, finding generation trips may not be trivial. Examine Figure 2-13 and notice how the generation trip signature does not appear distinguishable based upon some threshold.

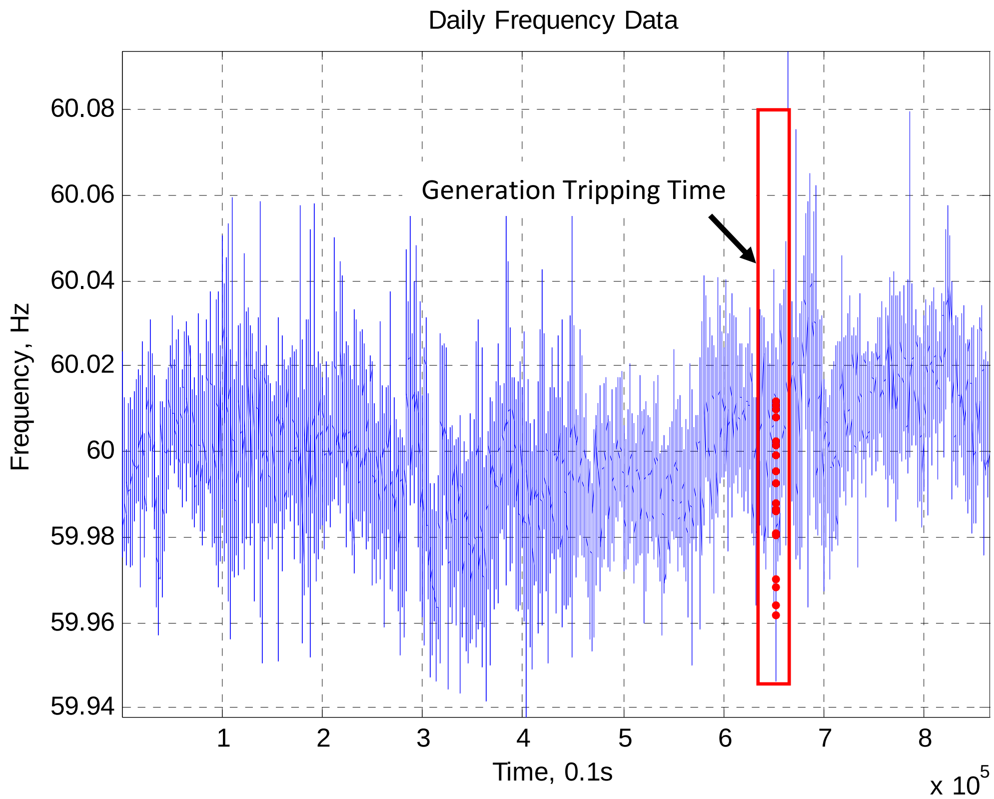

Figure 2-13: Daily frequency data (EI) with generation trip.

Having spoken about the observation of generation trips through wide-area frequency data, we yet have to deal with the question of motivation. Why detect generation trips using wide-area frequency data? There are two main reasons for attempting a detection strategy. First, and perhaps more practically, generation trips are events that pose a technical problem requiring a technical response. Beyond resulting in a mismatch between generation and load, generation trips can also cause a redistribution of power flows on the interconnection, they can induce dynamic phenomena such as power system oscillations which may or may not be dangerous, and they necessitate a re-examination of reliability constraints (such as the well-known N-1 criterion). Second, generation trips have financial consequences. Energy markets must adjust in situations where generation facilities are unable to meet their contracted power output levels. This situation is suboptimal for both the plant owner/operator and the buyer. Plant owners and operators can be fined for failing to deliver contracted power while the energy traders scramble to purchase power at a potential premium. In an environment where generation trips are communicated between utilities and operators across an interconnection via technology as simplistic as a phone call, there is significant room for the introduction of a technology that can detect and locate generation trips using wide-area frequency data (which is widely available) [37]. Hence, in order to estimate the amount and location of a generation trip, we begin by discussing methods event detection.

Statistical Event Location

We begin by examining frequency measurements from two arbitrary sensors (FDRs) under normal operating conditions. Since we are interested in the behavior of multiple data points we form a matrix from two vectors as follows:

$$\mathbf{F} = \begin{bmatrix} \mathbf{F}_i & \mathbf{F}_j \end{bmatrix} = \begin{bmatrix} f_{i,k-N} & f_{i,k-N+1} & \cdots & f_{i,k-2} & f_{i,k-1} \\ f_{j,k-N} & f_{j,k-N+1} & \cdots & f_{j,k-2} & f_{j,k-1} \end{bmatrix}^T \in \mathbb{R}^{N \times 2}$$

Figure 2-14 displays a scatter plot of the data in vectors $\mathbf{F}_i$ and $\mathbf{F}_j$ with error ellipses.

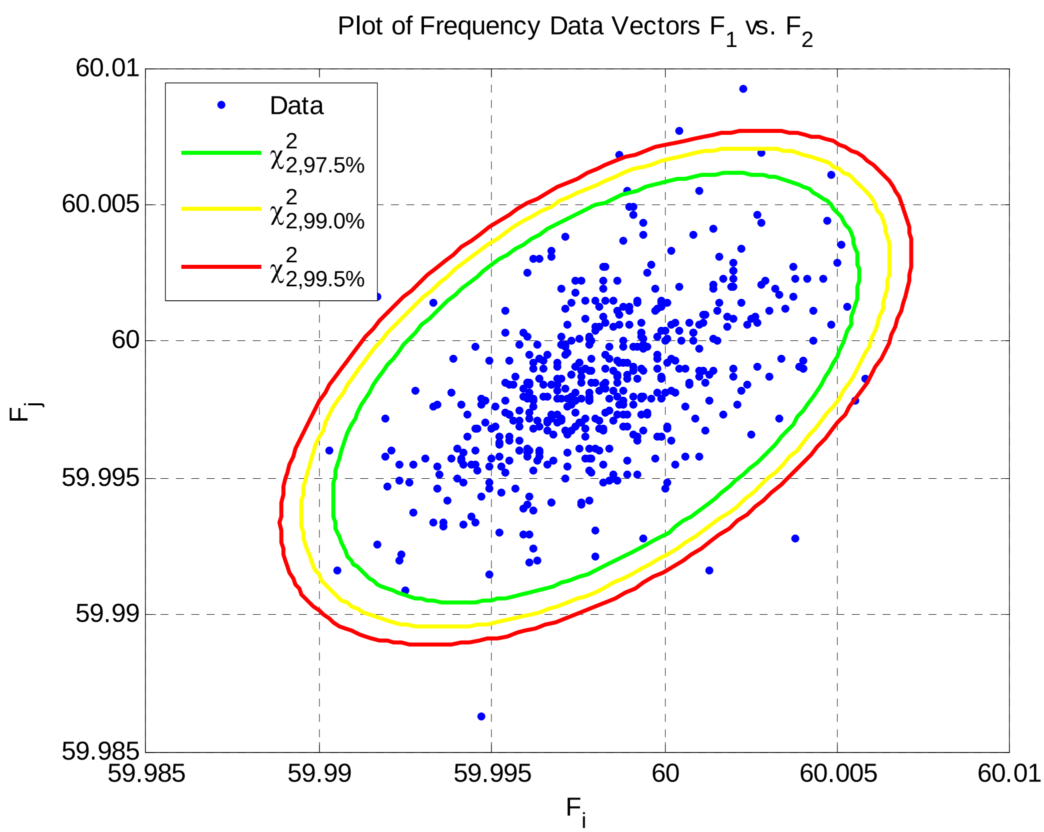

Figure 2-14: Scatter plot of frequency data as observed by two FDRs (i,j).

The error ellipses of Figure 2-14 are defined by points, $\mathbf{x} = \begin{bmatrix} x_1 \\ x_2 \end{bmatrix}$, that satisfy:

$$MD^2\left(\mathbf{x} \middle| \boldsymbol{\mu}, \mathbf{C}\right) = 7.38$$
$$MD^2\left(\mathbf{x} \middle| \boldsymbol{\mu}, \mathbf{C}\right) = 9.21$$
$$MD^2\left(\mathbf{x} \middle| \boldsymbol{\mu}, \mathbf{C}\right) = 10.6$$

respectively. These ellipse employ the Mahalanobis Distance metric defined by:

$$MD^2\left(\mathbf{x}\middle|\boldsymbol{\mu},\mathbf{C}\right)=\left(\mathbf{x}-\boldsymbol{\mu}\right)^T\mathbf{C}^{-1}\left(\mathbf{x}-\boldsymbol{\mu}\right)\in\mathbb{R}^1$$

where $\boldsymbol{\mu}$ is the sample mean vector defined:

$$\boldsymbol{\mu}=\begin{bmatrix}\frac{1}{N}\sum_{q=k-N}^{k-1} f_{i,q}\\ \frac{1}{N}\sum_{q=k-N}^{k-1} f_{j,q}\end{bmatrix}\in\mathbb{R}^{2\times1}$$

and $\mathbf{C}$ is the sample covariance which is an estimator of the covariance, $\boldsymbol{\Sigma}$, of the probability distribution from which the data in $\mathbf{F}$ are drawn. We calculate $\mathbf{C}$ as:

$$\mathbf{C}=\frac{1}{N-1}\sum_{q=k-N}^{k-1}\left(\begin{bmatrix}f_{i,q}\\ f_{j,q}\end{bmatrix}-\boldsymbol{\mu}\right)\left(\begin{bmatrix}f_{i,q}\\ f_{j,q}\end{bmatrix}-\boldsymbol{\mu}\right)^T\in\mathbb{R}^{2\times2}$$

The distance parameters are chosen based upon the 97.5%, 99.0%, and 99.5% quantiles of the Chi-Squared distribution specified by the degrees of freedom in the data (2). The Chi-Squared distribution is a common basis used in applied statistics for making inferences about the variance of an arbitrary population based upon a sample set of data [38]. We also remind ourselves that the principle axes of the confidence ellipses are defined by the eigenvectors of the sample covariance matrix, $\mathbf{C}$. Correspondingly, the lengths of the semi-major and semi-minor axes, ℓ_i, can be calculated from the eigenvalues of the sample covariance matrix:

$$\begin{aligned}\ell_{i,97.5\%}&=\sqrt{\lambda_i\chi^2_{2,97.5\%}}=\sqrt{7.38\lambda_i}\\ \ell_{i,99.0\%}&=\sqrt{\lambda_i\chi^2_{2,99.0\%}}=\sqrt{9.21\lambda_i}\\ \ell_{i,99.5\%}&=\sqrt{\lambda_i\chi^2_{2,99.5\%}}=\sqrt{10.6\lambda_i}\end{aligned}$$

Given these definitions, let us consider the position of the centroid of *new* points, $\mathbf{F}^*$, defined in similar manner as $\mathbf{F}$ by:

$$\mathbf{F}^*=\begin{bmatrix}\mathbf{F}_i^* & \mathbf{F}_j^*\end{bmatrix}=\begin{bmatrix}f_{i,k} & f_{i,k+1} & \cdots & f_{i,k+M-2} & f_{i,k+M-1}\\ f_{j,k} & f_{j,k+1} & \cdots & f_{j,k+M-2} & f_{j,k+M-1}\end{bmatrix}^T\in\mathbb{R}^{M\times2}$$

where, for our purposes, we stipulate:

$$M\ll N$$

The centroid of $\mathbf{F}^*$ is $\boldsymbol{\mu}^*$ and is calculated in a robust fashion using the median:

$$\boldsymbol{\mu}^* = \begin{bmatrix} \text{median}\begin{bmatrix} f_{i,k} & f_{i,k+1} & \cdots & f_{i,k+M-2} & f_{i,k+M-1} \end{bmatrix} \\ \text{median}\begin{bmatrix} f_{j,k} & f_{j,k+1} & \cdots & f_{j,k+M-2} & f_{j,k+M-1} \end{bmatrix} \end{bmatrix} \in \mathbb{R}^{2\times 1}$$

The location of the *new* centroid can now be compared with that of the existing point cloud. In this sense, we are using the point cloud defined by the previous N measurements to serve as an estimator for the location of where the new centroid should exist. For stationary or wide-sense stationary data we should expect, according to our definitions:

$$\boldsymbol{\mu} \approx \boldsymbol{\mu}^*$$

In the absence of an event having occurred during the time spanned by the new set of data samples, we might expect the centroid of the new point cloud to reside within the bounds of the confidence ellipses. Figure 2-15 displays the old point cloud in blue along with the new data points in red. The centroid of the new data points is also indicated and can be seen to be situated within the tolerance ellipses.

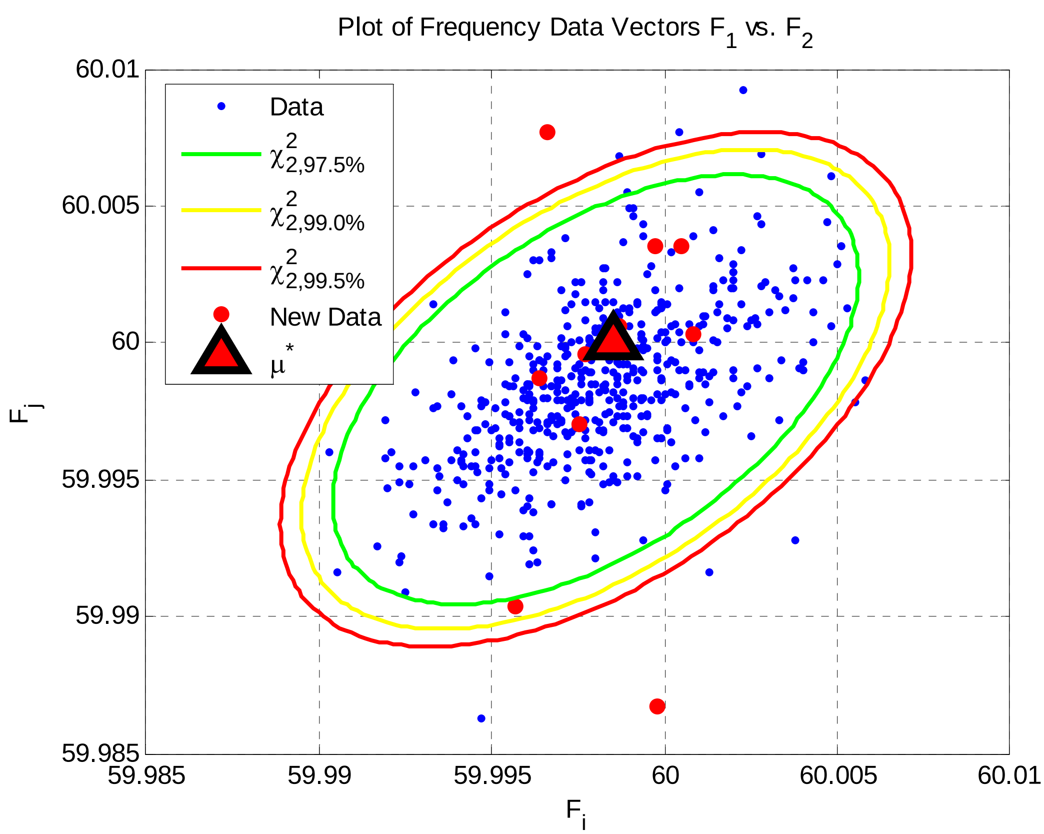

Figure 2-15: Old point cloud (in blue) plotted with new point cloud (in red).

To verify the situation of the centroid of the new data within the confidence ellipses numerically, we calculate the Mahalanobis Distance of the new centroid, $\boldsymbol{\mu}^*$, from the old centroid, $\boldsymbol{\mu}$:

$$MD^2\left(\boldsymbol{\mu}^*\middle|\boldsymbol{\mu},\mathbf{C}\right)=\left(\boldsymbol{\mu}^*-\boldsymbol{\mu}\right)^T\mathbf{C}^{-1}\left(\boldsymbol{\mu}^*-\boldsymbol{\mu}\right)\in\mathbb{R}^1$$

In the example of Figure 2-15, the Mahalanobis Distance (squared) of the new centroid from the old is calculated to be 0.342. This value is well below the squared distance of the nearest tolerance ellipse (7.38). The Mahalanobis Distance is a scalar representing a distance. However, our data is a vector. Though the distance itself is a scalar, it represents the *activity* of a vector of frequency measurements. We therefore associate $MD^2\left(\boldsymbol{\mu}^*\middle|\boldsymbol{\mu},\mathbf{C}\right)$ with an activity vector the length of $\mathbf{F}^*$ as follows:

$$\mathbf{A}=\left[MD^2\left(\boldsymbol{\mu}^*\middle|\boldsymbol{\mu},\mathbf{C}\right)\quad MD^2\left(\boldsymbol{\mu}^*\middle|\boldsymbol{\mu},\mathbf{C}\right)\quad\cdots\quad MD^2\left(\boldsymbol{\mu}^*\middle|\boldsymbol{\mu},\mathbf{C}\right)\quad MD^2\left(\boldsymbol{\mu}^*\middle|\boldsymbol{\mu},\mathbf{C}\right)\right]^T\in\mathbb{R}^{M\times1}$$

It is through the monitoring of this activity vector that we trigger the event detection algorithm.

This process involved data indexed from $k-N$ (in the matrix, $\mathbf{F}$, which we shall call the *parent cluster*) through $k+M-1$ (in the matrix, $\mathbf{F}^*$, which we shall call the *candidate cluster*), a total of $N+M$ frequency measurements from two FDRs. In a near real-time setting, the most recently available data point will have index $k+M-1$. It is worth noting that this algorithm will have a delay D, calculated as:

$$D=\frac{M}{f_s}+T_c$$

due to the formation requirements of the candidate cluster where f_s is the data sampling frequency. The computation time, which in most cases will be negligible, is accounted for in T_c. Figure 2-16 represents the process visually. Figure 2-17 represents the construction of the activity vector, $\mathbf{A}$.

Having populated (or updated) the activity vector, the iteration variable, k, can be incremented for the analysis of a newly arrived set of data. Therefore, k is incremented as follows:

$$k_{\text{new}}\Leftarrow k_{\text{old}}+M$$

The parent cluster can then be dismantled as follows:

$$\mathbf{F}=\left[\begin{array}{c}\mathbf{F}^{\text{discard}}\\\hline\mathbf{F}^{\text{remain}}\end{array}\right]=\left[\begin{array}{cc}\mathbf{F}_i^{\text{discard}} & \mathbf{F}_j^{\text{discard}}\\\hline\mathbf{F}_i^{\text{remain}} & \mathbf{F}_j^{\text{remain}}\end{array}\right]\in\mathbb{R}^{N\times2}$$

$$\left[\mathbf{F}_i^{\text{remain}}\quad\mathbf{F}_j^{\text{remain}}\right]=\begin{bmatrix}f_{i,k_{\text{old}}-N} & f_{i,k_{\text{old}}-N+1} & \cdots & f_{i,k_{\text{old}}-N+M-2} & f_{i,k_{\text{old}}-N+M-1}\\ f_{j,k_{\text{old}}-N} & f_{j,k_{\text{old}}-N+1} & \cdots & f_{j,k_{\text{old}}-N+M-2} & f_{j,k_{\text{old}}-N+M-1}\end{bmatrix}^T\in\mathbb{R}^{M\times2}$$

$$\left[\mathbf{F}_i^{\text{discard}}\quad\mathbf{F}_j^{\text{discard}}\right]=\begin{bmatrix}f_{i,k_{\text{old}}-N+M} & f_{i,k_{\text{old}}-N+M+1} & \cdots & f_{i,k_{\text{old}}-2} & f_{i,k_{\text{old}}-1}\\ f_{j,k_{\text{old}}-N+M} & f_{j,k_{\text{old}}-N+M+1} & \cdots & f_{j,k_{\text{old}}-2} & f_{j,k_{\text{old}}-1}\end{bmatrix}^T\in\mathbb{R}^{(N-M)\times2}$$

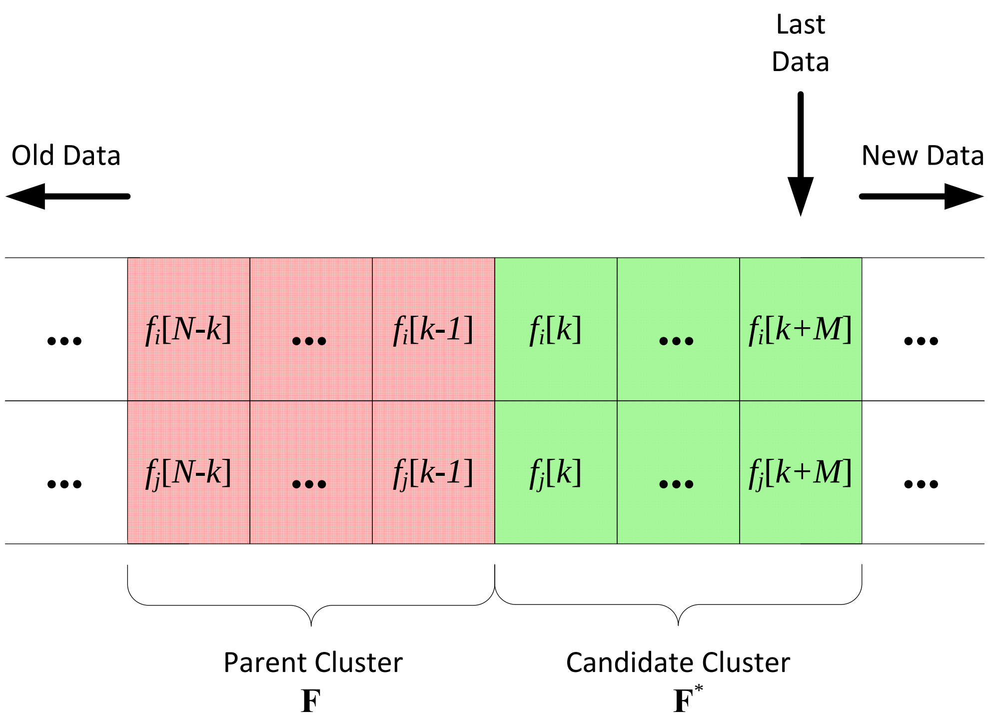

Figure 2-16: Event detection data vectors.

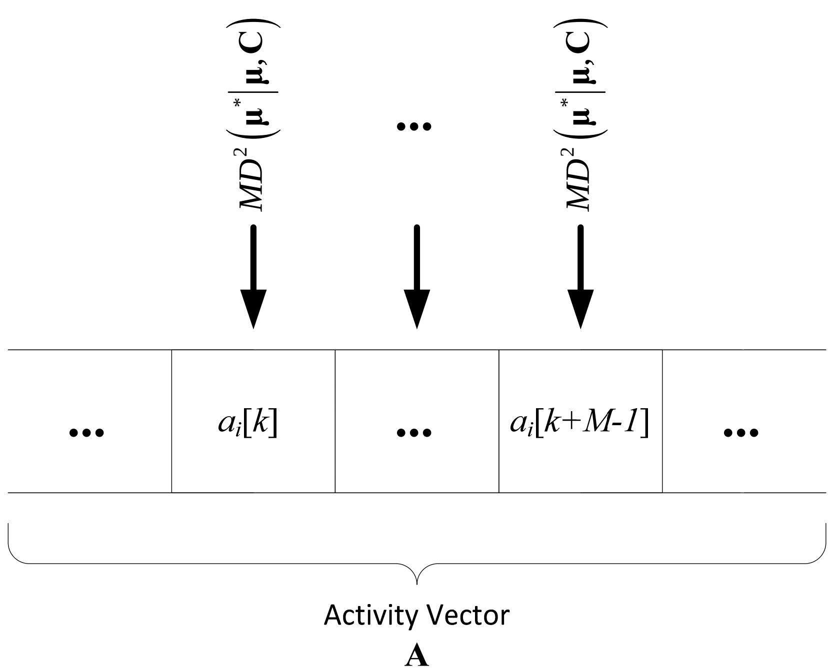

Figure 2-17: Construction of activity vector.

A *new* parent cluster can be formed using the remaining portion of the *old* parent cluster augmented with the previous candidate cluster as follows:

$$\mathbf{F}^{\text{new}} = \left[\frac{\mathbf{F}^{\text{remain}}}{\mathbf{F}^{*}}\right]$$

The process continues with the formation of a new matrix describing a new candidate cluster, $\mathbf{F}^{*,\text{new}}$, and the eventual calculation of a new activity vector, $\mathbf{A}^{\text{new}}$. For the moment, we have considered data from only two of the possibly multiple FDRs online. Wishing to base any form of event triggering on a consensus of triggers from all FDRs, the entire triggering process can be expanded (either in series or in parallel) to examine data from all FDRs. For the purposes of online implementation, pairs of FDRs are considered such that:

$$\wp\left(\begin{bmatrix}\mathbf{F}_i \\ \mathbf{F}_{i+1}\end{bmatrix}\right) \Rightarrow \mathbf{A}_i$$

where $\wp(\bullet)$ denotes the process of forming the activity vector using the Mahalanobis Distance methodology described above. For example,

$$\wp\left(\begin{bmatrix}\mathbf{F}_1 \\ \mathbf{F}_2\end{bmatrix}\right) \Rightarrow \mathbf{A}_1,\ \wp\left(\begin{bmatrix}\mathbf{F}_2 \\ \mathbf{F}_3\end{bmatrix}\right) \Rightarrow \mathbf{A}_2, \cdots, \wp\left(\begin{bmatrix}\mathbf{F}_Q \\ \mathbf{F}_1\end{bmatrix}\right) \Rightarrow \mathbf{A}_Q$$

for any Q FDRs online at any given time. Therefore, the analysis of any single activity vector, as a function of the data from any two arbitrary FDRs, will not necessarily serve as a single means of event triggering.

This particular method of event triggering has its strengths in the fact that the event triggering is not based upon any fixed frequency threshold. Rather, the thresholds are based upon the statistical behavior of the data as a cluster. The Mahalanobis Distance of the data cluster is constantly changing as the covariance of the frequency data changes (as new data are added and old data are discarded). Figure 2-19 provides an overview of the data processing methods to make this type of trigger possible.

It is important to note that the use of the Mahalanobis Distance as an affine invariant distance measure is a common and classical tool widely used in pattern recognition and outlier detection [26, 39]. Other methods, such as the use of so called projection statistics, are also suitable for this type of analysis [40-46].

Figure 2-20 through Figure 2-27 display the results of the Mahalanobis Distance triggering scheme. The upper left window displays the raw frequency data from two FDRs. A green stripe indicates the current data under analysis. The upper right window presents a scatter plot of the raw data. As data is analyzed, it is added to this window. A red ellipse marks the 97.5% error tolerance of the last N data points (in this example, $N = 500$). A red marker denotes the centroid of this parent cluster. A green ellipse marks the 97.5% error tolerance of the candidate cluster of size M (in this example, $M = 10$). A green marker denotes the centroid of the candidate cluster. The lower left window is a plot of the activity vector. The lower right window maintains an archive of the tolerance ellipses. The most recent ellipse is plotted in red whereas previous ellipses are plotted in blue. Events, when detected, are marked in red in the upper left window. See Figure 2-24 and following.

A triggering of any single unit pair is not sufficient evidence to announce that a generation trip (or load shedding) has occurred. We seek further proof. Therefore, if any single unit pair triggers off of the migration of the activity vector outside of a set bound, an examination is carried out that addresses data from the activity vectors of every other unit pair. Two questions need to be addressed: 1) Which FDRs detected the event? 2) To what extreme did each unit experience the event? To help answer these questions, consider an example the results associated with the La Cygne generator trip in January of 2007. The left window displays raw data from each FDR and the right window shows the activity of the Mahalanobis Distance event trigger. Each red (yellow/green) dot indicates a passing of the candidate cluster's centroid outside of the 99.5% (99.0%/97.5%) tolerance ellipse of the parent cluster.

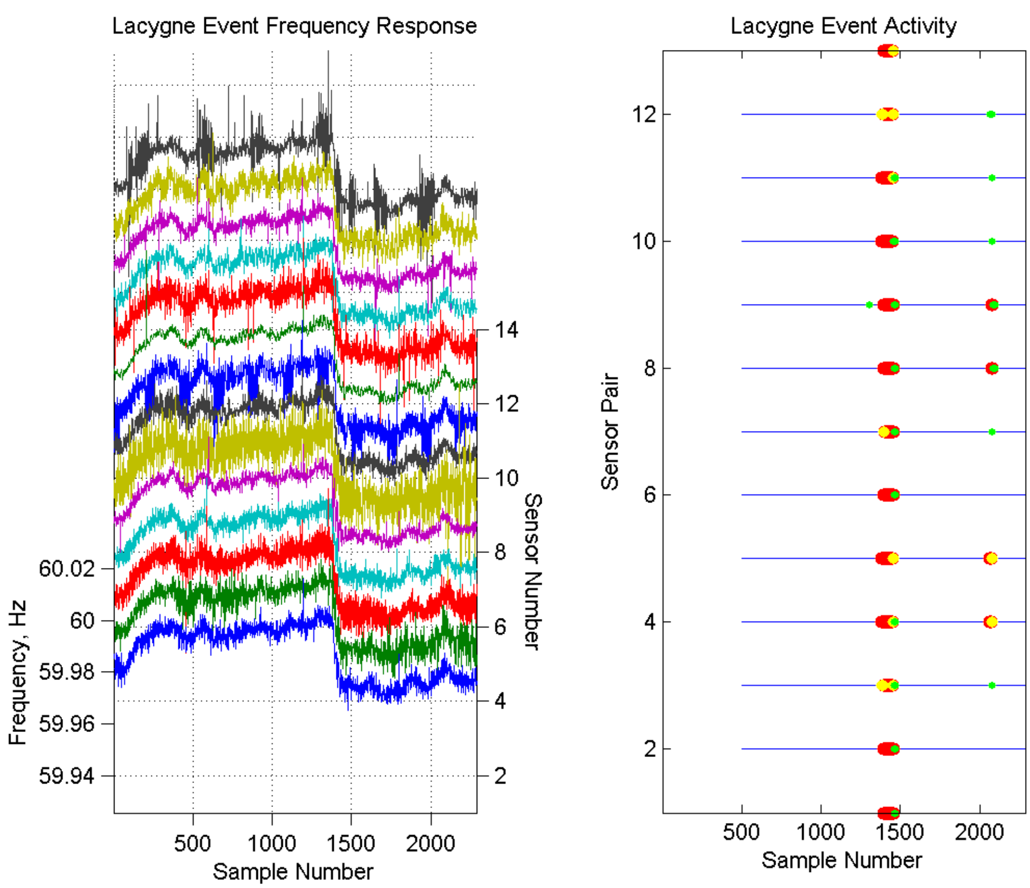

Figure 2-18: Event detection results (La Cygne Event - 01/02/2007)

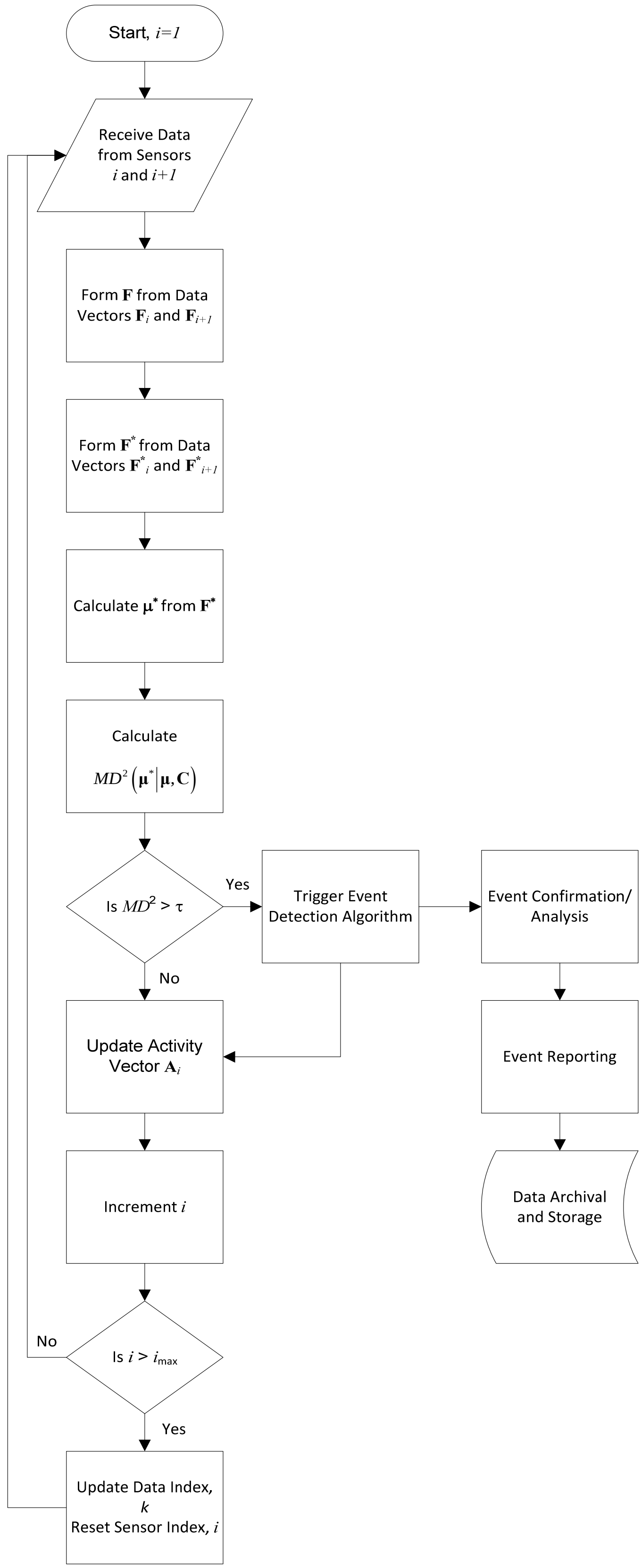

Figure 2-19: Event detection flowchart.

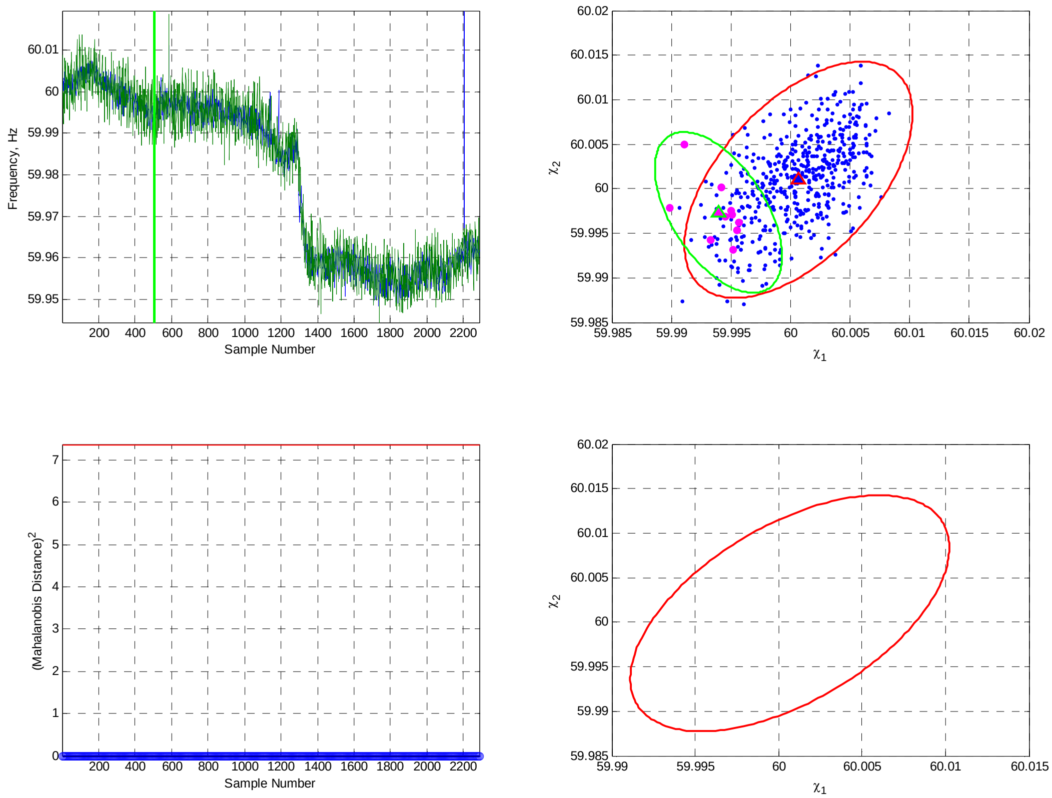

Figure 2-20: MD Event Trigger (t=500).

From the activity window (right Figure 2-18) it is quite clear to see that every pair of units triggered for the main event (at $t \approx 140$ s). There is, however, spurious activity around $t \approx 200$ s. We notice that not every unit pair triggers for this particular "event," and that most unit pairs that did trigger did so based upon the migration of the candidate cluster centroid outside of the 97.5% confidence ellipse (not outside of the 99.0% or 99.5% ellipses). Though some unit pairs triggered, this activity in frequency was indeed not an event. Therefore, we see the value of triggering based upon a consensus between all unit pairs as opposed to a few pairs. We gain this principle not only from this practical example but also from our original understanding that long term frequency behavior within a synchronous interconnection is consistent throughout.

A summary of the various constants needed thus far for the Mahalanobis Distance event detection algorithm:

- N is the length of the parent cluster (e.g., $N = 500$).
- M is the length of the candidate cluster (and also the analysis step size, e.g., $M = 10$).
- p_1, p_2, p_3 are the tolerance thresholds (giving rise to $\chi^2_{2,p_1}, \chi^2_{2,p_2}, \chi^2_{2,p_3}$, e.g., $p_1 = 7.38$, $p_2 = 9.21$, $p_3 = 10.6$).

It is important to note that the number of tolerance thresholds is indeed arbitrary to the extent that it is both a matter of taste and computational complexity. Having now formed the Q activity vectors, $\mathbf{A}_i$, we wish to condense the vectors into a single informative vector that will inform the end user of the occurrence of a generation tripping or load shedding event. This is accomplished by analyzing one entry from all activity vectors and comparing them to the tolerance thresholds. We now introduce a final set of tunable weights: w_1, w_2, w_3 corresponding to p_1, p_2, p_3. These weights are used in the vector-by-vector comparison of the frequency signal's activity. Figure 2-28 displays the process for event determination. In short, this process reduces the information from all activity vectors at some arbitrary time step, k, into a single value between 0% and 100%. This process, applied to the data of Figure 2-18, results in a value of 100% for the actual event data around $t \approx 140$ s and 44% for the erroneous event data around $t \approx 200$ s. A value of 0% is calculated for all other data. Appendix VI gives full results for each of the cases presented in Appendix IV.

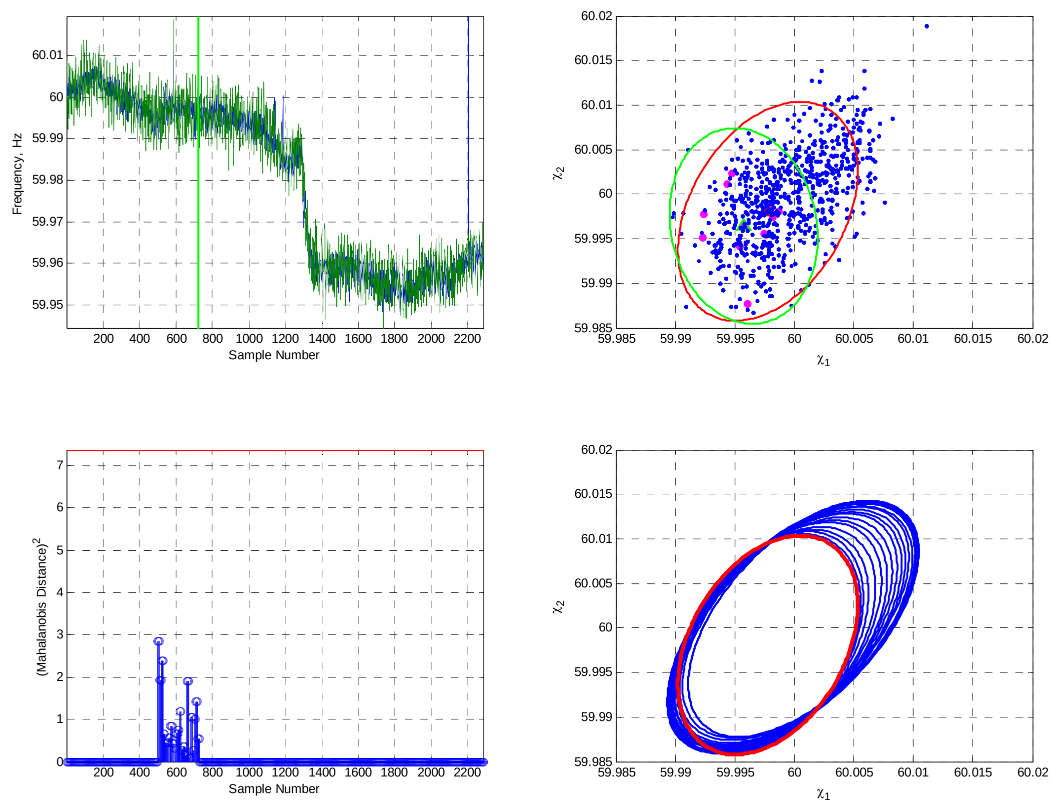

Figure 2-21: MD Event Trigger (t=720).

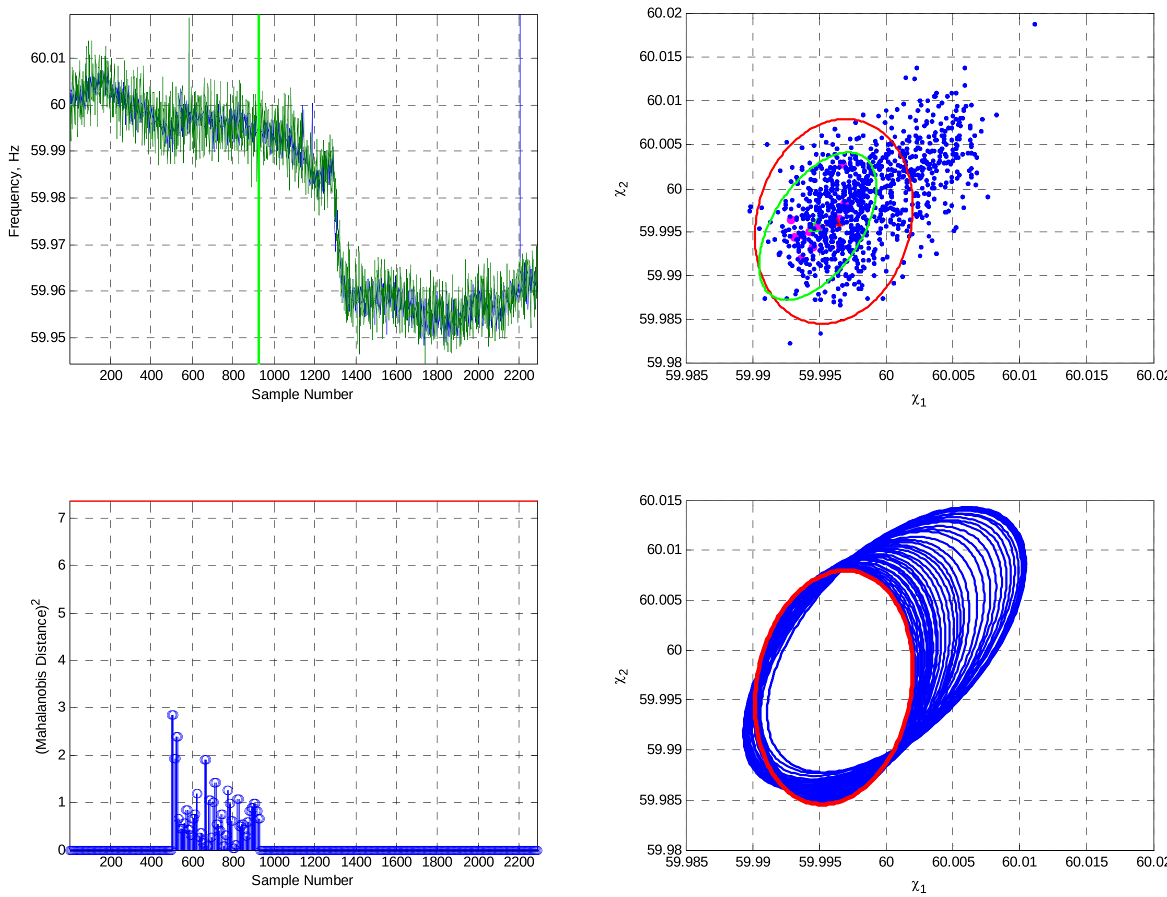

Figure 2-22: MD Event Trigger (t=920).

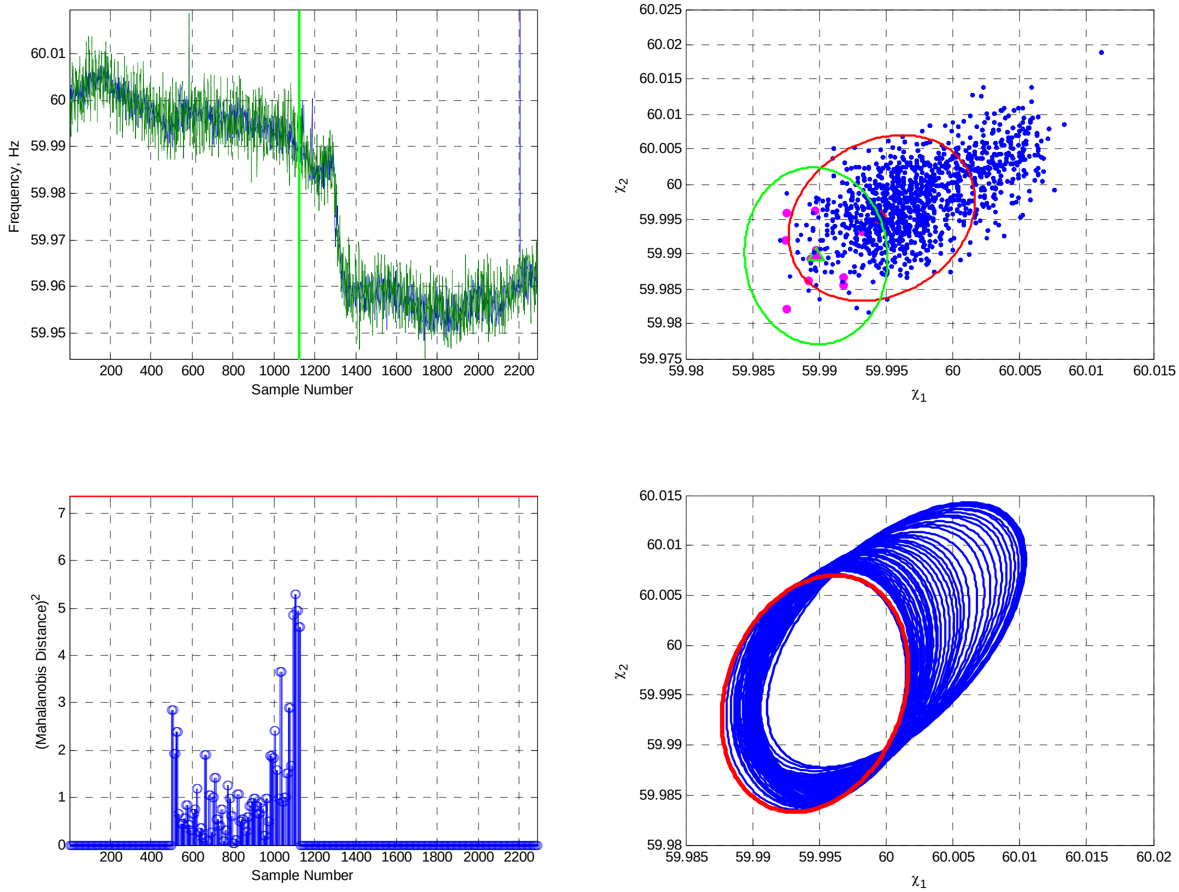

Figure 2-23: MD Event Trigger (t=1120).

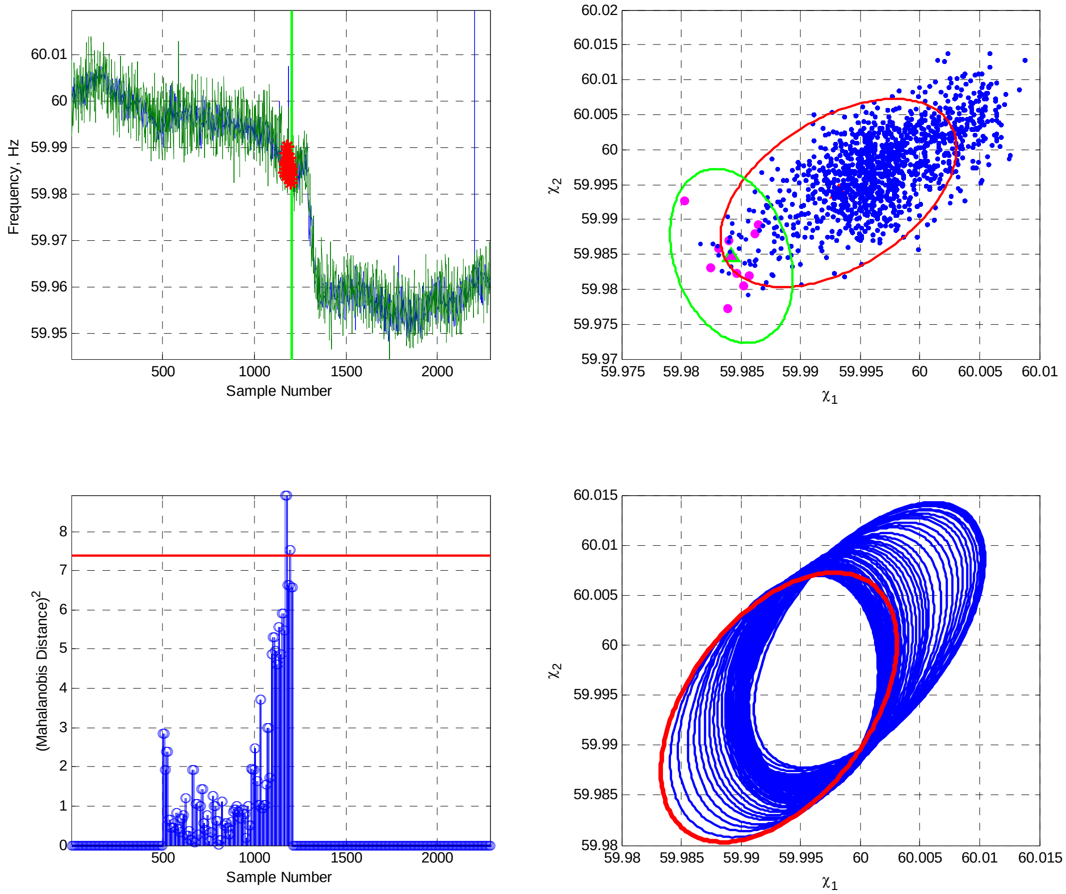

Figure 2-24: MD Event Trigger (t=1200).

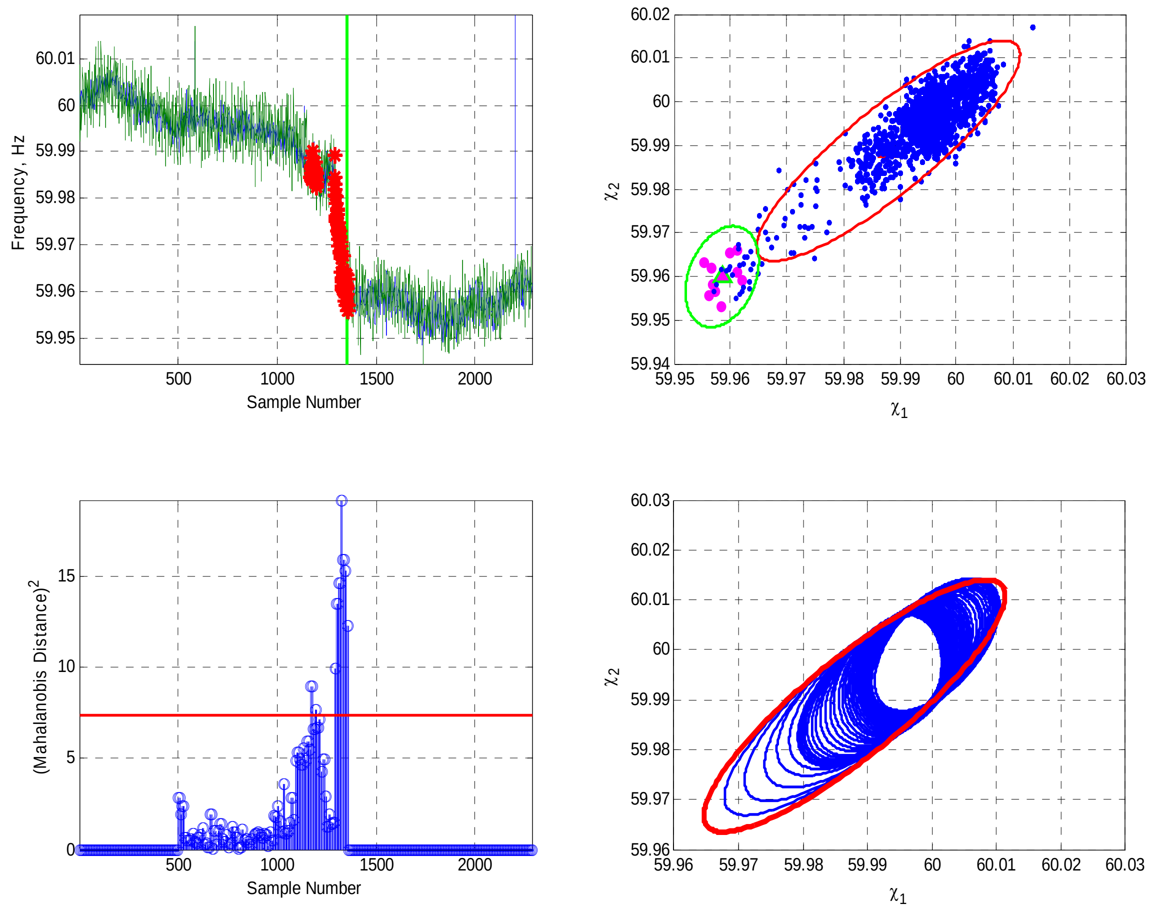

Figure 2-25: MD Event Trigger (t=1400).

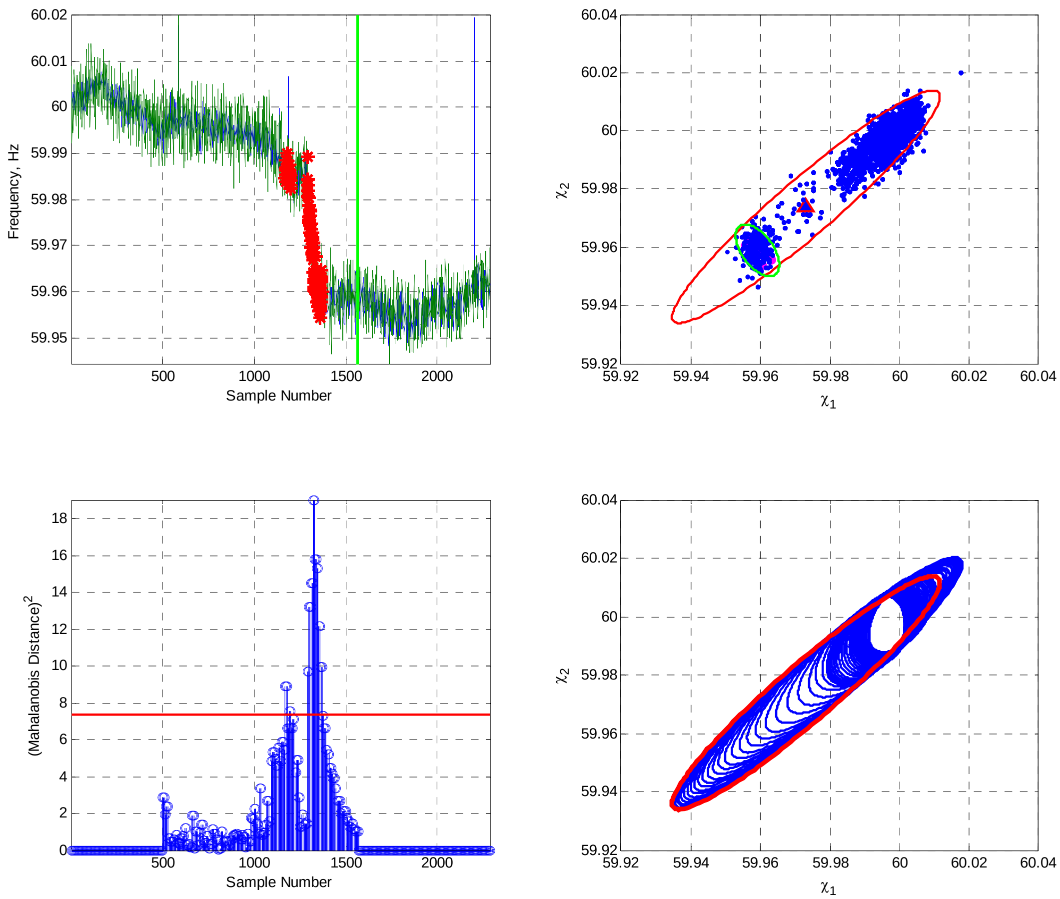

Figure 2-26: MD Event Trigger (t=1600).

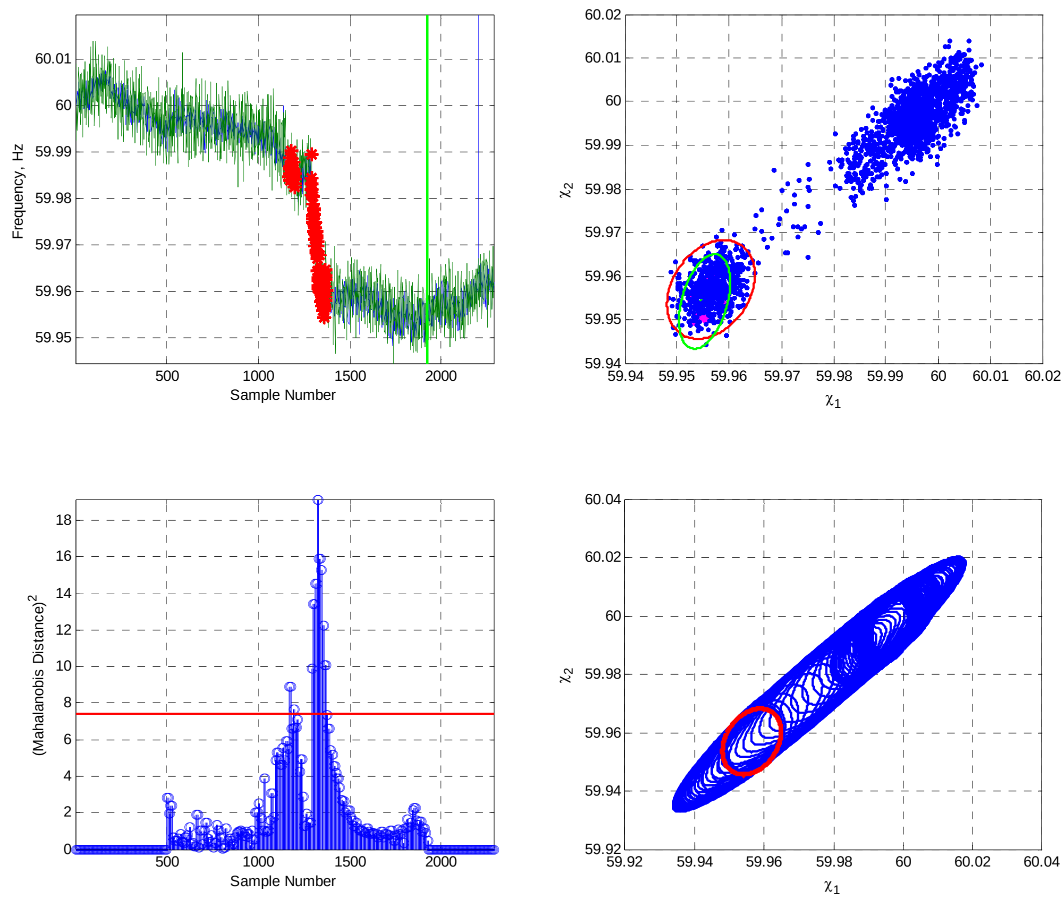

Figure 2-27: MD Event Trigger (t=1920).

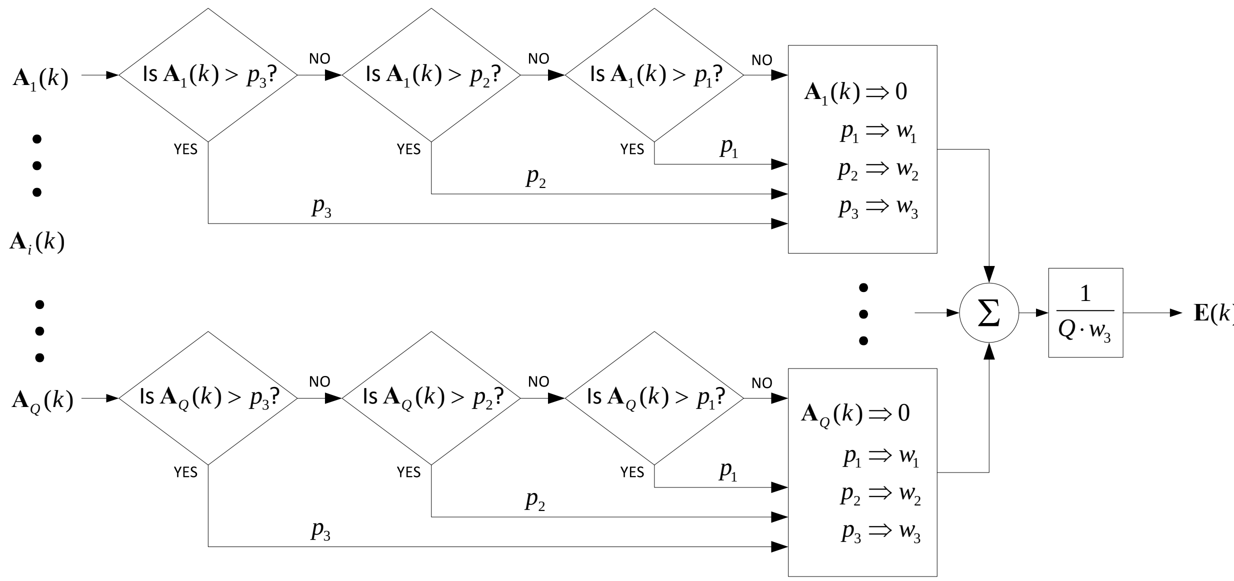

Figure 2-28: Process for event determination.

Generation-Load Mismatch Estimation

For certain generation-load mismatch events, namely generation trips, the NERC has specified methods for estimating the so called *frequency response characteristic* or *load-frequency sensitivity*, denoted as β and measured in MW/0.1 Hz [22, 30]. This particular parameter has been closely monitored and a significant level of apprehension has been expressed over the past several years about this parameter's decline in the EI [37]. Concisely, the decline of this parameter indicates an increased frequency sensitivity of the EI to generation trips. Per NERC standards, this parameter is calculated as:

$$\beta = \frac{-\Delta P}{\Delta f}$$

where ΔP is the generation trip amount (in MW) and Δf is the difference in steady-state pre-disturbance system frequency and pseudo-steady-state frequency post-disturbance (settling value of frequency after disturbance but before the response of supplementary control). Actually, this parameter is directly related to the system's load frequency sensitivity (D) and collective generator drooping governor characteristic in the following manner [9]:

$$\beta = \frac{2\pi}{\frac{1}{R_1} + \frac{1}{R_2} + \cdots + \frac{1}{R_n} + D}$$

where R_i is the governor drooping characteristic for each of the n machines online within an interconnection (in this case the EI). Regular or seasonal updates of this parameter are needed for generation-load mismatch estimation following a disturbance that influences frequency.

Consider the following situation: Say a utility (or system operator) in the EI (or any arbitrary interconnection) experiences frequency phenomena that seem to indicate a generation trip somewhere within the interconnection. Perhaps the detection method discussed in the previous section was used. Per the utility's metering, it is found that the contingency did not occur within its control area. The operations manager will be interested in knowing, as soon as possible, the magnitude of the generation trip that induced the generation-load mismatch. He/she classically has two options:

- Wait for the proverbial "phone call" for the trip information.
- Calculate the generation trip amount using the NERC guidelines (or "beta" method).

In most instances both options, in fact, will be executed (the latter by either computer or hand calculation). However, with a β parameter that may be updated as infrequently as the seasons, the operator has no facility to indicate the "goodness" of the megawatt drop estimation. Depending on the pre-disturbance frequency level and governing characteristics of the generators online, this parameter may change.

A means of supplementing the mismatch estimate calculated using the "beta" method proceeds from the aggregate Swing Equation (2.2). This method, as opposed to relating Δf via β to a power mismatch, ΔP, relates the slope of the frequency, $\frac{df(t)}{dt}$ as estimated by $\frac{\Delta f}{\Delta t}$, to the power mismatch[6]. From the swing equation we can see that, during an event, maximum power mismatch will correspond to a maximum slope in frequency. This method also presents a linear method of relating Δf to ΔP although our definition of Δf does change slightly to approximate a slope as opposed to a step change. Rather than using β, which relies heavily on the system's aggregate governor response (and load frequency sensitivity to perhaps a lesser extent), the proposed method relies on an estimate of the system's inertia. Yet another advantage of this proposed method is the ability to calculate an interconnection's generation-load mismatch based upon the slope of the system average frequency at any arbitrary moment in time. This is a significant advantage over the "beta" method which is actually meant only for use with step disturbances.

A lack of known generator output values at the time of tripping deprives this method of present application. However, the method shows promise when comparing $\max\left(\frac{df(t)}{dt}\right)$ versus Δf. These results are presented as preliminary indicators of promise for future studies on the variation of system inertia, H_{system}, over time (primarily between the seasons). The volatility of the aggregate system inertia compared to the NERC beta factor is as of yet unknown. However, we might postulate that mismatch estimation using inertia as opposed to the "beta" method is less volatile. We make this postulation on the grounds that the "beta" method is affected by system governor response which is in turn affected by the pre-disturbance nominal frequency (activation of dead bands, etc.). Inertia-based estimation is not.

[6] Slope of pre-disturbance frequency must be equal to zero for an accurate estimation. While this requirement is seldom met, often the pre-disturbance slope of frequency is very small compared to the mid-disturbance slope.

The following figures plot pre- and post-event frequency deviation versus the maximum frequency slope for each of the events listed in Appendix IV. The plots also sectionalize the data by season for further analysis of the regression between slope and deviation.[7]

The data in the following figures were obtained in an organized fashion as follows: For each event, a window of data, uniform in length across each event and for each FDR was analyzed. The derivative of frequency with respect to time was calculated on moving average (MA) filtered frequency data from each FDR. The maximum magnitude of the derivative was then found for each unit and compared with the total frequency deviation. The frequency deviation was prescribed as the difference in median frequency before and after point of maximum slope. This process resulted in a locus of points for each event. This locus of points was condensed via the sample median to a single point for each event. These results are plotted in Figure 2-29. A full exposition of this process for each event is listed in Appendix VII.

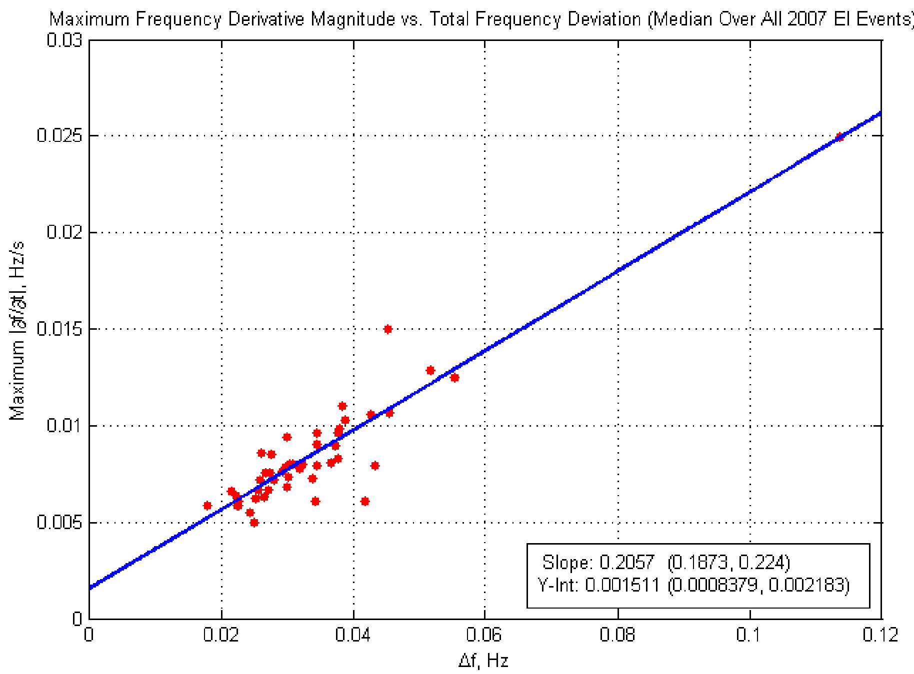

Figure 2-29: Frequency deviation versus frequency slope for all events in 2007.

[7] Fall data is incomplete and therefore it is understood that a regression analysis of the data is perhaps ill-advised. The results are nevertheless presented for completeness.

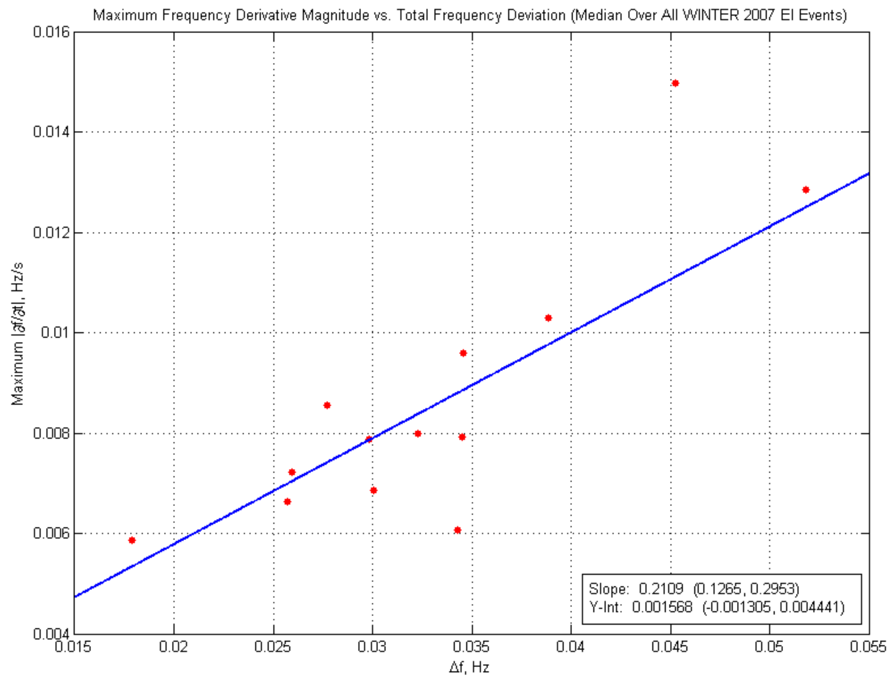

Figure 2-30: Frequency deviation versus frequency slope for winter events in 2007.

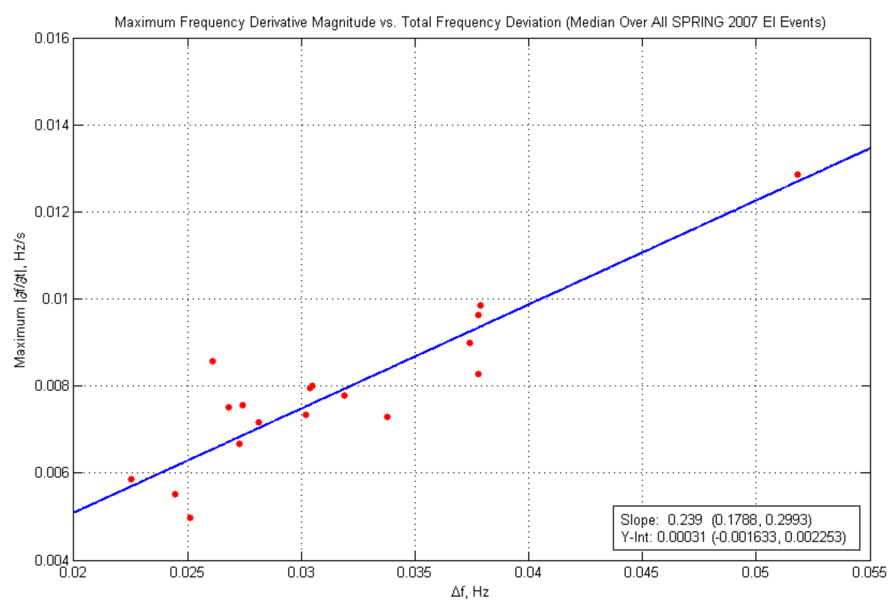

Figure 2-31: Frequency deviation versus frequency slope for spring events in 2007.

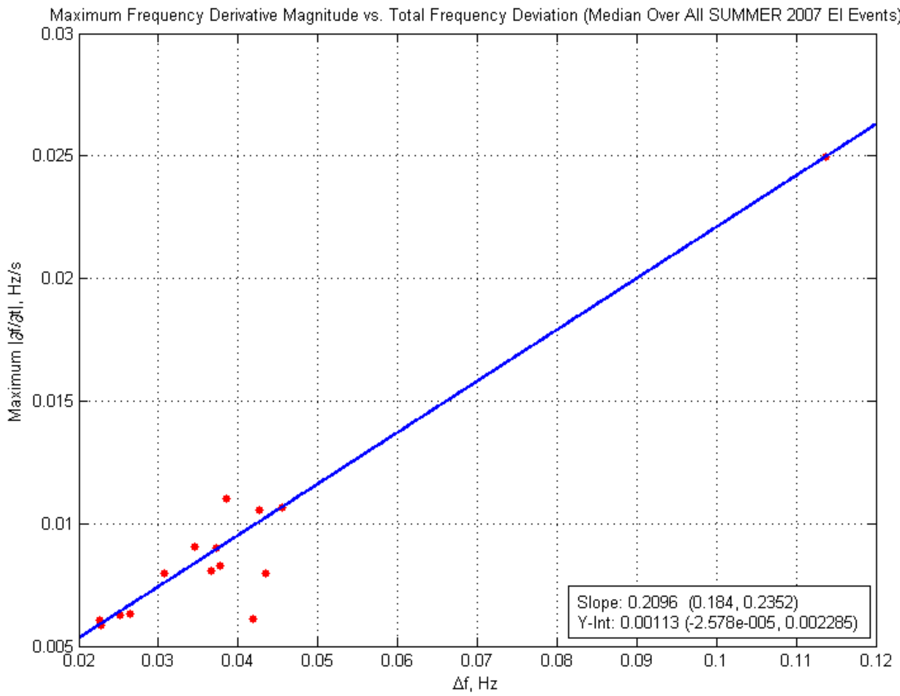

Figure 2-32: Frequency deviation versus frequency slope for summer events in 2007.

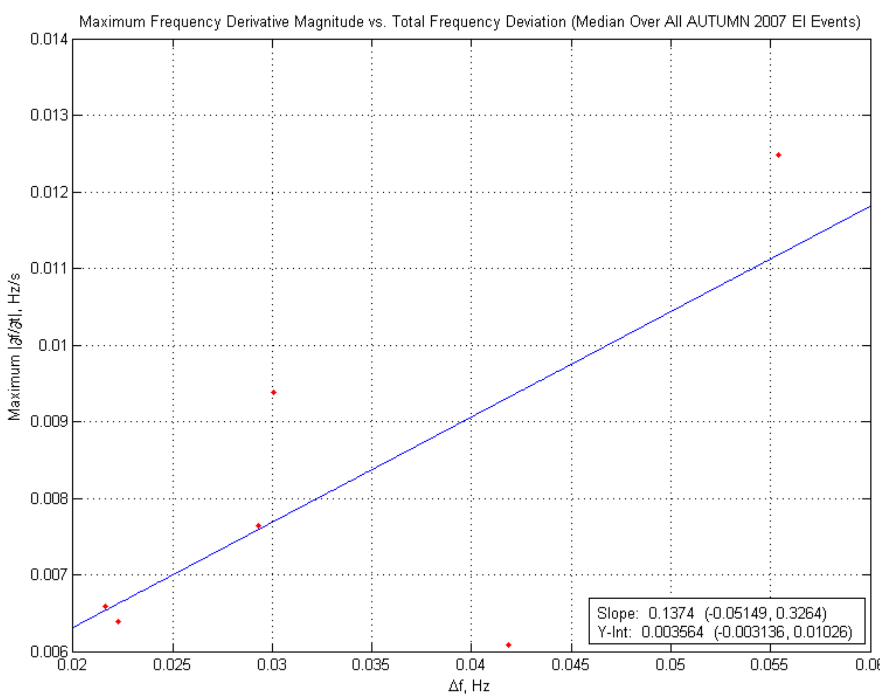

Figure 2-33: Frequency deviation versus frequency slope for fall 2007 (incomplete).

Chapter 3: Power System Oscillation Detection and Analysis Based on Wide-Area Frequency Measurements

Heretofore the focus of this report has been on the behavior of the U.S. interconnections as observed through wide-area frequency measurements during discrete mismatch events such as generation trips or load shedding events. However, wide-area frequency measurements also reflect the presence of oscillations on the electric grid. Oscillations in system frequency are an indicator of oscillations in system voltage angles which further indicate oscillations in the speeds of the machines within the interconnection. Machine speed oscillations are relevant both for the problems that they pose to the operation of an interconnection and for their rather frequent occurrence. Sustained inter-area oscillations can potentially reduce the effective capacity of transmission lines within the system. Oscillations that are negatively damped also have the capability to cause system break-up and/or instability in which case the hazard of a blackout is ever increased. Also, depending on the magnitude of the oscillations, system voltage can also fluctuate (as was seen in the case of the Florida blackout in February of 2008).

This chapter has a threefold focus. First, a method for the detection of oscillations in wide-area frequency data is presented. Detection methods are necessary for triggering event alarms (to be developed later) and the identification of oscillations in noisy, non-stationary wide-area frequency data. Second, the so called matrix pencil method of decomposing a signal into a sum of damped sinusoids is introduced, applied to wide-area frequency data, and extended for simultaneous application to multiple channels of frequency data. The study of power system oscillations is not new. Classically, the use of Prony's method of modal identification has been used in the power systems arena [47-52]. This method is perhaps best treated from an engineering and signal-processing perspective by Marple in [53]. The behavior of Prony's method (also commonly called the polynomial method) has been found unsatisfactory when applied to wide-area frequency data due to the relatively high signal-to-noise ratio of this type of data. We therefore resort to the use of the Matrix Pencil as concisely defined and analyzed by Hua [54]. The drive behind the application of the Matrix Pencil method to wide-area frequency measurements is threefold. First, methods for event identification (and therefore, location) have been developed that use the modal content of voltage frequency as an input [14]. Second, as more efforts are under way to further enlarge power system capacity using flexible AC transmission systems (FACTS) and the like, we should like to propose the use of wide-area frequency measurements for the tuning of said device's controllers. Finally, we seek to add the analysis of oscillations in wide-area frequency data to the power system situational awareness toolbox. The chapter concludes with a case study of oscillations in both the WECC and EI.

Oscillation Detection

We wish to detect frequency oscillations in our inherently noisy frequency data. Figure 3-1 presents a flowchart of our method.

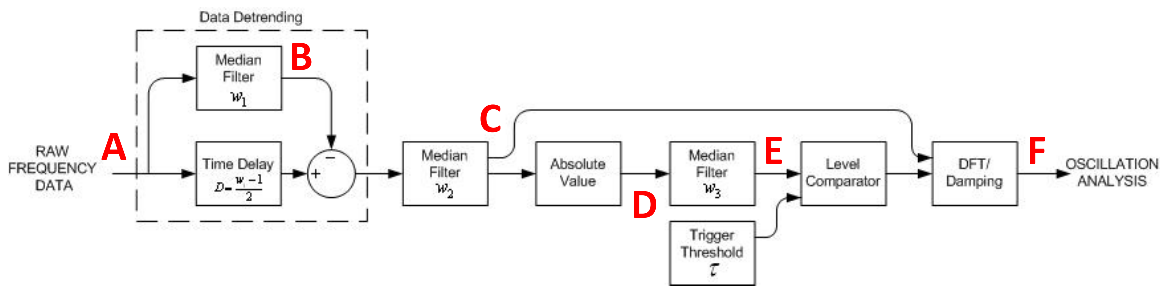

Figure 3-1: Oscillation triggering flowchart.

We have three reasons for using such a system as shown in Figure 3-1 for oscillation detection. First, we should like to detect oscillations in a signal that resides in a neighborhood around 60Hz. The discrete Fourier transform (DFT) applied directly to raw frequency data would result in output coefficients that include a large overshadowing DC component. Second, we wish to detect the envelope in which any oscillations might occur without including other events (such as generator trips and load shedding). Thirdly, our raw data contains outliers that might otherwise contaminate DFT- or envelope-based oscillation detection schemes.

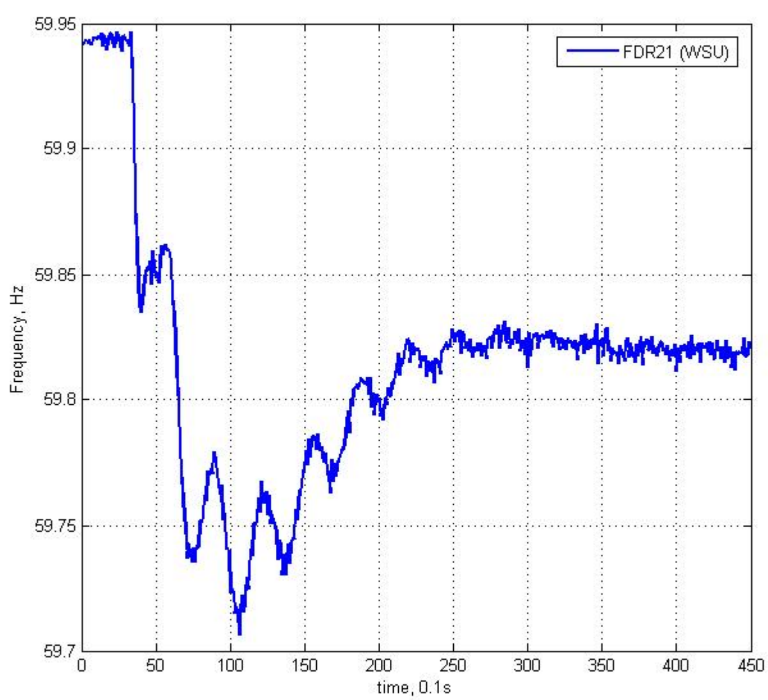

Figure 3-2: Raw data including oscillation.

Consider the frequency oscillation riding on a generation trip event signature in Figure 3-2. The data of this figure is applied at point **A** in the schematic of Figure 3-1. If we should immediately take the DFT of this signal, we would have the output as shown in Figure 3-3.

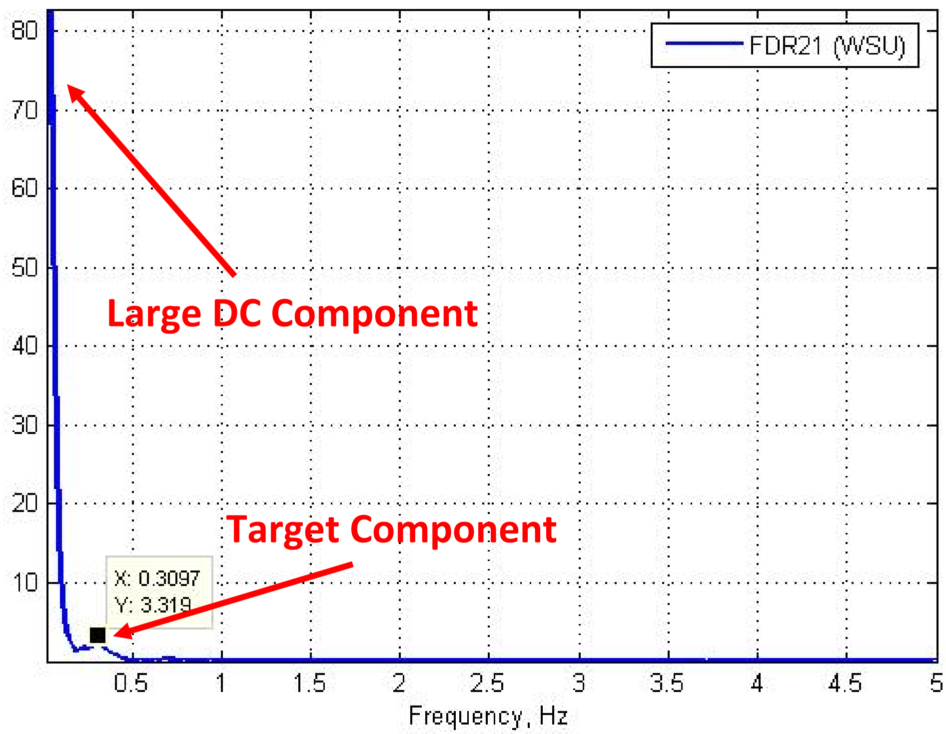

Figure 3-3: DFT of raw frequency data.

We can obviously see how the component in which we are interested is completely washed out by leakage from the large DC component and event signature. If we can estimate the trend of the frequency data and remove the trend from the raw data, we will be left with a signal stationary about zero that we can use to determine the parameters of the oscillation riding on the trend. The trend is estimated with a 31-point moving median (w_1 = 31 in flowchart). The median filter is a non-linear filter and therefore we cannot design it spectrally. However, in loose terms due to the non-recursive nature of the median filter, we shall consider it to be an MA-type process. Experimentation gives the final window size of the median filter used. Figure 3-4 shows our estimation of the trend at point **B** in the flowchart.

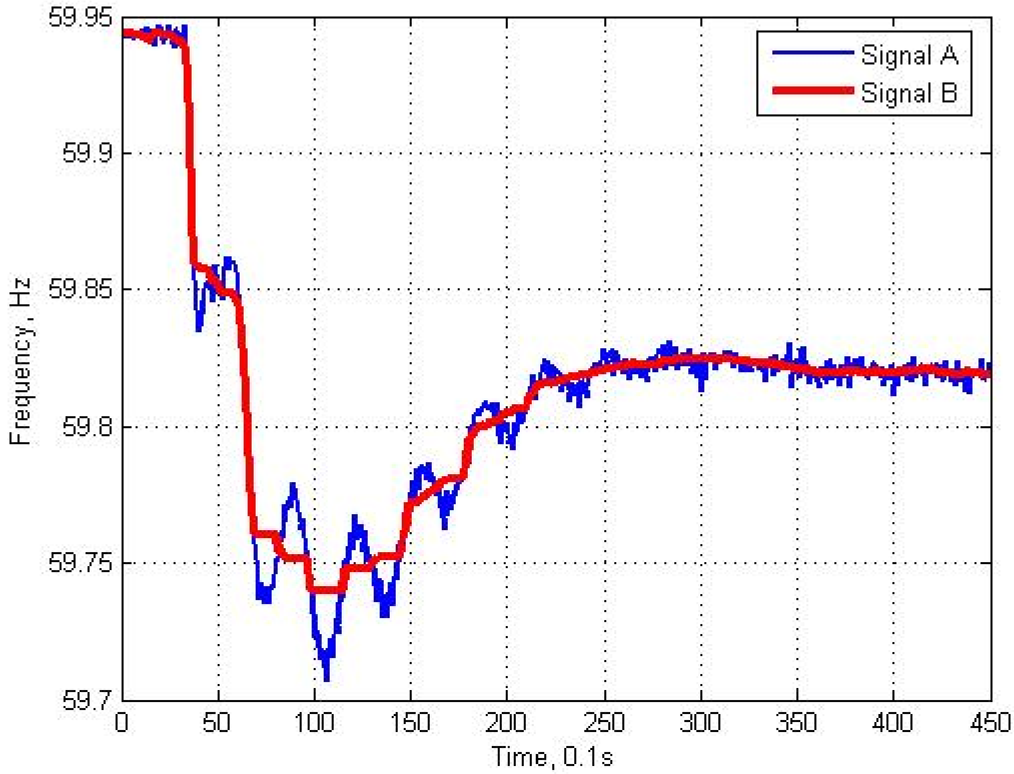

Figure 3-4: Raw data and trend estimation.

We see from Figure 3-4 that the trend estimation made by the 31-point median filter excludes the oscillation but includes the frequency drop due to the generation trip. This inclusion of the generation trip into the trend might be undesirable if we were constructing a generation trip trigger. However, remember that we are temporarily focusing on the triggering of *oscillations*. Figure 3-5 shows the filtering capabilities of the median filter. We notice that the component we are seeking at 0.3 Hz is not included in the trend estimate. If we subtract the trend estimate from the raw data we shall be left with a stationary zero-centered signal containing our target oscillation. This subtraction is performed by the signed summer in the de-trending block of the flowchart above. The effectual behavior of this component is that of a high-pass filter. As a matter of practicality (as we are constrained to causality), we must insert a delay in the raw data signal so as to align the median filter output with the raw data (the median window is centered on the data point it is estimating). As with any causal filter, some delay will be incurred during the data filtration process. We do note, however, that this robust MA-type filter when compensated with the use of the delay block introduces zero phase distortion. Zero phase filtering is possible with ARMA-type (or IIR-type) filters but only acausally. Between the summer and point **C**, we filter the data again. This filter is not necessarily needed for the purpose of event triggering. However, it is placed for practical reasons discussed in later this section.

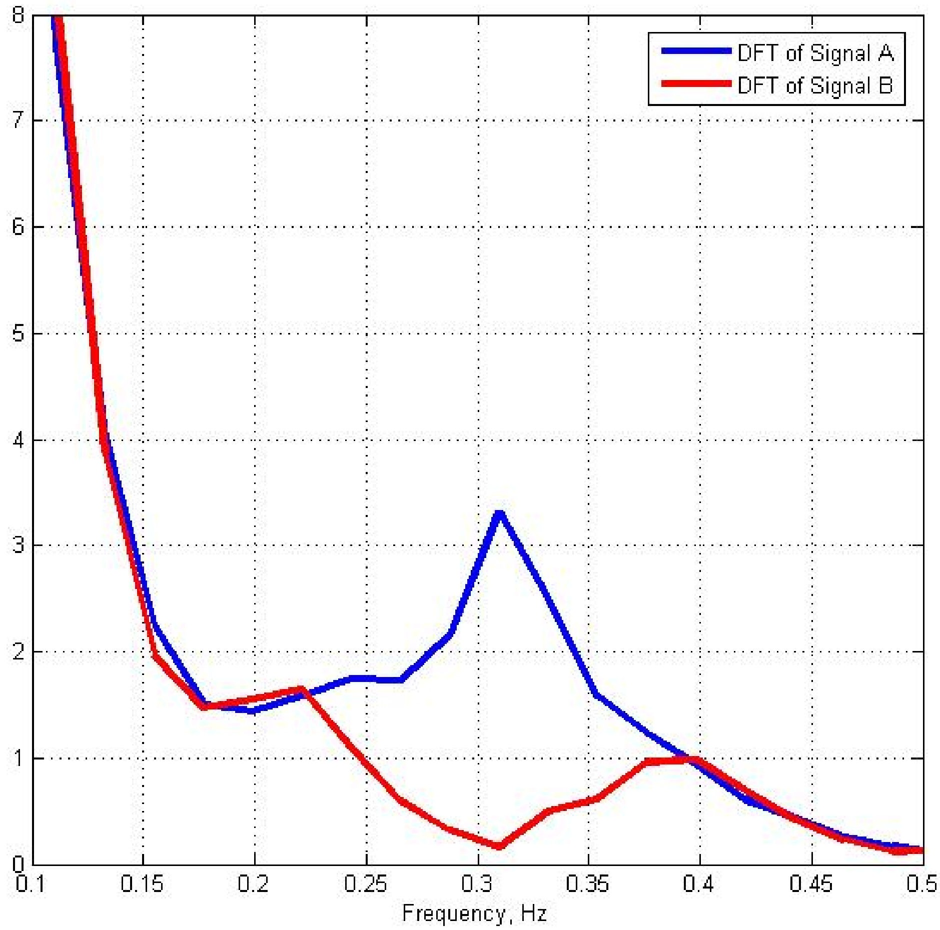

Figure 3-5: Spectrum of raw data and trend estimation.

Figure 3-6 shows the signal's residual after de-trending. This signal has also been filtered slightly using the second median filter in the flowchart ($w_2 = 7$). As mentioned previously, this filter is not necessary to the oscillation detection process but is useful in calculating the DFT of the candidate signal if it is triggered later. Hence, there is the direct feed forward to the DFT/damping block. The DFT damping block only acts when triggered by the signal from the comparator. Figure 3-7 displays the absolute value of the de-trended data. This data corresponds to the signal at point **D** in the flowchart. We are now not far from the signal we want to act as a trigger signal. The last median filter ($w_3 = 51$) acts to "de-bounce" signal **D**. This produces signal **E** which is fed to the comparator. The comparator checks the level of signal **E** against a threshold value. If **E** is above a certain threshold, τ, then the signal is captured and analyzed. Figure 3-9 contains the output of this analysis, signal **F**. Many days and much data have been scanned for oscillations using this method. The method is extremely tunable depending on its application and the noise content of the signal. We have chosen to use median filtering because of the robust qualities intrinsic to the median. Appendix VIII contains one day's worth of data showing the output of this algorithm.

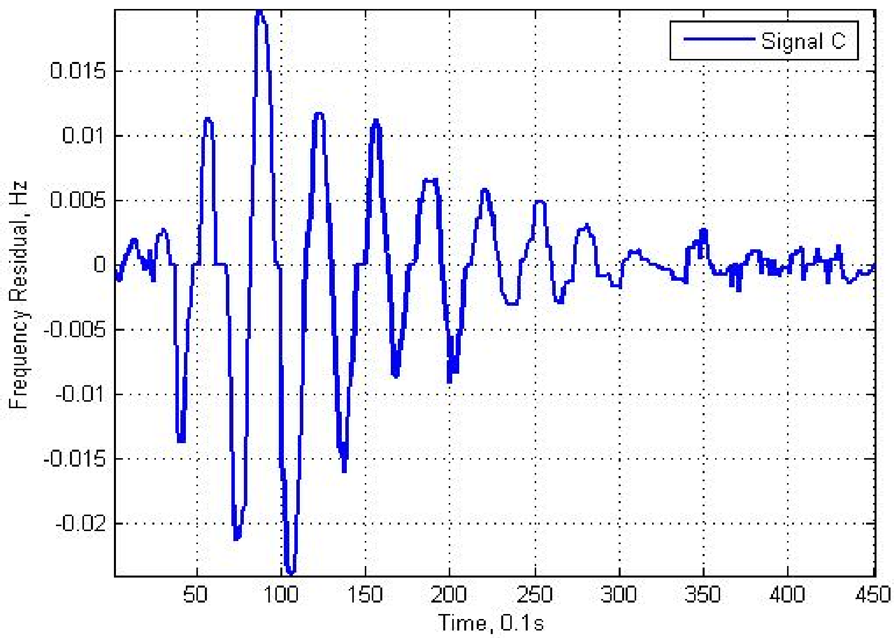

Figure 3-6: Residual after de-trending.

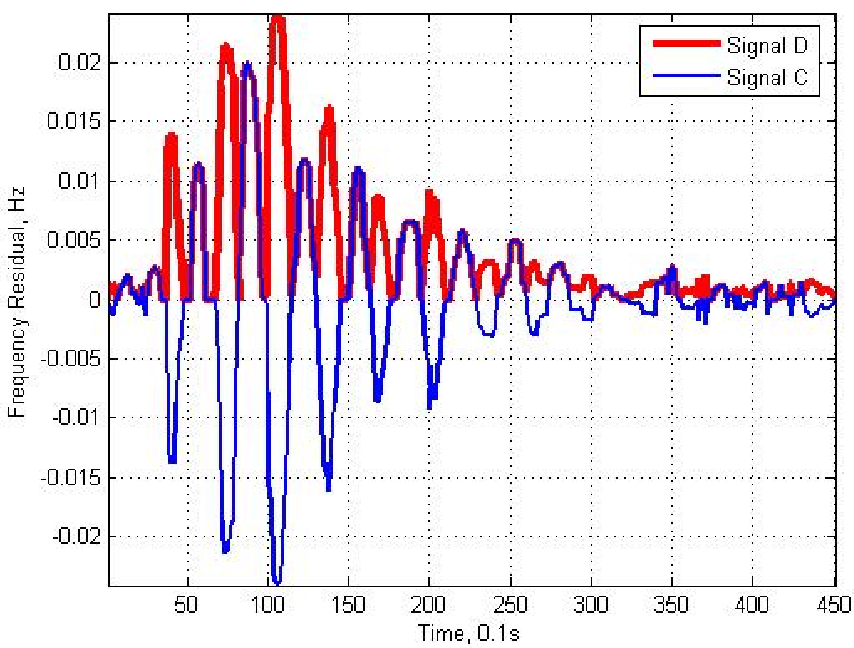

Figure 3-7: Absolute value of de-trended data.

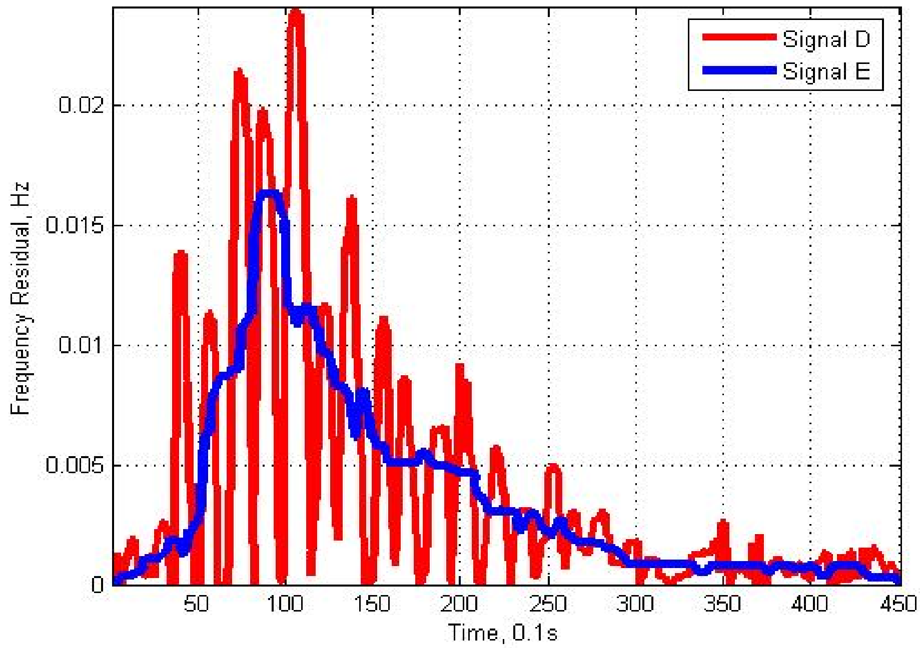

Figure 3-8: The oscillation trigger signal.

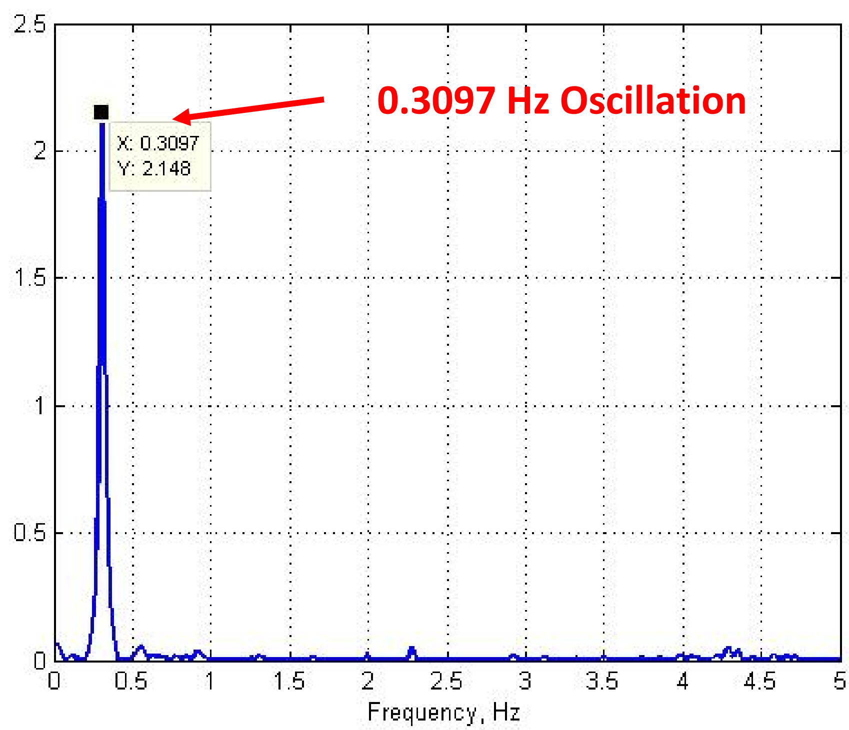

Figure 3-9: DFT of frequency oscillation.

We have found the aforementioned method of oscillation detection to be well suited for online implementation. When implemented using sample mean blocks this method reduces to a classical signal detection routine (similar to AM signal demodulation) attached to an all-zero (MA) band-pass filter. In the off-line or post-mortem sense there are in fact better methods of de-trending the frequency data. An ARMA-type (IIR) filter such as the classical Butterworth filter has given exceptional results. This filter has only been applied to wide-area frequency data offline where zero phase filtering is possible. Zero phase filtering is accomplished by filtering the raw data (signal A), reversing the signal, and then filtering the signal again. Since power system oscillations typically occur in the 0.2Hz to 2.5 Hz band, a tenth-order sugar-dipped Butterworth filter with the following response has been used for oscillation extraction.

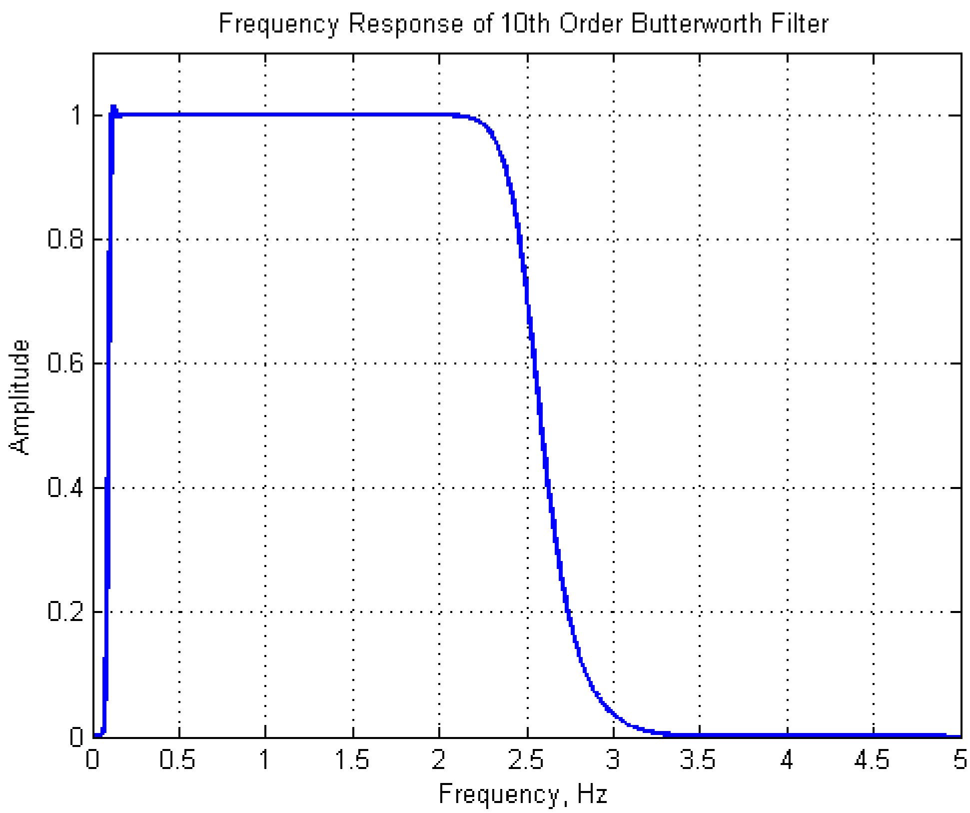

Figure 3-10: Frequency response of Butterworth filter used in oscillation extraction.

It is important to note that one further reason exists to de-trend wide-area frequency data. The Matrix Pencil method, discussed next, necessarily operates on zero-mean data. Especially during load-mismatch events, it is of utmost importance to remove not only the signal's sample mean over a window, but also the signal's trend, offsets, and any other extraneous effects that might be in the signal.

Power System Modeling and FNET Data

Conventionally, modal analysis of power systems has been carried out using small-signal state models of the system. The behavior of this model is determined by a homogeneous vector-matrix differential equation of the form:

$$\dot{\mathbf{x}}(t) = \mathbf{A}\mathbf{x}(t)$$

The state vector, $\mathbf{x}(t) \in \mathbb{R}^{n\times 1}$, and the plant matrix, $\mathbf{A} \in \mathbb{R}^{n\times n}$, with real and constant entries completely describe the system assuming that any inputs to the system are accounted for in the initial conditions. The model (presumably the result of some form of linearization) can either be described in terms of parameter differences or absolute parameter values. Either way, our development here remains unaffected. This state equation, subject to initial condition $\mathbf{x}(t_0) = \mathbf{x}_0$, has a solution of the form:

$$\mathbf{x}(t) = e^{\mathbf{A}t}\mathbf{x}_0$$

where $e^{\mathbf{A}t}$ is the transition matrix which can be represented by a power series expansion of the exponential [55]. In the case of a practical system, the plant matrix will have distinct eigenvalues allowing for diagonalization of the plant matrix as follows [56]:

$$\begin{aligned} \mathbf{A}\mathbf{R} &= \mathbf{R}\Lambda \\ \mathbf{L}^T\mathbf{A} &= \Lambda\mathbf{L}^T \\ \mathbf{A} &= \mathbf{R}\Lambda\mathbf{L}^T \\ \mathbf{R} &= \mathbf{L}^{-T} \end{aligned}$$

with a diagonal matrix of eigenvalues:

$$\Lambda = \begin{bmatrix} \lambda_1 & & \mathbf{0} \\ & \ddots & \\ \mathbf{0} & & \lambda_n \end{bmatrix} \in \mathbb{C}^{n\times n}$$

and matrices of left and (normalized[8]) right eigenvectors, $\mathbf{L}$ and $\mathbf{R}$ respectively, of the form:

$$\begin{aligned} \mathbf{L} &= \begin{bmatrix} \mathbf{l}_1 & \mathbf{l}_2 & \cdots & \mathbf{l}_n \end{bmatrix} \in \mathbb{C}^{n\times n} \\ \mathbf{R} &= \begin{bmatrix} \mathbf{r}_1 & \mathbf{r}_2 & \cdots & \mathbf{r}_n \end{bmatrix} \in \mathbb{C}^{n\times n} \end{aligned}$$

yielding a solution of the state vector, given initial conditions as:

$$\mathbf{x}(t) = \mathbf{R}\,\mathrm{e}^{\mathbf{A}t}\,\mathbf{L}^T\mathbf{x}_0 = \sum_{i=1}^{n} \mathbf{r}_i e^{\lambda_i t}\mathbf{l}_i^T\mathbf{x}_0$$

[8] The right and left eigenvectors are not uniquely defined thus introducing another degree of freedom in to the solution of the state equation. Thus it is common to normalize the set of right eigenvalues to reduce this freedom.

Each term in this summation corresponds directly to a mode in the natural response of the system (determined by the plant matrix) in a linearly independent fashion. In general, the eigenvalues of any practical system are complex (occurring in conjugate pairs due to the fact that the entries in the plant matrix are purely real for any practical system that we should consider). That is,

$$\lambda_i = \alpha_i \pm j\beta_i$$

These eigenvalues can also be referred to as the poles of the plant matrix. Upon this note, we take a quick moment to review a few concepts from basic control theory [57]. Several scenarios can exist based upon the values of both α_i and β_i. In the case of a pure real (single) eigenvalue, $\lambda_i \in \mathbb{R}^1$, the i^{th} mode in the system's natural response will either exponentially decay or exponentially grow in a non-oscillatory fashion as determined by:

$$\begin{aligned}\alpha_i > 0 &\rightarrow \text{pole in RHP} \rightarrow \text{growth}\\ \alpha_i < 0 &\rightarrow \text{pole in LHP} \rightarrow \text{decay}\end{aligned}$$

In the case of a purely imaginary pair of complex poles, $\alpha_i = 0$, the i^{th} mode in the system's natural response will be purely sinusoidal with no damping. In the case of a pair of complex poles with both nonzero real and nonzero imaginary components, the i^{th} mode will exhibit damped sinusoidal behavior where the sign of the damping is, again, determined by the sign of α_i. We now take interest in several descriptors of the modal behavior. The first descriptor is the natural frequency of the i^{th} mode, $\omega_i^{\,n}$, which we shall define in radians per second as:

$$\omega_i^{\,n} \triangleq \sqrt{\alpha_i^2 + \beta_i^2}$$

Notice that in the case where $\alpha_i = 0$, the purely sinusoidal case, that $\omega_i^{\,n} = \beta_i$. Actually, this is a case where the natural frequency is, in fact, equal to the damped frequency (since damping is zero) whereby we introduce the damped frequency descriptor (in radians per second):

$$\omega_i^{\,d} \triangleq \beta_i$$

The final descriptor of premier importance for our study hence forward is the damping ratio of the i^{th} mode written as ξ_i and defined as:

$$\xi_i \triangleq -\frac{\alpha_i}{\omega_{n,i}}$$

and sometimes calculated as $\xi_i \triangleq \cos(\theta)$ where θ is the angle formed between the negative real axis and the position of the pole (either towards $-j\infty$ or $+j\infty$). By this definition of damping ratio, we see that poles in the LHP have positive damping, poles in the RHP have negative damping, and poles on the imaginary axis have no damping. The eigenvalues of the plant matrix give an indication of the modal content of the system's natural response but not an indication of the mode shape. The mode shape of the response is governed by the normalized right eigenvectors of the plant matrix, $\mathbf{r}_i$. The components of this right eigenvector determine the relative activity of each state in the i^{th} mode.

The work in the report is not driven by system models or even, in reality, the study or consideration thereof. Rather we focus on measurement data from some real system with a largely unknown model – the EI. We have access to frequency at certain points within the grid but certainly we do not have access to all or even many of the systems states. Therefore, in modeling terms we have an output vector $\mathbf{y}(t)$ of m measurements translated by some $m \times n$ output matrix $\mathbf{C}$ as follows[9]:

$$\begin{aligned}\dot{\mathbf{x}}(t) &= \mathbf{A}\mathbf{x}(t)\\ \mathbf{y}(t) &= \mathbf{C}\mathbf{x}(t)\end{aligned}$$

Therefore, in an attempt to better understand the natural response(s) of the EI, we examine closely that which we have available – measurement data. We examine the eigenvalue of our signal data in the $\mathbf{y}(t)$ vector. We understand that, in doing so, we lose particular relevance and calculability of the right eigenvectors of the plant matrix. For now, we relent in our pursuit of that information. According to basic linear system theory, if the matrix pair $(\mathbf{C}, \mathbf{A})$ is completely observable, then every system mode will appear in the output vector. We realize that our number and placement of sensors, or FDRs, may or may not satisfy this observability criterion. However, we do expect that our data shall reflect those modes which are strongly coupled throughout the electrical interconnection. Topics associated with the in-depth modeling of power systems in the context of wide-area frequency measurements and continuum theory can be found in [14, 33, 58-62].

In order to determine parameters determined by system eigenvalues such as damping ratio, etc., using wide-area frequency data we estimate the Laplace transform of our measurement signal, $\mathcal{L}\{y(t)\}$, to form a M^{th} order fraction of the form:

$$\hat{Y}(s) = \frac{b_M s^M + b_{M-1}s^{M-1} + \cdots + b_1 s + b_0}{a_M s^M + a_{M-1}s^{M-1} + \cdots + a_1 s + a_0}$$

which can be expanded through partial fraction expansion to take the form:

$$\hat{Y}(s) = \frac{k_1}{s - p_1} + \frac{k_2}{s - p_2} + \cdots + \frac{k_M}{s - p_M}$$

---

[9] Several simplifications and idealizations are made here. Mainly, we understand that $\mathbf{A}$ and $\mathbf{C}$ are in fact functions of time, $\mathbf{A}(t)$ and $\mathbf{C}(t)$, respectively. However these matrices are assumed to change so slowly that we can consider them to be time invariant. Also, since our measurements are discrete, that is they are sampled versions of system frequency, our data vector is better described as $\mathbf{y}(kT_s)$.

Note that because we are limiting the order of the system and acknowledging that noise may well exist in the measurement signal, we write $\hat{Y}(s)$ as opposed to $Y(s)$. Complex poles are accommodated in the partial fraction expansion procedure. For example, if $p_1 = \alpha - j\beta$ and $p_2 = \alpha + j\beta$, then the partial fraction expansion would take the form:

$$\hat{Y}(s) = \frac{k_1}{s - \alpha + j\beta} + \frac{k_1^*}{s - \alpha - j\beta} + \cdots + \frac{k_M}{s - p_M}$$

keeping in mind that k^* is the complex conjugate of k. (We continue to maintain the assumption that all poles or eigenvalues will be distinct as they should be for any practical system.) Decomposing our signal in this manner as opposed to using, say for instance the Fourier transform, allows us to consider system poles that may have nonzero real parts. The Fourier transform will estimate our measurement signal with a set of undamped sinusoids therefore placing system poles along the imaginary axis. It is important to note that the above partial fraction expansion amounts to a sum of damped exponentials (potentially sinusoids) in the time domain. We find this particularly attractive over, say, wavelet techniques as the solution of the differential equations that govern our multiple-input multiple-output (MIMO) linear time-invariant (LTI) system should be a weighted sum of damped exponentials.

Having noted that our measurement signal is in fact set of discrete data points in a vector we must need to have some process of to deal with discrete data and compute the discrete Laplace transform (yielding in effect a discrete partial fraction expansion). To accomplish this effort we employ the so-called Matrix Pencil method.

Treatment of Wide-Area Frequency Data using Matrix Pencils

Perhaps the best in-depth treatment of the Matrix Pencil method has been presented by Hua in [54] and well condensed by Sarkar in [63]. We now wish to exploit the properties of the Matrix Pencil method to estimate the eigenvalues and residues of our discrete wide-area frequency data. Previously in this report we have used the notation $f(\mathbf{x}_i, t)$ to indicate frequency at location $\mathbf{x}_i$ at time t. Now, to be consistent with notation commonly used in signal processing studies, our observed signal $f(\mathbf{x}_i, t)$ will assume the notation $y(t)$ with a temporary suppression of the location vector. We therefore write our observed (properly detrended) frequency signal leaving only the small signal behavior as:

$$y(t) = f(t) - \mu(t)$$

where $f(t)$ is our frequency signal with $\mu(t)$ containing the signal trend. We look to the Matrix Pencil method to estimate our observed signal through a process that will disclose the signal's eigenvalues (or poles) and residues (or zeros). Concisely,

$$\hat{y}(t) = \sum_{i=1}^{M} R_i e^{s_i t}$$

with residues, R_i, which in familiar terms is a phasor with a magnitude and phase, and poles $s_i = -\alpha_i + j\beta_i = -\alpha_i + j\omega_i^d$. Again, however, our data is discrete formed from the sampling of the continuous electric grid frequency. Therefore, in fact, our signal takes the form:

$$\begin{aligned}
\mathbf{y} &= \begin{bmatrix} y(0) & y(T_s) & \cdots & y(kT_s) \end{bmatrix}^T \\
\hat{\mathbf{y}} &= \begin{bmatrix} \hat{y}(0) & \hat{y}(T_s) & \cdots & \hat{y}(kT_s) \end{bmatrix}^T \\
\hat{y}(kT_s) &= \sum_{i=1}^{M} R_i z_i^k \\
k &= \begin{bmatrix} 0 & 1 & \cdots & N-1 \end{bmatrix}
\end{aligned}$$

In this discrete case, the discrete poles z_i can be described in terms of continuous poles via:

$$z_i = e^{s_i T_s} = e^{\left(-\alpha_i + j\omega_i^d\right)T_s}$$

In essence, the Matrix Pencil method will help us determine approximations the parameters: R_i, z_i, and M. The Matrix Pencil method, developed by Hua and published in 1988, is relatively new compared to the long history of the problem of estimating a function by a sum of complex exponentials first treated by Baron Gaspard Riche de Prony in 1795 [64]. The method takes its name from the term used to describe the combination of two functions by a scalar parameter λ in the following way:

$$f(t,\lambda) = g(t) + \lambda h(t)$$

The resultant function, $f(t,\lambda)$, is a pencil of the two functions $g(t)$ and $h(t)$[10]. The first step in the decomposition of our data vector is the formation of the matrix $\mathbf{Y}$ with Hankel structure as follows:

$$\mathbf{Y} = \begin{bmatrix} y_0 & y_1 & \cdots & y_L \\ y_1 & y_2 & \cdots & y_{L+1} \\ \vdots & \vdots & & \vdots \\ y_{N-L-1} & y_{N-L} & \cdots & y_{N-1} \end{bmatrix} \in \mathbb{R}^{N-L \times L+1}$$

The matrix then is partitioned:

[10] Not allowing the trivial case where $g(t)$ is a scalar multiple of $h(t)$.

$$\mathbf{Y} = \left[\begin{array}{c|cccc|c} y_0 & y_1 & y_2 & \cdots & y_{L-1} & y_L \\ y_1 & y_2 & y_3 & \cdots & y_L & y_{L+1} \\ \vdots & \vdots & \vdots & & \vdots & \vdots \\ y_{N-L-1} & y_{N-L} & y_{N-L+1} & \cdots & y_{N-2} & y_{N-1} \end{array}\right]$$
$$\mathbf{Y} = \left[\mathbf{Y}_L \mid \mathbf{Y}_C \mid \mathbf{Y}_R\right]$$

and two further matrices are formed brining us ever closer to the disclosure of the matrix pencil:

$$\mathbf{Y}_1 = \left[\mathbf{Y}_L \mid \mathbf{Y}_C\right] \quad \text{and} \quad \mathbf{Y}_2 = \left[\mathbf{Y}_C \mid \mathbf{Y}_R\right]$$

The length of our measurement data vector is N, our desired model order is M, and the pencil parameter is L [11] with a few handy pointers for selecting the parameter provided in [63]. We now introduce a decomposition of the Hankel matrices, $\mathbf{Y}_1$ and $\mathbf{Y}_2$, that will allow access to the eigenvalues of the measurement vector.

$$\begin{aligned} \mathbf{Y}_1 &= \mathbf{Z}_1 \mathbf{R} \mathbf{Z}_0 \mathbf{Z}_2 \\ \mathbf{Y}_2 &= \mathbf{Z}_1 \mathbf{R} \mathbf{Z}_2 \end{aligned}$$

where $\mathbf{Z}_1$ and $\mathbf{Z}_2$ are matrices with Vandermonde structure:

$$\mathbf{Z}_1 = \begin{bmatrix} 1 & 1 & \cdots & 1 \\ z_0 & z_1 & \cdots & z_{M-1} \\ \vdots & \vdots & & \vdots \\ z_0^{N-L-1} & z_1^{N-L-1} & \cdots & z_{M-1}^{N-L-1} \end{bmatrix} \in \mathbb{C}^{(N-L)\times M}$$
$$\mathbf{Z}_2 = \begin{bmatrix} 1 & z_0 & \cdots & z_0^{L-1} \\ 1 & z_1 & \cdots & z_1^{L-1} \\ \vdots & \vdots & & \vdots \\ 1 & z_{M-1} & \cdots & z_{M-1}^{L-1} \end{bmatrix} \in \mathbb{C}^{M\times L}$$

and the matrices $\mathbf{R}$ and $\mathbf{Z}_0$ are diagonal matrices:

[11] For later use, we choose $L = \text{round}(0.4 \cdot N)$.

$$\mathbf{Z}_0 = \begin{bmatrix} z_1 & & \mathbf{0} \\ & \ddots & \\ \mathbf{0} & & z_M \end{bmatrix} \in \mathbb{C}^{M \times M}$$

$$\mathbf{R} = \begin{bmatrix} R_1 & & \mathbf{0} \\ & \ddots & \\ \mathbf{0} & & R_M \end{bmatrix} \in \mathbb{C}^{M \times M}$$

The matrices $\mathbf{Y}_1$ and $\mathbf{Y}_2$ are the matrix analogs of the functions $g(t)$ and $h(t)$ used earlier to describe the pencil of functions. In like manner, we construct a *matrix pencil* in the following fashion:

$$\mathbf{Y}_2 - \lambda \mathbf{Y}_1 = \mathbf{Z}_1 \mathbf{R} \left(\mathbf{Z}_0 - \lambda \mathbf{I} \right) \mathbf{Z}_2$$

given that $\mathbf{I} \in \mathbb{R}^{M \times M}$ is the identity matrix. In general, it has been demonstrated by Hua and Sarkar that:

$$\text{rank}\left(\left[\mathbf{Y}_2 - \lambda \mathbf{Y}_1 \right] \right) = M \text{ if } M \leq L \leq N - M$$

However, this will not be true in the case where any one of the values, λ, is a rank-reducing parameter. That is:

$$\text{rank}\left(\left[\mathbf{Y}_2 - \lambda \mathbf{Y}_1 \right] \right) = M - 1 \text{ iff } \lambda = z_i \text{ for } i = 1, 2, \cdots, M$$

Therefore, the parameters, z_i, are the generalized eigenvalues of the matrix pair $\left(\mathbf{Y}_2, \mathbf{Y}_1 \right)$ or the solution of the ordinary eigenvalue problem for the matrix $\left[\mathbf{Y}_1^{\dagger} \mathbf{Y}_2 - \lambda \mathbf{I} \right]$[12]. These values for z_i, because of the Hankel structure of the data matrix $\mathbf{Y}$, are also the poles of our signal sampled into the data vector $\mathbf{y}$. Once the poles of the signal are known, the residues can be solved for as follows:

$$\mathbf{y} = \begin{bmatrix} 1 & 1 & \cdots & 1 \\ z_1 & z_2 & \cdots & z_M \\ \vdots & \vdots & & \vdots \\ z_1^{N-1} & z_2^{N-1} & \cdots & z_M^{N-1} \end{bmatrix} \begin{bmatrix} R_1 \\ R_2 \\ \vdots \\ R_M \end{bmatrix} \Rightarrow \begin{bmatrix} 1 & 1 & \cdots & 1 \\ z_1 & z_2 & \cdots & z_M \\ \vdots & \vdots & & \vdots \\ z_1^{N-1} & z_2^{N-1} & \cdots & z_M^{N-1} \end{bmatrix}^{\dagger} \mathbf{y} = \begin{bmatrix} \hat{R}_1 \\ \hat{R}_2 \\ \vdots \\ \hat{R}_M \end{bmatrix}$$

Since the data in our signal vector will likely contain noise, a system reduction is performed on $\mathbf{y}$ to achieve some form of filtering. Making use of the singular value decomposition (SVD), this method becomes the total least-squares Matrix Pencil method. We shall provide a very simplistic overview of

[12] For an arbitrary matrix $\mathbf{A}$, $\mathbf{A}^{\dagger}$ denotes the Moore-Penrose pseudoinverse of $\mathbf{A}$. Superscript H indicates complex conjugate transpose operation.

the SVD-based method. Returning to our Hankel matrix, $\mathbf{Y}$, we achieve filtration via discarding insignificant singular values and appropriately reducing matrix dimensions in the following manner:

- First $\mathbf{Y}$ is decomposed: $\mathbf{Y} = \mathbf{U}\Sigma\mathbf{V}^H$ with $\mathbf{U}$ and $\mathbf{V}$ unitary and Σ a diagonal matrix of singular values.
- Singular values are examined and the first M kept while the rest are discarded. This step determines the value of M based upon the decay of the singular values.
- The matrix $\mathbf{V}$ is truncated to include only the first M right singular vectors: $\mathbf{V}' = \begin{bmatrix} \mathbf{v}_1 & \mathbf{v}_2 & \cdots & \mathbf{v}_M \end{bmatrix}$ yielding $\hat{\mathbf{Y}}_1 = \mathbf{U}_1\Sigma'\left(\mathbf{V}_1'\right)^H$ and $\hat{\mathbf{Y}}_2 = \mathbf{U}_2\Sigma'\left(\mathbf{V}_2'\right)^H$.
- The poles of the "noise-free" system need not be calculated from the generalized eigenvalues of the matrix pair $\left(\hat{\mathbf{Y}}_2, \hat{\mathbf{Y}}_1\right)$, but can be calculated via the ordinary eigenvalue problem for the matrix $\left[\left\{\left(\mathbf{V}_1'\right)^H\right\}^\dagger \left\{\left(\mathbf{V}_2'\right)^H\right\} - \lambda\mathbf{I}\right]$ [65-69].

Having formed $\hat{\mathbf{Y}}_1$ and $\hat{\mathbf{Y}}_2$ as "denoised" Hankel matrices, we can estimate the poles of the system as:

$$\hat{\mathbf{z}} = \begin{bmatrix} \hat{z}_1 \\ \hat{z}_2 \\ \vdots \\ \hat{z}_M \end{bmatrix} = \mathrm{eig}\left(\hat{\mathbf{Y}}_1^\dagger \hat{\mathbf{Y}}_2\right) = \mathrm{eig}\left(\left\{\left(\mathbf{V}_1'\right)^H\right\}^\dagger \left\{\left(\mathbf{V}_2'\right)^H\right\}\right)$$

This process has been implemented for use both with FNET formatted data and PSS/E™ ASCII output format. The associated MATLAB™ code is located in Appendix IX. A subtlety of note is that we operate on discrete data. Therefore our results will be in terms of discrete poles. Several mappings exist and are well known such as Tustin's rule, etc. For our purposes it suffices to compute the continuous poles from the discrete poles by:

$$\hat{s}_i \approx \frac{\log\left(\hat{z}_i\right)}{T_s}$$

Application of the Matrix Pencil Method to Single Channel FNET Data

We now return to the WECC test cases presented originally in Chapter 1. For each of the tests D1 through D5 (omitting D3), several FDRs were online and reporting data to the FNET server at Virginia Tech. Table 3-1 contains analysis results based upon FDR5 in Seattle, WA to serve as an example. A comprehensive library of plots from all tests, all FDRs, and all PMUs is contained in Appendix X. Table 3-2 contains single channel WECC results based upon PMU data. Table 3-3 addresses the Florida blackout event and provides data from two FDRs (one in Florida and the other across the grid in North Dakota) and a PMU located near Virginia Tech. The following battery of figures demonstrates the operation of the single channel matrix pencil method on both FDR and PMU measured data.

Extending the Single Channel Matrix Pencil Method to Multiple Channels

Since we are measuring frequency at several points within the North American electric grids, we wish to extend the operation of the Matrix Pencil algorithm to accommodate a simultaneous analysis of multiple channels. The reasoning behind this endeavor extends from the notion that, in fact, each of the multiple sensors is measuring the same grid differing only by location in the system topology. We do not wish to propose that any oscillation within the electric grid is observable at every point. However in many cases, such as the WECC tests and the Florida blackout, severe inter-area oscillations are observable throughout an interconnection. These oscillations are a result of the natural response of the interconnection in which they occur and therefore should contain the same modes. The mode shapes may differ as the residues at each sensor location change, but the set of modes should be consistent. In cases where modes are unobservable at certain points, the corresponding residue would have a magnitude of zero. The single channel matrix pencil method estimates a set of poles and residues for each signal. Therefore, the possibility exists for inconsistency in the estimated modal parameters across an interconnection. We now develop a rather simple extension of the single channel Matrix Pencil algorithm to form the multiple channel Matrix Pencil algorithm.

WECC TEST D1 – FNET Perspective

WECC Test D1: Insertion of Chief Joseph Dynamic Brake (First Insertion)

Virginia Tech Sensor: FDR 5 – Seattle, WA

Virginia Tech Modes:	BPA Modes:
0.90 Hz at 16.3%	0.89 Hz at 10.7%
0.32 Hz at 9.4%	0.31 Hz at 8.3%
0.31 Hz at 39.5%	--
--	0.63 Hz at 15.4%
--	0.72 Hz at 22.5%

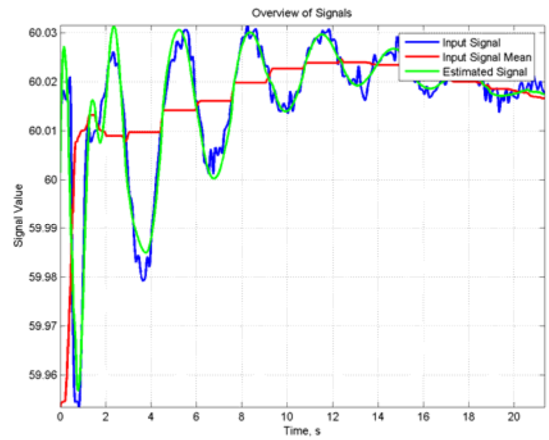

Figure 3-11: Original signal with trend and estimate.

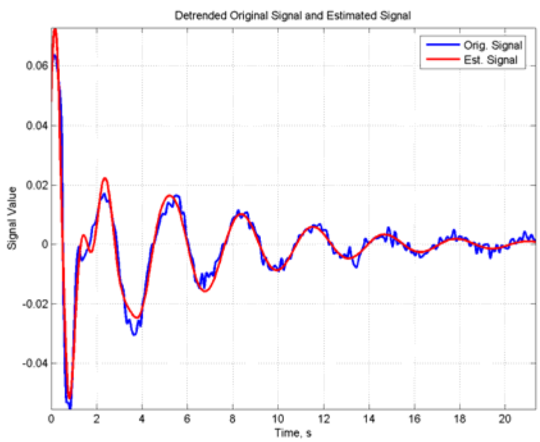

Figure 3-12: Detrended signal with estimate.

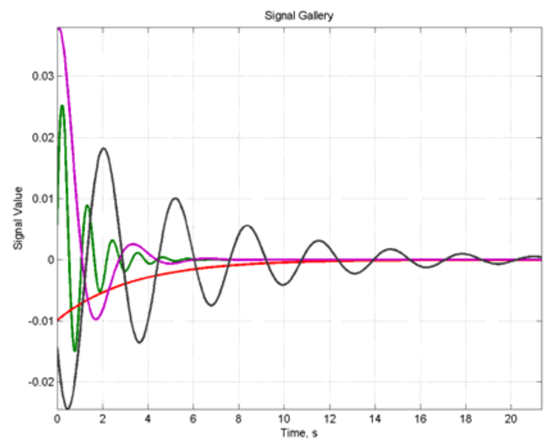

Figure 3-13: Modes used in estimation.

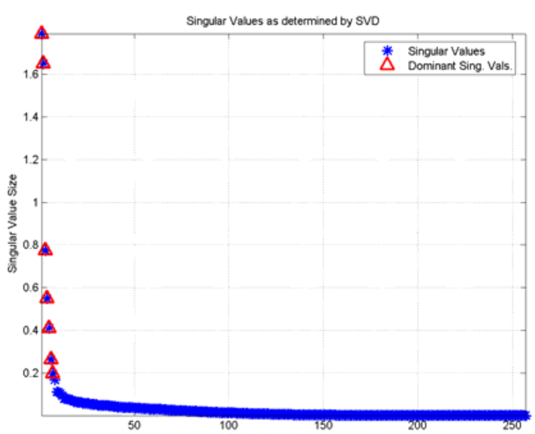

Figure 3-14: Singular values used in reduction.

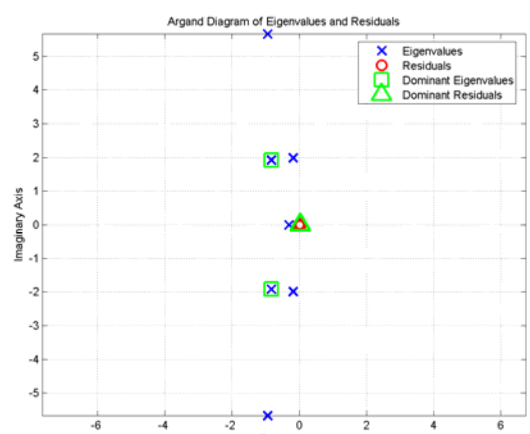

Figure 3-15: Estimated signal eigenvalues.

WECC TEST D2 – FNET Perspective

WECC Test D2: Insertion of Chief Joseph Dynamic Brake (Second Insertion)

Virginia Tech Sensor: FDR 5 – Seattle, WA

Virginia Tech Modes:	BPA Modes (from D1):
--	0.89 Hz at 10.7%
0.31 Hz at 8.3%	0.31 Hz at 8.3%
0.08 Hz at 89.6%	Similar Low
--	0.63 Hz at 15.4%
0.74 Hz at 26.7%	0.72 Hz at 22.5%

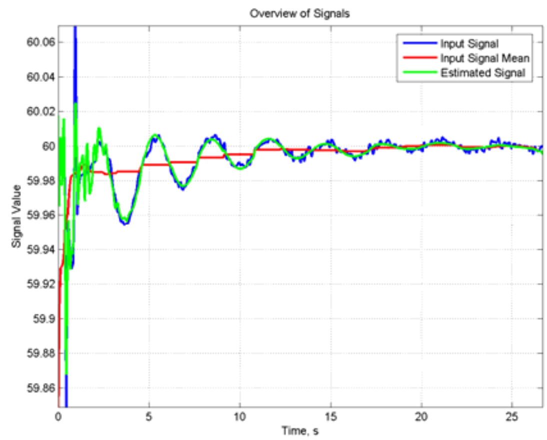

Figure 3-16: Original signal with trend and estimate.

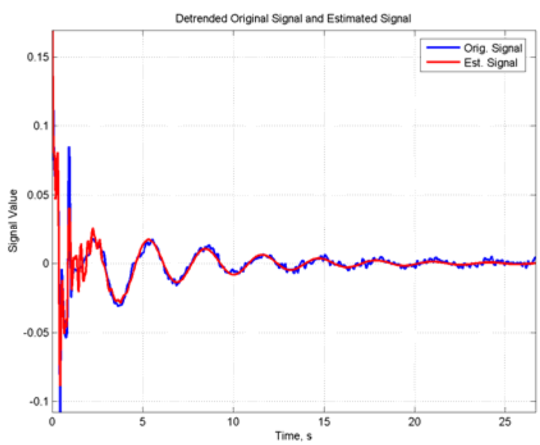

Figure 3-17: Detrended signal with estimate.

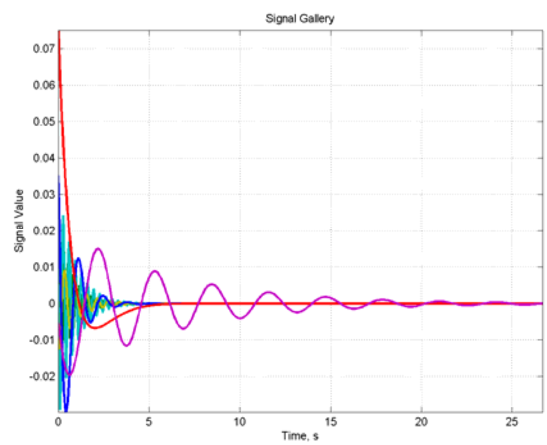

Figure 3-18: Modes used in estimation.

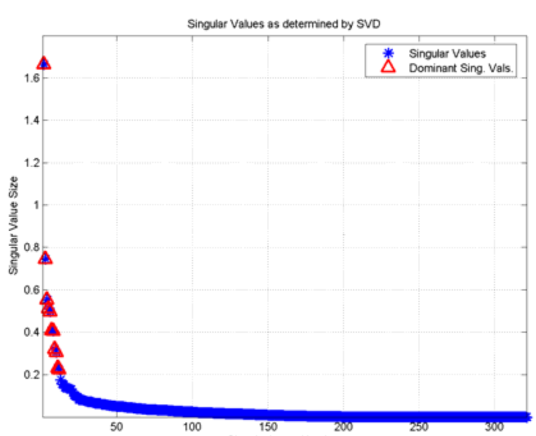

Figure 3-19: Singular values used reduction.

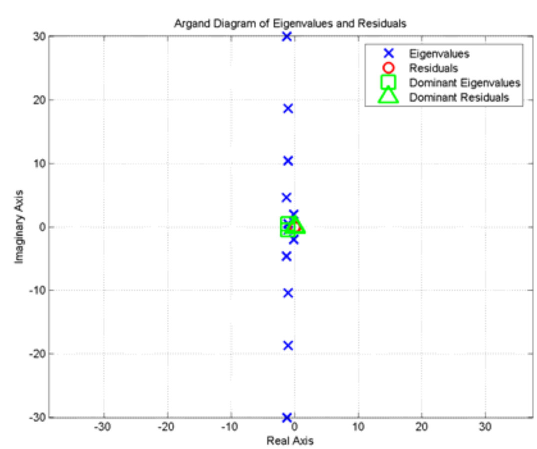

Figure 3-20: Estimated signal eigenvalues.

WECC TEST D4 – FNET Perspective

WECC Test D4: “Square Wave” Modulation of PDCI at 0.25 Hz for Three Cycles at ± 125 MW Peak-to-Peak Amplitude.

Virginia Tech Sensor: FDR 5 – Seattle, WA

Virginia Tech Modes:	BPA Modes:
0.28 Hz at 5.4% 0.22 Hz at 7.8% 0.32 Hz at 0.2%	0.25 Hz 3 cycles

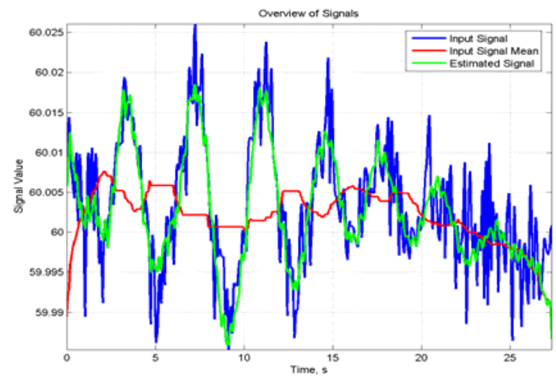

Figure 3-21: Original signal with trend and estimate.

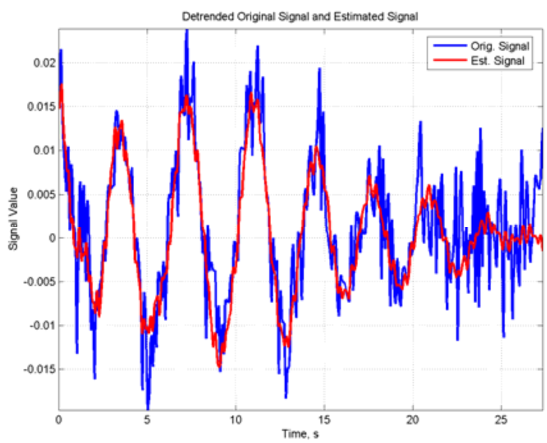

Figure 3-22: Detrended signal with estimate.

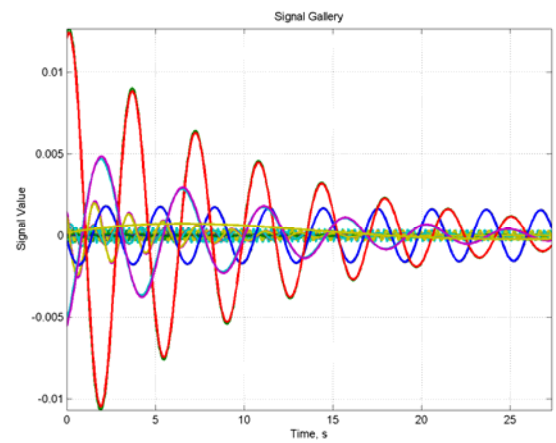

Figure 3-23: Modes used in estimation.

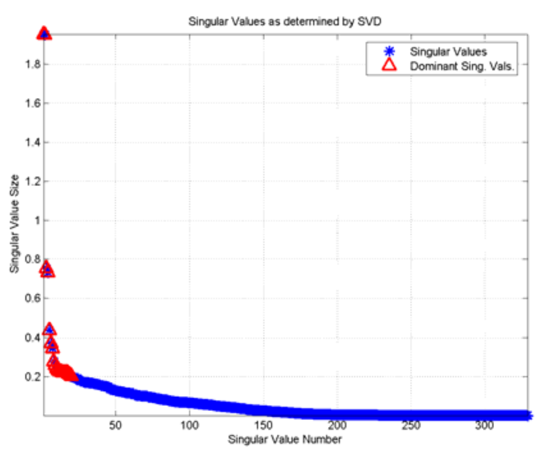

Figure 3-24: Singular values used reduction.

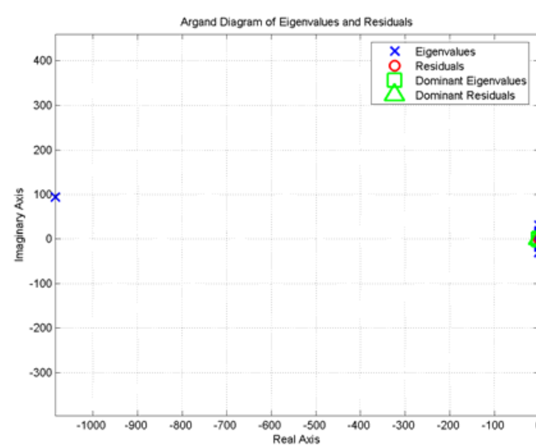

Figure 3-25: Estimated signal eigenvalues.

WECC TEST D5 – FNET Perspective

WECC Test D5: Sine Wave Modulation of PDCI at 0.25 Hz for Three Cycles at ± 125 MW Peak-to-Peak Amplitude.

Virginia Tech Sensor: FDR 5 – Seattle, WA

Virginia Tech Modes:	BPA Modes:
0.33 Hz at 3.5% 0.29 Hz at 4.8%	0.25 Hz 3 cycles

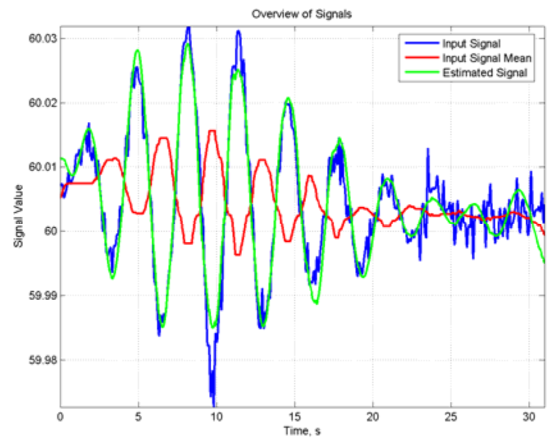

Figure 3-26: Original signal with trend and estimate.

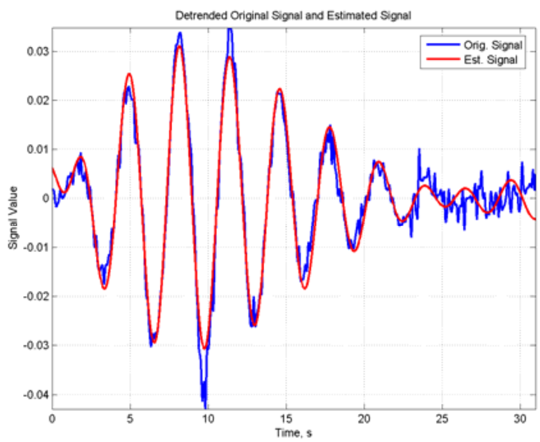

Figure 3-27: Detrended signal with estimate.

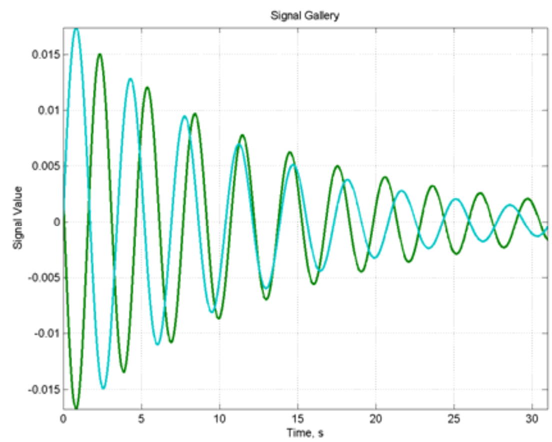

Figure 3-28: Modes used in estimation.

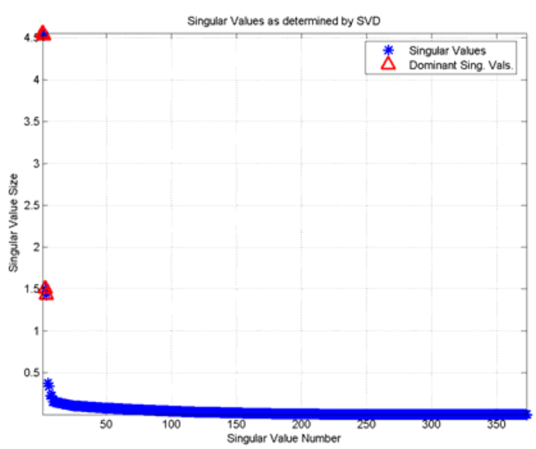

Figure 3-29: Singular values used reduction.

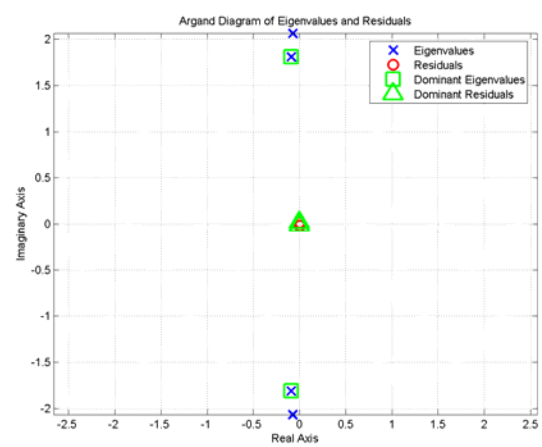

Figure 3-30: Estimated signal eigenvalues.

WECC TEST D1 – PMU Perspective

WECC Test D1: Insertion of Chief Joseph Dynamic Brake (First Insertion)

WECC PMU at Colstrip Generating Station

PMU Modes:	BPA Modes:
0.84 Hz at 6.9%	0.89 Hz at 10.7%
0.33 Hz at 7.7%	0.31 Hz at 8.3%
0.68 Hz at 7.7%	0.63 Hz at 15.4%
--	0.72 Hz at 22.5%

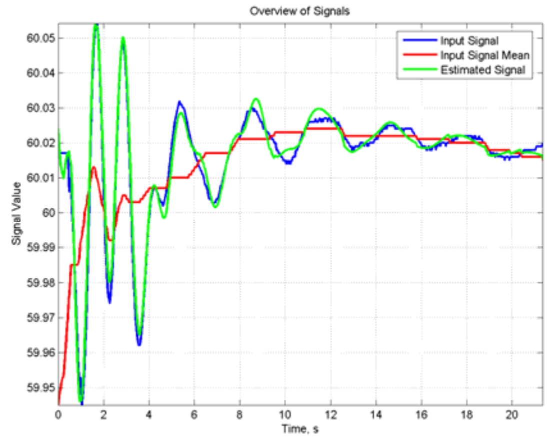

Figure 3-31: Original signal with trend and estimate.

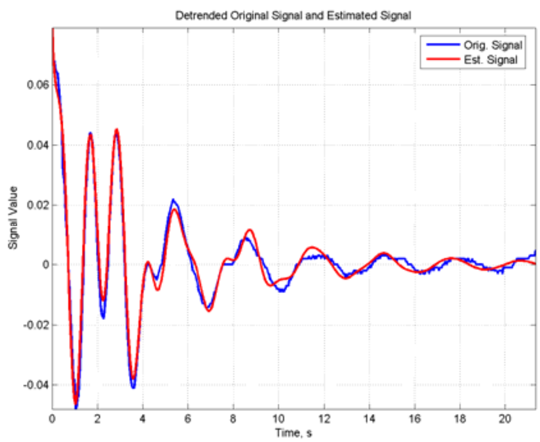

Figure 3-32: Detrended signal with estimate.

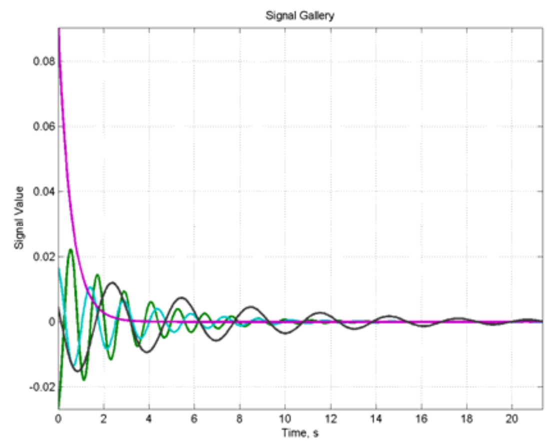

Figure 3-33: Modes used in estimation.

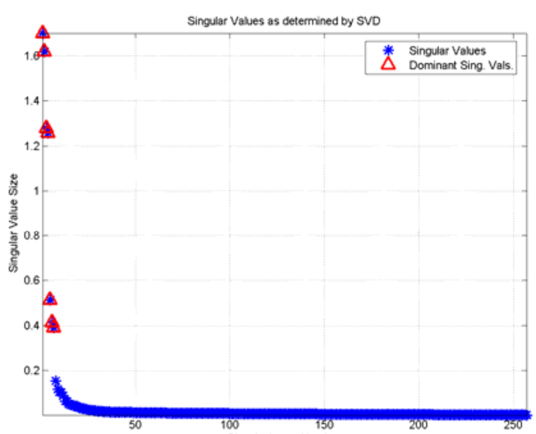

Figure 3-34: Singular values used reduction.

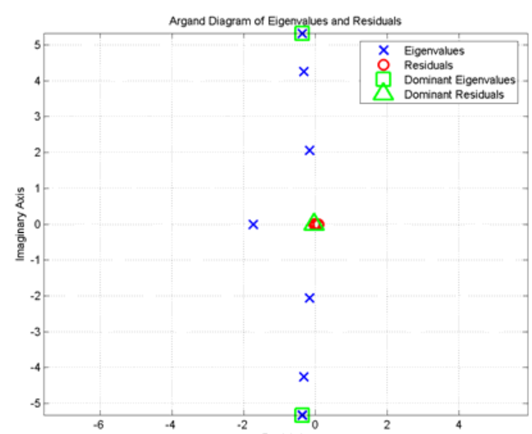

Figure 3-35: Estimated signal eigenvalues.

WECC TEST D2 – PMU Perspective

WECC Test D2: Insertion of Chief Joseph Dynamic Brake (Second Insertion)

WECC PMU at Colstrip Generating Station

PMU Modes:	BPA Modes (From D1):
0.89 Hz at 7.9%	0.89 Hz at 10.7%
0.32 Hz at 11.3%	0.31 Hz at 8.3%
--	0.63 Hz at 15.4%
0.71 Hz at 9.9%	0.72 Hz at 22.5%
0.32 Hz at 37.0%	--

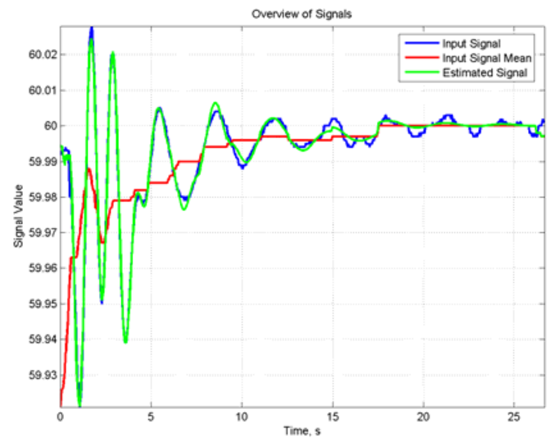

Figure 3-36: Original signal with trend and estimate.

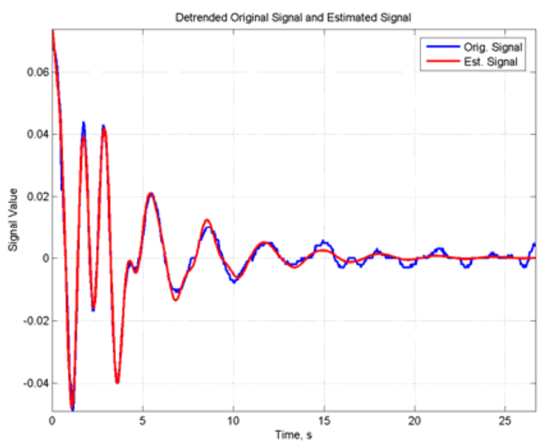

Figure 3-37: Detrended signal with estimate.

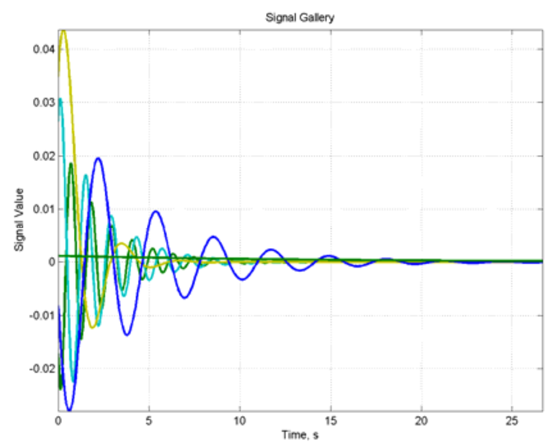

Figure 3-38: Modes used in estimation.

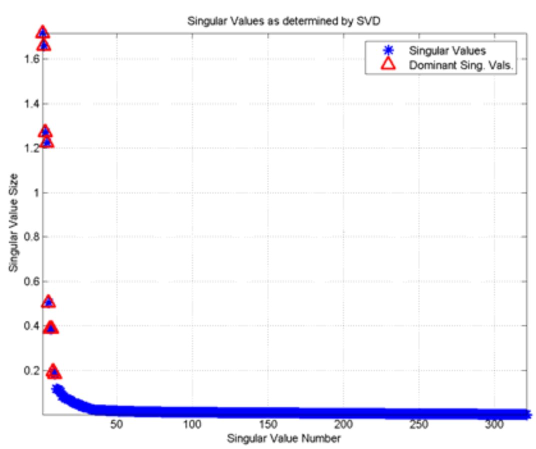

Figure 3-39: Singular values used reduction.

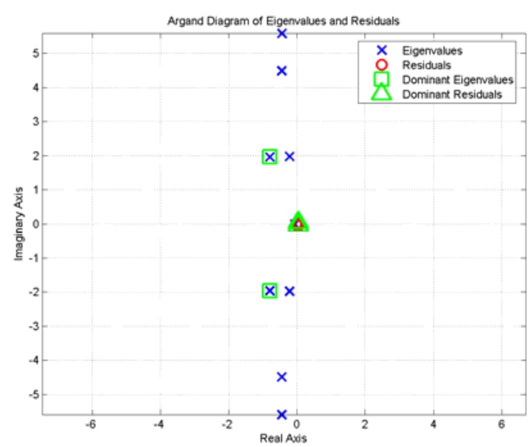

Figure 3-40: Estimated signal eigenvalues.

WECC TEST D4 – PMU Perspective

WECC Test D4: "Square Wave" Modulation of PDCI at 0.25 Hz for Three Cycles at ± 125 MW Peak-to-Peak Amplitude.

WECC PMU at Colstrip Generating Station

PMU Modes:	BPA Modes:
0.29 Hz at 4.0% 0.24 Hz at 5.0% 0.35 Hz at 0.1%	0.25 Hz for 3 cycles

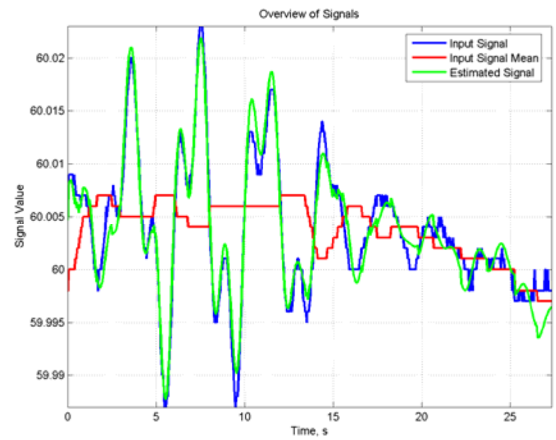

Figure 3-41: Original signal with trend and estimate.

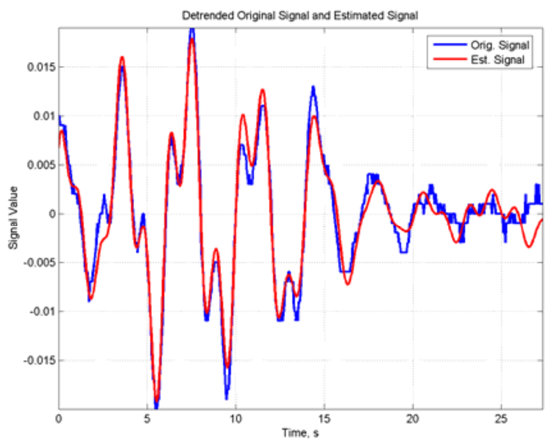

Figure 3-42: Detrended signal with estimate.

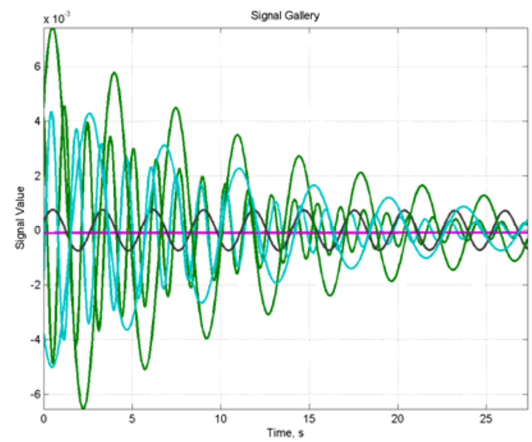

Figure 3-43: Modes used in estimation.

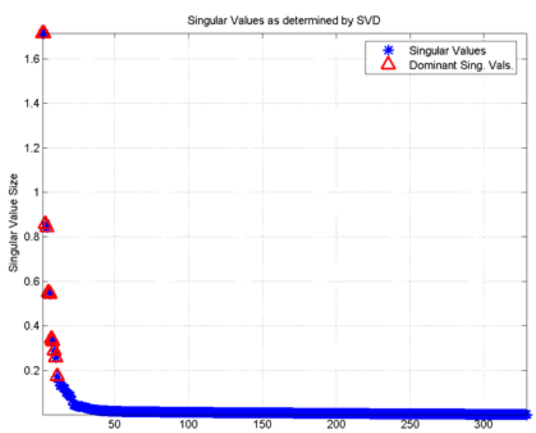

Figure 3-44: Singular values used reduction.

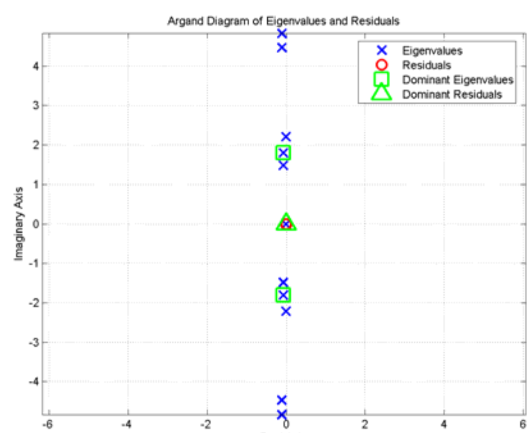

Figure 3-45: Estimated signal eigenvalues.

WECC TEST D5 – PMU Perspective

WECC Test D5: Sine Wave Modulation of PDCI at 0.25 Hz for Three Cycles at ±125 MW Peak-to-Peak Amplitude.

WECC PMU at Colstrip Generating Station

PMU Modes:	BPA Modes:
0.29 Hz at 4.5%	
0.33 Hz at 3.4%	0.25 Hz for 3 cycles
0.89 Hz at 1.2%	

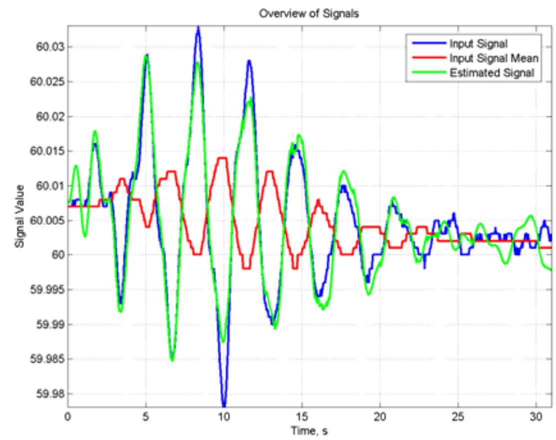

Figure 3-46: Original signal with trend and estimate.

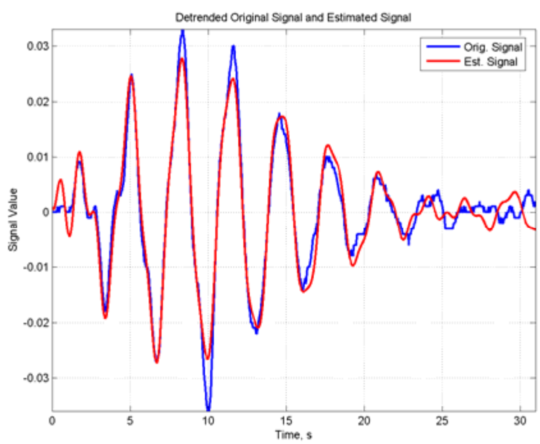

Figure 3-47: Detrended signal with estimate.

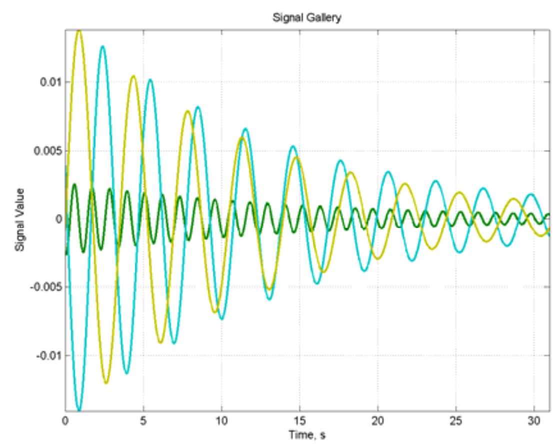

Figure 3-48: Modes used in estimation.

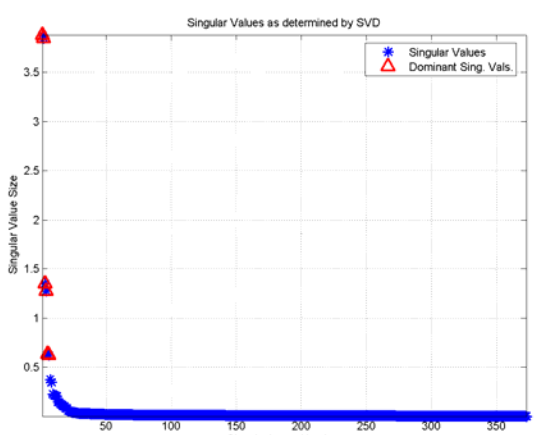

Figure 3-49: Singular values used reduction.

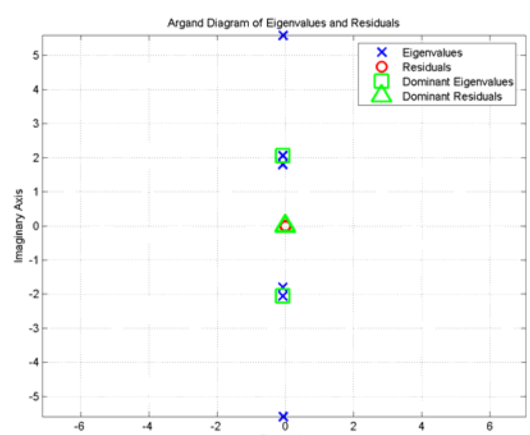

Figure 3-50: Estimated signal eigenvalues.

Florida Blackout (February 2008) – FNET Perspective

Virginia Tech Sensor: FDR 42 – Tallahassee, FL

FDR Modes:
0.51 Hz at 7.7%
0.25 Hz at 16.9%
0.12 Hz at 24.0%

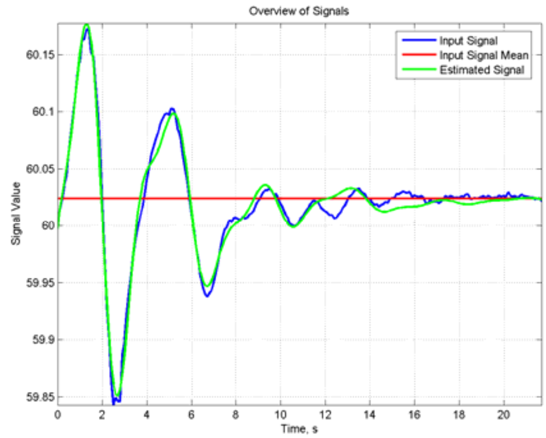

Figure 3-51: Original signal with trend and estimate.

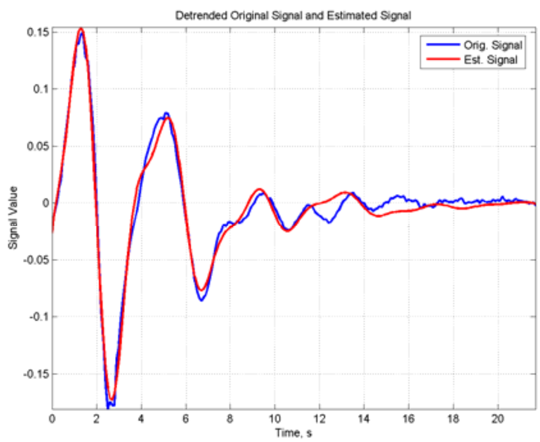

Figure 3-52: Detrended signal with estimate.

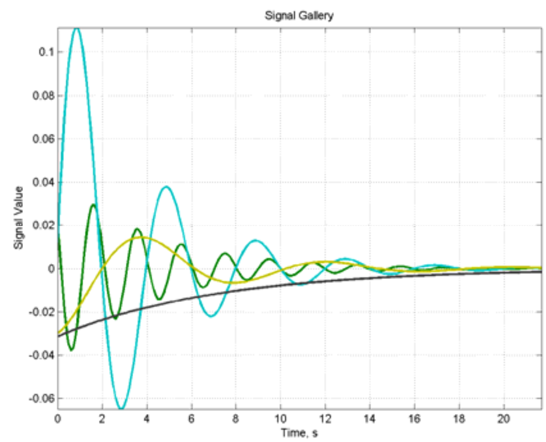

Figure 3-53: Modes used in estimation.

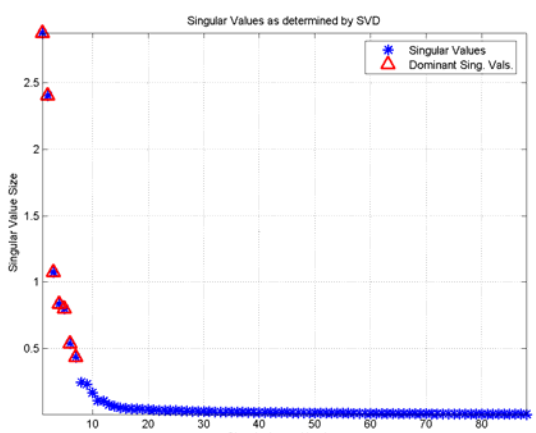

Figure 3-54: Singular values used reduction.

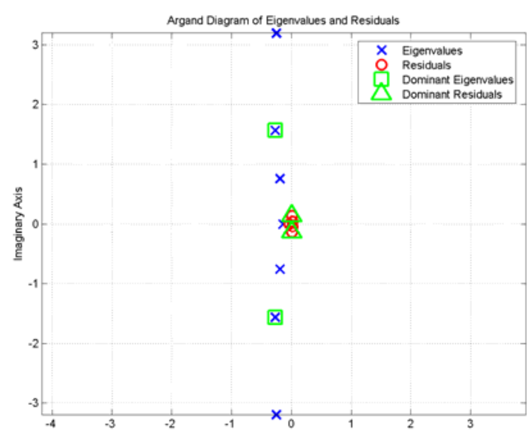

Figure 3-55: Estimated signal eigenvalues.

Florida Blackout (February 2008) – FNET Perspective

Virginia Tech Sensor: FDR 43 – Bismarck, ND

FDR Modes:
0.50 Hz at 4.9%
0.27 Hz at 13.2%
0.21 Hz at 28.9%

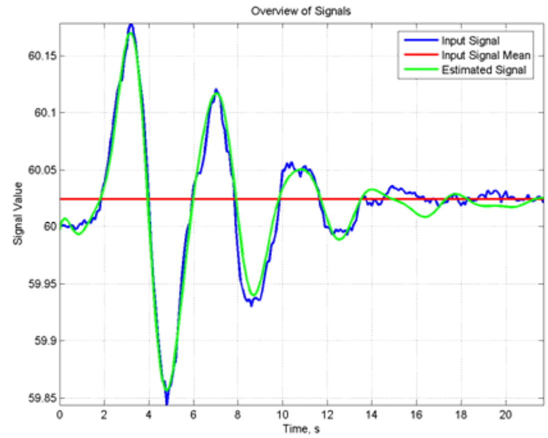

Figure 3-56: Original signal with trend and estimate.

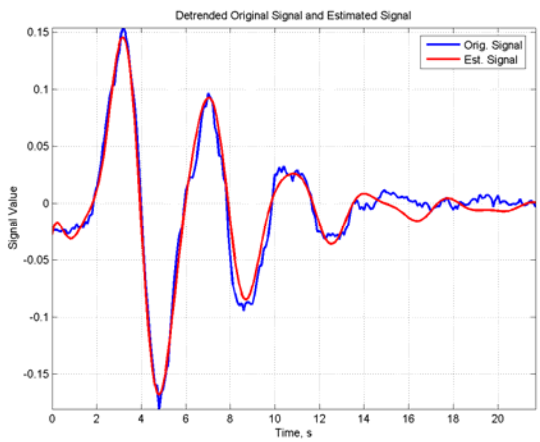

Figure 3-57: Detrended signal with estimate.

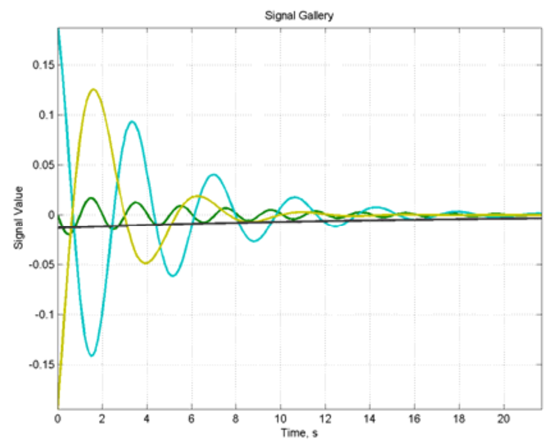

Figure 3-58: Modes used in estimation.

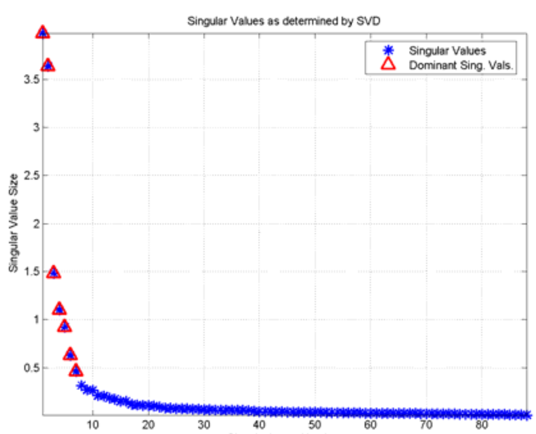

Figure 3-59: Singular values used reduction.

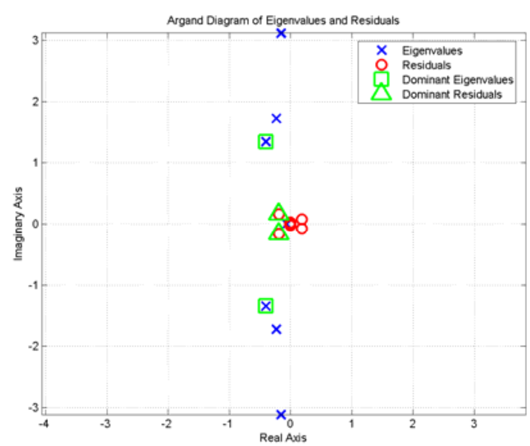

Figure 3-60: Estimated signal eigenvalues.

Florida Blackout (February 2008) – PMU Perspective

AEP PMU: Matt Funk Substation

PMU Modes:
0.52 Hz at 6.0%
0.28 Hz at 20.9%
0.30 Hz at 2.0%

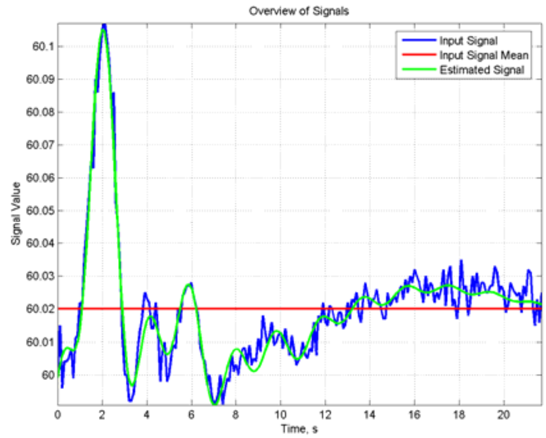

Figure 3-61: Original signal with trend and estimate.

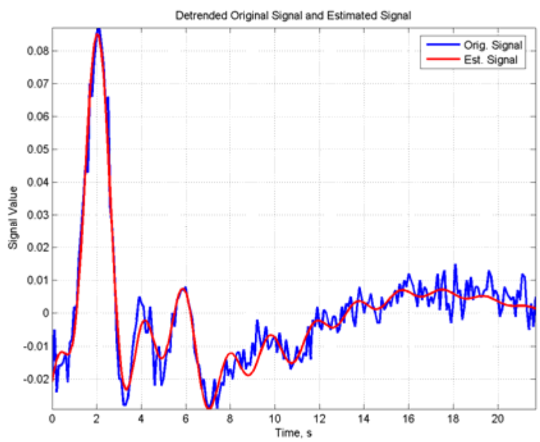

Figure 3-62: Detrended signal with estimate.

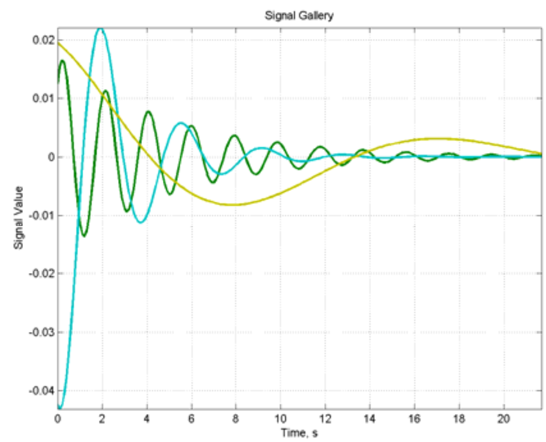

Figure 3-63: Modes used in estimation.

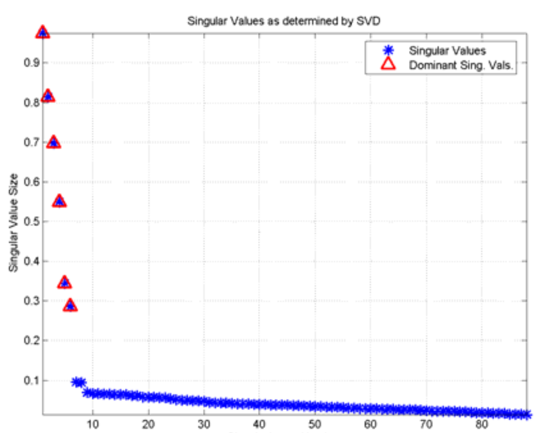

Figure 3-64: Singular values used reduction.

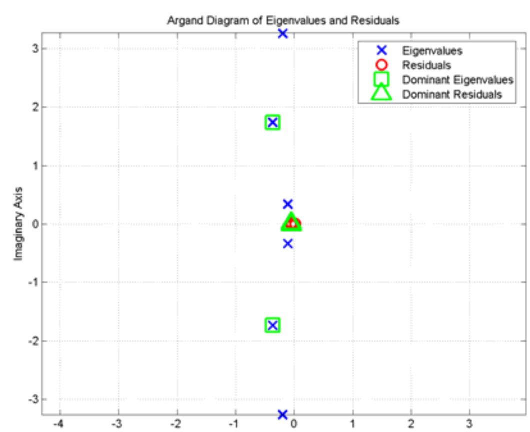

Figure 3-65: Estimated signal eigenvalues.

Overview of FNET Results for WECC Tests

Table 3-1: Single channel matrix pencil results for WECC tests (FDR5).

Test D1			Test D2			Test D4[13]			Test D5		
ω^d	ξ	$\|R\|$	ω^d	ξ	$\|R\|$	ω^d	ξ	$\|R\|$	ω^d	ξ	$\|R\|$
0.902488	0.163355	0.031426	4.786442	0.041127	0.021619	4.954193	0.002462	0.000458	0.328704	0.034946	0.017803
0.902488	0.163355	0.031426	4.786442	0.041127	0.021619	4.954193	0.002462	0.000459	0.328704	0.034946	0.017803
0	0	0.009928	2.976616	0.056548	0.032305	2.99118	0.000877	0.000497	0.288149	0.048486	0.018728
0.30572	0.395475	0.043447	2.976616	0.056548	0.032305	2.99118	0.000877	0.000503	0.288149	0.048486	0.018728
0.30572	0.395475	0.043447	1.66295	0.097212	0.013163	2.07481	0.000502	0.000333			
0.316508	0.093647	0.02676	1.66295	0.097212	0.013163	2.07481	0.000502	0.000337			
0.316508	0.093647	0.02676	0.742288	0.267468	0.053927	15.00015	0.996247	0.001365			
			0.742288	0.267468	0.053927	1.076312	0.009819	0.000067			
			0.083842	0.896078	0.130871	1.076312	0.009819	0.000104			
			0.083842	0.896078	0.130871	0.747338	0.01952	0.000721			
			0.319299	0.083129	0.021759	0.747338	0.01952	0.000702			
			0.319299	0.083129	0.021759	0.518671	0.065768	0.002968			
						0.518671	0.065768	0.002776			
						0.326441	0.00287	0.001837			
						0.326441	0.00287	0.001811			
						0.280862	0.05401	0.012821			
						0.280862	0.05401	0.012574			
						0.218096	0.078299	0.005768			
						0.218096	0.078299	0.005992			
						0.026451	0.339169	0.00113			

[13] Square wave modulation of the line caused significant harmonics. Reference Table 1-3.

Overview of PMU Results for WECC Tests

Table 3-2: Single channel matrix pencil results for WECC tests (Colstrip Generating Station PMU).

Test D1			Test D2			Test D4[14]			Test D5		
ω^d	ξ	$\|R\|$	ω^d	ξ	$\|R\|$	ω^d	ξ	$\|R\|$	ω^d	ξ	$\|R\|$
0.847064	0.068851	0.027209	0.889607	0.079043	0.025511	0.768862	0.022229	0.005181	0.890439	0.011591	0.002652
0.847064	0.068851	0.027209	0.889607	0.079043	0.025511	0.768862	0.022229	0.005181	0.890439	0.011591	0.002652
0.677307	0.077413	0.016952	0.714569	0.099322	0.032546	0.710591	0.025044	0.004581	0.328482	0.03442	0.014963
0.677307	0.077413	0.016952	0.714569	0.099322	0.032546	0.710591	0.025044	0.004581	0.328482	0.03442	0.014963
0	0	0.090281	0.312877	0.372925	0.058832	0	0	0.000106	0.287618	0.044593	0.014852
0.328032	0.077336	0.017504	0.312877	0.372925	0.058832	0.352413	0.000805	0.000762	0.287618	0.044593	0.014852
0.328032	0.077336	0.017504	0.315161	0.112681	0.032247	0.352413	0.000805	0.000762			
			0.315161	0.112681	0.032247	0.287326	0.039878	0.007706			
						0.287326	0.039878	0.007706			
						0.236694	0.050434	0.00521			
						0.236694	0.050434	0.00521			

[14] Square wave modulation of the line caused significant harmonics. Reference Table 1-3.

Overview of February 2008 Florida Blackout

Table 3-3: Single channel matrix pencil results for Florida Blackout

FDR42: Tallahassee, FL			FDR43: Bismarck, ND			Matt Funk PMU		
ω^d	ξ	$\lVert R \rVert$	ω^d	ξ	$\lVert R \rVert$	ω^d	ξ	$\lVert R \rVert$
0.508186	0.076946	0.044293	0.496202	0.048834	0.021341	0.519432	0.060069	0.017313
0.508186	0.076946	0.044293	0.496202	0.048834	0.021341	0.519432	0.060069	0.017313
0.24899	0.169224	0.141816	0.274571	0.131599	0.202344	0.276582	0.20857	0.045822
0.24899	0.169224	0.141816	0.274571	0.131599	0.202344	0.276582	0.20857	0.045822
0.120926	0.239439	0.02986	0.214104	0.289128	0.251824	0.054352	0.295716	0.019708
0.120926	0.239439	0.02986	0.214104	0.289128	0.251824	0.054352	0.295716	0.019708

Consider the Hankel matrix formed by the zero-mean frequency values:

$$\mathbf{Y} = \begin{bmatrix} y_0 & y_1 & \cdots & y_L \\ y_1 & y_2 & \cdots & y_{L+1} \\ \vdots & \vdots & & \vdots \\ y_{N-L-1} & y_{N-L} & \cdots & y_{N-1} \end{bmatrix} \in \mathbb{R}^{N-L \times L+1}$$

This matrix is formed from a vector of length N of sampled frequency measurements. Supposing the signal sampled in the vector is noise-free, the order of the signal's minimal modal representation is equal to the rank of $\mathbf{Y}$. Now let us consider the concatenation of two matrices formed by the arrangement of uniformly sampled frequency data of equal length as observed at two points in a synchronized interconnection, $\mathbf{Y}^{(1)}$ and $\mathbf{Y}^{(2)}$. If both signals are composed of the same modes, then the rank of each of the Hankel matrices is the same:

$$\text{rank}\left(\mathbf{Y}^{(1)}\right) = \text{rank}\left(\mathbf{Y}^{(2)}\right) = A$$

where A is the signals' order. Also, the following would hold true for the concatenated matrix:

$$\text{rank}\left(\left[\mathbf{Y}^{(1)} \;\vdots\; \mathbf{Y}^{(2)}\right]\right) = A$$

However, should $\mathbf{Y}^{(1)}$ be of rank A and $\mathbf{Y}^{(2)}$ be of rank B, then the following would be true for the concatenated matrix given that the modal contents of each of the signals in Hankel matrices are distinct from each other:

$$\text{rank}\left(\left[\mathbf{Y}^{(1)} \;\vdots\; \mathbf{Y}^{(2)}\right]\right) = A + B$$

We can quickly begin to see that concatenating the matrix $\mathbf{Y}^{(2)}$ onto the matrix $\mathbf{Y}^{(1)}$ shall only increase the rank of the matrix $\left[\mathbf{Y}^{(1)} \;\vdots\; \mathbf{Y}^{(2)}\right]$ if the modal content of $\mathbf{Y}^{(2)}$ is not already contained in $\mathbf{Y}^{(1)}$. The increase of the rank is directly determined by the number of modes in $\mathbf{Y}^{(2)}$ that are not already in $\mathbf{Y}^{(1)}$. The multiple channel Matrix Pencil algorithm is based on this principle. Suppose now that we concatenate Q Hankel matrices together to form a single interconnection Hankel matrix where Q is the number of FDRs reporting during the occurrence of an oscillation. We would then form:

$$\mathbf{Y} = \left[\mathbf{Y}^{(1)} \;\vdots\; \mathbf{Y}^{(2)} \;\vdots\; \cdots \;\vdots\; \mathbf{Y}^{(Q)}\right]$$

With partitions similar unto the single channel case:

$$\mathbf{Y} = \left[\left\{\mathbf{Y}_L^{(1)} \;\vdots\; \mathbf{Y}_C^{(1)} \;\vdots\; \mathbf{Y}_R^{(1)}\right\} \;\vdots\; \left\{\mathbf{Y}_L^{(2)} \;\vdots\; \mathbf{Y}_C^{(2)} \;\vdots\; \mathbf{Y}_R^{(2)}\right\} \;\vdots\; \cdots \;\vdots\; \left\{\mathbf{Y}_L^{(Q)} \;\vdots\; \mathbf{Y}_C^{(Q)} \;\vdots\; \mathbf{Y}_R^{(Q)}\right\}\right]$$

The components of the matrix pencil, $\mathbf{Y}_1$ and $\mathbf{Y}_2$, are also similarly formed as:

$$\mathbf{Y}_1 = \left[\left\{ \mathbf{Y}_L^{(1)} \;\vdots\; \mathbf{Y}_C^{(1)} \right\} \;\vdots\; \left\{ \mathbf{Y}_L^{(2)} \;\vdots\; \mathbf{Y}_C^{(2)} \right\} \;\vdots\; \cdots \;\vdots\; \left\{ \mathbf{Y}_L^{(Q)} \;\vdots\; \mathbf{Y}_C^{(Q)} \right\} \right]$$
$$\mathbf{Y}_2 = \left[\left\{ \mathbf{Y}_C^{(1)} \;\vdots\; \mathbf{Y}_R^{(1)} \right\} \;\vdots\; \left\{ \mathbf{Y}_C^{(2)} \;\vdots\; \mathbf{Y}_R^{(2)} \right\} \;\vdots\; \cdots \;\vdots\; \left\{ \mathbf{Y}_C^{(Q)} \;\vdots\; \mathbf{Y}_R^{(Q)} \right\} \right]$$

With these extensions of the Matrix Pencil method setup, the entire process as delineated for the single channel case can be applied from this point to completely define the multiple channel Matrix Pencil method. The multiple channel Matrix Pencil algorithm will result in a single set of modes from which the frequency signals at each sensor location can be constructed through the calculation of the appropriate residues. It should be highlighted perhaps once more that the estimation of the signals' residues at each point remains a single-channel problem, per se. Therefore we can write for sensors $i = 1, 2, \cdots, Q$:

$$\mathbf{y}^{(i)} = \begin{bmatrix} 1 & 1 & \cdots & 1 \\ z_1 & z_2 & \cdots & z_M \\ \vdots & \vdots & & \vdots \\ z_1^{N-1} & z_2^{N-1} & \cdots & z_M^{N-1} \end{bmatrix} \begin{bmatrix} R_1^{(i)} \\ R_2^{(i)} \\ \vdots \\ R_M^{(i)} \end{bmatrix} \Rightarrow \begin{bmatrix} 1 & 1 & \cdots & 1 \\ z_1 & z_2 & \cdots & z_M \\ \vdots & \vdots & & \vdots \\ z_1^{N-1} & z_2^{N-1} & \cdots & z_M^{N-1} \end{bmatrix}^{\dagger} \mathbf{y} = \begin{bmatrix} \hat{R}_1^{(i)} \\ \hat{R}_2^{(i)} \\ \vdots \\ \hat{R}_M^{(i)} \end{bmatrix}$$

This process has been automated for use with frequency data observed by FNET and the code has been placed in Appendix XII. In the interests of brevity, we shall not exhaustively include here the signal fitting graphs as was shown in the single channel case. However the following figures represent the general results of the multiple channel method when applied to the WECC tests and Florida blackout data. The participation of certain modes in the frequency data from various sensors is indicated by the magnitude of the residues (vertical axis).

Multiple Channel Matrix Pencil Analysis of WECC Tests Based Upon FDR Data

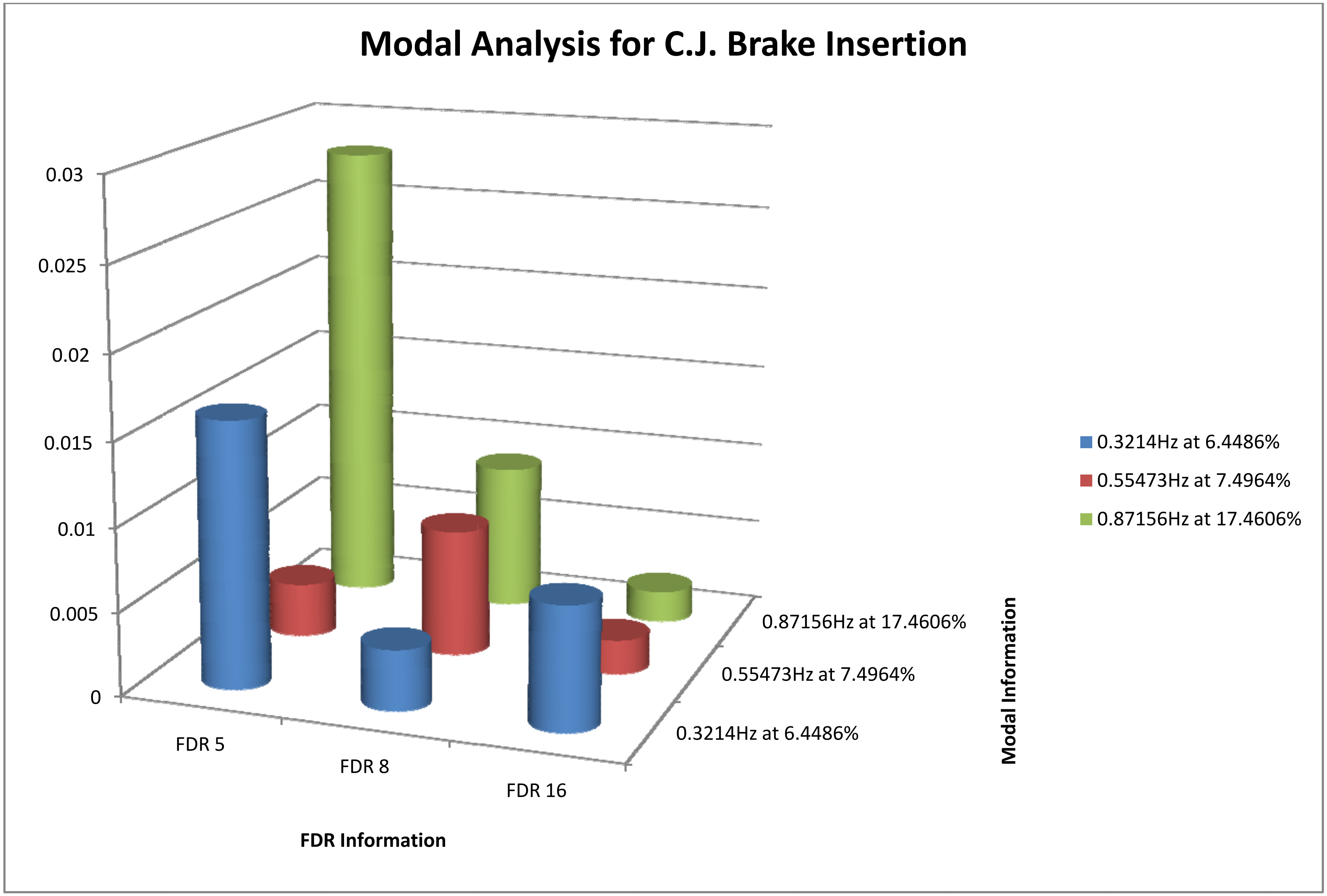

Figure 3-66: Multiple channel Matrix Pencil analysis of WECC test D1 based on FDR data.

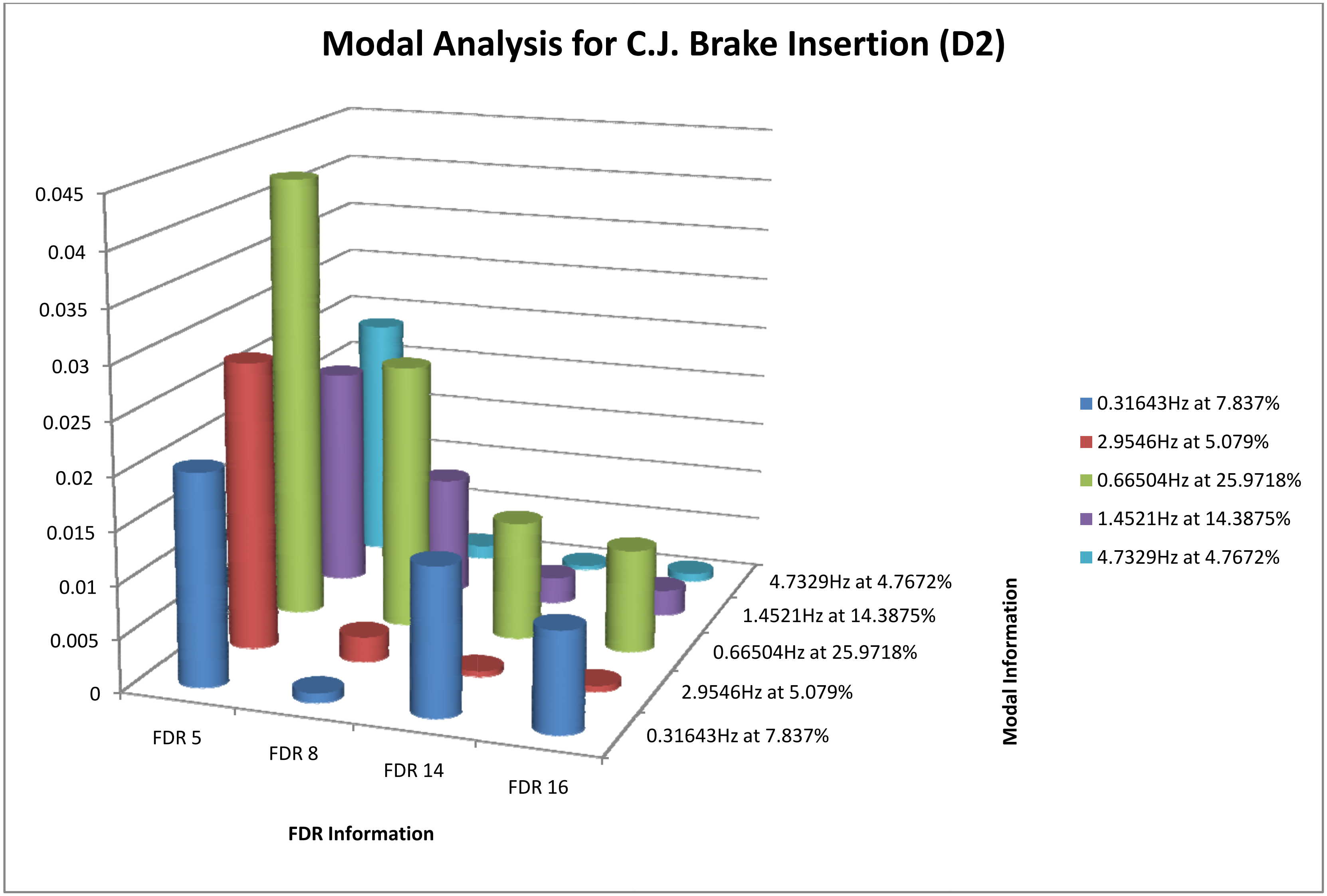

Figure 3-67: Multiple channel Matrix Pencil analysis of WECC test D2 based on FDR data.

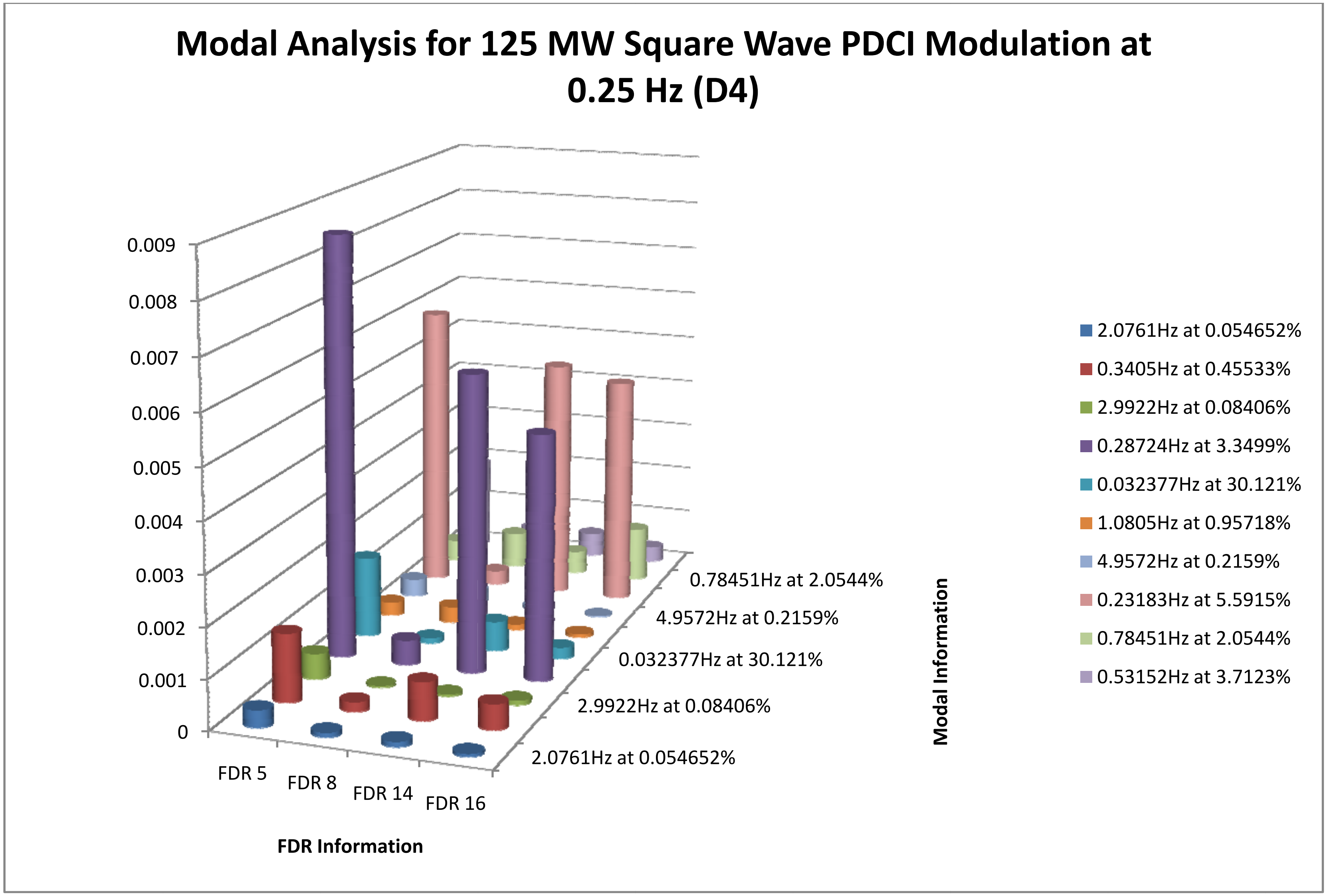

Figure 3-68: Multiple channel Matrix Pencil analysis of WECC test D4 based on FDR data.

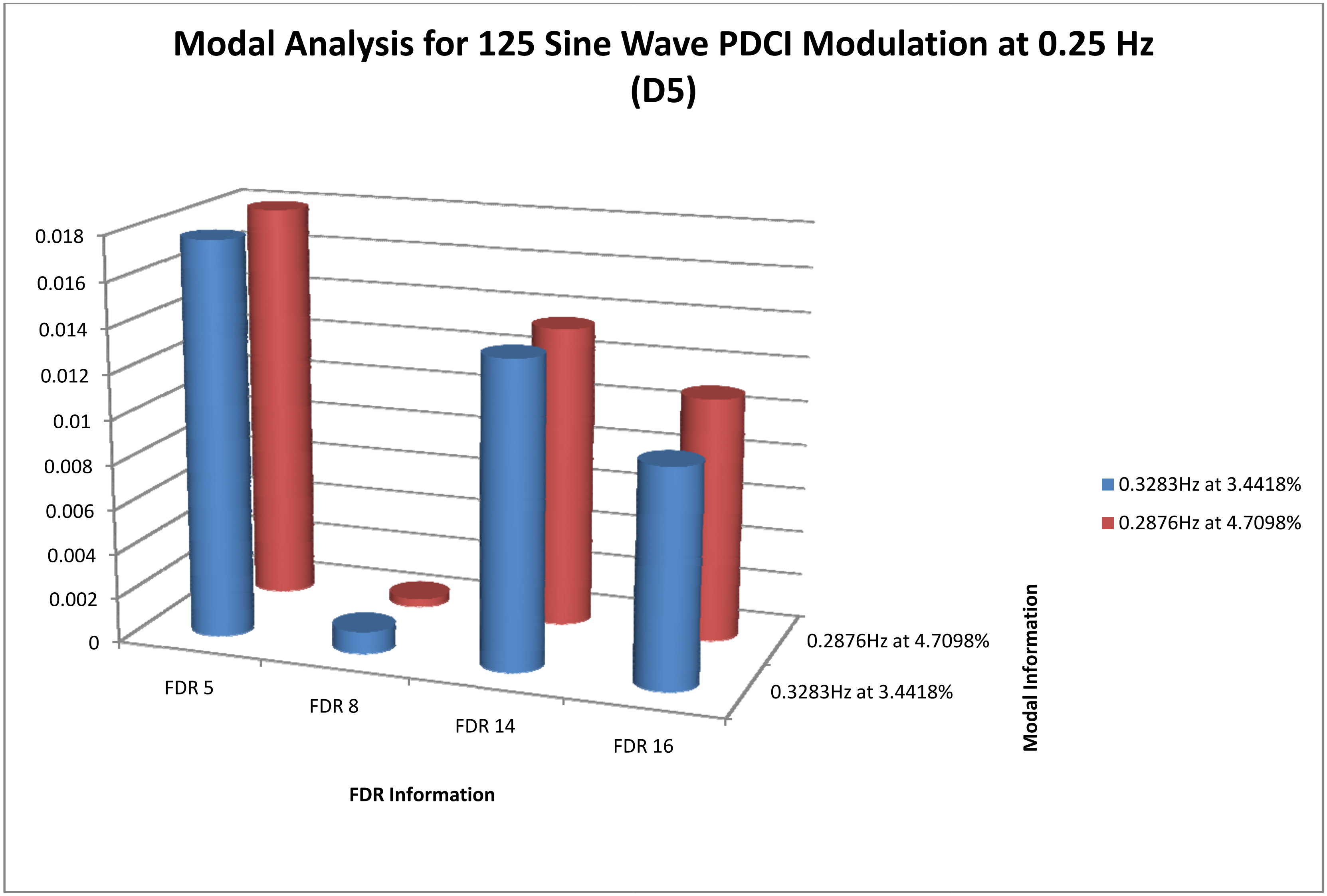

Figure 3-69: Multiple channel Matrix Pencil analysis of WECC test D5 based on FDR data.

Multiple Channel Matrix Pencil Analysis of WECC Tests Based Upon PMU Data

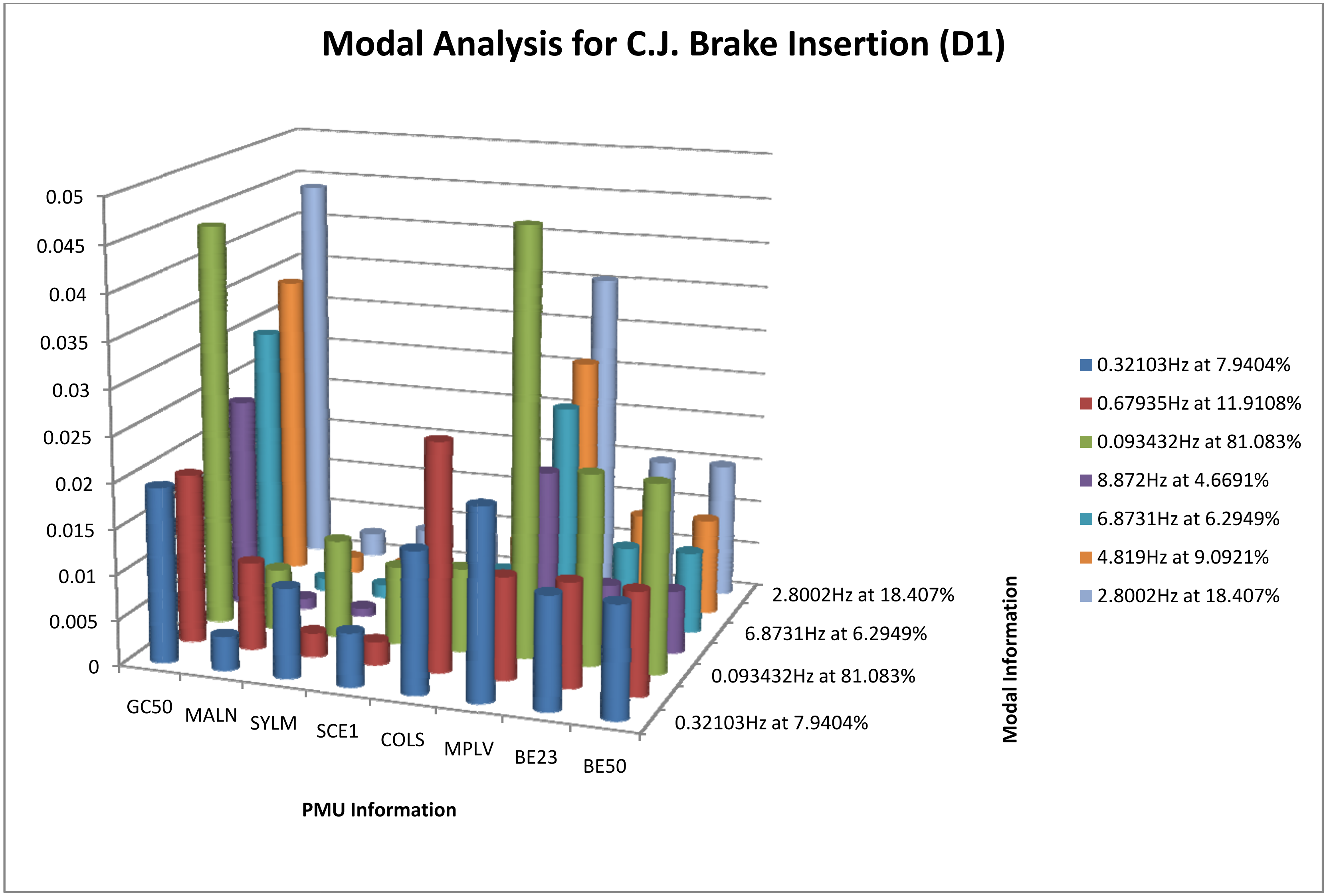

Figure 3-70: Multiple channel Matrix Pencil analysis of WECC test D1 based on PMU data.

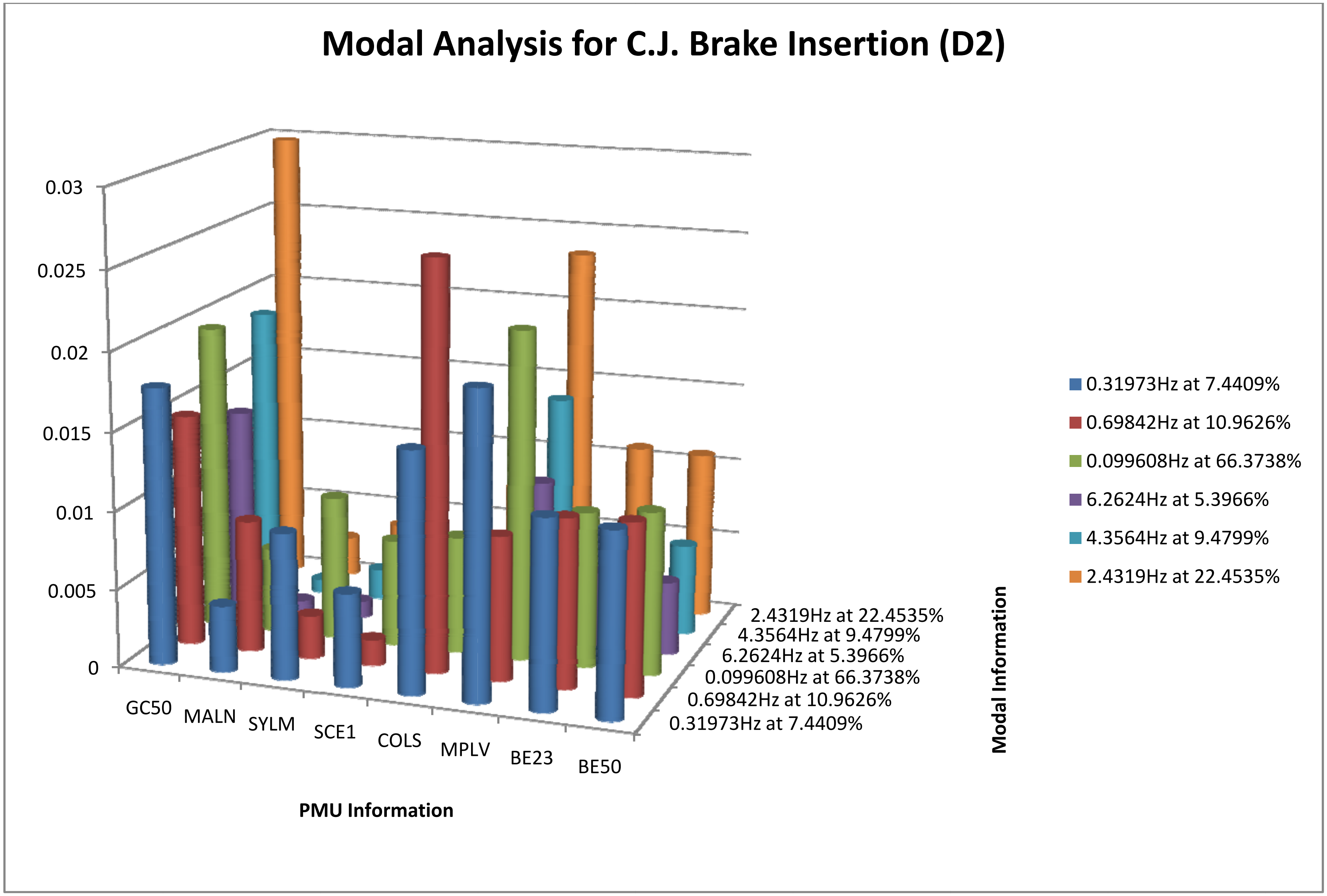

Figure 3-71: Multiple channel Matrix Pencil analysis of WECC test D2 based on PMU data.

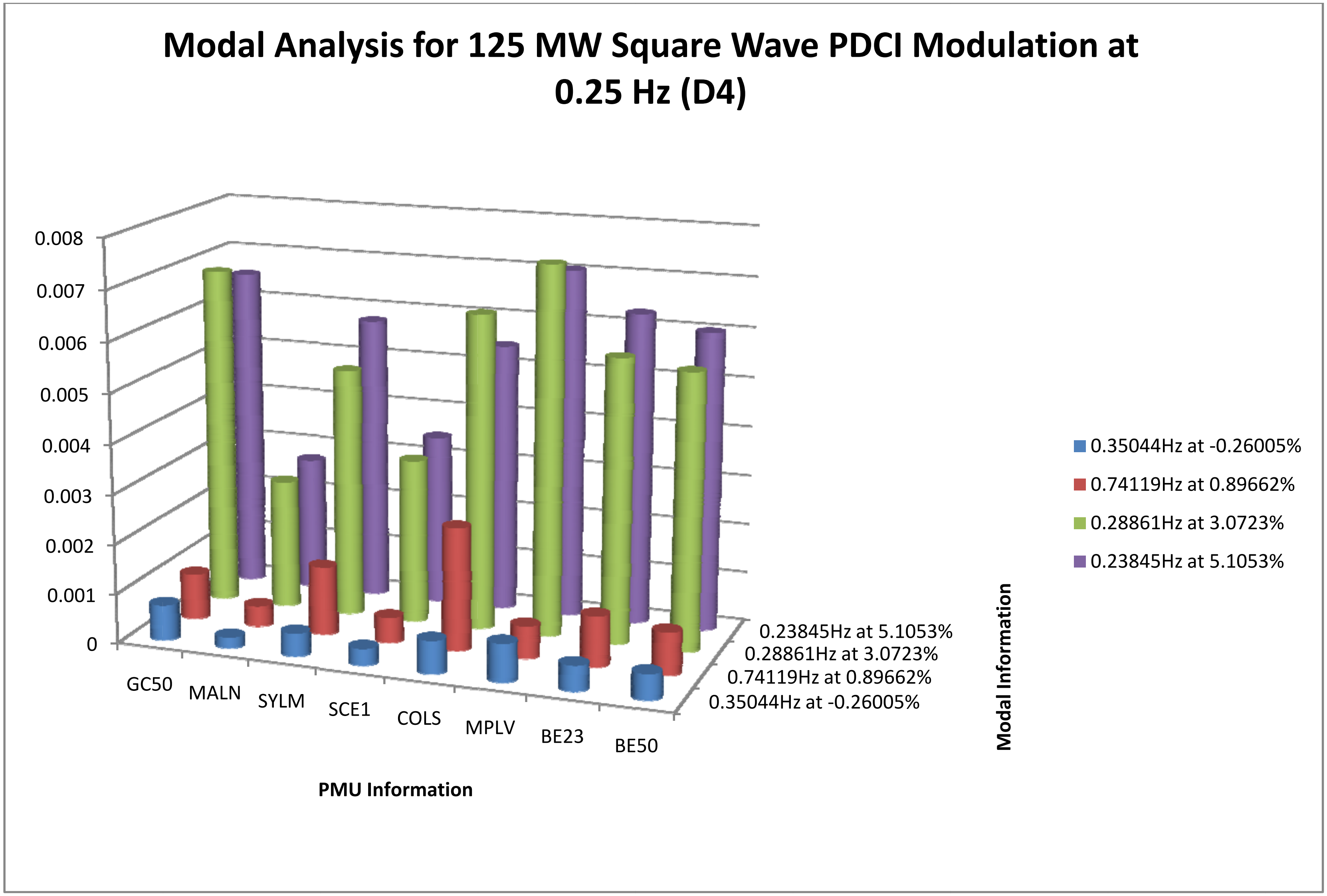

Figure 3-72: Multiple channel Matrix Pencil analysis of WECC test D4 based on PMU data.

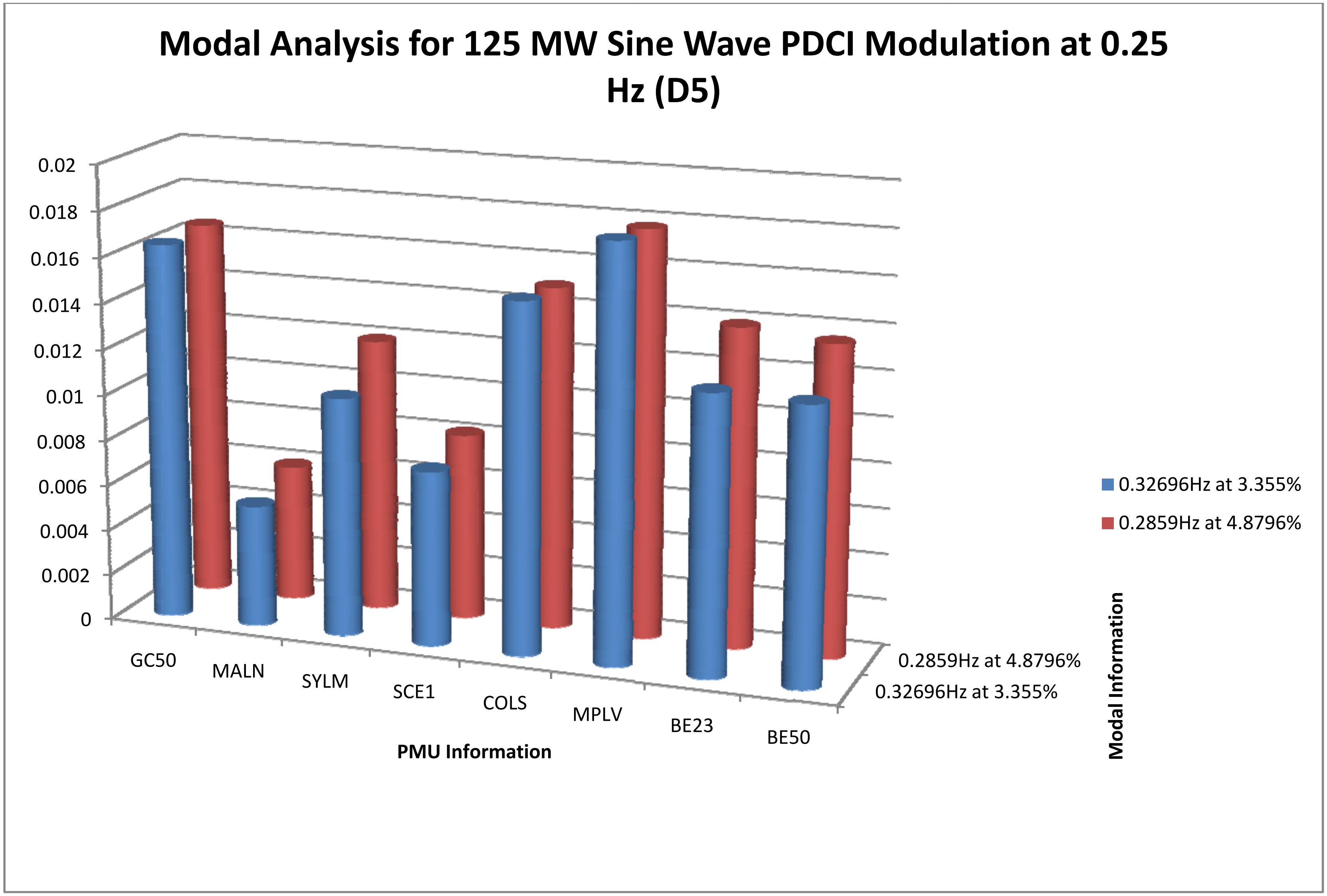

Figure 3-73: Multiple channel Matrix Pencil analysis of WECC test D5 based on PMU data.

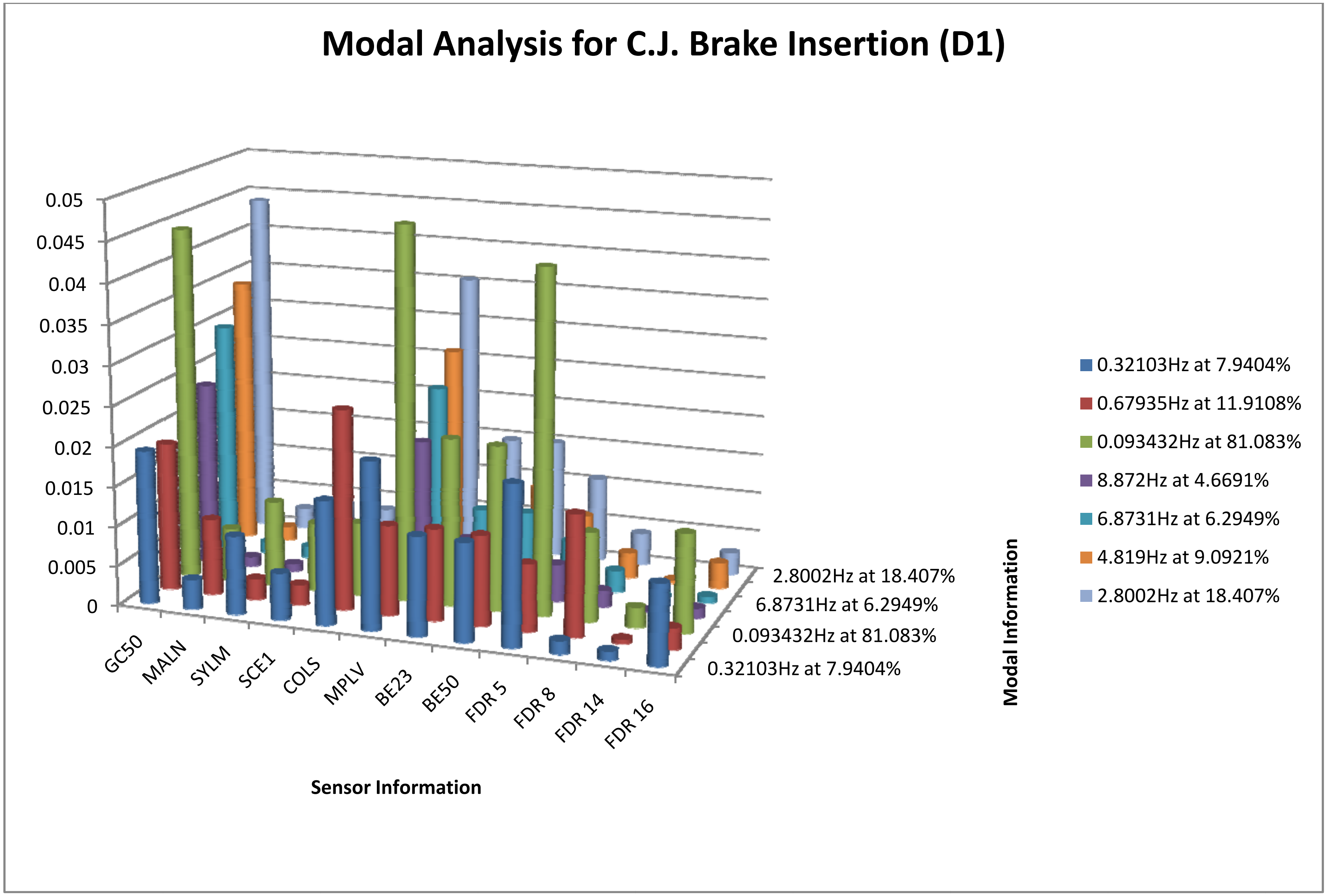

Figure 3-74: Multiple channel Matrix Pencil analysis of WECC test D1 based upon both FDR and PMU data.

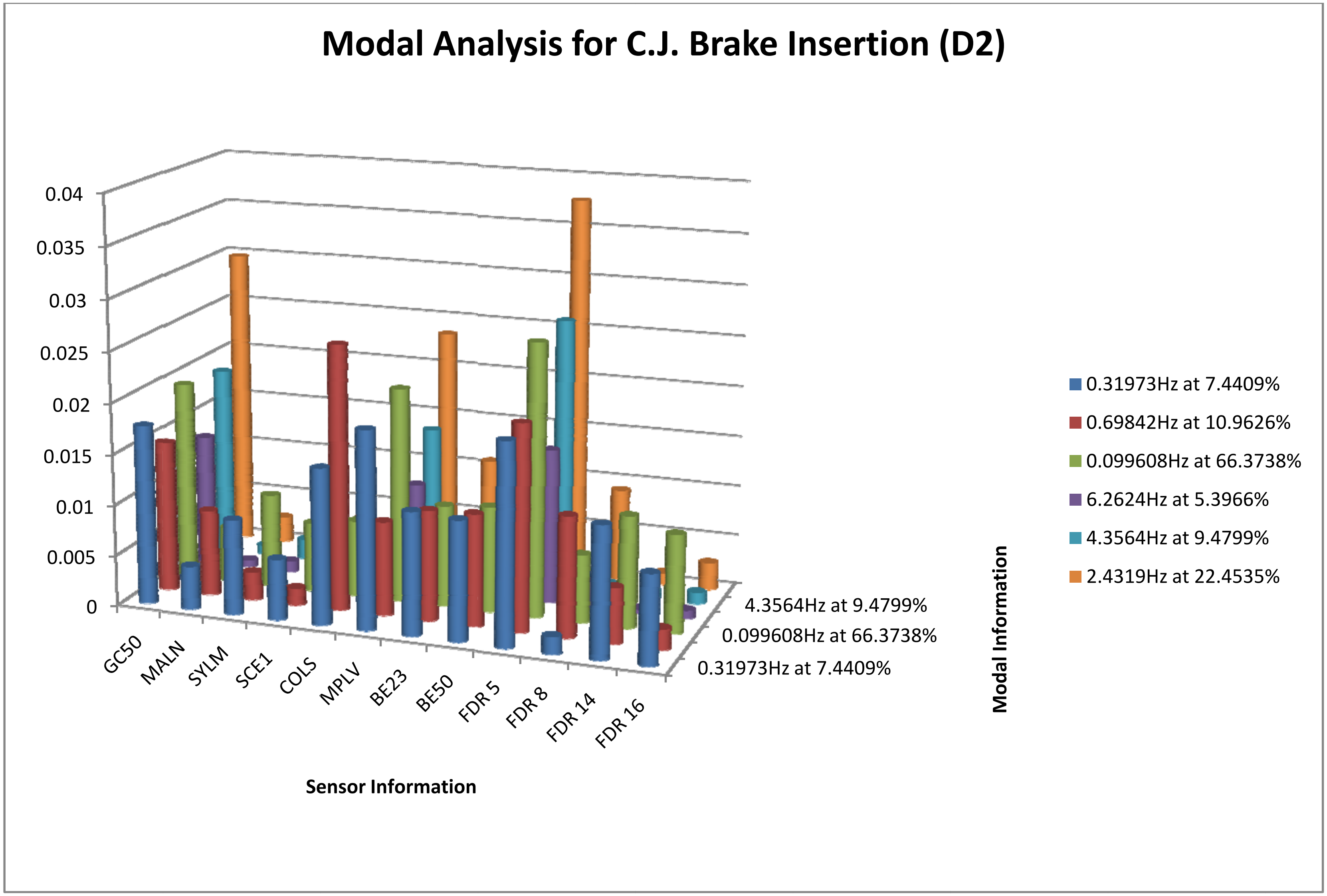

Figure 3-75: Multiple channel Matrix Pencil analysis of WECC test D2 based upon both FDR and PMU data.

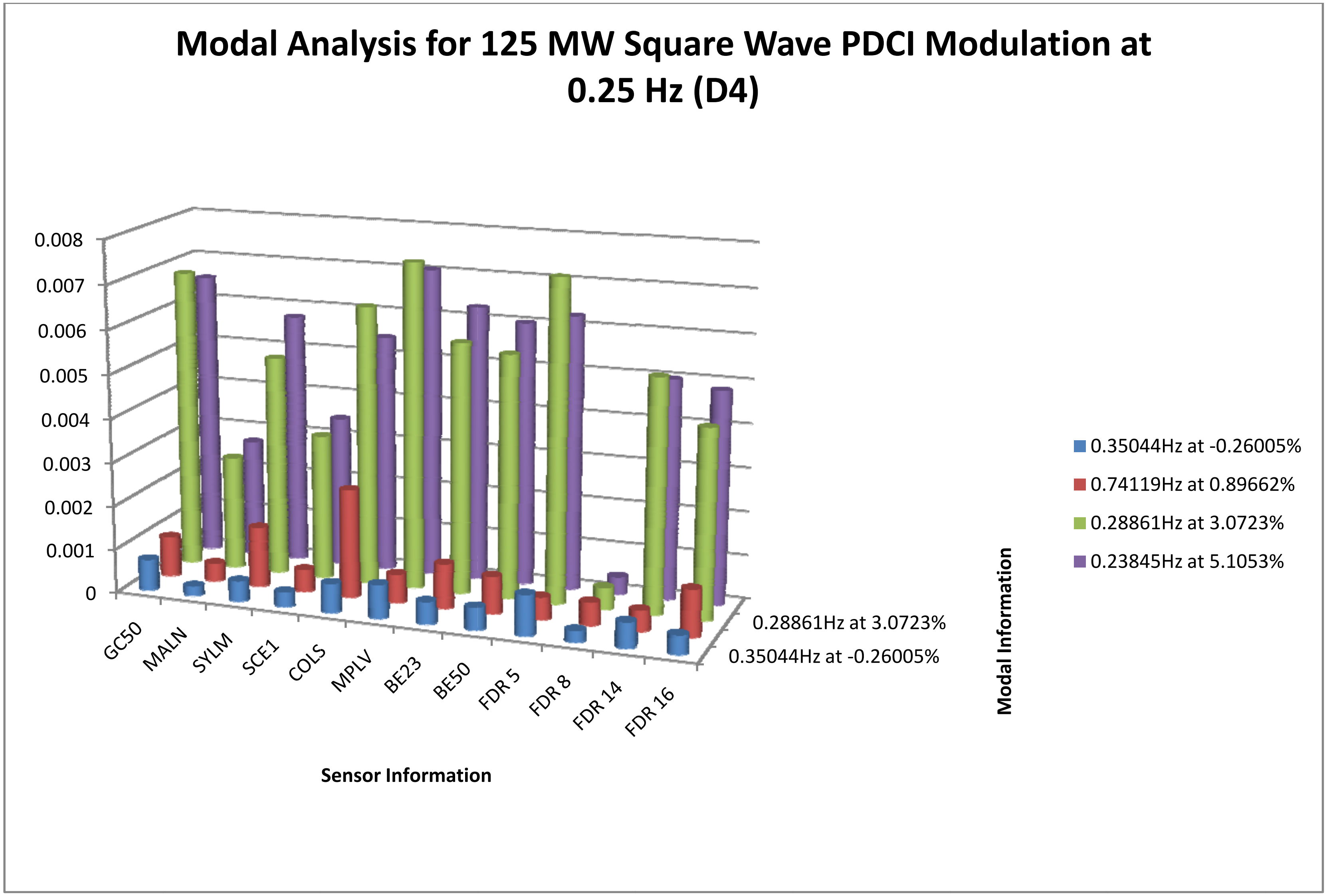

Figure 3-76: Multiple channel Matrix Pencil analysis of WECC test D4 based upon both FDR and PMU data.

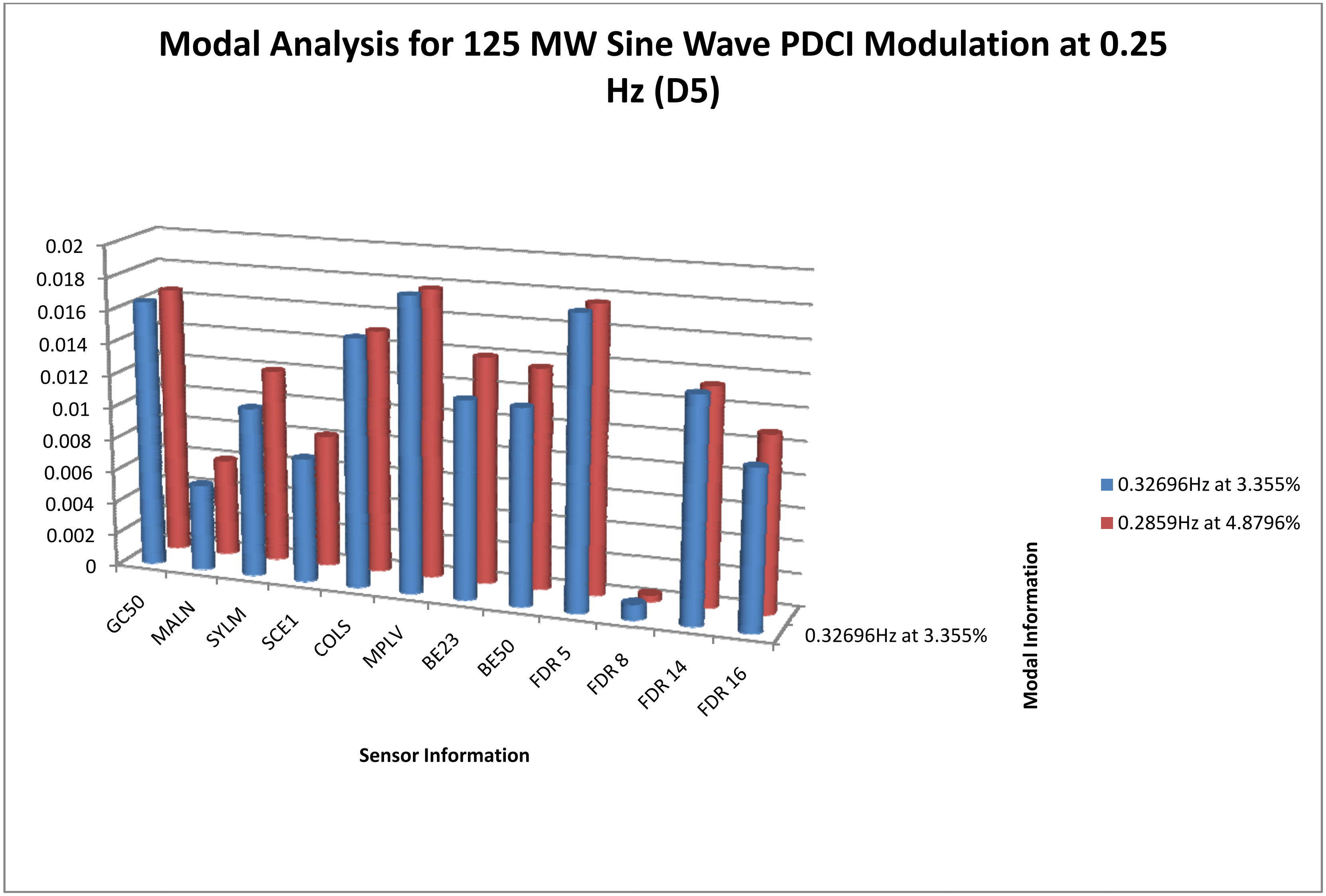

Figure 3-77: Multiple channel Matrix Pencil analysis of WECC test D5 based upon both FDR and PMU data.

Multiple Channel Matrix Pencil Analysis of Florida Blackout

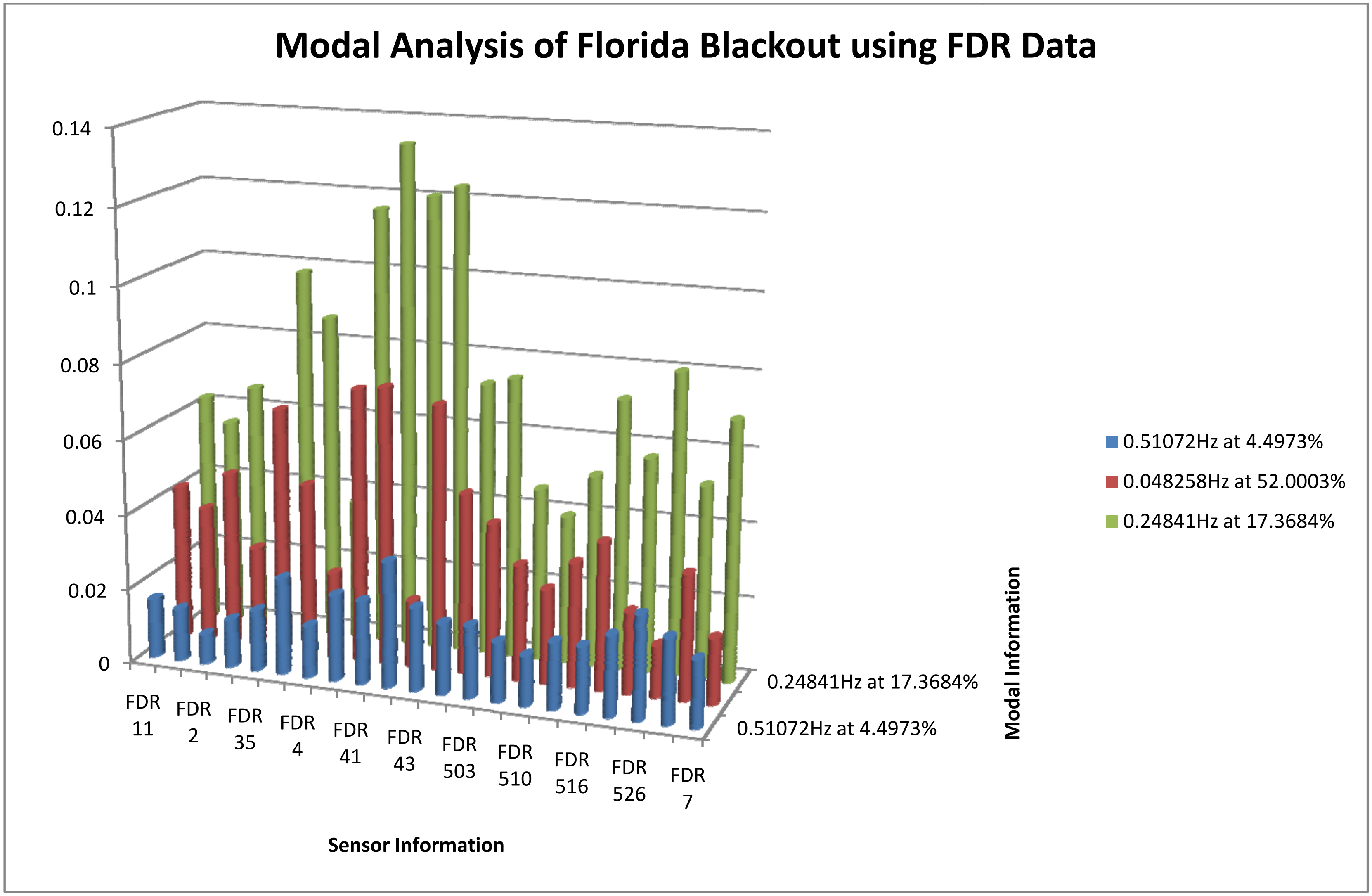

Figure 3-78: Multiple channel Matrix Pencil analysis of Florida blackout based on FDR data.

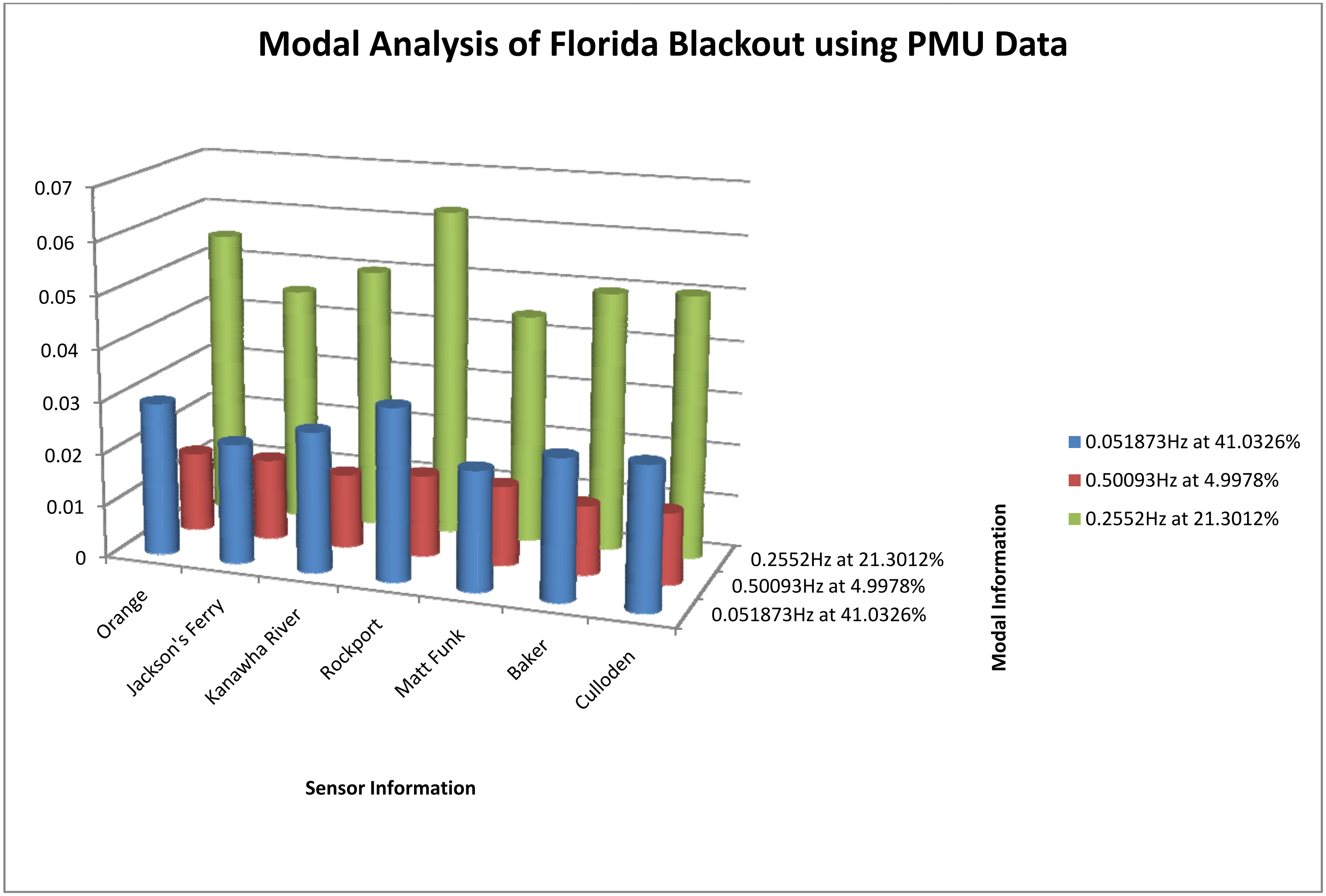

Figure 3-79: Multiple channel Matrix Pencil analysis of Florida blackout based on PMU data.

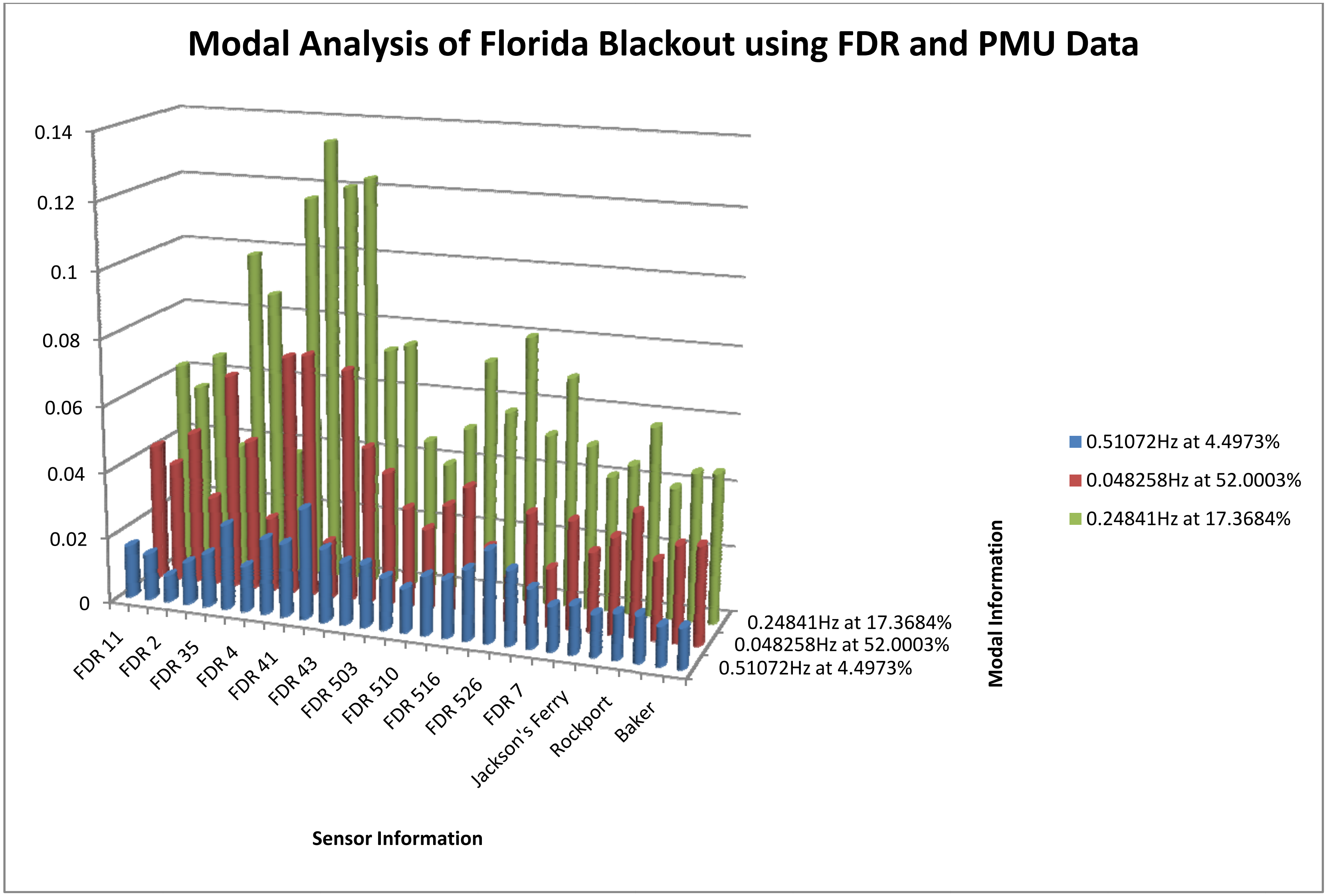

Figure 3-80: Multiple channel Matrix Pencil analysis of Florida blackout based on FDR and PMU data.

Pole Placement Comparisons Between Single and Multiple Channel Matrix Pencil Methods

As earlier developed, the multiple channel Matrix Pencil method estimates a single set of signal poles based upon the inputs of multiple channels of data. The following figures show the location of signal poles for each of the three modes identified during the Florida blackout (shown in figures above). The blue crosses indicate pole locations based upon single channel analysis. The blue triangle marker indicates the average single channel pole location. The two green triangles indicate the location of the pole locations according to the estimation of the multiple channel method. (One of the green markers indicates the pole location based upon FDR data while the other uses PMU data.)

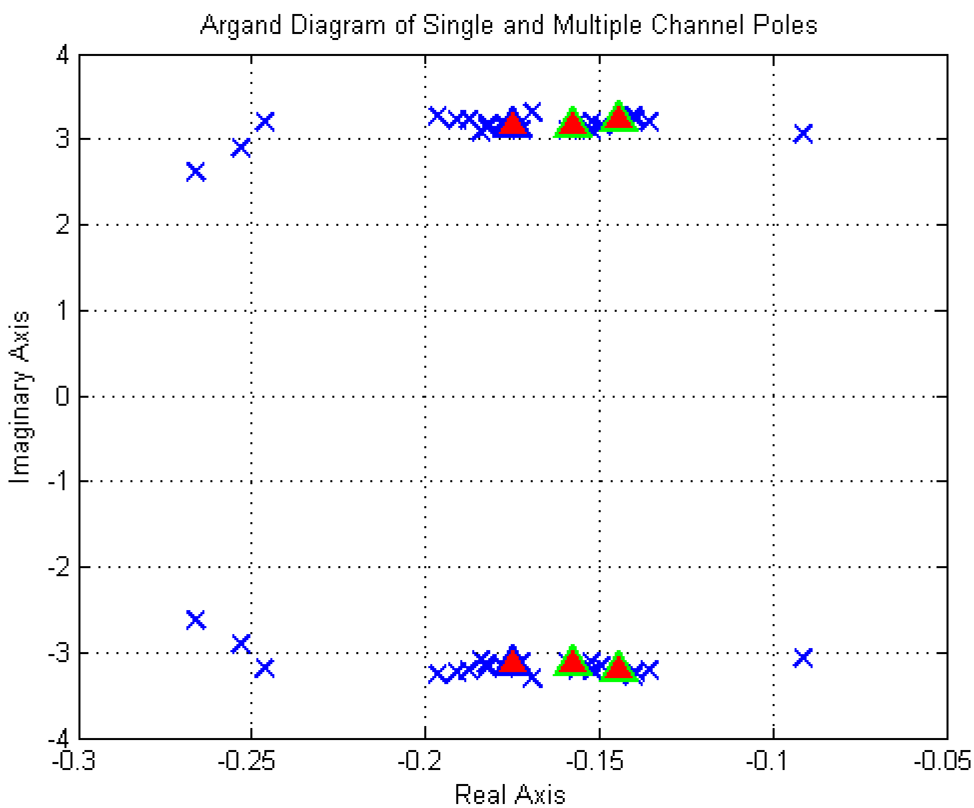

Figure 3-81: Pole locations of 0.51 Hz mode (FL blackout).

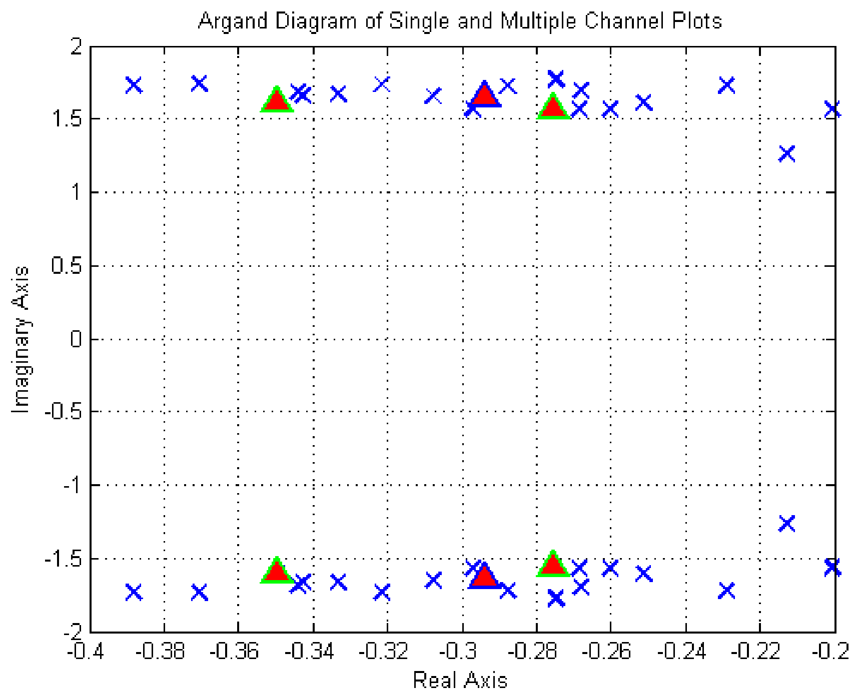

Figure 3-82: Pole locations of 0.25 Hz mode (FL blackout).

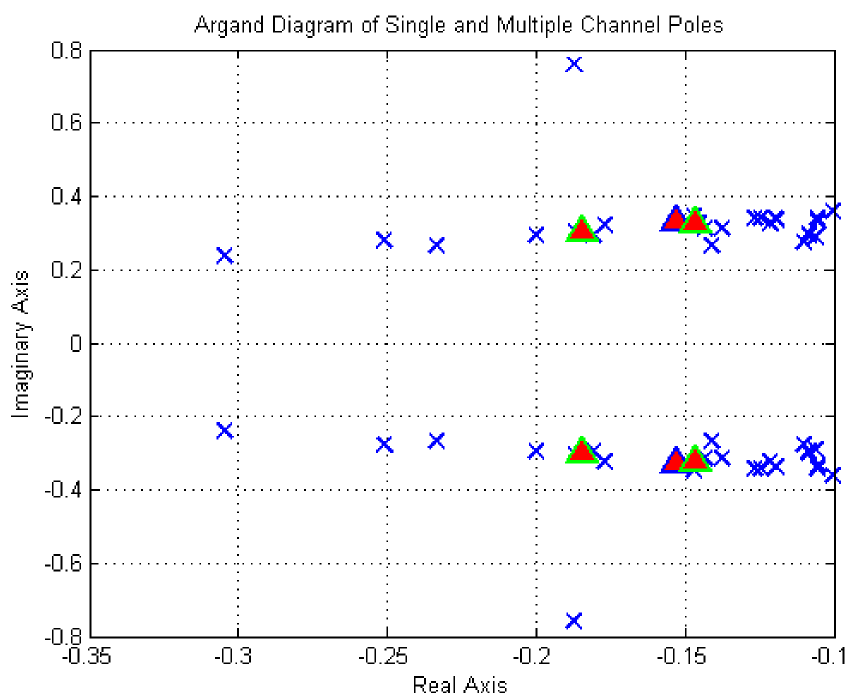

Figure 3-83: Pole locations of 0.05 Hz mode (FL blackout).

Further Considerations in Oscillation Detection and Analysis

The analysis of power system oscillations is rarely straight forward. However, the proper detection of system oscillations is quite easily developed, tuned, and implemented. In the course of oscillation analysis, proper care is required for the production of meaningful results. For instance, wholesale analysis of an entire oscillatory event may not be advised in all situations. In some cases, *during* an oscillatory event system changes occur that introduce nonlinearities. The work of this chapter is not indicated for real-time use but rather for the exploration of power system behavior via the use of wide-area time-synchronized frequency measurements. Perhaps a topic of future research would be the addition of expert system-like intelligence between the oscillation detection routines and the oscillation analysis routines. Such a system could perhaps introduce a way to either segment a detected oscillation into proper windows for analysis or even suggest that the fitting of damped sinusoids to the oscillation data is not advised.

The previous two chapters have discussed the nature of wide-area frequency data and set fourth methods of finding and analyzing events as detected by such measurements. The next chapter will switch focus from the detection and analysis of events to the location thereof.

Chapter 4: Generation Trip Location Using Wide-Area Frequency Measurements

Power system frequency can tell volumes about the health and state of a power system. Moreover, the manner in which angle and frequency perturbations travel throughout the power grid has been closely studied in the past [61, 70]. Such perturbations are known to propagate throughout the grid as a function of time and space [58]. Using measurements from FNET, one can observe the electromechanical wave signature of power system events in frequency data. In this section, a brief analysis of several generator tripping events is presented. The analysis comprises several event location methods and resulting observations. The eventual goal of this research is to formulate a practical event location algorithm that can be used online and in real-time to locate with sufficient accuracy the hypocenter of power system events irrespective of utility boundaries. We wish to take a first step in the direction of developing a reliable and comprehensive method of using real-time wide-area frequency measurements to locate the approximate, yet accurate, location of power system disturbances, such as generator trips. The stage for this study is set in the EI.

Simulation-Based Event Propagation Maps

There is no control within our domain over the power system events that serve as the base cases for this study. Hence, this work is meant to serve as a first effort in the area of power system event location using only wide-area frequency measurements. Actually, a main goal of this experimentation was to determine whether it is possible to use frequency measurements alone to locate the origin of a disturbance on the electric grid. In using the term “frequency measurements alone” it should be understood that system topology, parameters, and state are ignored.

Electromechanical Wave Propagation in EI – A Frequency Perspective

The following figures demonstrate the apparent electromechanical wave propagation throughout the EI due to several generation trip events. The figures indicate generation units that have experienced a 5 mHz drop in frequency due to the generation trip. A comprehensive list of generators of interest in the EI model can be found in Appendix V. This analysis is intended to provide a broad sampling of events from across the EI. It is this analysis that gives us inspiration for the use of wide-area frequency measurements in the location of large-scale (>500 MW) events.

Brown's Ferry Unit Trip -- Frequency Wave Propagation (5 mHz Decline – from simulation)

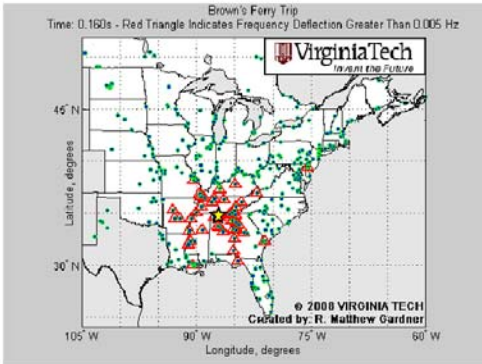

Figure 4-1: 5 mHz deviation at 160ms.

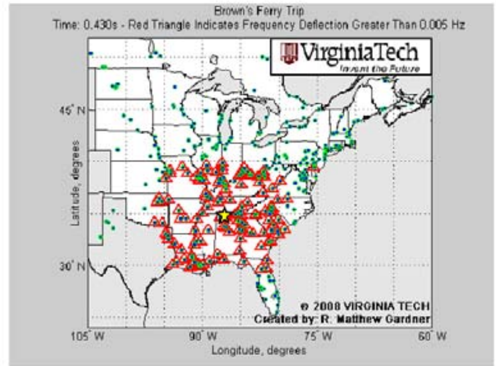

Figure 4-2: 5 mHz deviation at 430ms.

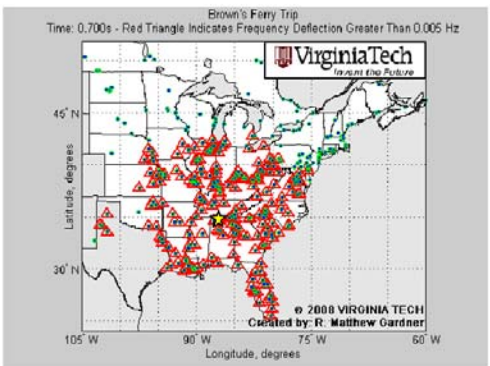

Figure 4-3: 5 mHz deviation at 700ms.

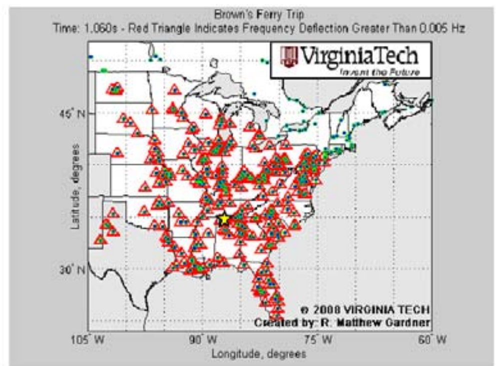

Figure 4-4: 5 mHz deviation at 1060ms.

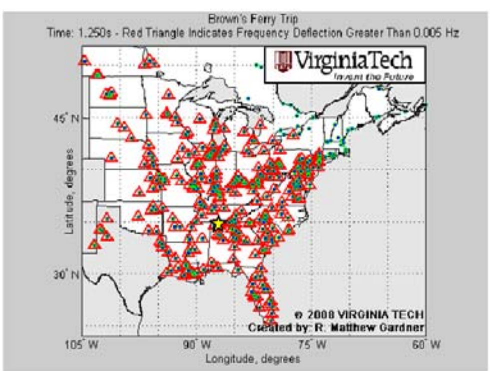

Figure 4-5: 5 mHz deviation at 1250ms.

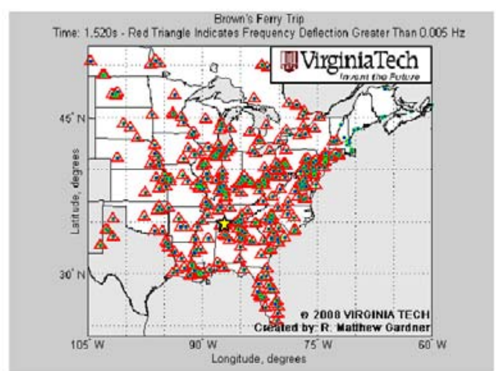

Figure 4-6: 5 mHz deviation at 1520ms.

La Cygne Unit Trip -- Frequency Wave Propagation (5 mHz Decline – from simulation)

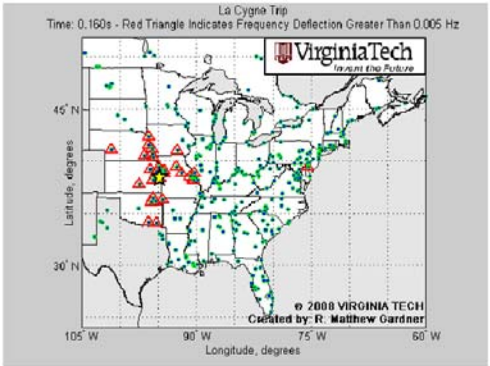

Figure 4-7: 5 mHz deviation at 160ms.

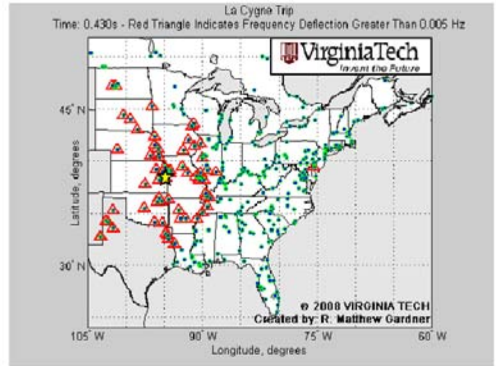

Figure 4-8: 5 mHz deviation at 430ms.

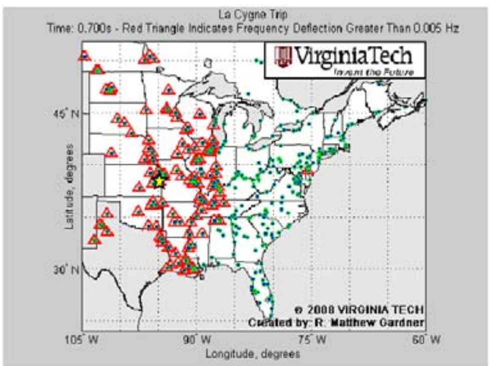

Figure 4-9: 5 mHz deviation at 700ms.

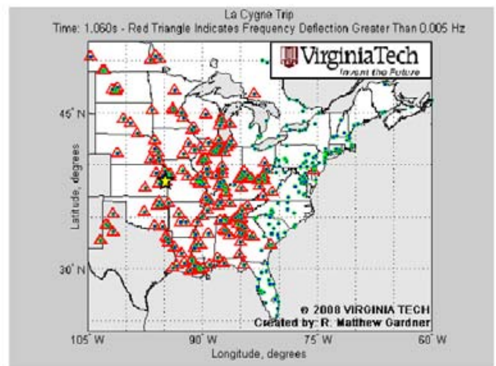

Figure 4-10: 5 mHz deviation at 1060ms.

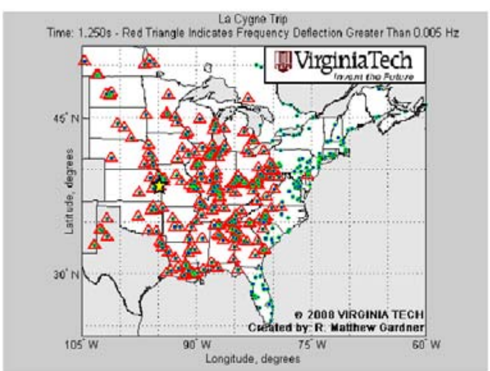

Figure 4-11: 5 mHz deviation at 1250ms.

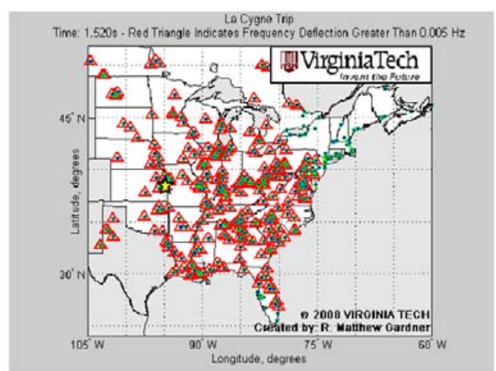

Figure 4-12: 5 mHz deviation at 1520ms.

North Anna Unit Trip -- Frequency Wave Propagation (5 mHz Decline – from simulation)

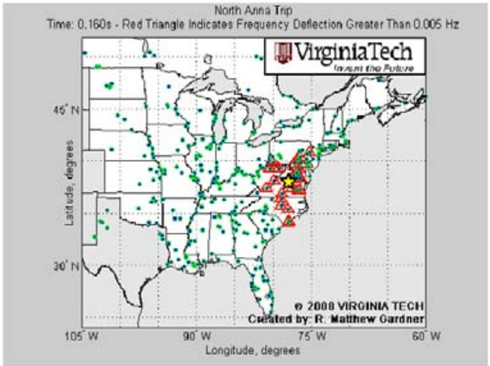

Figure 4-13: 5 mHz deviation at 160ms.

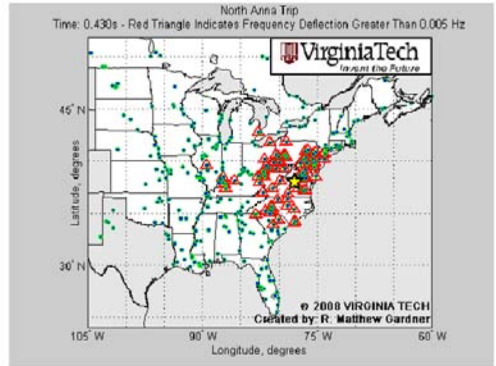

Figure 4-14: 5 mHz deviation at 430ms.

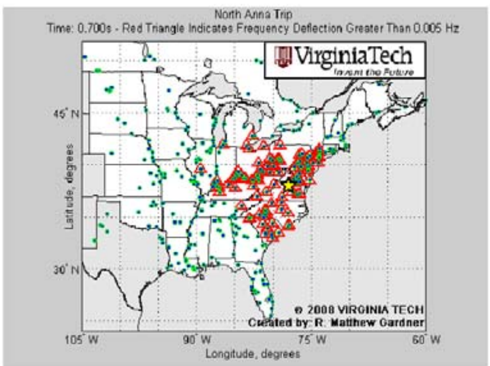

Figure 4-15: 5 mHz deviation at 700ms.

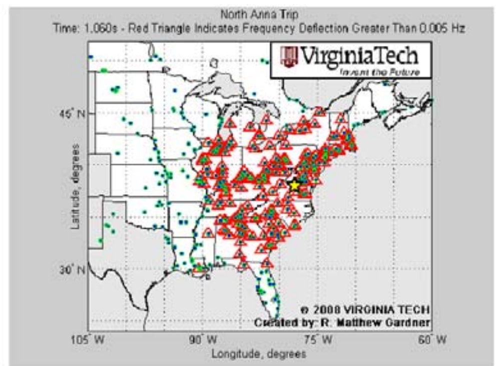

Figure 4-16: 5 mHz deviation at 1060ms.

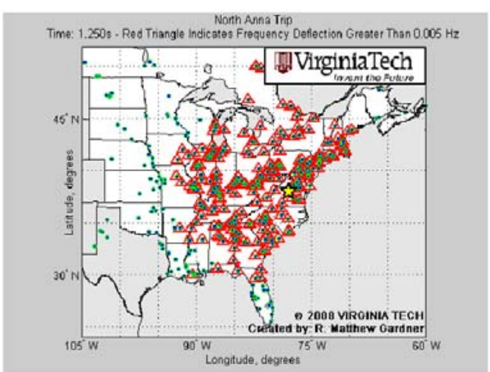

Figure 4-17: 5 mHz deviation at 1250ms.

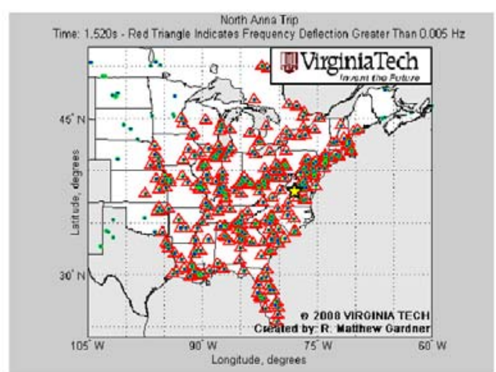

Figure 4-18: 5 mHz deviation at 1520ms.

Palisades Unit Trip -- Frequency Wave Propagation (5 mHz Decline – from simulation)

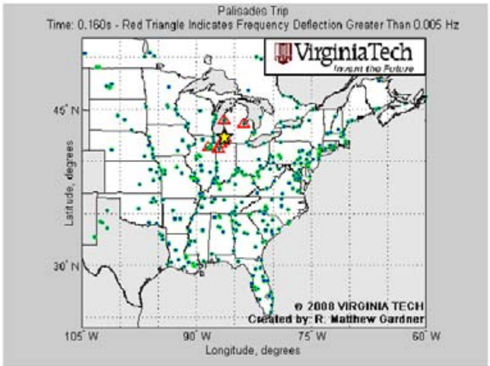

Figure 4-19: 5 mHz deviation at 160ms.

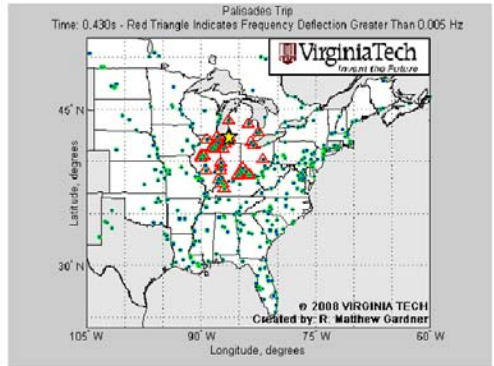

Figure 4-20: 5 mHz deviation at 430ms.

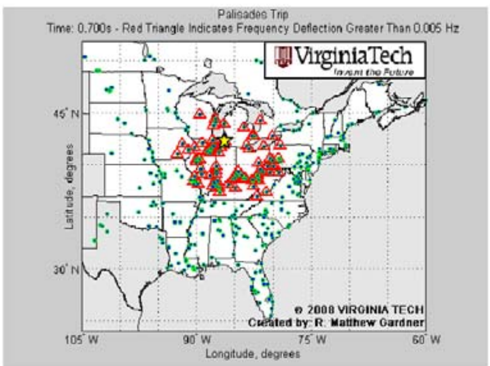

Figure 4-21: 5 mHz deviation at 700ms.

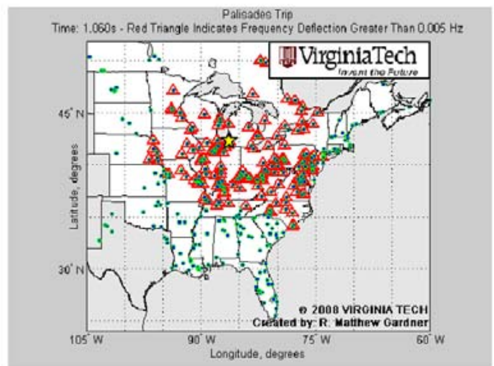

Figure 4-22: 5 mHz deviation at 1060ms.

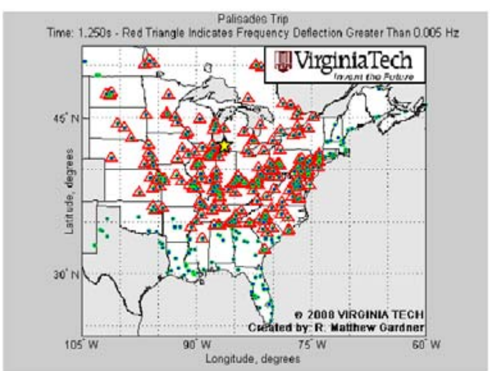

Figure 4-23: 5 mHz deviation at 1250ms.

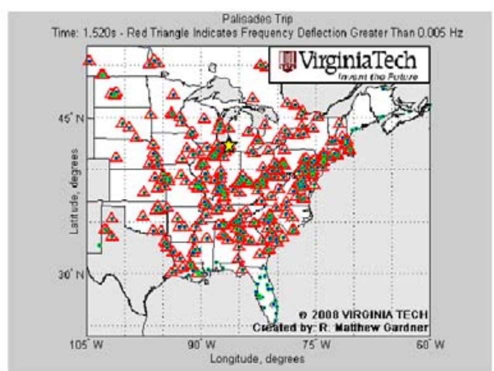

Figure 4-24: 5 mHz deviation at 1520ms.

This analysis grows out of an analysis of frequency waveforms following events. Notice the definite delay in the decline of frequency after the event time in the following figures. From the discussions in Chapter 1, we know that voltage magnitude is not an optimal parameter to examine in the event location effort. Thus far we have been focusing on voltage frequency; however, we also have the facility to measure voltage angle in a wide-area sense using FNET system. So we shall also examine the self-deviation of angle across the grid after an event in an effort to verify this metric for use in wide-area event location.

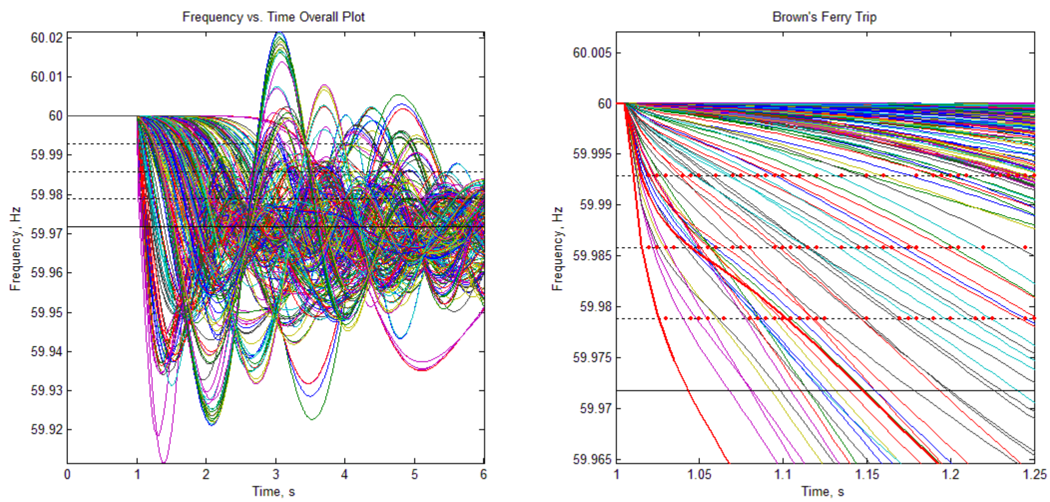

Figure 4-25: Frequency signature of Brown's Ferry event (simulation).

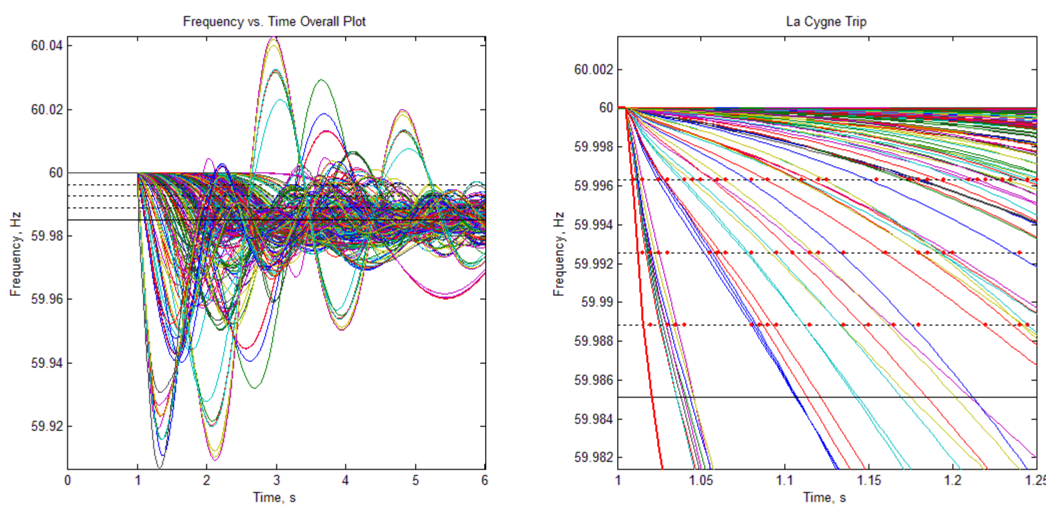

Figure 4-26: Frequency signature of La Cygne event (simulation).

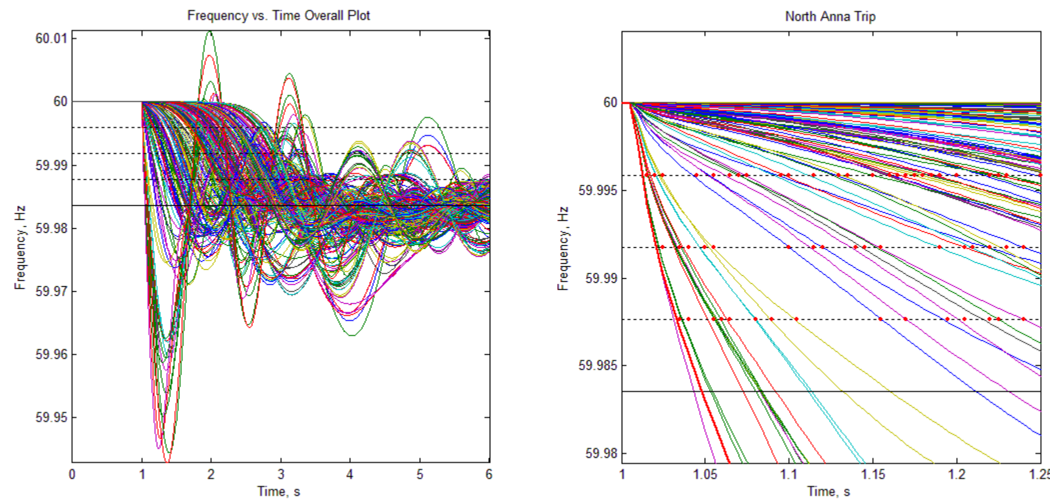

Figure 4-27: Frequency signature of North Anna event (simulation).

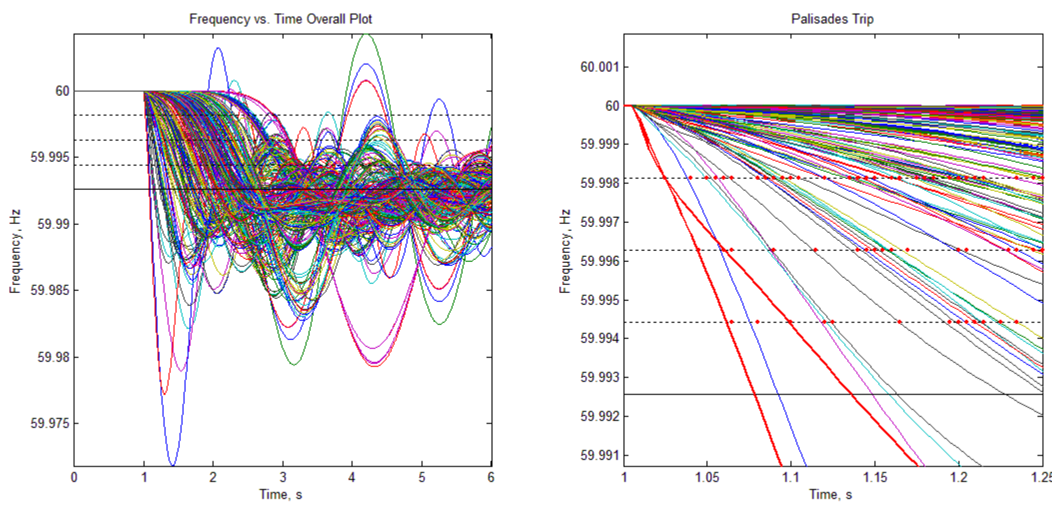

Figure 4-28: Frequency signature of Palisades event (simulation).

Electromechanical Wave Propagation in EI – An Angular Perspective

Voltage angle is presented in this section in a significantly different manner than in conventional power system analysis. Conventionally, voltage angle is measured with respect to some swing or slack bus in the system (usually TVA's Brown's Ferry nuclear generating station for EI studies and Palo Verde nuclear generating station in the WECC). However, in this analysis, we calculate angle in terms of self deviation:

$$\phi_i^{\text{dev}}(t) = \phi_i(t_0) - \phi_i(t)$$

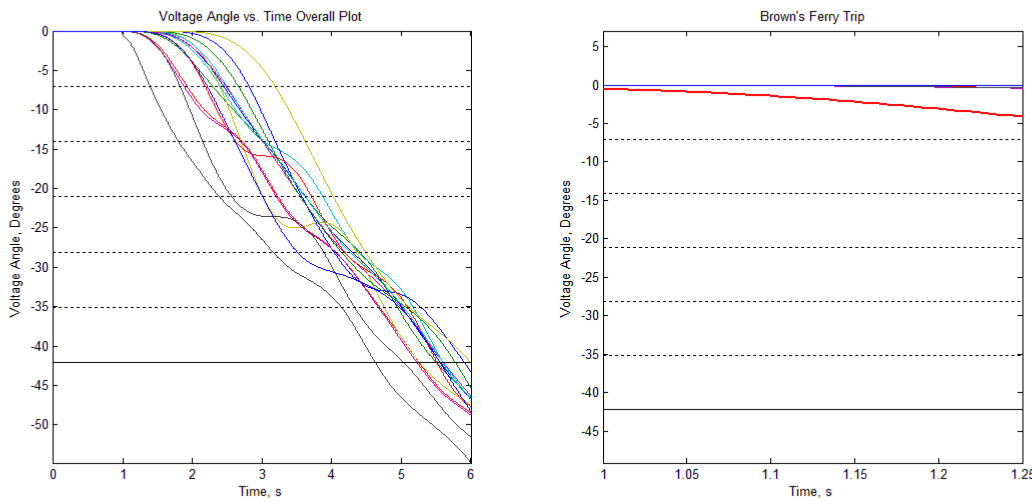

Figure 4-29: Angular signature of Brown's Ferry event (simulation).

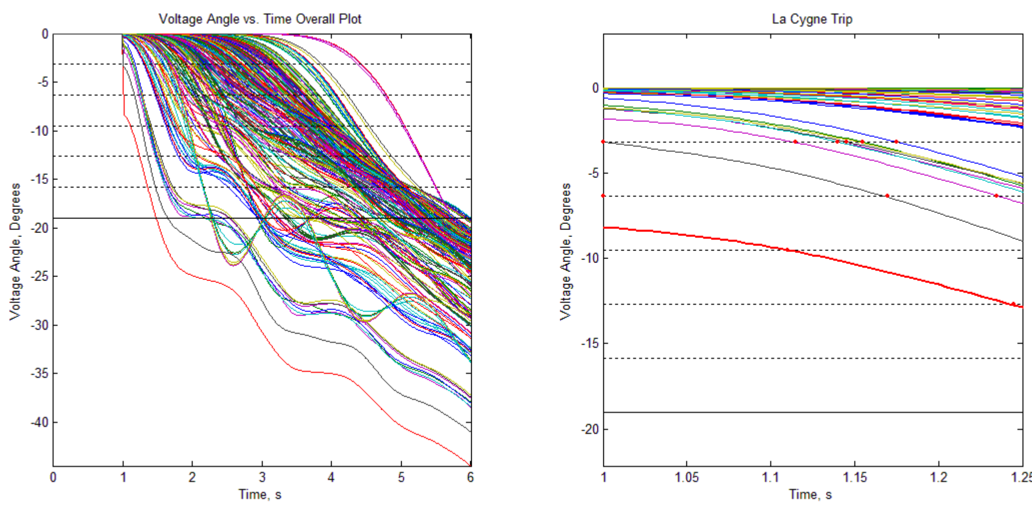

Figure 4-30: Angular signature of La Cygne event (simulation).

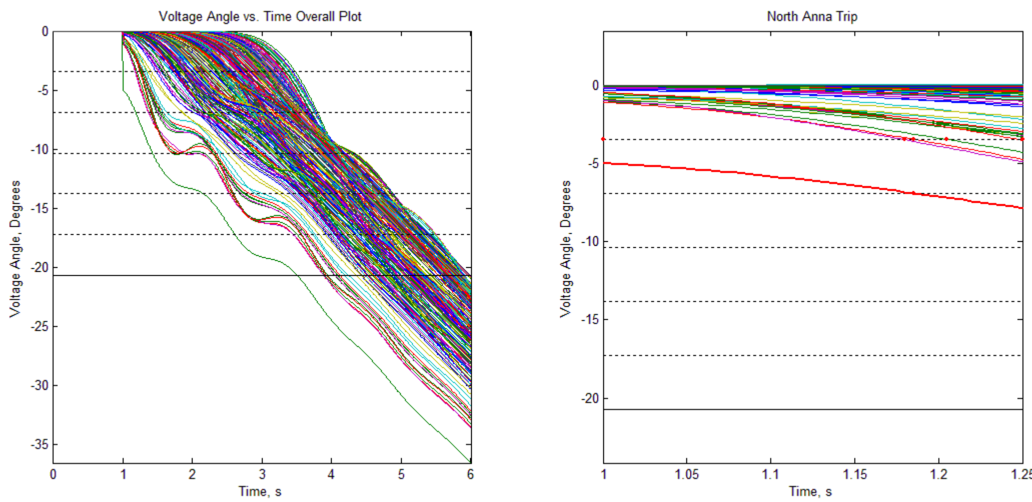

Figure 4-31: Angular signature of North Anna event (simulation).

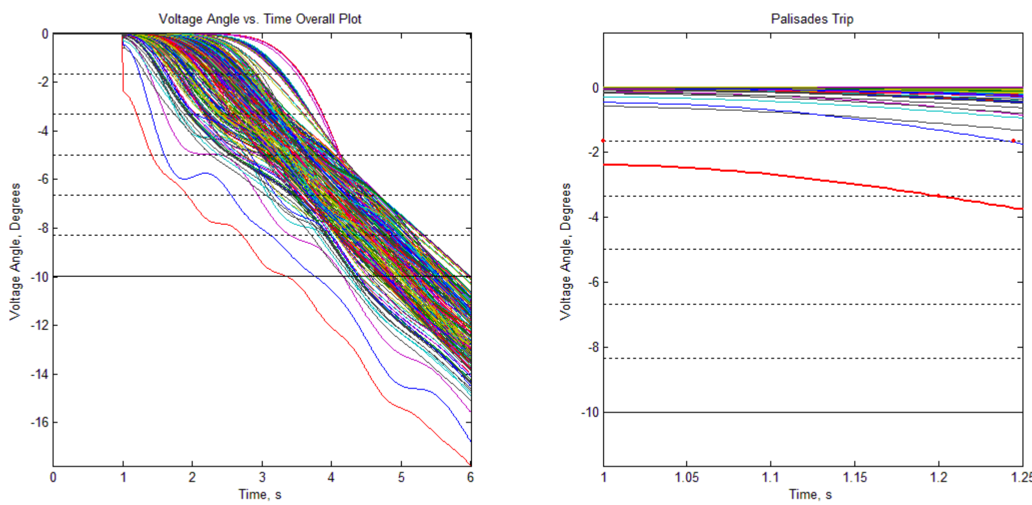

Figure 4-32: Angular signature of Palisades event (simulation).

Brown’s Ferry Unit Trip -- Angular Wave Propagation (5 degree Decline – from simulation)

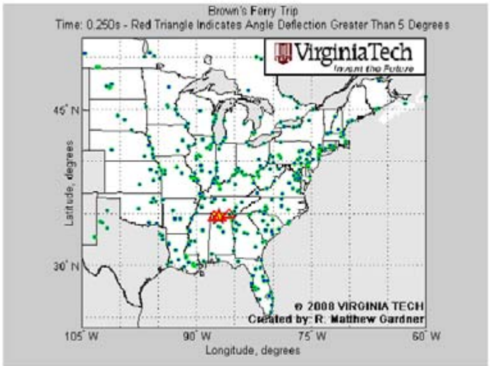

Figure 4-33: 5 degree deviation at 250ms.

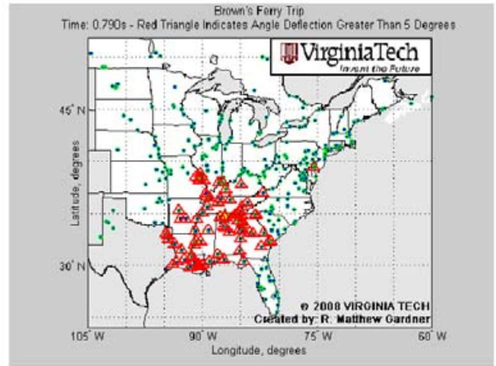

Figure 4-34: 5 degree deviation at 790ms.

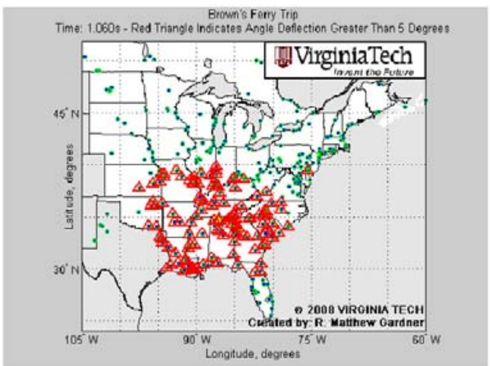

Figure 4-35: 5 degree deviation at 1060ms.

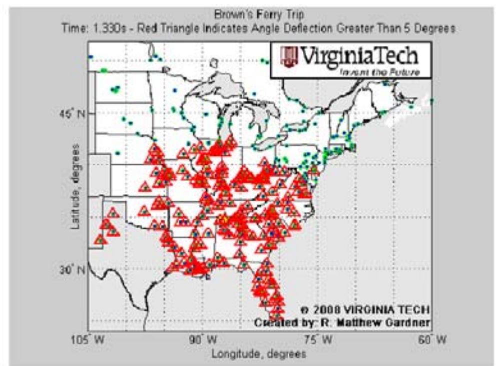

Figure 4-36: 5 degree deviation at 1330ms.

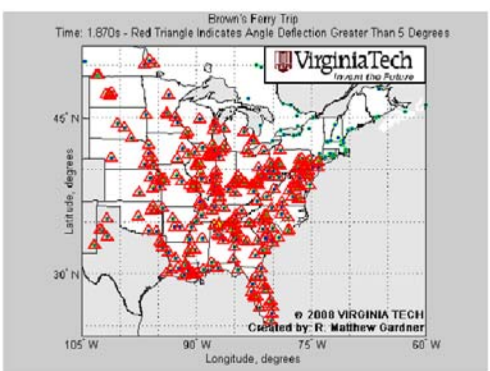

Figure 4-37: 5 degree deviation at 1870ms.

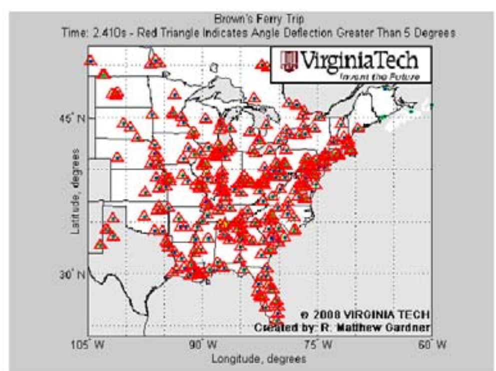

Figure 4-38: 5 degree deviation at 2410ms.

La Cygne Unit Trip -- Angular Wave Propagation (5 degree Decline – from simulation)

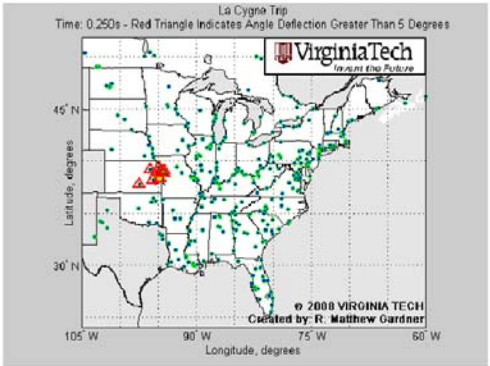

Figure 4-39: 5 degree deviation at 250ms.

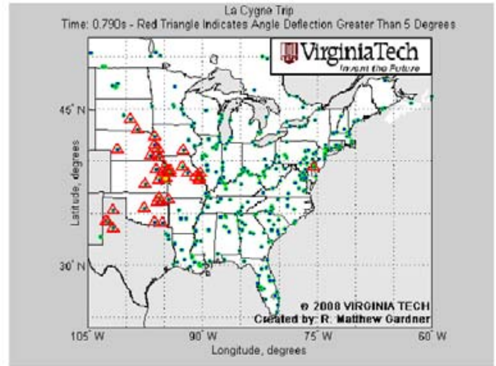

Figure 4-40: 5 degree deviation at 790ms.

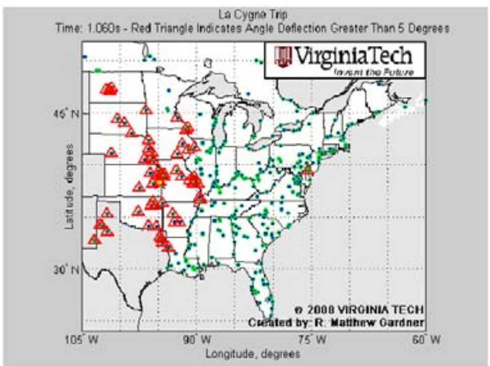

Figure 4-41: 5 degree deviation at 1060ms.

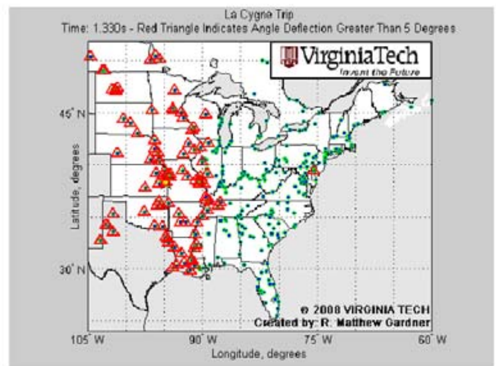

Figure 4-42: 5 degree deviation at 1330ms.

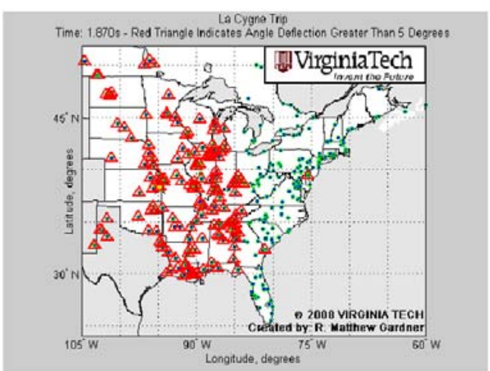

Figure 4-43: 5 degree deviation at 1870ms.

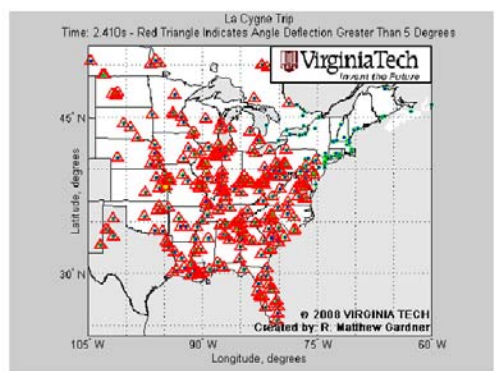

Figure 4-44: 5 degree deviation at 2410ms.

North Anna Unit Trip -- Angular Wave Propagation (5 degree Decline – from simulation)

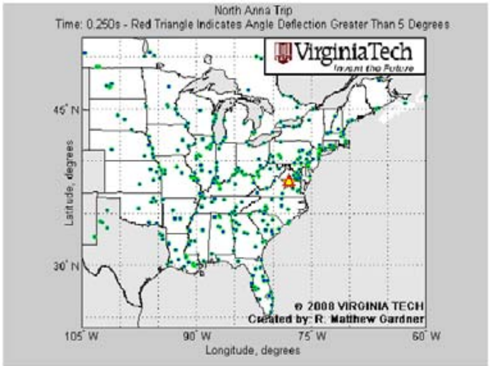

Figure 4-45: 5 degree deviation at 250ms.

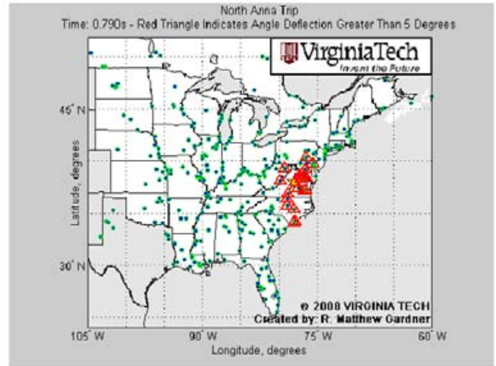

Figure 4-46: 5 degree deviation at 790ms.

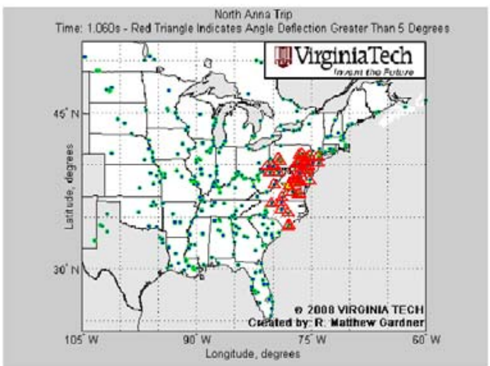

Figure 4-47: 5 degree deviation at 1060ms.

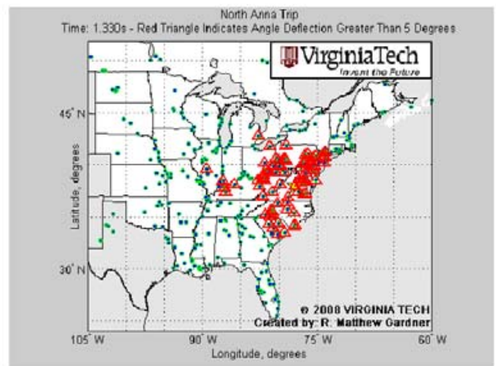

Figure 4-48: 5 degree deviation at 1330ms.

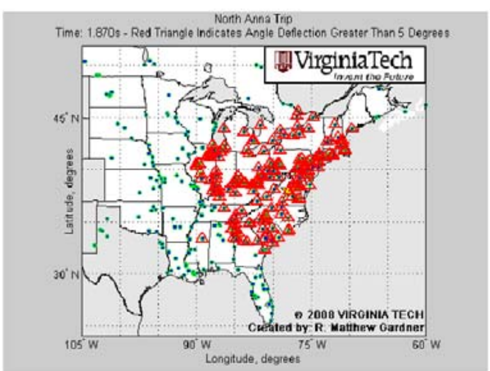

Figure 4-49: 5 degree deviation at 1870ms.

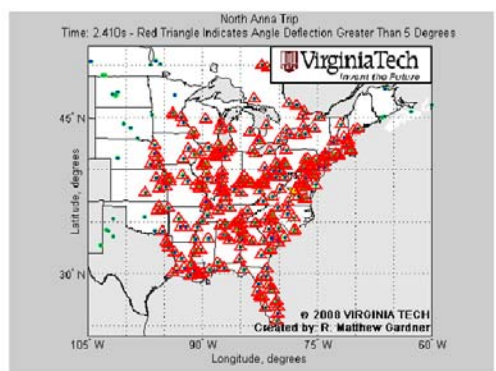

Figure 4-50: 5 degree deviation at 2410ms.

Palisades Unit Trip -- Angular Wave Propagation (5 degree Decline – from simulation)

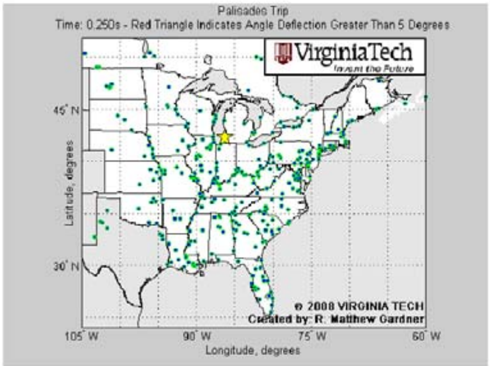

Figure 4-51: 5 degree deviation at 250ms.

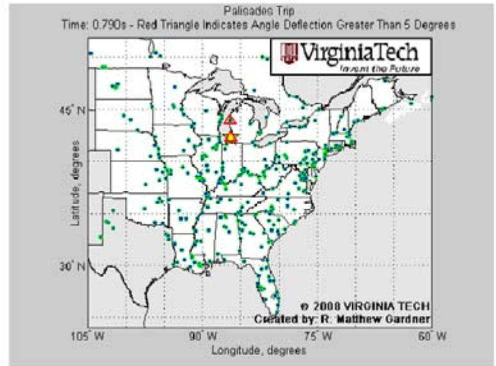

Figure 4-52: 5 degree deviation at 790ms.

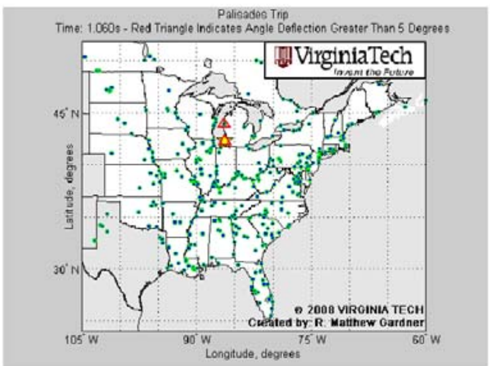

Figure 4-53: 5 degree deviation at 1060ms.

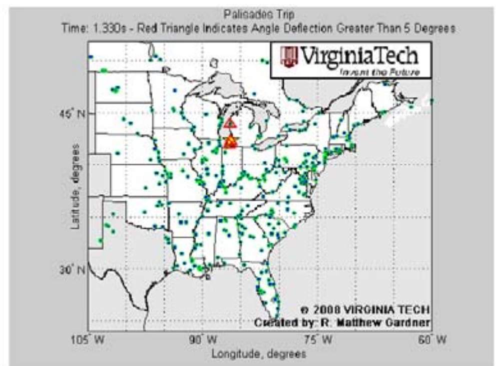

Figure 4-54: 5 degree deviation at 1330ms.

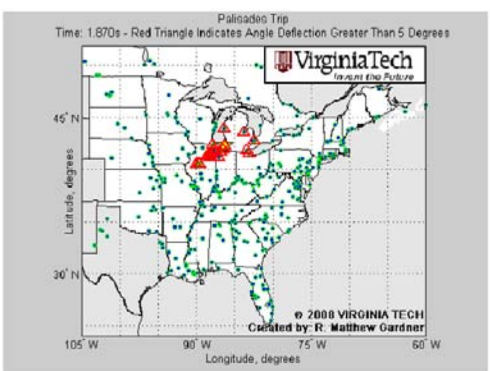

Figure 4-55: 5 degree deviation at 1870ms.

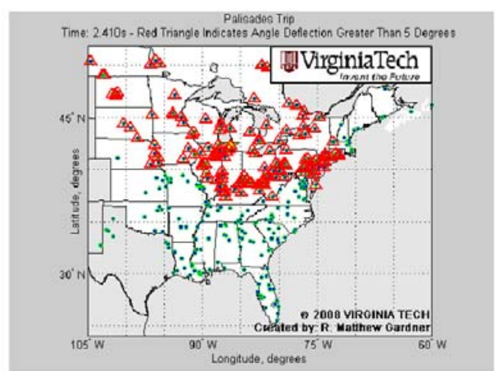

Figure 4-56: 5 degree deviation at 2410ms.

The main point for presenting the above figures is to show, through simulation, that the electromechanical disturbance resulting from a generation trip does in fact propagate throughout the electric grid at a finite speed. Further, we wish to capitalize on this propagation phenomena to use distribution-level wide-area frequency and angle data to locate such events. This type of analysis is a first in the field of electrical engineering.

Least-Squares Event Location

Frequency perturbations travel throughout the EI and in any general power system with finite speed [58, 61, 70, 71]. In the EI, frequency perturbations tend to travel with velocity on the order of 500 mi/s and in the WECC, frequency perturbations have been observed to travel with velocity on the order of 1000 mi/s [12]. The event location algorithms herein capitalize on the fact that frequency perturbations after events like generation trips will be measured by each FDR at different times. This time delay of arrival then gives a parameter by which to order the response of each unit. Figure 4-57 shows the frequency signature of a typical generation tripping event. Notice the very discernible delay in the frequency drop as measured by several FDRs. It is discernable that the frequency plotted in red drops first at time, t_1, and the frequency plotted in green drops last at time, t_{end}. This frequency drop is expected as the result of a generation/load mismatch in the few seconds following a significant loss of generation. These delays are not due to communication delays or latency in some stage of the signal processing. Each frequency measurement is GPS time-stamped at its point of origin (FDR sensor).

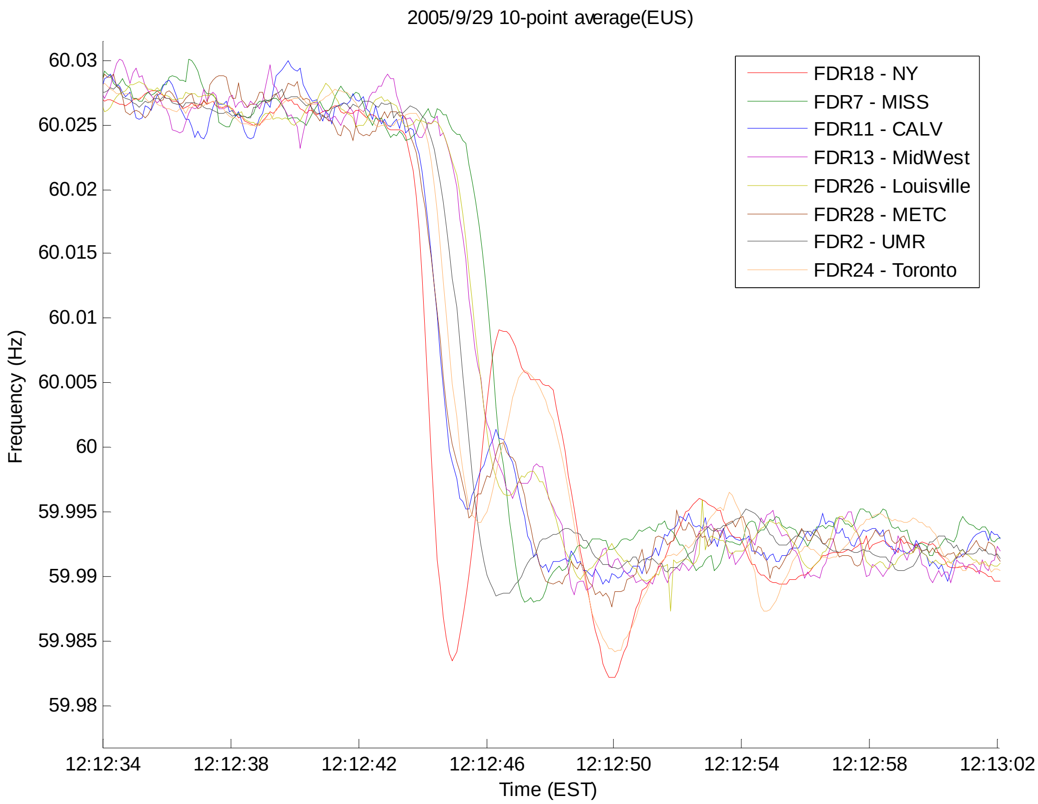

Figure 4-57: Typical frequency signature of a generator trip.

Therefore, the input parameters for the following event location algorithms are the times: t_1, t_2, ... , t_n corresponding to the times at which FDR_1, FDR_2, FDR_n measured the frequency disturbance. It is also important to note that all of the location algorithms solve for the hypocentral location (the location at which the disturbance is suspected to originate) in terms of Cartesian coordinates, (x_h, y_h). We map the Greenwich coordinates of each unit $(\text{Lat}_i, \text{Lon}_i)$ to Cartesian coordinates (x_i, y_i) before performing the locational analysis and reverse the mapping after the analysis.

From basic physics we obtain the key concept used in least-squares event location. Below we have the basic equation that relates mean velocity, time of travel, and distance traveled:

$$\text{Distance} = \text{Velocity} \times \text{Time}$$

Applying this concept to electromechanical waves with the assumption that such waves travel throughout the electric grid as a uniform continuum, we use the Pythagorean relation written in terms or our data and FDR locations:

$$(x_i - x_h)^2 + (y_i - y_h)^2 = V^2 (t_i - t_h)^2$$

For each responding FDR, we can write:

$$
\begin{aligned}
(x_1 - x_h)^2 + (y_1 - y_h)^2 &= V^2(t_1 - t_h)^2 \\
(x_2 - x_h)^2 + (y_2 - y_h)^2 &= V^2(t_2 - t_h)^2 \\
\vdots \qquad\qquad \vdots \qquad\quad &\qquad \vdots \\
(x_n - x_h)^2 + (y_n - y_h)^2 &= V^2(t_n - t_h)^2
\end{aligned}
$$

where (x_i, y_i) are the Cartesian coordinates of the i^{th} FDR to respond; (x_h, y_h) are the Cartesian coordinates of the hypocenter (origin of disturbance); t_i is the time at which the i^{th} FDR measures the electromechanical wave; t_h is the time at which the event occurred; and *V* is the mean velocity at which the frequency perturbation travels throughout the electric grid. The unknowns in the above equation set are: (x_h, y_h), and t_h. A set of mean velocities, $\{V_1, V_2, \cdots, V_k\}$, are assumed rendering a set of hypocentral coordinates, $\left\{\left(x_h^{(1)}, y_h^{(1)}\right), \left(x_h^{(2)}, y_h^{(2)}\right), \cdots, \left(x_h^{(k)}, y_h^{(k)}\right)\right\}$, in the solution of the system. To find a set of solutions, we seek a linear system in terms of the hypocentral coordinates such that the least-squares (LS) method of solving an over-constrained system of equations can be used. In general, our system of equations will be over-constrained since many more FDRs typically respond than there are variables. By subtracting successive pairs of equations, a linear equation in terms of the hypocentral coordinates is produced:

$$
(x_{i+1} - x_i)x_h + (y_{i+1} - y_i)y_h - V^2(t_{i+1} - t_i)t_h = \frac{1}{2}\left[V^2\left(t_i^2 - t_{i+1}^2\right) + x_{i+1}^2 + y_{i+1}^2 - x_i^2 - y_i^2\right]
$$

The above equation is linear in terms of our three hypocentral coordinates and the LS method can be applied. To accomplish this, we first form the following system of equations while collapsing the right-hand side into a constant C_i:

$$
\begin{aligned}
(x_2 - x_1)x_h + (y_2 - y_1)y_h - V^2(t_2 - t_1)t_h &= C_1 \\
(x_3 - x_2)x_h + (y_3 - y_2)y_h - V^2(t_3 - t_2)t_h &= C_2 \\
\vdots \qquad\qquad \vdots \qquad\qquad \vdots \qquad &\quad \vdots \\
(x_1 - x_n)x_h + (y_1 - y_n)y_h - V^2(t_1 - t_n)t_h &= C_n
\end{aligned}
$$

represented in matrix form as:

$$
\mathbf{C} = \mathbf{H}\mathbf{x}
$$

with matrix variables defined as:

$$\mathbf{C} = \begin{bmatrix} C_1 \\ C_2 \\ \vdots \\ C_{n-1} \\ C_n \end{bmatrix} \qquad \mathbf{H} = \begin{bmatrix} x_2 - x_1 & y_2 - y_1 & V^2(t_2 - t_1) \\ x_3 - x_2 & y_3 - y_2 & V^2(t_3 - t_2) \\ \vdots & \vdots & \vdots \\ x_n - x_{n-1} & y_n - y_{n-1} & V^2(t_n - t_{n-1}) \\ x_1 - x_n & y_1 - y_n & V^2(t_1 - t_n) \end{bmatrix} \qquad \mathbf{x} = \begin{bmatrix} x_h \\ y_h \\ t_h \end{bmatrix}$$

The hypocentral coordinates can then be solved for via the LS method using the Moore-Penrose pseudo-inverse:

$$\mathbf{H}^{\dagger} = \left(\mathbf{H}^{\mathrm{T}}\mathbf{H}\right)^{-1}\mathbf{H}^{\mathrm{T}}$$

yielding the final solution:

$$\mathbf{x} = \mathbf{H}^{\dagger}\mathbf{C}$$

A disadvantage of using the LS method to find the hypocentral coordinates is that one must assume that the electromechanical waves are traveling in a continuum at a constant velocity in each direction. Therefore, the velocity set, $\{V_1, V_2, \cdots, V_k\}$, must be assumed before solving. To date, there is no accepted velocity model for the travel of electromechanical waves in the EI. The following figures show the results of the LS method, plotted with red asterisks, using velocities, $V_j \in \{V_1, V_2, \cdots, V_k\}$, that vary from 100 mi/s to 1000 mi/s. This range for V_j was chosen based upon past observations of disturbances traveling between 350 mi/s and 660 mi/s in the EI [12]. In the following figures, the closest solution location is enlarged and pointed out with an arrow. The base case location (true value) being estimated is plotted with a square and the FDR locations are shown using blue dots.

Errors Associated with the Straight-Line Wave Propagation Assumption

The largest disadvantage of the LS location method perhaps stems out of the uniform continuum implications of straight-line event propagation. In a uniform continuum, we should expect that the distance of a sensor away from the origin of the event would be a linear function of time (straight-line wave propagation). To explore this notion, we again resort to simulation of the EI. Figure 4-61 and Figure 4-62 present a simulated regression analysis. It is clear to see that the distance versus time measurements stray from linearity. In general this has found to be the case as is borne out by an exhaustive regression analysis of the 2007 events seen in Appendices XIII and XIV. There has been a great push for the development of interconnection “speed maps.” This type of construction can be based on a similar regression analysis. These results for both frequency and angle are presented in

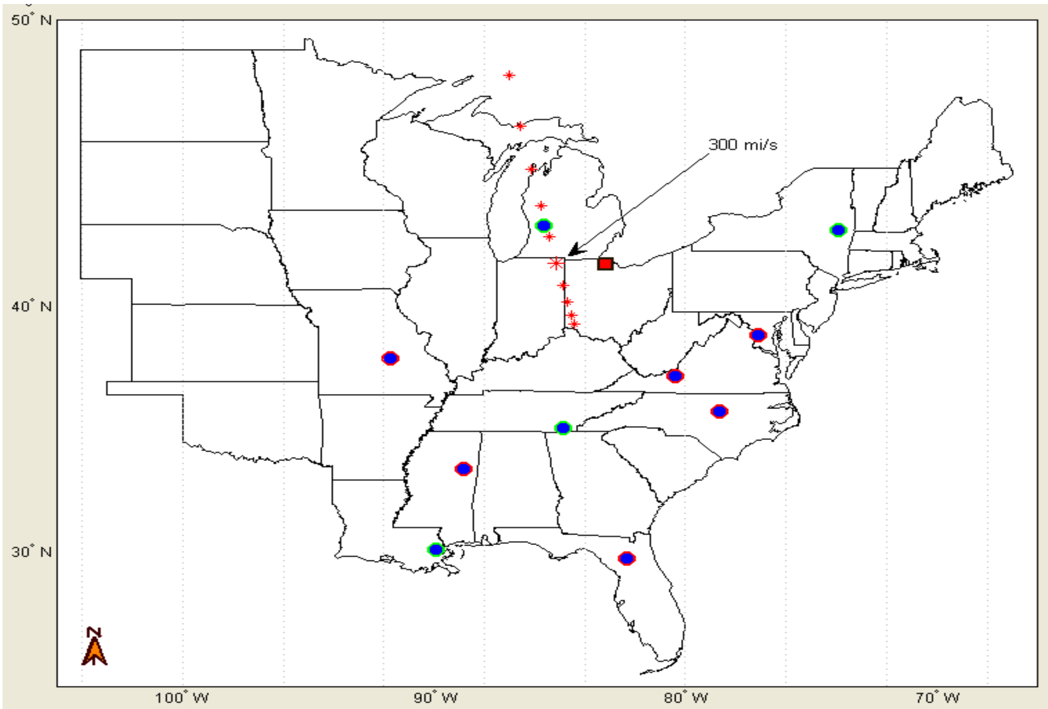

Figure 4-58: LS event location estimate for base case 1.

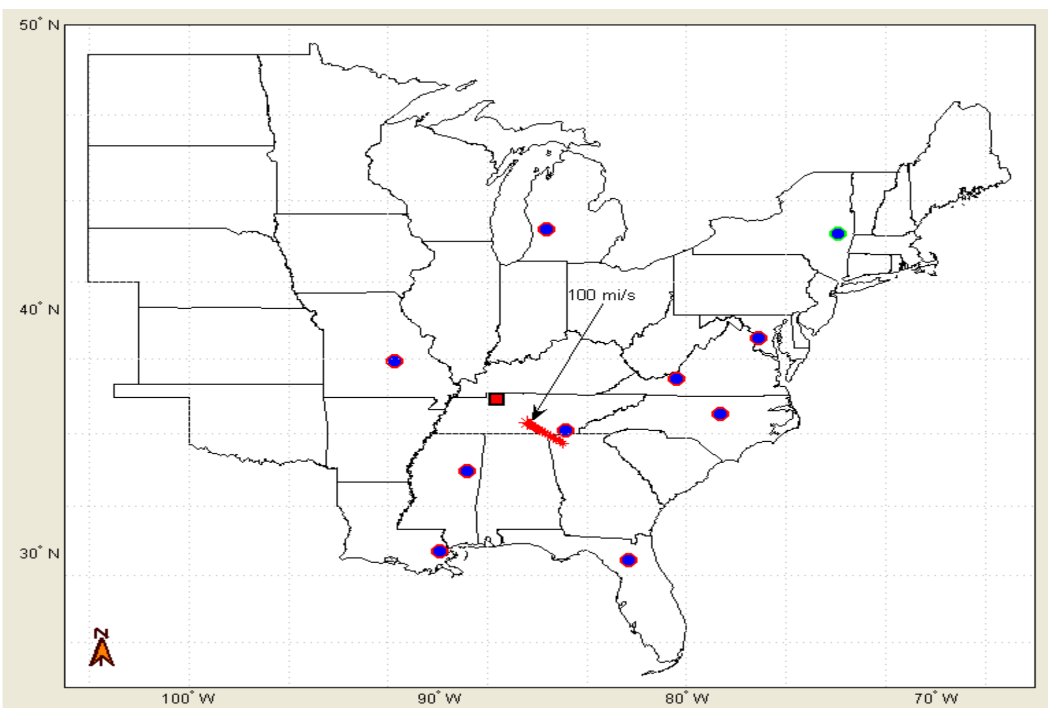

Figure 4-59: LS event location estimate for base case 2.

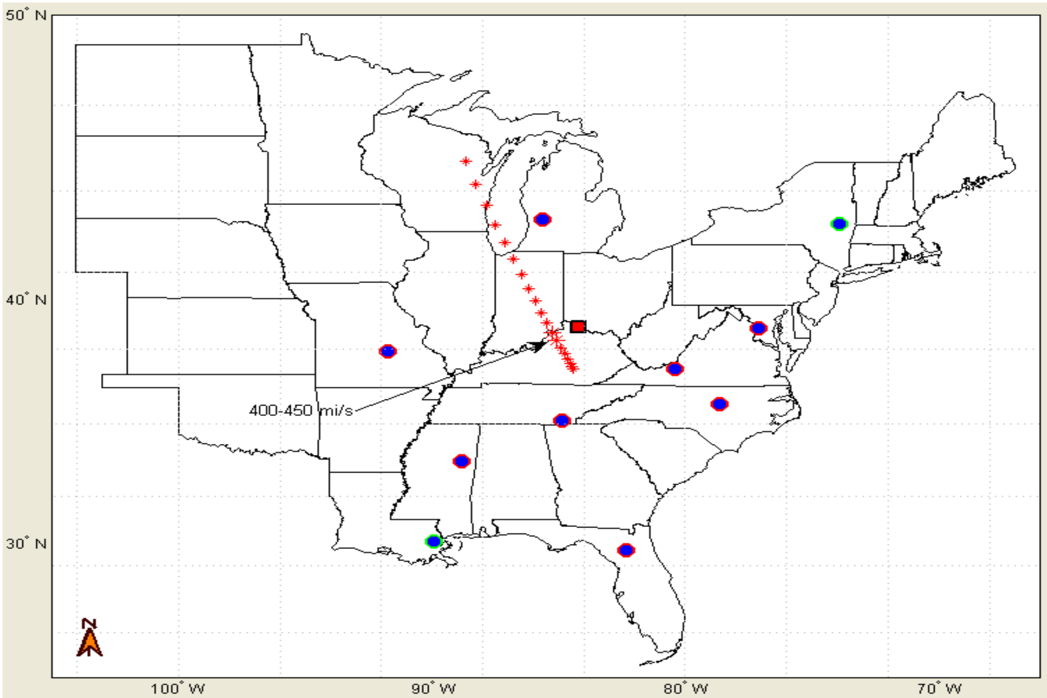

Figure 4-60: LS event location estimate for base case 2.

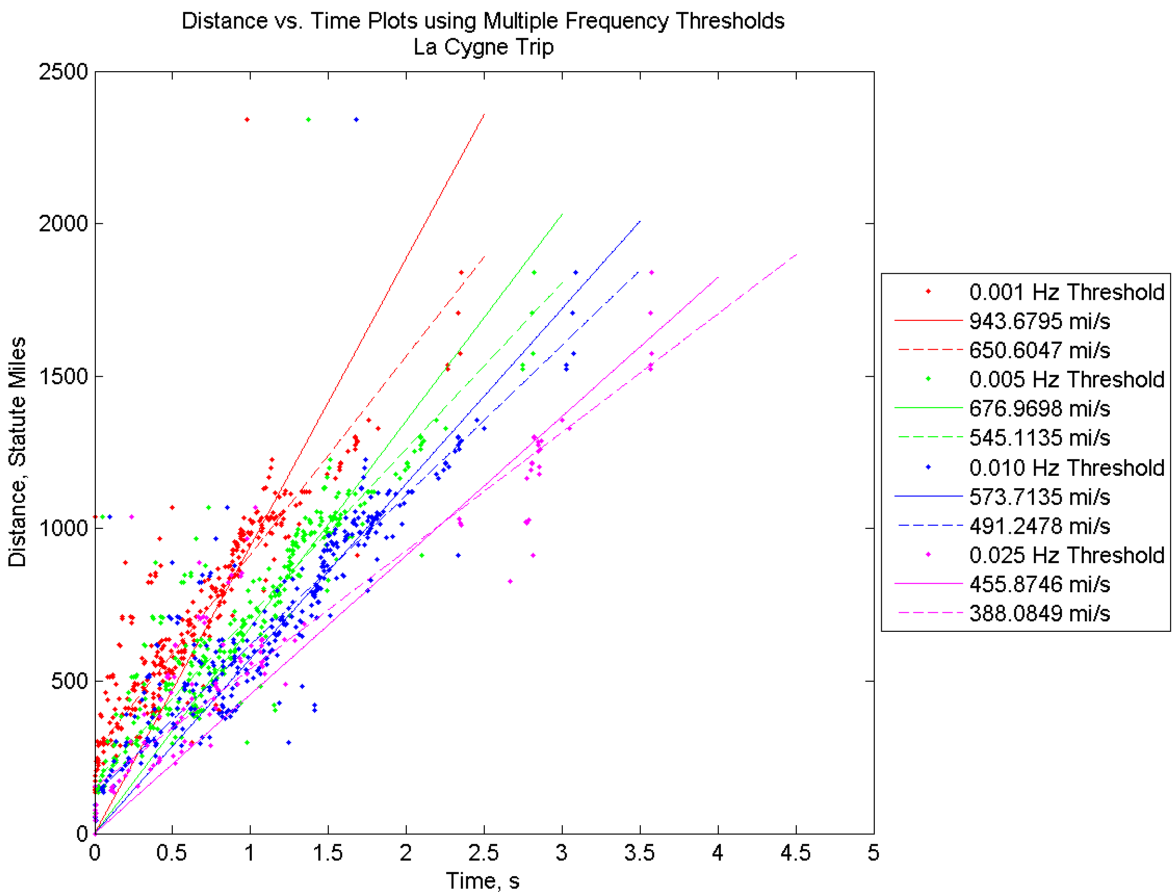

Figure 4-61: Distance versus time regression for frequency-based velocity calculation.

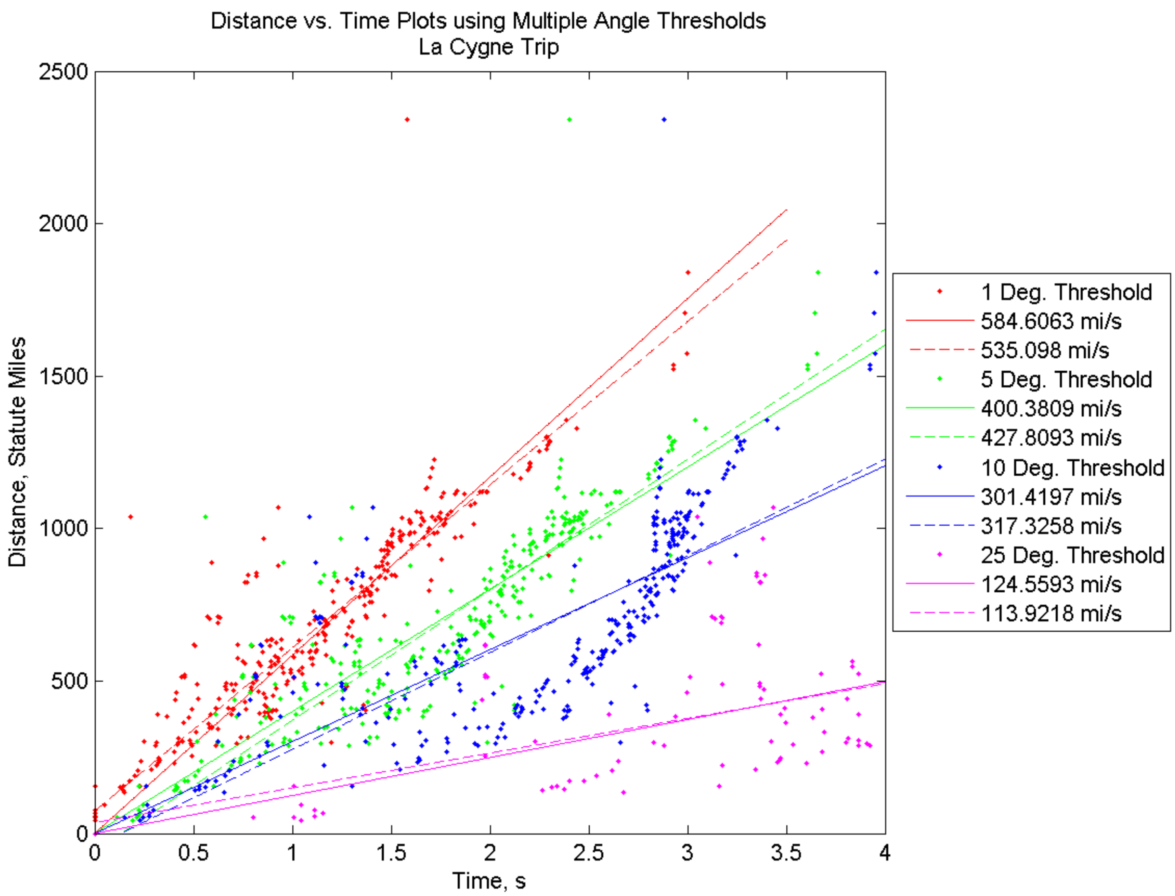

Figure 4-62: Distance versus time regression for angle-based velocity calculation.

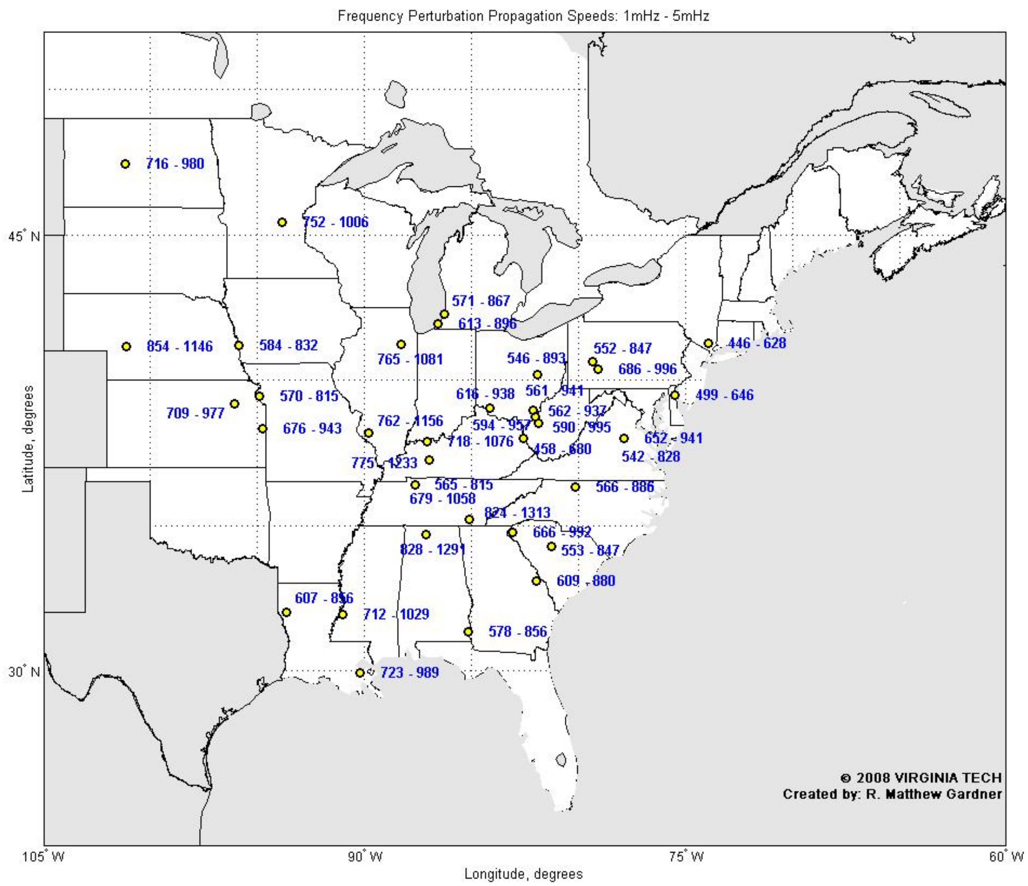

Figure 4-63: Frequency-based interconnection electromechanical wave speed propagation map (estimated from simulation data).

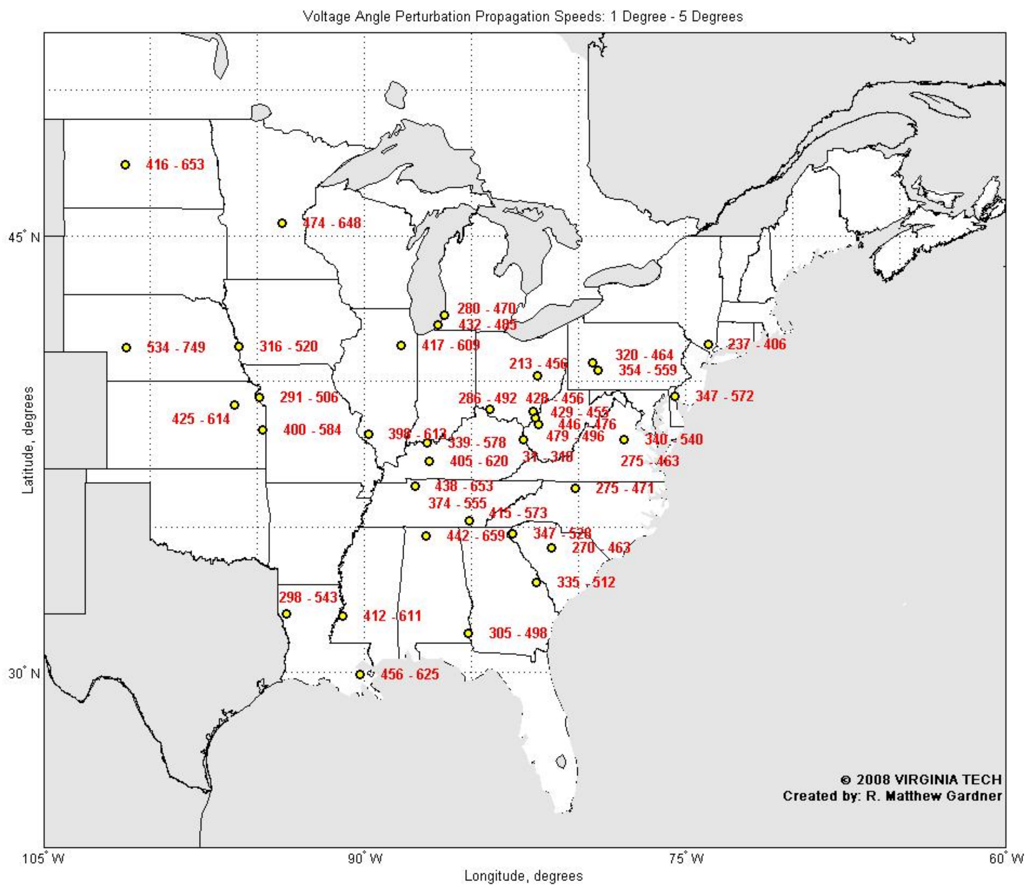

Figure 4-64: Angle-based interconnection electromechanical wave speed propagation map (estimated from simulation data).

Non-Parametric Event Location

Thus far, we are unsatisfied with least-squares event location method for two main reasons. First, we have to assume a mean electromechanical wave propagation speed. Second, preliminary results have shown that a "one size fits all" approach does not give consistent results. We thus resort to a less deterministic method of event location.

Consider a plane containing two points as shown in Figure 4-65. Suppose a wave, symmetrical in both directions on the level of the plane, is observed by sensors at points (x_1, y_1) and (x_n, y_n) where the subscript of each point indicates the order in which the wave was detected. If the spread of the wave is uniform in speed and propagation then we can assert that the origin of the wave is in the half-plane of the sensor that first detected the wave. This region is shaded in the figure. With just two sensors, we have reduced the locus of all possible points of origin by half. Here again, we are assuming that the electric grid is a nearly uniform continuum.

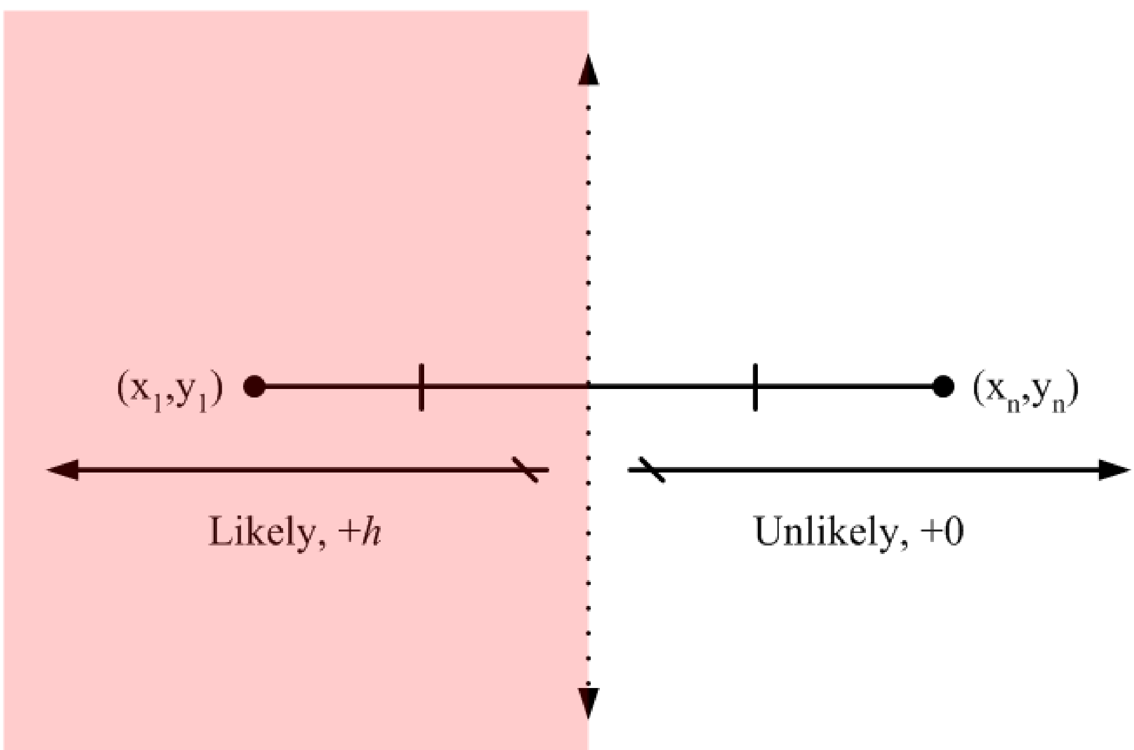

Figure 4-65: An example of a plane containing two sensor points.

Perhaps we have more than just two sensors. Say, for example, we have four sensors as shown in Figure 4-66. In this case we can construct three half-planes and observe a region of overlap. If these half-planes are labeled $\mathcal{R}_1$, $\mathcal{R}_2$, and $\mathcal{R}_3$, then the region of overlap can be described as:

$$\mathcal{R}_{\text{overlap}} = \mathcal{R}_1 \cap \mathcal{R}_2 \cap \mathcal{R}_3$$

Continuing with our logic, we can now assert with confidence (again assuming that the wave travels with even propagation) that the origin of the wave is in the overlapping portions of the planes of Figure 4-66. This overlapping region, $\mathcal{R}_{\text{overlap}}$, is shaded separately in Figure 4-67. One can imagine that, as the number of sensors increases, $\mathcal{R}_{\text{overlap}}$ tends to get smaller. Therefore, the higher the number of FDRs that respond to any arbitrary event in the EI, the smaller the region of the supposed origin.

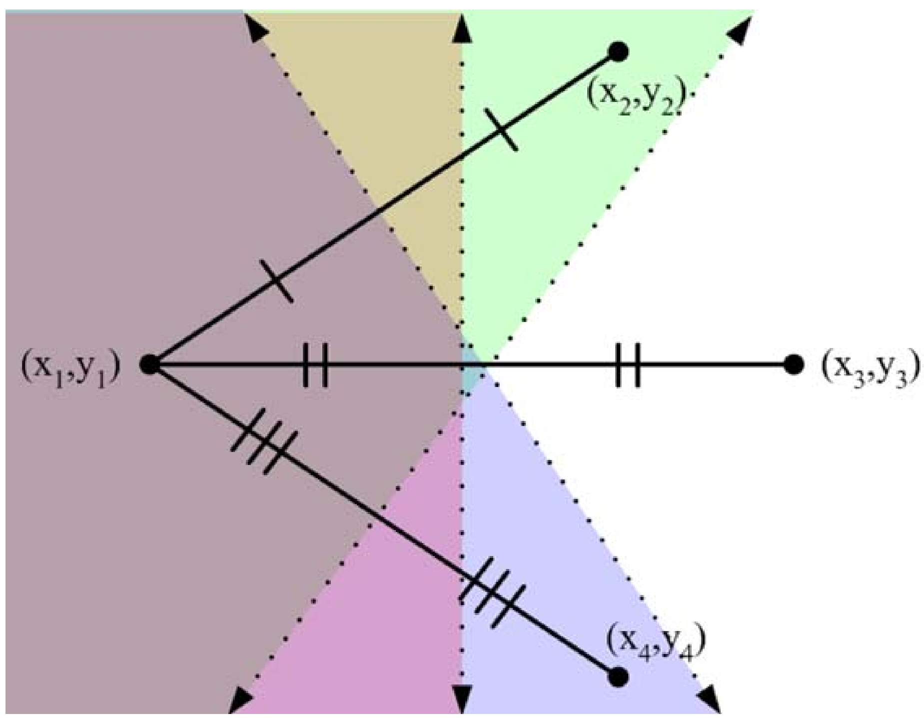

Figure 4-66: An example of a plane containing 4 sensor points.

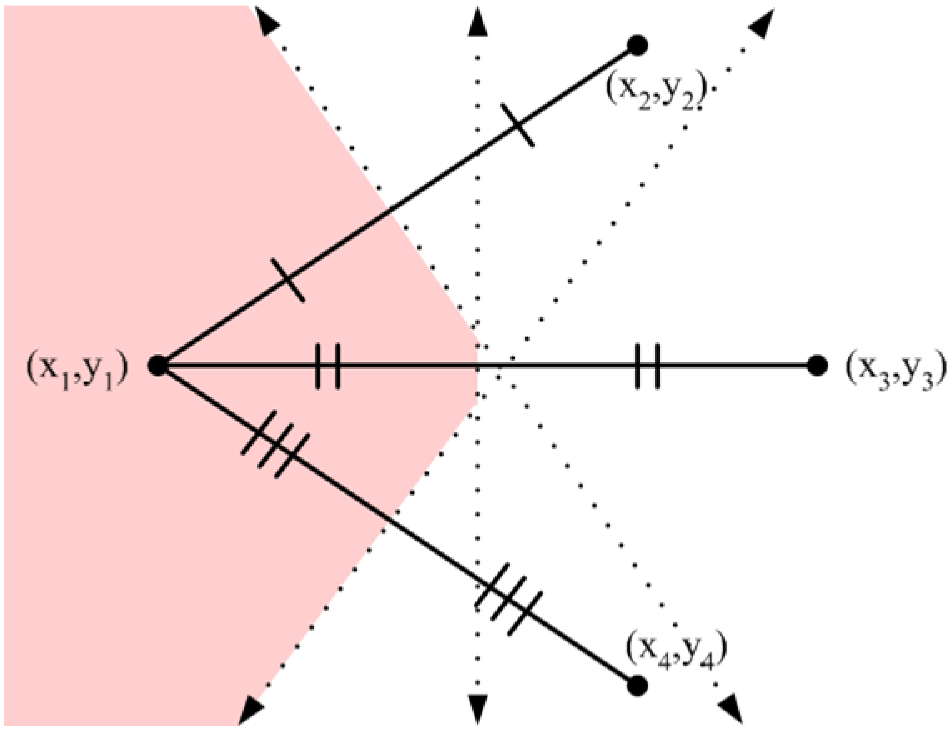

Figure 4-67: An example of a plane containing 4 sensor points with region selected.

The following figure represents an example of how the lines defining such half-planes might be constructed given a certain event detection sequence. The red star shows the actual location of the EI disturbance, but the green dot corresponding to the FDR at Virginia Tech was the first to measure the disturbance in this example.

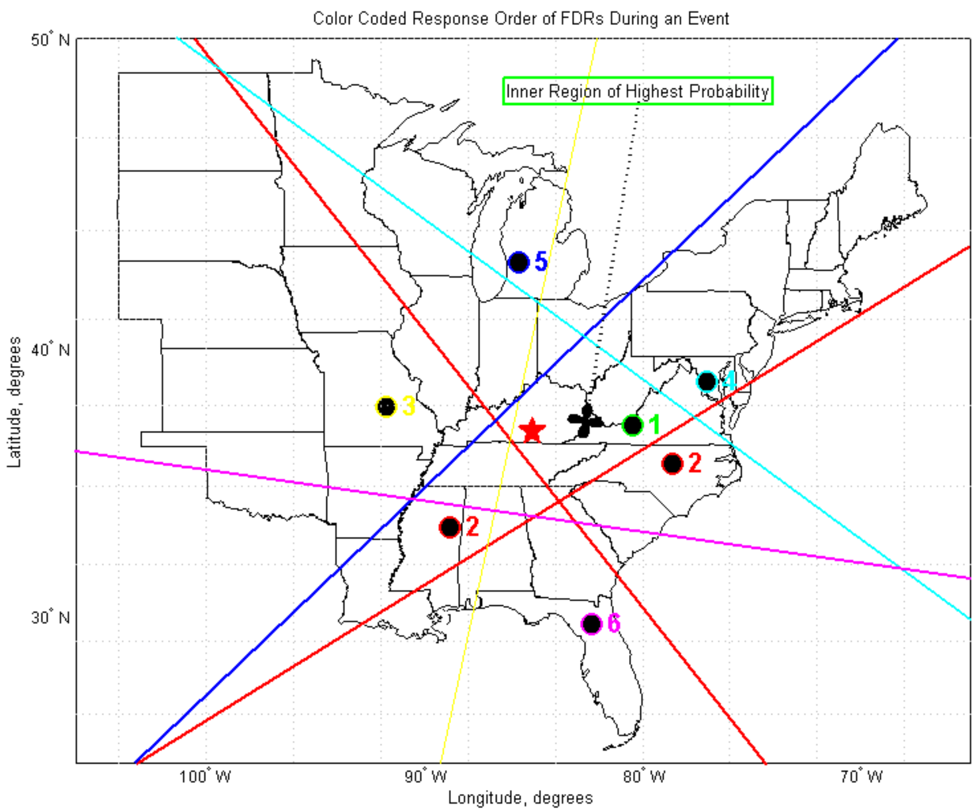

Figure 4-68: A cartoon of lines representing half-planes in the EI.

As opposed to eliminating half-planes outright, let us form regions of probability. We refer to this method as a Parzen window approach because we wish to estimate a probability density with a series of windowing functions [39]. In this case, these windowing functions are entire half-planes. As opposed to the situation of Figure 4-67, we can construct probability regions shown in Figure 4-69. The regions shaded the darkest correspond to the estimated regions of highest probability and the regions shaded lightest or not at all represent the estimated regions of least probability. We have, in essence created something akin to a probability density estimate that describes the probability of a detected disturbance having its origin in any given location.

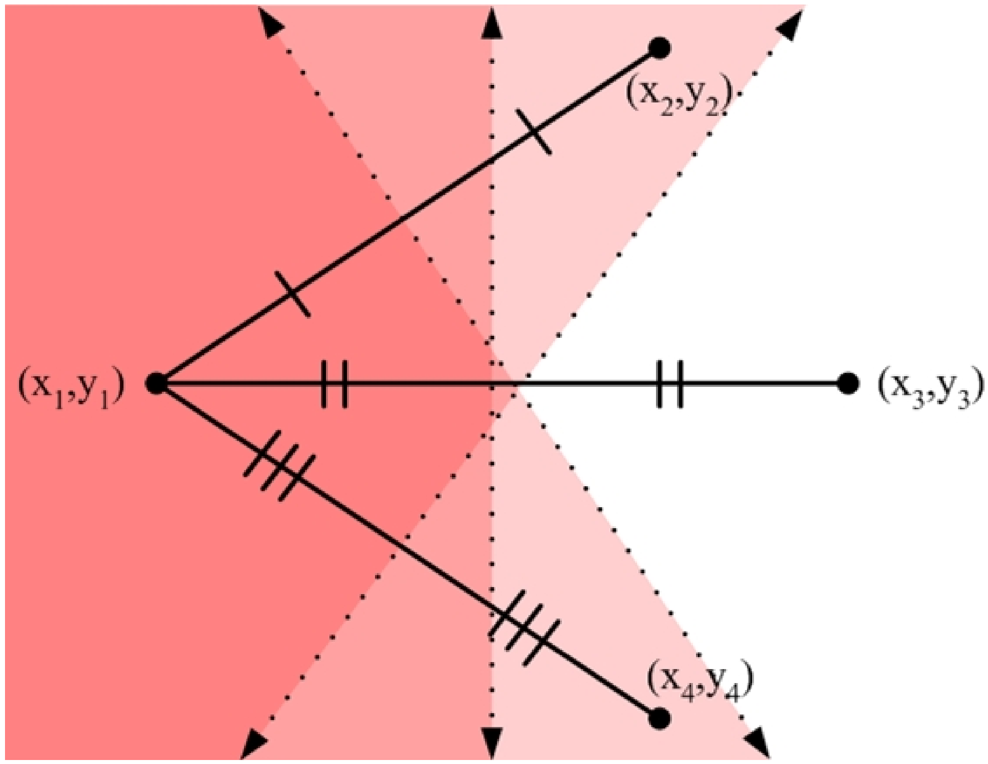

Figure 4-69: An example showing regions of probability.

As an example, let us assume that we have a set of five sensors as shown in Figure 4-70. In this figure, each sensor is plotted in its own panel with a green dot except for the first sensor to detect the disturbance which is represented as a red star. Four windowing functions are created corresponding to each sensor pair (x_1, y_1) and (x_i, y_i). One can see that to each point in the half plane of the first sensor, an arbitrary but consistent value is added. Each of the windowing functions can be summed to create our probability density estimate as shown in Figure 4-71. From Figure 4-71 we learn that, given the response of the sensors, we can create probability regions. For this example the region of highest probability is raised.

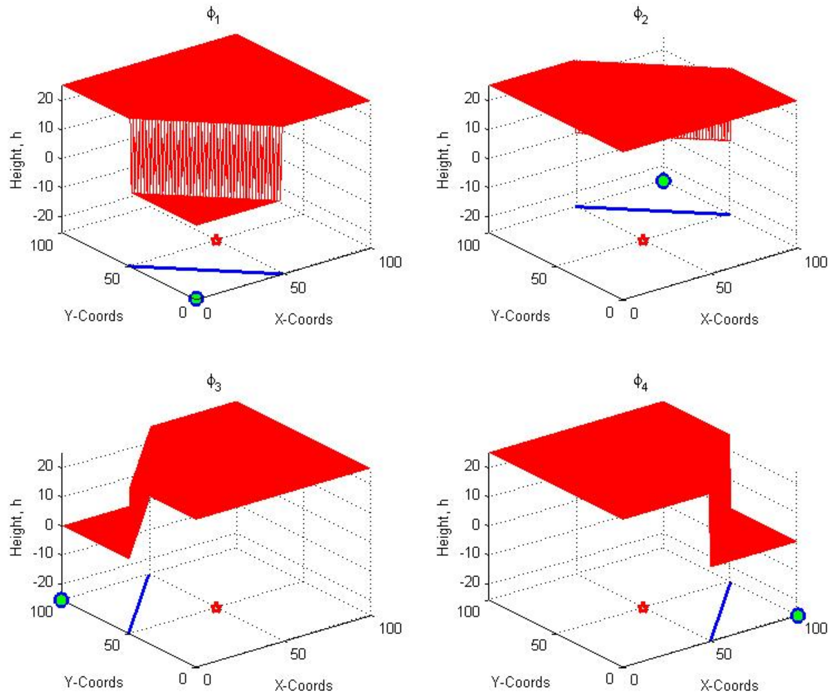

Figure 4-70: An example showing windowing functions for the Parzen window approach.

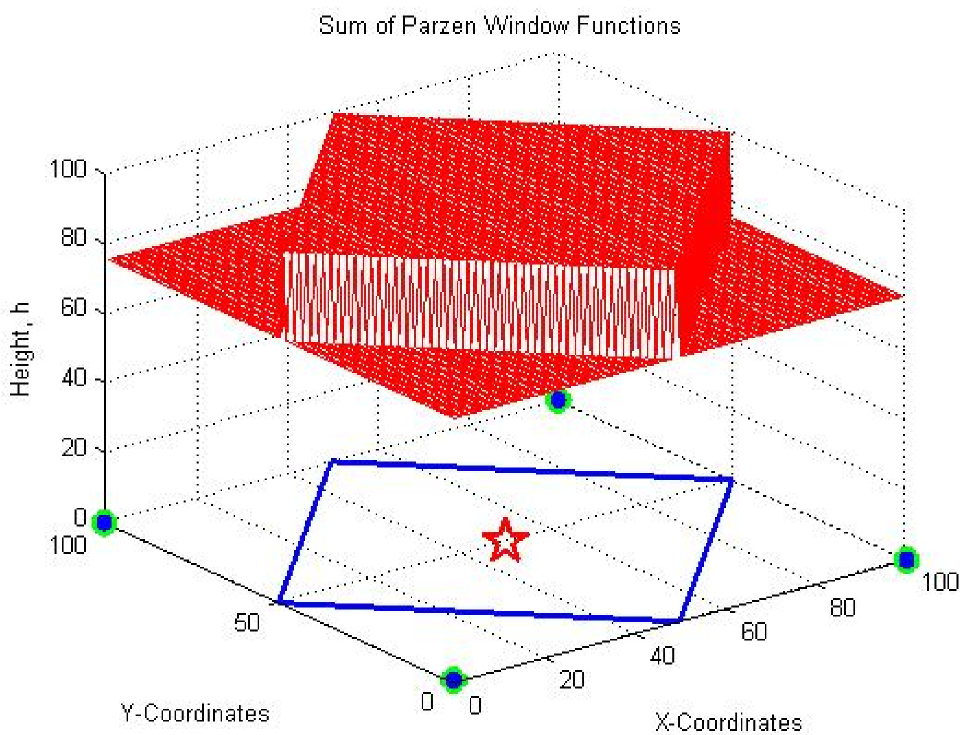

Figure 4-71: Sum of windowing functions creating event probability density estimate.

The Parzen window approach has been applied to a number of events in the EI. Figure 4-72 shows a view of the probability density estimate from above for the Cumberland generator trip. The lowest points are in deep blue and the highest points are in dark red. Obviously points outside the EI are of no relevance (for instance, points in the ocean) since there is no grid connectivity at these points. These points can be ignored. The actual location obtained from historical data is shown with a red and white star. Ideally, we should like to see this star falling in the region of highest probability (dark red). The location of each FDR is indicated with a blue dot and beside each dot there is a number that corresponds to the order in which that sensor detected the event. Figure 4-73 is the same except for the fact that this density is formed by summing the density estimates obtained using a variety of ordering methods.

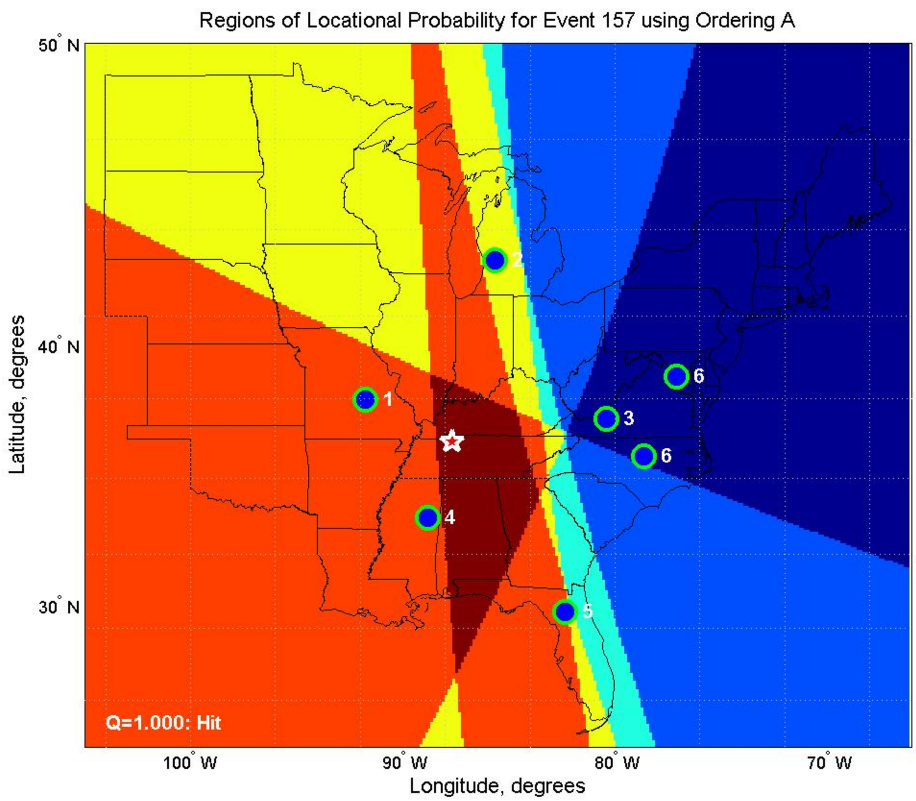

Figure 4-72: Probability density estimate: Cumberland generator trip.

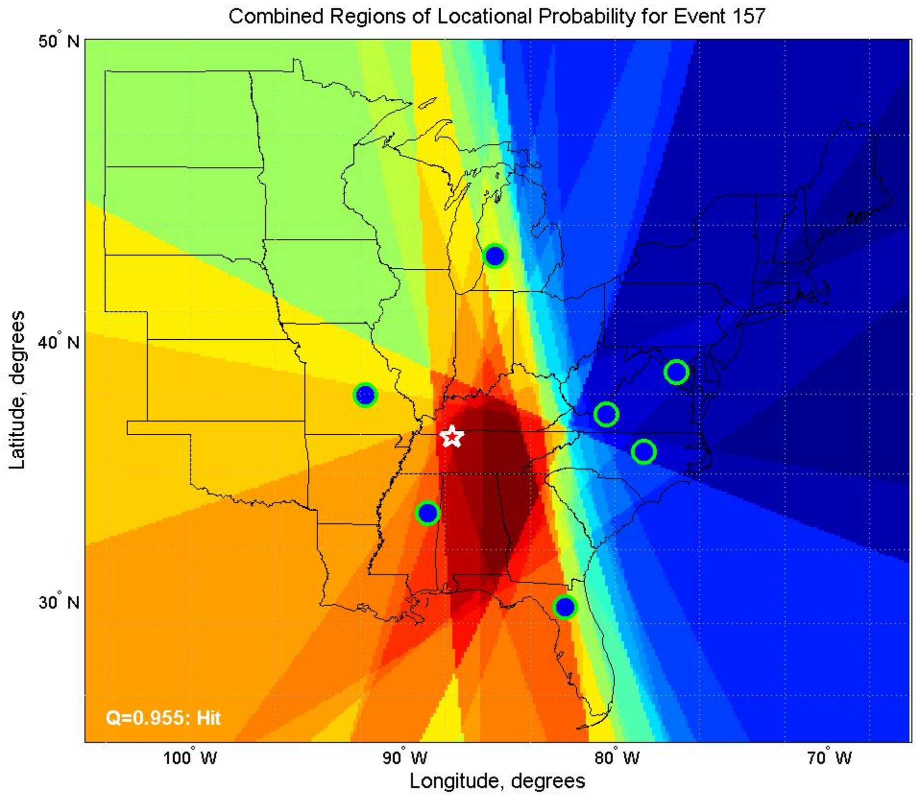

Figure 4-73: Probability density estimate using several event ordering methods.

How do we determine our hits or misses from historical data? We consider the result a hit if the actual location is in the upper quantiles of the formed probability density estimate. If $\beta > 0.5$, then we say that the estimated probability density represents a hit. If $\beta < 0.5$, then we say that the estimated density does not contain the actual location and is therefore a miss. A β-quantile of data set *X* is any value *x* such that:

$$\Pr(X \leq x) = \beta$$

Experiments have been made with other windowing functions as well. For instance, we can taper the windowing function so as to not resemble a sudden step in three dimensions. Figure 4-74 presents a comparison of the original windowing method against an alternate windowing method. This tapering method amounts to a spatial “Hanning” of the locational weights.

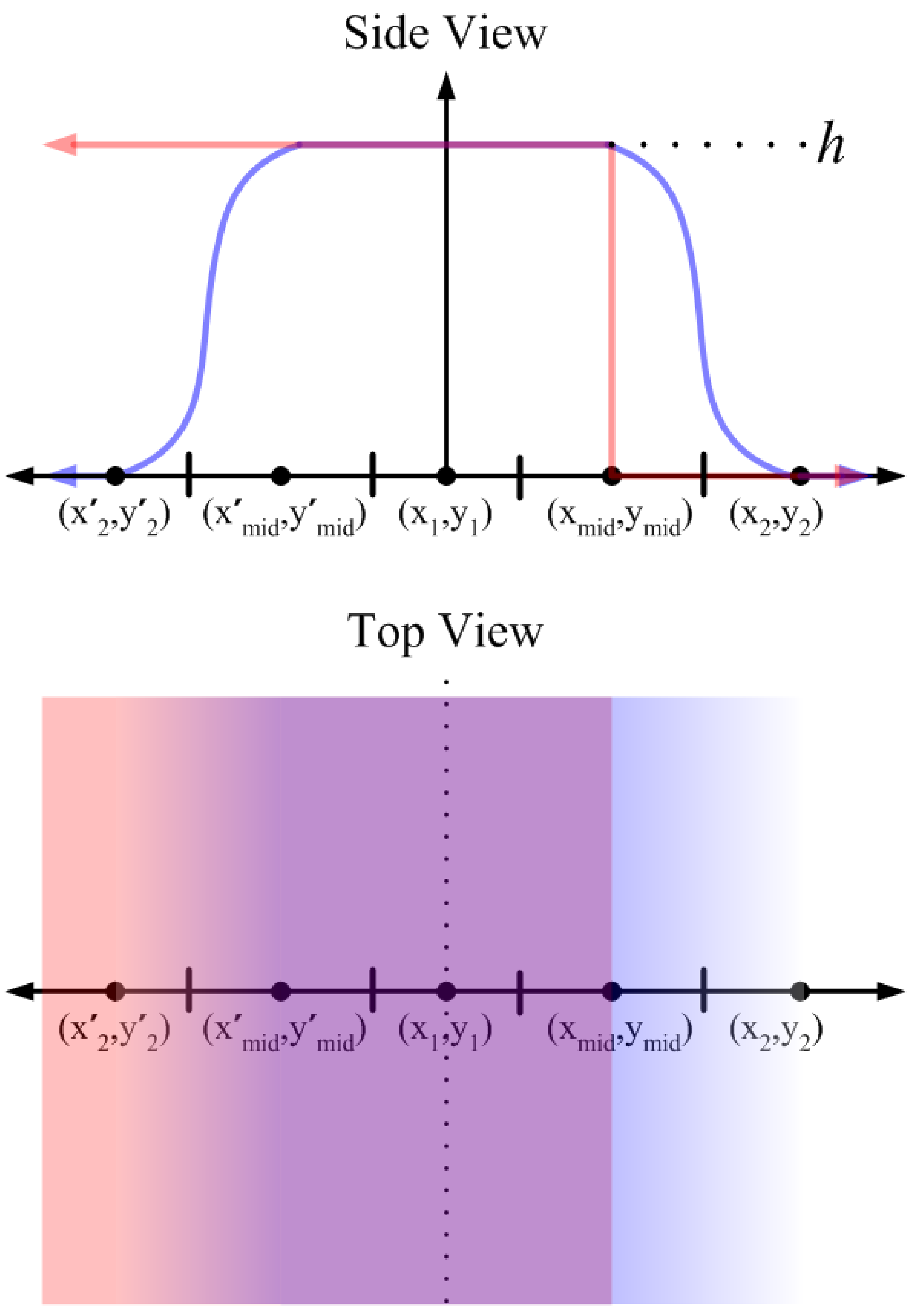

Figure 4-74: Example of an alternate windowing method.

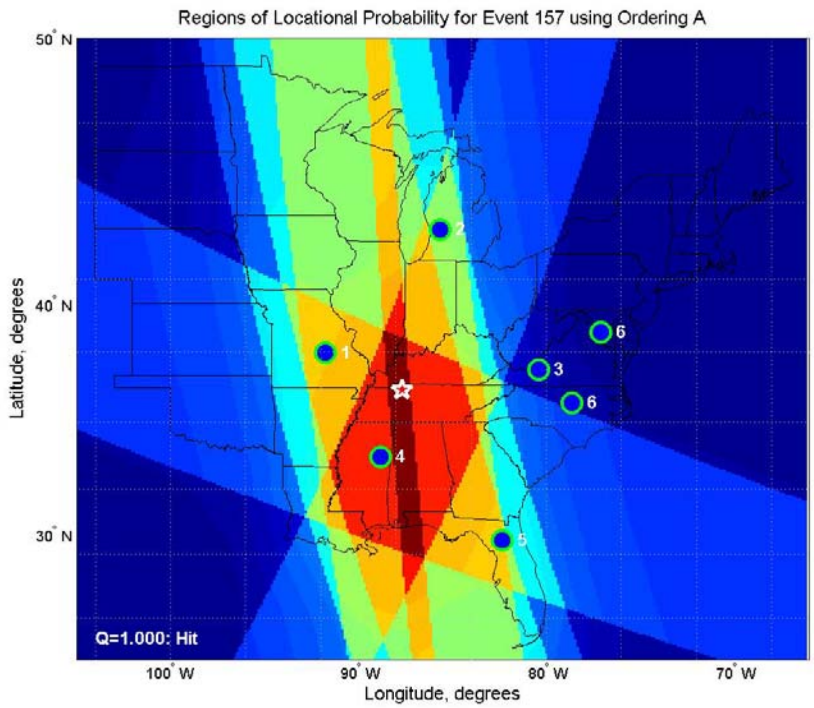

Figure 4-75: Probability density estimate: Cumberland generator trip. (alternate windowing method)

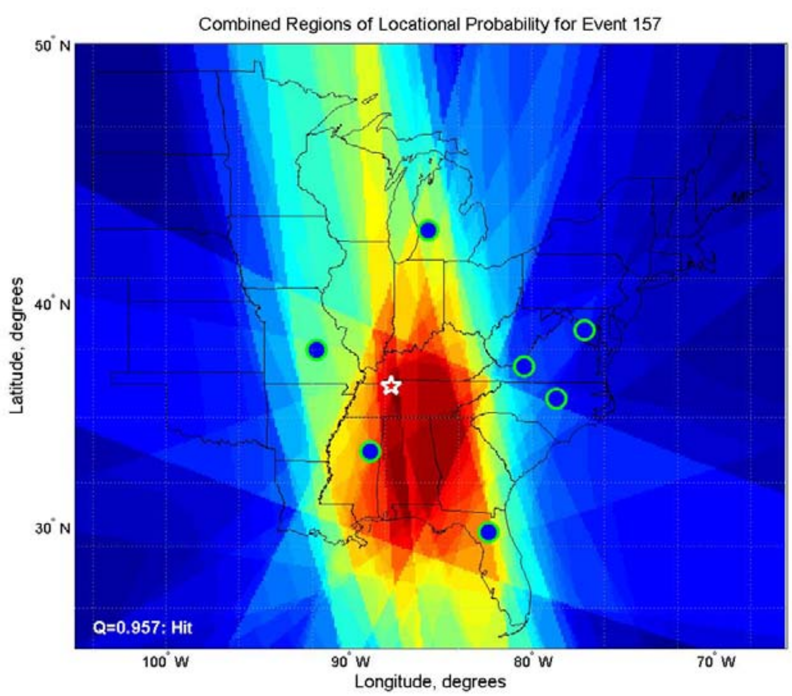

Figure 4-76: Probability density estimate using several event ordering methods. (alternate windowing method)

The results of the Parzen method are promising. The hit-to-miss ratios show room for improvement. Given the fact that we are attempting to locate a disturbance using only seven sensors over half of the United States, the results are satisfactory. As the number of FDRs increases it is plausible that our hit-to-miss ratio will improve. This will allow us to increase our quantile threshold from 0.5 to perhaps upwards of 0.95. Future work will continue to focus in the area of non-parametric and less deterministic methods of event location.

Using Multiple Thresholds in Event Location

Due to errors inherently in the frequency (and, in the future, angle) data, we wish to create a response order based upon the crossing of frequency and/or angle below (or above) multiple thresholds. Figure 4-25 and following demonstrate this action on simulated data.

Overview of Methodology and Testing via Random Methods

This windowing method uses entire half planes to construct the "probability regions" shown in Figure 4-67 and Figure 4-69. In the discrete case, which is our computational foundation, we consider every candidate point in our region of interest (the EI or some other interconnection geography). We tessellate this region into sufficiently small sub-regions in the $X-Y$ plane. The height parameter (extending in the $Z-\text{direction}$) for each of these small sub-regions is then determined by an analysis of candidate points $\left(x_i^*, y_i^*\right)$. If the region of interest is tessellated into an $N \times M$ grid, then there are $N \cdot M$ such candidate points. Each candidate point is addressed $(Q-1)\cdot P$ times as half planes are constructed for each sensor pair and for every frequency threshold:

$$\left\{\left(x_0^{(p)}, y_0^{(p)}\right) \quad \left(x_k^{(p)}, y_k^{(p)}\right)\right\}, \qquad \begin{array}{l} k=1,2,\cdots,Q-1 \\ p=1,2,\cdots,P-1 \end{array}$$

Therefore, for each sensor pair and each candidate point in the grid, we construct vectors $\mathbf{u}$ and $\mathbf{w}$ as shown in Figure 4-77.

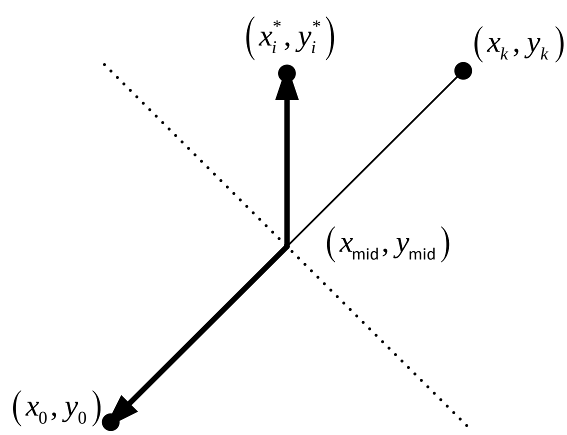

Figure 4-77: A cartoon showing vector relationships governing the half-plane Parzen approach to event location.

A density matrix, $\mathbf{H}^{(p)} \in \mathbb{R}^{N \times M}$, can be constructed based upon a summation of constituent matrices, $\mathbf{D}_k^{(p)}$, whose entries are determined based upon the half-plane methodology as follows:

$$\mathbf{D}_k^{(p)}(i,j) = \frac{h}{2} \cdot \operatorname{sgn}\left(\mathbf{w}^T \mathbf{u}(i,j)\right) + \frac{h}{2}$$
$$\mathbf{H}^{(p)}(i,j) = \sum_{k=0}^{Q-1} \mathbf{D}_k^{(p)}(i,j)$$
$$\mathbf{H}(i,j) = \sum_{p=0}^{P-1} \mathbf{H}^{(p)} \cdot w_p$$

where P is the number of thresholds chosen each weighted based by magnitude from nominal. Each entry in our density matrix, determines the likelihood of the generation trip event (or load shedding event) having occurred at the location corresponding to that entry. To force this density matrix to conform to a discrete and finite version a of a true probability density, h can be chosen such that:

$$1 - \sum_i^N \sum_j^M \mathbf{H}(i,j) \Delta x \Delta y = 0$$

A battery of full simulation results for both frequency and angle associated with the 2007 events are included in Appendices XV and XVI. Results from measured data associated with the 2007 events are included in Appendix XVII.

In order to simulate the effects of a less than optimal number of reporting sensors, we randomly choose a number of units and consider only the data from said units. Units are chosen in batches of 15, 50, and 161 sensors. These results are contained in Appendix XVIII for frequency data and Appendix XIX for angle data.

Finally, we introduce a method to capitalize on agreement in the event location process to further refine the location estimates. We wish, therefore, to weight each entry in the density matrix, $\mathbf{H}$, based upon agreement amongst the constituent matrices, $\mathbf{D}_k$. Concisely,

$$\mathbf{H}^{(p)}(i,j) = \frac{\mathbf{H}^{(p)}(i,j)}{\max\left\{ \underset{\forall k}{\text{var}}\left\{\mathbf{D}_k(i,j)\right\} \quad w_{\mathbf{D}} \right\}}$$

where $w_{\mathbf{D}}$ is some small weight to circumvent the unusual case of complete or near complete agreement where the variance of data in the constituent matrices approaches zero. This weighting capitalizes on agreement in the constituent matrices of the density matrix. In an effort to be mindful of space, we place frequency based simulation results in Appendix XX and frequency based observed results in Appendix XXI.

Having discussed event detection, classification, analysis and location up to this point, we begin to draw the concepts in this report together in the next chapter. Chapter 5 discusses the reporting of power system events.

Performance of Disturbance Location Methods

The methods presented in this chapter to locate disturbances have been tested and evaluated for their performance. The battery of 2007 events listed in Appendix IV, have been evaluated against both measured event data and simulated event data. It is important to note that the simulation data also expands the event location algorithms to operate on voltage phase angle since this parameter is also available, in theory, in distribution-level measurements. Appendices XV through XXI provide the results of these methods. Appendix XXII provides histograms that show the performance of these methods based upon the knowledge of the actual event hypocenter. We measure the performance of these methods based upon the location of the actual event hypocenter in our pseudo-probability density. A perfect hit would land on the peak of the probability density and a poor location would lie in the tails of the empirically formulated density. Based upon the histograms presented in Appendix XXII, we can see that the non-parametric event location algorithms presented in this chapter perform quite well. However, there is significant room for improvement in the variance-weighted algorithms.

Chapter 5: Power System Event Reporting

We have discussed the treatment of bulk transmission level power system events based upon distribution level measurements in the following contexts:

- Power system event detection and classification
- Oscillation event detection and analysis
- Event location based solely on frequency and angular measurements

On the practical side, we now fit the proverbial puzzle pieces together to form a high-level diagram of an automatic power system event reporting system. The purpose of a reporting system is aimed at addressing the needs for improvement in electric grid situational awareness. To date, the standard method for communicating the occurrence significant power system events across an interconnection from utility to utility is a phone call [72]. More modern solutions are now being implemented amongst utilities such as the Open-Access Same time Information System (OASIS). The existence of a system like unto the FNET system is justified by the need for increased inputs into system like OASIS for improved situational awareness. Reconsider Figure 1-2; the following figure now provides greater insight into the components of the FNET system.

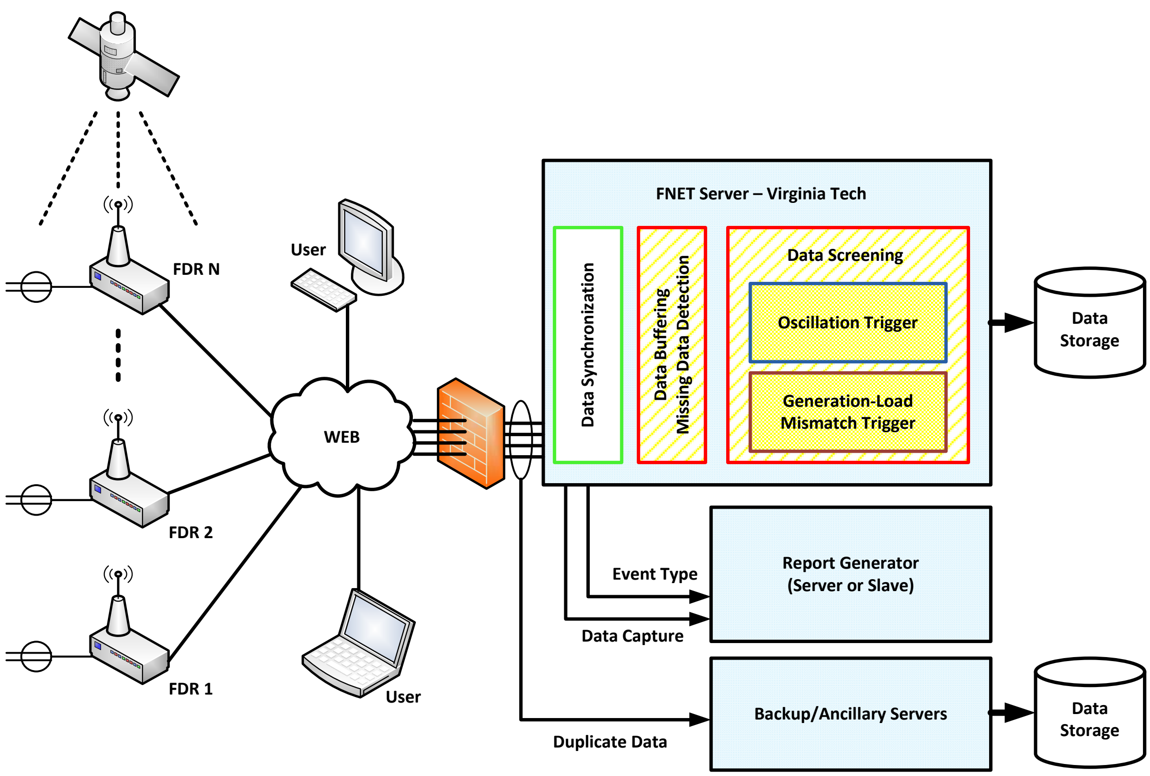

Figure 5-1: FNET system exposing event triggering components.

Within the main FNET server, three operations are germane to the topics discussed in this report – data synchronization, data buffering (and bad data detection), and event screening. The frequency data is time synchronized for the purposes of simultaneous analysis. Synchronization is especially important in determining event location (because of the sensitivity of detection ordering algorithms to timing) and oscillation phase analysis. Second, it is important to identify bad data and appropriately replace the errant data (via interpolation or some other method). In the case of missing data, it is key to appropriately pad the system data vectors (see Figure 5-2).

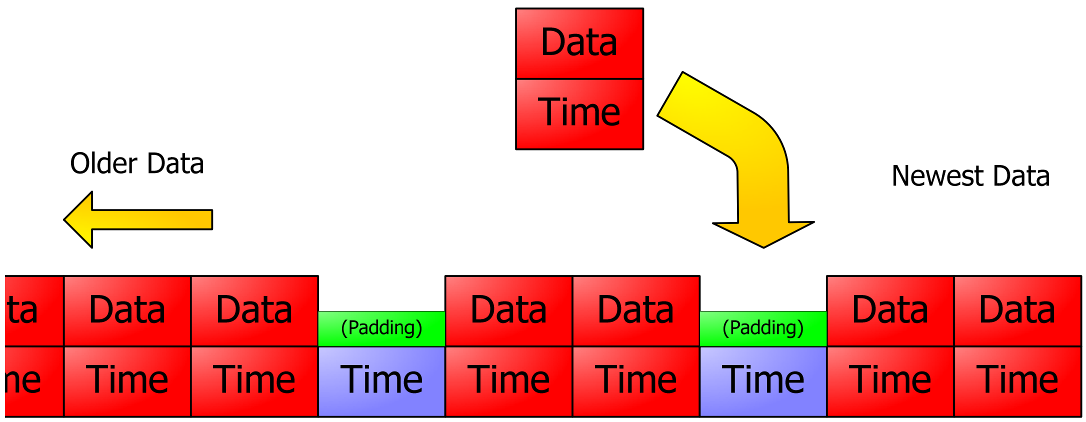

Figure 5-2: A cartoon of the FNET server's data buffer. As new data arrives, the synchronization process correctly assigns valid data addresses within the buffer.

Third, simplistic event detection routines, based upon the material presented herein, are applied repeatedly to the frequency measurements as they arrive. The event detection routines make use of several layers of data filtering. Therefore, filtered data is also stacked in the system's buffer.

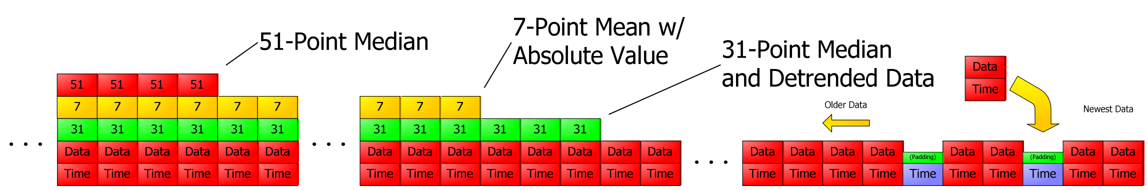

Figure 5-3: Data buffer with raw and filtered data vectors.

Upon detecting an event, the server is designed to trigger a report generation routine. Triggering the report generation routine does not necessarily result in the generation of an event report. Since the server's event detection routines are intended for real time operation, the event detection algorithms are given freedom to be rudimentary – tending towards false alarm. Therefore, the report generation routines have a built-in secondary analysis layer. The following figure presents a high-level description of the report generation routine. The reports generated are intended for immediate online distribution after completion. In this respect, automatic report generation adds significant resolution to classical power system situational awareness.

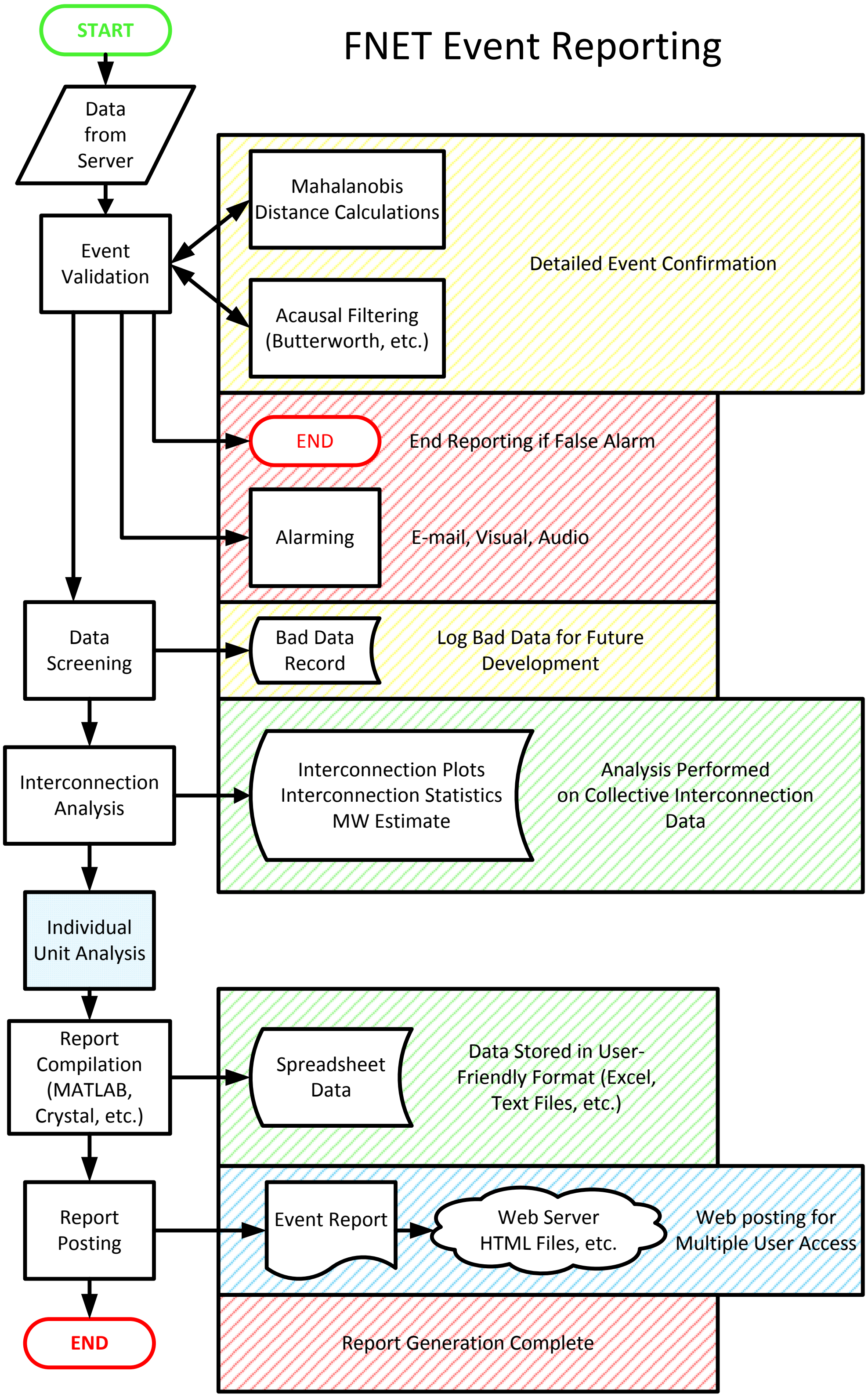

Figure 5-4: FNET event reporting routine flowchart.

Figure 5-4 presents the four major functions of the report generator:

- Event confirmation and supplemental bad data detection
- Interconnection-wide analysis
- Individual sensor analysis
- Report compilation

Interconnection-wide analysis draws data from all FDRs for the calculation of interconnection "averages" such as minimum/maximum frequency deviation, megawatt change estimation, event location, overall event plotting, and other interconnection statistics. Individual sensor analysis primarily focuses on system oscillation studies. Finally, the report compilation process is focused on the distillation of event analyses into a single report and online report distribution. For an overview of the individual sensor analysis functionality see Figure 5-5.

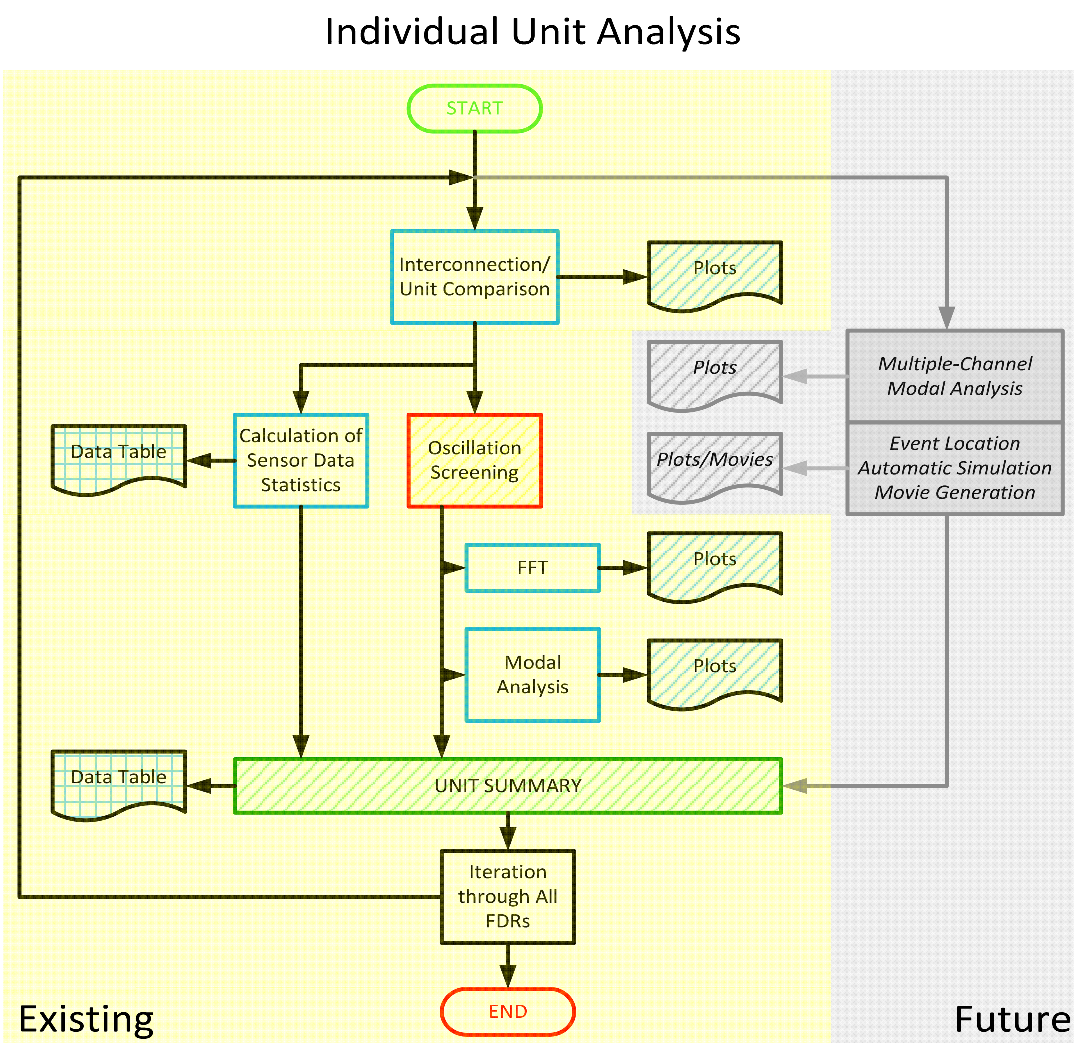

Figure 5-5: Flowchart for the analysis of individual FDRs in the report generation process.

Chapter 6: Conclusions, Contributions, and Future Directions

Through this report we have directly observed the viability of certain distribution-level wide-area measurements for the analysis of bulk transmission-level power system operation and dynamics. Classically, such measurements made at relatively low voltage levels have been overlooked for several reasons:

- The availability of a wide array of measurements and sensor points has been either non-existent or quite scarce.
- The metering of current, power consumption/injection, and power factor at the distribution level is both difficult to measure with meaning and considered irrelevant.
- Low level voltage waveforms are dominated by distribution level noise and local load influences.
- Modeling of the Eastern Interconnection with known major generator locations has been not been attempted.

The data-intensive perspectives of this report lead to contributions in the areas of wide-area event detection, classification, location, and analysis.

Contributions

Perhaps the largest contribution of this work is the very perspective from which it is written. The data set forth in this report as measured by the FNET system is exclusively obtained from calculations applied to observations of 120 V voltage waveforms from across the EI. The measured data is also analyzed without the aid of system models. Extensive modeling has been used for the establishment of best-case scenarios – especially in the location of disturbance efforts. Another unique facet of this research is the attempt at a correlation between power system disturbance propagation and geographical sensor placement (as opposed to sensor placement in the context of location in an electrical topology).

The behavior of a large electrical interconnection during the occurrence of generation/load mismatch events has been well-studied in the past – from a bulk transmission level perspective. In Chapter 2, this report presents such behavior from a distribution level perspective. We were not surprised by an overall agreement between the two perspectives. However, no conclusive results or procedures on the topic of event detection from distribution level perspective have been previously presented. This work shows how event detection is possible through the exclusive use of wide-area frequency measurements and presents a method for the execution thereof. In Chapter 2, we also begin to see the effects of electromechanical wave propagation in frequency measurements. In fact, not all sensors simultaneously detect disturbances – data from some sensors reflect a measureable delay. Finally, Chapter 2 closes with a contribution through the presentation of a linear relationship between frequency excursion and frequency slope during generation/load mismatch events. This relationship is submitted for further examination when exact mismatch amounts are known.

The transient behavior of power systems has been a topic historically associated with both a known (or well-estimated) system model and (usually well-placed) transmission-level measurements. While this association is certainly recognized as a solid foundation, we begin to examine the transient "ringdown" behavior of power system transient from a distribution-level perspective. Chapter 3 recapitulated the so-called Matrix Pencil method and introduced the method, first presented in the electromagnetics arena, to wide-area frequency data in the electric power arena. Agreement was found and presented between both PMU (transmission-level) and FDR (distribution-level) measurements. The Matrix Pencil method was subsequently expanded to address the multiple channel problem associated with power system measurements (regardless of the voltage level at which said measurements are obtained). Chapter 3 concluded by contributing a battery of results that reflect the existence of commonly known modes in both the WECC and EI.

Chapter 4 is perhaps the crown of this report. The viability of such an effort was shown through interconnection modeling and exhaustive application. Multiple routines for event location, sans model, are presented an applied to a comprehensive battery of observed power system events for the year 2007. Wide-area event location has proven quite useful and drawn significant attention from utilities, system operators, and energy markets. However, an event location algorithm like unto the one presented herein is perhaps most valuable when applied to data from a network of sensors that extends across an entire synchronous interconnection (like FNET).

Chapter 5 presented a methodology by which the contributions from the previous chapters can be condensed into a single system. The subject matter of Chapter 5 lays the foundation for the use of FNET-based information for the purpose of interconnection-wide situational awareness.

Future Directions

This report does not pretend to be a comprehensive treatment of the use and benefits of distribution-level wide-area measurements. Significant work lay ahead in nearly all areas addressed by this report. Specifically, in the area of event detection and classification, there are great challenges in detecting and rightly classifying line trips. Inadvertent line outages can be as critical if not more dangerous than generation trips and load shedding. However, these types of events are quite difficult to detect in system frequency. Perhaps this difficulty is due to the relationship between a line's loading and it influence on system frequency. For instance, a line connecting generation to the rest of the interconnection when tripped may have effects similar unto a generator trip. Or, rather consider the opposite scenario in terms of system load. This report establishes wide-area frequency measurements as a diagnostic tool for certain disturbances in hopes of lighting the way towards an eventual comprehensive examination of all major system disturbances.

The realm of wide area oscillation analysis is perhaps the subject needing most attention in any future work. The expansion of wide-area disturbance detection and classification rests directly on this topic. It is suspected that many oscillations detected by the FNET system are due to line outages. Groundwork has been laid by other research that establishes the correlation between the oscillatory behavior of an interconnection and the change of system model parameters [14]. However, such work has typically stopped with models infinitesimal in size compared to the whole of the EI or WECC. The use of expert systems in the diagnosis of events is suggested based upon the notion that no effort to ensure linear behavior during the analysis of detected oscillations has been made by this research effort. Detected oscillations are directly and automatically analyzed by the FNET system as it exists now. However, it is not beyond the realm of imagination and experience to consider that changes in system topology can occur during oscillations. In such cases, a direct analysis of the whole triggered signal would be ill advised. Therefore, some effort needs to be made to pre-analyze and partition any detected oscillation prior to the application of the Matrix Pencil method.

Wide-area power system event detection is perhaps the most exciting frontier explored in this report. It is the author's opinion that four key elements are required for the furtherance of this field. First, more sensors are necessary to provide richer resolution to both parametric and non-parametric event location techniques. Second, more known cases to serve as training samples are a needed for the honing of tools in this field. Perhaps these first two elements are more functions of finance and time rather than intellectual efforts. Third, greater near real time signal processing efforts are required for the improvement of the location of disturbance algorithms. It has been observed by the author that, in many cases, the failure of the non-parametric event location methods has been largely due to a failure to reject bad data properly. Finally, this report has focused on methods that do not rely on system model information but rather a combination of geographical sensor location and disturbance measurement data. Perhaps an "all or none" mentality is less than optimal in this particular effort. Perhaps it would be better to use some model data in combination with sensor information and measurement data. For example, perhaps better event location results could be obtained with the windowing method if said windows were deflected based upon the inertial profile of the system. The inertial profile should not change much in a large interconnection from day to day. Season-to-season alterations are, however, possible.

References

1. Phadke, A.G., *Synchronized phasor measurements in power systems.* Computer Applications in Power, IEEE, 1993. **6**(2): p. 10.
2. Tsai, S.J.S., *Study of Global Power System Frequency Behavior Based on Simulations and FNET Measurements*, in *Bradley Department of Electrical and Computer Engineering*. 2005, Virginia Tech: Blacksburg.
3. Zhian, Z., et al., *Power system frequency monitoring network (FNET) implementation.* Power Systems, IEEE Transactions on, 2005. **20**(4): p. 1914.
4. Bin, Q., et al. *Internet based frequency monitoring network (FNET)*. 2001.
5. Fromm, W., A. Halinka, and W. Winkler. *Accurate measurement of wide-range power system frequency changes for generator protection*. 1997.
6. Girgis, A.A. and W.L. Peterson, *Adaptive estimation of power system frequency deviation and its rate of change for calculating sudden power system overloads.* Power Delivery, IEEE Transactions on, 1990. **5**(2): p. 585.
7. Karimi, H., M. Karimi-Ghartemani, and M.R. Iravani, *Estimation of frequency and its rate of change for applications in power systems.* Power Delivery, IEEE Transactions on, 2004. **19**(2): p. 472.
8. Kundur, P., N.J. Balu, and M.G. Lauby, *Power system stability and control*. The EPRI power system engineering series. 1994, New York: McGraw-Hill. xxiii, 1176 p.
9. Wood, A.J. and B.F. Wollenberg, *Power generation, operation, and control*. 2nd ed. 1996, New York: J. Wiley & Sons. xv, 569 p.
10. Chapman, S.J., *Electric machinery and power system fundamentals*. McGraw-Hill series in electrical and computer engineering. 2002, Boston: McGraw-Hill. xix, 673 p.
11. Dugan, R.C. and R.C. Dugan, *Electrical power systems quality*. 2nd ed. 2003, New York: McGraw-Hill. xv, 528 p.
12. Tsai, S.S., et al. *Study of global frequency dynamic behavior of large power systems*. 2004.
13. Tsai, S.J.S., et al. *Frequency visualization in large electric power systems*. 2005.
14. Baldwin, M.W., *Modal Analysis Techniques in Wide-Area Frequency Monitoring Systems*, in *Bradley Department of Electrical and Computer Engineering*. 2008, Virginia Tech: Blacksburg.
15. *September 2005 Staged System Tests for Validation of WECC System Performance and Modeling*, J. Hauer, Editor. 2006, Western Electricity Coordinating Council.
16. Litzenberger, W. *A Short History of the Pacific HVDC Intertie*. in *Power Systems Conference and Exposition*. 2006: IEEE.
17. ABB. *The Western USA interconnection (Pacific Intertie)*. 2005 12/7/2005 [cited 2008 2/15/2008]; Available from: www.abb.com.
18. Shelton, M.L., Winkelman, P. F., Mittelstadt, W. A., Bellerby, W. J., *Bonneville Power Administration 1400-MW Braking Resistor*, in *Power Engineering Society*. 1974, IEEE: Anahiem, CA.
19. Samuelsson, O., Hemmingsson, M., Nielsen, A. H., Pederson, K. O. H., Rasmussen, J., *Monitoring of Power System Events at Transmission and Distribution Level.* IEEE Transactions on Power Systems, 2006. **21**(2).
20. Lyon, A.J., *Dealing with data*. 1st ed. 1970, Oxford: Pergamon Press. xvii, 392.
21. Trudnowski, D.J. and J.E. Dagle, *Effects of generator and static-load nonlinearities on electromechanical oscillations.* Power Systems, IEEE Transactions on, 1997. **12**(3): p. 1283.

22. NERC, *Understand and Calculate Frequency Response*. 2003, NERC Training Resources Working Group.
23. YongJune, S., et al. *Time-frequency analysis of power system disturbance signals for power quality*. 1999.
24. Bertsch, J., et al. *Experiences with and perspectives of the system for wide area monitoring of power systems*. 2003.
25. Staudte, R.G. and S.J. Sheather, *Robust estimation and testing*. Wiley series in probability and mathematical statistics. Applied probability and statistics. 1990, New York: Wiley. xix, 351 p.
26. Rousseeuw, P.J. and A.M. Leroy, *Robust regression and outlier detection*. Wiley series in probability and mathematical statistics. Applied probability and statistics,. 1987, New York: Wiley. xiv, 329 p.
27. Hoaglin, D.C., F. Mosteller, and J.W. Tukey, *Understanding robust and exploratory data analysis*. Wiley classics library ed. 2000, New York: Wiley. xx, 447 p.
28. Huber, P.J., *Robust statistics*. Wiley series in probability and statistics. 2004, Hoboken, N.J.: Wiley-Interscience. ix, 308 p.
29. *http://www.census.gov/cgi-bin/gazetteer*. 2005, US Census Bureau.
30. NERC, *Frequency Response Characteristic Survery Training Document*. 1989.
31. Anderson, P.M., *Power system protection*. IEEE Press power engineering series. 1999, New York: McGraw-Hill : IEEE Press. xxviii, 1307 p.
32. Allen, E., Cummings, R., *Personal Communications on EI Frequency Response*. 2007.
33. Parashar, M., *Continuum Modeling of Power Networks*, in *Electrical Engineering*. 2003, Cornell University: Ithaca.
34. Huang, L., *Electromechanical Wave Propagation in Large Electric Power Systems*, in *Bradley Department of Electrical and Computer Engineering*. 2003, Virginia Tech: Blacksburg, VA USA.
35. Zhong, Z. and Y. Liu, *Estimation of Event Location and Tripped Generation of Generator Tripping Fault Based on FNET Frequency Information*, in *Final Report Submitted to ABB/TVA*. 2004, Virginia Tech: Blacksburg.
36. NERC, *Frequency Response Standard Whitepaper*, F.T.F.o.N.R. SubCommittee, Editor. 2004.
37. Ingleson, J.W., Ellis, D.M. *Tracking the Eastern Interconnection Frequency Governing Characteristic*. in *IEEE Power Engineering Society General Meeting*. 2005: IEEE.
38. Milton, J.S. and J.C. Arnold, *Introduction to probability and statistics : principles and applications for engineering and the computing sciences*. 3rd ed. Schaum's solved problems series. 1995, New York: McGraw-Hill. xx, 811 p.
39. Duda, R.O., P.E. Hart, and D.G. Stork, *Pattern classification*. 2nd ed. 2001, New York: Wiley. xx, 654 p.
40. Mili, L., et al., *Robust state estimation based on projection statistics [of power systems].* Power Systems, IEEE Transactions on, 1996. **11**(2): p. 1118-1127.
41. Mili, L., et al., *Robustification of the least absolute value estimator by means of projection statistics [power system state estimation].* Power Systems, IEEE Transactions on, 1996. **11**(1): p. 216-225.
42. Mili, L., et al. *Robust Mahalanobis distances in power system state estimation*. in *Circuits and Systems, 1993., Proceedings of the 36th Midwest Symposium on*. 1993.
43. Rousseeuw, P.J. and K. Van Driessen, *A Fast Algorithm for the Minimum Covariance Determinant Estimator.* Technometrics, 1999. **31**(3): p. 212-223.
44. Rousseeuw, P.J. and B.C. Van Zomeren, *Robust Distances: Simulations and Cutoff Values.* Directions in Robust Statistics and Diagnostics, 1991. **34**: p. 195.

45. Van Cutsem, T., M. Ribbens-Pavella, and L. Mili, *Bad Data Identification Methods In Power System State Estimation-A Comparative Study.* IEEE Transactions on Power Apparatus and Systems, 1985. **PAS-104**(11): p. 3037-3049.
46. Thomas, L. and L. Mili, *A Robust GM-Estimator for the Automated Detection of External Defects on Barked Hardwood Logs and Stems.* Signal Processing, IEEE Transactions on [see also Acoustics, Speech, and Signal Processing, IEEE Transactions on], 2007. **55**(7): p. 3568-3576.
47. Hauer, J., et al., *Keeping an eye on power system dynamics.* Computer Applications in Power, IEEE, 1997. **10**(4): p. 50.
48. Hauer, J.F., *Application of Prony analysis to the determination of modal content and equivalent models for measured power system response.* Power Systems, IEEE Transactions on, 1991. **6**(3): p. 1062.
49. Hauer, J.F., C.J. Demeure, and L.L. Scharf, *Initial results in Prony analysis of power system response signals.* Power Systems, IEEE Transactions on, 1990. **5**(1): p. 80.
50. Hauer, J.F. and F. Vakili, *An oscillation detector used in the BPA power system disturbance monitor.* Power Systems, IEEE Transactions on, 1990. **5**(1): p. 74.
51. Trudnowski, D.J., M.K. Donnelly, and J.F. Hauer, *A procedure for oscillatory parameter identification.* Power Systems, IEEE Transactions on, 1994. **9**(4): p. 2049.
52. Trudnowski, D.J., J.M. Johnson, and J.F. Hauer, *Making Prony analysis more accurate using multiple signals.* Power Systems, IEEE Transactions on, 1999. **14**(1): p. 226.
53. Marple, S.L., *Digital spectral analysis : with applications*. Prentice-Hall signal processing series. 1987, Englewood Cliffs, N.J.: Prentice-Hall. xx, 492 p.
54. Hua, Y., *On Techniques for Estimating Parameters of Exponentially Damped/Undamped Sinusoids in Noise*, in *Electrical Engineering*. 1988, Syracuse Univeristy: Syracuse.
55. Rugh, W.J., *Linear system theory*. 2nd ed. 1996, Upper Saddle River, N.J.: Prentice Hall. xv, 581 p.
56. Franklin, J.N., *Matrix theory*. 1968, Englewood Cliffs, N.J.,: Prentice-Hall. xii, 292 p.
57. Phillips, C.L. and J.M. Parr, *Signals, systems, and transforms*. 2nd ed. 1999, Upper Saddle River, N.J.: Prentice Hall. xxii, 663 p.
58. Parashar, M., J.S. Thorp, and C.E. Seyler, *Continuum modeling of electromechanical dynamics in large-scale power systems.* Circuits and Systems I: Regular Papers, IEEE Transactions on [Circuits and Systems I: Fundamental Theory and Applications, IEEE Transactions on], 2004. **51**(9): p. 1848.
59. Semlyen, A., *Analysis of Disturbance Propagation in Power Systems Based on a Homogeneous Dynamic Model.* Power Apparatus and Systems, IEEE Transactions on, 1974. **93**(2): p. 676-684.
60. Thorp, J.S., et al., *The large scale electric power system as a distributed continuum.* Power Engineering Review, IEEE, 1998. **18**(1): p. 49.
61. Thorp, J.S., C.E. Seyler, and A.G. Phadke, *Electromechanical wave propagation in large electric power systems.* Circuits and Systems I: Fundamental Theory and Applications, IEEE Transactions on [see also Circuits and Systems I: Regular Papers, IEEE Transactions on], 1998. **45**(6): p. 614.
62. Wong, D.Y., et al., *Eigenvalue analysis of very large power systems.* Power Systems, IEEE Transactions on, 1988. **3**(2): p. 472.
63. Sarkar, T.K. and O. Pereira, *Using the matrix pencil method to estimate the parameters of a sum of complex exponentials.* Antennas and Propagation Magazine, IEEE, 1995. **37**(1): p. 48.
64. de Prony, B.G.R., *Essai éxperimental et analytique: sur les lois de la dilatabilité de fluides élastique et sur celles de la force expansive de la vapeur de l'alkool, à différentes températures.* Journal de l'École Polytechnique, 1795. **1**(22): p. 24-76.
65. Hua, Y. and T.K. Sarkar, *Matrix pencil method for estimating parameters of exponentially damped/undamped sinusoids in noise.* Acoustics, Speech, and Signal Processing [see also IEEE Transactions on Signal Processing], IEEE Transactions on, 1990. **38**(5): p. 814.

66. Hua, Y. and T.K. Sarkar, *On SVD for estimating generalized eigenvalues of singular matrix pencil in noise.* Signal Processing, IEEE Transactions on [see also Acoustics, Speech, and Signal Processing, IEEE Transactions on], 1991. **39**(4): p. 892-900.
67. Hua, Y. and T.K. Sarkar. *Matrix pencil method and its performance*. 1988.
68. Hua, Y. and T.K. Sarkar, *Perturbation analysis of TK method for harmonic retrieval problems.* Acoustics, Speech, and Signal Processing [see also IEEE Transactions on Signal Processing], IEEE Transactions on, 1988. **36**(2): p. 228-240.
69. Hua, Y. and T.K. Sarkar, *A perturbation property of the TLS-LP method.* Acoustics, Speech, and Signal Processing [see also IEEE Transactions on Signal Processing], IEEE Transactions on, 1990. **38**(11): p. 2004-2005.
70. Huang, L. and M. Parashar. *Impact of Electromechanical Wave Propagation on Power System Protection and Control*. in *CIGRE conference*. 2001.
71. Abdel-Rahman, K., et al. *Internet based wide area information sharing and its roles in power system state estimation*. 2001.
72. Ingleson, J.W. and D.M. Ellis. *Tracking the Eastern interconnection frequency governing characteristic*. in *Power Engineering Society General Meeting, 2005. IEEE*. 2005.
73. Proakis, J.G. and D.G. Manolakis, *Digital signal processing : principles, algorithms, and applications*. 3rd ed. 1996, Upper Saddle River, N.J.: Prentice Hall. 1 v. (various pagings).
74. Weisstein, E.W. *"Moving Average"*. [cited; Available from: http://mathworld.wolfram.com/MovingAverage.html
75. Mili, L., *Robust Estimation and Filtering (ECE 5714)*. 2005, Virginia Tech.
76. Milton, J.S. and J.C. Arnold, *Introduction to probability and statistics : principles and applications for engineering and the computing sciences*. 3rd ed. Schaum's solved problems series. 1995, New York: McGraw-Hill. xx, 811.
77. Helstrom, C.W., *Probability and stochastic processes for engineers*. 2nd ed. 1991, New York Toronto Canada: Macmillan ; Collier Macmillan Publishers. xi, 610.
78. Bendat, J.S. and A.G. Piersol, *Random data : analysis and measurement procedures*. 2nd ed. 1986, New York: Wiley. xvii, 566.
79. Walpole, R.E. and R.H. Myers, *Probability and statistics for engineers and scientists*. 5th ed. 1993, New York, Toronto, New York: Macmillan ; Maxwell Macmillan Canada ; Maxwell Macmillan International. xiv, 766.
80. Aki, K. and P.G. Richards, *Quantitative seismology : theory and methods*. 1980, San Francisco: W. H. Freeman. 2 v. (xiv, 932, 16).

Appendix I: FDR Information

Unit #:	Name:	Location:	Latitude:	Longitude:
2	University of Missouri, Rolla	Rolla, Missouri	37.9487	-91.7658
3	Advanced Research Institute	Vienna, VA	38.9352	-77.2995
4	Virginia Tech	FNET Lab, VT	37.2327	-80.4284
5	Seattle	Seattle, WA	47.6218	-122.3503
6	ABB	Raleigh, NC	35.8220	-78.6588
7	Mississippi State University	Mississippi State, MS	33.4567	-88.8222
8	EPRI	Palo Alto, CA	37.3992	-122.1394
9	University of Florida	Gainesville, FL	29.6742	-82.3363
10	TVA1-Chattanooga	Chattanooga, TN	35.0662	-85.2570
11	Calvin	Grand Rapids, MI	42.9613	-85.6557
12	Houston	Sugar Land, TX	29.6188	-95.6162
13	Midwest ISO	Carmel, IN	39.9693	-86.1095
14	Arizona State University	Tempe, AZ	33.3884	-111.9306
15	TVA3-Nashville	Nashville, TN	36.1716	-86.7848
16	Los Angeles	Pasadena, CA	34.1427	-118.1325
17	TVA4-Jackson	Jackson, TN	36.1653	-86.7843
21	National Science Foundation (WSU)	Pullman, WA	46.7318	-117.1783
23	Duluth	Duluth, MN	46.7874	-92.0991
25	Enernex	Knoxville, TN	35.9135	-84.0920
27	Rennselear Polytechnic Institute	Troy, NY	42.7312	-73.6842
28	Michigan Electric Transmission Company	Grand Rapids, MI	42.9109	-85.5262
29	Alberta	Alberta, Canada	53.5455	-113.4901
30	Tiffin	Tiffin, OH	41.1133	-83.1778
31	University of Kentucky	Lexington, KY	38.0500	-84.5000
32	TVA7_Hopkinsville	Hopkinsville, KY	36.8216	-87.4745
34	Troy	Troy, NY	42.7312	-73.6842
35	Iowa State University	Ames, IA	42.0228	-93.6502
36	TVA5-Chattanooga	Chattanooga, TN	34.7737	-87.6510
38	New England ISO	Holyoke, MA	42.2135	-72.6424
40	MISO_StPaul	St. Paul, MN	44.9477	-93.1037
41	Winnipeg	Winnipeg, M.B. Canada	49.8107	-97.0836
42	Florida State University	Tallahassee, FL	30.4204	-84.3181
43	MDU_Bismarck	Bismarck, ND	46.8088	-100.7867
500	Chicago	Orland Park, IL	41.5615	-87.8779
502	Toronto	Markham, ON	43.6670	-79.3670
504	Wayne State University	Detroit, MI	42.3562	-83.0703
508	Roanoke Valley Christian Schools	Roanoke, VA	37.2784	-79.9584
509	West Virginia University	Morgantown, WV	39.6460	-79.9728

Unit # (cont'd):	**Name (cont'd):**	**Location (cont'd):**	**Latitude (cont'd):**	**Longitude (cont'd):**
510	Blacksburg	Blacksburg, VA	37.2253	-80.3781
513	Penn State University	University Park, PA	40.7951	-77.8639
514	South Carolina	Simpsonville, SC	34.8050	-82.2546
516	LeRoy	LeRoy, NY	43.1511	-77.7130
518	NERC	Princeton, NJ	40.3556	-74.6128
519	Newport-News	Newport-News, VA	37.0823	-76.4843
523	Tennessee Tech University	Cookeville, TN	36.1756	-85.5076
535	PJM	Norristown, PA	40.1997	-75.5229

Appendix II: WECC Frequency and Voltage Comparison

230 kV PMU Voltage Magnitude Data

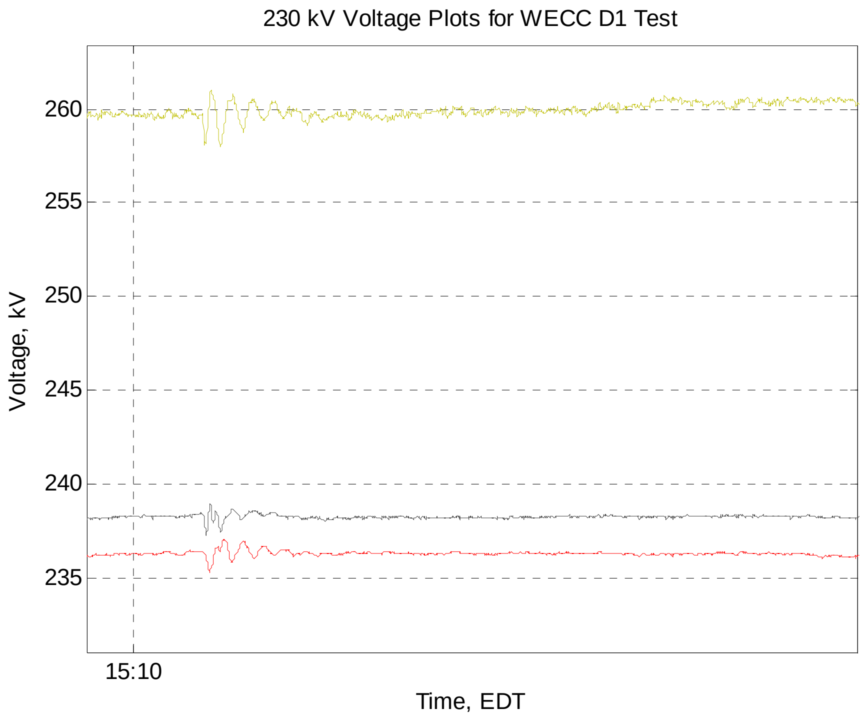

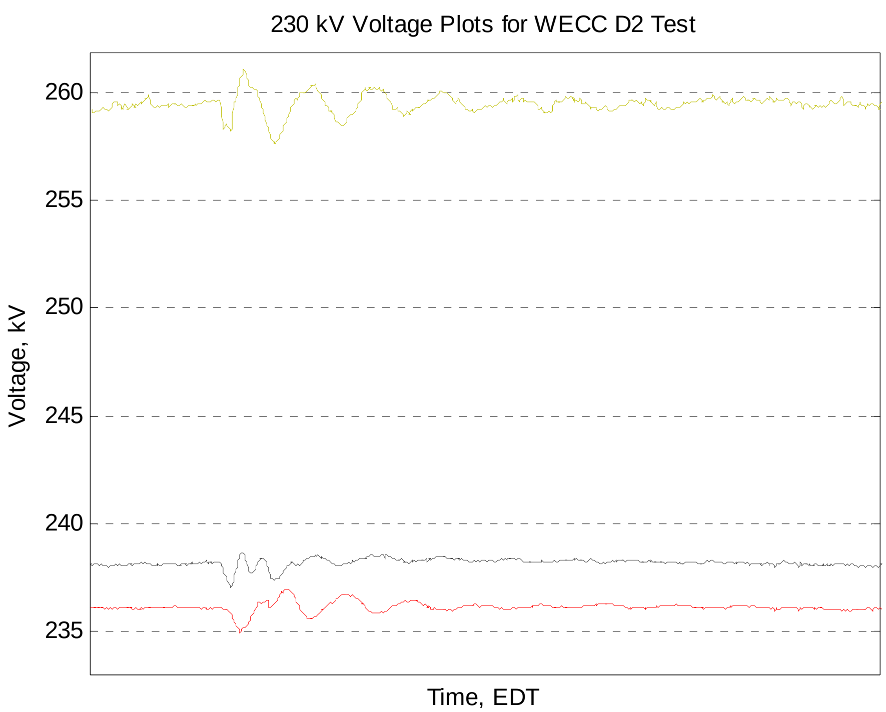

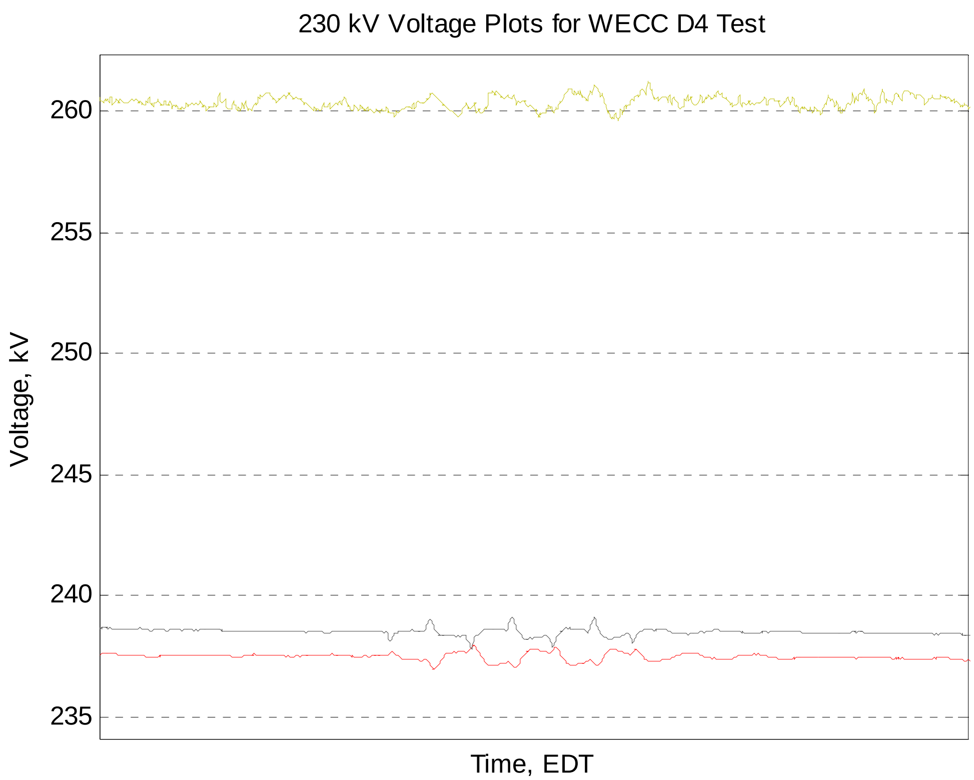
230 kV Voltage Plots for WECC D4 Test
Voltage, kV
260
255
250
245
240
235
Time, EDT

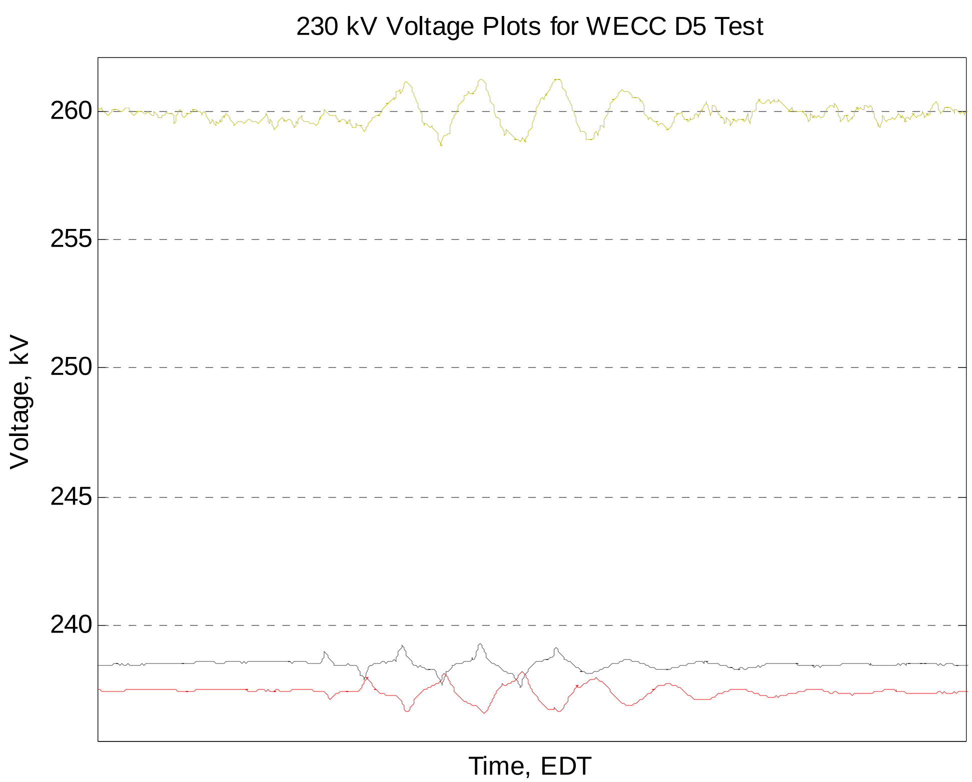
230 kV Voltage Plots for WECC D5 Test
Voltage, kV
260
255
250
245
240
Time, EDT

500 kV PMU Voltage Magnitude Data

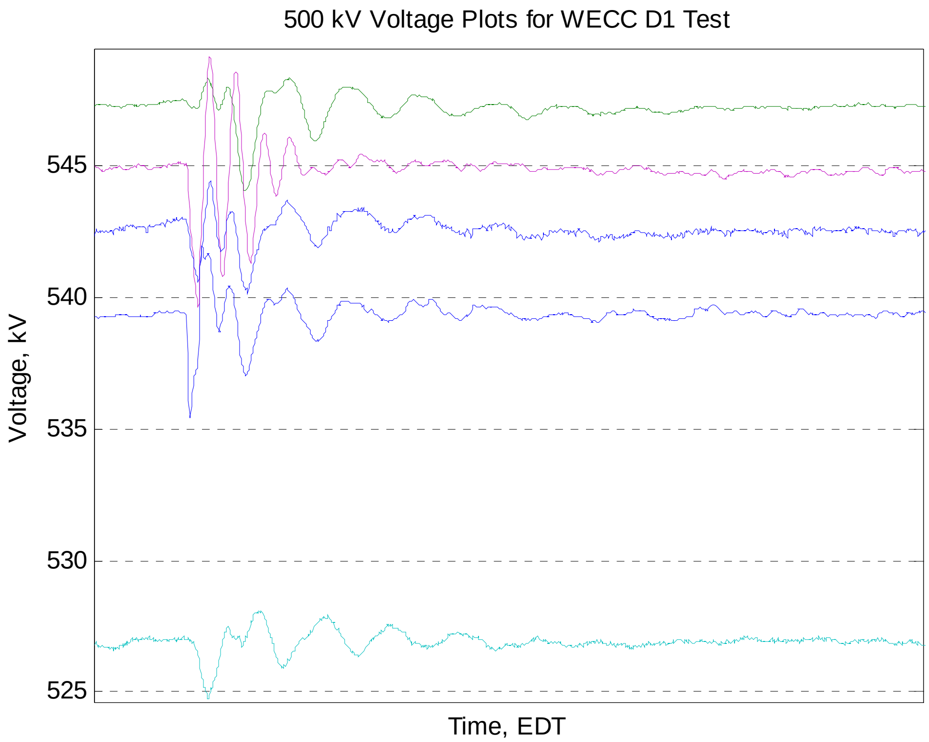

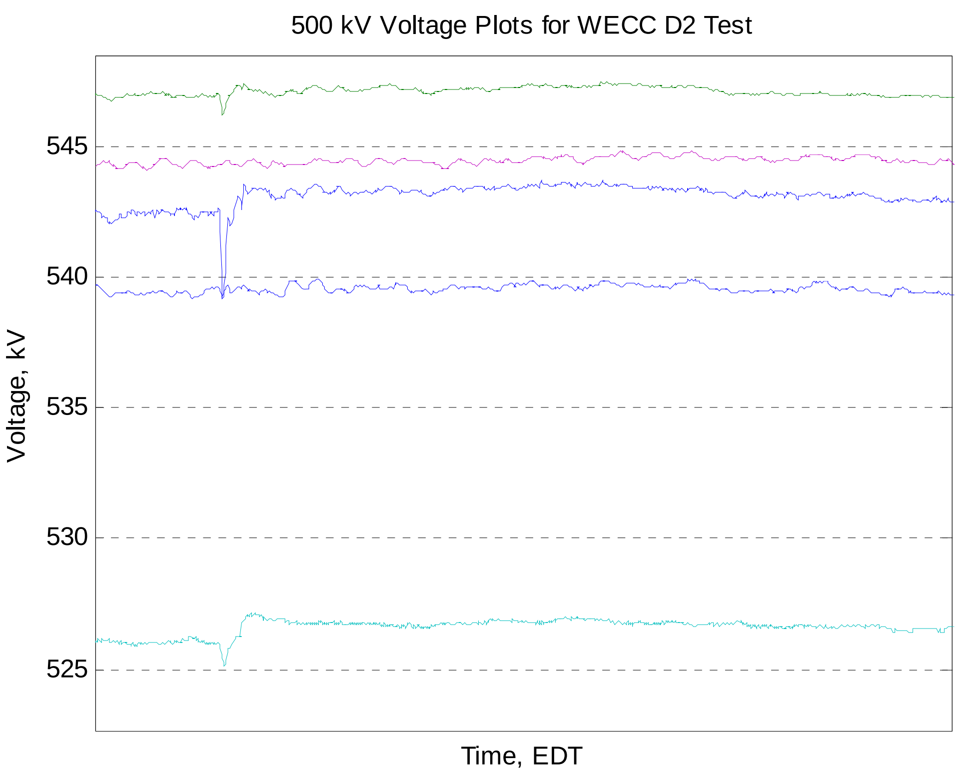

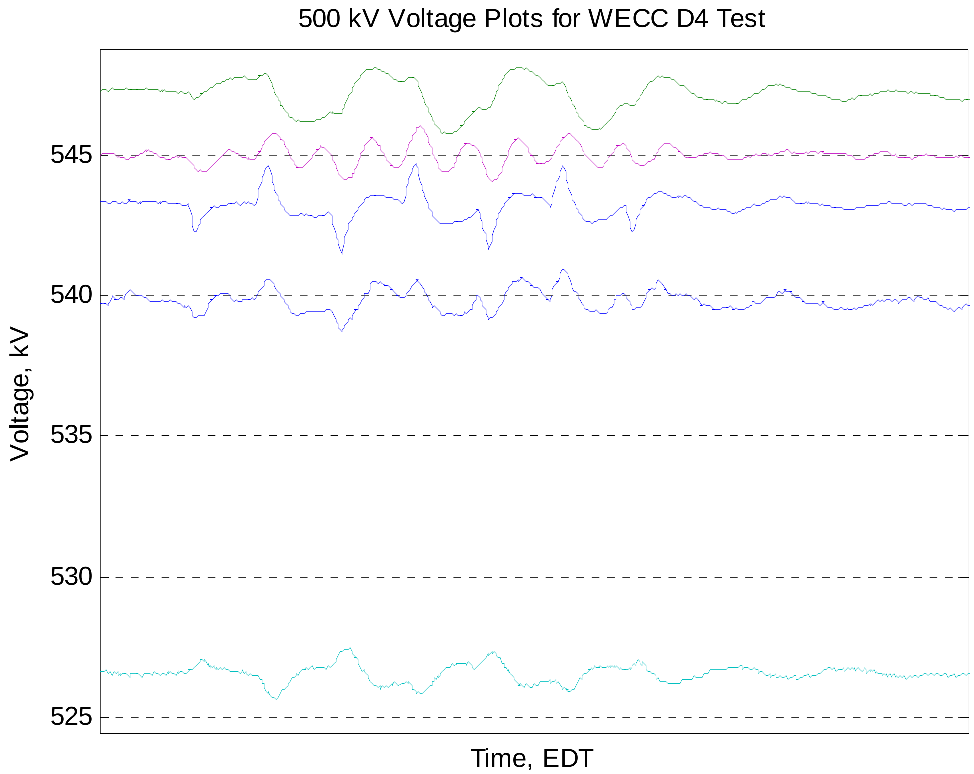
500 kV Voltage Plots for WECC D4 Test
Voltage, kV
545
540
535
530
525
Time, EDT

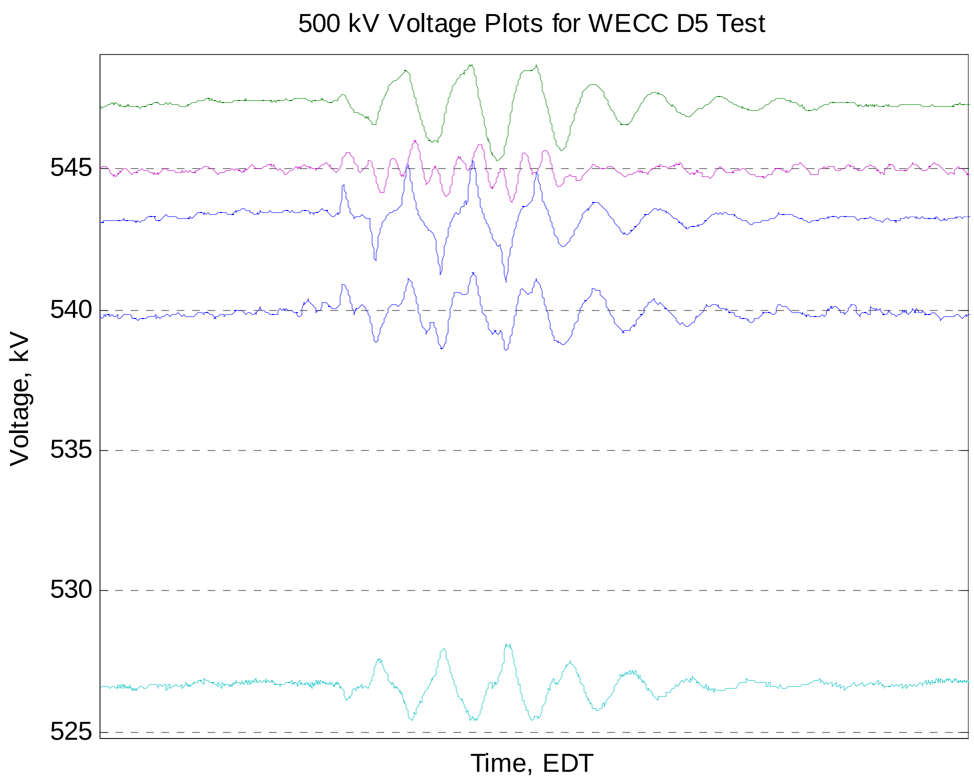
500 kV Voltage Plots for WECC D5 Test
Voltage, kV
545
540
535
530
525
Time, EDT

120 V FDR Voltage Magnitude Data

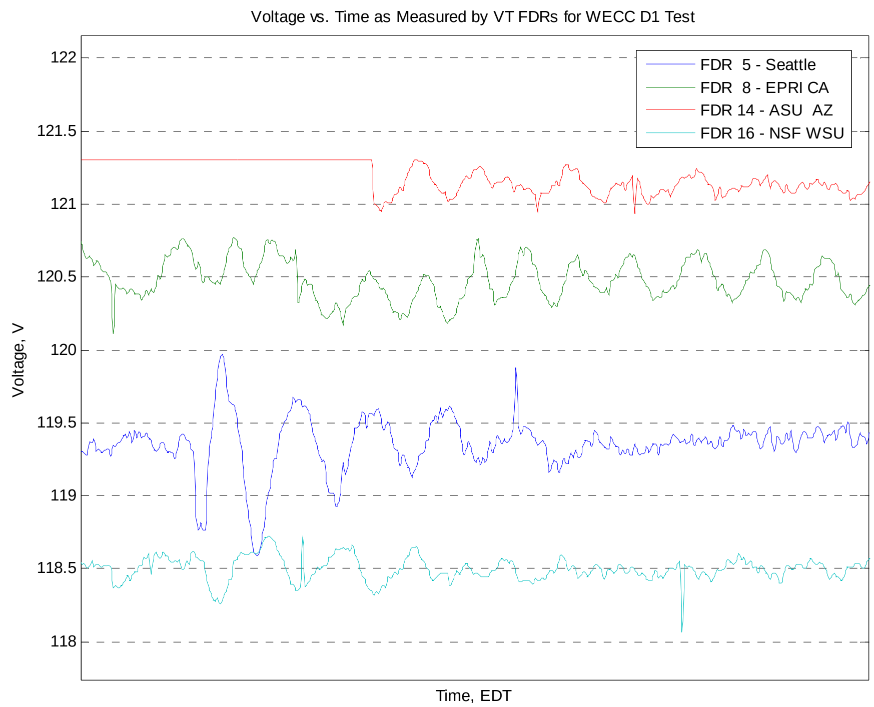

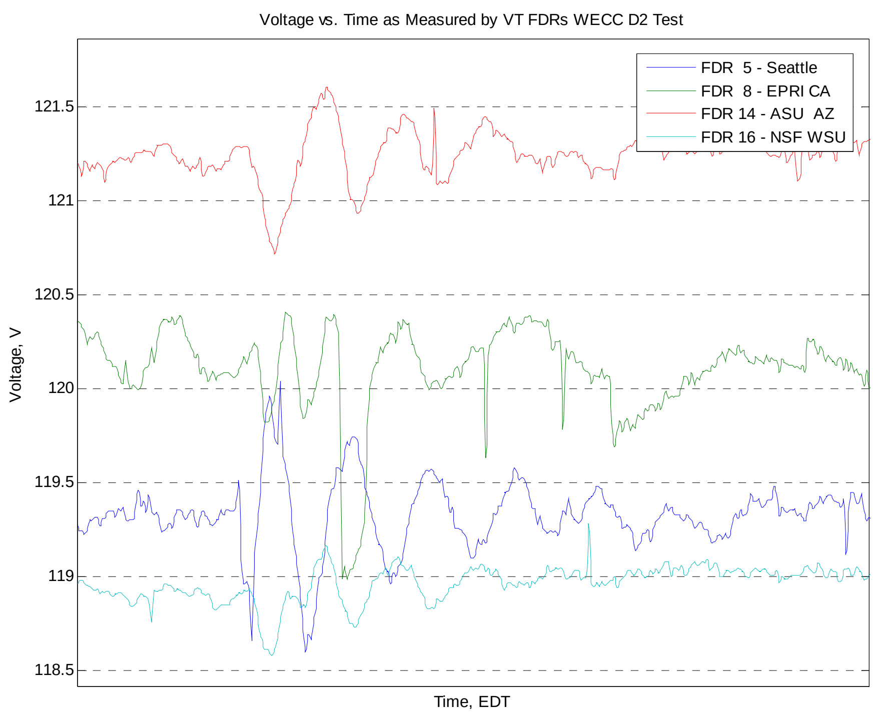

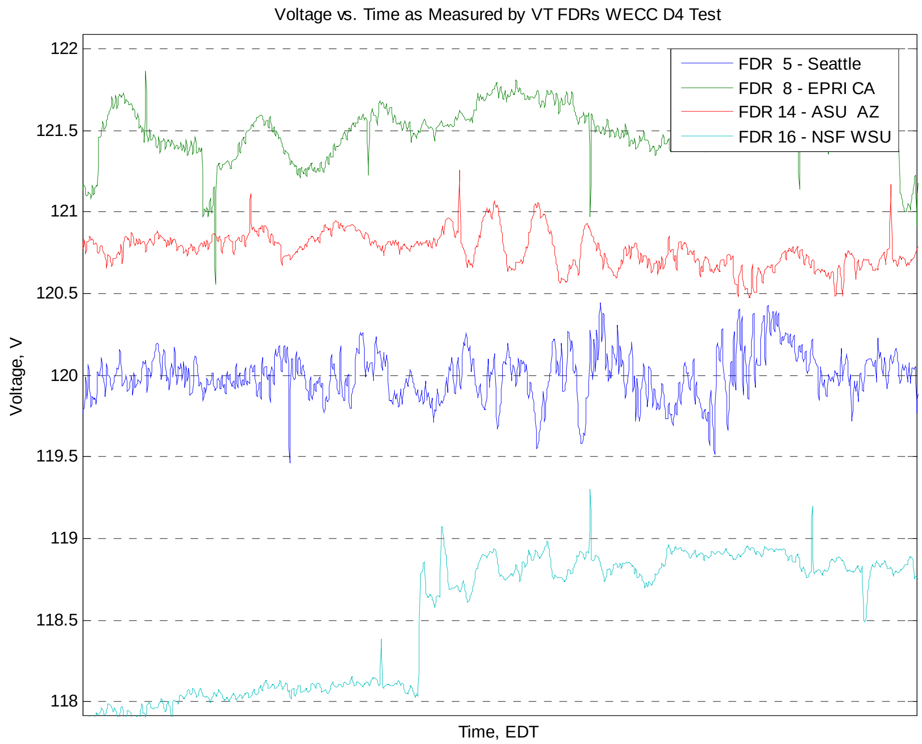

Voltage vs. Time as Measured by VT FDRs WECC D4 Test
FDR 5 - Seattle
FDR 8 - EPRI CA
FDR 14 - ASU AZ
FDR 16 - NSF WSU
Voltage, V
Time, EDT
122
121.5
121
120.5
120
119.5
119
118.5
118

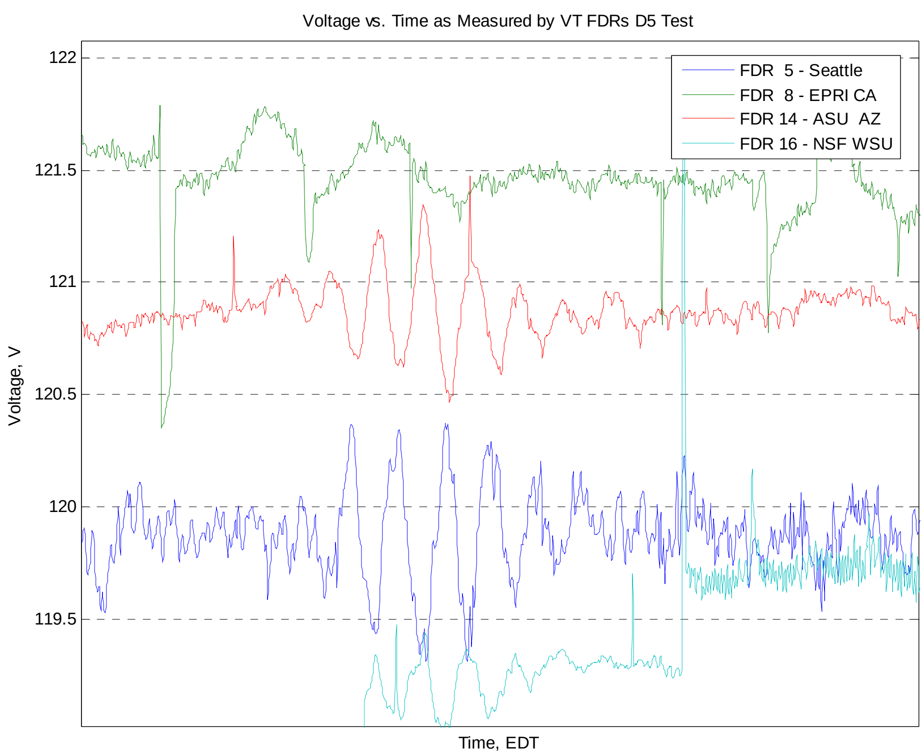

Voltage vs. Time as Measured by VT FDRs D5 Test
FDR 5 - Seattle
FDR 8 - EPRI CA
FDR 14 - ASU AZ
FDR 16 - NSF WSU
Voltage, V
Time, EDT
122
121.5
121
120.5
120
119.5

PMU Frequency Data (230 kV and 500 kV)

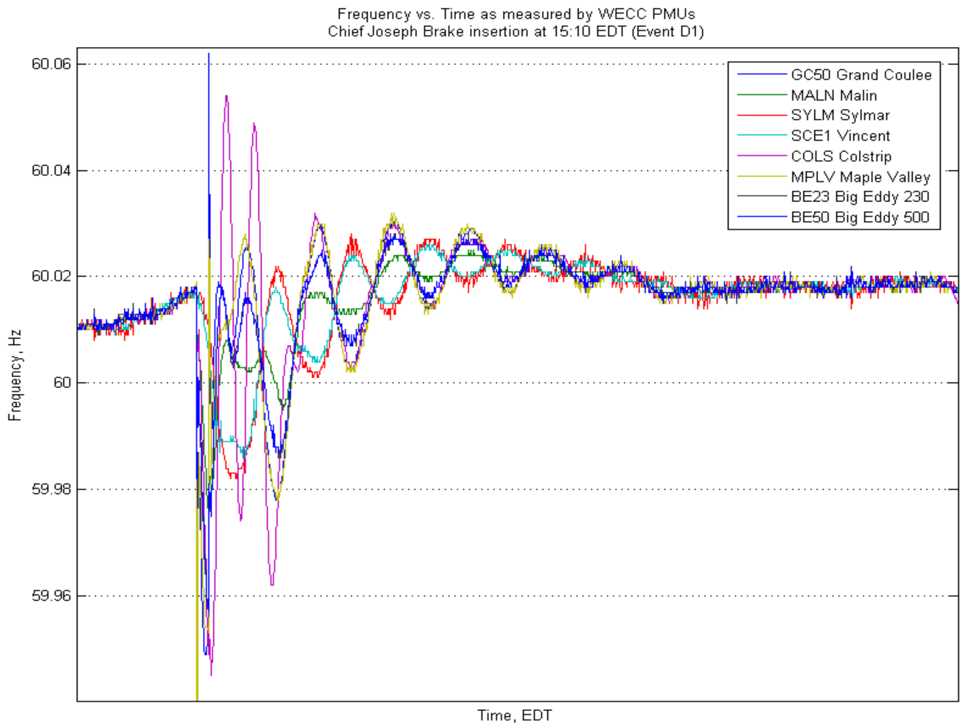

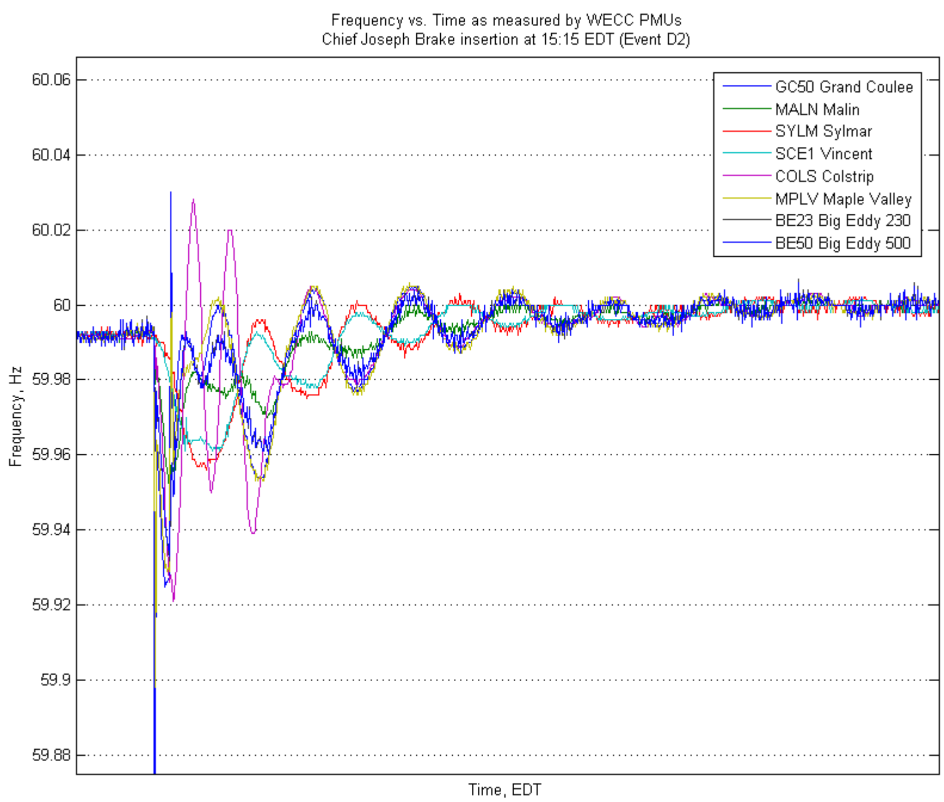

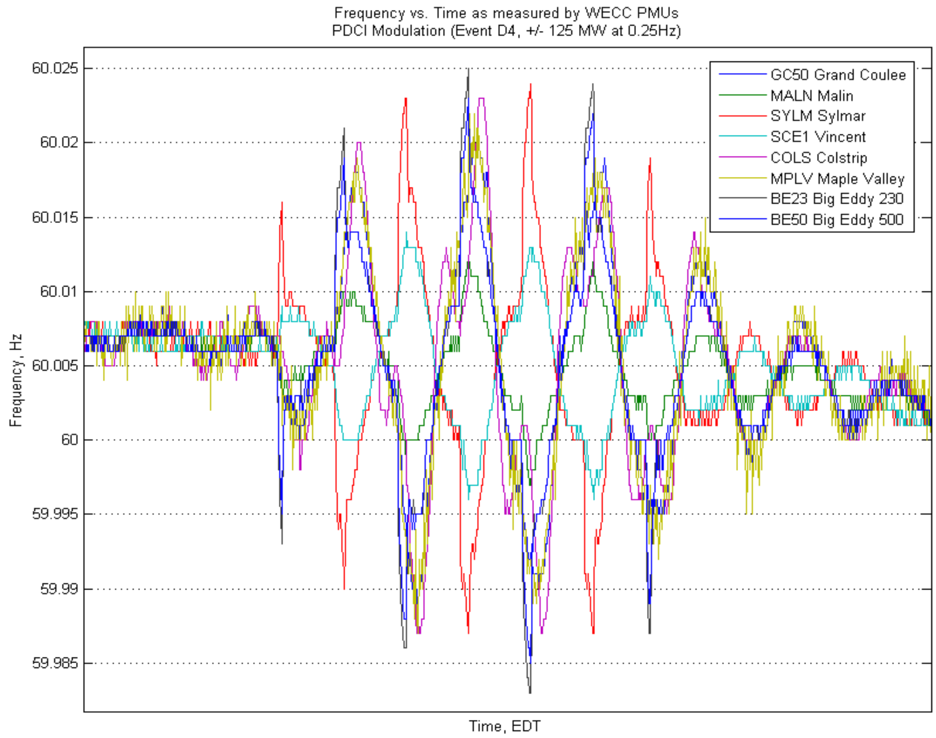
Frequency vs. Time as measured by WECC PMUs
PDCI Modulation (Event D4, +/- 125 MW at 0.25Hz)
60.025
60.02
60.015
60.01
60.005
60
59.995
59.99
59.985
Frequency, Hz
Time, EDT
GC50 Grand Coulee
MALN Malin
SYLM Sylmar
SCE1 Vincent
COLS Colstrip
MPLV Maple Valley
BE23 Big Eddy 230
BE50 Big Eddy 500

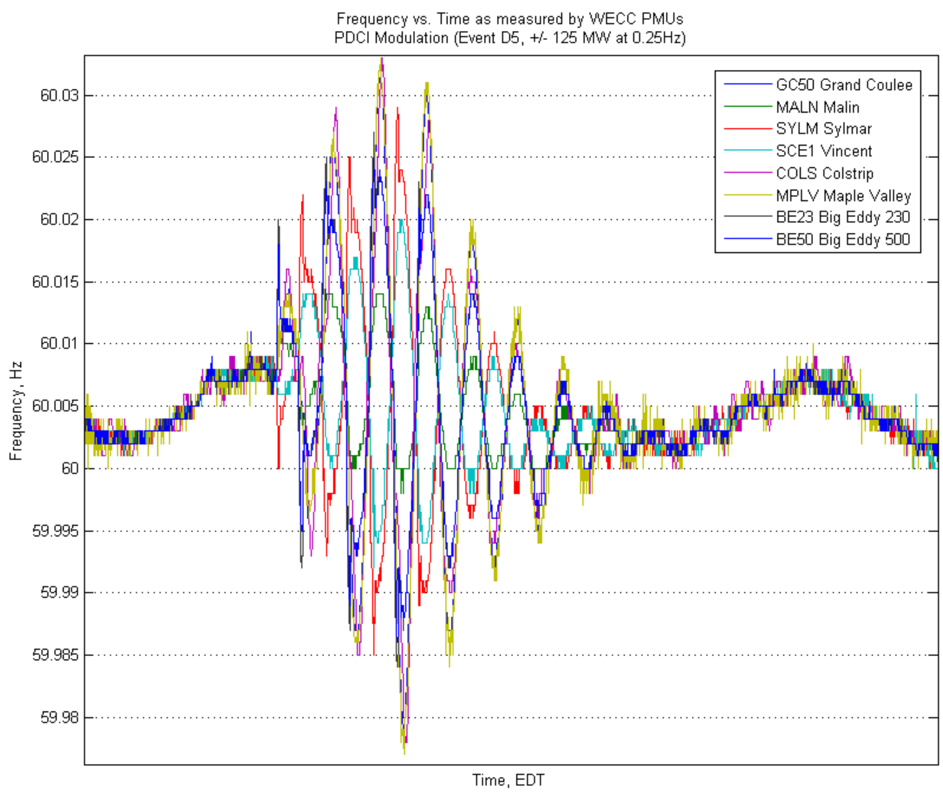
Frequency vs. Time as measured by WECC PMUs
PDCI Modulation (Event D5, +/- 125 MW at 0.25Hz)
60.03
60.025
60.02
60.015
60.01
60.005
60
59.995
59.99
59.985
59.98
Frequency, Hz
Time, EDT
GC50 Grand Coulee
MALN Malin
SYLM Sylmar
SCE1 Vincent
COLS Colstrip
MPLV Maple Valley
BE23 Big Eddy 230
BE50 Big Eddy 500

FDR Frequency Data

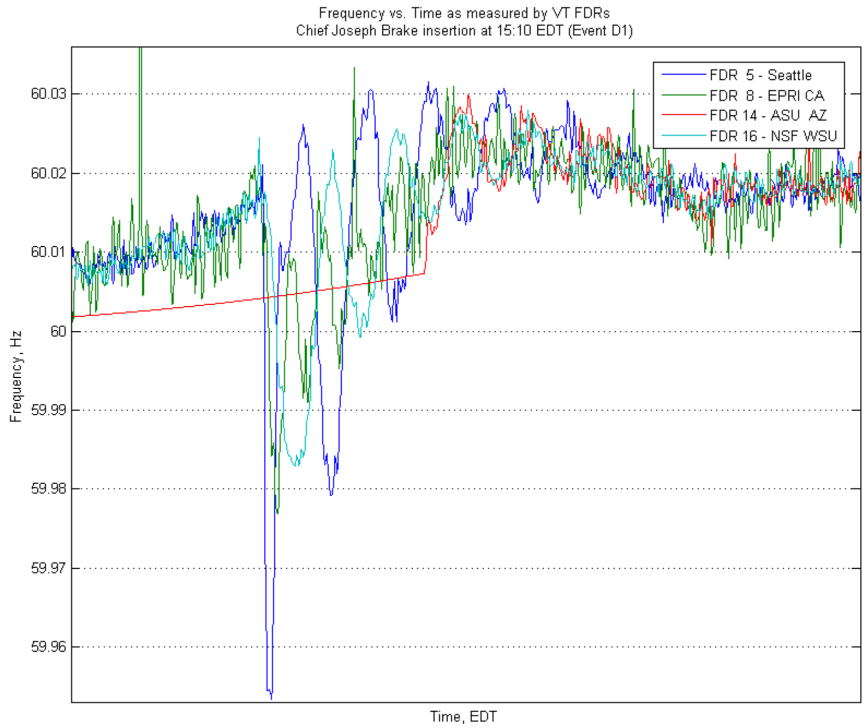

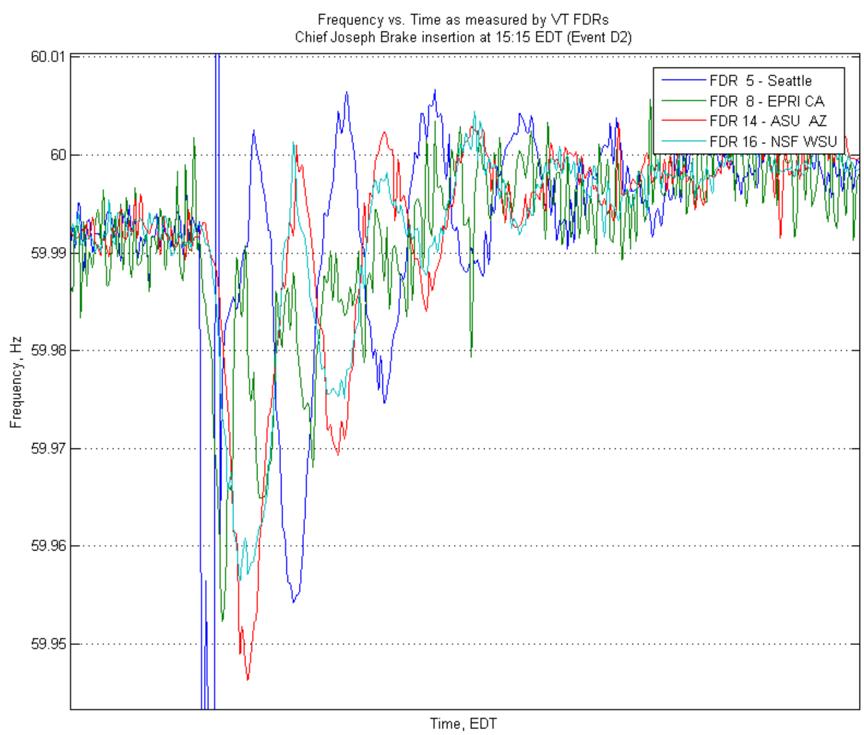

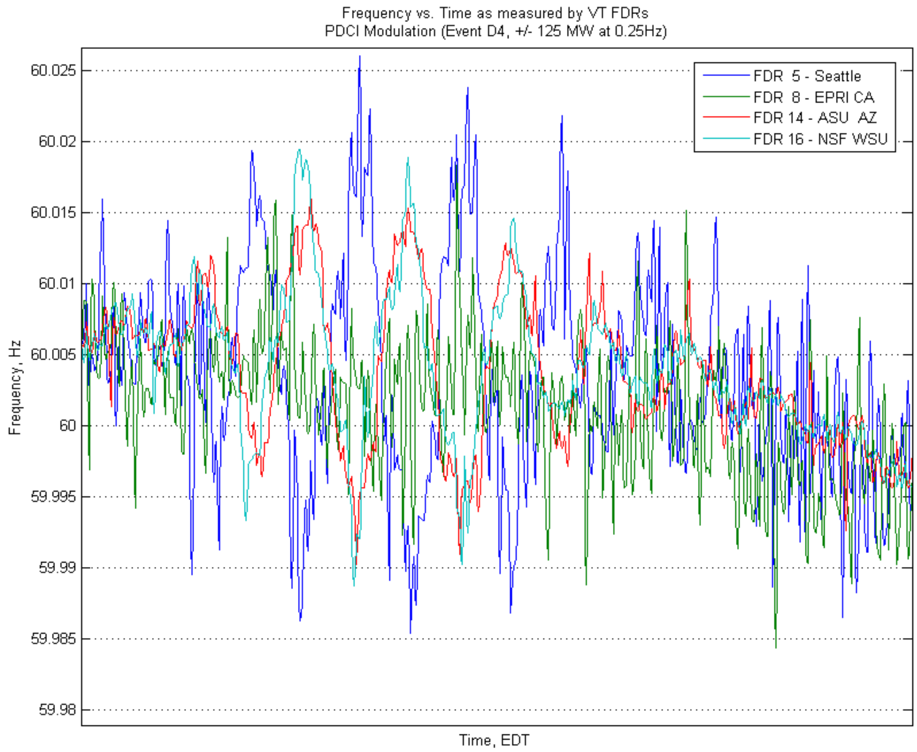
Frequency vs. Time as measured by VT FDRs
PDCI Modulation (Event D4, +/- 125 MW at 0.25Hz)
FDR 5 - Seattle
FDR 8 - EPRI CA
FDR 14 - ASU AZ
FDR 16 - NSF WSU
60.025
60.02
60.015
60.01
60.005
60
59.995
59.99
59.985
59.98
Frequency, Hz
Time, EDT

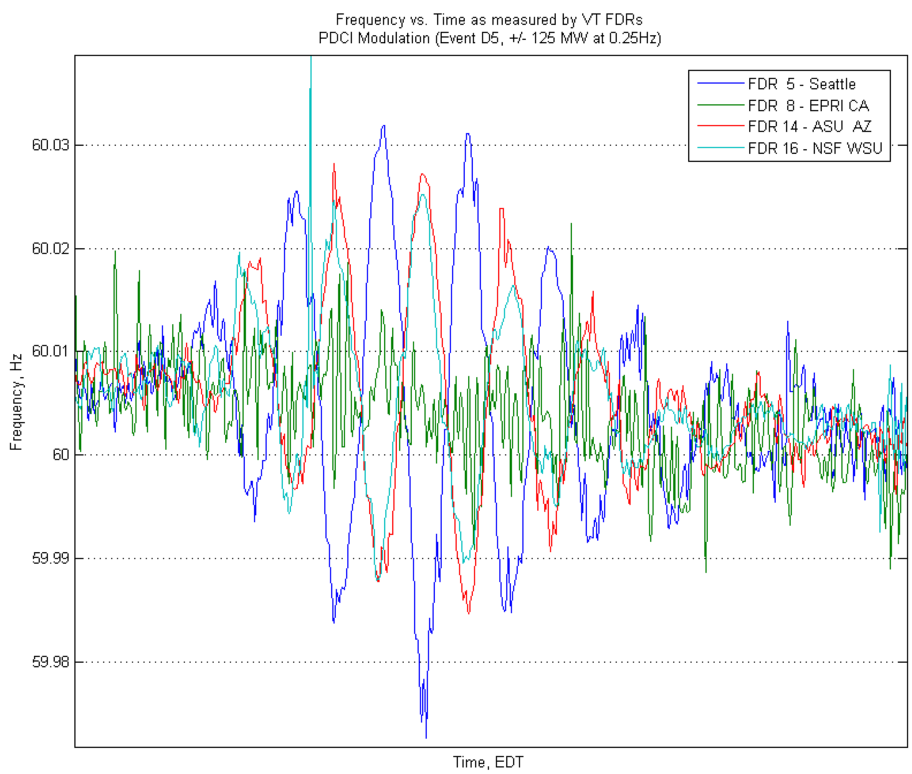
Frequency vs. Time as measured by VT FDRs
PDCI Modulation (Event D5, +/- 125 MW at 0.25Hz)
FDR 5 - Seattle
FDR 8 - EPRI CA
FDR 14 - ASU AZ
FDR 16 - NSF WSU
60.03
60.02
60.01
60
59.99
59.98
Frequency, Hz
Time, EDT

Comparison betwixt PMU and FDR Data Frequency Data

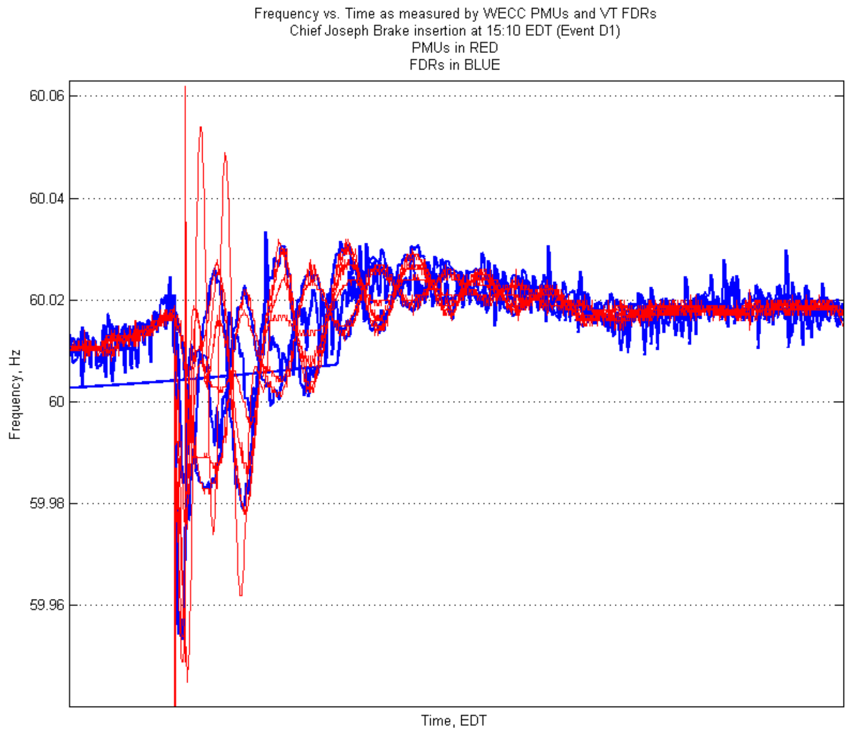

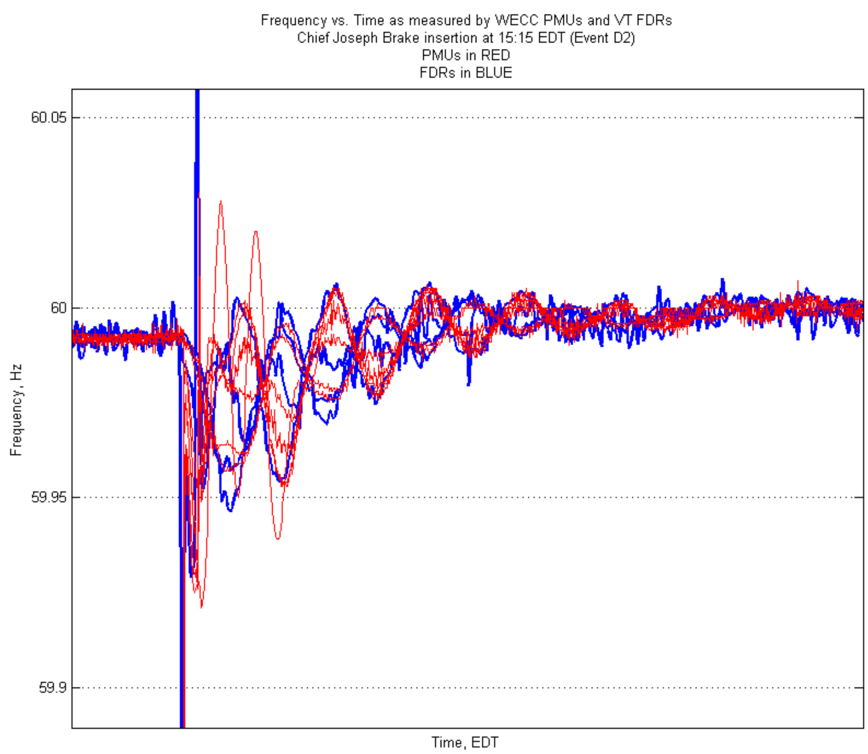

Frequency vs. Time as measured by WECC PMUs and VT FDRs
PDCI Modulation (Event D4, +/-125 MW at 0.25 Hz)
PMUs in RED
FDRs in BLUE

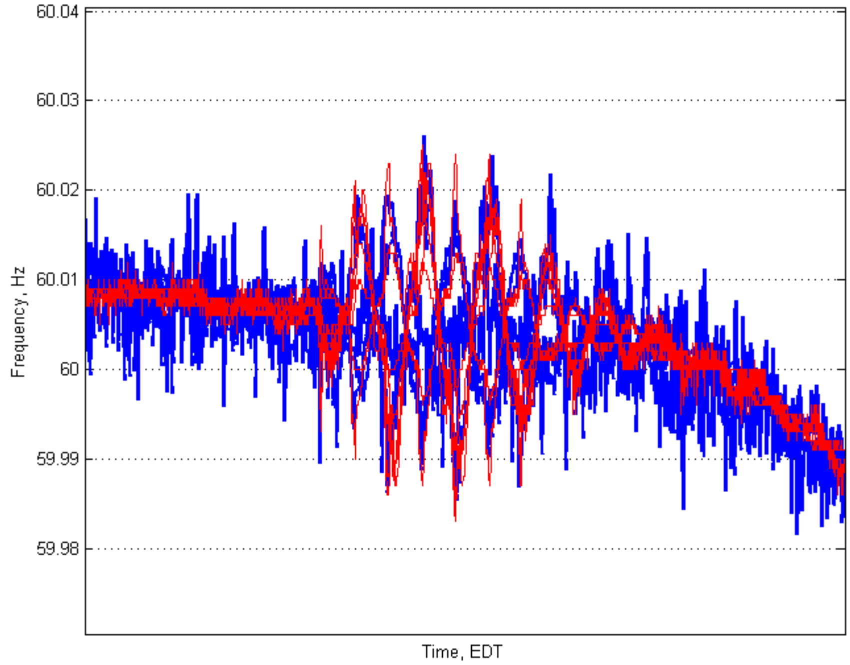

Frequency vs. Time as measured by WECC PMUs and VT FDRs
PDCI Modulation (Event D5, +/-125 MW at 0.25 Hz)
PMUs in RED
FDRs in BLUE

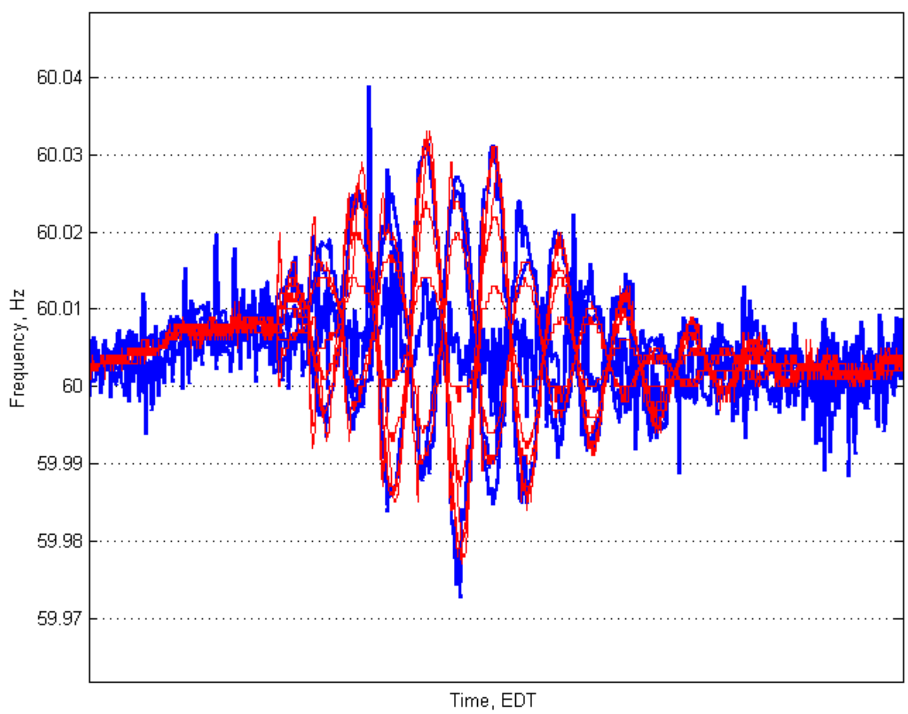

Appendix III: Basic Data Filtering

The purpose of this appendix is to reveal some of the basic aspects of filtering used within this report. The moving average filter and moving median filters are typically used within the report as smoothing filters and low-pass filters. Window sizes were chosen based upon the frequency responses needed for various applications. For example a window size of 31 points for wide-area frequency data sampled at 10 Hz has been found adequate for the removal step generation-load mismatch event signatures. The frequency response properties of the following filters are well documented and shall be treated only briefly here [73]. Figure III-1 gives a few frequency response plots for filters commonly used within the body of the report.

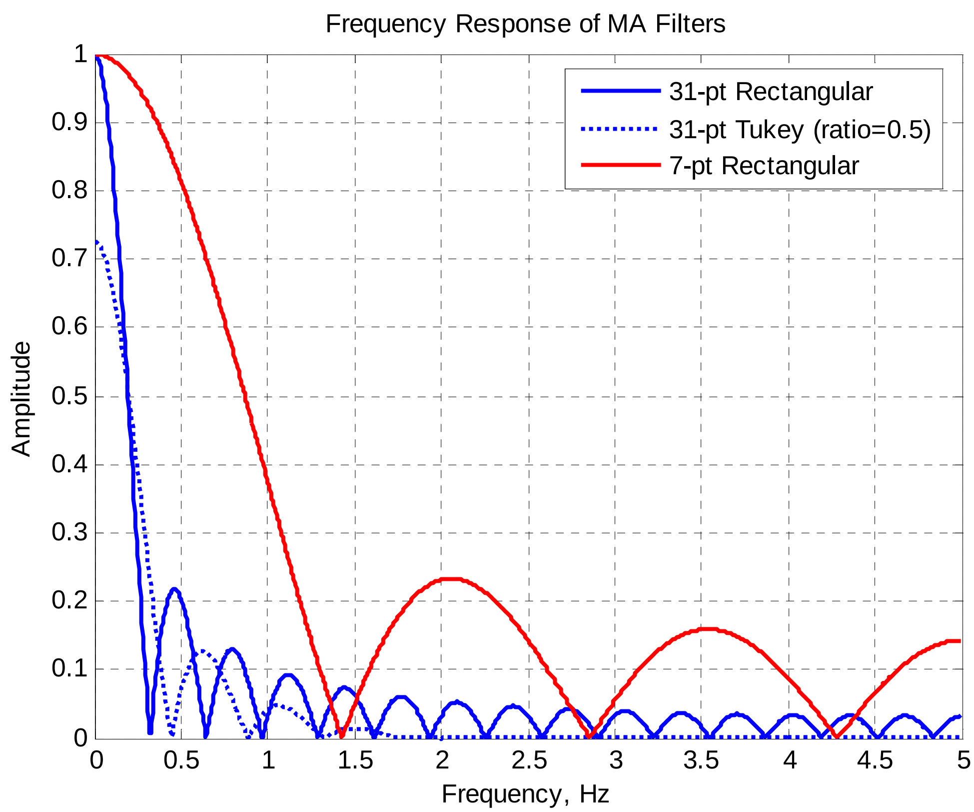

Figure III-1: Frequency response of filters commonly used within this report for processing of FNET data.

The Moving Average

One method used to estimate the true value of the frequency, f_t, measured by each individual FDR is the "moving average" or "moving mean" [35]. The moving mean is defined as follows [74]: given a sequence $\{f_i\}_{i=1}^{N}$, an n-moving mean is another sequence $\{\bar{f}_i\}_{i=1}^{N-n+1}$ defined from f_i by taking the mean as:

$$\bar{f}_i = \frac{1}{n}\sum_{j=1}^{i+n-1} f_j$$

Thus the estimate of the true value of the frequency is defined as:

$$\hat{f}_t \equiv \left\{\bar{f}_i\right\}_{i=1}^{N-n+1}$$

Although the actual true value of the frequency f_t only exists in theory. This approach estimates f_t and we write this value as $\hat{f}_t$. The moving mean is actually a moving least squares estimator that minimizes the following objective function:

$$\phi(f_t) = \sum_{i=1}^{n} r_i^2 = \sum_{i=1}^{n}(f_i - f_t)^2$$

It is important to note that the least squares (LS) estimator is the maximum (ML) likelihood, or optimal, estimator of normally distributed data [75]. Normal, or Gaussian, distributed data has a probability density function of the form [76-78]:

$$f(x) = \frac{1}{\sigma\sqrt{2\pi}} e^{-\frac{(x-\mu)^2}{2\sigma^2}}$$

And can be viewed pictorially as:

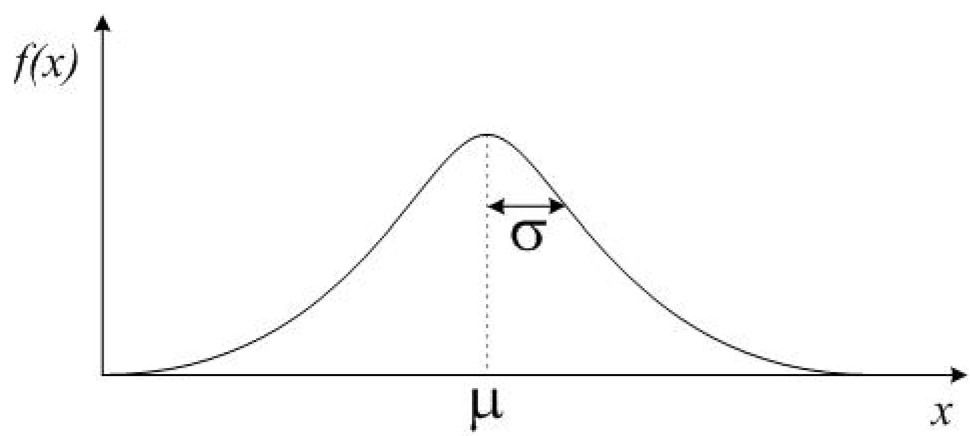

Figure III-2: The Gaussian distribution.

The following figure shows an example of raw frequency data, f, and the estimate of the true value using the moving mean, $\hat{f}_t$.

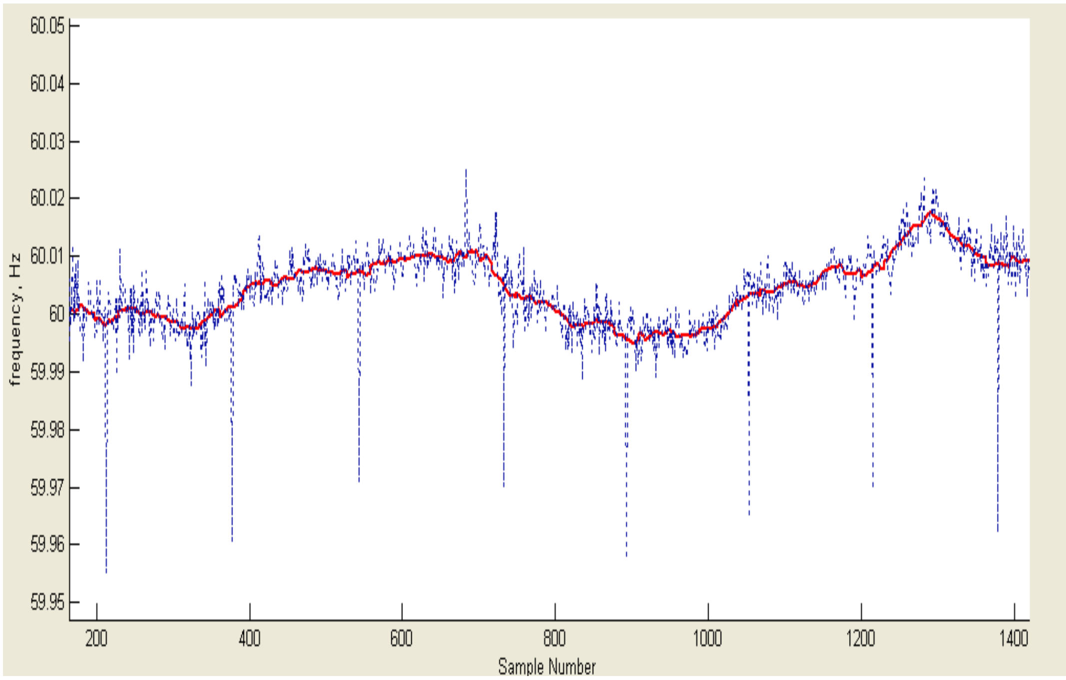

Figure III-3: Raw FDR data plotted with moving mean.

The above figure shows both the raw FDR data plotted in blue and the moving mean plotted in red. A window size of 30 ($n = 30$) has been selected for the computation of the moving mean. From this figure the smoothing capabilities of the moving mean are evident and, at first glance, this method looks an excellent estimator of true value of the frequency. However, let us introduce a disturbance, not unlike one that might result from an actual scenario, and examine the moving mean closer. In the next figure, the actual data has been perturbed by adding eight data points at 59.9 Hz near one another. It is clearly visible, that the moving mean is not robust against these outliers because the mean is also perturbed. The mean is perturbed because we are breaking from Gaussianity by adding outliers that are common to real data. As can be seen from Figure III-2, the Gaussian distribution has relatively thin tails and such outliers as added are not accommodated by the tails in the distribution. Therefore the LS estimator which is optimal at the Gaussian distribution will break down when non-Gaussian data is introduced.

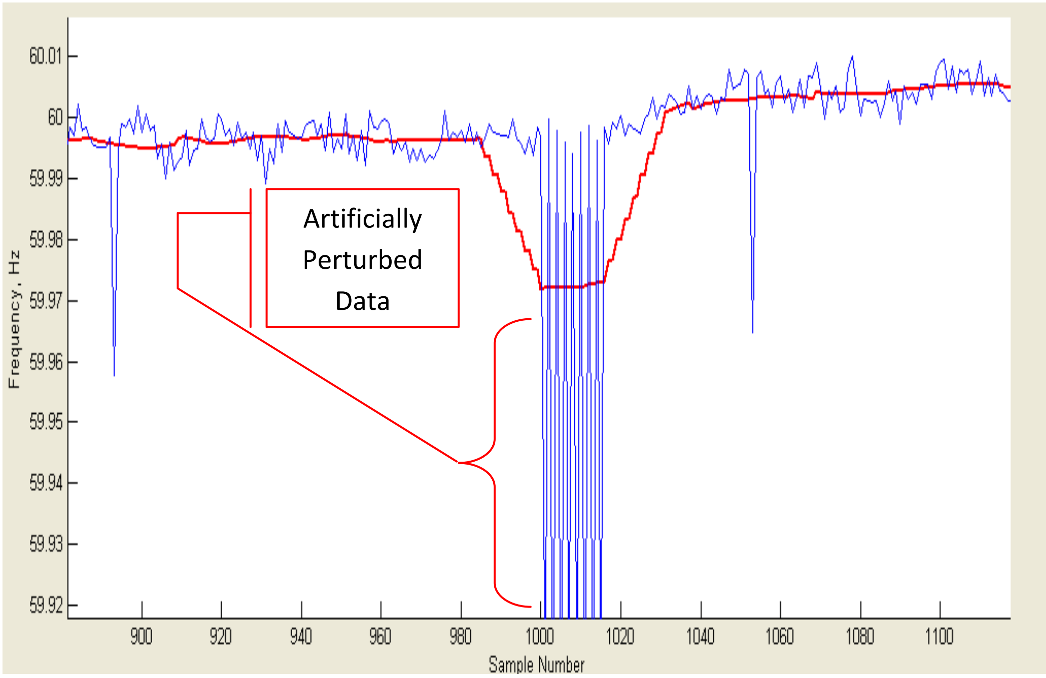

Figure III-4: Raw perturbed data plotted with moving mean.

In the figure above, the data plotted in blue is the raw data and the data plotted in red is the moving mean with a window size of 30. Such a disturbance that lasts less than two seconds is not uncommon at the distribution level [11]. We seek an estimator of f_t that is robust against such common occurrences of outliers. We turn from classical statistics to robust statistics for the solution [25, 26].

To calculate the frequency response of the moving average (MA) filter, we present the discrete-time Fourier transform (DTFT) as follows:

$$H(\omega) = \sum_{n=-\infty}^{\infty} h(n)e^{-j\omega n}$$

where $h(n)$ is the impulse response of the of our filter. For example, an L-point MA filter will have an impulse response defined by:

$$h(n) = \begin{cases} \frac{1}{L} & \text{if } n = 0,1,\cdots,L-1 \\ 0 & \text{otherwise} \end{cases}$$

For our common 31-point MA filter, $L = 31$. The MA filter is actually a finite impulse response (FIR) filter since the output of the filter will eventually decay to zero after being excited by a Kronecker delta function. This feature of the MA filter is perhaps intuitive after realizing that the simple MA filter is an all-zero filter (no internal feedback, compare to autoregressive, AR, and autoregressive moving average, ARMA, filters, etc.). Since the MA filter is in fact an FIR filter we can reduce the infinite sum of the DTFT as follows:

$$H(\omega)=\frac{1}{L}\sum_{n=0}^{L-1}e^{-j\omega n}$$

We now employ the following identity:

$$\sum_{n=N}^{M}a^{n}=\frac{a^{N}-a^{M+1}}{1-a}$$

to compute:

$$H(\omega)=\left(\frac{1}{L}\right)\left(\frac{1-e^{-j\omega L}}{1-e^{-j\omega}}\right)$$

given that:

$$\begin{aligned}a&=e^{-j\omega}\\N&=0\\M&=L-1\end{aligned}$$

We now can compute the frequency response of the filters used in this report by plotting $\left\|H\left(\omega\right)\right\|$ versus ω scaling the abscissa by the sampling frequency of data (in our case, $f_s=10\text{ Hz}$). Re-examine Figure III-1. For oscillation analysis, as discussed in Chapter 3, band-pass filters are employed. Figure III-5 shows the frequency response of a band-pass filter constructed using parallel (and properly delayed) MA filters. The band-pass properties of the MA filter leave significant room for improvement. However, for purposes of speed and ease of implementation, we consider these filters to be satisfactory.

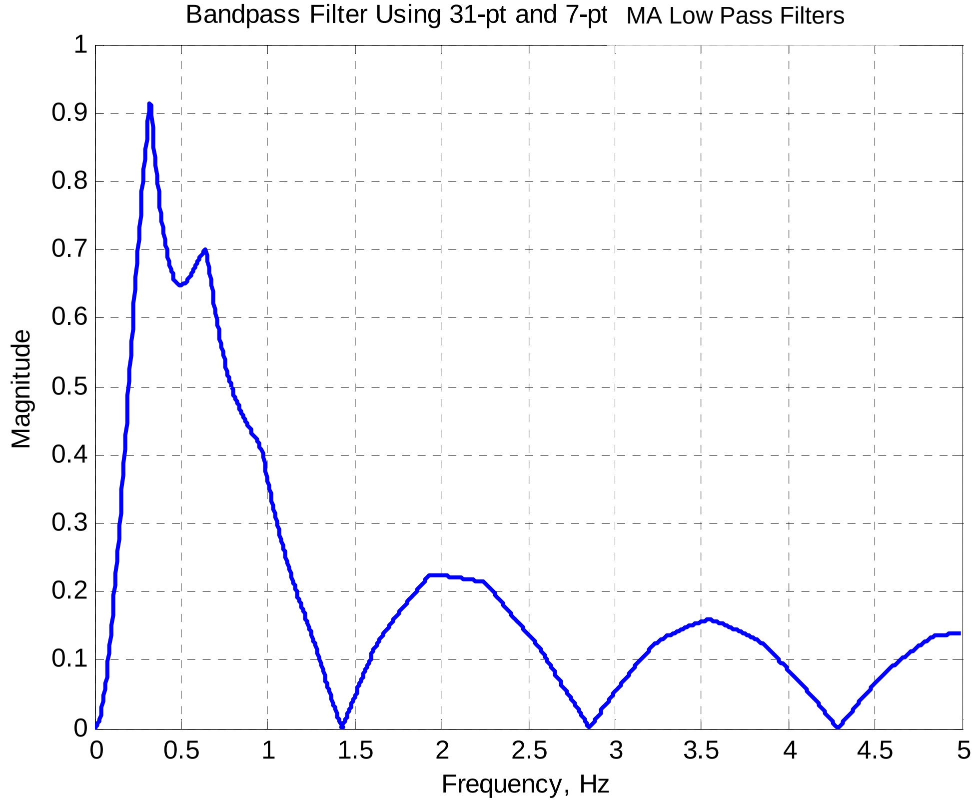

Figure III-5: Band-pass frequency response using MA filtering.

The Moving Median

We define the moving median in much the same way as the moving mean. The concept of a moving window each encompassing 30 elements remains the same but the mean is replaced with the median. In closed form, the moving median is defined: given a sequence $\{f_i\}_{i=1}^{N}$, an *n*-moving median is another sequence $\{\bar{f}_i\}_{i=1}^{N-n+1}$ defined from f_i by taking the median as [74, 76, 79]:

$$\bar{f}_i = \text{median}[f_i, f_{i+1}, \cdots, f_{i+n-1}]$$

The estimation of the true value of the frequency can then be defined as:

$$\hat{f}_t \equiv \{\bar{f}_i\}_{i=1}^{N-n+1}$$

The moving median is the ML estimator of the Laplacian or Double-Exponential distribution which minimizes the L_1 norm given by [75]:

$$\phi(f_t) = \sum_{i=1}^{n} |f_i|$$

And the probability density function of the Laplacian distribution is given by [75-78]:

$$f(x) = \frac{1}{2a} e^{-\frac{|x-b|}{a}}$$

The following figure presents the Laplacian distribution pictorially. Notice that the Laplacian distribution has thicker tails than those of the Gaussian distribution.

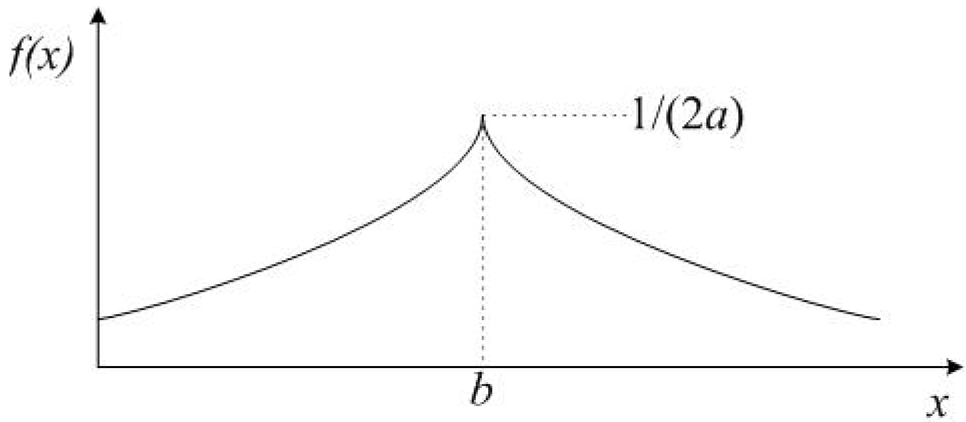

Figure III-6: The Laplacian Distribution

The following figure shows a sample of perturbed FDR data plotted along with both the moving mean and the moving median. The raw data is plotted in blue, the moving mean in red, and the moving median in green. From this figure the robustness of the moving median becomes evident as the moving median is not at all perturbed by the simulated disturbance. The thicker tails in the Laplacian distribution allow for the greater possibility of outliers and thus the moving median does not break down when outliers are present. The "ride-through" capability of the median is quite desirable for our application, thus we shall consider the moving median as a viable, though not as computationally efficient, replacement of the moving mean.

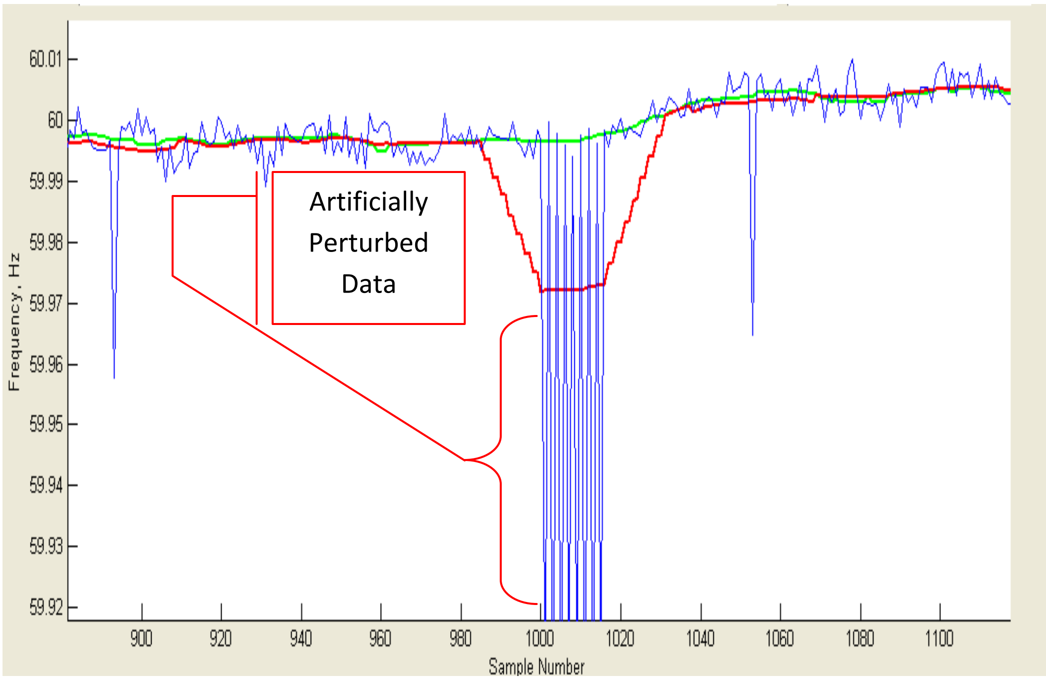

Figure III-7: Raw perturbed data with moving mean and moving median.

The frequency response of the median filter is not calculable in the same manner as the MA filter given the fact that the moving median filter is, in fact, a non-linear filter. Therefore, the filter parameter, or window size is obtained empirically.

Appendix IV: Scenario Information

Fuel Type:	Plant:	Date:	Time (UTC):	MW Est.:	Latitude:	Longitude:	Data Found?	Bus Found?
	Lacygne	1/2/2007	17:16:32	604	38.3335	-94.7608	Yes	Yes
Nuclear	North Anna	1/3/2007	23:03:27	905	37.99861	-77.8781	Yes	Yes
Nuclear	Browns Ferry	1/11/2007	14:18:45	1019	34.70549	-87.1173	Yes	Yes
Coal	Paradise	1/24/2007	14:56:01	921	37.25782	-86.9792	Yes	Yes
Coal	W H Zimmer	1/25/2007	22:07:29	694	39.05232	-84.1505	Yes	Yes
Nuclear	Summer	2/5/2007	8:07:40	865	34.27169	-81.2712	Yes	Yes
Nuclear	Oconee U1&U2	2/15/2007	21:54:10	1385	34.75382	-83.0674	Yes	Yes
Nuclear	Indian Point	2/28/2007	11:33:50	955	41.26966	-73.9524	Yes	Yes
Nuclear	Sequoyah	3/13/2007	19:27:12	1181	35.22723	-85.0943	Yes	Yes
	Conemaugh	3/16/2007	7:18:31	657	40.38227	-79.0968	Yes	Yes
	Gentleman	3/18/2007	4:06:43	771	41.15575	-101.136	No	Yes
Coal	Gavin 1	3/31/2007	2:39:56	1487	38.95868	-82.1235	No	Yes
Nuclear	Vogtle Unit 2	4/23/2007	14:25:30	770	33.0894	-81.978	Yes	Yes
Nuclear	Salem Unit 1	4/30/2007	19:02:50	706	39.4956	-75.4733	Yes	Yes

Fuel Type:	Plant:	Date:	Time (UTC):	MW Est.:	Latitude:	Longitude:	Data Found?	Bus Found?
	Mitchell Unit 2	5/1/2007	0:24:37	639	39.91482	-80.731	No	Yes
Coal	Coal Creek	5/6/2007	7:54:50	598	47.46016	-101.19	Yes	Yes
Nuclear	Palisades	5/8/2007	17:23:42	902	42.2857	-86.2695	Yes	Yes
coal	Council Bluffs	5/10/2007	17:54:46	786	41.2146	-95.8574	Yes	Yes
Coal	Brunner Island 3	5/12/2007	2:36:46	598	40.12215	-76.7737	No	Yes
Coal	Sherburne	5/14/2007	14:21:02	738	45.43654	-93.841	Yes	Yes
Nuclear	Grand Gulf	5/19/2007	16:27:12	808	31.9266	-91.023	Yes	Yes
Nuclear	Salem Unit 2	5/24/2007	6:32:29	765	39.4956	-75.4733	Yes	Yes
Coal	Dolet Hills	5/25/2007	11:36:41	609	32.0037	-93.6731	Yes	Yes
Coal	Petersburg	5/29/2007	2:26:46	578	38.4723	-87.3105	No	Yes
Coal	Keystone	6/9/2007	5:59:25	908	40.63879	-79.3191	Yes	Yes
Nuclear	Browns Ferry Unit 1	6/9/2007	16:00:34	742	34.70549	-87.1173	Yes	Yes
	Belews Creek U1	6/12/2007	15:40:52	870	36.31887	-80.1484	Yes	Yes
	Iatan	6/16/2007	4:50:52	697	39.44529	-94.9145	No	Yes
	Belews Creek U2	6/19/2007	5:09:01	693	36.31887	-80.1484	Yes	Yes
	Cumberland	6/23/2007	14:23:10	1052	36.38453	-87.6569	No	Yes
Nuclear	Braidwood	6/27/2007	14:21:13	875	41.22879	-88.269	Yes	Yes

Fuel Type:	Plant:	Date:	Time (UTC):	MW Est.:	Latitude:	Longitude:	Data Found?	Bus Found?
Nuclear	North Anna2	6/29/2007	21:53:56	864	37.99861	-77.8781	Yes	Yes
	Amos U3	7/2/2007	16:49:42	1076	38.50718	-81.89	Yes	Yes
	Bull Run U1	7/3/2007	13:55:35	663	36.01885	-84.1586	Yes	Yes
Coal	Cumberland unit 1	7/21/2007	2:44:25	686	36.38453	-87.6569	No	Yes
Coal	Baldwin	7/25/2007	19:01:41	872	38.1764	-89.8265	Yes	Yes
	Rockport,Petersburg,Newton	8/4/2007	21:44:14	2387			Yes	Yes
Nuclear	Nine Mile Point Nuclear	8/20/2007	12:32:14	570	29.9137	-90.2078	Yes	Yes
Nuclear	Donald C. Cook Unit 1 (1020 MW Capacity)	8/28/2007	17:53:13	920	41.9362	-86.5543	Yes	Yes
	Mountaineer U1 (1300 MW Capacity)	9/1/2007	13:48:00	1090	38.7292	-82.0223	Yes	Yes
	Rockport Unit2 (1300 MW Capacity)	9/4/2007	16:57:07	745	37.8858	-87.077	Yes	Yes
	Jeffrey Energy Center U2 U3	10/3/2007	15:26:37	1112	39.19867	-96.0683	Yes	Yes
Nuclear	Farley Unit 2	10/3/2007	19:10:11	740	31.33524	-85.1455	Yes	Yes
	Amos U2 (800 MW Capacity)	11/1/2007	14:48:00		38.50718	-81.89	No	Yes
	Connesville U4 (780 MW Capacity)	11/4/2007	22:20:10	569	40.18044	-81.8951	Yes	Yes
	Big Sandy U2 (800 MW Capacity)	11/9/2007	13:00:00	1426	37.9848	-82.5857	Yes	Yes
	McWilliams – Vann	2/7/2007	16:03:44	818	N/A	N/A	Yes	No

Fuel Type:	Plant:	Date:	Time (UTC):	MW Est.:	Latitude:	Longitude:	Data Found?	Bus Found?
	Cardinal U1	6/7/2007	2:50:41	605	N/A	N/A	No	No
	Lacygne	5/3/2007	14:58:59	729	38.3335	-94.7608	Yes	Yes
	Paradise	3/20/2007	10:06:41	457	37.25782	-86.9792	Yes	Yes
	W H Zimmer	3/24/2007	3:13:17	1547	39.05232	-84.1505	Yes	Yes
	W H Zimmer	11/14/2007	15:56:56	1295	39.05232	-84.1505	Yes	Yes
Nuclear	Indian Point Unit3	4/6/2007	15:09:07	753	41.26966	-73.9524	Yes	Yes
Nuclear	Sequoyah	8/24/2007	7:50:13	690	35.22723	-85.0943	Yes	Yes
	Conemaugh	3/21/2007	20:41:41	797	40.38227	-79.0968	Yes	Yes
	Conemaugh	7/1/2007	23:34:16	756	40.38227	-79.0968	Yes	Yes
	Gavin U1	7/4/2007	13:27:43	1038	38.95868	-82.1235	Yes	Yes
	Mitchell U2 (800 MW Capacity)	11/4/2007	9:26:35	634	39.91482	-80.731	Yes	Yes
Coal	Council Bluffs	6/9/2007	5:08:19	732	41.2146	-95.8574	Yes	Yes
Nuclear	Salem U2	8/6/2007	17:11:22	952	39.4956	-75.4733	Yes	Yes
	Keystone	6/27/2007	8:50:07	774	40.63879	-79.3191	Yes	Yes
Nuclear	Browns Ferry Unit 1	10/12/2007	13:02:35	778	34.70549	-87.1173	Yes	Yes
	Iatan	7/7/2007	20:37:54	570	39.44529	-94.9145	Yes	Yes
Nuclear	Braidwood Nuclear	8/18/2007	19:10:21	690	41.22879	-88.269	Yes	Yes

Fuel Type:	Plant:	Date:	Time (UTC):	MW Est.:	Latitude:	Longitude:	Data Found?	Bus Found?
Nuclear	Braidwood Unit 2	8/23/2007	20:30:52	870	41.22879	-88.269	No	Yes
	Amos U3 (1300MW capacity)	8/6/2007	19:39:22	1037	38.50718	-81.89	Yes	Yes
	Amos U3 (1300 MW capacity)	11/9/2007	2:49:25	1095	38.50718	-81.89	No	Yes

Appendix V: Model Information

Plant Name	Plant City	Plant State	Approx. Lat.	Approx. Lon.
A B Brown	Posey	IN	37.950569	-87.856887
AES Petersburg	Pike	IN	38.4723	-87.3105
Ashtabula	Ashtabula	OH	41.867877	-80.794681
Beaver Valley	Beaver	PA	40.626012	-80.419866
Belle River	St Clair	MI	42.82473	-82.49291
Big Sandy	Lawrence	KY	37.9848	-82.5857
Bruce Mansfield	Beaver	PA	40.626012	-80.419866
Cayuga	Vermillion	IN	39.878	-87.444
Cheswick Power Plant	Allegheny	PA	40.455569	-80.061056
Clinch River	Russell	VA	36.92584	-82.09273
Conesville	Coshocton	OH	40.180441	-81.895074
D B Wilson	Ohio	KY	37.407918	-87.00902
Dan E Karn	Bay	MI	43.6045	-83.7801
Davis Besse	Ottawa	OH	41.523556	-83.127764
E W Brown	Mercer	KY	37.7856	-84.8966
East Bend	Boone	KY	38.97368	-84.72964
Eastlake	Lake	OH	41.649822	-81.447887
Elmer Smith	Daviess	KY	37.762	-87.0519
F B Culley	Warrick	IN	37.9629	-87.3632
Fermi	Monroe	MI	41.9895	-83.2915
General James M Gavin	Gallia	OH	38.958678	-82.123537

Plant Name	Plant City	Plant State	Approx. Lat.	Approx. Lon.
Ghent	Carroll	KY	38.7126	-85.0472
Gibson	Gibson	IN	38.274414	-87.709052
Glen Lyn	Glen Lyn	VA	37.37098	-80.86633
Greenwood	St Clair	MI	43.056424	-82.678141
Hanging Rock Energy Facility	Lawrence	OH	38.529429	-82.665351
Harding Street	Marion	IN	39.673	-86.1937
Harrison Power Station	Harrison	WV	39.28667	-80.38329
Hatfields Ferry Power Station	Greene	PA	39.83495	-79.893813
J H Campbell	Ottawa	MI	42.9384	-86.1343
J M Stuart	Adams	OH	38.670864	-83.763723
John E Amos	Putnam	WV	38.507178	-81.889965
Killen Station	Adams	OH	38.698167	-83.618064
Ludington	Mason	MI	43.9737	-86.4001
Merom	Sullivan	IN	39.101018	-87.410235
Miami Fort	Hamilton	OH	39.39075	-84.56409
Michigan City	La Porte	IN	41.687	-86.8677
Mill Creek	Jefferson	KY	38.0866	-85.8492
Mitchell	Marshall	WV	39.914819	-80.730971
Monroe	Monroe	MI	41.9088	-83.4727
Mountaineer	Mason	WV	38.7292	-82.02231
Muskingum River	Washington	OH	39.571435	-81.634588
Palisades	Van Buren	MI	42.2857	-86.2695
Perry	Lake	OH	41.767916	-81.143312
Philip Sporn	Mason	WV	39.01885	-82.03244

Plant Name	**Plant City**	**Plant State**	**Approx. Lat.**	**Approx. Lon.**
Pleasants Power Station	Pleasants	WV	39.367927	-81.27881
R M Schahfer	Jasper	IN	41.177948	-87.069876
Rockport	Spencer	IN	37.885803	-87.07701
St Clair	St Clair	MI	42.7808	-82.6288
Tanners Creek	Dearborn	IN	39.1597	-84.8764
Trimble County	Trimble	KY	38.586363	-85.313331
W H Sammis	Jefferson	OH	39.87045	-84.76551
W H Zimmer	Clermont	OH	39.05232	-84.15045
Wabash River	Vigo	IN	39.434	-87.41
Walter C Beckjord	Clermont	OH	39.05232	-84.15045
Anclote	Pasco	FL	28.184527	-82.787476
Arvah B Hopkins	Leon	FL	30.39797	-84.65054
Big Bend	Hillsborough	FL	27.795028	-82.403641
C D McIntosh Jr	Polk	FL	27.727849	-81.989851
Cape Canaveral	Brevard	FL	28.46921	-80.76628
Crystal River	Citrus	FL	28.95879	-82.6857
Deerhaven Generating Station	Alachua	FL	29.65095	-82.32156
Fort Myers	Lee	FL	26.69843	-81.76972
H. L. Culbreath Bayside	Hillsborough	FL	27.90703	-82.417846
Indiantown Cogeneration LP	Martin	FL	27.040918	-80.513214
Manatee	Manatee	FL	27.605604	-82.344847
Martin	Martin	FL	27.056527	-80.564976
Northside Generating Station	Duval	FL	30.417323	-81.55264
Port Everglades	Broward	FL	26.08439	-80.1248

Plant Name	Plant City	Plant State	Approx. Lat.	Approx. Lon.
Riviera	Palm Beach	FL	26.76511	-80.05549
Sanford	Volusia	FL	28.842926	-81.325457
Seminole	Putnam	FL	29.73293	-81.632516
St Johns River Power Park	Duval	FL	30.434373	-81.554604
St Lucie	St Lucie	FL	27.348746	-80.246286
Stanton Energy Center	Orange	FL	28.48475	-81.156
Turkey Point	Miami-Dade	FL	25.433915	-80.331087
AES Ironwood LLC	Lebanon	PA	40.335912	-76.425895
Benning	District of Columbia	DC	38.8914	-76.9418
Bergen Generating Station	Bergen	NJ	40.8313	-74.0134
Brandon Shores	Anne Arundel	MD	39.1918	-76.5466
Calvert Cliffs Nuclear Power P	Calvert	MD	38.366128	-76.43464
Chalk Point LLC	Prince Georges	MD	38.5884	-76.7103
Conemaugh	Indiana	PA	40.382266	-79.096803
Eddystone Generating Station	Delaware	PA	39.868457	-75.337397
Edge Moor	New Castle	DE	39.772	-75.4963
Herbert A Wagner	Anne Arundel	MD	39.1918	-76.5466
Homer City Station	Indiana	PA	40.538375	-79.183942
Hunterstown	Adams	PA	39.832044	-77.222313
Indian River Generating Statio	Sussex	DE	38.5628	75.2319
Keystone	Armstrong	PA	40.638787	-79.31907
Limerick	Montgomery	PA	40.242989	-75.639256
Morgantown Generating Plant	Charles	MD	38.3457	-76.9162
Oyster Creek	Ocean	NJ	40.2492	-74.0521

Plant Name	Plant City	Plant State	Approx. Lat.	Approx. Lon.
Peach Bottom	York	PA	39.751754	-76.344101
Portland	Northampton	PA	40.688	-75.48869
PPL Brunner Island	York	PA	40.122154	-76.773725
PPL Martins Creek	Northampton	PA	40.854907	-75.195644
PPL Montour	Montour	PA	40.97647	-76.50155
PPL Susquehanna	Columbia	PA	41.066477	-76.244269
PSEG Hope Creek Generating Sta	Salem	NJ	39.56804	-75.47316
PSEG Hudson Generating Station	Hudson	NJ	40.7351	-74.0685
PSEG Mercer Generating Station	Mercer	NJ	40.1951	-74.7448
PSEG Salem Generating Station	Salem	NJ	39.4956	-75.4733
Seward	Indiana	PA	40.382266	-79.096803
Three Mile Island	Dauphin	PA	40.204086	-76.733127
Baldwin Energy Complex	Randolph	IL	38.1764	-89.8265
Braidwood Generation Station	Will	IL	41.228788	-88.269042
Byron Generating Station	Ogle	IL	42.129236	-89.265887
Callaway	Callaway	MO	38.851821	-91.96055
Coffeen	Montgomery	IL	39.1049	-89.4043
Collins	Grundy	IL	41.367233	-88.417769
Crawford	Cook	IL	41.8466	-87.7191
Dresden Generating Station	Grundy	IL	41.3973	-88.4715
Duck Creek	Fulton	IL	40.560137	-90.024151
E D Edwards	Peoria	IL	40.6465	-89.6859

Plant Name	Plant City	Plant State	Approx. Lat.	Approx. Lon.
Edgewater	Sheboygan	WI	43.7849	-87.76643
Fisk Street	Cook	IL	41.8491	-87.6709
Havana	Mason	IL	40.2774	-90.0095
Joliet 29	Will	IL	41.4941	-88.1457
Joliet 9	Will	IL	41.4941	-88.1457
Kewaunee	Kewaunee	WI	44.440143	-87.559442
Kincaid Generation LLC	Christian	IL	39.5893	-89.4176
Labadie	Franklin	MO	38.5268	-90.8765
LaSalle Generating Station	La Salle	IL	41.330201	-88.694678
Meramec	St Louis	MO	38.4581	-90.3236
Newton	Jasper	IL	38.984678	-88.170386
Point Beach	Manitowoc	WI	44.166008	-87.585504
Powerton	Tazewell	IL	40.5452	-89.6011
Quad Cities Generating Station	Rock Island	IL	41.6978	-90.2741
Rush Island	Jefferson	MO	38.187889	-90.42859
Sioux	St Charles	MO	38.871	-90.219
Waukegan	Lake	IL	42.4068	-87.8529
Weston	Marathon	WI	44.88429	-89.619262
Will County	Will	IL	41.6499	-88.0888
Allen S King	Washington	MN	45.0174	-92.7808
Antelope Valley	Mercer	ND	47.270664	-101.807468
Big Bend	Buffalo	SD	44.04059	-99.44011
Big Stone	Grant	SD	45.28504	-96.561434
Boundary Dam	Estevan	SK	49.14864	-103.09265

Plant Name	Plant City	Plant State	Approx. Lat.	Approx. Lon.
Clay Boswell	Itasca	MN	47.2371	-93.6985
Coal Creek	McLean	ND	47.460163	-101.189807
Cooper	Nemaha	NE	40.399447	-95.69348
Coteau Creek (Gardiner Dam)	Lake Diefenbaker	SK	51.2732	-106.86901
Council Bluffs	Pottawattamie	IA	41.2146	-95.8574
Coyote	Mercer	ND	47.270664	-101.807468
Duane Arnold	Linn	IA	42.0483	-91.7982
Fort Calhoun	Washington	NE	41.5565	-96.2448
Fort Peck	McCone	MT	48.01237	-106.41145
Fort Randall	Charles Mix	SD	43.06325	-98.55568
Genoa	Vernon	WI	43.605134	-91.134999
George Neal North	Woodbury	IA	42.3446	-96.2663
Gerald Gentleman	Lincoln	NE	41.15575	-101.136029
Great Falls Generating Station	Great Falls	MB	50.56815	-96.17755
Lansing	Allamakee	IA	43.3826	-91.3585
Leland Olds	Mercer	ND	47.2948	-101.4091
Louisa	Louisa	IA	41.430378	-91.050928
Milton R Young	Oliver	ND	47.121912	-101.328643
Monticello	Wright	MN	45.2795	-93.7941
Nebraska City	Otoe	NE	40.674746	-95.8619
Oahe	Hughes	SD	44.45007	-100.38923
Ottumwa	Wapello	IA	41.077041	-92.532762
Prairie Island	Goodhue	MN	44.5193	-92.5587
Regina	Regina	SK	50.46296	-104.61553

Plant Name	Plant City	Plant State	Approx. Lat.	Approx. Lon.
Selkirk Generating Station	Selkirk	MB	50.15128	-96.87988
Shand	Estevan	SK	49.088391	-102.864518
Sheldon	Lancaster	NE	40.55889	-96.78417
Sherburne County	Sherburne	MN	45.436539	-93.840966
Slave Falls Generating Station	Pointe du Bois	MB	50.228759	-95.569296
Abitibi GS	Abitibi	ON	49.881667	-81.561667
AES Somerset LLC	Niagara	NY	43.353	-78.59628
Arnprior GS	Arnprior	ON	45.41919	-76.34681
Astoria Generating Station	Queens	NY	40.7841	-73.91258
Aubrey Falls GS	Aubrey Falls	ON	46.85	-83.2833
Bear Swamp	Berkshire	MA	42.68529	-72.976706
Belledune	Calhoun	NB	47.78	-66.16
Bowline Point	Rockland	NY	41.20544	-73.96697
Brayton Point	Bristol	MA	41.73459	-71.14998
Bruce Nuclear	Tiverton	ON	44.326	-81.59532
Canal	Barnstable	MA	41.77056	-70.50972
Chenaux GS	Chenaux	ON	45.58291	-76.67715
Coleson Cove	Etowah	NB	45.156389	-66.204167
Comerford	Grafton	NH	44.33625	-71.874104
Darlington GS	Ketchikan Gateway	ON	43.871944	-77.278611
Des Joachim GS	Rolphton	ON	46.18053	-77.69734
James A Fitzpatrick	Oswego	NY	43.52235	-76.39506
Kipling GS	Kipling	ON	50.13666	-82.208333
Lambton GS	Juneau	ON	42.796645	-82.466877

Plant Name	Plant City	Plant State	Approx. Lat.	Approx. Lon.
Lennox GS	Fairbanks North Star	ON	44.17893	-76.78229
Lingan GS	Lingan	NS	46.2357	-60.0402
Little Long GS	Little Long	ON	50.00333	-82.16667
Lower Notch GS	North Cobalt	ON	47.1375	49.454167
Mason Station	Wiscasset	ME	43.991352	-69.669848
Merrimack	Merrimack	NH	43.14241	-71.47829
Middletown	Middlesex	CT	41.55472	-72.57944
Milford Power Project	New Haven	CT	41.223908	-73.099052
Millstone	New London	CT	41.311533	-72.168288
Montville Station	New London	CT	41.4275	-72.10111
Mountain Chute GS	Mountain Chute	ON	45.19612	-76.90711
Mystic Generating Station	Middlesex	MA	42.39001	-71.07126
Nanticoke GS	Ketchikan Gateway	ON	42.798676	-80.051794
Nine Mile Point Nuclear Statio	Oswego	NY	43.52152	-76.40413
O. Holden GS	Mattawa	ON	46.37556	-78.72952
Oswego Harbor Power	Oswego	NY	43.45858	-76.53164
Pickering A GS	McKinley	ON	43.809741	-79.066672
Pilgrim Nuclear Power Station	Plymouth	MA	41.94372	-70.57859
Point Lepreau	Elmore	NB	45.06667	-66.46667
R. E. Ginna Nuclear Power Plan	Wayne	NY	43.27679	-77.30934
Roseton Generating Station	Orange	NY	41.55959	-73.98881
Salem Harbor	Essex	MA	42.52667	-70.87639
Saunders GS	Wrangell-Petersburg	ON	45.010315	-74.789128
Seabrook	Rockingham	NH	42.898399	-70.851216

Plant Name	Plant City	Plant State	Approx. Lat.	Approx. Lon.
Taylorville	Lewis	NY	43.92144	-75.27709
Trenton GS	Trenton	NS	45.65319	-62.71804
Vermont Yankee	Windham	VT	42.778803	-72.514014
Wells GS	Iron Bridge	ON	46.31441	-83.29021
William F Wyman	Cumberland	ME	43.75056	-70.15639
Seneca	Warren	PA	41.83754	-79.00486
Allen Steam Plant	Shelby	TN	35.042538	-90.073238
Arkansas Nuclear One	Pope	AR	35.284208	-93.131476
Bad Creek	Oconee	SC	34.872836	-82.960687
Barry	Mobile	AL	31.0113	-88.0226
Bath County	Bath	VA	38.085119	-79.807792
Baxter Wilson	Warren	MS	32.3263	-90.8614
Belews Creek	Stokes	NC	36.318872	-80.148414
Big Cajun 2	Pointe Coupee	LA	30.701356	-91.442124
Birchwood Power	King George	VA	38.281142	-77.126023
Bowen	Bartow	GA	34.1498	84.8279
Browns Ferry	Limestone	AL	34.705485	-87.117258
Brunswick	Brunswick	NC	34.012137	-78.045551
Bull Run	Anderson	TN	36.018846	-84.15861
Catawba	York	SC	34.994669	-81.224462
Chesterfield	Chesterfield	VA	37.342934	-77.41557
Cliffside	Cleveland	NC	35.2381	-81.7701
Clover	Halifax	VA	36.863695	-78.78618
Colbert	Colbert	AL	34.6544	-87.6611

Plant Name	Plant City	Plant State	Approx. Lat.	Approx. Lon.
Cope	Orangeburg	SC	33.372555	-80.963111
Crist	Escambia	FL	30.5313	-87.2216
Cross	Berkeley	SC	33.3003	-80.2017
Cumberland	Stewart	TN	36.384531	-87.656908
E C Gaston	Shelby	AL	33.243	-86.5295
Edwin I Hatch	Appling	GA	31.783663	-82.348643
G G Allen	Gaston	NC	35.2342	-81.041
Gallatin	Sumner	TN	36.315384	-86.400561
Gerald Andrus	Washington	MS	33.28552	-90.94751
Gleason Gas Turbine	Gleason	TN	36.432332	-88.976555
Gorgas	Walker	AL	33.708	-87.255
Grand Gulf	Claiborne	MS	31.926604	-91.02303
H Allen Franklin Combined Cycl	Lee	AL	32.520072	-85.100027
H B Robinson	Darlington	SC	34.375616	-80.084237
H L Spurlock	Mason	KY	38.619716	-83.758858
Hammond	Floyd	GA	34.2539	-85.3548
Harllee Branch	Putnam	GA	33.0769	-83.3032
Harris	Wake	NC	35.680877	-78.936534
Jack McDonough	Cobb	GA	33.8714	-84.4998
Jack Watson	Harrison	MS	30.3896	-89.0988
James H Miller Jr	Jefferson	AL	33.63356	-86.948221
Jasper	Jasper	SC	32.263512	-81.066865
Johnsonville Fossil	Waverly	TN	36.077476	-87.948132
Joseph M Farley	Houston	AL	31.335235	-85.145488

Plant Name	Plant City	Plant State	Approx. Lat.	Approx. Lon.
L V Sutton	New Hanover	NC	34.2436	-77.9363
Lagoon Creek Gas Turbine	Haywood County	TN	35.658333	-89.4
Lake Catherine	Hot Spring	AR	34.4668	-92.843
Lee	Wayne	NC	35.4141	-78.0215
Little Gypsy	St Charles	LA	30.1499	-90.4621
Marshall	Catawba	NC	35.587	-80.9648
Mayo	Person	NC	36.405902	-78.973698
McGuire	Mecklenburg	NC	35.421992	-80.864664
McIntosh Combined Cycle Facili	Effingham	GA	32.235632	-81.287777
Michoud	Orleans	LA	30.0733	-89.8781
Morgan Energy Center	Morgan	AL	34.589599	-86.98868
Mt Storm	Grant	WV	39.265224	-79.225454
Murray Energy Facility	Murray	GA	34.77922	-84.933871
Nine Mile Point	Jefferson	LA	29.9137	-90.2078
North Anna	Louisa	VA	37.998609	-77.878069
Oconee	Oconee	SC	34.75382	-83.06743
Paradise	Muhlenberg	KY	37.25782	-86.9792
Possum Point	Prince William	VA	38.602344	-77.338704
R S Nelson	Calcasieu	LA	30.2637	-93.2773
Raccoon Mountain	Hamilton	TN	35.056361	-85.406561
Red Hills Generating Facility	Choctaw	MS	33.351684	-89.20139
Reliant Energy Choctaw County	Choctaw	MS	33.338319	-89.394585
River Bend	West Feliciana	LA	30.858658	-91.392266
Robert E Ritchie	Phillips	AR	34.4952	-90.7117

Plant Name	Plant City	Plant State	Approx. Lat.	Approx. Lon.
Rocky Mountain Hydro	Floyd	GA	34.283679	-85.223122
Roxboro	Person	NC	36.4067	-78.98
Sabine	Orange	TX	30.02509	-93.85664
Scherer	Monroe	GA	33.119412	-83.823529
Sequoyah	Hamilton	TN	35.227234	-85.094326
Surry	Surry	VA	37.126024	-76.76514
Taft Cogeneration Facility	St Charles	LA	30.000094	-90.488581
V C Summer	Fairfield	SC	34.271693	-81.271153
Victor J Daniel Jr	Jackson	MS	32.3205	-90.20759
Vogtle	Burke	GA	33.0894	-81.978
Wansley	Heard	GA	33.432226	-85.167148
Wateree	Richland	SC	33.915274	-80.699647
Waterford 3	St Charles	LA	29.91179	-90.35675
Watts Bar Nuclear Plant	Rhea	TN	35.60464	-84.79529
White Bluff	Jefferson	AR	34.452647	-92.17579
Widows Creek	Jackson	AL	34.887409	-85.754492
Williams	Berkeley	SC	32.988699	-80.019948
Willow Glen	Iberville	LA	30.2802	-91.0796
Winyah	Georgetown	SC	33.430776	-79.323459
Yates	Coweta	GA	33.3807	-84.7999
Yorktown	York	VA	37.228657	-76.542346
Acadia Energy Center	Acadia	LA	30.51158	-92.398474
Aries Power Project	Cass	MO	38.785856	-94.243961
Cunningham	Lea	NM	32.713012	-103.353152

Plant Name	Plant City	Plant State	Approx. Lat.	Approx. Lon.
Dolet Hills	De Soto	LA	32.0037	-93.6731
Flint Creek	Benton	AR	36.26516	-94.475131
Gordon Evans Energy Center	Sedgwick	KS	37.7627	-97.5442
GRDA	Mayes	OK	36.141	-95.3638
Harrington	Potter	TX	35.29944	-101.74667
Hawthorn	Jackson	MO	39.1239	-94.5339
Holcomb	Finney	KS	37.9567	-101.0244
Hugo	Choctaw	OK	34.051968	-95.253015
Iatan	Platte	MO	39.445294	-94.914453
Jeffrey Energy Center	Pottawatomie	KS	39.198674	-96.068277
Jones	Lubbock	TX	33.524152	-101.739471
La Cygne	Linn	KS	38.3335	-94.7608
Lawrence Energy Center	Douglas	KS	38.9886	-95.3029
Maddox	Lea	NM	32.71433	-103.301686
Mustang	Canadian	OK	35.483371	-97.629927
New Madrid	New Madrid	MO	36.6317	-89.5078
Northeastern	Rogers	OK	36.443723	-95.72901
Pirkey	Harrison	TX	32.45357	-94.48713
Plant X	Lamb	TX	34.166008	-102.410538
Riverside	Tulsa	OK	36.014834	-95.979711
Rodemacher	Rapides	LA	31.418481	-92.77185
Sibley	Jackson	MO	39.1591	-94.1879
Sikeston Power Station	Scott	MO	36.891111	-89.59197
Southwestern	Caddo	OK	34.13131	-96.26906

Plant Name	Plant City	Plant State	Approx. Lat.	Approx. Lon.
Teche	St Mary	LA	29.827	-91.5738
Thomas Hill	Randolph	MO	39.4237	-92.6667
Tolk	Lamb	TX	34.18472	-102.56861
Welsh	Titus	TX	33.055067	-94.839499
Wilkes	Marion	TX	32.848307	-94.548061
Wolf Creek Generating Station	Coffey	KS	38.1931	-95.748

Appendix VI: Mahalanobis Distance Event Detection Results

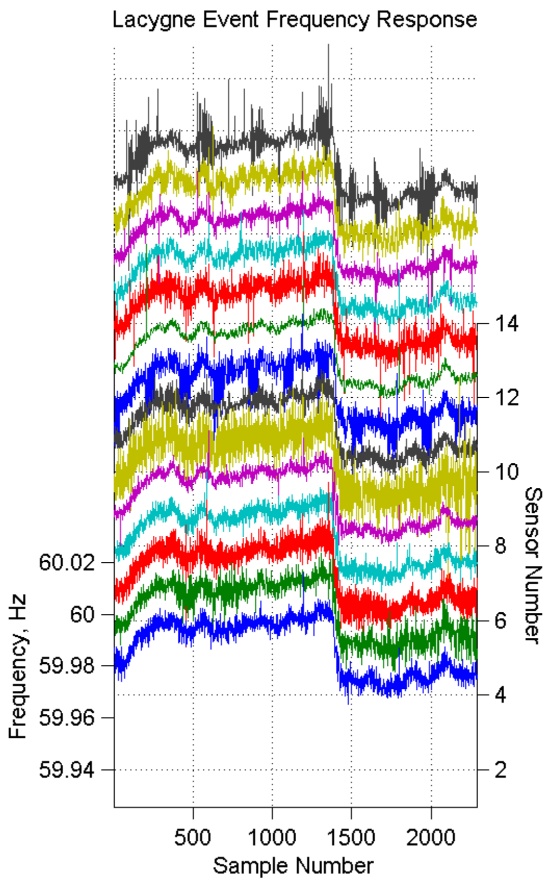

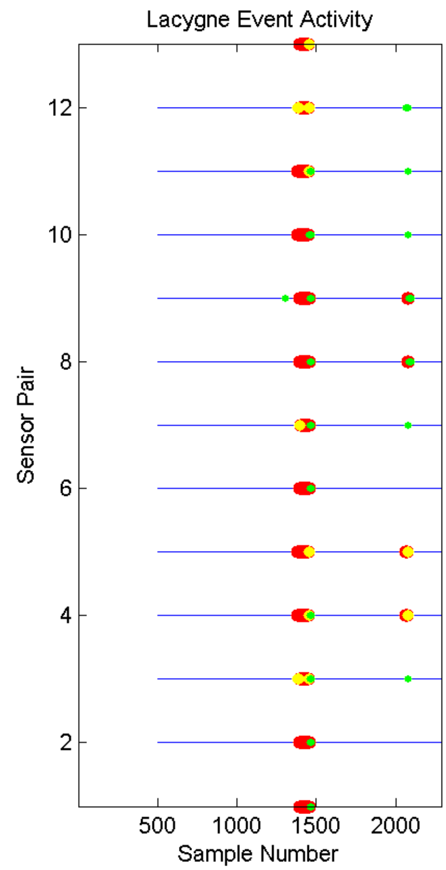

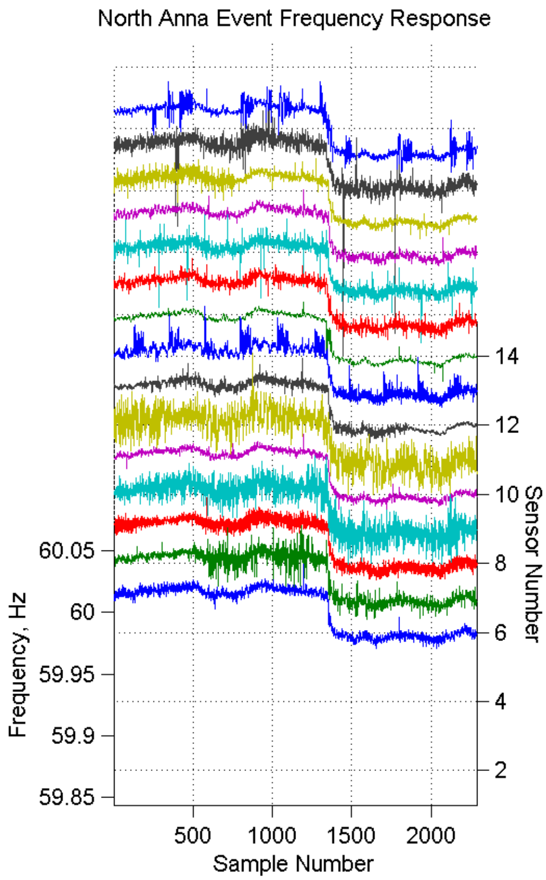
North Anna Event Frequency Response
60.05
60
59.95
59.9
59.85
Frequency, Hz
500
1000
1500
2000
Sample Number
14
12
10
8
6
4
2
Sensor Number

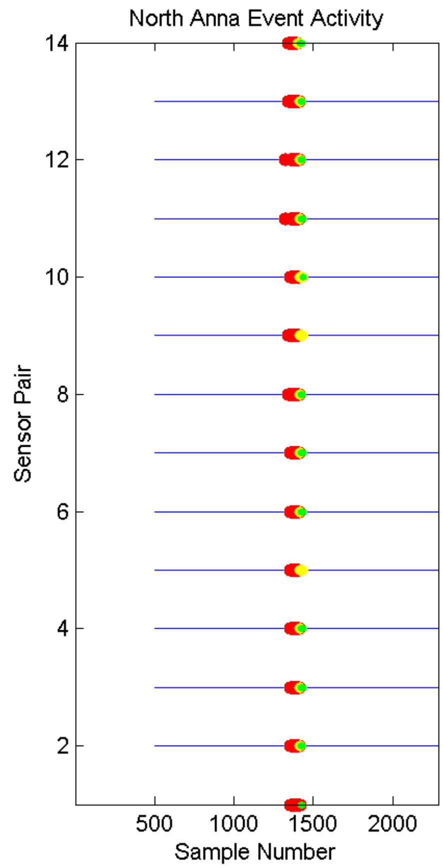
North Anna Event Activity
14
12
10
8
6
4
2
Sensor Pair
500
1000
1500
2000
Sample Number

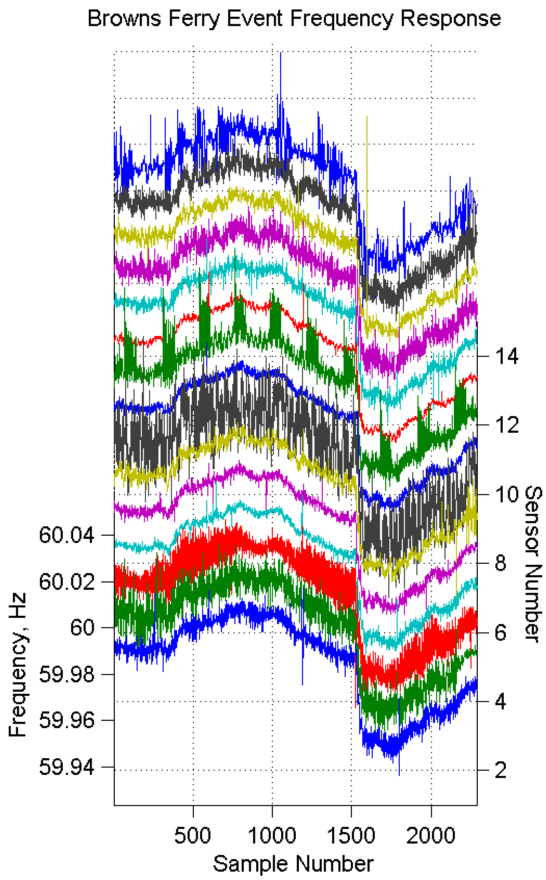
Browns Ferry Event Frequency Response
Frequency, Hz
60.04
60.02
60
59.98
59.96
59.94
500
1000
1500
2000
Sample Number
Sensor Number
14
12
10
8
6
4
2

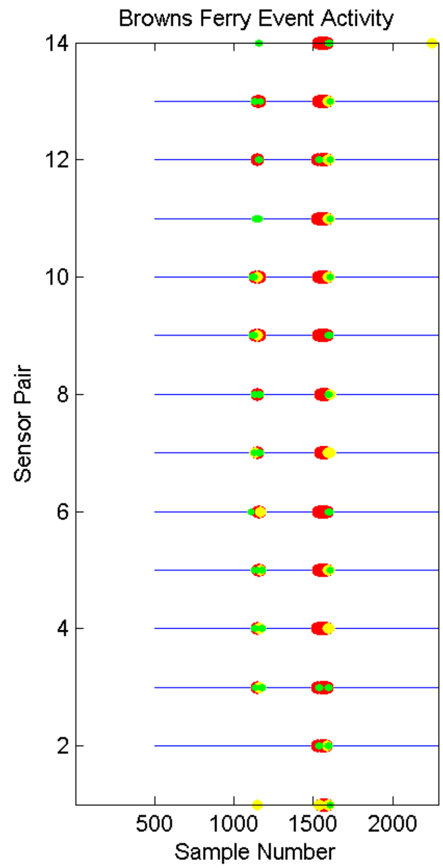
Browns Ferry Event Activity
Sensor Pair
14
12
10
8
6
4
2
500
1000
1500
2000
Sample Number

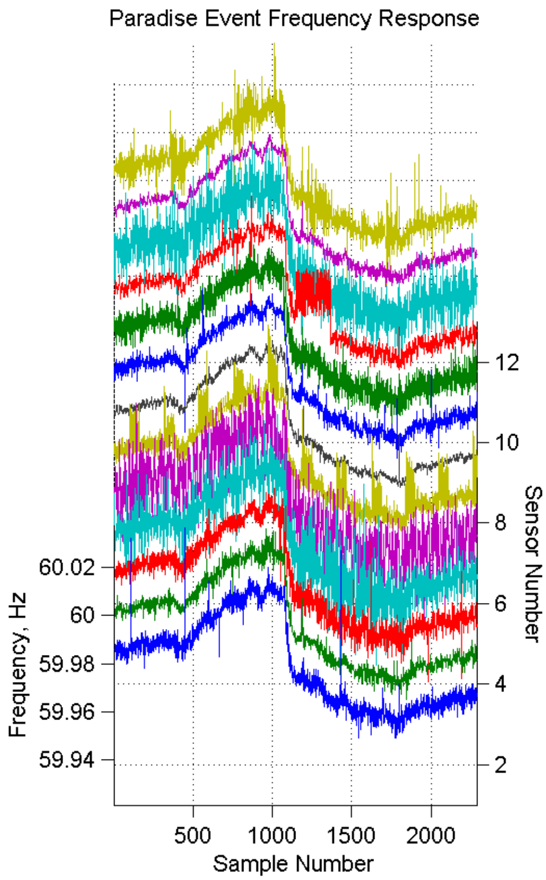
Paradise Event Frequency Response
60.02
60
59.98
59.96
59.94
Frequency, Hz
500
1000
1500
2000
Sample Number
12
10
8
6
4
2
Sensor Number

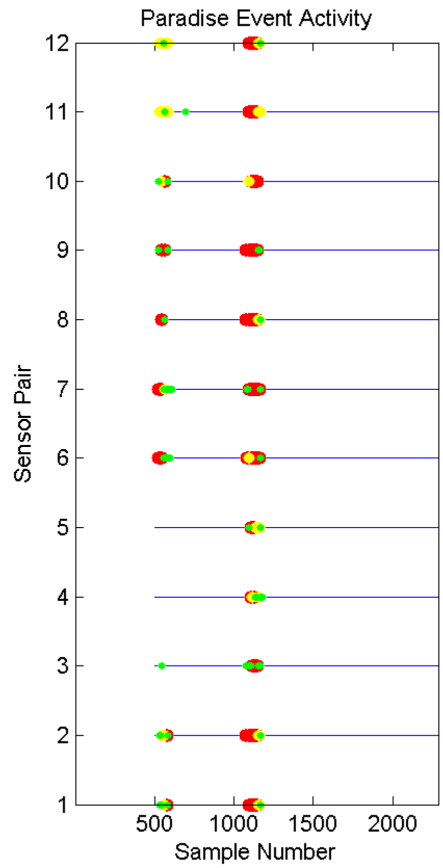
Paradise Event Activity
12
11
10
9
8
7
6
5
4
3
2
1
Sensor Pair
500
1000
1500
2000
Sample Number

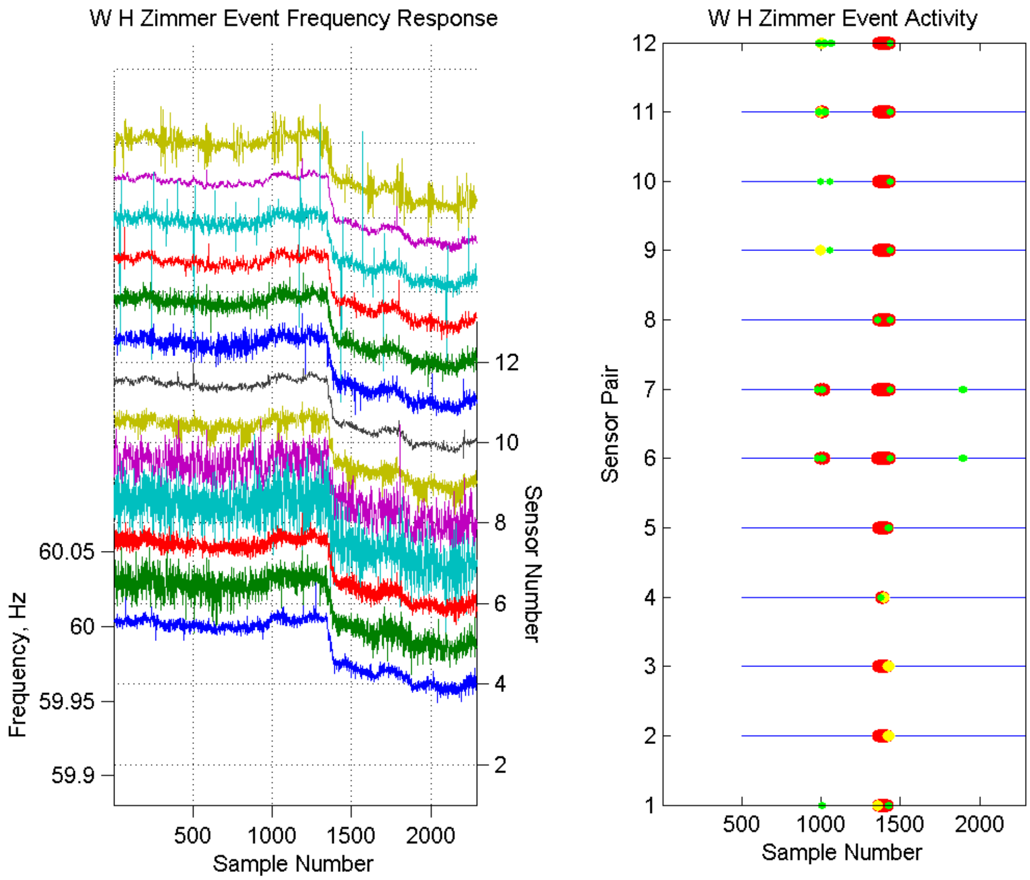
W H Zimmer Event Frequency Response
Frequency, Hz
60.05
60
59.95
59.9
500
1000
1500
2000
Sample Number
Sensor Number
12
10
8
6
4
2
W H Zimmer Event Activity
Sensor Pair
1
2
3
4
5
6
7
8
9
10
11
12
500
1000
1500
2000
Sample Number

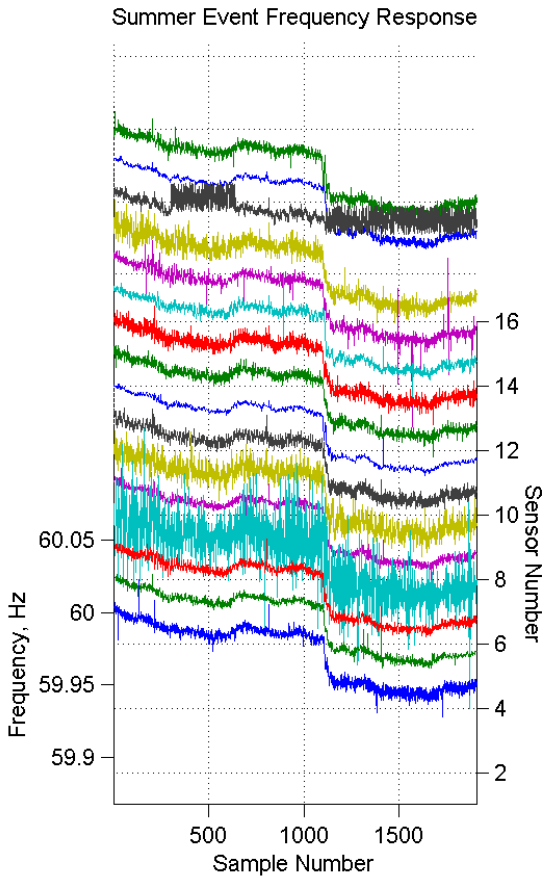

Summer Event Frequency Response
Frequency, Hz
60.05
60
59.95
59.9
500
1000
1500
Sample Number
Sensor Number
16
14
12
10
8
6
4
2

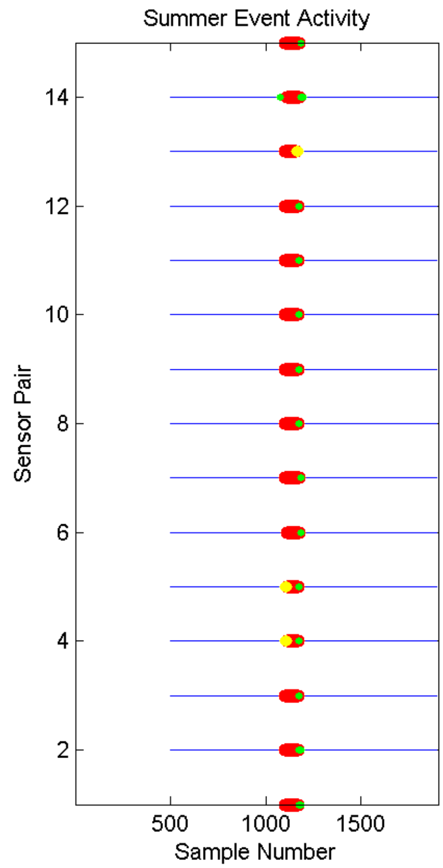

Summer Event Activity
Sensor Pair
14
12
10
8
6
4
2
500
1000
1500
Sample Number

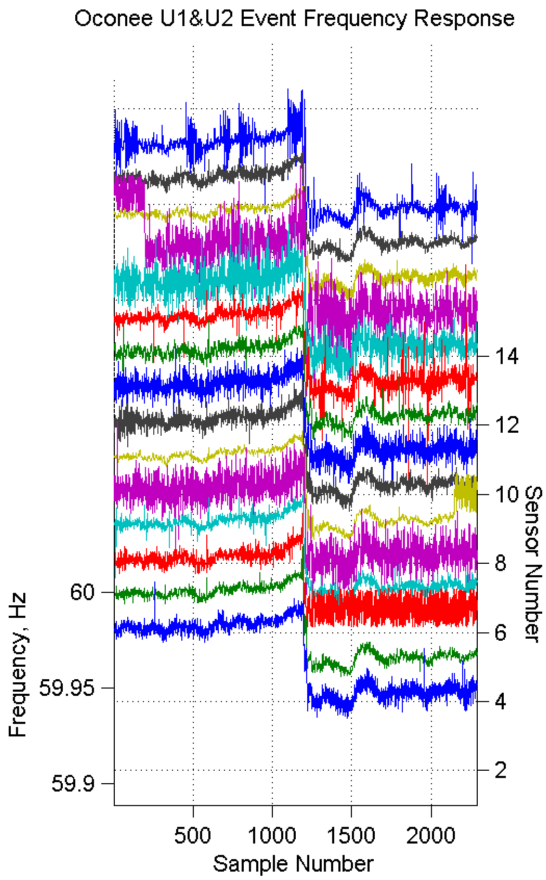
Oconee U1&U2 Event Frequency Response
Frequency, Hz
60
59.95
59.9
500
1000
1500
2000
Sample Number
14
12
10
8
6
4
2
Sensor Number

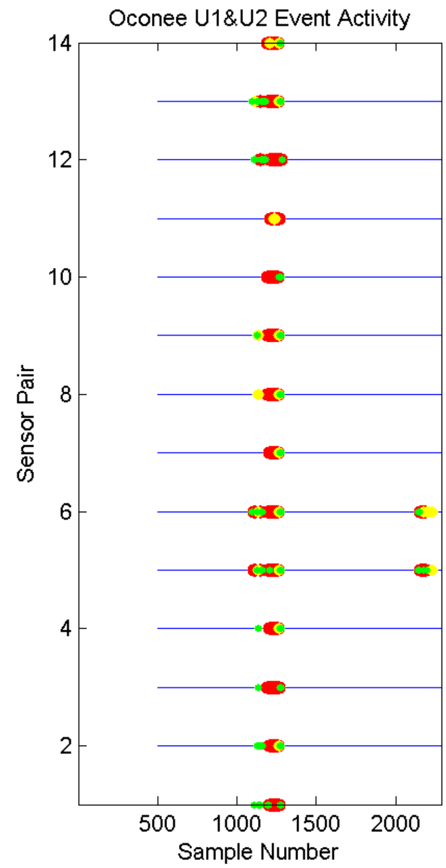
Oconee U1&U2 Event Activity
Sensor Pair
14
12
10
8
6
4
2
500
1000
1500
2000
Sample Number

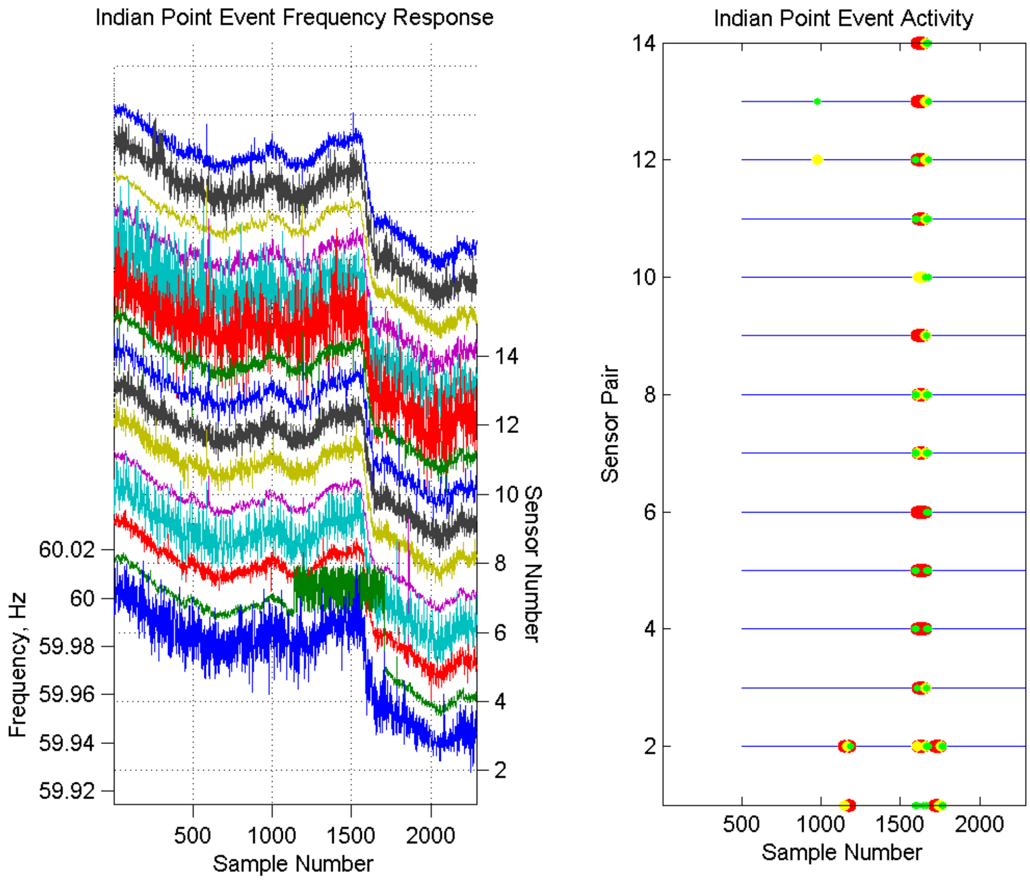
Indian Point Event Frequency Response
Frequency, Hz
Sample Number
Sensor Number
Indian Point Event Activity
Sensor Pair
Sample Number

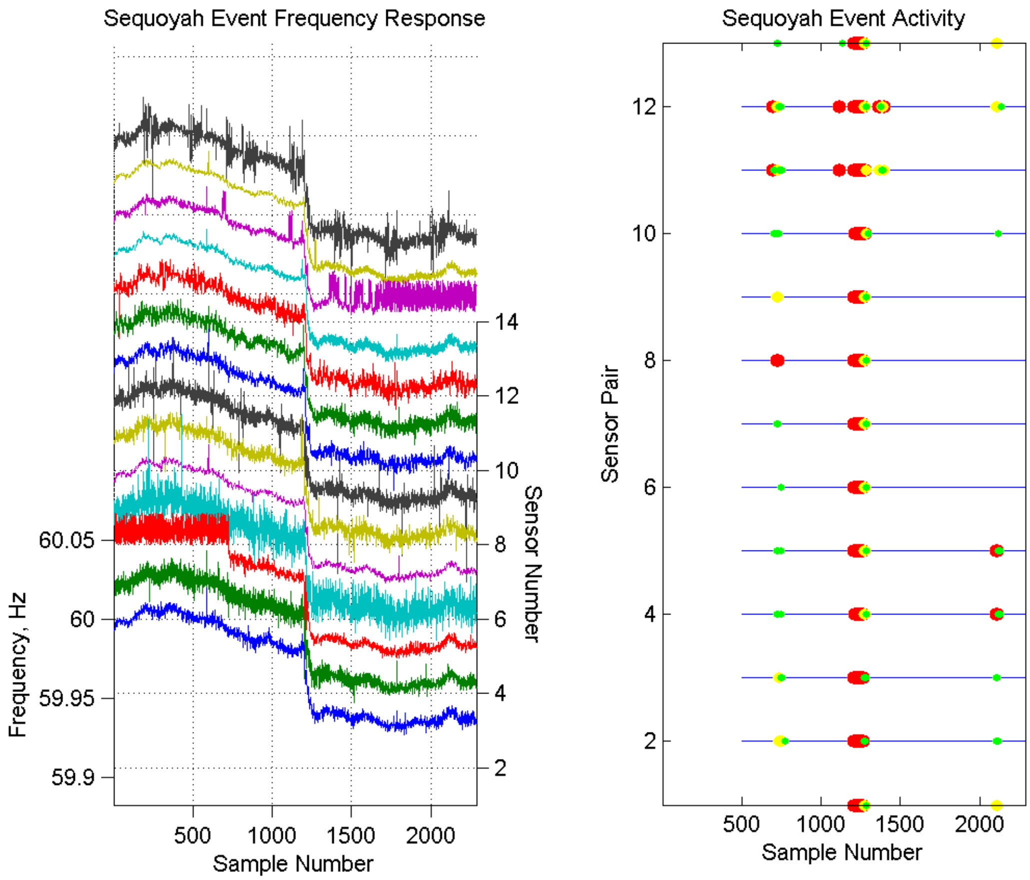
Sequoyah Event Frequency Response
Frequency, Hz
60.05
60
59.95
59.9
500
1000
1500
2000
Sample Number
Sensor Number
14
12
10
8
6
4
2
Sequoyah Event Activity
Sensor Pair
12
10
8
6
4
2
500
1000
1500
2000
Sample Number

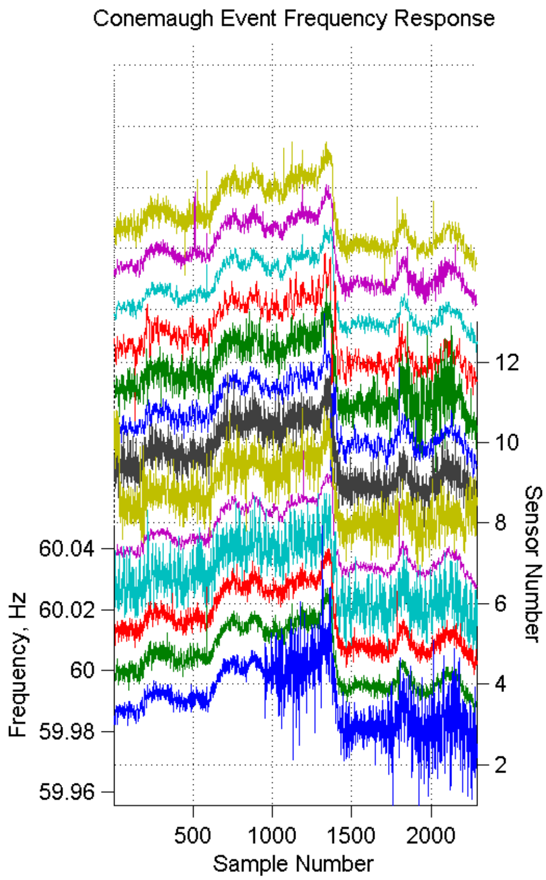
Conemaugh Event Frequency Response
60.04
60.02
60
59.98
59.96
Frequency, Hz
500
1000
1500
2000
Sample Number
12
10
8
6
4
2
Sensor Number

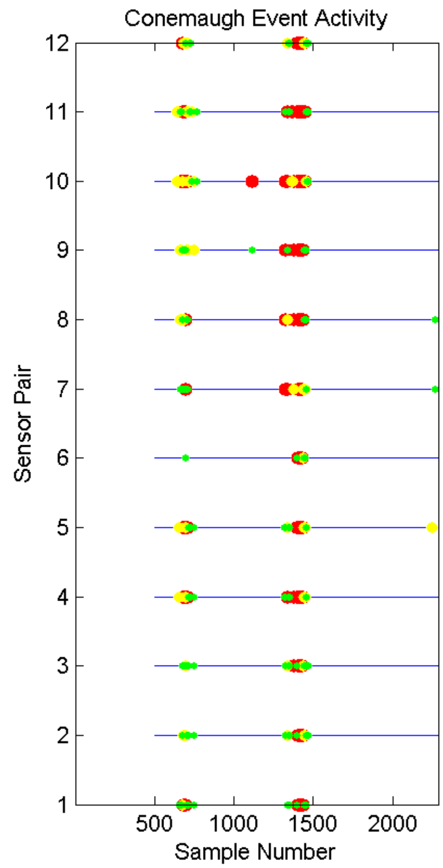
Conemaugh Event Activity
12
11
10
9
8
7
6
5
4
3
2
1
Sensor Pair
500
1000
1500
2000
Sample Number

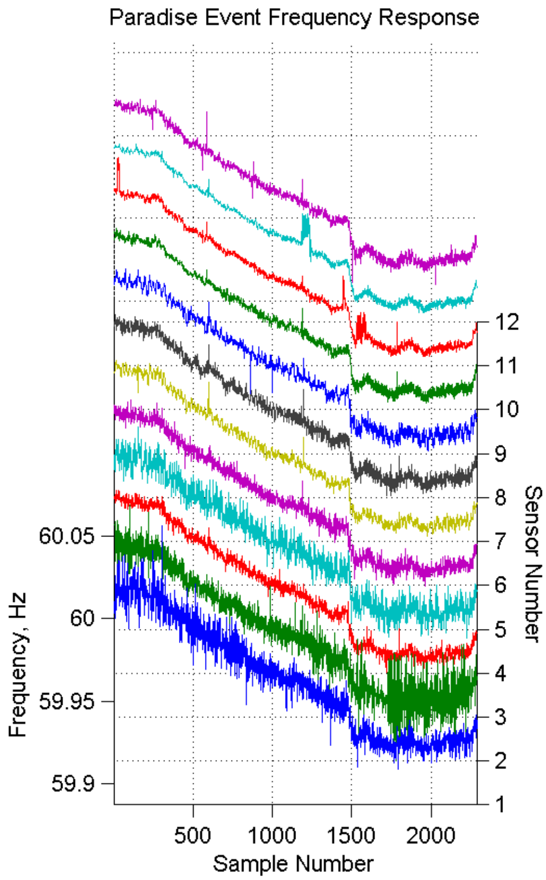
Paradise Event Frequency Response
Frequency, Hz
60.05
60
59.95
59.9
500
1000
1500
2000
Sample Number
Sensor Number
12
11
10
9
8
7
6
5
4
3
2
1

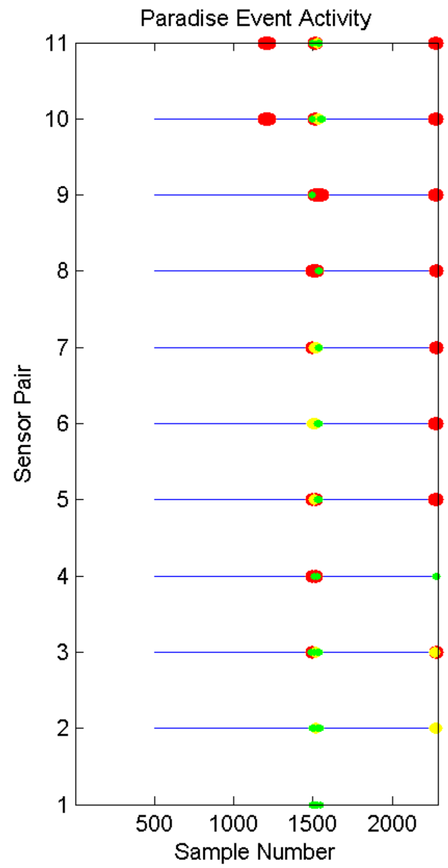
Paradise Event Activity
Sensor Pair
11
10
9
8
7
6
5
4
3
2
1
500
1000
1500
2000
Sample Number

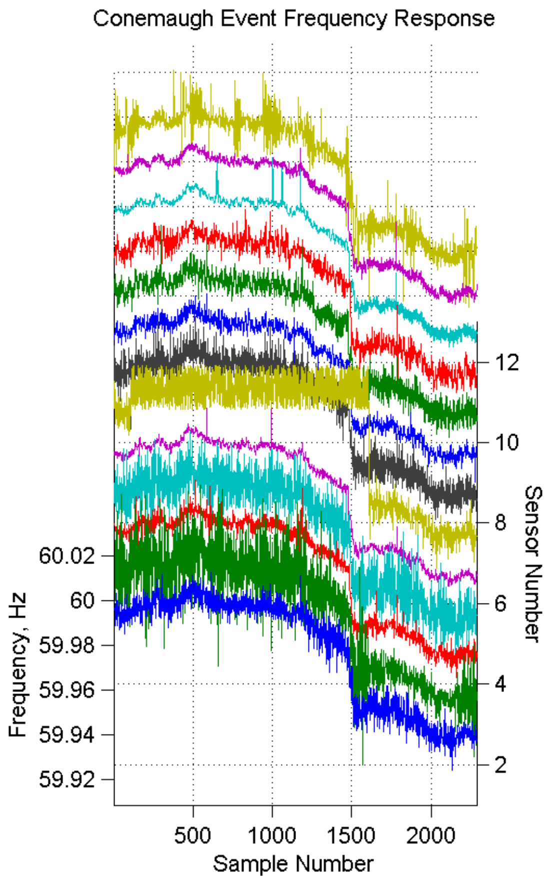
Conemaugh Event Frequency Response
Frequency, Hz
60.02
60
59.98
59.96
59.94
59.92
500
1000
1500
2000
Sample Number
Sensor Number
12
10
8
6
4
2

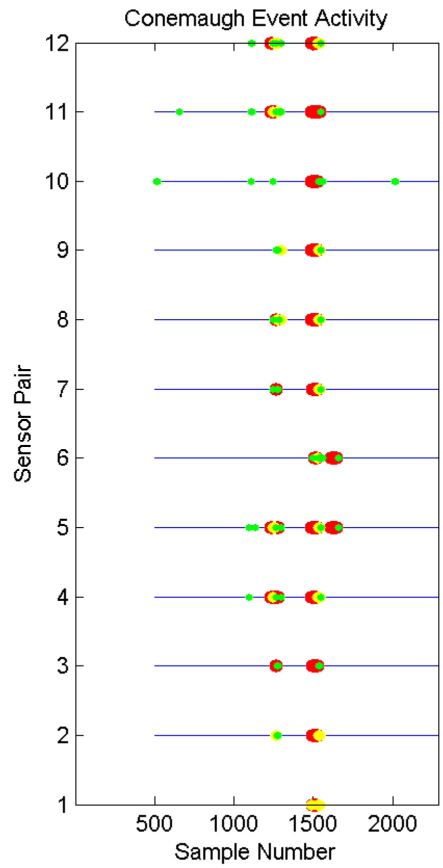
Conemaugh Event Activity
Sensor Pair
12
11
10
9
8
7
6
5
4
3
2
1
500
1000
1500
2000
Sample Number

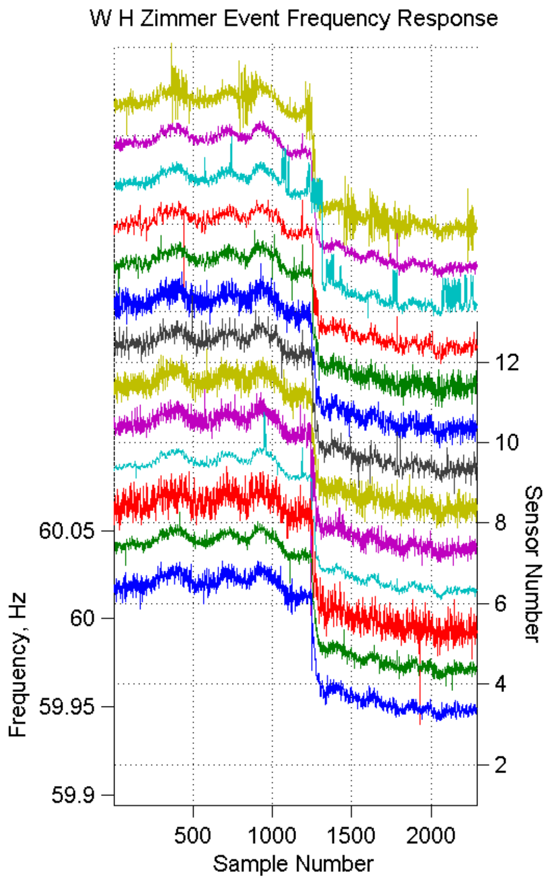
W H Zimmer Event Frequency Response
Frequency, Hz
60.05
60
59.95
59.9
500
1000
1500
2000
Sample Number
Sensor Number
12
10
8
6
4
2

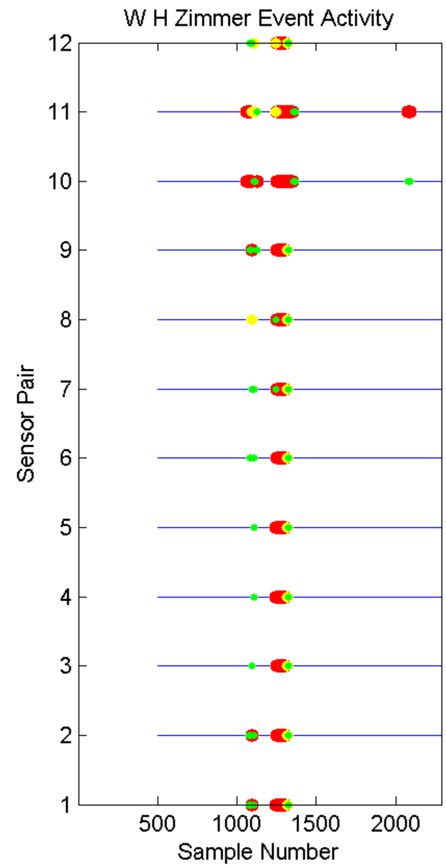
W H Zimmer Event Activity
Sensor Pair
12
11
10
9
8
7
6
5
4
3
2
1
500
1000
1500
2000
Sample Number

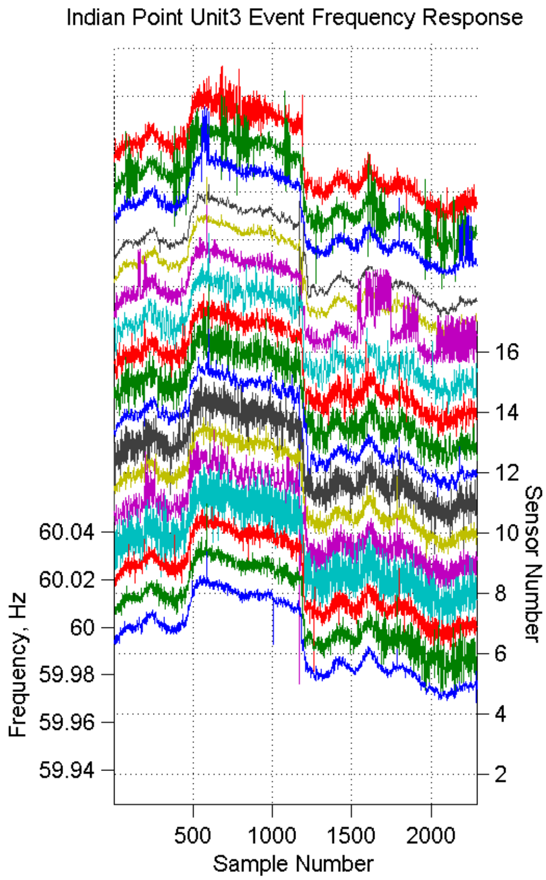
Indian Point Unit3 Event Frequency Response
Frequency, Hz
60.04
60.02
60
59.98
59.96
59.94
500
1000
1500
2000
Sample Number
Sensor Number
16
14
12
10
8
6
4
2

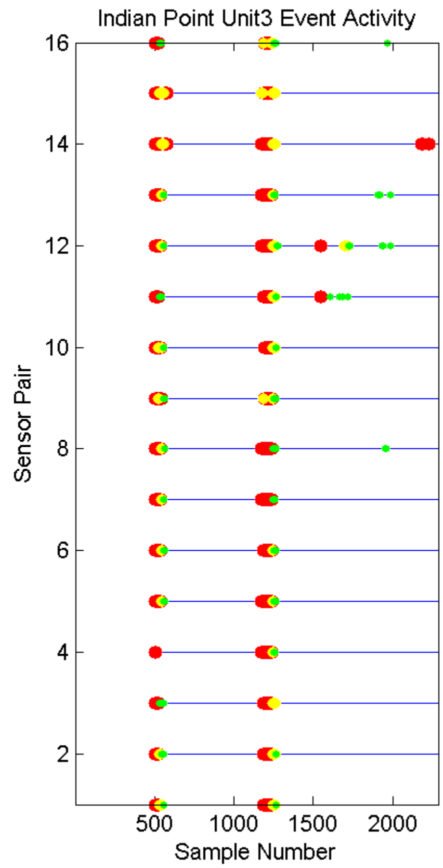
Indian Point Unit3 Event Activity
Sensor Pair
16
14
12
10
8
6
4
2
500
1000
1500
2000
Sample Number

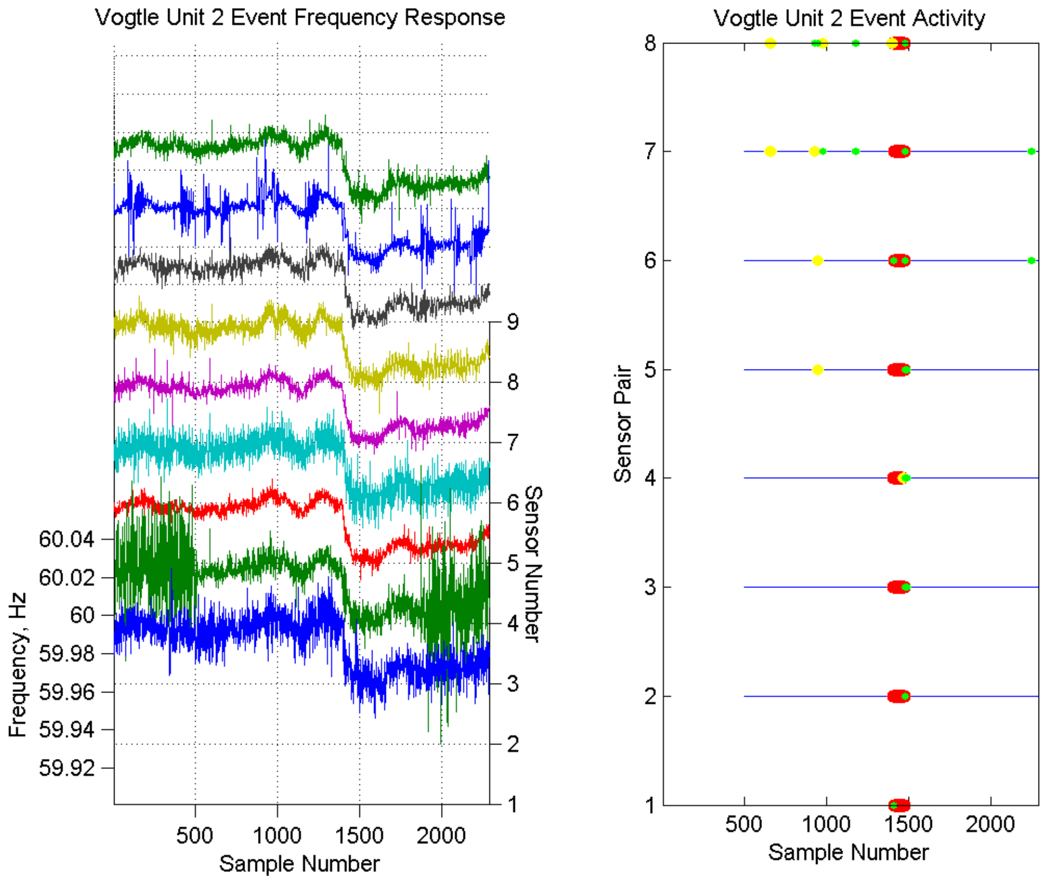
Vogtle Unit 2 Event Frequency Response
Frequency, Hz
60.04
60.02
60
59.98
59.96
59.94
59.92
500
1000
1500
2000
Sample Number
Sensor Number
1
2
3
4
5
6
7
8
9
Vogtle Unit 2 Event Activity
Sensor Pair
1
2
3
4
5
6
7
8
500
1000
1500
2000
Sample Number

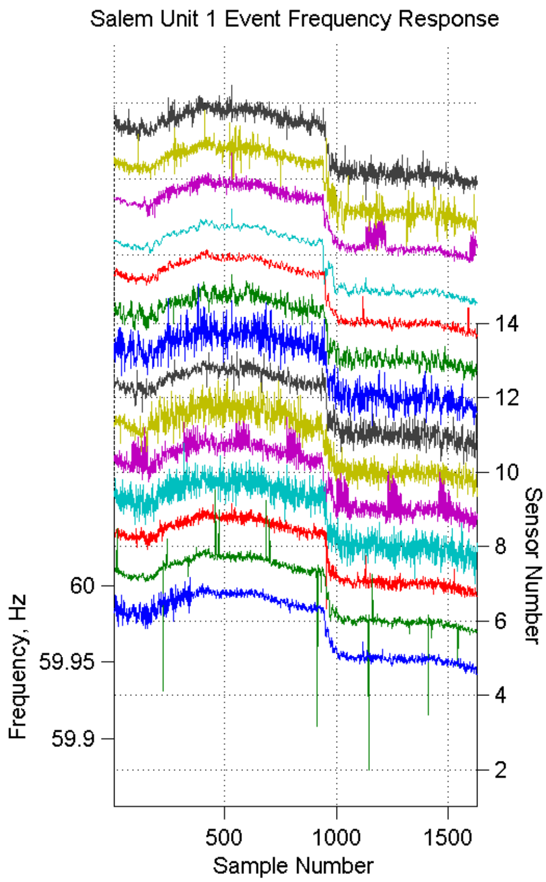
Salem Unit 1 Event Frequency Response
Frequency, Hz
60
59.95
59.9
500
1000
1500
Sample Number
Sensor Number
14
12
10
8
6
4
2

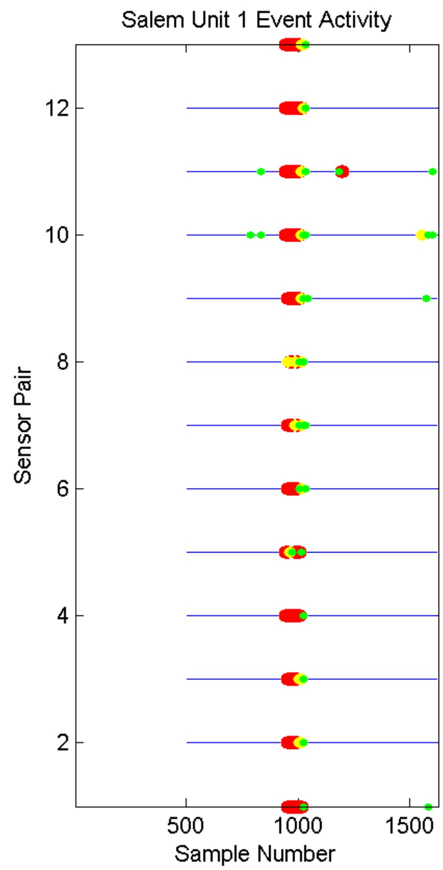
Salem Unit 1 Event Activity
Sensor Pair
12
10
8
6
4
2
500
1000
1500
Sample Number

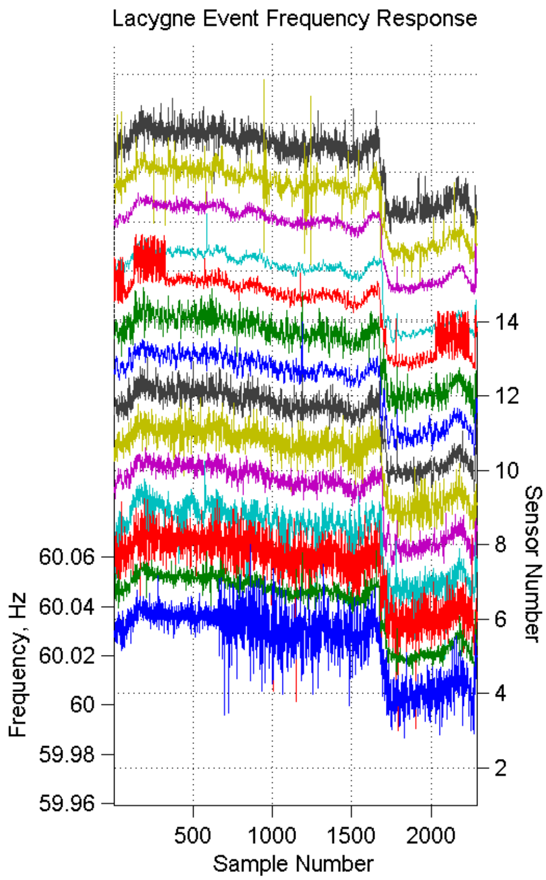
Lacygne Event Frequency Response
Frequency, Hz
Sample Number
Sensor Number
60.06
60.04
60.02
60
59.98
59.96
500
1000
1500
2000
14
12
10
8
6
4
2

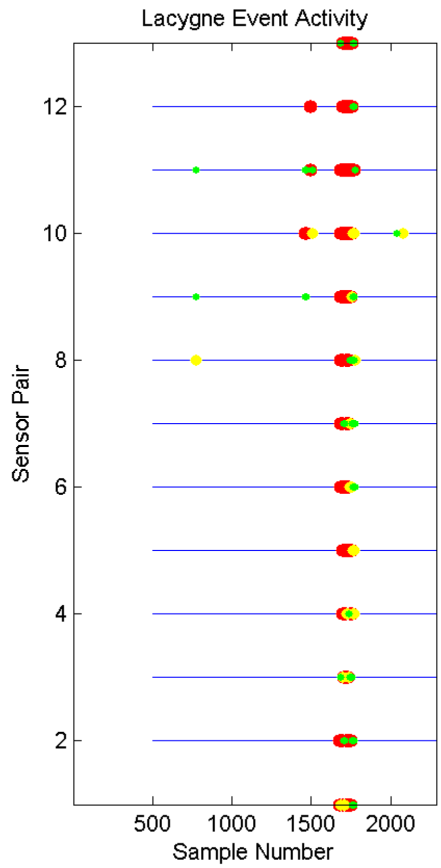
Lacygne Event Activity
Sensor Pair
Sample Number
12
10
8
6
4
2
500
1000
1500
2000

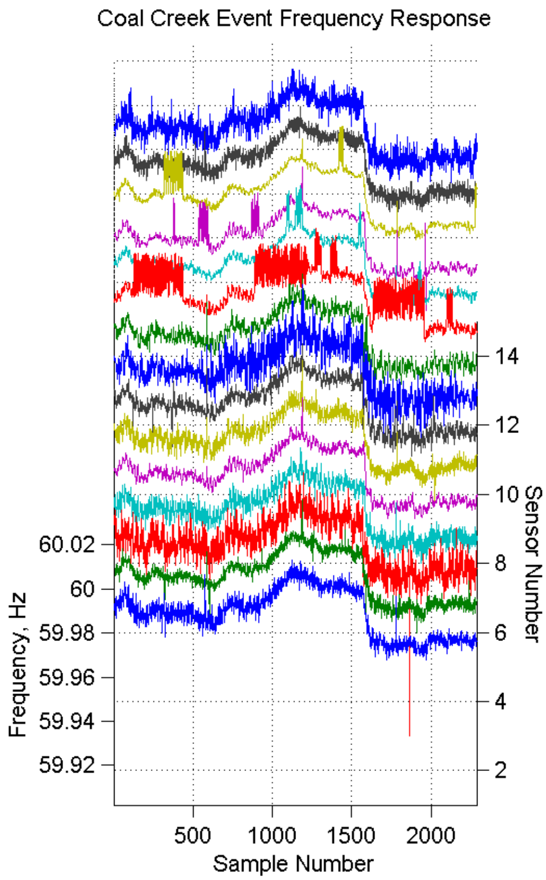
Coal Creek Event Frequency Response
60.02
60
59.98
59.96
59.94
59.92
Frequency, Hz
500
1000
1500
2000
Sample Number
14
12
10
8
6
4
2
Sensor Number

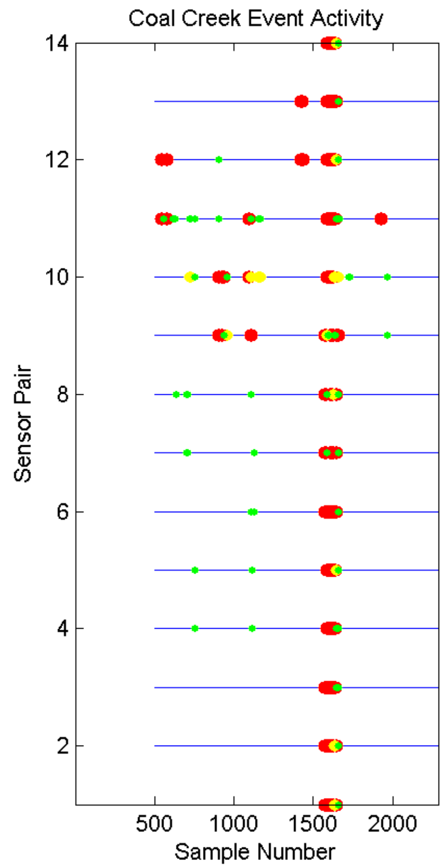
Coal Creek Event Activity
14
12
10
8
6
4
2
Sensor Pair
500
1000
1500
2000
Sample Number

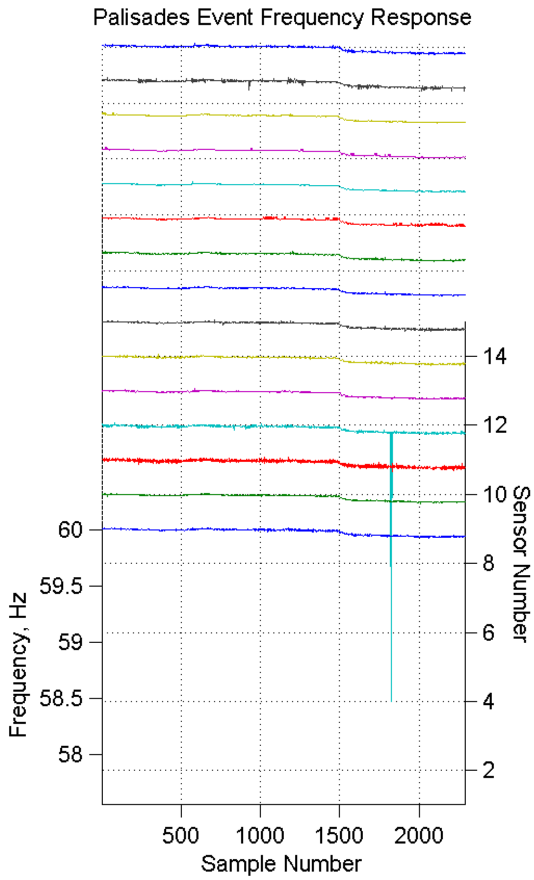
Palisades Event Frequency Response
60
59.5
59
58.5
58
Frequency, Hz
500
1000
1500
2000
Sample Number
14
12
10
8
6
4
2
Sensor Number

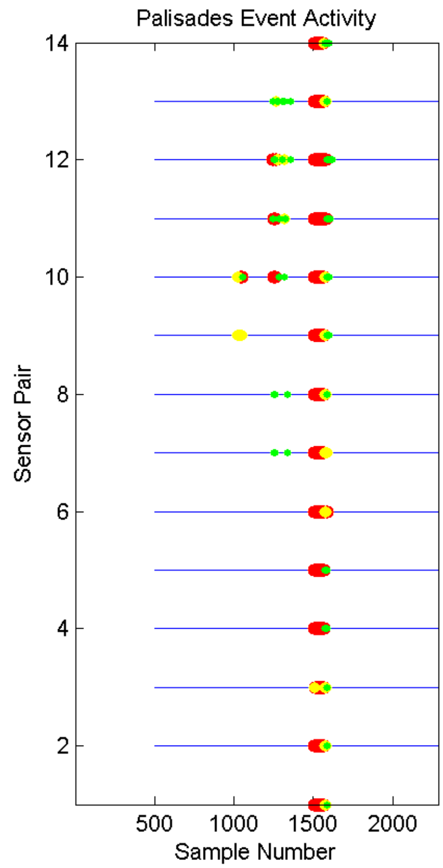
Palisades Event Activity
14
12
10
8
6
4
2
Sensor Pair
500
1000
1500
2000
Sample Number

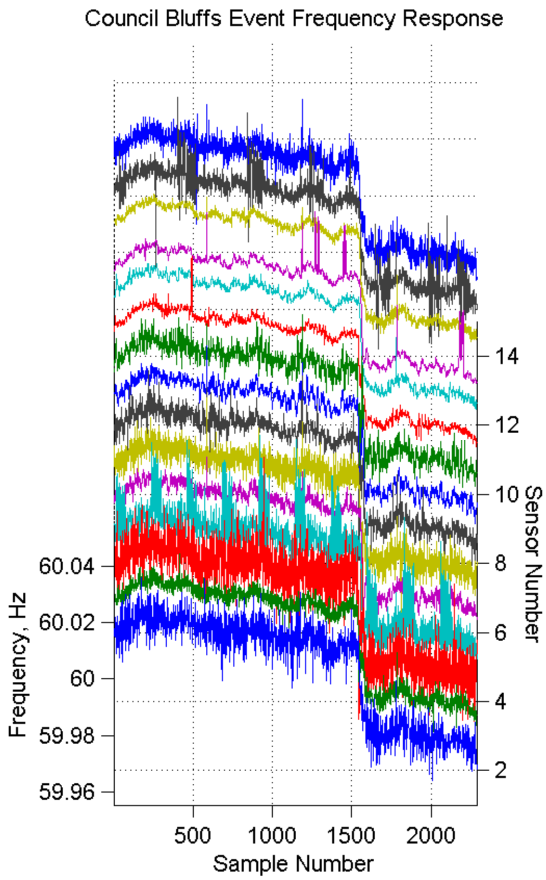
Council Bluffs Event Frequency Response
Frequency, Hz
60.04
60.02
60
59.98
59.96
500
1000
1500
2000
Sample Number
14
12
10
8
6
4
2
Sensor Number

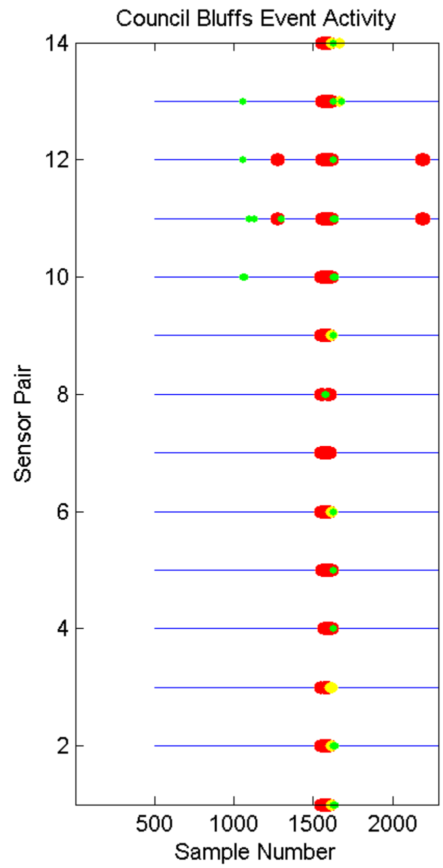
Council Bluffs Event Activity
Sensor Pair
14
12
10
8
6
4
2
500
1000
1500
2000
Sample Number

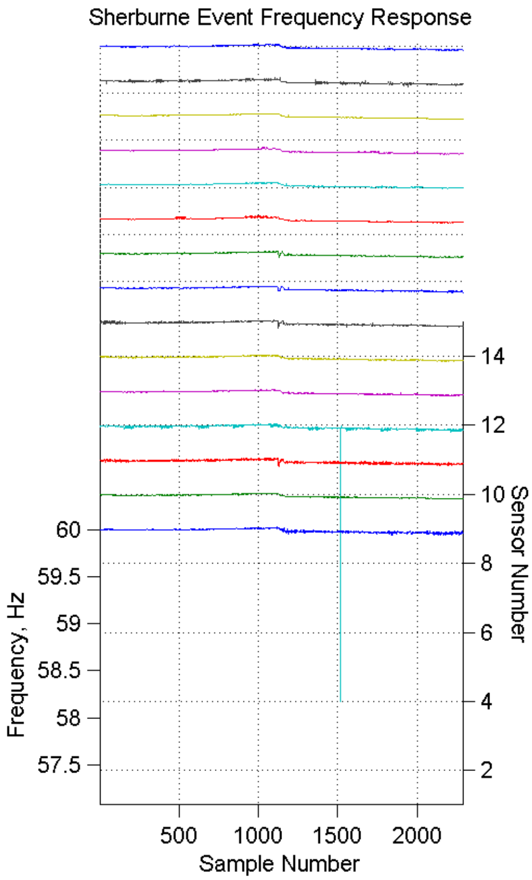
Sherburne Event Frequency Response
Frequency, Hz
60
59.5
59
58.5
58
57.5
Sensor Number
14
12
10
8
6
4
2
500
1000
1500
2000
Sample Number

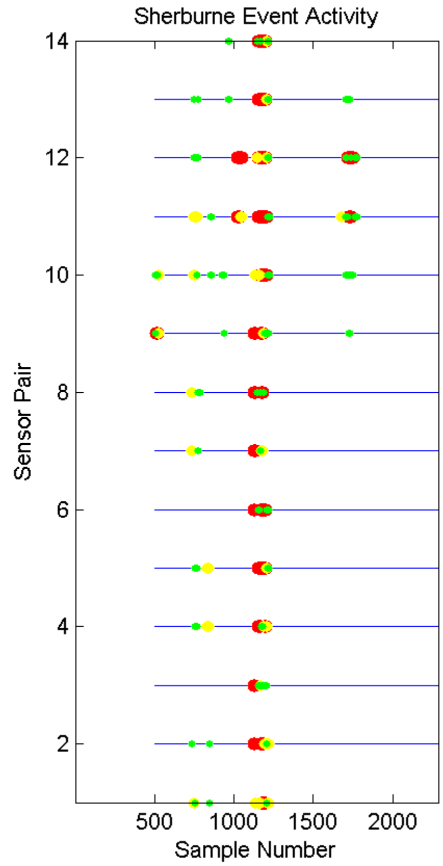
Sherburne Event Activity
Sensor Pair
14
12
10
8
6
4
2
500
1000
1500
2000
Sample Number

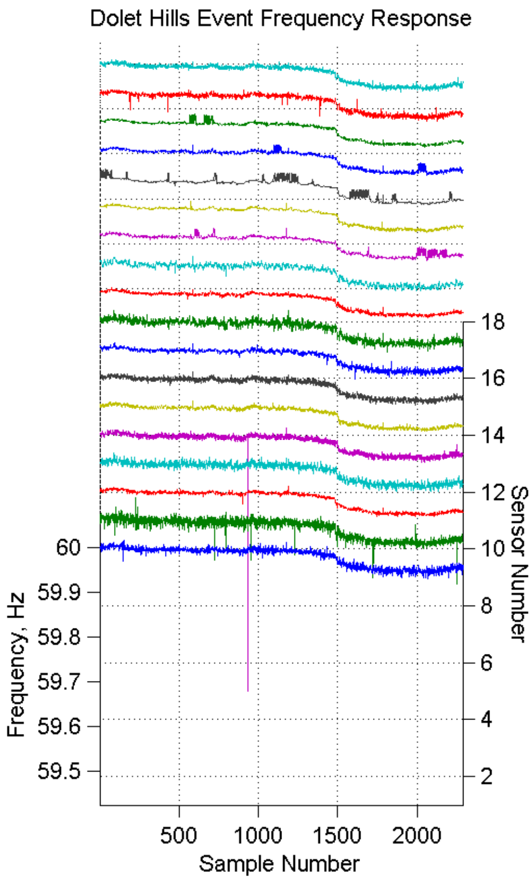
Dolet Hills Event Frequency Response
Frequency, Hz
60
59.9
59.8
59.7
59.6
59.5
500
1000
1500
2000
Sample Number
Sensor Number
18
16
14
12
10
8
6
4
2

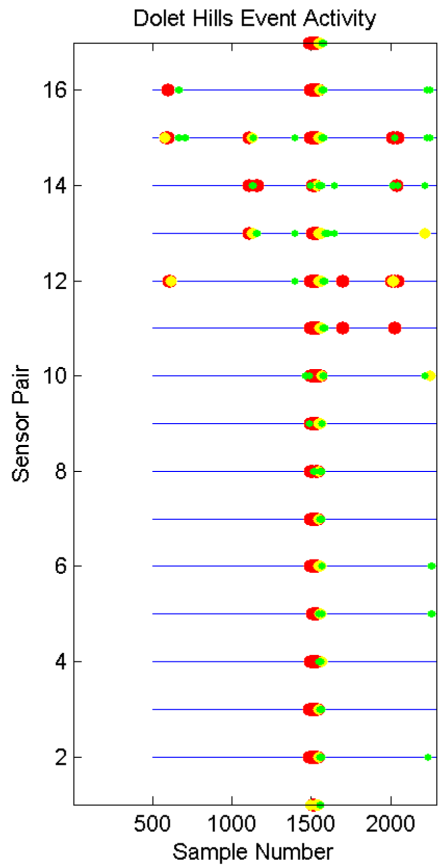
Dolet Hills Event Activity
Sensor Pair
16
14
12
10
8
6
4
2
500
1000
1500
2000
Sample Number

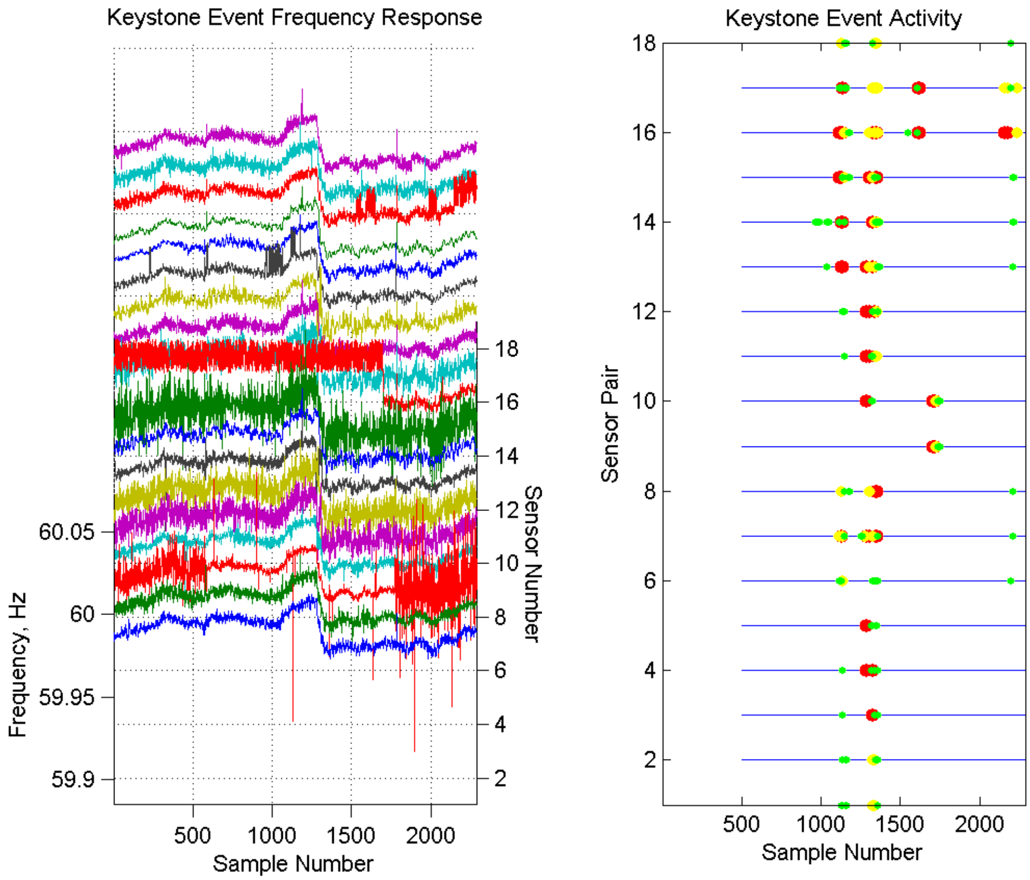
Keystone Event Frequency Response
Frequency, Hz
Sample Number
Sensor Number
60.05
60
59.95
59.9
500
1000
1500
2000
18
16
14
12
10
8
6
4
2
Keystone Event Activity
Sensor Pair

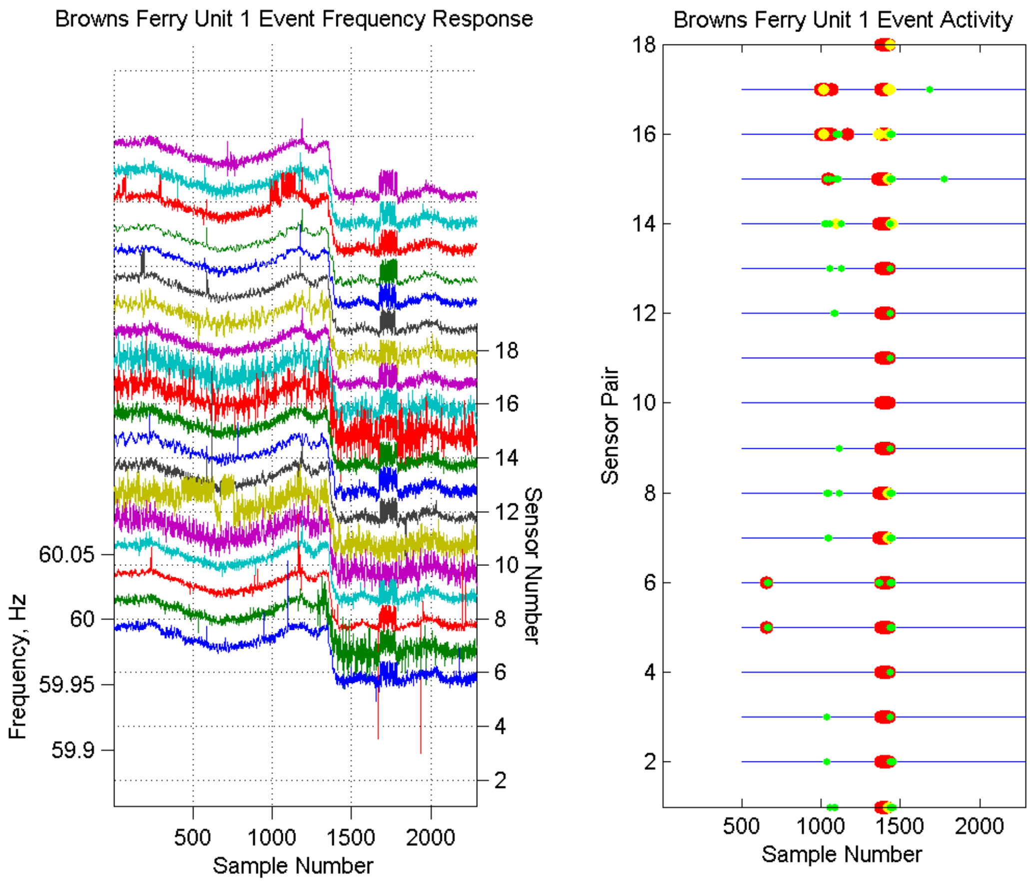

Browns Ferry Unit 1 Event Frequency Response
Frequency, Hz
60.05
60
59.95
59.9
500
1000
1500
2000
Sample Number
Sensor Number
18
16
14
12
10
8
6
4
2
Browns Ferry Unit 1 Event Activity
Sensor Pair
18
16
14
12
10
8
6
4
2
500
1000
1500
2000
Sample Number

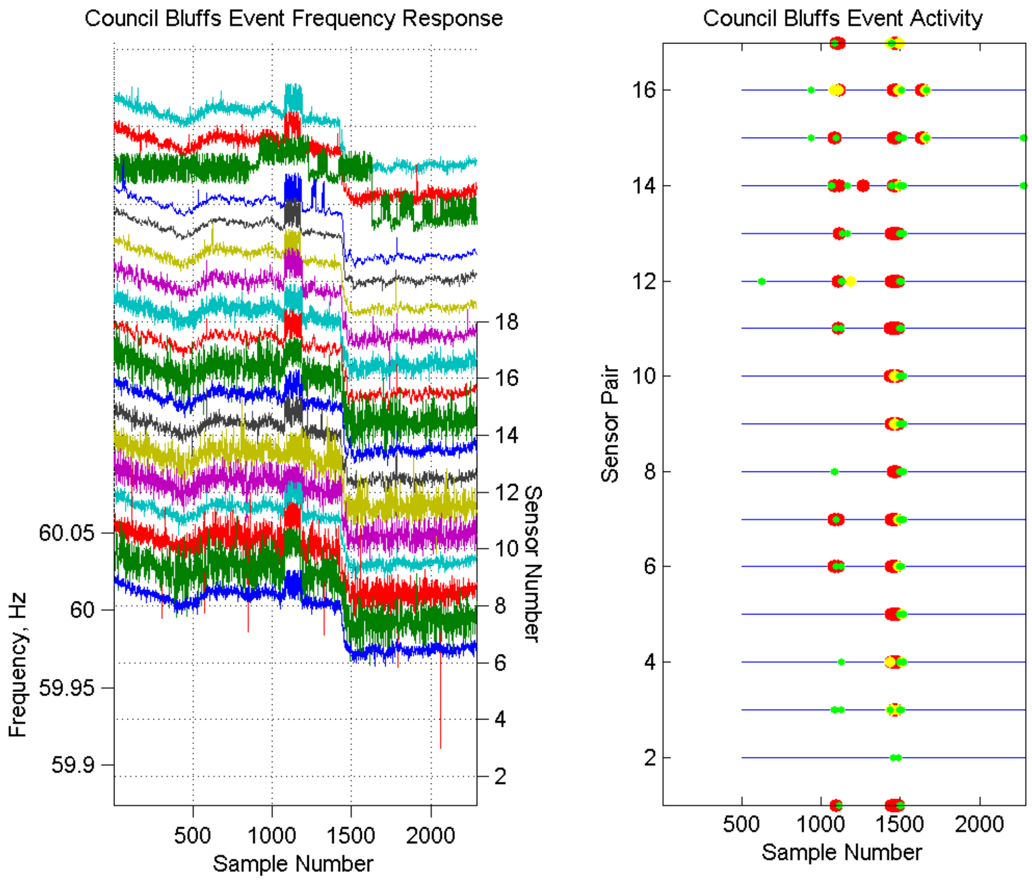
Council Bluffs Event Frequency Response
Frequency, Hz
60.05
60
59.95
59.9
500
1000
1500
2000
Sample Number
18
16
14
12
10
8
6
4
2
Sensor Number
Council Bluffs Event Activity
Sensor Pair
16
14
12
10
8
6
4
2
500
1000
1500
2000
Sample Number

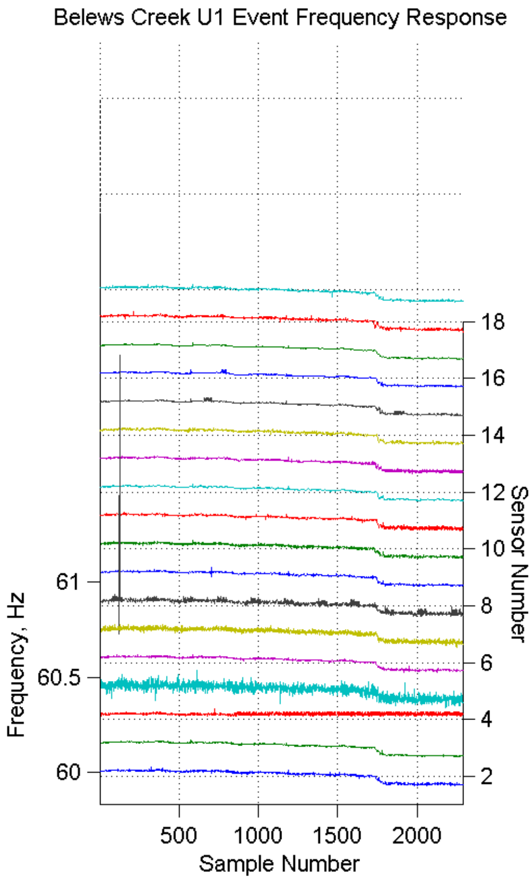
Belews Creek U1 Event Frequency Response
Frequency, Hz
61
60.5
60
500
1000
1500
2000
Sample Number
Sensor Number
18
16
14
12
10
8
6
4
2

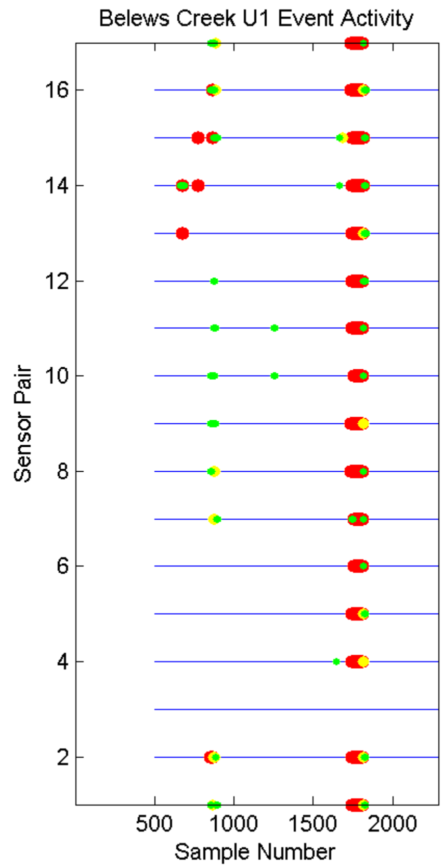
Belews Creek U1 Event Activity
Sensor Pair
16
14
12
10
8
6
4
2
500
1000
1500
2000
Sample Number

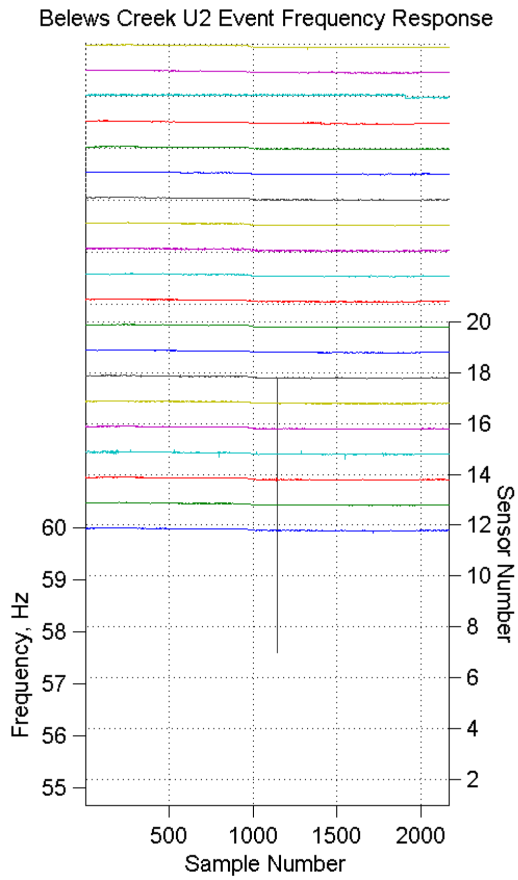
Belews Creek U2 Event Frequency Response
Frequency, Hz
60
59
58
57
56
55
500
1000
1500
2000
Sample Number
Sensor Number
20
18
16
14
12
10
8
6
4
2

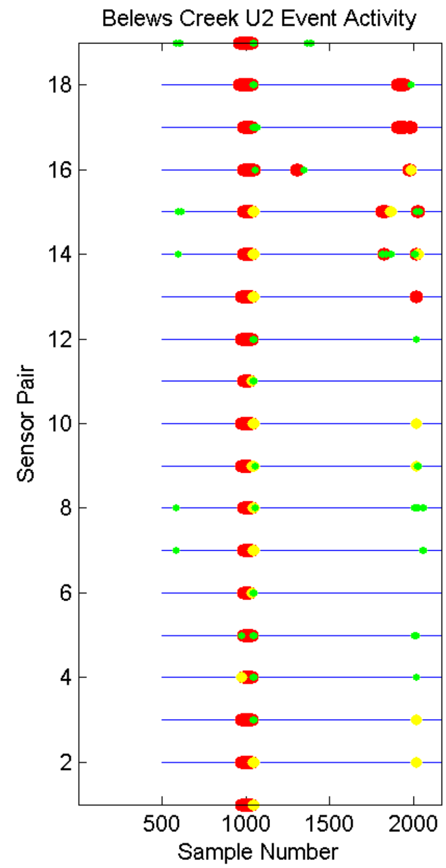
Belews Creek U2 Event Activity
Sensor Pair
18
16
14
12
10
8
6
4
2
500
1000
1500
2000
Sample Number

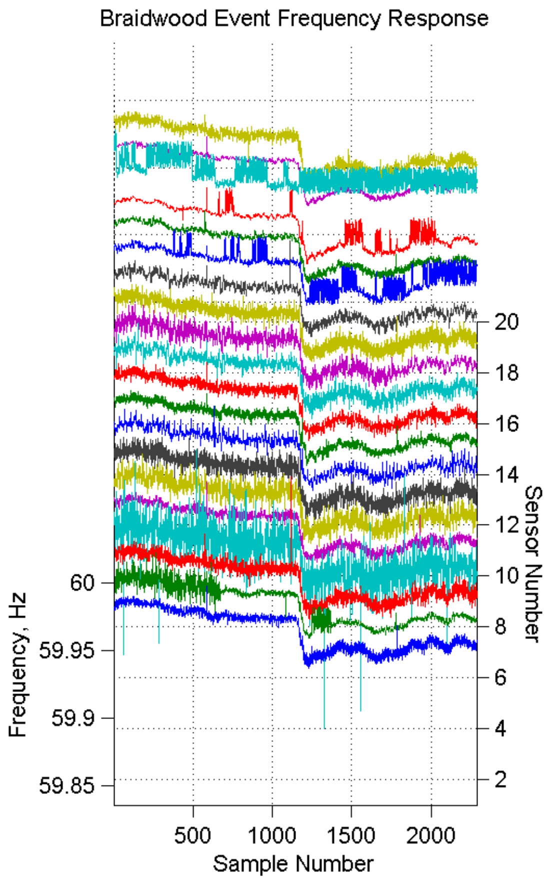
Braidwood Event Frequency Response
Frequency, Hz
60
59.95
59.9
59.85
500
1000
1500
2000
Sample Number
20
18
16
14
12
10
8
6
4
2
Sensor Number

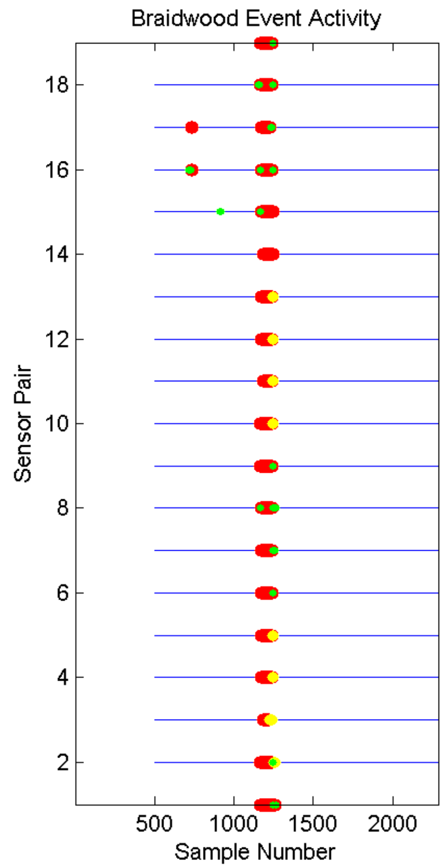
Braidwood Event Activity
Sensor Pair
18
16
14
12
10
8
6
4
2
500
1000
1500
2000
Sample Number

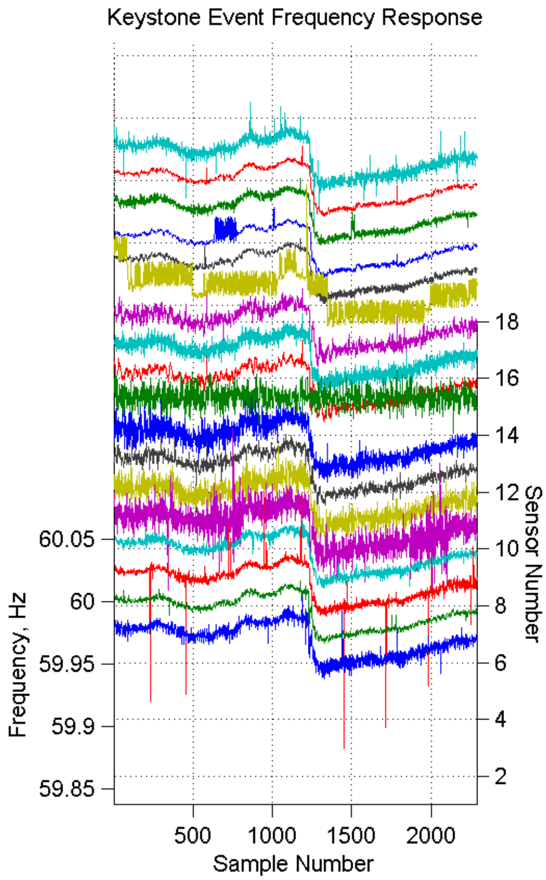
Keystone Event Frequency Response
Frequency, Hz
60.05
60
59.95
59.9
59.85
500
1000
1500
2000
Sample Number
Sensor Number
18
16
14
12
10
8
6
4
2

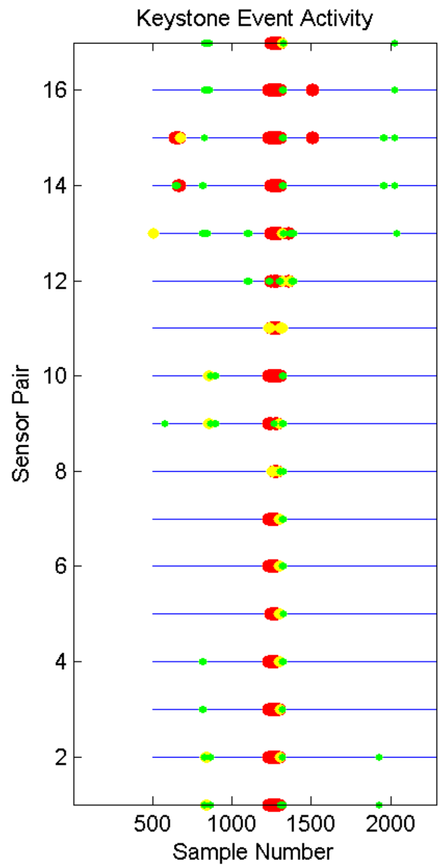
Keystone Event Activity
Sensor Pair
16
14
12
10
8
6
4
2
500
1000
1500
2000
Sample Number

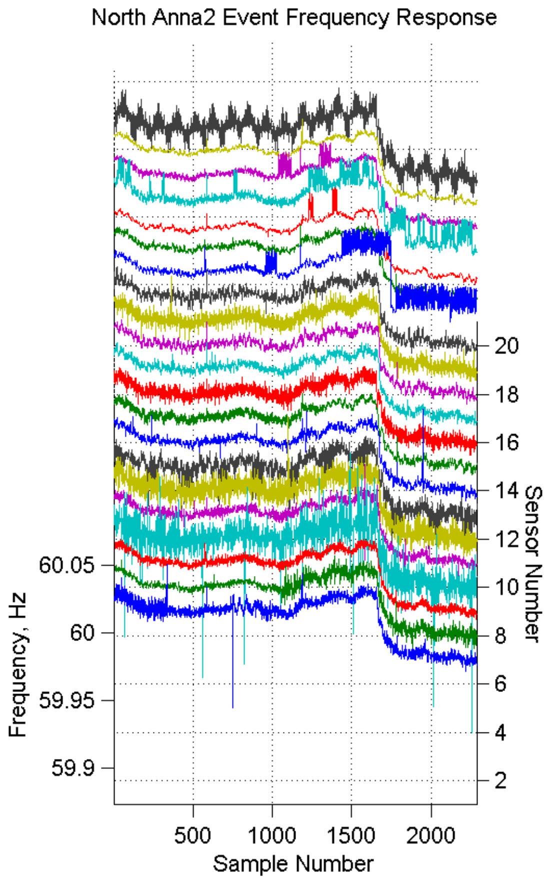
North Anna2 Event Frequency Response
Frequency, Hz
60.05
60
59.95
59.9
500
1000
1500
2000
Sample Number
Sensor Number
20
18
16
14
12
10
8
6
4
2

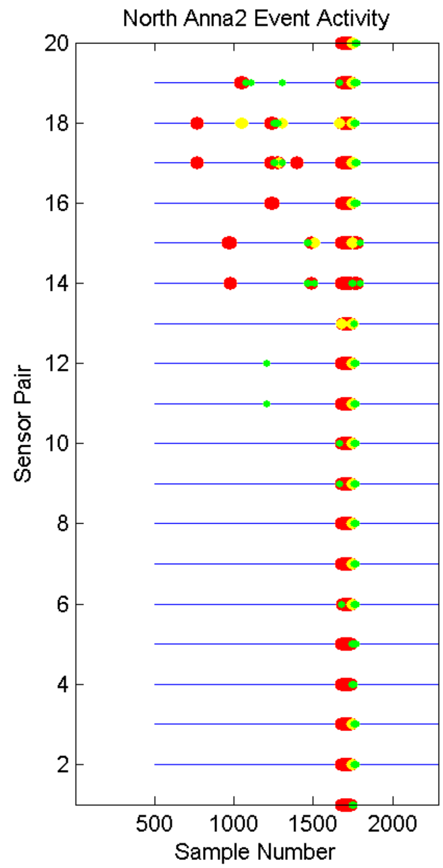
North Anna2 Event Activity
Sensor Pair
20
18
16
14
12
10
8
6
4
2
500
1000
1500
2000
Sample Number

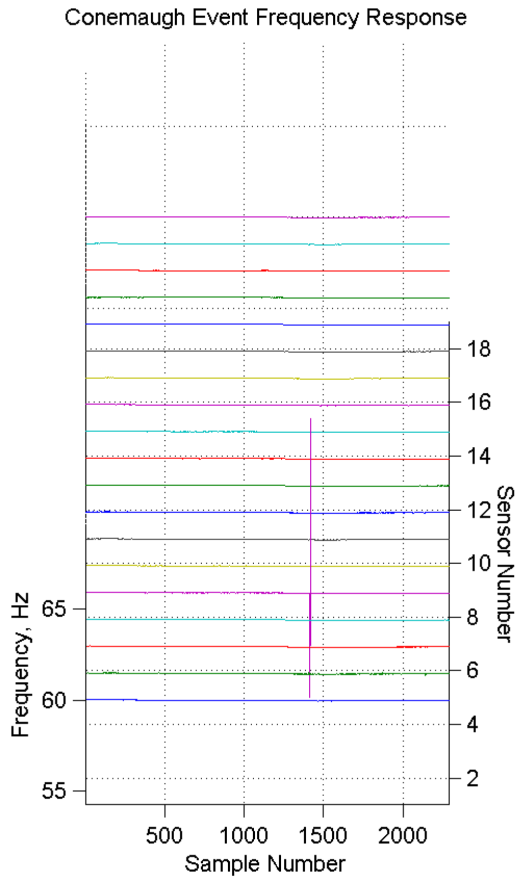
Conemaugh Event Frequency Response
Frequency, Hz
55
60
65
Sample Number
500
1000
1500
2000
Sensor Number
2
4
6
8
10
12
14
16
18

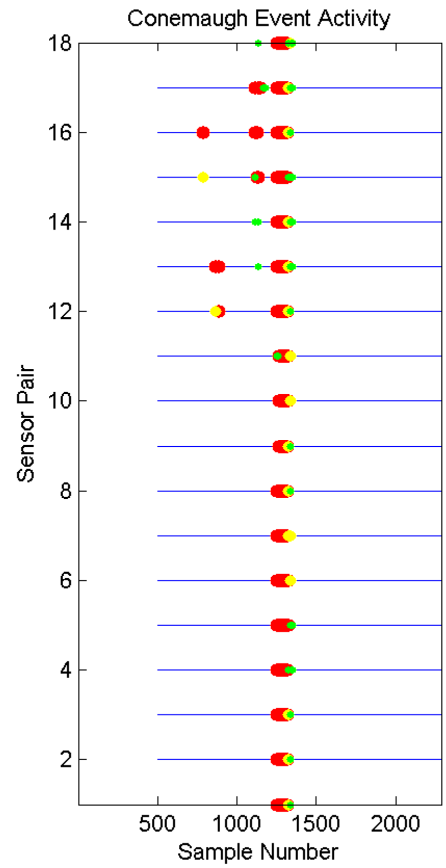
Conemaugh Event Activity
Sensor Pair
2
4
6
8
10
12
14
16
18
Sample Number
500
1000
1500
2000

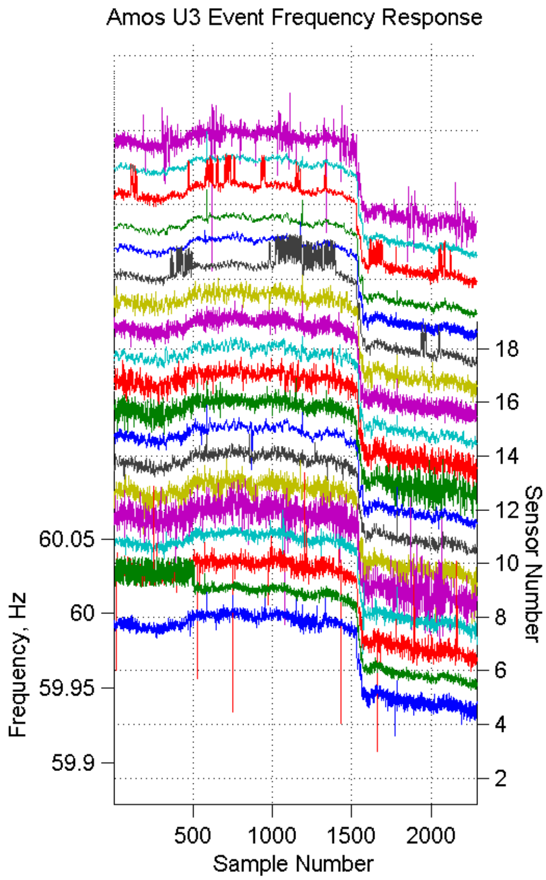
Amos U3 Event Frequency Response
60.05
60
59.95
59.9
Frequency, Hz
500
1000
1500
2000
Sample Number
18
16
14
12
10
8
6
4
2
Sensor Number

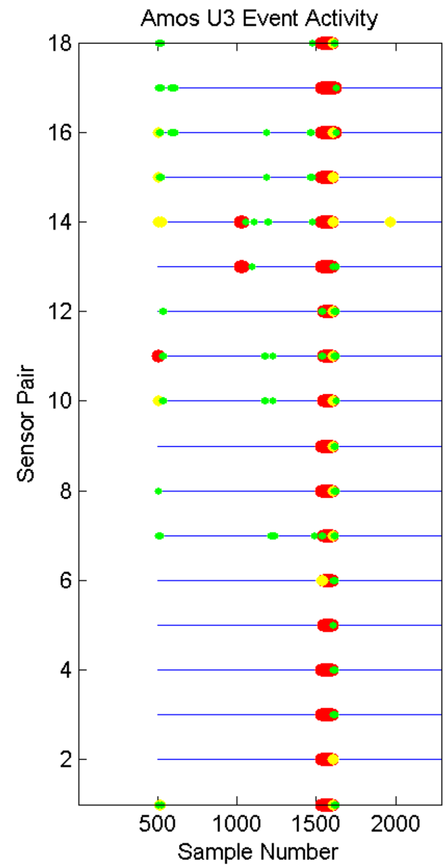
Amos U3 Event Activity
18
16
14
12
10
8
6
4
2
Sensor Pair
500
1000
1500
2000
Sample Number

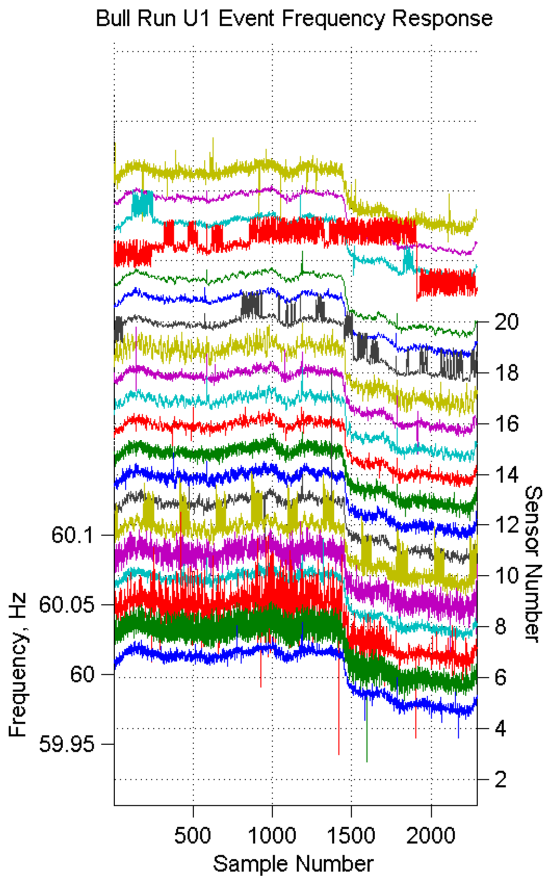
Bull Run U1 Event Frequency Response
Frequency, Hz
60.1
60.05
60
59.95
Sensor Number
20
18
16
14
12
10
8
6
4
2
500
1000
1500
2000
Sample Number

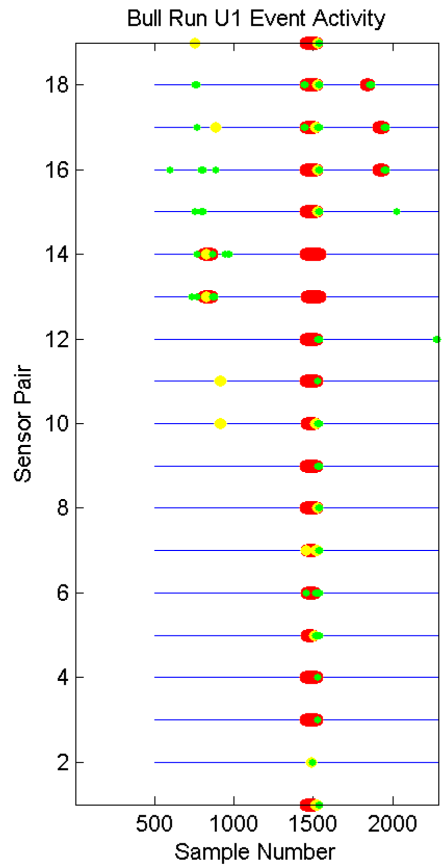
Bull Run U1 Event Activity
Sensor Pair
18
16
14
12
10
8
6
4
2
500
1000
1500
2000
Sample Number

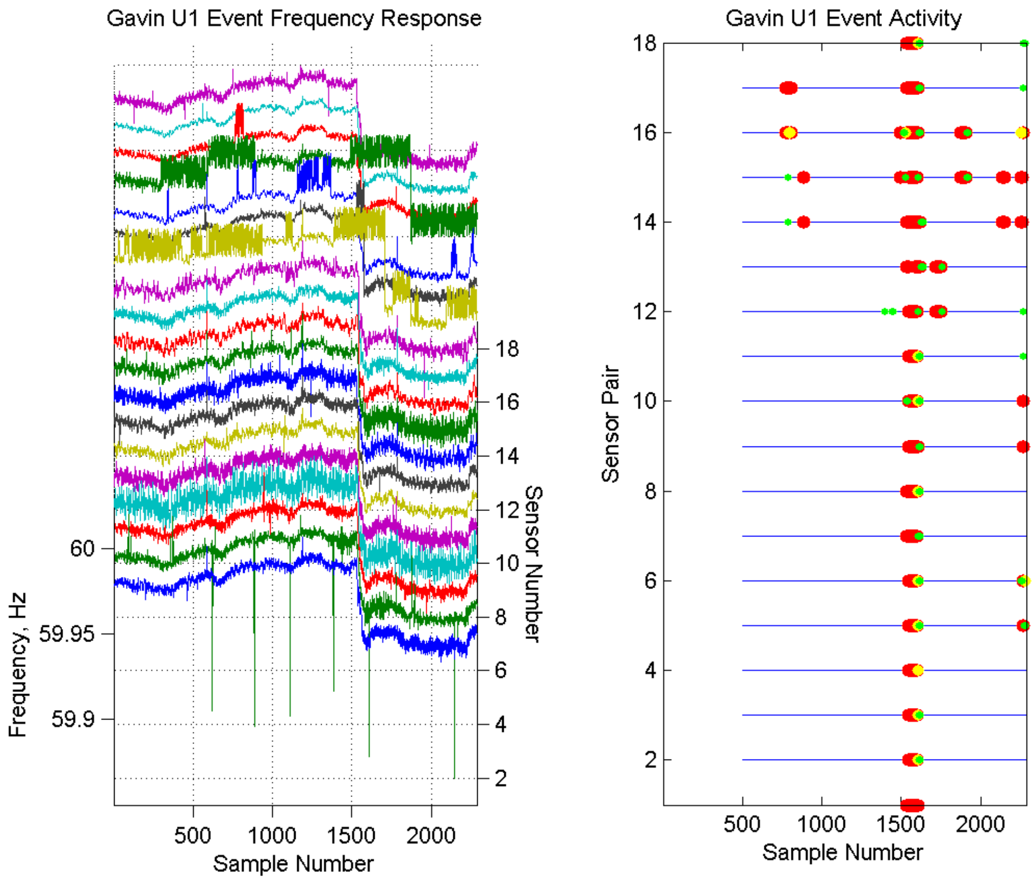
Gavin U1 Event Frequency Response
Frequency, Hz
60
59.95
59.9
500
1000
1500
2000
Sample Number
Sensor Number
18
16
14
12
10
8
6
4
2
Gavin U1 Event Activity
Sensor Pair
Sample Number

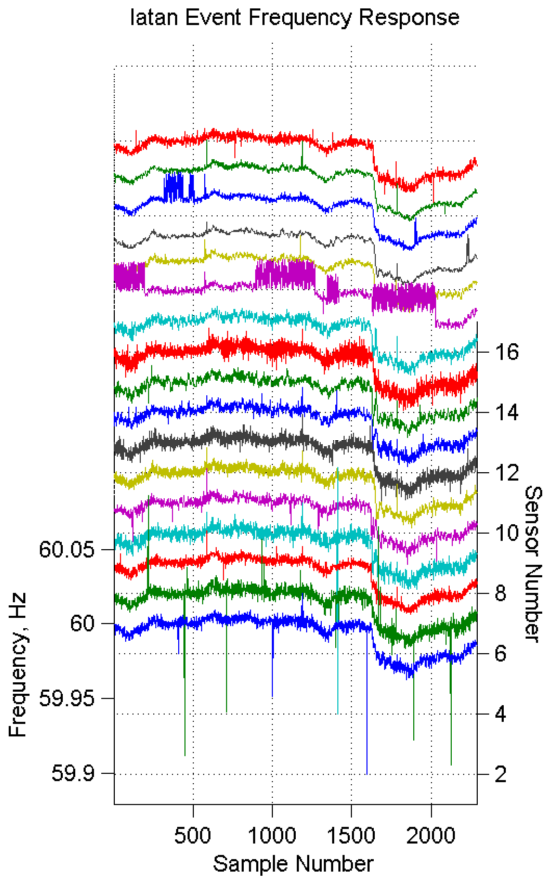
Iatan Event Frequency Response
60.05
60
59.95
59.9
Frequency, Hz
500
1000
1500
2000
Sample Number
16
14
12
10
8
6
4
2
Sensor Number

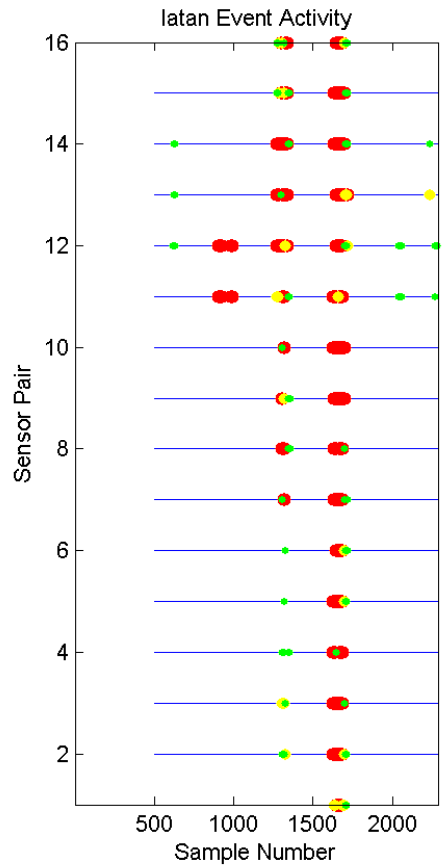
Iatan Event Activity
16
14
12
10
8
6
4
2
Sensor Pair
500
1000
1500
2000
Sample Number

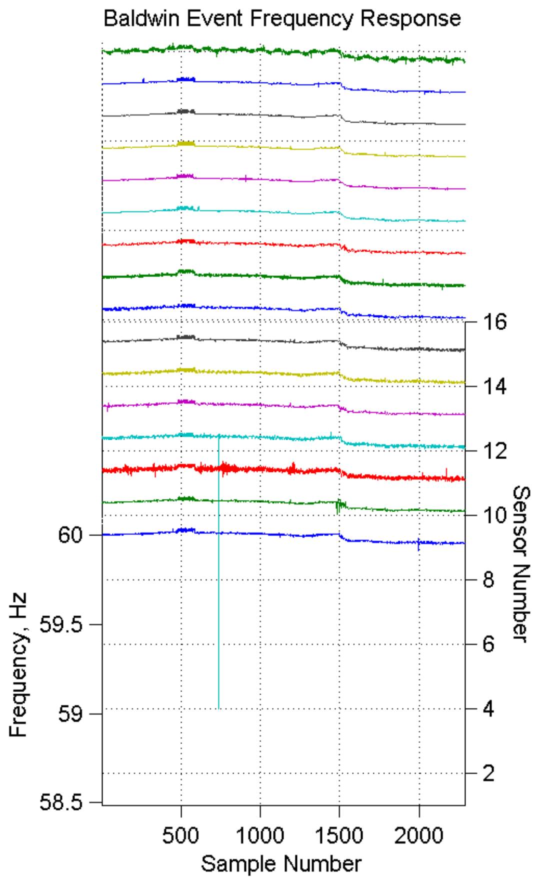
Baldwin Event Frequency Response
Frequency, Hz
60
59.5
59
58.5
500
1000
1500
2000
Sample Number
16
14
12
10
8
6
4
2
Sensor Number

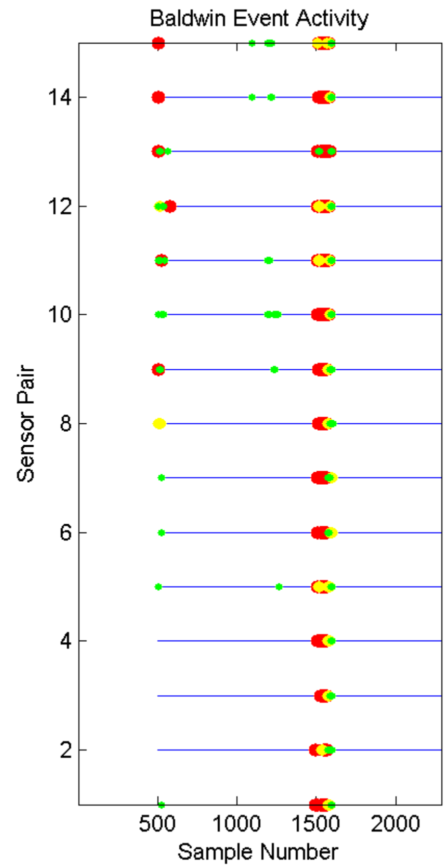
Baldwin Event Activity
Sensor Pair
14
12
10
8
6
4
2
500
1000
1500
2000
Sample Number

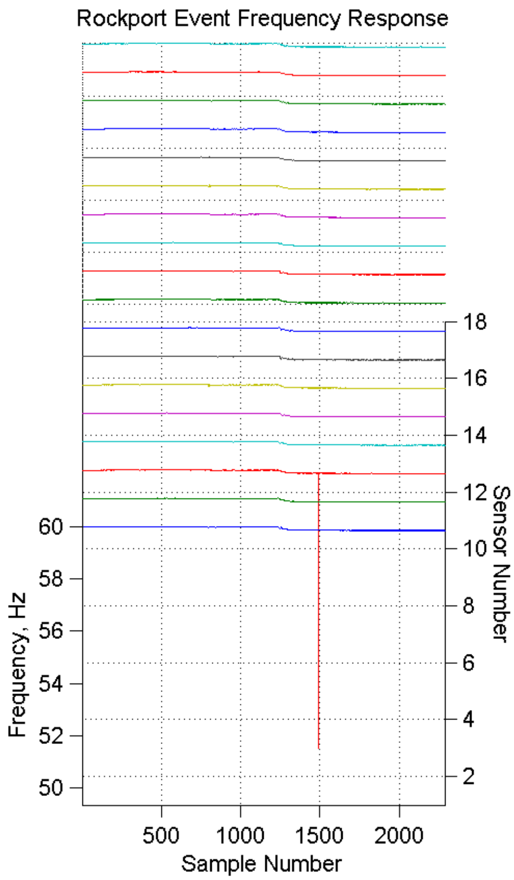

Rockport Event Frequency Response
Frequency, Hz
60
58
56
54
52
50
500
1000
1500
2000
Sample Number
18
16
14
12
10
8
6
4
2
Sensor Number

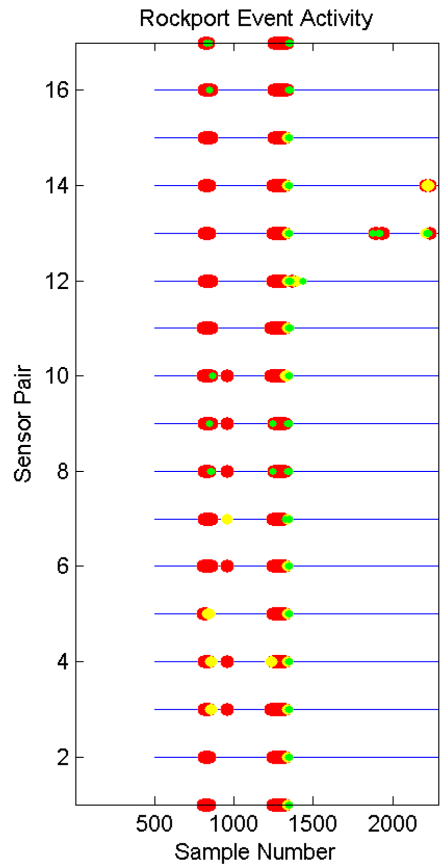

Rockport Event Activity
Sensor Pair
16
14
12
10
8
6
4
2
500
1000
1500
2000
Sample Number

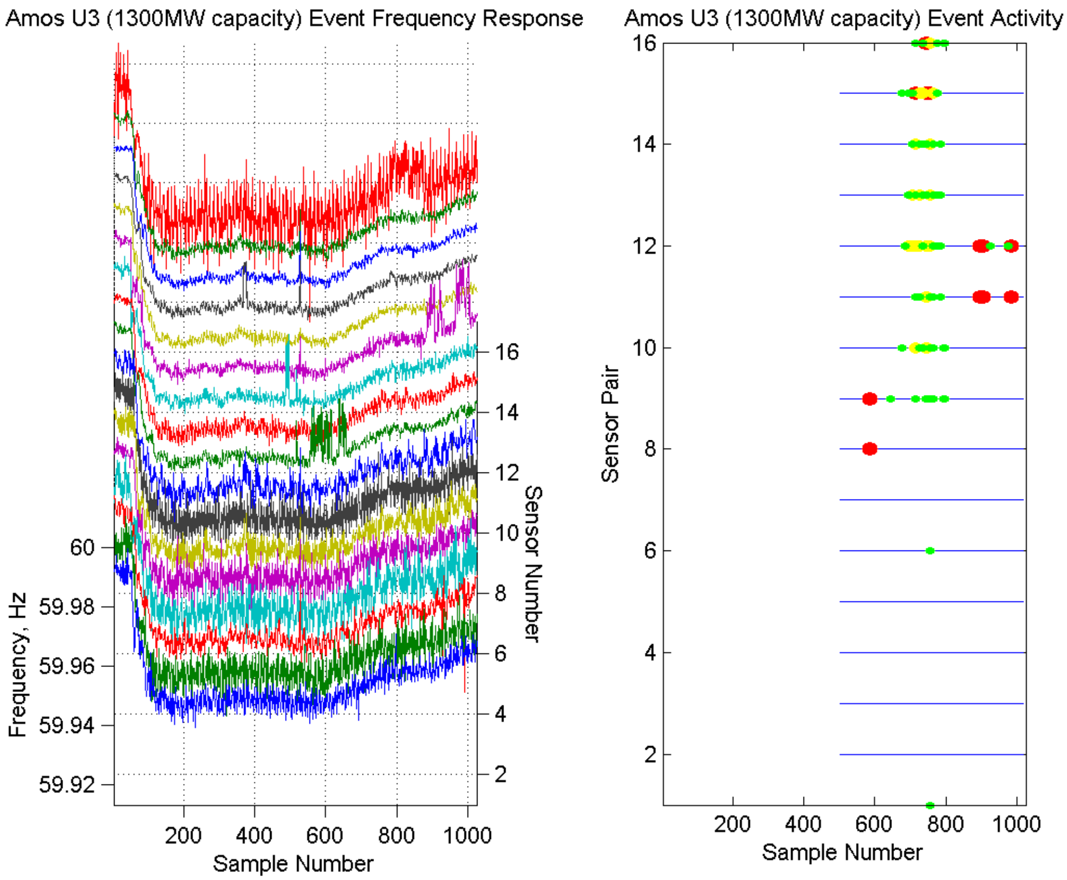
Amos U3 (1300MW capacity) Event Frequency Response
Frequency, Hz
60
59.98
59.96
59.94
59.92
200
400
600
800
1000
Sample Number
Sensor Number
16
14
12
10
8
6
4
2
Amos U3 (1300MW capacity) Event Activity
Sensor Pair
16
14
12
10
8
6
4
2
200
400
600
800
1000
Sample Number

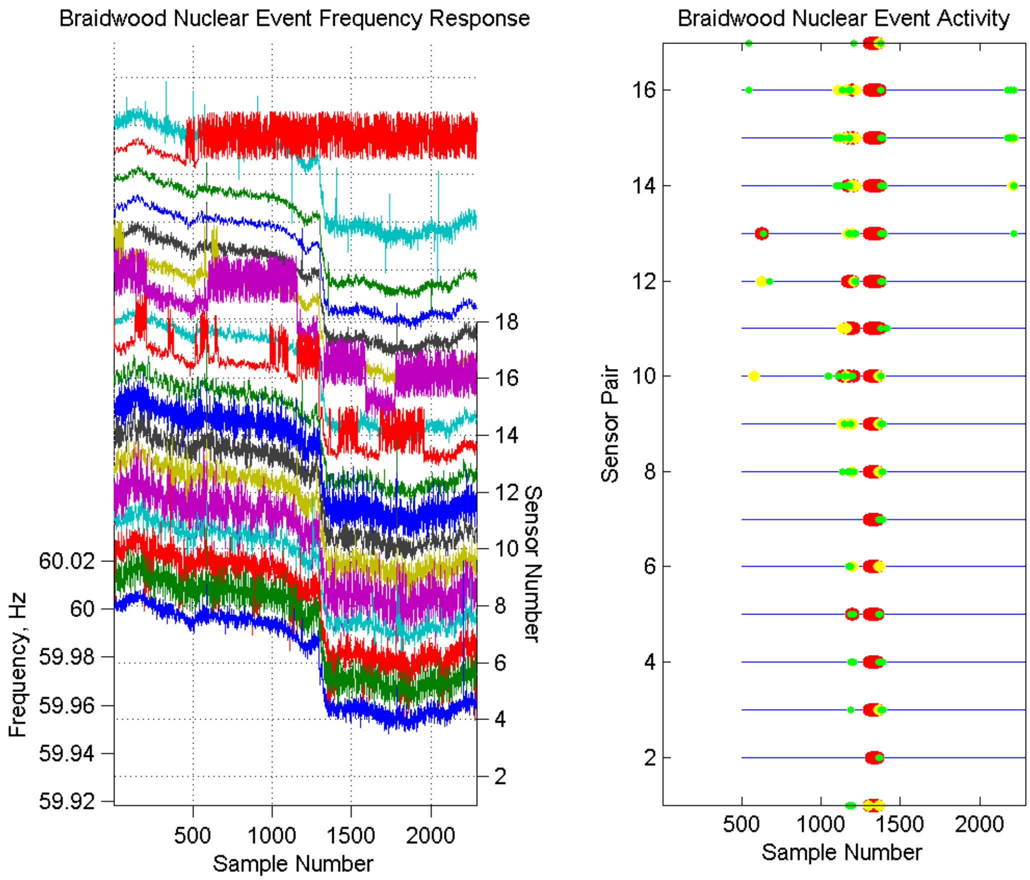
Braidwood Nuclear Event Frequency Response
Frequency, Hz
60.02
60
59.98
59.96
59.94
59.92
500
1000
1500
2000
Sample Number
Sensor Number
18
16
14
12
10
8
6
4
2
Braidwood Nuclear Event Activity
Sensor Pair
16
14
12
10
8
6
4
2
500
1000
1500
2000
Sample Number

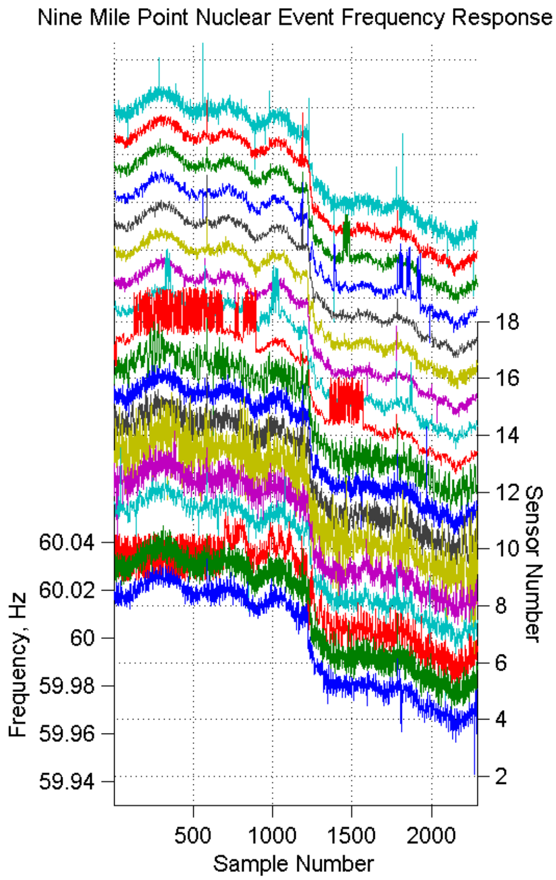
Nine Mile Point Nuclear Event Frequency Response
Frequency, Hz
60.04
60.02
60
59.98
59.96
59.94
500
1000
1500
2000
Sample Number
Sensor Number
18
16
14
12
10
8
6
4
2

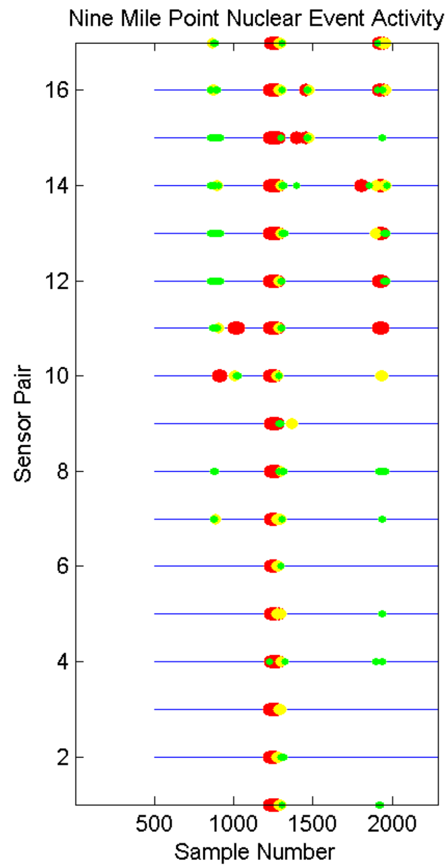
Nine Mile Point Nuclear Event Activity
Sensor Pair
16
14
12
10
8
6
4
2
500
1000
1500
2000
Sample Number

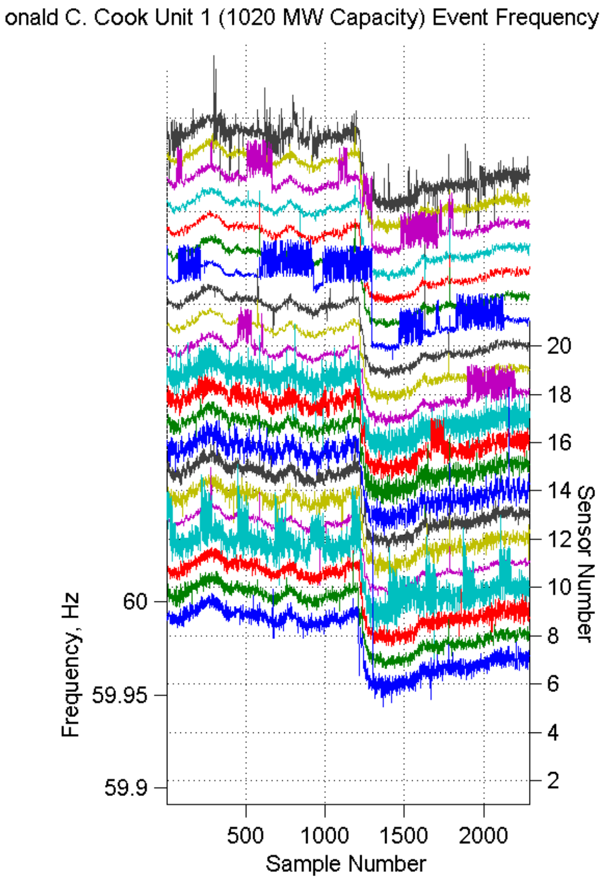
onald C. Cook Unit 1 (1020 MW Capacity) Event Frequency Response
Frequency, Hz
60
59.95
59.9
500
1000
1500
2000
Sample Number
20
18
16
14
12
10
8
6
4
2
Sensor Number

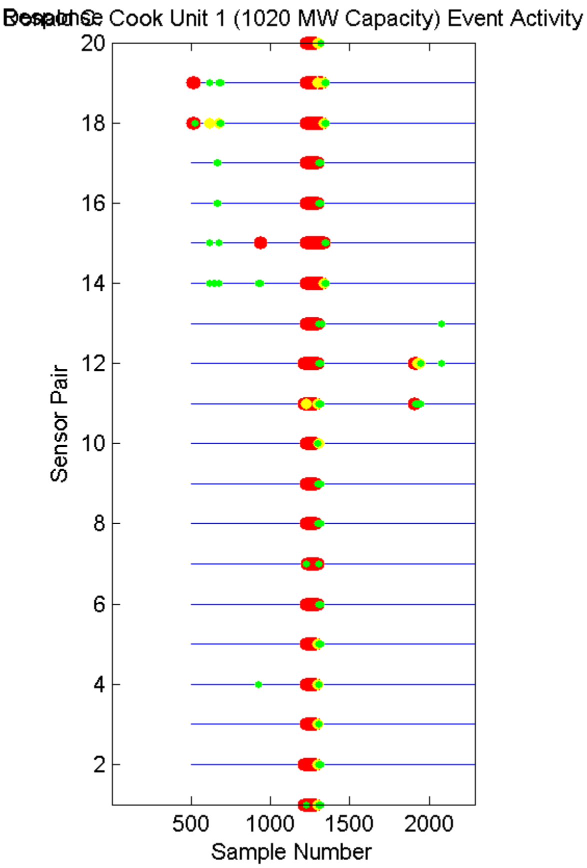
Cook Unit 1 (1020 MW Capacity) Event Activity
Sensor Pair
20
18
16
14
12
10
8
6
4
2
500
1000
1500
2000
Sample Number

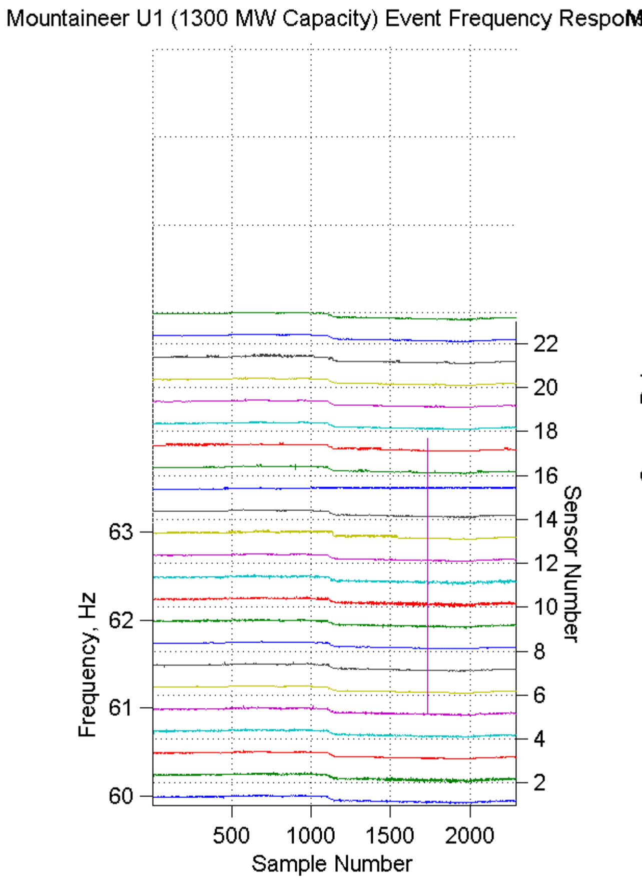
Mountaineer U1 (1300 MW Capacity) Event Frequency Response
Frequency, Hz
60
61
62
63
Sample Number
500
1000
1500
2000
Sensor Number
2
4
6
8
10
12
14
16
18
20
22

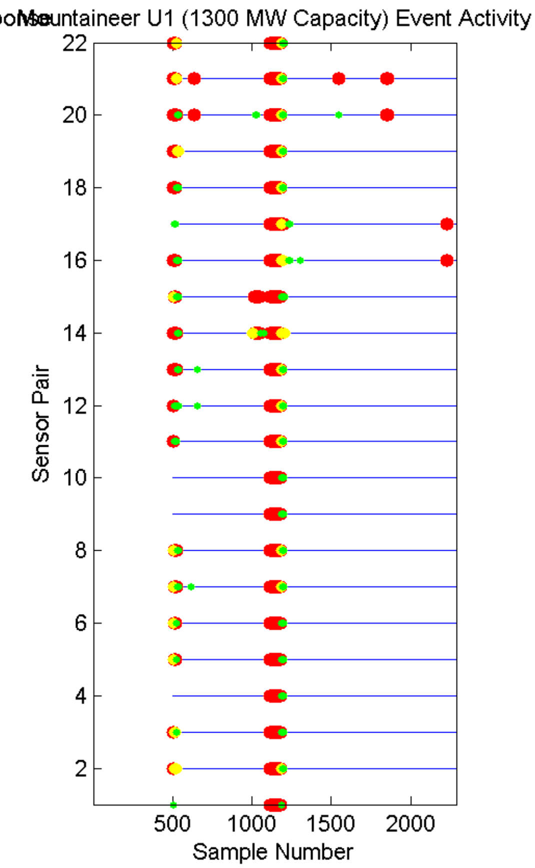
Mountaineer U1 (1300 MW Capacity) Event Activity
Sensor Pair
2
4
6
8
10
12
14
16
18
20
22
Sample Number
500
1000
1500
2000

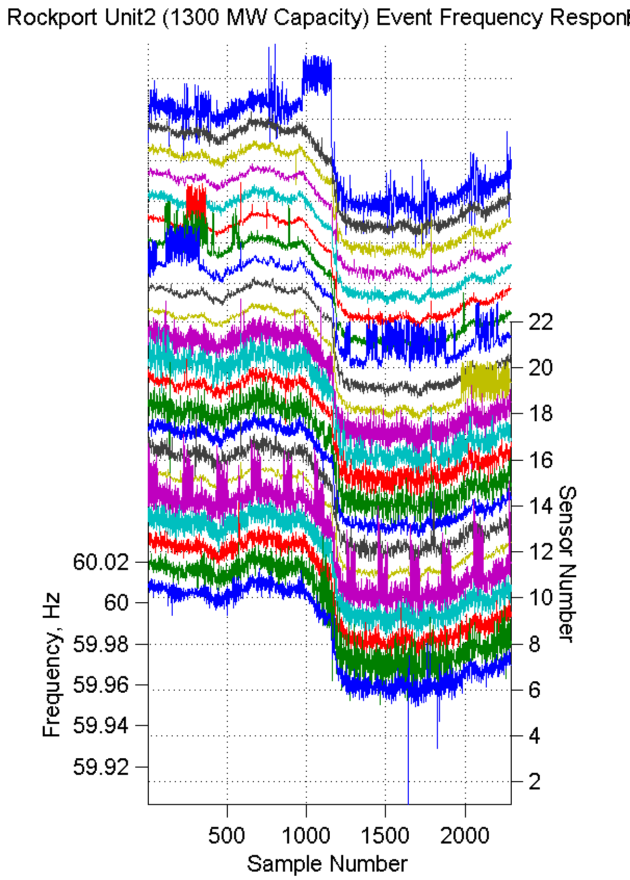
Rockport Unit2 (1300 MW Capacity) Event Frequency Response
Frequency, Hz
Sample Number
Sensor Number
60.02
60
59.98
59.96
59.94
59.92
500
1000
1500
2000
22
20
18
16
14
12
10
8
6
4
2

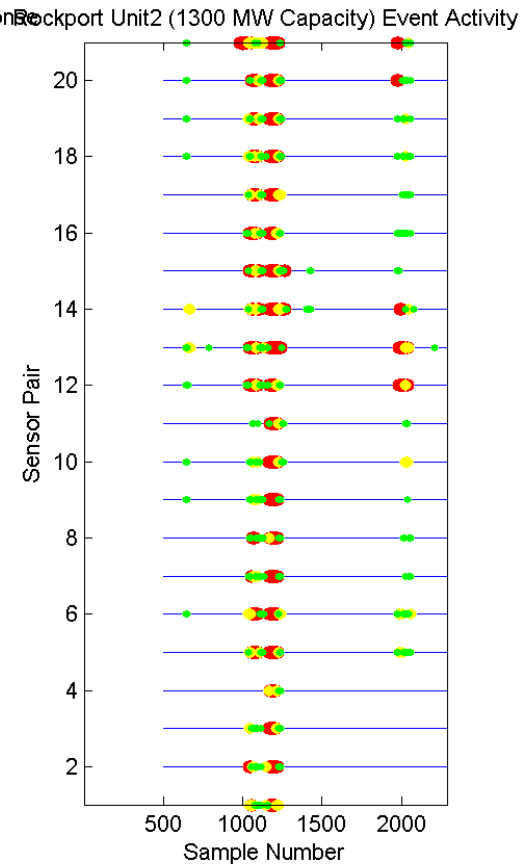
Rockport Unit2 (1300 MW Capacity) Event Activity
Sensor Pair
Sample Number
20
18
16
14
12
10
8
6
4
2
500
1000
1500
2000

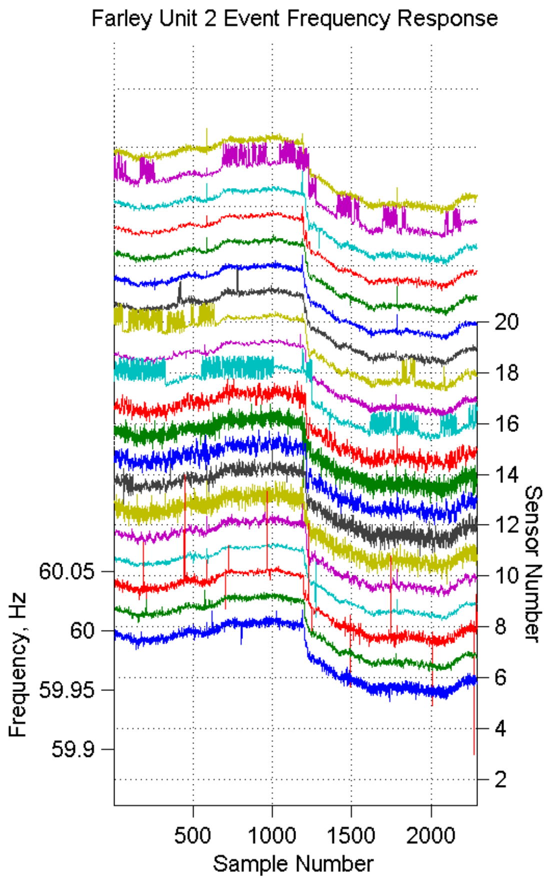
Farley Unit 2 Event Frequency Response
Frequency, Hz
60.05
60
59.95
59.9
500
1000
1500
2000
Sample Number
Sensor Number
20
18
16
14
12
10
8
6
4
2

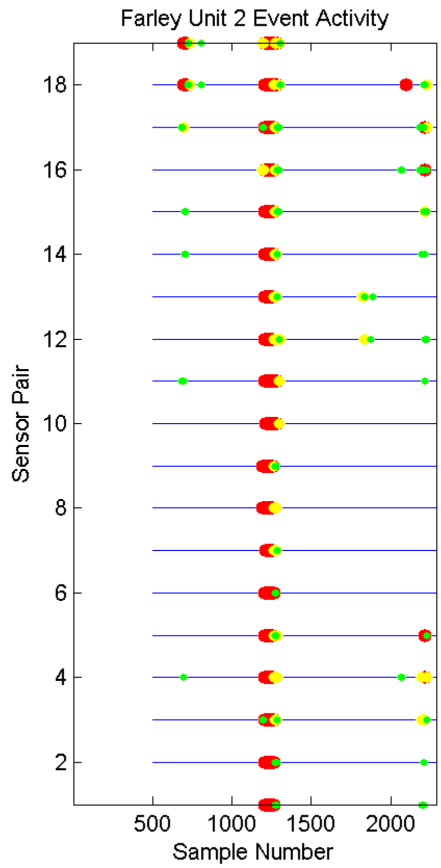
Farley Unit 2 Event Activity
Sensor Pair
18
16
14
12
10
8
6
4
2
500
1000
1500
2000
Sample Number

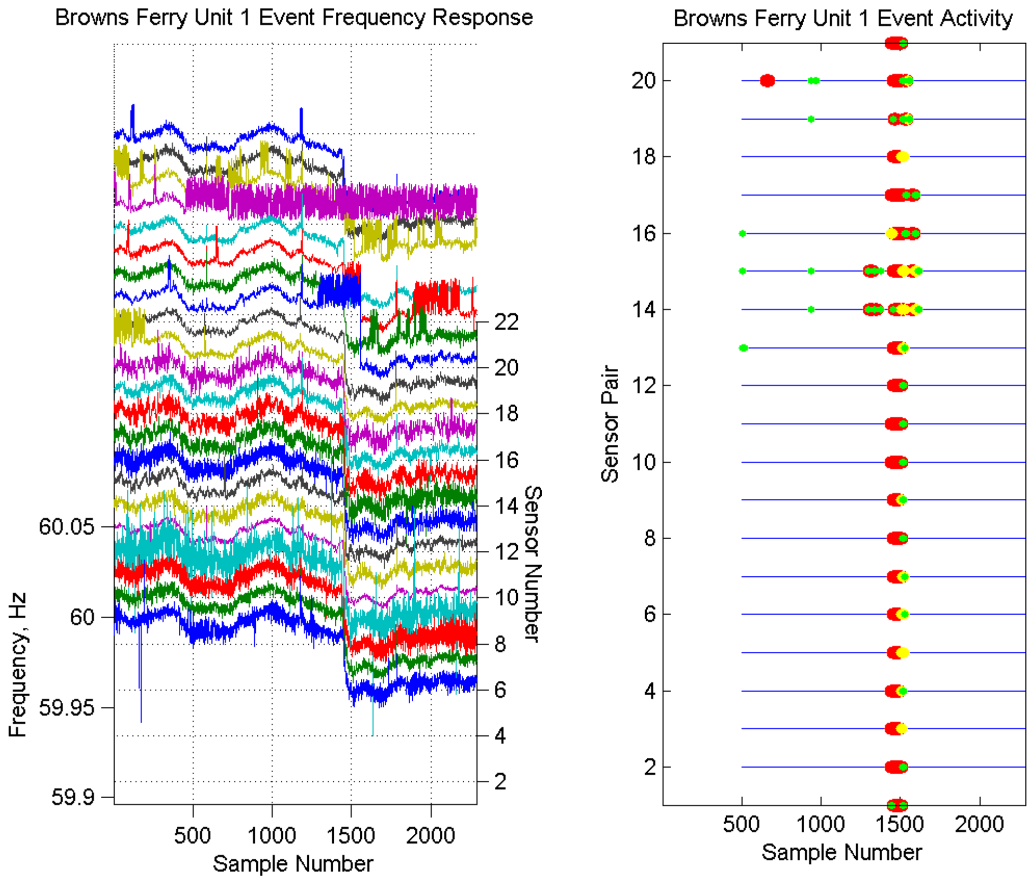
Browns Ferry Unit 1 Event Frequency Response
Frequency, Hz
60.05
60
59.95
59.9
500
1000
1500
2000
Sample Number
22
20
18
16
14
12
10
8
6
4
2
Sensor Number
Browns Ferry Unit 1 Event Activity
Sensor Pair
20
18
16
14
12
10
8
6
4
2
500
1000
1500
2000
Sample Number

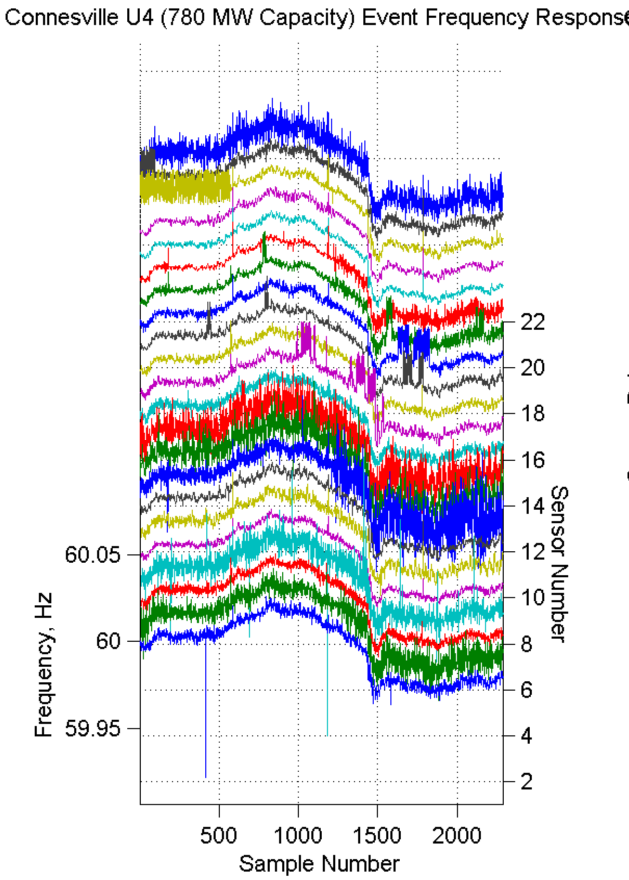
Connesville U4 (780 MW Capacity) Event Frequency Response
Frequency, Hz
Sample Number
Sensor Number
60.05
60
59.95
500
1000
1500
2000
22
20
18
16
14
12
10
8
6
4
2

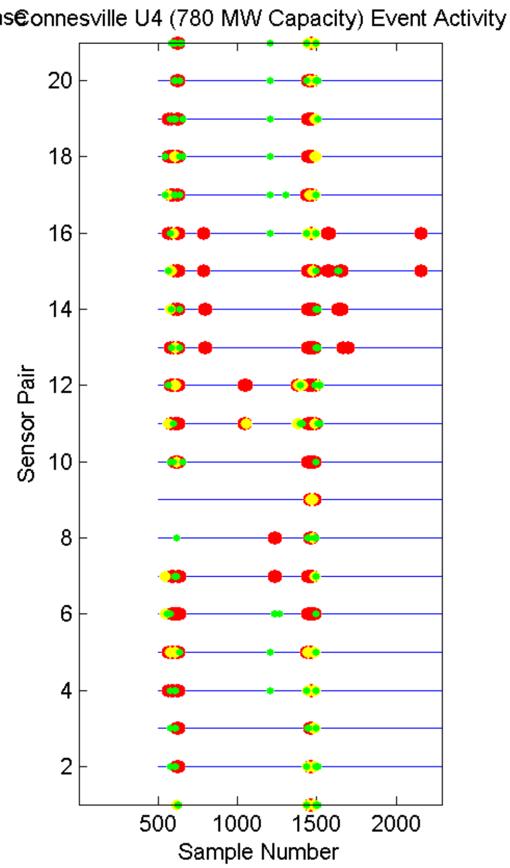
Connesville U4 (780 MW Capacity) Event Activity
Sensor Pair
Sample Number
20
18
16
14
12
10
8
6
4
2
500
1000
1500
2000

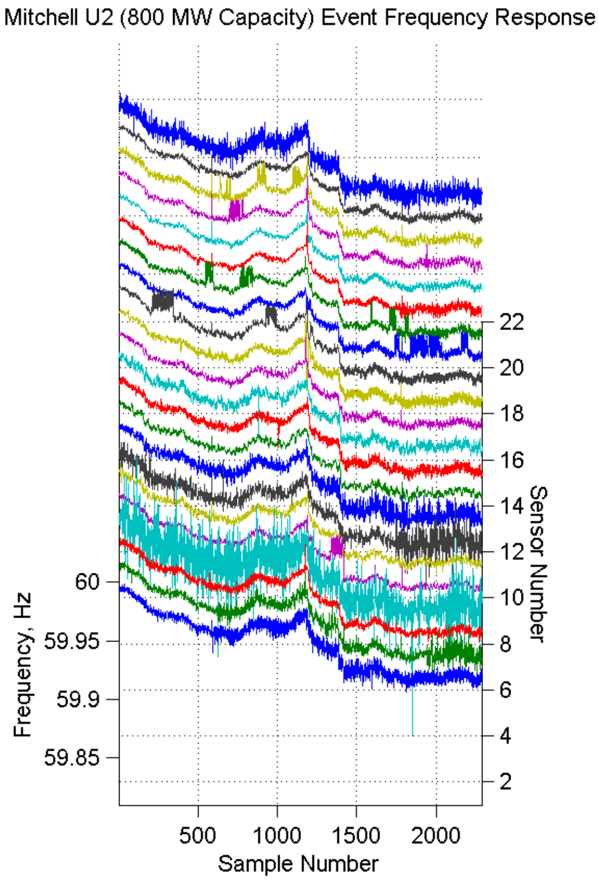
Mitchell U2 (800 MW Capacity) Event Frequency Response
Frequency, Hz
60
59.95
59.9
59.85
500
1000
1500
2000
Sample Number
Sensor Number
22
20
18
16
14
12
10
8
6
4
2

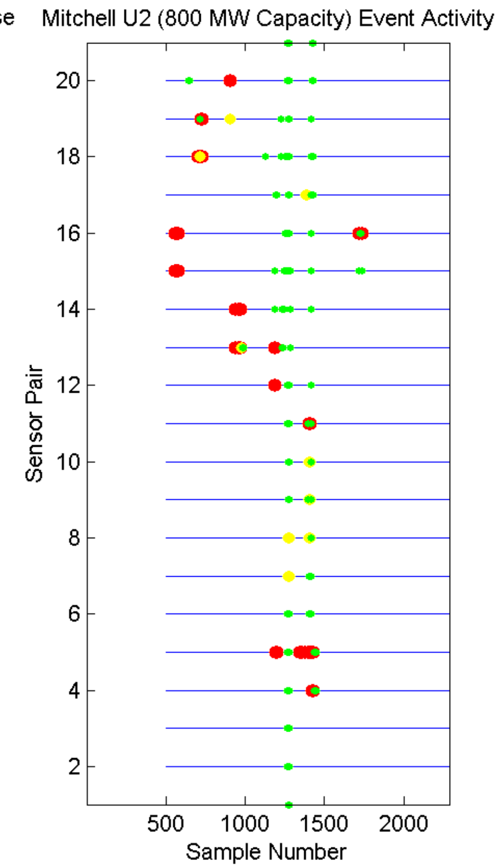
Mitchell U2 (800 MW Capacity) Event Activity
Sensor Pair
20
18
16
14
12
10
8
6
4
2
500
1000
1500
2000
Sample Number

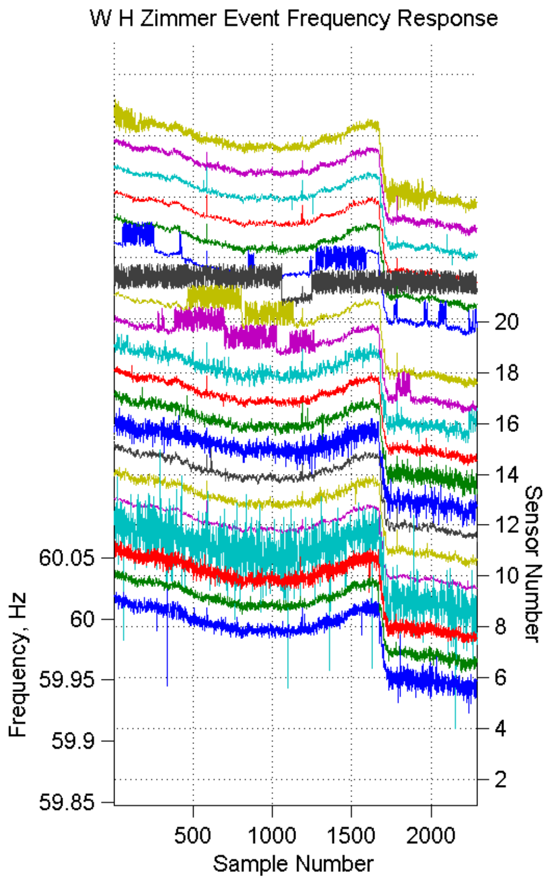
W H Zimmer Event Frequency Response
Frequency, Hz
60.05
60
59.95
59.9
59.85
500
1000
1500
2000
Sample Number
Sensor Number
20
18
16
14
12
10
8
6
4
2

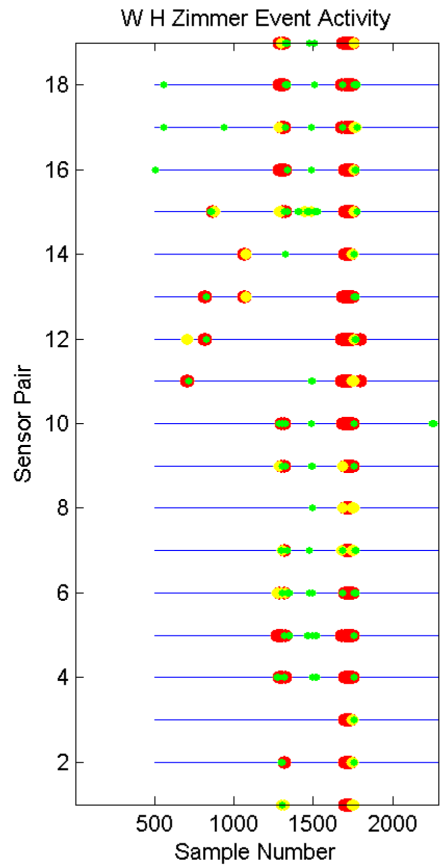
W H Zimmer Event Activity
Sensor Pair
18
16
14
12
10
8
6
4
2
500
1000
1500
2000
Sample Number

Appendix VII: Generation-Load Mismatch Plots and Derivatives

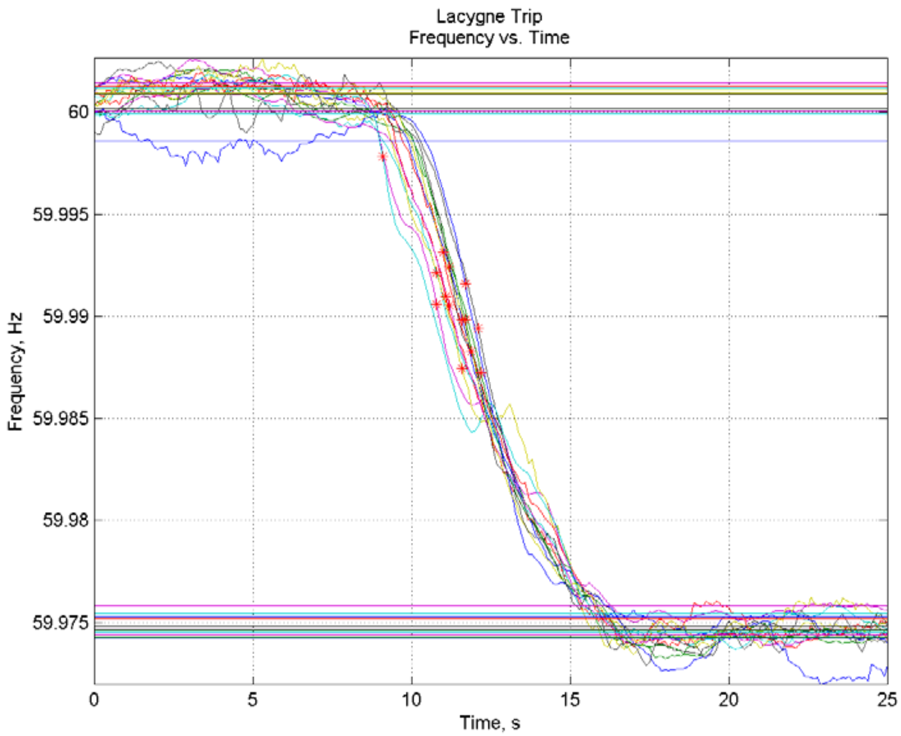

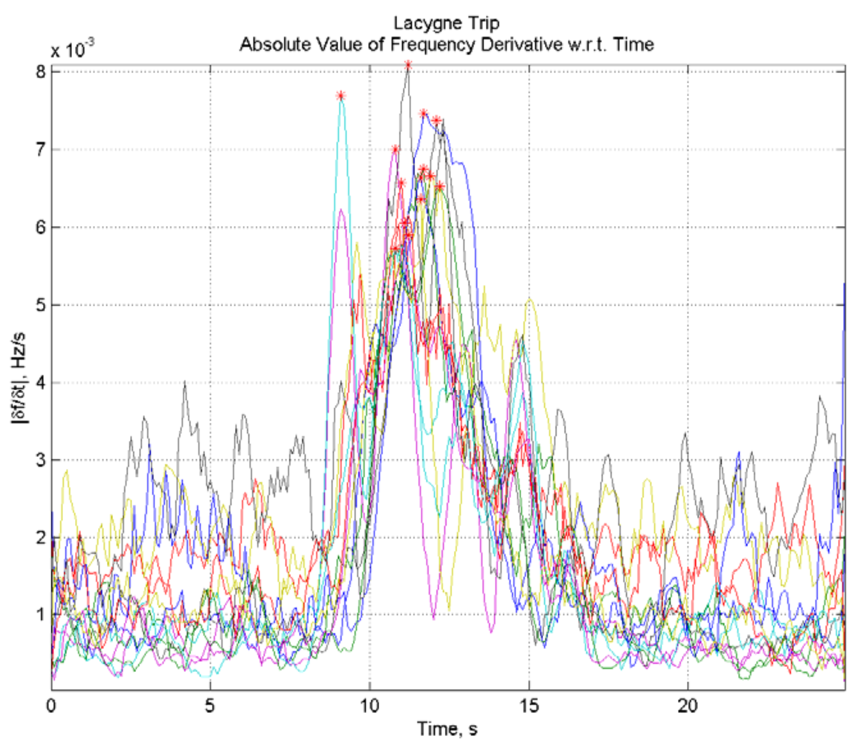

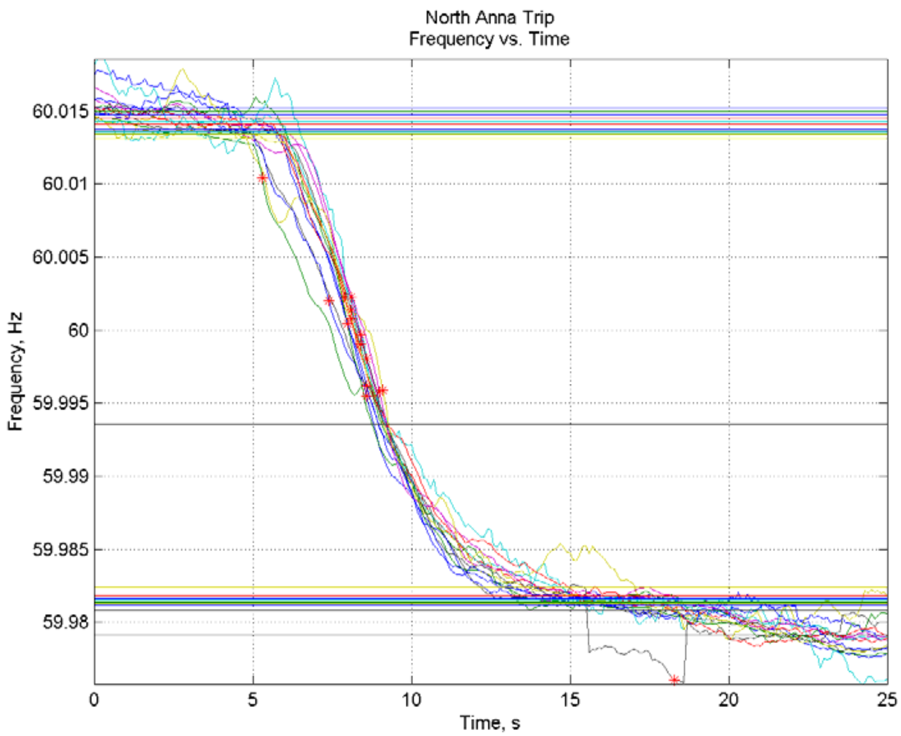
North Anna Trip
Frequency vs. Time
60.015
60.01
60.005
60
59.995
59.99
59.985
59.98
Frequency, Hz
0
5
10
15
20
25
Time, s

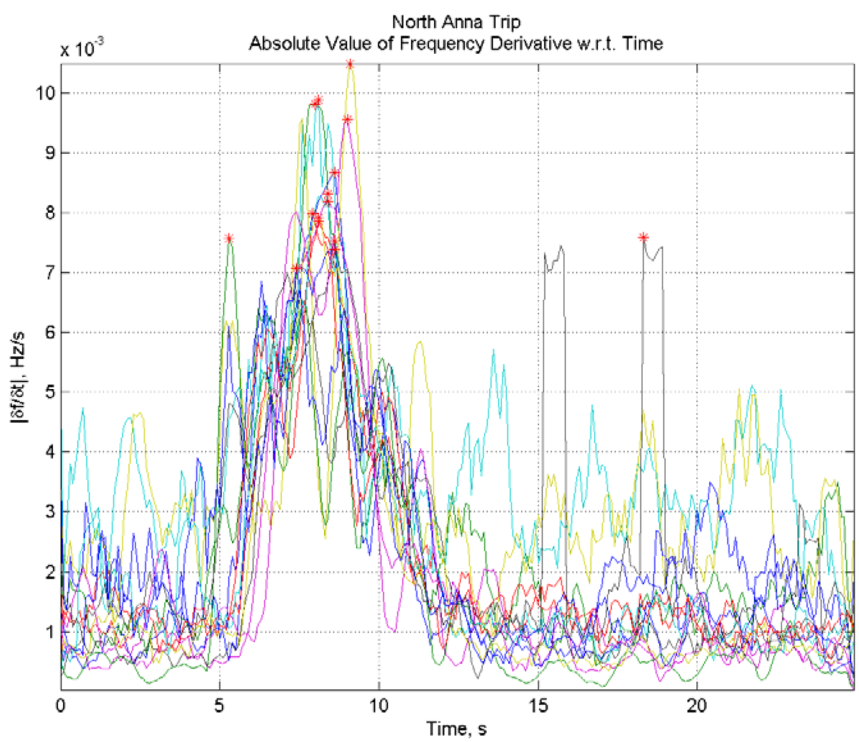
North Anna Trip
Absolute Value of Frequency Derivative w.r.t. Time
x 10^{-3}
10
9
8
7
6
5
4
3
2
1
|δf/δt|, Hz/s
0
5
10
15
20
Time, s

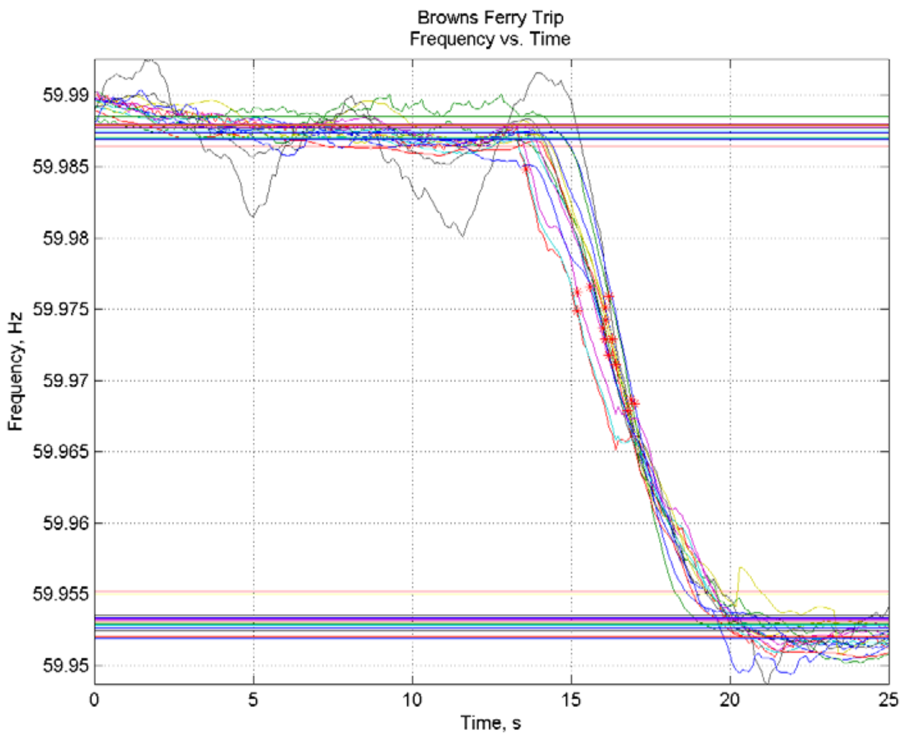
Browns Ferry Trip
Frequency vs. Time
Frequency, Hz
59.99
59.985
59.98
59.975
59.97
59.965
59.96
59.955
59.95
0
5
10
15
20
25
Time, s

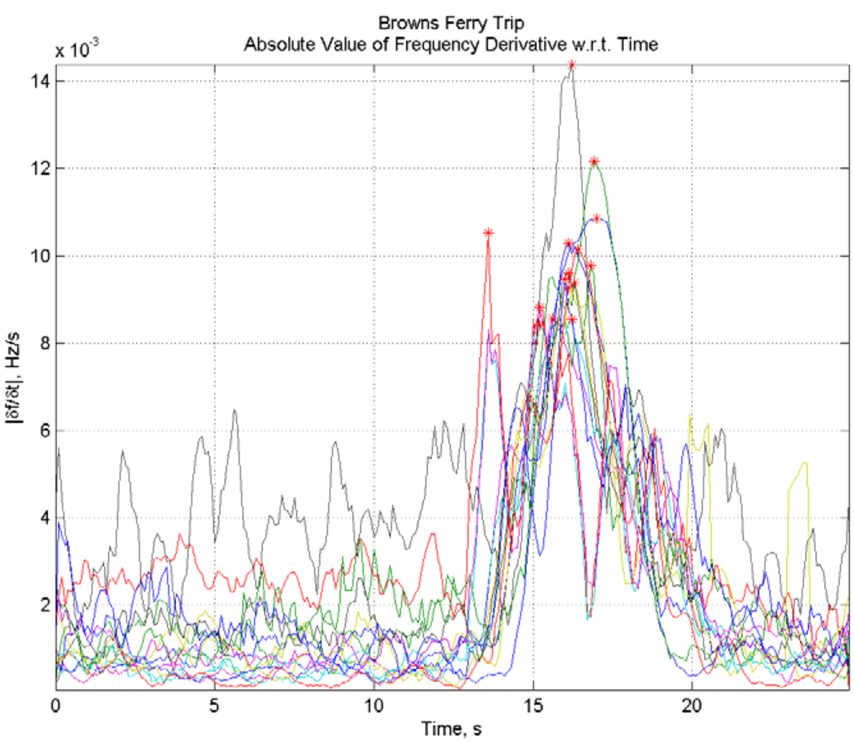
Browns Ferry Trip
Absolute Value of Frequency Derivative w.r.t. Time
x 10^-3
|δf/δt|, Hz/s
14
12
10
8
6
4
2
0
5
10
15
20
Time, s

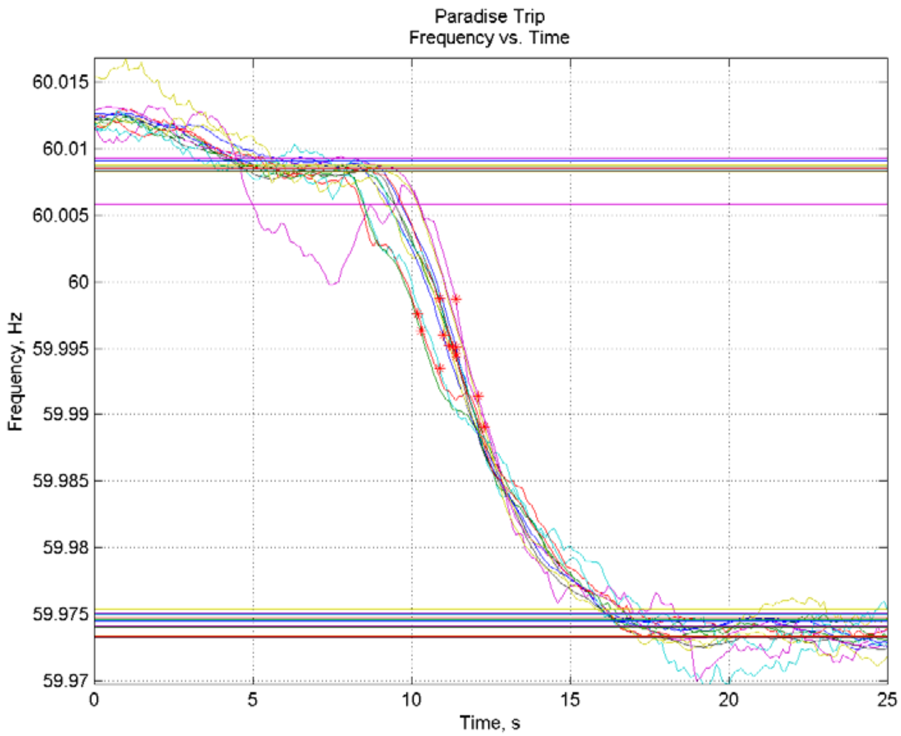
Paradise Trip
Frequency vs. Time
Frequency, Hz
60.015
60.01
60.005
60
59.995
59.99
59.985
59.98
59.975
59.97
0
5
10
15
20
25
Time, s

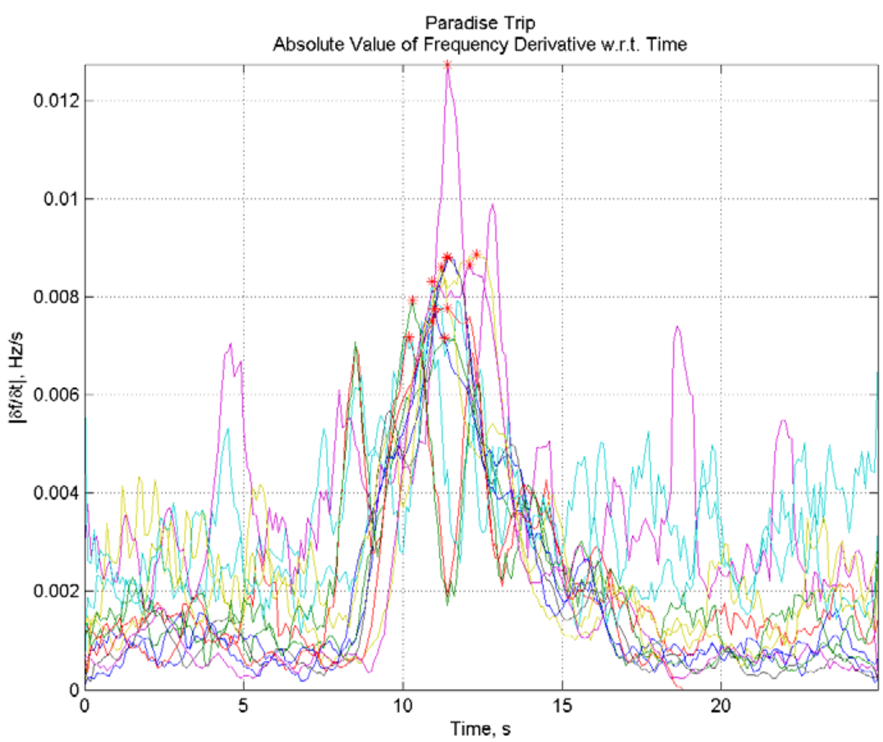
Paradise Trip
Absolute Value of Frequency Derivative w.r.t. Time
|δf/δt|, Hz/s
0.012
0.01
0.008
0.006
0.004
0.002
0
0
5
10
15
20
Time, s

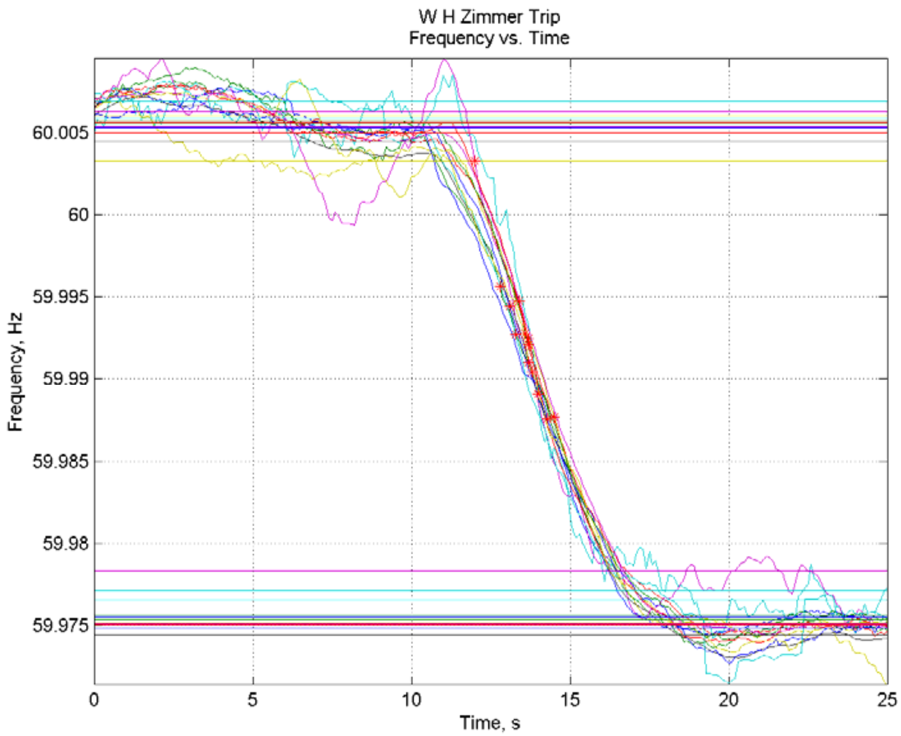
W H Zimmer Trip
Frequency vs. Time
Frequency, Hz
60.005
60
59.995
59.99
59.985
59.98
59.975
0
5
10
15
20
25
Time, s

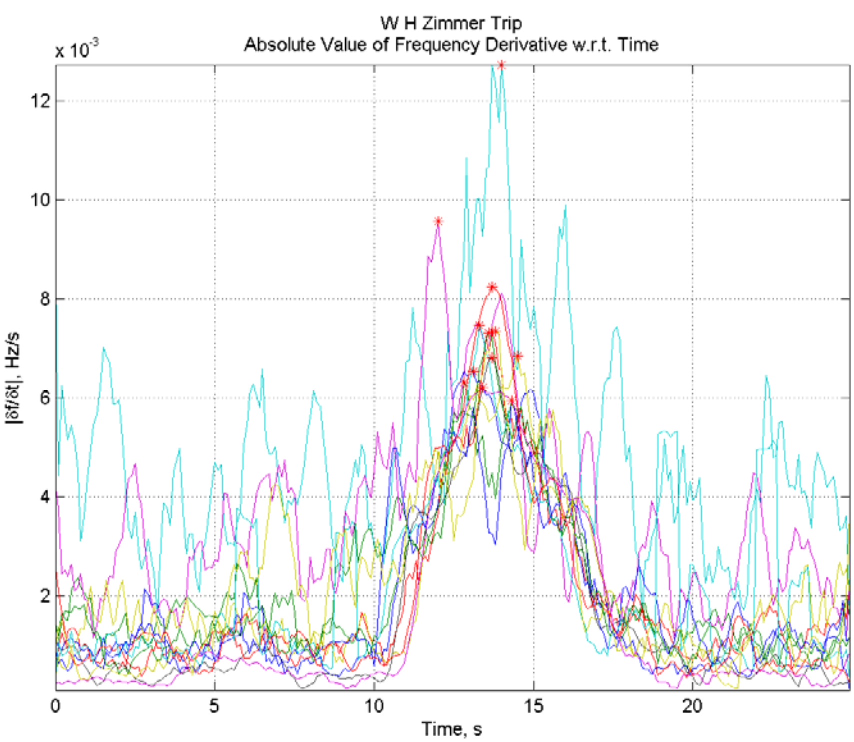
W H Zimmer Trip
Absolute Value of Frequency Derivative w.r.t. Time
x 10^-3
|δf/δt|, Hz/s
12
10
8
6
4
2
0
5
10
15
20
Time, s

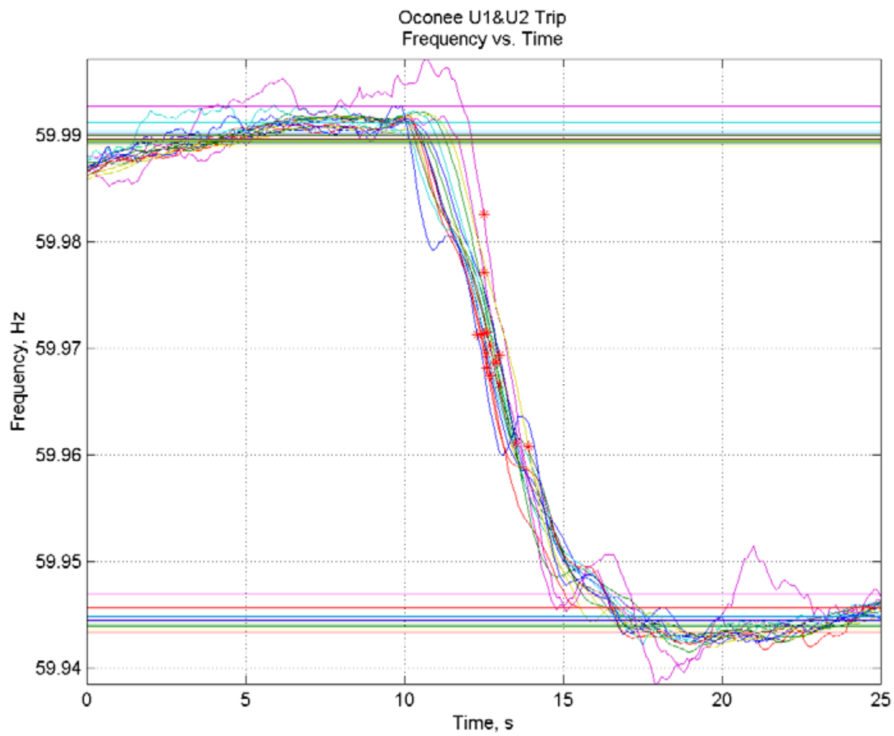
Oconee U1&U2 Trip
Frequency vs. Time
Frequency, Hz
59.99
59.98
59.97
59.96
59.95
59.94
0
5
10
15
20
25
Time, s

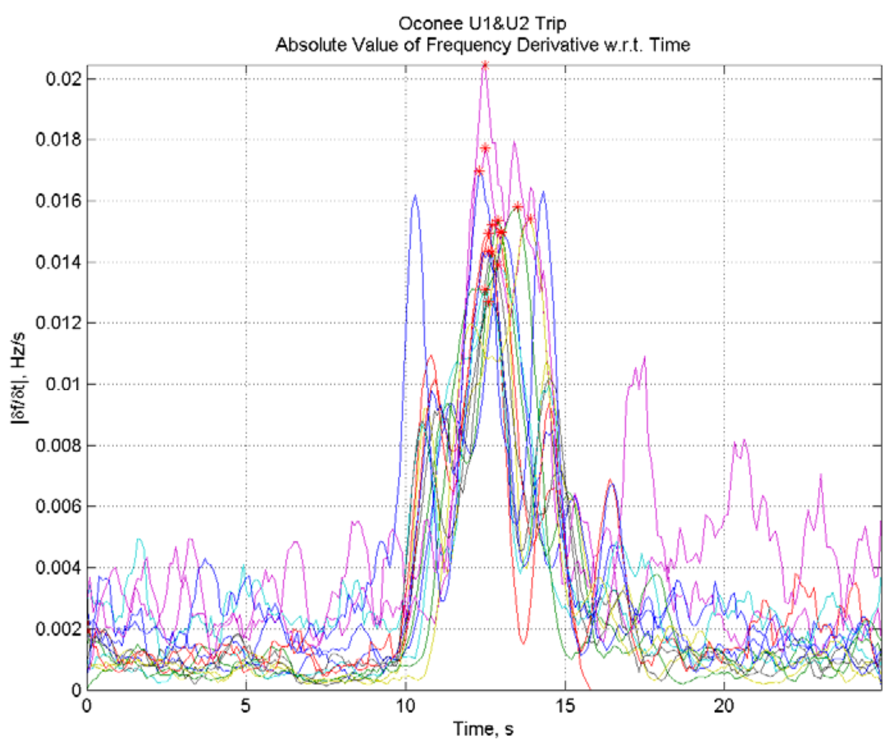
Oconee U1&U2 Trip
Absolute Value of Frequency Derivative w.r.t. Time
|δf/δt|, Hz/s
0.02
0.018
0.016
0.014
0.012
0.01
0.008
0.006
0.004
0.002
0
0
5
10
15
20
Time, s

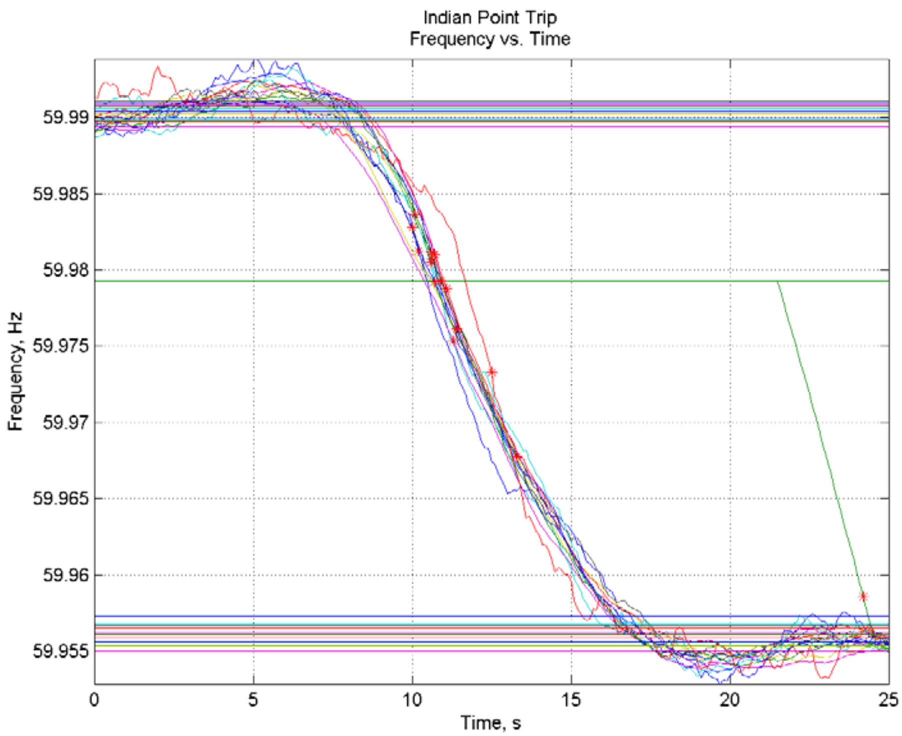
Indian Point Trip
Frequency vs. Time
Frequency, Hz
59.99
59.985
59.98
59.975
59.97
59.965
59.96
59.955
0
5
10
15
20
25
Time, s

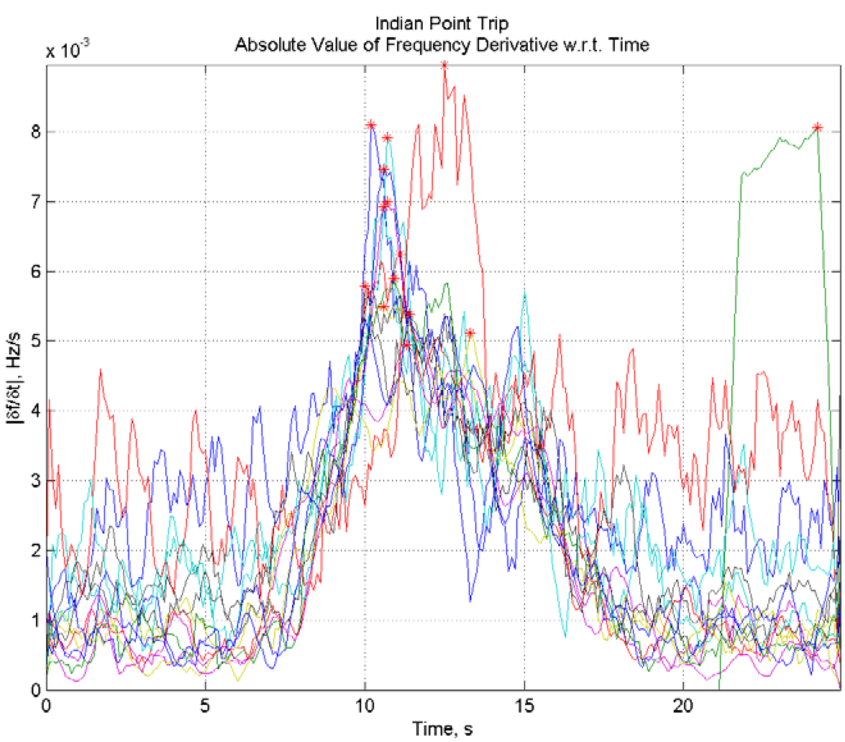
Indian Point Trip
Absolute Value of Frequency Derivative w.r.t. Time
x 10^-3
|δf/δt|, Hz/s
8
7
6
5
4
3
2
1
0
0
5
10
15
20
Time, s

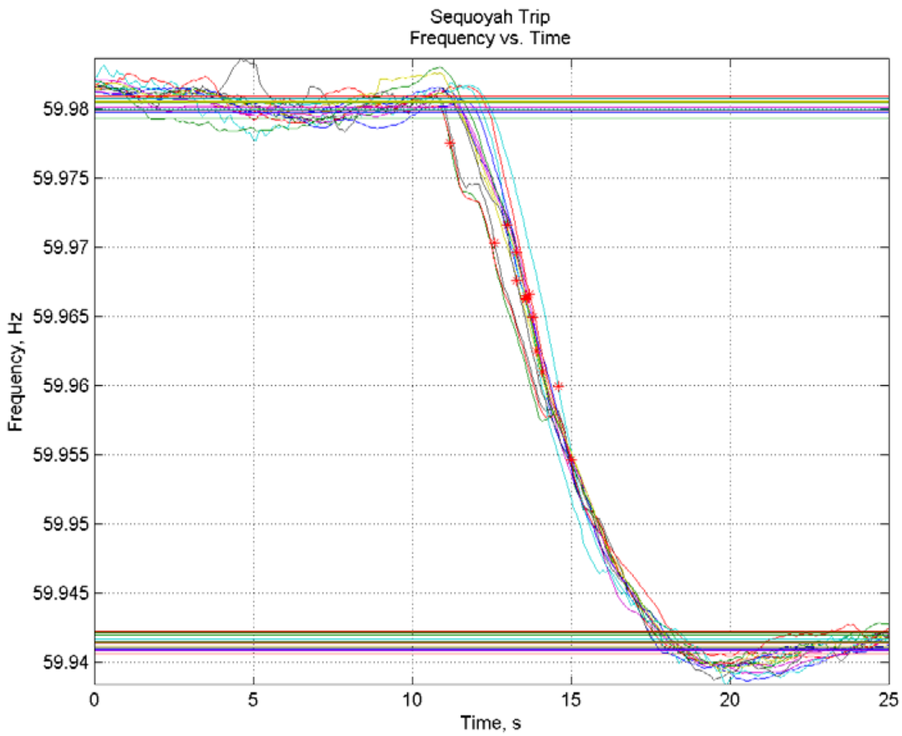
Sequoyah Trip
Frequency vs. Time
Frequency, Hz
Time, s

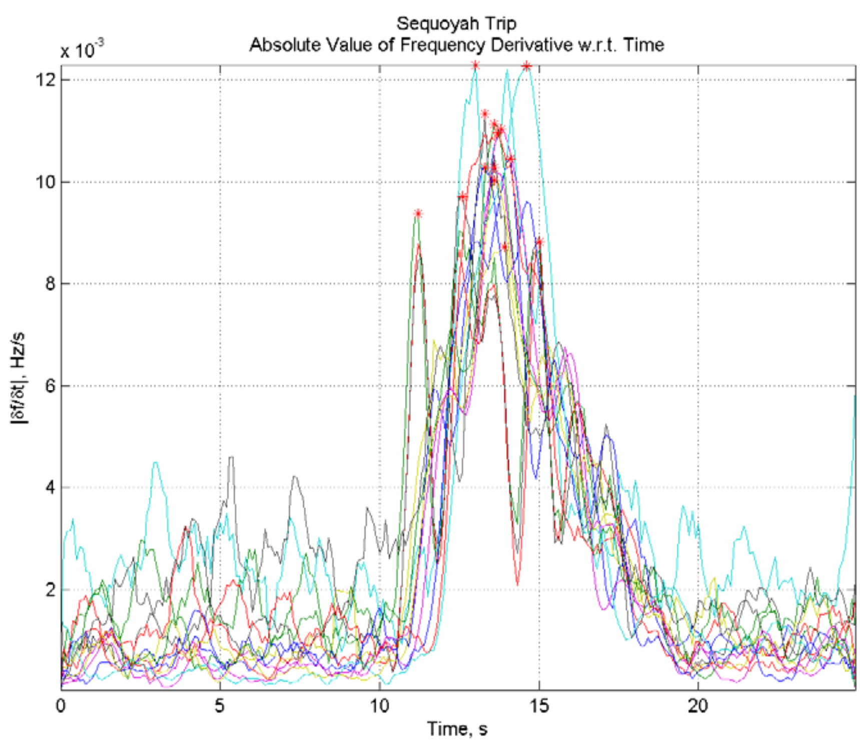
Sequoyah Trip
Absolute Value of Frequency Derivative w.r.t. Time
x 10^-3
|δf/δt|, Hz/s
Time, s

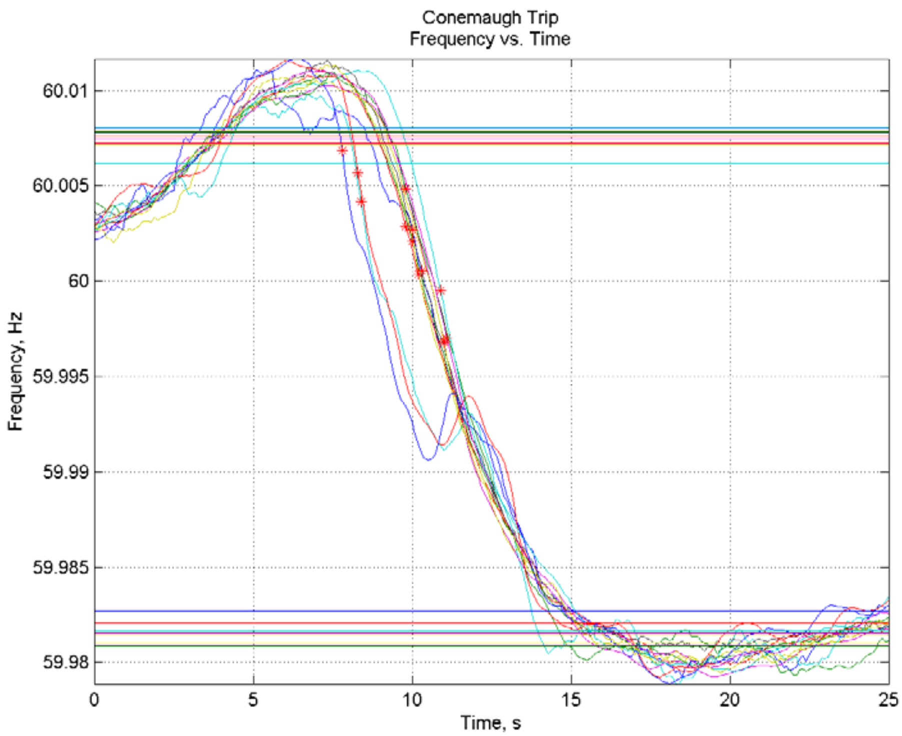
Conemaugh Trip
Frequency vs. Time
Frequency, Hz
Time, s
60.01
60.005
60
59.995
59.99
59.985
59.98
0
5
10
15
20
25

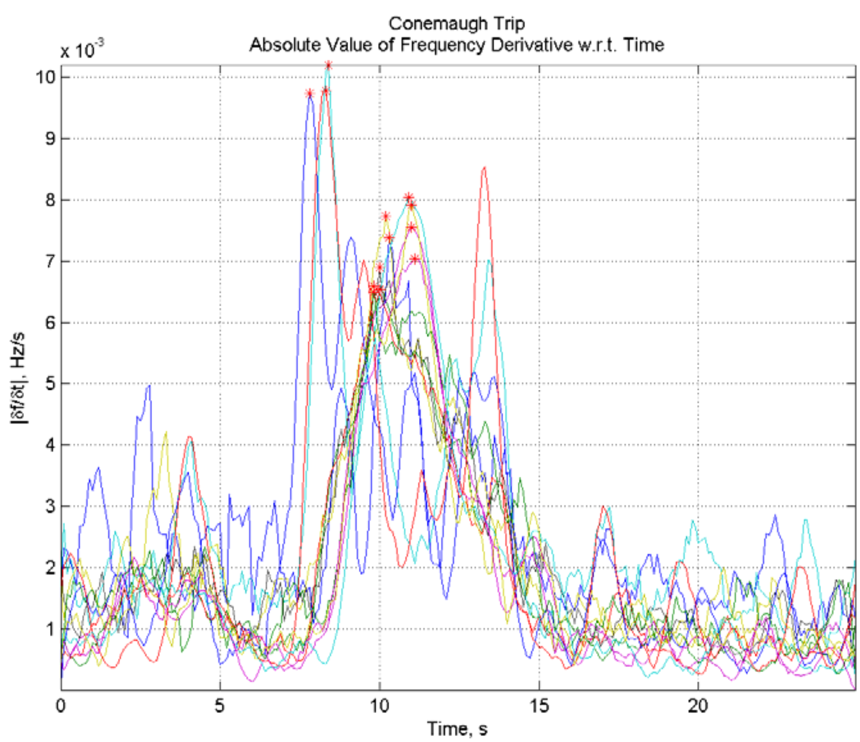
Conemaugh Trip
Absolute Value of Frequency Derivative w.r.t. Time
x 10^-3
|δf/δt|, Hz/s
Time, s
10
9
8
7
6
5
4
3
2
1
0
5
10
15
20

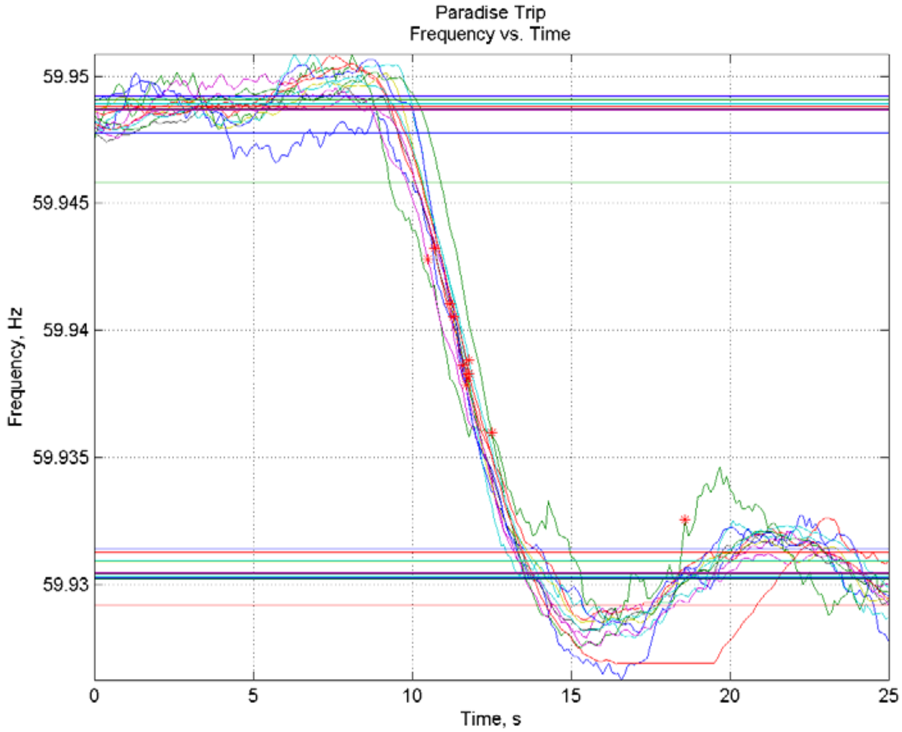
Paradise Trip
Frequency vs. Time
Frequency, Hz
Time, s
59.95
59.945
59.94
59.935
59.93
0
5
10
15
20
25

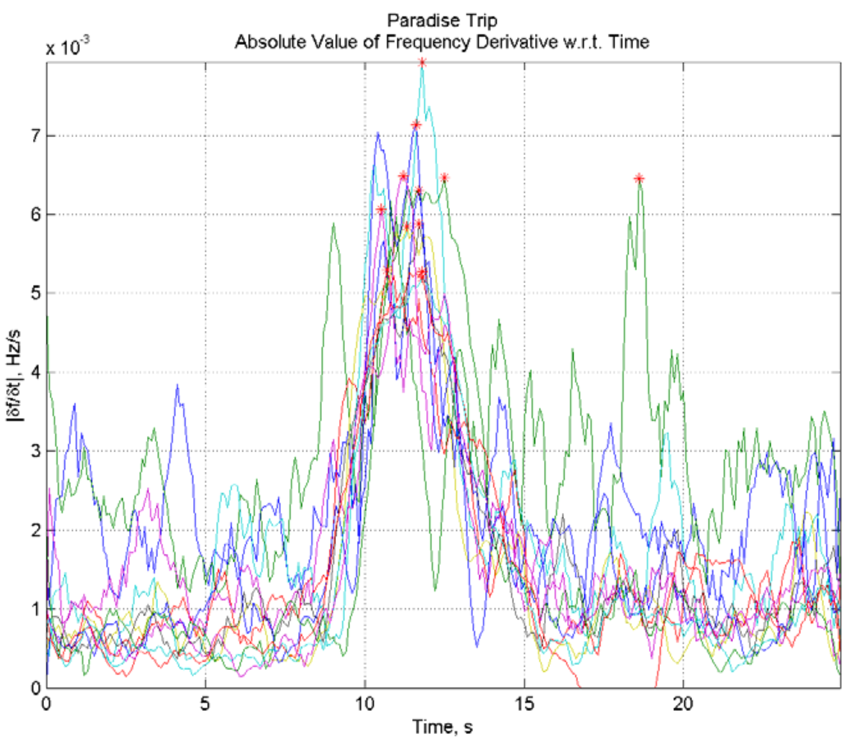
Paradise Trip
Absolute Value of Frequency Derivative w.r.t. Time
x 10^-3
|δf/δt|, Hz/s
Time, s
0
1
2
3
4
5
6
7
0
5
10
15
20

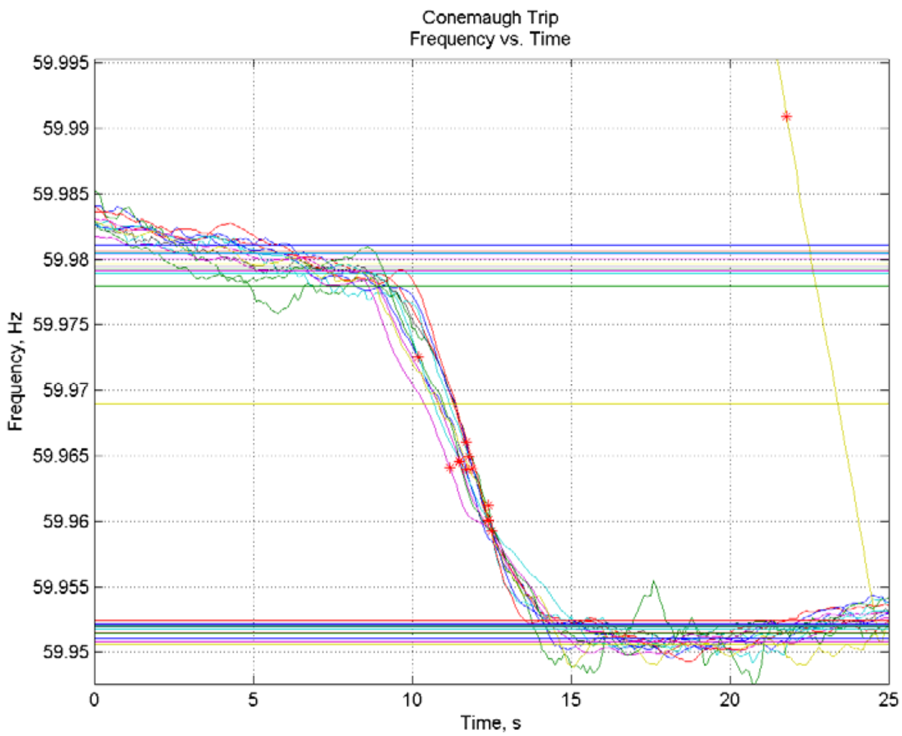
Conemaugh Trip
Frequency vs. Time
59.995
59.99
59.985
59.98
59.975
59.97
59.965
59.96
59.955
59.95
Frequency, Hz
0
5
10
15
20
25
Time, s

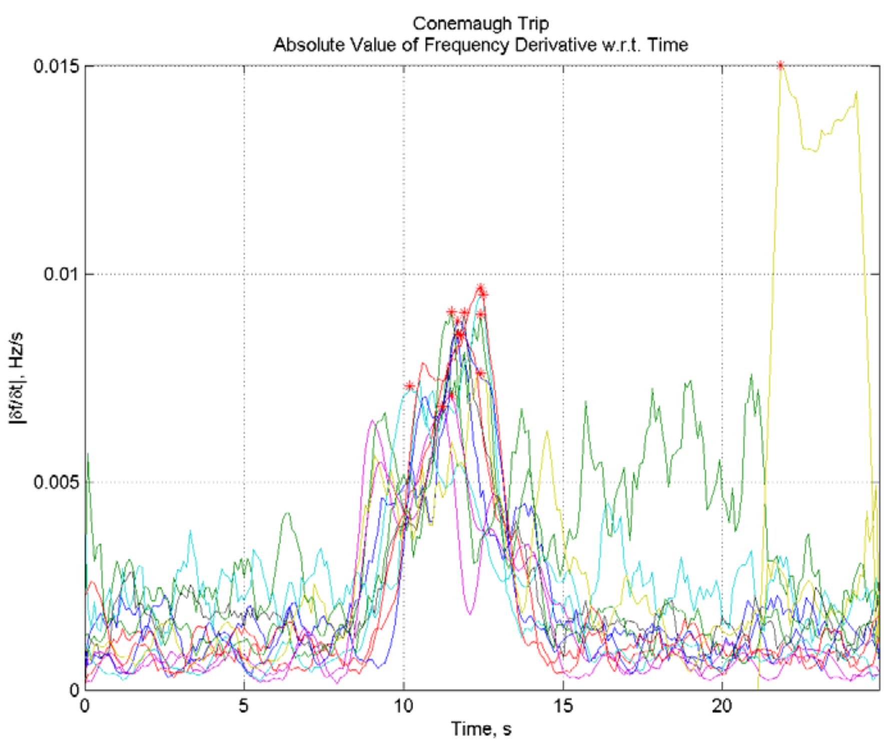
Conemaugh Trip
Absolute Value of Frequency Derivative w.r.t. Time
0.015
0.01
0.005
0
|δf/δt|, Hz/s
0
5
10
15
20
Time, s

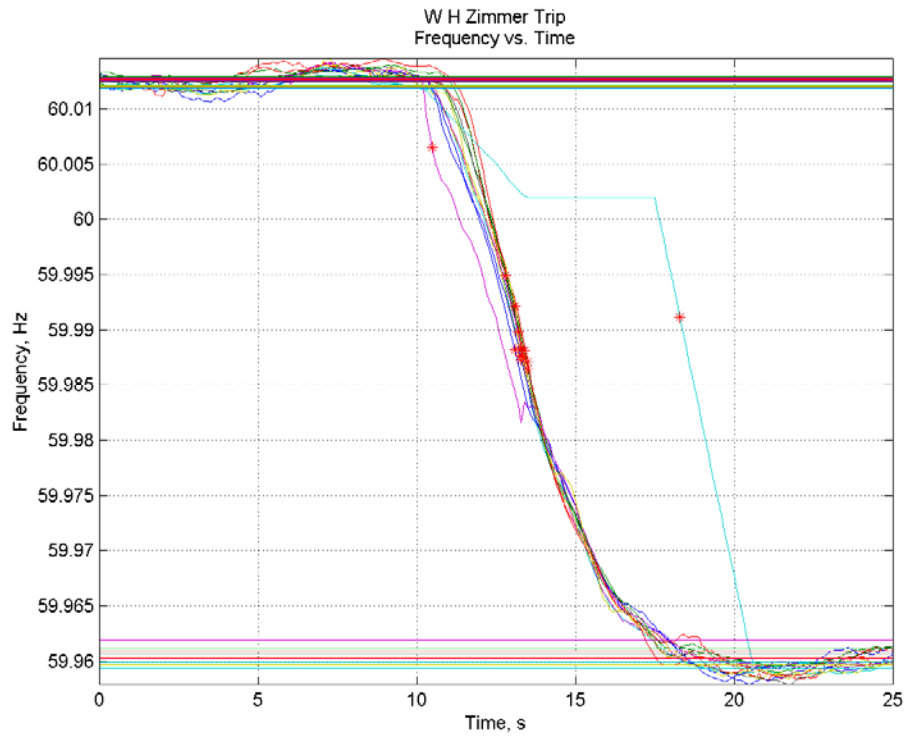
W H Zimmer Trip
Frequency vs. Time
Frequency, Hz
60.01
60.005
60
59.995
59.99
59.985
59.98
59.975
59.97
59.965
59.96
0
5
10
15
20
25
Time, s

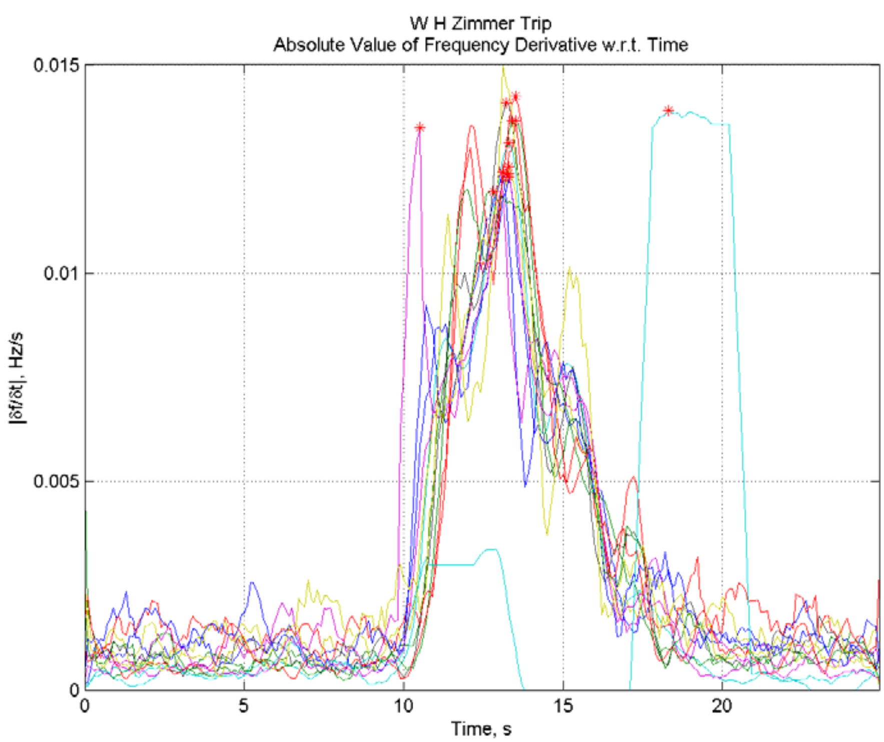
W H Zimmer Trip
Absolute Value of Frequency Derivative w.r.t. Time
|δf/δt|, Hz/s
0.015
0.01
0.005
0
0
5
10
15
20
Time, s

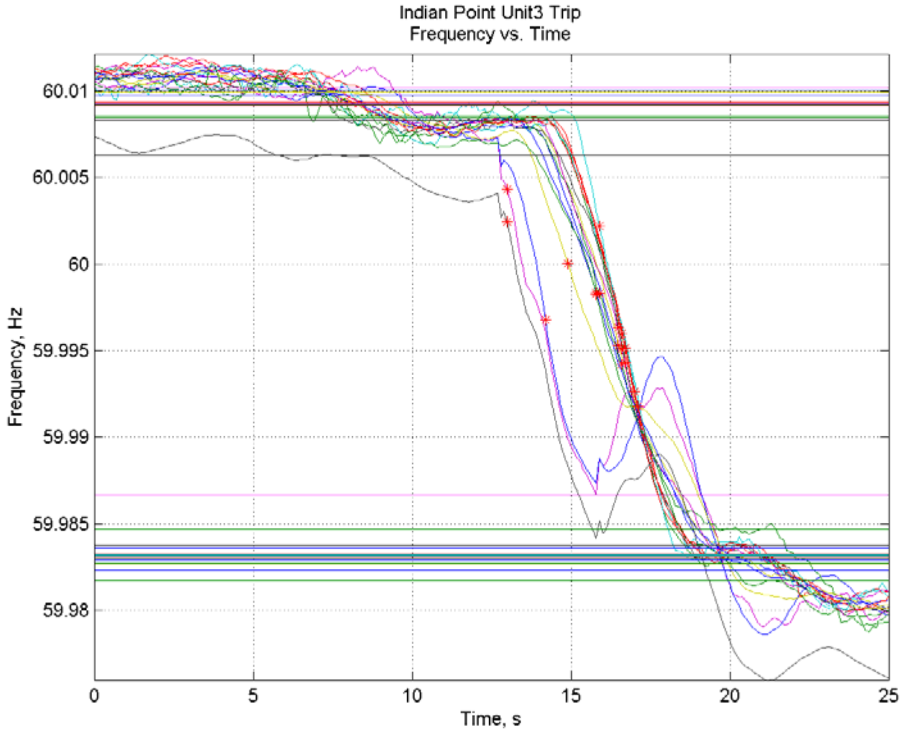
Indian Point Unit3 Trip
Frequency vs. Time
Frequency, Hz
60.01
60.005
60
59.995
59.99
59.985
59.98
0
5
10
15
20
25
Time, s

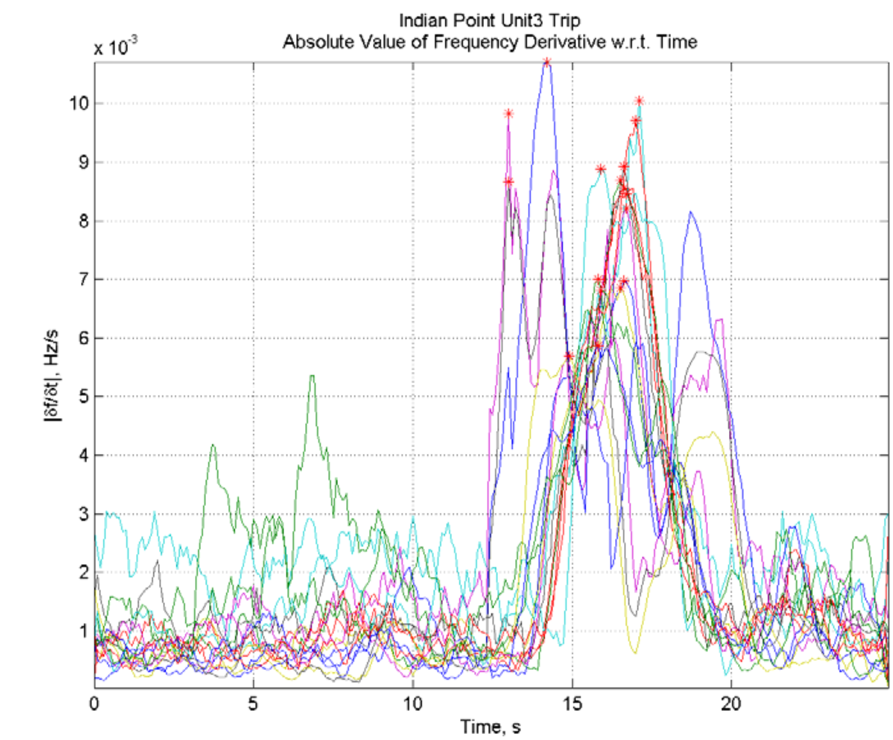
Indian Point Unit3 Trip
Absolute Value of Frequency Derivative w.r.t. Time
x 10^-3
|δf/δt|, Hz/s
10
9
8
7
6
5
4
3
2
1
0
5
10
15
20
Time, s

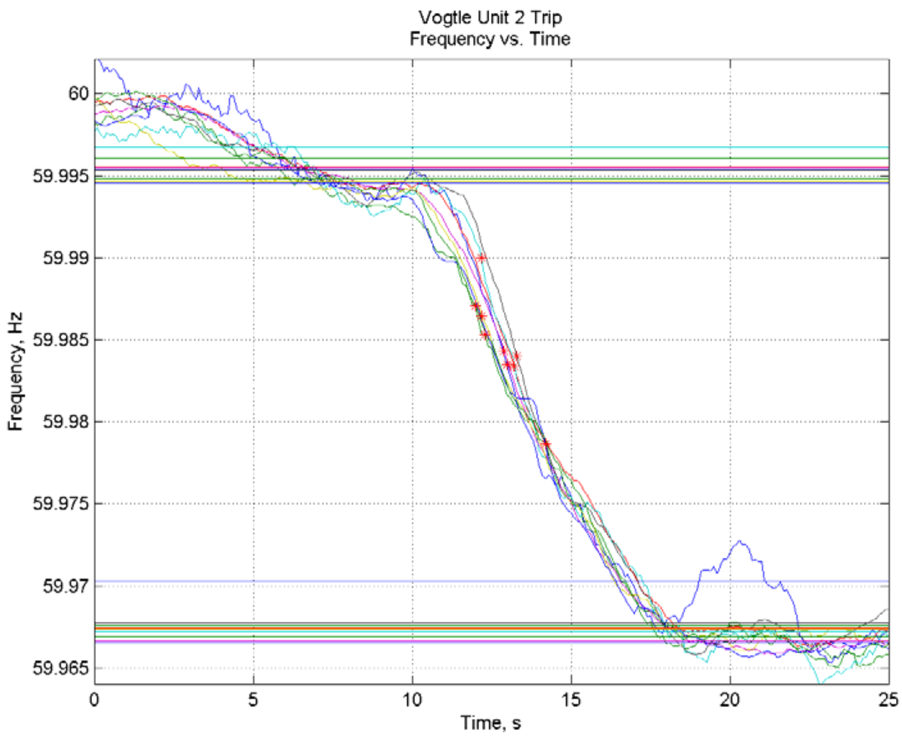
Vogtle Unit 2 Trip
Frequency vs. Time
Frequency, Hz
Time, s
60
59.995
59.99
59.985
59.98
59.975
59.97
59.965
0
5
10
15
20
25

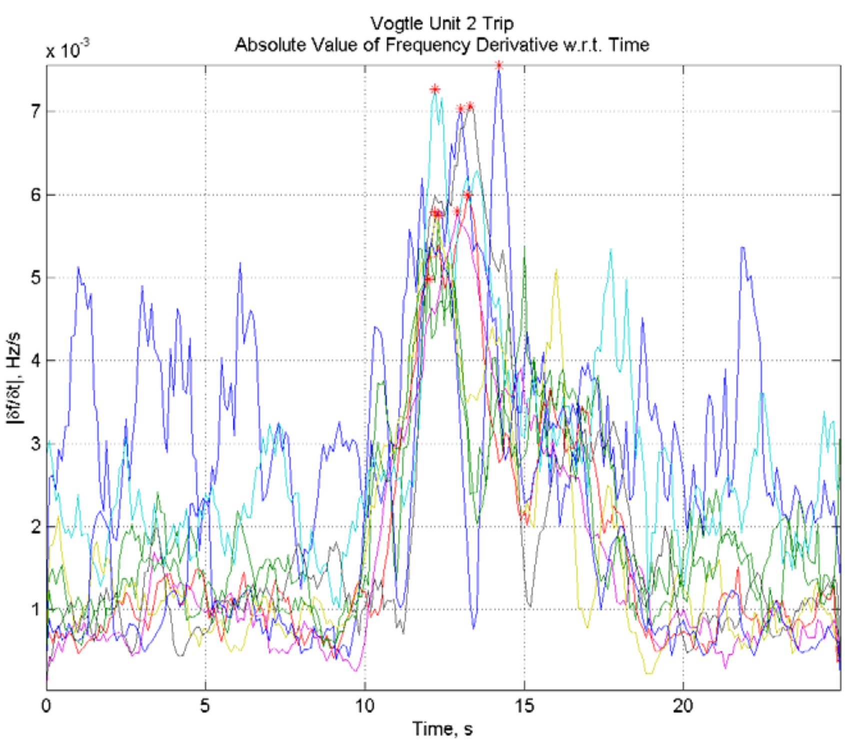
Vogtle Unit 2 Trip
Absolute Value of Frequency Derivative w.r.t. Time
x 10^-3
|δf/δt|, Hz/s
Time, s
7
6
5
4
3
2
1
0
5
10
15
20

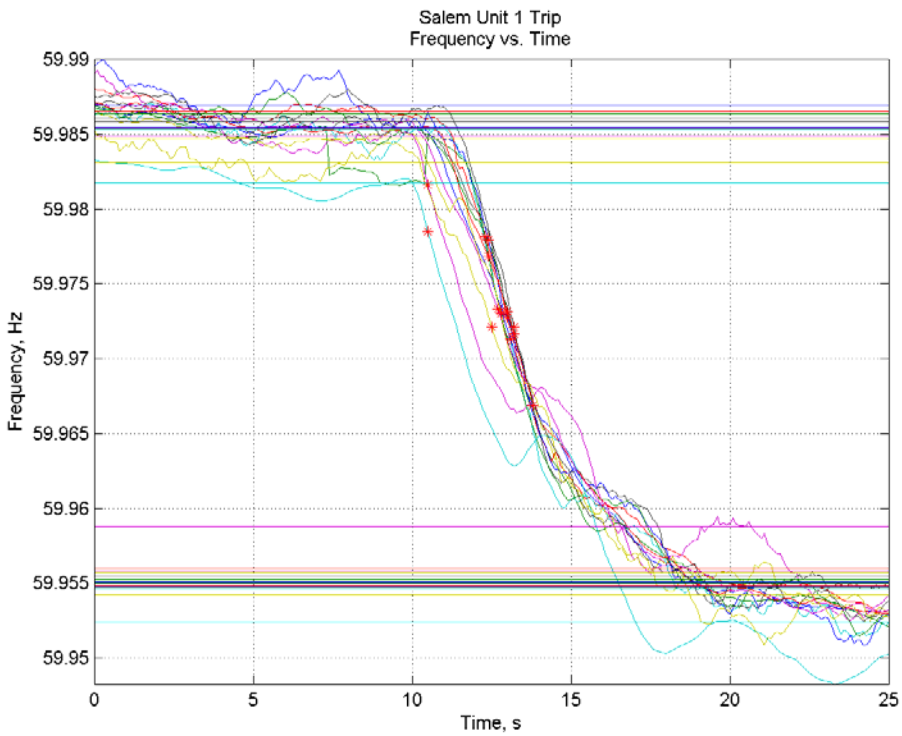
Salem Unit 1 Trip
Frequency vs. Time
Frequency, Hz
Time, s
59.99
59.985
59.98
59.975
59.97
59.965
59.96
59.955
59.95
0
5
10
15
20
25

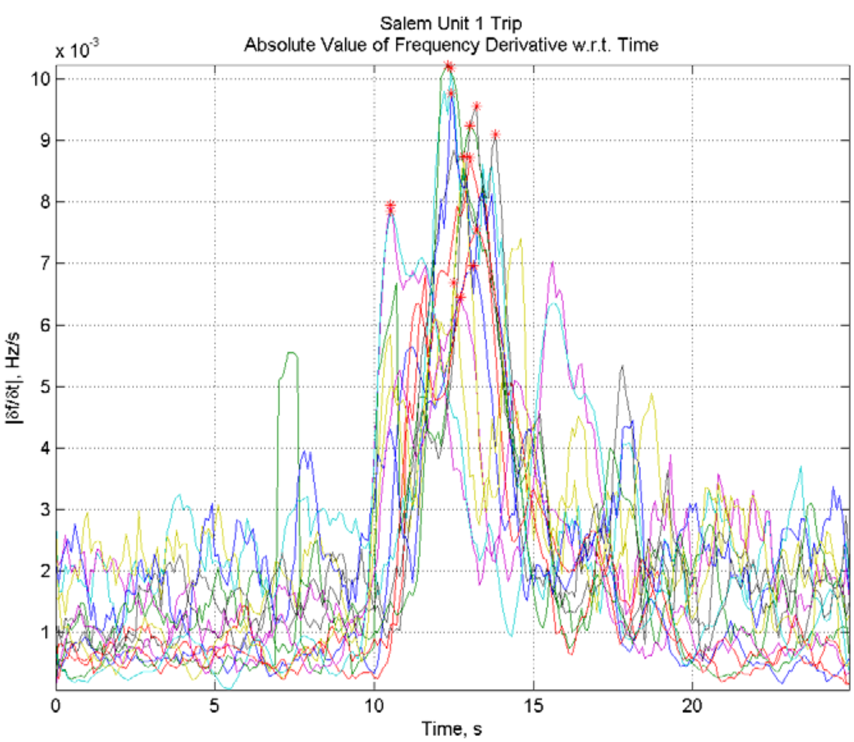
Salem Unit 1 Trip
Absolute Value of Frequency Derivative w.r.t. Time
x 10^-3
|δf/δt|, Hz/s
Time, s
10
9
8
7
6
5
4
3
2
1
0
5
10
15
20

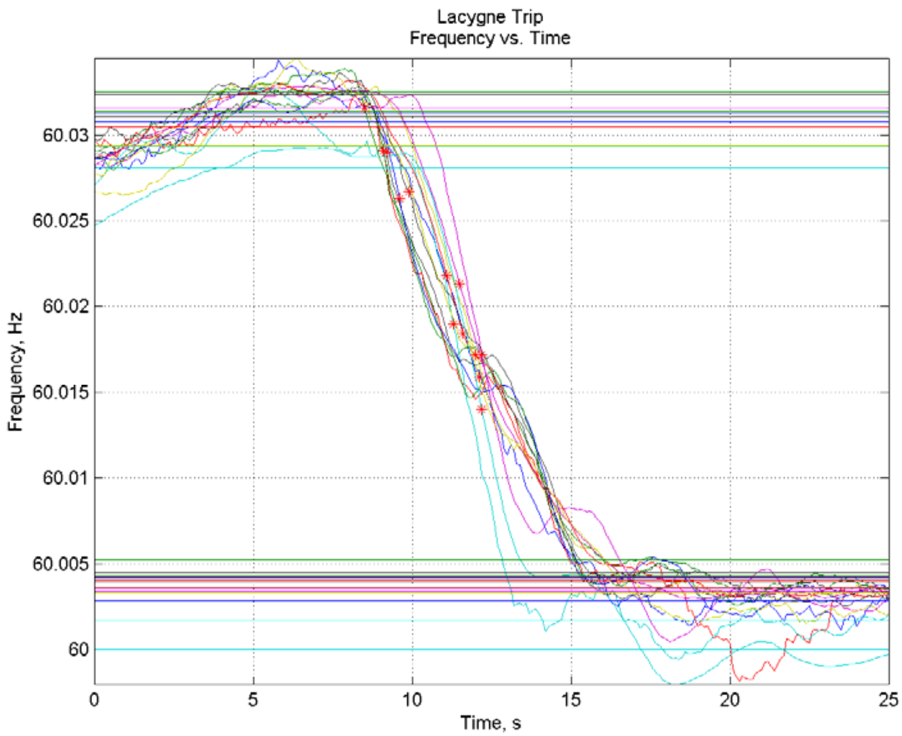
Lacygne Trip
Frequency vs. Time
Frequency, Hz
Time, s
60.03
60.025
60.02
60.015
60.01
60.005
60
0
5
10
15
20
25

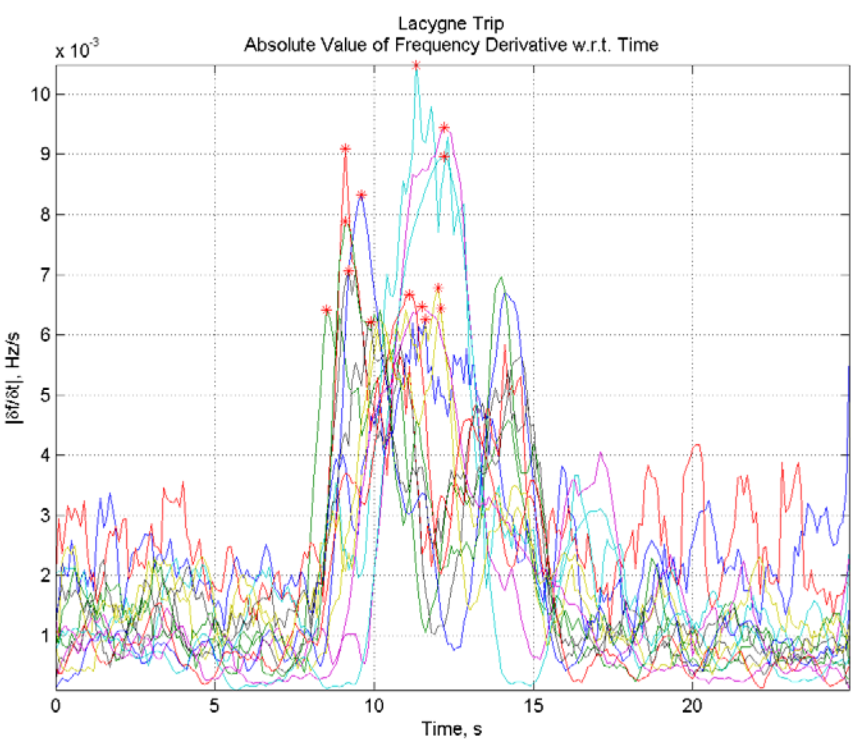
Lacygne Trip
Absolute Value of Frequency Derivative w.r.t. Time
x 10^-3
|δf/δt|, Hz/s
Time, s
10
9
8
7
6
5
4
3
2
1
0
5
10
15
20

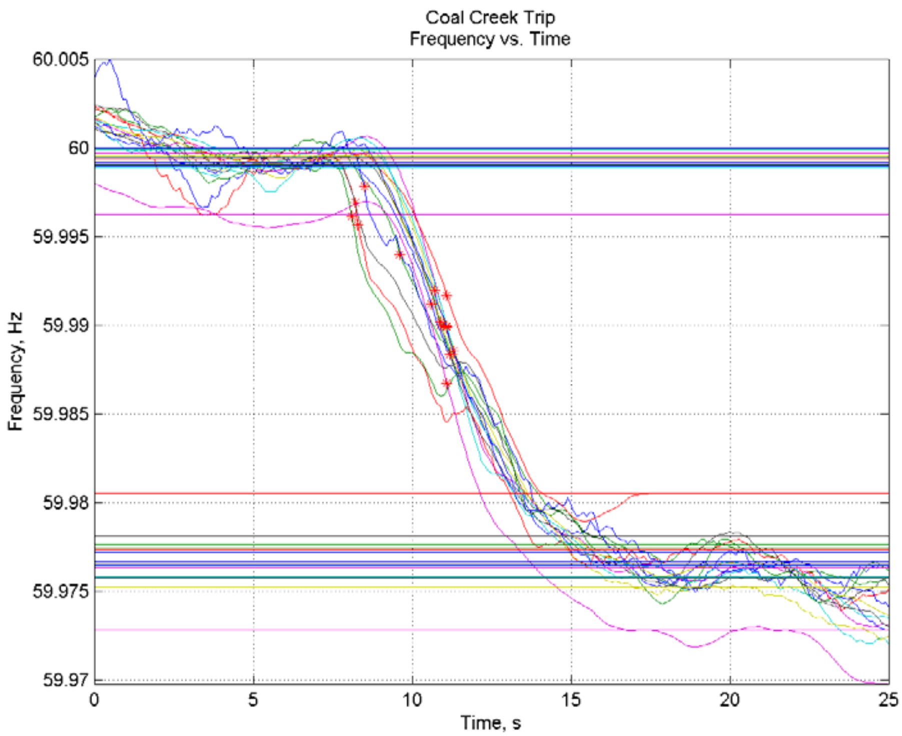
Coal Creek Trip
Frequency vs. Time
60.005
60
59.995
59.99
59.985
59.98
59.975
59.97
Frequency, Hz
0
5
10
15
20
25
Time, s

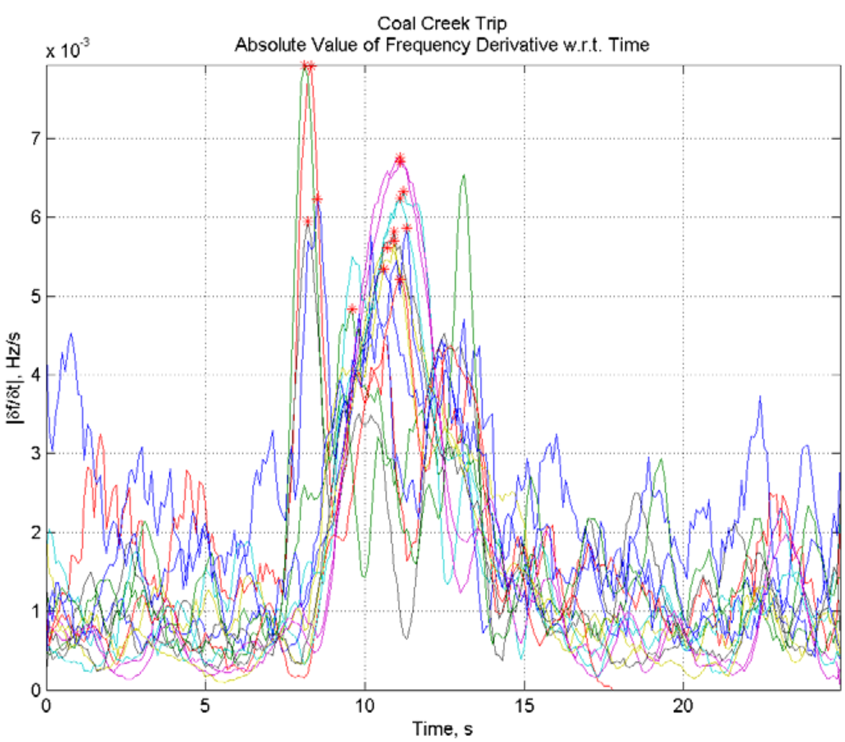
Coal Creek Trip
Absolute Value of Frequency Derivative w.r.t. Time
x 10^-3
7
6
5
4
3
2
1
0
|δf/δt|, Hz/s
0
5
10
15
20
Time, s

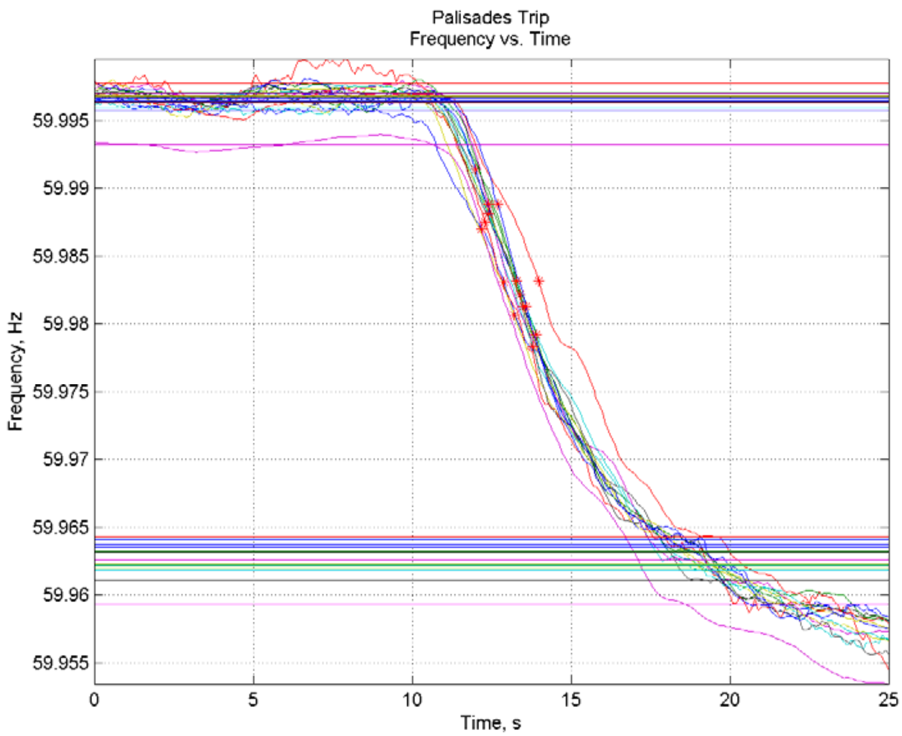
Palisades Trip
Frequency vs. Time
Frequency, Hz
Time, s
59.995
59.99
59.985
59.98
59.975
59.97
59.965
59.96
59.955
0
5
10
15
20
25

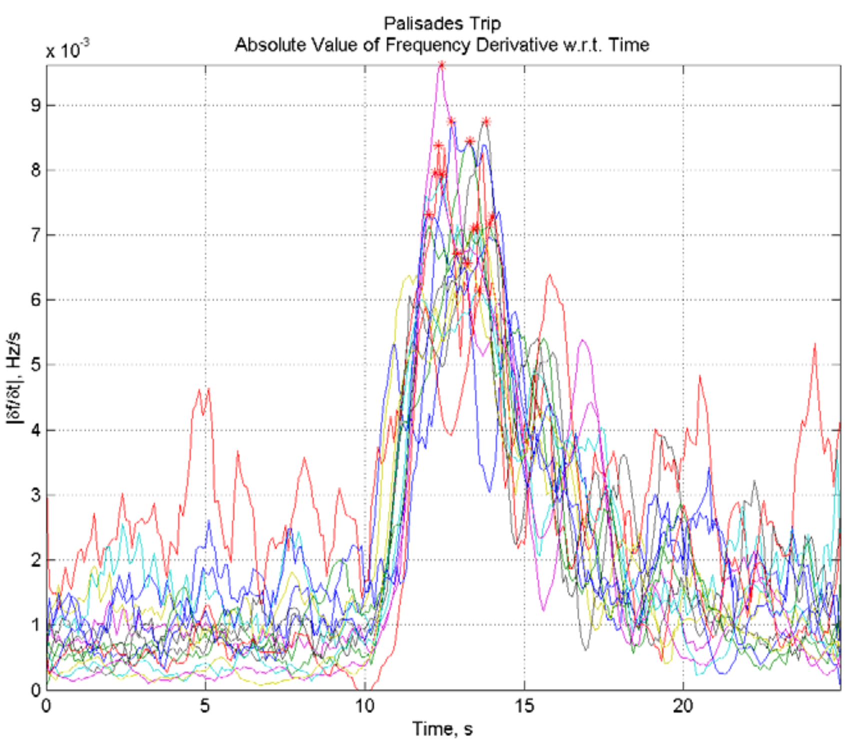
Palisades Trip
Absolute Value of Frequency Derivative w.r.t. Time
x 10^-3
|δf/δt|, Hz/s
Time, s
0
1
2
3
4
5
6
7
8
9
10
15
20

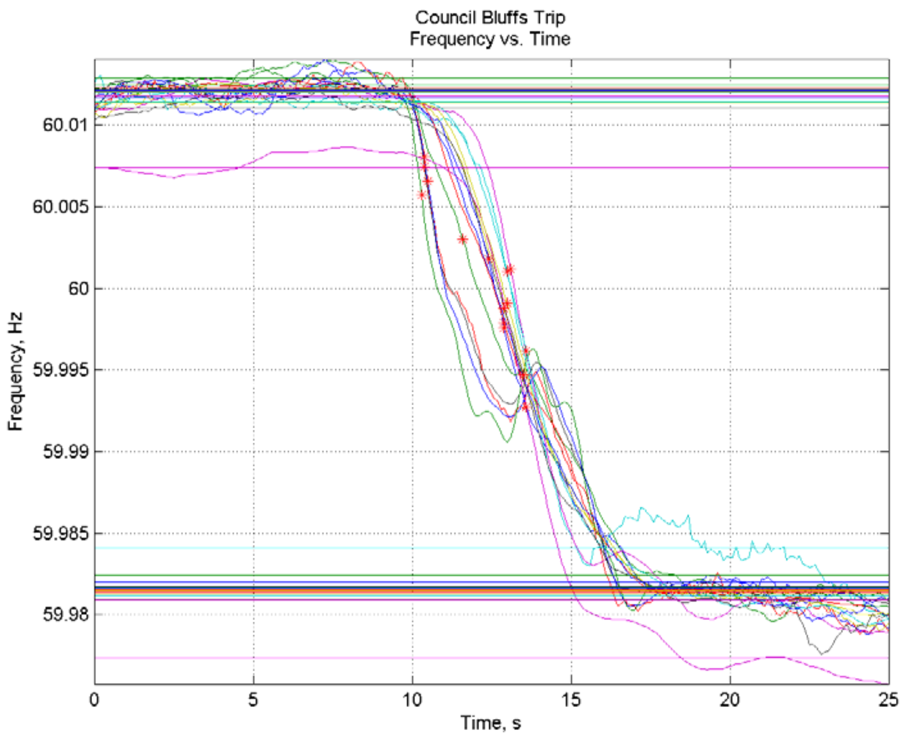
Council Bluffs Trip
Frequency vs. Time
Frequency, Hz
60.01
60.005
60
59.995
59.99
59.985
59.98
0
5
10
15
20
25
Time, s

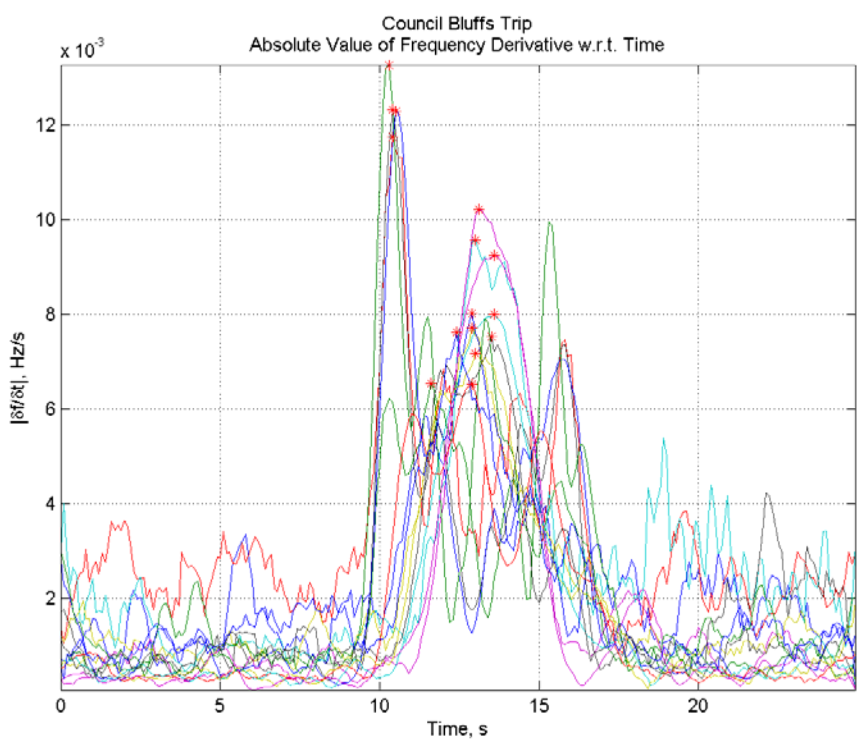
Council Bluffs Trip
Absolute Value of Frequency Derivative w.r.t. Time
x 10^-3
|δf/δt|, Hz/s
12
10
8
6
4
2
0
5
10
15
20
Time, s

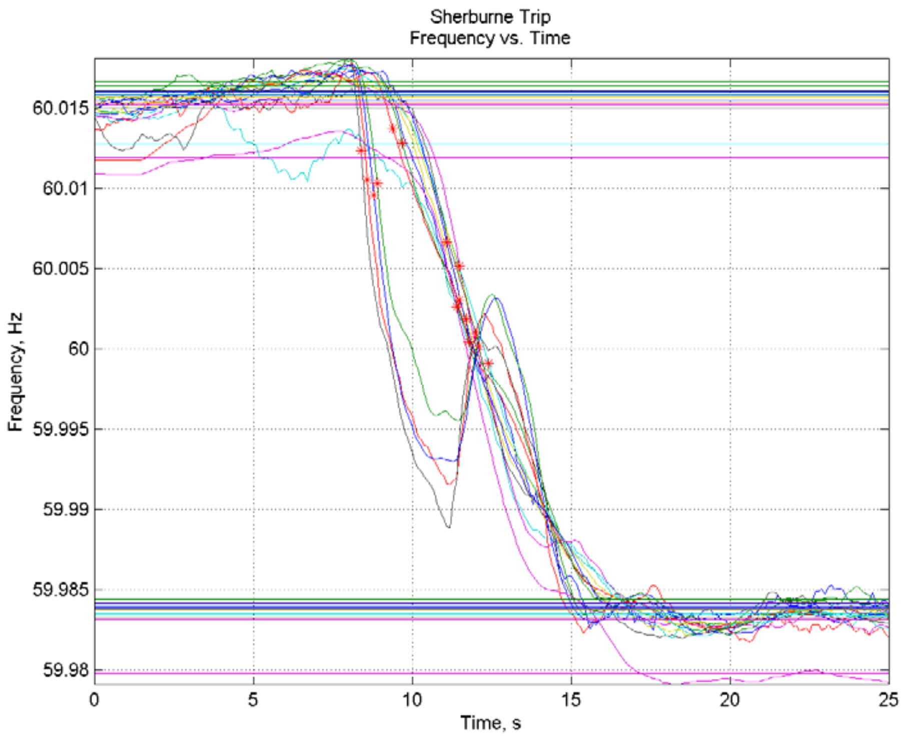
Sherburne Trip
Frequency vs. Time
Frequency, Hz
Time, s
60.015
60.01
60.005
60
59.995
59.99
59.985
59.98
0
5
10
15
20
25

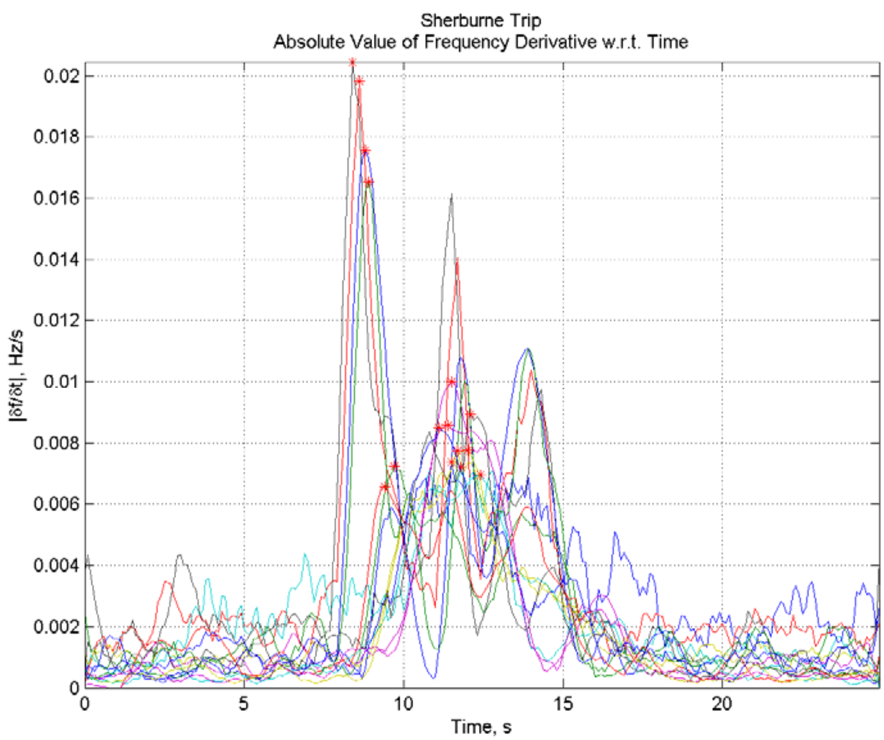
Sherburne Trip
Absolute Value of Frequency Derivative w.r.t. Time
|δf/δt|, Hz/s
Time, s
0.02
0.018
0.016
0.014
0.012
0.01
0.008
0.006
0.004
0.002
0
0
5
10
15
20

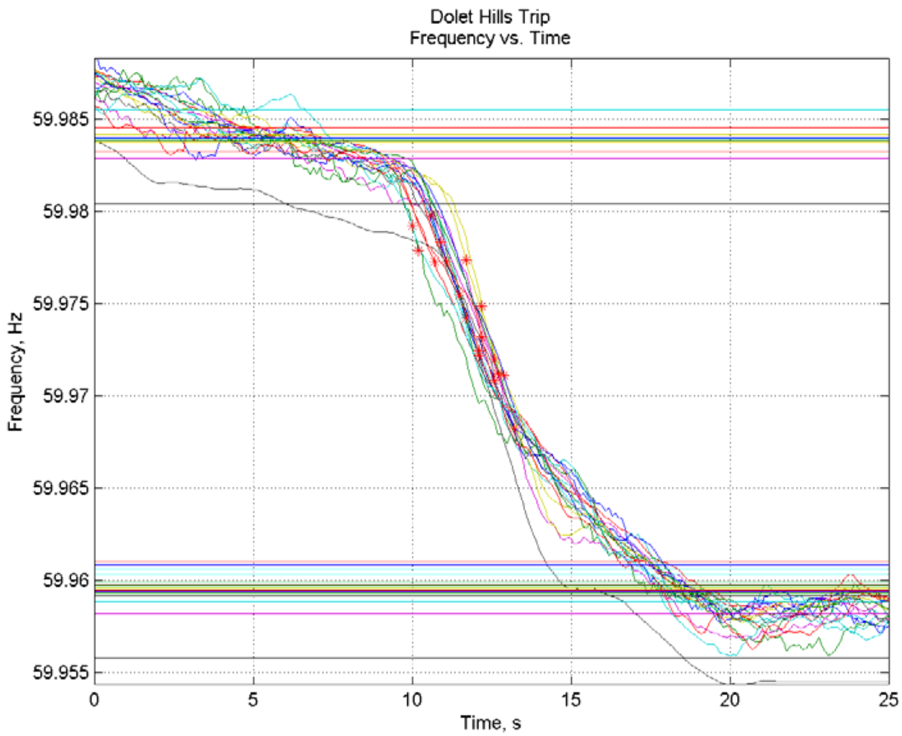
Dolet Hills Trip
Frequency vs. Time
Frequency, Hz
59.985
59.98
59.975
59.97
59.965
59.96
59.955
0
5
10
15
20
25
Time, s

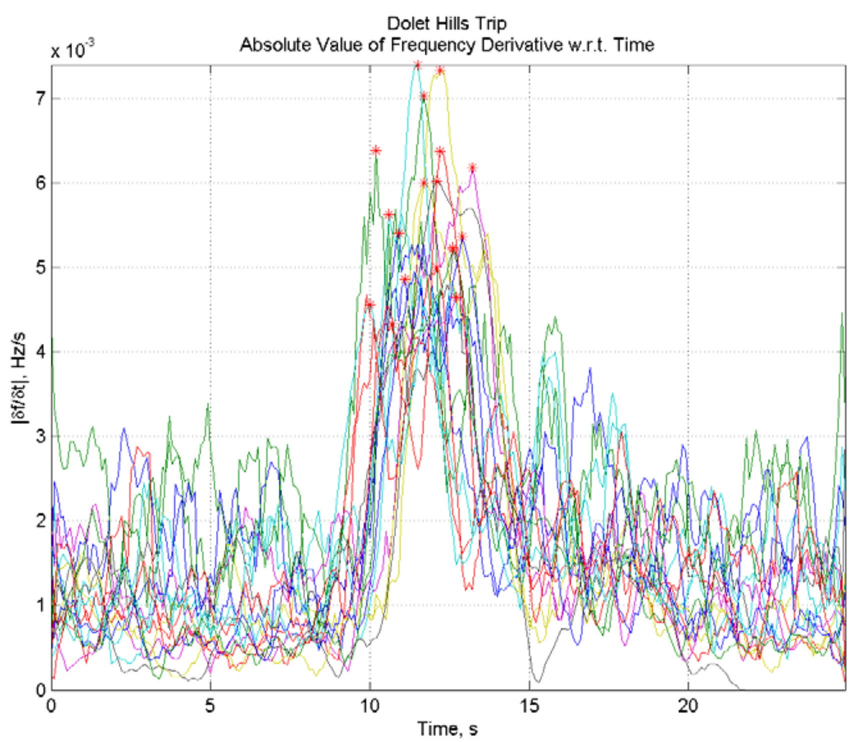
Dolet Hills Trip
Absolute Value of Frequency Derivative w.r.t. Time
x 10^-3
|δf/δt|, Hz/s
7
6
5
4
3
2
1
0
0
5
10
15
20
Time, s

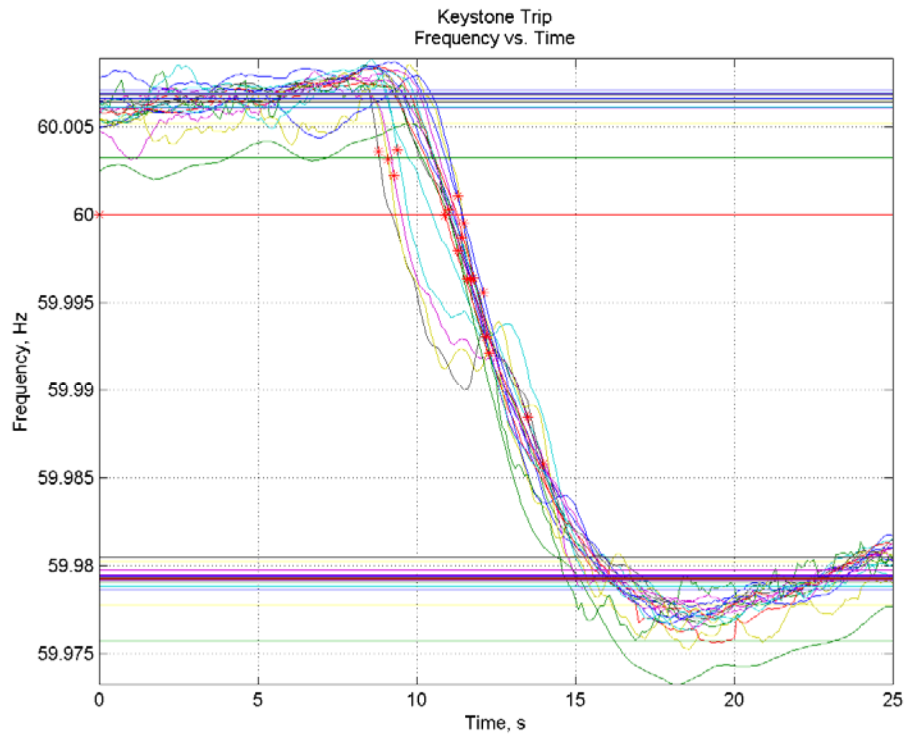
Keystone Trip
Frequency vs. Time
Frequency, Hz
60.005
60
59.995
59.99
59.985
59.98
59.975
0
5
10
15
20
25
Time, s

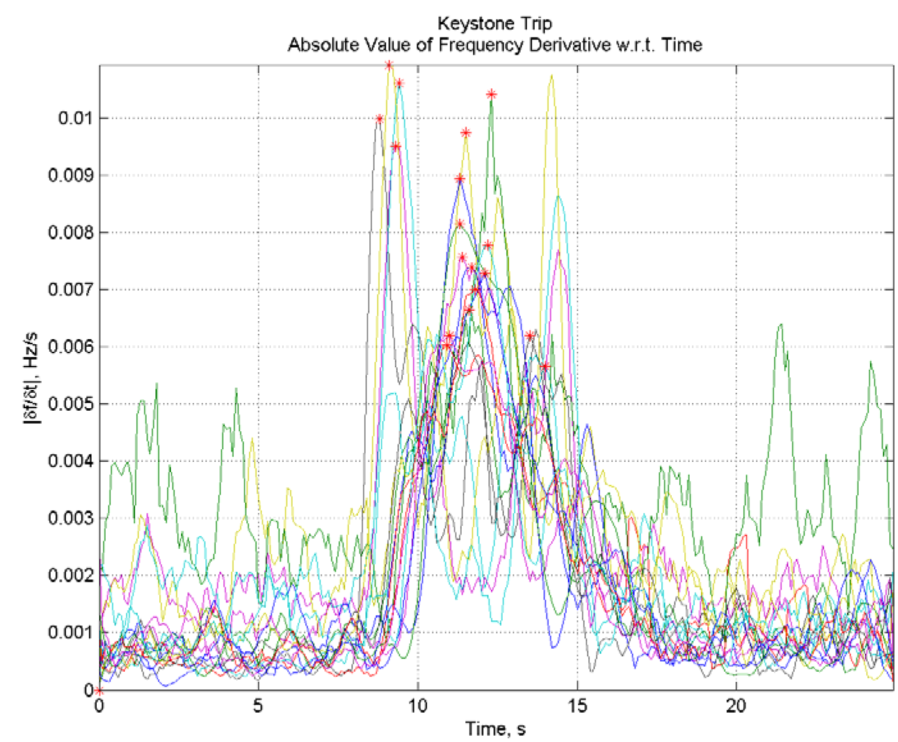
Keystone Trip
Absolute Value of Frequency Derivative w.r.t. Time
|δf/δt|, Hz/s
0.01
0.009
0.008
0.007
0.006
0.005
0.004
0.003
0.002
0.001
0
0
5
10
15
20
Time, s

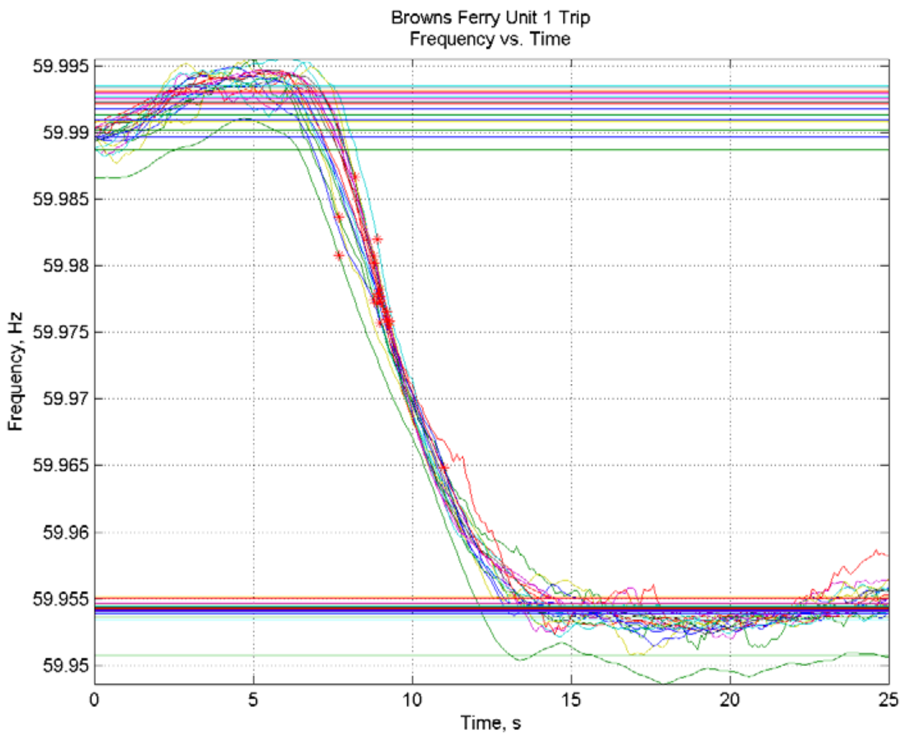
Browns Ferry Unit 1 Trip
Frequency vs. Time
Frequency, Hz
59.995
59.99
59.985
59.98
59.975
59.97
59.965
59.96
59.955
59.95
0
5
10
15
20
25
Time, s

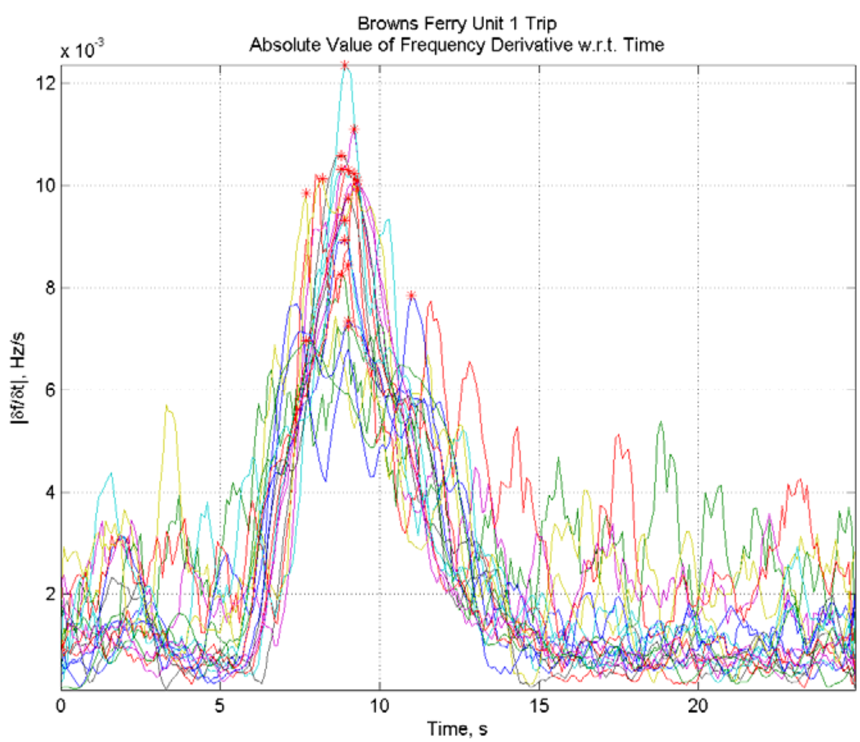
Browns Ferry Unit 1 Trip
Absolute Value of Frequency Derivative w.r.t. Time
x 10^-3
|δf/δt|, Hz/s
12
10
8
6
4
2
0
5
10
15
20
Time, s

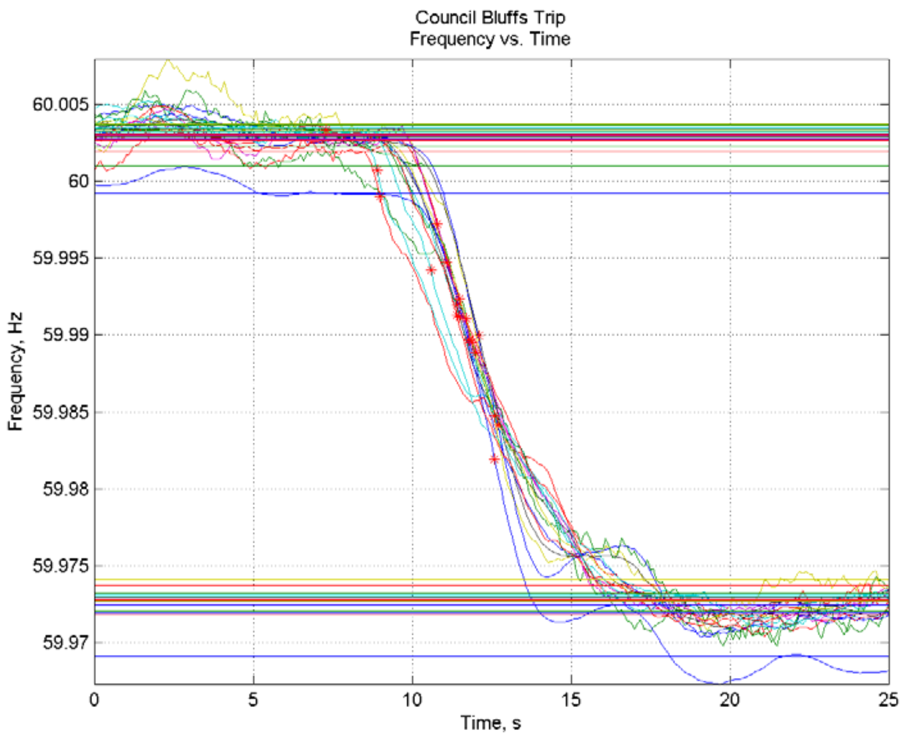
Council Bluffs Trip
Frequency vs. Time
Frequency, Hz
60.005
60
59.995
59.99
59.985
59.98
59.975
59.97
0
5
10
15
20
25
Time, s

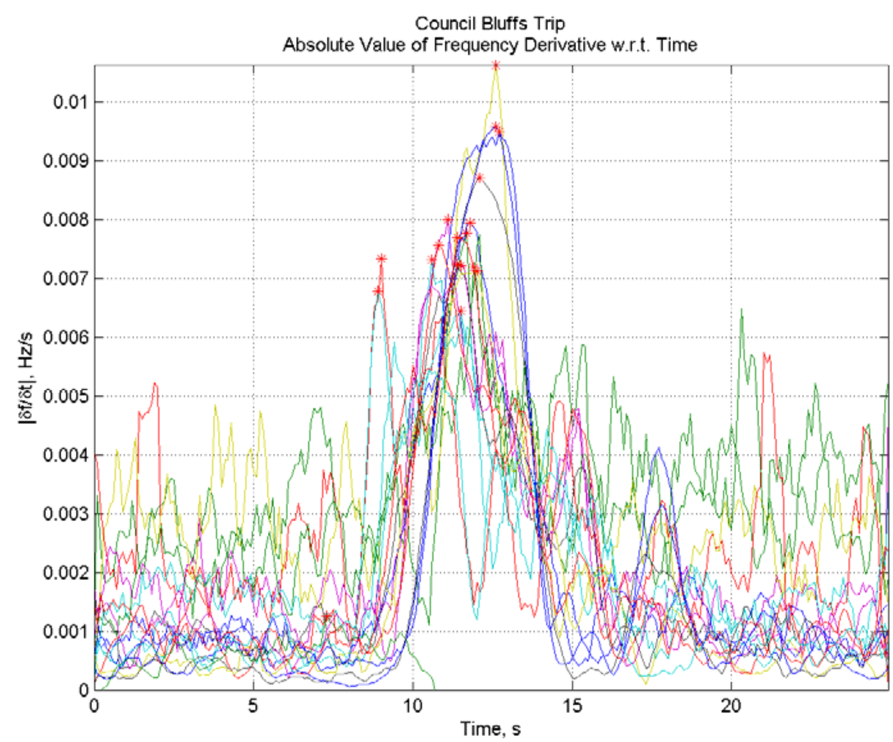
Council Bluffs Trip
Absolute Value of Frequency Derivative w.r.t. Time
|δf/δt|, Hz/s
0.01
0.009
0.008
0.007
0.006
0.005
0.004
0.003
0.002
0.001
0
0
5
10
15
20
Time, s

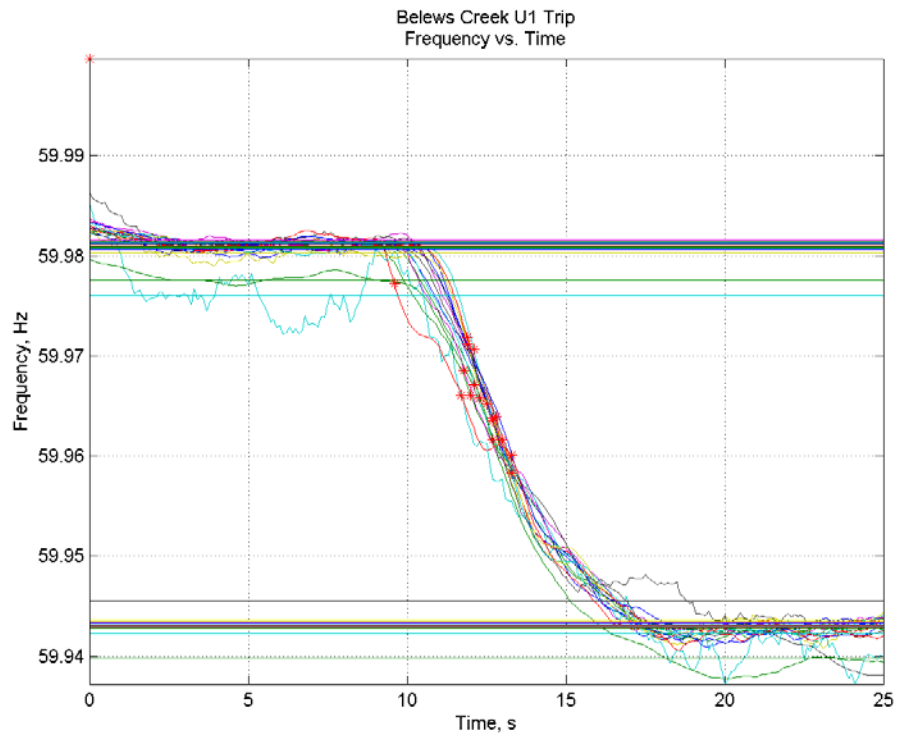
Belews Creek U1 Trip
Frequency vs. Time
Frequency, Hz
Time, s

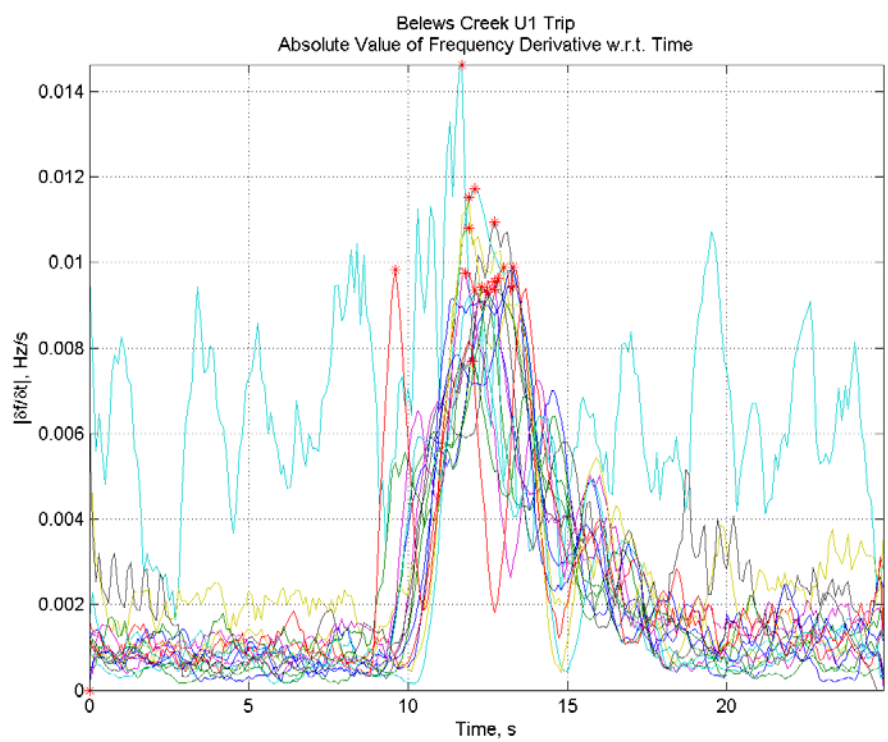
Belews Creek U1 Trip
Absolute Value of Frequency Derivative w.r.t. Time
|δf/δt|, Hz/s
Time, s

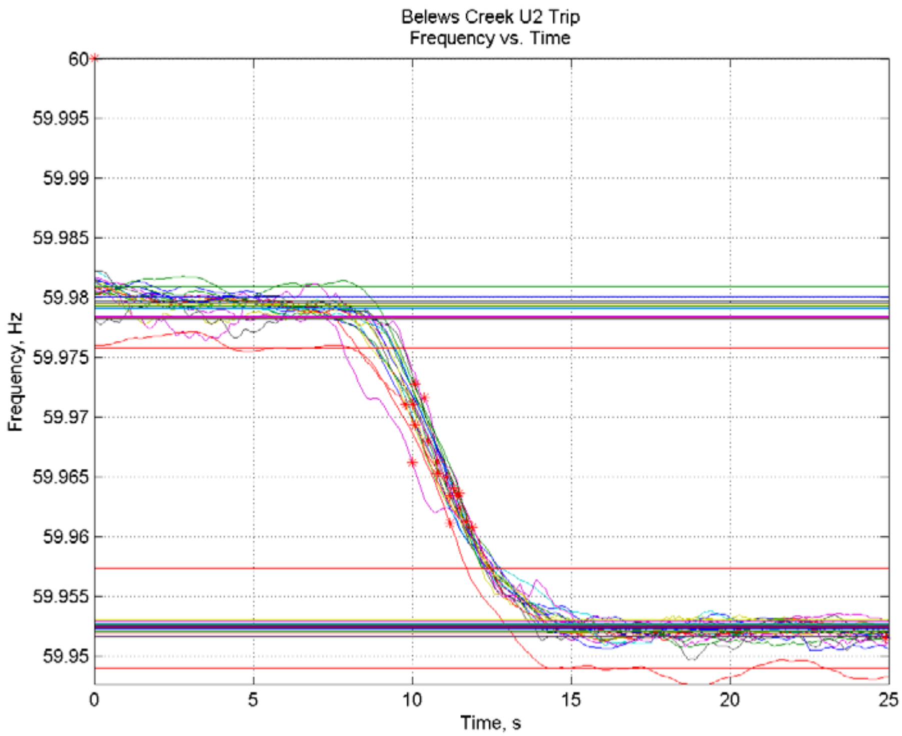
Belews Creek U2 Trip
Frequency vs. Time
Frequency, Hz
Time, s
60
59.995
59.99
59.985
59.98
59.975
59.97
59.965
59.96
59.955
59.95
0
5
10
15
20
25

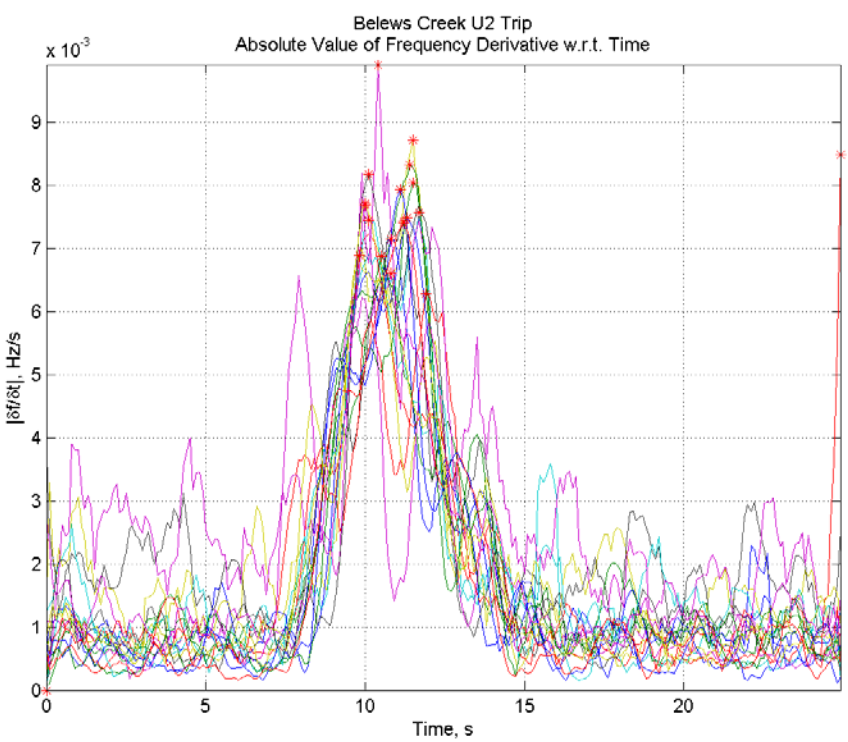
Belews Creek U2 Trip
Absolute Value of Frequency Derivative w.r.t. Time
x 10⁻³
|δf/δt|, Hz/s
Time, s
9
8
7
6
5
4
3
2
1
0
0
5
10
15
20

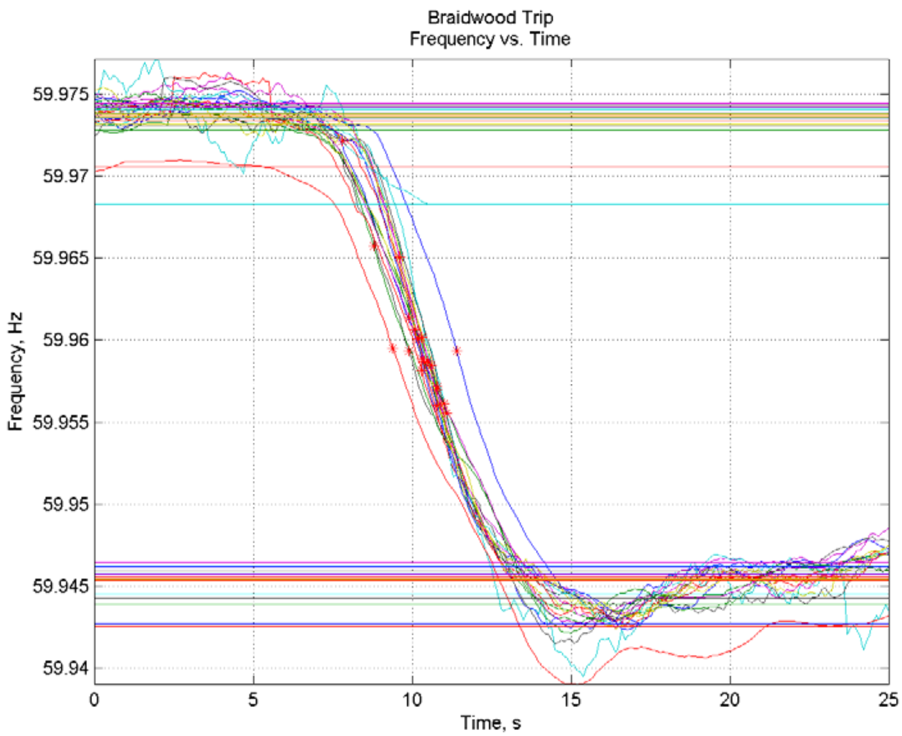
Braidwood Trip
Frequency vs. Time
Frequency, Hz
59.975
59.97
59.965
59.96
59.955
59.95
59.945
59.94
0
5
10
15
20
25
Time, s

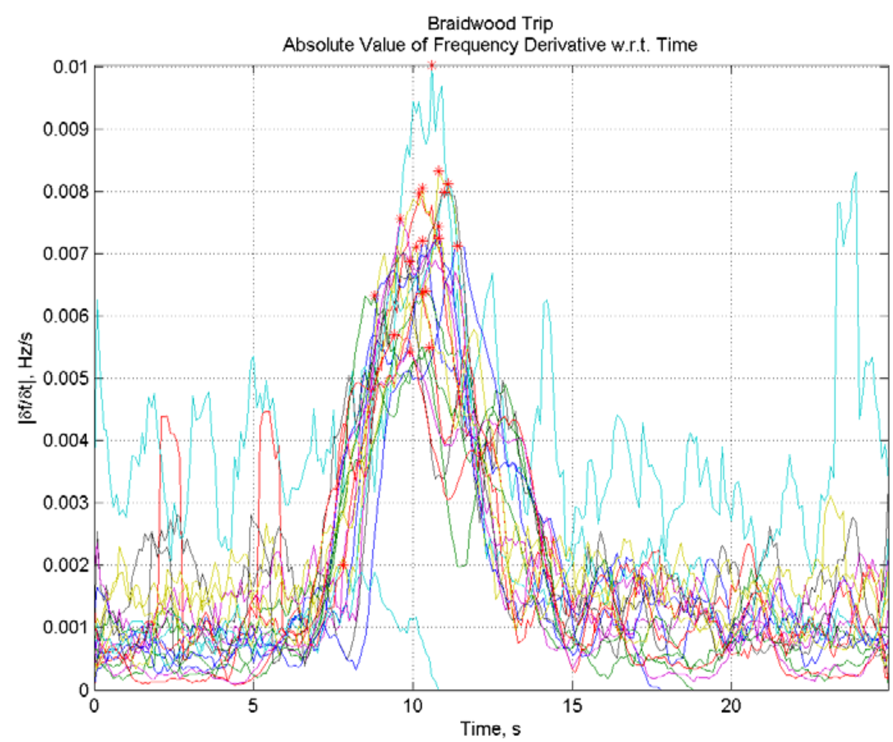
Braidwood Trip
Absolute Value of Frequency Derivative w.r.t. Time
|δf/δt|, Hz/s
0.01
0.009
0.008
0.007
0.006
0.005
0.004
0.003
0.002
0.001
0
0
5
10
15
20
Time, s

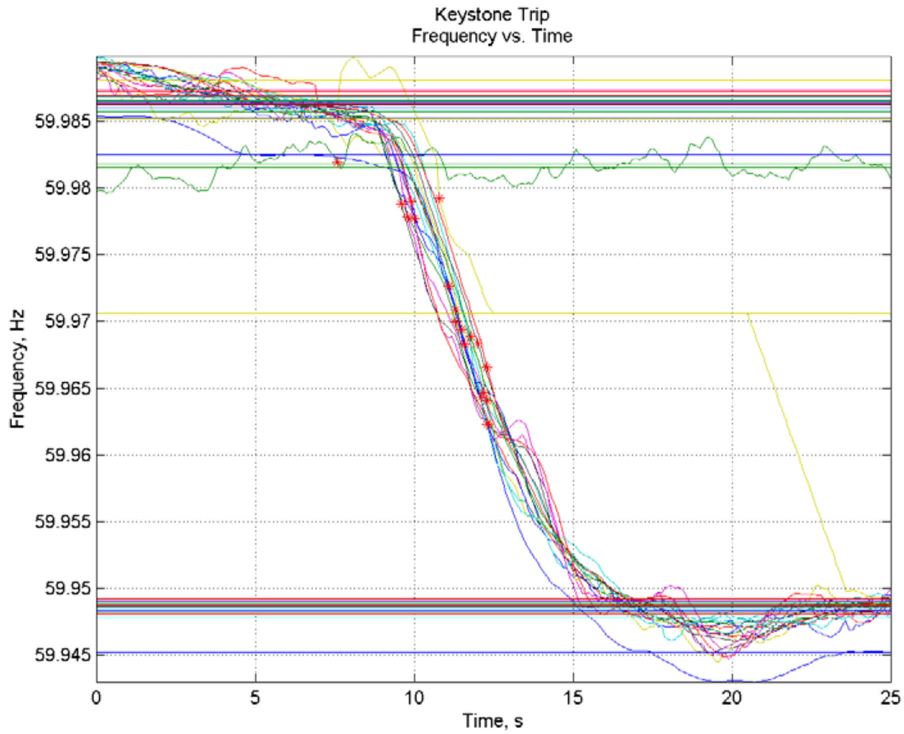
Keystone Trip
Frequency vs. Time
Frequency, Hz
59.985
59.98
59.975
59.97
59.965
59.96
59.955
59.95
59.945
0
5
10
15
20
25
Time, s

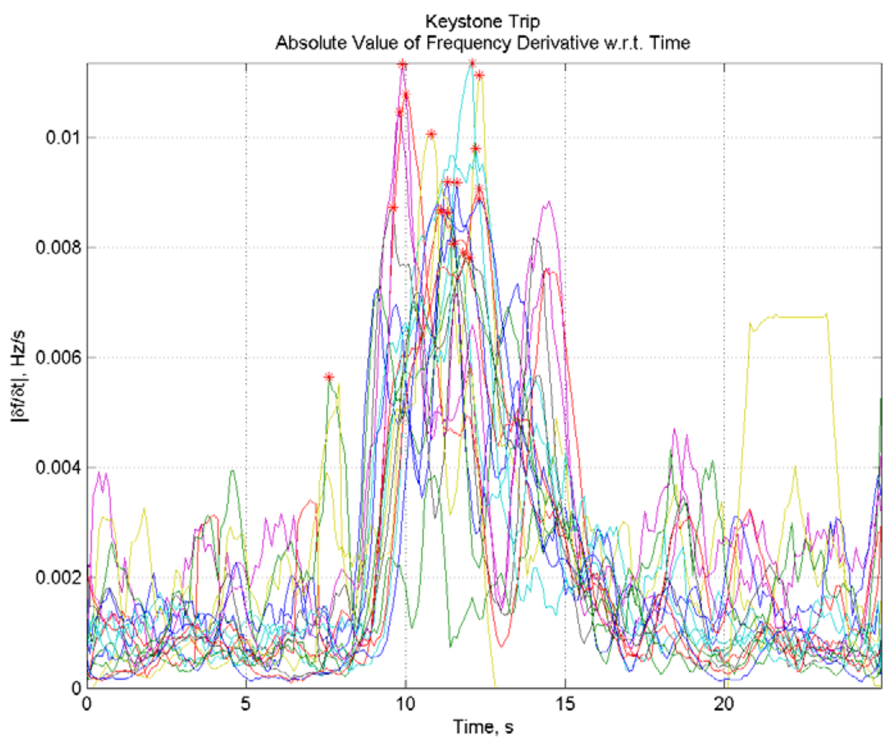
Keystone Trip
Absolute Value of Frequency Derivative w.r.t. Time
|δf/δt|, Hz/s
0.01
0.008
0.006
0.004
0.002
0
0
5
10
15
20
Time, s

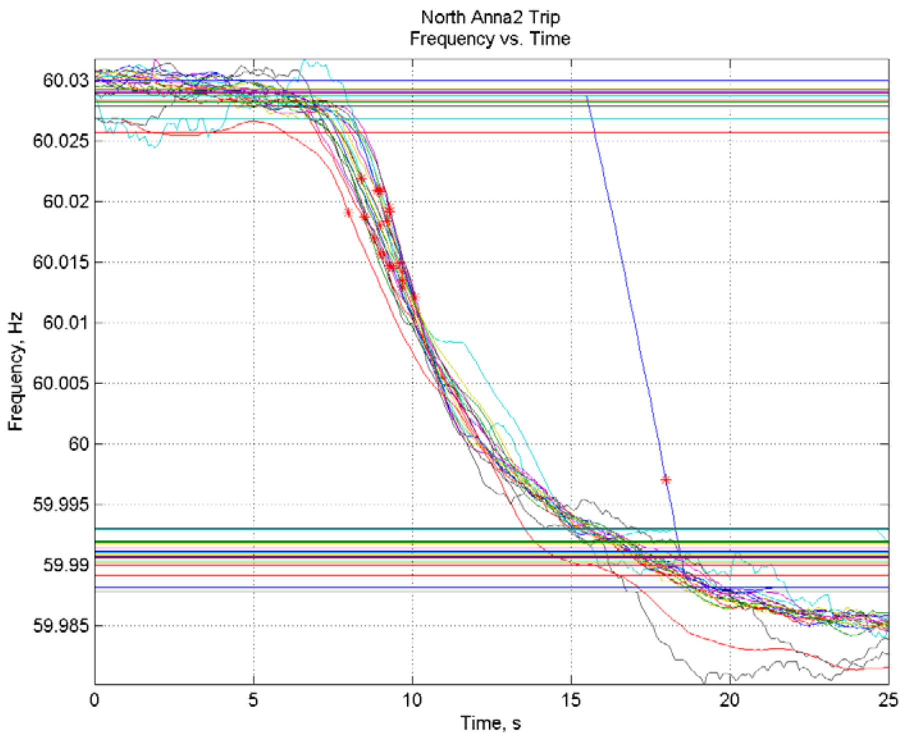
North Anna2 Trip
Frequency vs. Time
Frequency, Hz
60.03
60.025
60.02
60.015
60.01
60.005
60
59.995
59.99
59.985
0
5
10
15
20
25
Time, s

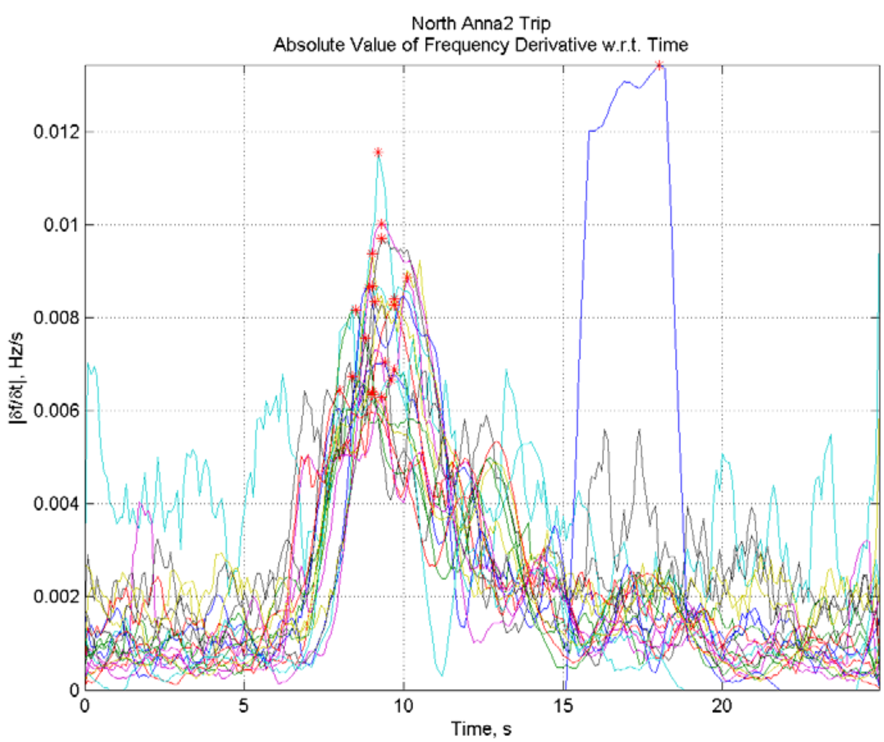
North Anna2 Trip
Absolute Value of Frequency Derivative w.r.t. Time
|δf/δt|, Hz/s
0.012
0.01
0.008
0.006
0.004
0.002
0
0
5
10
15
20
Time, s

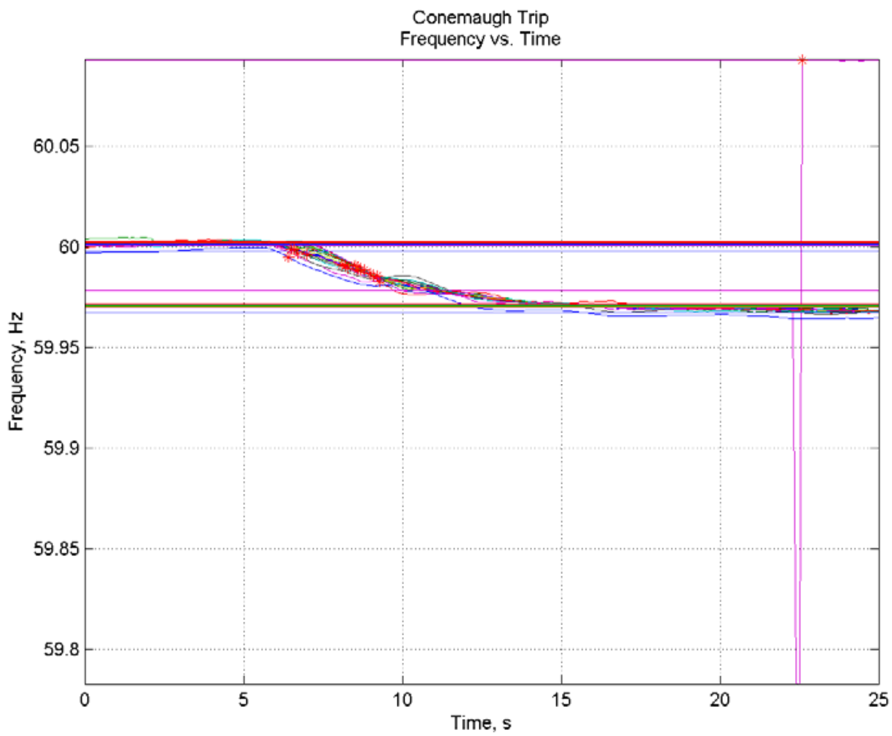
Conemaugh Trip
Frequency vs. Time
60.05
60
59.95
59.9
59.85
59.8
Frequency, Hz
0
5
10
15
20
25
Time, s

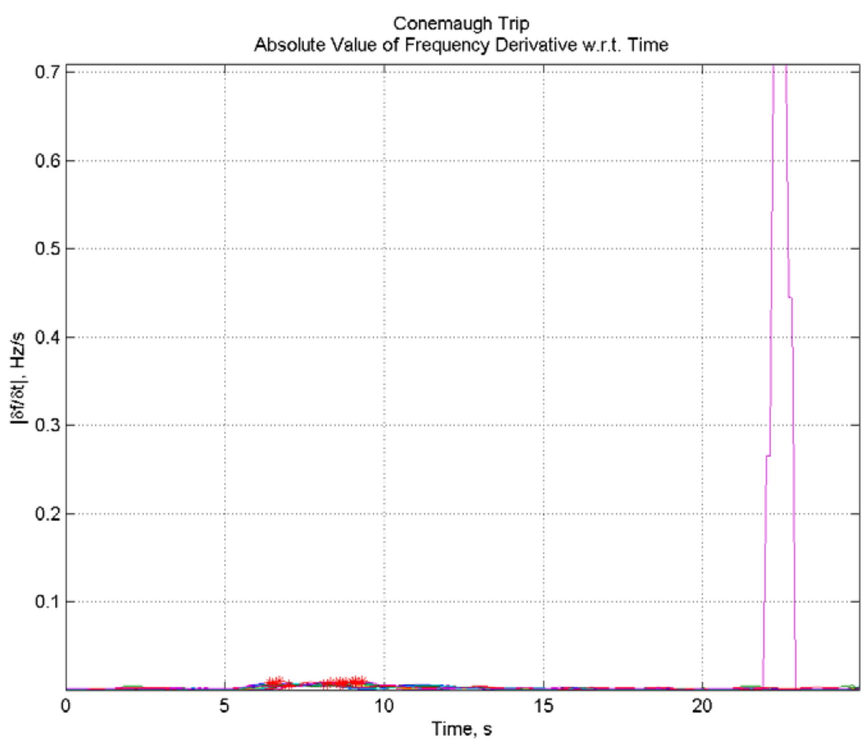
Conemaugh Trip
Absolute Value of Frequency Derivative w.r.t. Time
0.7
0.6
0.5
0.4
0.3
0.2
0.1
|δf/δt|, Hz/s
0
5
10
15
20
Time, s

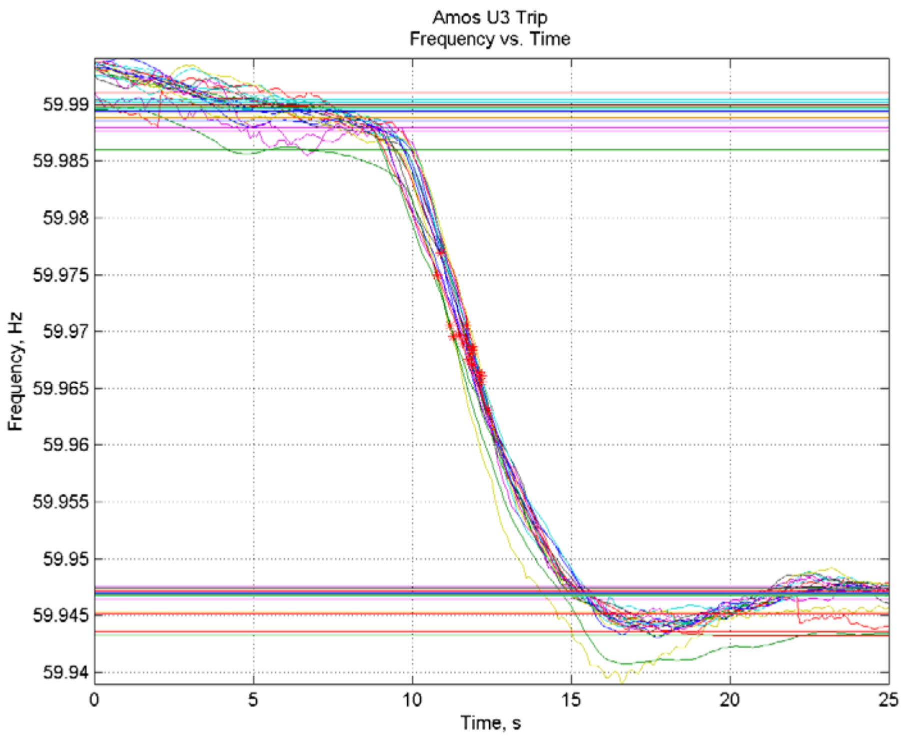
Amos U3 Trip
Frequency vs. Time
Frequency, Hz
59.99
59.985
59.98
59.975
59.97
59.965
59.96
59.955
59.95
59.945
59.94
0
5
10
15
20
25
Time, s

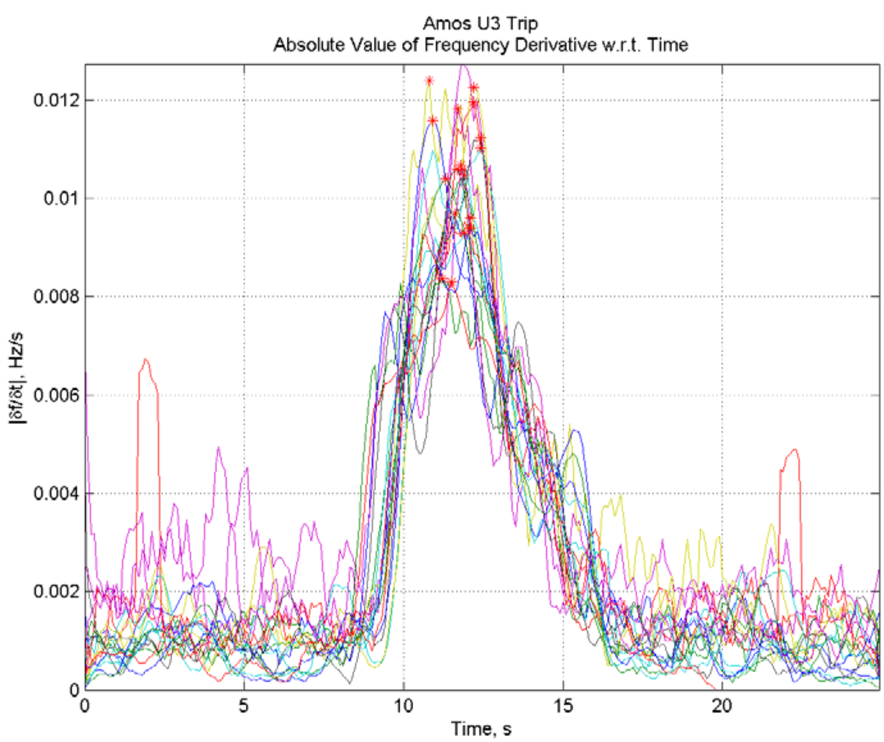
Amos U3 Trip
Absolute Value of Frequency Derivative w.r.t. Time
|δf/δt|, Hz/s
0.012
0.01
0.008
0.006
0.004
0.002
0
0
5
10
15
20
Time, s

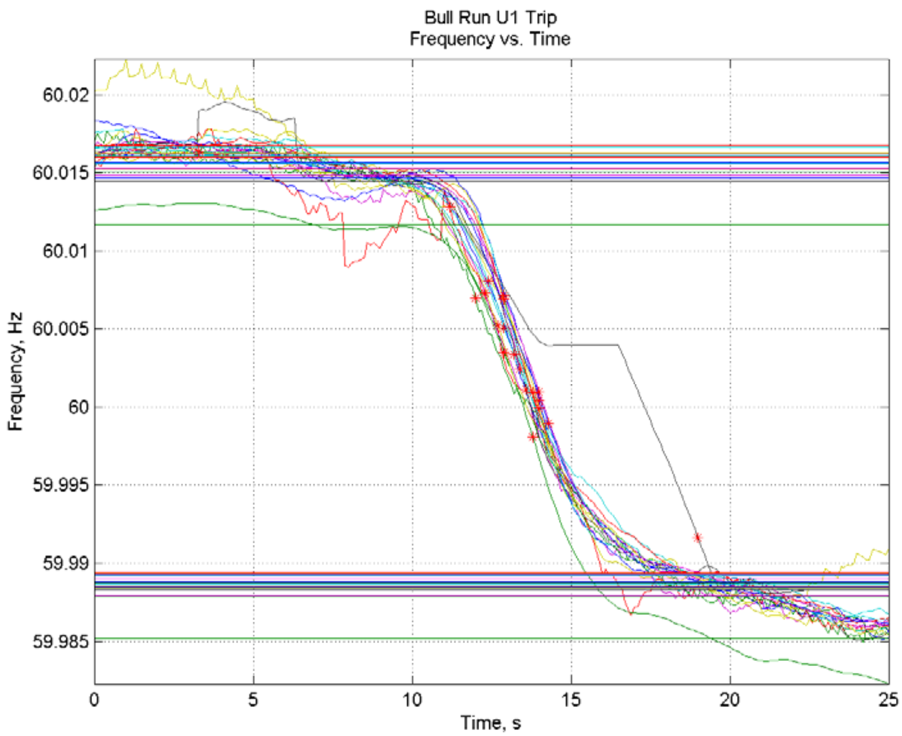
Bull Run U1 Trip
Frequency vs. Time
Frequency, Hz
Time, s
60.02
60.015
60.01
60.005
60
59.995
59.99
59.985
0
5
10
15
20
25

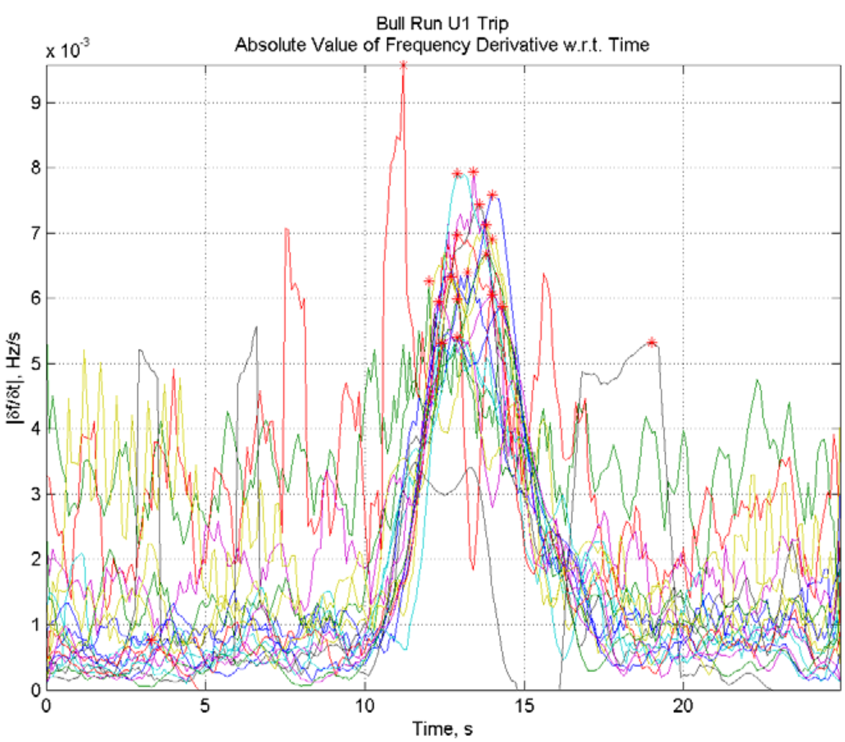
Bull Run U1 Trip
Absolute Value of Frequency Derivative w.r.t. Time
x 10^-3
|δf/δt|, Hz/s
Time, s
9
8
7
6
5
4
3
2
1
0
0
5
10
15
20

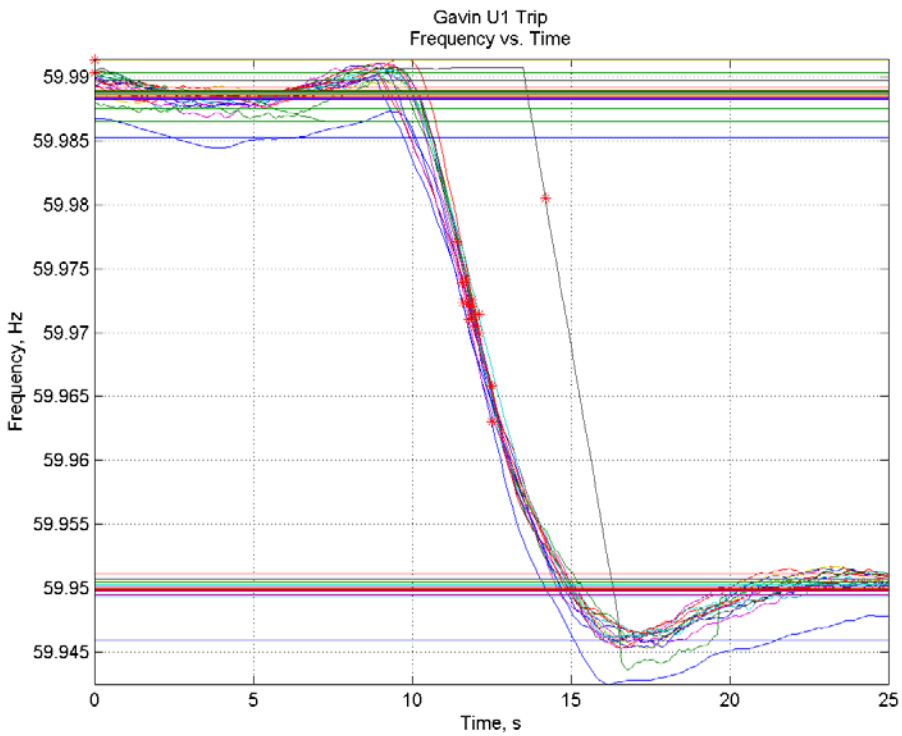
Gavin U1 Trip
Frequency vs. Time
Frequency, Hz
59.99
59.985
59.98
59.975
59.97
59.965
59.96
59.955
59.95
59.945
0
5
10
15
20
25
Time, s

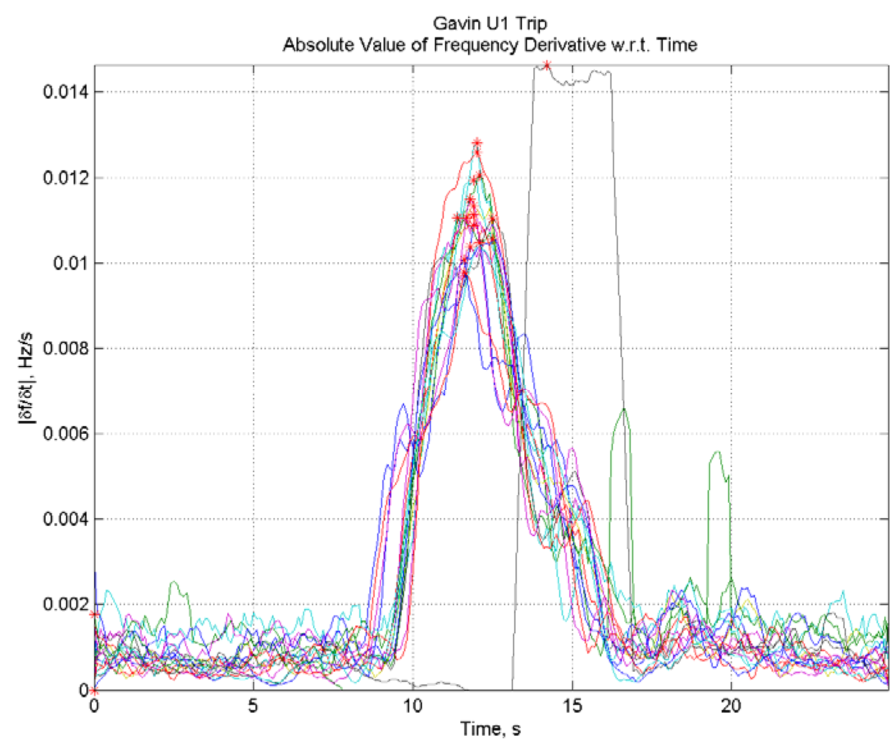
Gavin U1 Trip
Absolute Value of Frequency Derivative w.r.t. Time
|δf/δt|, Hz/s
0.014
0.012
0.01
0.008
0.006
0.004
0.002
0
0
5
10
15
20
Time, s

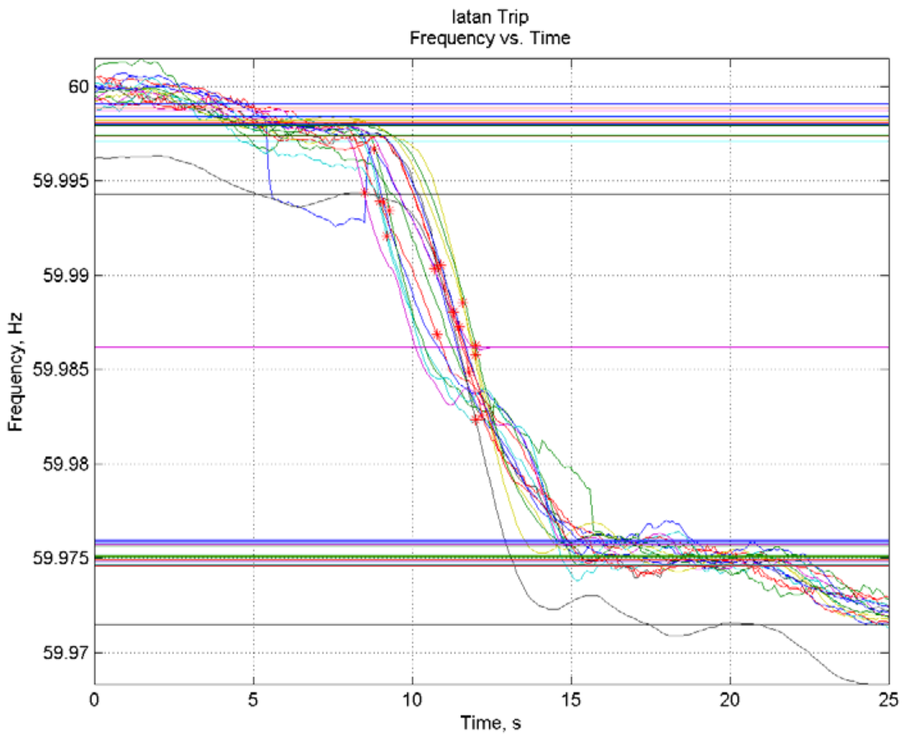
Iatan Trip
Frequency vs. Time
Frequency, Hz
Time, s
60
59.995
59.99
59.985
59.98
59.975
59.97
0
5
10
15
20
25

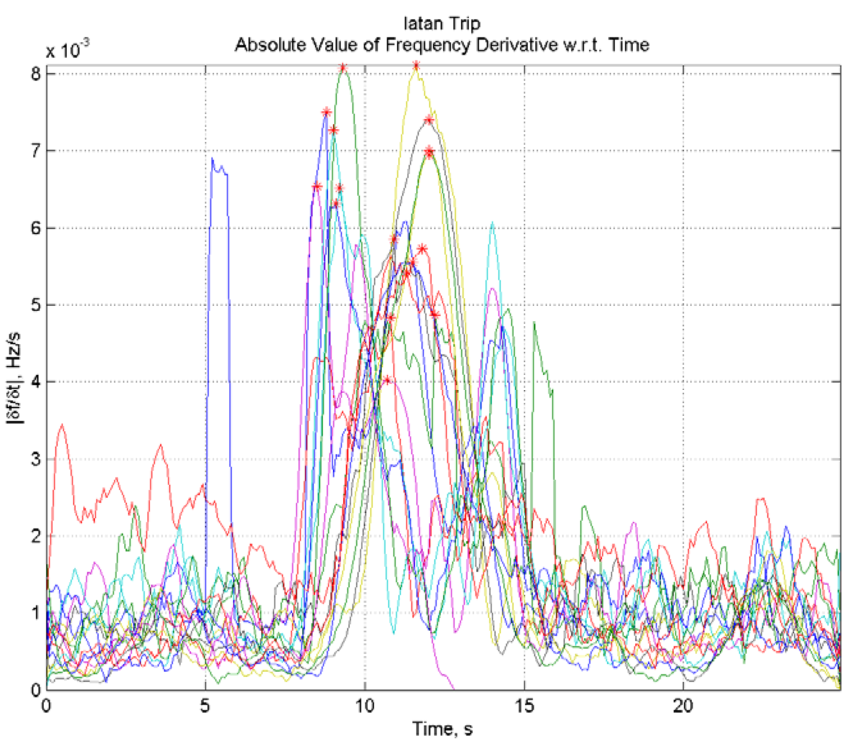
Iatan Trip
Absolute Value of Frequency Derivative w.r.t. Time
x 10^-3
|δf/δt|, Hz/s
Time, s
0
1
2
3
4
5
6
7
8
0
5
10
15
20

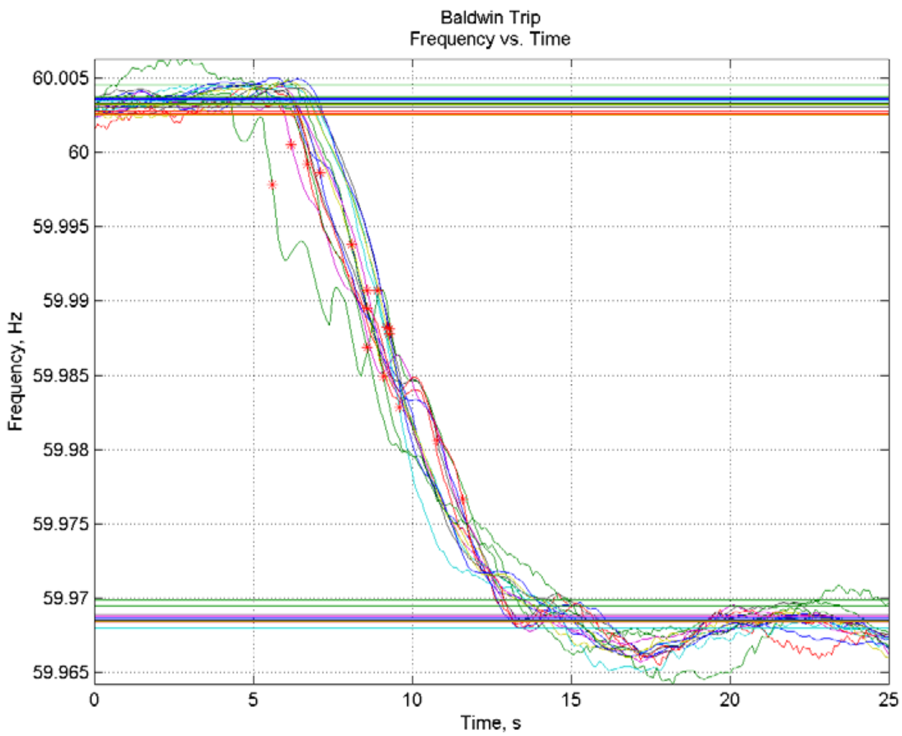
Baldwin Trip
Frequency vs. Time
Frequency, Hz
Time, s
60.005
60
59.995
59.99
59.985
59.98
59.975
59.97
59.965
0
5
10
15
20
25

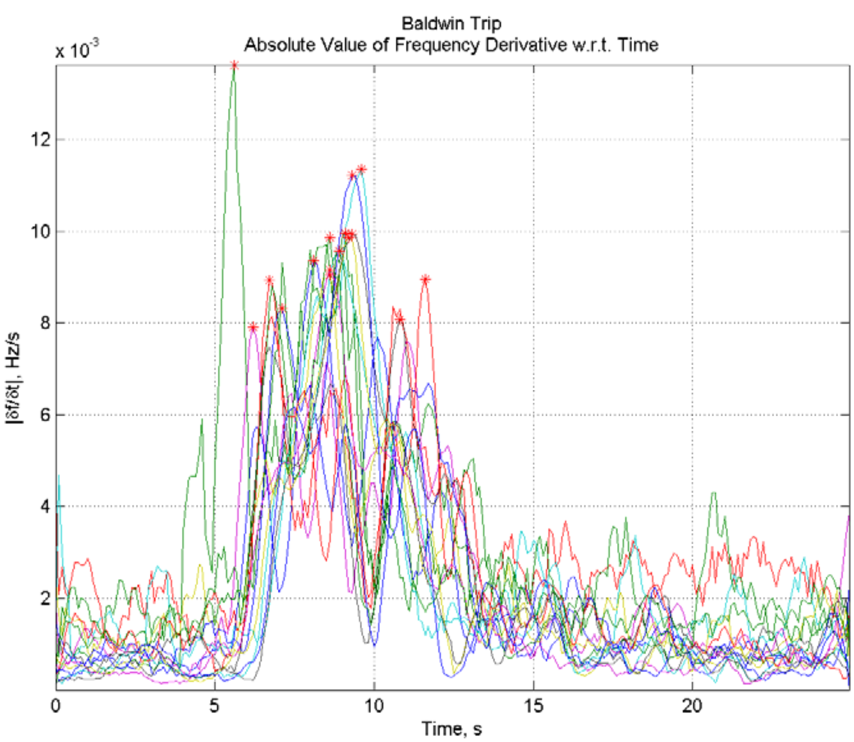
Baldwin Trip
Absolute Value of Frequency Derivative w.r.t. Time
x 10-3
|δf/δt|, Hz/s
Time, s
12
10
8
6
4
2
0
5
10
15
20

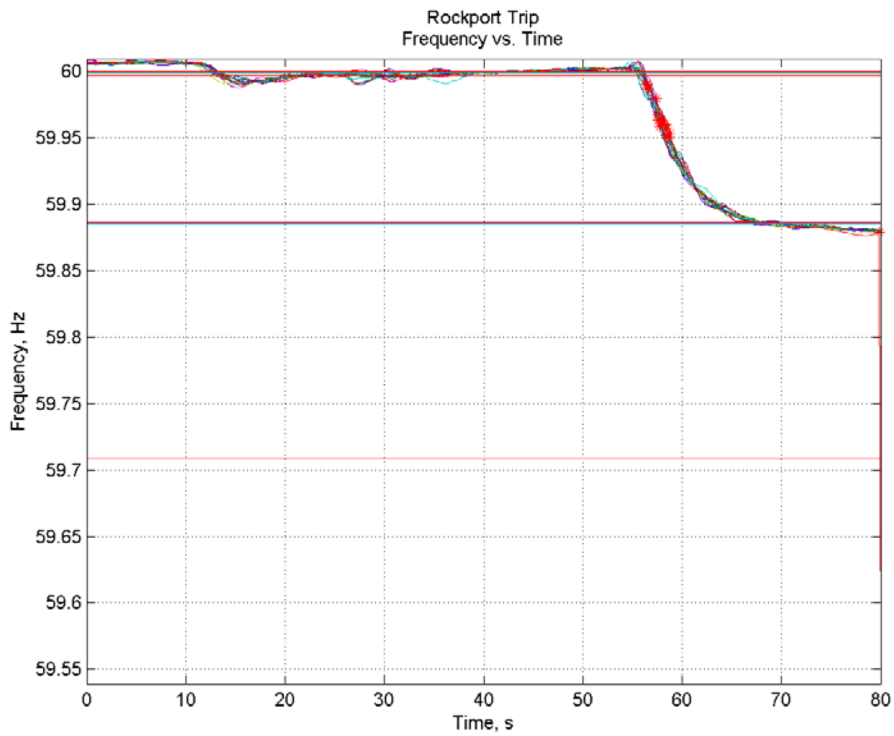
Rockport Trip
Frequency vs. Time
Frequency, Hz
Time, s
60
59.95
59.9
59.85
59.8
59.75
59.7
59.65
59.6
59.55
0
10
20
30
40
50
60
70
80

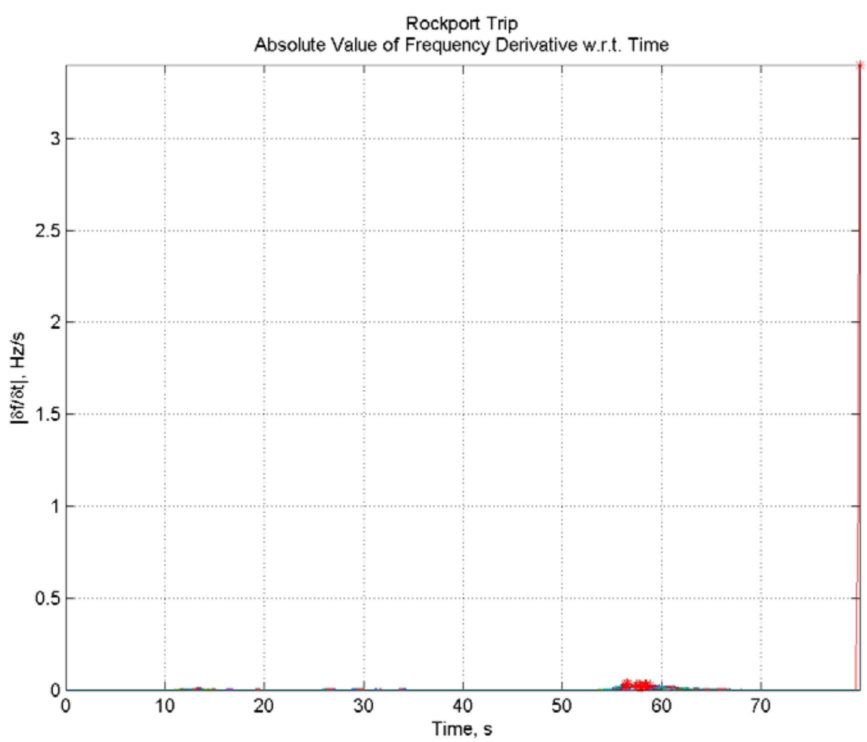
Rockport Trip
Absolute Value of Frequency Derivative w.r.t. Time
|δf/δt|, Hz/s
Time, s
3
2.5
2
1.5
1
0.5
0
0
10
20
30
40
50
60
70

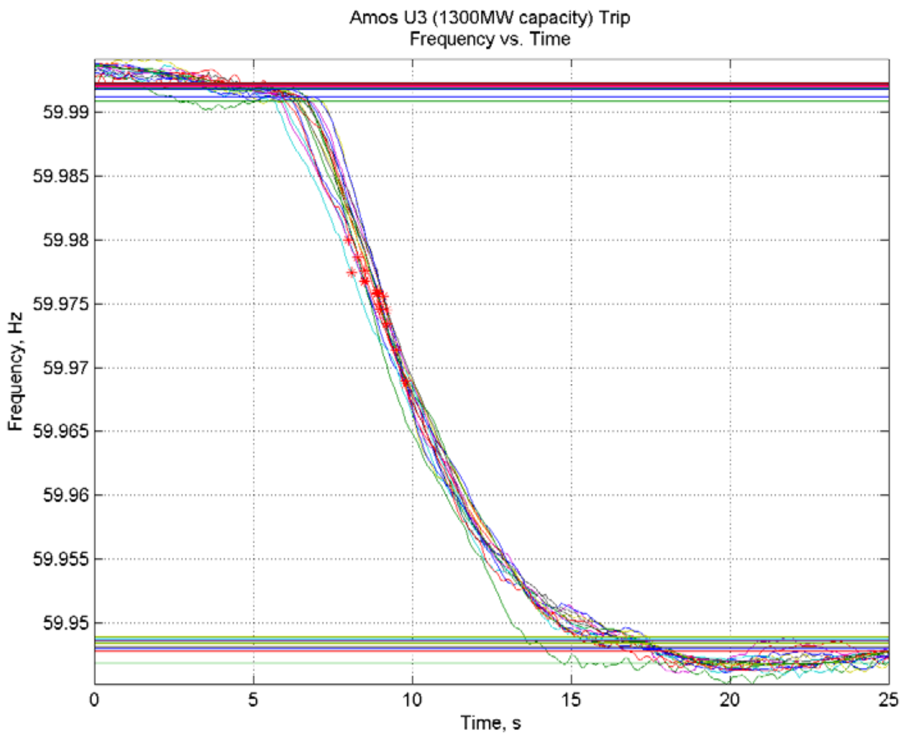
Amos U3 (1300MW capacity) Trip
Frequency vs. Time
Frequency, Hz
Time, s
59.99
59.985
59.98
59.975
59.97
59.965
59.96
59.955
59.95
0
5
10
15
20
25

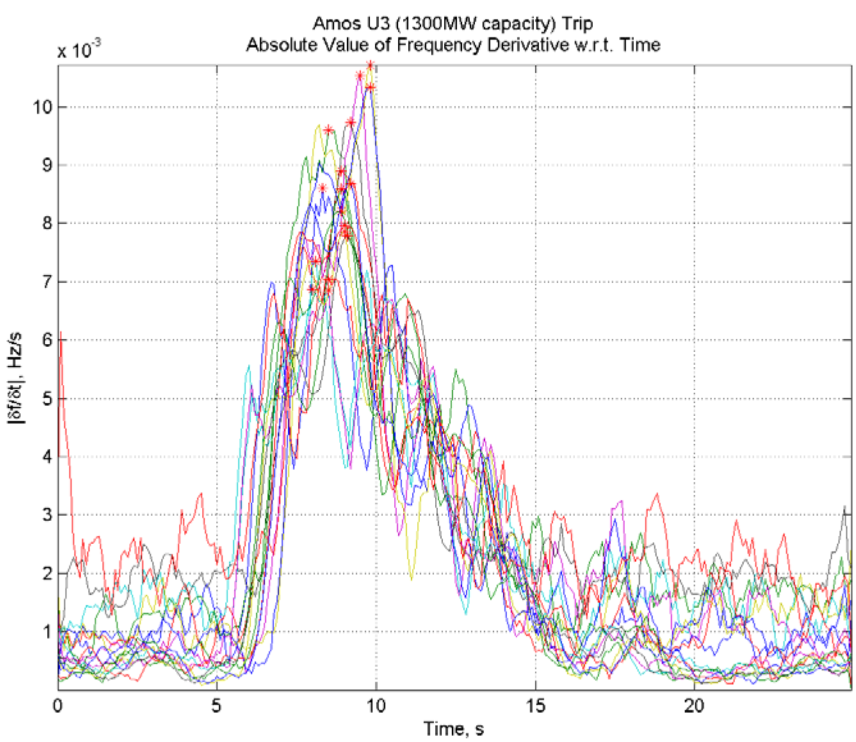
Amos U3 (1300MW capacity) Trip
Absolute Value of Frequency Derivative w.r.t. Time
x 10-3
|δf/δt|, Hz/s
Time, s
10
9
8
7
6
5
4
3
2
1
0
5
10
15
20

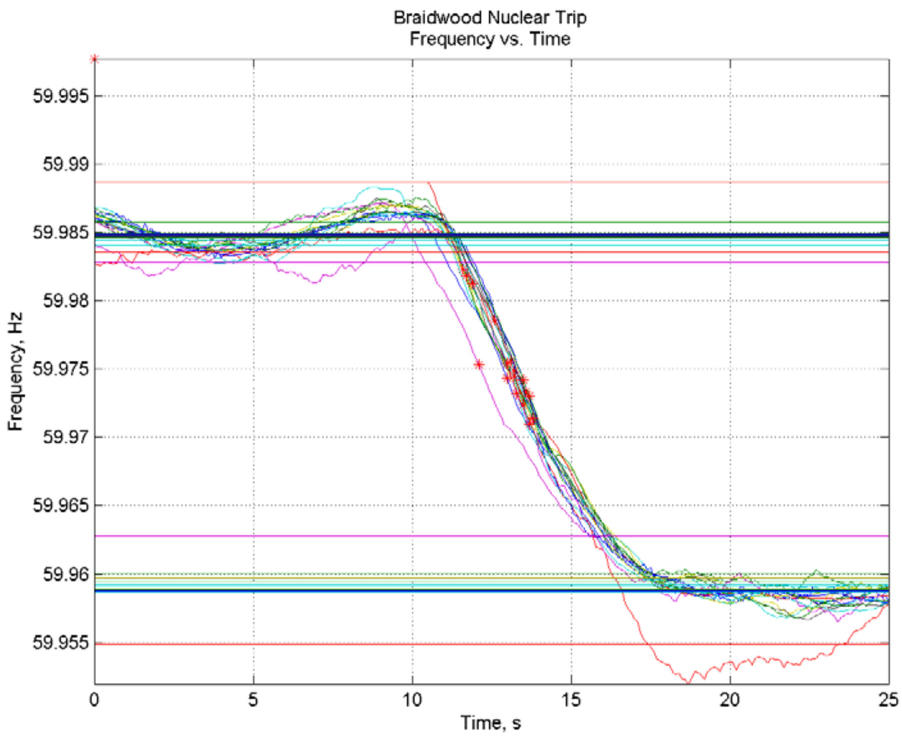
Braidwood Nuclear Trip
Frequency vs. Time
Frequency, Hz
Time, s
59.995
59.99
59.985
59.98
59.975
59.97
59.965
59.96
59.955
0
5
10
15
20
25

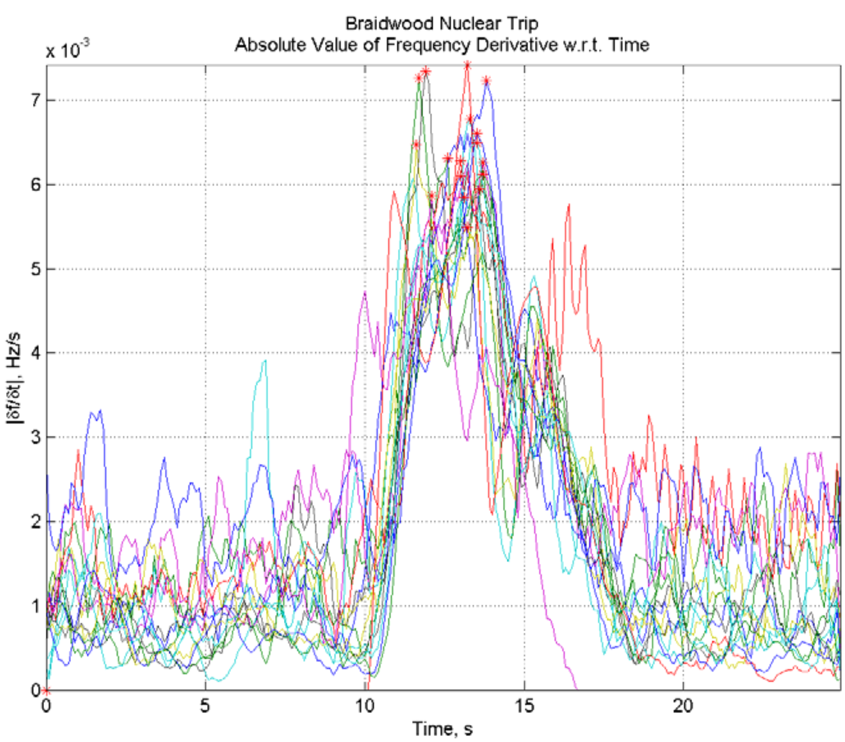
Braidwood Nuclear Trip
Absolute Value of Frequency Derivative w.r.t. Time
x 10^-3
|δf/δt|, Hz/s
Time, s
0
1
2
3
4
5
6
7
0
5
10
15
20

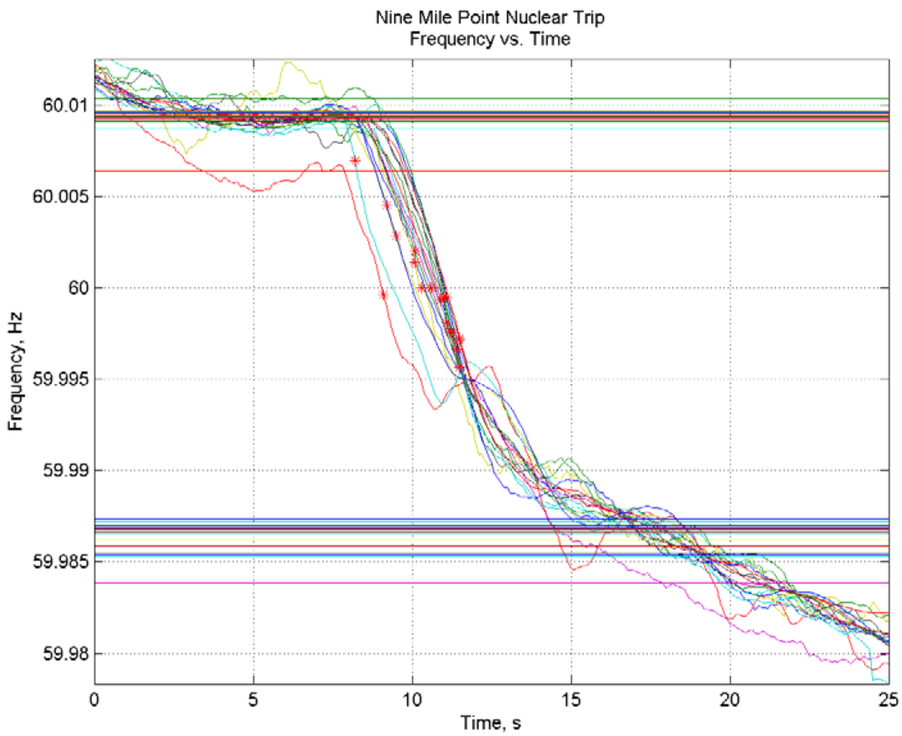
Nine Mile Point Nuclear Trip
Frequency vs. Time
Frequency, Hz
Time, s
60.01
60.005
60
59.995
59.99
59.985
59.98
0
5
10
15
20
25

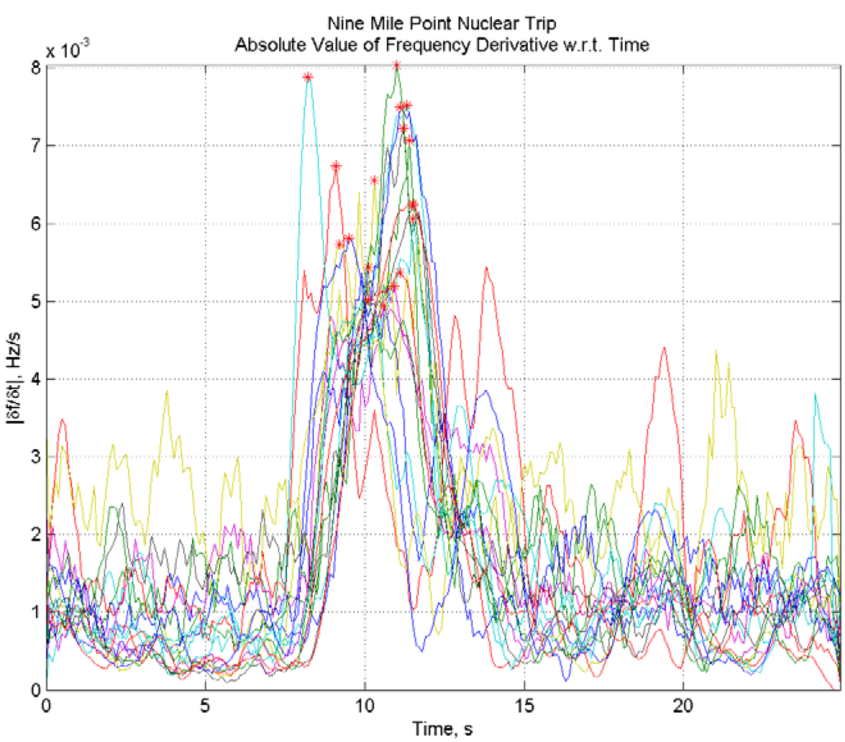
Nine Mile Point Nuclear Trip
Absolute Value of Frequency Derivative w.r.t. Time
x 10-3
|δf/δt|, Hz/s
Time, s
8
7
6
5
4
3
2
1
0
0
5
10
15
20

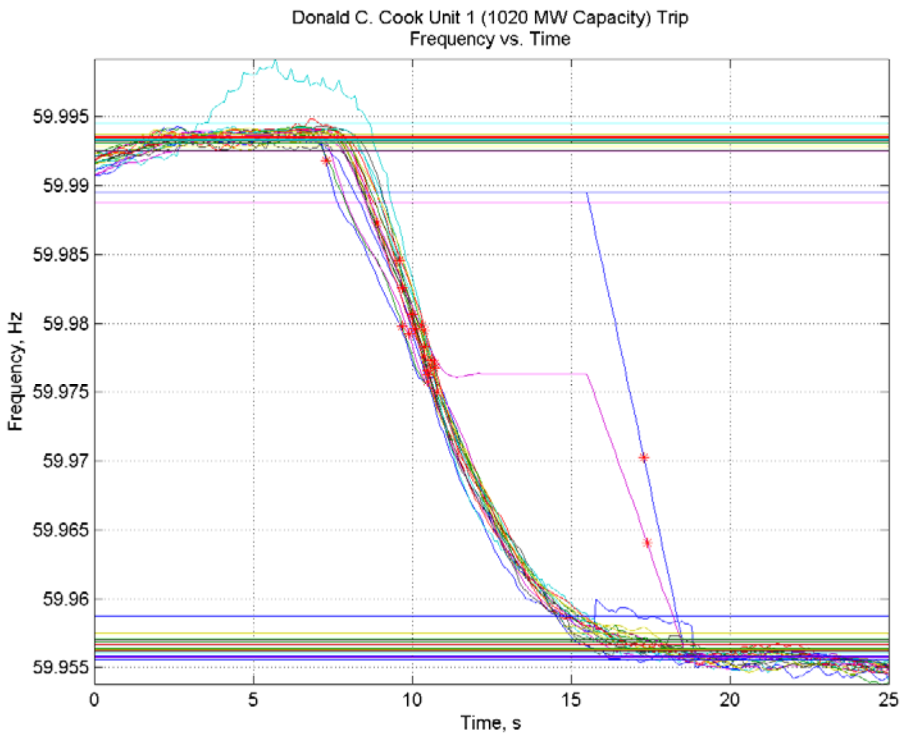
Donald C. Cook Unit 1 (1020 MW Capacity) Trip
Frequency vs. Time
Frequency, Hz
59.995
59.99
59.985
59.98
59.975
59.97
59.965
59.96
59.955
0
5
10
15
20
25
Time, s

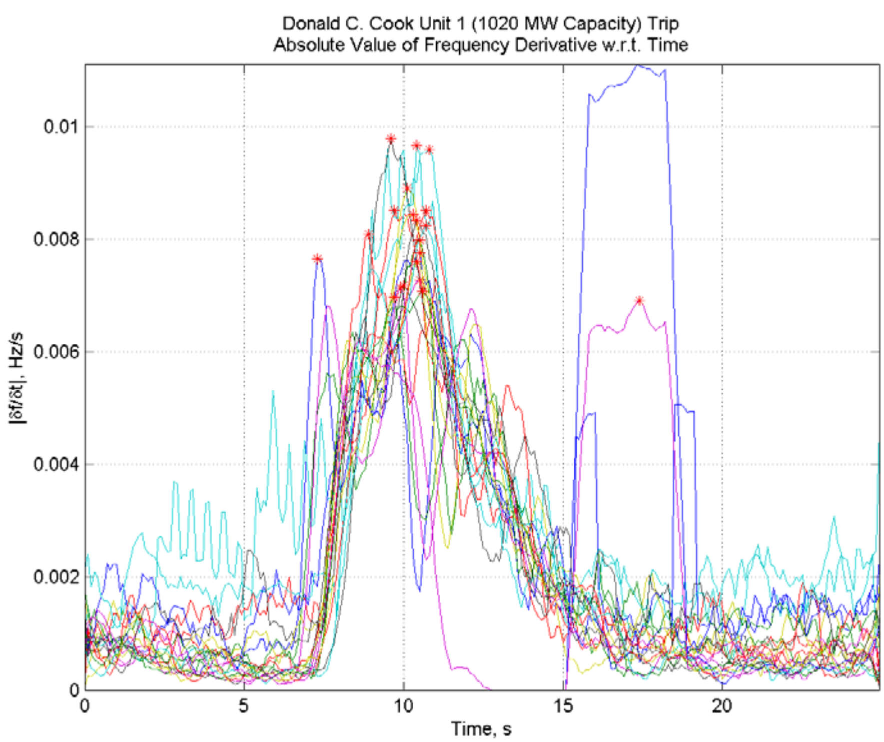
Donald C. Cook Unit 1 (1020 MW Capacity) Trip
Absolute Value of Frequency Derivative w.r.t. Time
|δf/δt|, Hz/s
0.01
0.008
0.006
0.004
0.002
0
0
5
10
15
20
Time, s

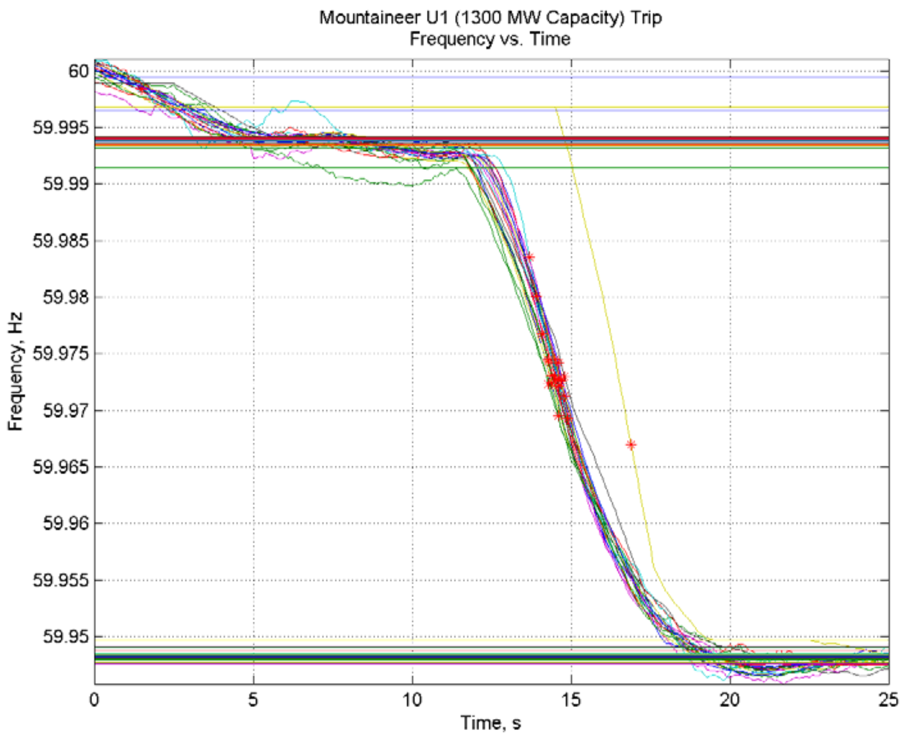
Mountaineer U1 (1300 MW Capacity) Trip
Frequency vs. Time
Frequency, Hz
Time, s
60
59.995
59.99
59.985
59.98
59.975
59.97
59.965
59.96
59.955
59.95
0
5
10
15
20
25

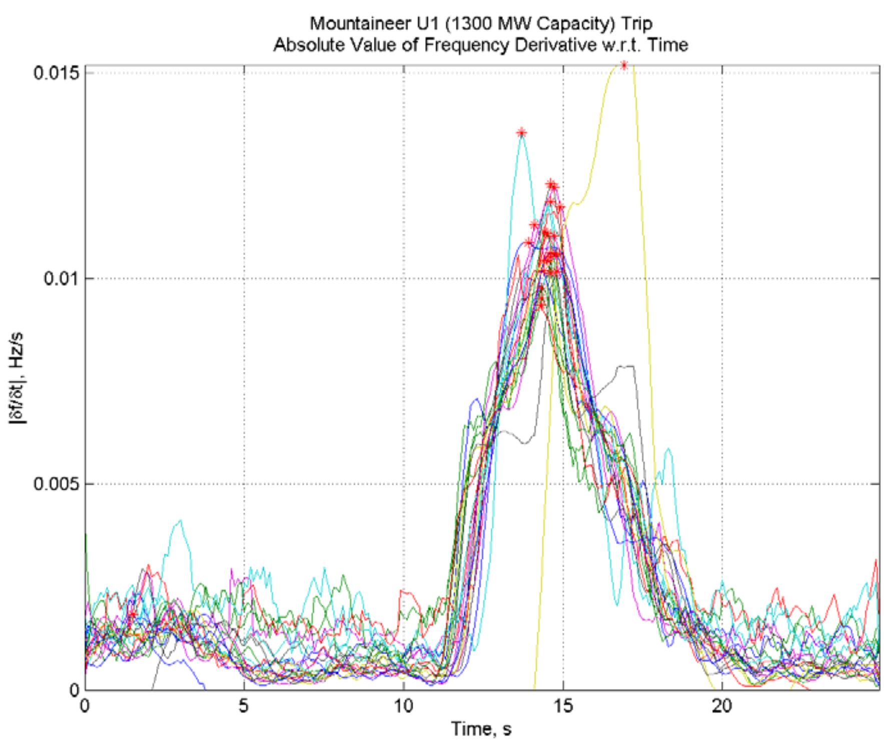
Mountaineer U1 (1300 MW Capacity) Trip
Absolute Value of Frequency Derivative w.r.t. Time
|δf/δt|, Hz/s
Time, s
0.015
0.01
0.005
0
0
5
10
15
20

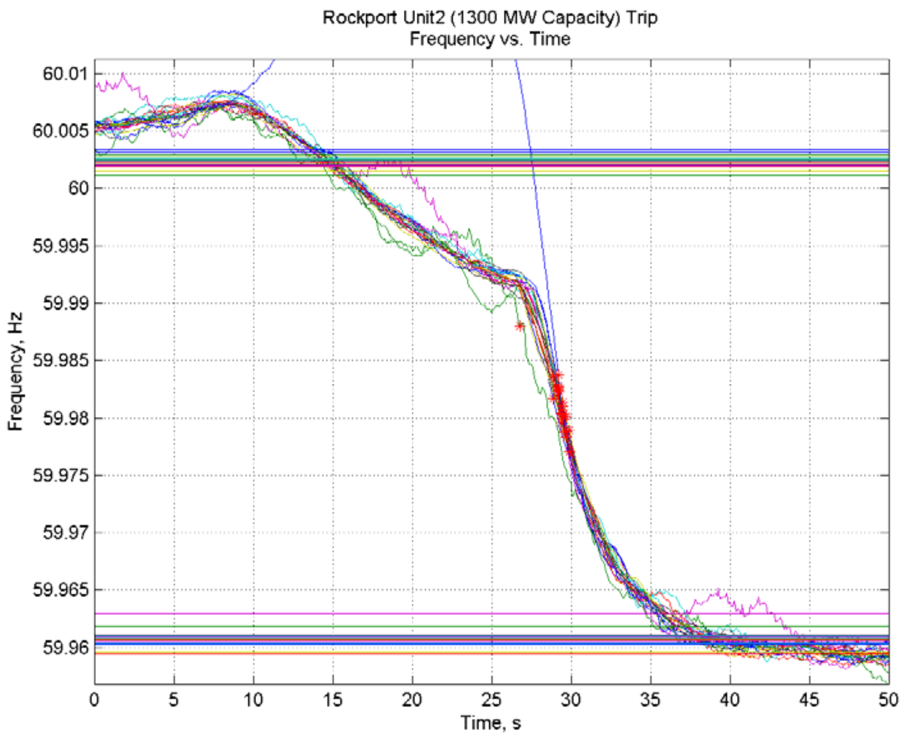
Rockport Unit2 (1300 MW Capacity) Trip
Frequency vs. Time
Frequency, Hz
60.01
60.005
60
59.995
59.99
59.985
59.98
59.975
59.97
59.965
59.96
0
5
10
15
20
25
30
35
40
45
50
Time, s

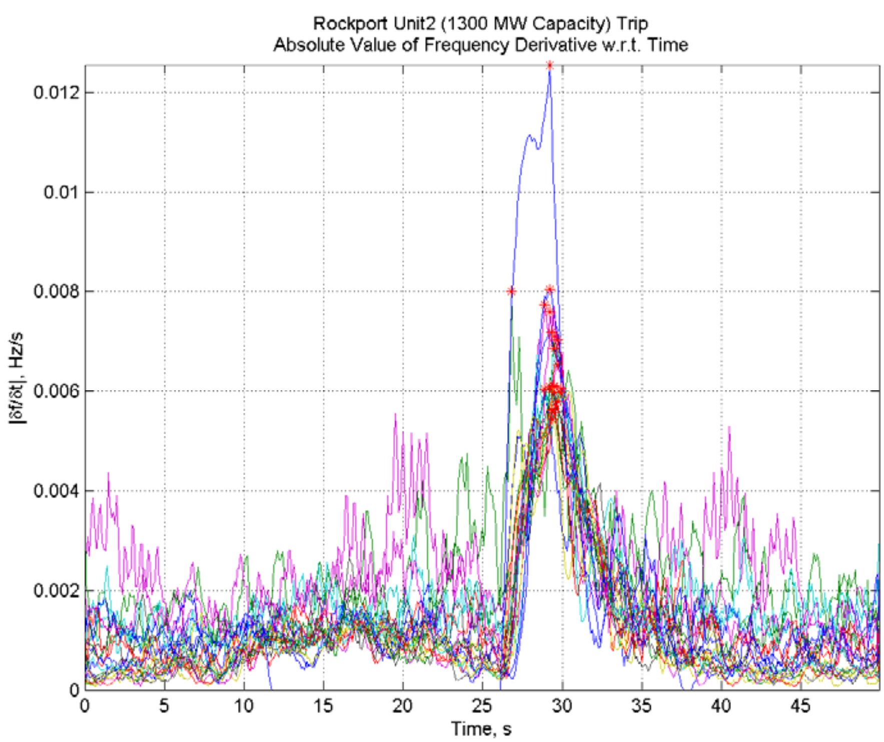
Rockport Unit2 (1300 MW Capacity) Trip
Absolute Value of Frequency Derivative w.r.t. Time
|δf/δt|, Hz/s
0.012
0.01
0.008
0.006
0.004
0.002
0
0
5
10
15
20
25
30
35
40
45
Time, s

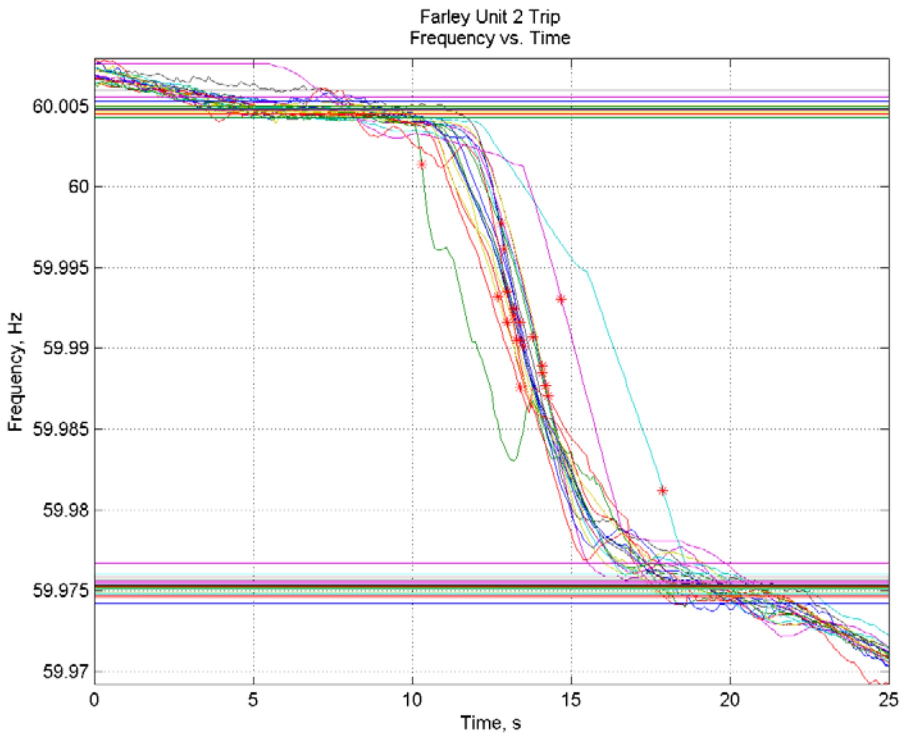
Farley Unit 2 Trip
Frequency vs. Time
Frequency, Hz
Time, s
60.005
60
59.995
59.99
59.985
59.98
59.975
59.97
0
5
10
15
20
25

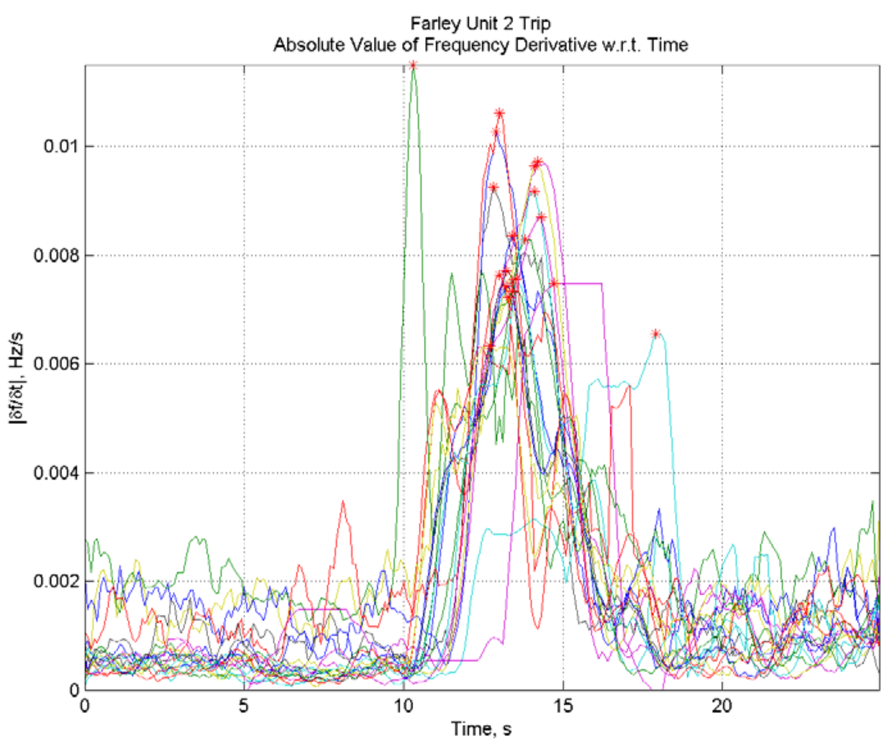
Farley Unit 2 Trip
Absolute Value of Frequency Derivative w.r.t. Time
|δf/δt|, Hz/s
Time, s
0.01
0.008
0.006
0.004
0.002
0
0
5
10
15
20

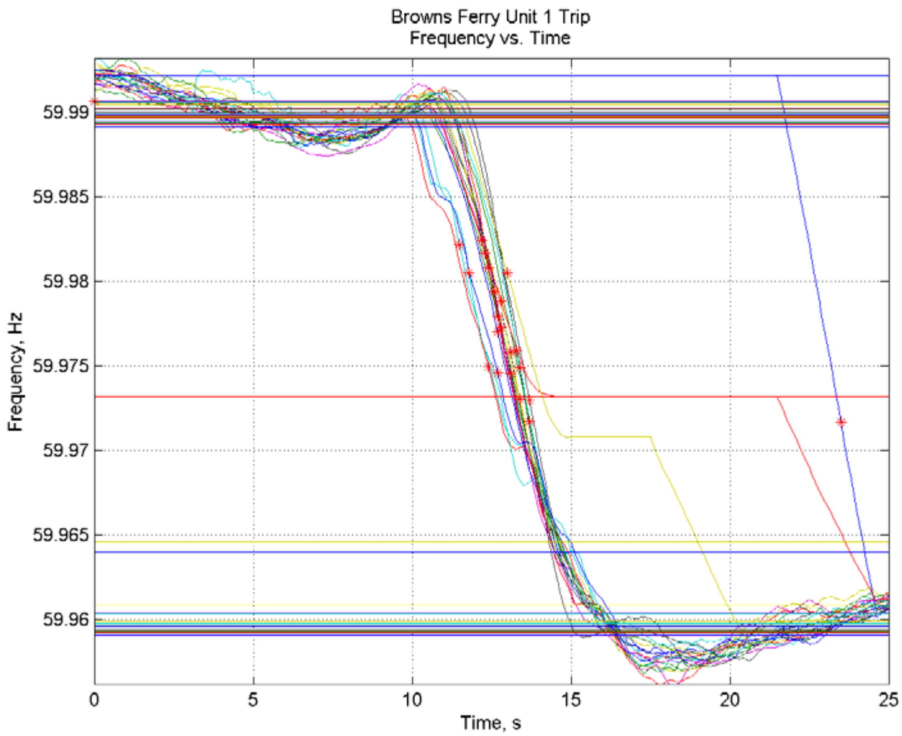
Browns Ferry Unit 1 Trip
Frequency vs. Time
Frequency, Hz
59.99
59.985
59.98
59.975
59.97
59.965
59.96
0
5
10
15
20
25
Time, s

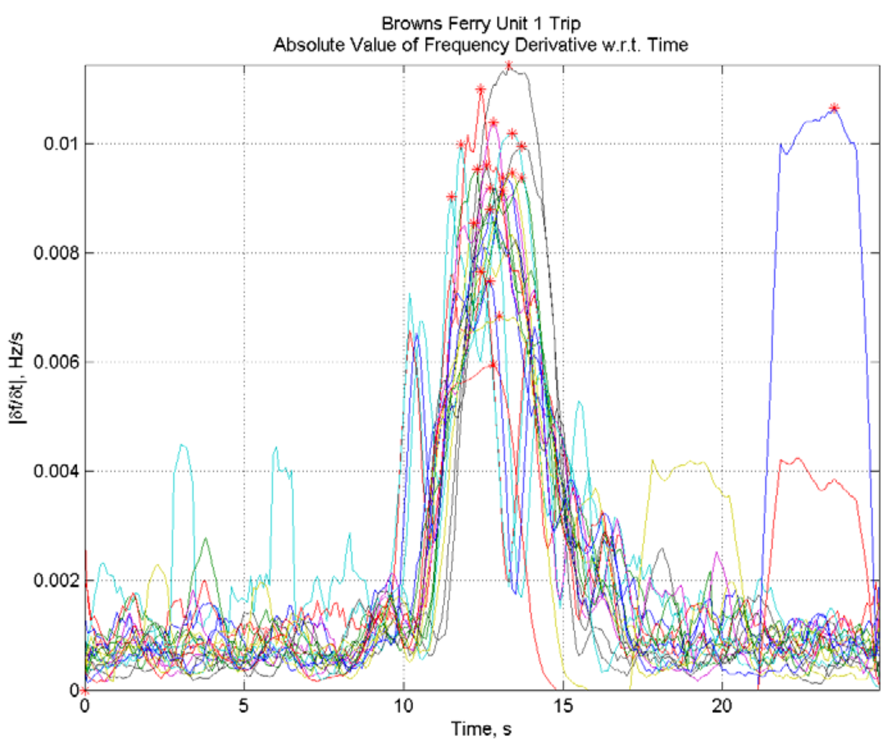
Browns Ferry Unit 1 Trip
Absolute Value of Frequency Derivative w.r.t. Time
|δf/δt|, Hz/s
0.01
0.008
0.006
0.004
0.002
0
0
5
10
15
20
Time, s

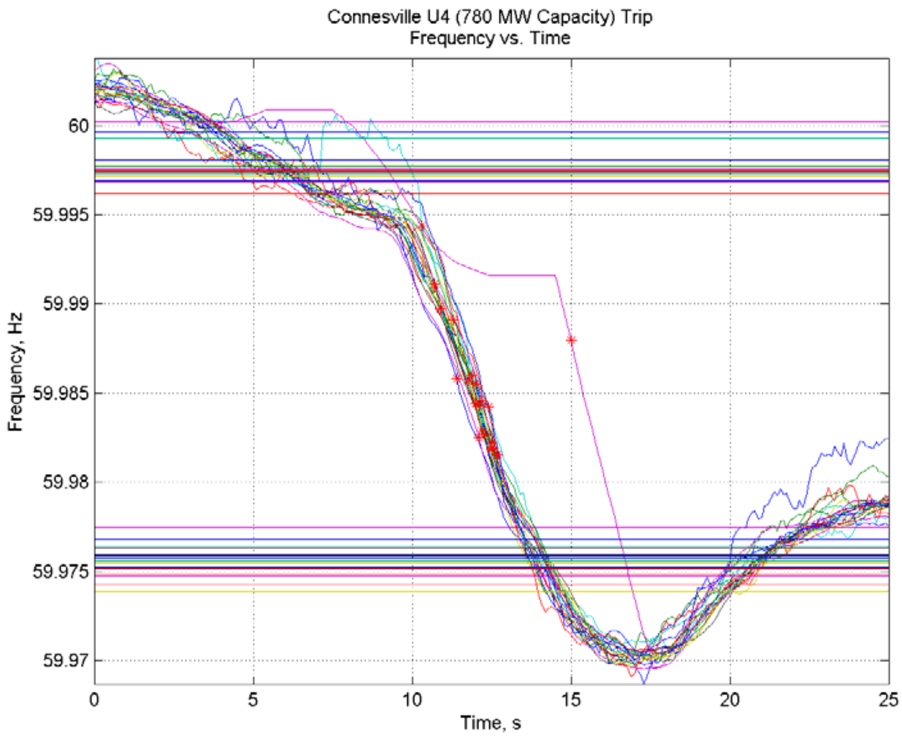
Connesville U4 (780 MW Capacity) Trip
Frequency vs. Time
Frequency, Hz
60
59.995
59.99
59.985
59.98
59.975
59.97
0
5
10
15
20
25
Time, s

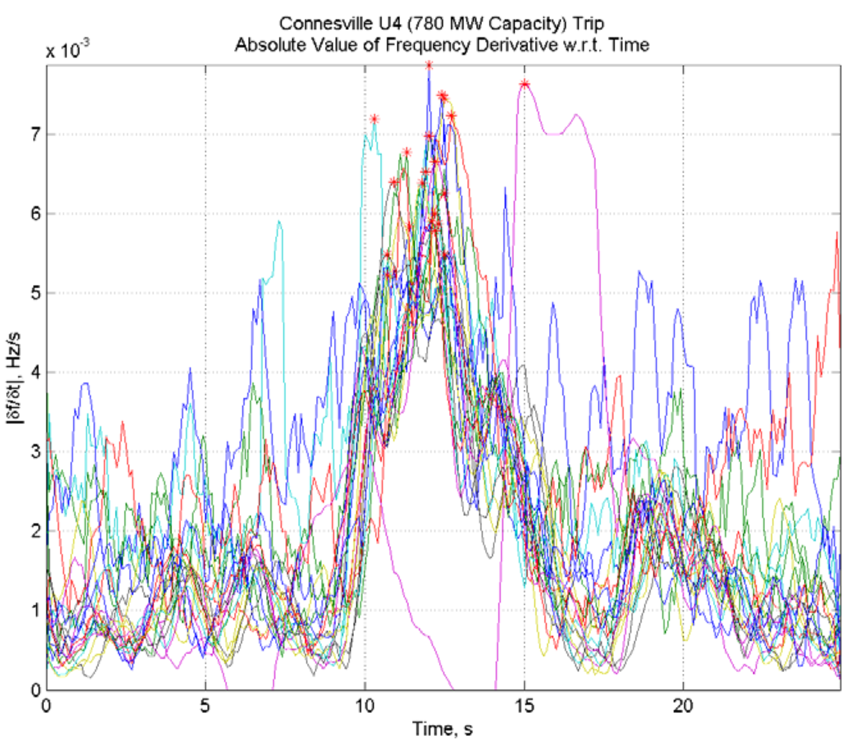
Connesville U4 (780 MW Capacity) Trip
Absolute Value of Frequency Derivative w.r.t. Time
x 10-3
|δf/δt|, Hz/s
0
1
2
3
4
5
6
7
0
5
10
15
20
Time, s

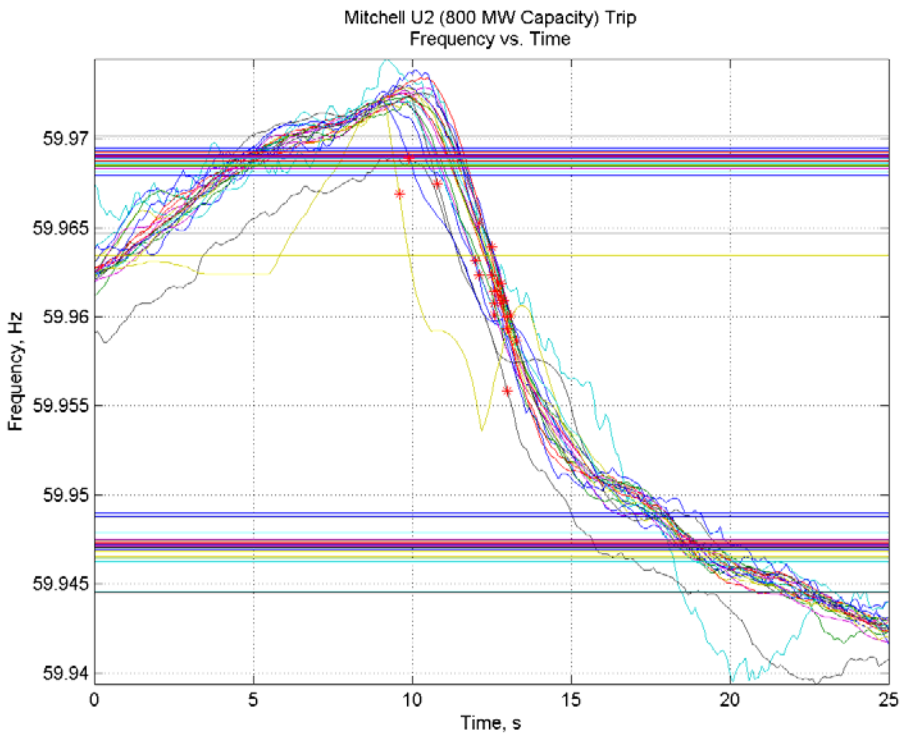

Mitchell U2 (800 MW Capacity) Trip
Frequency vs. Time
Frequency, Hz
Time, s

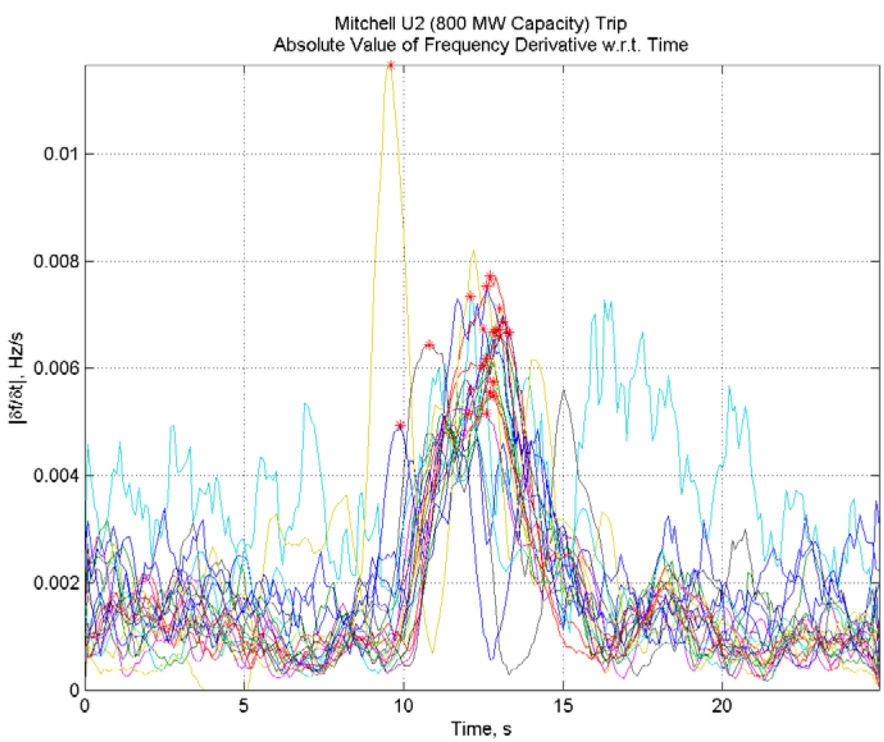

Mitchell U2 (800 MW Capacity) Trip
Absolute Value of Frequency Derivative w.r.t. Time
|δf/δt|, Hz/s
Time, s

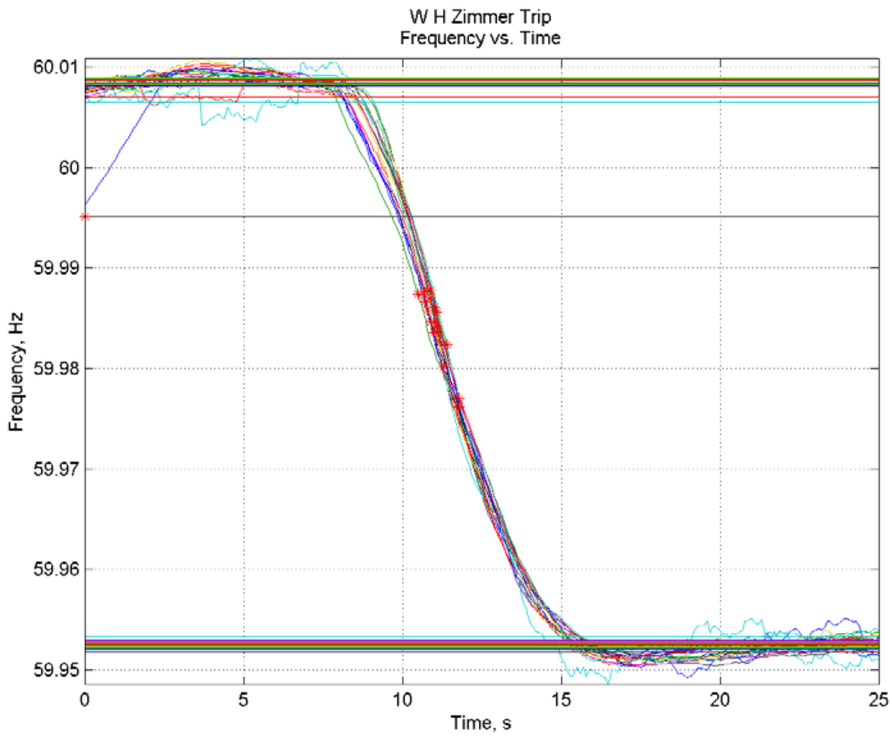
W H Zimmer Trip
Frequency vs. Time
Frequency, Hz
60.01
60
59.99
59.98
59.97
59.96
59.95
0
5
10
15
20
25
Time, s

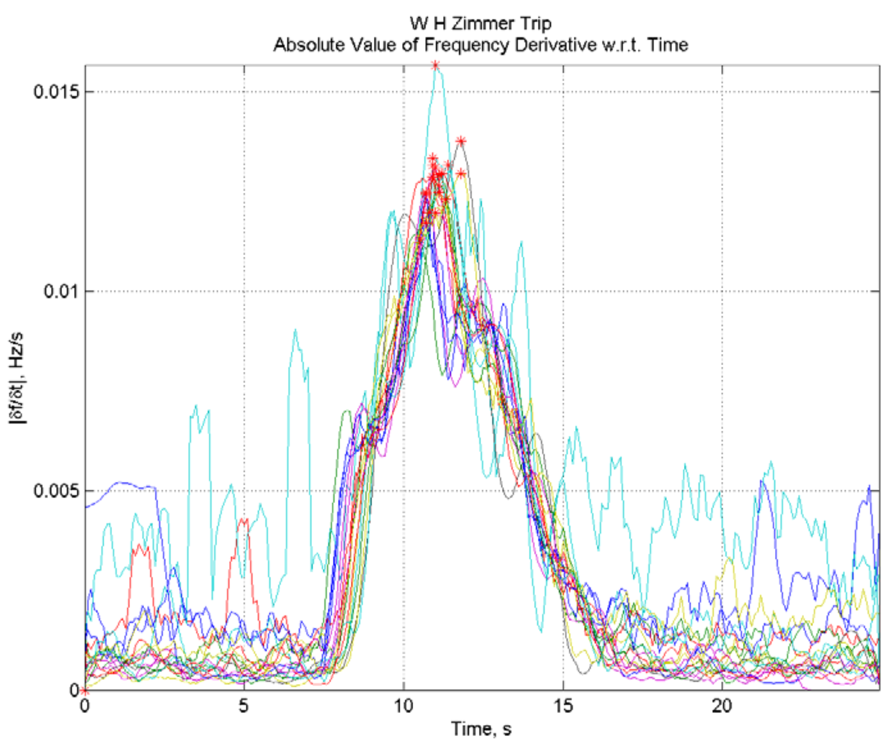
W H Zimmer Trip
Absolute Value of Frequency Derivative w.r.t. Time
|δf/δt|, Hz/s
0.015
0.01
0.005
0
0
5
10
15
20
Time, s

Appendix VIII: Operation of Wide-Area Frequency Oscillation Detection Algorithms

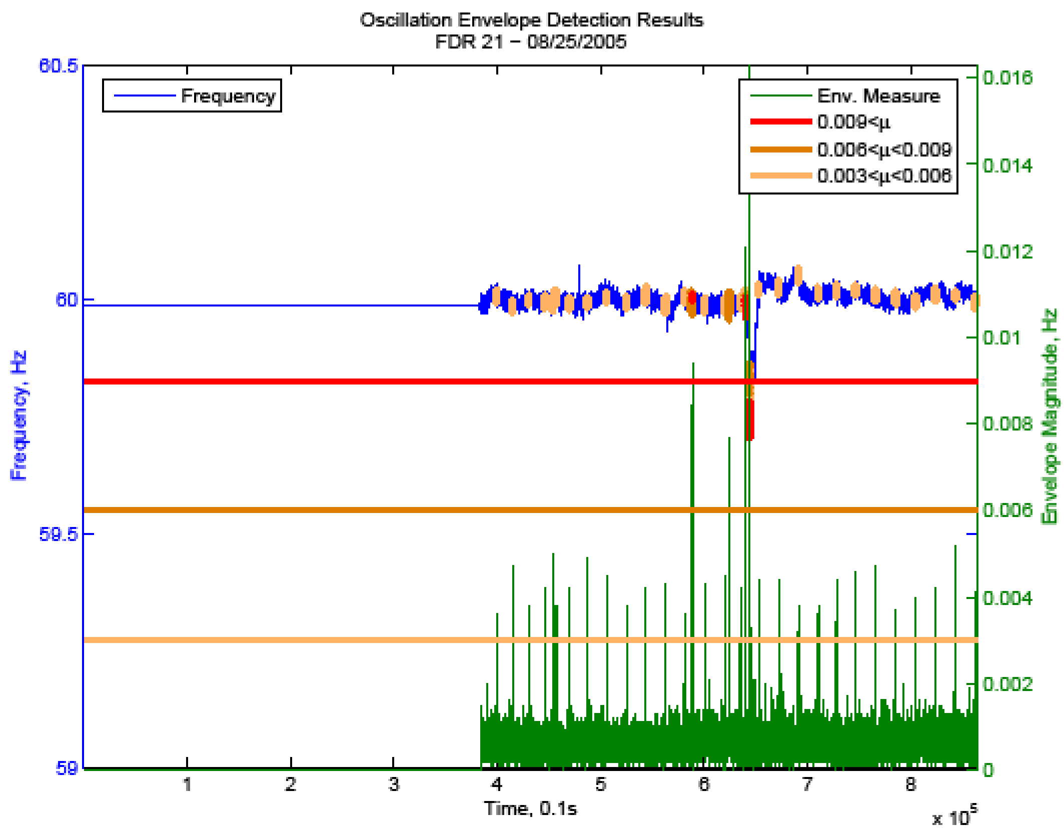

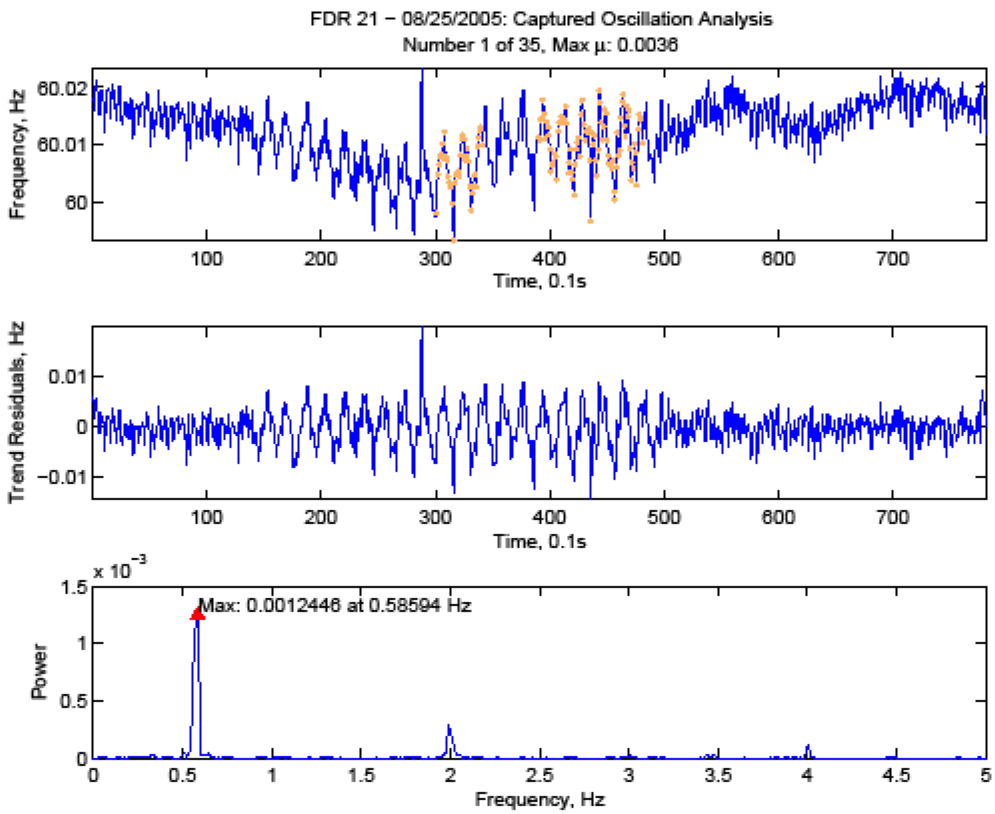
FDR 21 − 08/25/2005: Captured Oscillation Analysis
Number 1 of 35, Max μ: 0.0036
Frequency, Hz
60.02
60.01
60
100
200
300
400
500
600
700
Time, 0.1s
Trend Residuals, Hz
0.01
0
−0.01
Time, 0.1s
x 10^-3
1.5
1
0.5
Power
Max: 0.0012446 at 0.58594 Hz
Frequency, Hz

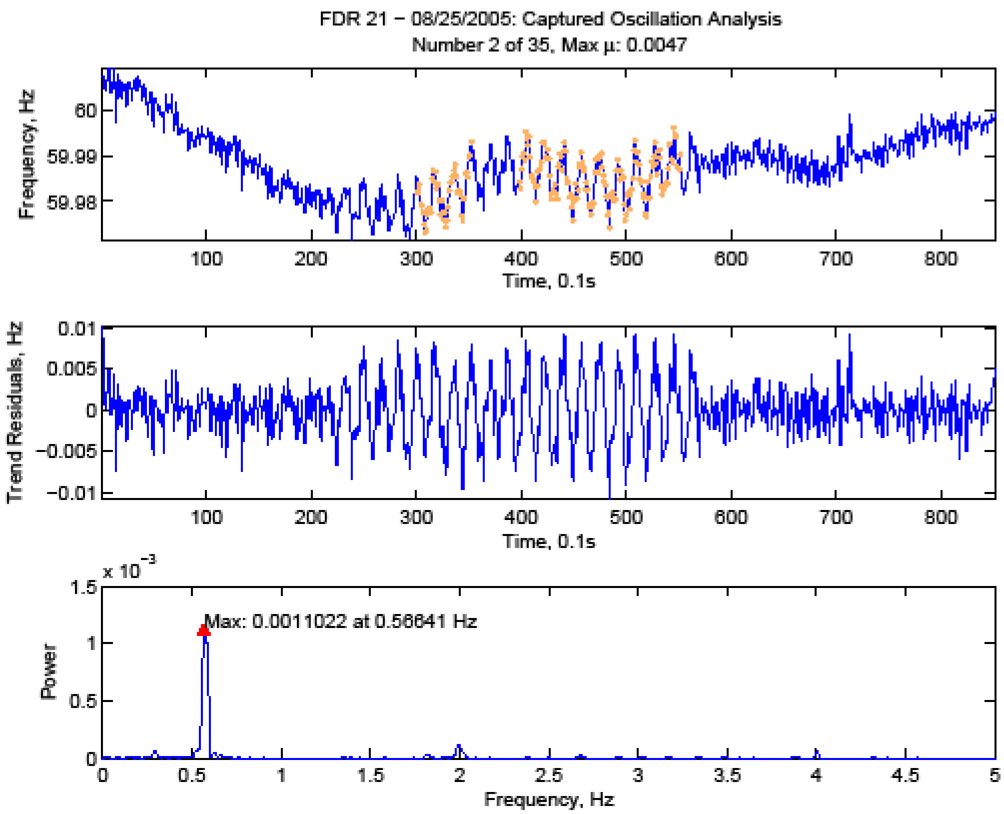
FDR 21 − 08/25/2005: Captured Oscillation Analysis
Number 2 of 35, Max μ: 0.0047
Frequency, Hz
60
59.99
59.98
100
200
300
400
500
600
700
800
Time, 0.1s
Trend Residuals, Hz
0.01
0.005
0
−0.005
−0.01
Time, 0.1s
x 10^-3
1.5
1
0.5
Power
Max: 0.0011022 at 0.56641 Hz
0
0.5
1
1.5
2
2.5
3
3.5
4
4.5
5
Frequency, Hz

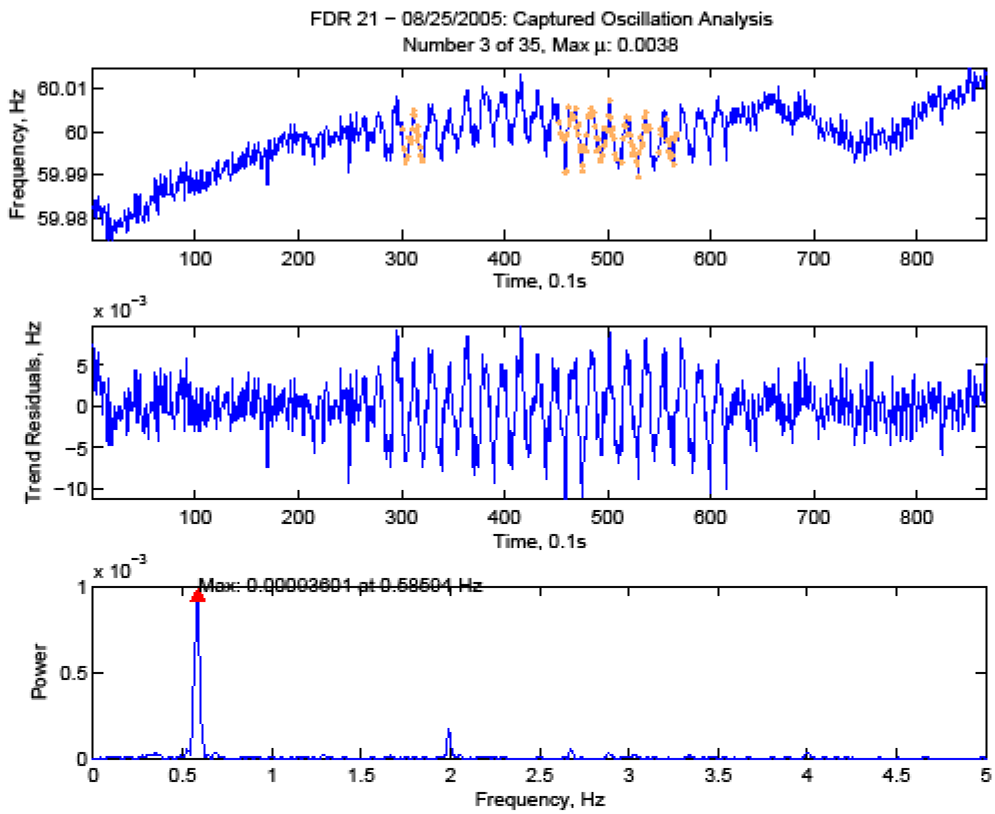
FDR 21 – 08/25/2005: Captured Oscillation Analysis
Number 3 of 35, Max μ: 0.0038
Frequency, Hz
Time, 0.1s
Trend Residuals, Hz
x 10^-3
Max: 0.00003601 at 0.58504 Hz
Power
Frequency, Hz

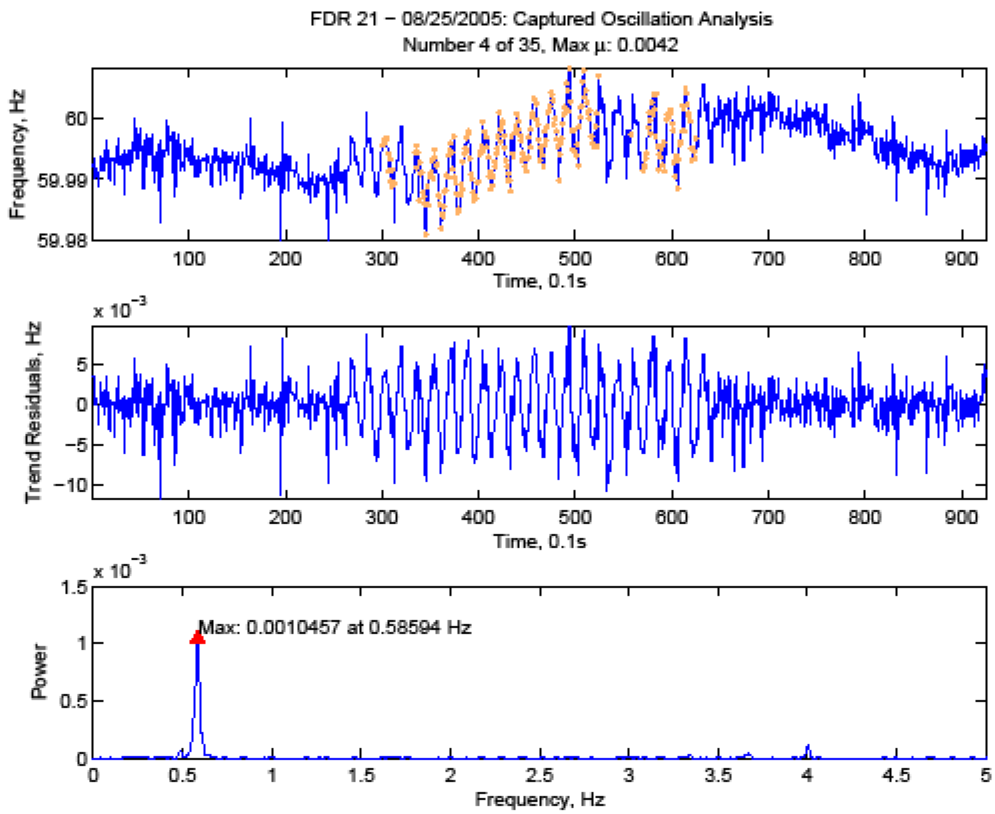

FDR 21 – 08/25/2005: Captured Oscillation Analysis
Number 4 of 35, Max μ: 0.0042
Frequency, Hz
60
59.99
59.98
100
200
300
400
500
600
700
800
900
Time, 0.1s
x 10^-3
Trend Residuals, Hz
5
0
−5
−10
Time, 0.1s
x 10^-3
Power
1.5
1
0.5
0
Max: 0.0010457 at 0.58594 Hz
0
0.5
1
1.5
2
2.5
3
3.5
4
4.5
5
Frequency, Hz

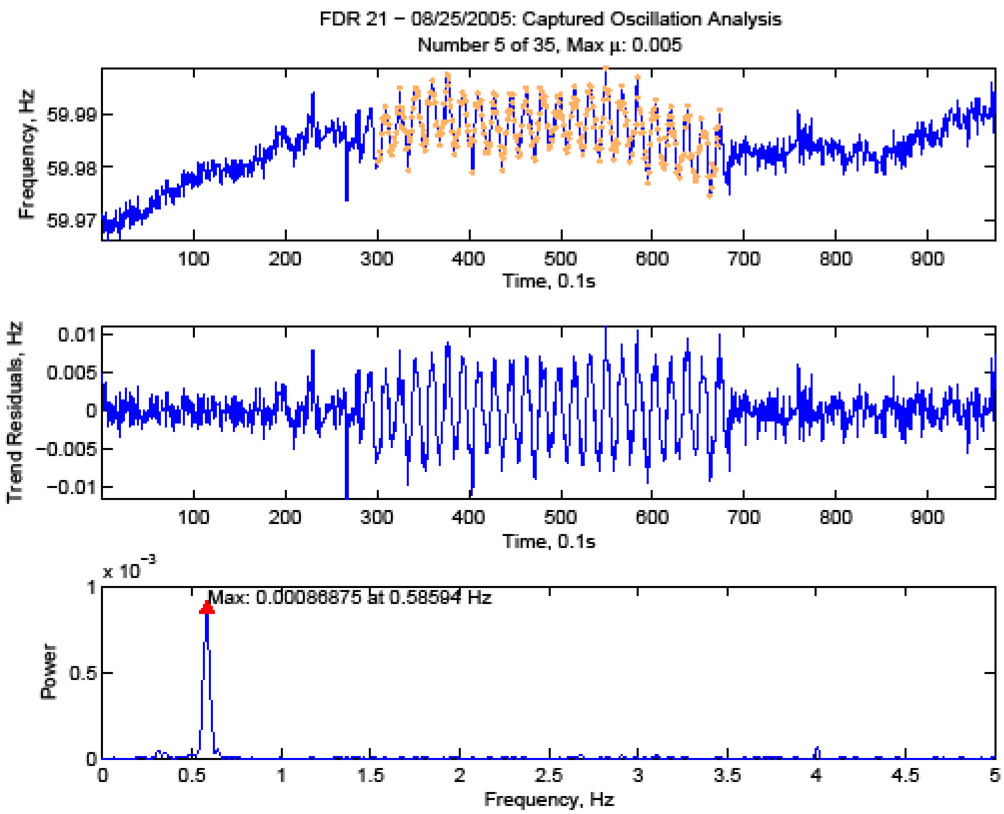
FDR 21 − 08/25/2005: Captured Oscillation Analysis
Number 5 of 35, Max μ: 0.005
Frequency, Hz
59.99
59.98
59.97
100
200
300
400
500
600
700
800
900
Time, 0.1s
Trend Residuals, Hz
0.01
0.005
0
−0.005
−0.01
Time, 0.1s
x 10^-3
Max: 0.00086875 at 0.58594 Hz
Power
1
0.5
0
Frequency, Hz

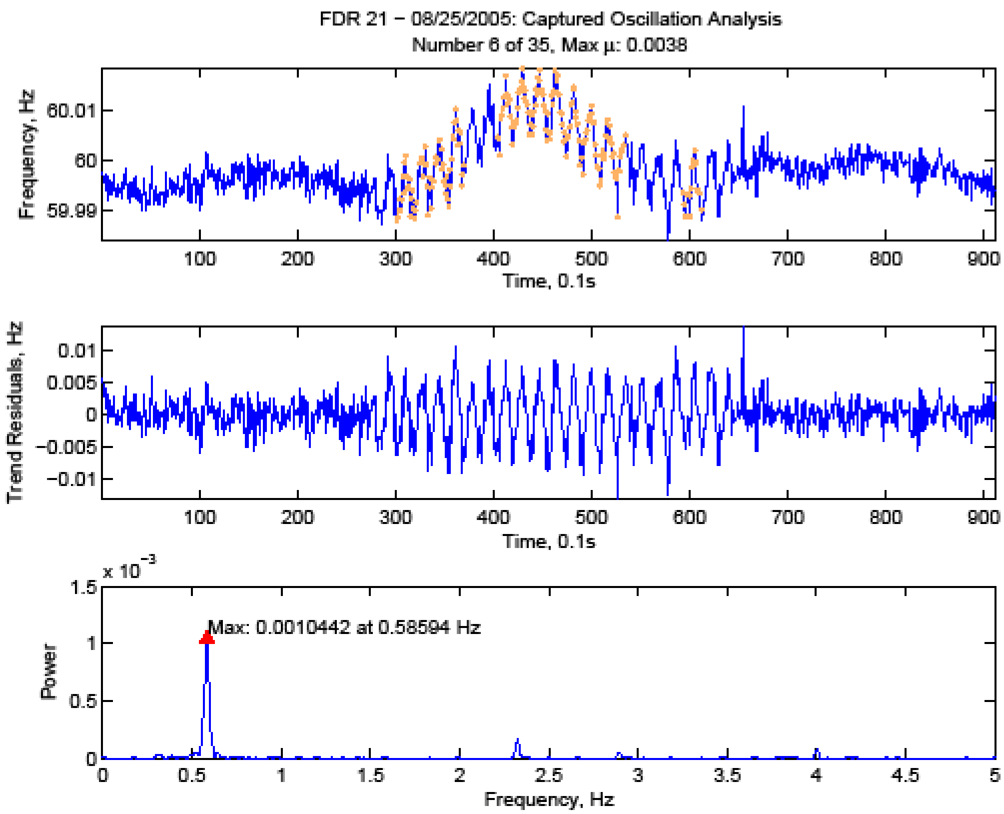

FDR 21 – 08/25/2005: Captured Oscillation Analysis
Number 6 of 35, Max μ: 0.0038
Frequency, Hz
60.01
60
59.99
100
200
300
400
500
600
700
800
900
Time, 0.1s
Trend Residuals, Hz
0.01
0.005
0
−0.005
−0.01
Time, 0.1s
x 10^−3
Power
1.5
1
0.5
Max: 0.0010442 at 0.58594 Hz
0
0.5
1
1.5
2
2.5
3
3.5
4
4.5
5
Frequency, Hz

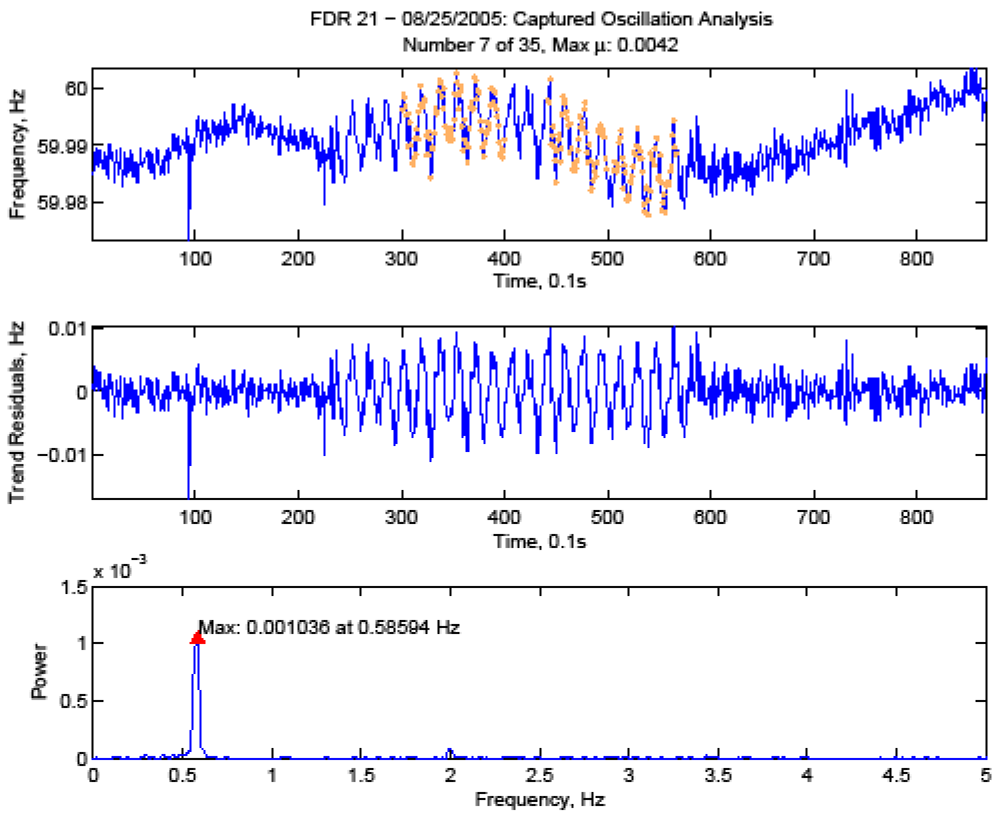

FDR 21 − 08/25/2005: Captured Oscillation Analysis
Number 7 of 35, Max μ: 0.0042
Frequency, Hz
60
59.99
59.98
100
200
300
400
500
600
700
800
Time, 0.1s
Trend Residuals, Hz
0.01
0
−0.01
Time, 0.1s
x 10^−3
1.5
1
0.5
0
Power
Max: 0.001036 at 0.58594 Hz
0.5
1.5
2
2.5
3
3.5
4
4.5
5
Frequency, Hz

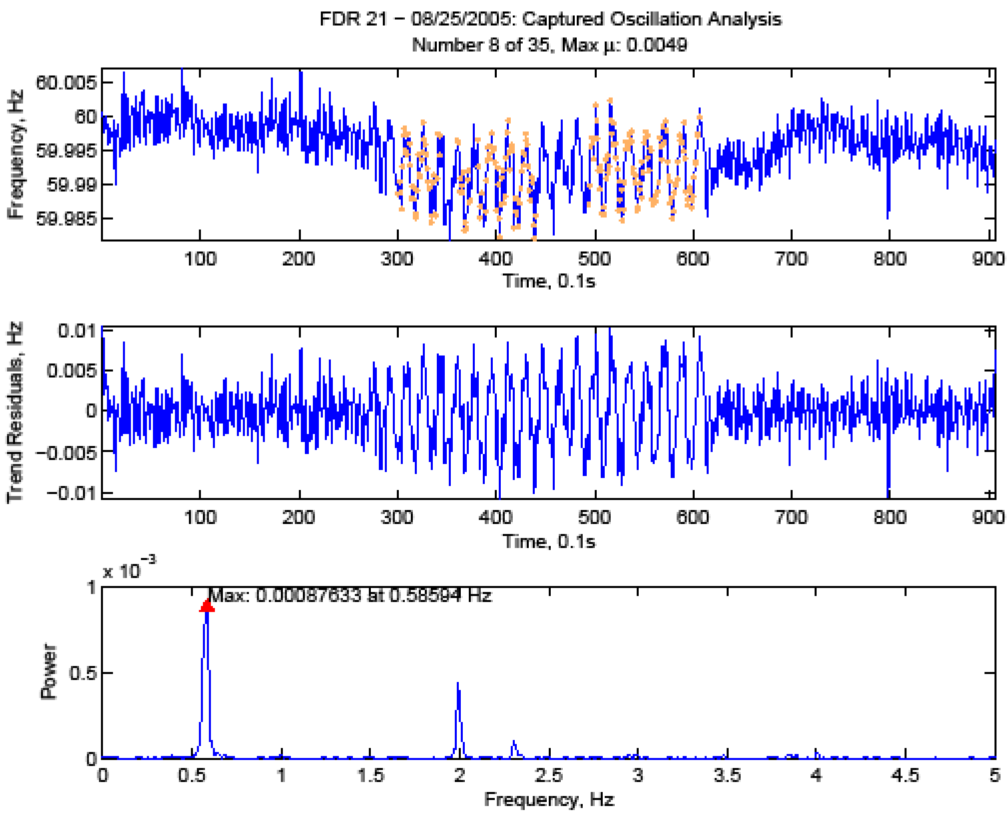

FDR 21 − 08/25/2005: Captured Oscillation Analysis
Number 8 of 35, Max μ: 0.0049
Frequency, Hz
Time, 0.1s
Trend Residuals, Hz
Time, 0.1s
x 10^-3
Max: 0.00087633 at 0.58594 Hz
Power
Frequency, Hz

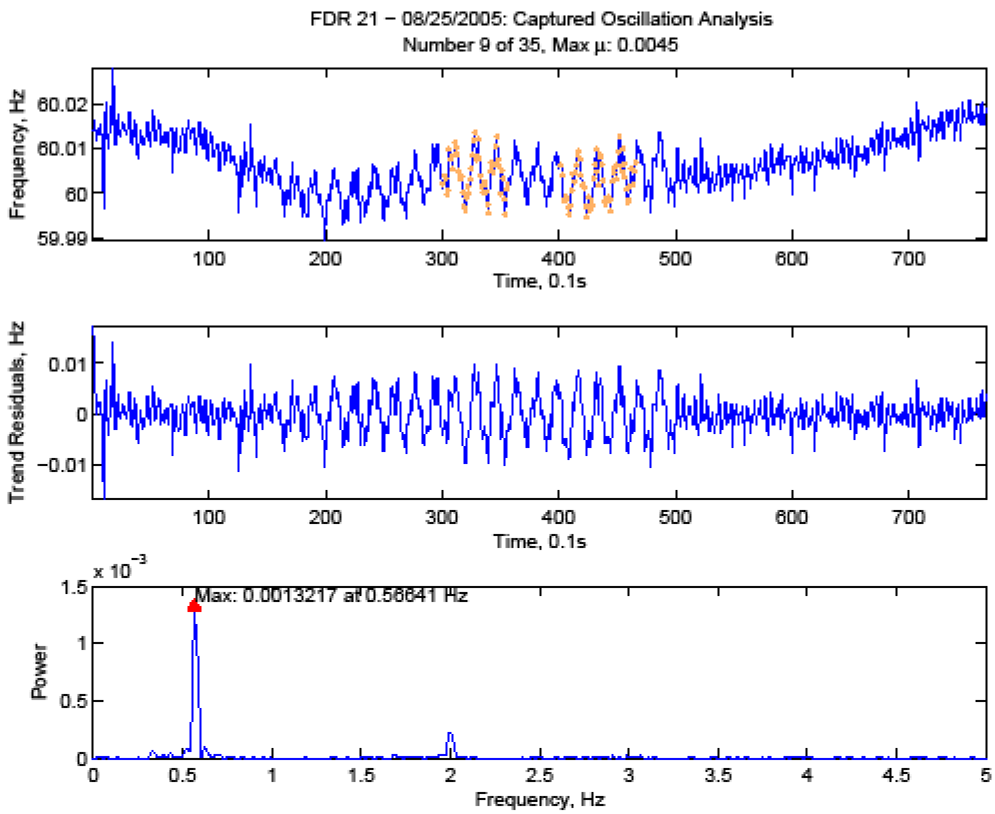
FDR 21 − 08/25/2005: Captured Oscillation Analysis
Number 9 of 35, Max μ: 0.0045
Frequency, Hz
60.02
60.01
60
59.99
100
200
300
400
500
600
700
Time, 0.1s
Trend Residuals, Hz
0.01
0
−0.01
100
200
300
400
500
600
700
Time, 0.1s
x 10^−3
1.5
1
0.5
0
Power
Max: 0.0013217 at 0.56641 Hz
0
0.5
1
1.5
2
2.5
3
3.5
4
4.5
5
Frequency, Hz

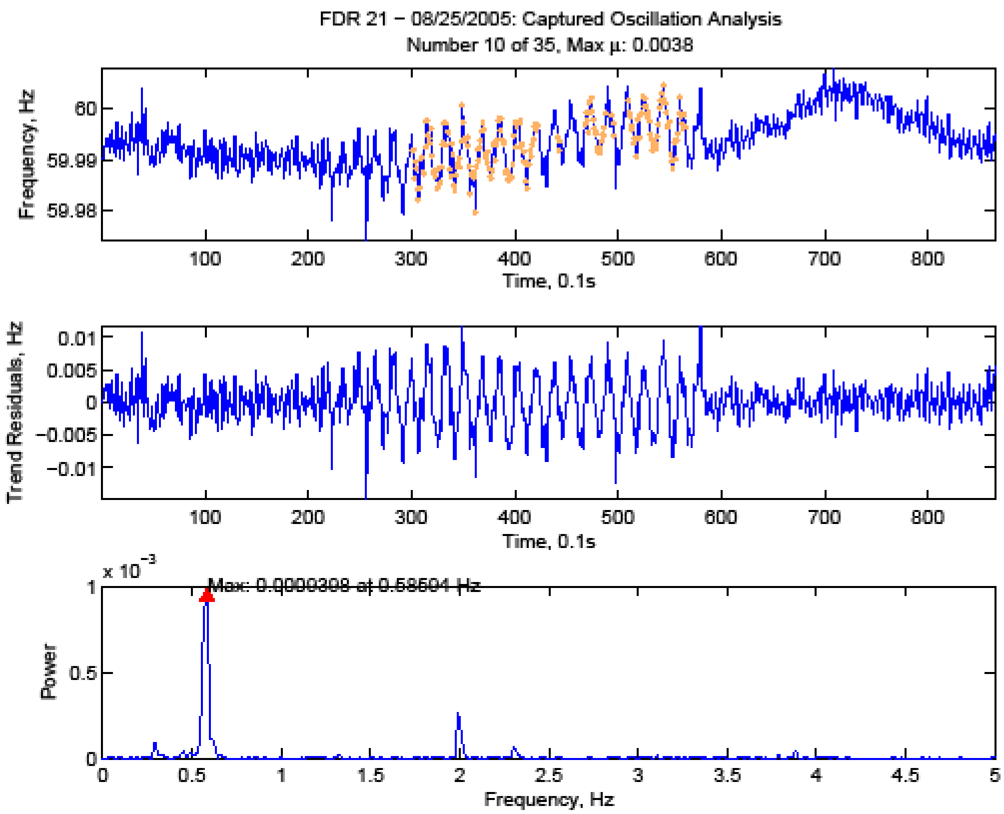
FDR 21 − 08/25/2005: Captured Oscillation Analysis
Number 10 of 35, Max μ: 0.0038
Frequency, Hz
Time, 0.1s
Trend Residuals, Hz
Time, 0.1s
x 10^-3
Max: 0.0000308 at 0.58504 Hz
Power
Frequency, Hz

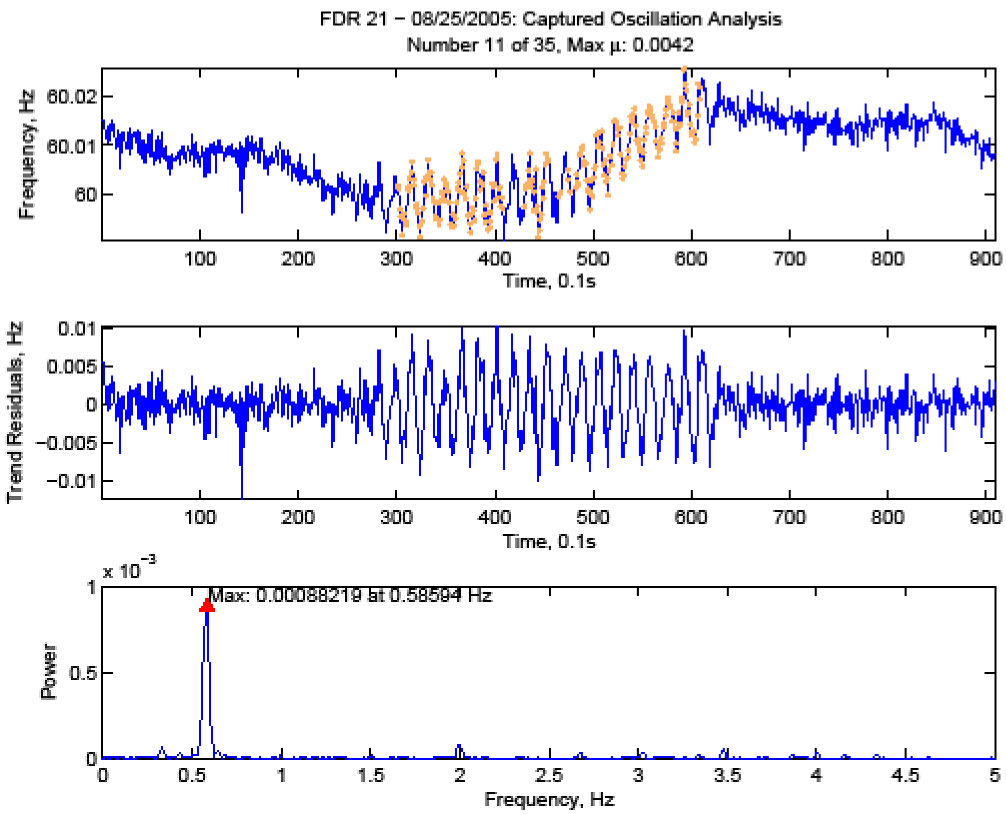
FDR 21 – 08/25/2005: Captured Oscillation Analysis
Number 11 of 35, Max μ: 0.0042
Frequency, Hz
Time, 0.1s
Trend Residuals, Hz
Time, 0.1s
x 10^-3
Max: 0.00088219 at 0.58594 Hz
Power
Frequency, Hz

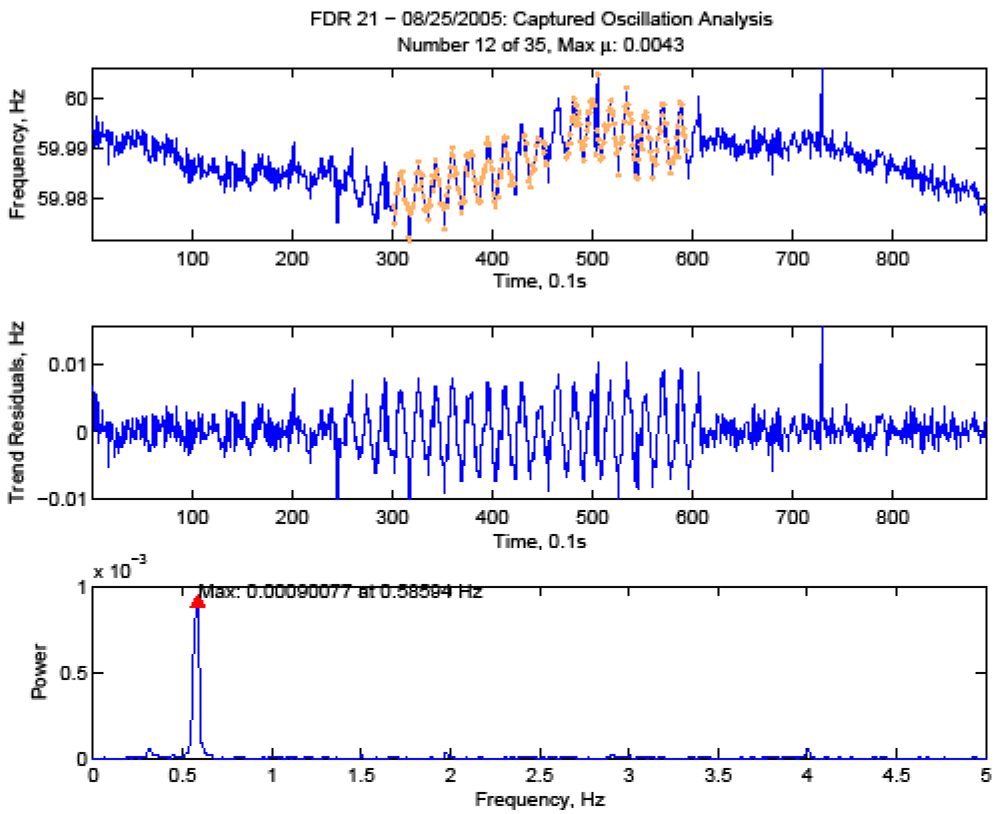
FDR 21 − 08/25/2005: Captured Oscillation Analysis
Number 12 of 35, Max μ: 0.0043
Frequency, Hz
60
59.99
59.98
100
200
300
400
500
600
700
800
Time, 0.1s
Trend Residuals, Hz
0.01
0
−0.01
100
200
300
400
500
600
700
800
Time, 0.1s
x 10^−3
1
Max: 0.00090077 at 0.58594 Hz
Power
0.5
0
0
0.5
1
1.5
2
2.5
3
3.5
4
4.5
5
Frequency, Hz

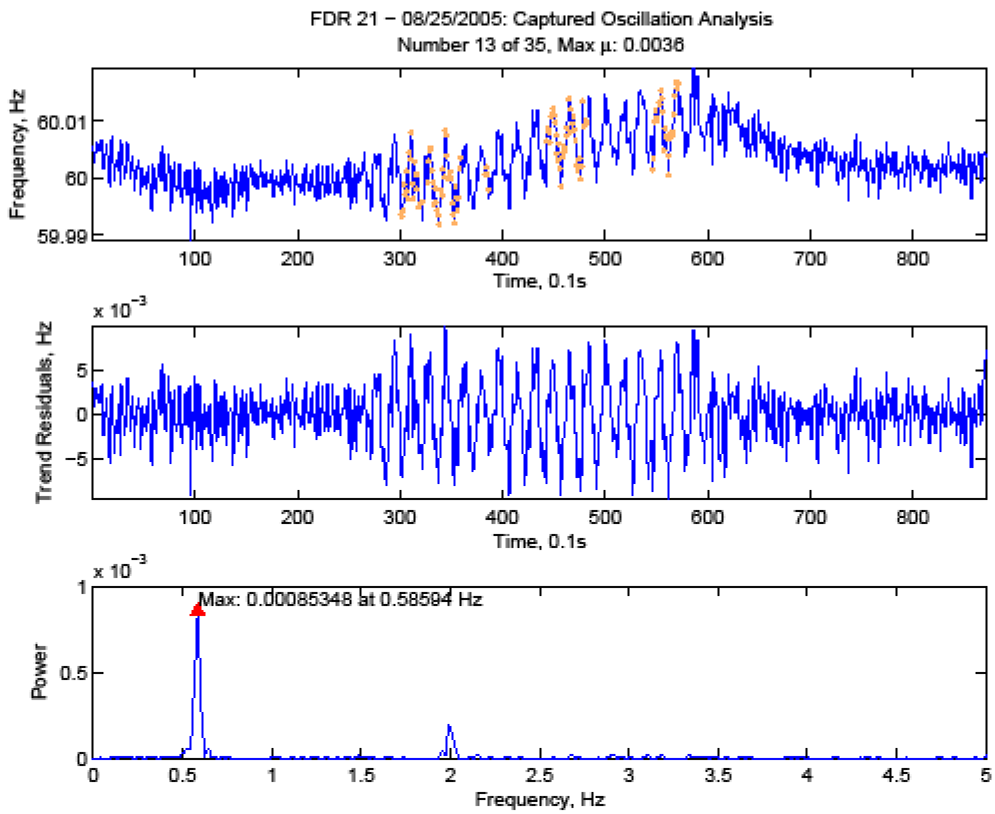
FDR 21 − 08/25/2005: Captured Oscillation Analysis
Number 13 of 35, Max μ: 0.0036
Frequency, Hz
60.01
60
59.99
100
200
300
400
500
600
700
800
Time, 0.1s
x 10^−3
Trend Residuals, Hz
5
0
−5
Time, 0.1s
x 10^−3
Power
1
0.5
0
Max: 0.00085348 at 0.58594 Hz
0.5
1
1.5
2
2.5
3
3.5
4
4.5
5
Frequency, Hz

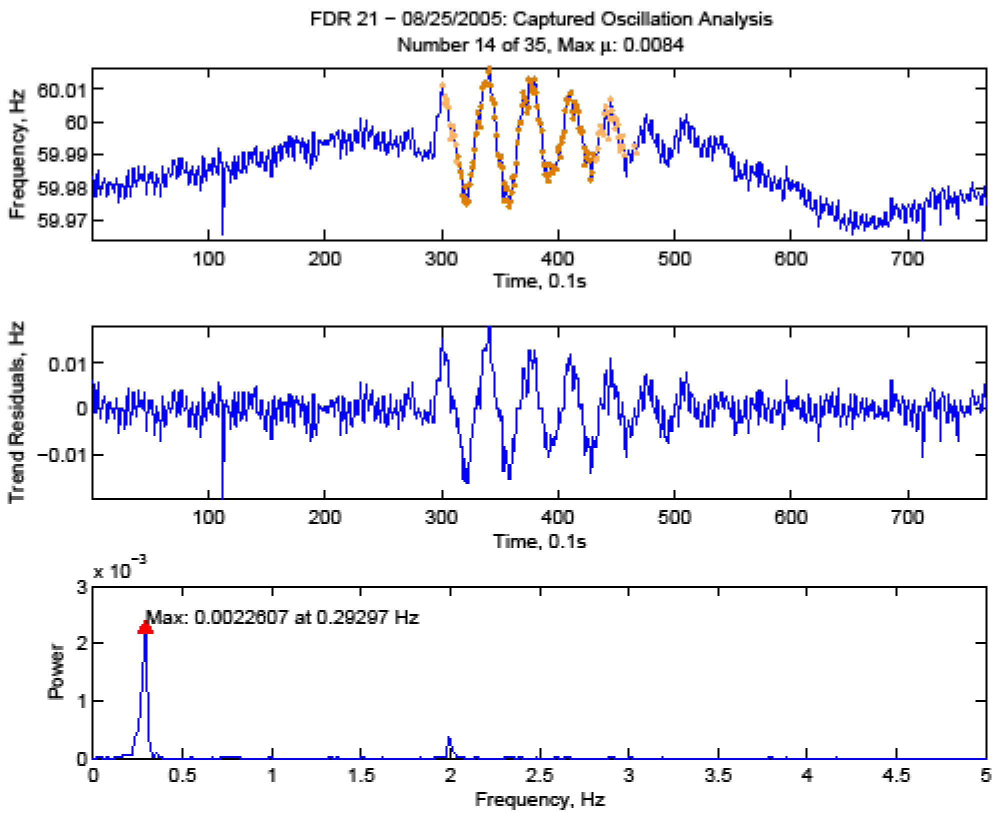
FDR 21 − 08/25/2005: Captured Oscillation Analysis
Number 14 of 35, Max μ: 0.0084
Frequency, Hz
60.01
60
59.99
59.98
59.97
100
200
300
400
500
600
700
Time, 0.1s
Trend Residuals, Hz
0.01
0
−0.01
100
200
300
400
500
600
700
Time, 0.1s
x 10^−3
3
2
1
0
Power
Max: 0.0022607 at 0.29297 Hz
0
0.5
1
1.5
2
2.5
3
3.5
4
4.5
5
Frequency, Hz

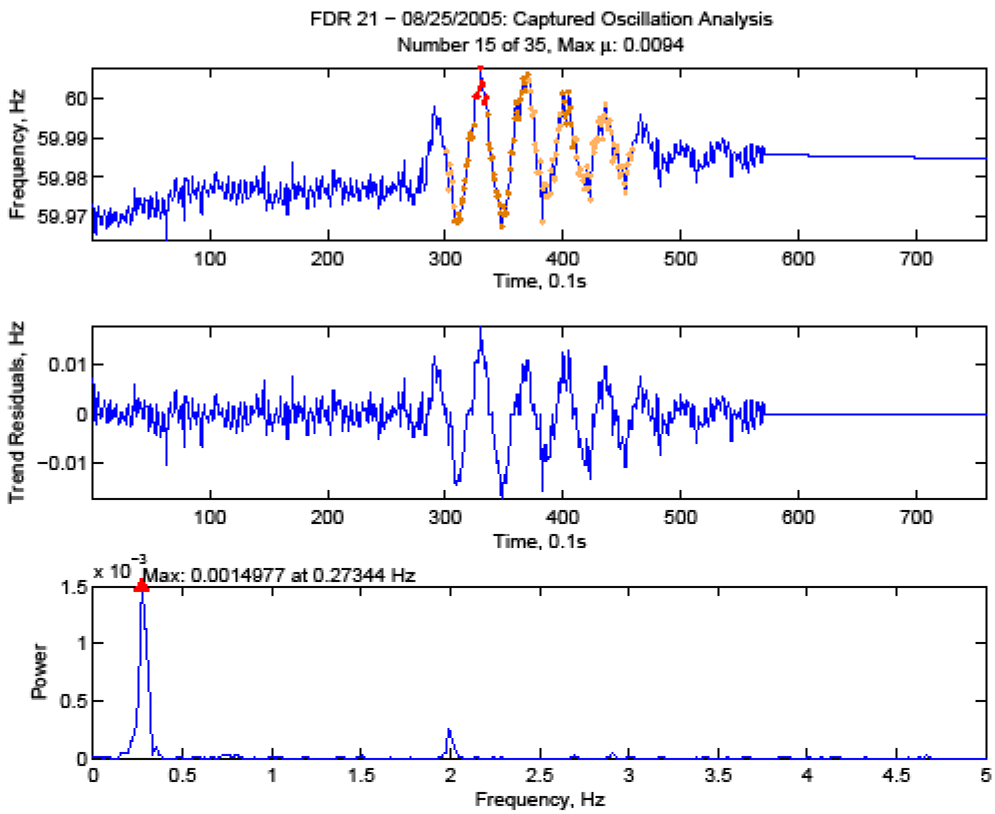
FDR 21 − 08/25/2005: Captured Oscillation Analysis
Number 15 of 35, Max μ: 0.0094
Frequency, Hz
Time, 0.1s
Trend Residuals, Hz
Time, 0.1s
x 10^-3 Max: 0.0014977 at 0.27344 Hz
Power
Frequency, Hz

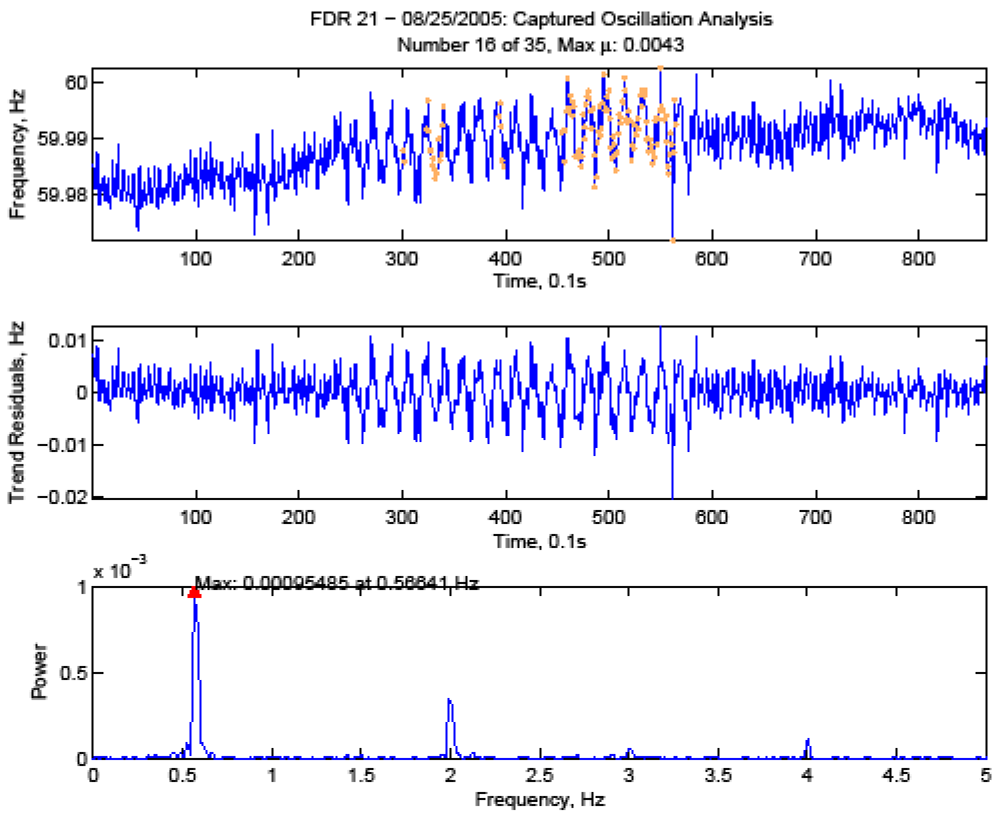
FDR 21 − 08/25/2005: Captured Oscillation Analysis
Number 16 of 35, Max μ: 0.0043
Frequency, Hz
60
59.99
59.98
100
200
300
400
500
600
700
800
Time, 0.1s
Trend Residuals, Hz
0.01
0
−0.01
−0.02
Time, 0.1s
x 10^−3
Max: 0.00095485 at 0.56641 Hz
Power
1
0.5
0
0.5
1
1.5
2
2.5
3
3.5
4
4.5
5
Frequency, Hz

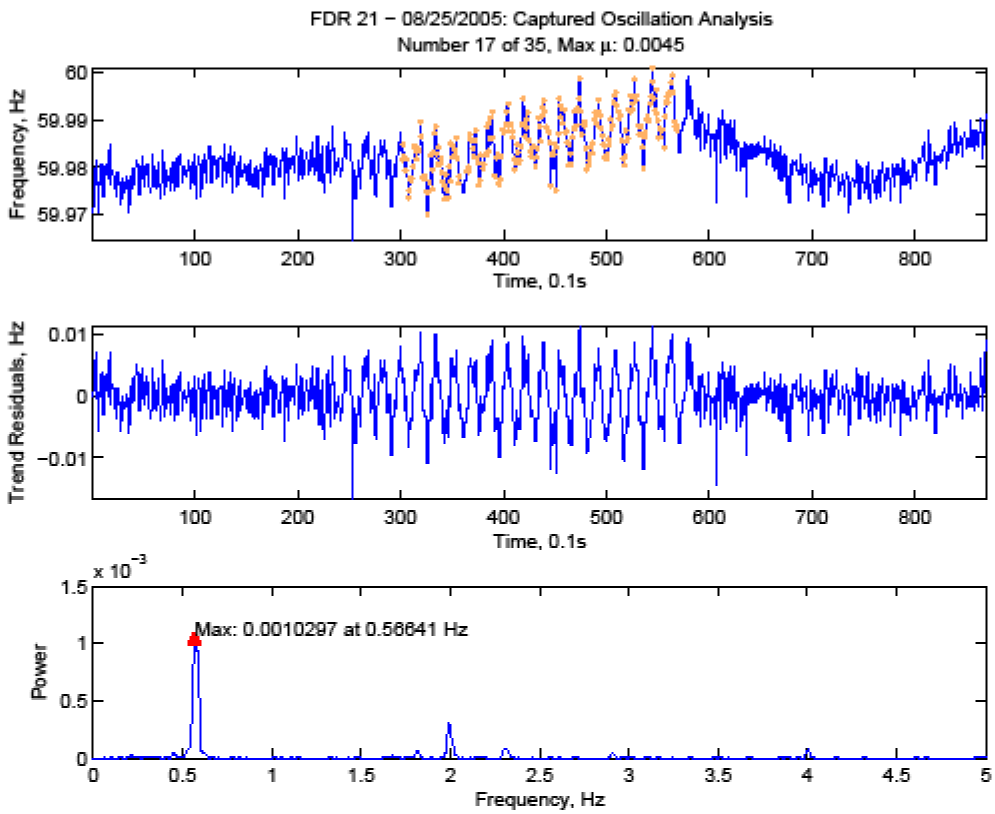
FDR 21 – 08/25/2005: Captured Oscillation Analysis
Number 17 of 35, Max μ: 0.0045
Frequency, Hz
60
59.99
59.98
59.97
100 200 300 400 500 600 700 800
Time, 0.1s
Trend Residuals, Hz
0.01
0
−0.01
100 200 300 400 500 600 700 800
Time, 0.1s
x 10^-3
1.5
1
0.5
0
Power
Max: 0.0010297 at 0.56641 Hz
0 0.5 1 1.5 2 2.5 3 3.5 4 4.5 5
Frequency, Hz

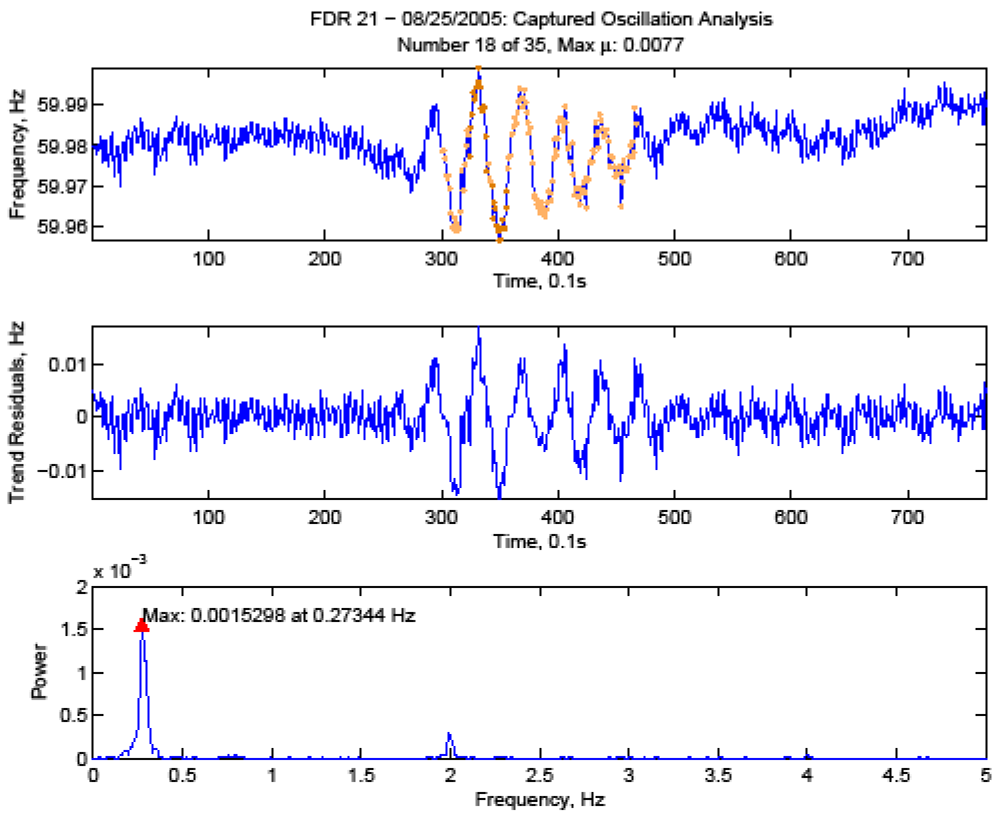
FDR 21 − 08/25/2005: Captured Oscillation Analysis
Number 18 of 35, Max μ: 0.0077
Frequency, Hz
59.99
59.98
59.97
59.96
100
200
300
400
500
600
700
Time, 0.1s
Trend Residuals, Hz
0.01
0
−0.01
100
200
300
400
500
600
700
Time, 0.1s
x 10−3
Power
Max: 0.0015298 at 0.27344 Hz
0
0.5
1
1.5
2
2.5
3
3.5
4
4.5
5
Frequency, Hz

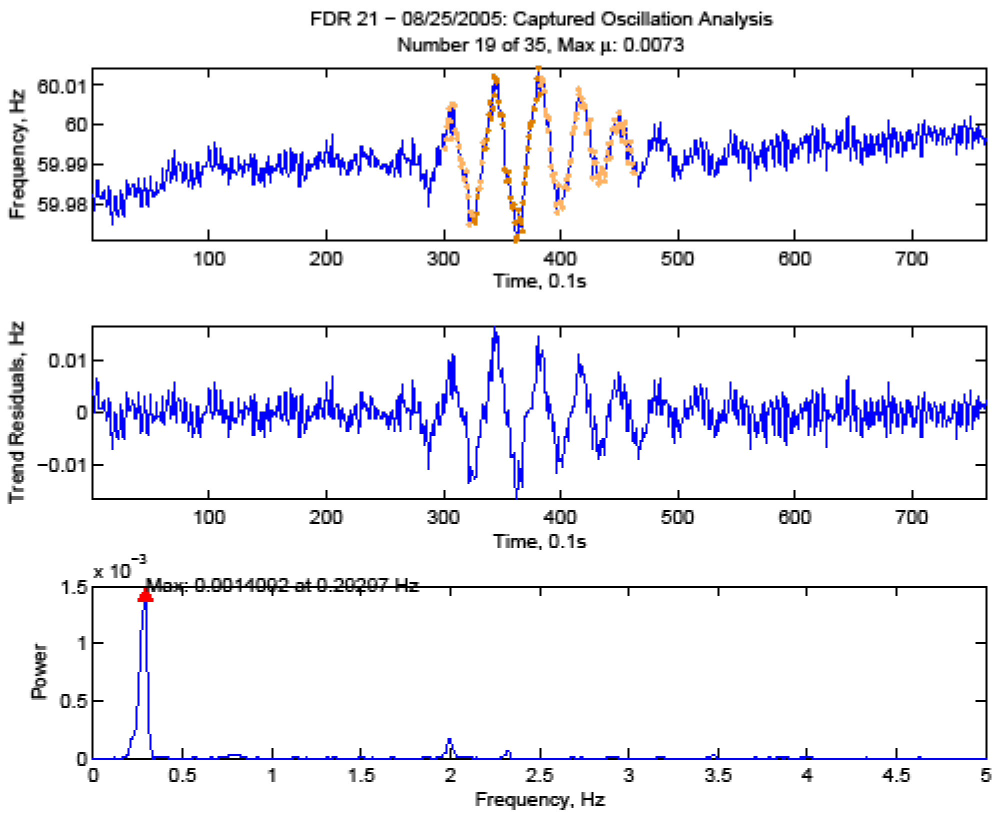
FDR 21 – 08/25/2005: Captured Oscillation Analysis
Number 19 of 35, Max μ: 0.0073
Frequency, Hz
60.01
60
59.99
59.98
100
200
300
400
500
600
700
Time, 0.1s
Trend Residuals, Hz
0.01
0
−0.01
Time, 0.1s
x 10^−3
Max: 0.0014002 at 0.28207 Hz
Power
1.5
1
0.5
0
0
0.5
1
1.5
2
2.5
3
3.5
4
4.5
5
Frequency, Hz

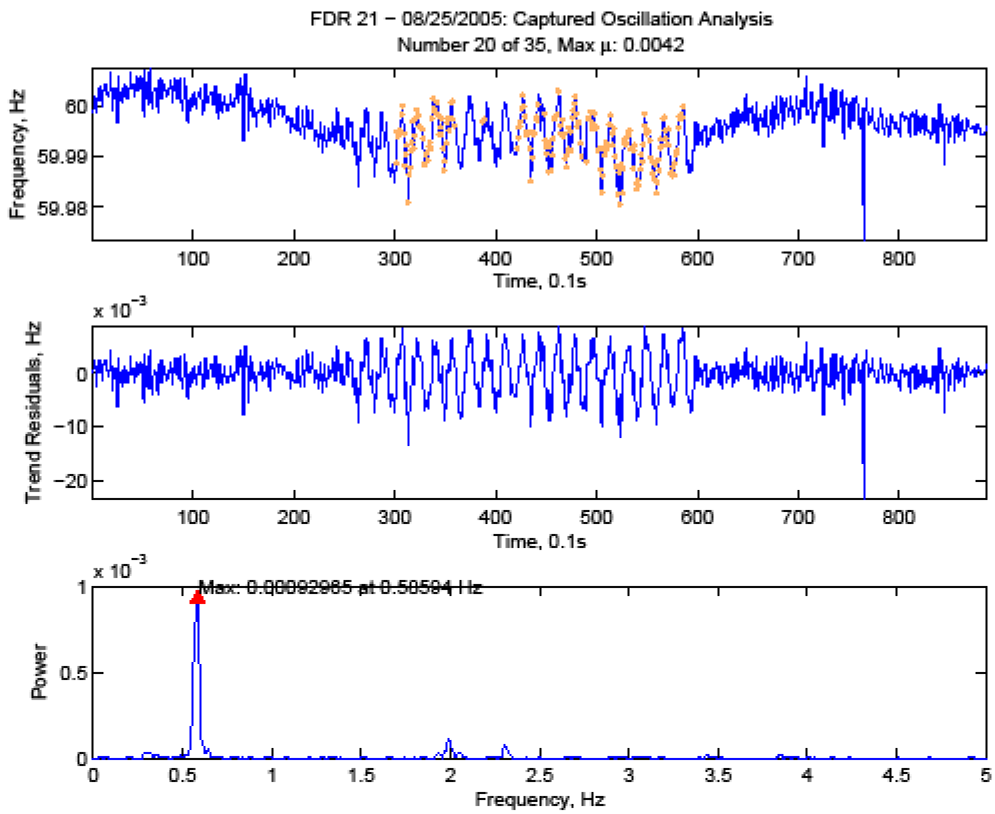

FDR 21 − 08/25/2005: Captured Oscillation Analysis
Number 20 of 35, Max μ: 0.0042
Frequency, Hz
Time, 0.1s
Trend Residuals, Hz
x 10^-3
Time, 0.1s
x 10^-3
Max: 0.00092965 at 0.58594 Hz
Power
Frequency, Hz

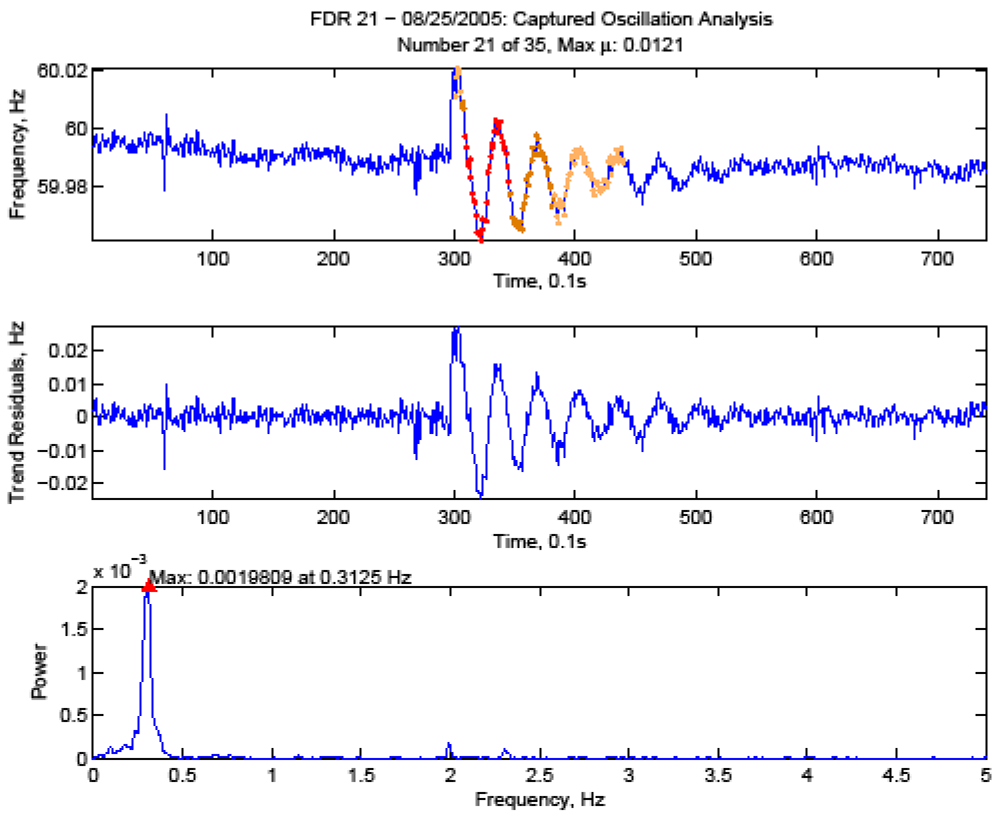
FDR 21 − 08/25/2005: Captured Oscillation Analysis
Number 21 of 35, Max μ: 0.0121
Frequency, Hz
60.02
60
59.98
100
200
300
400
500
600
700
Time, 0.1s
Trend Residuals, Hz
0.02
0.01
0
−0.01
−0.02
Time, 0.1s
x 10^−3
Max: 0.0019809 at 0.3125 Hz
Power
2
1.5
1
0.5
0
0.5
1
1.5
2
2.5
3
3.5
4
4.5
5
Frequency, Hz

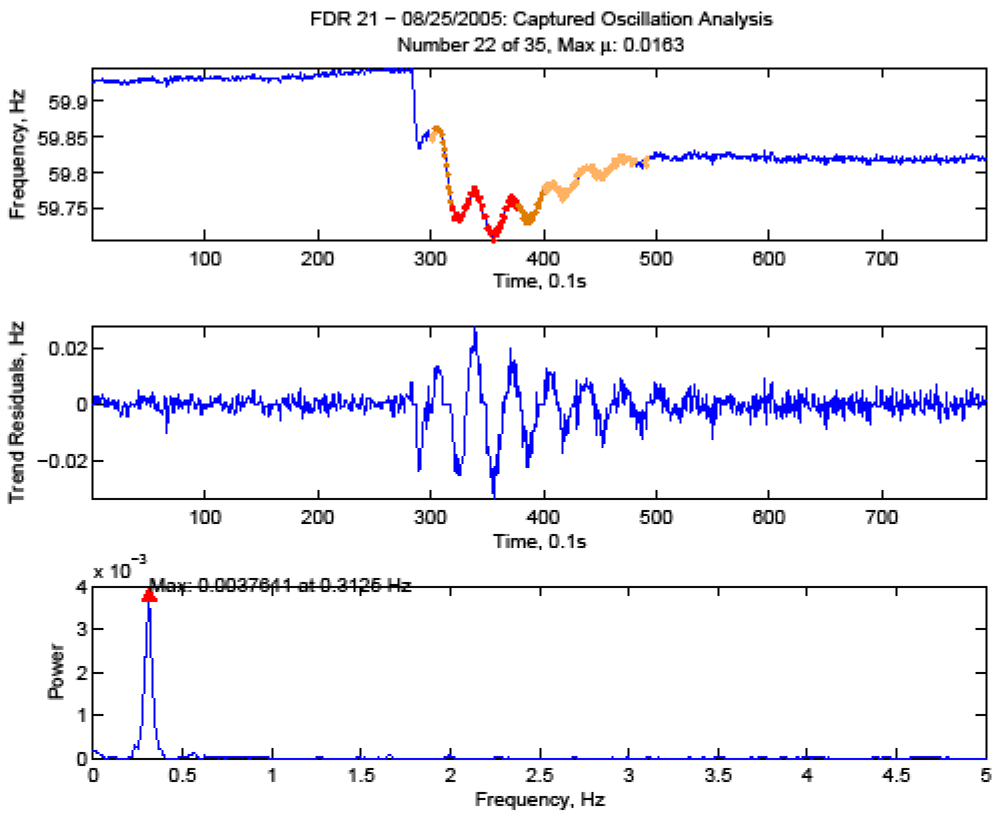
FDR 21 – 08/25/2005: Captured Oscillation Analysis
Number 22 of 35, Max µ: 0.0163
Frequency, Hz
Time, 0.1s
Trend Residuals, Hz
Time, 0.1s
x 10^-3
Max: 0.0037641 at 0.3125 Hz
Power
Frequency, Hz

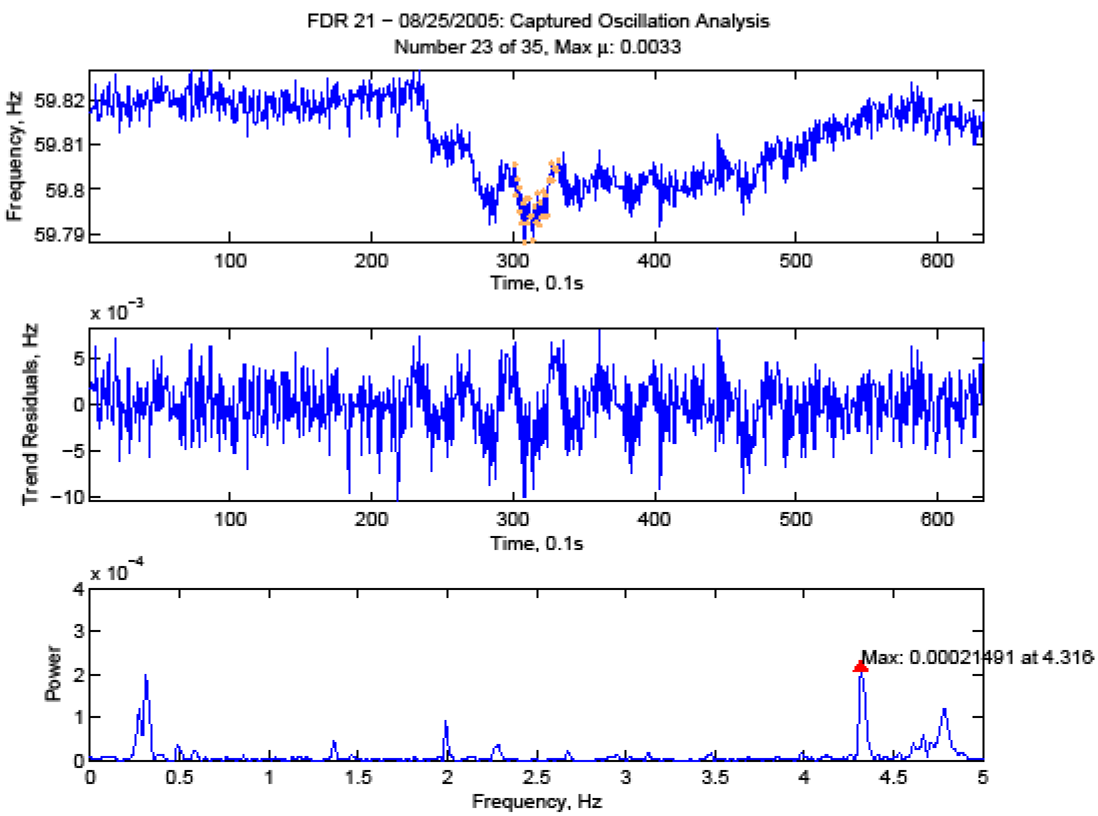
FDR 21 − 08/25/2005: Captured Oscillation Analysis
Number 23 of 35, Max µ: 0.0033
Frequency, Hz
59.82
59.81
59.8
59.79
100
200
300
400
500
600
Time, 0.1s
x 10^-3
Trend Residuals, Hz
5
0
−5
−10
100
200
300
400
500
600
Time, 0.1s
x 10^-4
Power
4
3
2
1
0
Max: 0.00021491 at 4.316
0
0.5
1
1.5
2
2.5
3
3.5
4
4.5
5
Frequency, Hz

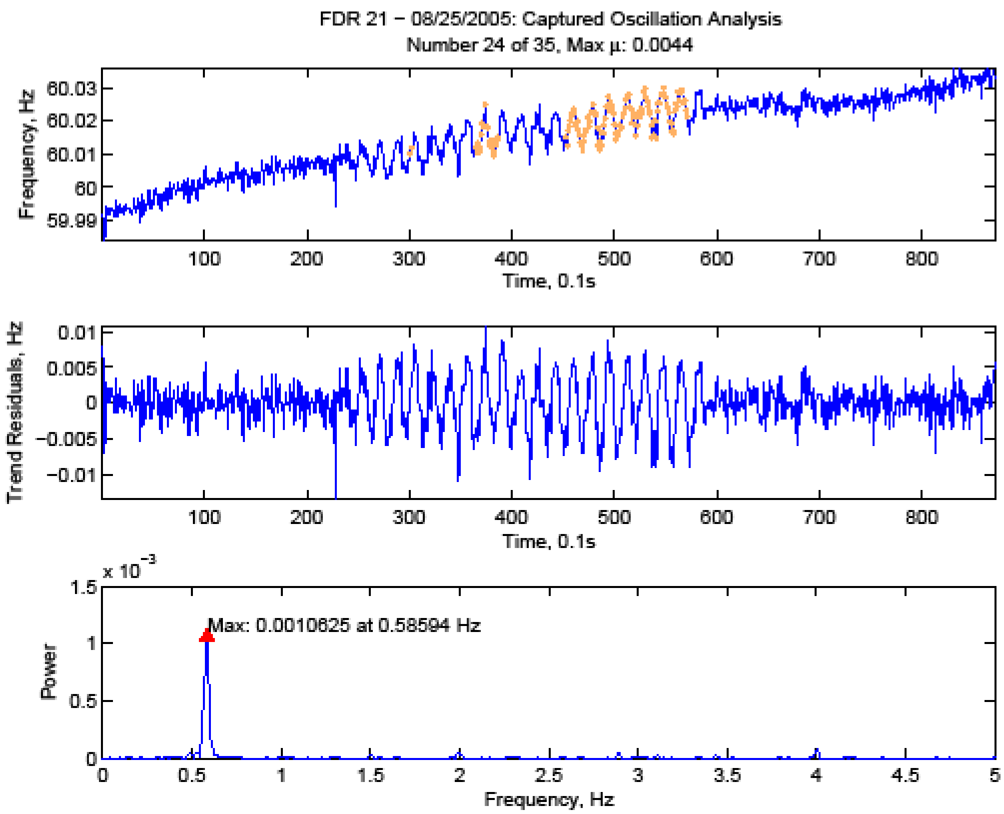
FDR 21 – 08/25/2005: Captured Oscillation Analysis
Number 24 of 35, Max μ: 0.0044
Frequency, Hz
60.03
60.02
60.01
60
59.99
100
200
300
400
500
600
700
800
Time, 0.1s
Trend Residuals, Hz
0.01
0.005
0
−0.005
−0.01
Time, 0.1s
x 10^−3
1.5
1
0.5
0
Power
Max: 0.0010625 at 0.58594 Hz
0
0.5
1
1.5
2
2.5
3
3.5
4
4.5
5
Frequency, Hz

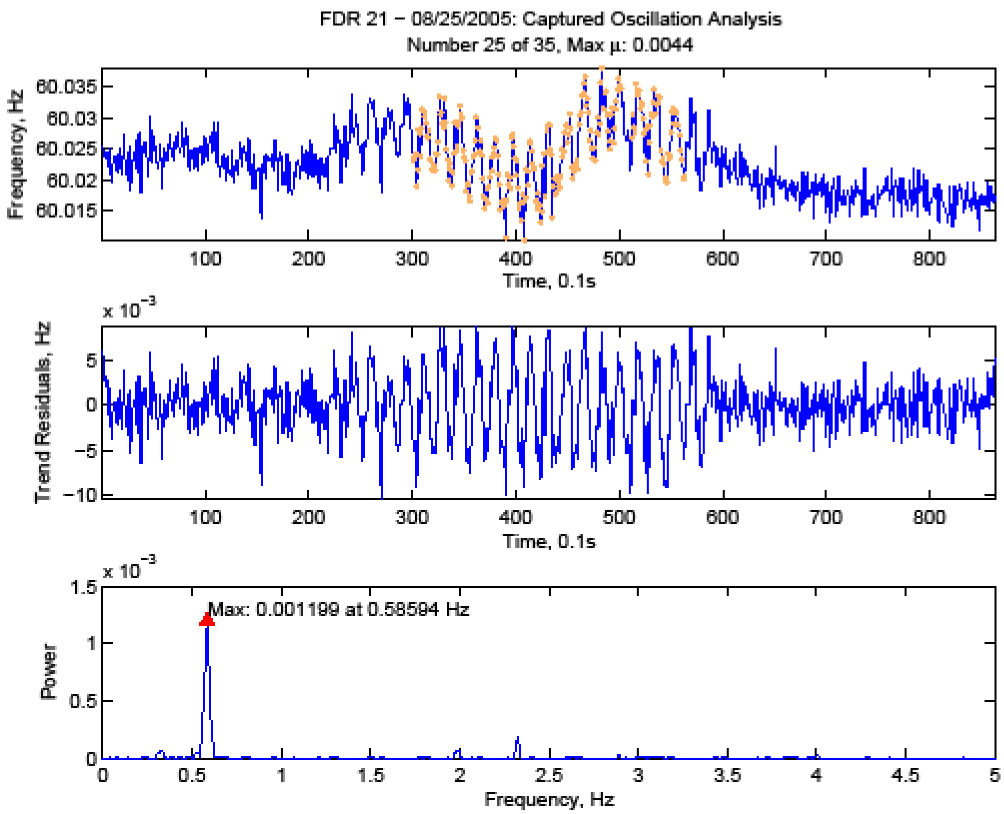
FDR 21 − 08/25/2005: Captured Oscillation Analysis
Number 25 of 35, Max μ: 0.0044
Frequency, Hz
60.035
60.03
60.025
60.02
60.015
100
200
300
400
500
600
700
800
Time, 0.1s
x 10^-3
Trend Residuals, Hz
5
0
−5
−10
Time, 0.1s
x 10^-3
Power
1.5
1
0.5
0
Max: 0.001199 at 0.58594 Hz
0
0.5
1
1.5
2
2.5
3
3.5
4
4.5
5
Frequency, Hz

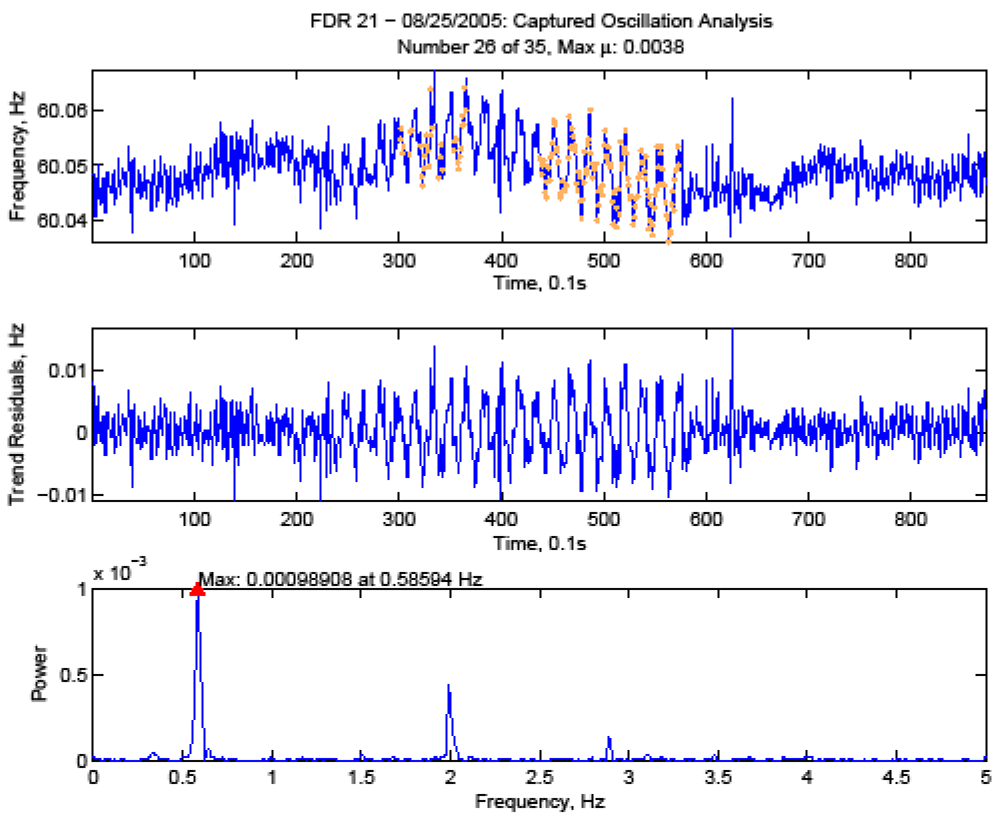
FDR 21 – 08/25/2005: Captured Oscillation Analysis
Number 26 of 35, Max μ: 0.0038
Frequency, Hz
Time, 0.1s
Trend Residuals, Hz
Time, 0.1s
Power
Max: 0.00098908 at 0.58594 Hz
Frequency, Hz

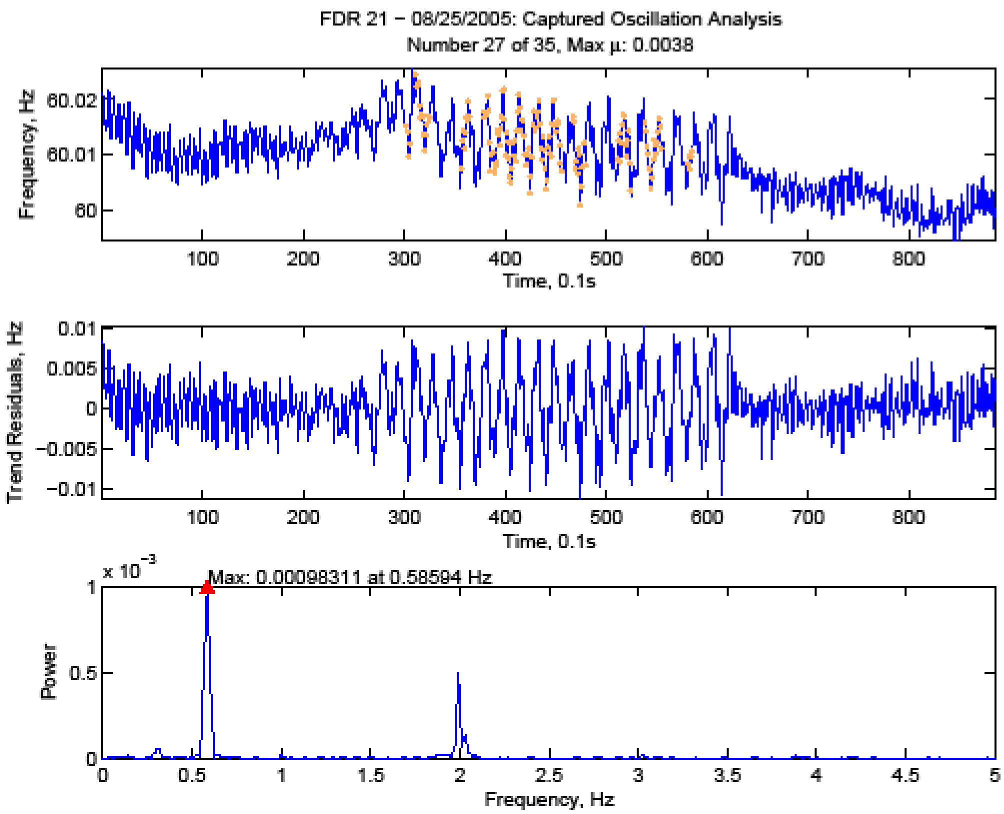
FDR 21 – 08/25/2005: Captured Oscillation Analysis
Number 27 of 35, Max μ: 0.0038
Frequency, Hz
Time, 0.1s
Trend Residuals, Hz
Time, 0.1s
Max: 0.00098311 at 0.58594 Hz
Power
Frequency, Hz

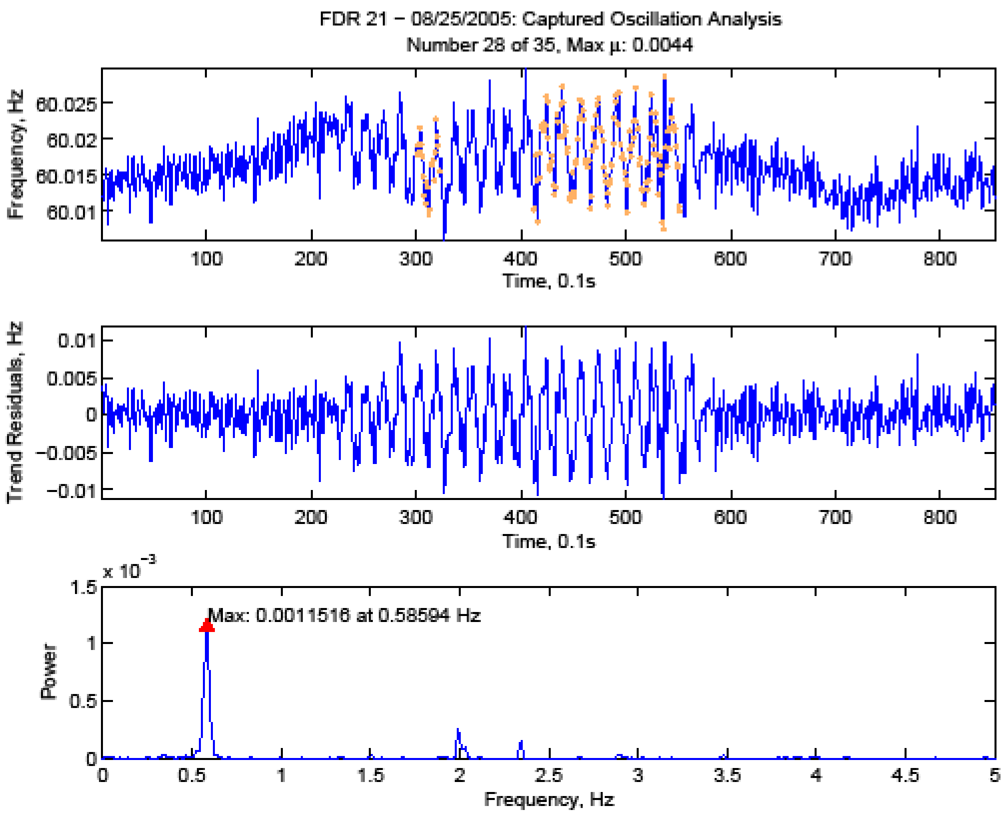
FDR 21 − 08/25/2005: Captured Oscillation Analysis
Number 28 of 35, Max µ: 0.0044
Frequency, Hz
60.025
60.02
60.015
60.01
100
200
300
400
500
600
700
800
Time, 0.1s
Trend Residuals, Hz
0.01
0.005
0
−0.005
−0.01
Time, 0.1s
x 10^−3
Power
1.5
1
0.5
0
Max: 0.0011516 at 0.58594 Hz
0.5
1
1.5
2
2.5
3
3.5
4
4.5
5
Frequency, Hz

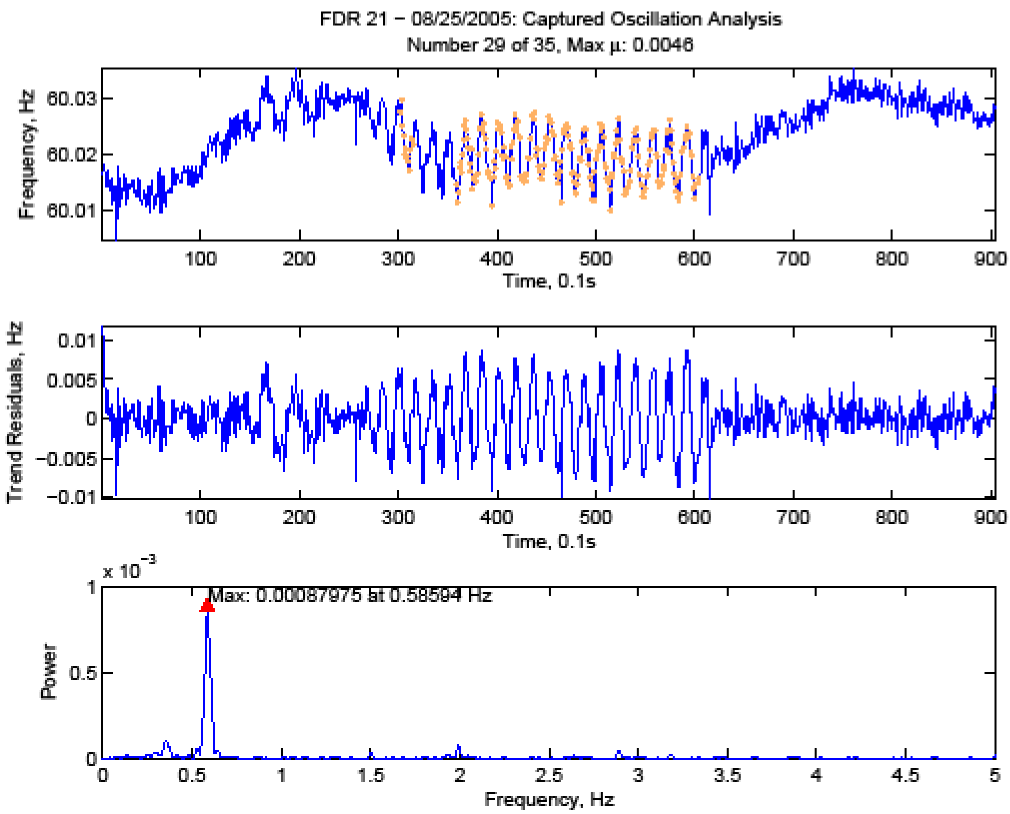
FDR 21 − 08/25/2005: Captured Oscillation Analysis
Number 29 of 35, Max μ: 0.0046
Frequency, Hz
60.03
60.02
60.01
100
200
300
400
500
600
700
800
900
Time, 0.1s
Trend Residuals, Hz
0.01
0.005
0
−0.005
−0.01
Time, 0.1s
x 10^−3
1
0.5
0
Power
Max: 0.00087975 at 0.58594 Hz
0
0.5
1
1.5
2
2.5
3
3.5
4
4.5
5
Frequency, Hz

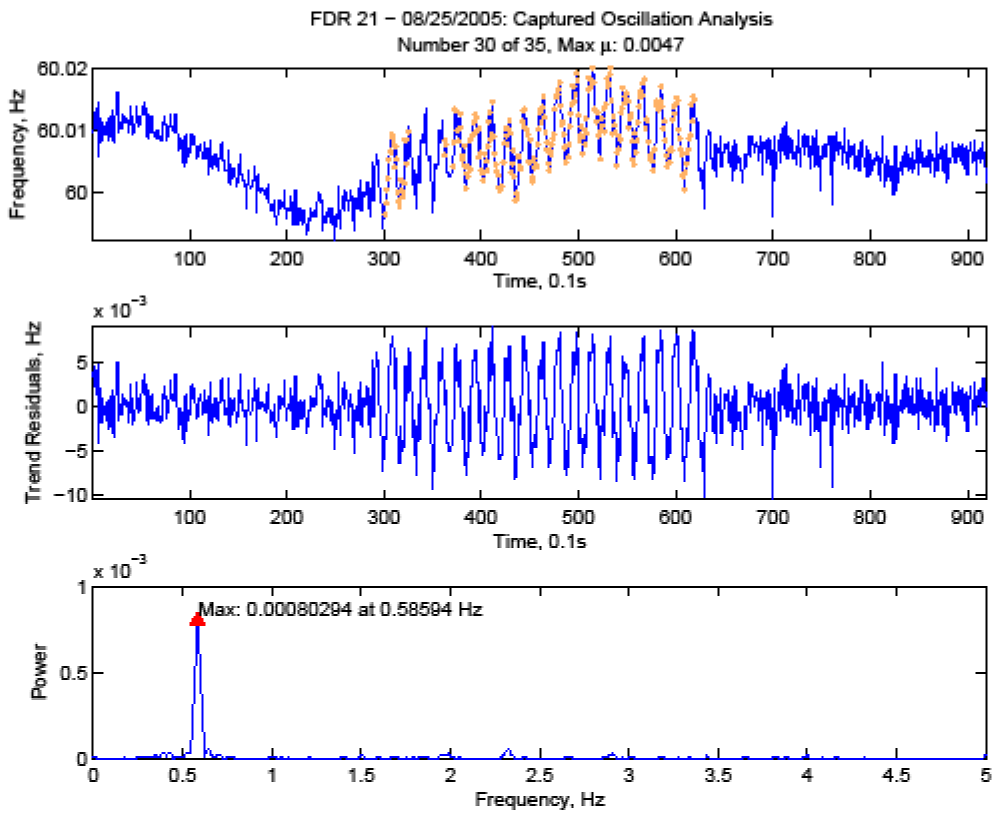
FDR 21 − 08/25/2005: Captured Oscillation Analysis
Number 30 of 35, Max µ: 0.0047
Frequency, Hz
60.02
60.01
60
100
200
300
400
500
600
700
800
900
Time, 0.1s
x 10^-3
Trend Residuals, Hz
5
0
−5
−10
Time, 0.1s
Power
1
0.5
0
Max: 0.00080294 at 0.58594 Hz
0.5
1
1.5
2
2.5
3
3.5
4
4.5
5
Frequency, Hz

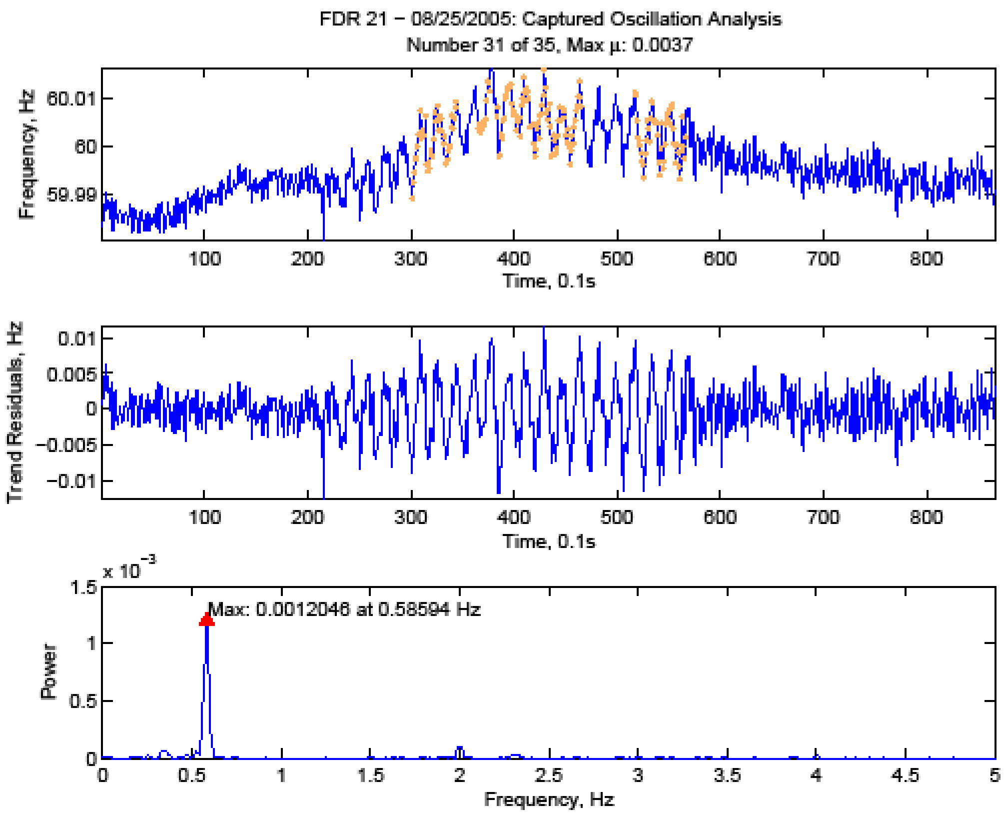
FDR 21 − 08/25/2005: Captured Oscillation Analysis
Number 31 of 35, Max µ: 0.0037
Frequency, Hz
60.01
60
59.99
100
200
300
400
500
600
700
800
Time, 0.1s
Trend Residuals, Hz
0.01
0.005
0
−0.005
−0.01
Time, 0.1s
x 10⁻³
Power
1.5
1
0.5
0
Max: 0.0012046 at 0.58594 Hz
0.5
1
1.5
2
2.5
3
3.5
4
4.5
5
Frequency, Hz

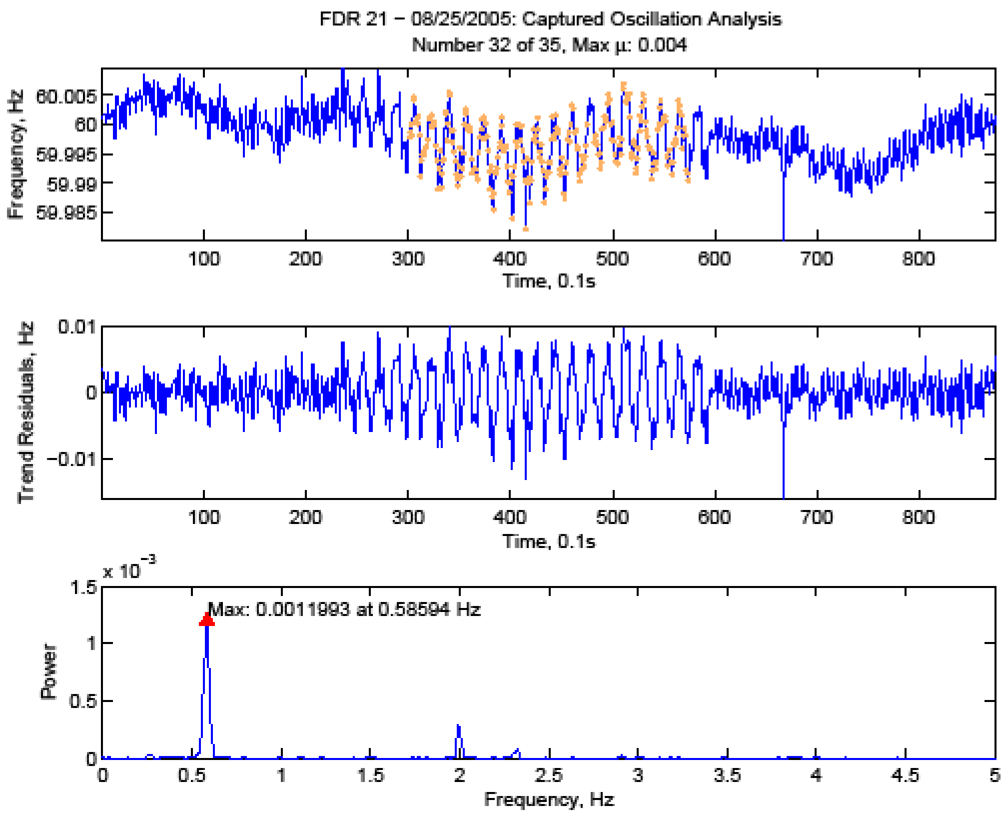
FDR 21 − 08/25/2005: Captured Oscillation Analysis
Number 32 of 35, Max μ: 0.004
Frequency, Hz
60.005
60
59.995
59.99
59.985
100
200
300
400
500
600
700
800
Time, 0.1s
Trend Residuals, Hz
0.01
0
−0.01
Time, 0.1s
x 10^-3
1.5
1
0.5
Power
Max: 0.0011993 at 0.58594 Hz
0
0.5
1
1.5
2
2.5
3
3.5
4
4.5
5
Frequency, Hz

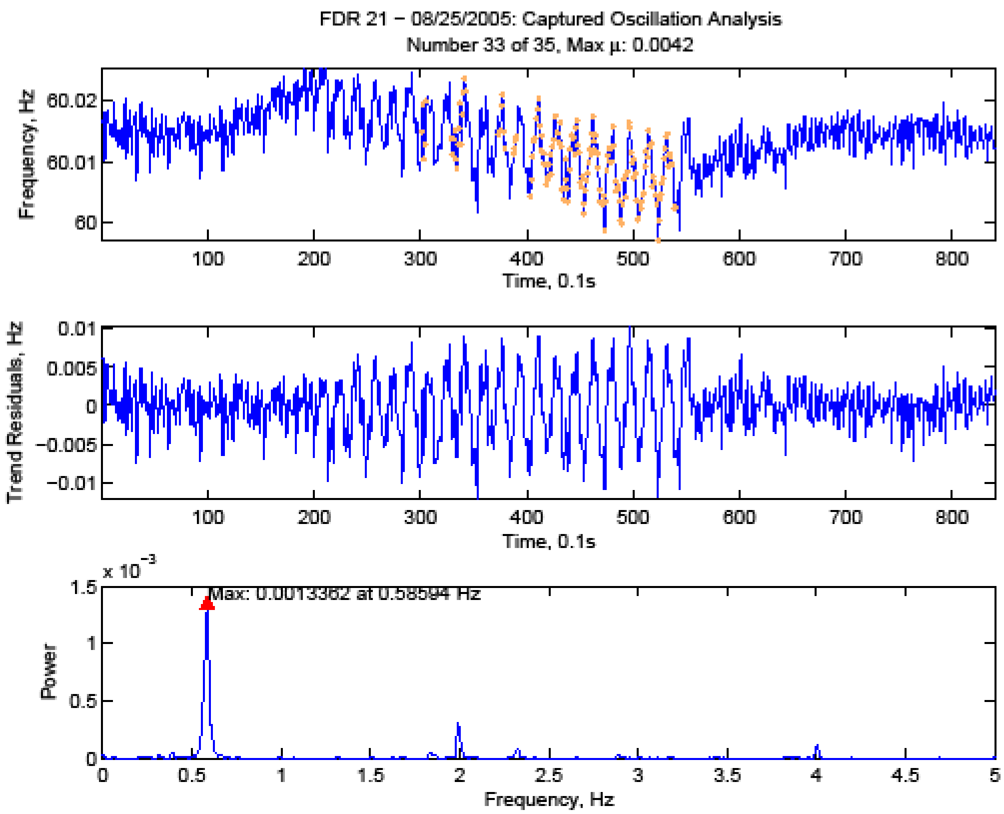
FDR 21 – 08/25/2005: Captured Oscillation Analysis
Number 33 of 35, Max μ: 0.0042
Frequency, Hz
Time, 0.1s
Trend Residuals, Hz
Time, 0.1s
Power
Max: 0.0013362 at 0.58594 Hz
Frequency, Hz

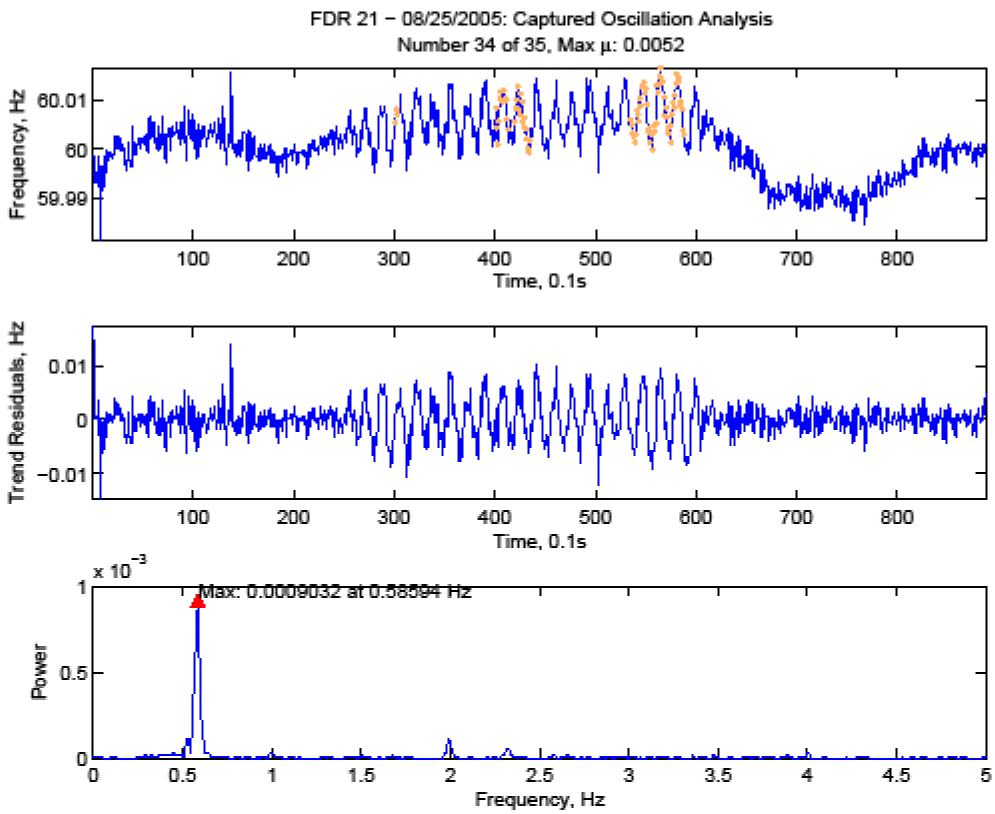

FDR 21 − 08/25/2005: Captured Oscillation Analysis
Number 34 of 35, Max μ: 0.0052
Frequency, Hz
60.01
60
59.99
100
200
300
400
500
600
700
800
Time, 0.1s
Trend Residuals, Hz
0.01
0
−0.01
100
200
300
400
500
600
700
800
Time, 0.1s
x 10^−3
1
Max: 0.0009032 at 0.58594 Hz
Power
0.5
0
0
0.5
1
1.5
2
2.5
3
3.5
4
4.5
5
Frequency, Hz

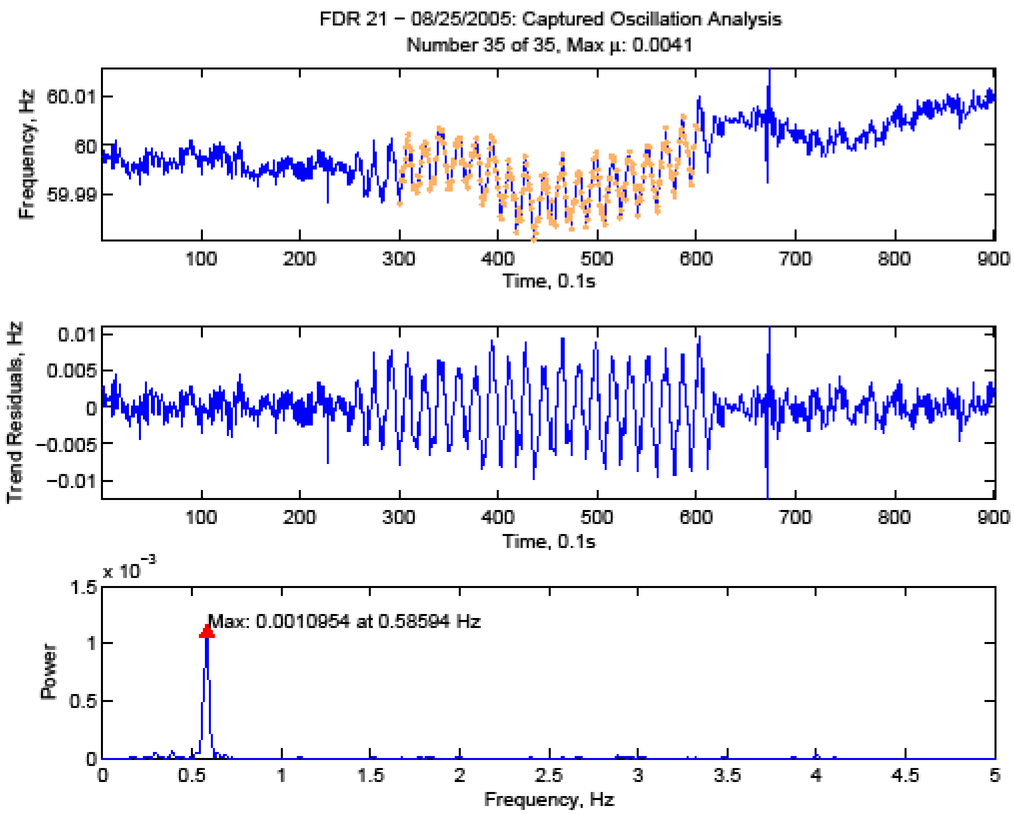
FDR 21 − 08/25/2005: Captured Oscillation Analysis
Number 35 of 35, Max μ: 0.0041
Frequency, Hz
60.01
60
59.99
100
200
300
400
500
600
700
800
900
Time, 0.1s
Trend Residuals, Hz
0.01
0.005
0
−0.005
−0.01
Time, 0.1s
x 10^-3
1.5
1
0.5
Power
Max: 0.0010954 at 0.58594 Hz
0
0.5
1
1.5
2
2.5
3
3.5
4
4.5
5
Frequency, Hz

Appendix IX: MATLAB™ Code for Matrix Pencil Calculations

PSS/E™ Data Conversion Code

```
function [t,S,L] = psseconv(fname)
%Program psseconv: Convert ASCII PSS/E file into MATLAB format
%t-timing vector (output)
%S-signal matrix (output)
%L-label structure (output)

%Initialize variables
idx=1;
cmidx=0;
t=[];
L=[];
S=[];
temp=[];
mat=[];

%Open PSS/E File
fid=fopen(fname);

%Scan file
C=textscan(fid,'%s',-1);

%Close file
fclose(fid);
stc=strcmp(C{1},'TIME');
tidx=find(stc==1);
tidx=[1; tidx; length(C{:})];
ch=nan(5,length(tidx)-2);
for i=1:length(tidx)-2
    cidx=find(strcmp(C{1}(tidx(i):tidx(i+1)),'CHANNEL')==1);
    cidx=cidx+tidx(i)-1;
    for j=1:length(cidx)
        ch(j,i)=str2num(C{1}{cidx(j)+2}(1:5));
    end
end
ch=[nan(5,1),ch];
for i=1:length(C{1})
    if strcmp(C{1}{i},'TIME')   %Locate "TIME" string data typically follows
        idx=idx+1;
        if (ch(:,idx)~=ch(:,idx-1))
            L=[L,C{1}(i+1:i+sum(~isnan(ch(:,idx))))'];
            cmult=cmidx*sum(~isnan(ch(:,idx)));
            cmidx=cmidx+1;
            S=[S, mat];
            mat=[];
        end
        j=i+sum(~isnan(ch(:,idx)))+1;
        numflag=true;           %Set numeric flag
        while numflag           %While input is numeric, iterate through data
            if j<=length(C{1})  %Don't attempt to read past end of cell
                if ~isempty(str2num(C{1}{j}))
```

```
                    temp=[temp str2num(C{1}{j})];
                    j=j+1;
                else
                    numflag=false;
                end
            else
                numflag=false;
            end
        end
        ttidx=1:1+sum(~isnan(ch(:,idx))):length(temp);
        if cmidx==1
            t=[t; temp(ttidx)'];
        end
        temp(ttidx)=[];
        mat=[mat; vec2mat(temp,sum(~isnan(ch(:,idx))))];
        temp=[];
    end
end
S=[S, mat];
i=2:length(t);
tdel=find(t(i)==t(i-1));
t(tdel)=[];
S(tdel,:)=[];
t=t(1:min(length(t),size(S,1)));
S=S(1:min(length(t),size(S,1)),:);
```

Damping Tool Manager

```
function DampBatchMgr(varargin)
global Sout Xout Yout tout CALC_OUT SC
%Program DampBatchMgr - Feed CalcDamping.m with files for batch processing.
%Program attempts to open text file Batch.txt which should be in same
%working directory as this script.  Batch.txt should contain the names of
%PSS/E text channel output files to be processed.  IMPORTANT: LEAVE *.txt
%EXTENSION OFF FILE NAME.  An extension may be passed into this program
%that specifies the type of plot file to save.  For instance,
%DampBatchMgr('pdf') will create Adobe PDF files from the plots rendered in
%CalcDamping.  See end of script for acceptable plotting file extensions.
%Calling this program with no arguments will execute CalcDamping without
%making any plots.
%
%COMMENTS:
%None
%
%INTERNALLY ADJUSTABLE PARAMETERS:
%Noise filtering parameter: kfilt
%Model order reduction parameter: p
%Model order reduction continuation factor: prcf
%Default model order used if singular values do not rapidly decay: defordr
%Resampling frequency parameter: fs
%Signal fitting offset time: toff
%
%AUTHOR: R. Matthew Gardner
%Created for TVA: Tennessee Valley Authority Transmission Planning Dept.
%
%VERSION: 2
```

```
%
%REVISED BY: R. Matthew Gardner
%DATE REVISED: 8/10/2007
tic
warning off MATLAB:xlswrite:AddSheet
if nargin>1                         %Check number of input arguments
    disp('Warning: Number of input arguments greater than 1.  Excess inputs
ignored.');
end
fid=fopen('Batch.txt');             %Open batch file
fid1=fopen('Batch_out.txt','w');    %Open batch overveiw file
if exist('Batch_ctrl.txt')          %Check for control file containing input
constants
    try                             %Try to load properly formatted file
        Vars=load('Batch_ctrl.txt');%Load constants in from file
        if length(Vars)~=6
            disp('Incorrect number of constants listed in Batch_ctrl.txt.
Switching to default parameters.');
            CTRL_IN=populatectrl([]);   %Incorrect number of constants in
file, Use default control constant values
        else
            CTRL_IN=populatectrl(Vars); %Arrange constant in proper structure
for passing to CalcDamping
        end
    catch                           %Control file improperly formatted
        disp('Problem loading control constants.  Switching to default
parameters.');
        CTRL_IN=populatectrl([]);   %Use default control constant values
    end
else                                %No control file was found
    disp('No control file Batch_ctrl.txt found.  Using default solution
parameters.');
    CTRL_IN=populatectrl([]);       %Use default control constant values
end
fprintf(fid1,'INPUT PARAMETERS:\r\n');  %Print constants used to batch output
file
fprintf(fid1,'kfilt = %6.6f\r\n',CTRL_IN.kfilt);
fprintf(fid1,'p = %6.6f\r\n',CTRL_IN.p);
fprintf(fid1,'prcf = %6.6f\r\n',CTRL_IN.prcf);
fprintf(fid1,'defordr = %6.6f\r\n',CTRL_IN.defordr);
fprintf(fid1,'fs = %6.6f\r\n',CTRL_IN.fs);
fprintf(fid1,'toff = %6.6f\r\n\r\n',CTRL_IN.toff);
fprintf(fid1,'BEGIN OUTPUT OF DAMPING ANALYSIS:\r\n');
if fid==-1|fid1==-1                 %Check for error opening file
    disp('Program terminated: Error opening Batch R/W file.  Check file type,
location, and extension.');
    return
end
try                                 %Scan in file listings, terminate if
error
    C=textscan(fid,'%s',-1);
catch
    disp('Program terminated: Error scanning Batch text file.  Check file
contents to ensure compliance with input rules.');
    return
end
fclose(fid);                                %Close file stream
```

```
for i=1:length(C{1})                            %Iterate though file listings and
call CalcDamping
    disp(['Processing ' num2str(i) ' of ' num2str(length(C{1})) ' input
file(s).']);
    FILE_IN.infile=[C{1}{i} '.txt'];        %Form input file name to pass
into CalcDamping
    try
        [t,S,L]=psseconv(FILE_IN.infile);   %Read and convert multichannel
PSS/E file
        disp(['Found ' num2str(length(L)) ' channel(s) in file: '
FILE_IN.infile]);
        try
            for j=1:length(L)
                disp(['Processing channel: ' L{j}]);
                FILE_IN.outfile=[C{1}{i} '_ch' L{j} '_out.txt'];   %Form
output file name to pass into CalcDamping
                if nargin>0                 %Executes if plotting is desired
                    FILE_IN.pfile=[C{1}{i} '_ch' L{j} '_plot.' varargin{1}];
%Form plotting file name to pass into CalcDamping
                else                        %Otherwise no plots
                    FILE_IN.pfile=[];       %No plot desired, do not pass
plotting file
                end
                CALC_OUT=CalcDamping(t,S(:,j),FILE_IN,CTRL_IN);
                fprintf(fid1,'%s\t%6.6f\t%6.6f\r\n',[C{1}{i} '_ch'
L{j}],CALC_OUT.domdamp,CALC_OUT.err);
                tout=CALC_OUT.t';
                Sout(:,j)=CALC_OUT.S;
                Xout(:,j)=CALC_OUT.Xo;
                Yout(:,j)=CALC_OUT.Yo;
                SC{j}=CALC_OUT;
            end
        catch                               %Skip any files with errors
            disp(['Error in execution of program "CalcDamping.m" for file: '
C{1}{i} ' - File skipped.']);
        end
        disp(['Writing Excel file: ' C{1}{i} '_out.xls']);
        try                                 %Write data to Excel file
%              xlswrite([C{1}{i} '_out.xls'],{'TIME'},'INPUT DATA','A1');
%              xlswrite([C{1}{i} '_out.xls'],L,'INPUT DATA','B1');
%              xlswrite([C{1}{i} '_out.xls'],[t,S],'INPUT DATA','A2');
%              disp('Input data written to Excel.');
%              xlswrite([C{1}{i} '_out.xls'],{'TIME'},'RESAMPLED DATA','A1');
%              xlswrite([C{1}{i} '_out.xls'],L,'RESAMPLED DATA','B1');
%              xlswrite([C{1}{i} '_out.xls'],[tout,Xout],'RESAMPLED
DATA','A2');
%              disp('Resampled data written to Excel.');
%              xlswrite([C{1}{i} '_out.xls'],{'TIME'},'ESTIMATED DATA','A1');
%              xlswrite([C{1}{i} '_out.xls'],L,'ESTIMATED DATA','B1');
%              xlswrite([C{1}{i} '_out.xls'],[tout,Sout],'ESTIMATED
DATA','A2');
%              disp('Estimated data written to Excel.');
%              Sout=[];
%              Xout=[];
        catch
            disp('Error writing MS Excel file.  No Excel file created');
        end
```

```
    catch
        disp(['Error in execution of program "psseconv.m" for file: ' C{1}{i}
' - File skipped.']);
    end
end
fclose(fid1);   %close file stream
disp('Batch program execution complete.');
toct=toc;
disp(['Program execution time = ' num2str(toct) ' seconds.']);

function CTRL_IN = populatectrl(Vars)   %Populate structure containing
constants
    if ~isempty(Vars)
        CTRL_IN.kfilt=Vars(1);
        CTRL_IN.p=Vars(2);
        CTRL_IN.prcf=Vars(3);
        CTRL_IN.defordr=Vars(4);
        CTRL_IN.fs=Vars(5);
        CTRL_IN.toff=Vars(6);
    else
        CTRL_IN.kfilt=0.4;
        CTRL_IN.p=1;
        CTRL_IN.prcf=0.6667;
        CTRL_IN.defordr=4;
        CTRL_IN.fs=60;
        CTRL_IN.toff=7;
    end

%Accepatable plot file extensions:
%'bmp'Windows Bitmap (BMP)
%'cur'Windows Cursor resources (CUR)
%'gif'Graphics Interchange Format (GIF)
%'hdf'Hierarchical Data Format (HDF)
%'ico'Windows Icon resources (ICO)
%'jpg' or 'jpeg'Joint Photographic Experts Group (JPEG)
%'pbm'Portable Bitmap (PBM)
%'pcx'Windows Paintbrush (PCX)
%'pgm'Portable Graymap (PGM)
%'png'Portable Network Graphics (PNG)
%'pnm'Portable Anymap (PNM)
%'ppm'Portable Pixmap (PPM)
%'ras'Sun Raster (RAS)
%'tif' or 'tiff'Tagged Image File Format (TIFF)
%'xwd'X Windows Dump (XWD)
%'pdf' Adobe Portable Document Format
```

Damping Calculation Code (Called by Damping Tool Manager)

```
function CALC_OUT=CalcDamping(t,S,FILE_IN,CTRL_IN)
%Program CalcDamping - Calculate the damping of a signal stored as a text
%file.
%CalcDamping(INFILE,OUTFILE,pfile) approximates the data stored in
%INFILE.txt with a series of damped sinusoids.  The input file is assumed
%consist of a single column whose first entry indicates the sampling period
%of the data.  All other entries compose the signal. OUTFILE should contain
%a string to be used as a file name for the results.  The output file name
```

```
%should not contain any illegal characters.  If pfile is provided, then
%MATLAB will save plots that are generated during estimation process.
%Files will be saved using the legal extension provided.  See MATLAB Help
%for comprehensive list of plot file formats.
%
%COMMENTS:
%
%Input data need not have zero mean.  Input data is automatically detrended
%before fitting.
%
%INTERNALLY ADJUSTABLE PARAMETERS:
%None
%
%AUTHOR: R. Matthew Gardner
%Created for TVA: Tennessee Valley Authority Transmission Planning Dept.
%
%VERSION: 2.1
%
%REVISED BY: R. Matthew Gardner
%DATE REVISED: 8/10/2007

%***************************************************************************
%MAIN~MAIN~MAIN~MAIN~MAIN~MAIN~MAIN~MAIN~MAIN~MAIN~MAIN~MAIN~MAIN~MAIN~MAIN
%***************************************************************************
toff=CTRL_IN.toff;                                %Set signal fitting offset time
if toff>min(t) & ~isempty(find(t>toff))
    S=S(find(t>toff));                           %Delete signal values at t<toff
    t=t(find(t>toff));                           %Truncate timing vector
else
    disp('Warning: Either toff not greater than minimum time in vector OR 
signal length does not exceed time toff.');
end
disp('Re-sampling data...');
fs=CTRL_IN.fs;                                   %Set resampling frequency
[tsamp,Xo]=ReSamp(t,S,fs);                       %Resample original signal via 
linear interpolation
CALC_OUT.Yo=Xo;
Xo=awgn(Xo,25,'measured');                      %TEST CODE: Adds 30 dB of AWGN to 
input signal (REMOVE BEFORE STANDARD OPERATION)
disp('Re-sampling complete.  Detrending data...');
[X,Xt]=detrend(Xo);                              %De-trend Signal
disp('Data detrending complete.  Forming Hankel matrix...');
kfilt=CTRL_IN.kfilt;                             %Adjustable noise filtering 
parameter: best results 0.333<kfilt<0.5
[N,L,Y]=form_Hankel(X,kfilt);                    %Specify dimensions and create 
Hankel matrix
p=CTRL_IN.p;                                     %Adjustable model order reduction 
parameter
prcf=CTRL_IN.prcf;                               %p-reduction continuation factor
defordr=CTRL_IN.defordr;                         %Adjustable default model order 
if singular values do not decay
disp('Hankel matrix complete.  Reducing system and calculating needed 
eigenvalues...');
err1=true;                                       %Set error flag for Moore-Penrose 
pseudo inverse
while err1                                       %Loop until model order yields 
system considered to be solution to BAP
```

```
    [M,dS,Y1,Y2]=reduce_sys(Y,p,defordr);   %System reduction
    [E,R,yout,youtgal,err1]=calc_eig(M,Y1,Y2,N,X);%Calculate eigenvalues and
estimate signal
    p=p*prcf;                               %Continued model reduction
(implied Moore-Penrose pseudoinverse problems)
    if err1                                 %Inform user about reduction in p
        disp(['Reduction factor found to be too large. p reduced to '
num2str(p)]);
    end
end
disp('System reduction complete.  Calculating damping factors...');
[Ec,dfactor,nfreq,dfreq,domdamp,didx]=calc_damp(E,R,tsamp);%Calculate damping
factor, natural frequency, and damped frequency
CALC_OUT.Ec=Ec;
CALC_OUT.R=R;
CALC_OUT.didx=didx;
if ~isempty(FILE_IN.pfile)
    disp('Plotting results...');
    plot_results(FILE_IN.pfile,Xo,Xt,tsamp,X,yout,dS,Ec,R,youtgal,didx);%Plot
results if requested
end
disp('Writing output file...');
CALC_OUT.err=norm(Xo-(Xt+yout));
write_txt(FILE_IN.outfile,M,dfactor,nfreq,dfreq,Ec,R,Xo,Xt,yout,dS,CALC_OUT.e
rr,didx);%Write output text file
disp('Program CalcDamping.m complete.');
CALC_OUT.domdamp=domdamp;
CALC_OUT.S=yout+Xt;
CALC_OUT.Xo=Xo;
CALC_OUT.t=(0:(length(Xo)-1))*tsamp;

%**************************************************************************
%RESAMPLE DATA
%**************************************************************************
function [tsamp,Xo]=ReSamp(t,S,fs)
    i=2:length(S);                        %Create index for comparison
    delidx=find(t(i)==t(i-1));            %Compare timing pairs
    t(delidx)=[];                         %Delete timing vector entries with
consecutive duplicate time
    S(delidx)=[];                         %Also, delete corresponding signal
vector entries
    tsamp=1/fs;                           %Calculate sampling period
    Xo=interp1(t,S,t(1):tsamp:t(end))'; %Interpolate signal

%**************************************************************************
%DE-TREND SIGNAL
%**************************************************************************
function [X,Xt]=detrend(Xo,tsamp)
    X=Xo-mean(Xo);
    Xt=Xo-X;                          %Calculate trend

%**************************************************************************
%FORMATION OF HANKEL MATRIX --- DIM:(N-L)x(L+1)
%**************************************************************************
function [N,L,Y]=form_Hankel(X,kfilt)
    N=length(X);                      %Length of input signal vector
```

```
    L=round(N*kfilt);
    hank=hankel(1:(N-L),(N-L):N);   %Create Hankel matrix index numbers
    Y=X(hank);                      %Populate Hankel matrix using index
numbers

%***************************************************************************
%SYSTEM REDUCTION VIA SVD: SINGULAR VALUE DECOMPOSITION OF HANKEL MATRIX
%***************************************************************************
function [M,dS,Y1,Y2]=reduce_sys(Y,p,defordr)
    [U,S,V]=svd(Y);             %Calculate SVD of Y
    dS=diag(S);                     %Extract singular value from diagonal
matrix S
    idx=find(dS/max(dS)>10^(-p));   %Calculate ratio of all singular values
to maximum singular value and determine model order cutoff point
    if idx==1                       %Determine system order from idx or
default to defordr
        M=round(defordr);           %Try to estimate signal even if singular
values do not decay
    else
        M=idx(end);                 %Model order set IF singular values decay
        M=min(M,length(dS)-1);      %Limit size of M to be comformable with
Y1, Y2 in further steps
    end
    Vp=V(:,1:M);                    %Calculated "filtered" matrix Vp (from V)
    Vp1=Vp(1:end-1,:);              %Set up intermediate matrices
    Vp2=Vp(2:end,:);
    Sp=S(:,1:M);                    %Remove columns of S to ensure rank(S)=M
leaving only dominant singular values
    Y1=U*Sp*Vp1';                   %Create matrices Y1 and Y2 to form matrix
pencil
    Y2=U*Sp*Vp2';

%***************************************************************************
%EIGENVALUE ANALYSIS OF MATRIX PENCIL
%***************************************************************************
function [E,R,yout,youtgal,err]=calc_eig(M,Y1,Y2,N,X)
    E=eig(pinv(Y1)*Y2);          %Find eigenvalues of matrix pencil
    E=E(1:M);                    %Pare down eigenvalues based on model order
    for h=0:N-1                  %Form Vandermonde-esque matrix
        Zmat(h+1,:)=E'.^h;
    end
    try                          %Error catching if model order acidentally
set too big
        R=pinv(Zmat)*X;          %Calculate phase vector
        yout=real(Zmat*R);       %yout now contains signal estimate
        for i=1:length(R)        %Create signal gallery
            youtgal(:,i)=Zmat(:,i)*R(i);
        end
        err=false;               %Clear error flag
    catch
        yout=[];                 %Set error flag if problem calculating
pseudoinverse
        err=true;
    end

%***************************************************************************
```

```
%CALCULATE DAMPING PERCENTAGES
%***************************************************************************
function [Ec,dfactor,nfreq,dfreq,domdamp,didx]=calc_damp(E,R,tsamp)
    domdamp=NaN;
    pridx=0;
    if imag(E)<pi
        Ec=log(E)/tsamp;                                %Convert discrete system
poles to continuous system poles
    else
        Ec=(2/tsamp)*((E-1)./(E+1));
        disp('Warning: Imaginary component of Eigenvalue found to be greater
than Pi.  Switching to Tustin''s Method for discrete to cont. pole
mapping.');
    end
    for i=1:length(Ec)
        if real(Ec(i))>0
                pridx=pridx+1;
        end
        if ~isreal(Ec(i))                           %Do not attempt to calculate
frequencies for real eigenvalues
            %pole=log(E(i))/tsamp;                  %Convert discrete system
poles to continuous system poles
            dfactor(i)=-real(Ec(i))/abs(Ec(i)); %Calculate damping factor
from pole locations in complex plane
            nfreq(i)=abs(Ec(i))/2/pi;               %Calculate natural frequency
in Hz
            dfreq(i)=abs(imag(Ec(i)))/2/pi;     %Calculate damped frequency
in Hz
        end
    end
    if pridx>0
        disp(['Warning: ' num2str(pridx) ' Eigenvalues with positive real
components calculated.']);
    end
    [sR,sidx]=sort(R,'descend');                    %Sort residual vector
    for i=1:length(R)                               %Find largest R with complex
corresponding eigenvalue
        if ~isreal(Ec(sidx(i)))                     %Test complexity of
eigenvalue
            domdamp=dfactor(sidx(i));               %Calculate dominant damping
            didx=[sidx(i),find(Ec==Ec(sidx(i))')];%Find index of compex
conjugate if exists
            break;
        end
    end

%***************************************************************************
%PLOT RESULTS
%***************************************************************************
function plot_results(pfile,Xo,Xt,tsamp,X,yout,dS,E,R,youtgal,didx)
    [tok,rem]=strtok(pfile,'.');                %Determine plot file name and
desired plot file extension
    figure                                      %Plot original signal
    plot((0:(length(Xo)-1))*tsamp,Xo,'b','linewidth',2);        %Plot
original signal
    hold on;
```

```
    plot((0:(length(Xt)-1))*tsamp,Xt,'r','linewidth',2);        %Plot signal
mean (or trend)
    plot((0:(length(Xt)-1))*tsamp,(Xt+yout),'g','linewidth',2); %Plot signal
estimate
    grid on;                                %Misc. plot formatting
    axis on;
    ylabel('Signal Value');
    xlabel('Time, s');
    title('Overview of Signals');
    legend('Input Signal','Input Signal Mean','Estimated Signal');
    axis tight
    drawnow                                 %Flush graphics buffer
    try                                     %File saving error catching
        saveas(gcf,[tok '_original' rem]);  %Save file
    catch
        disp(['Error writing file: ' pfile ' Check file extension.']);
    end
    close all                               %Close plot
    figure                                  %Plot signal gallery
    plot((0:(length(Xo)-1))*tsamp,real(youtgal),'linewidth',2); %Plot signal
gallery
    grid on;                                %Misc. plot formatting
    axis on;
    ylabel('Signal Value');
    xlabel('Time, s');
    title('Signal Gallery');
    axis tight
    drawnow                                 %Flush graphics buffer
    try                                     %File saving error catching
        saveas(gcf,[tok '_gallery' rem]);   %Save file
    catch
        disp(['Error writing file: ' pfile ' Check file extension.']);
    end
    close all
    figure                                  %Plot signal overlay
    subplot(2,1,1);
    plot((0:(length(Xo)-1))*tsamp,Xo,'b','linewidth',2);        %Plot
original signal
    hold on;
    plot((0:(length(Xt)-1))*tsamp,Xt,'r','linewidth',2);        %Plot signal
mean (or trend)
    plot((0:(length(Xt)-1))*tsamp,(Xt+yout),'g','linewidth',2); %Plot signal
estimate
    grid on;                                %Misc. plot formatting
    axis on;
    ylabel('Signal Value');
    xlabel('Time, s');
    title('Overview of Signals');
    legend('Input Signal','Input Signal Mean','Estimated Signal');
    axis tight
    drawnow
    subplot(2,1,2);
    plot((0:(length(Xo)-1))*tsamp,real(youtgal),'linewidth',2); %Plot signal
gallery
    grid on;                                %Misc. plot formatting
    axis on;
    ylabel('Signal Value');
```

```
    xlabel('Time, s');
    title('Signal Gallery');
    axis tight
    drawnow                                 %Flush graphics buffer
    try                                     %File saving error catching
        saveas(gcf,[tok '_overlay' rem]);   %Save file
    catch
        disp(['Error writing file: ' pfile ' Check file extension.']);
    end
    close all
    figure                                  %Plot detrended signals (both
original detrend and estimate to detrend)
    plot((0:(length(X)-1))*tsamp,X,'b','linewidth',2);  %Plot zero-mean
(detrended) original signal
    hold on;                                %Misc. plot formatting
    grid on;
    axis on;
    plot((0:(length(yout)-1))*tsamp,real(yout),'r','linewidth',2);  %Plot
zero-mean signal estimate
    legend('Orig. Signal','Est. Signal');   %Misc. plot formatting
    ylabel('Signal Value');
    xlabel('Time, s');
    title('Detrended Original Signal and Estimated Signal');
    axis tight
    drawnow                                 %Flush graphics buffer
    try                                     %File saving error catching
        saveas(gcf,[tok '_zeromean' rem]);  %Save file
    catch
        disp(['Error writing file: ' pfile ' Check file extension.']);
    end
    close all                               %Close plot
    figure                                  %Plot singular values
    plot(dS,'b*','linewidth',1.5,'markersize',10);  %Plot singular values
    hold on;                                %Misc. plot formatting
    grid on;
    plot(dS(1:length(E)),'r^','linewidth',2,'markersize',12);   %Plot
selected singular values
    legend('Singular Values','Dominant Sing. Vals.');           %Misc. plot
formatting
    ylabel('Singular Value Size');
    xlabel('Singular Value Number');
    title('Singular Values as determined by SVD');
    axis on;
    axis tight
    drawnow                                 %Flush graphics buffer
    try                                     %File saving error catching
        saveas(gcf,[tok '_singvals' rem]);  %Save file
    catch
        disp(['Error writing file: ' pfile ' Check file extension.']);
    end
    close all                               %Close plot
    figure                                  %Plot eigenvalues (poles) of
signal in Argand diagram
    plot(E,'bx','linewidth',2,'markersize',12); %Plot eigenvalues
    hold on;
    plot(R,'ro','linewidth',2,'markersize',10); %Plot residuals
```

```
    plot(E(didx),'gs','linewidth',2,'markersize',16); %Plot dominant
eigenvalues
    plot(R(didx),'g^','linewidth',2,'markersize',16); %Plot dominant
residuals
    grid on;                                %Misc. plot formatting
    axis equal;
    axis on;
    ylabel('Imaginary Axis');
    xlabel('Real Axis');
    title('Argand Diagram of Eigenvalues and Residuals');
    legend('Eigenvalues','Residuals','Dominant Eigenvalues','Dominant
Residuals');
    drawnow                                 %Flush graphics buffer
    try                                     %File saving error catching
        saveas(gcf,[tok '_argand' rem]);    %Save file
    catch
        disp(['Error writing file: ' pfile ' Check file extension.']);
    end
    close all                               %Close plot
    drawnow                                 %Flush graphics buffer

%**************************************************************************
%CREATE OUTPUT FILE
%**************************************************************************
function
write_txt(outfile,M,dfactor,nfreq,dfreq,Ec,R,Xo,Xt,yout,dS,ferr,didx)
    dmark=32*ones(M,1);                 %ASCII vector of spaces
    dmark(didx)=42;                     %Mark with stars as proper
    fid = fopen(outfile,'w');           %Open file stream for writing
    if fid==-1                          %File stream error checking
        disp('Error opening output file for reporting.  No report created.
Output printed to screen.');
        fid=1;                          %fid=1 prints data to screen
    end
    fprintf(fid,'MODEL ORDER:\r\n');        %Data labeling
    fprintf(fid,'%6.0f\r\n',M);             %Write model order
    fprintf(fid,'\r\n');                    %Line feed carriage return
    fprintf(fid,'RMS ERROR:\r\n');          %Data labeling
    fprintf(fid,'%6.6f\r\n',ferr);          %Write fitting error
    fprintf(fid,'\r\n');                    %Line feed carriage return
    fprintf(fid,'DAMPING FACTORS:\r\n');    %Data labeling
    fprintf(fid,'%6.6f\r\n',dfactor);       %Write damping factors
    fprintf(fid,'\r\n');                    %Line feed carriage return
    fprintf(fid,'NATURAL FREQUENCIES (Hz):\r\n');%Data labeling
    fprintf(fid,'%6.6f\r\n',nfreq);         %Write natural frequencies
    fprintf(fid,'\r\n');                    %Line feed carriage return
    fprintf(fid,'DAMPED FREQUENCIES (Hz):\r\n'); %Data labeling
    fprintf(fid,'%6.6f\r\n',dfreq);         %Write damped frequencies
    fprintf(fid,'\r\n');                    %Line feed carriage return
    fprintf(fid,'EIGENVALUES (cont.):\r\n');%Data labeling
    fprintf(fid,'%6.6f%+6.6fj%c\r\n',[real(Ec),imag(Ec),dmark]'); %Write
eigenvalues
    fprintf(fid,'\r\n');                    %Line feed carriage return
    fprintf(fid,'RESIDUALS (cont.):\r\n');  %Data labeling

fprintf(fid,'%6.6f%+6.6fj\t(%6.6f)%c\r\n',[real(R),imag(R),abs(R),dmark]');
%Write residuals (complex amplitudes)
```

```
    fprintf(fid,'\r\n');                    %Line feed carriage return
    fprintf(fid,'SINGULAR VALUES:\r\n');    %Data labeling
    fprintf(fid,'%6.6f\r\n',dS);            %Write singular values
    fprintf(fid,'\r\n');                    %Line feed carriage return
    fprintf(fid,'ORIGINAL SIGNAL:\r\n');    %Data labeling
    fprintf(fid,'%6.6f\r\n',Xo);            %Repeat original signal (for
convenience)
    fprintf(fid,'\r\n');                    %Line feed carriage return
    fprintf(fid,'ESTIMATED SIGNAL:\r\n');   %Data labeling
    fprintf(fid,'%6.6f\r\n',Xt+yout);       %Write estimated signal
    if fid~=1
        status = fclose(fid);               %Close file stream
    end
```

Appendix X: Single Channel Matrix Pencil Analysis of WECC Tests and Florida Blackout

Table X-1: WECC test D1 FDR data.

	Argand Diagram	Plot of Signal and Modes	Singular Values
FDR 5: Seattle, WA	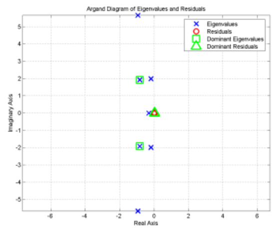	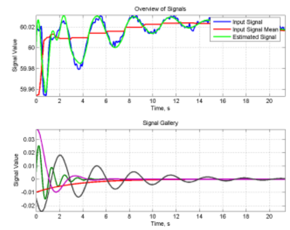	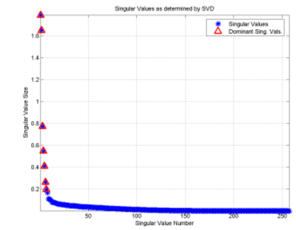
FDR 8: Palo Alto, CA	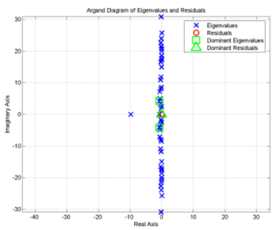	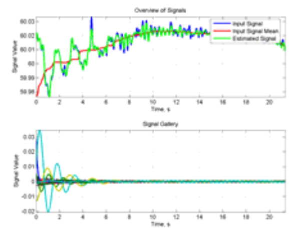	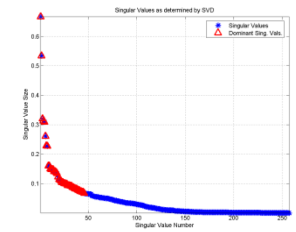
FDR 14: Tempe, AZ	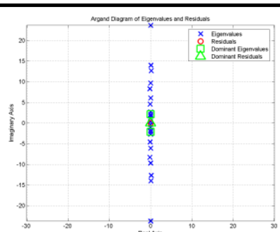	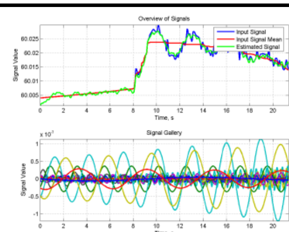	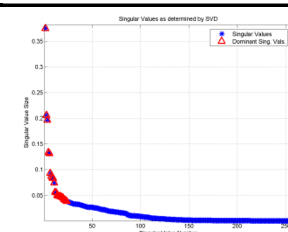
FDR 16: Pullman, WA	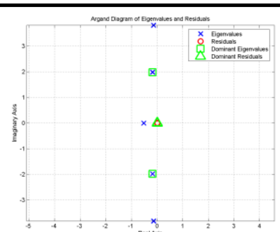	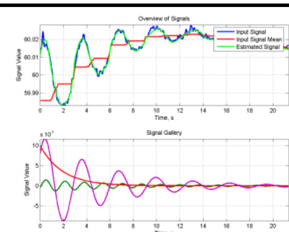	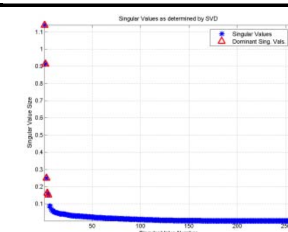

Table X-2: WECC test D1 PMU data.

	Argand Diagram	Plot of Signal and Modes	Singular Values
Big Eddy 230kV PMU	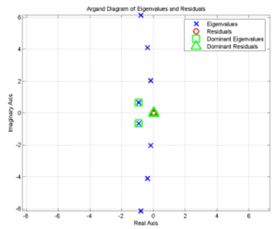	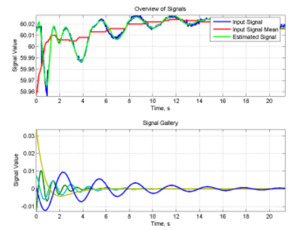	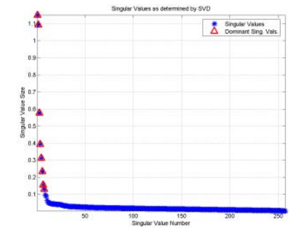
Big Eddy 500kV PMU	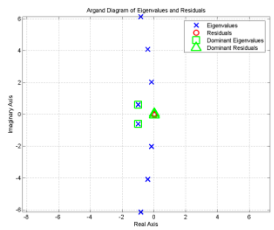	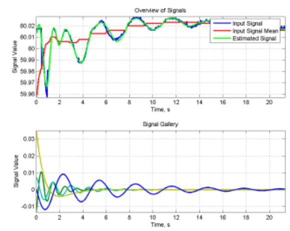	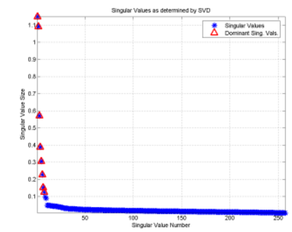
Colstrip PMU	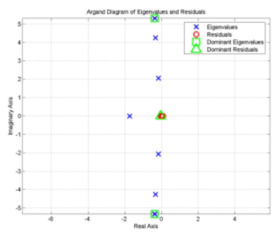	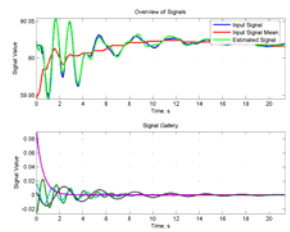	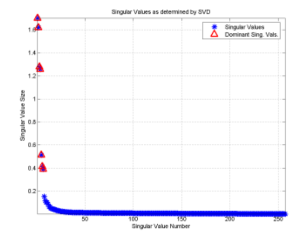
Grand Coulee Dam PMU	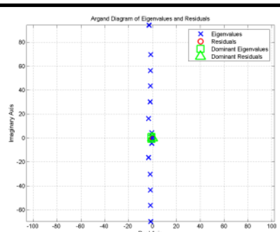	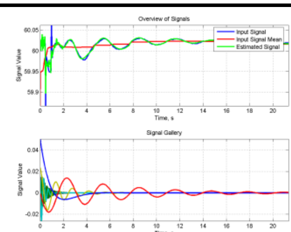	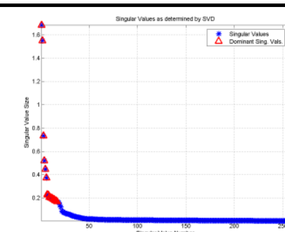

Malin PMU	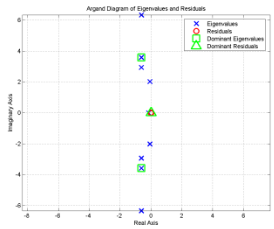	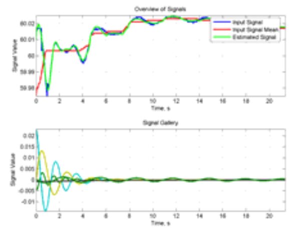	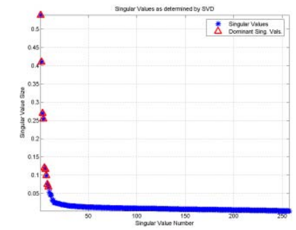
Maple Valley PMU	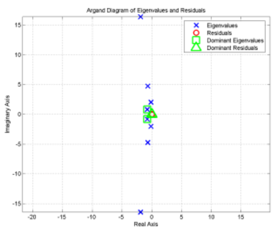	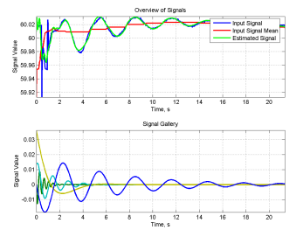	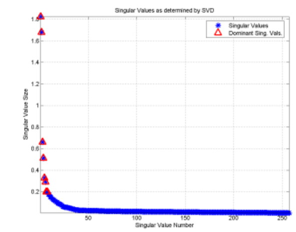
Vincent PMU	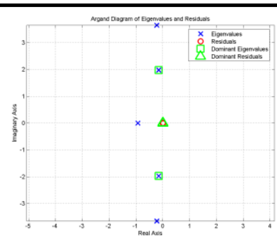	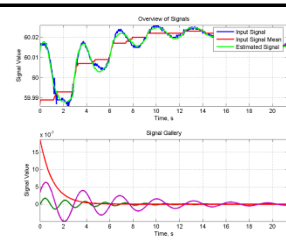	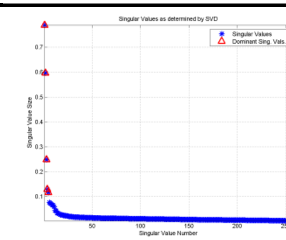
Sylmar PMU	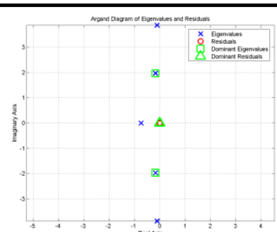	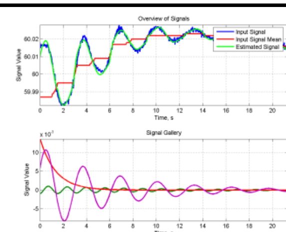	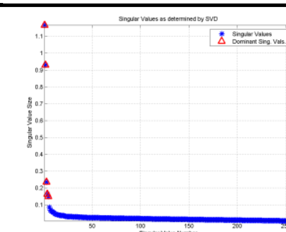

Table X-3: WECC test D2 FDR data.

	Argand Diagram	Plot of Signal and Modes	Singular Values
FDR 5: Seattle, WA	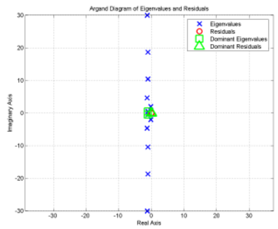	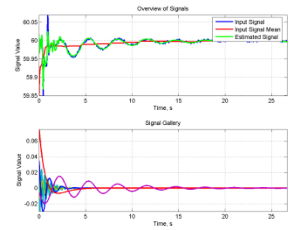	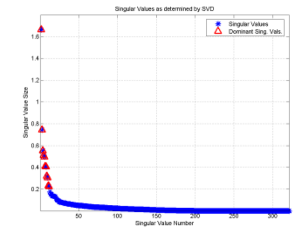
FDR 8: Palo Alto, CA	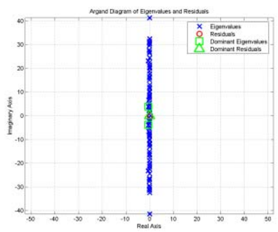	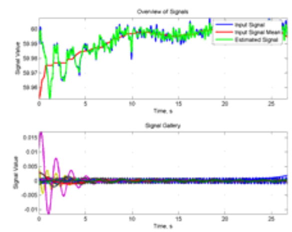	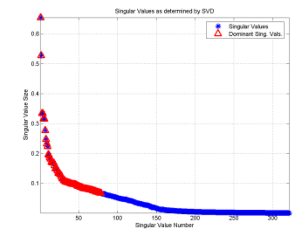
FDR 14: Tempe, AZ	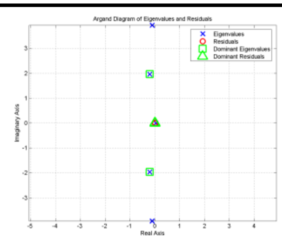	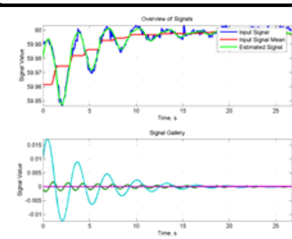	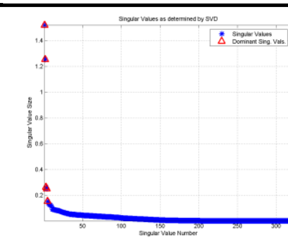
FDR 16: Pullman, WA	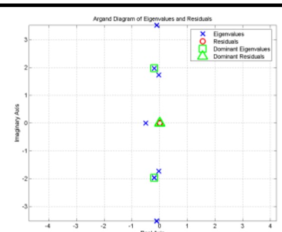	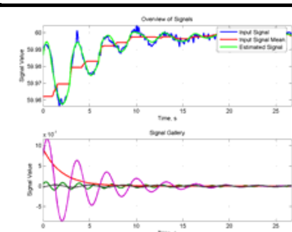	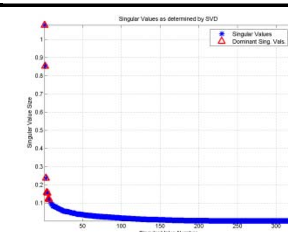

Table X-4: WECC test D2 PMU data.

	Argand Diagram	Plot of Signal and Modes	Singular Values
Big Eddy 230kV PMU	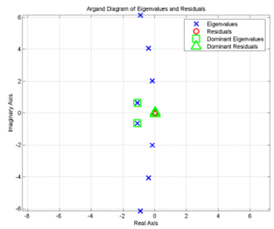	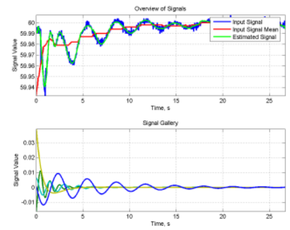	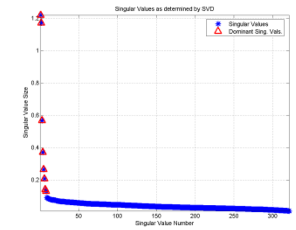
Big Eddy 500kV PMU	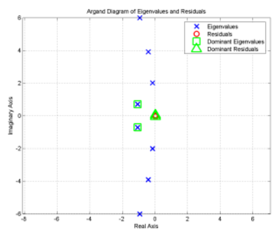	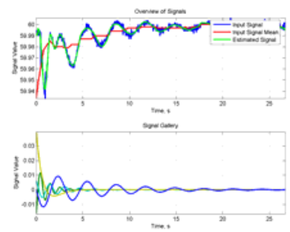	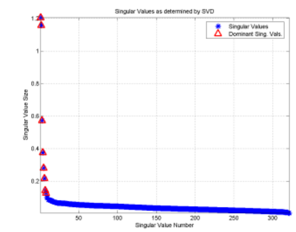
Colstrip PMU	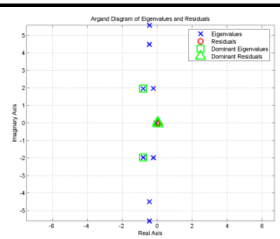	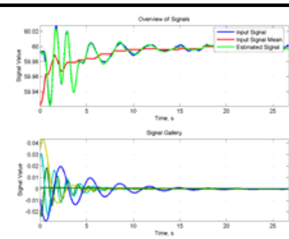	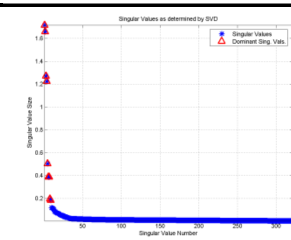
Grand Coulee Dam PMU	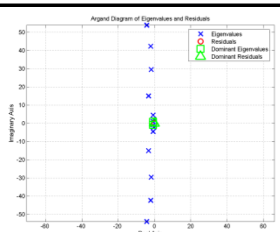	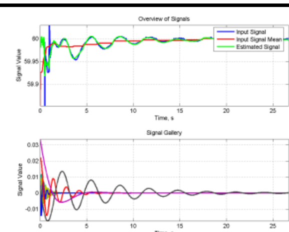	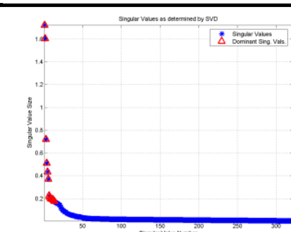

Malin PMU	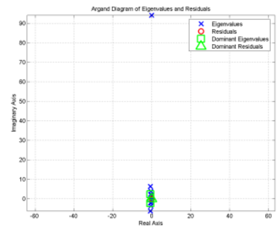	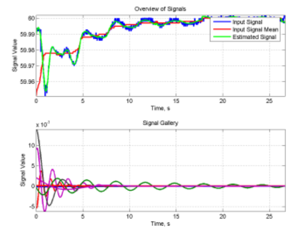	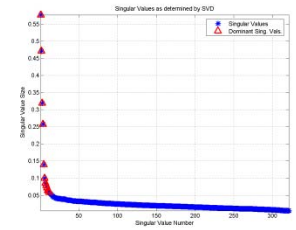
Maple Valley PMU	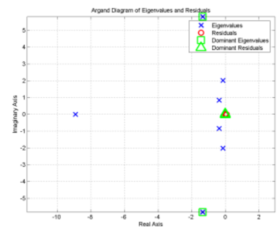	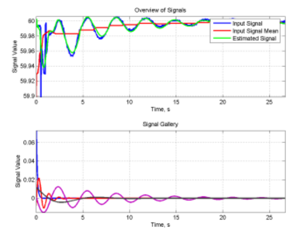	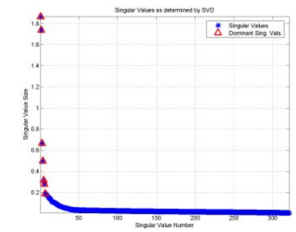
Vincent PMU	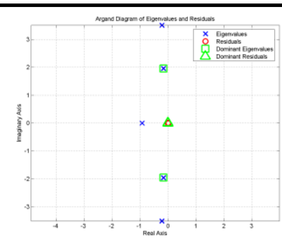	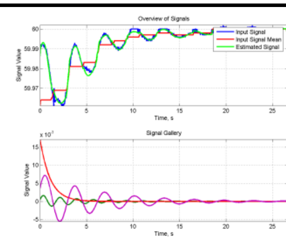	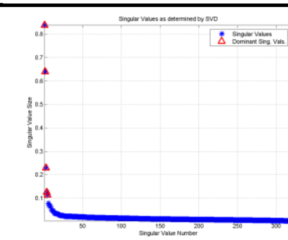
Sylmar PMU	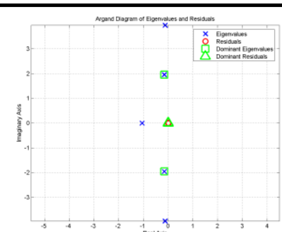	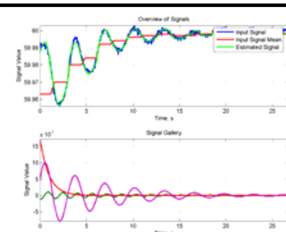	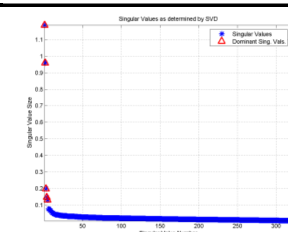

Table X-5: WECC test D4 FDR data.

	Argand Diagram	Plot of Signal and Modes	Singular Values
FDR 5: Seattle, WA	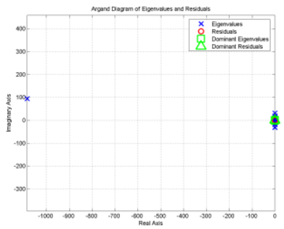	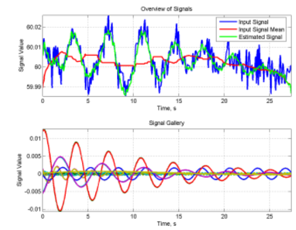	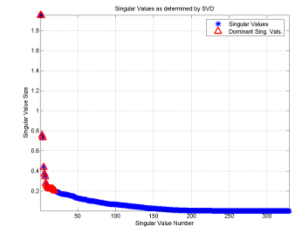
FDR 8: Palo Alto, CA	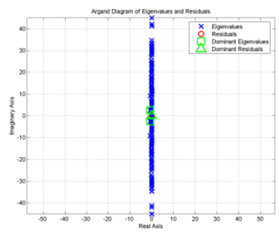	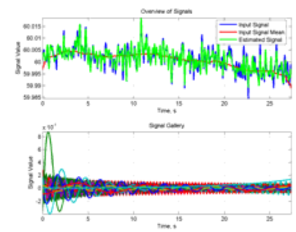	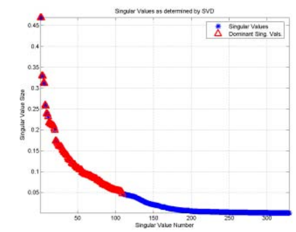
FDR 14: Tempe, AZ	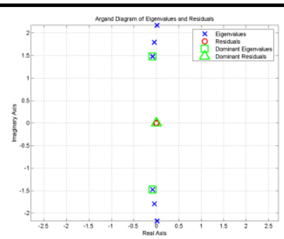	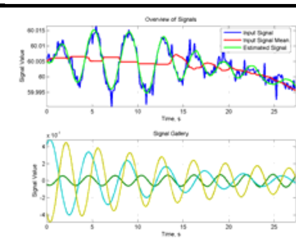	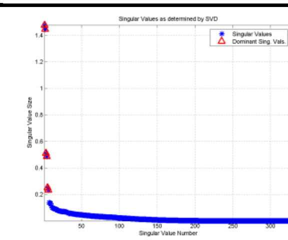
FDR 16: Pullman, WA	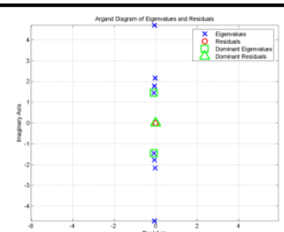	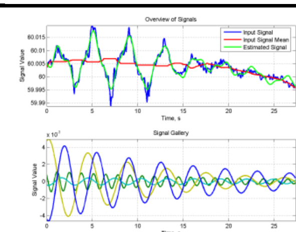	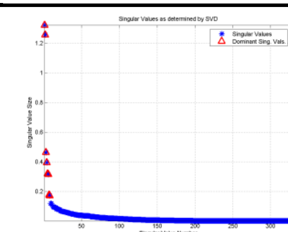

Table X-6: WECC test D4 PMU data.

	Argand Diagram	Plot of Signal and Modes	Singular Values
Big Eddy 230kV PMU	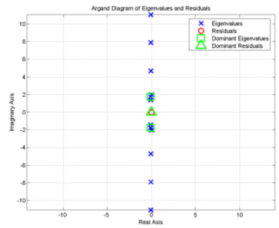	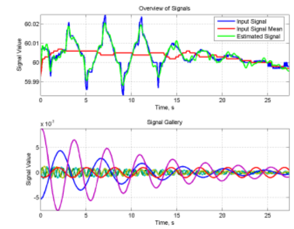	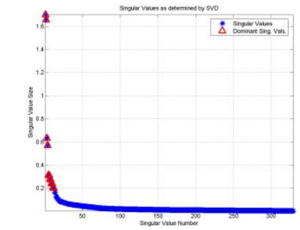
Big Eddy 500kV PMU	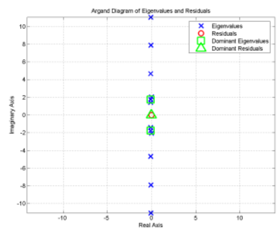	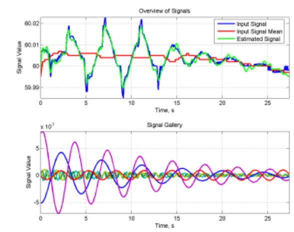	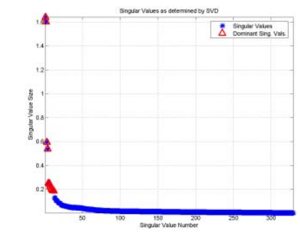
Colstrip PMU	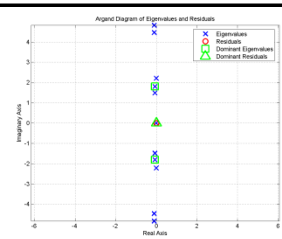	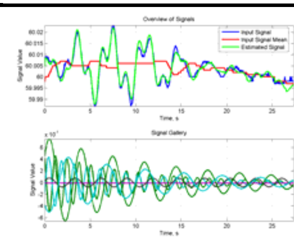	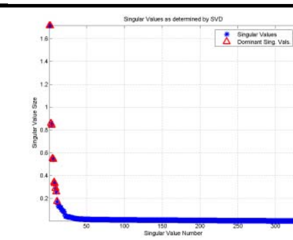
Grand Coulee Dam PMU	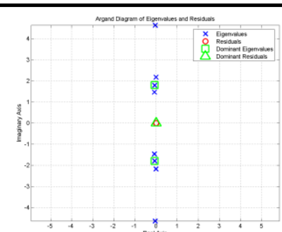	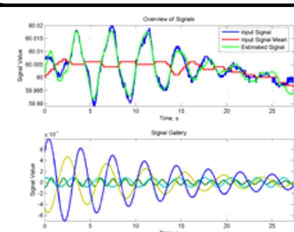	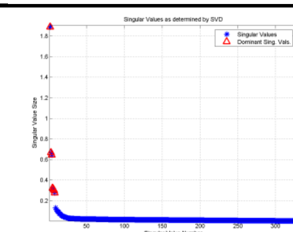

Malin PMU

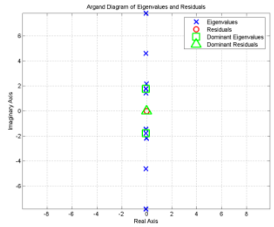

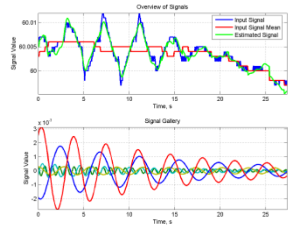

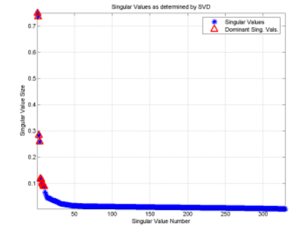

Maple Valley PMU

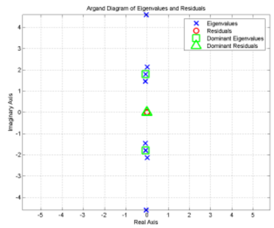

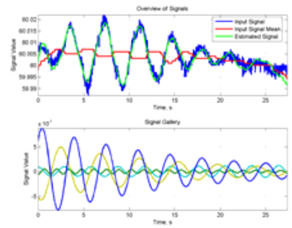

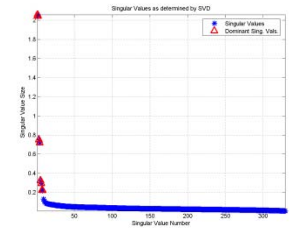

Vincent PMU

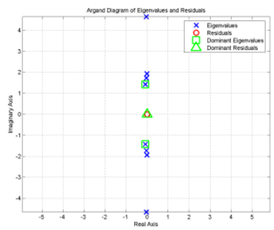

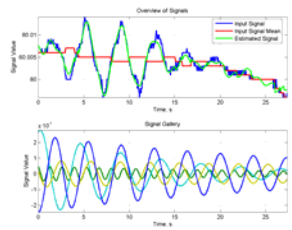

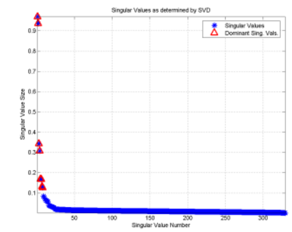

Sylmar PMU

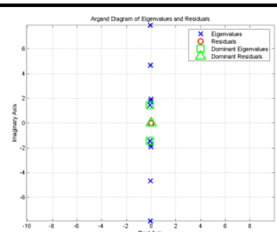

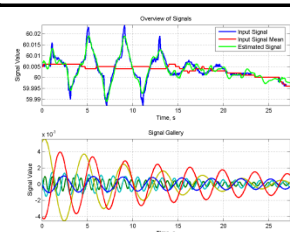

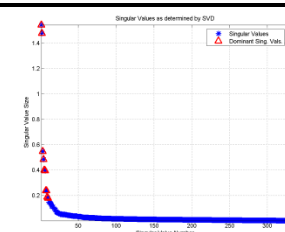

Table X-7: WECC test D5 FDR data.

	Argand Diagram	Plot of Signal and Modes	Singular Values
FDR 5: Seattle, WA	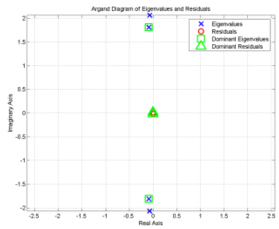	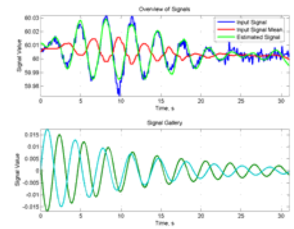	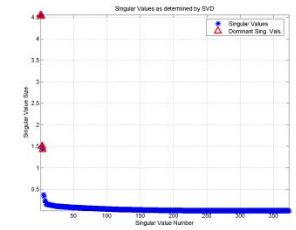
FDR 8: Palo Alto, CA	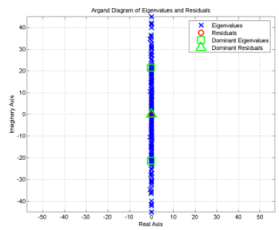	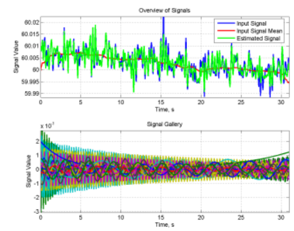	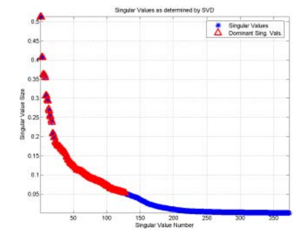
FDR 14: Tempe, AZ	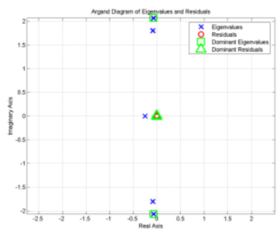	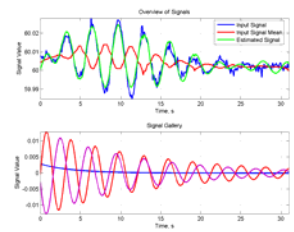	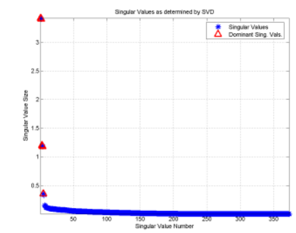
FDR 16: Pullman, WA	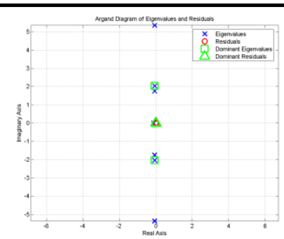	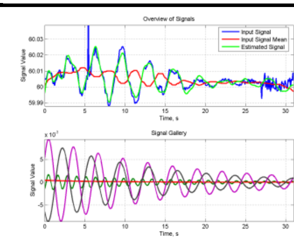	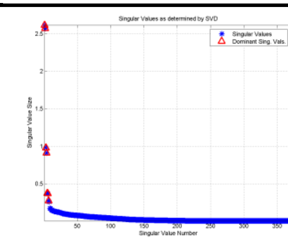

Table X-8: WECC test D5 PMU data.

	Argand Diagram	Plot of Signal and Modes	Singular Values
Big Eddy 230kV PMU	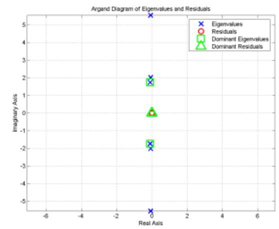	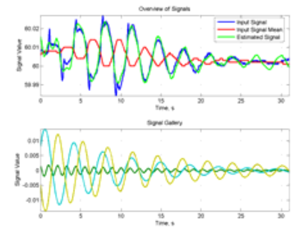	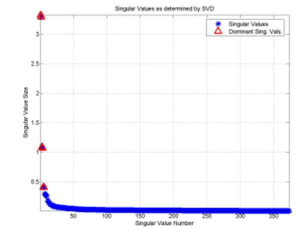
Big Eddy 500kV PMU	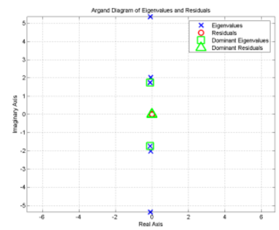	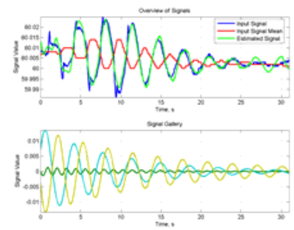	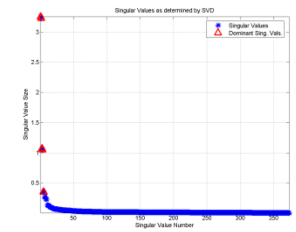
Colstrip PMU	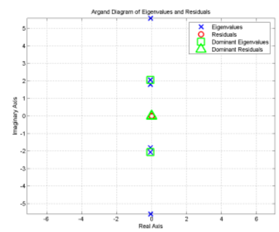	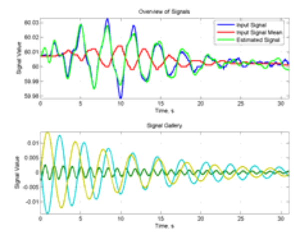	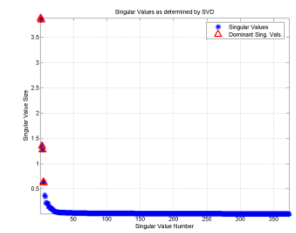
Grand Coulee Dam PMU	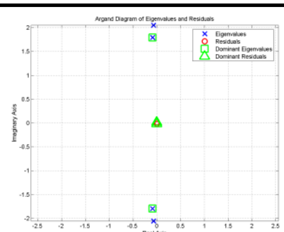	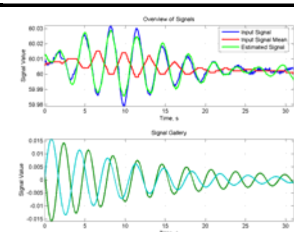	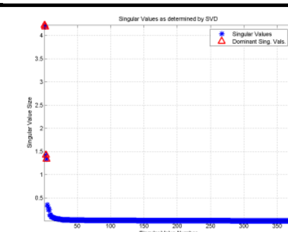

Malin PMU	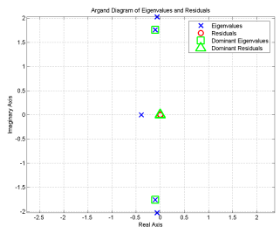	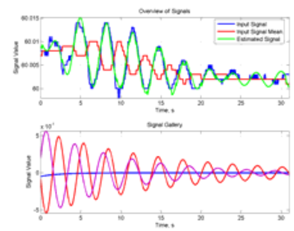	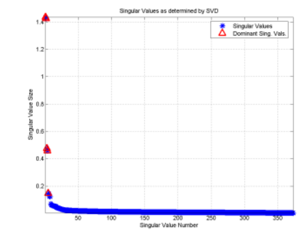
Maple Valley PMU	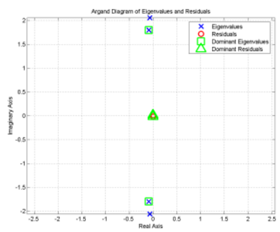	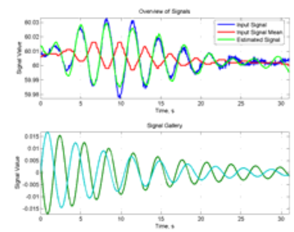	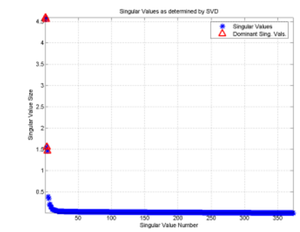
Vincent PMU	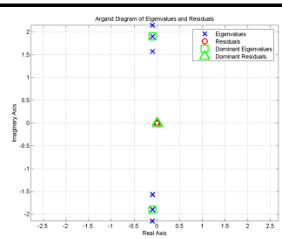	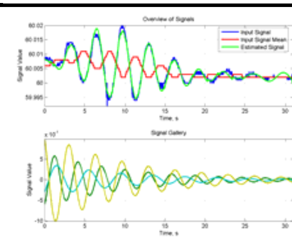	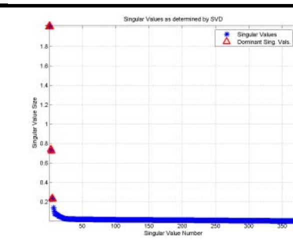
Sylmar PMU	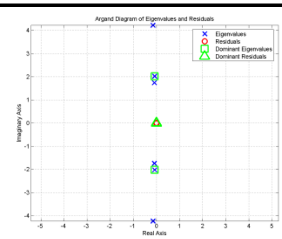	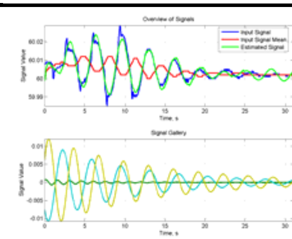	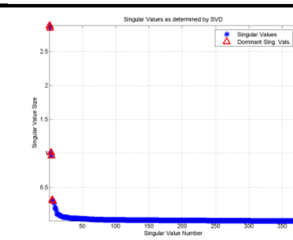

Table X-9: Florida blackout FDR data.

	Argand Diagram	Plot of Signal and Modes	Singular Values
FDR 11: Grand Rapids, MI	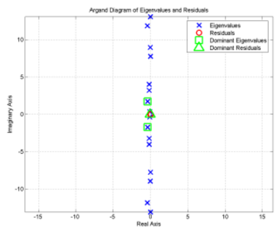	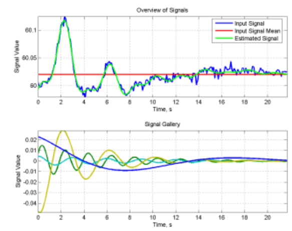	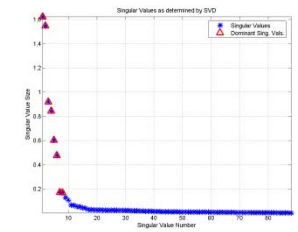
FDR 13: Carmel, IN	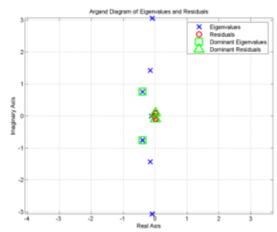	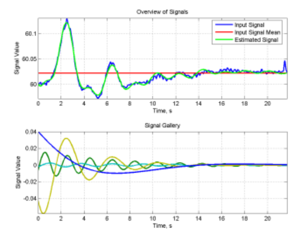	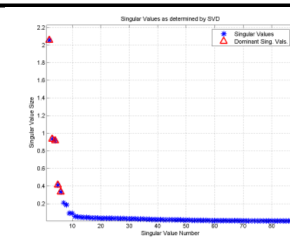
FDR 2: Rolla, MO	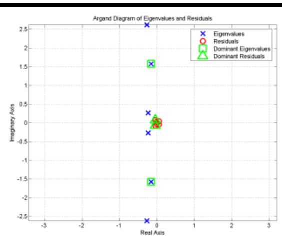	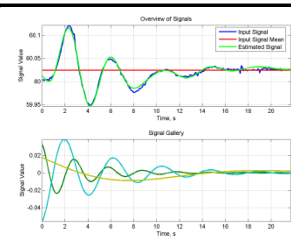	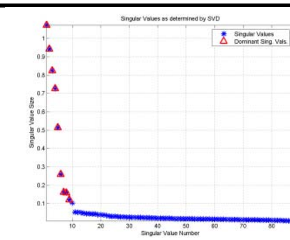
FDR 3: Vienna, VA	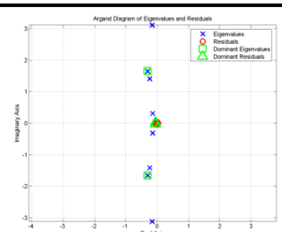	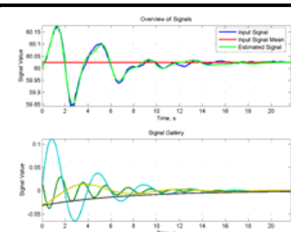	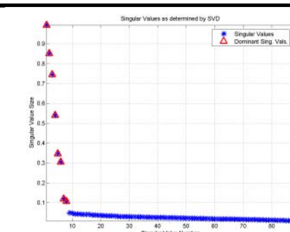

FDR 35: Ames, IA	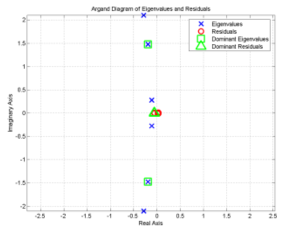	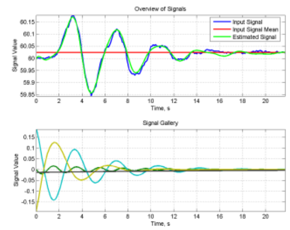	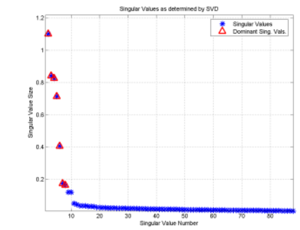
FDR 38: Holyoke, MA	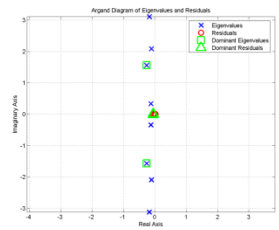	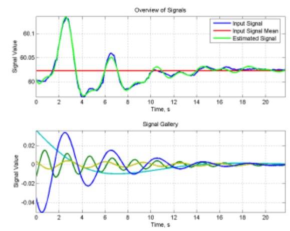	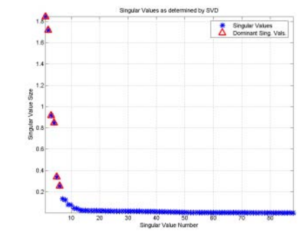
FDR 4: Blacksburg, VA	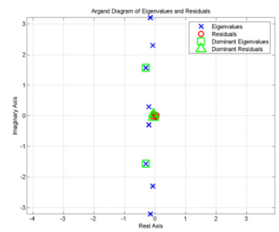	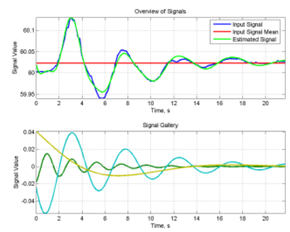	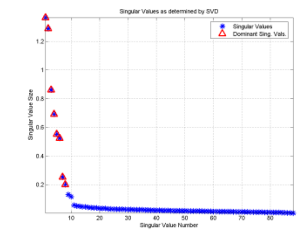
FDR 40: St. Paul, MN	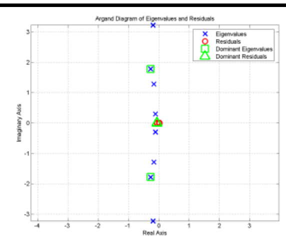	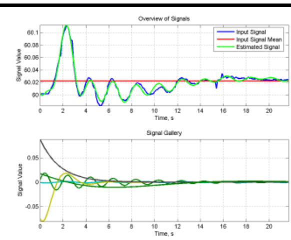	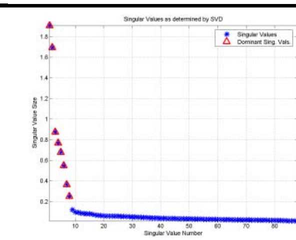
FDR 41: Winnipeg, MB	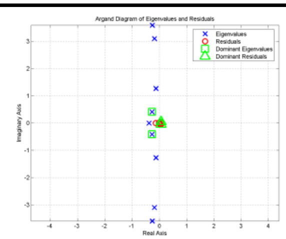	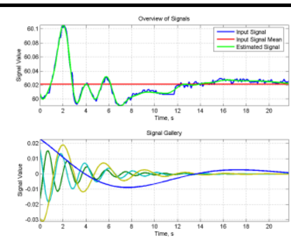	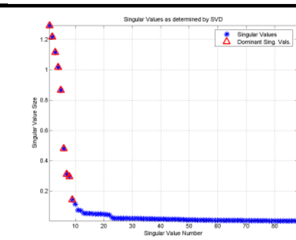

FDR 42: Tallahassee, FL	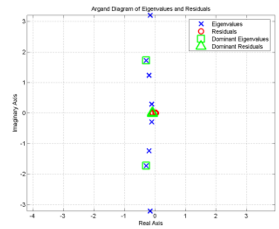	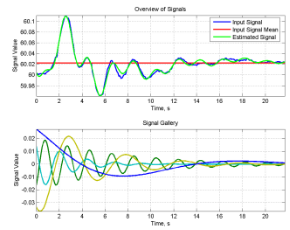	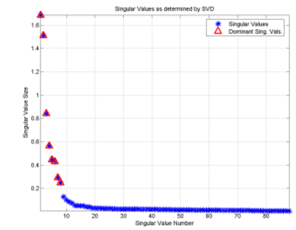
FDR 43: Bismarck, ND	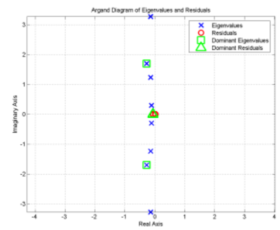	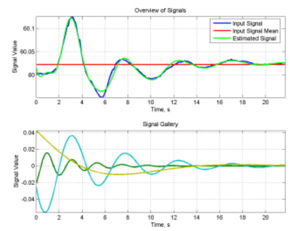	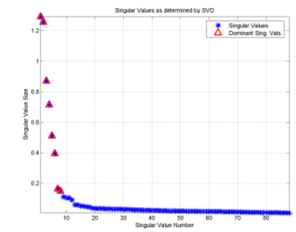
FDR 500: Chicago, IL	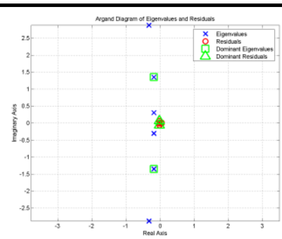	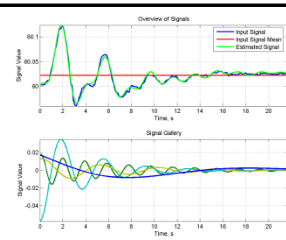	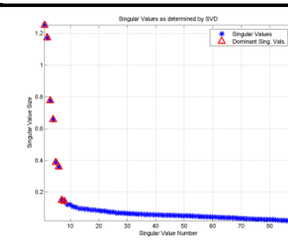
FDR 503: Danbury, CT	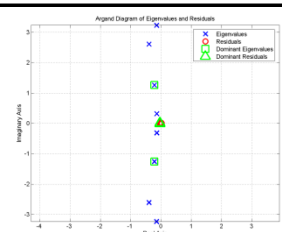	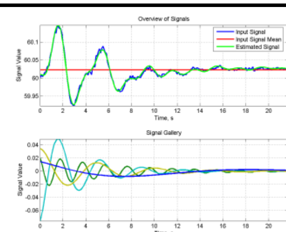	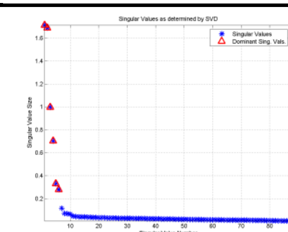
FDR 509: Morgantown, WV	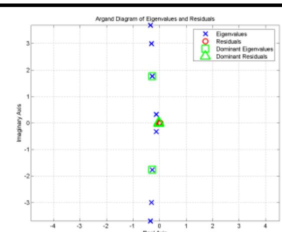	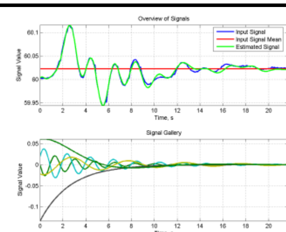	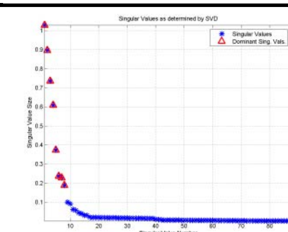

FDR 510: Blacksburg, VA	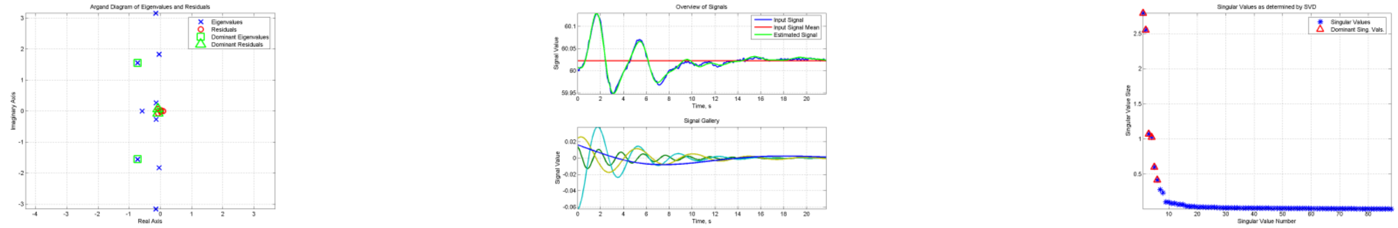
FDR 513: University Park, PA	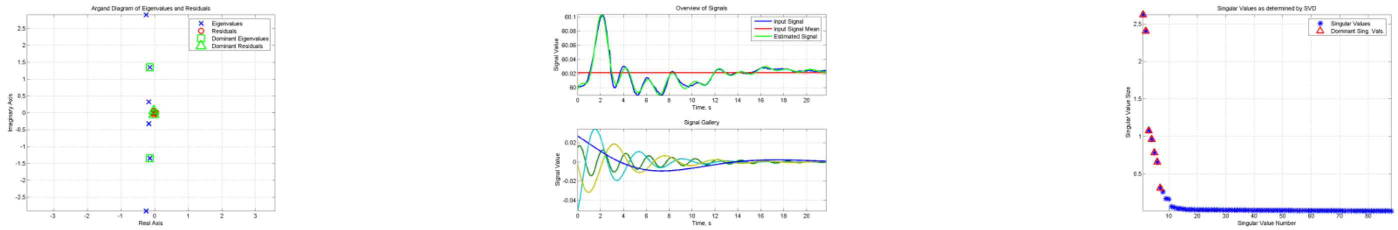
FDR 516: LeRoy, NY	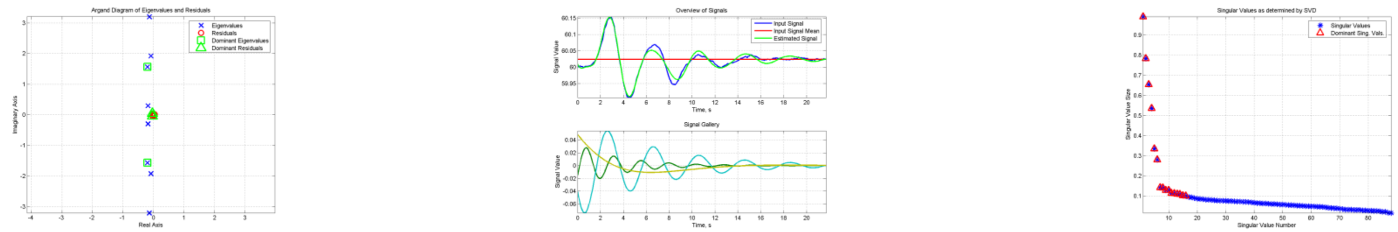
FDR 523: Cookeville, TN	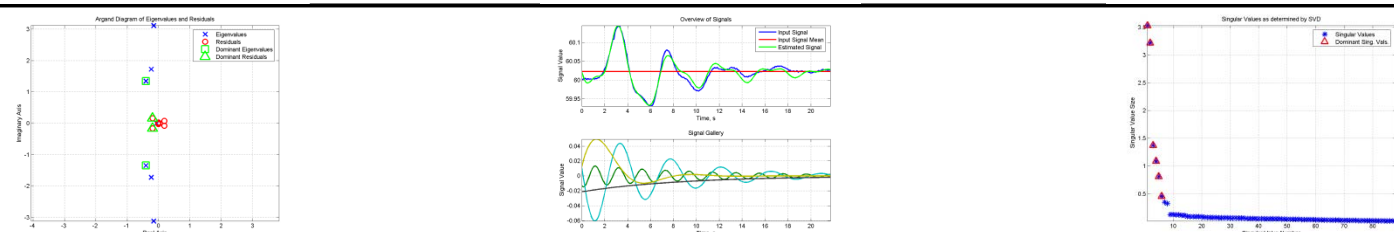
FDR 526: Birmingham, AL	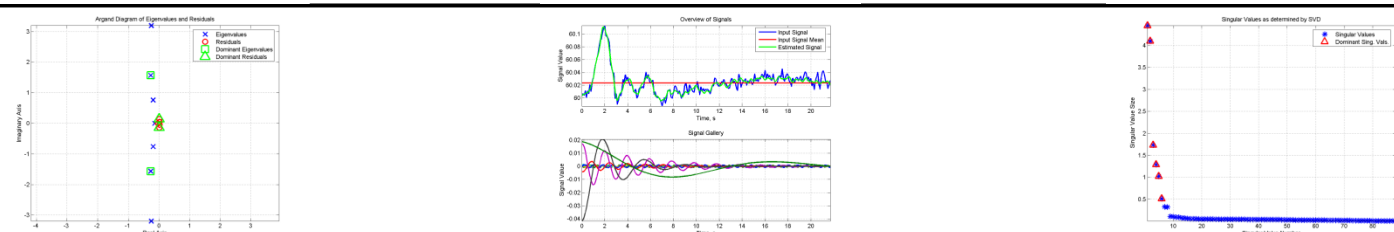

FDR 535: Norristown, PA	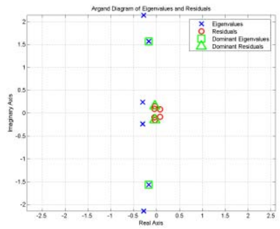	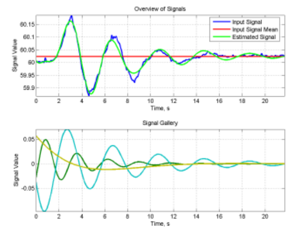	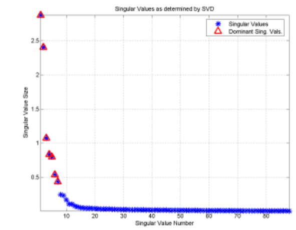
FDR 7: Jackson, MS	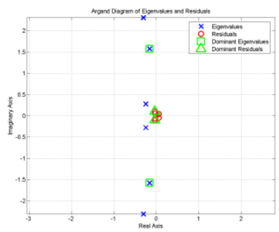	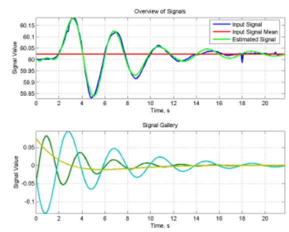	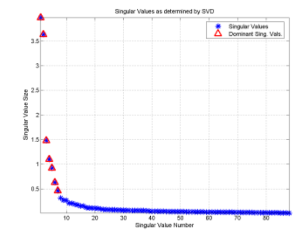

Table X-10: Florida blackout PMU data.

	Argand Diagram	Plot of Signal and Modes	Singular Values
Baker PMU	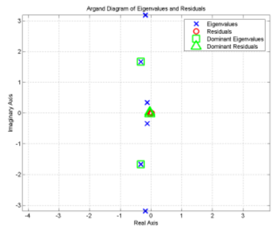	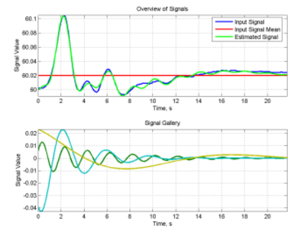	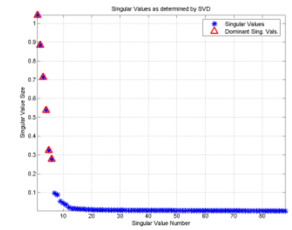
Culloden PMU	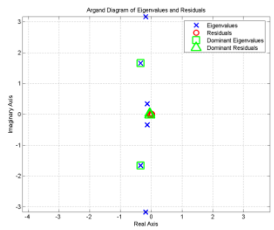	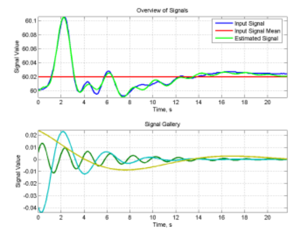	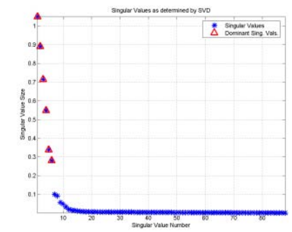
Jackson's Ferry PMU	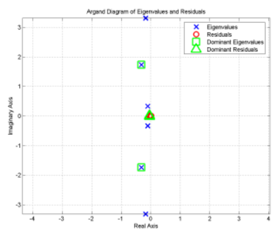	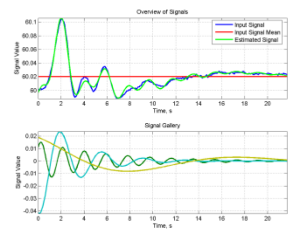	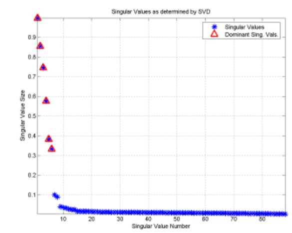
Kanawha River PMU	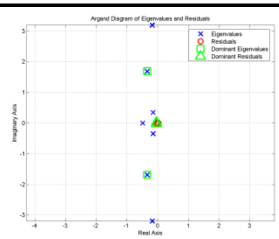	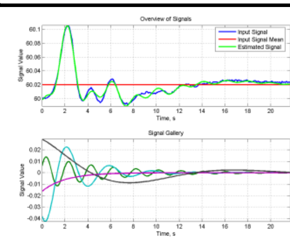	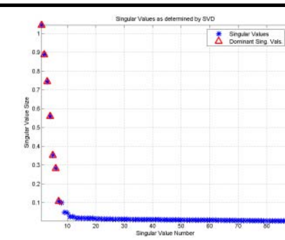

Matt Funk PMU	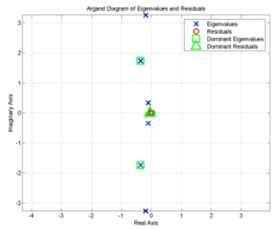	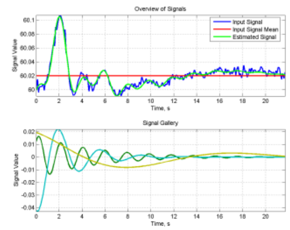	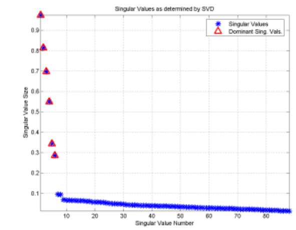
Orange PMU	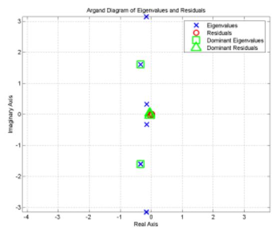	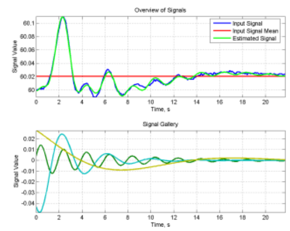	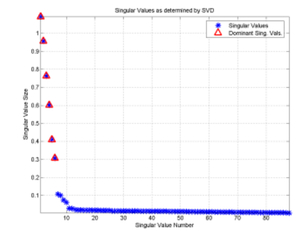
Rockport PMU	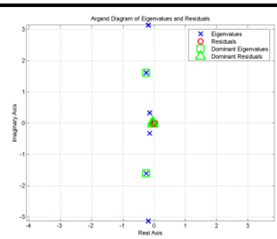	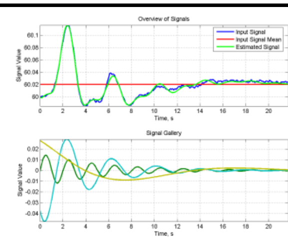	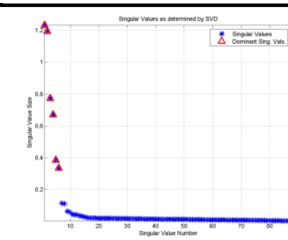

Appendix XI: Multiple Channel Matrix Pencil Analysis of WECC Tests and Florida Blackout

Table XI-1: WECC test D1 FDR data.

	Signals and Modes (FDRs only)	Signals and Modes (FDRs and PMUs)
FDR 5: Seattle, WA	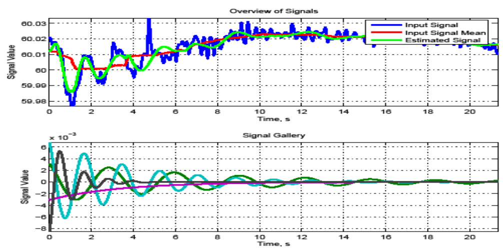	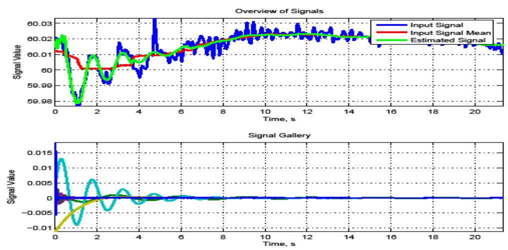
FDR 8: Palo Alto, CA	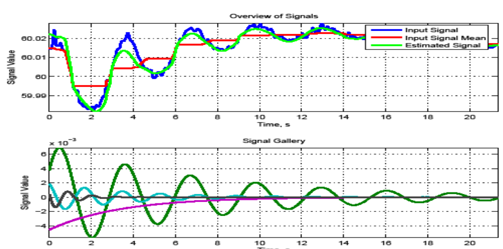	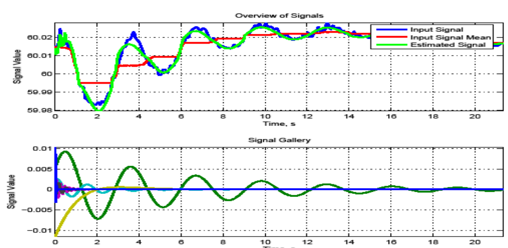

FDR 14: Tempe, AZ

FDR 16: Pullman, WA

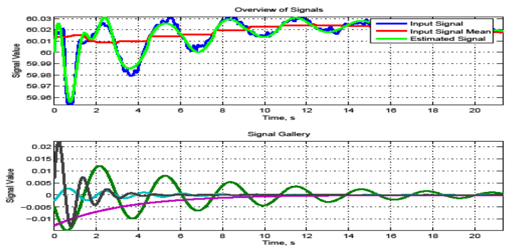

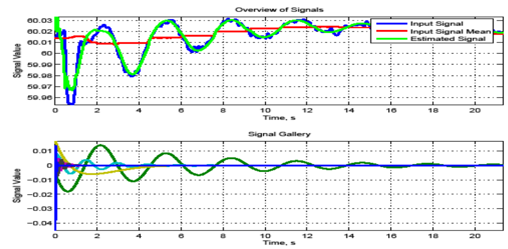

Table XI-2: WECC test D1 PMU data.

	Signals and Modes (PMUs only)	Signals and Modes (FDRs and PMUs)
Big Eddy 230kV PMU	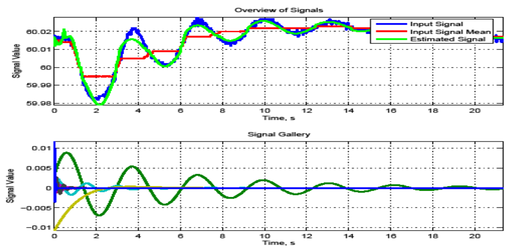	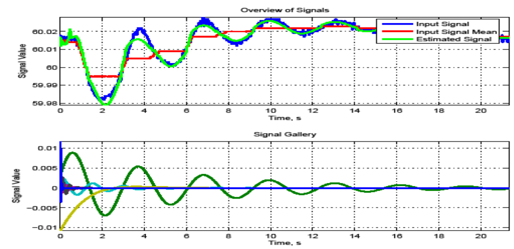
Big Eddy 500kV PMU	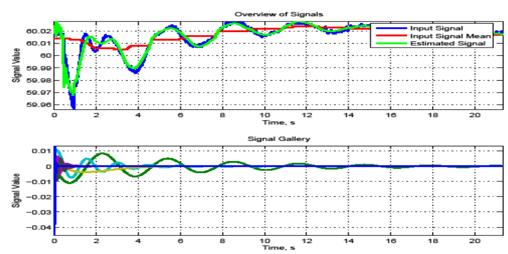	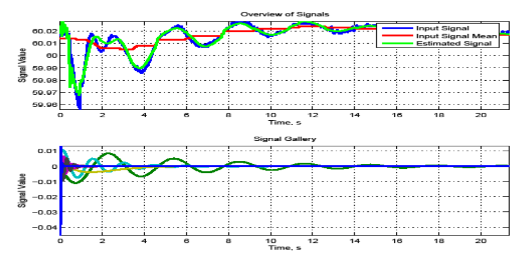

Colstrip PMU	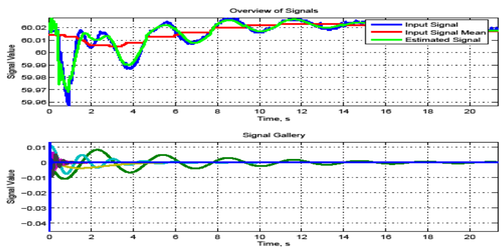	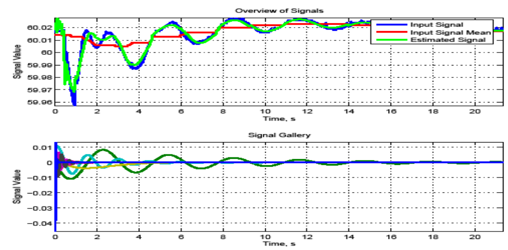
Grand Coulee Dam PMU	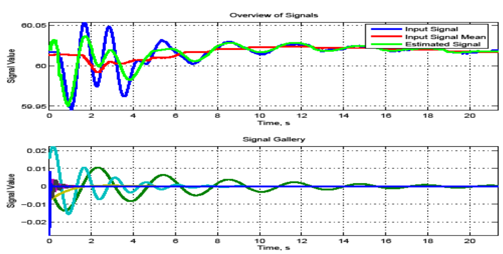	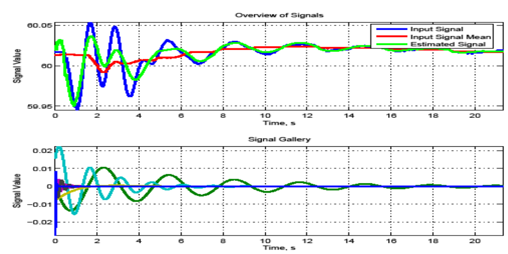

Malin PMU	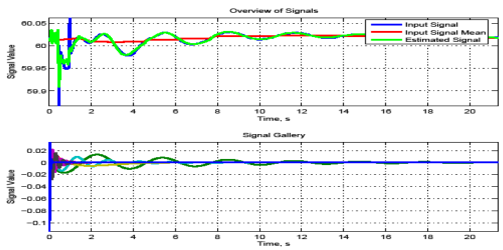	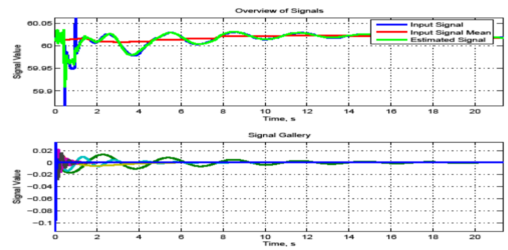
Maple Valley PMU	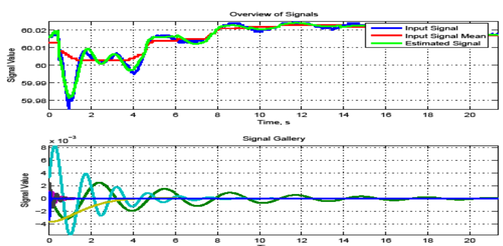	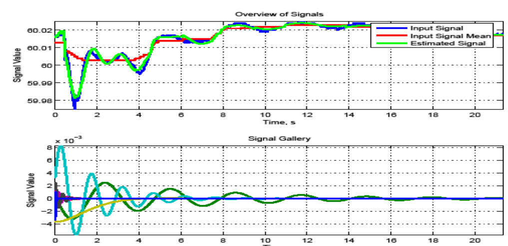

Vincent PMU

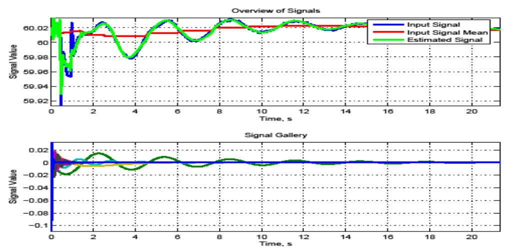

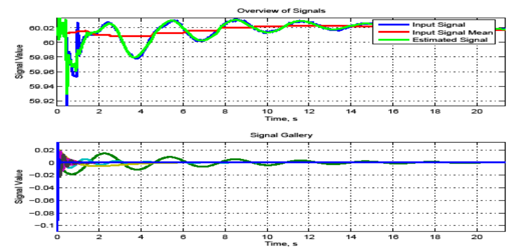

Sylmar PMU

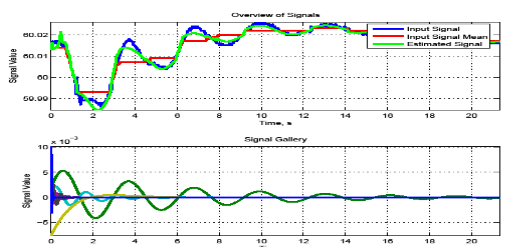

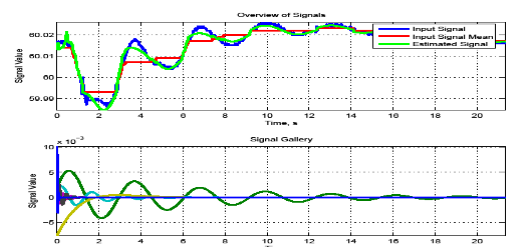

Table XI-3: WECC test D2 FDR data.

<table>
<tr><th></th><th>Signals and Modes (FDRs only)</th><th>Signals and Modes (FDRs and PMUs)</th></tr>
<tr><td>FDR 5: Seattle, WA</td><td>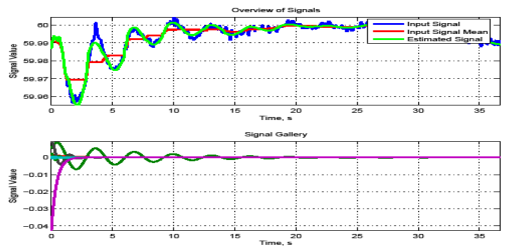
</td><td>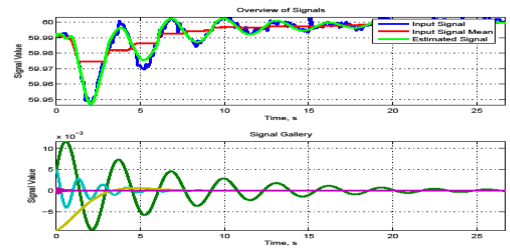
</td></tr>
<tr><td>FDR 8: Palo Alto, CA</td><td>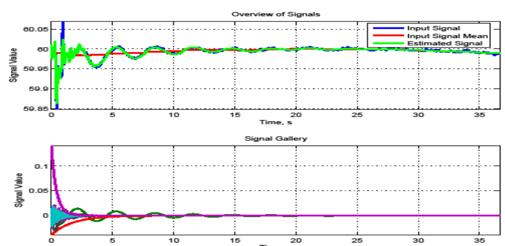
</td><td>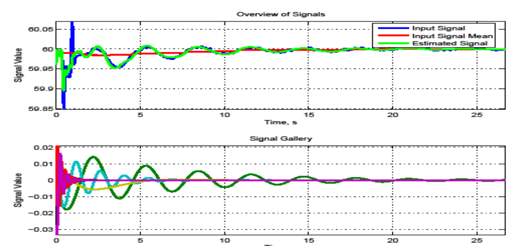
</td></tr>
</table>

FDR 14: Tempe, AZ

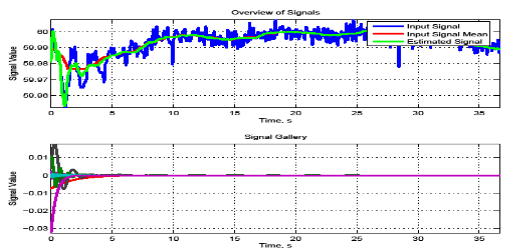

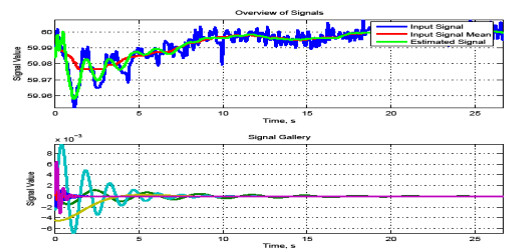

FDR 16: Pullman, WA

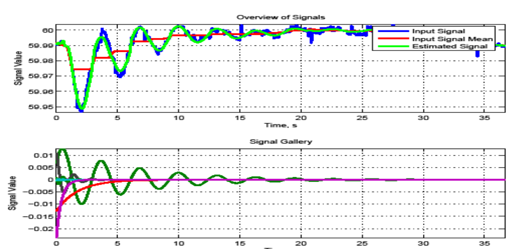

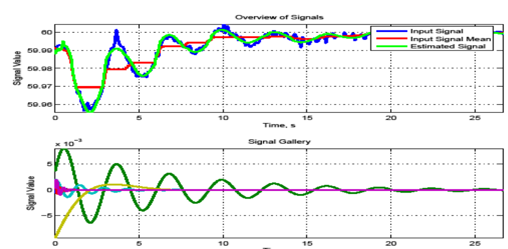

Table XI-4: WECC test D2 PMU data.

	Signals and Modes (PMUs only)	Signals and Modes (FDRs and PMUs)
Big Eddy 230kV PMU	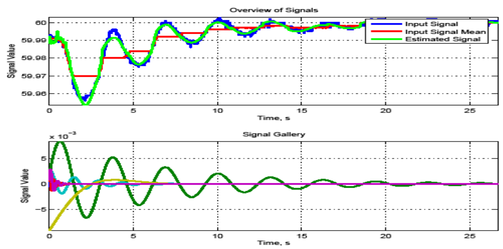	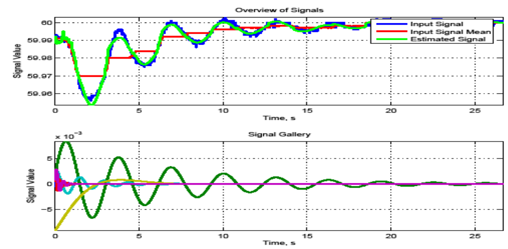
Big Eddy 500kV PMU	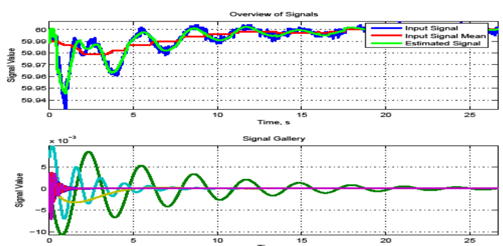	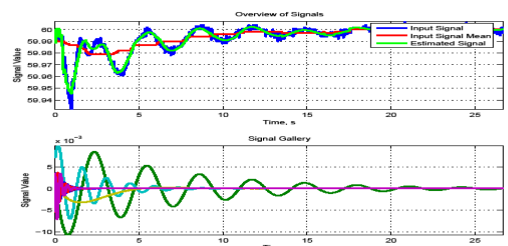

Colstrip PMU	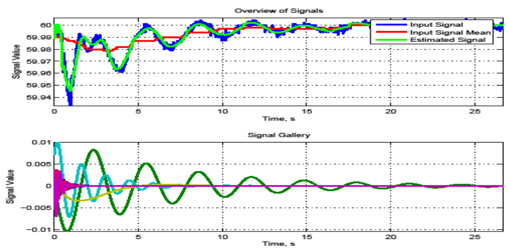	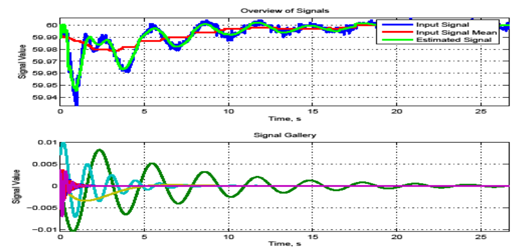
Grand Coulee Dam PMU	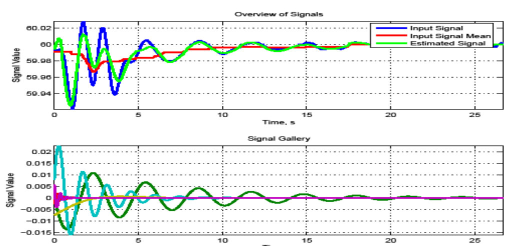	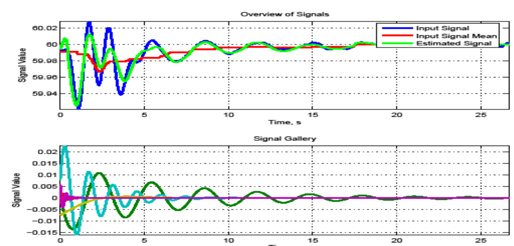

Malin PMU	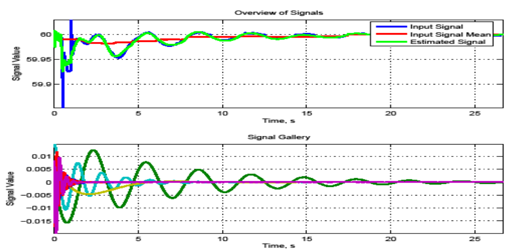	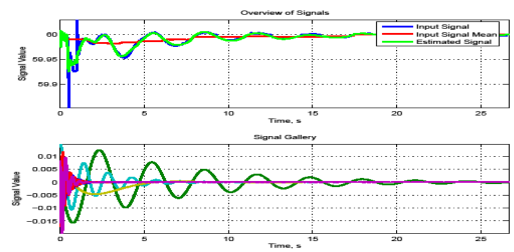
Maple Valley PMU	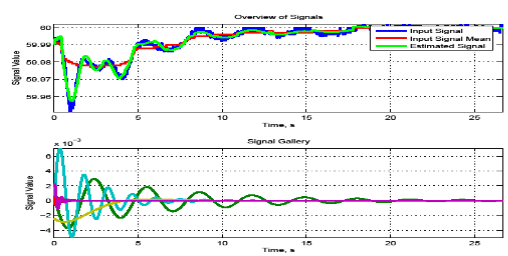	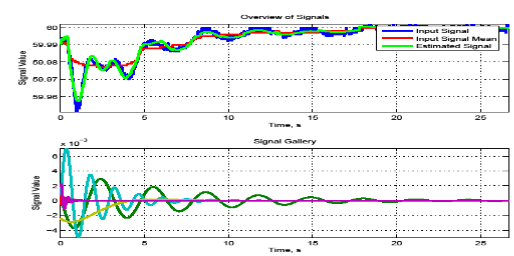

Vincent PMU	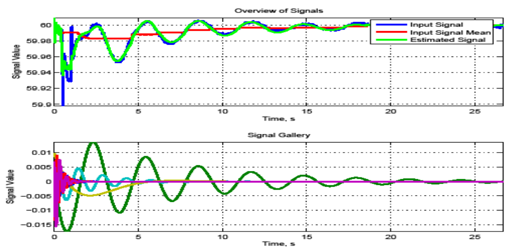	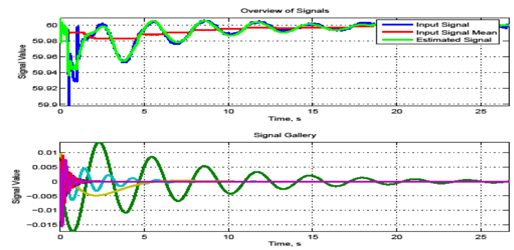
Sylmar PMU	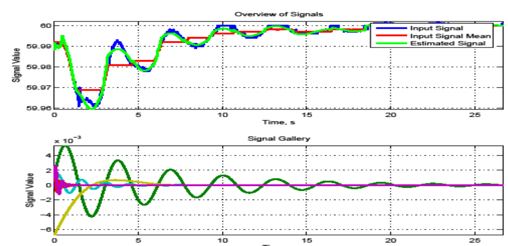	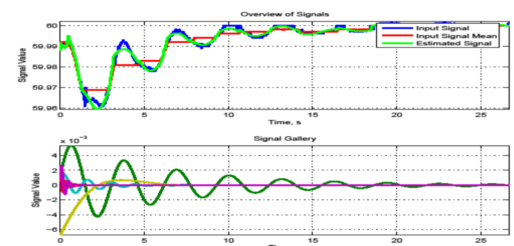

Table XI-5: WECC test D4 FDR data.

	Signals and Modes (FDRs only)	Signals and Modes (FDRs and PMUs)
FDR 5: Seattle, WA	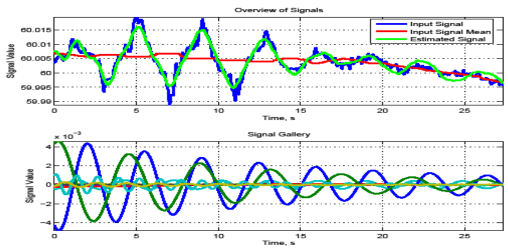	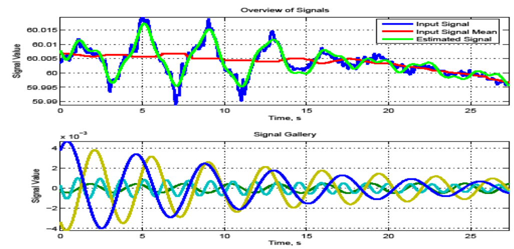
FDR 8: Palo Alto, CA	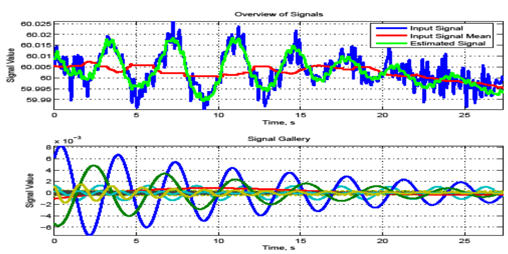	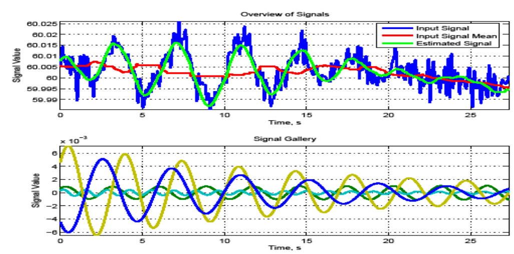

FDR 14: Tempe, AZ

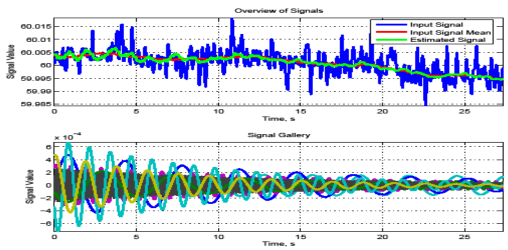

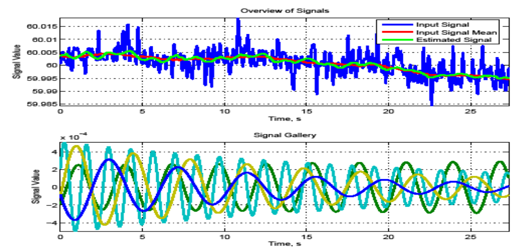

FDR 16: Pullman, WA

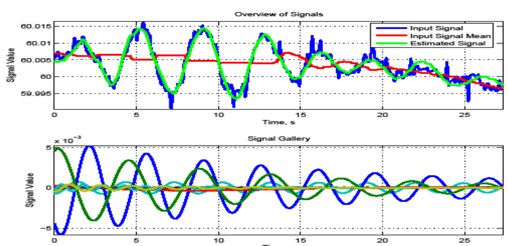

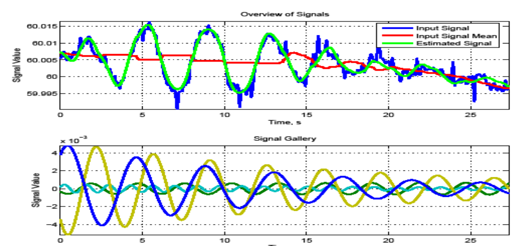

Table XI-6: WECC test D4 PMU data.

	Signals and Modes (PMUs only)	Signals and Modes (FDRs and PMUs)
Big Eddy 230kV PMU	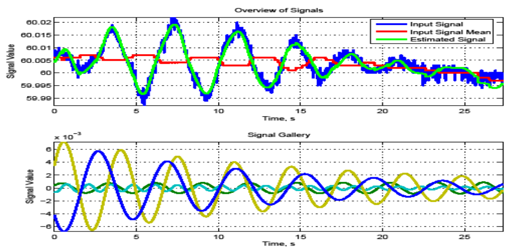	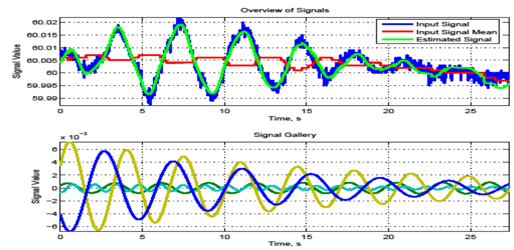
Big Eddy 500kV PMU	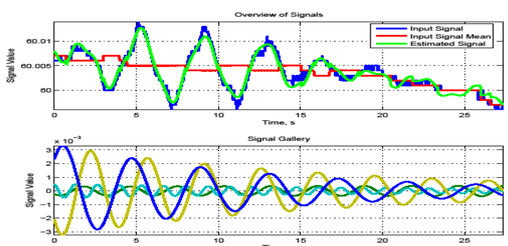	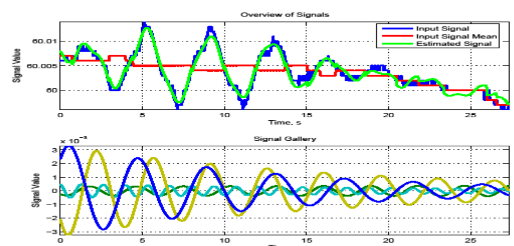

Colstrip PMU

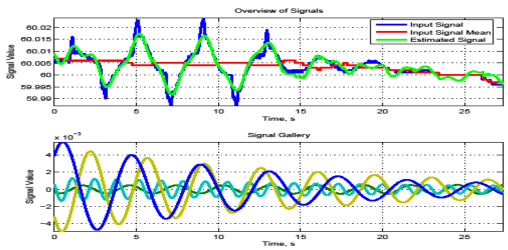

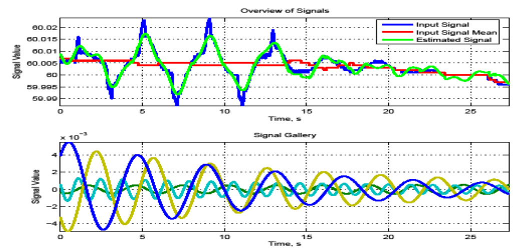

Grand Coulee Dam PMU

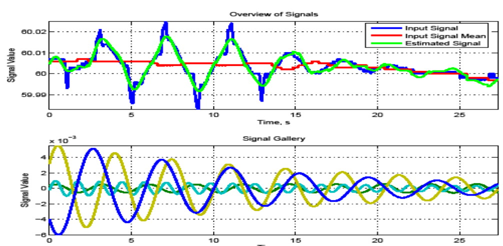

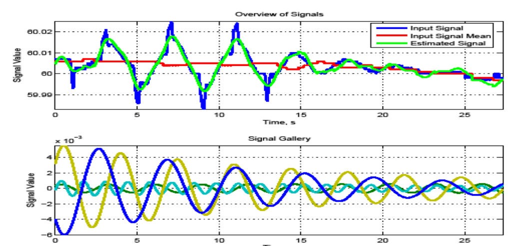

Malin PMU	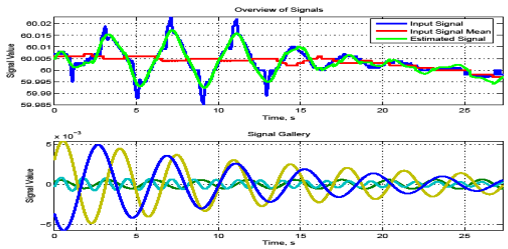	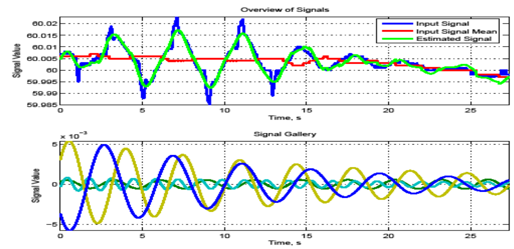
Maple Valley PMU	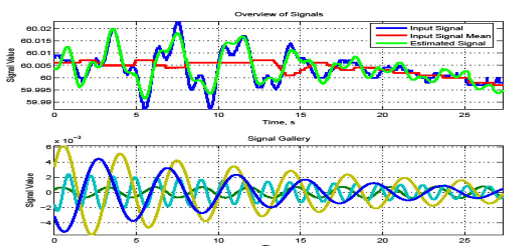	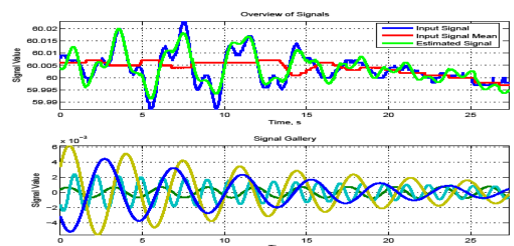

Vincent PMU

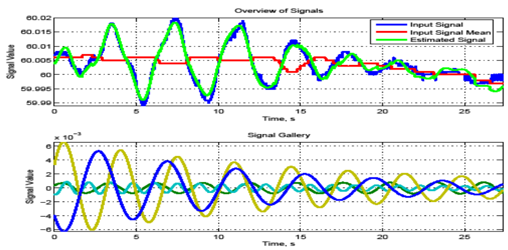

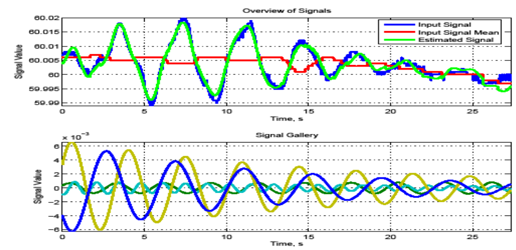

Sylmar PMU

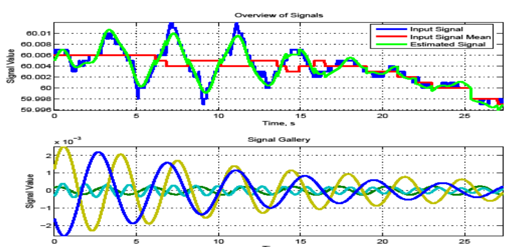

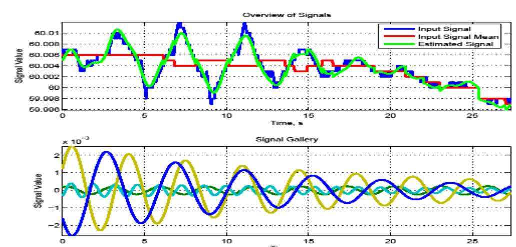

Table XI-7: WECC test D5 FDR data.

	Signals and Modes (FDRs only)	Signals and Modes (FDRs and PMUs)
FDR 5: Seattle, WA	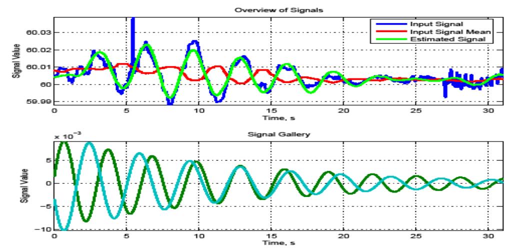	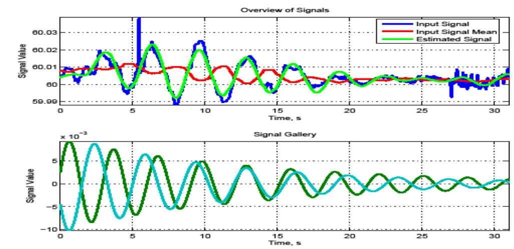
FDR 8: Palo Alto, CA	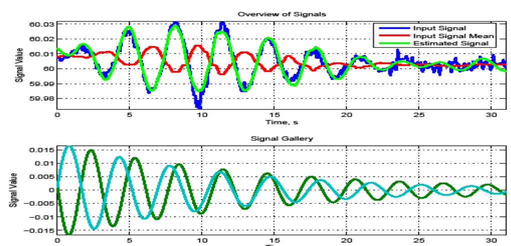	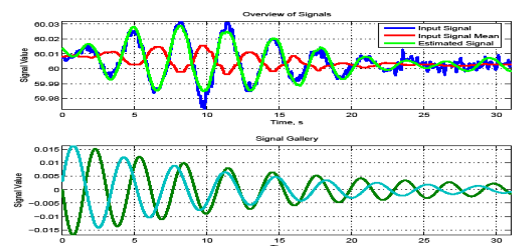

FDR 14: Tempe, AZ

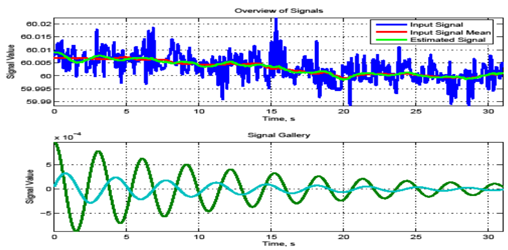

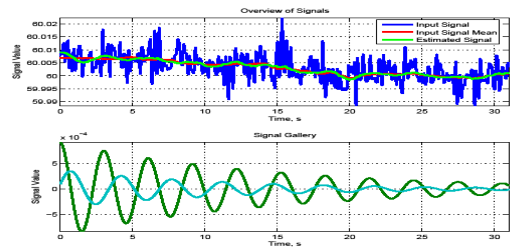

FDR 16: Pullman, WA

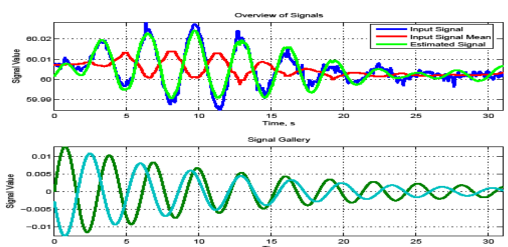

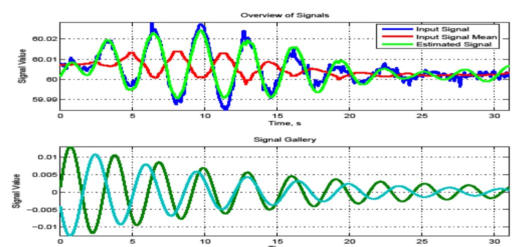

Table XI-8: WECC test D5 PMU data.

	Signals and Modes (PMUs only)	Signals and Modes (FDRs and PMUs)
Big Eddy 230kV PMU	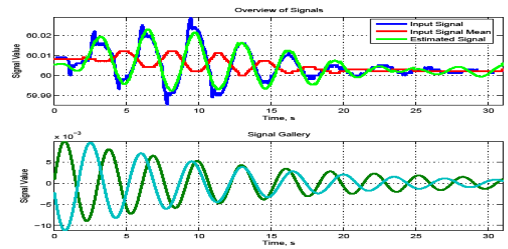	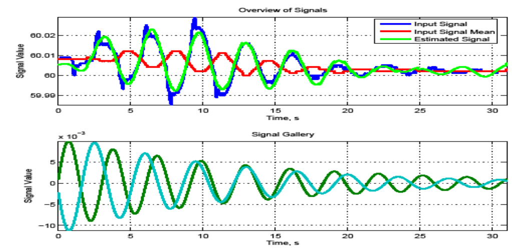
Big Eddy 500kV PMU	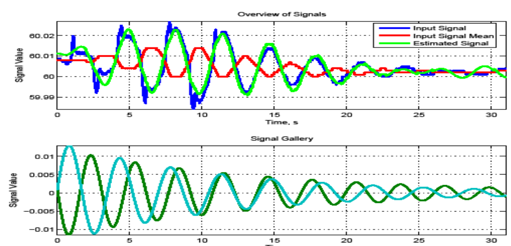	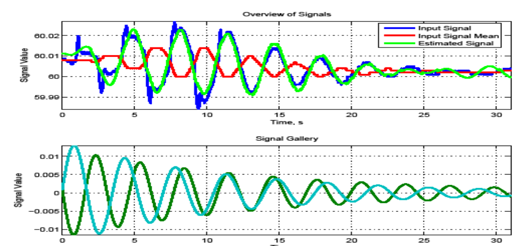

Colstrip PMU	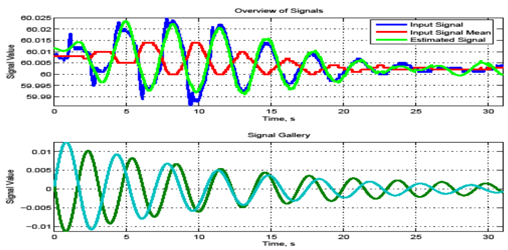	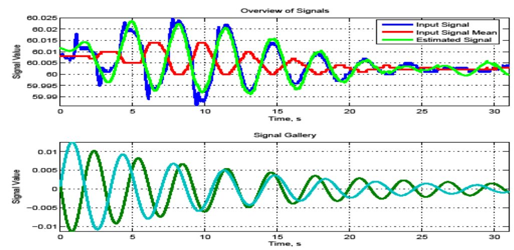
Grand Coulee Dam PMU	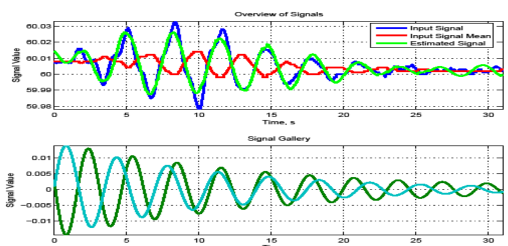	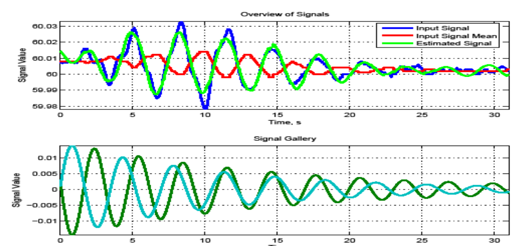

Malin PMU	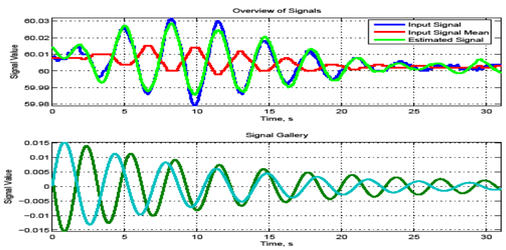	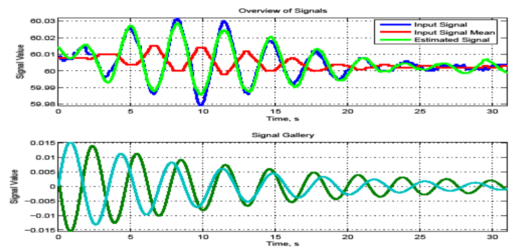
Maple Valley PMU	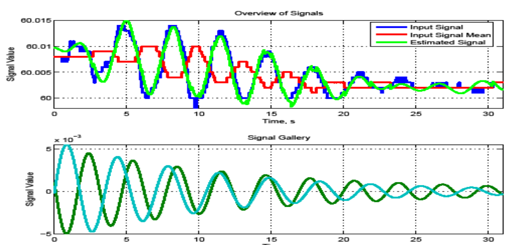	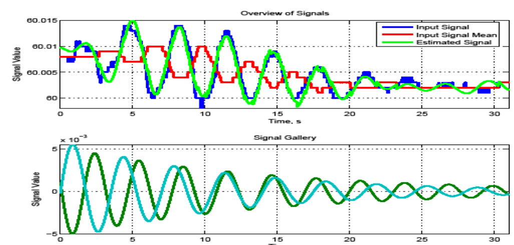

Vincent PMU

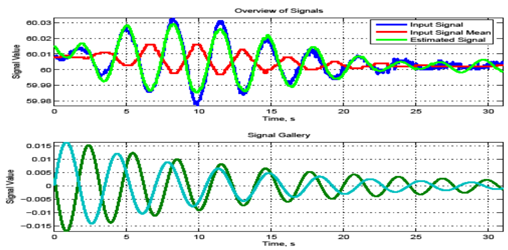

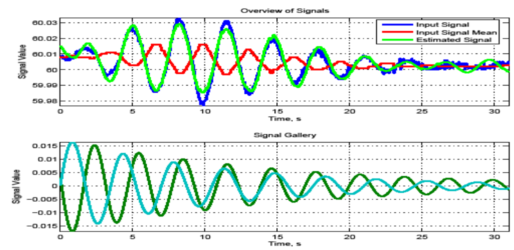

Sylmar PMU

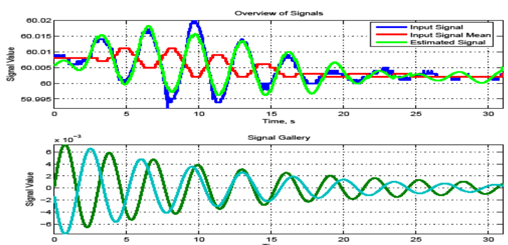

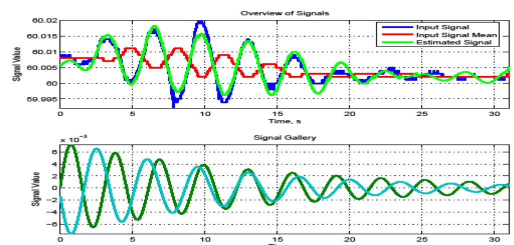

Table XI-9: Florida blackout FDR data.

	Signals and Modes (FDRs only)	Signals and Modes (FDRs and PMUs)
FDR 11: Grand Rapids, MI	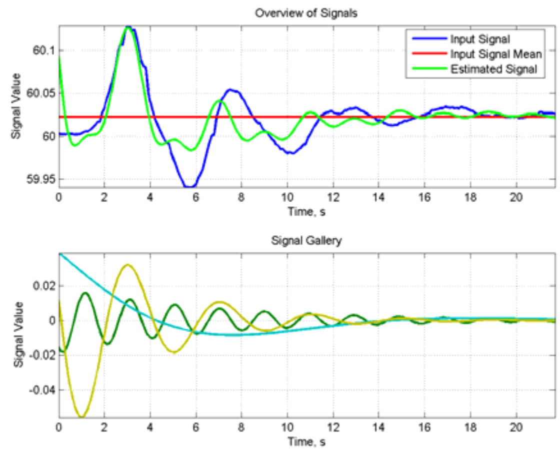	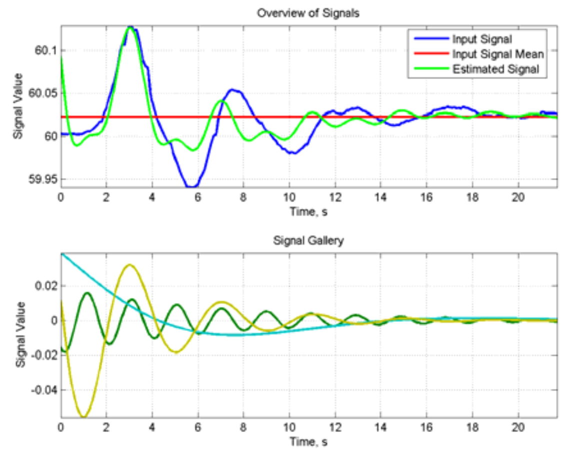
FDR 13: Carmel, IN	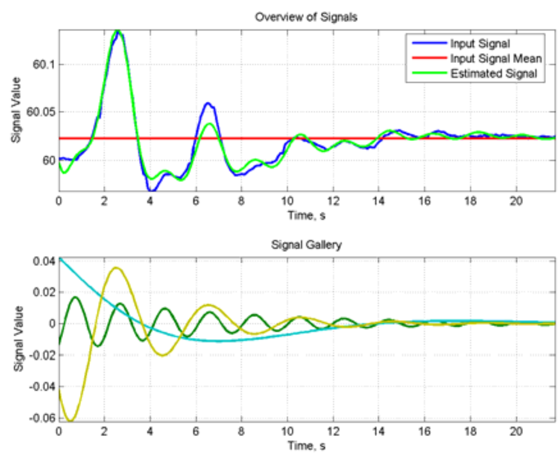	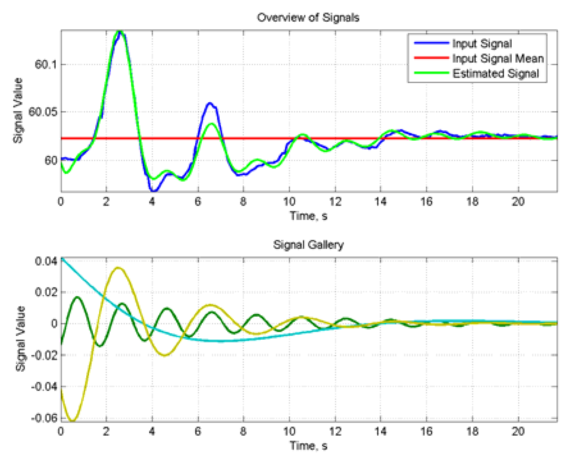

FDR 2: Rolla, MO

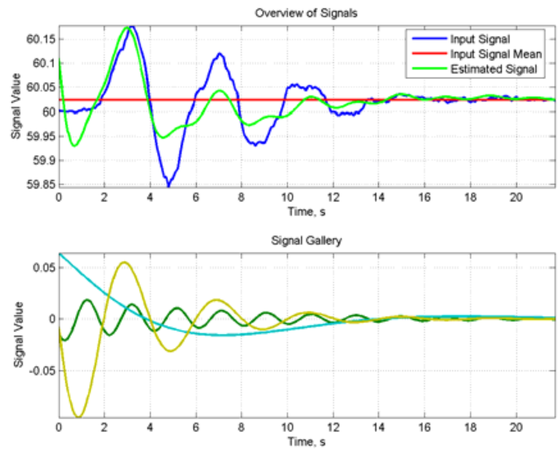

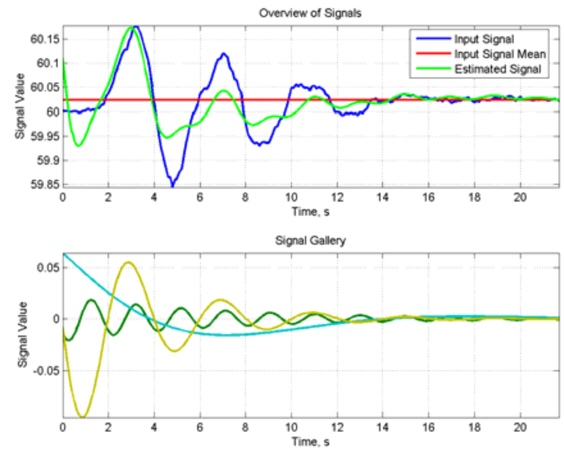

FDR 3: Vienna, VA

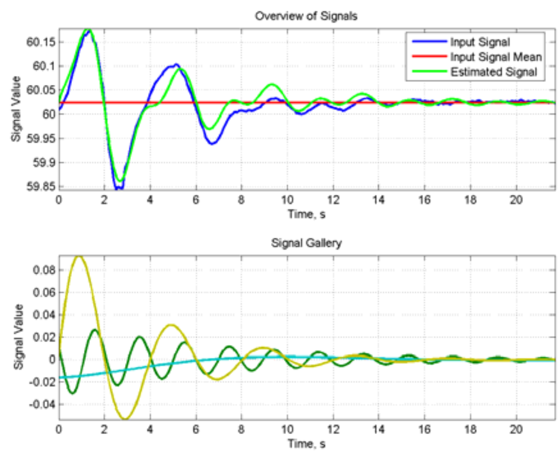

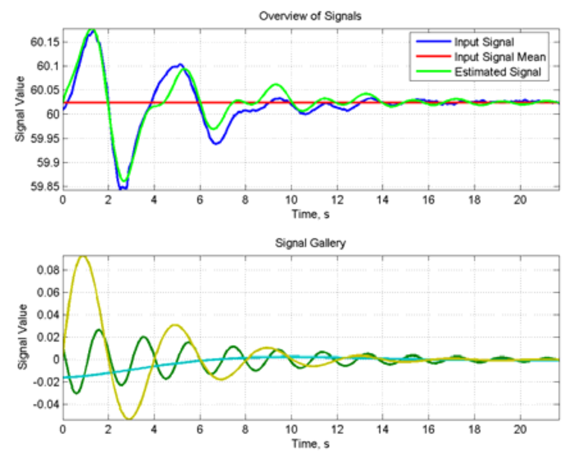

FDR 35: Ames, IA

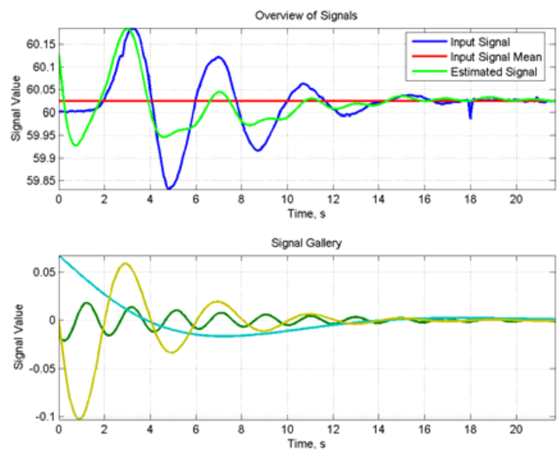

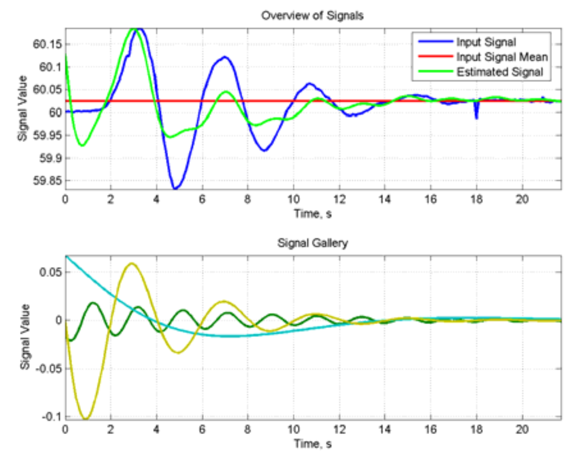

FDR 38: Holyoke, MA

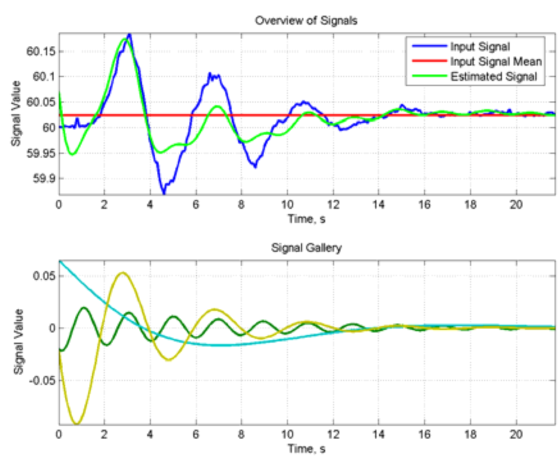

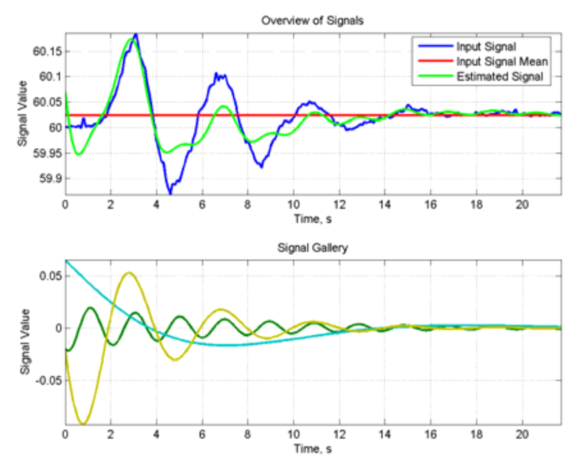

FDR 4: Blacksburg, VA

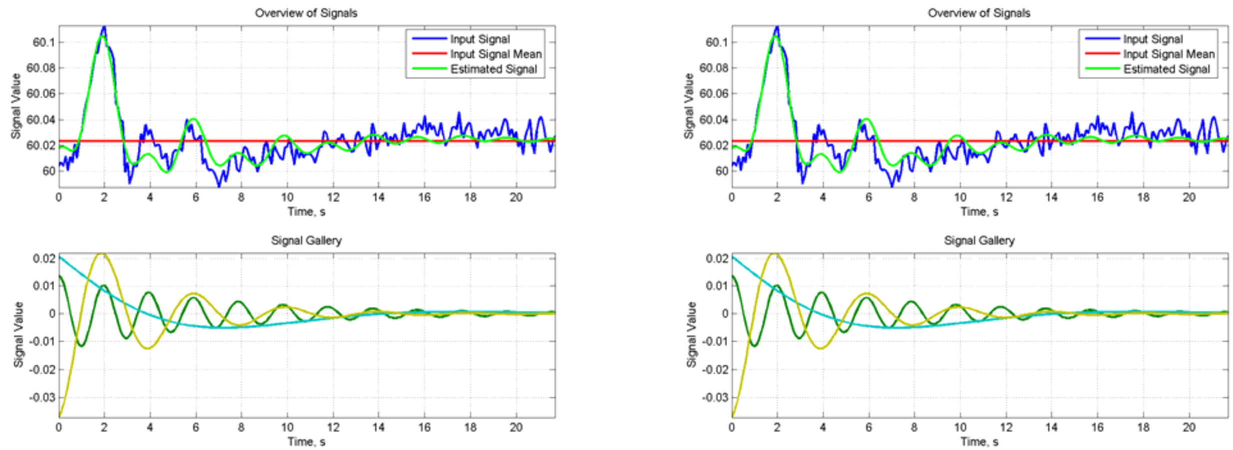

FDR 40: St. Paul, MN

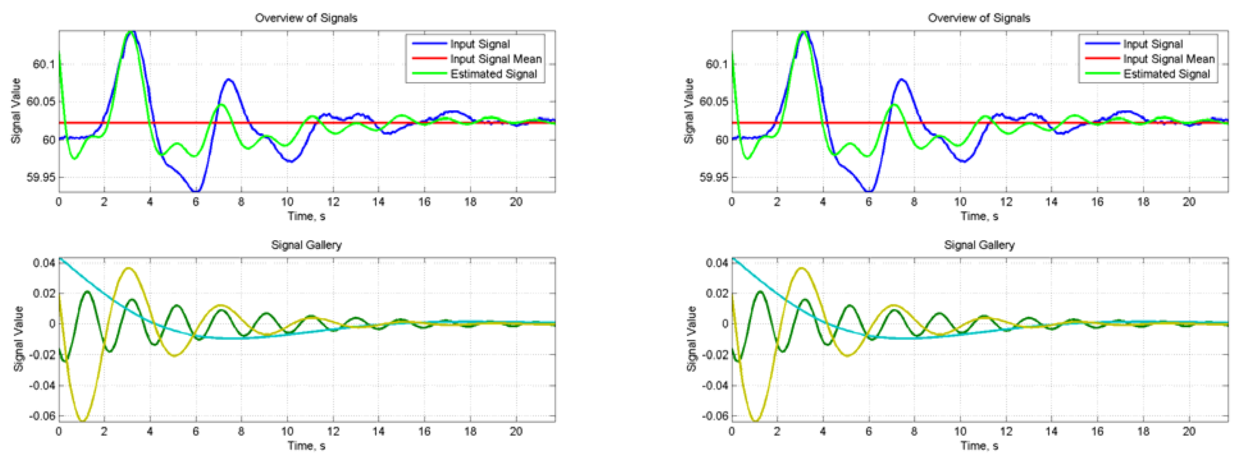

FDR 41: Winnipeg, MB

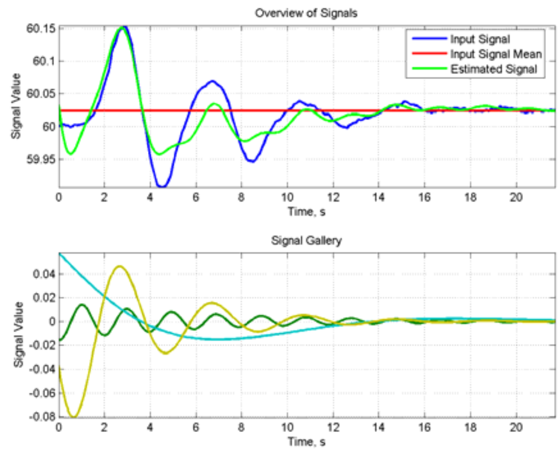

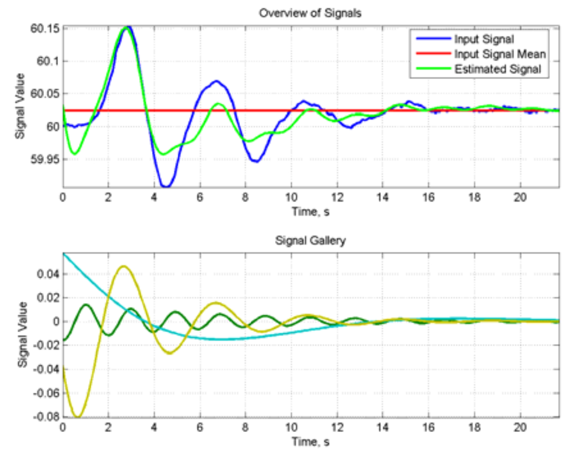

FDR 42: Tallahassee, FL

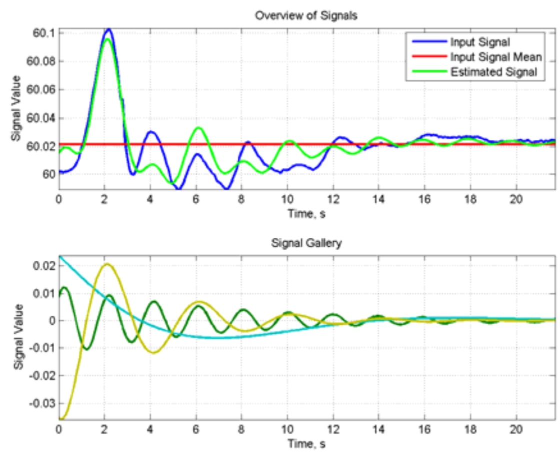

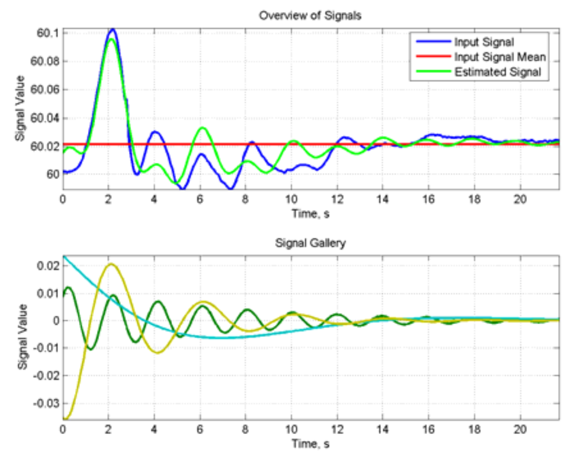

FDR 43: Bismarck, ND

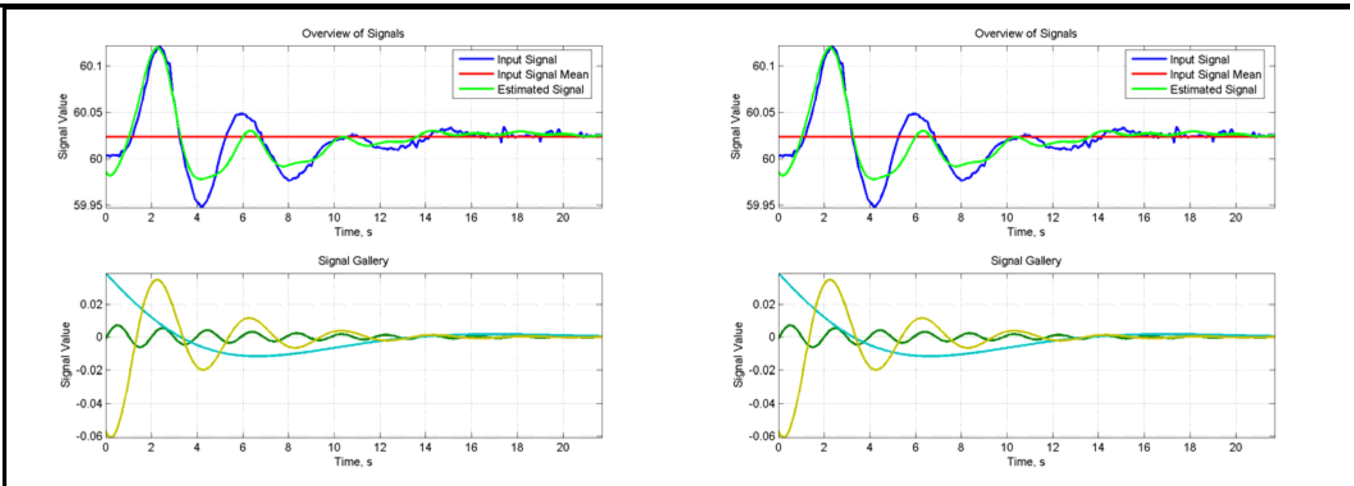

FDR 500: Chicago, IL

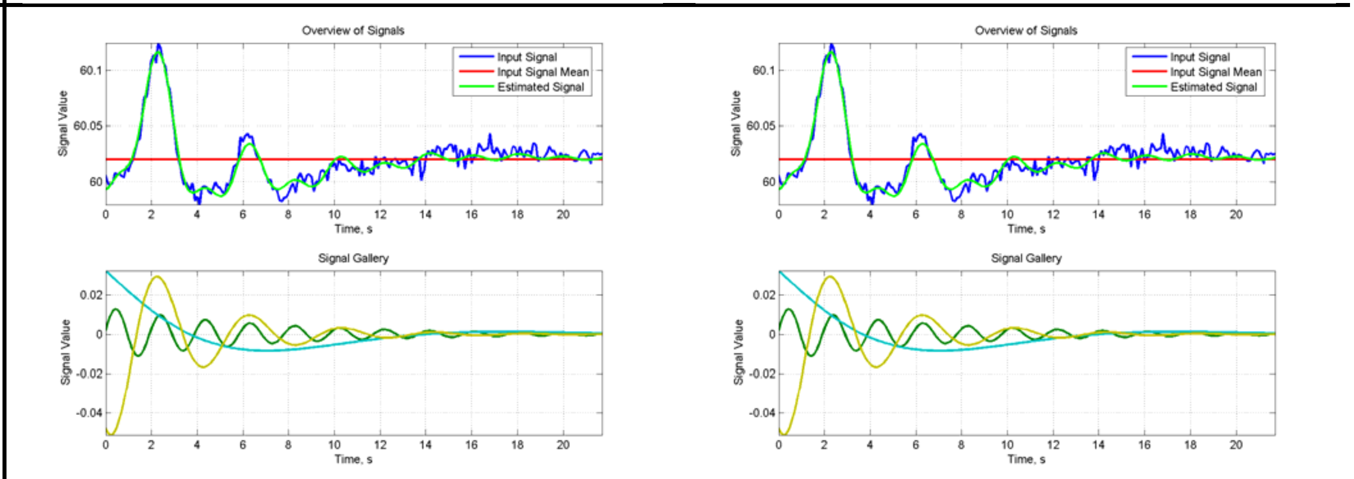

FDR 503: Danbury, CT

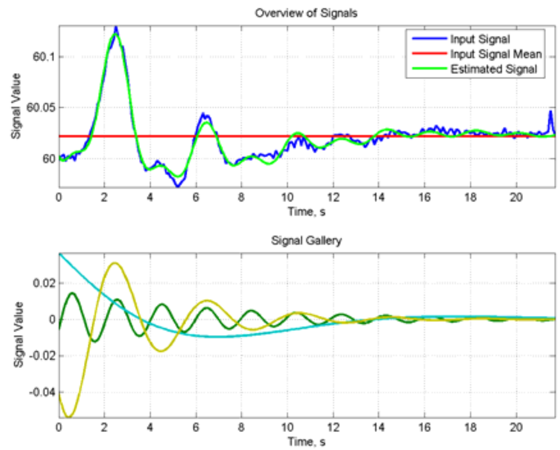

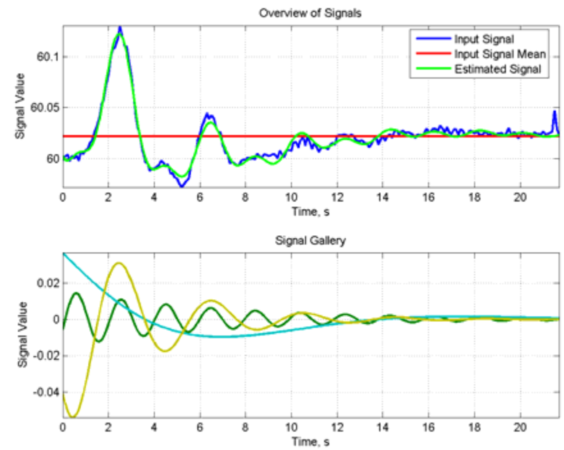

FDR 509: Morgantown, WV

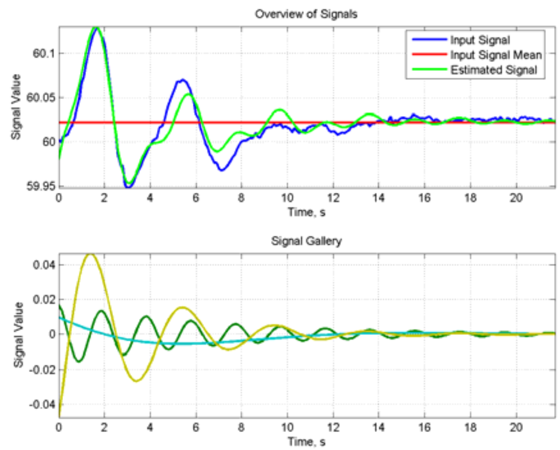

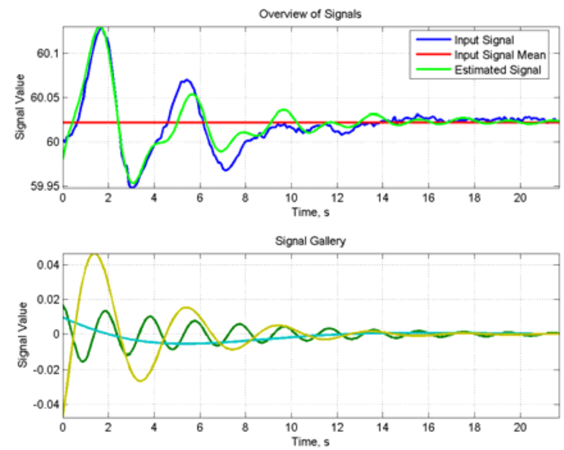

FDR 510: Blacksburg, VA

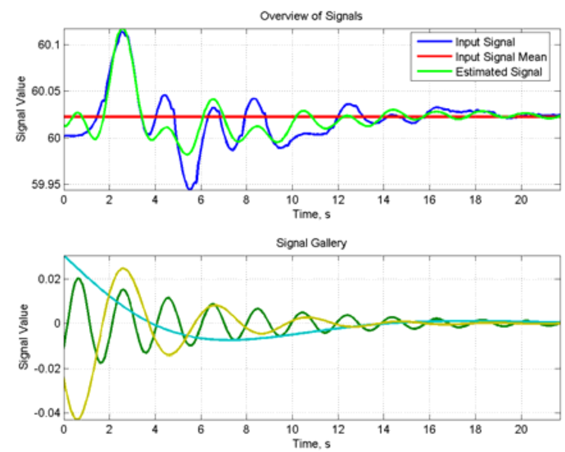

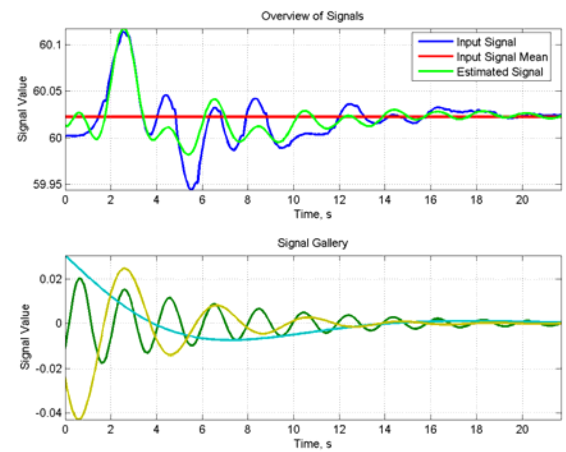

FDR 513: University Park, PA

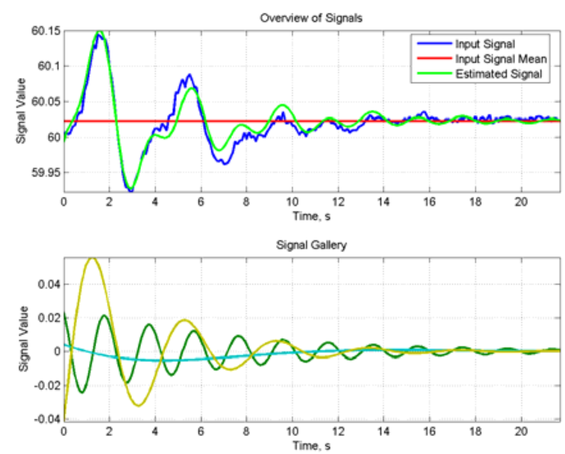

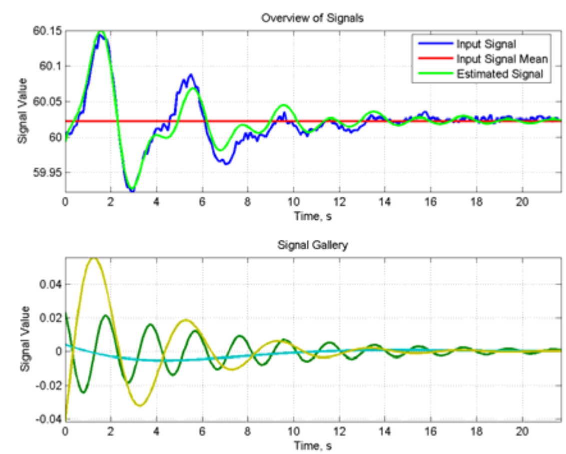

FDR 516: LeRoy, NY	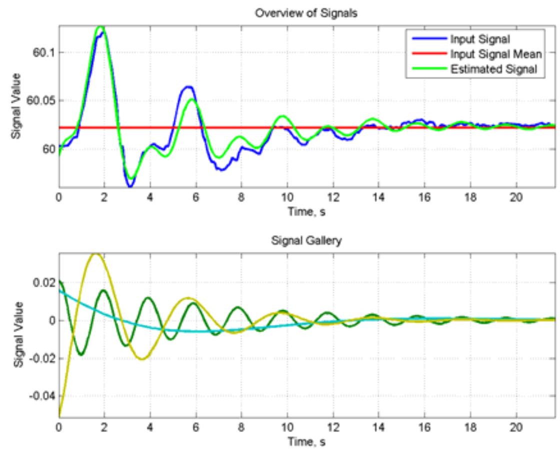	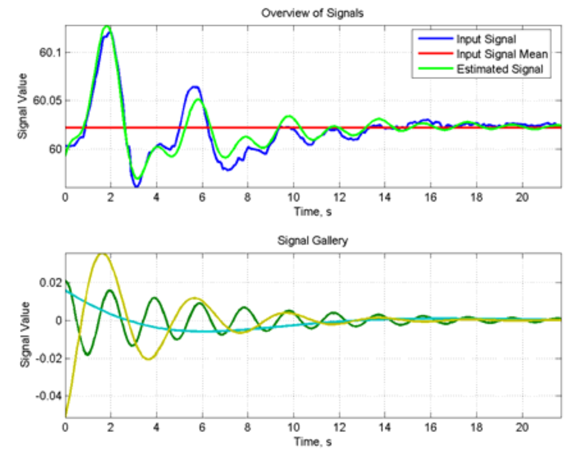
FDR 523: Cookeville, TN	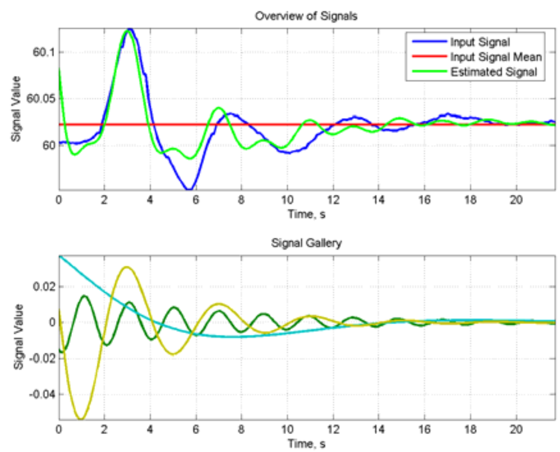	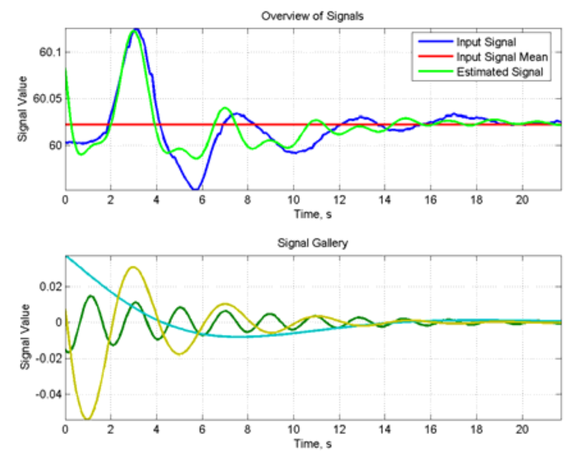

FDR 526: Birmingham, AL

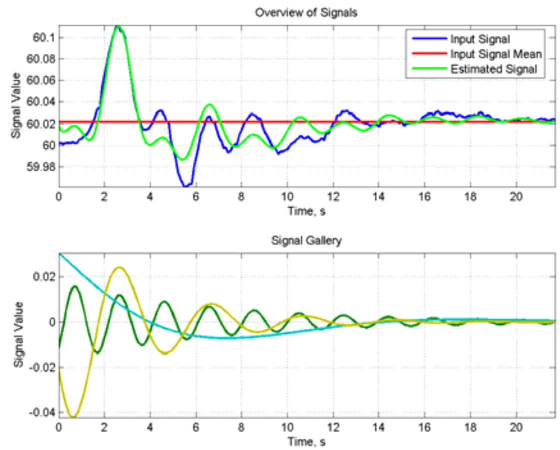

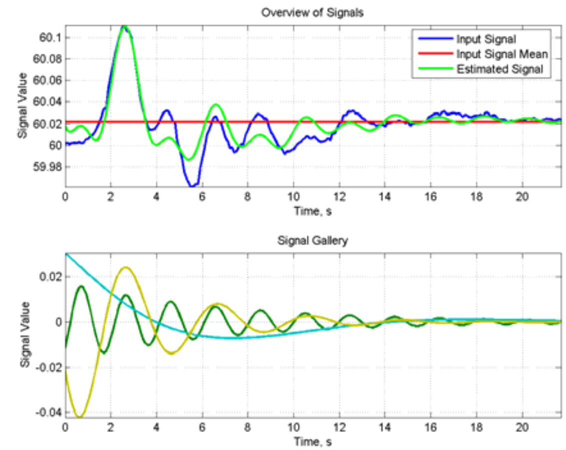

FDR 535: Norristown, PA

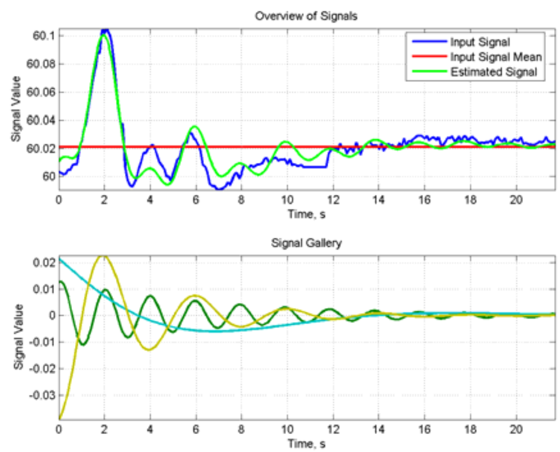

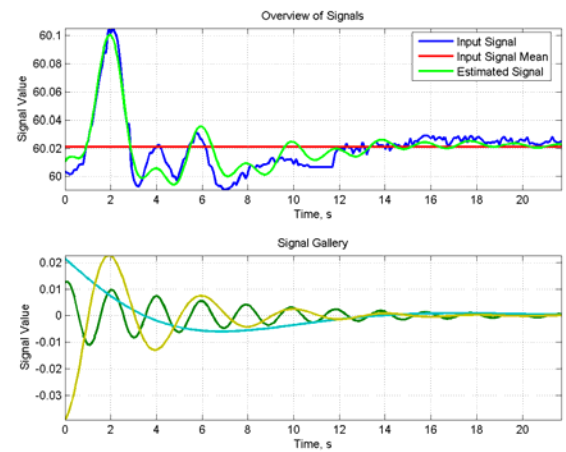

FDR 7: Jackson, MS	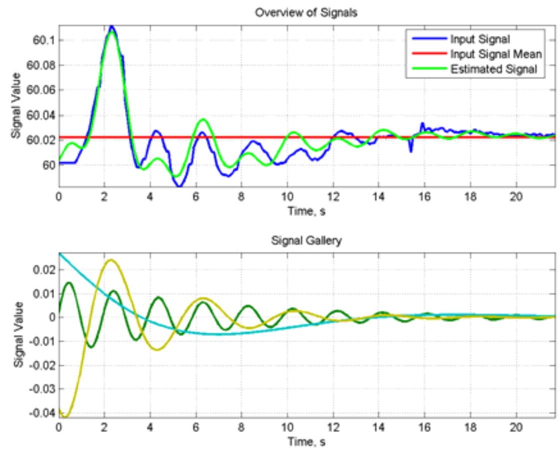	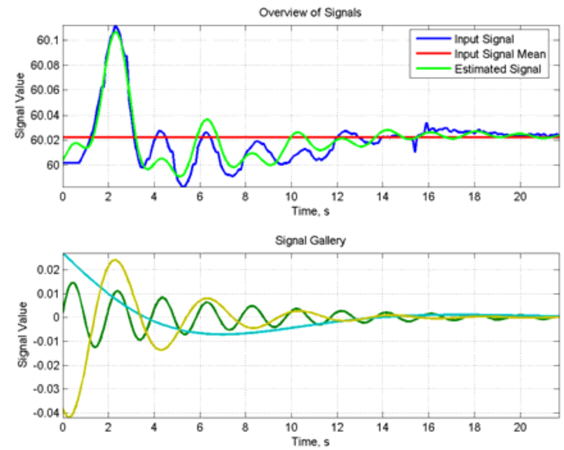

Table XI-10: Florida blackout PMU data.

<table>
<tr><th></th><th>Signals and Modes (PMUs only)</th><th>Signals and Modes (FDRs and PMUs)</th></tr>
<tr><td>Baker PMU</td><td>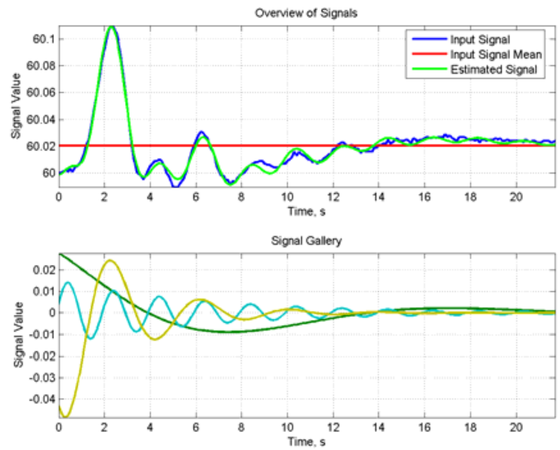
</td><td>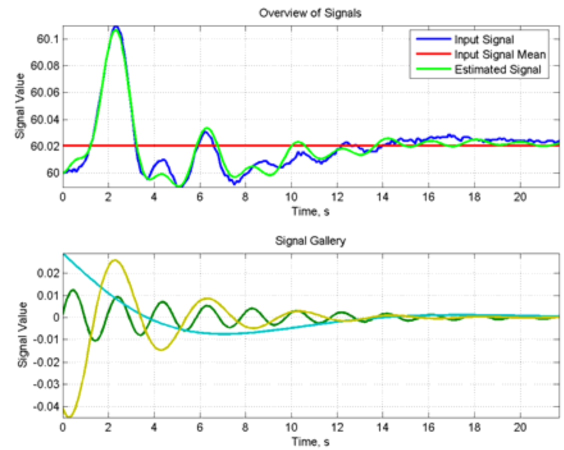
</td></tr>
<tr><td>Culloden PMU</td><td>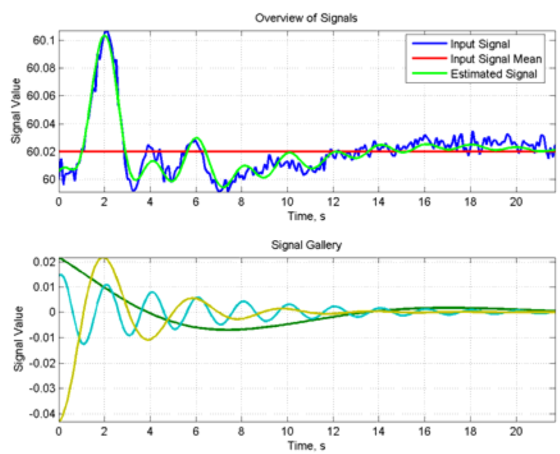
</td><td>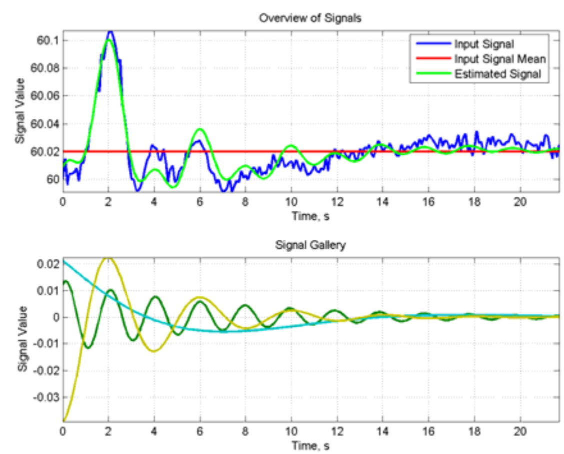
</td></tr>
</table>

Jackson's Ferry PMU	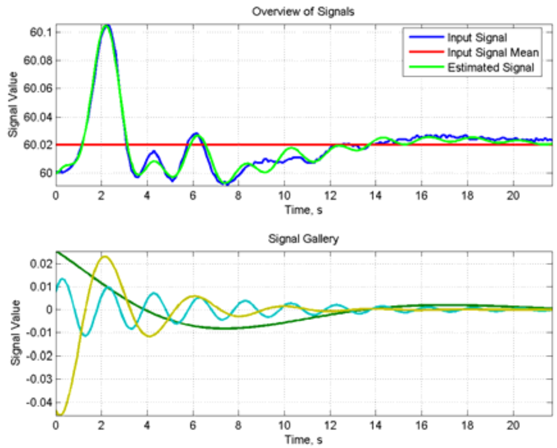	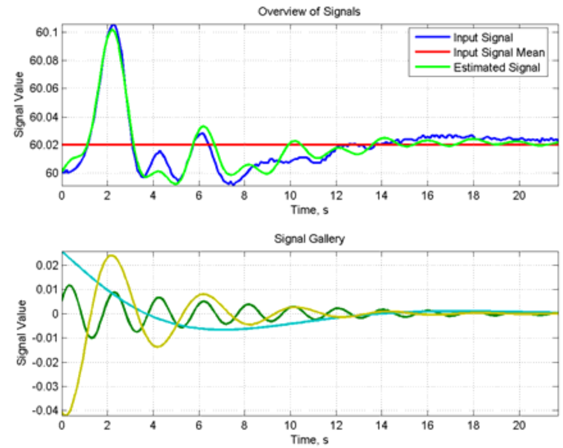
Kanawha River PMU	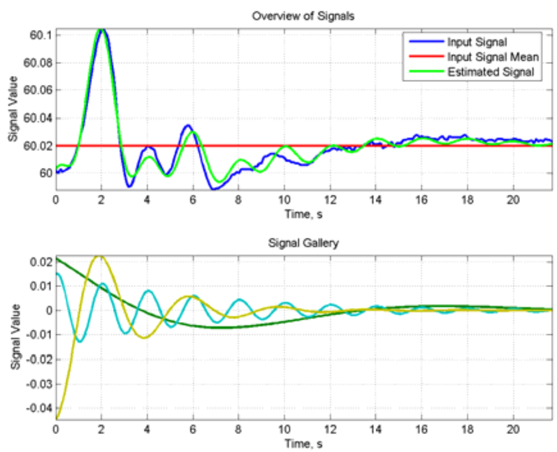	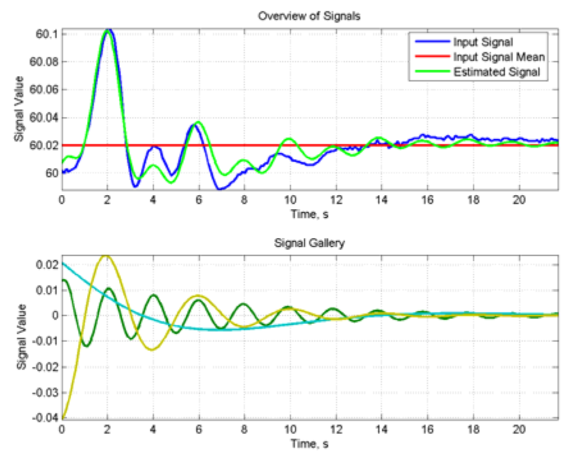

Matt Funk PMU

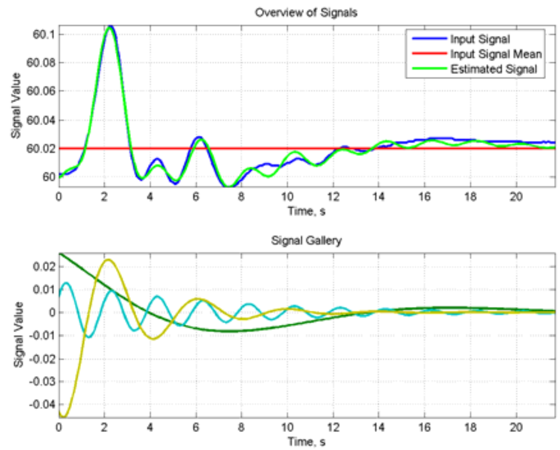

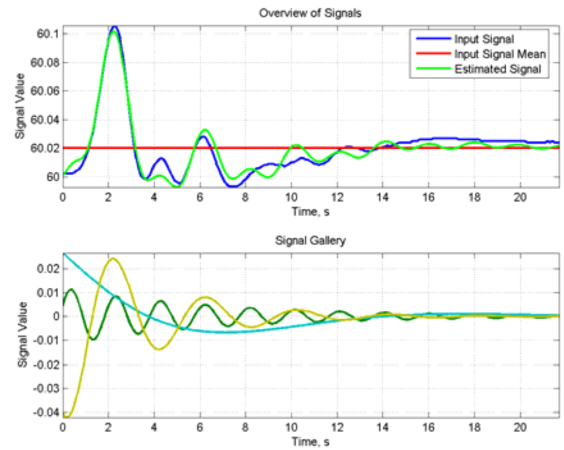

Orange PMU

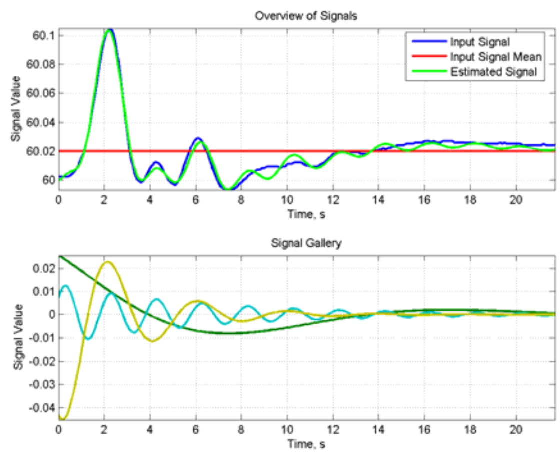

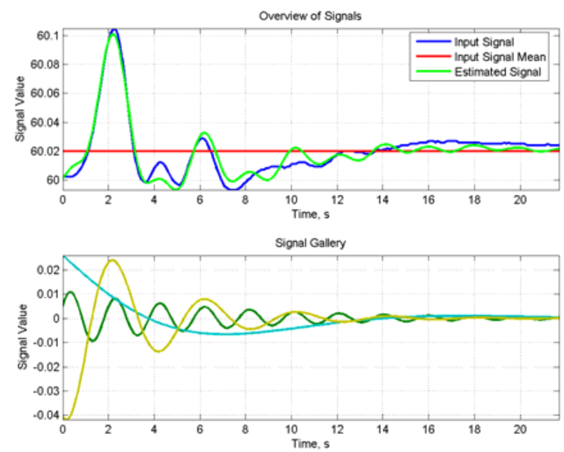

Rockport PMU

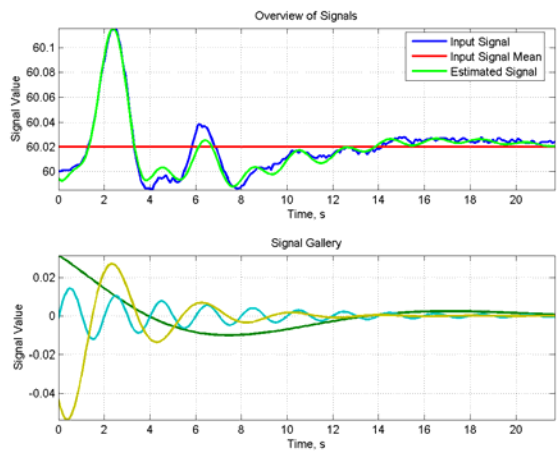

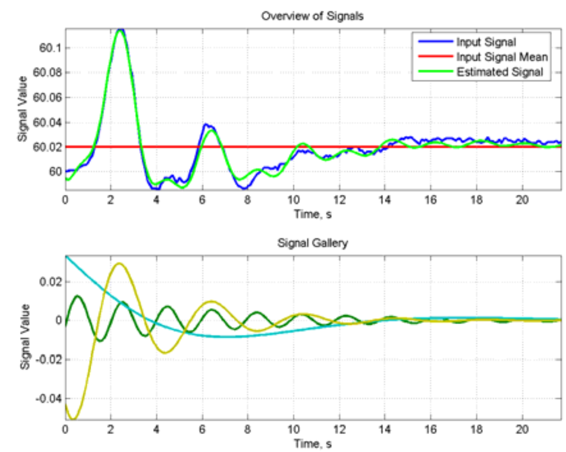

Appendix XII: MATLAB™ Code for Multiple Channel Matrix Pencil Calculations

```
function CALC_OUT=CalcDampingMC(fldnames,frequencymat)
%Program CalcDampingMC.m authored by R. Matthew Gardner accepts two input
%structures.  The structure 'fldnames' is an Qx1 cell structure with the
%names of data sensors.  The structure 'frequencymat' is a QxN array of N
%frequency measurements from Q sensors.  Output are both plotted and
%printed in a text file is shown below.
pfile='PlotFileName.png';
outfile='OutputTextFileName.txt';
Xo=frequencymat';
tsamp=0.1;
t=0:tsamp:length(Xo)/10;
[X,Xt]=detrend(frequencymat');    %De-trend Signal
disp('Data detrending complete.  Forming Hankel matrix...');
kfilt=0.4;                        %Adjustable noise filtering parameter: best
results 0.333<kfilt<0.5
[N,L,Y]=form_Hankel(X,kfilt);     %Specify dimensions and create Hankel
matrix
p=0.8;                            %Adjustable model order reduction parameter
prcf=0.6667;                      %p-reduction continuation factor
defordr=4;                        %Adjustable default model order if singular
values do not decay
disp('Hankel matrix complete.  Reducing system and calculating needed
eigenvalues...');
err1=true;                                  %Set error flag for Moore-Penrose
pseudo inverse
while err1                                  %Loop until model order yields
system considered to be solution to BAP
    [M,dS,Vp1,Vp2]=reduce_sys(Y,size(Xo,2),p,defordr,frequencymat);   %System
reduction
    [E,R,yout,youtgal,err1]=calc_eig(M,Vp1,Vp2,N,X);%Calculate eigenvalues
and estimate signal
    p=p*prcf;                               %Continued model reduction
(implied Moore-Penrose pseudoinverse problems)
    if err1                                 %Inform user about reduction in p
        disp(['Reduction factor found to be too large. p reduced to '
num2str(p)]);
    end
end
disp('System reduction complete.  Calculating damping factors...');
[Ec,dfactor,nfreq,dfreq,domdamp,didx,dtext]=calc_damp(E,R,tsamp);%Calculate
damping factor, natural frequency, and damped frequency
CALC_OUT.Ec=Ec;
CALC_OUT.Rmag=abs(R);
%CALC_OUT.didx=didx;
if ~isempty(pfile)
    disp('Plotting results...');
    for i=1:size(Xo,2)
        [a,b]=strtok(pfile,'_plot');
        fileconstruct=[a '_MC_' fldnames{i} b];
```

```
plot_results(fileconstruct,Xo(:,i),Xt(:,i),tsamp,X(:,i),yout(:,i),dS,Ec,R(:,i
),youtgal{i},didx);%Plot results if requested
    end
end
disp('Writing output file...');
CALC_OUT.err=norm(Xo-(Xt+yout));
for i=1:size(Xo,2)
    [a,b]=strtok(outfile,'_out');
    fileconstruct=[a '_MC_' fldnames{i} b];

write_txt(fileconstruct,M,dfactor,nfreq,dfreq,Ec,R(:,i),Xo(:,i),Xt(:,i),yout(
:,i),dS,CALC_OUT.err,didx);%Write output text file
end
disp('Program CalcDamping.m complete.');
%CALC_OUT.domdamp=domdamp;
CALC_OUT.S=yout+Xt;
CALC_OUT.Xo=Xo;
CALC_OUT.t=(0:(length(Xo)-1))*tsamp;
CALC_OUT.dfactor=dfactor';
CALC_OUT.dfreq=dfreq';
CALC_OUT.dtext=dtext';

%***************************************************************************
%DE-TREND SIGNAL
%***************************************************************************
function [X,Xt]=detrend(Xo,tsamp)
    %[b,a]=butter(10,[0.1/5 2.5/5]);
    for i=1:size(Xo,2)
        X(:,i)=Xo(:,i)-median(Xo(:,i));
        %X(:,i)=Xo(:,i)-medfilt1(Xo(:,i),121);
        %X(:,i)=filtfilt(b,a,Xo(:,i));
    end
    Xt=Xo-X;                        %Calculate trend

%***************************************************************************
%FORMATION OF HANKEL MATRIX --- DIM:(N-L)x(L+1)
%***************************************************************************
function [N,L,Y]=form_Hankel(X,kfilt)
    N=size(X,1);                    %Length of input signal vector
    L=round(N*kfilt);
    hank=hankel(1:(N-L),(N-L):N);   %Create Hankel matrix index numbers
    Y=[];
    for i=1:size(X,2)
        Y=[Y,X(hank)];                      %Populate Hankel matrix using
index numbers
    end

%***************************************************************************
%SYSTEM REDUCTION VIA SVD: SINGULAR VALUE DECOMPOSITION OF HANKEL MATRIX
%***************************************************************************
function [M,dS,Vp1,Vp2]=reduce_sys(Y,Q,p,defordr,frequencymat)
    L=size(frequencymat,1);
    [U,S,V]=svd(Y,'econ');          %Calculate SVD of Y
    dS=diag(S);                     %Extract singular value from diagonal
matrix S
```

```
    idx=find(dS/max(dS)>10^(-p));   %Calculate ratio of all singular values
to maximum singular value and determine model order cutoff point
    if idx==1                       %Determine system order from idx or
default to defordr
        M=round(defordr);           %Try to estimate signal even if singular
values do not decay
    else
        M=idx(end);                 %Model order set IF singular values decay
        M=min(M,length(dS)-1);      %Limit size of M to be comformable with
Y1, Y2 in further steps
    end
    %M=14
    Vp=V(:,1:M);                    %Calculated "filtered" matrix Vp (from V)
    Vp1=Vp;                         %Set up intermediate matrices
    Vp1(size(Y,2)/L:size(Y,2)/L:end,:)=[];%Remove Q rows
    Vp2=Vp;
    Vp2(1:size(Y,2)/L:end,:)=[];
    Sp=S(:,1:M);                    %Remove columns of S to ensure rank(S)=M
leaving only dominant singular values
    Y1=U*Sp*Vp1';                   %Create matrices Y1 and Y2 to form matrix
pencil
    Y2=U*Sp*Vp2';

%***************************************************************************
%EIGENVALUE ANALYSIS OF MATRIX PENCIL
%***************************************************************************
function [E,R,yout,youtgal,err]=calc_eig(M,Vp1,Vp2,N,X)
    E=eigs(pinv(Vp1')*Vp2',M);          %Find pared down eigenvalues of
matrix pencil based on model order
    for h=0:N-1                     %Form Vandermonde-esque matrix
        Zmat(h+1,:)=E'.^h;
    end
    try                             %Error catching if model order acidentally
set too big
        R=pinv(Zmat)*X;             %Calculate phase vector
        yout=real(Zmat*R);          %yout now contains signal estimate
        for ii=1:size(X,2)
            for i=1:size(R,1)           %Create signal gallery
                youtgal[80](:,i)=Zmat(:,i)*R(i,ii);
            end
        end
        err=false;                  %Clear error flag
    catch
        yout=[];                    %Set error flag if problem calculating
pseudoinverse
        err=true;
    end

%***************************************************************************
%CALCULATE DAMPING PERCENTAGES
%***************************************************************************
function [Ec,dfactor,nfreq,dfreq,domdamp,didx,dtext]=calc_damp(E,R,tsamp)
    domdamp=NaN;
    pridx=0;
    if imag(E)<pi
```

```
        Ec=log(E)/tsamp;                                %Convert discrete system
poles to continuous system poles
    else
        Ec=(2/tsamp)*((E-1)./(E+1));
        disp('Warning: Imaginary component of Eigenvalue found to be greater
than Pi.  Switching to Tustin''s Method for discrete to cont. pole
mapping.');
    end
    for i=1:length(Ec)
        if real(Ec(i))>0
                pridx=pridx+1;
        end
        if ~isreal(Ec(i))                           %Do not attempt to calculate
frequencies for real eigenvalues
            %pole=log(E(i))/tsamp;                  %Convert discrete system
poles to continuous system poles
            dfactor(i)=-real(Ec(i))/abs(Ec(i)); %Calculate damping factor
from pole locations in complex plane
            nfreq(i)=abs(Ec(i))/2/pi;               %Calculate natural frequency
in Hz
            dfreq(i)=abs(imag(Ec(i)))/2/pi;         %Calculate damped frequency
in Hz
            dtext{i}=[num2str(dfreq(i)) 'Hz at ' num2str(dfactor(i)*100)
'%'];
        end
    end
    if pridx>0
        disp(['Warning: ' num2str(pridx) ' Eigenvalues with positive real
components calculated.']);
    end
    [sR,sidx]=sort(R,'descend');                    %Sort residual vector
    for ii=size(R,2)
        for i=1:size(R,1)                               %Find largest R with
complex corresponding eigenvalue
            if ~isreal(Ec(sidx(i,ii)))                     %Test complexity of
eigenvalue
                domdamp=dfactor(sidx(i,ii));               %Calculate dominant
damping
                didx=[sidx(i,ii),find(Ec==Ec(sidx(i,ii))')];%Find index of
compex conjugate if exists
                break;
            end
        end
    end

%***************************************************************************
%PLOT RESULTS
%***************************************************************************
function plot_results(pfile,Xo,Xt,tsamp,X,yout,dS,E,R,youtgal,didx)
    [tok,rem]=strtok(pfile,'.');                %Determine plot file name and
desired plot file extension
    figure                                      %Plot original signal
    plot((0:(length(Xo)-1))*tsamp,Xo,'b','linewidth',2);        %Plot
original signal
    hold on;
    plot((0:(length(Xt)-1))*tsamp,Xt,'r','linewidth',2);        %Plot signal
mean (or trend)
```

```
    plot((0:(length(Xt)-1))*tsamp,(Xt+yout),'g','linewidth',2); %Plot signal
estimate
    grid on;                                %Misc. plot formatting
    axis on;
    ylabel('Signal Value');
    xlabel('Time, s');
    title('Overview of Signals');
    legend('Input Signal','Input Signal Mean','Estimated Signal');
    axis tight
    drawnow                                 %Flush graphics buffer
    try                                     %File saving error catching
        saveas(gcf,[tok '_original' rem]);  %Save file
    catch
        disp(['Error writing file: ' pfile ' Check file extension.']);
    end
    close all                               %Close plot
    figure                                  %Plot signal gallery
    plot((0:(length(Xo)-1))*tsamp,real(youtgal),'linewidth',2); %Plot signal
gallery
    grid on;                                %Misc. plot formatting
    axis on;
    ylabel('Signal Value');
    xlabel('Time, s');
    title('Signal Gallery');
    axis tight
    drawnow                                 %Flush graphics buffer
    try                                     %File saving error catching
        saveas(gcf,[tok '_gallery' rem]);   %Save file
    catch
        disp(['Error writing file: ' pfile ' Check file extension.']);
    end
    close all
    figure                                  %Plot signal overlay
    subplot(2,1,1);
    plot((0:(length(Xo)-1))*tsamp,Xo,'b','linewidth',2);        %Plot
original signal
    hold on;
    plot((0:(length(Xt)-1))*tsamp,Xt,'r','linewidth',2);        %Plot signal
mean (or trend)
    plot((0:(length(Xt)-1))*tsamp,(Xt+yout),'g','linewidth',2); %Plot signal
estimate
    grid on;                                %Misc. plot formatting
    axis on;
    ylabel('Signal Value');
    xlabel('Time, s');
    title('Overview of Signals');
    legend('Input Signal','Input Signal Mean','Estimated Signal');
    axis tight
    drawnow
    subplot(2,1,2);
    plot((0:(length(Xo)-1))*tsamp,real(youtgal),'linewidth',2); %Plot signal
gallery
    grid on;                                %Misc. plot formatting
    axis on;
    ylabel('Signal Value');
    xlabel('Time, s');
    title('Signal Gallery');
```

```
    axis tight
    drawnow                                  %Flush graphics buffer
    try                                      %File saving error catching
        saveas(gcf,[tok '_overlay' rem]);    %Save file
    catch
        disp(['Error writing file: ' pfile ' Check file extension.']);
    end
    close all
    figure                                   %Plot detrended signals (both
original detrend and estimate to detrend)
    plot((0:(length(X)-1))*tsamp,X,'b','linewidth',2);  %Plot zero-mean
(detrended) original signal
    hold on;                                 %Misc. plot formatting
    grid on;
    axis on;
    plot((0:(length(yout)-1))*tsamp,real(yout),'r','linewidth',2);  %Plot
zero-mean signal estimate
    legend('Orig. Signal','Est. Signal');    %Misc. plot formatting
    ylabel('Signal Value');
    xlabel('Time, s');
    title('Detrended Original Signal and Estimated Signal');
    axis tight
    drawnow                                  %Flush graphics buffer
    try                                      %File saving error catching
        saveas(gcf,[tok '_zeromean' rem]);   %Save file
    catch
        disp(['Error writing file: ' pfile ' Check file extension.']);
    end
    close all                                %Close plot
    figure                                   %Plot singular values
    plot(dS,'b*','linewidth',1.5,'markersize',10);  %Plot singular values
    hold on;                                 %Misc. plot formatting
    grid on;
    plot(dS(1:length(E)),'r^','linewidth',2,'markersize',12);   %Plot
selected singular values
    legend('Singular Values','Dominant Sing. Vals.');           %Misc. plot
formatting
    ylabel('Singular Value Size');
    xlabel('Singular Value Number');
    title('Singular Values as determined by SVD');
    axis on;
    axis tight
    drawnow                                  %Flush graphics buffer
    try                                      %File saving error catching
        saveas(gcf,[tok '_singvals' rem]);   %Save file
    catch
        disp(['Error writing file: ' pfile ' Check file extension.']);
    end
    close all                                %Close plot
    figure                                   %Plot eigenvalues (poles) of
signal in Argand diagram
    plot(E,'bx','linewidth',2,'markersize',12); %Plot eigenvalues
    hold on;
    plot(R,'ro','linewidth',2,'markersize',10); %Plot residuals
    plot(E(didx),'gs','linewidth',2,'markersize',16); %Plot dominant
eigenvalues
```

```
    plot(R(didx),'g^','linewidth',2,'markersize',16); %Plot dominant 
residuals
    grid on;                                 %Misc. plot formatting
    axis tight;
    axis on;
    ylabel('Imaginary Axis');
    xlabel('Real Axis');
    title('Argand Diagram of Eigenvalues and Residuals');
    legend('Eigenvalues','Residuals','Dominant Eigenvalues','Dominant 
Residuals','Location','NorthWest');
    drawnow                                  %Flush graphics buffer
    try                                      %File saving error catching
        saveas(gcf,[tok '_argand' rem]);     %Save file
    catch
        disp(['Error writing file: ' pfile ' Check file extension.']);
    end
    close all                                %Close plot
    drawnow                                  %Flush graphics buffer

%**************************************************************************
%CREATE OUTPUT FILE
%**************************************************************************
function 
write_txt(outfile,M,dfactor,nfreq,dfreq,Ec,R,Xo,Xt,yout,dS,ferr,didx)
    dmark=32*ones(M,1);                  %ASCII vector of spaces
    dmark(didx)=42;                      %Mark with stars as proper
    fid = fopen(outfile,'w');            %Open file stream for writing
    if fid==-1                           %File stream error checking
        disp('Error opening output file for reporting.  No report created. 
Output printed to screen.');
        fid=1;                           %fid=1 prints data to screen
    end
    fprintf(fid,'MODEL ORDER:\r\n');         %Data labeling
    fprintf(fid,'%6.0f\r\n',M);              %Write model order
    fprintf(fid,'\r\n');                     %Line feed carriage return
    fprintf(fid,'RMS ERROR:\r\n');           %Data labeling
    fprintf(fid,'%6.6f\r\n',ferr);           %Write fitting error
    fprintf(fid,'\r\n');                     %Line feed carriage return
    fprintf(fid,'DAMPING FACTORS:\r\n');     %Data labeling
    fprintf(fid,'%6.6f\r\n',dfactor);        %Write damping factors
    fprintf(fid,'\r\n');                     %Line feed carriage return
    fprintf(fid,'NATURAL FREQUENCIES (Hz):\r\n');%Data labeling
    fprintf(fid,'%6.6f\r\n',nfreq);          %Write natural frequencies
    fprintf(fid,'\r\n');                     %Line feed carriage return
    fprintf(fid,'DAMPED FREQUENCIES (Hz):\r\n'); %Data labeling
    fprintf(fid,'%6.6f\r\n',dfreq);          %Write damped frequencies
    fprintf(fid,'\r\n');                     %Line feed carriage return
    fprintf(fid,'EIGENVALUES (cont.):\r\n');%Data labeling
    fprintf(fid,'%6.6f%+6.6fj%c\r\n',[real(Ec),imag(Ec),dmark]'); %Write 
eigenvalues
    fprintf(fid,'\r\n');                     %Line feed carriage return
    fprintf(fid,'RESIDUALS (cont.):\r\n');   %Data labeling

fprintf(fid,'%6.6f%+6.6fj\t(%6.6f)%c\r\n',[real(R),imag(R),abs(R),dmark]'); 
%Write residuals (complex amplitudes)
    fprintf(fid,'\r\n');                     %Line feed carriage return
    fprintf(fid,'SINGULAR VALUES:\r\n');     %Data labeling
```

```
    fprintf(fid,'%6.6f\r\n',dS);            %Write singular values
    fprintf(fid,'\r\n');                    %Line feed carriage return
    fprintf(fid,'ORIGINAL SIGNAL:\r\n');    %Data labeling
    fprintf(fid,'%6.6f\r\n',Xo);            %Repeat original signal (for
convenience)
    fprintf(fid,'\r\n');                    %Line feed carriage return
    fprintf(fid,'ESTIMATED SIGNAL:\r\n');   %Data labeling
    fprintf(fid,'%6.6f\r\n',Xt+yout);       %Write estimated signal
    if fid~=1
        status = fclose(fid);               %Close file stream
    end
```

Appendix XIII: Distance vs. Time Regression for Calculation of Frequency Velocity

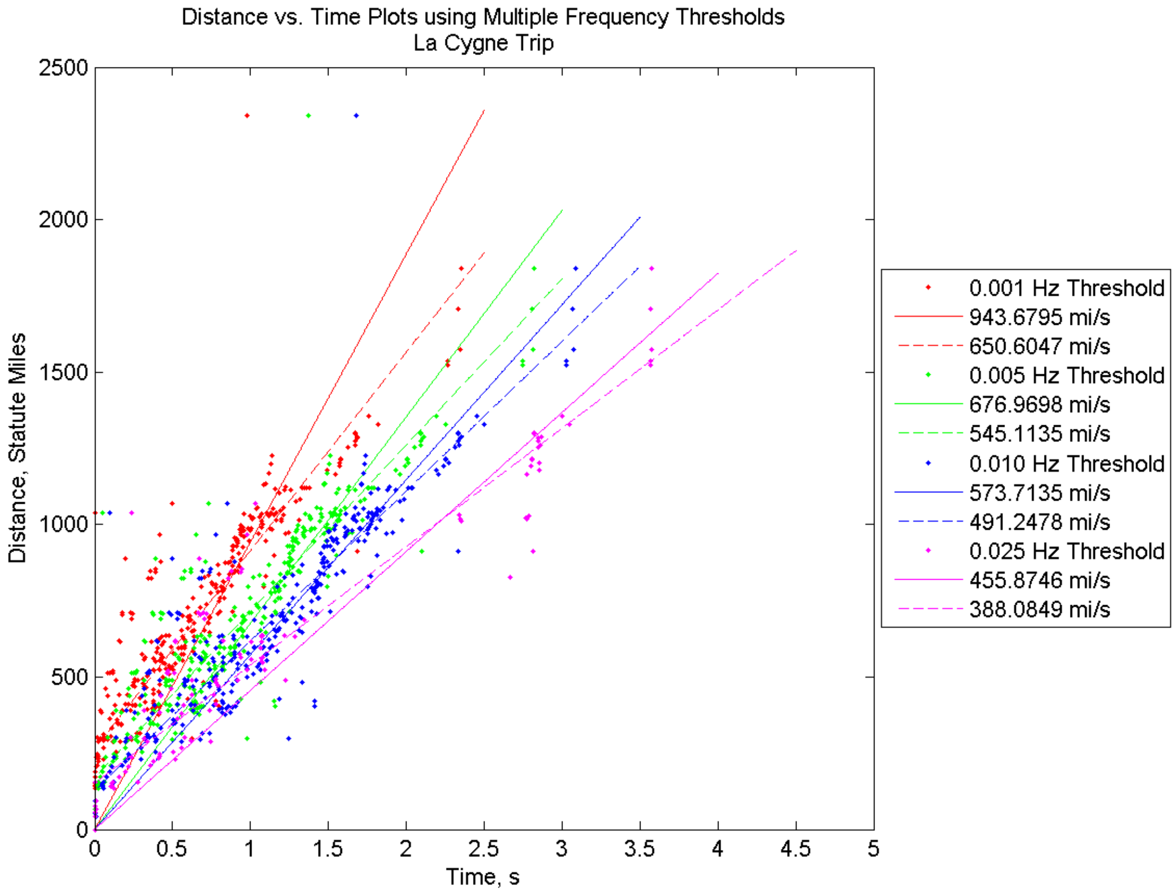

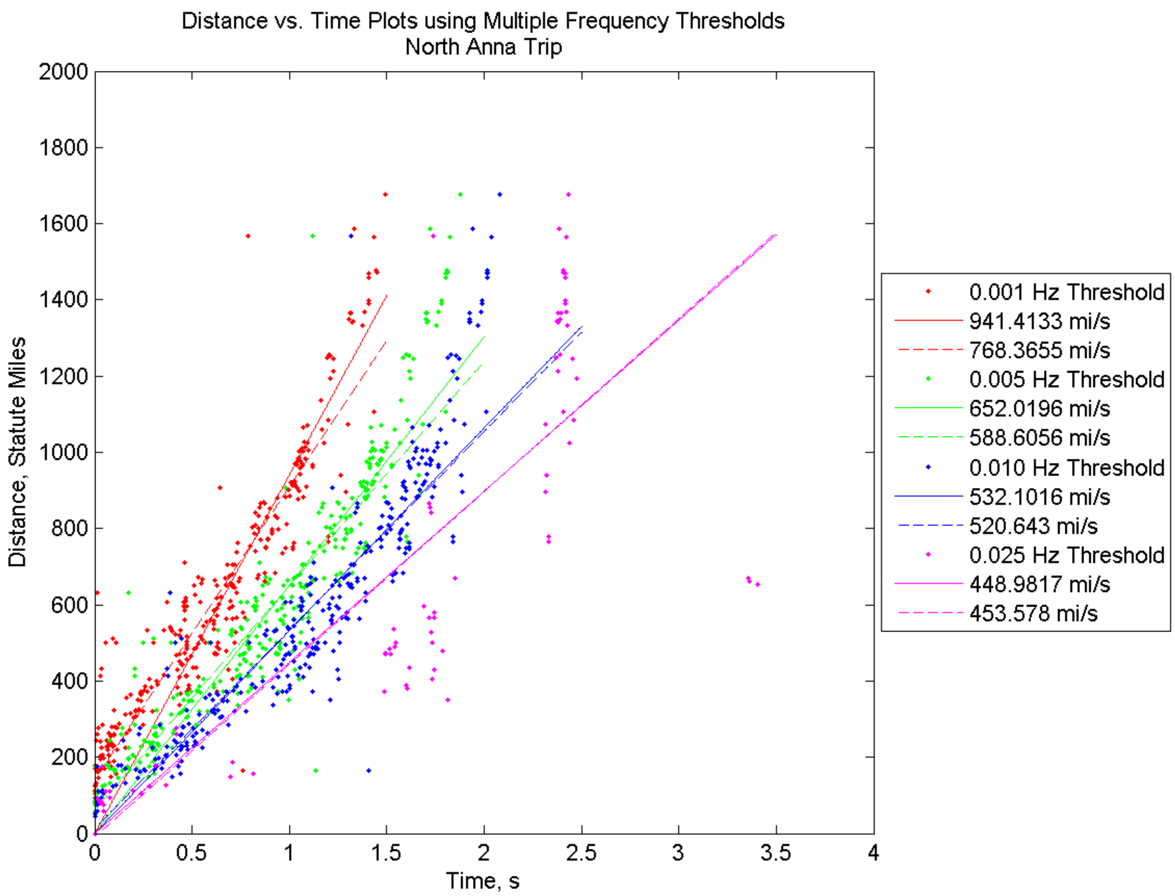
Distance vs. Time Plots using Multiple Frequency Thresholds
North Anna Trip
Distance, Statute Miles
Time, s
0
200
400
600
800
1000
1200
1400
1600
1800
2000
0
0.5
1
1.5
2
2.5
3
3.5
4
0.001 Hz Threshold
941.4133 mi/s
768.3655 mi/s
0.005 Hz Threshold
652.0196 mi/s
588.6056 mi/s
0.010 Hz Threshold
532.1016 mi/s
520.643 mi/s
0.025 Hz Threshold
448.9817 mi/s
453.578 mi/s

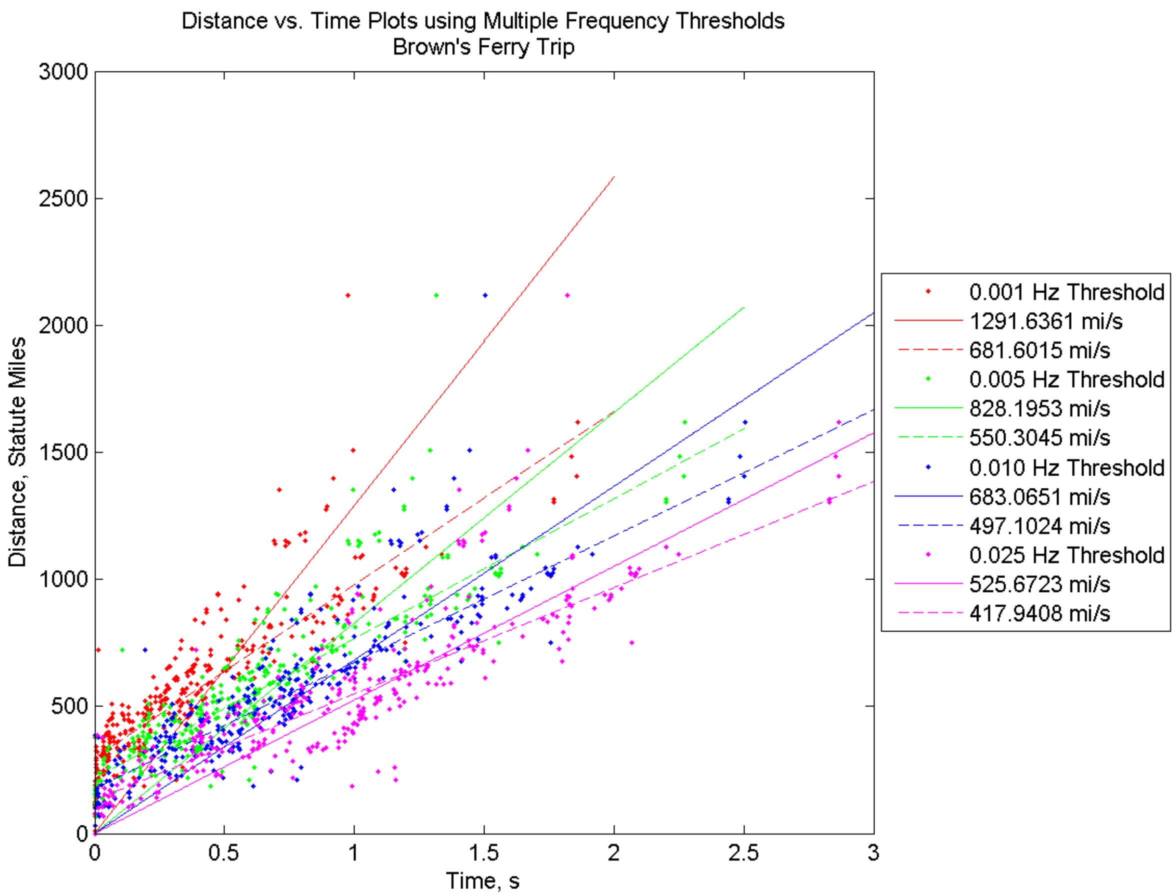
Distance vs. Time Plots using Multiple Frequency Thresholds
Brown's Ferry Trip
Distance, Statute Miles
Time, s
0.001 Hz Threshold
1291.6361 mi/s
681.6015 mi/s
0.005 Hz Threshold
828.1953 mi/s
550.3045 mi/s
0.010 Hz Threshold
683.0651 mi/s
497.1024 mi/s
0.025 Hz Threshold
525.6723 mi/s
417.9408 mi/s

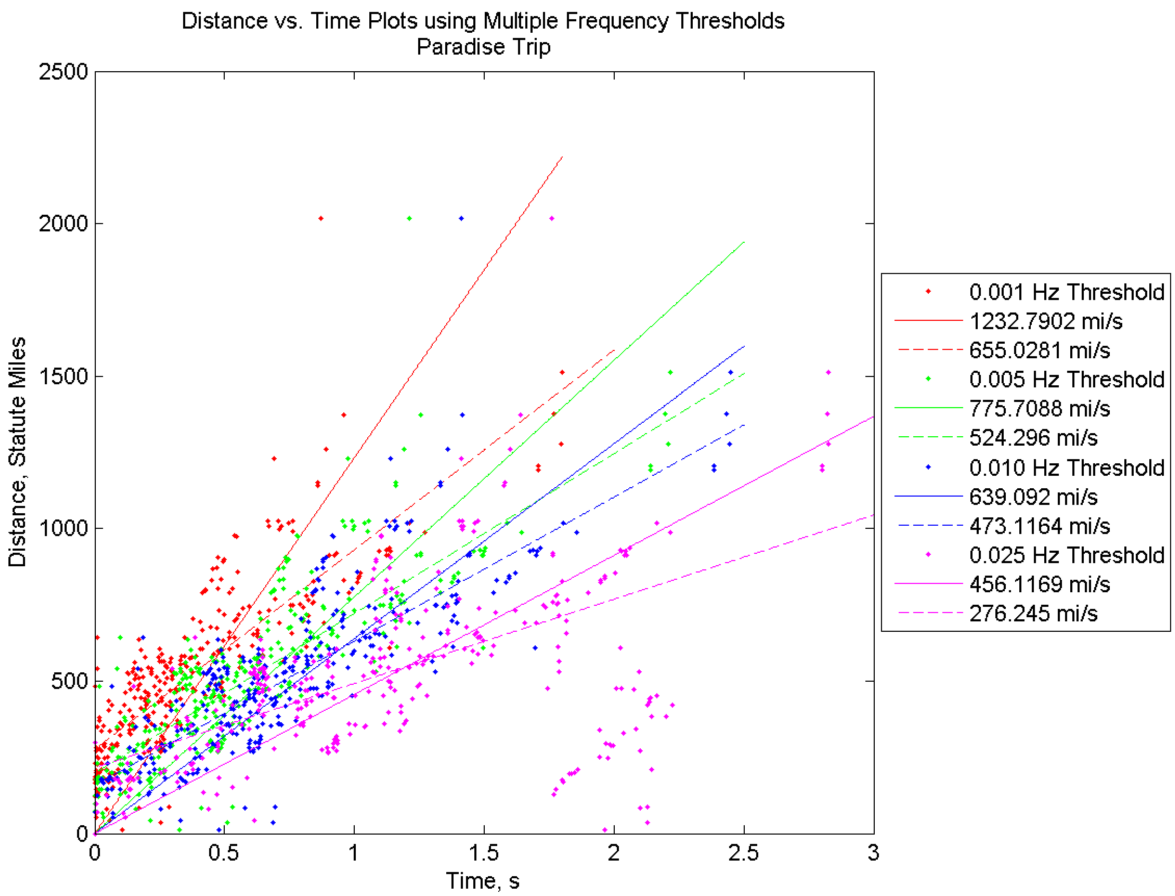
Distance vs. Time Plots using Multiple Frequency Thresholds
Paradise Trip
Distance, Statute Miles
Time, s
0
500
1000
1500
2000
2500
0
0.5
1
1.5
2
2.5
3
0.001 Hz Threshold
1232.7902 mi/s
655.0281 mi/s
0.005 Hz Threshold
775.7088 mi/s
524.296 mi/s
0.010 Hz Threshold
639.092 mi/s
473.1164 mi/s
0.025 Hz Threshold
456.1169 mi/s
276.245 mi/s

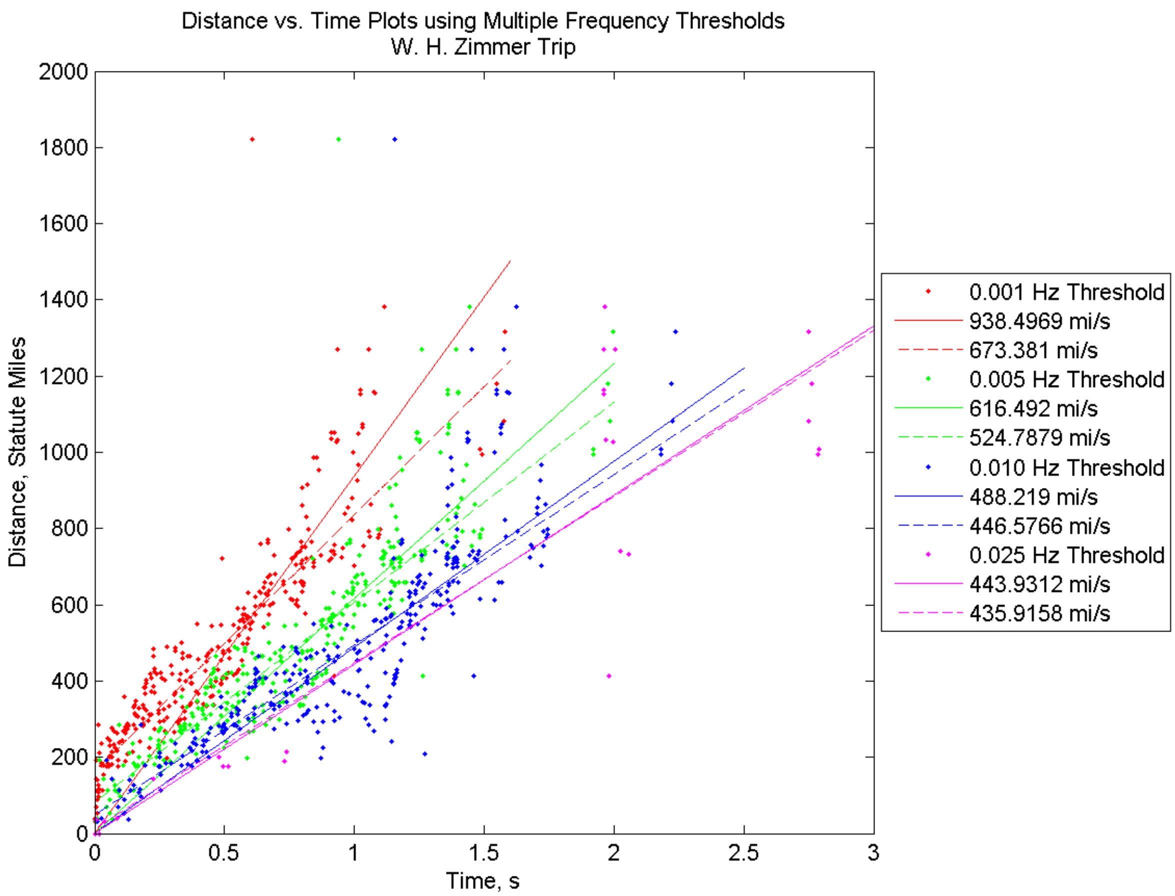
Distance vs. Time Plots using Multiple Frequency Thresholds
W. H. Zimmer Trip
Distance, Statute Miles
Time, s
0
200
400
600
800
1000
1200
1400
1600
1800
2000
0
0.5
1
1.5
2
2.5
3
0.001 Hz Threshold
938.4969 mi/s
673.381 mi/s
0.005 Hz Threshold
616.492 mi/s
524.7879 mi/s
0.010 Hz Threshold
488.219 mi/s
446.5766 mi/s
0.025 Hz Threshold
443.9312 mi/s
435.9158 mi/s

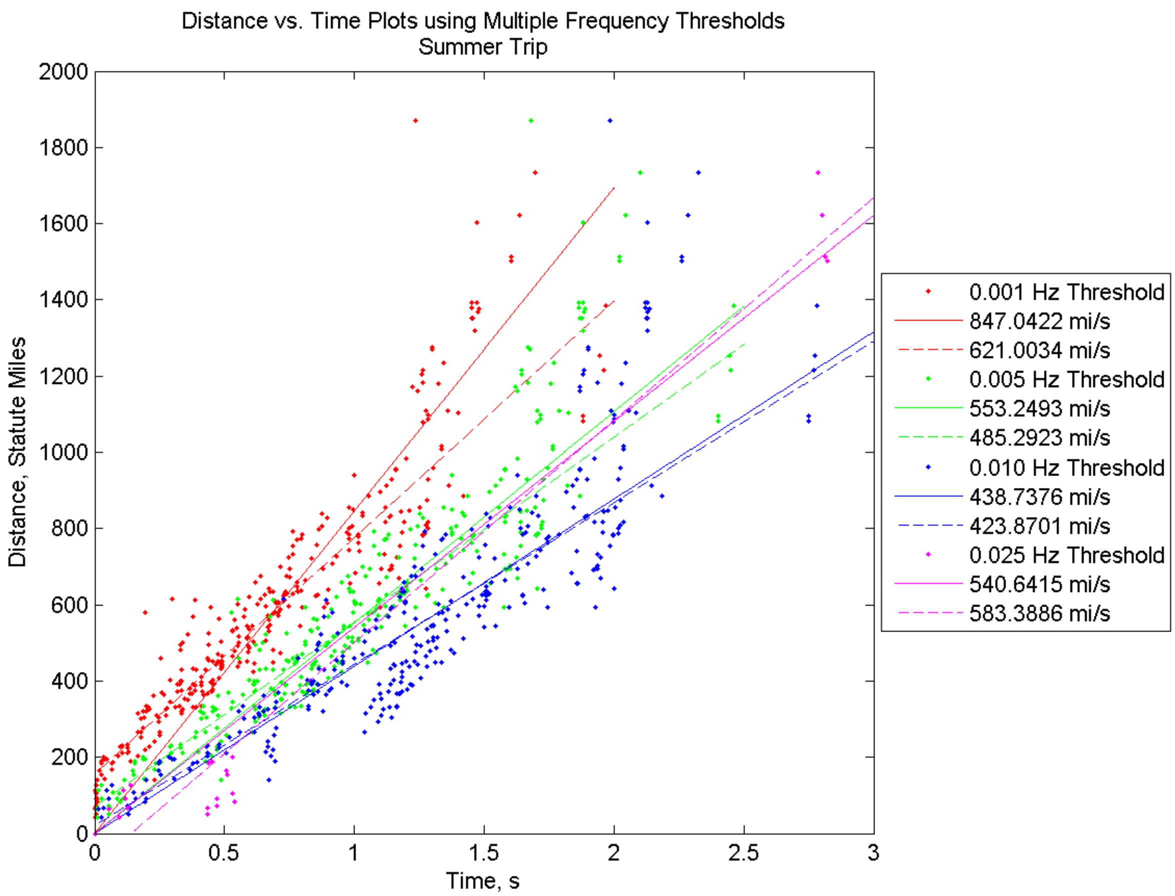
Distance vs. Time Plots using Multiple Frequency Thresholds
Summer Trip
Distance, Statute Miles
Time, s
0
200
400
600
800
1000
1200
1400
1600
1800
2000
0
0.5
1
1.5
2
2.5
3
0.001 Hz Threshold
847.0422 mi/s
621.0034 mi/s
0.005 Hz Threshold
553.2493 mi/s
485.2923 mi/s
0.010 Hz Threshold
438.7376 mi/s
423.8701 mi/s
0.025 Hz Threshold
540.6415 mi/s
583.3886 mi/s

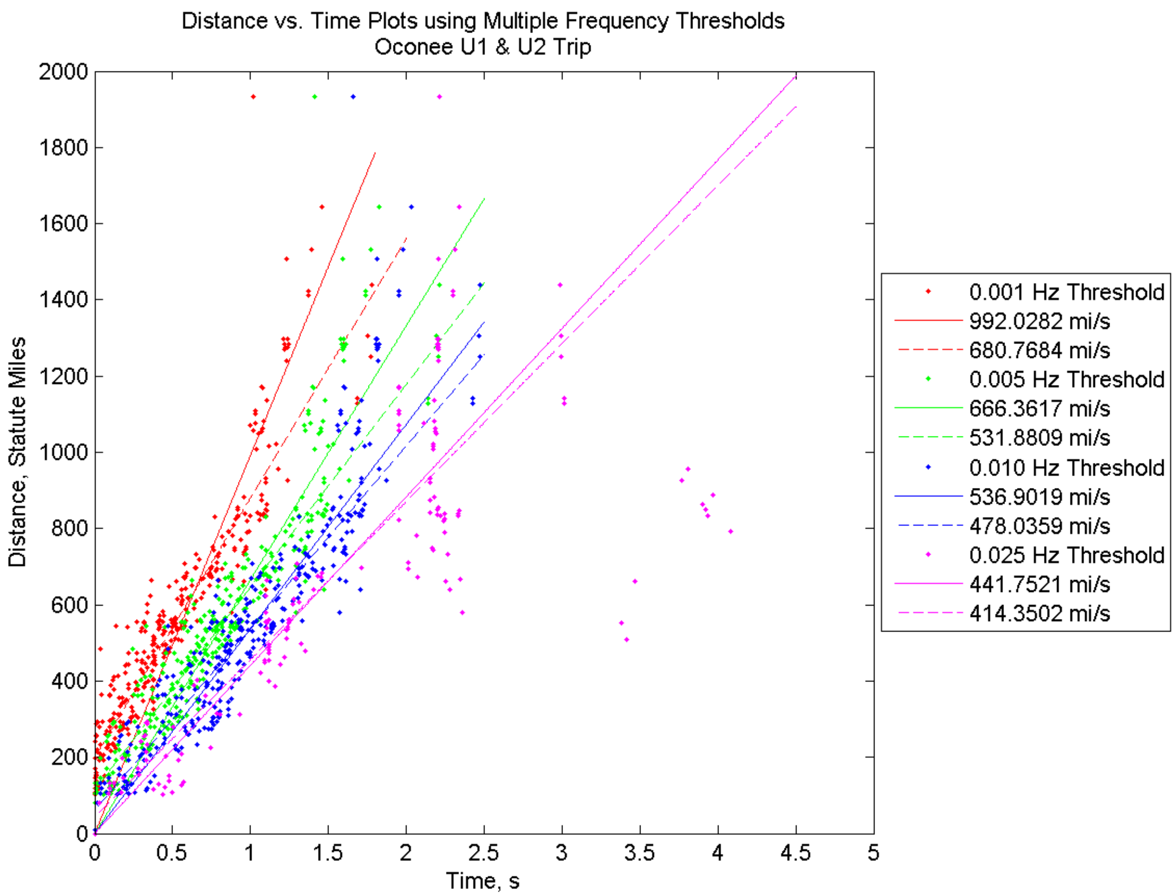
Distance vs. Time Plots using Multiple Frequency Thresholds
Oconee U1 & U2 Trip
Distance, Statute Miles
Time, s
0.001 Hz Threshold
992.0282 mi/s
680.7684 mi/s
0.005 Hz Threshold
666.3617 mi/s
531.8809 mi/s
0.010 Hz Threshold
536.9019 mi/s
478.0359 mi/s
0.025 Hz Threshold
441.7521 mi/s
414.3502 mi/s

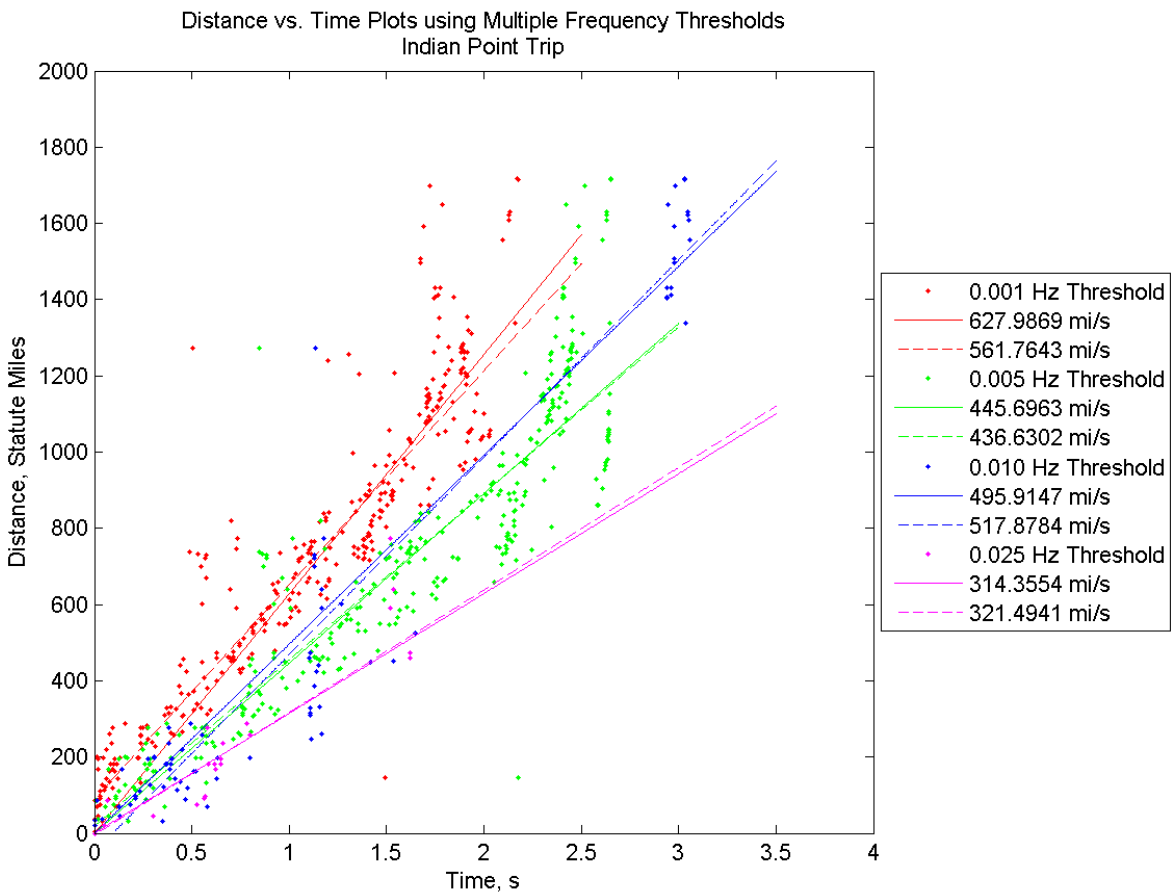
Distance vs. Time Plots using Multiple Frequency Thresholds
Indian Point Trip
Distance, Statute Miles
Time, s
0
200
400
600
800
1000
1200
1400
1600
1800
2000
0
0.5
1
1.5
2
2.5
3
3.5
4
0.001 Hz Threshold
627.9869 mi/s
561.7643 mi/s
0.005 Hz Threshold
445.6963 mi/s
436.6302 mi/s
0.010 Hz Threshold
495.9147 mi/s
517.8784 mi/s
0.025 Hz Threshold
314.3554 mi/s
321.4941 mi/s

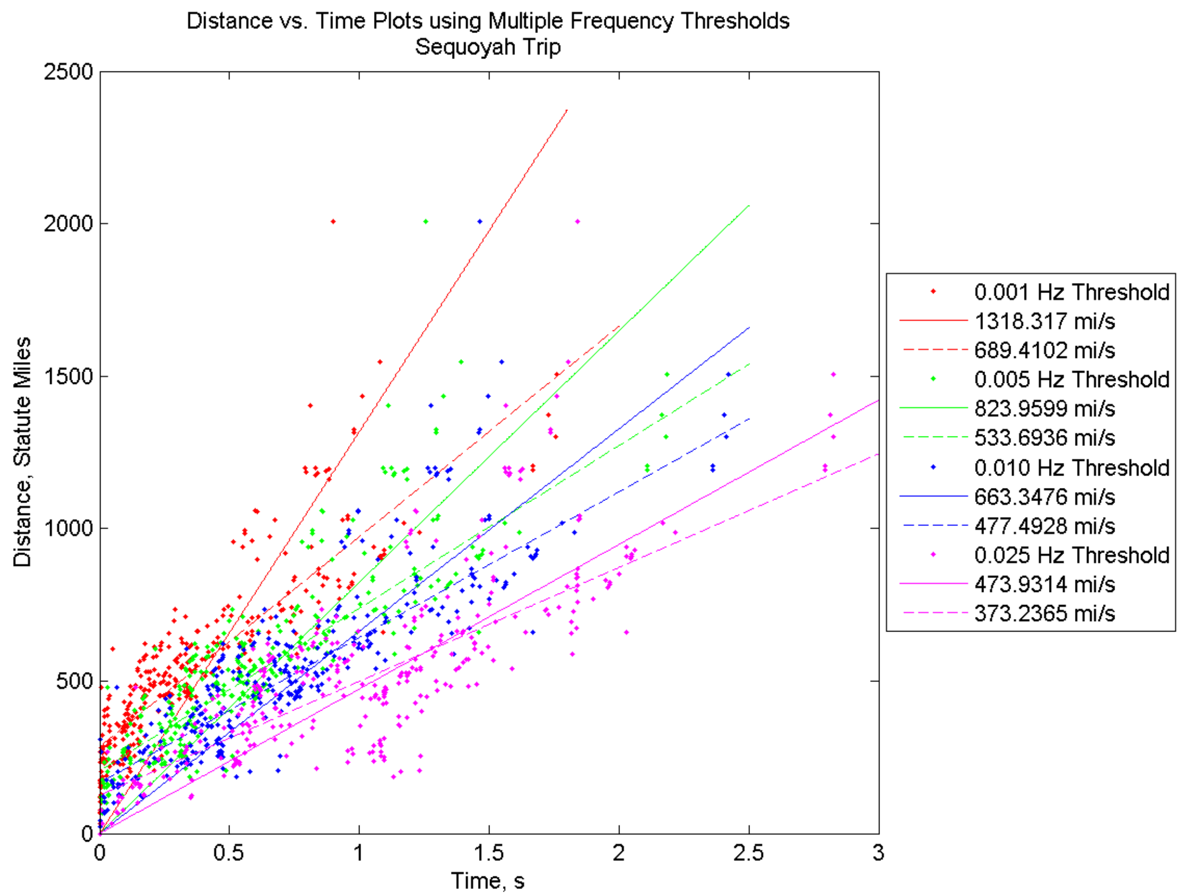
Distance vs. Time Plots using Multiple Frequency Thresholds
Sequoyah Trip
Distance, Statute Miles
Time, s
0
500
1000
1500
2000
2500
0
0.5
1
1.5
2
2.5
3
0.001 Hz Threshold
1318.317 mi/s
689.4102 mi/s
0.005 Hz Threshold
823.9599 mi/s
533.6936 mi/s
0.010 Hz Threshold
663.3476 mi/s
477.4928 mi/s
0.025 Hz Threshold
473.9314 mi/s
373.2365 mi/s

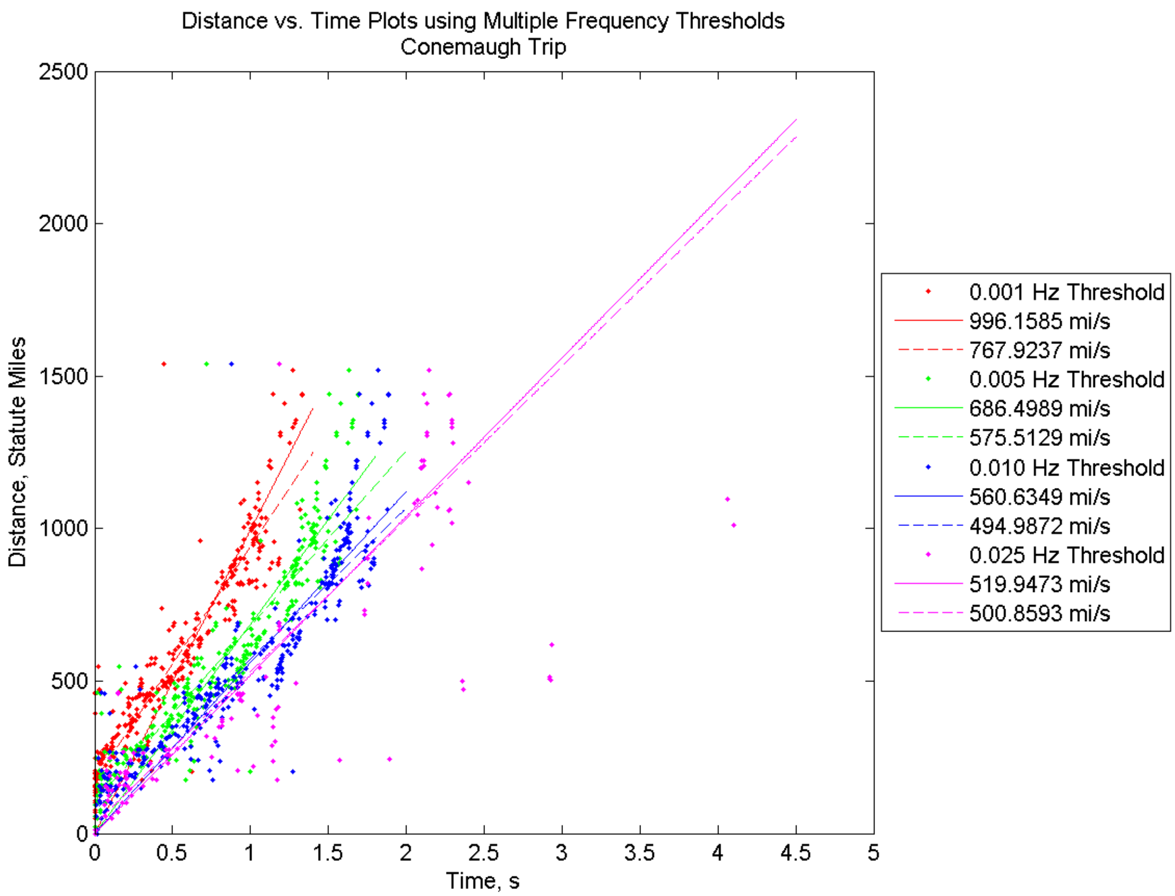
Distance vs. Time Plots using Multiple Frequency Thresholds
Conemaugh Trip
Distance, Statute Miles
Time, s
0
500
1000
1500
2000
2500
0.5
1
1.5
2
2.5
3
3.5
4
4.5
5
0.001 Hz Threshold
996.1585 mi/s
767.9237 mi/s
0.005 Hz Threshold
686.4989 mi/s
575.5129 mi/s
0.010 Hz Threshold
560.6349 mi/s
494.9872 mi/s
0.025 Hz Threshold
519.9473 mi/s
500.8593 mi/s

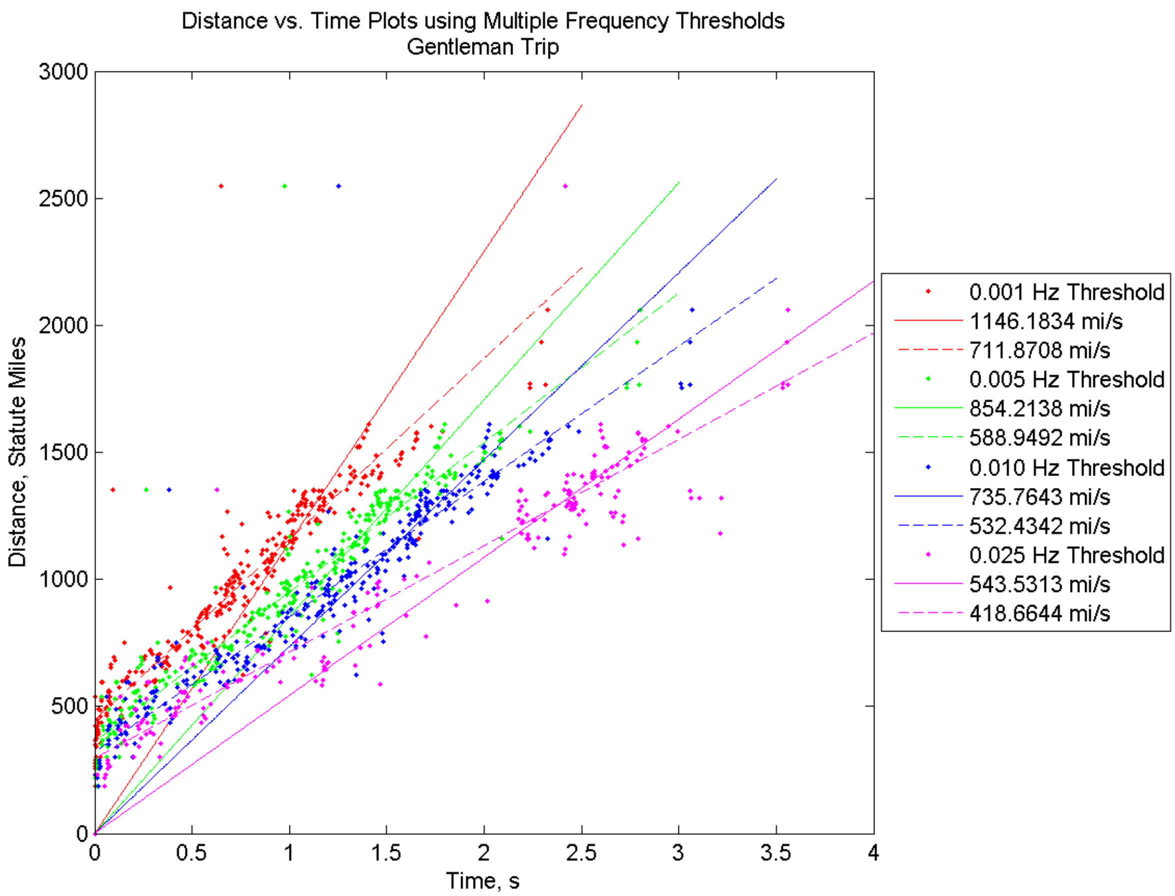
Distance vs. Time Plots using Multiple Frequency Thresholds
Gentleman Trip
Distance, Statute Miles
Time, s
0
0.5
1
1.5
2
2.5
3
3.5
4
500
1000
1500
2000
2500
3000
0.001 Hz Threshold
1146.1834 mi/s
711.8708 mi/s
0.005 Hz Threshold
854.2138 mi/s
588.9492 mi/s
0.010 Hz Threshold
735.7643 mi/s
532.4342 mi/s
0.025 Hz Threshold
543.5313 mi/s
418.6644 mi/s

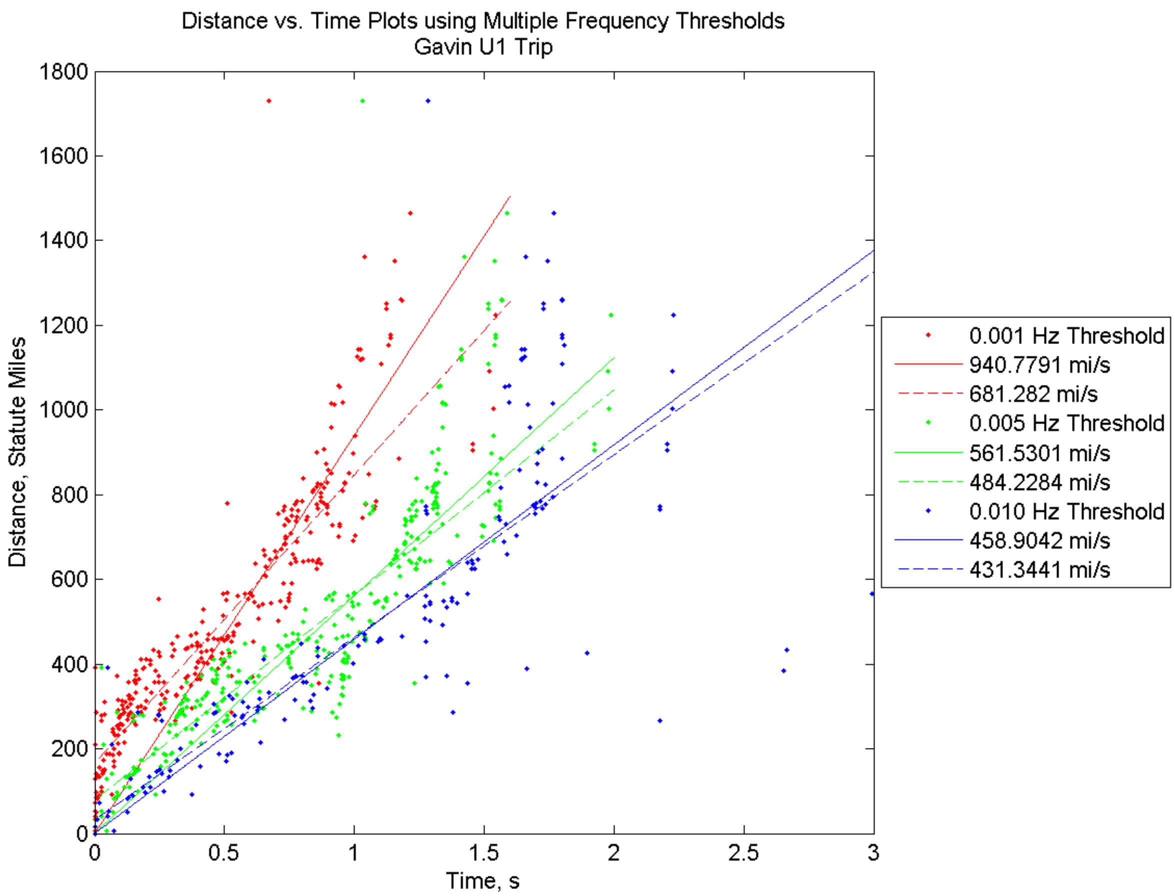

Distance vs. Time Plots using Multiple Frequency Thresholds
Gavin U1 Trip
Distance, Statute Miles
Time, s
0.001 Hz Threshold
940.7791 mi/s
681.282 mi/s
0.005 Hz Threshold
561.5301 mi/s
484.2284 mi/s
0.010 Hz Threshold
458.9042 mi/s
431.3441 mi/s

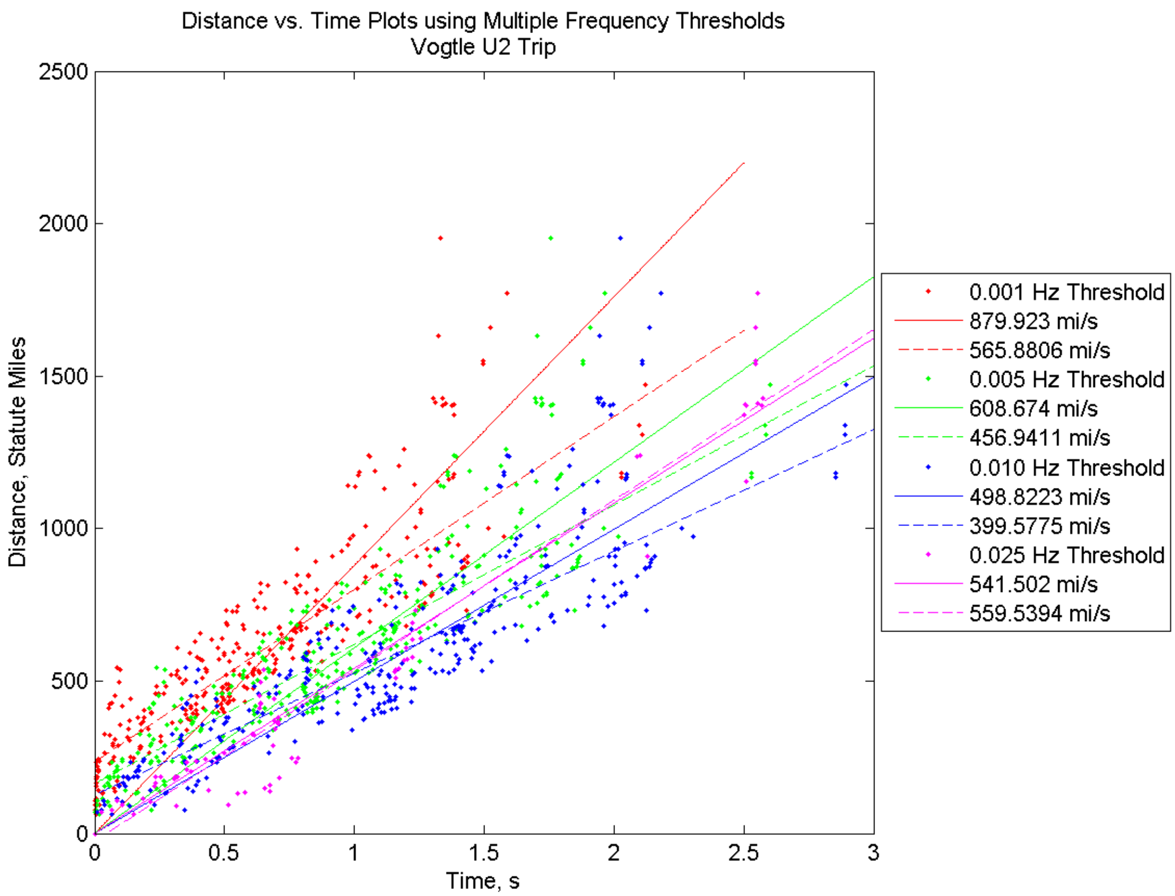

Distance vs. Time Plots using Multiple Frequency Thresholds
Vogtle U2 Trip
Distance, Statute Miles
Time, s
0
500
1000
1500
2000
2500
0.5
1
1.5
2
2.5
3
0.001 Hz Threshold
879.923 mi/s
565.8806 mi/s
0.005 Hz Threshold
608.674 mi/s
456.9411 mi/s
0.010 Hz Threshold
498.8223 mi/s
399.5775 mi/s
0.025 Hz Threshold
541.502 mi/s
559.5394 mi/s

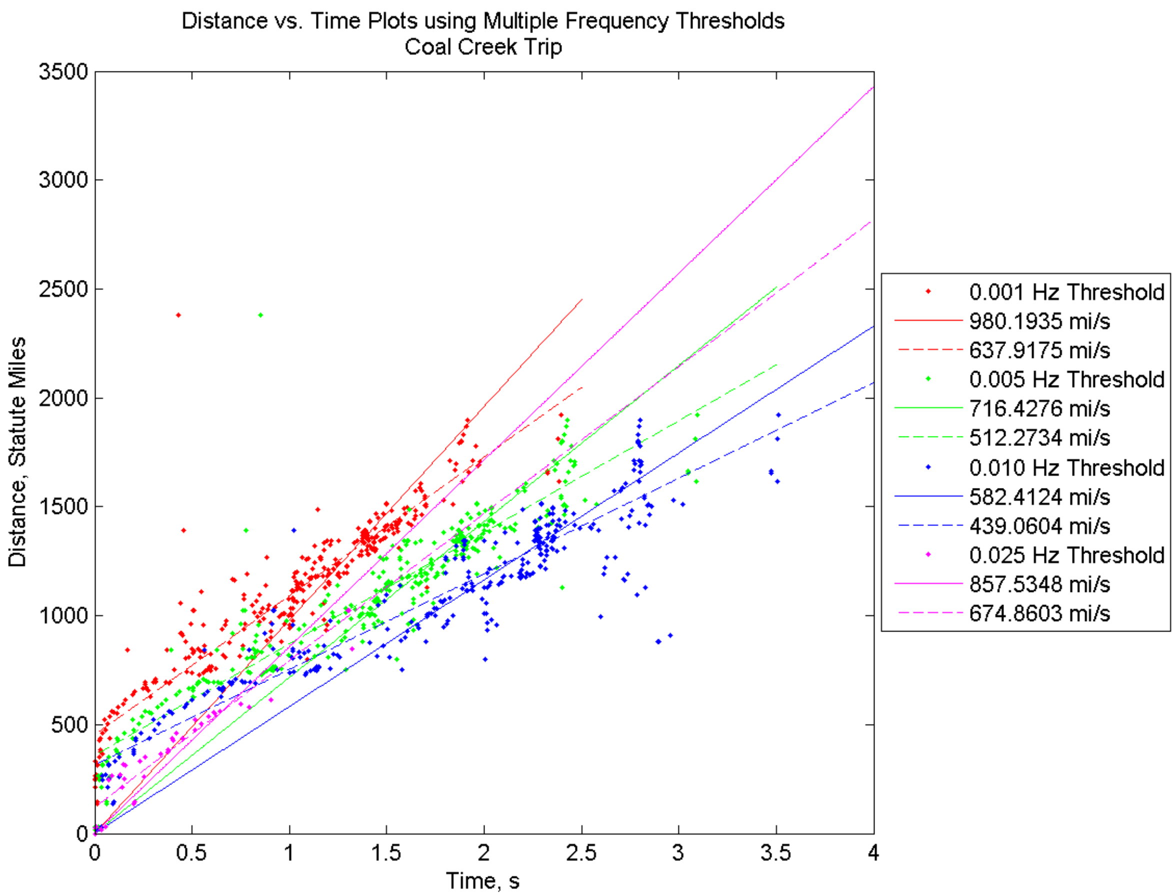
Distance vs. Time Plots using Multiple Frequency Thresholds
Coal Creek Trip
Distance, Statute Miles
Time, s
0.001 Hz Threshold
980.1935 mi/s
637.9175 mi/s
0.005 Hz Threshold
716.4276 mi/s
512.2734 mi/s
0.010 Hz Threshold
582.4124 mi/s
439.0604 mi/s
0.025 Hz Threshold
857.5348 mi/s
674.8603 mi/s

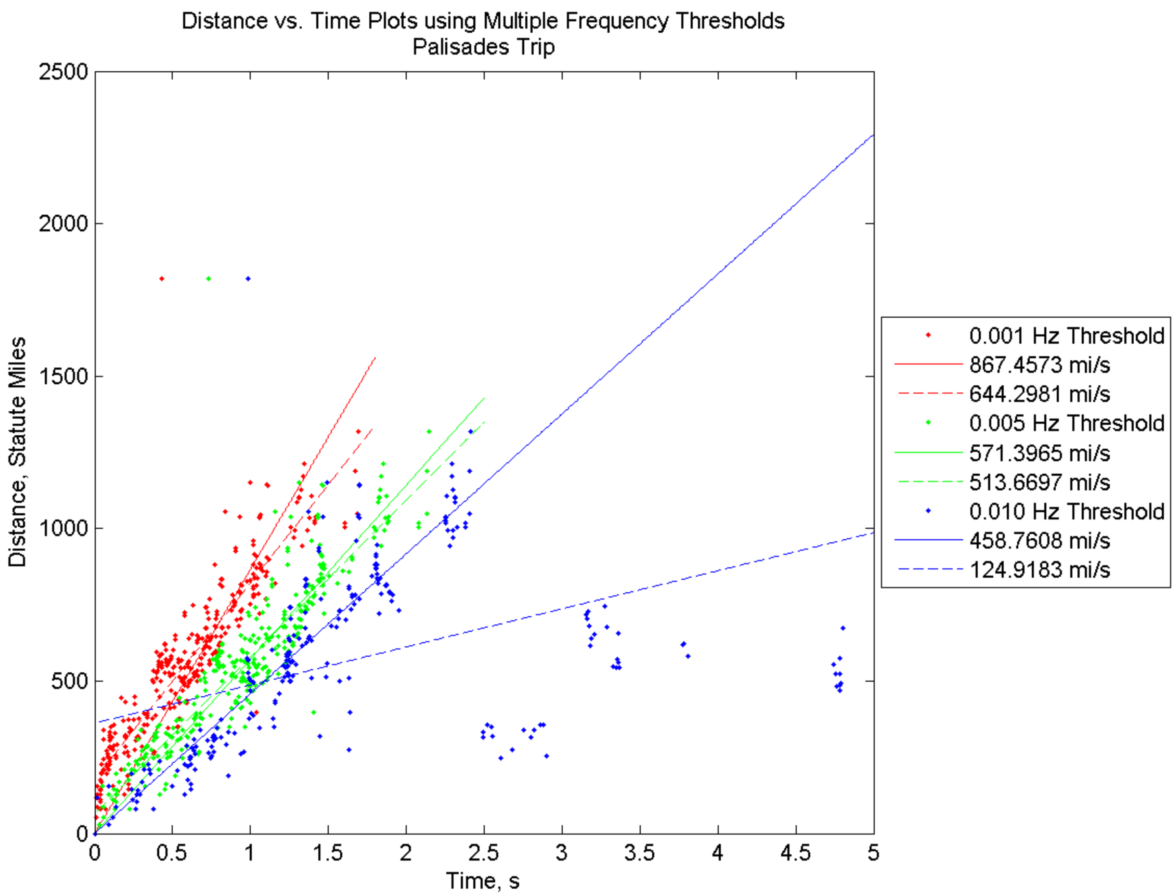
Distance vs. Time Plots using Multiple Frequency Thresholds
Palisades Trip
Distance, Statute Miles
Time, s
0
500
1000
1500
2000
2500
0
0.5
1
1.5
2
2.5
3
3.5
4
4.5
5
0.001 Hz Threshold
867.4573 mi/s
644.2981 mi/s
0.005 Hz Threshold
571.3965 mi/s
513.6697 mi/s
0.010 Hz Threshold
458.7608 mi/s
124.9183 mi/s

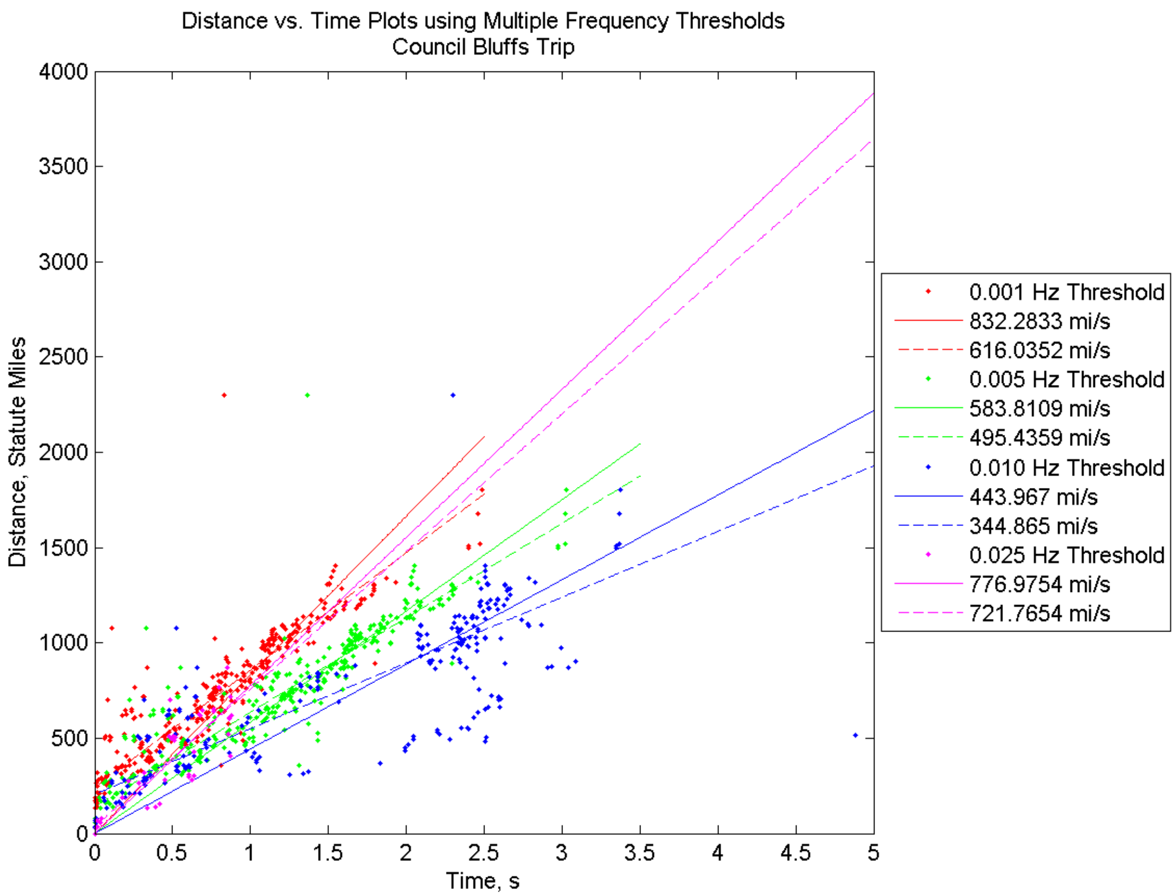
Distance vs. Time Plots using Multiple Frequency Thresholds
Council Bluffs Trip
Distance, Statute Miles
Time, s
0 0.5 1 1.5 2 2.5 3 3.5 4 4.5 5
0 500 1000 1500 2000 2500 3000 3500 4000
0.001 Hz Threshold
832.2833 mi/s
616.0352 mi/s
0.005 Hz Threshold
583.8109 mi/s
495.4359 mi/s
0.010 Hz Threshold
443.967 mi/s
344.865 mi/s
0.025 Hz Threshold
776.9754 mi/s
721.7654 mi/s

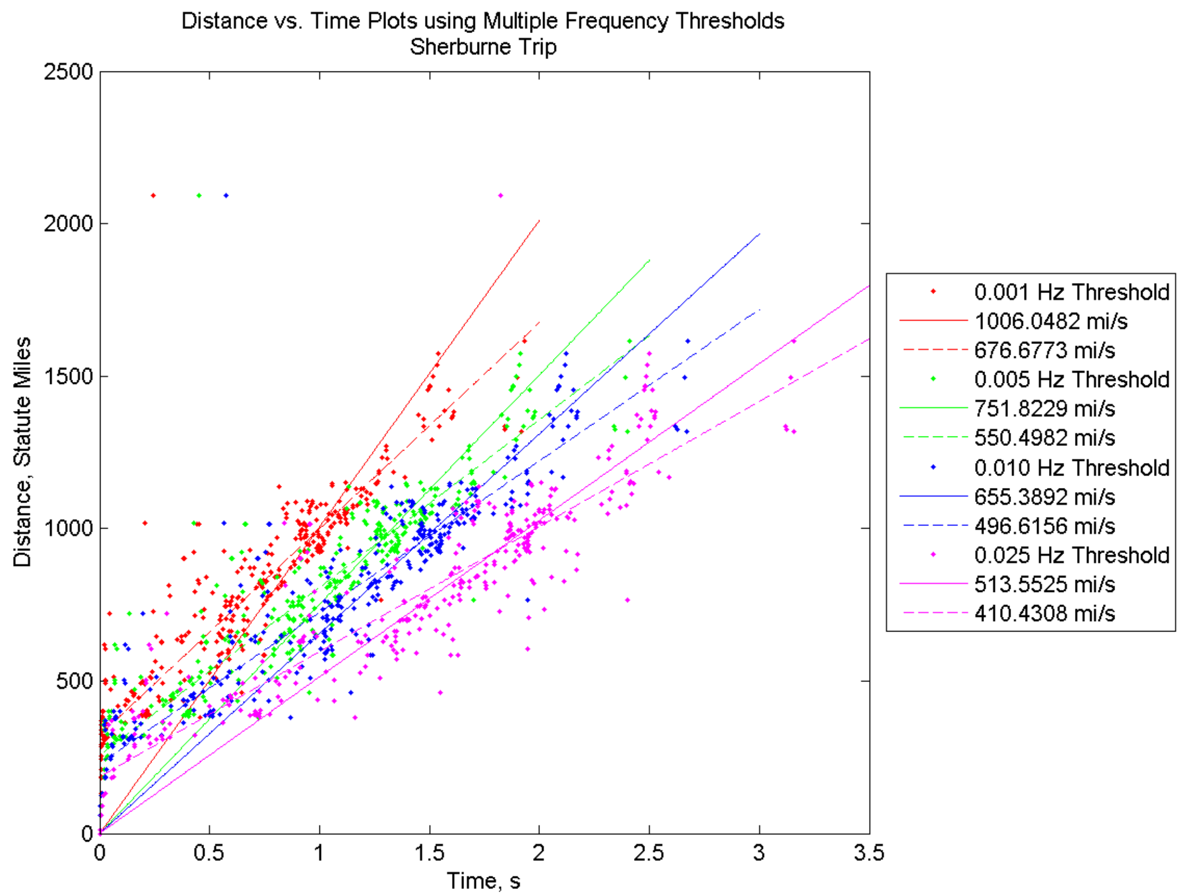
Distance vs. Time Plots using Multiple Frequency Thresholds
Sherburne Trip
Distance, Statute Miles
Time, s
2500
2000
1500
1000
500
0
0
0.5
1
1.5
2
2.5
3
3.5
0.001 Hz Threshold
1006.0482 mi/s
676.6773 mi/s
0.005 Hz Threshold
751.8229 mi/s
550.4982 mi/s
0.010 Hz Threshold
655.3892 mi/s
496.6156 mi/s
0.025 Hz Threshold
513.5525 mi/s
410.4308 mi/s

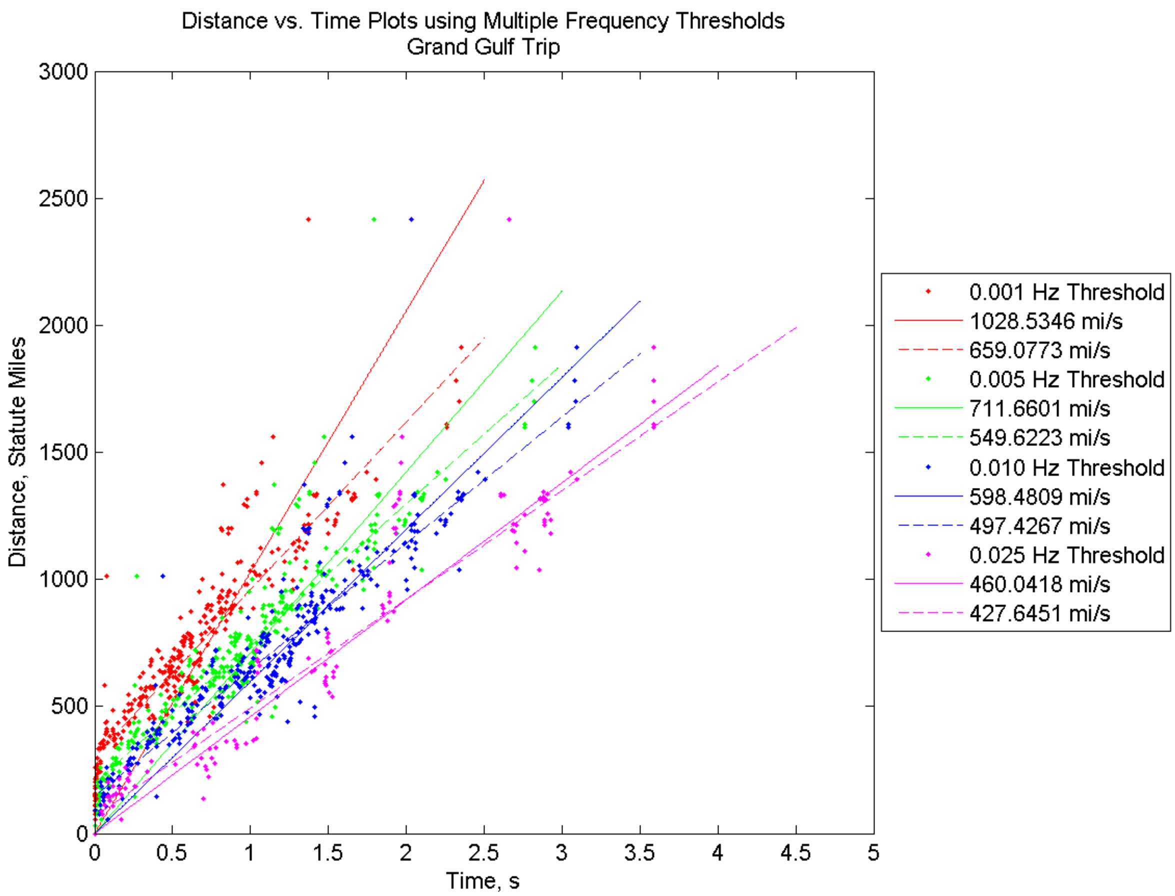
Distance vs. Time Plots using Multiple Frequency Thresholds
Grand Gulf Trip
Distance, Statute Miles
Time, s
0.001 Hz Threshold
1028.5346 mi/s
659.0773 mi/s
0.005 Hz Threshold
711.6601 mi/s
549.6223 mi/s
0.010 Hz Threshold
598.4809 mi/s
497.4267 mi/s
0.025 Hz Threshold
460.0418 mi/s
427.6451 mi/s

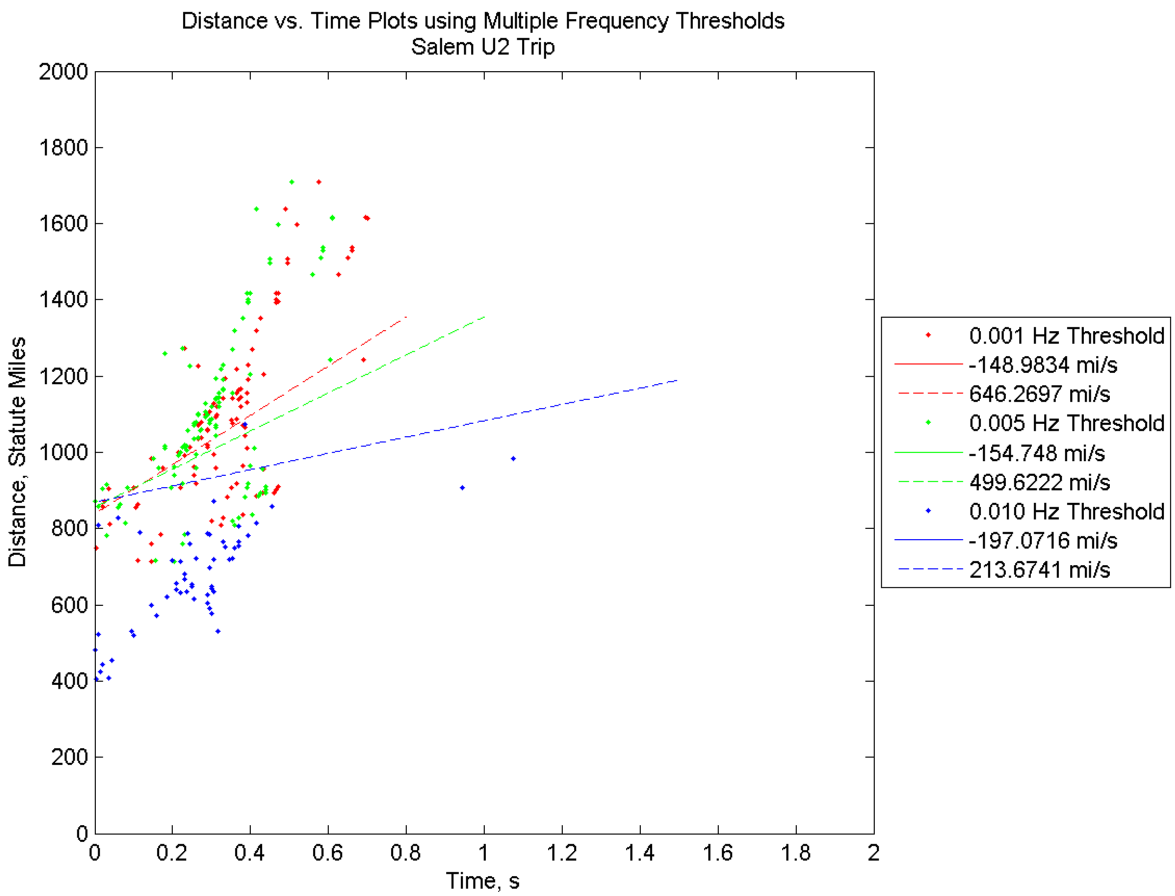

Distance vs. Time Plots using Multiple Frequency Thresholds
Salem U2 Trip
Distance, Statute Miles
Time, s
0
200
400
600
800
1000
1200
1400
1600
1800
2000
0
0.2
0.4
0.6
0.8
1
1.2
1.4
1.6
1.8
2
0.001 Hz Threshold
-148.9834 mi/s
646.2697 mi/s
0.005 Hz Threshold
-154.748 mi/s
499.6222 mi/s
0.010 Hz Threshold
-197.0716 mi/s
213.6741 mi/s

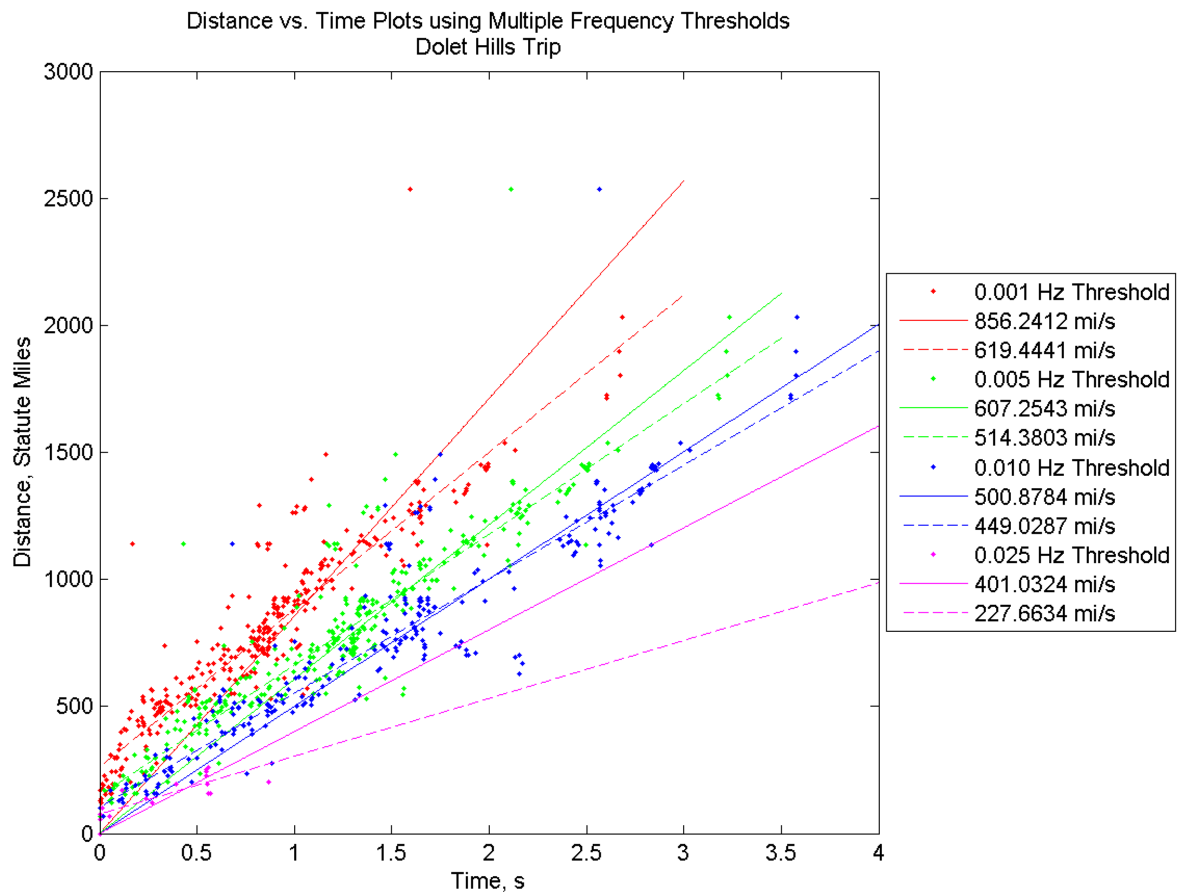
Distance vs. Time Plots using Multiple Frequency Thresholds
Dolet Hills Trip
Distance, Statute Miles
Time, s
0
500
1000
1500
2000
2500
3000
0
0.5
1
1.5
2
2.5
3
3.5
4
0.001 Hz Threshold
856.2412 mi/s
619.4441 mi/s
0.005 Hz Threshold
607.2543 mi/s
514.3803 mi/s
0.010 Hz Threshold
500.8784 mi/s
449.0287 mi/s
0.025 Hz Threshold
401.0324 mi/s
227.6634 mi/s

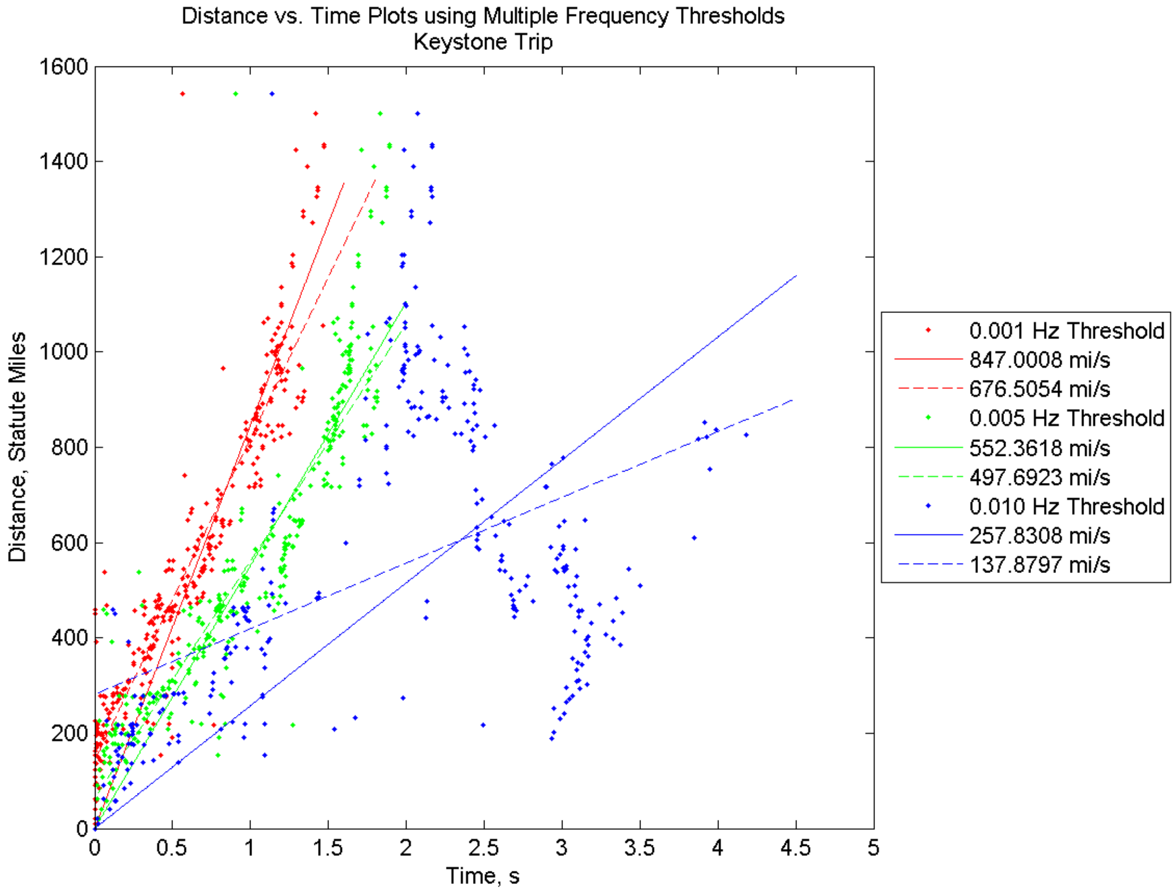
Distance vs. Time Plots using Multiple Frequency Thresholds
Keystone Trip
Distance, Statute Miles
Time, s
0
200
400
600
800
1000
1200
1400
1600
0
0.5
1
1.5
2
2.5
3
3.5
4
4.5
5
0.001 Hz Threshold
847.0008 mi/s
676.5054 mi/s
0.005 Hz Threshold
552.3618 mi/s
497.6923 mi/s
0.010 Hz Threshold
257.8308 mi/s
137.8797 mi/s

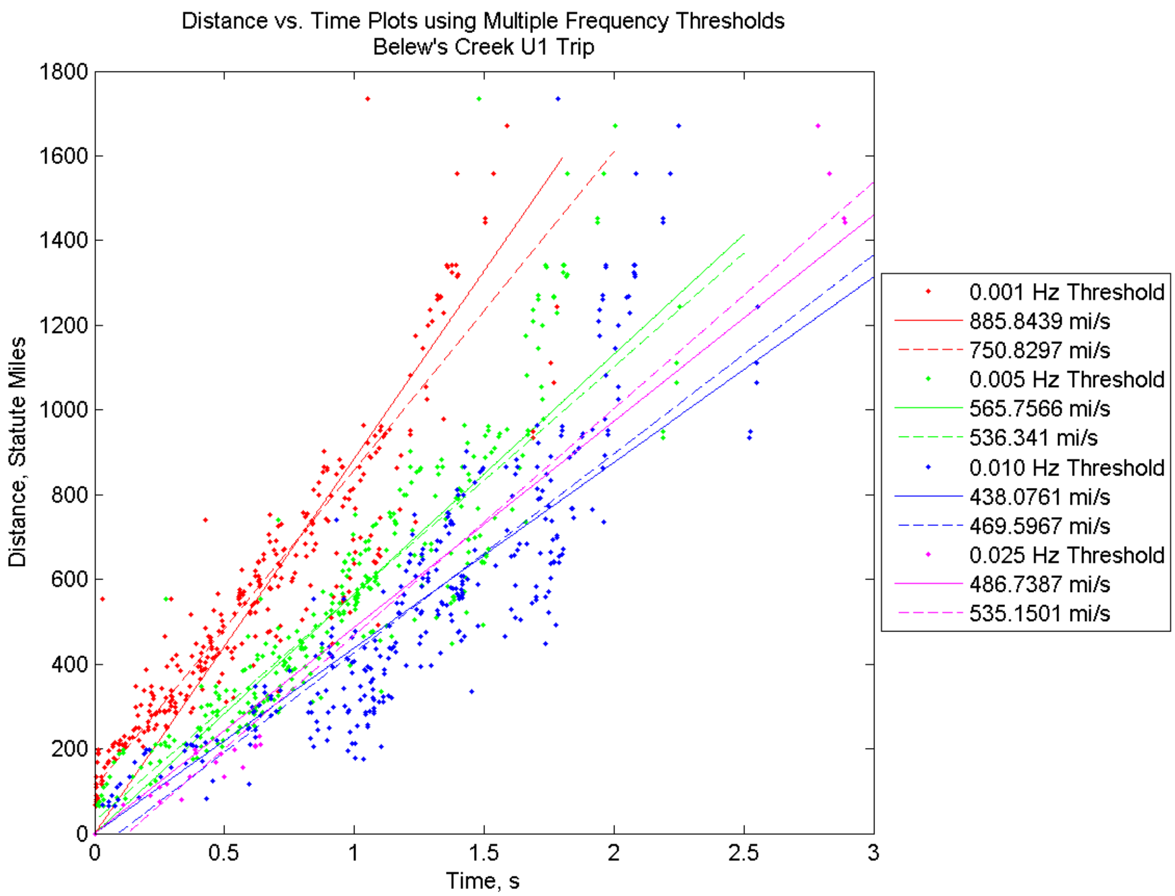
Distance vs. Time Plots using Multiple Frequency Thresholds
Belew's Creek U1 Trip
Distance, Statute Miles
Time, s
0
200
400
600
800
1000
1200
1400
1600
1800
0
0.5
1
1.5
2
2.5
3
0.001 Hz Threshold
885.8439 mi/s
750.8297 mi/s
0.005 Hz Threshold
565.7566 mi/s
536.341 mi/s
0.010 Hz Threshold
438.0761 mi/s
469.5967 mi/s
0.025 Hz Threshold
486.7387 mi/s
535.1501 mi/s

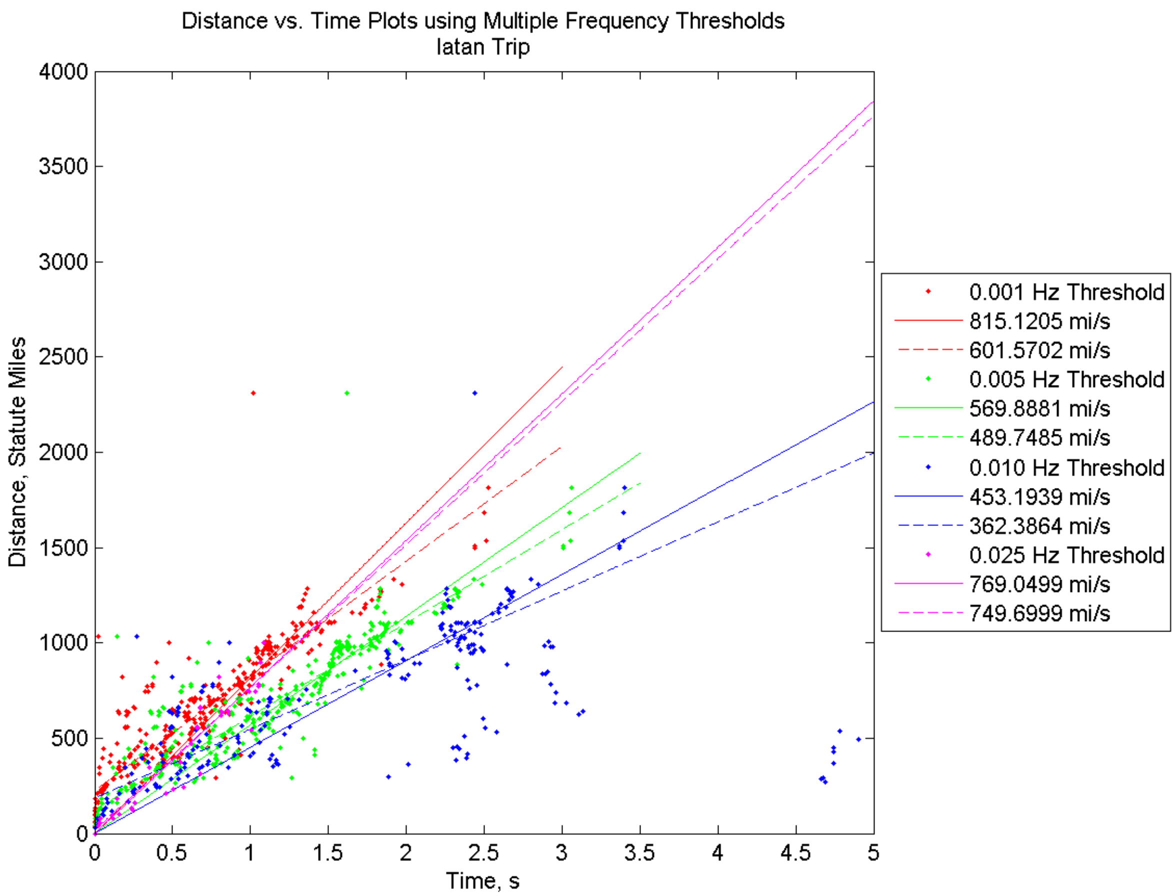
Distance vs. Time Plots using Multiple Frequency Thresholds
Iatan Trip
Distance, Statute Miles
Time, s
0.001 Hz Threshold
815.1205 mi/s
601.5702 mi/s
0.005 Hz Threshold
569.8881 mi/s
489.7485 mi/s
0.010 Hz Threshold
453.1939 mi/s
362.3864 mi/s
0.025 Hz Threshold
769.0499 mi/s
749.6999 mi/s

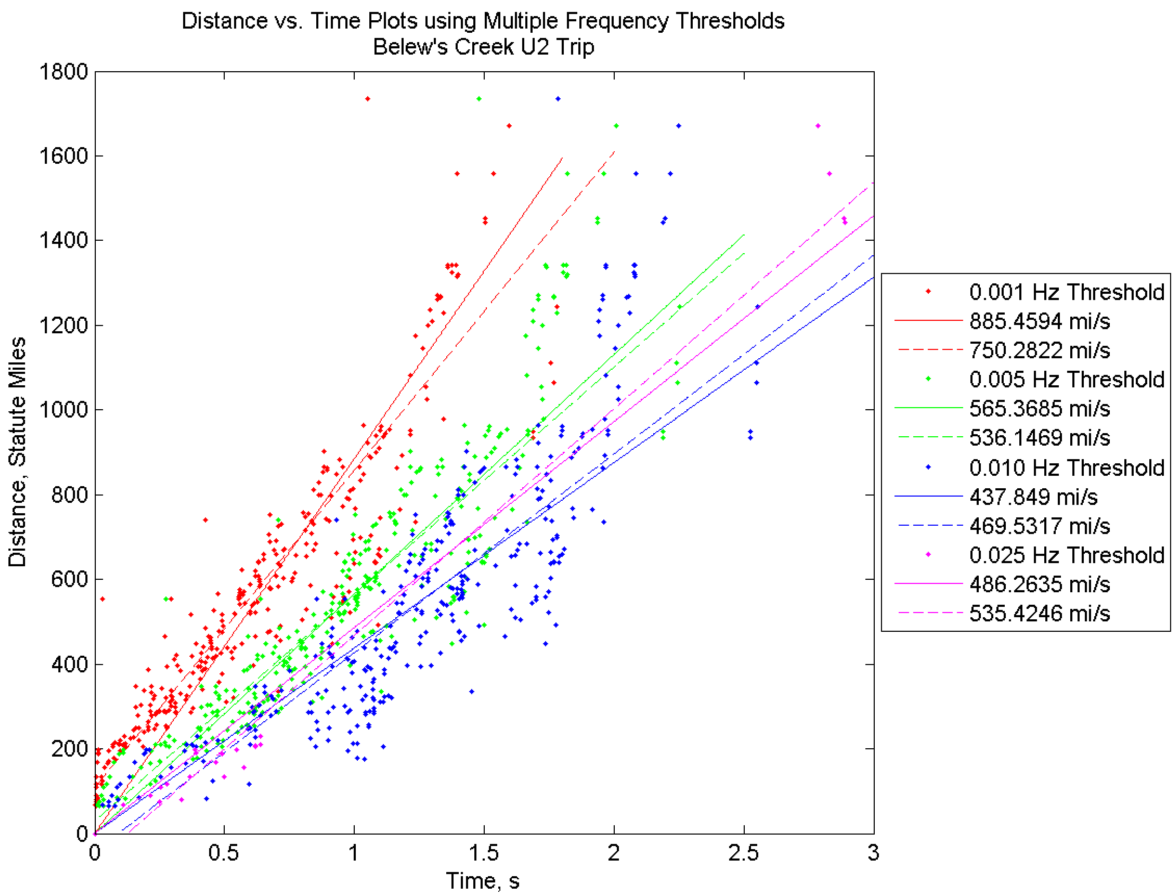
Distance vs. Time Plots using Multiple Frequency Thresholds
Belew's Creek U2 Trip
Distance, Statute Miles
Time, s
0
200
400
600
800
1000
1200
1400
1600
1800
0
0.5
1
1.5
2
2.5
3
0.001 Hz Threshold
885.4594 mi/s
750.2822 mi/s
0.005 Hz Threshold
565.3685 mi/s
536.1469 mi/s
0.010 Hz Threshold
437.849 mi/s
469.5317 mi/s
0.025 Hz Threshold
486.2635 mi/s
535.4246 mi/s

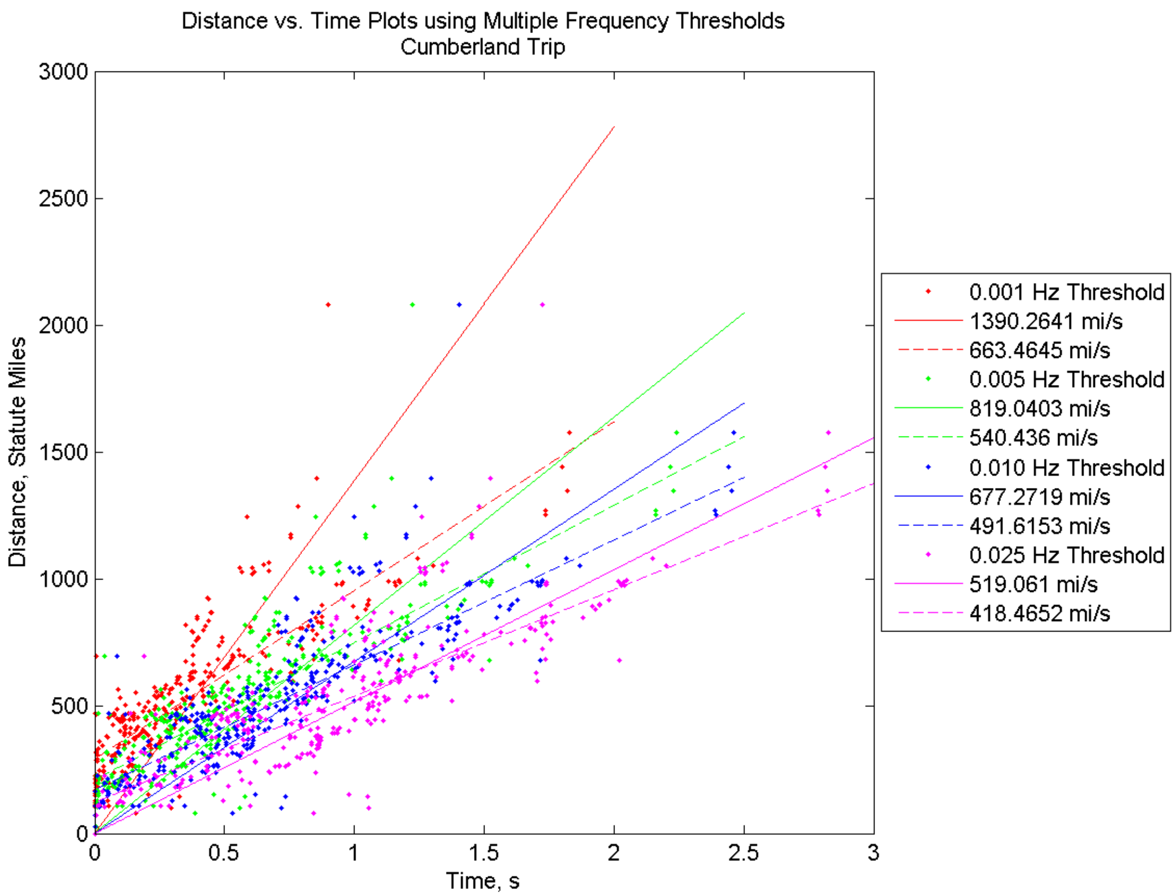
Distance vs. Time Plots using Multiple Frequency Thresholds
Cumberland Trip
Distance, Statute Miles
Time, s
0
500
1000
1500
2000
2500
3000
0
0.5
1
1.5
2
2.5
3
0.001 Hz Threshold
1390.2641 mi/s
663.4645 mi/s
0.005 Hz Threshold
819.0403 mi/s
540.436 mi/s
0.010 Hz Threshold
677.2719 mi/s
491.6153 mi/s
0.025 Hz Threshold
519.061 mi/s
418.4652 mi/s

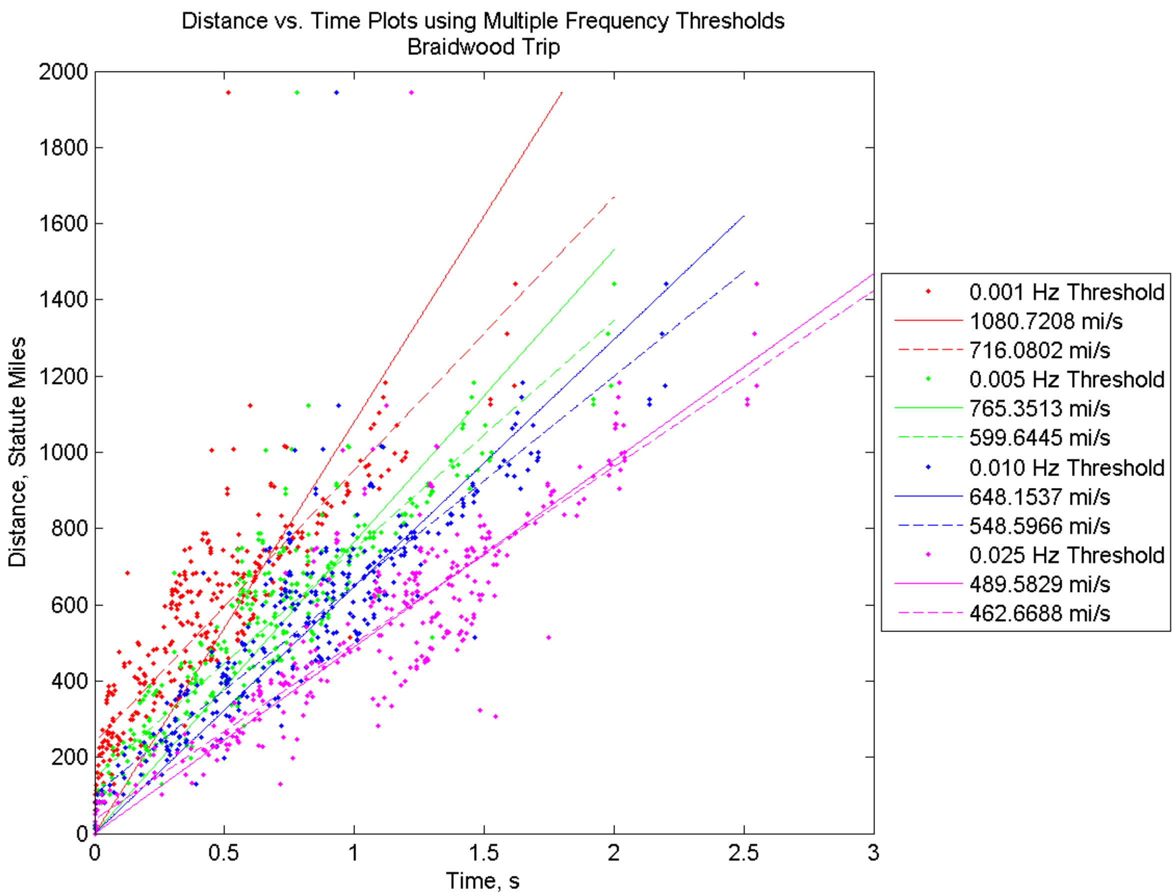
Distance vs. Time Plots using Multiple Frequency Thresholds
Braidwood Trip
Distance, Statute Miles
Time, s
0
200
400
600
800
1000
1200
1400
1600
1800
2000
0
0.5
1
1.5
2
2.5
3
0.001 Hz Threshold
1080.7208 mi/s
716.0802 mi/s
0.005 Hz Threshold
765.3513 mi/s
599.6445 mi/s
0.010 Hz Threshold
648.1537 mi/s
548.5966 mi/s
0.025 Hz Threshold
489.5829 mi/s
462.6688 mi/s

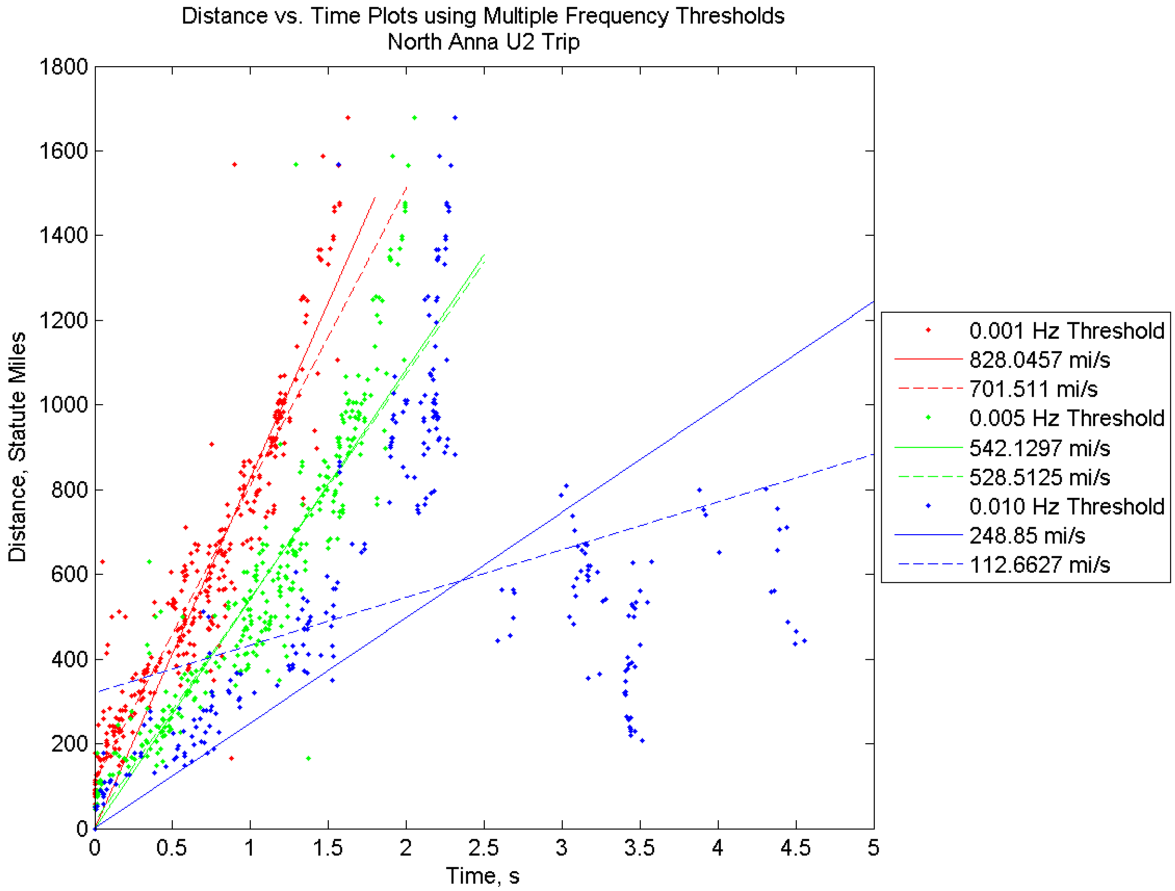

Distance vs. Time Plots using Multiple Frequency Thresholds
North Anna U2 Trip
Distance, Statute Miles
Time, s
0.001 Hz Threshold
828.0457 mi/s
701.511 mi/s
0.005 Hz Threshold
542.1297 mi/s
528.5125 mi/s
0.010 Hz Threshold
248.85 mi/s
112.6627 mi/s

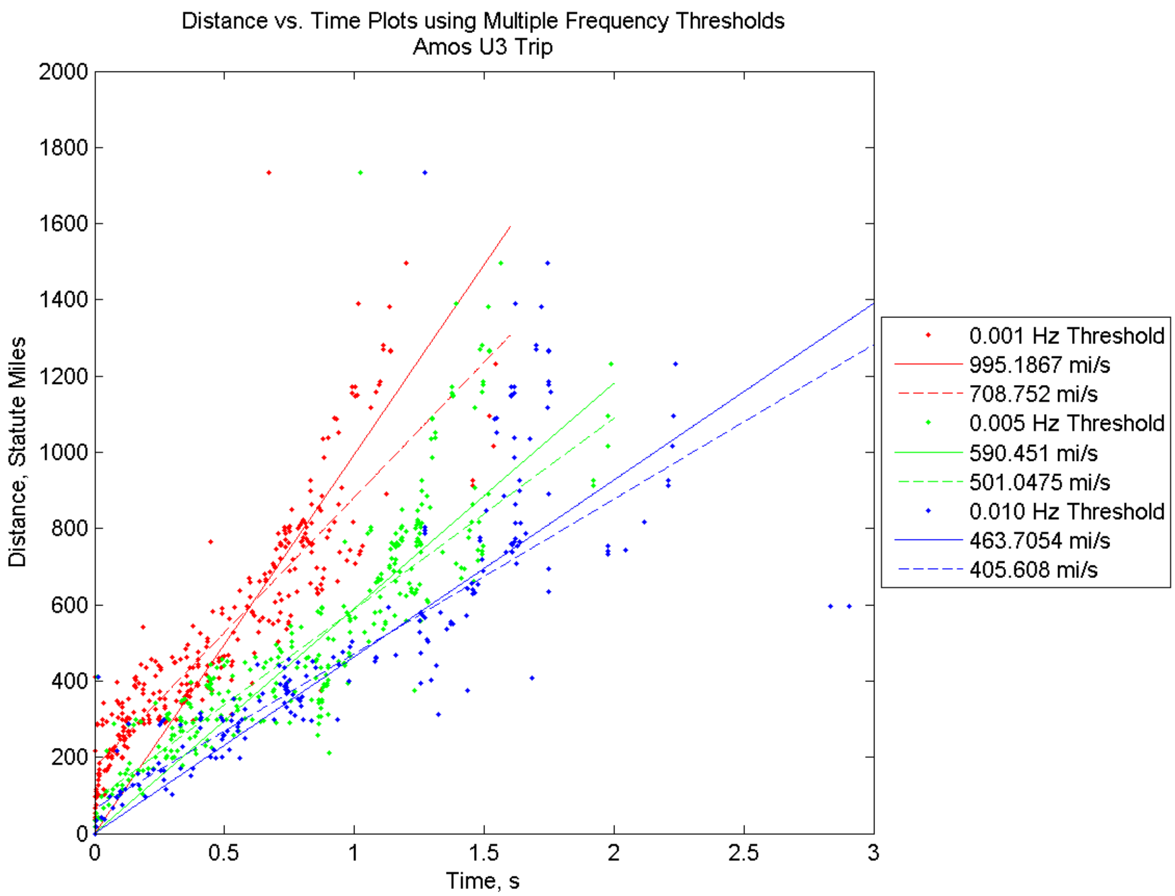

Distance vs. Time Plots using Multiple Frequency Thresholds
Amos U3 Trip
Distance, Statute Miles
Time, s
0.001 Hz Threshold
995.1867 mi/s
708.752 mi/s
0.005 Hz Threshold
590.451 mi/s
501.0475 mi/s
0.010 Hz Threshold
463.7054 mi/s
405.608 mi/s

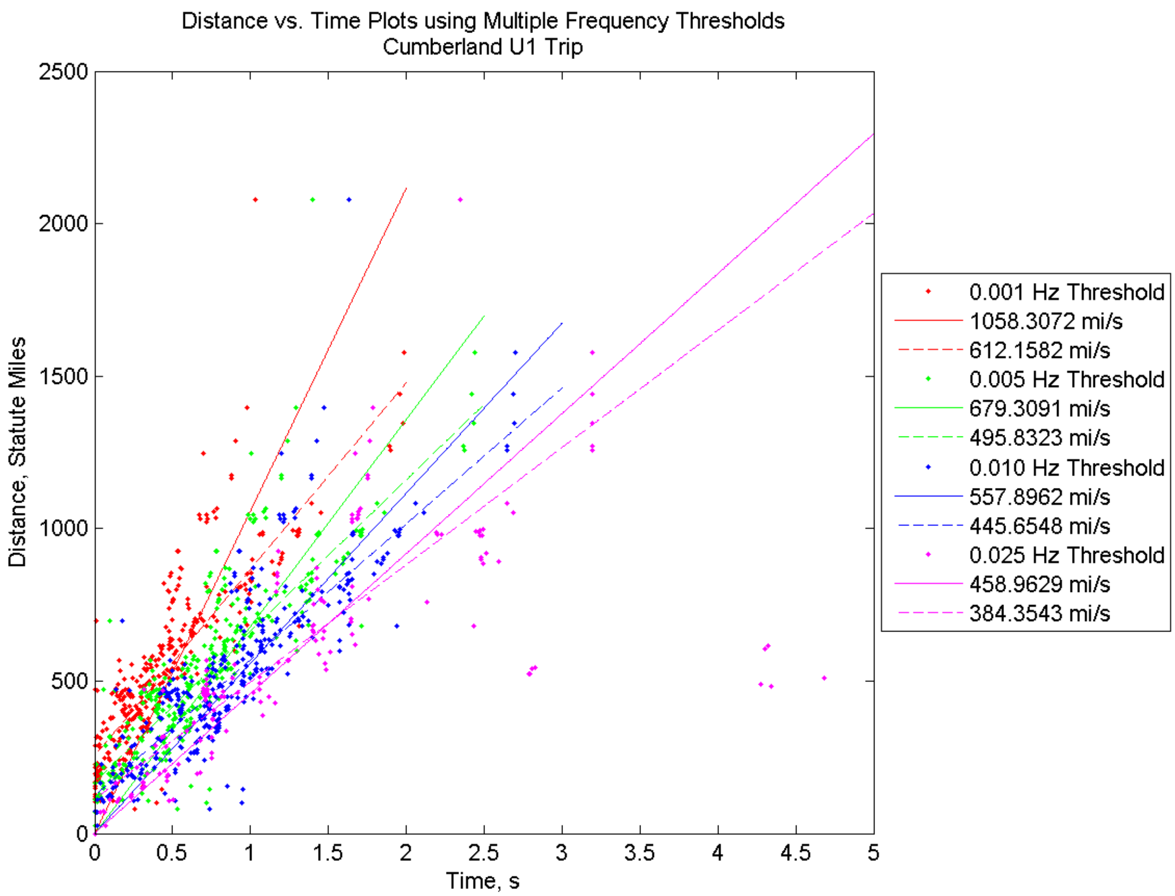
Distance vs. Time Plots using Multiple Frequency Thresholds
Cumberland U1 Trip
Distance, Statute Miles
Time, s
0.001 Hz Threshold
1058.3072 mi/s
612.1582 mi/s
0.005 Hz Threshold
679.3091 mi/s
495.8323 mi/s
0.010 Hz Threshold
557.8962 mi/s
445.6548 mi/s
0.025 Hz Threshold
458.9629 mi/s
384.3543 mi/s

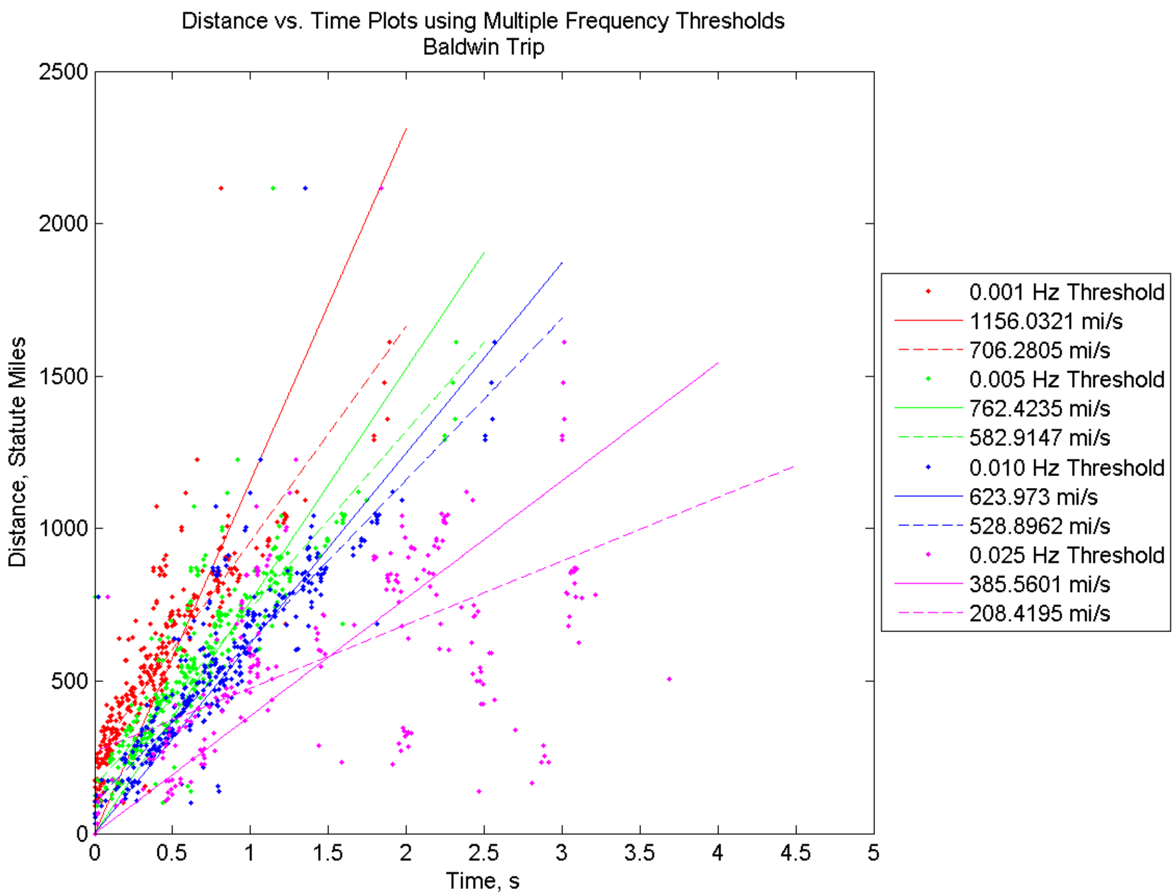
Distance vs. Time Plots using Multiple Frequency Thresholds
Baldwin Trip
Distance, Statute Miles
Time, s
0
0.5
1
1.5
2
2.5
3
3.5
4
4.5
5
500
1000
1500
2000
2500
0.001 Hz Threshold
1156.0321 mi/s
706.2805 mi/s
0.005 Hz Threshold
762.4235 mi/s
582.9147 mi/s
0.010 Hz Threshold
623.973 mi/s
528.8962 mi/s
0.025 Hz Threshold
385.5601 mi/s
208.4195 mi/s

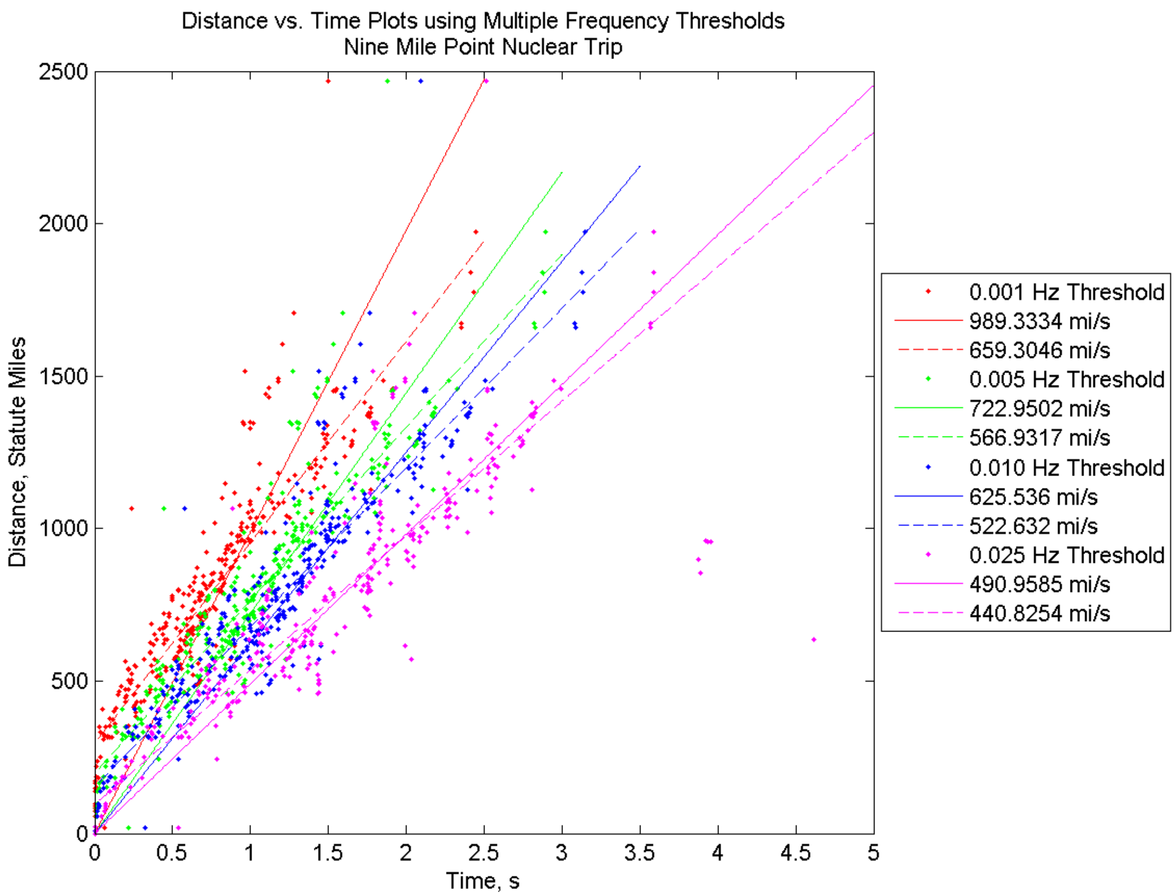
Distance vs. Time Plots using Multiple Frequency Thresholds
Nine Mile Point Nuclear Trip
Distance, Statute Miles
Time, s
0.001 Hz Threshold
989.3334 mi/s
659.3046 mi/s
0.005 Hz Threshold
722.9502 mi/s
566.9317 mi/s
0.010 Hz Threshold
625.536 mi/s
522.632 mi/s
0.025 Hz Threshold
490.9585 mi/s
440.8254 mi/s

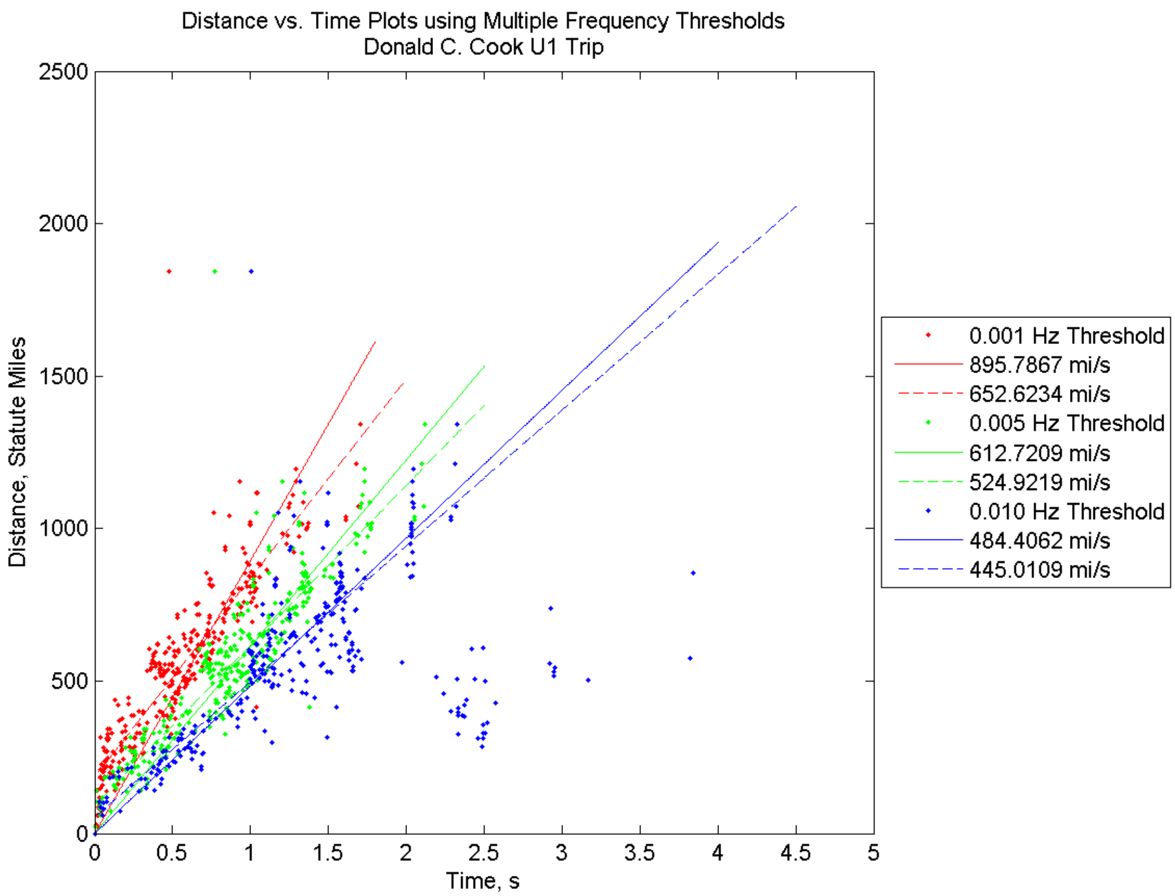

Distance vs. Time Plots using Multiple Frequency Thresholds
Donald C. Cook U1 Trip
Distance, Statute Miles
Time, s
0
500
1000
1500
2000
2500
0.5
1
1.5
2
2.5
3
3.5
4
4.5
5
0.001 Hz Threshold
895.7867 mi/s
652.6234 mi/s
0.005 Hz Threshold
612.7209 mi/s
524.9219 mi/s
0.010 Hz Threshold
484.4062 mi/s
445.0109 mi/s

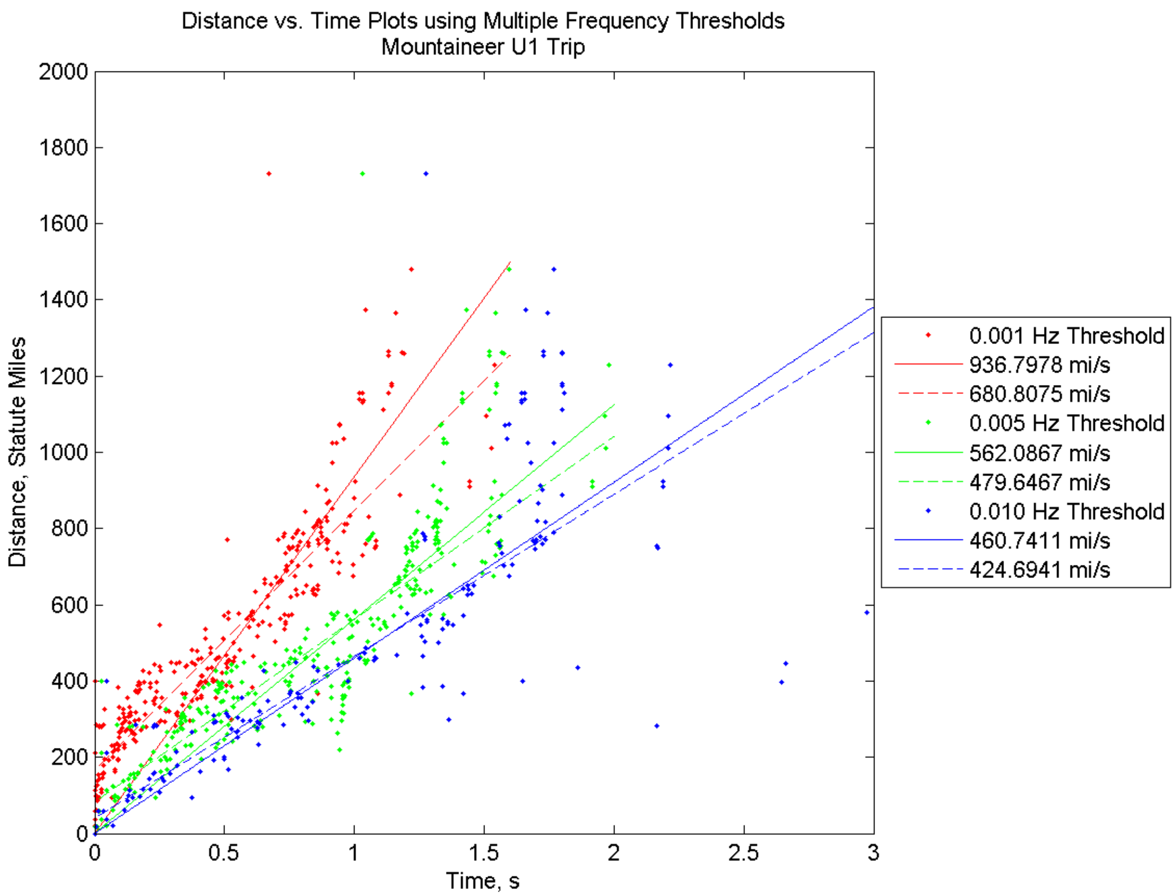
Distance vs. Time Plots using Multiple Frequency Thresholds
Mountaineer U1 Trip
Distance, Statute Miles
Time, s
0
200
400
600
800
1000
1200
1400
1600
1800
2000
0
0.5
1
1.5
2
2.5
3
0.001 Hz Threshold
936.7978 mi/s
680.8075 mi/s
0.005 Hz Threshold
562.0867 mi/s
479.6467 mi/s
0.010 Hz Threshold
460.7411 mi/s
424.6941 mi/s

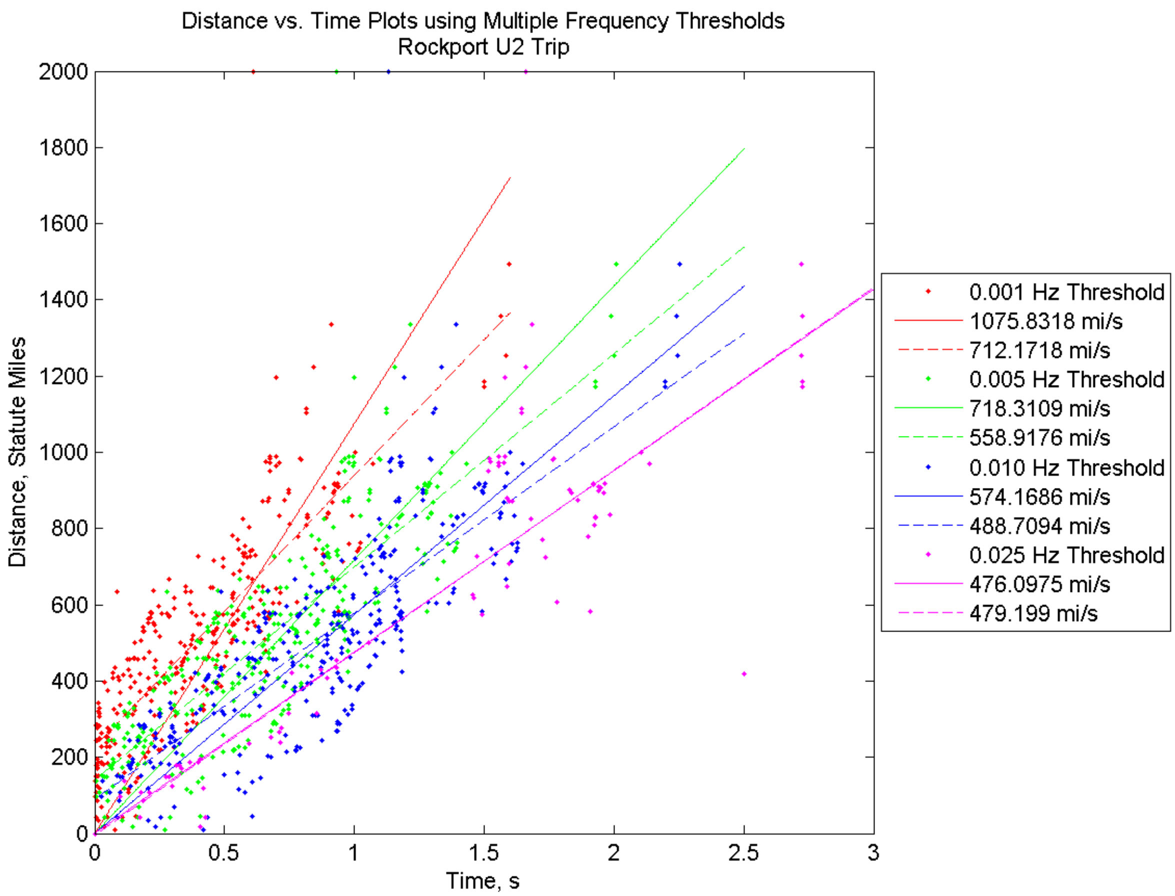
Distance vs. Time Plots using Multiple Frequency Thresholds
Rockport U2 Trip
Distance, Statute Miles
Time, s
0
200
400
600
800
1000
1200
1400
1600
1800
2000
0
0.5
1
1.5
2
2.5
3
0.001 Hz Threshold
1075.8318 mi/s
712.1718 mi/s
0.005 Hz Threshold
718.3109 mi/s
558.9176 mi/s
0.010 Hz Threshold
574.1686 mi/s
488.7094 mi/s
0.025 Hz Threshold
476.0975 mi/s
479.199 mi/s

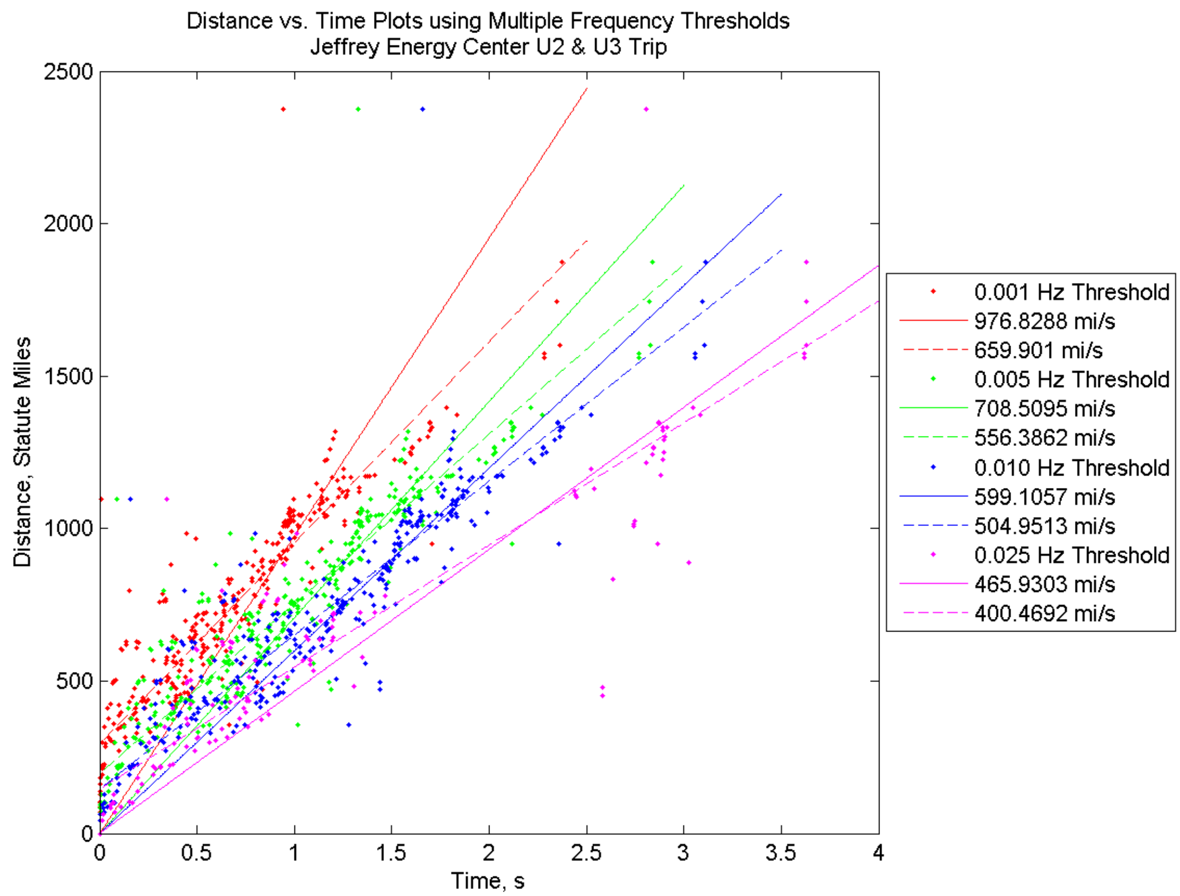

Distance vs. Time Plots using Multiple Frequency Thresholds
Jeffrey Energy Center U2 & U3 Trip
Distance, Statute Miles
Time, s
0
500
1000
1500
2000
2500
0.5
1
1.5
2
2.5
3
3.5
4
0.001 Hz Threshold
976.8288 mi/s
659.901 mi/s
0.005 Hz Threshold
708.5095 mi/s
556.3862 mi/s
0.010 Hz Threshold
599.1057 mi/s
504.9513 mi/s
0.025 Hz Threshold
465.9303 mi/s
400.4692 mi/s

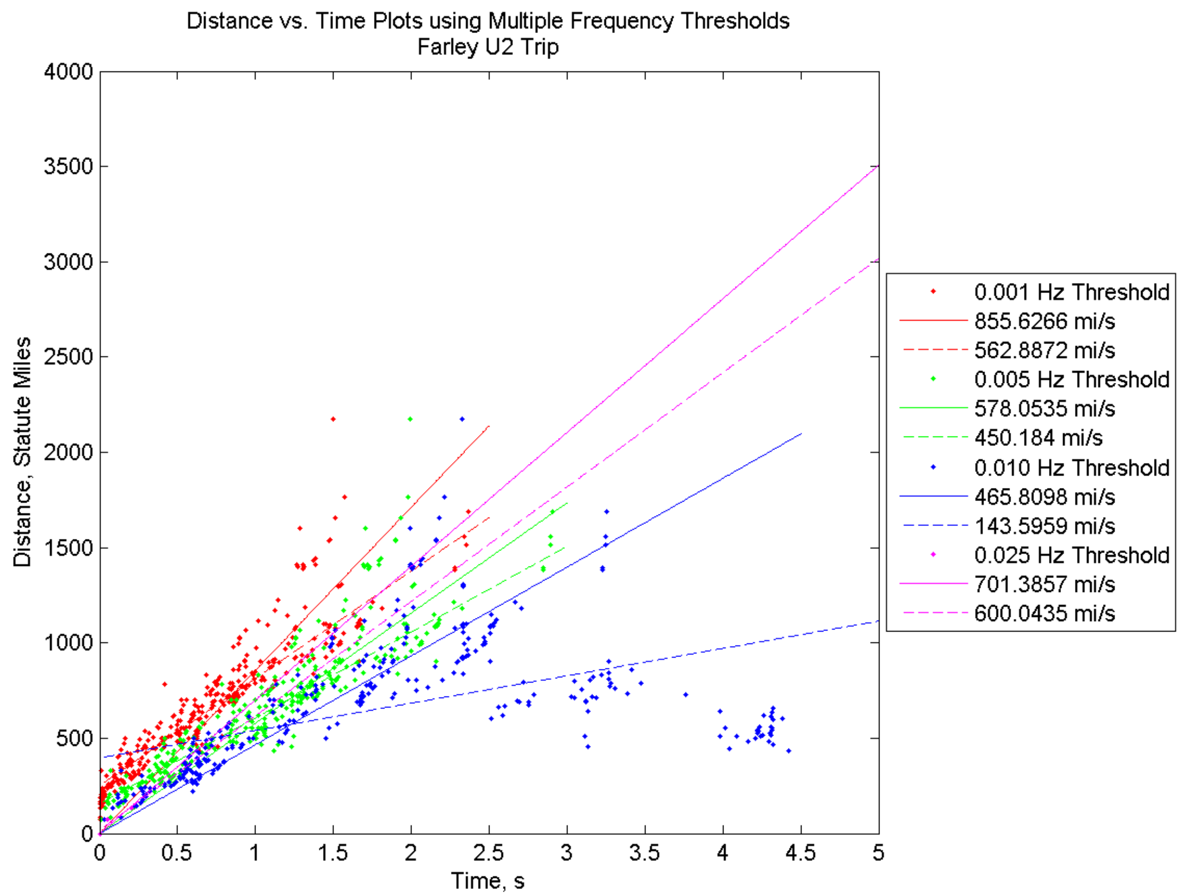

Distance vs. Time Plots using Multiple Frequency Thresholds
Farley U2 Trip
Distance, Statute Miles
Time, s
0
500
1000
1500
2000
2500
3000
3500
4000
0
0.5
1
1.5
2
2.5
3
3.5
4
4.5
5
0.001 Hz Threshold
855.6266 mi/s
562.8872 mi/s
0.005 Hz Threshold
578.0535 mi/s
450.184 mi/s
0.010 Hz Threshold
465.8098 mi/s
143.5959 mi/s
0.025 Hz Threshold
701.3857 mi/s
600.0435 mi/s

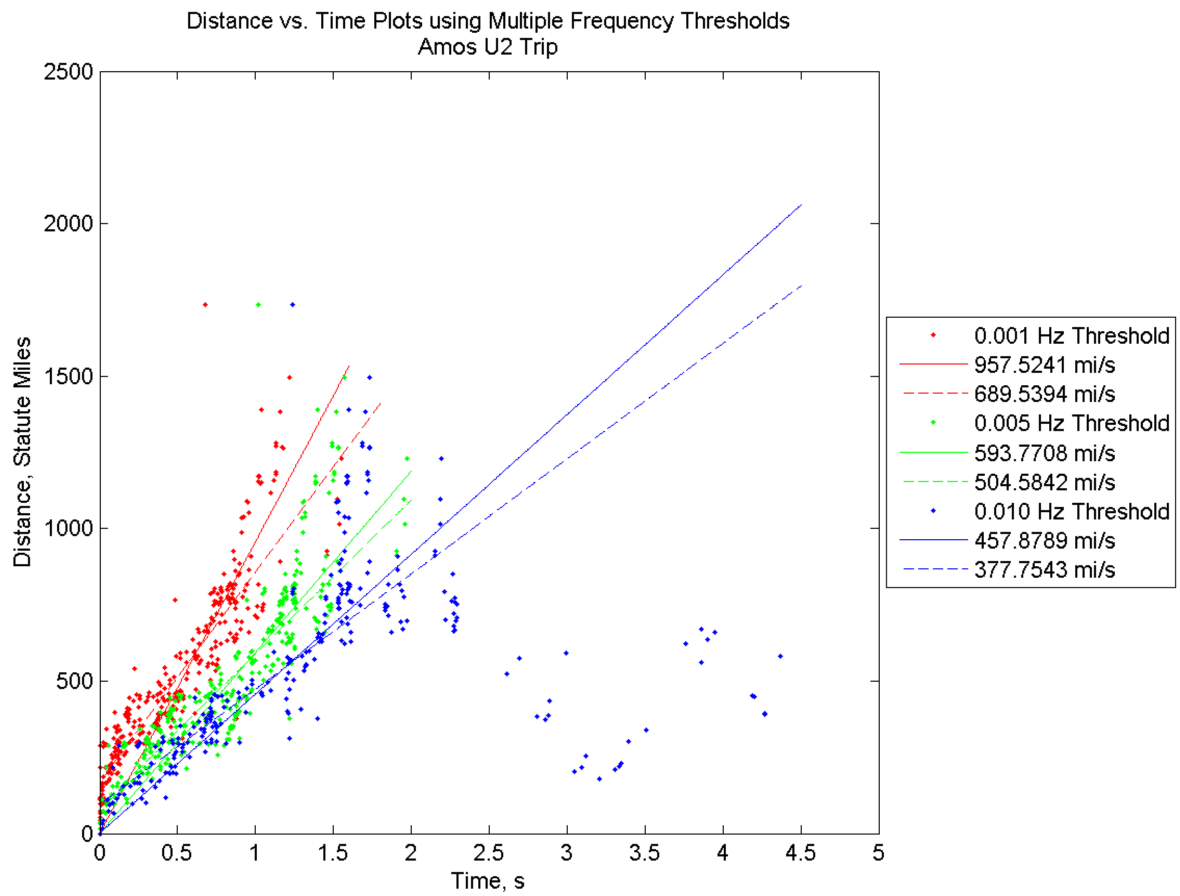
Distance vs. Time Plots using Multiple Frequency Thresholds
Amos U2 Trip
Distance, Statute Miles
Time, s
0
500
1000
1500
2000
2500
0
0.5
1
1.5
2
2.5
3
3.5
4
4.5
5
0.001 Hz Threshold
957.5241 mi/s
689.5394 mi/s
0.005 Hz Threshold
593.7708 mi/s
504.5842 mi/s
0.010 Hz Threshold
457.8789 mi/s
377.7543 mi/s

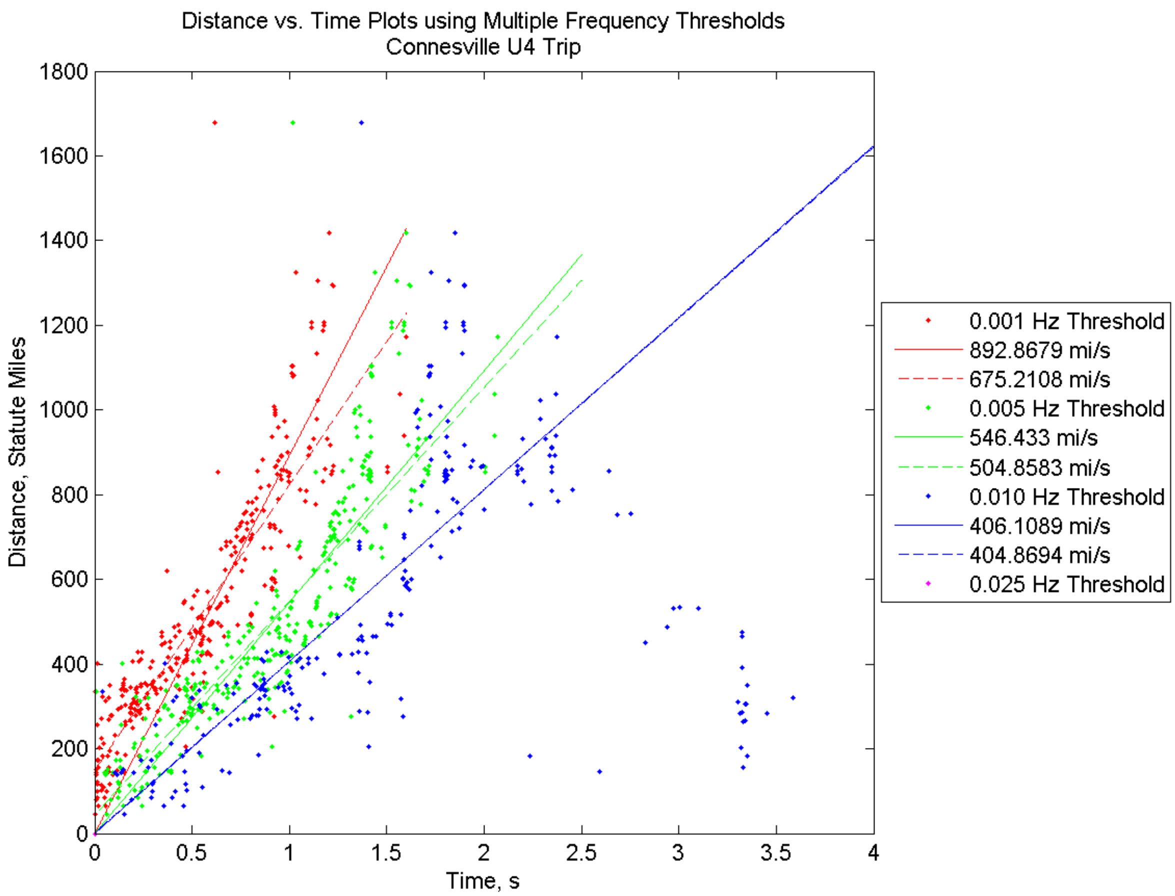

Distance vs. Time Plots using Multiple Frequency Thresholds
Connesville U4 Trip
Distance, Statute Miles
Time, s
0
200
400
600
800
1000
1200
1400
1600
1800
0
0.5
1
1.5
2
2.5
3
3.5
4
0.001 Hz Threshold
892.8679 mi/s
675.2108 mi/s
0.005 Hz Threshold
546.433 mi/s
504.8583 mi/s
0.010 Hz Threshold
406.1089 mi/s
404.8694 mi/s
0.025 Hz Threshold

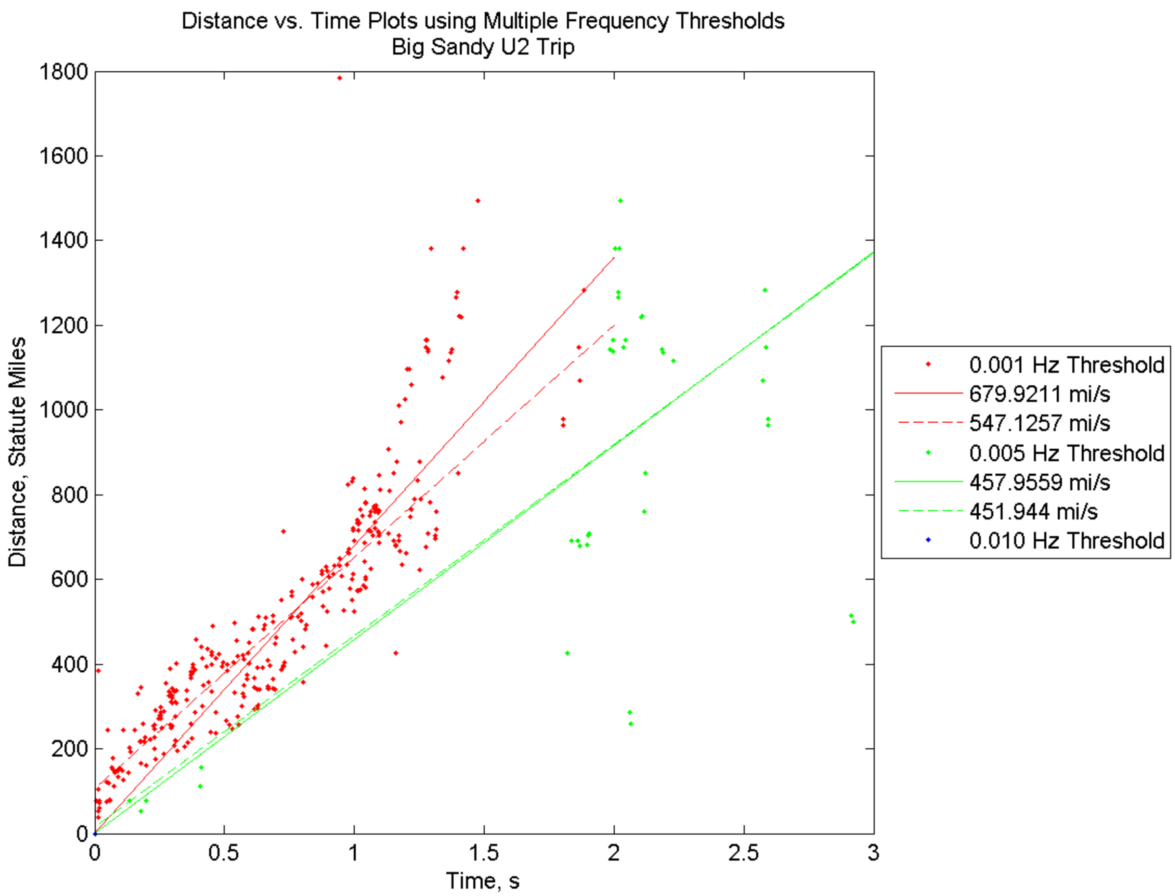
Distance vs. Time Plots using Multiple Frequency Thresholds
Big Sandy U2 Trip
Distance, Statute Miles
Time, s
0.001 Hz Threshold
679.9211 mi/s
547.1257 mi/s
0.005 Hz Threshold
457.9559 mi/s
451.944 mi/s
0.010 Hz Threshold

Appendix XIV: Distance vs. Time Regression for Calculation of Angular Velocity

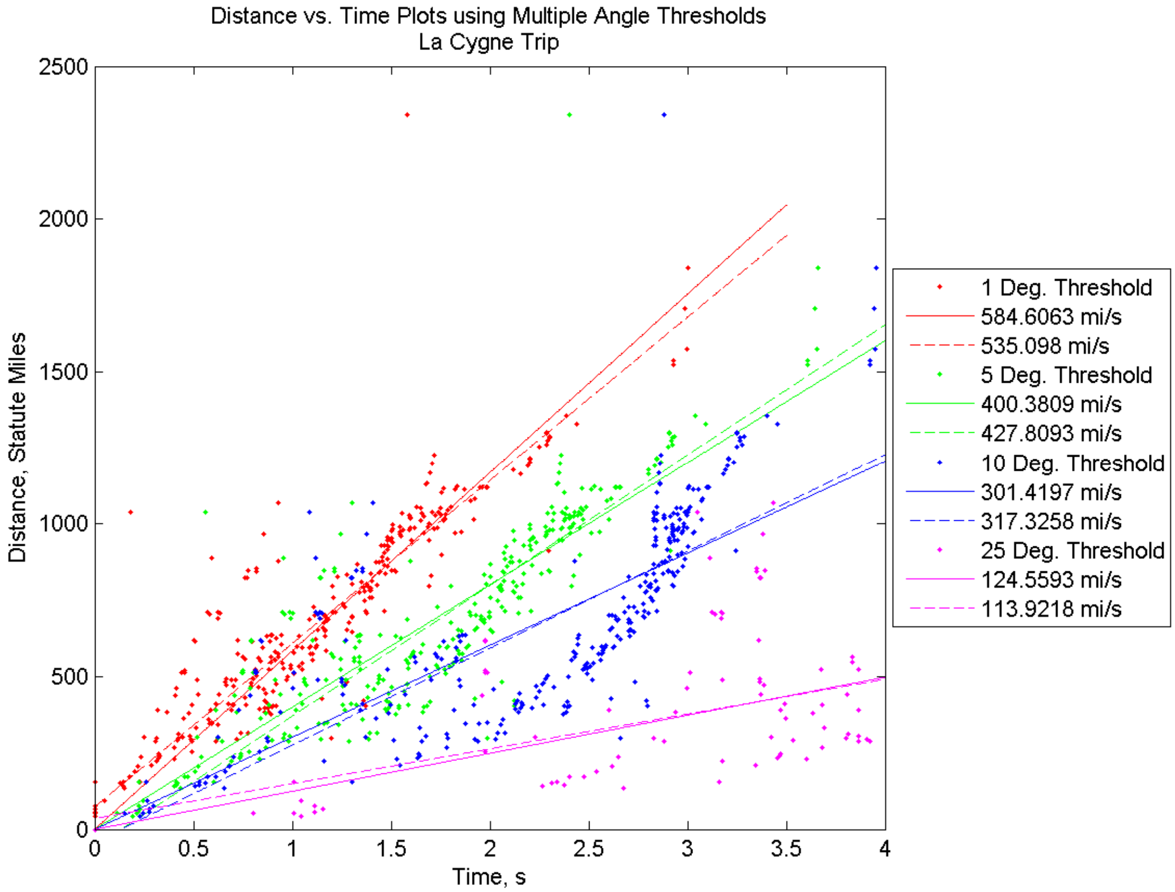

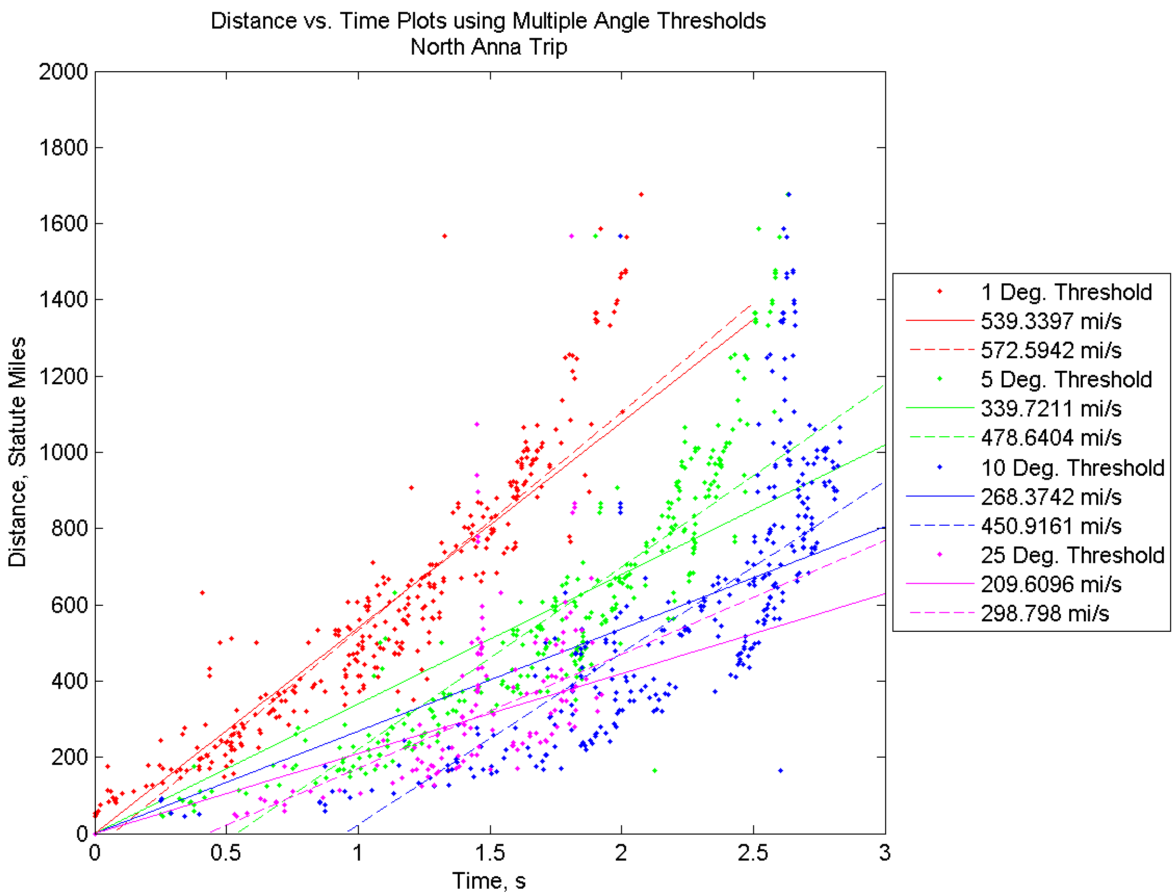

Distance vs. Time Plots using Multiple Angle Thresholds
North Anna Trip
Distance, Statute Miles
Time, s
0
200
400
600
800
1000
1200
1400
1600
1800
2000
0
0.5
1
1.5
2
2.5
3
1 Deg. Threshold
539.3397 mi/s
572.5942 mi/s
5 Deg. Threshold
339.7211 mi/s
478.6404 mi/s
10 Deg. Threshold
268.3742 mi/s
450.9161 mi/s
25 Deg. Threshold
209.6096 mi/s
298.798 mi/s

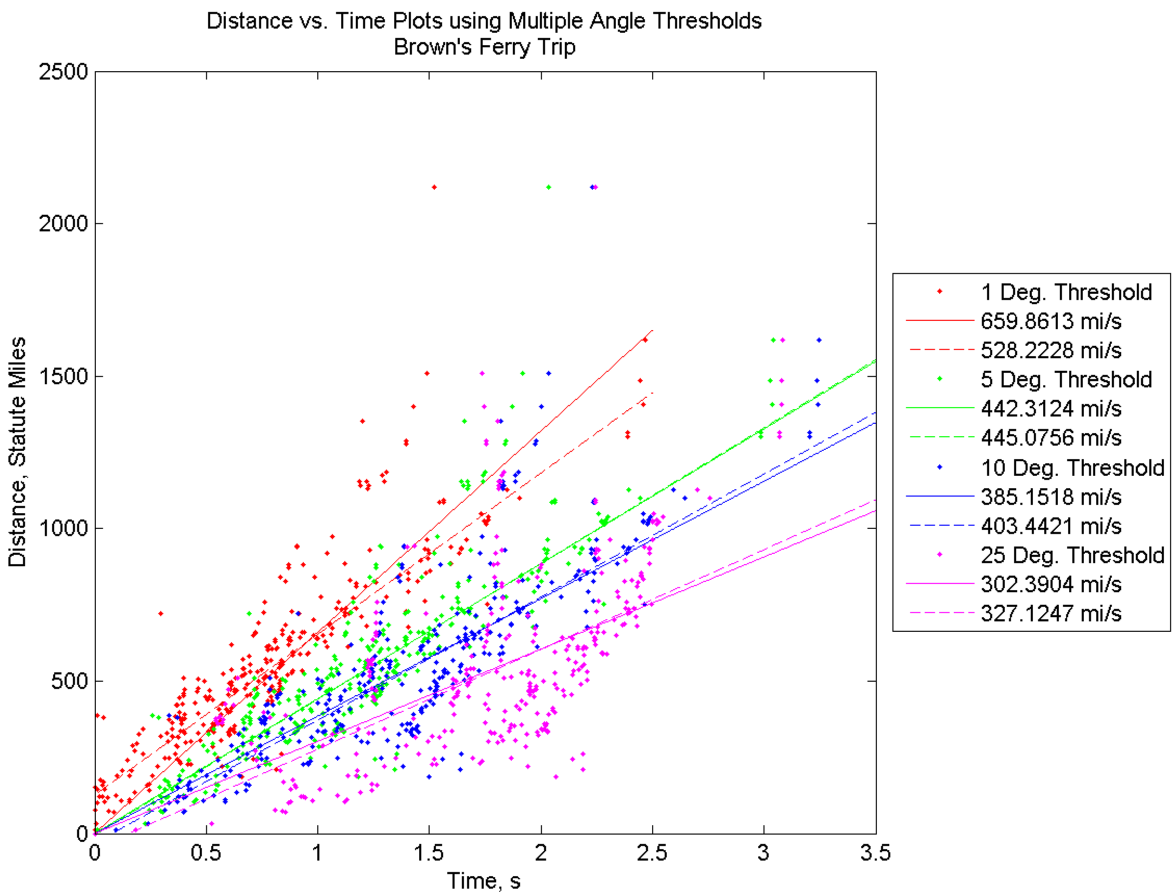
Distance vs. Time Plots using Multiple Angle Thresholds
Brown's Ferry Trip
Distance, Statute Miles
Time, s
0
500
1000
1500
2000
2500
0
0.5
1
1.5
2
2.5
3
3.5
1 Deg. Threshold
659.8613 mi/s
528.2228 mi/s
5 Deg. Threshold
442.3124 mi/s
445.0756 mi/s
10 Deg. Threshold
385.1518 mi/s
403.4421 mi/s
25 Deg. Threshold
302.3904 mi/s
327.1247 mi/s

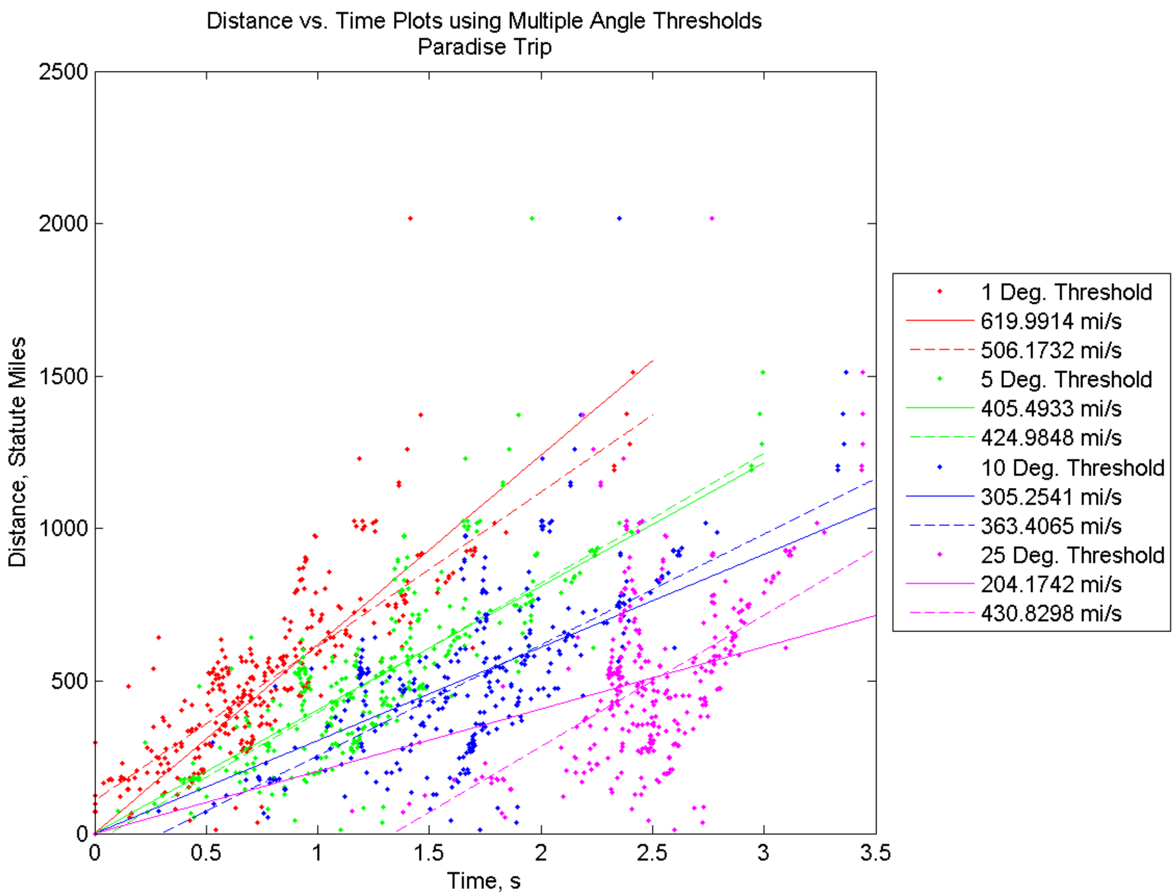

Distance vs. Time Plots using Multiple Angle Thresholds
Paradise Trip
Distance, Statute Miles
Time, s
0
500
1000
1500
2000
2500
0
0.5
1
1.5
2
2.5
3
3.5
1 Deg. Threshold
619.9914 mi/s
506.1732 mi/s
5 Deg. Threshold
405.4933 mi/s
424.9848 mi/s
10 Deg. Threshold
305.2541 mi/s
363.4065 mi/s
25 Deg. Threshold
204.1742 mi/s
430.8298 mi/s

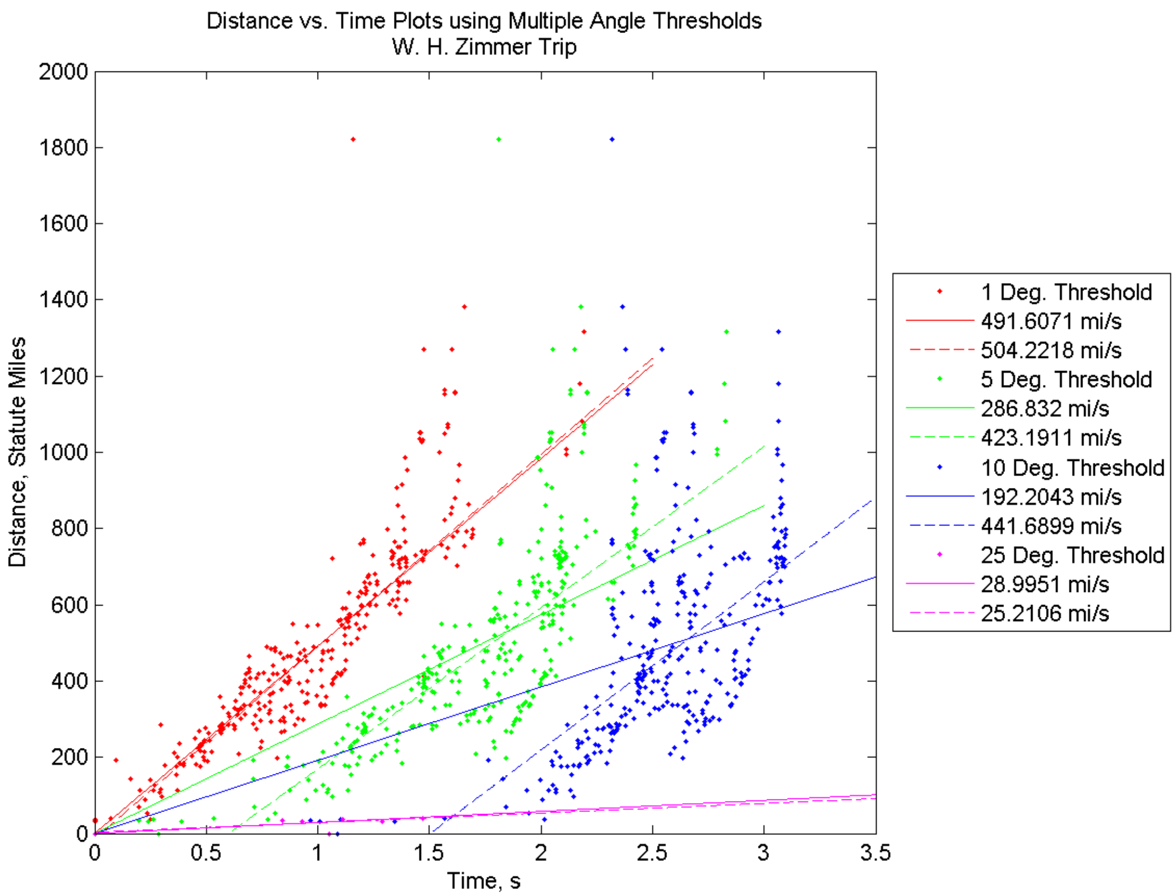
Distance vs. Time Plots using Multiple Angle Thresholds
W. H. Zimmer Trip
Distance, Statute Miles
Time, s
0
200
400
600
800
1000
1200
1400
1600
1800
2000
0
0.5
1
1.5
2
2.5
3
3.5
1 Deg. Threshold
491.6071 mi/s
504.2218 mi/s
5 Deg. Threshold
286.832 mi/s
423.1911 mi/s
10 Deg. Threshold
192.2043 mi/s
441.6899 mi/s
25 Deg. Threshold
28.9951 mi/s
25.2106 mi/s

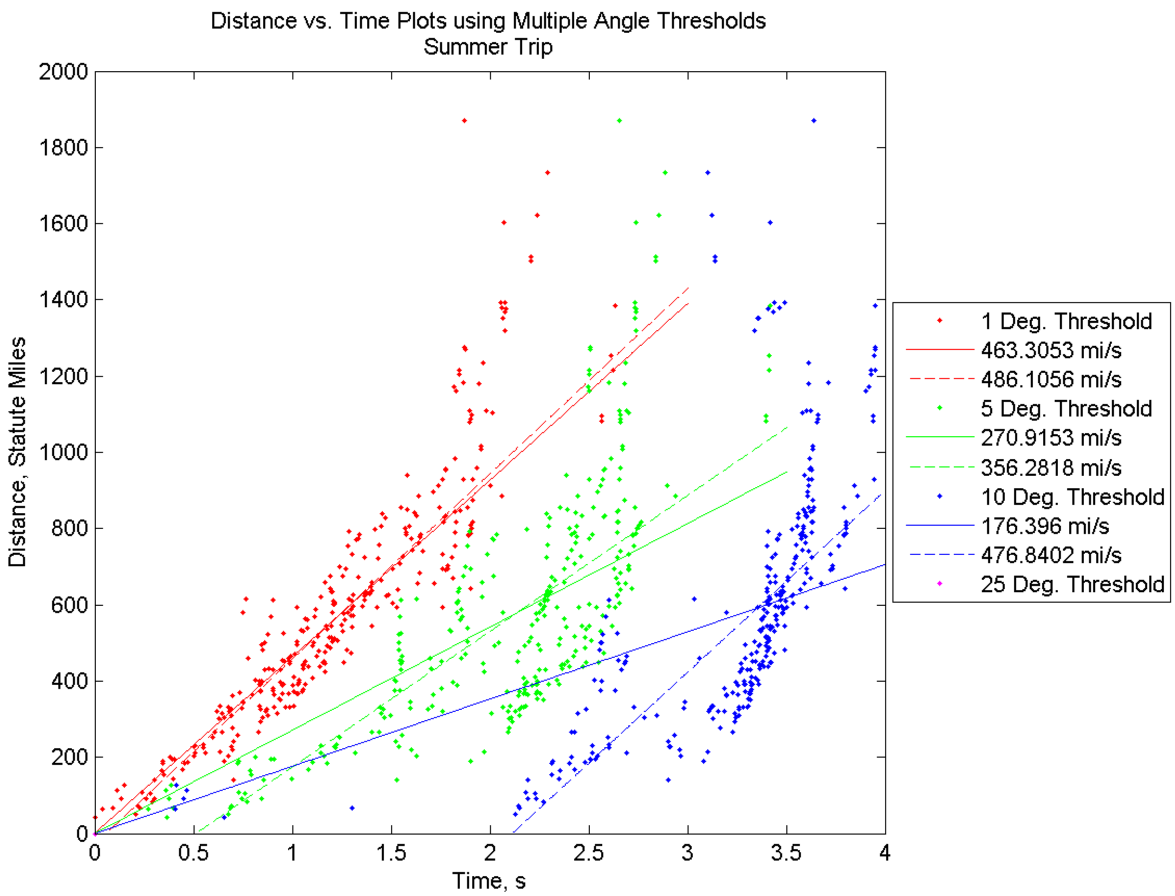
Distance vs. Time Plots using Multiple Angle Thresholds
Summer Trip
Distance, Statute Miles
Time, s
2000
1800
1600
1400
1200
1000
800
600
400
200
0
0
0.5
1
1.5
2
2.5
3
3.5
4
1 Deg. Threshold
463.3053 mi/s
486.1056 mi/s
5 Deg. Threshold
270.9153 mi/s
356.2818 mi/s
10 Deg. Threshold
176.396 mi/s
476.8402 mi/s
25 Deg. Threshold

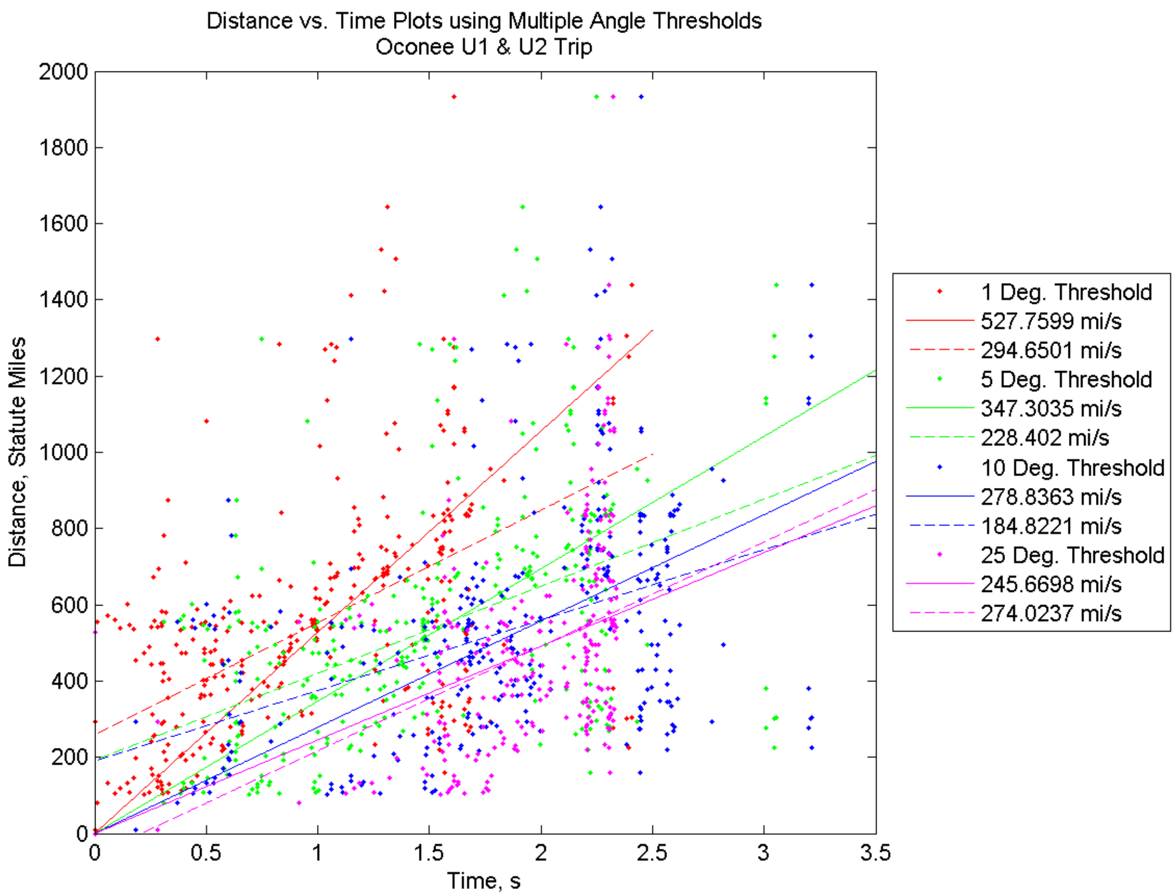
Distance vs. Time Plots using Multiple Angle Thresholds
Oconee U1 & U2 Trip
Distance, Statute Miles
Time, s
0
200
400
600
800
1000
1200
1400
1600
1800
2000
0.5
1
1.5
2
2.5
3
3.5
1 Deg. Threshold
527.7599 mi/s
294.6501 mi/s
5 Deg. Threshold
347.3035 mi/s
228.402 mi/s
10 Deg. Threshold
278.8363 mi/s
184.8221 mi/s
25 Deg. Threshold
245.6698 mi/s
274.0237 mi/s

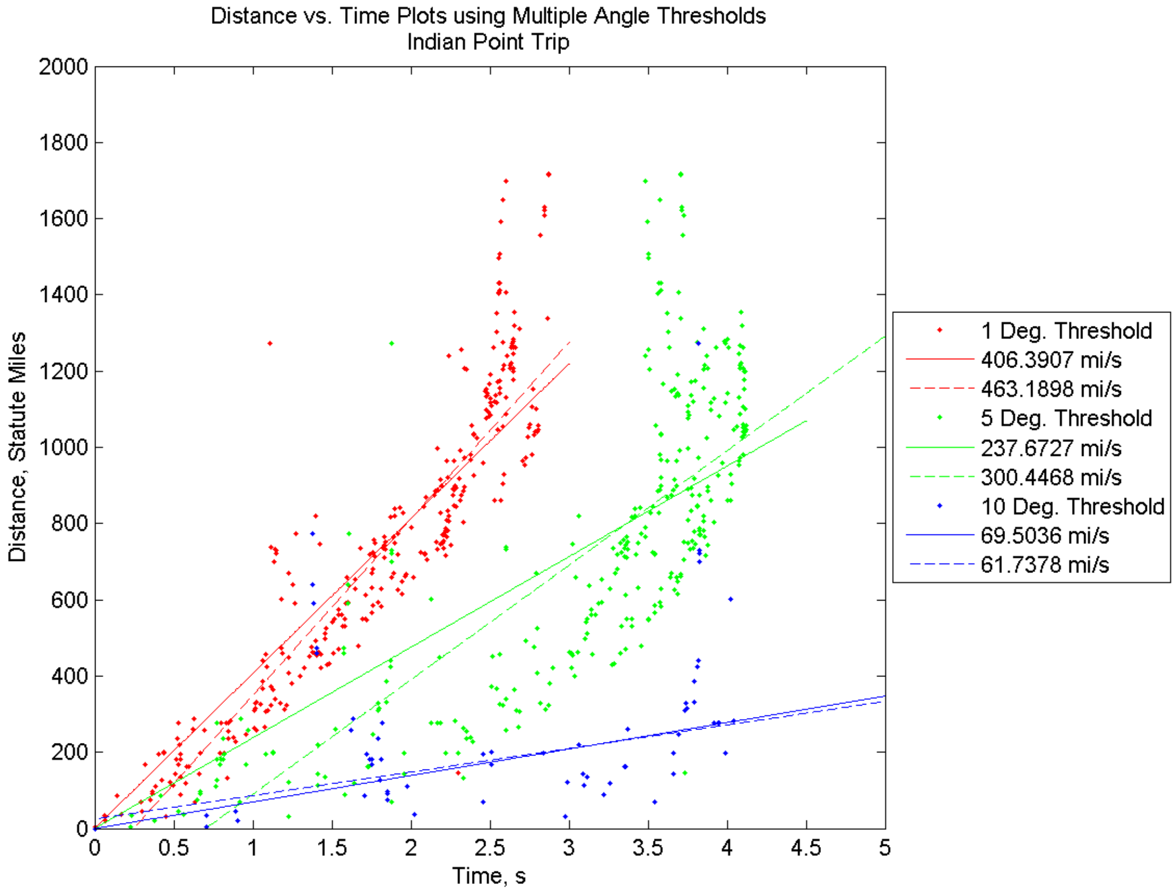
Distance vs. Time Plots using Multiple Angle Thresholds
Indian Point Trip
Distance, Statute Miles
Time, s
0
200
400
600
800
1000
1200
1400
1600
1800
2000
0
0.5
1
1.5
2
2.5
3
3.5
4
4.5
5
1 Deg. Threshold
406.3907 mi/s
463.1898 mi/s
5 Deg. Threshold
237.6727 mi/s
300.4468 mi/s
10 Deg. Threshold
69.5036 mi/s
61.7378 mi/s

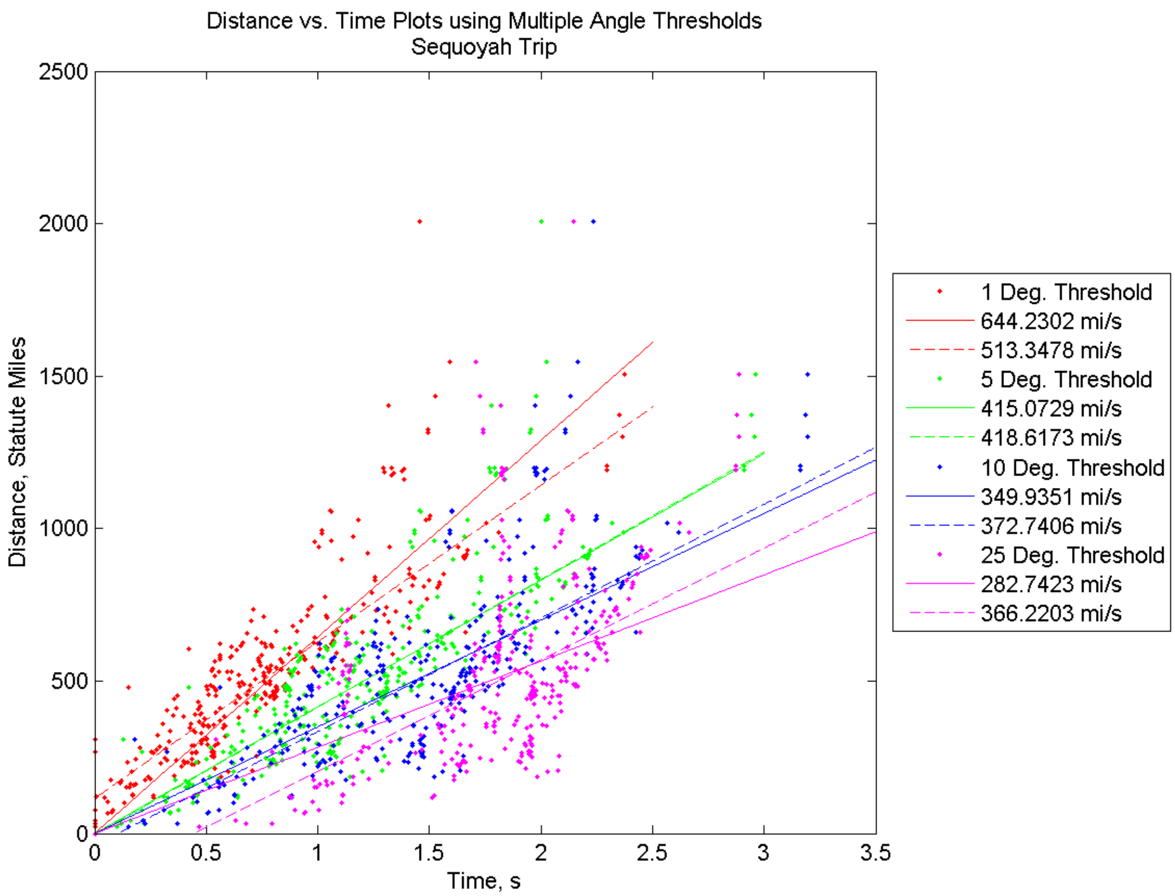
Distance vs. Time Plots using Multiple Angle Thresholds
Sequoyah Trip
Distance, Statute Miles
Time, s
0
500
1000
1500
2000
2500
0
0.5
1
1.5
2
2.5
3
3.5
1 Deg. Threshold
644.2302 mi/s
513.3478 mi/s
5 Deg. Threshold
415.0729 mi/s
418.6173 mi/s
10 Deg. Threshold
349.9351 mi/s
372.7406 mi/s
25 Deg. Threshold
282.7423 mi/s
366.2203 mi/s

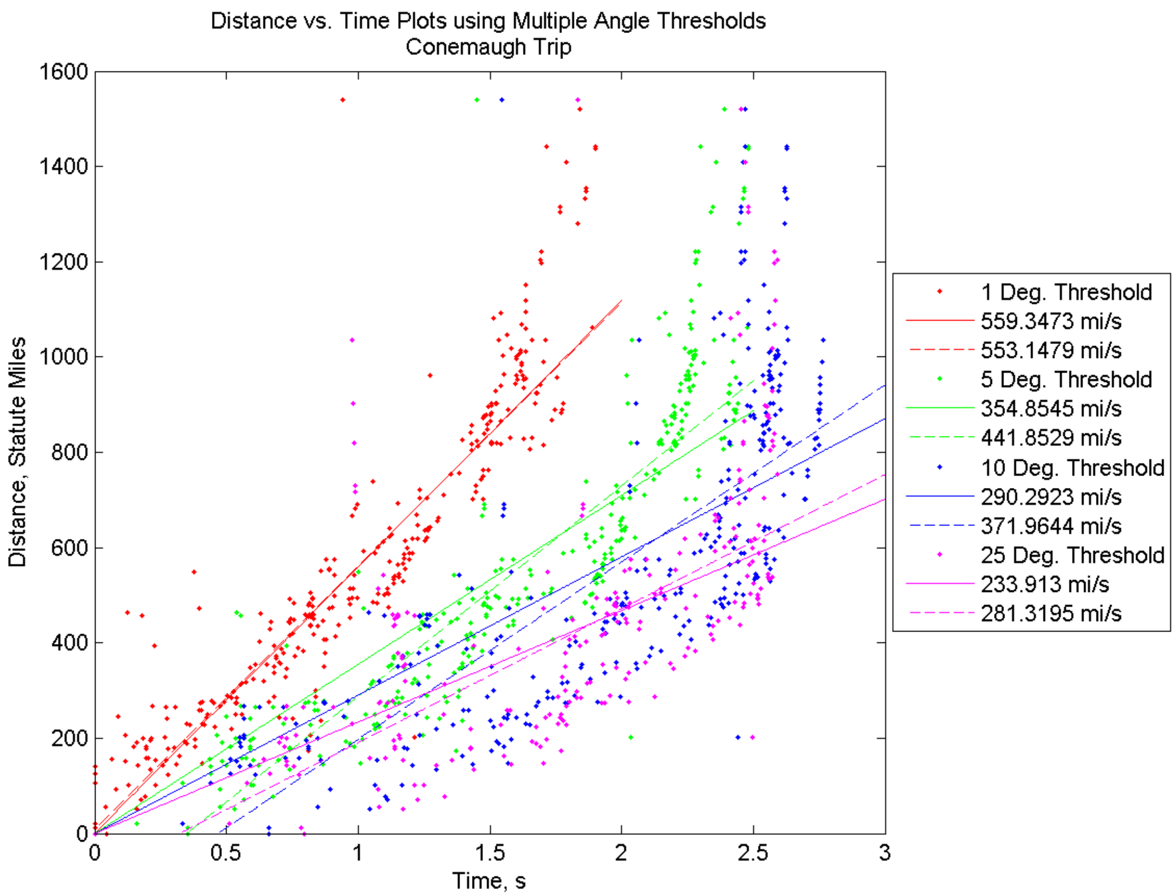
Distance vs. Time Plots using Multiple Angle Thresholds
Conemaugh Trip
Distance, Statute Miles
Time, s
0
200
400
600
800
1000
1200
1400
1600
0
0.5
1
1.5
2
2.5
3
1 Deg. Threshold
559.3473 mi/s
553.1479 mi/s
5 Deg. Threshold
354.8545 mi/s
441.8529 mi/s
10 Deg. Threshold
290.2923 mi/s
371.9644 mi/s
25 Deg. Threshold
233.913 mi/s
281.3195 mi/s

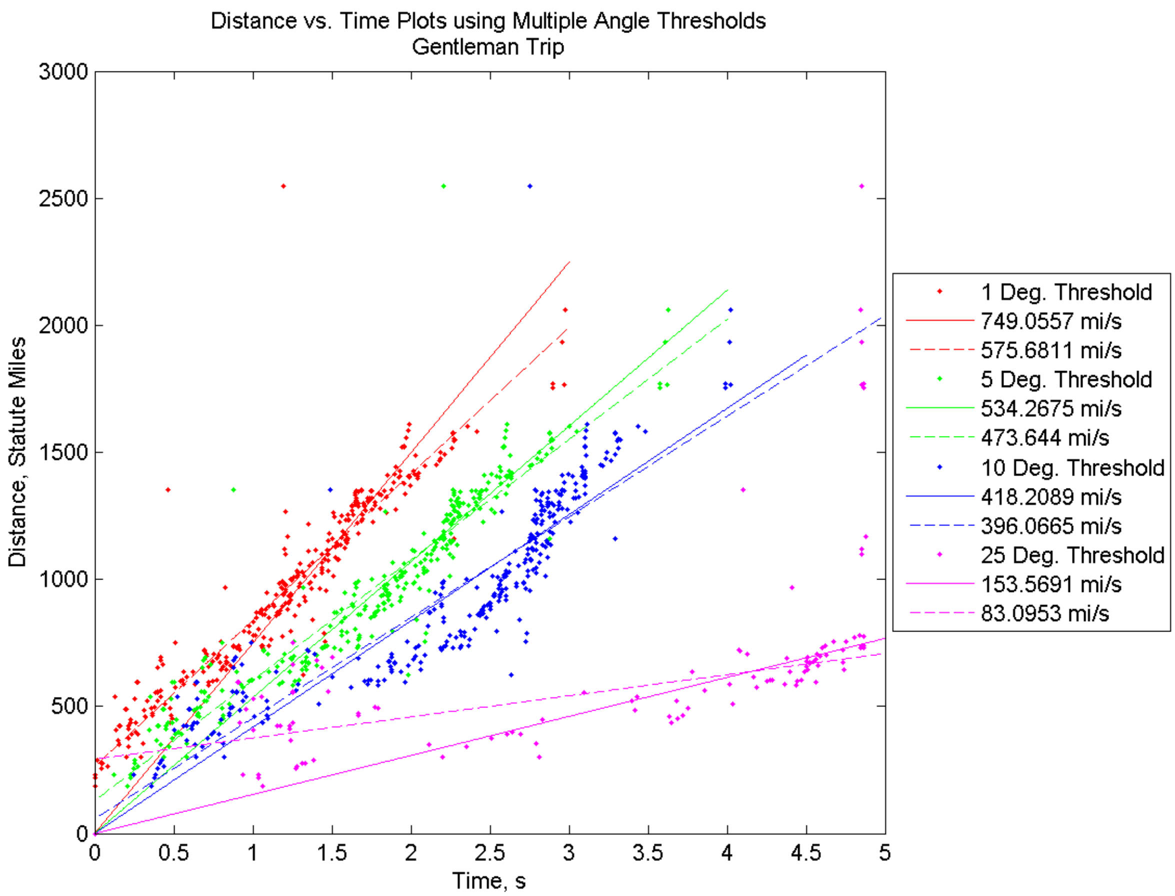
Distance vs. Time Plots using Multiple Angle Thresholds
Gentleman Trip
Distance, Statute Miles
Time, s
0
500
1000
1500
2000
2500
3000
0
0.5
1
1.5
2
2.5
3
3.5
4
4.5
5
1 Deg. Threshold
749.0557 mi/s
575.6811 mi/s
5 Deg. Threshold
534.2675 mi/s
473.644 mi/s
10 Deg. Threshold
418.2089 mi/s
396.0665 mi/s
25 Deg. Threshold
153.5691 mi/s
83.0953 mi/s

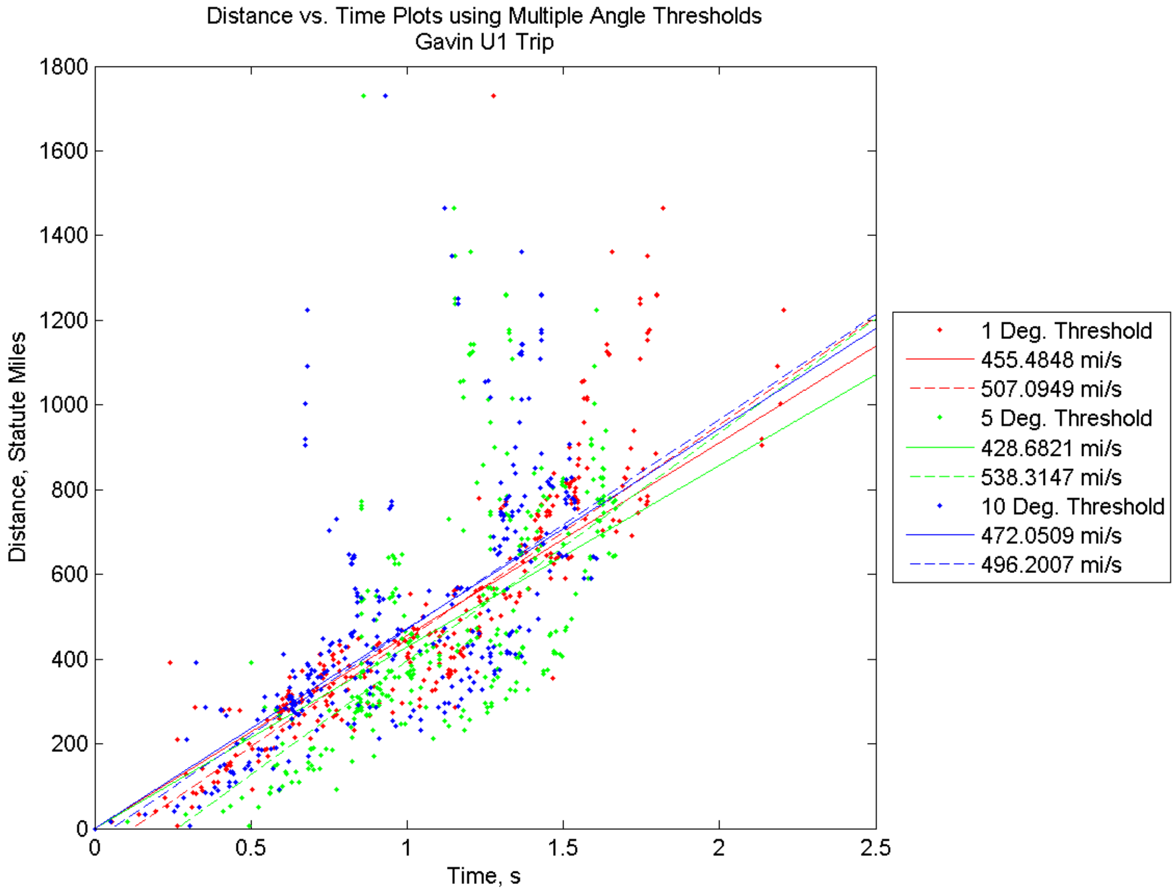
Distance vs. Time Plots using Multiple Angle Thresholds
Gavin U1 Trip
Distance, Statute Miles
Time, s
0
200
400
600
800
1000
1200
1400
1600
1800
0
0.5
1
1.5
2
2.5
1 Deg. Threshold
455.4848 mi/s
507.0949 mi/s
5 Deg. Threshold
428.6821 mi/s
538.3147 mi/s
10 Deg. Threshold
472.0509 mi/s
496.2007 mi/s

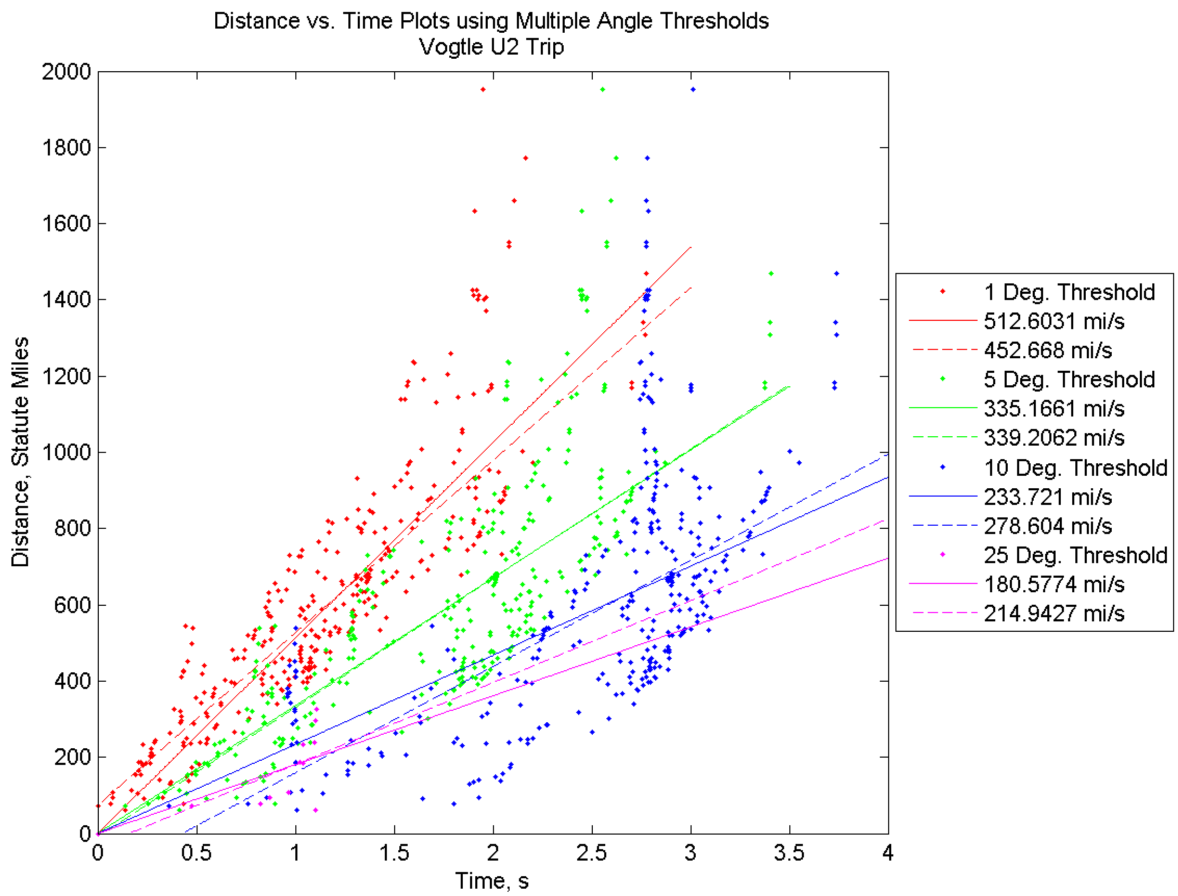

Distance vs. Time Plots using Multiple Angle Thresholds
Vogtle U2 Trip
Distance, Statute Miles
Time, s
0
200
400
600
800
1000
1200
1400
1600
1800
2000
0.5
1
1.5
2
2.5
3
3.5
4
1 Deg. Threshold
512.6031 mi/s
452.668 mi/s
5 Deg. Threshold
335.1661 mi/s
339.2062 mi/s
10 Deg. Threshold
233.721 mi/s
278.604 mi/s
25 Deg. Threshold
180.5774 mi/s
214.9427 mi/s

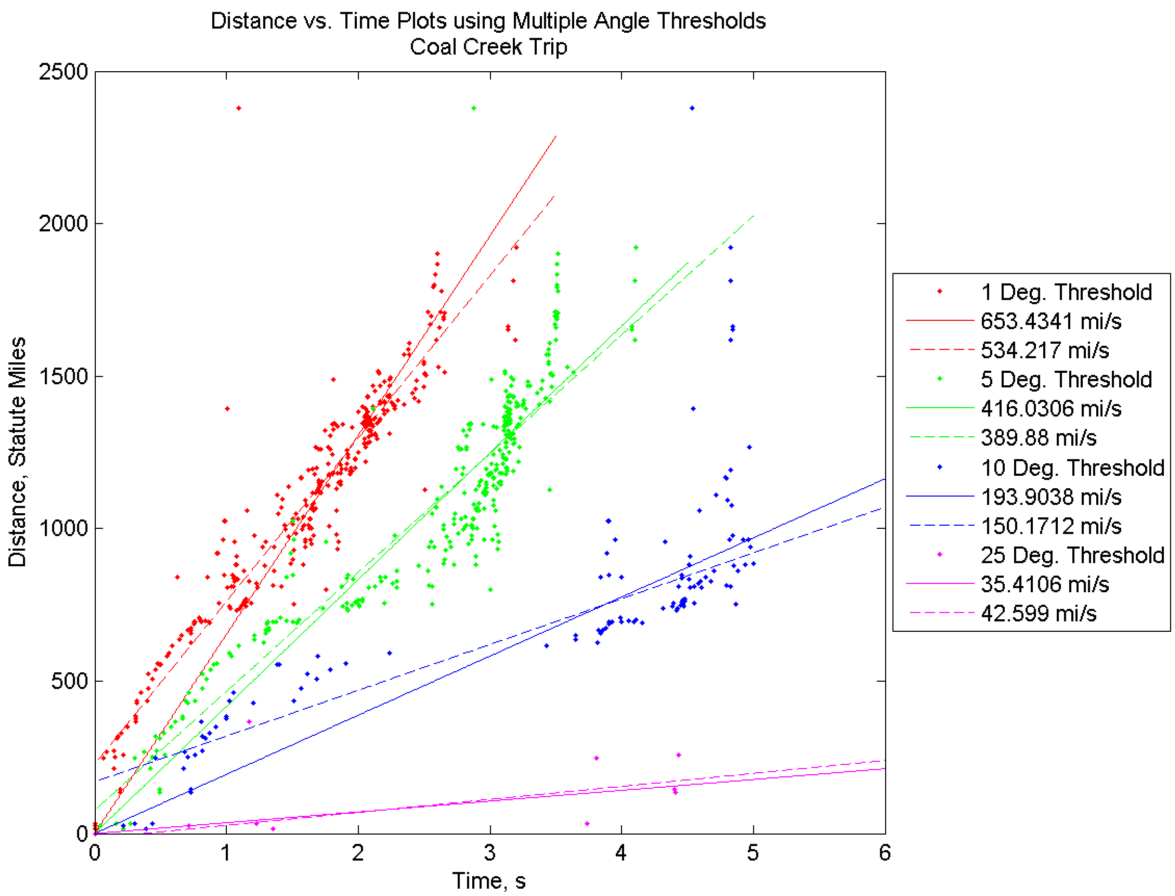
Distance vs. Time Plots using Multiple Angle Thresholds
Coal Creek Trip
Distance, Statute Miles
Time, s
0
500
1000
1500
2000
2500
0
1
2
3
4
5
6
1 Deg. Threshold
653.4341 mi/s
534.217 mi/s
5 Deg. Threshold
416.0306 mi/s
389.88 mi/s
10 Deg. Threshold
193.9038 mi/s
150.1712 mi/s
25 Deg. Threshold
35.4106 mi/s
42.599 mi/s

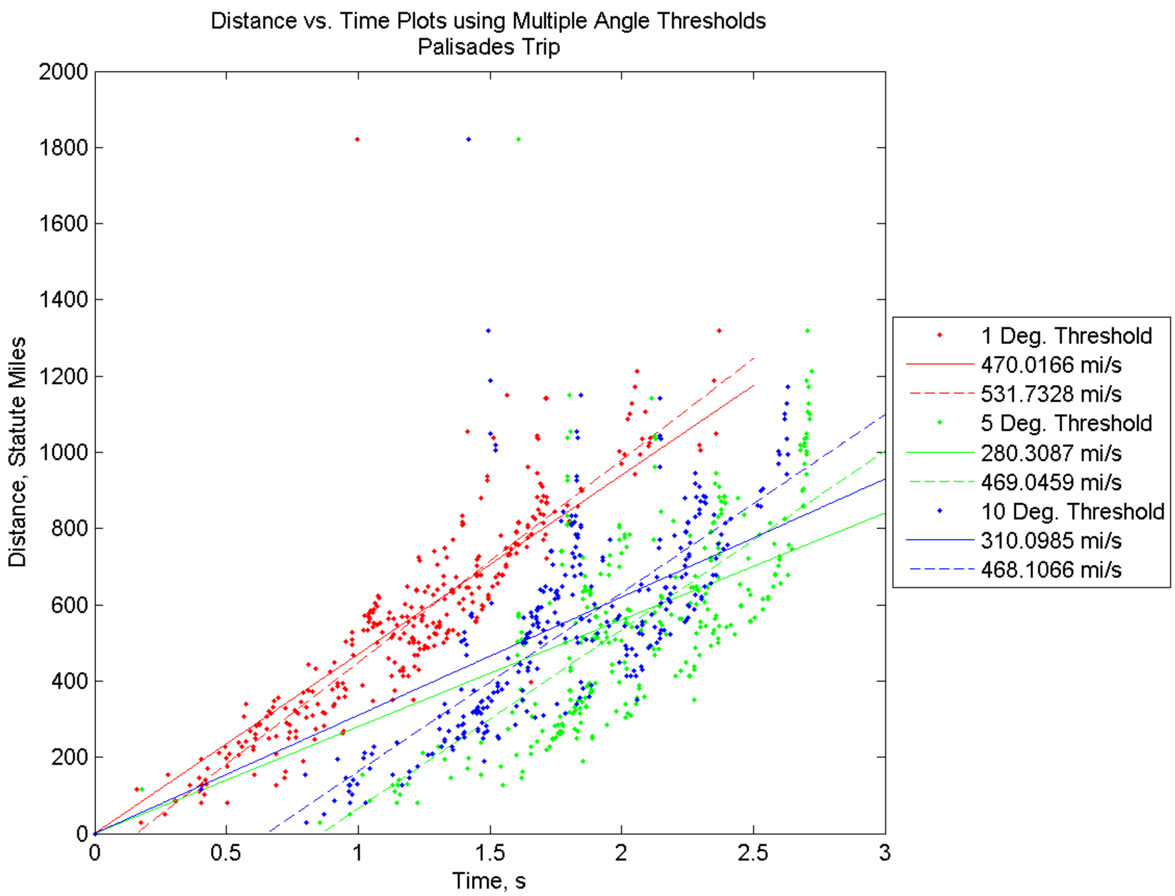
Distance vs. Time Plots using Multiple Angle Thresholds
Palisades Trip
2000
1800
1600
1400
1200
1000
800
600
400
200
0
Distance, Statute Miles
0
0.5
1
1.5
2
2.5
3
Time, s
1 Deg. Threshold
470.0166 mi/s
531.7328 mi/s
5 Deg. Threshold
280.3087 mi/s
469.0459 mi/s
10 Deg. Threshold
310.0985 mi/s
468.1066 mi/s

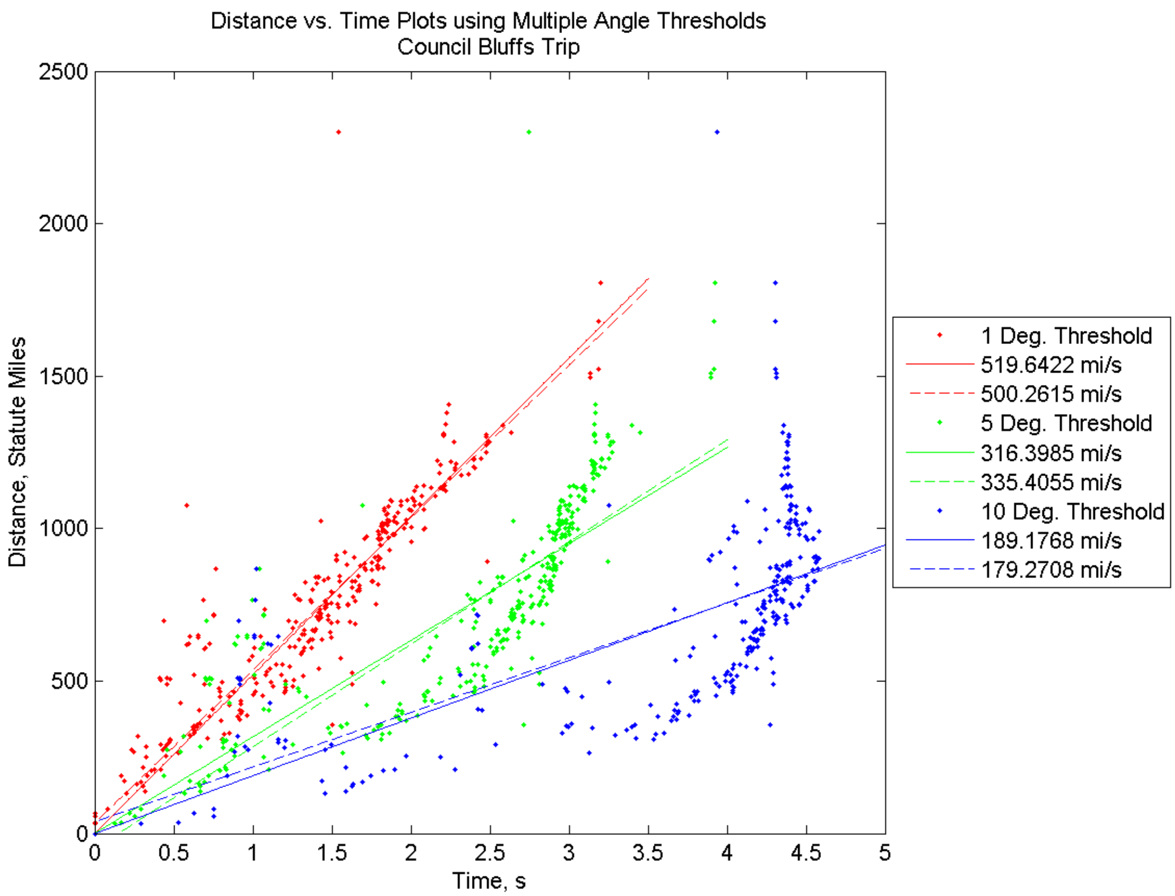
Distance vs. Time Plots using Multiple Angle Thresholds
Council Bluffs Trip
Distance, Statute Miles
Time, s
0
500
1000
1500
2000
2500
0
0.5
1
1.5
2
2.5
3
3.5
4
4.5
5
1 Deg. Threshold
519.6422 mi/s
500.2615 mi/s
5 Deg. Threshold
316.3985 mi/s
335.4055 mi/s
10 Deg. Threshold
189.1768 mi/s
179.2708 mi/s

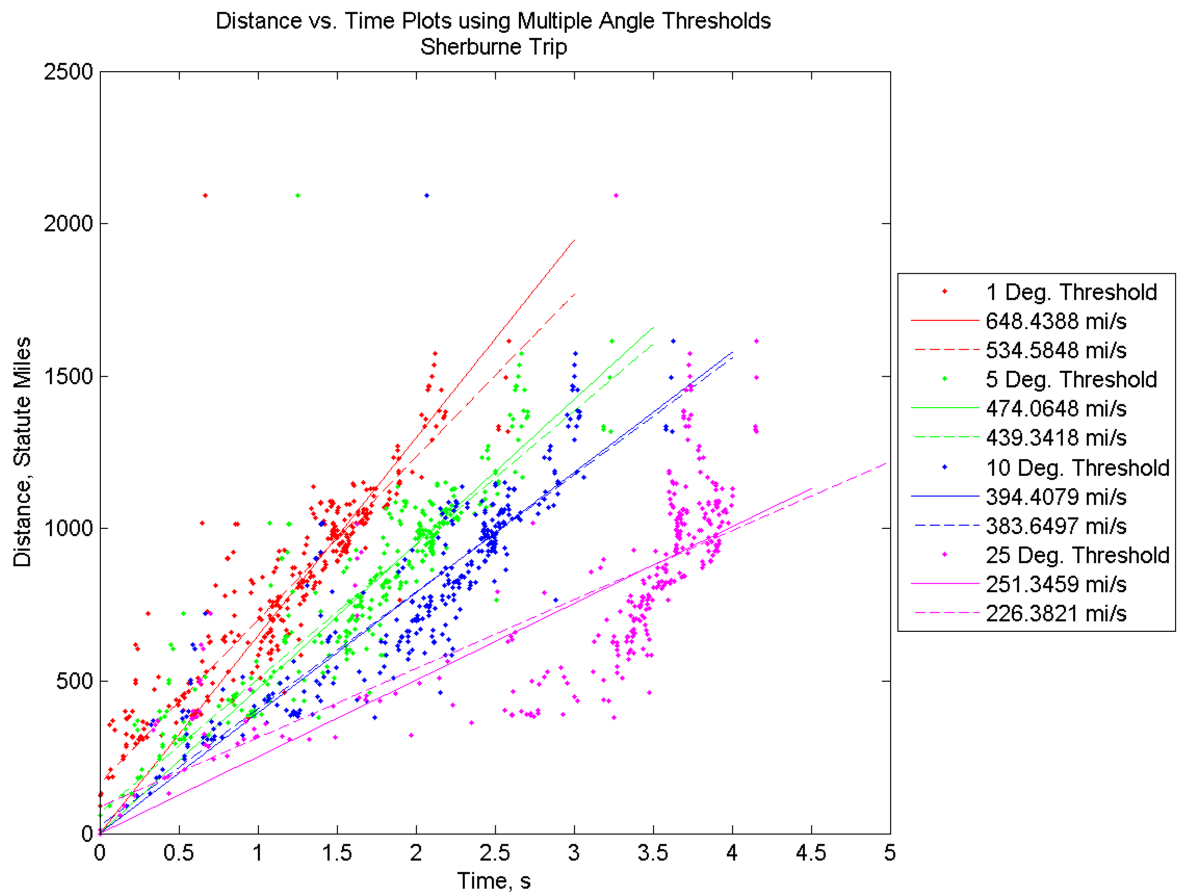
Distance vs. Time Plots using Multiple Angle Thresholds
Sherburne Trip
Distance, Statute Miles
Time, s
0
500
1000
1500
2000
2500
0.5
1
1.5
2
2.5
3
3.5
4
4.5
5
1 Deg. Threshold
648.4388 mi/s
534.5848 mi/s
5 Deg. Threshold
474.0648 mi/s
439.3418 mi/s
10 Deg. Threshold
394.4079 mi/s
383.6497 mi/s
25 Deg. Threshold
251.3459 mi/s
226.3821 mi/s

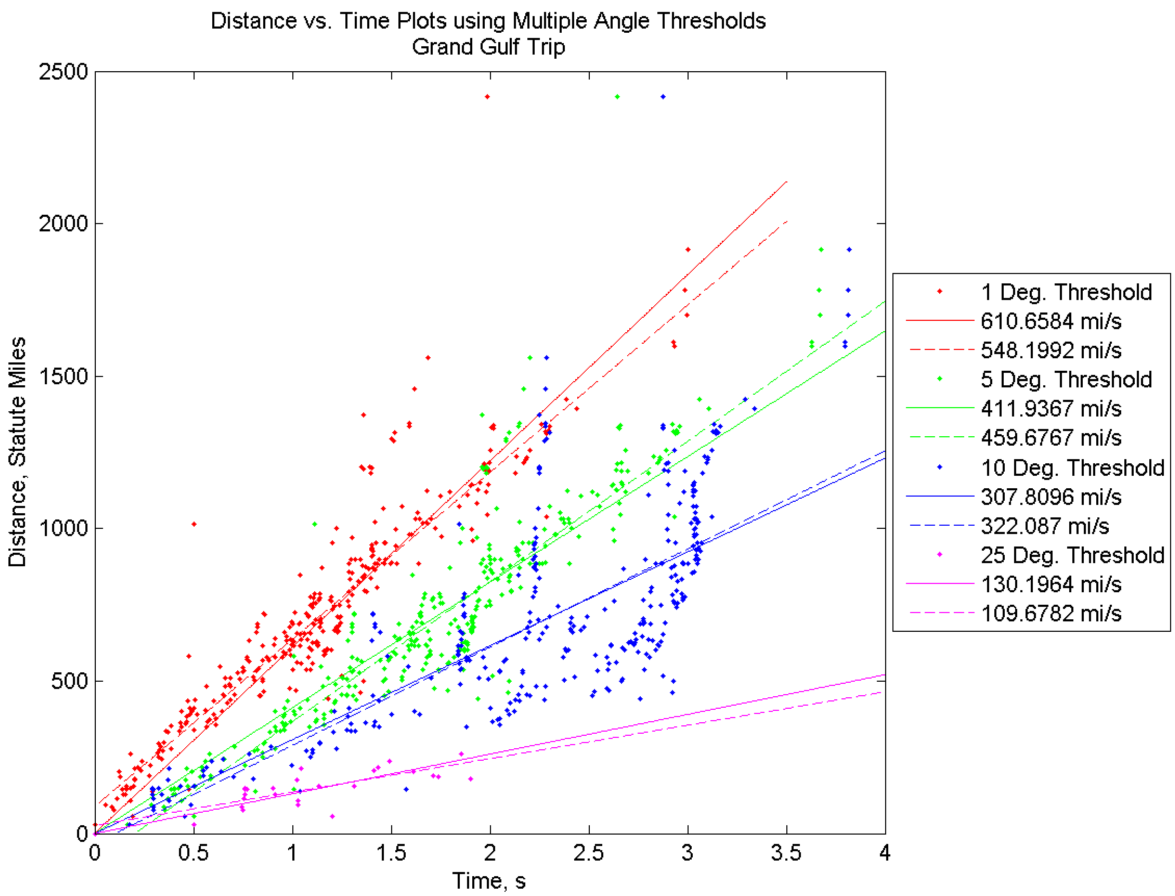
Distance vs. Time Plots using Multiple Angle Thresholds
Grand Gulf Trip
Distance, Statute Miles
Time, s
0
500
1000
1500
2000
2500
0
0.5
1
1.5
2
2.5
3
3.5
4
1 Deg. Threshold
610.6584 mi/s
548.1992 mi/s
5 Deg. Threshold
411.9367 mi/s
459.6767 mi/s
10 Deg. Threshold
307.8096 mi/s
322.087 mi/s
25 Deg. Threshold
130.1964 mi/s
109.6782 mi/s

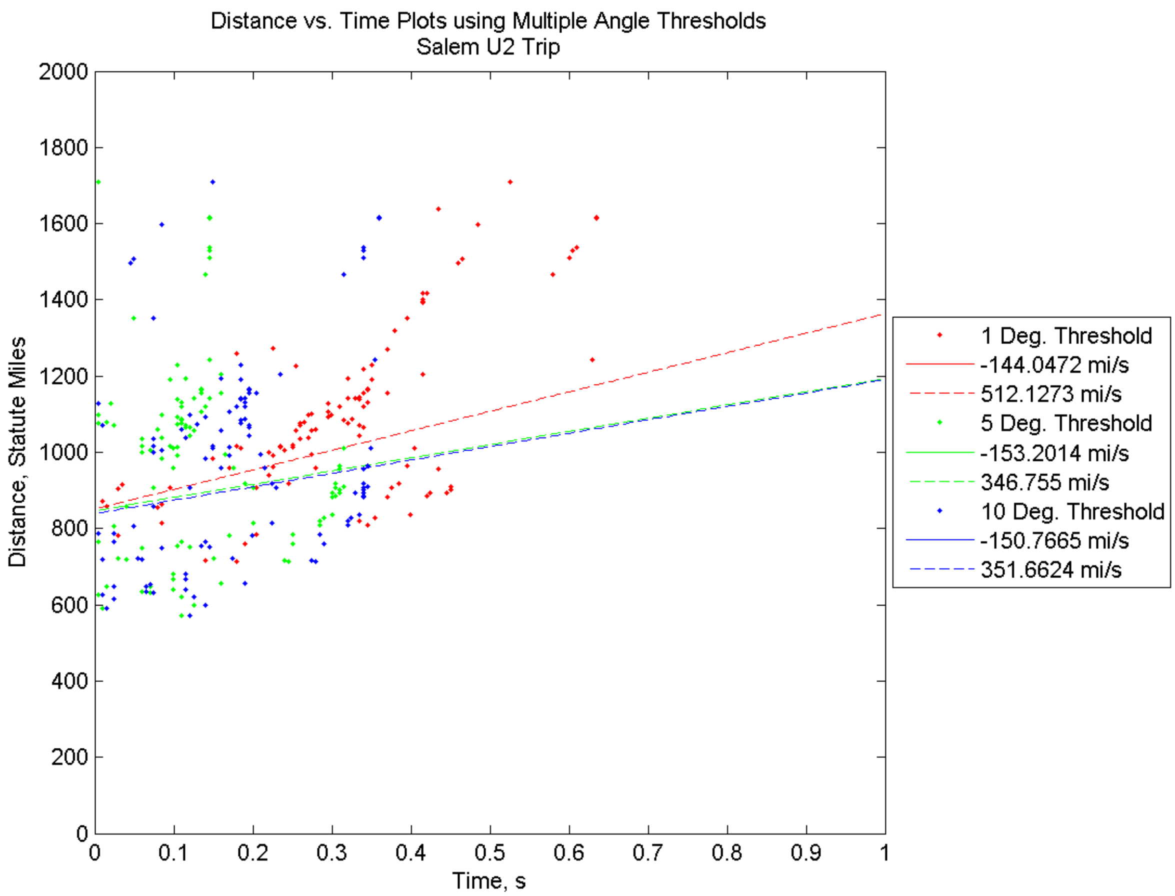
Distance vs. Time Plots using Multiple Angle Thresholds
Salem U2 Trip
Distance, Statute Miles
Time, s
0
200
400
600
800
1000
1200
1400
1600
1800
2000
0
0.1
0.2
0.3
0.4
0.5
0.6
0.7
0.8
0.9
1
1 Deg. Threshold
-144.0472 mi/s
512.1273 mi/s
5 Deg. Threshold
-153.2014 mi/s
346.755 mi/s
10 Deg. Threshold
-150.7665 mi/s
351.6624 mi/s

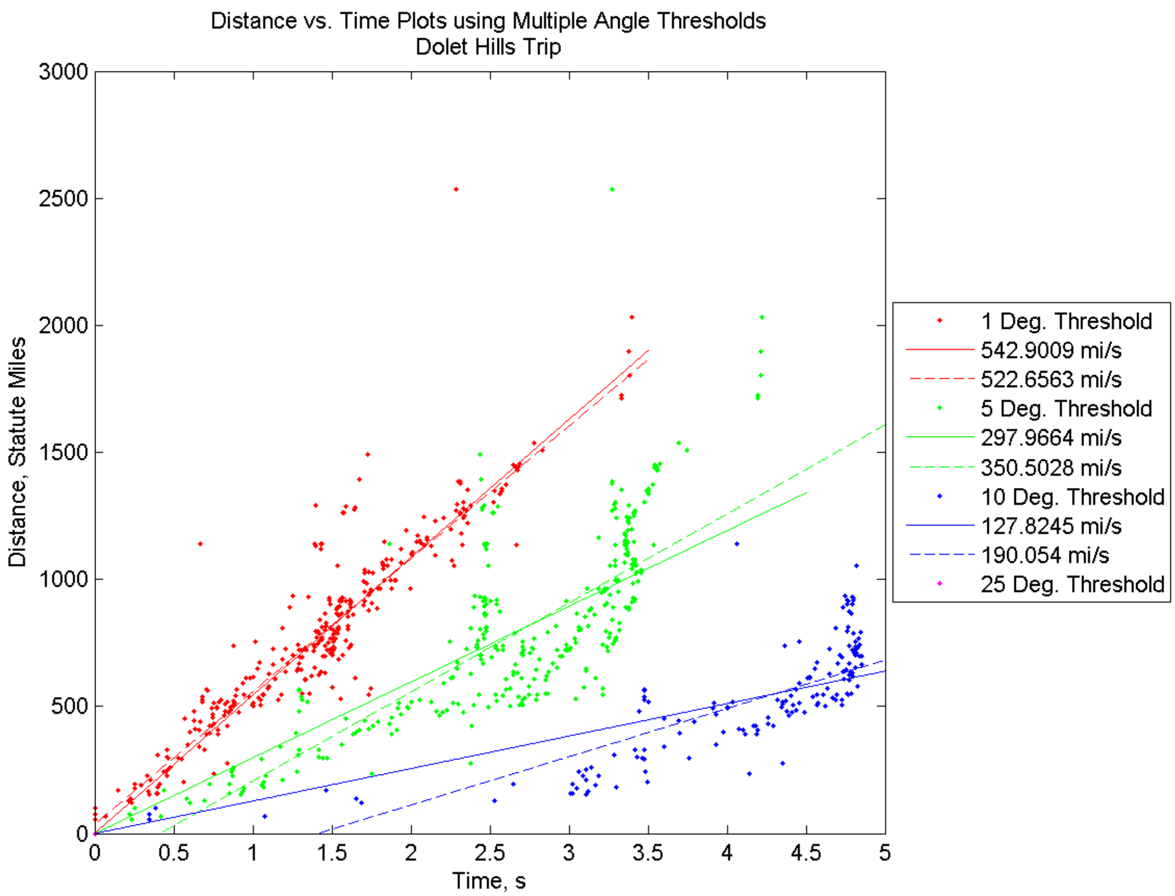
Distance vs. Time Plots using Multiple Angle Thresholds
Dolet Hills Trip
Distance, Statute Miles
Time, s
0
500
1000
1500
2000
2500
3000
0
0.5
1
1.5
2
2.5
3
3.5
4
4.5
5
1 Deg. Threshold
542.9009 mi/s
522.6563 mi/s
5 Deg. Threshold
297.9664 mi/s
350.5028 mi/s
10 Deg. Threshold
127.8245 mi/s
190.054 mi/s
25 Deg. Threshold

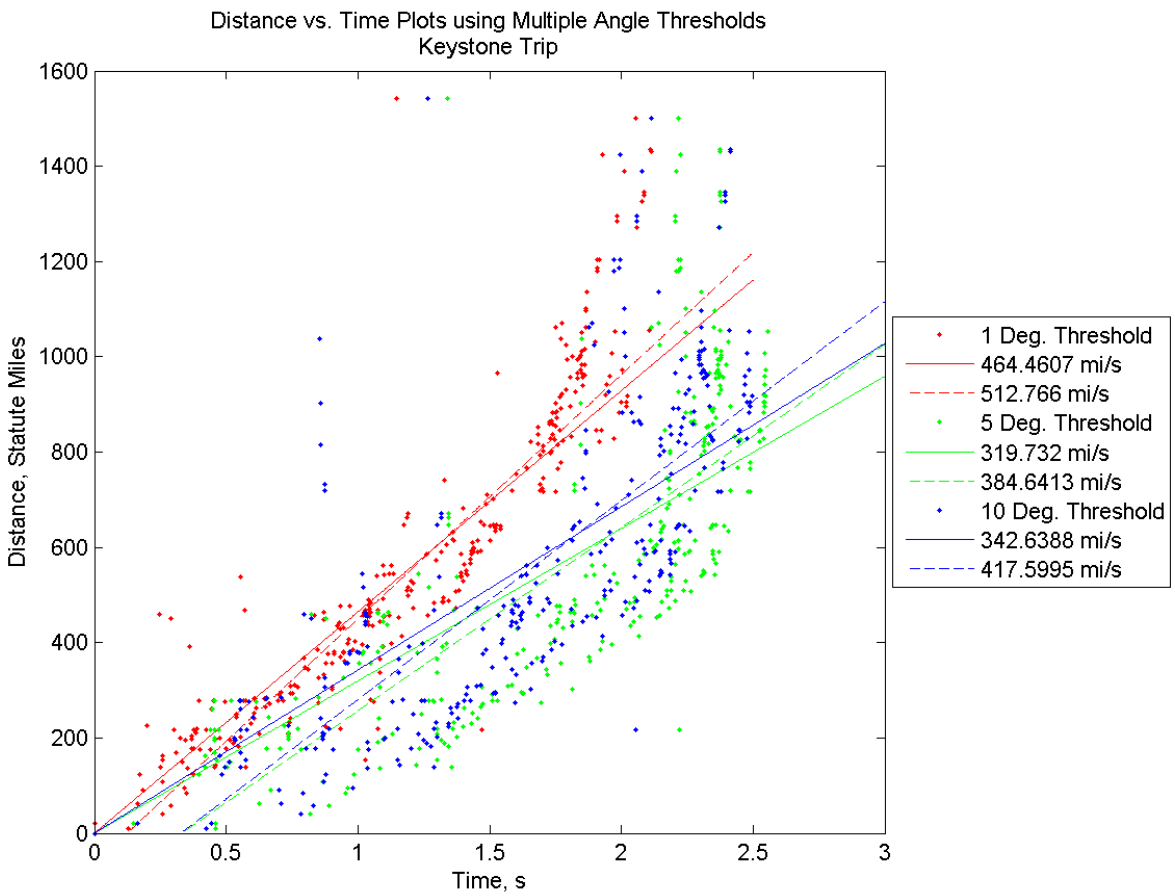
Distance vs. Time Plots using Multiple Angle Thresholds
Keystone Trip
Distance, Statute Miles
Time, s
0
200
400
600
800
1000
1200
1400
1600
0
0.5
1
1.5
2
2.5
3
1 Deg. Threshold
464.4607 mi/s
512.766 mi/s
5 Deg. Threshold
319.732 mi/s
384.6413 mi/s
10 Deg. Threshold
342.6388 mi/s
417.5995 mi/s

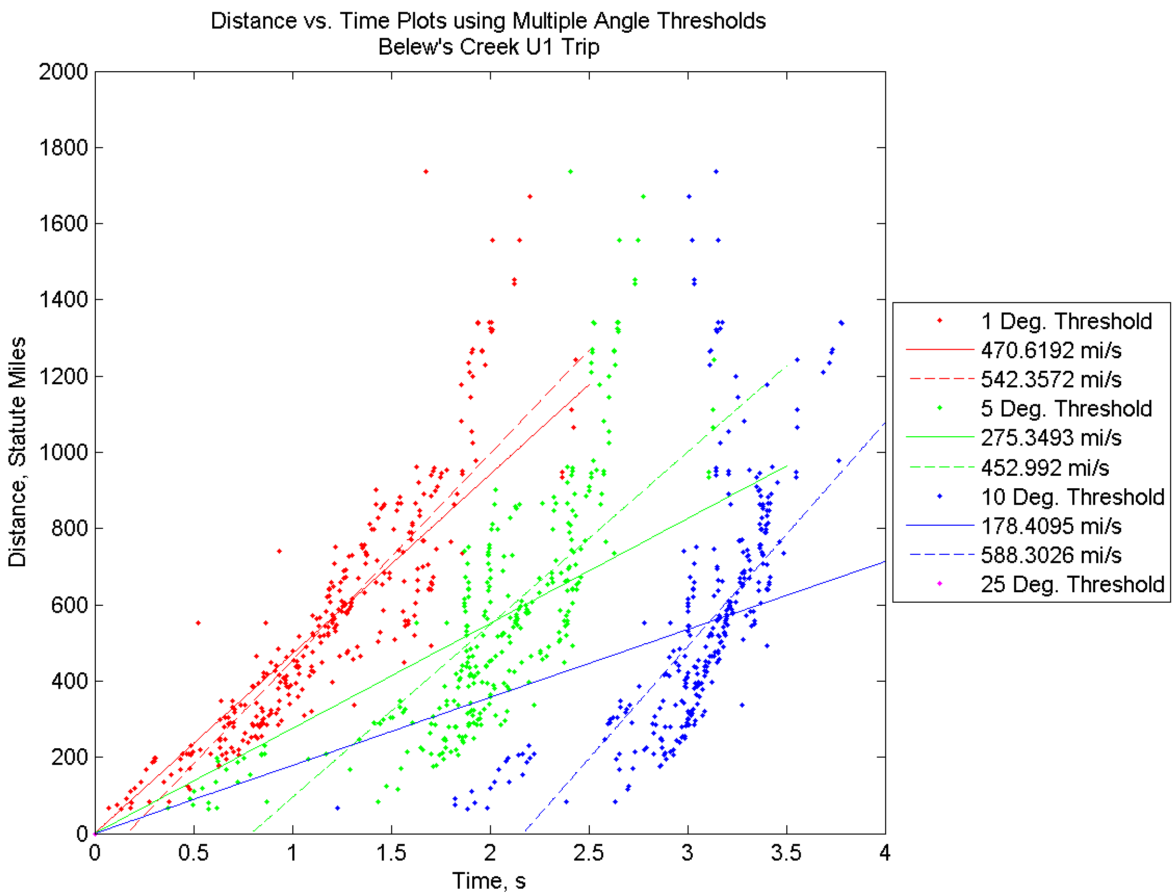

Distance vs. Time Plots using Multiple Angle Thresholds
Belew's Creek U1 Trip
Distance, Statute Miles
Time, s
0
200
400
600
800
1000
1200
1400
1600
1800
2000
0
0.5
1
1.5
2
2.5
3
3.5
4
1 Deg. Threshold
470.6192 mi/s
542.3572 mi/s
5 Deg. Threshold
275.3493 mi/s
452.992 mi/s
10 Deg. Threshold
178.4095 mi/s
588.3026 mi/s
25 Deg. Threshold

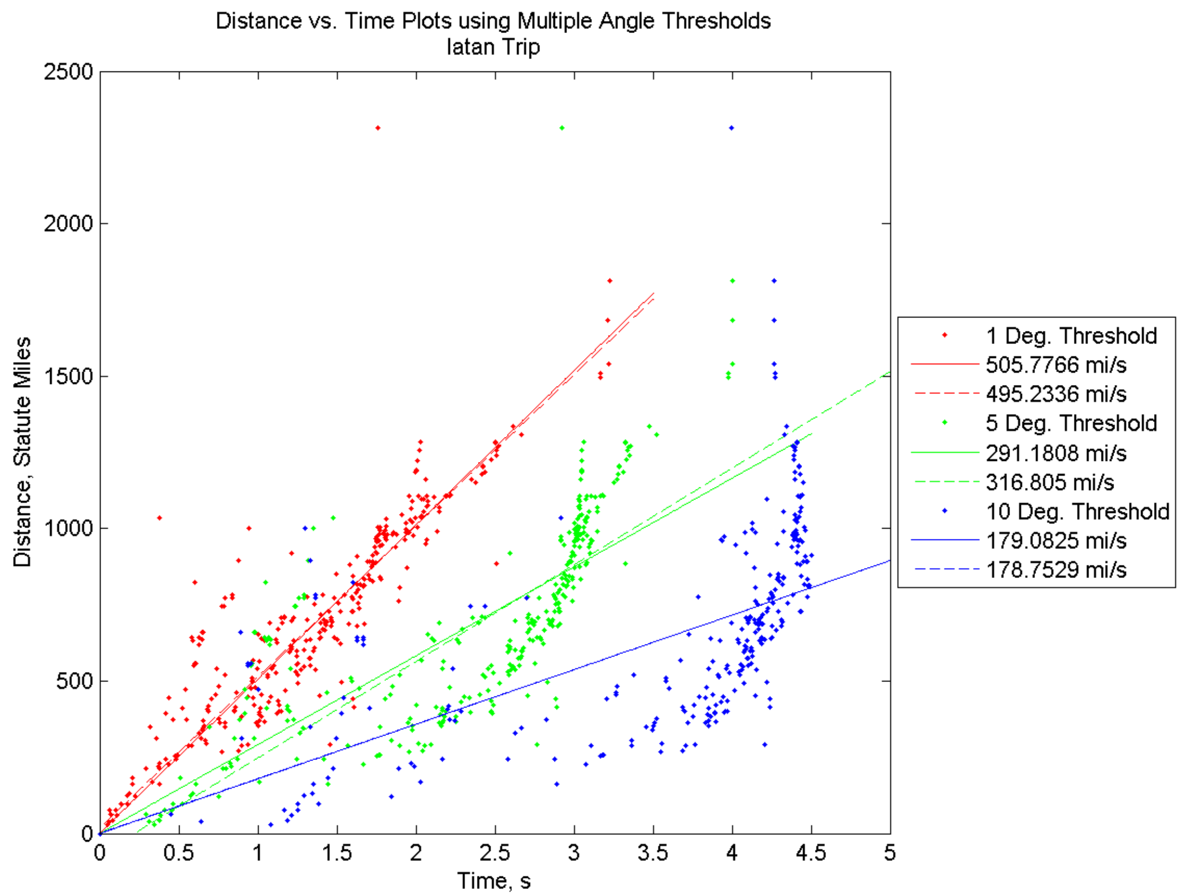
Distance vs. Time Plots using Multiple Angle Thresholds
Iatan Trip
Distance, Statute Miles
Time, s
1 Deg. Threshold
505.7766 mi/s
495.2336 mi/s
5 Deg. Threshold
291.1808 mi/s
316.805 mi/s
10 Deg. Threshold
179.0825 mi/s
178.7529 mi/s

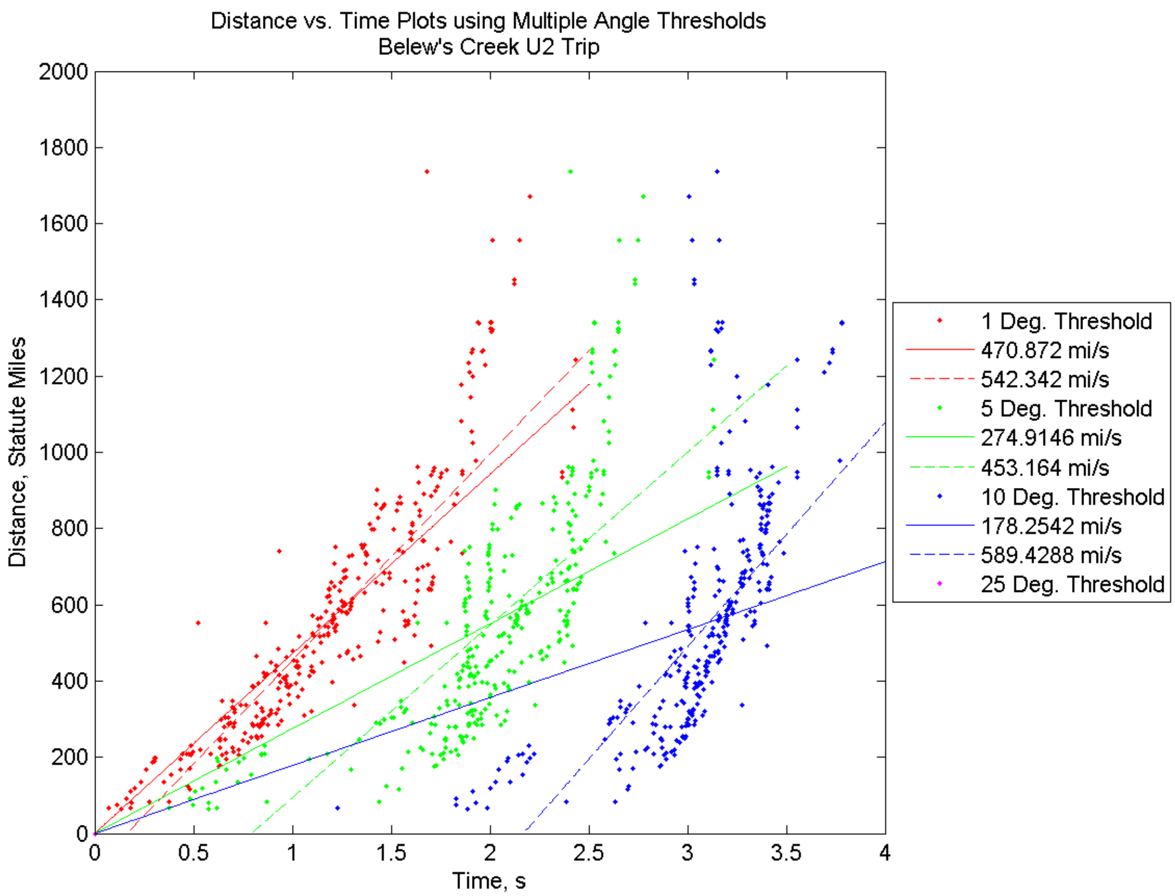
Distance vs. Time Plots using Multiple Angle Thresholds
Belew's Creek U2 Trip
Distance, Statute Miles
Time, s
0
200
400
600
800
1000
1200
1400
1600
1800
2000
0
0.5
1
1.5
2
2.5
3
3.5
4
1 Deg. Threshold
470.872 mi/s
542.342 mi/s
5 Deg. Threshold
274.9146 mi/s
453.164 mi/s
10 Deg. Threshold
178.2542 mi/s
589.4288 mi/s
25 Deg. Threshold

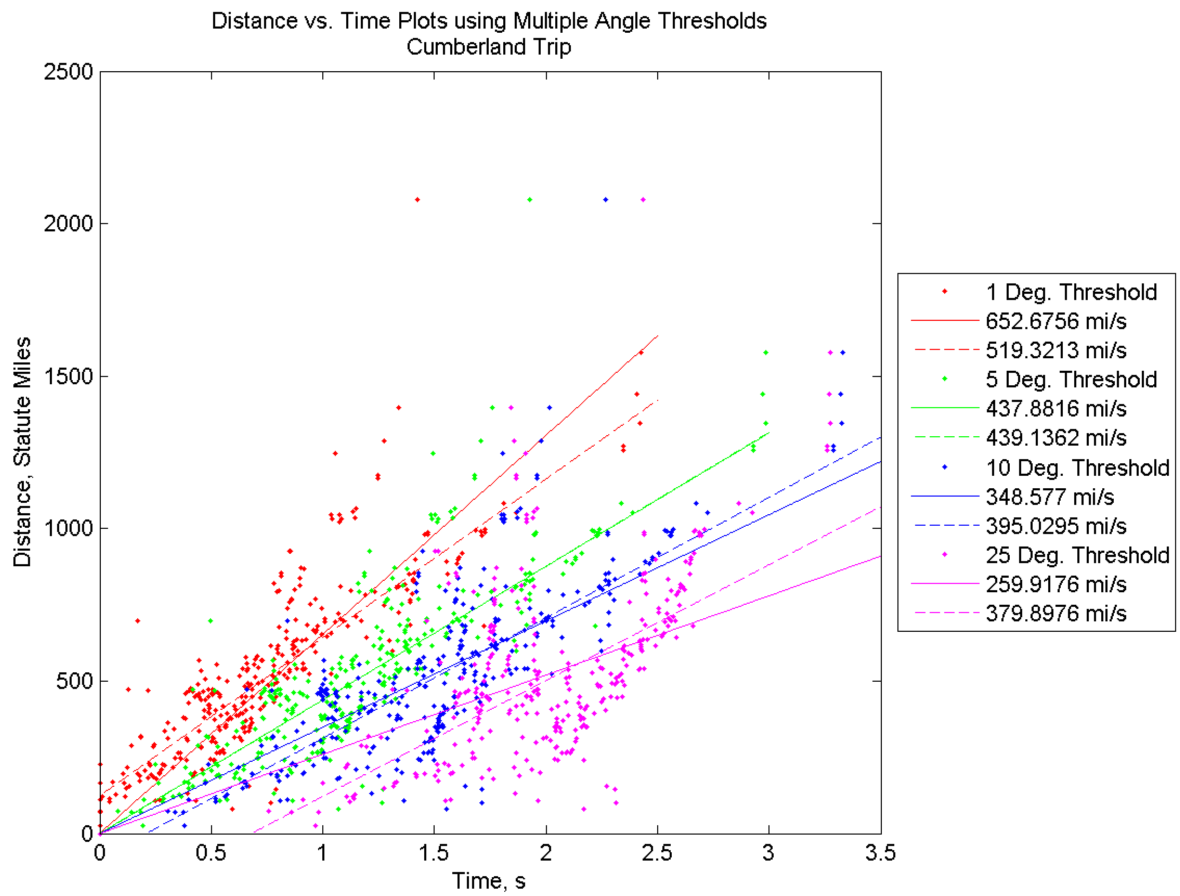
Distance vs. Time Plots using Multiple Angle Thresholds
Cumberland Trip
Distance, Statute Miles
Time, s
2500
2000
1500
1000
500
0
0.5
1
1.5
2
2.5
3
3.5
1 Deg. Threshold
652.6756 mi/s
519.3213 mi/s
5 Deg. Threshold
437.8816 mi/s
439.1362 mi/s
10 Deg. Threshold
348.577 mi/s
395.0295 mi/s
25 Deg. Threshold
259.9176 mi/s
379.8976 mi/s

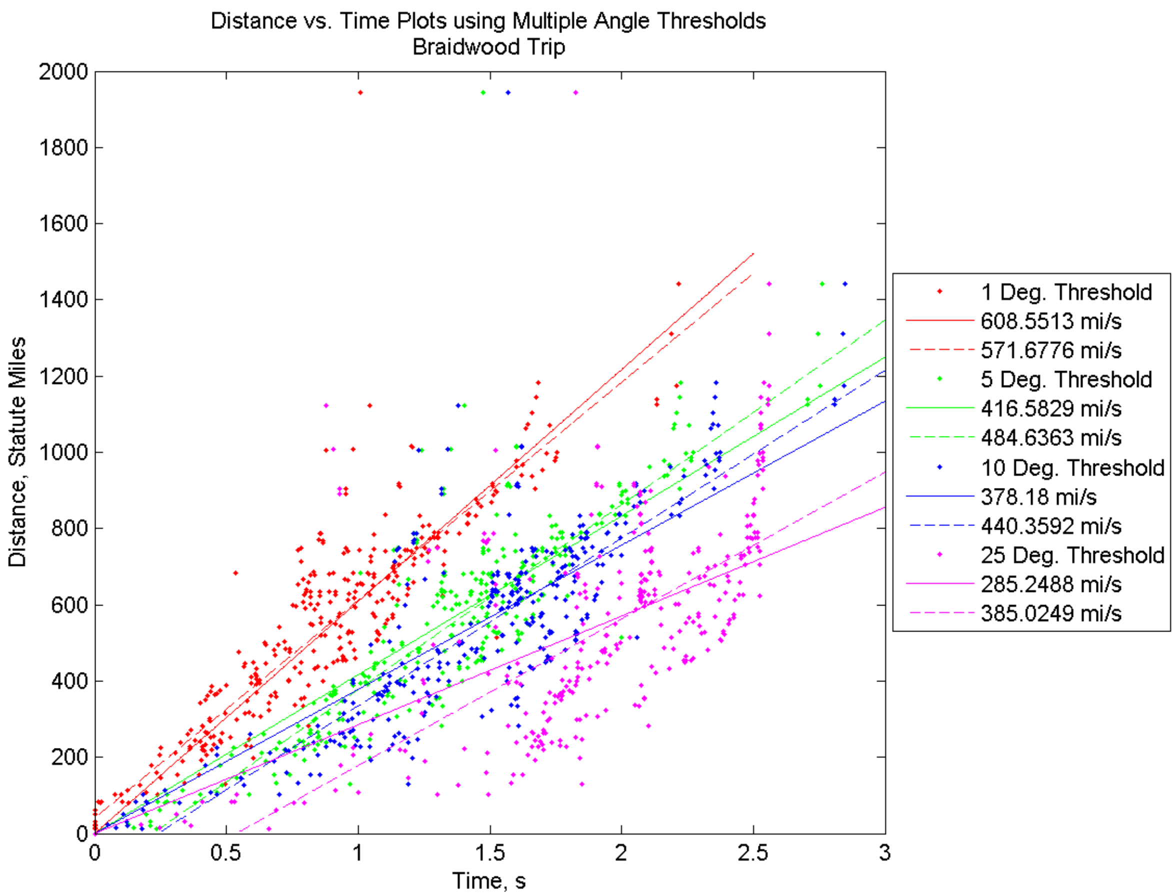
Distance vs. Time Plots using Multiple Angle Thresholds
Braidwood Trip
Distance, Statute Miles
Time, s
0
200
400
600
800
1000
1200
1400
1600
1800
2000
0
0.5
1
1.5
2
2.5
3
1 Deg. Threshold
608.5513 mi/s
571.6776 mi/s
5 Deg. Threshold
416.5829 mi/s
484.6363 mi/s
10 Deg. Threshold
378.18 mi/s
440.3592 mi/s
25 Deg. Threshold
285.2488 mi/s
385.0249 mi/s

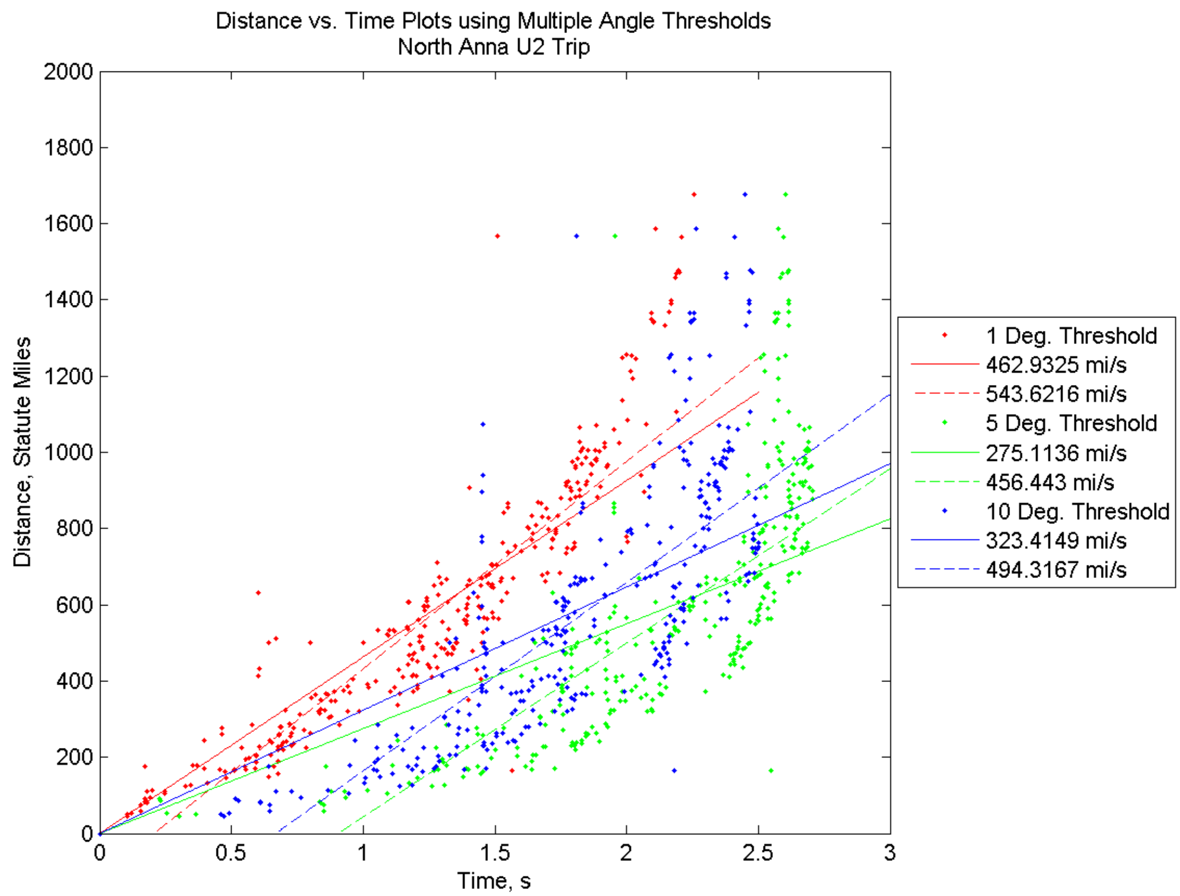

Distance vs. Time Plots using Multiple Angle Thresholds
North Anna U2 Trip
Distance, Statute Miles
Time, s
0
200
400
600
800
1000
1200
1400
1600
1800
2000
0.5
1
1.5
2
2.5
3
1 Deg. Threshold
462.9325 mi/s
543.6216 mi/s
5 Deg. Threshold
275.1136 mi/s
456.443 mi/s
10 Deg. Threshold
323.4149 mi/s
494.3167 mi/s

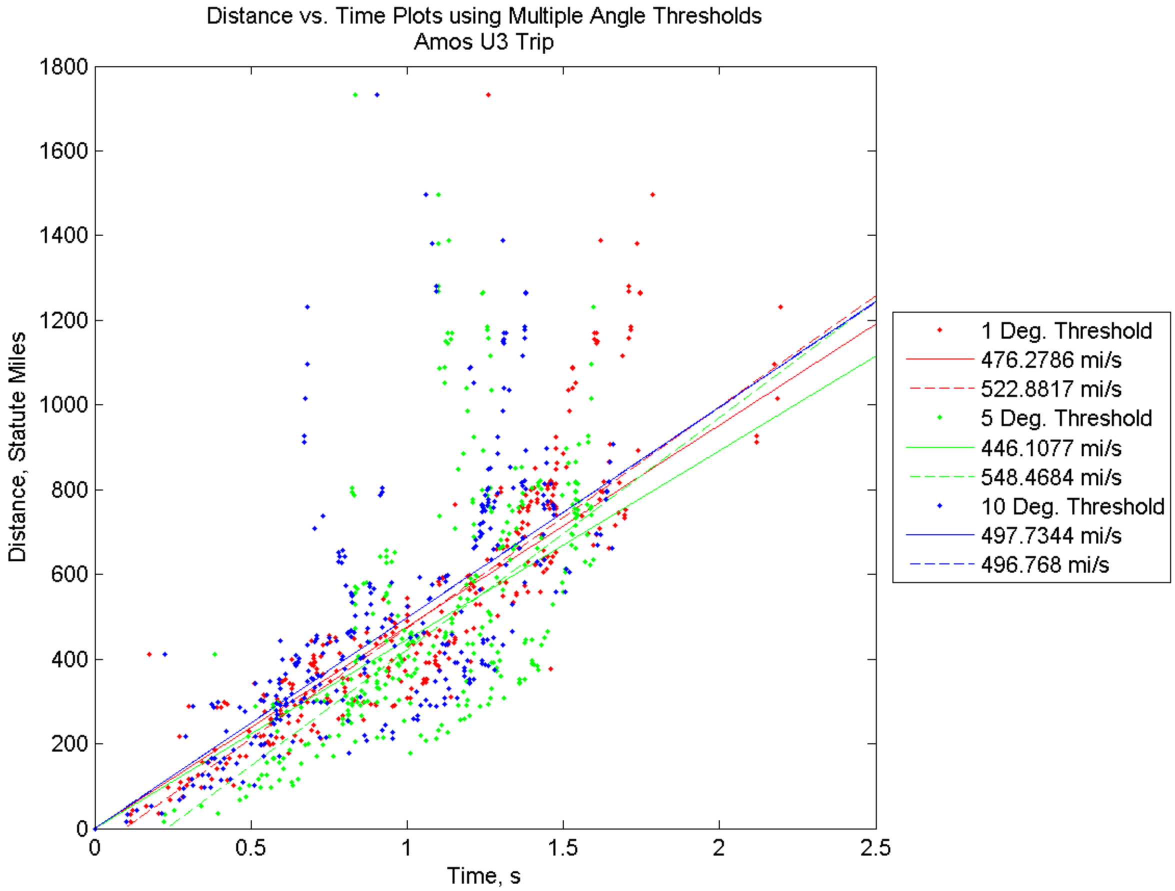
Distance vs. Time Plots using Multiple Angle Thresholds
Amos U3 Trip
Distance, Statute Miles
Time, s
1 Deg. Threshold
476.2786 mi/s
522.8817 mi/s
5 Deg. Threshold
446.1077 mi/s
548.4684 mi/s
10 Deg. Threshold
497.7344 mi/s
496.768 mi/s
0
200
400
600
800
1000
1200
1400
1600
1800
0
0.5
1
1.5
2
2.5

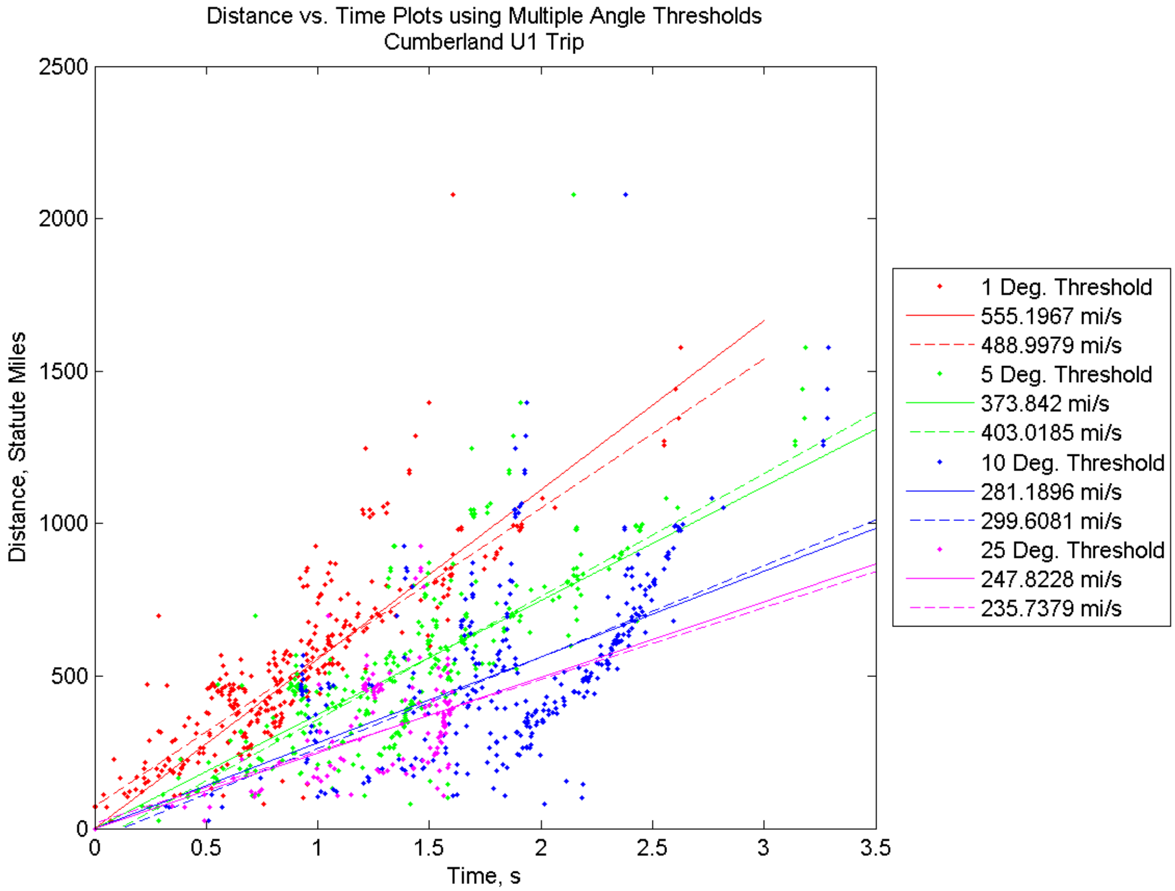
Distance vs. Time Plots using Multiple Angle Thresholds
Cumberland U1 Trip
Distance, Statute Miles
Time, s
0
500
1000
1500
2000
2500
0
0.5
1
1.5
2
2.5
3
3.5
1 Deg. Threshold
555.1967 mi/s
488.9979 mi/s
5 Deg. Threshold
373.842 mi/s
403.0185 mi/s
10 Deg. Threshold
281.1896 mi/s
299.6081 mi/s
25 Deg. Threshold
247.8228 mi/s
235.7379 mi/s

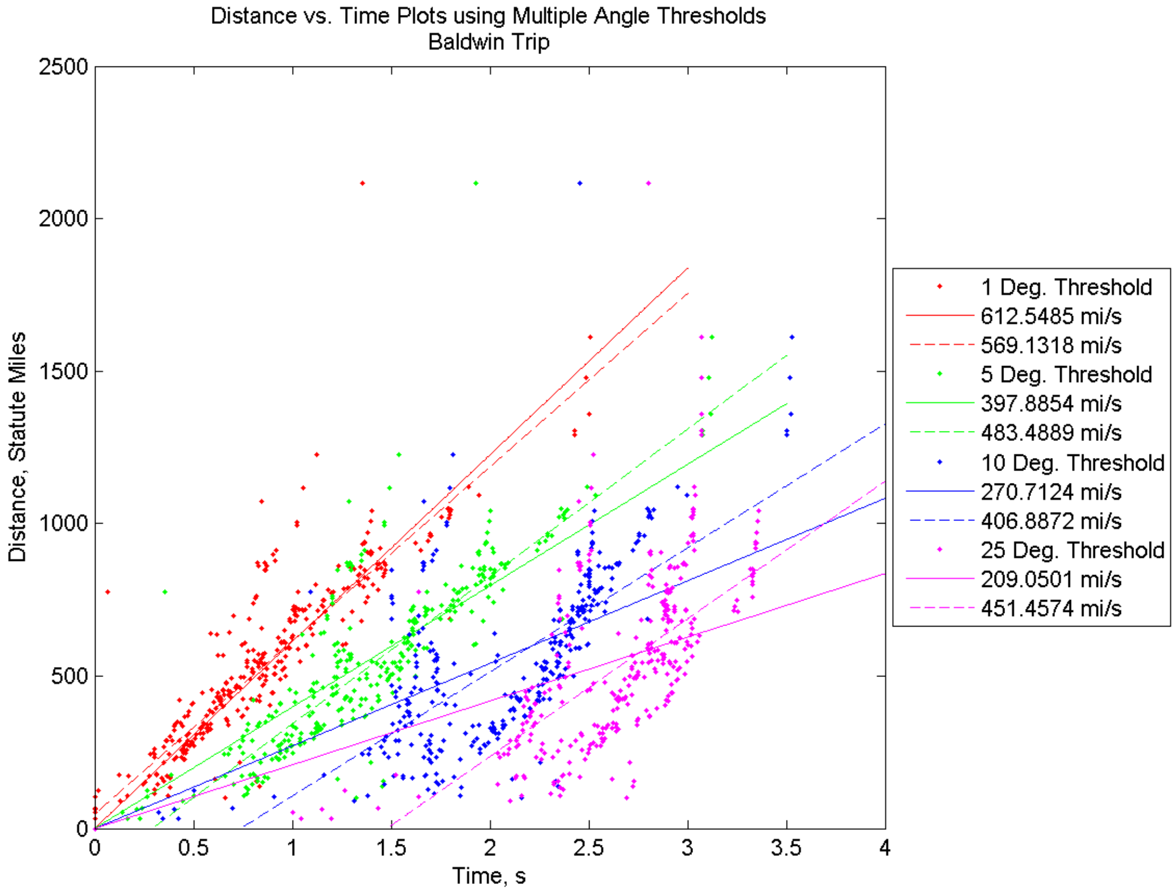
Distance vs. Time Plots using Multiple Angle Thresholds
Baldwin Trip
Distance, Statute Miles
Time, s
0
500
1000
1500
2000
2500
0.5
1
1.5
2
2.5
3
3.5
4
1 Deg. Threshold
612.5485 mi/s
569.1318 mi/s
5 Deg. Threshold
397.8854 mi/s
483.4889 mi/s
10 Deg. Threshold
270.7124 mi/s
406.8872 mi/s
25 Deg. Threshold
209.0501 mi/s
451.4574 mi/s

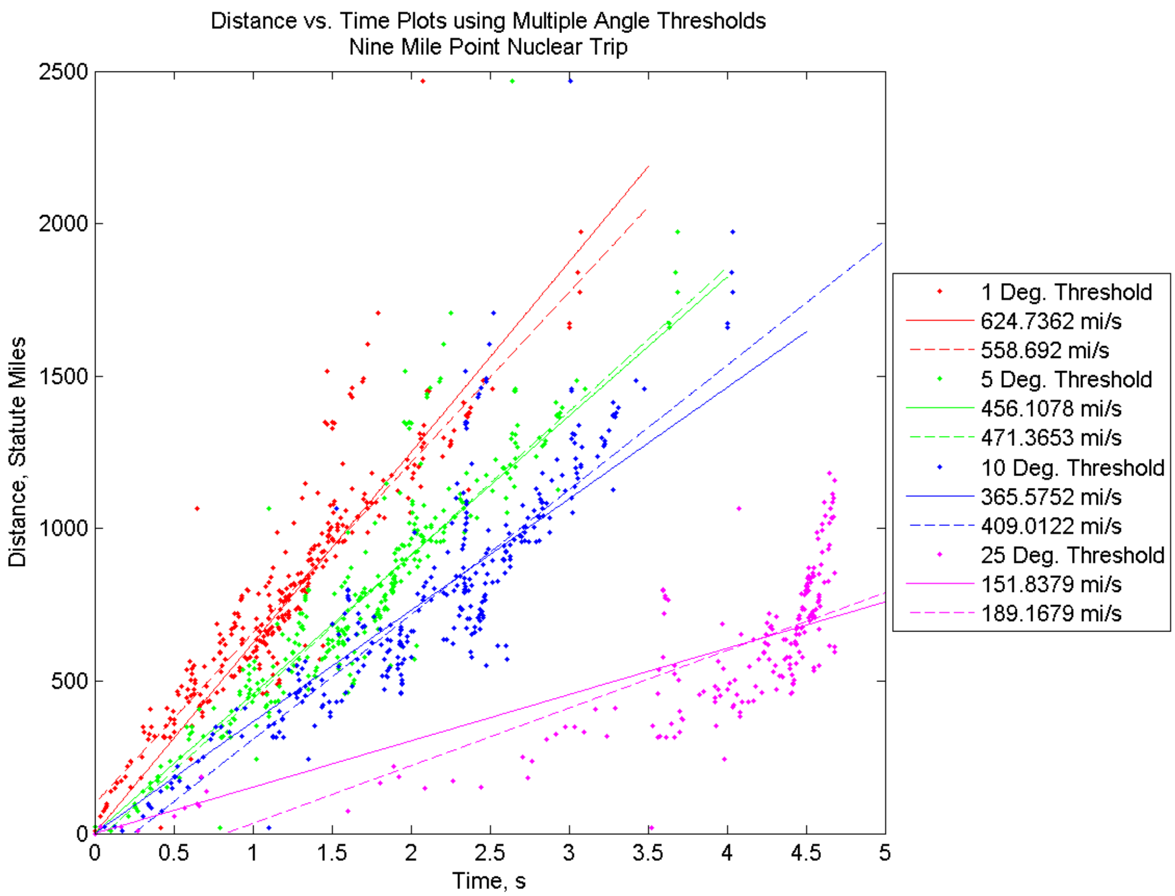
Distance vs. Time Plots using Multiple Angle Thresholds
Nine Mile Point Nuclear Trip
Distance, Statute Miles
Time, s
0
500
1000
1500
2000
2500
0
0.5
1
1.5
2
2.5
3
3.5
4
4.5
5
1 Deg. Threshold
624.7362 mi/s
558.692 mi/s
5 Deg. Threshold
456.1078 mi/s
471.3653 mi/s
10 Deg. Threshold
365.5752 mi/s
409.0122 mi/s
25 Deg. Threshold
151.8379 mi/s
189.1679 mi/s

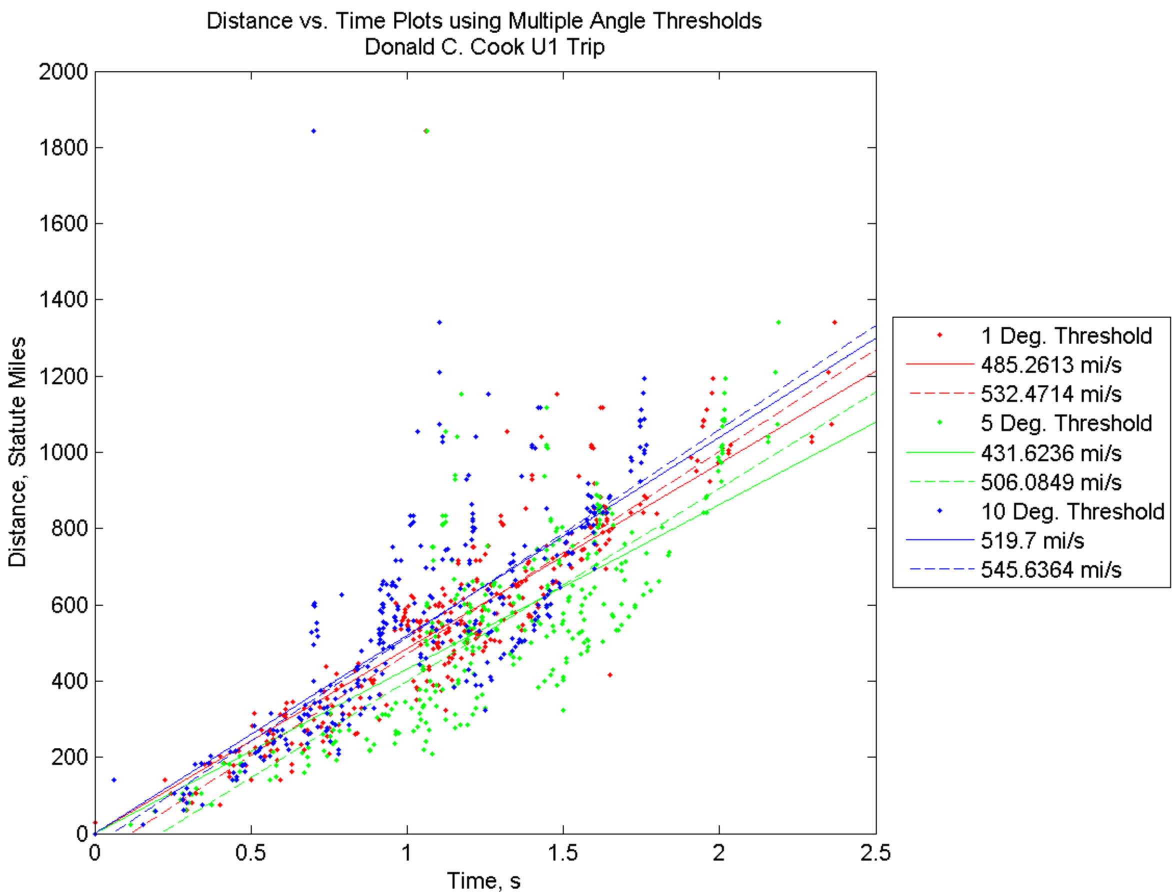
Distance vs. Time Plots using Multiple Angle Thresholds
Donald C. Cook U1 Trip
Distance, Statute Miles
Time, s
0
200
400
600
800
1000
1200
1400
1600
1800
2000
0.5
1
1.5
2
2.5
1 Deg. Threshold
485.2613 mi/s
532.4714 mi/s
5 Deg. Threshold
431.6236 mi/s
506.0849 mi/s
10 Deg. Threshold
519.7 mi/s
545.6364 mi/s

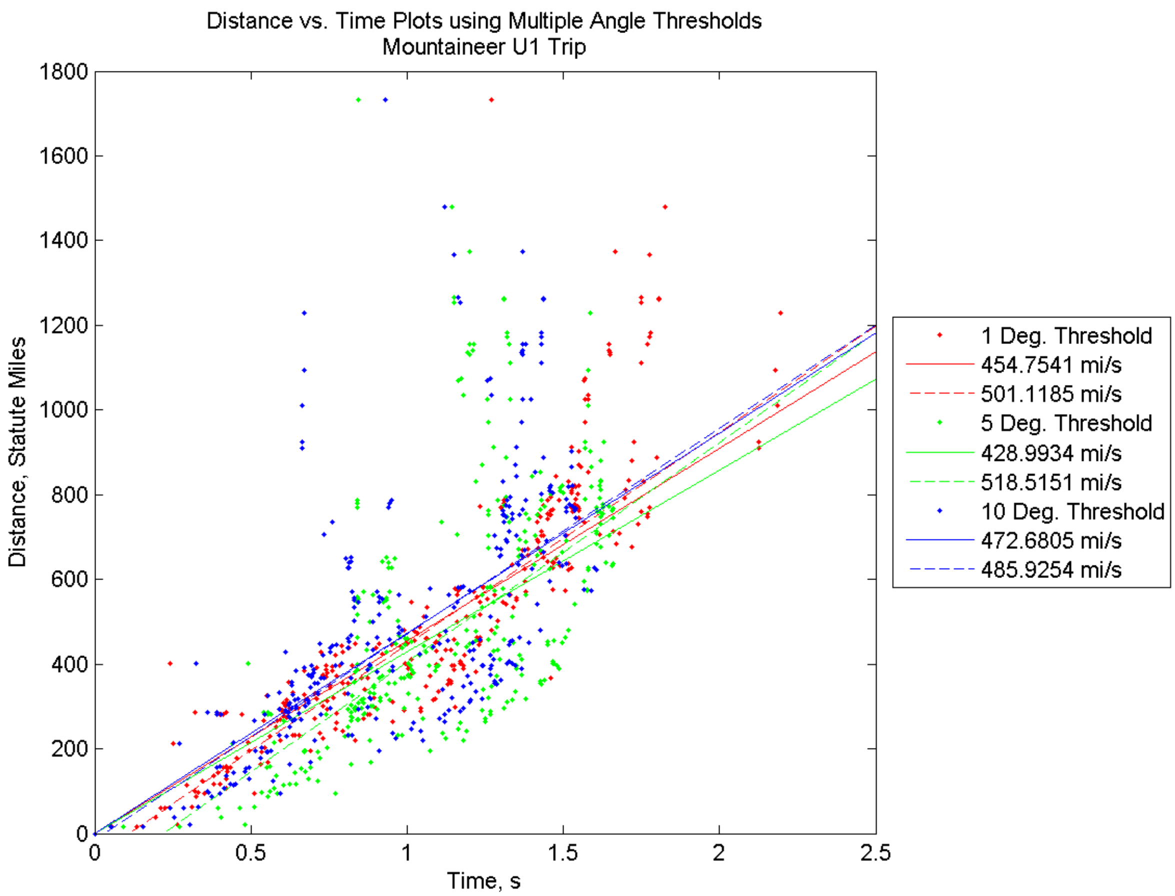
Distance vs. Time Plots using Multiple Angle Thresholds
Mountaineer U1 Trip
Distance, Statute Miles
Time, s
0
200
400
600
800
1000
1200
1400
1600
1800
0
0.5
1
1.5
2
2.5
1 Deg. Threshold
454.7541 mi/s
501.1185 mi/s
5 Deg. Threshold
428.9934 mi/s
518.5151 mi/s
10 Deg. Threshold
472.6805 mi/s
485.9254 mi/s

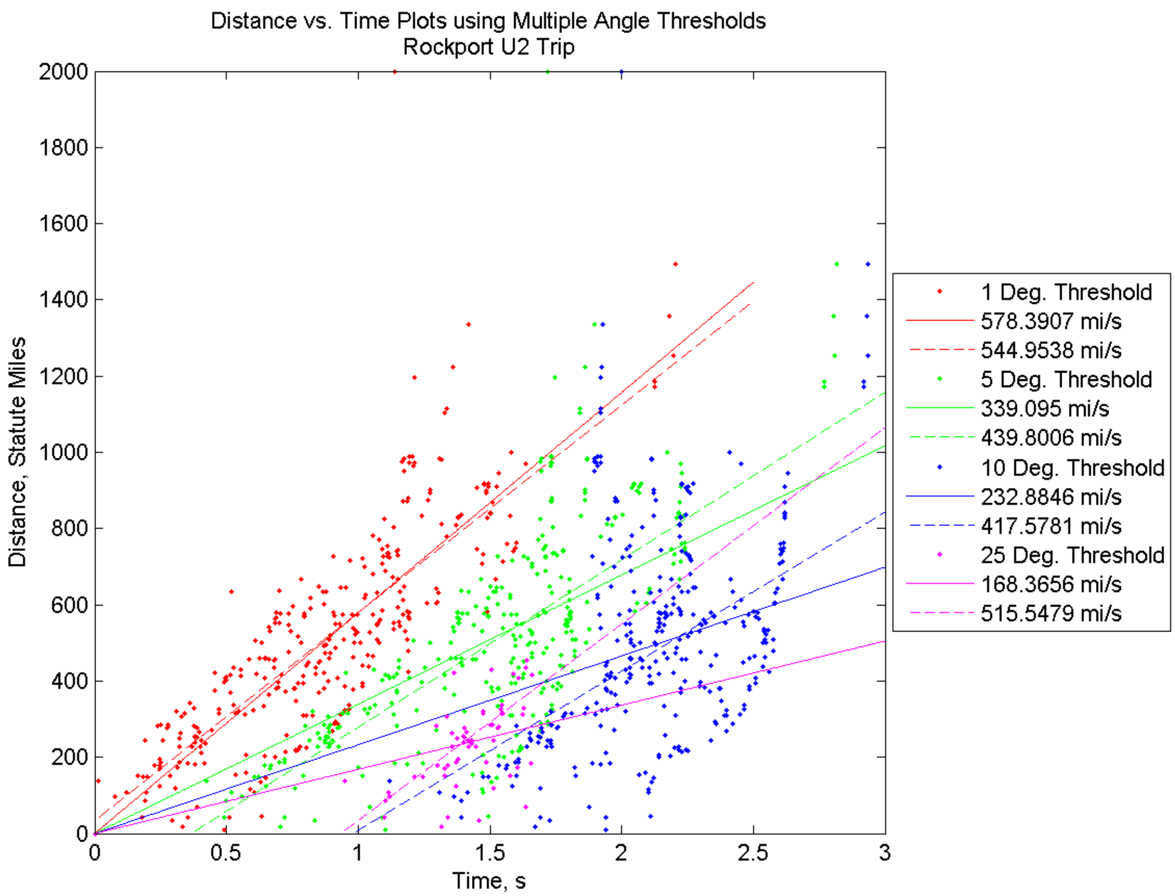
Distance vs. Time Plots using Multiple Angle Thresholds
Rockport U2 Trip
Distance, Statute Miles
Time, s
0
200
400
600
800
1000
1200
1400
1600
1800
2000
0
0.5
1
1.5
2
2.5
3
1 Deg. Threshold
578.3907 mi/s
544.9538 mi/s
5 Deg. Threshold
339.095 mi/s
439.8006 mi/s
10 Deg. Threshold
232.8846 mi/s
417.5781 mi/s
25 Deg. Threshold
168.3656 mi/s
515.5479 mi/s

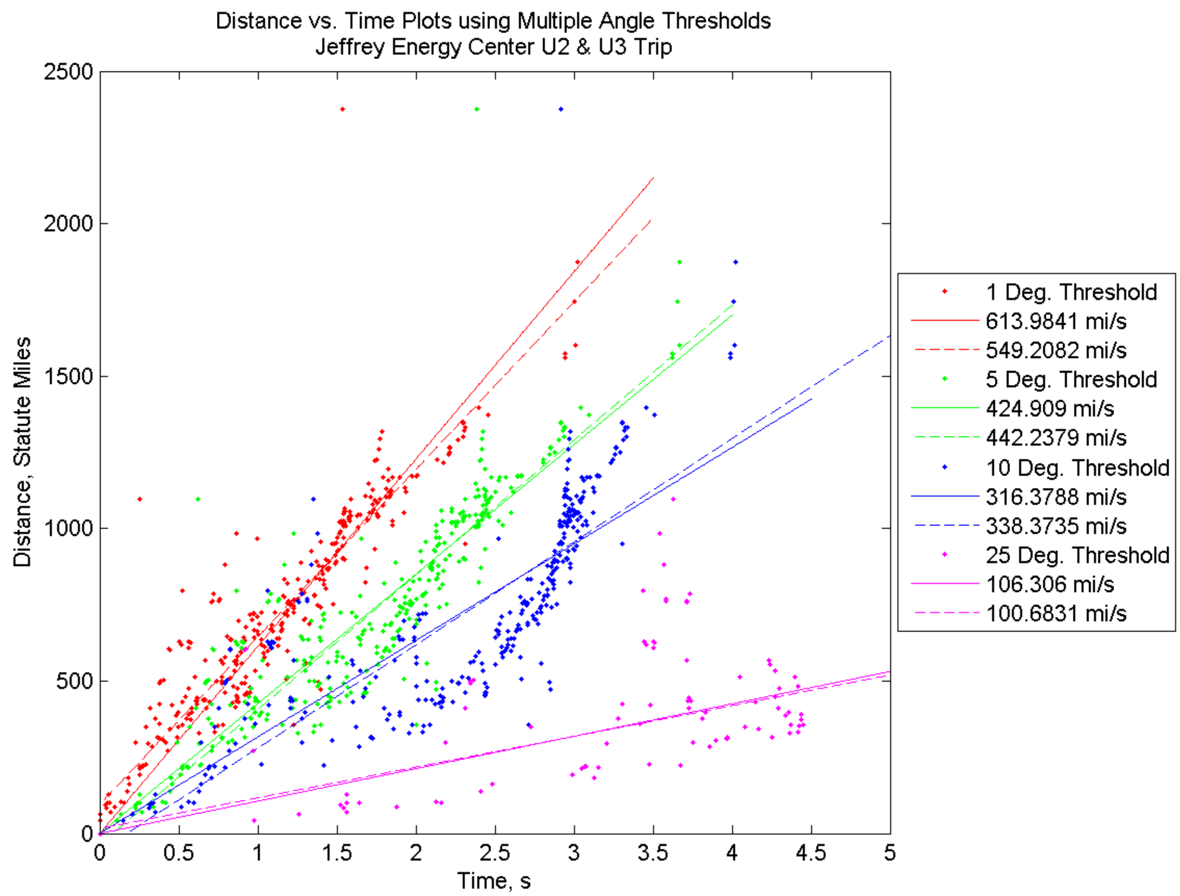

Distance vs. Time Plots using Multiple Angle Thresholds
Jeffrey Energy Center U2 & U3 Trip
Distance, Statute Miles
Time, s
0
500
1000
1500
2000
2500
0
0.5
1
1.5
2
2.5
3
3.5
4
4.5
5
1 Deg. Threshold
613.9841 mi/s
549.2082 mi/s
5 Deg. Threshold
424.909 mi/s
442.2379 mi/s
10 Deg. Threshold
316.3788 mi/s
338.3735 mi/s
25 Deg. Threshold
106.306 mi/s
100.6831 mi/s

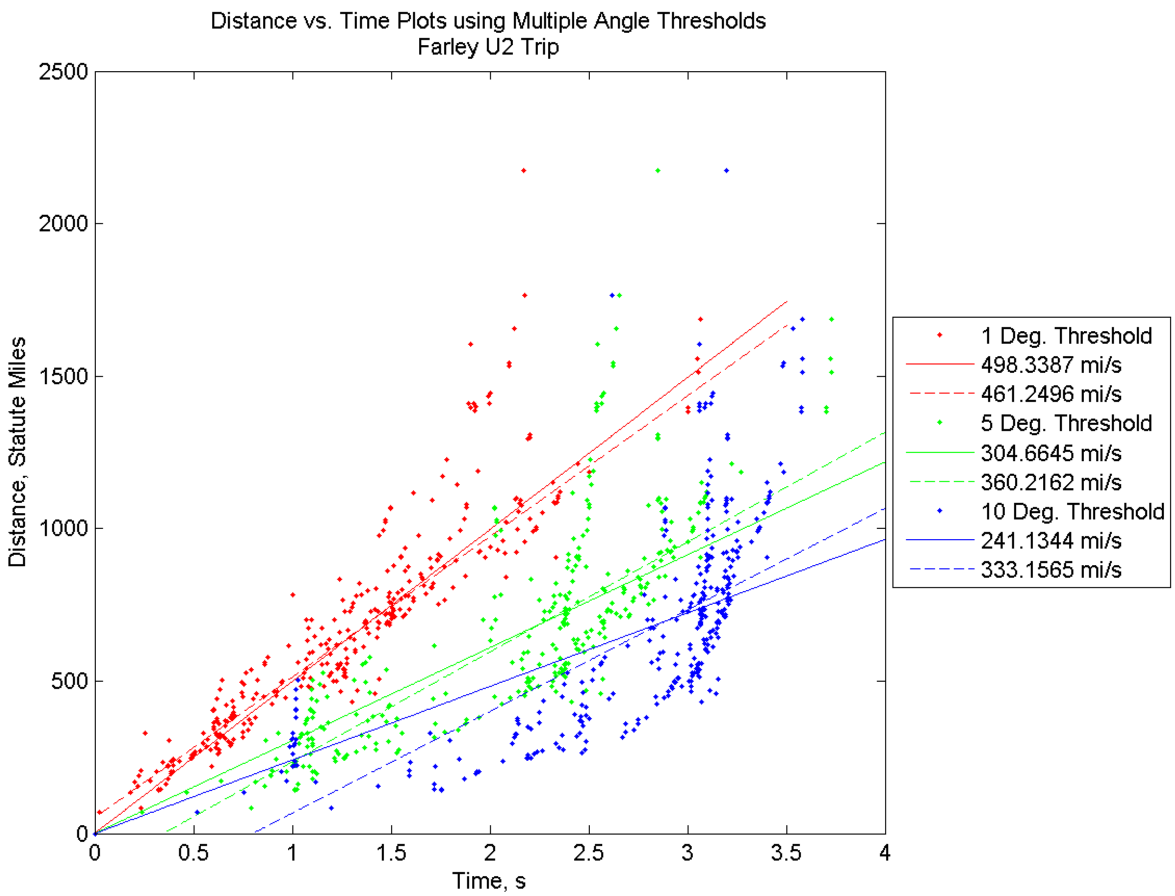
Distance vs. Time Plots using Multiple Angle Thresholds
Farley U2 Trip
Distance, Statute Miles
Time, s
0
500
1000
1500
2000
2500
0
0.5
1
1.5
2
2.5
3
3.5
4
1 Deg. Threshold
498.3387 mi/s
461.2496 mi/s
5 Deg. Threshold
304.6645 mi/s
360.2162 mi/s
10 Deg. Threshold
241.1344 mi/s
333.1565 mi/s

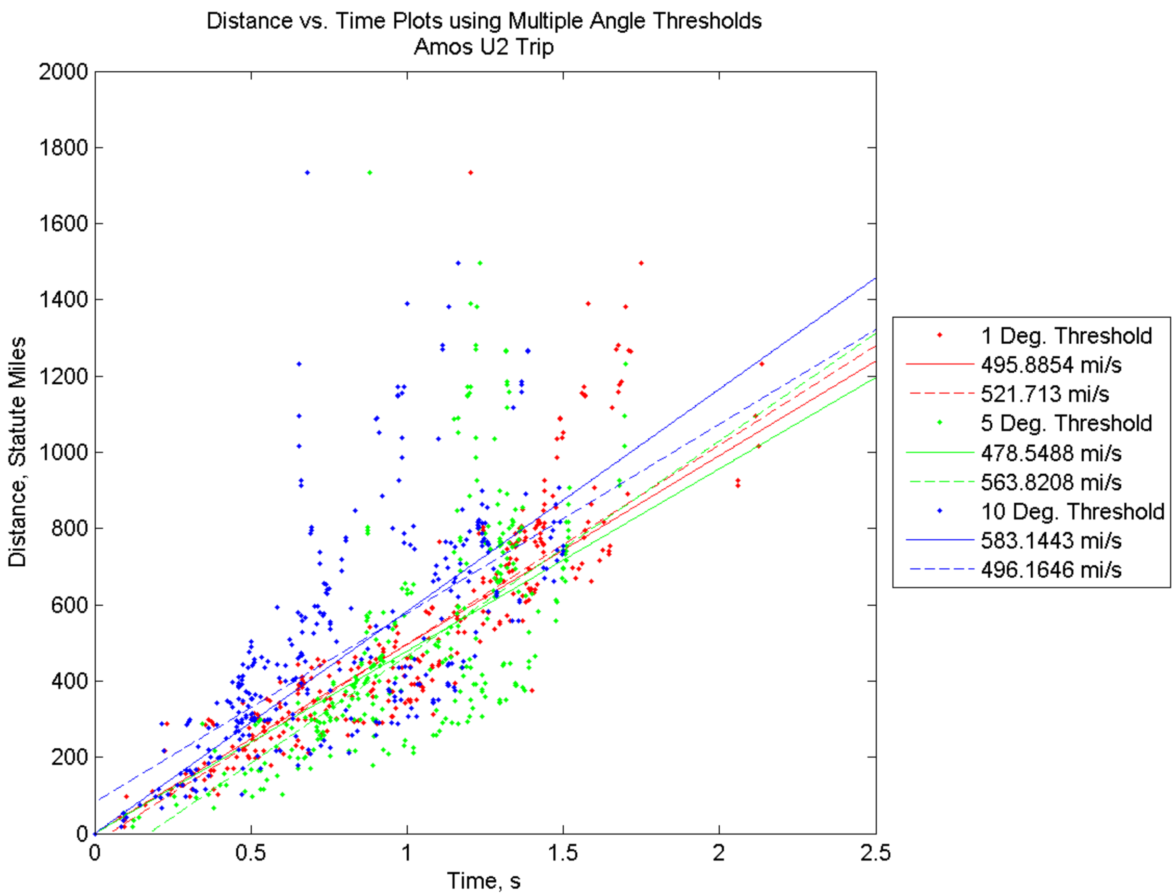
Distance vs. Time Plots using Multiple Angle Thresholds
Amos U2 Trip
Distance, Statute Miles
Time, s
0
200
400
600
800
1000
1200
1400
1600
1800
2000
0.5
1
1.5
2
2.5
1 Deg. Threshold
495.8854 mi/s
521.713 mi/s
5 Deg. Threshold
478.5488 mi/s
563.8208 mi/s
10 Deg. Threshold
583.1443 mi/s
496.1646 mi/s

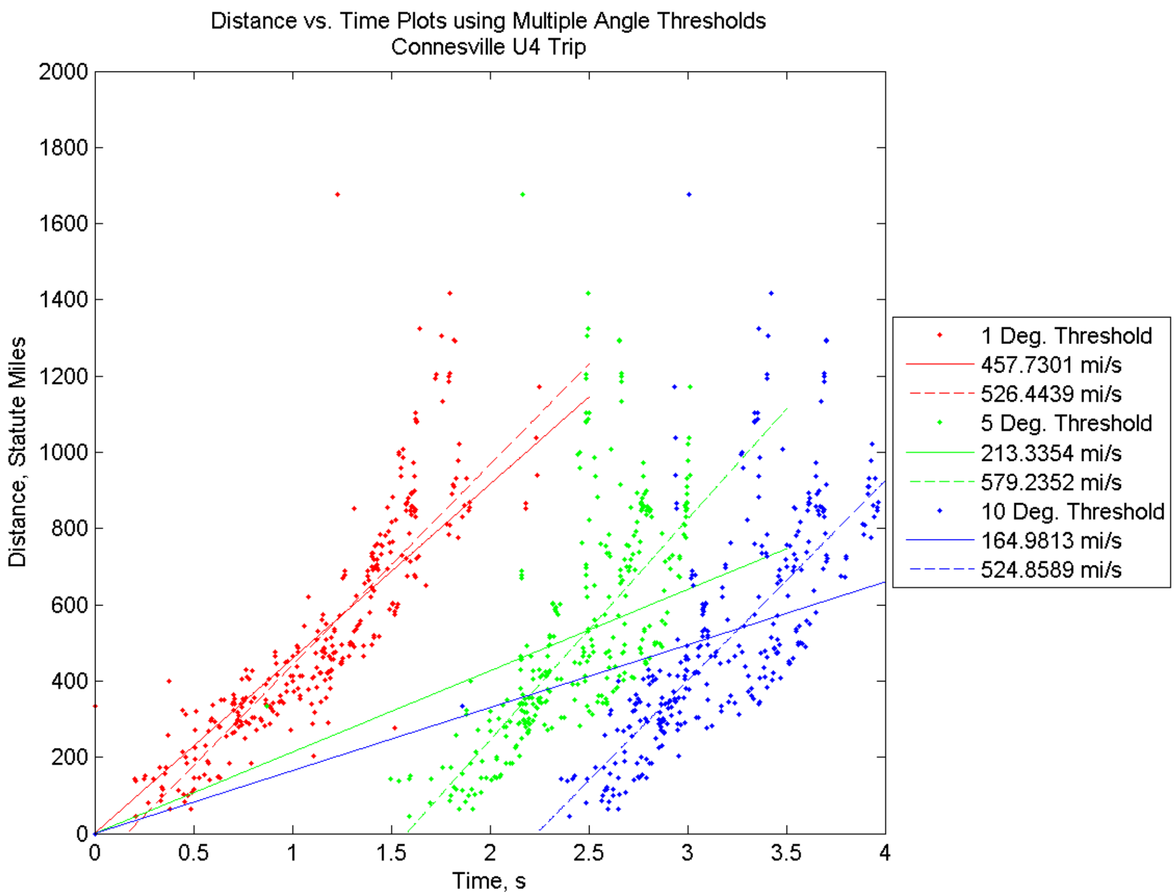
Distance vs. Time Plots using Multiple Angle Thresholds
Connesville U4 Trip
Distance, Statute Miles
Time, s
0
200
400
600
800
1000
1200
1400
1600
1800
2000
0
0.5
1
1.5
2
2.5
3
3.5
4
1 Deg. Threshold
457.7301 mi/s
526.4439 mi/s
5 Deg. Threshold
213.3354 mi/s
579.2352 mi/s
10 Deg. Threshold
164.9813 mi/s
524.8589 mi/s

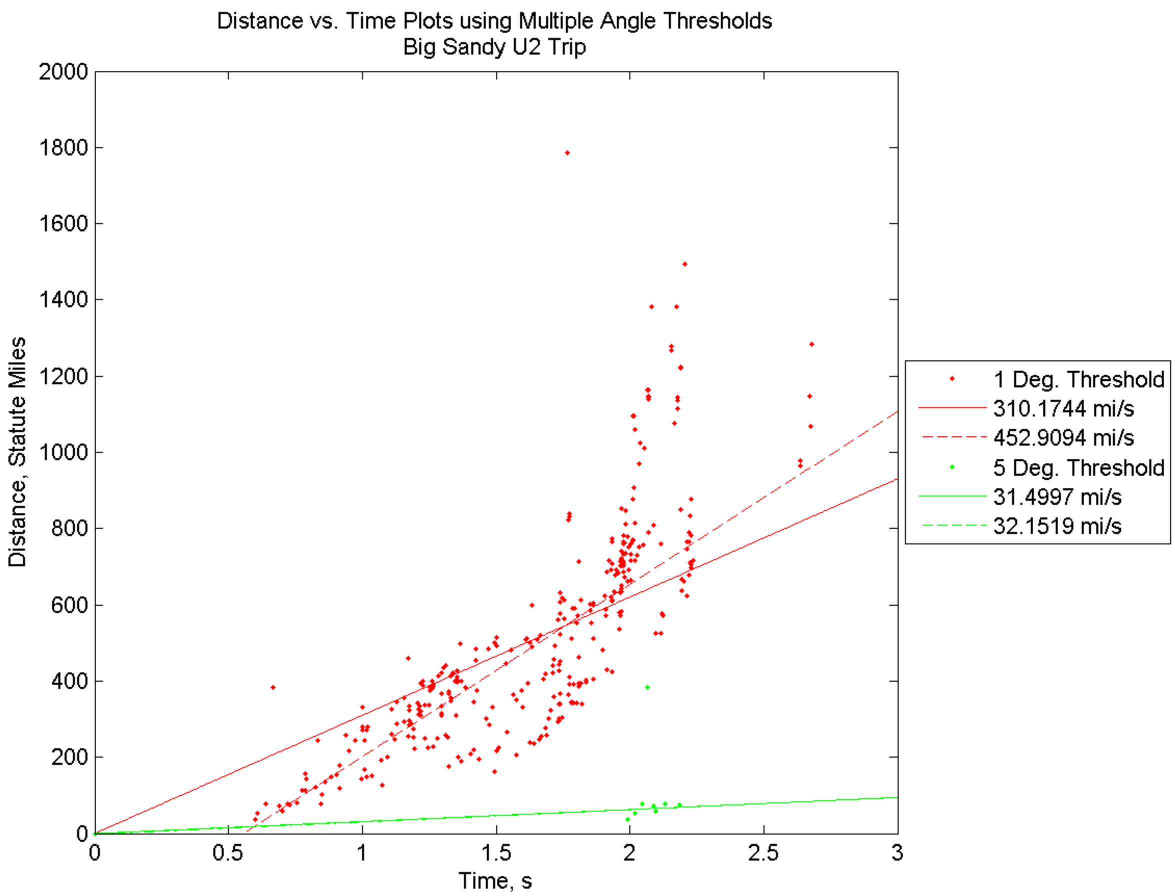
Distance vs. Time Plots using Multiple Angle Thresholds
Big Sandy U2 Trip
Distance, Statute Miles
Time, s
0
200
400
600
800
1000
1200
1400
1600
1800
2000
0
0.5
1
1.5
2
2.5
3
1 Deg. Threshold
310.1744 mi/s
452.9094 mi/s
5 Deg. Threshold
31.4997 mi/s
32.1519 mi/s

Appendix XV: Full Half-Plane Event Location Based Upon Full Simulation of EI Frequency

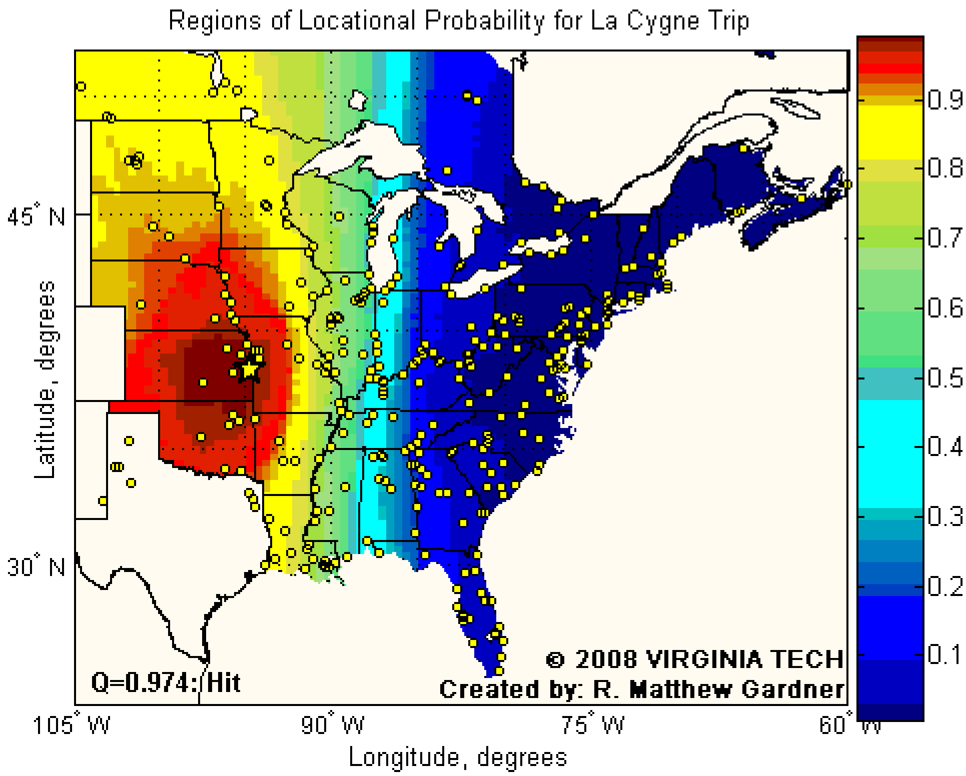

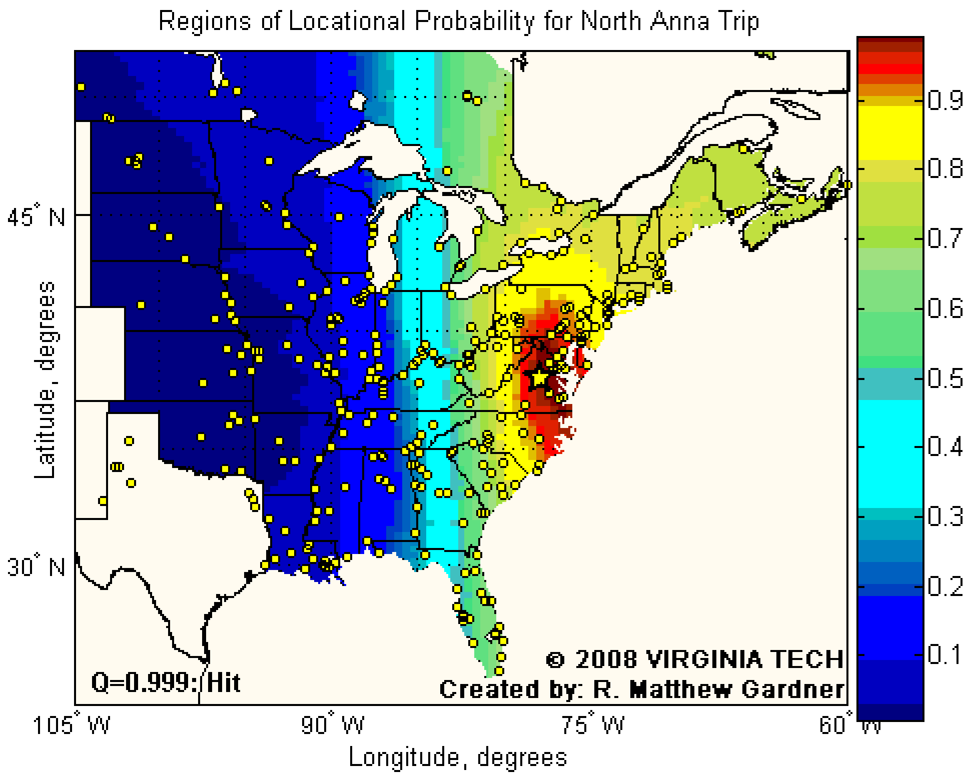
Regions of Locational Probability for North Anna Trip
45° N
30° N
Latitude, degrees
105° W
90° W
75° W
60° W
Longitude, degrees
Q=0.999: Hit
© 2008 VIRGINIA TECH
Created by: R. Matthew Gardner
0.9
0.8
0.7
0.6
0.5
0.4
0.3
0.2
0.1

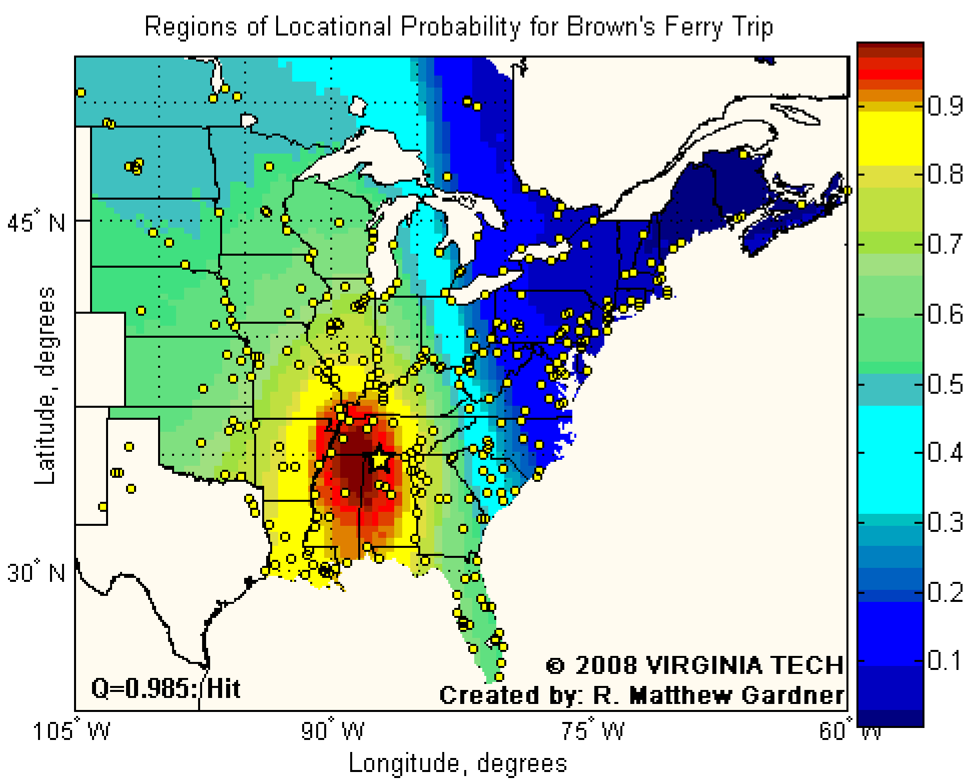
Regions of Locational Probability for Brown's Ferry Trip
45° N
30° N
Latitude, degrees
105° W
90° W
75° W
60° W
Longitude, degrees
Q=0.985: Hit
© 2008 VIRGINIA TECH
Created by: R. Matthew Gardner
0.9
0.8
0.7
0.6
0.5
0.4
0.3
0.2
0.1

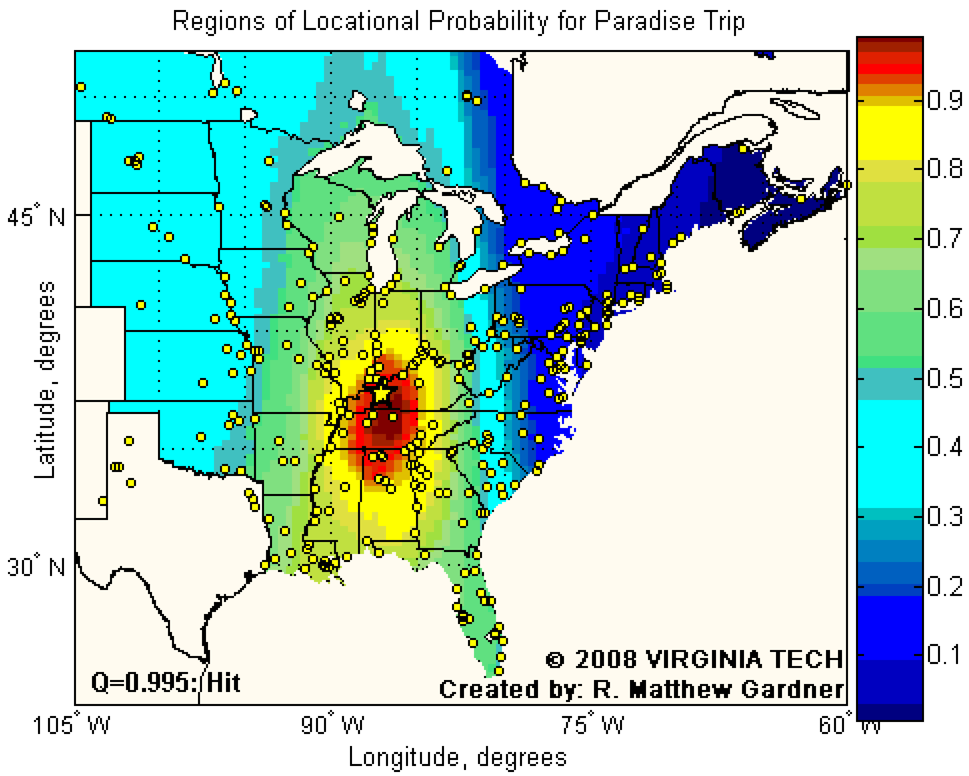
Regions of Locational Probability for Paradise Trip
Latitude, degrees
Longitude, degrees
45° N
30° N
105° W
90° W
75° W
60° W
0.1
0.2
0.3
0.4
0.5
0.6
0.7
0.8
0.9
Q=0.995: Hit
© 2008 VIRGINIA TECH
Created by: R. Matthew Gardner

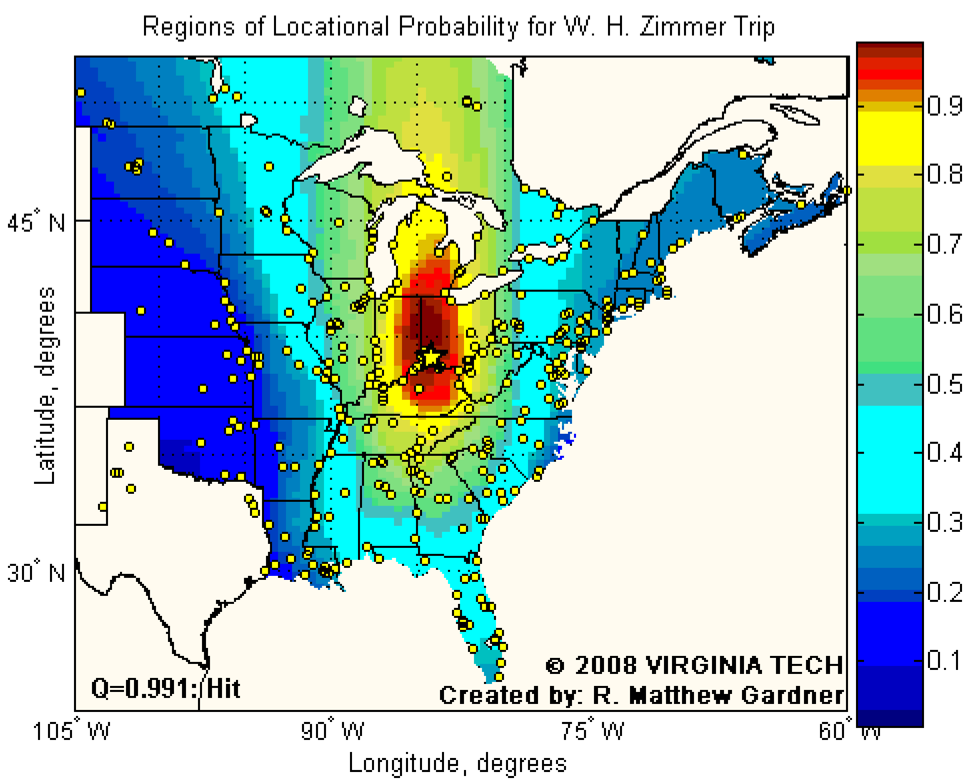
Regions of Locational Probability for W. H. Zimmer Trip
Latitude, degrees
Longitude, degrees
45° N
30° N
105° W
90° W
75° W
60° W
0.1
0.2
0.3
0.4
0.5
0.6
0.7
0.8
0.9
Q=0.991: Hit
© 2008 VIRGINIA TECH
Created by: R. Matthew Gardner

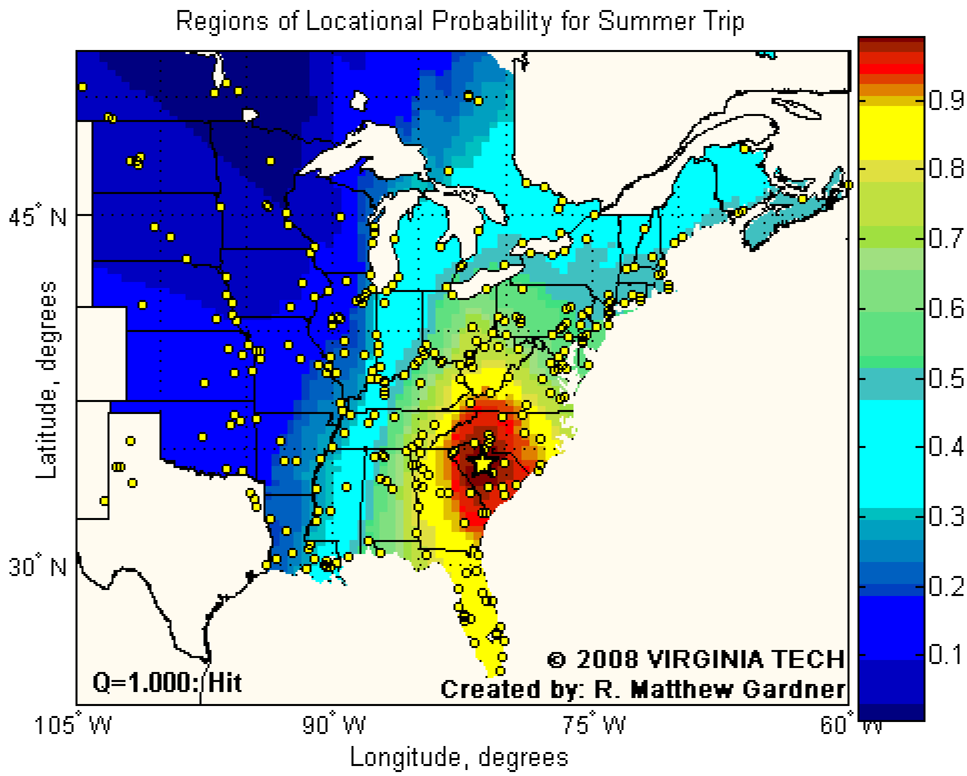
Regions of Locational Probability for Summer Trip
45° N
30° N
Latitude, degrees
105° W
90° W
75° W
60° W
Longitude, degrees
Q=1.000: Hit
© 2008 VIRGINIA TECH
Created by: R. Matthew Gardner
0.9
0.8
0.7
0.6
0.5
0.4
0.3
0.2
0.1

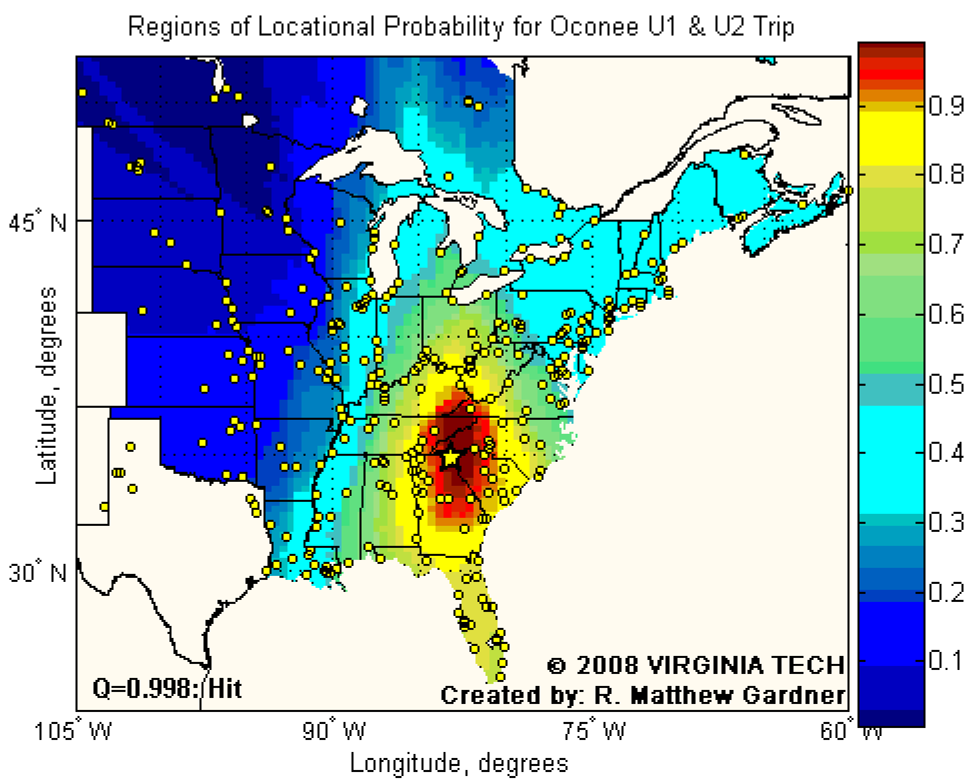
Regions of Locational Probability for Oconee U1 & U2 Trip
45° N
30° N
Latitude, degrees
105° W
90° W
75° W
60° W
Longitude, degrees
Q=0.998: Hit
© 2008 VIRGINIA TECH
Created by: R. Matthew Gardner
0.9
0.8
0.7
0.6
0.5
0.4
0.3
0.2
0.1

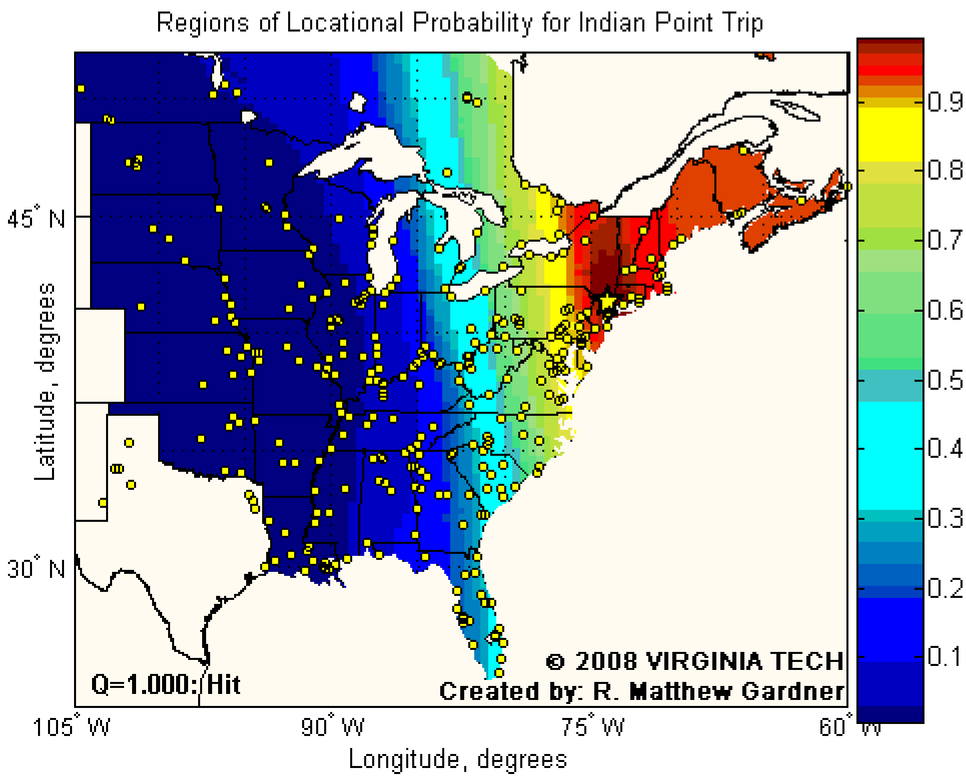
Regions of Locational Probability for Indian Point Trip
Latitude, degrees
45° N
30° N
105° W
90° W
75° W
60° W
Longitude, degrees
Q=1.000:/Hit
© 2008 VIRGINIA TECH
Created by: R. Matthew Gardner
0.9
0.8
0.7
0.6
0.5
0.4
0.3
0.2
0.1

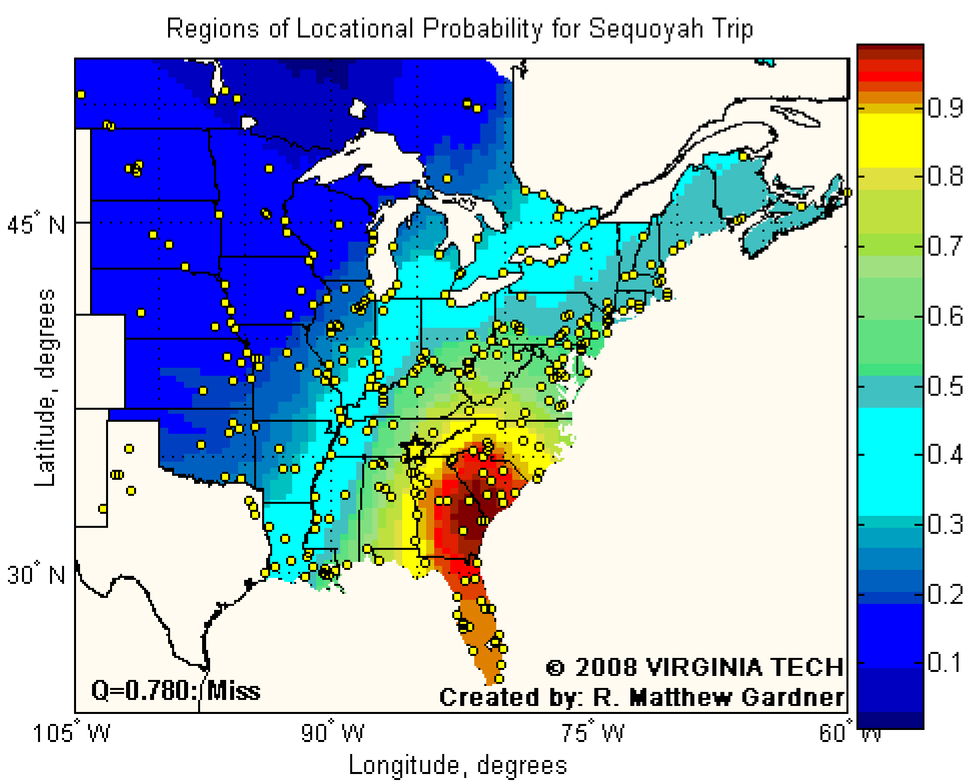
Regions of Locational Probability for Sequoyah Trip
Latitude, degrees
45° N
30° N
105° W
90° W
75° W
60° W
Longitude, degrees
Q=0.780:/Miss
© 2008 VIRGINIA TECH
Created by: R. Matthew Gardner
0.9
0.8
0.7
0.6
0.5
0.4
0.3
0.2
0.1

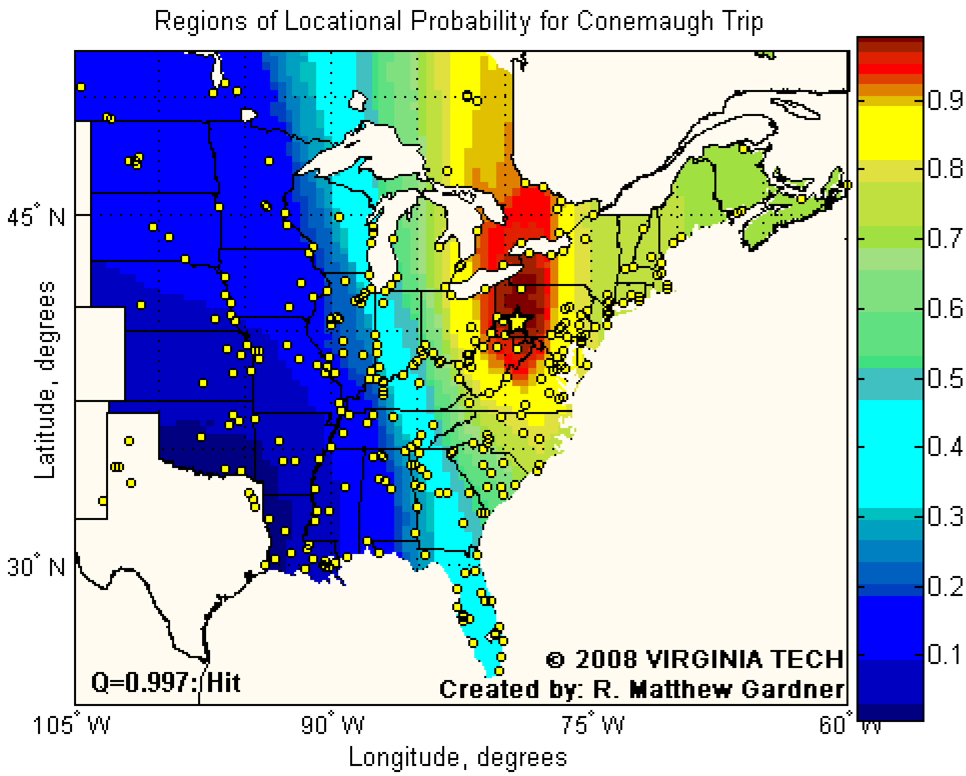
Regions of Locational Probability for Conemaugh Trip
45° N
30° N
Latitude, degrees
105° W
90° W
75° W
60° W
Longitude, degrees
Q=0.997: Hit
© 2008 VIRGINIA TECH
Created by: R. Matthew Gardner
0.9
0.8
0.7
0.6
0.5
0.4
0.3
0.2
0.1

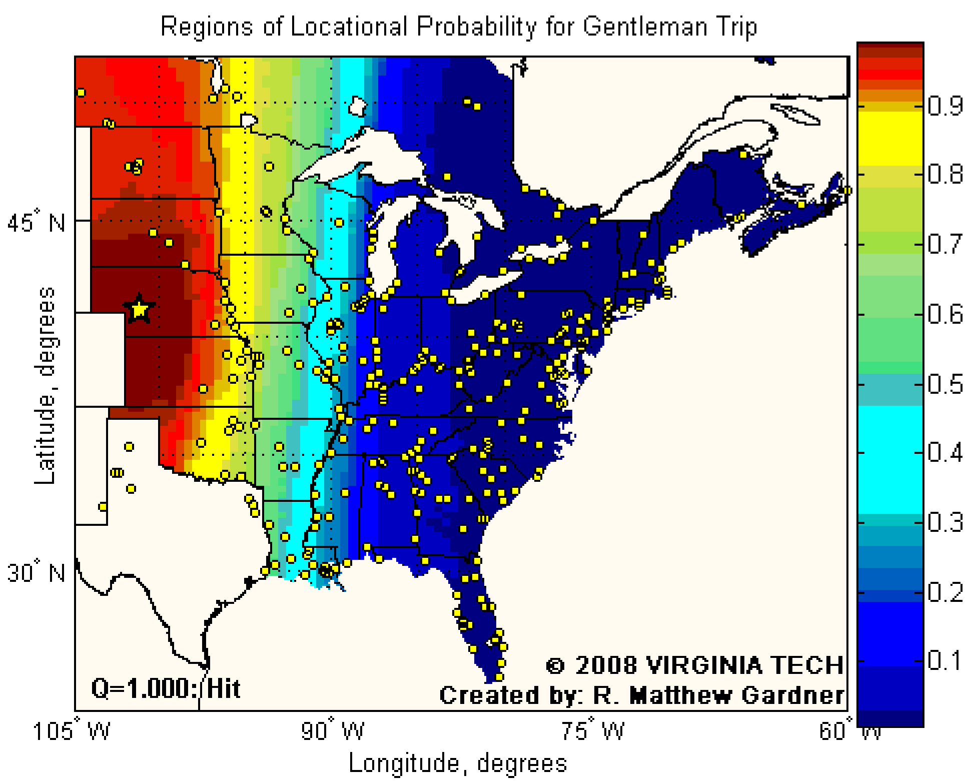
Regions of Locational Probability for Gentleman Trip
45° N
30° N
Latitude, degrees
105° W
90° W
75° W
60° W
Longitude, degrees
Q=1.000: Hit
© 2008 VIRGINIA TECH
Created by: R. Matthew Gardner
0.9
0.8
0.7
0.6
0.5
0.4
0.3
0.2
0.1

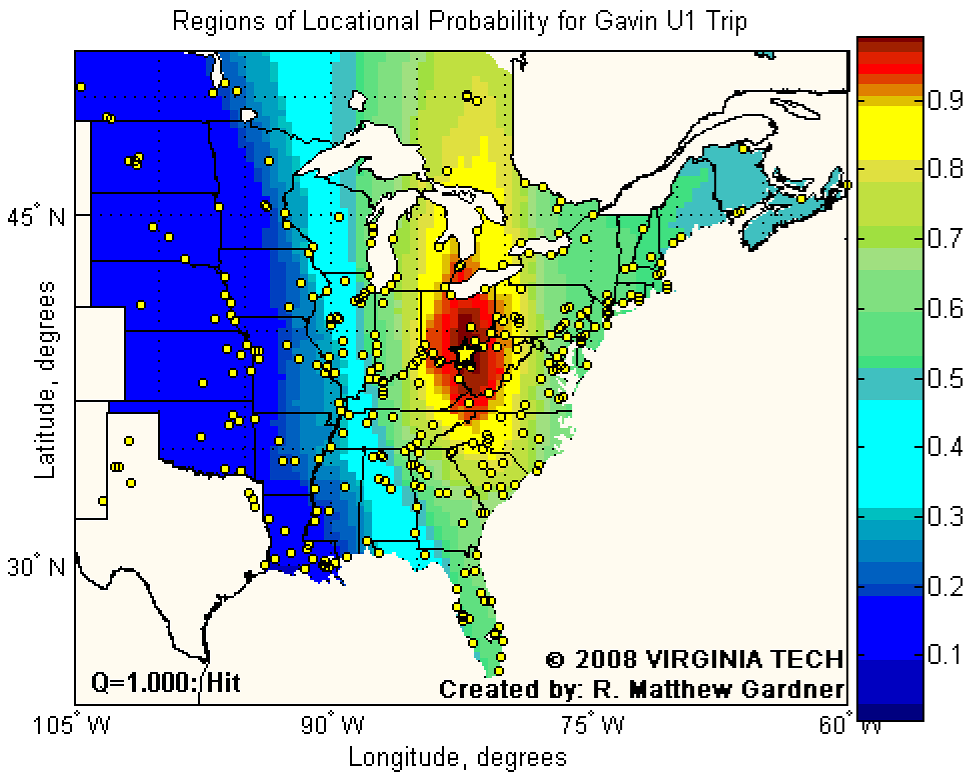
Regions of Locational Probability for Gavin U1 Trip
45° N
30° N
Latitude, degrees
105° W
90° W
75° W
60° W
Longitude, degrees
Q=1.000:/Hit
© 2008 VIRGINIA TECH
Created by: R. Matthew Gardner
0.9
0.8
0.7
0.6
0.5
0.4
0.3
0.2
0.1

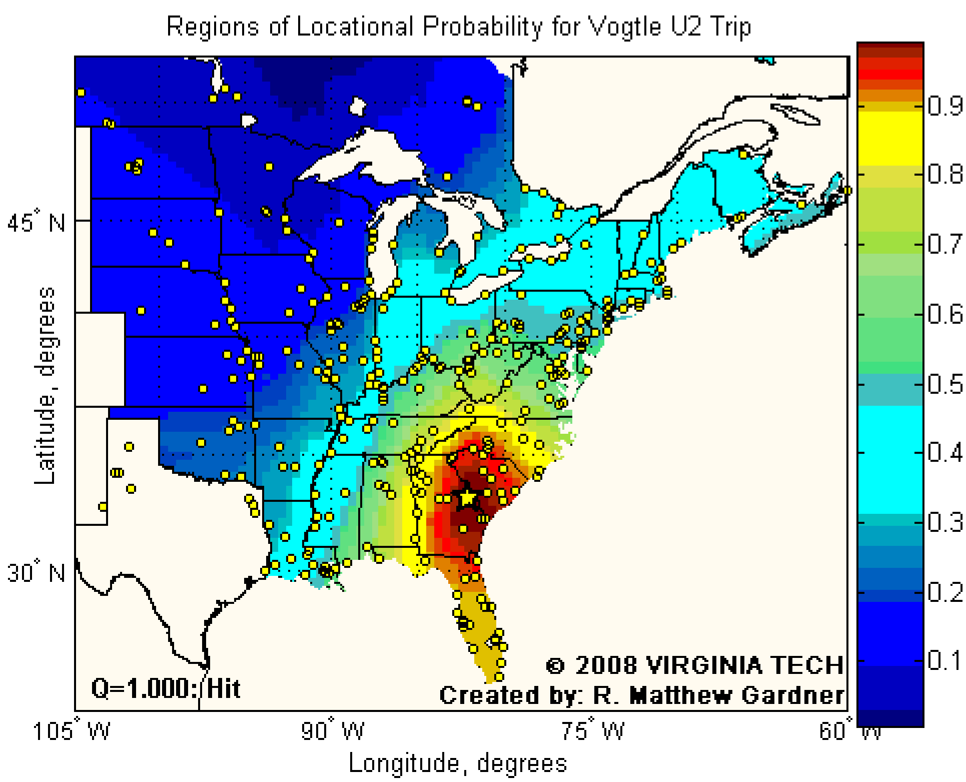
Regions of Locational Probability for Vogtle U2 Trip
45° N
30° N
Latitude, degrees
105° W
90° W
75° W
60° W
Longitude, degrees
Q=1.000:/Hit
© 2008 VIRGINIA TECH
Created by: R. Matthew Gardner
0.9
0.8
0.7
0.6
0.5
0.4
0.3
0.2
0.1

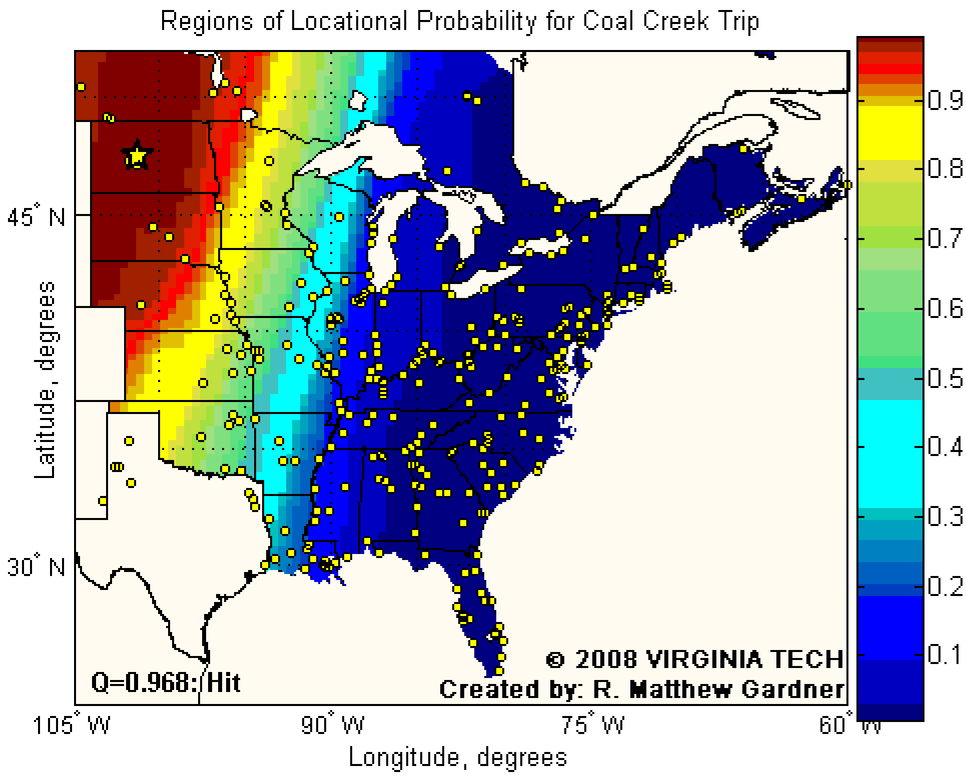
Regions of Locational Probability for Coal Creek Trip
45° N
30° N
Latitude, degrees
105° W
90° W
75° W
60° W
Longitude, degrees
Q=0.968: Hit
© 2008 VIRGINIA TECH
Created by: R. Matthew Gardner
0.9
0.8
0.7
0.6
0.5
0.4
0.3
0.2
0.1

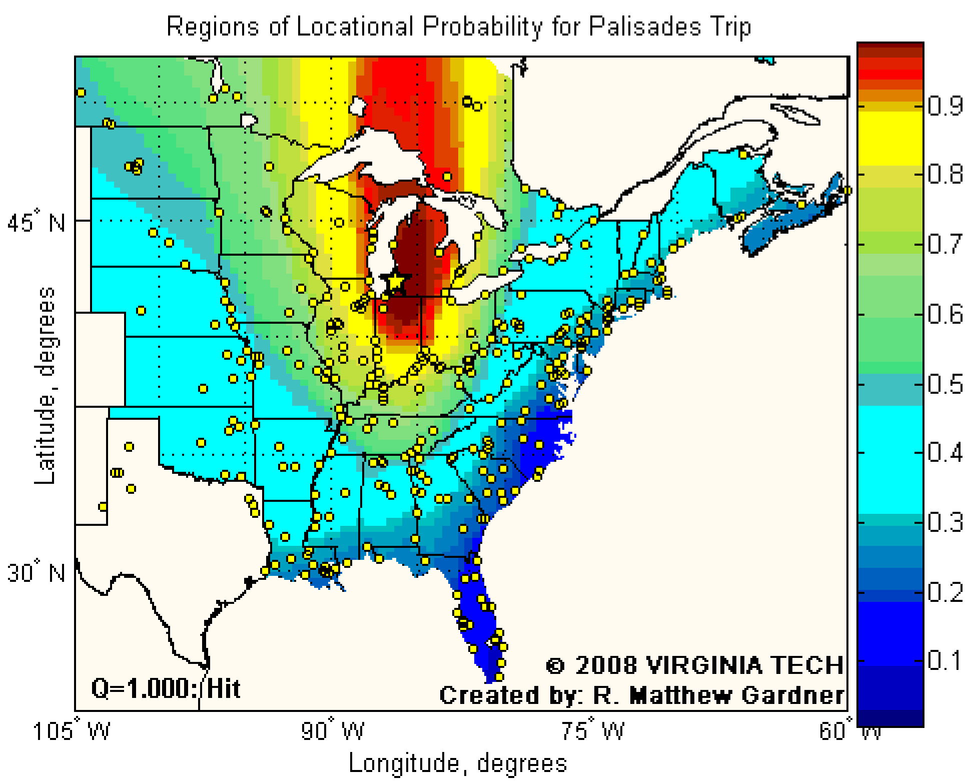
Regions of Locational Probability for Palisades Trip
45° N
30° N
Latitude, degrees
105° W
90° W
75° W
60° W
Longitude, degrees
Q=1.000: Hit
© 2008 VIRGINIA TECH
Created by: R. Matthew Gardner
0.9
0.8
0.7
0.6
0.5
0.4
0.3
0.2
0.1

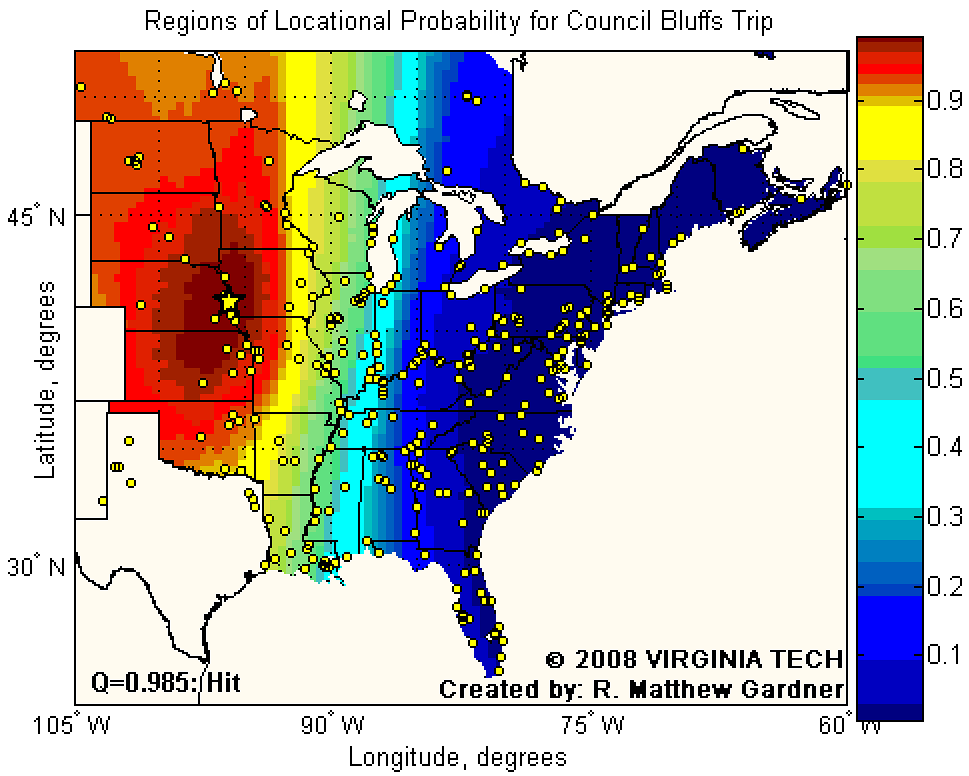
Regions of Locational Probability for Council Bluffs Trip
45° N
30° N
Latitude, degrees
105° W
90° W
75° W
60° W
Longitude, degrees
Q=0.985: Hit
© 2008 VIRGINIA TECH
Created by: R. Matthew Gardner
0.9
0.8
0.7
0.6
0.5
0.4
0.3
0.2
0.1

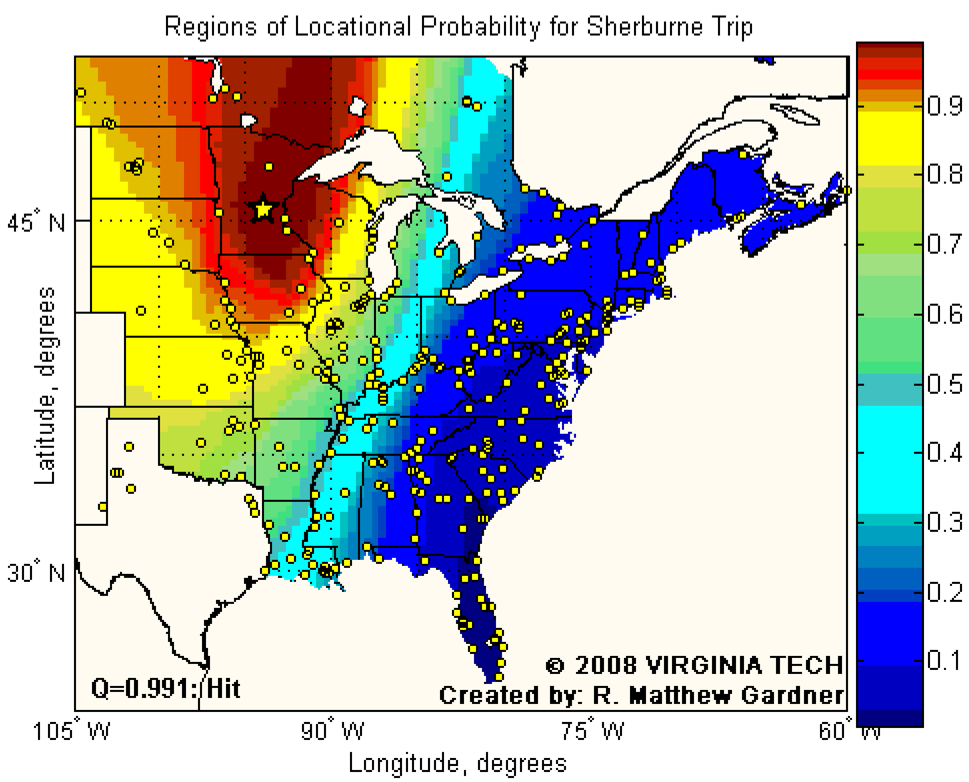
Regions of Locational Probability for Sherburne Trip
45° N
30° N
Latitude, degrees
105° W
90° W
75° W
60° W
Longitude, degrees
Q=0.991: Hit
© 2008 VIRGINIA TECH
Created by: R. Matthew Gardner
0.9
0.8
0.7
0.6
0.5
0.4
0.3
0.2
0.1

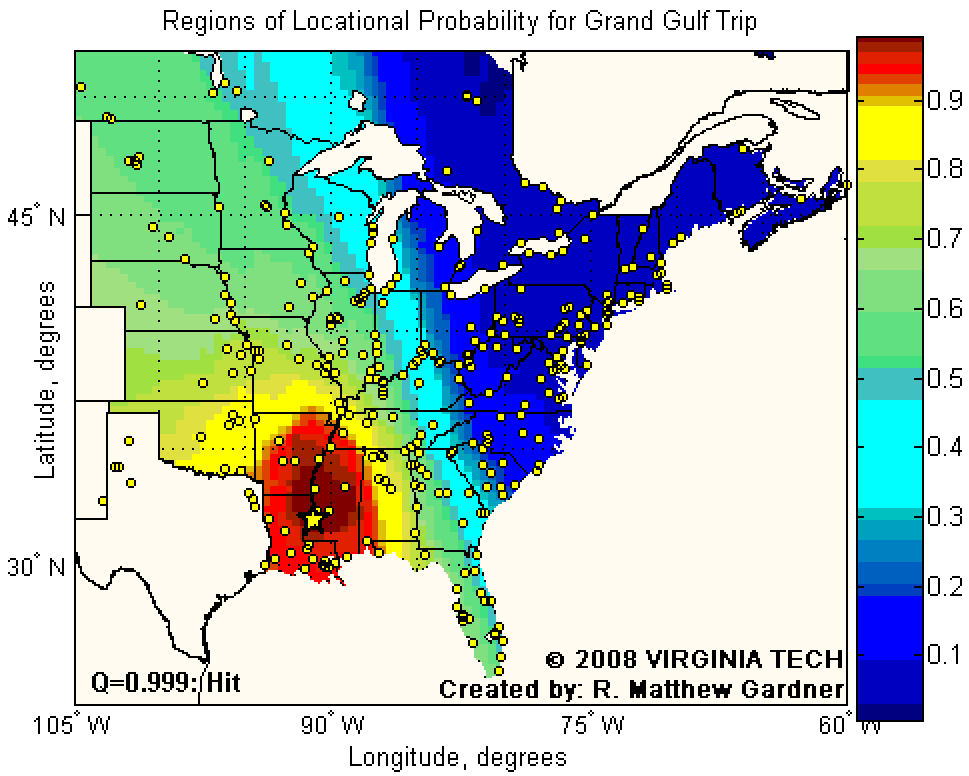
Regions of Locational Probability for Grand Gulf Trip
45° N
30° N
Latitude, degrees
105° W
90° W
75° W
60° W
Longitude, degrees
Q=0.999: Hit
© 2008 VIRGINIA TECH
Created by: R. Matthew Gardner
0.9
0.8
0.7
0.6
0.5
0.4
0.3
0.2
0.1

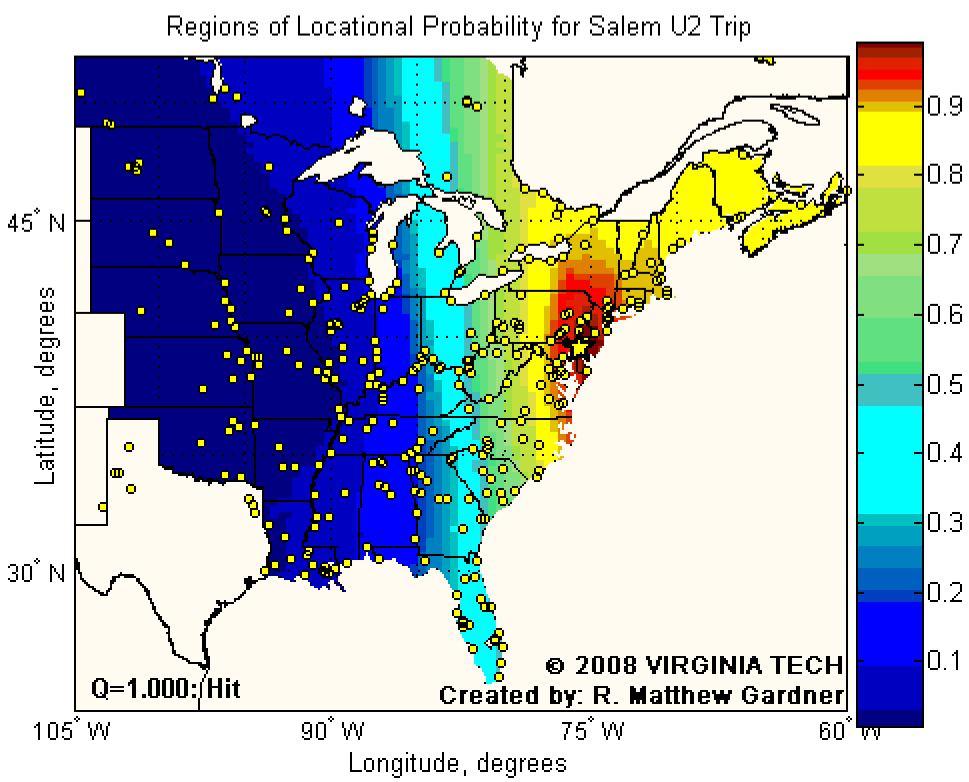
Regions of Locational Probability for Salem U2 Trip
45° N
30° N
Latitude, degrees
105° W
90° W
75° W
60° W
Longitude, degrees
Q=1.000: Hit
© 2008 VIRGINIA TECH
Created by: R. Matthew Gardner
0.9
0.8
0.7
0.6
0.5
0.4
0.3
0.2
0.1

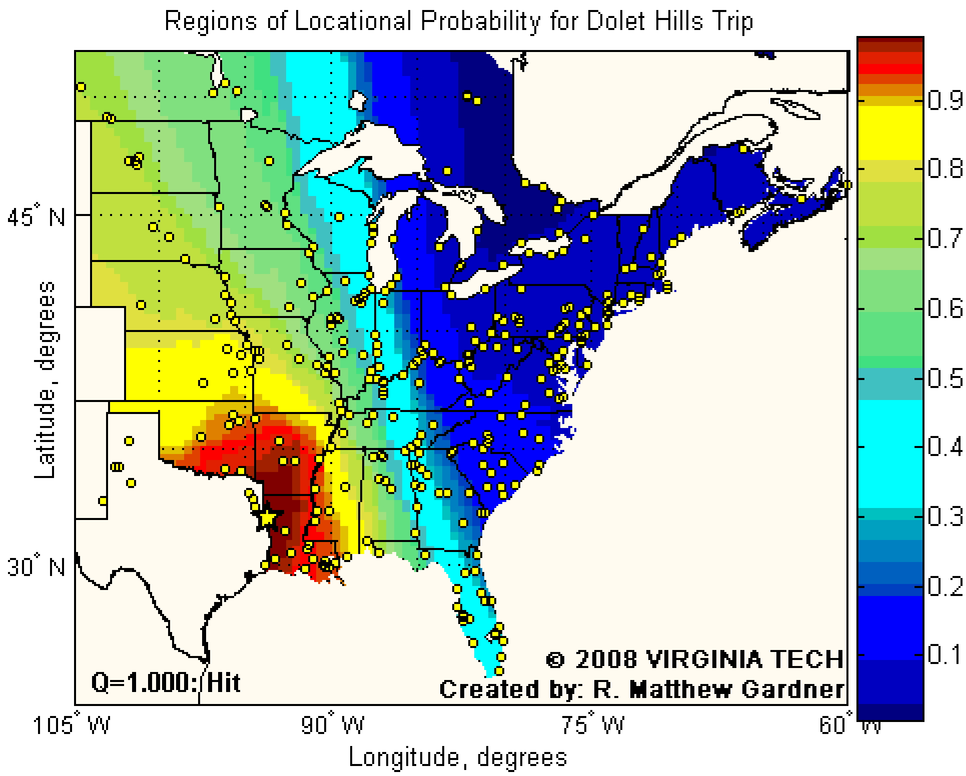
Regions of Locational Probability for Dolet Hills Trip
Latitude, degrees
45° N
30° N
105° W
90° W
75° W
60° W
Longitude, degrees
Q=1.000:/Hit
© 2008 VIRGINIA TECH
Created by: R. Matthew Gardner
0.9
0.8
0.7
0.6
0.5
0.4
0.3
0.2
0.1

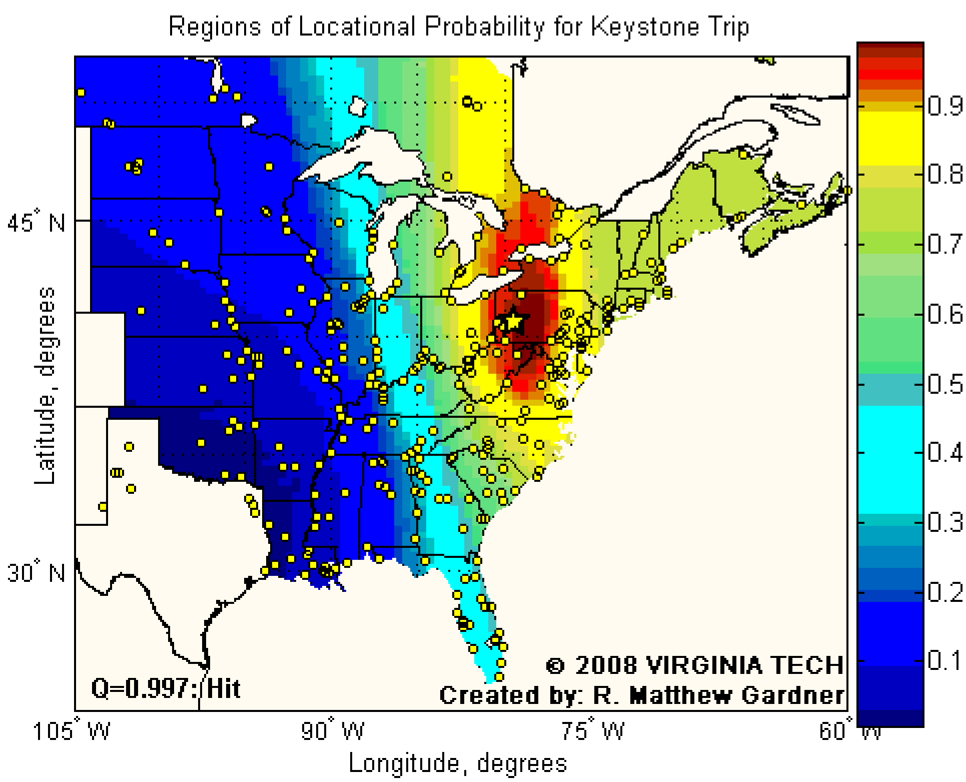
Regions of Locational Probability for Keystone Trip
Latitude, degrees
45° N
30° N
105° W
90° W
75° W
60° W
Longitude, degrees
Q=0.997:/Hit
© 2008 VIRGINIA TECH
Created by: R. Matthew Gardner
0.9
0.8
0.7
0.6
0.5
0.4
0.3
0.2
0.1

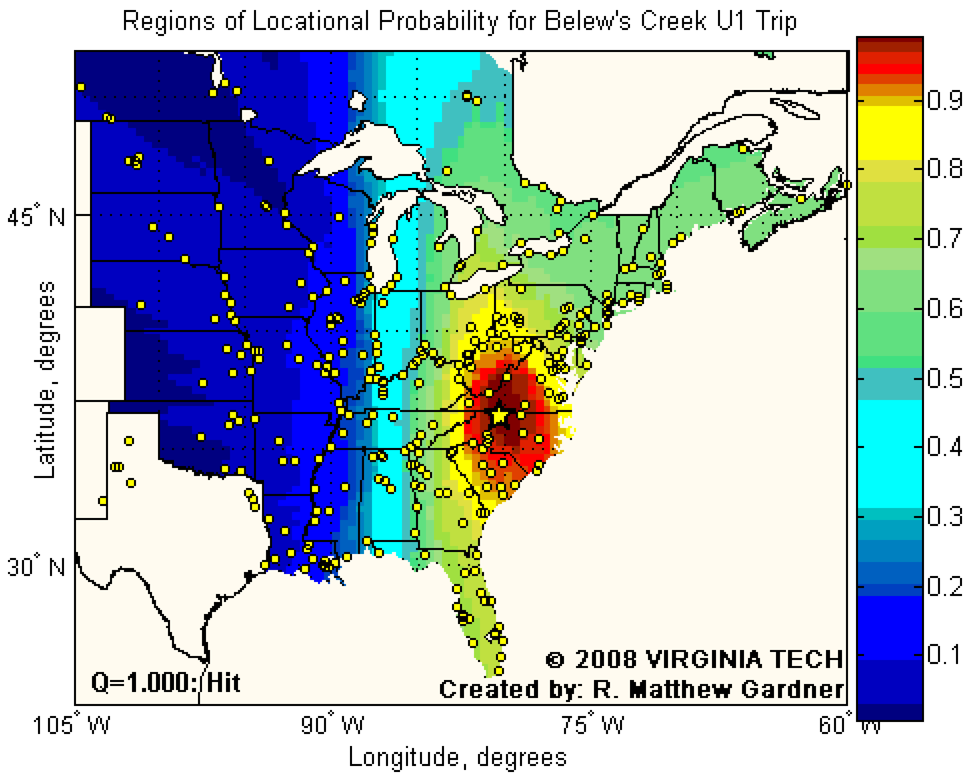
Regions of Locational Probability for Belew's Creek U1 Trip
45° N
30° N
Latitude, degrees
105° W
90° W
75° W
60° W
Longitude, degrees
Q=1.000: Hit
© 2008 VIRGINIA TECH
Created by: R. Matthew Gardner
0.9
0.8
0.7
0.6
0.5
0.4
0.3
0.2
0.1

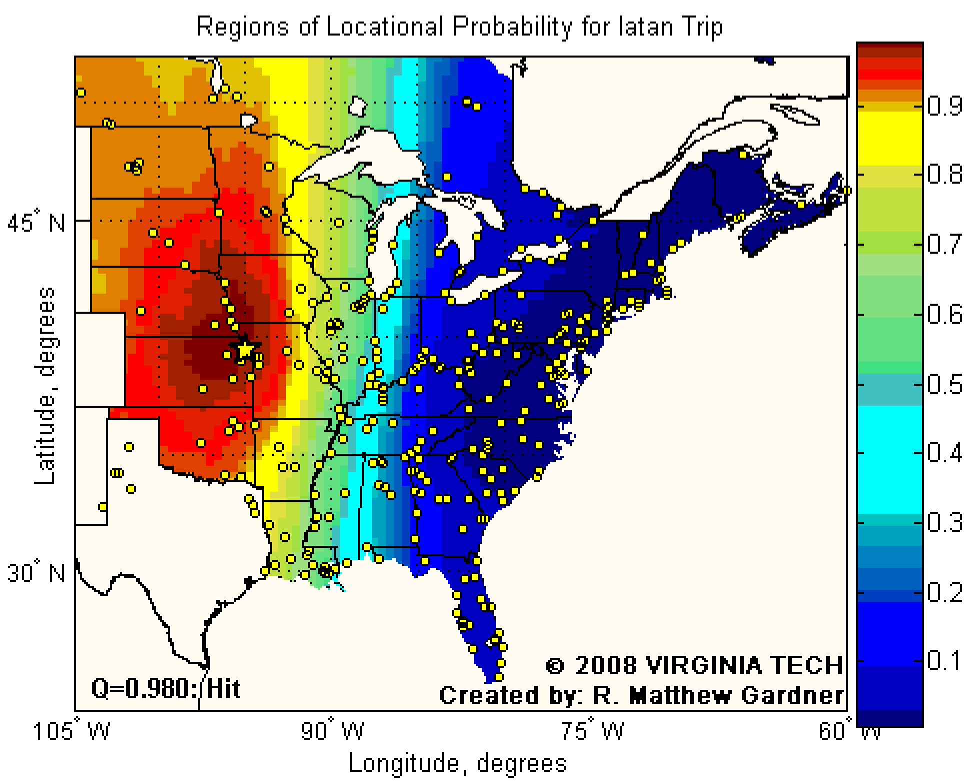
Regions of Locational Probability for Iatan Trip
45° N
30° N
Latitude, degrees
105° W
90° W
75° W
60° W
Longitude, degrees
Q=0.980: Hit
© 2008 VIRGINIA TECH
Created by: R. Matthew Gardner
0.9
0.8
0.7
0.6
0.5
0.4
0.3
0.2
0.1

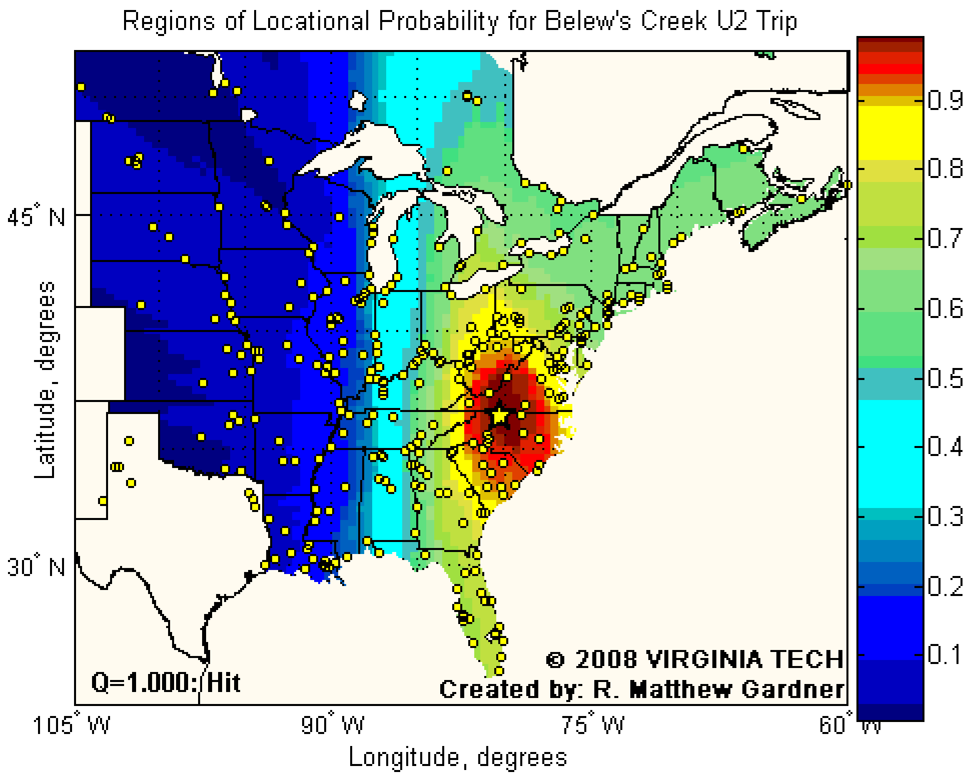
Regions of Locational Probability for Belew's Creek U2 Trip
45° N
30° N
Latitude, degrees
105° W
90° W
75° W
60° W
Longitude, degrees
Q=1.000: Hit
© 2008 VIRGINIA TECH
Created by: R. Matthew Gardner
0.9
0.8
0.7
0.6
0.5
0.4
0.3
0.2
0.1

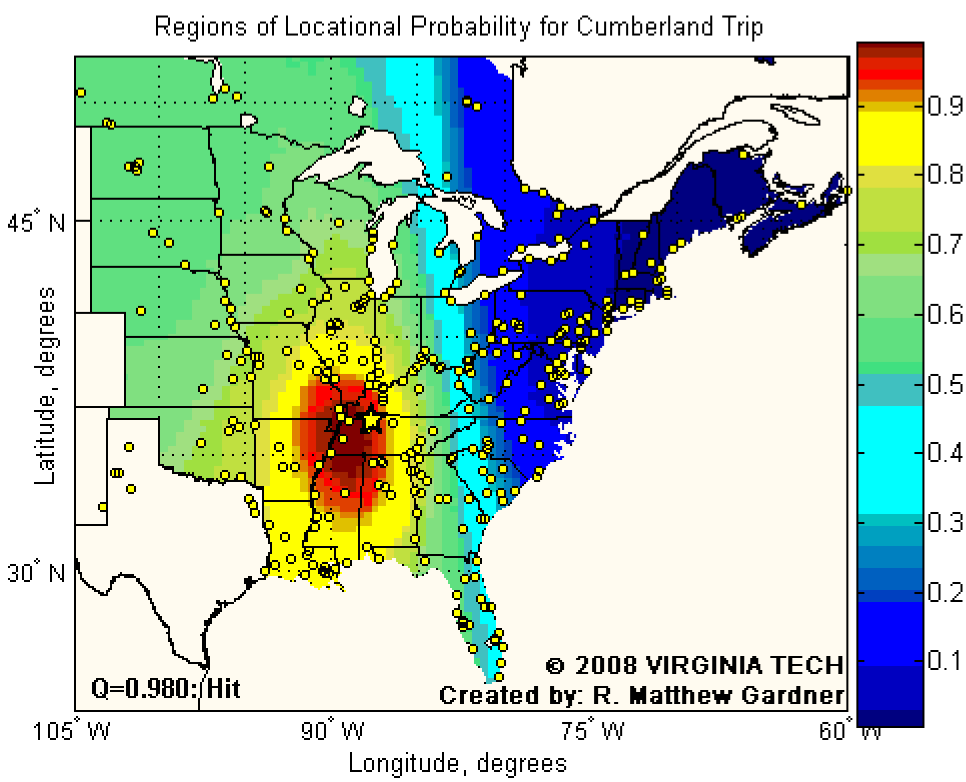
Regions of Locational Probability for Cumberland Trip
45° N
30° N
Latitude, degrees
105° W
90° W
75° W
60° W
Longitude, degrees
Q=0.980: Hit
© 2008 VIRGINIA TECH
Created by: R. Matthew Gardner
0.9
0.8
0.7
0.6
0.5
0.4
0.3
0.2
0.1

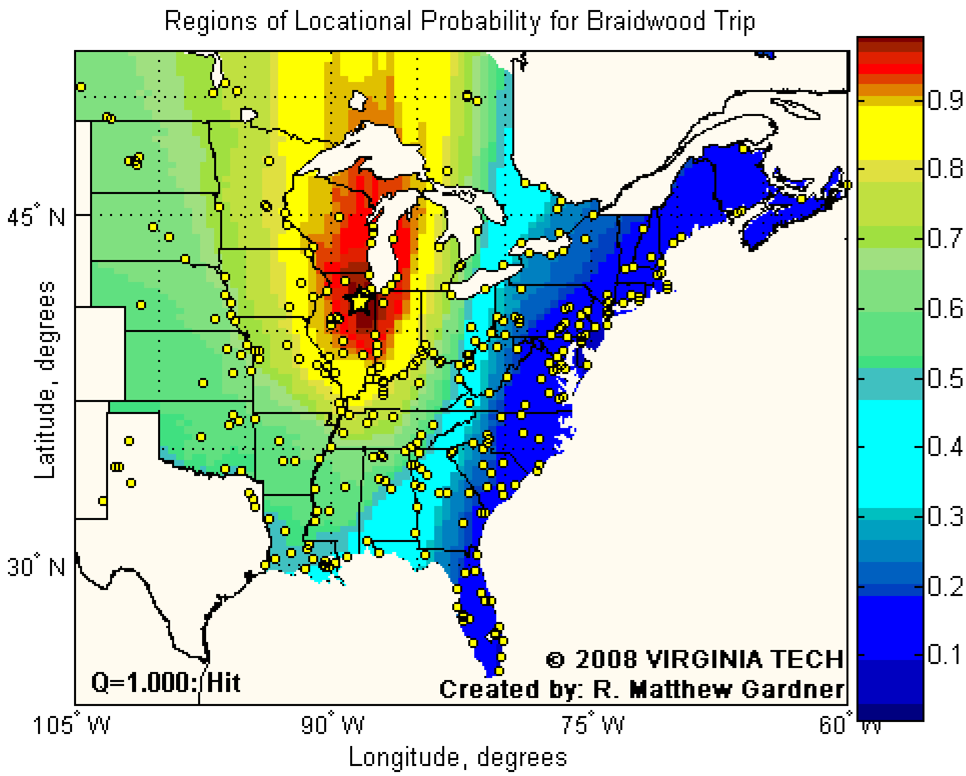
Regions of Locational Probability for Braidwood Trip
45° N
30° N
Latitude, degrees
105° W
90° W
75° W
60° W
Longitude, degrees
Q=1.000:/Hit
© 2008 VIRGINIA TECH
Created by: R. Matthew Gardner
0.9
0.8
0.7
0.6
0.5
0.4
0.3
0.2
0.1

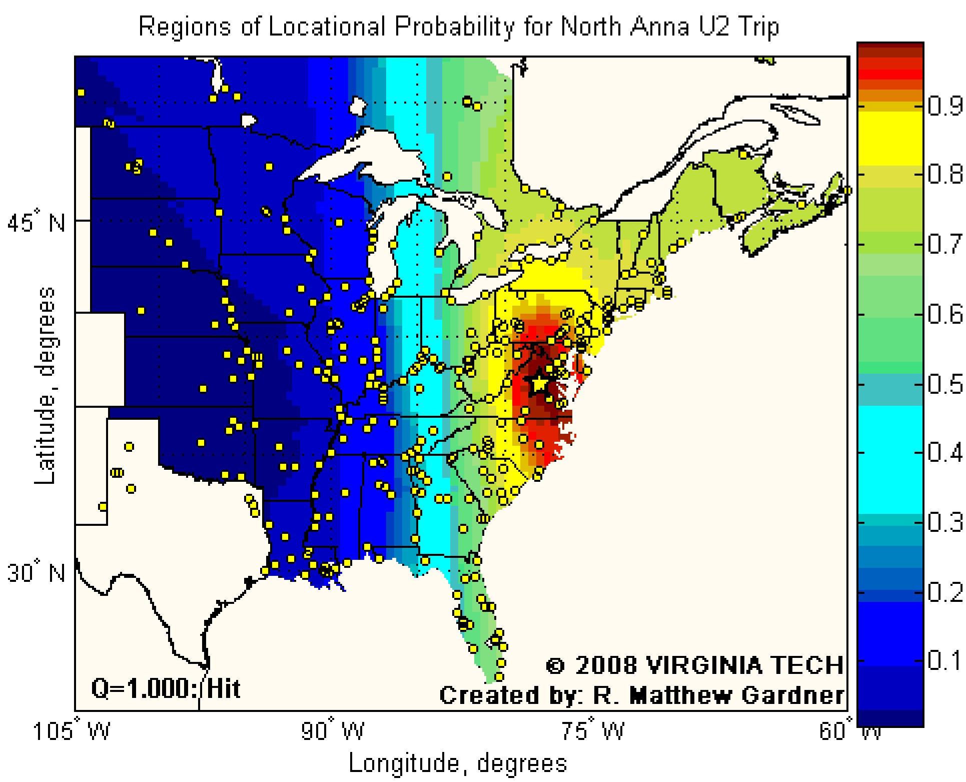
Regions of Locational Probability for North Anna U2 Trip
45° N
30° N
Latitude, degrees
105° W
90° W
75° W
60° W
Longitude, degrees
Q=1.000:/Hit
© 2008 VIRGINIA TECH
Created by: R. Matthew Gardner
0.9
0.8
0.7
0.6
0.5
0.4
0.3
0.2
0.1

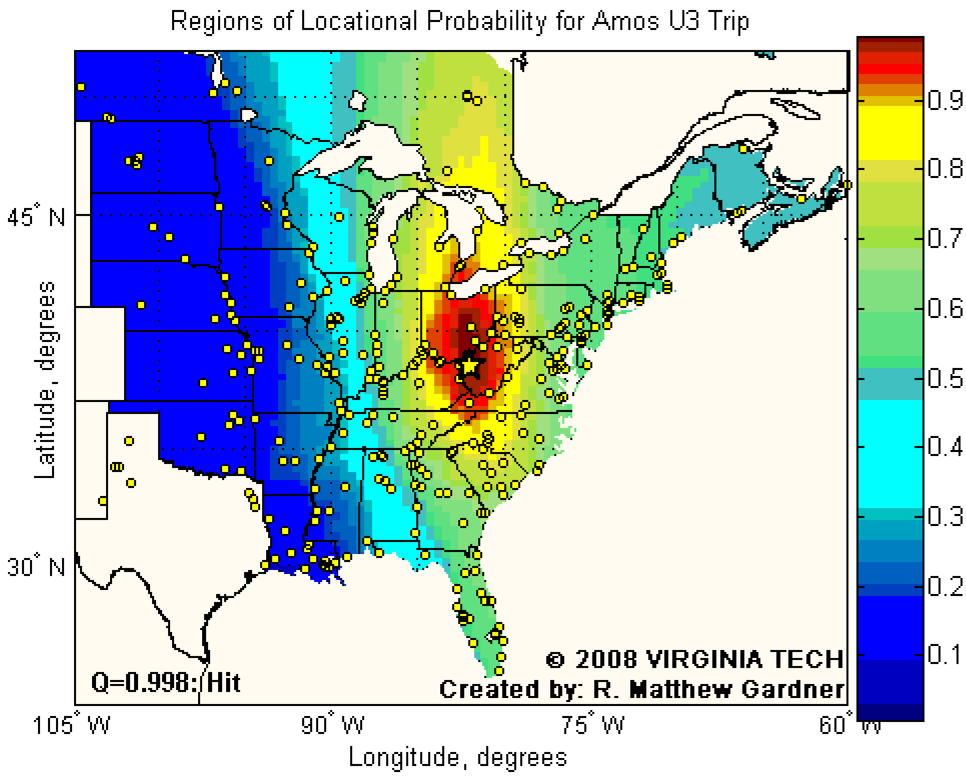
Regions of Locational Probability for Amos U3 Trip
45° N
30° N
Latitude, degrees
105° W
90° W
75° W
60° W
Longitude, degrees
Q=0.998: Hit
© 2008 VIRGINIA TECH
Created by: R. Matthew Gardner
0.9
0.8
0.7
0.6
0.5
0.4
0.3
0.2
0.1

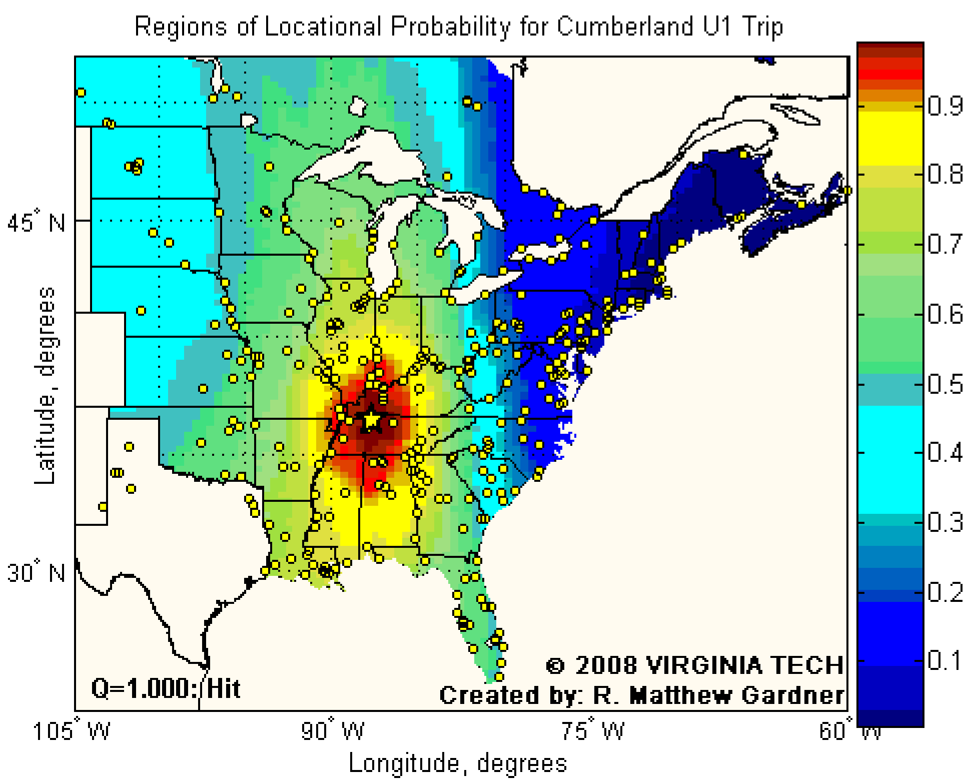
Regions of Locational Probability for Cumberland U1 Trip
45° N
30° N
Latitude, degrees
105° W
90° W
75° W
60° W
Longitude, degrees
Q=1.000: Hit
© 2008 VIRGINIA TECH
Created by: R. Matthew Gardner
0.9
0.8
0.7
0.6
0.5
0.4
0.3
0.2
0.1

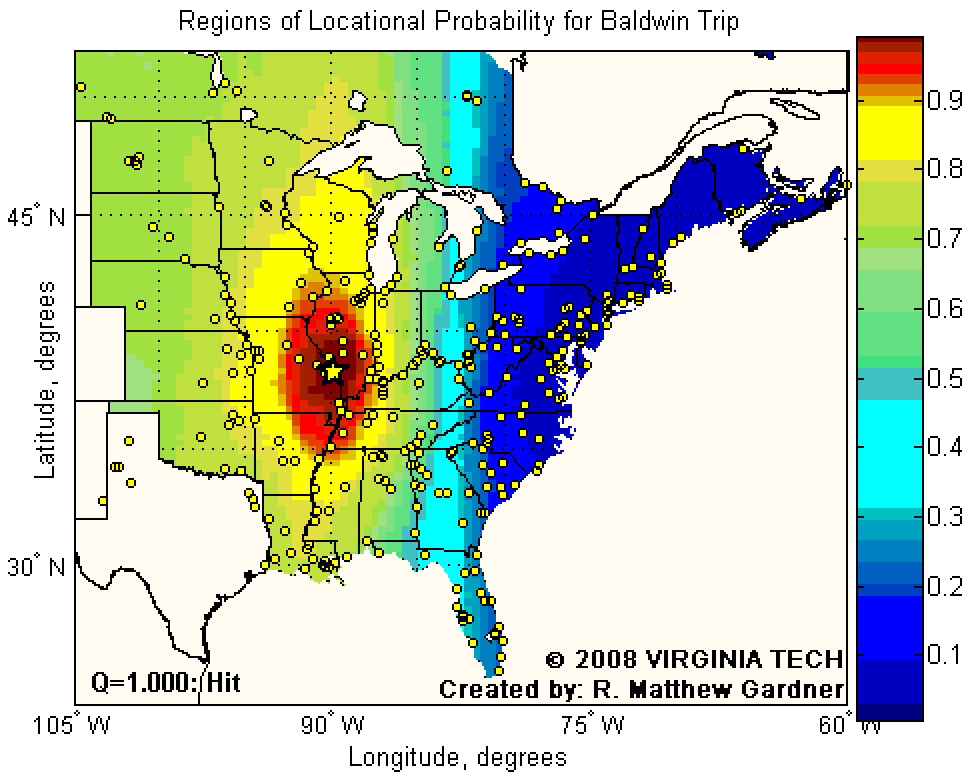
Regions of Locational Probability for Baldwin Trip
Latitude, degrees
45° N
30° N
105° W
90° W
75° W
60° W
Longitude, degrees
Q=1.000: Hit
© 2008 VIRGINIA TECH
Created by: R. Matthew Gardner
0.9
0.8
0.7
0.6
0.5
0.4
0.3
0.2
0.1

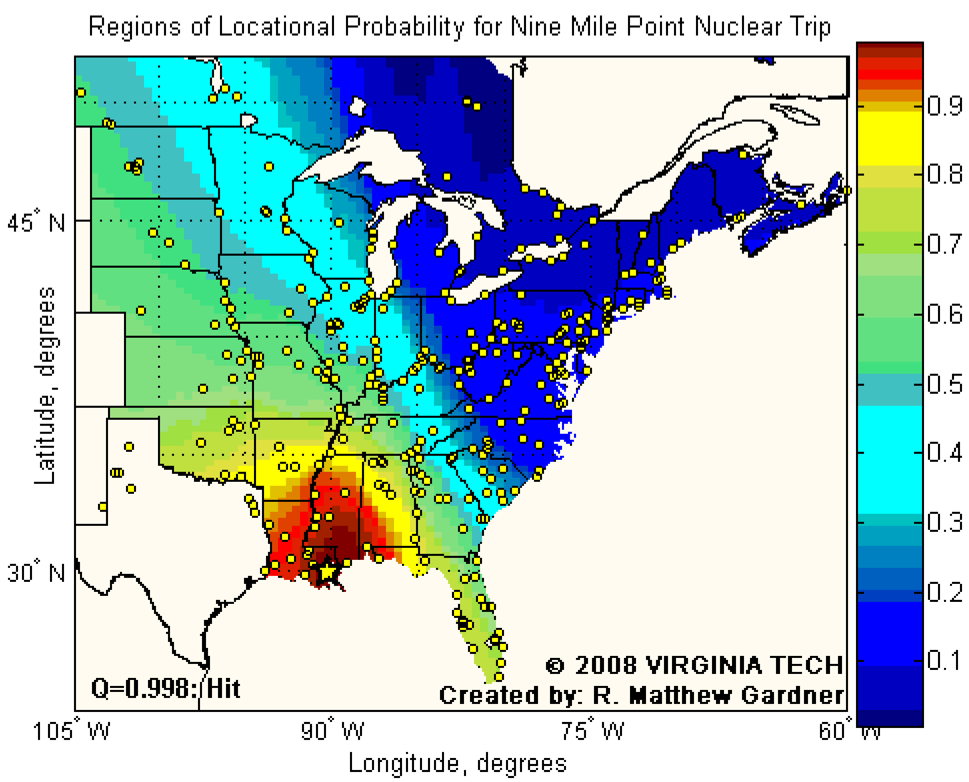
Regions of Locational Probability for Nine Mile Point Nuclear Trip
Latitude, degrees
45° N
30° N
105° W
90° W
75° W
60° W
Longitude, degrees
Q=0.998: Hit
© 2008 VIRGINIA TECH
Created by: R. Matthew Gardner
0.9
0.8
0.7
0.6
0.5
0.4
0.3
0.2
0.1

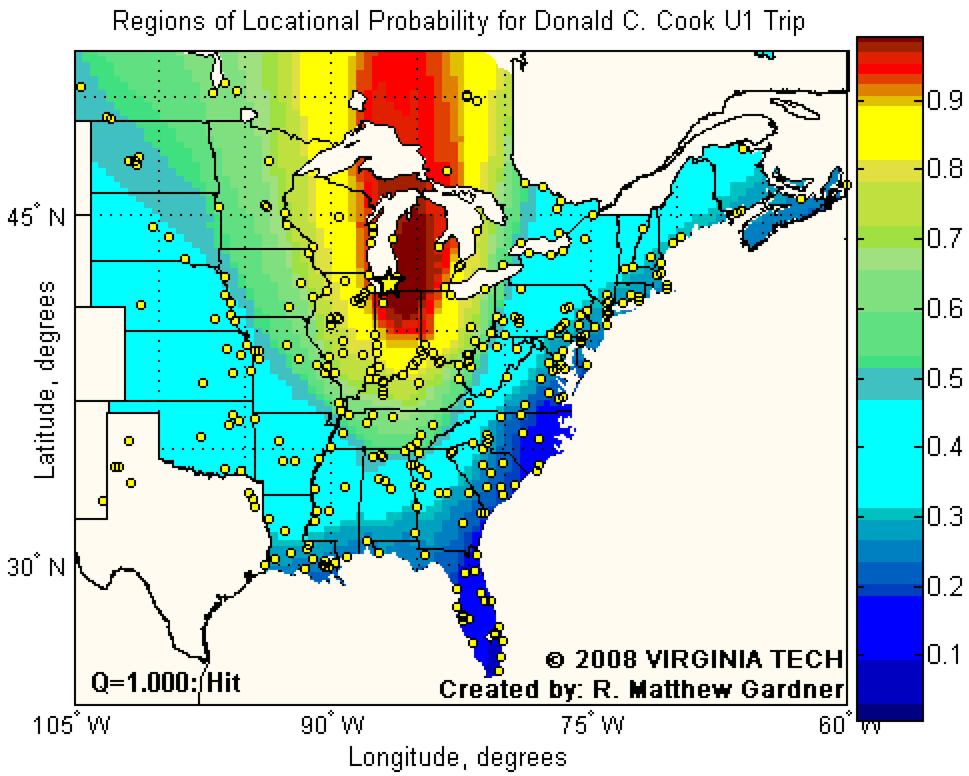
Regions of Locational Probability for Donald C. Cook U1 Trip
45° N
30° N
Latitude, degrees
105° W
90° W
75° W
60° W
Longitude, degrees
Q=1.000: Hit
© 2008 VIRGINIA TECH
Created by: R. Matthew Gardner
0.9
0.8
0.7
0.6
0.5
0.4
0.3
0.2
0.1

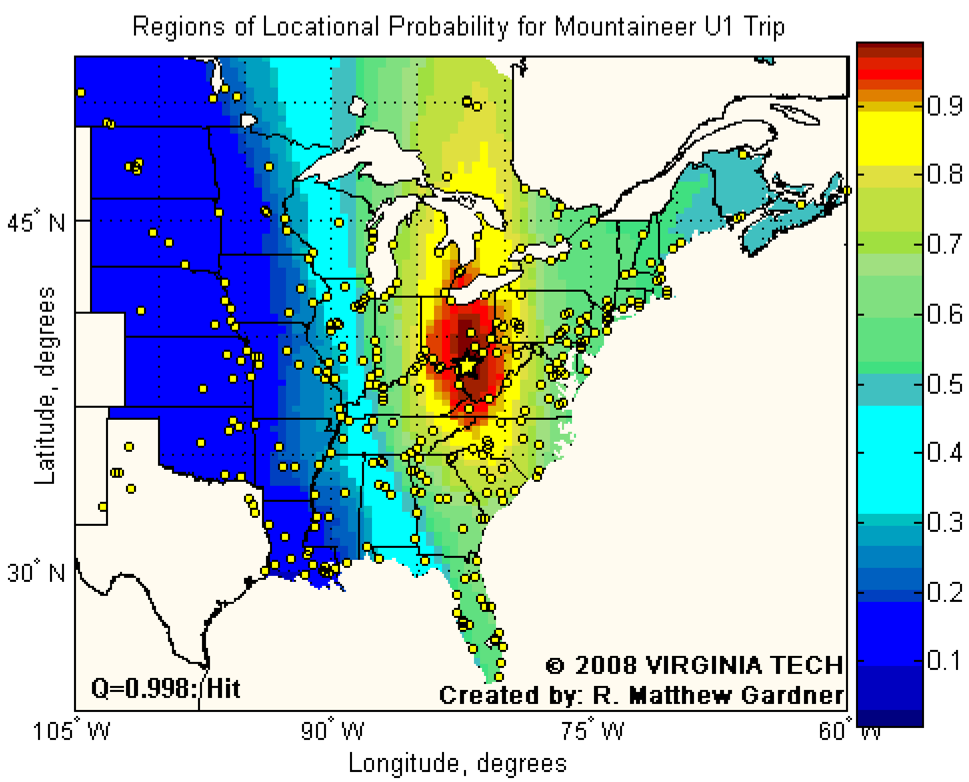
Regions of Locational Probability for Mountaineer U1 Trip
45° N
30° N
Latitude, degrees
105° W
90° W
75° W
60° W
Longitude, degrees
Q=0.998: Hit
© 2008 VIRGINIA TECH
Created by: R. Matthew Gardner
0.9
0.8
0.7
0.6
0.5
0.4
0.3
0.2
0.1

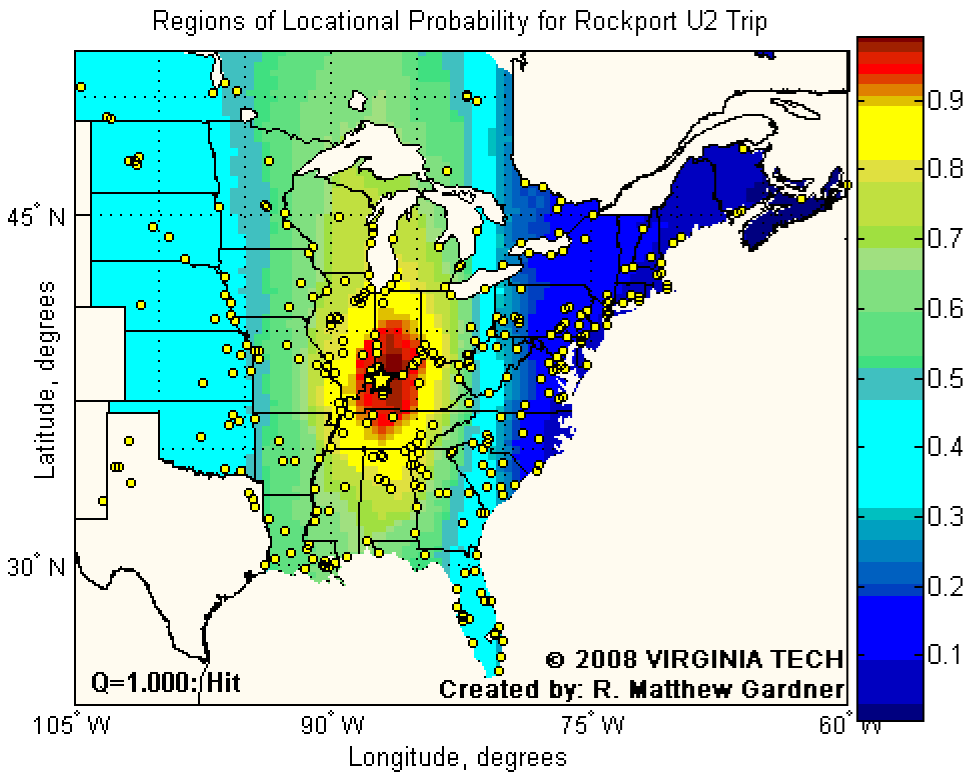
Regions of Locational Probability for Rockport U2 Trip
45° N
30° N
Latitude, degrees
105° W
90° W
75° W
60° W
Longitude, degrees
Q=1.000: Hit
© 2008 VIRGINIA TECH
Created by: R. Matthew Gardner
0.9
0.8
0.7
0.6
0.5
0.4
0.3
0.2
0.1

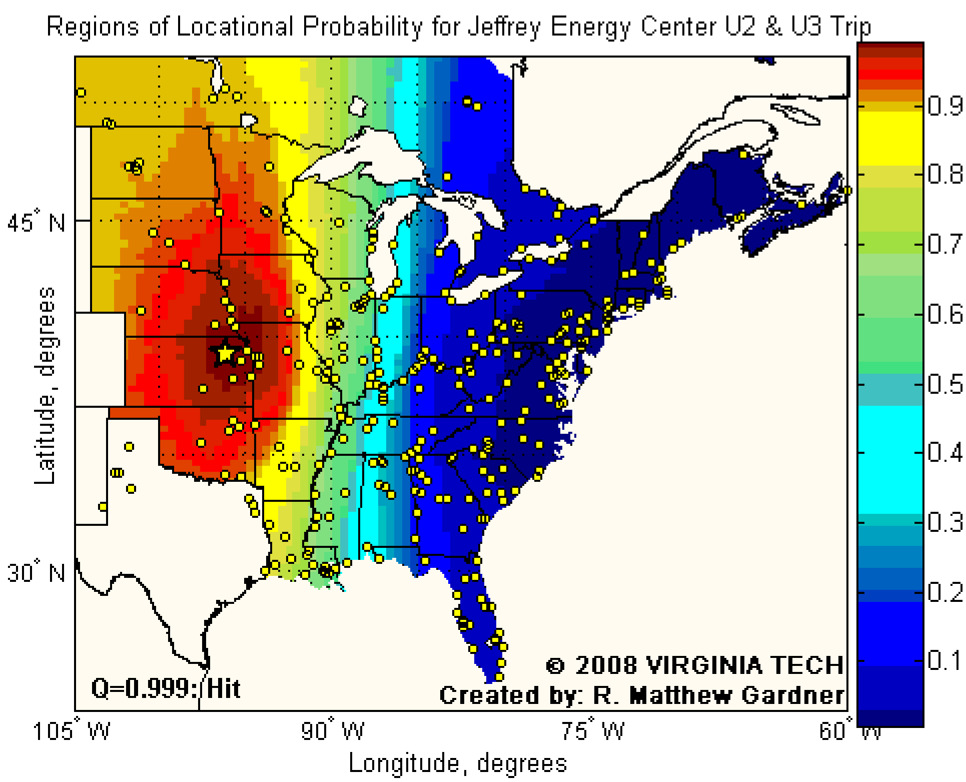
Regions of Locational Probability for Jeffrey Energy Center U2 & U3 Trip
45° N
30° N
Latitude, degrees
105° W
90° W
75° W
60° W
Longitude, degrees
Q=0.999: Hit
© 2008 VIRGINIA TECH
Created by: R. Matthew Gardner
0.9
0.8
0.7
0.6
0.5
0.4
0.3
0.2
0.1

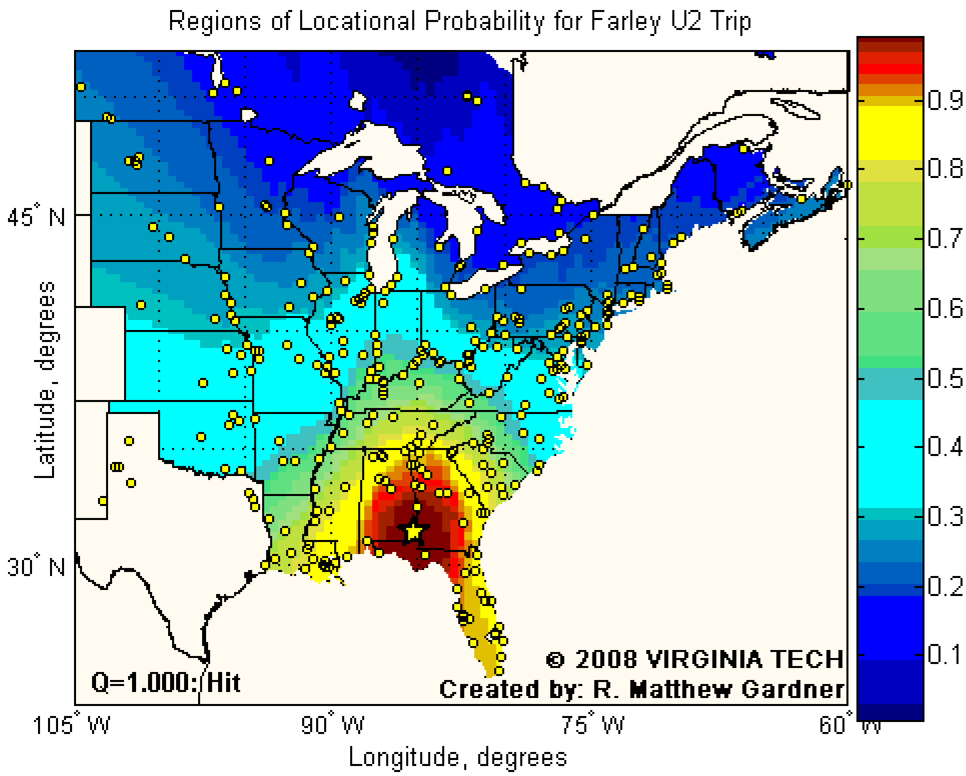
Regions of Locational Probability for Farley U2 Trip
Latitude, degrees
Longitude, degrees
45° N
30° N
105° W
90° W
75° W
60° W
0.1
0.2
0.3
0.4
0.5
0.6
0.7
0.8
0.9
Q=1.000: Hit
© 2008 VIRGINIA TECH
Created by: R. Matthew Gardner

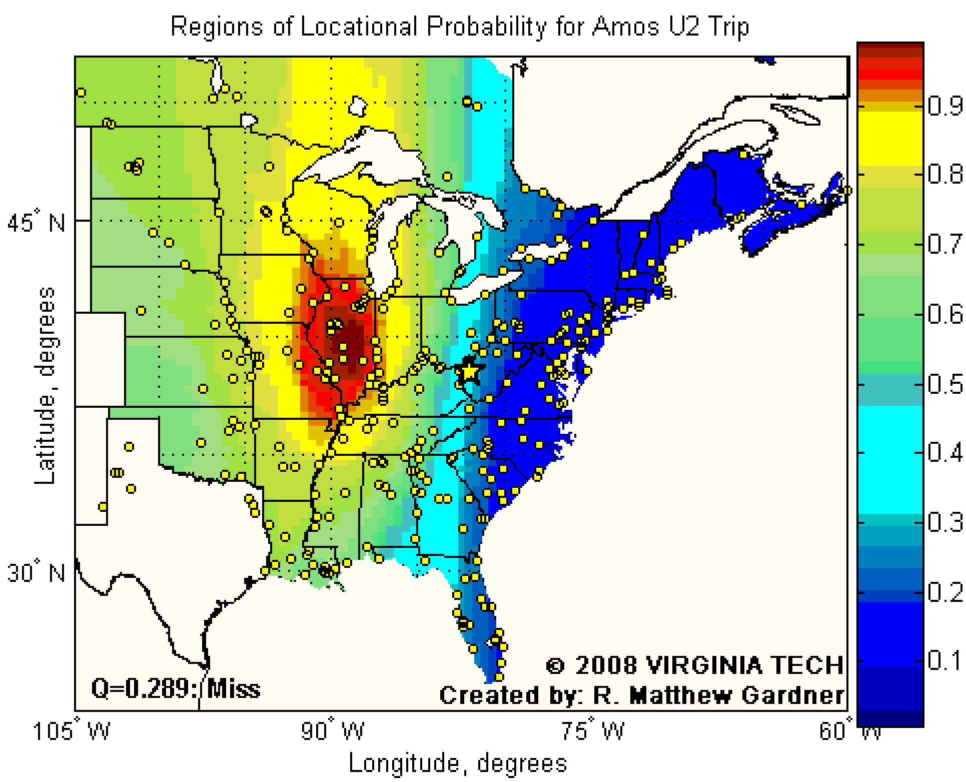
Regions of Locational Probability for Amos U2 Trip
Latitude, degrees
Longitude, degrees
45° N
30° N
105° W
90° W
75° W
60° W
0.1
0.2
0.3
0.4
0.5
0.6
0.7
0.8
0.9
Q=0.289: Miss
© 2008 VIRGINIA TECH
Created by: R. Matthew Gardner

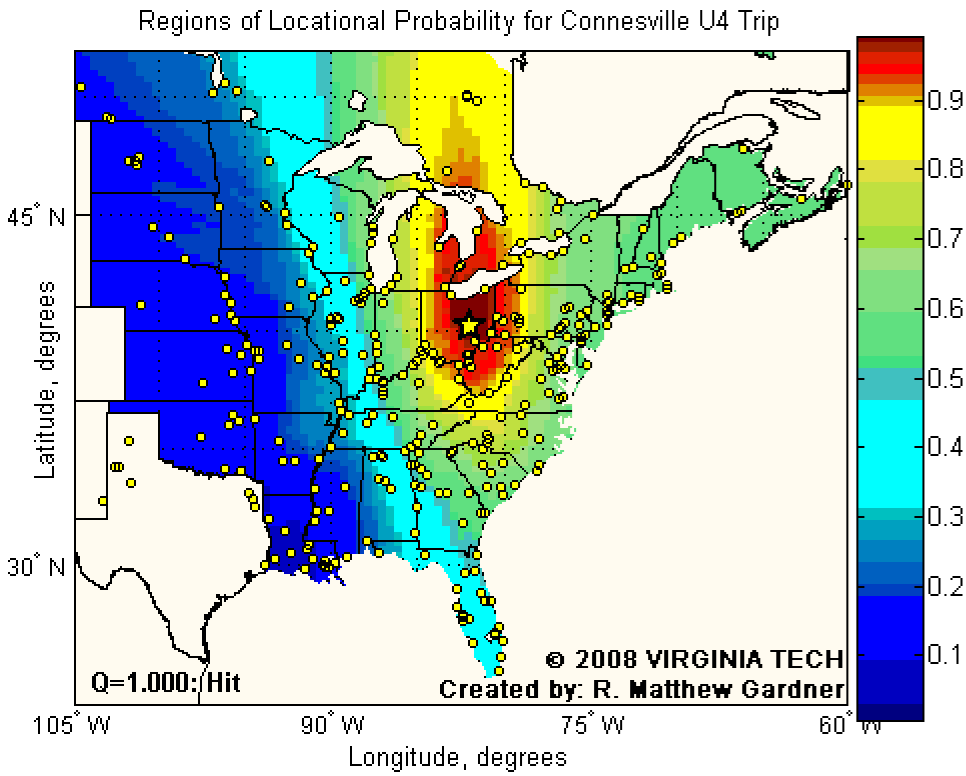
Regions of Locational Probability for Connesville U4 Trip
Latitude, degrees
Longitude, degrees
45° N
30° N
105° W
90° W
75° W
60° W
0.9
0.8
0.7
0.6
0.5
0.4
0.3
0.2
0.1
© 2008 VIRGINIA TECH
Created by: R. Matthew Gardner
Q=1.000: Hit

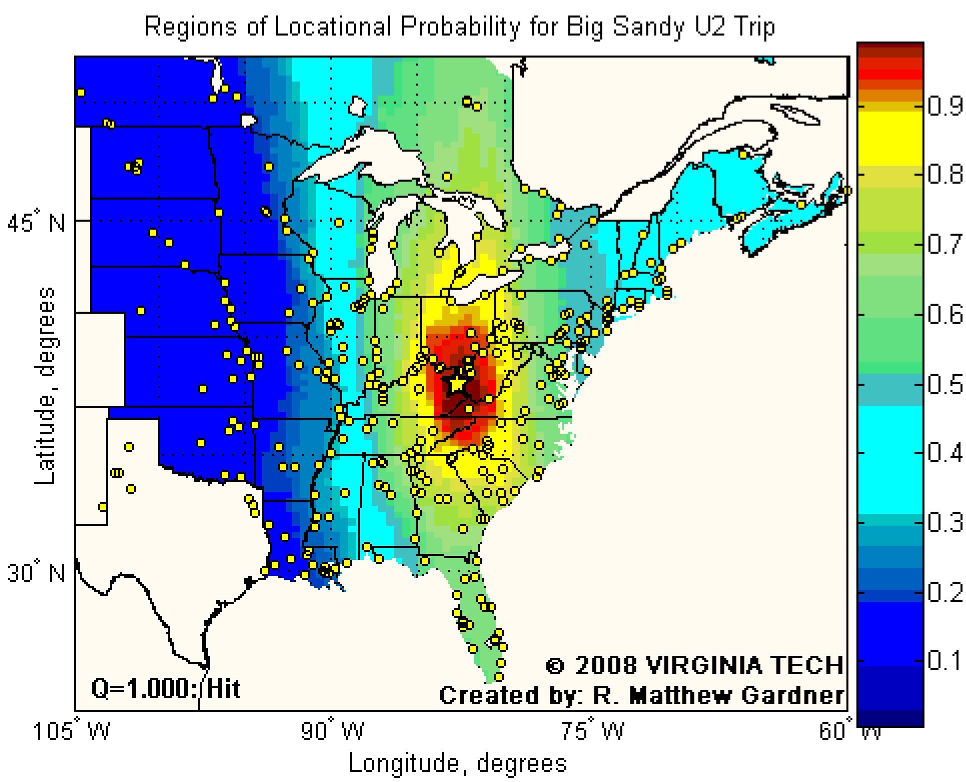
Regions of Locational Probability for Big Sandy U2 Trip
Latitude, degrees
Longitude, degrees
45° N
30° N
105° W
90° W
75° W
60° W
0.9
0.8
0.7
0.6
0.5
0.4
0.3
0.2
0.1
© 2008 VIRGINIA TECH
Created by: R. Matthew Gardner
Q=1.000: Hit

Appendix XVI: Full Half-Plane Event Location Based Upon Full Simulation of EI Angles

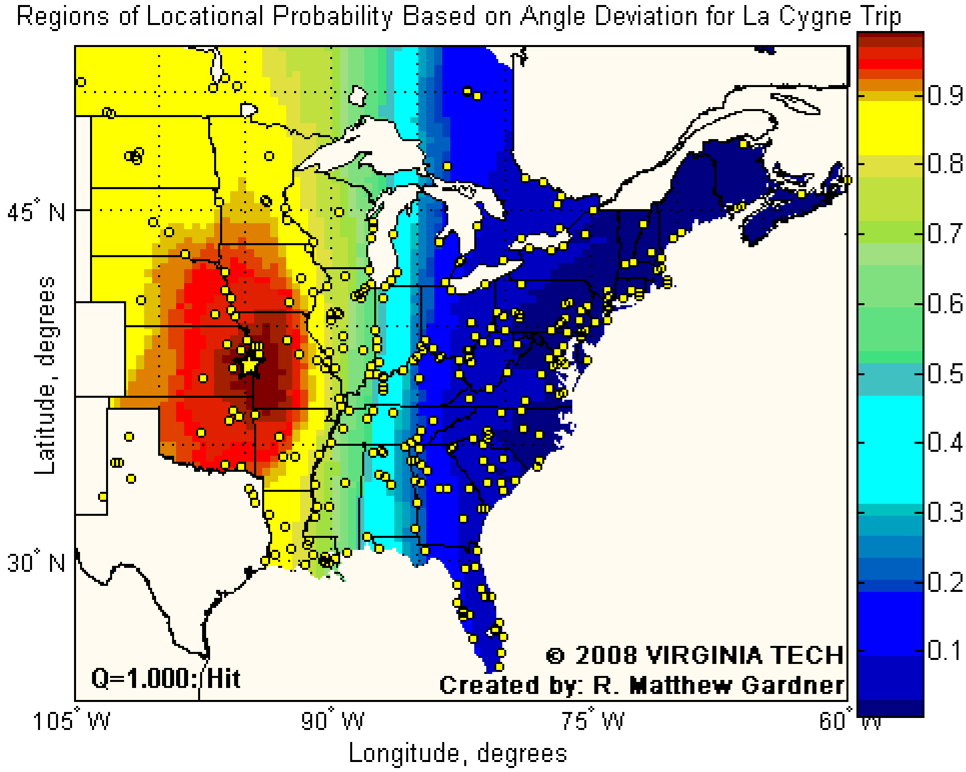

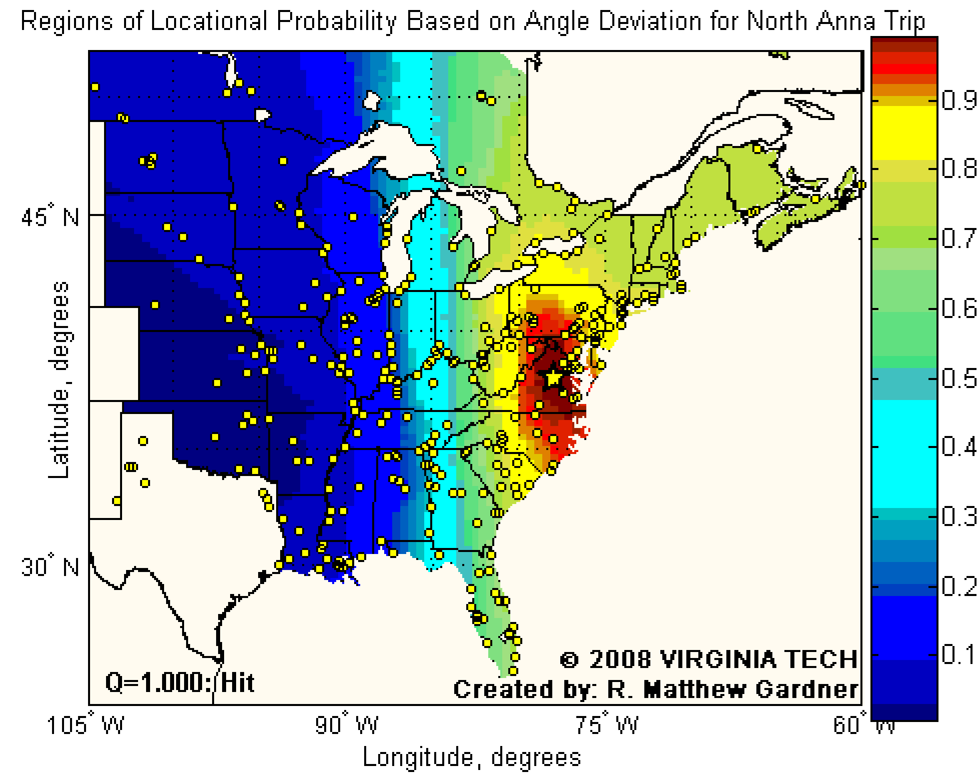
Regions of Locational Probability Based on Angle Deviation for North Anna Trip
Latitude, degrees
Longitude, degrees
45° N
30° N
105° W
90° W
75° W
60° W
0.9
0.8
0.7
0.6
0.5
0.4
0.3
0.2
0.1
Q=1.000:/Hit
© 2008 VIRGINIA TECH
Created by: R. Matthew Gardner

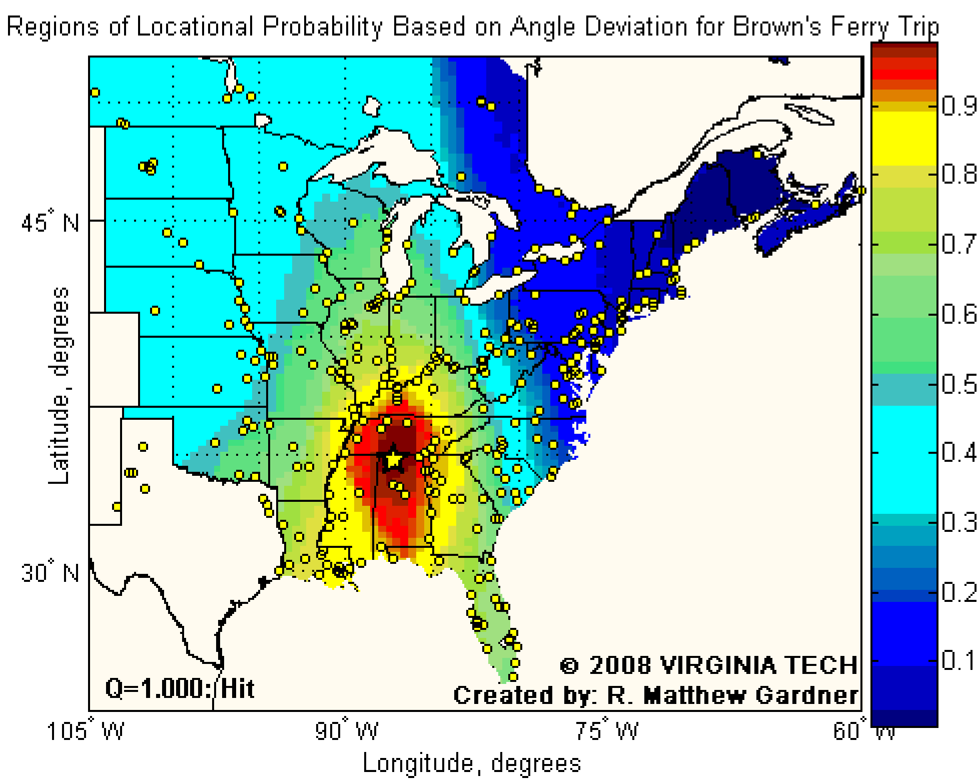
Regions of Locational Probability Based on Angle Deviation for Brown's Ferry Trip
Latitude, degrees
Longitude, degrees
45° N
30° N
105° W
90° W
75° W
60° W
0.9
0.8
0.7
0.6
0.5
0.4
0.3
0.2
0.1
Q=1.000:/Hit
© 2008 VIRGINIA TECH
Created by: R. Matthew Gardner

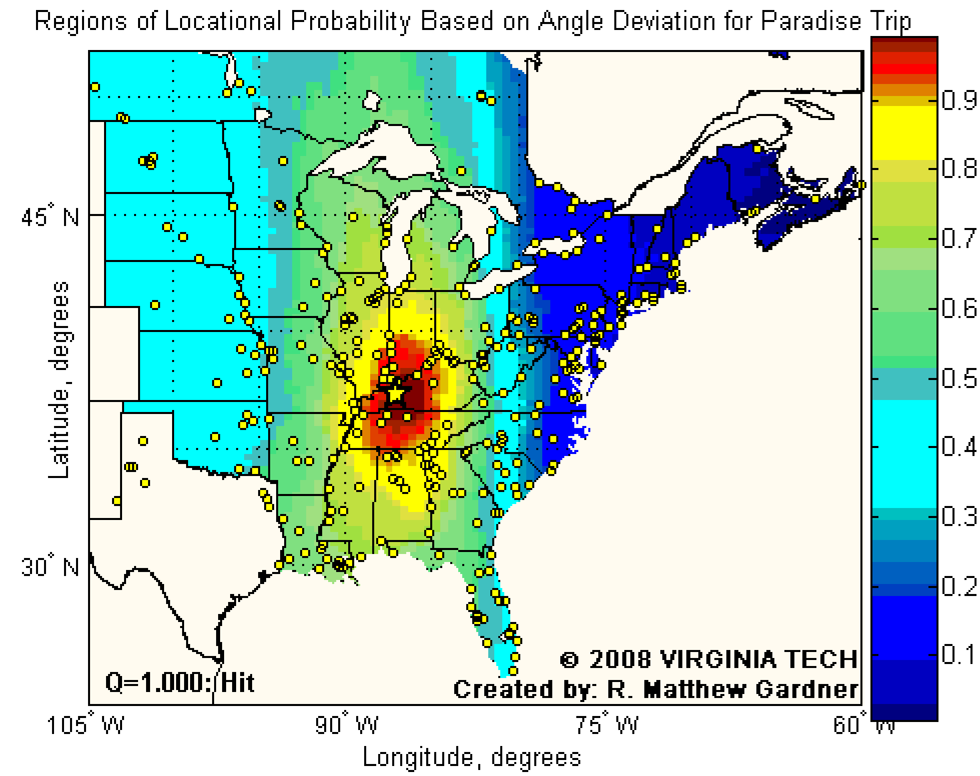
Regions of Locational Probability Based on Angle Deviation for Paradise Trip
Latitude, degrees
Longitude, degrees
45° N
30° N
105° W
90° W
75° W
60° W
0.9
0.8
0.7
0.6
0.5
0.4
0.3
0.2
0.1
Q=1.000:/Hit
© 2008 VIRGINIA TECH
Created by: R. Matthew Gardner

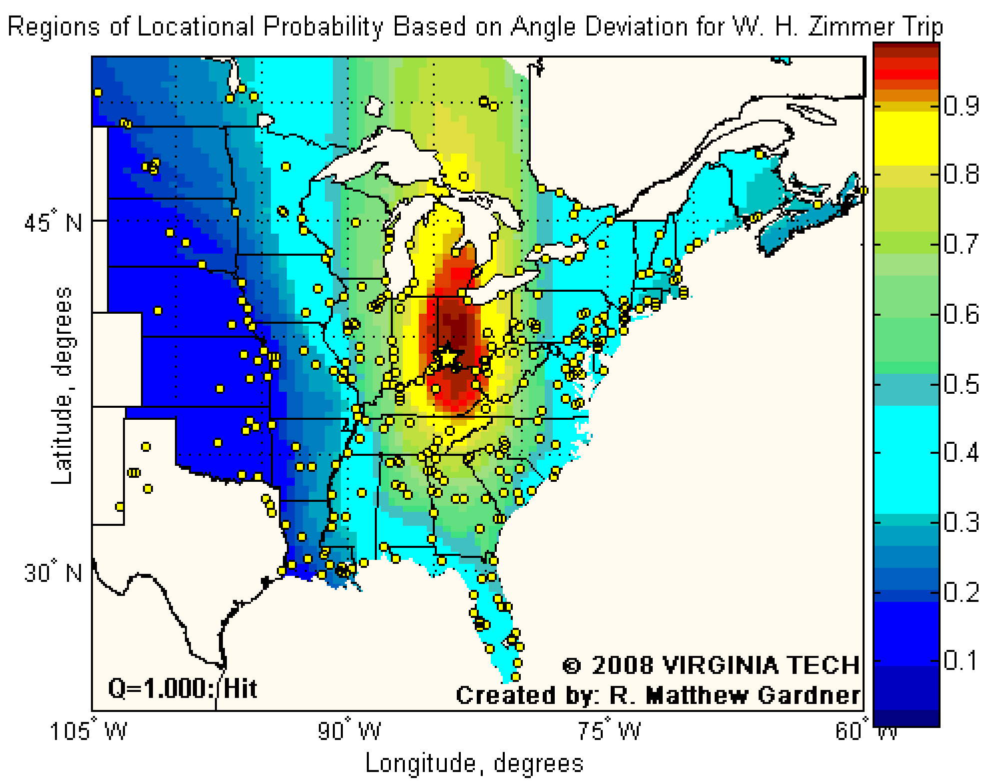
Regions of Locational Probability Based on Angle Deviation for W. H. Zimmer Trip
Latitude, degrees
Longitude, degrees
45° N
30° N
105° W
90° W
75° W
60° W
0.9
0.8
0.7
0.6
0.5
0.4
0.3
0.2
0.1
Q=1.000:/Hit
© 2008 VIRGINIA TECH
Created by: R. Matthew Gardner

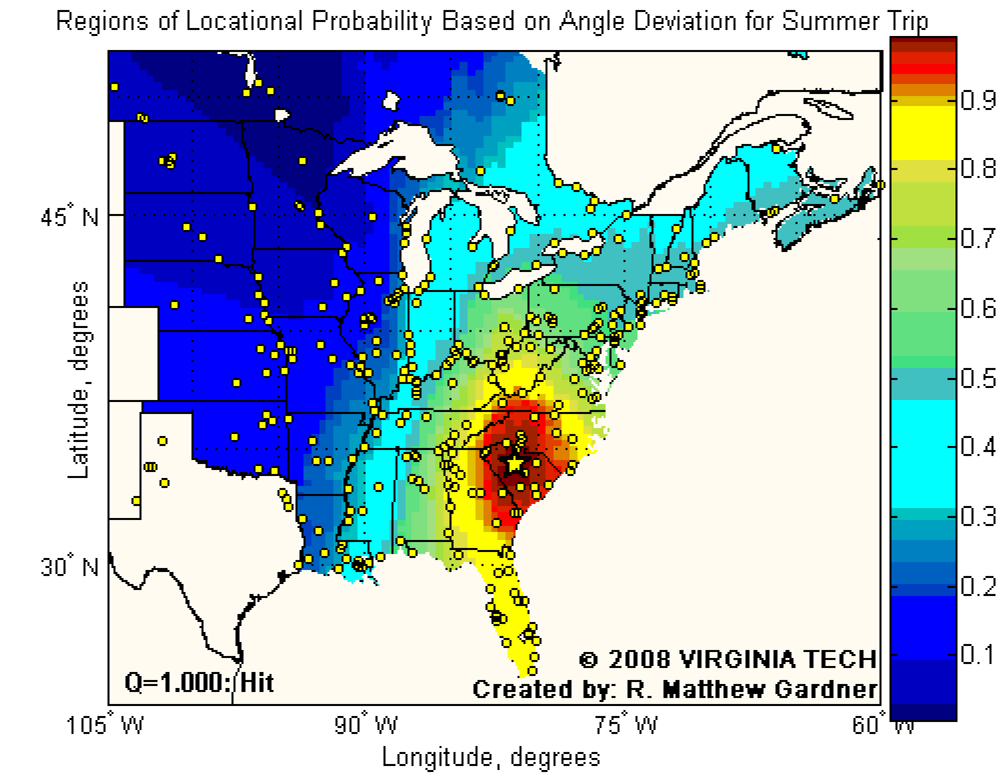
Regions of Locational Probability Based on Angle Deviation for Summer Trip
Latitude, degrees
45° N
30° N
105° W
90° W
75° W
60° W
Longitude, degrees
Q=1.000:/Hit
© 2008 VIRGINIA TECH
Created by: R. Matthew Gardner
0.9
0.8
0.7
0.6
0.5
0.4
0.3
0.2
0.1

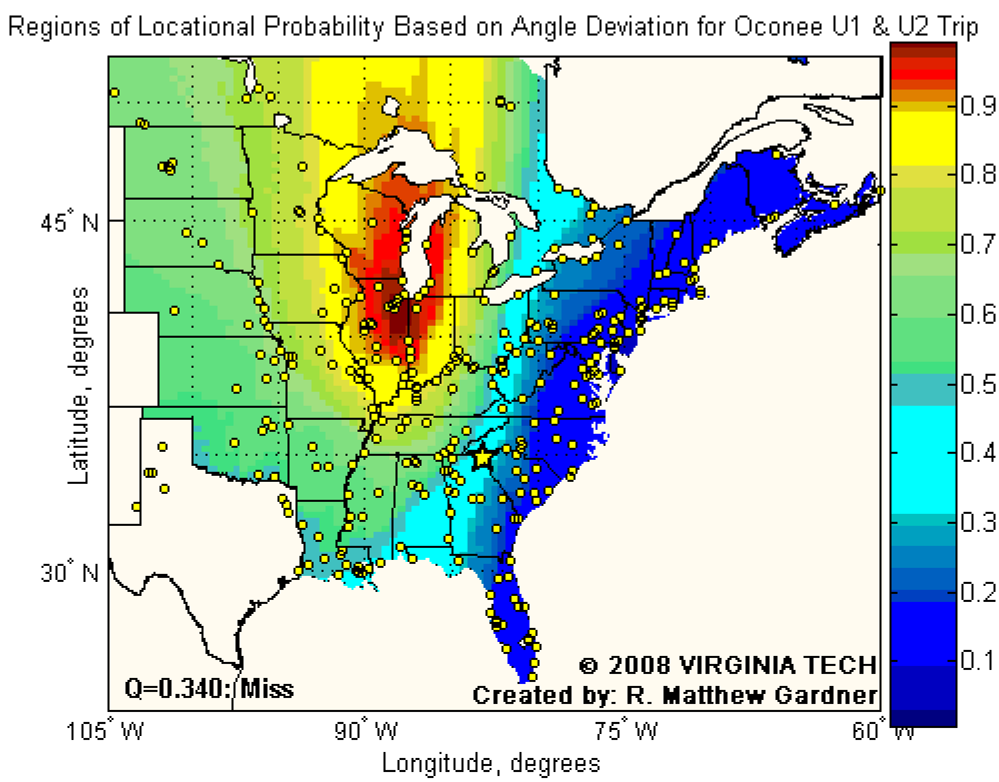
Regions of Locational Probability Based on Angle Deviation for Oconee U1 & U2 Trip
Latitude, degrees
45° N
30° N
105° W
90° W
75° W
60° W
Longitude, degrees
Q=0.340:/Miss
© 2008 VIRGINIA TECH
Created by: R. Matthew Gardner
0.9
0.8
0.7
0.6
0.5
0.4
0.3
0.2
0.1

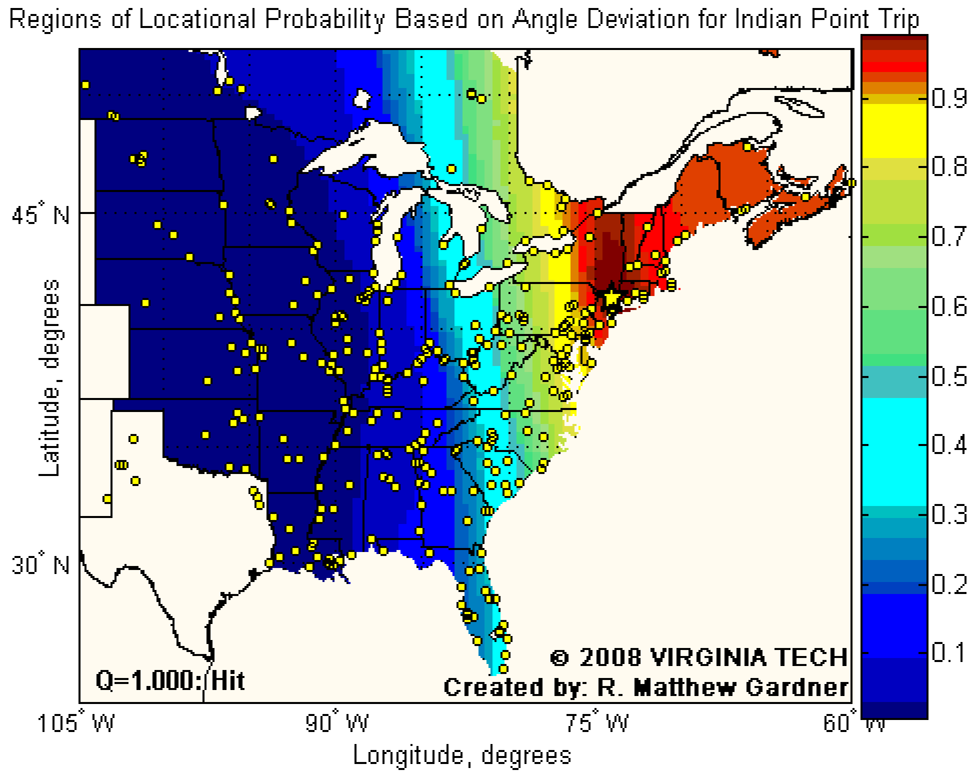
Regions of Locational Probability Based on Angle Deviation for Indian Point Trip
Latitude, degrees
Longitude, degrees
45° N
30° N
105° W
90° W
75° W
60° W
0.9
0.8
0.7
0.6
0.5
0.4
0.3
0.2
0.1
Q=1.000: Hit
© 2008 VIRGINIA TECH
Created by: R. Matthew Gardner

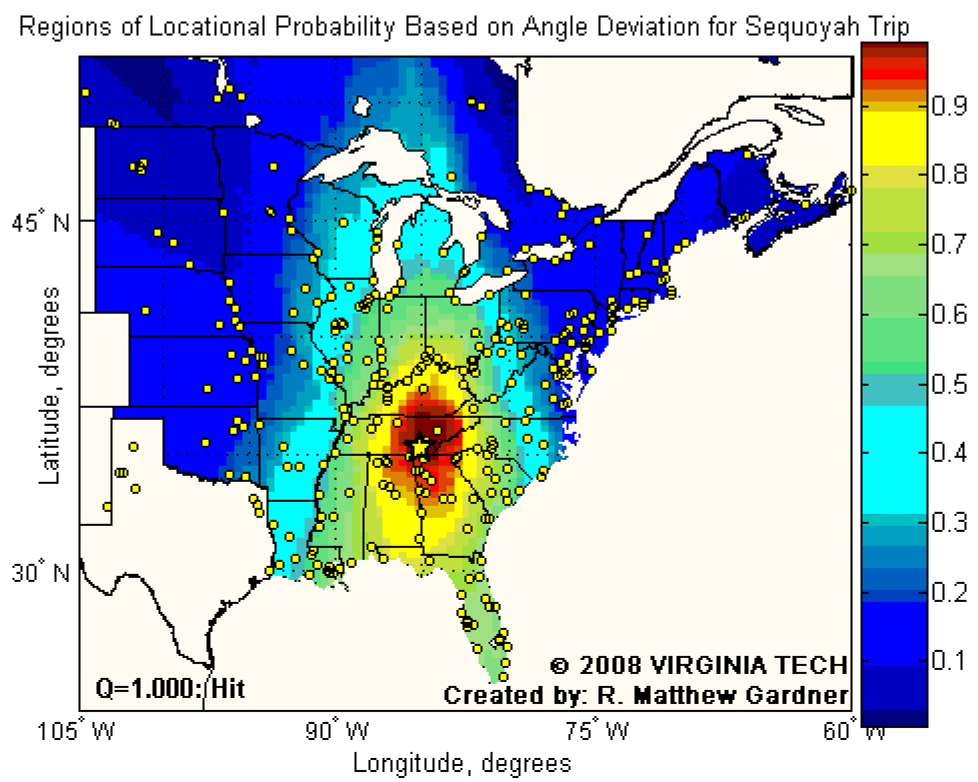
Regions of Locational Probability Based on Angle Deviation for Sequoyah Trip
Latitude, degrees
Longitude, degrees
45° N
30° N
105° W
90° W
75° W
60° W
0.9
0.8
0.7
0.6
0.5
0.4
0.3
0.2
0.1
Q=1.000: Hit
© 2008 VIRGINIA TECH
Created by: R. Matthew Gardner

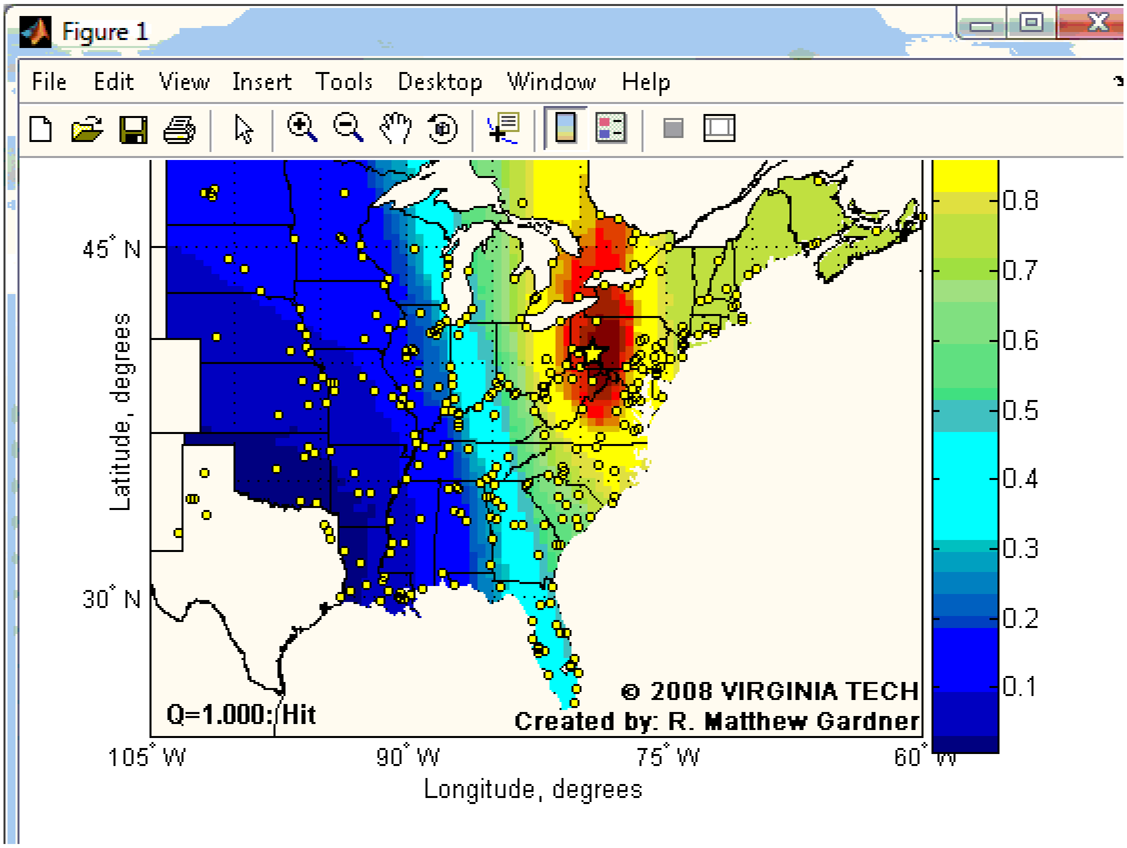
Figure 1
File Edit View Insert Tools Desktop Window Help
45° N
30° N
Latitude, degrees
105° W
90° W
75° W
60° W
Longitude, degrees
Q=1.000:/Hit
© 2008 VIRGINIA TECH
Created by: R. Matthew Gardner
0.8
0.7
0.6
0.5
0.4
0.3
0.2
0.1

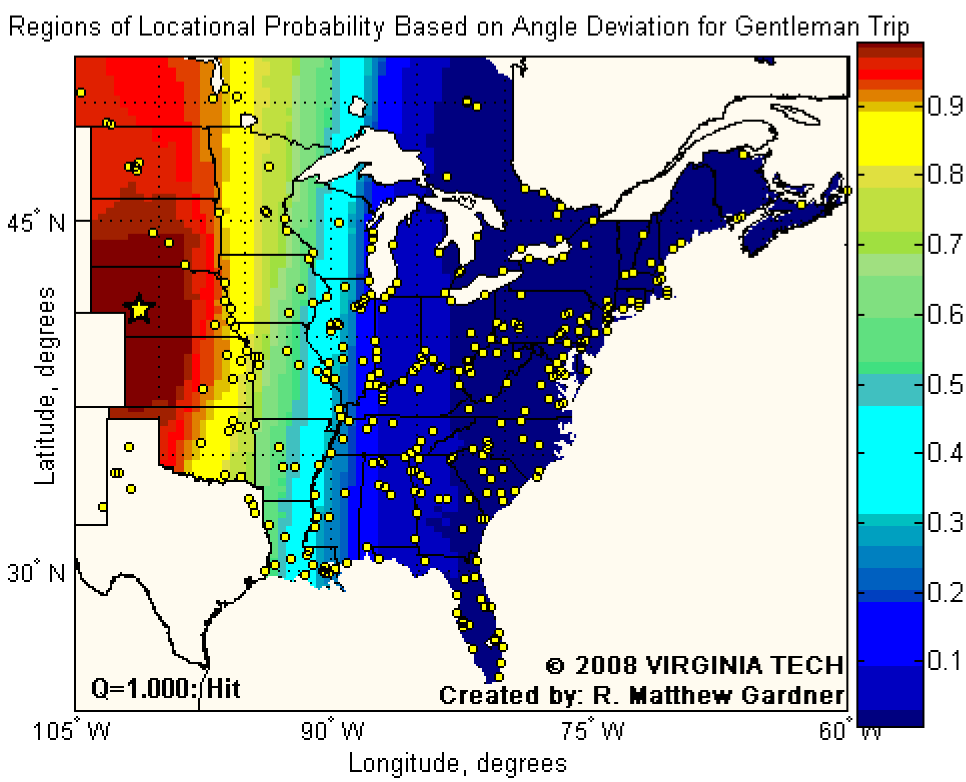
Regions of Locational Probability Based on Angle Deviation for Gentleman Trip
45° N
30° N
Latitude, degrees
105° W
90° W
75° W
60° W
Longitude, degrees
Q=1.000:/Hit
© 2008 VIRGINIA TECH
Created by: R. Matthew Gardner
0.9
0.8
0.7
0.6
0.5
0.4
0.3
0.2
0.1

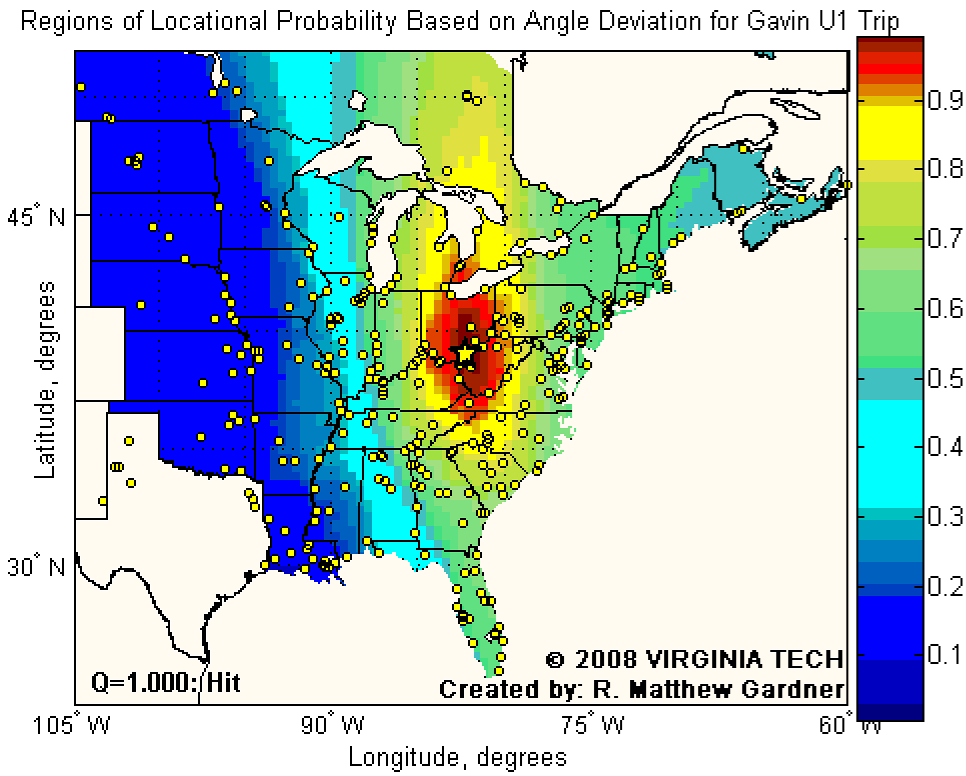
Regions of Locational Probability Based on Angle Deviation for Gavin U1 Trip
45° N
30° N
Latitude, degrees
105° W
90° W
75° W
60° W
Longitude, degrees
Q=1.000:/Hit
© 2008 VIRGINIA TECH
Created by: R. Matthew Gardner
0.9
0.8
0.7
0.6
0.5
0.4
0.3
0.2
0.1

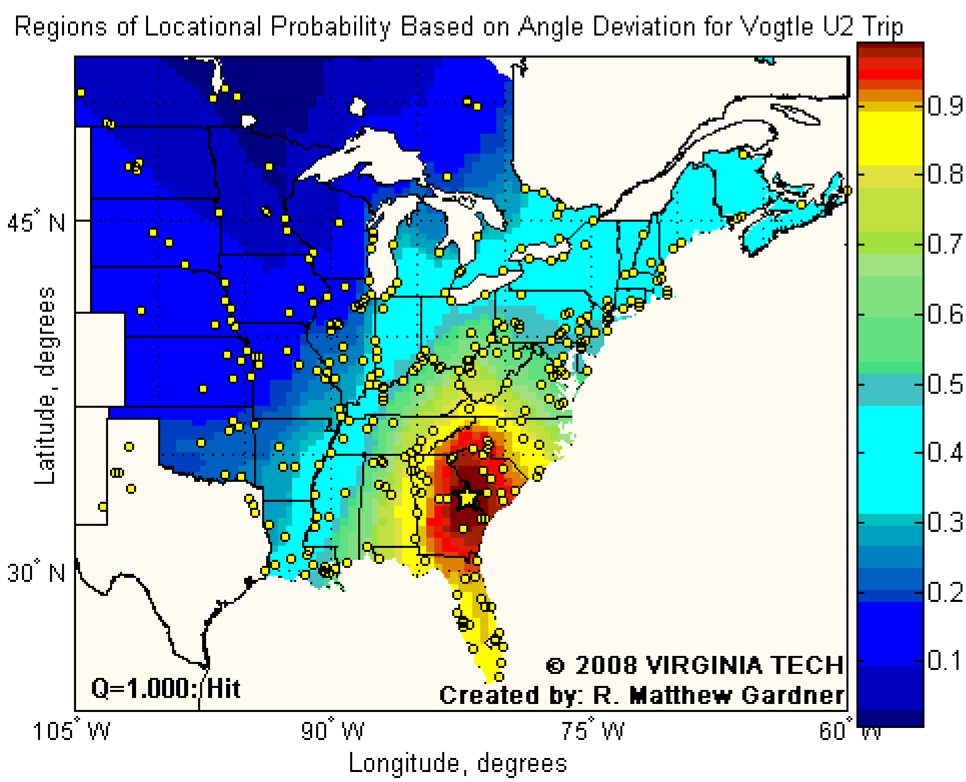
Regions of Locational Probability Based on Angle Deviation for Vogtle U2 Trip
45° N
30° N
Latitude, degrees
105° W
90° W
75° W
60° W
Longitude, degrees
Q=1.000:/Hit
© 2008 VIRGINIA TECH
Created by: R. Matthew Gardner
0.9
0.8
0.7
0.6
0.5
0.4
0.3
0.2
0.1

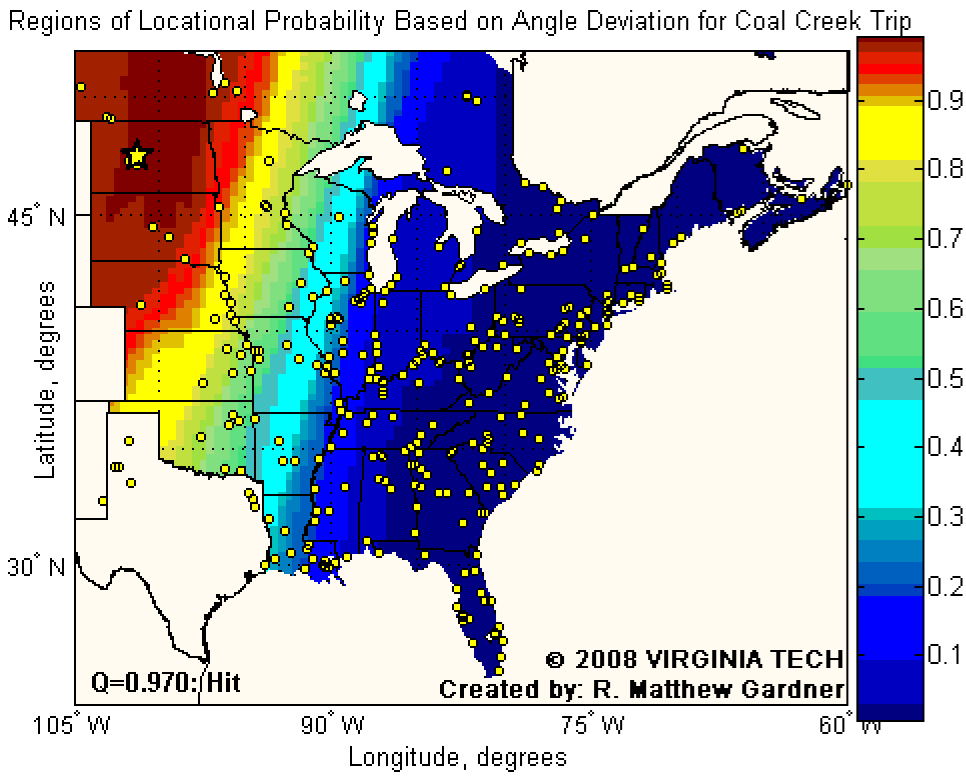
Regions of Locational Probability Based on Angle Deviation for Coal Creek Trip
45° N
30° N
Latitude, degrees
105° W
90° W
75° W
60° W
Longitude, degrees
Q=0.970: Hit
© 2008 VIRGINIA TECH
Created by: R. Matthew Gardner
0.9
0.8
0.7
0.6
0.5
0.4
0.3
0.2
0.1

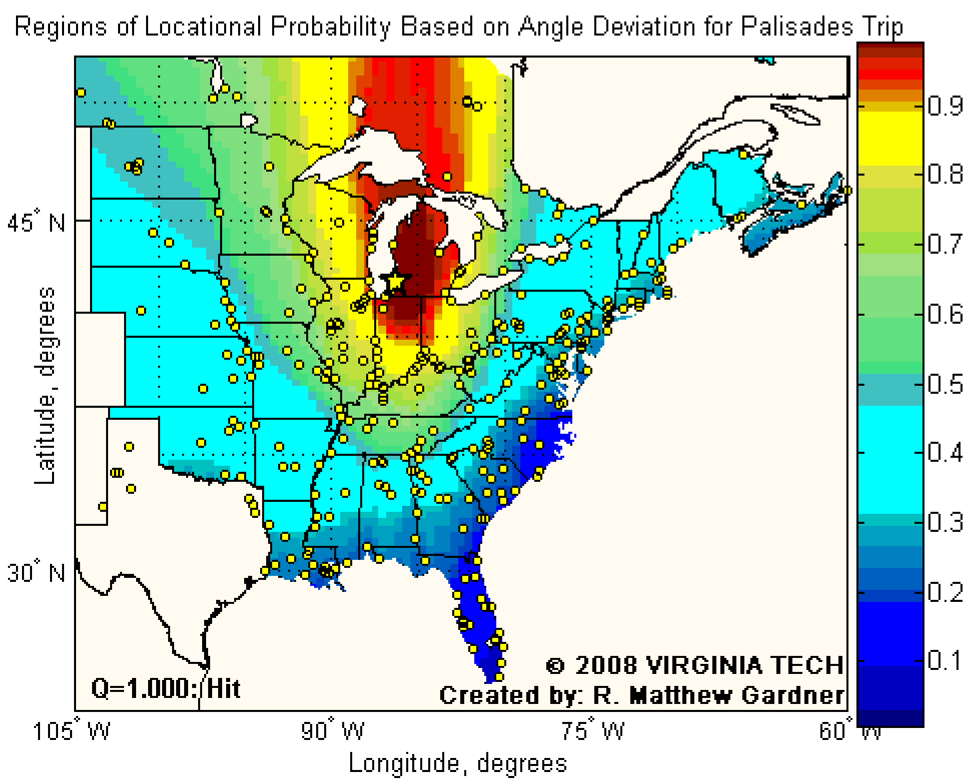
Regions of Locational Probability Based on Angle Deviation for Palisades Trip
45° N
30° N
Latitude, degrees
105° W
90° W
75° W
60° W
Longitude, degrees
Q=1.000: Hit
© 2008 VIRGINIA TECH
Created by: R. Matthew Gardner
0.9
0.8
0.7
0.6
0.5
0.4
0.3
0.2
0.1

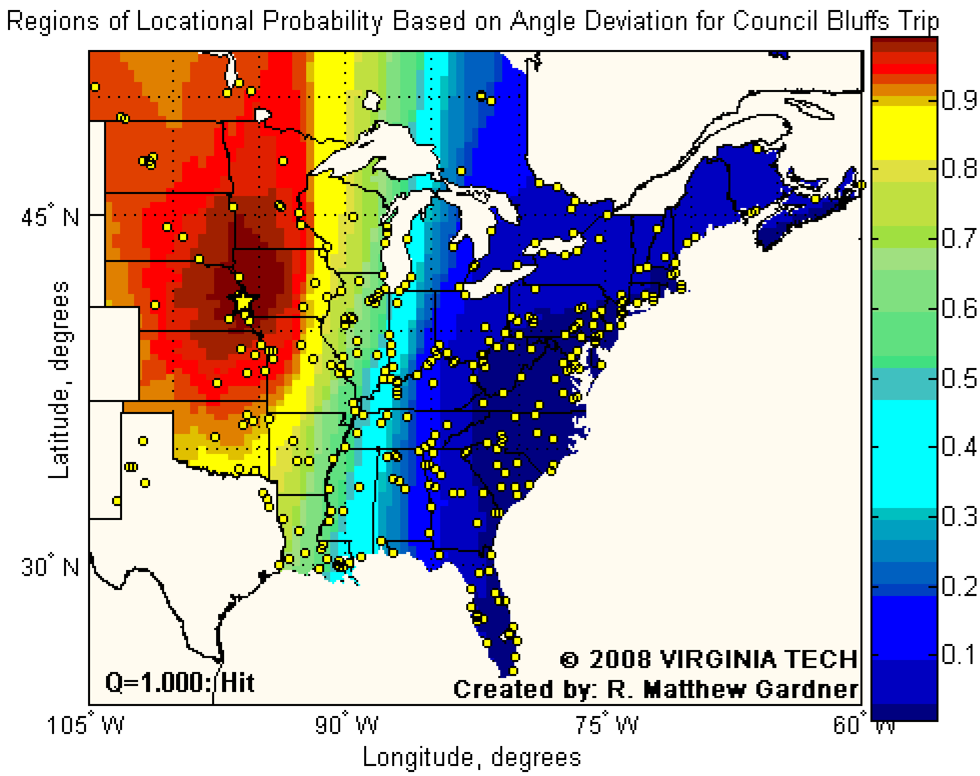
Regions of Locational Probability Based on Angle Deviation for Council Bluffs Trip
45° N
30° N
Latitude, degrees
105° W
90° W
75° W
60° W
Longitude, degrees
Q=1.000:/Hit
© 2008 VIRGINIA TECH
Created by: R. Matthew Gardner
0.9
0.8
0.7
0.6
0.5
0.4
0.3
0.2
0.1

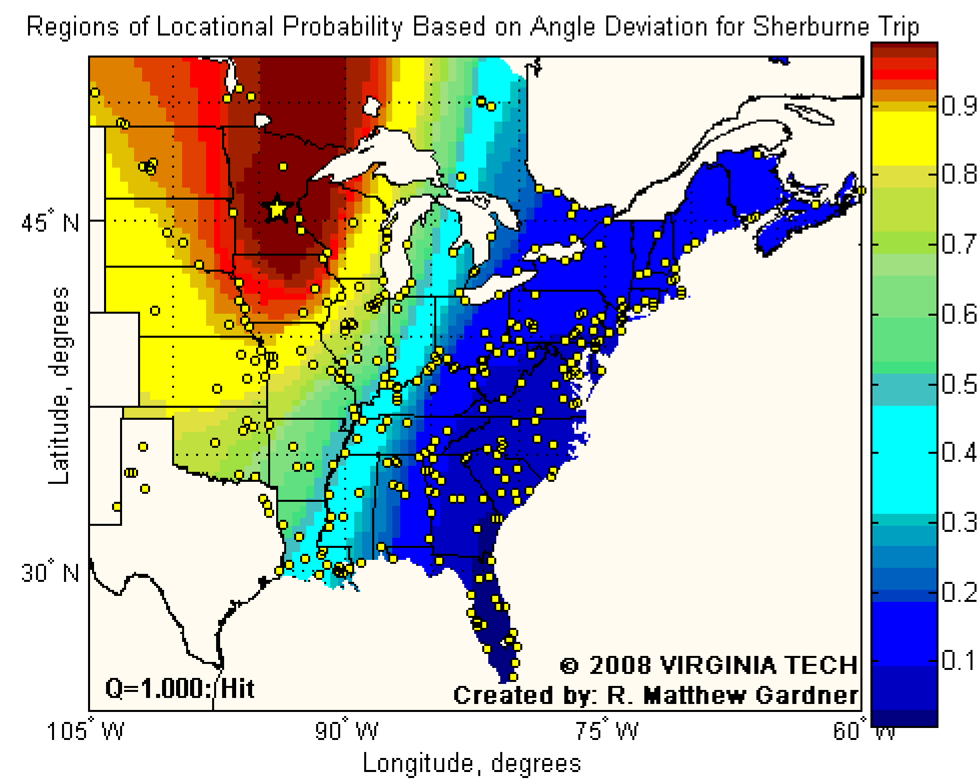
Regions of Locational Probability Based on Angle Deviation for Sherburne Trip
45° N
30° N
Latitude, degrees
105° W
90° W
75° W
60° W
Longitude, degrees
Q=1.000:/Hit
© 2008 VIRGINIA TECH
Created by: R. Matthew Gardner
0.9
0.8
0.7
0.6
0.5
0.4
0.3
0.2
0.1

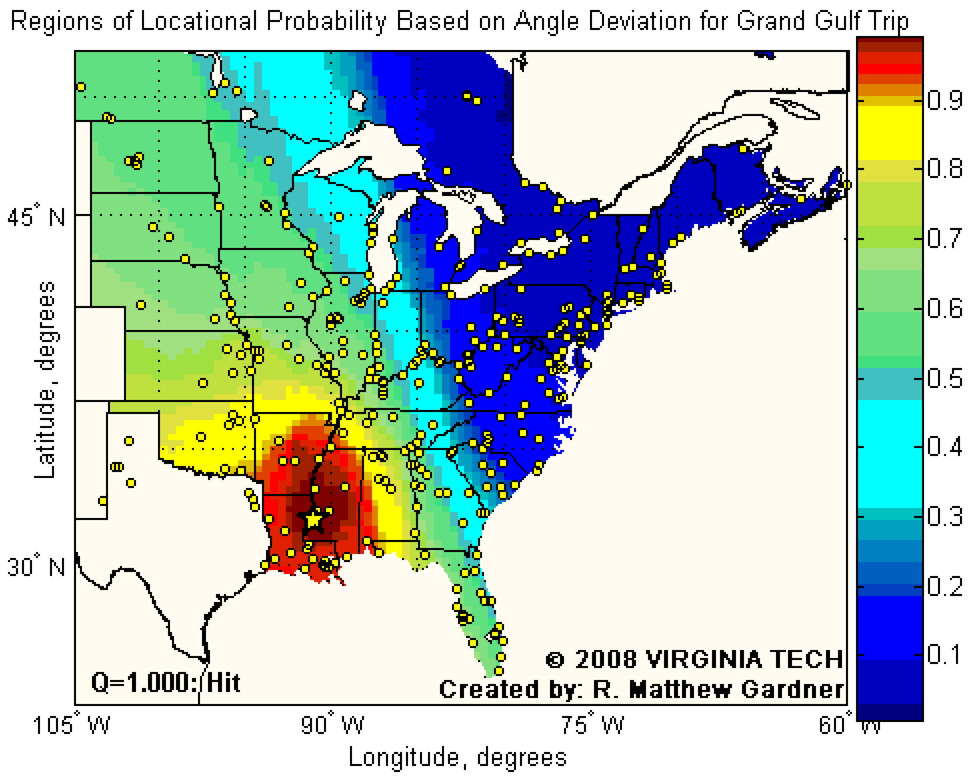
Regions of Locational Probability Based on Angle Deviation for Grand Gulf Trip
45° N
30° N
Latitude, degrees
105° W
90° W
75° W
60° W
Longitude, degrees
Q=1.000:/Hit
© 2008 VIRGINIA TECH
Created by: R. Matthew Gardner
0.9
0.8
0.7
0.6
0.5
0.4
0.3
0.2
0.1

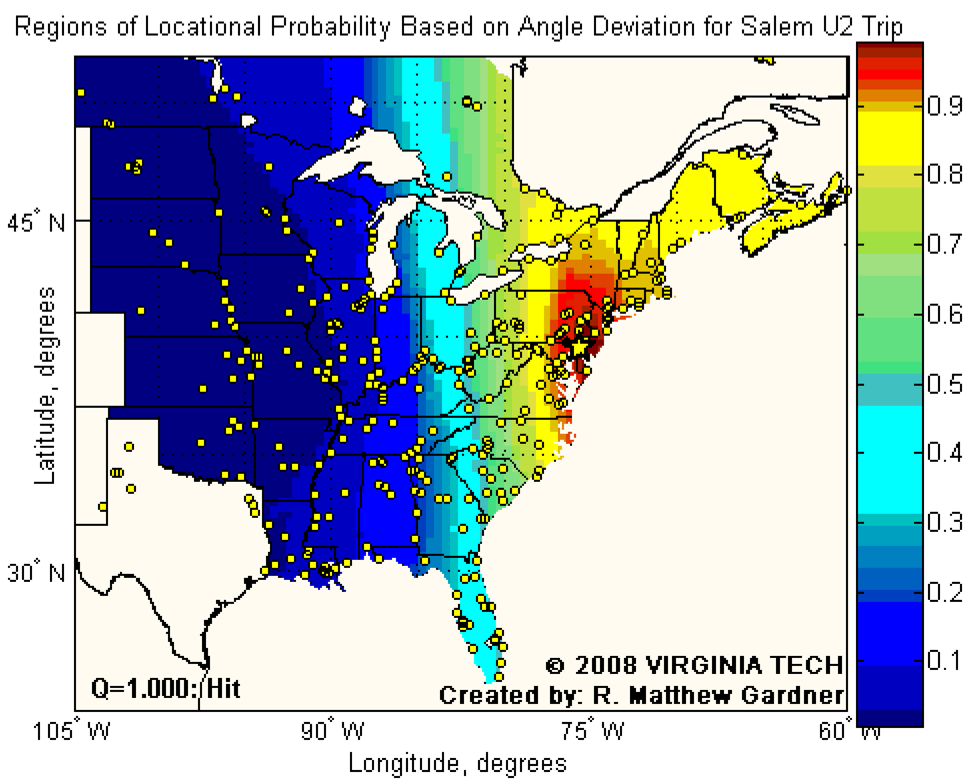
Regions of Locational Probability Based on Angle Deviation for Salem U2 Trip
45° N
30° N
Latitude, degrees
105° W
90° W
75° W
60° W
Longitude, degrees
Q=1.000:/Hit
© 2008 VIRGINIA TECH
Created by: R. Matthew Gardner
0.9
0.8
0.7
0.6
0.5
0.4
0.3
0.2
0.1

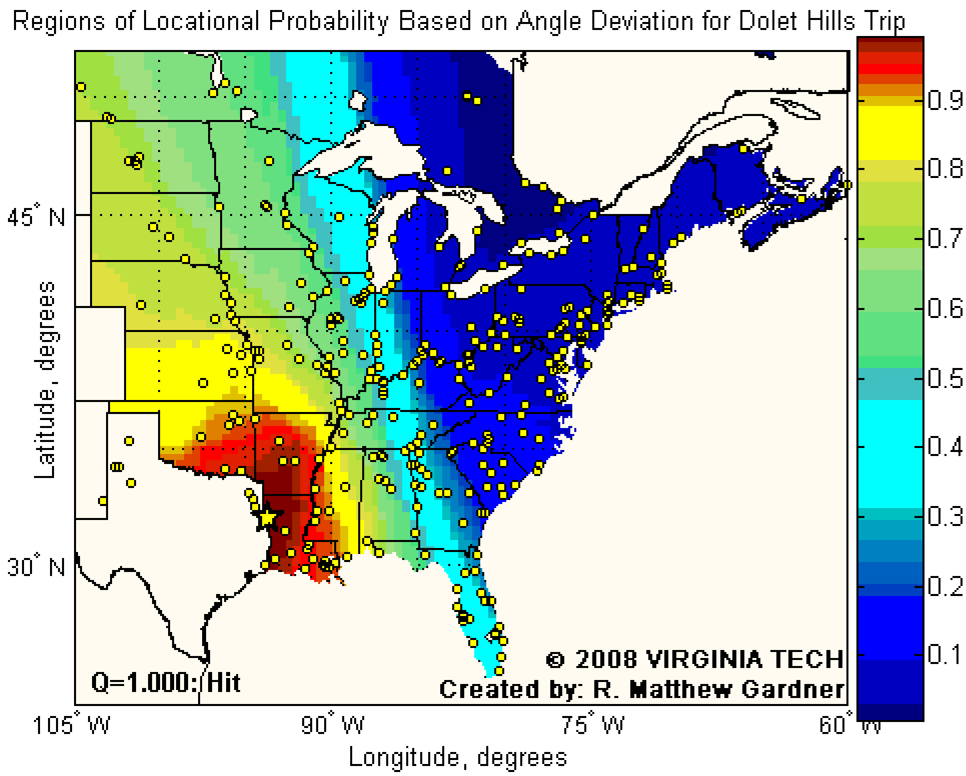
Regions of Locational Probability Based on Angle Deviation for Dolet Hills Trip
Latitude, degrees
45° N
30° N
105° W
90° W
75° W
60° W
Longitude, degrees
0.9
0.8
0.7
0.6
0.5
0.4
0.3
0.2
0.1
Q=1.000:/Hit
© 2008 VIRGINIA TECH
Created by: R. Matthew Gardner

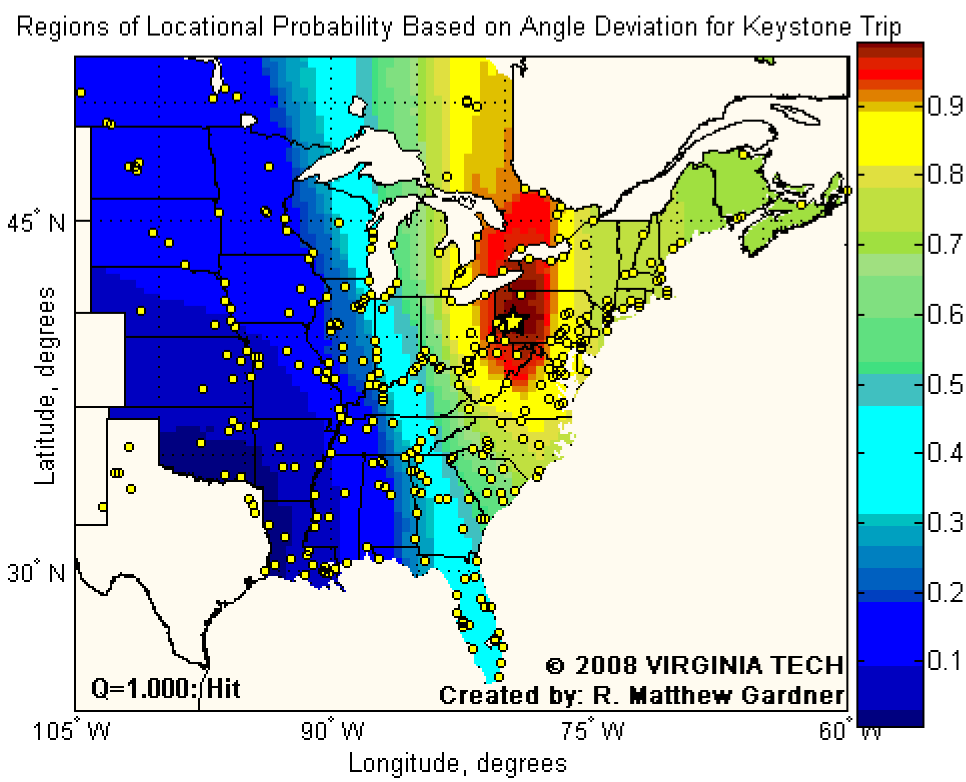
Regions of Locational Probability Based on Angle Deviation for Keystone Trip
Latitude, degrees
45° N
30° N
105° W
90° W
75° W
60° W
Longitude, degrees
0.9
0.8
0.7
0.6
0.5
0.4
0.3
0.2
0.1
Q=1.000:/Hit
© 2008 VIRGINIA TECH
Created by: R. Matthew Gardner

Regions of Locational Probability Based on Angle Deviation for Belew's Creek U1 Trip

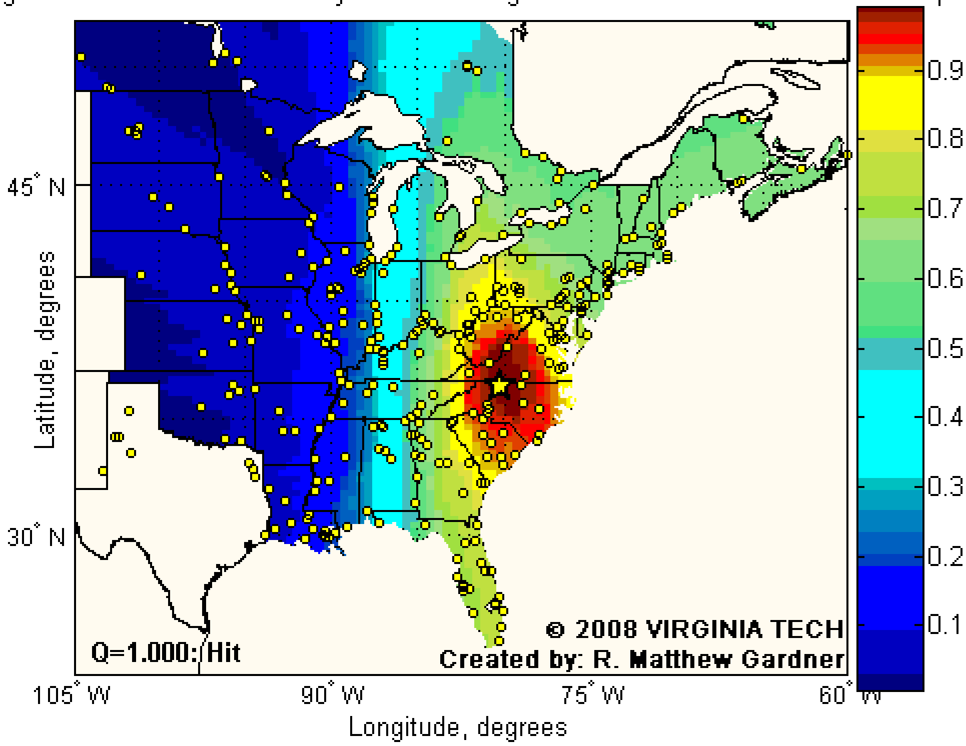

Regions of Locational Probability Based on Angle Deviation for Iatan Trip

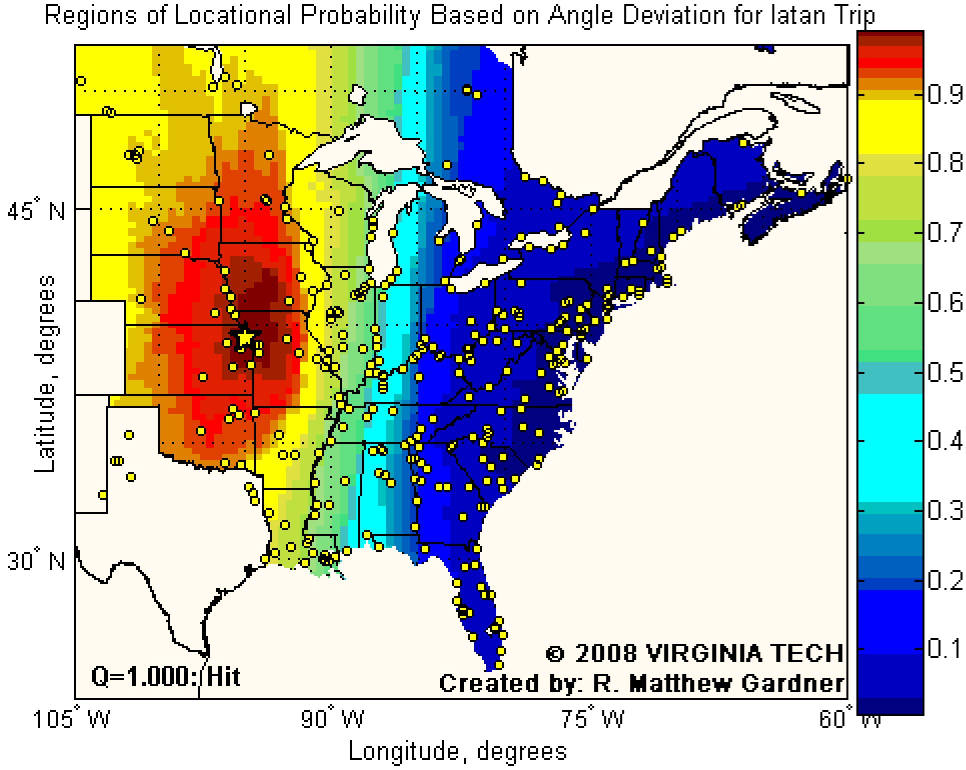

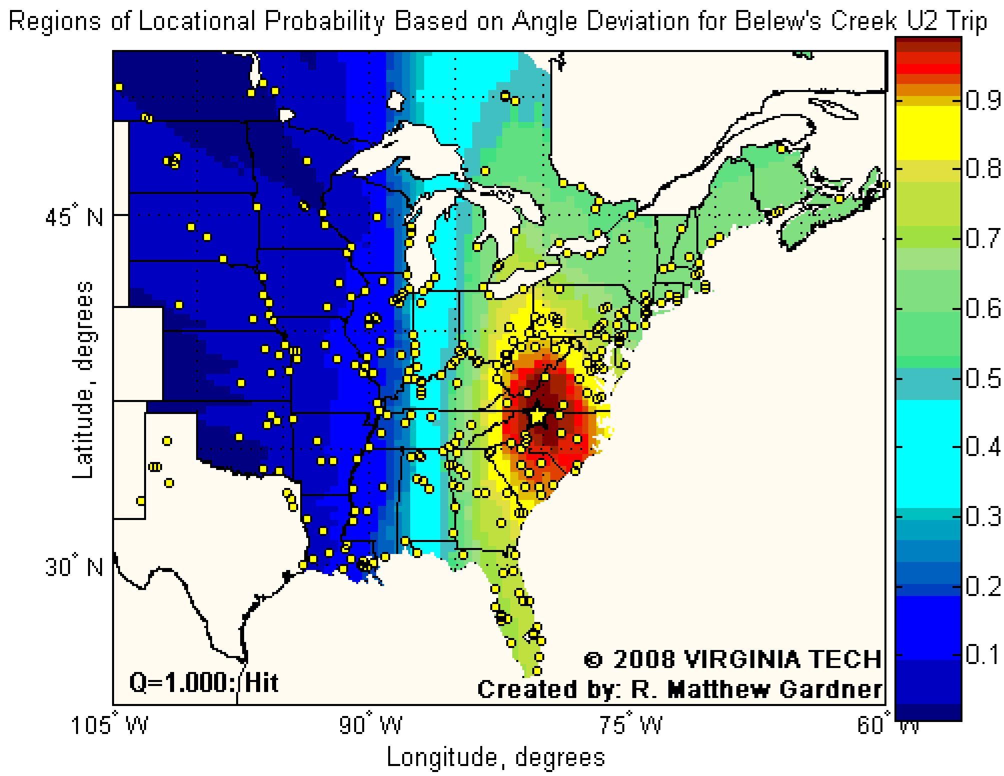
Regions of Locational Probability Based on Angle Deviation for Belew's Creek U2 Trip
45° N
30° N
Latitude, degrees
105° W
90° W
75° W
60° W
Longitude, degrees
Q=1.000:/Hit
© 2008 VIRGINIA TECH
Created by: R. Matthew Gardner
0.9
0.8
0.7
0.6
0.5
0.4
0.3
0.2
0.1

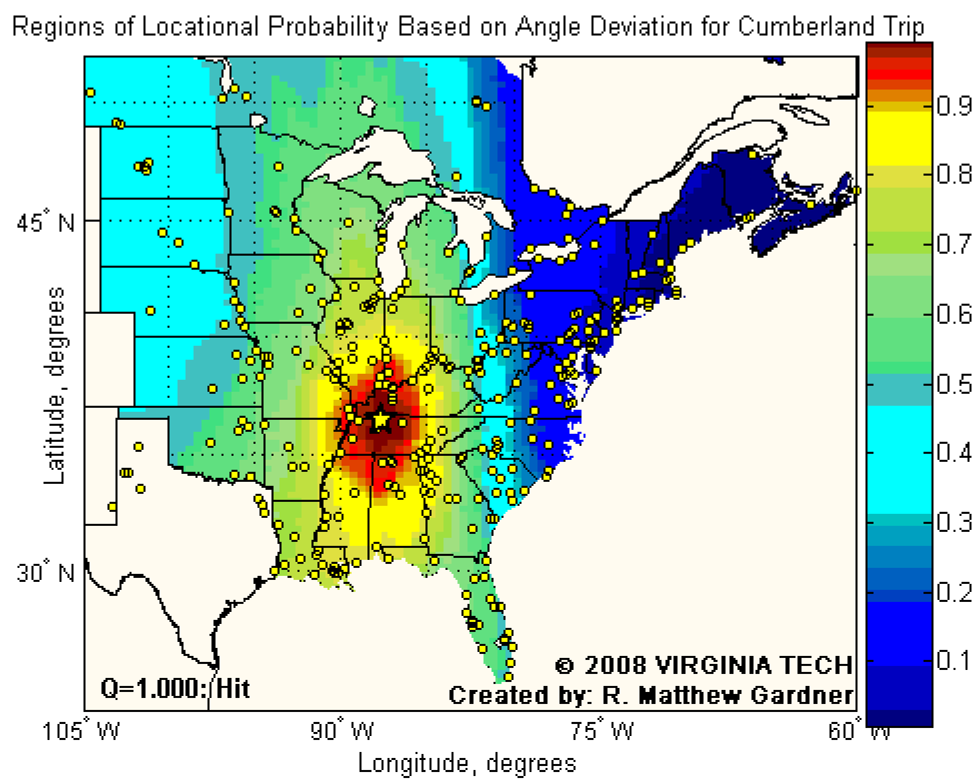
Regions of Locational Probability Based on Angle Deviation for Cumberland Trip
45° N
30° N
Latitude, degrees
105° W
90° W
75° W
60° W
Longitude, degrees
Q=1.000:/Hit
© 2008 VIRGINIA TECH
Created by: R. Matthew Gardner
0.9
0.8
0.7
0.6
0.5
0.4
0.3
0.2
0.1

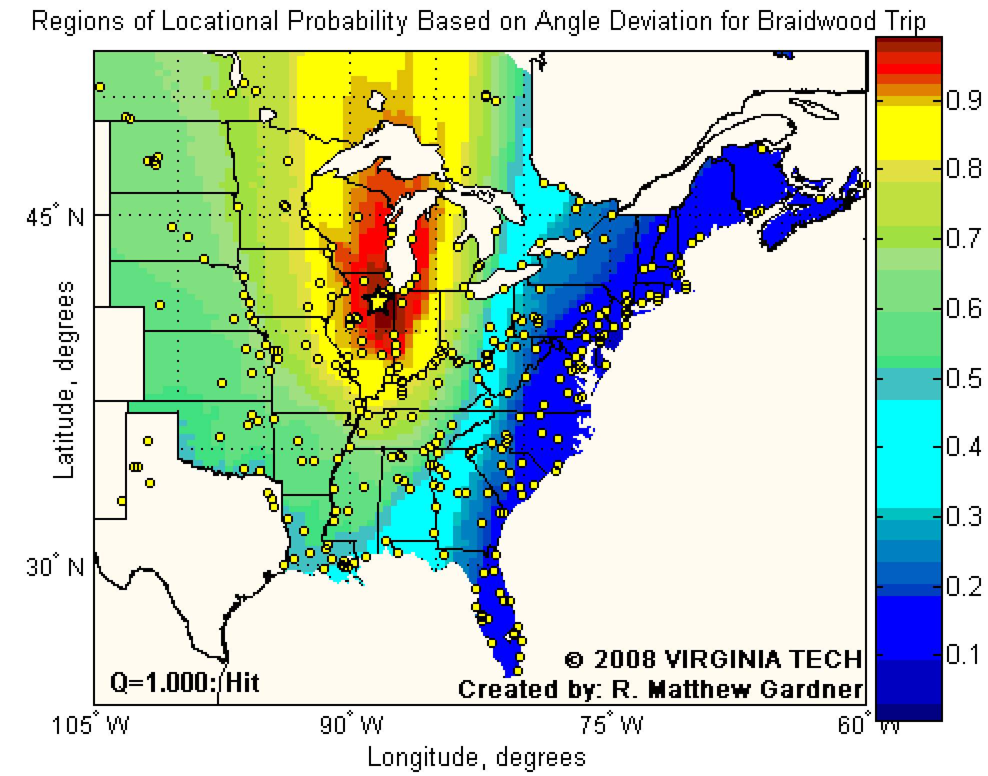
Regions of Locational Probability Based on Angle Deviation for Braidwood Trip
Latitude, degrees
45° N
30° N
105° W
90° W
75° W
60° W
Longitude, degrees
Q=1.000:/Hit
© 2008 VIRGINIA TECH
Created by: R. Matthew Gardner
0.9
0.8
0.7
0.6
0.5
0.4
0.3
0.2
0.1

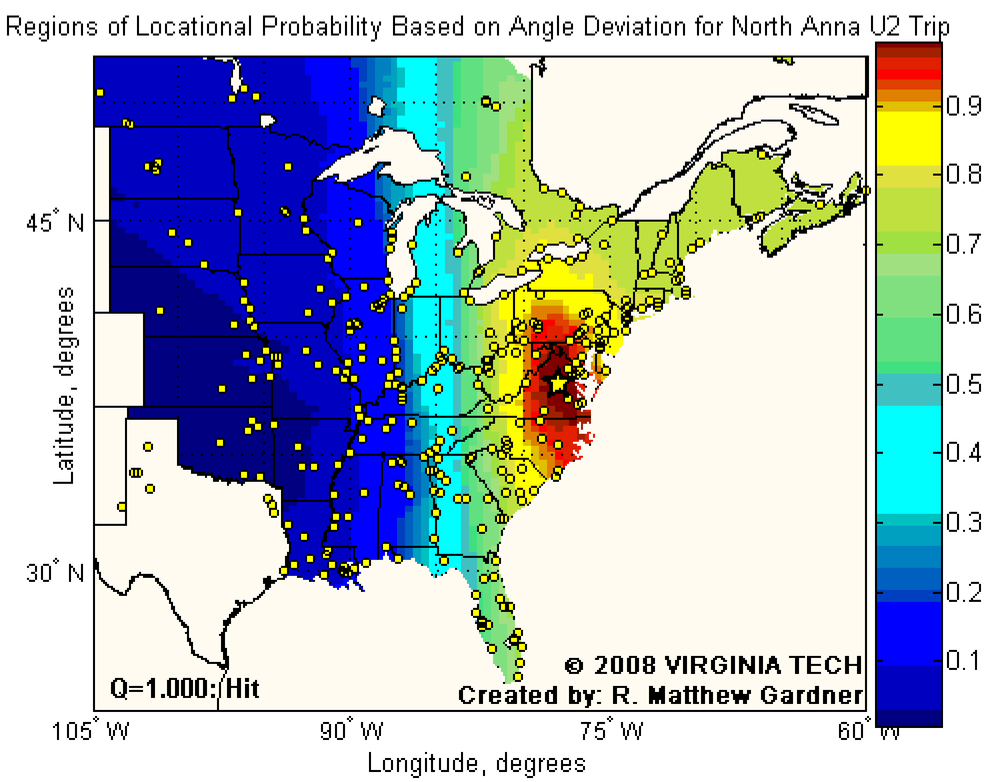
Regions of Locational Probability Based on Angle Deviation for North Anna U2 Trip
Latitude, degrees
45° N
30° N
105° W
90° W
75° W
60° W
Longitude, degrees
Q=1.000:/Hit
© 2008 VIRGINIA TECH
Created by: R. Matthew Gardner
0.9
0.8
0.7
0.6
0.5
0.4
0.3
0.2
0.1

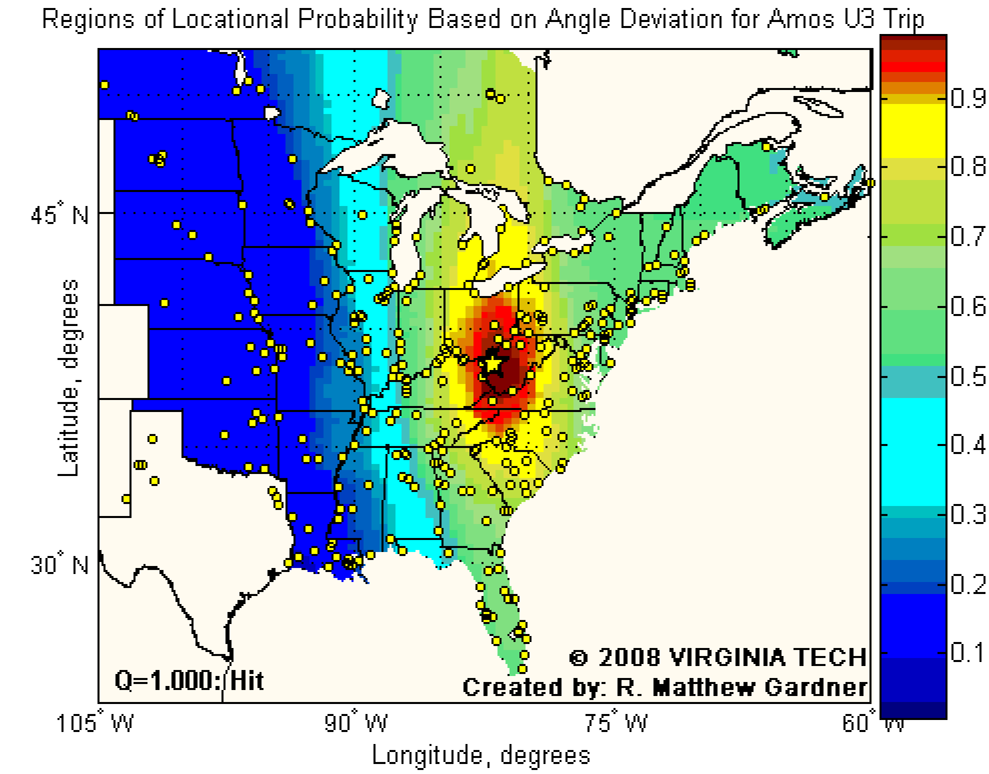
Regions of Locational Probability Based on Angle Deviation for Amos U3 Trip
Latitude, degrees
45° N
30° N
105° W
90° W
75° W
60° W
Longitude, degrees
0.9
0.8
0.7
0.6
0.5
0.4
0.3
0.2
0.1
Q=1.000:/Hit
© 2008 VIRGINIA TECH
Created by: R. Matthew Gardner

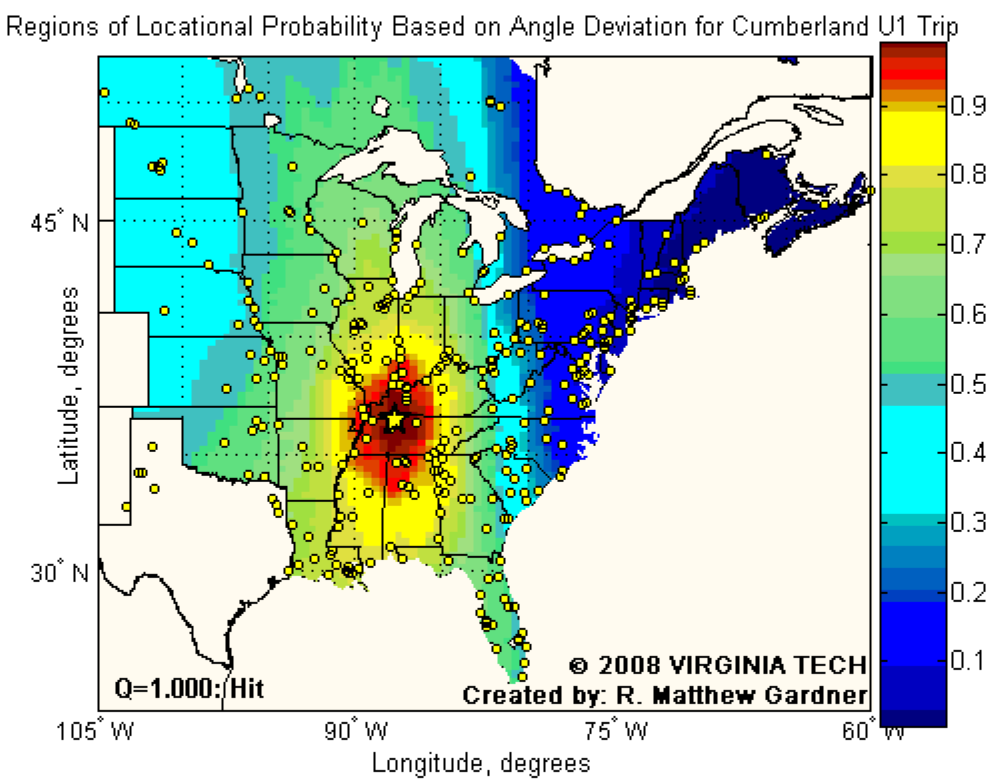
Regions of Locational Probability Based on Angle Deviation for Cumberland U1 Trip
Latitude, degrees
45° N
30° N
105° W
90° W
75° W
60° W
Longitude, degrees
0.9
0.8
0.7
0.6
0.5
0.4
0.3
0.2
0.1
Q=1.000:/Hit
© 2008 VIRGINIA TECH
Created by: R. Matthew Gardner

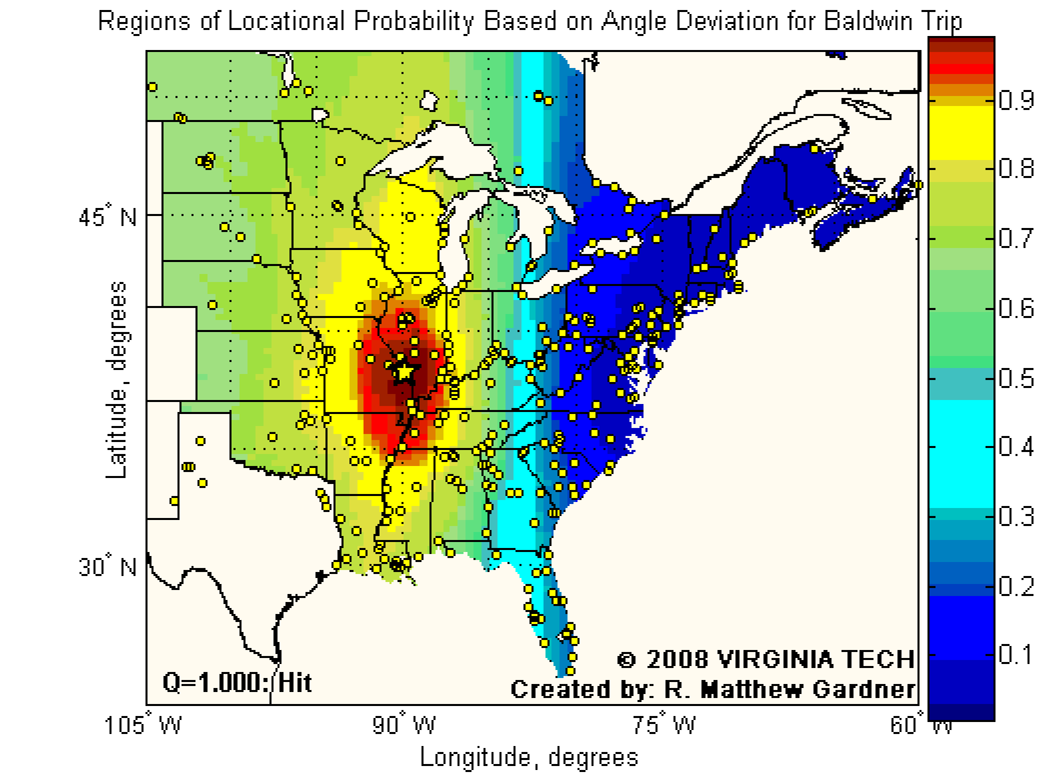
Regions of Locational Probability Based on Angle Deviation for Baldwin Trip
Latitude, degrees
Longitude, degrees
45° N
30° N
105° W
90° W
75° W
60° W
0.9
0.8
0.7
0.6
0.5
0.4
0.3
0.2
0.1
© 2008 VIRGINIA TECH
Created by: R. Matthew Gardner
Q=1.000:/Hit

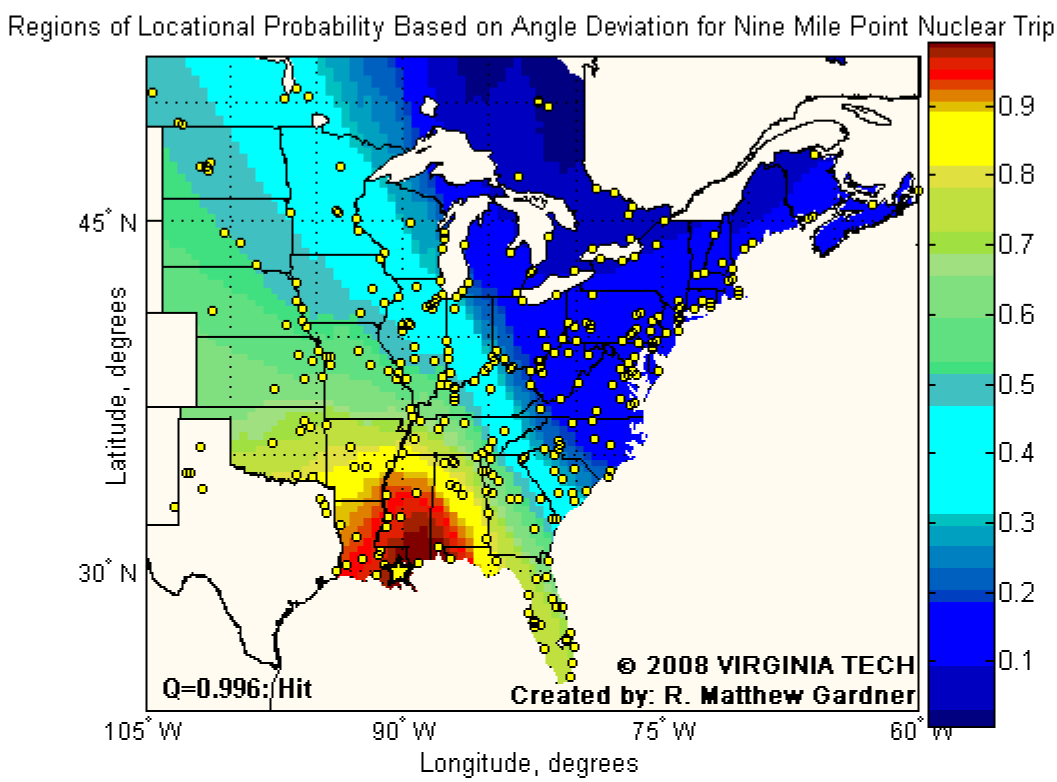
Regions of Locational Probability Based on Angle Deviation for Nine Mile Point Nuclear Trip
Latitude, degrees
Longitude, degrees
45° N
30° N
105° W
90° W
75° W
60° W
0.9
0.8
0.7
0.6
0.5
0.4
0.3
0.2
0.1
© 2008 VIRGINIA TECH
Created by: R. Matthew Gardner
Q=0.996:/Hit

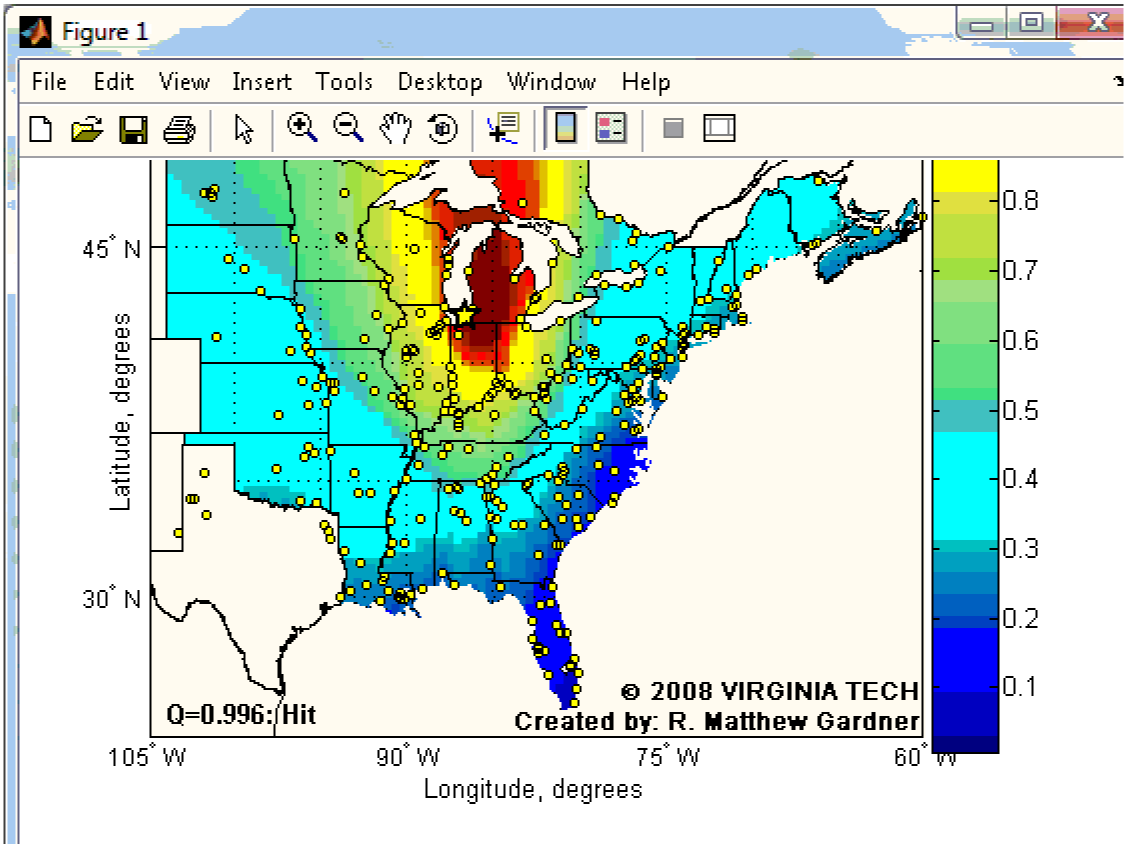
Figure 1
File Edit View Insert Tools Desktop Window Help
45° N
30° N
Latitude, degrees
105° W
90° W
75° W
60° W
Longitude, degrees
Q=0.996:/Hit
© 2008 VIRGINIA TECH
Created by: R. Matthew Gardner
0.8
0.7
0.6
0.5
0.4
0.3
0.2
0.1

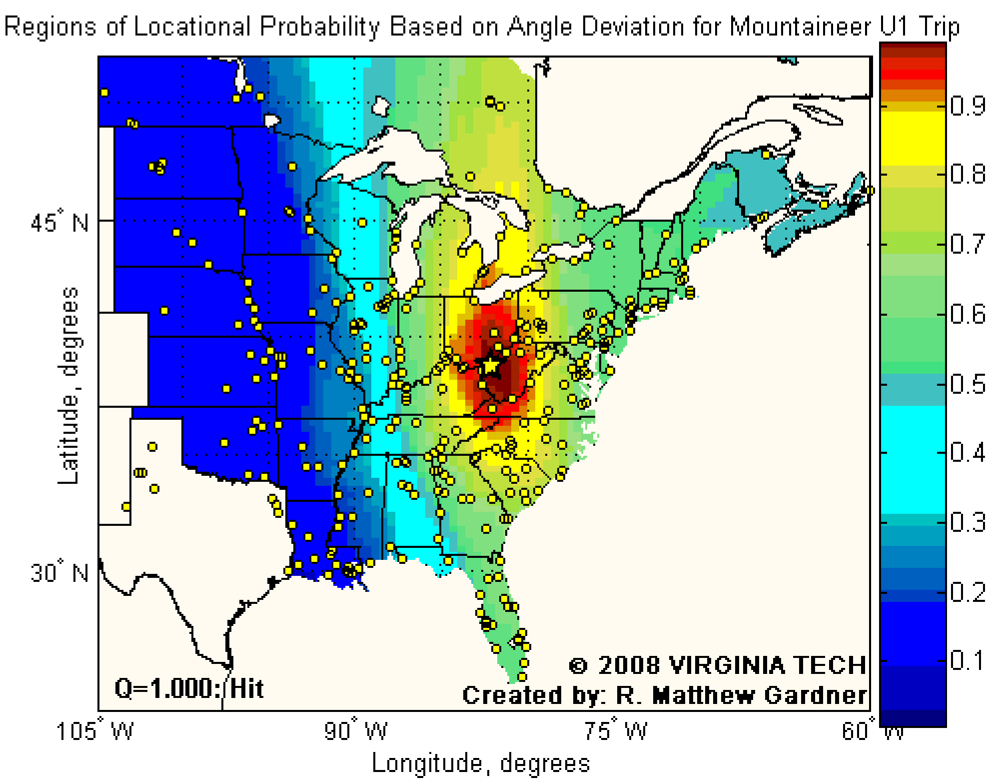
Regions of Locational Probability Based on Angle Deviation for Mountaineer U1 Trip
45° N
30° N
Latitude, degrees
105° W
90° W
75° W
60° W
Longitude, degrees
Q=1.000:/Hit
© 2008 VIRGINIA TECH
Created by: R. Matthew Gardner
0.9
0.8
0.7
0.6
0.5
0.4
0.3
0.2
0.1

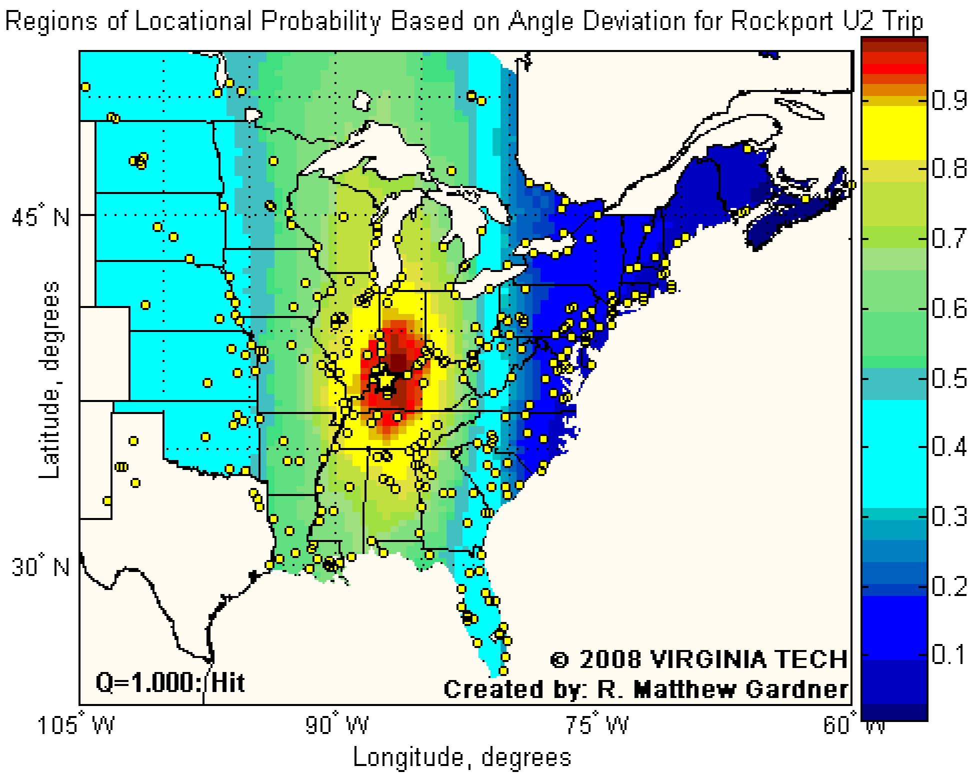
Regions of Locational Probability Based on Angle Deviation for Rockport U2 Trip
45° N
30° N
Latitude, degrees
105° W
90° W
75° W
60° W
Longitude, degrees
Q=1.000:/Hit
© 2008 VIRGINIA TECH
Created by: R. Matthew Gardner
0.9
0.8
0.7
0.6
0.5
0.4
0.3
0.2
0.1

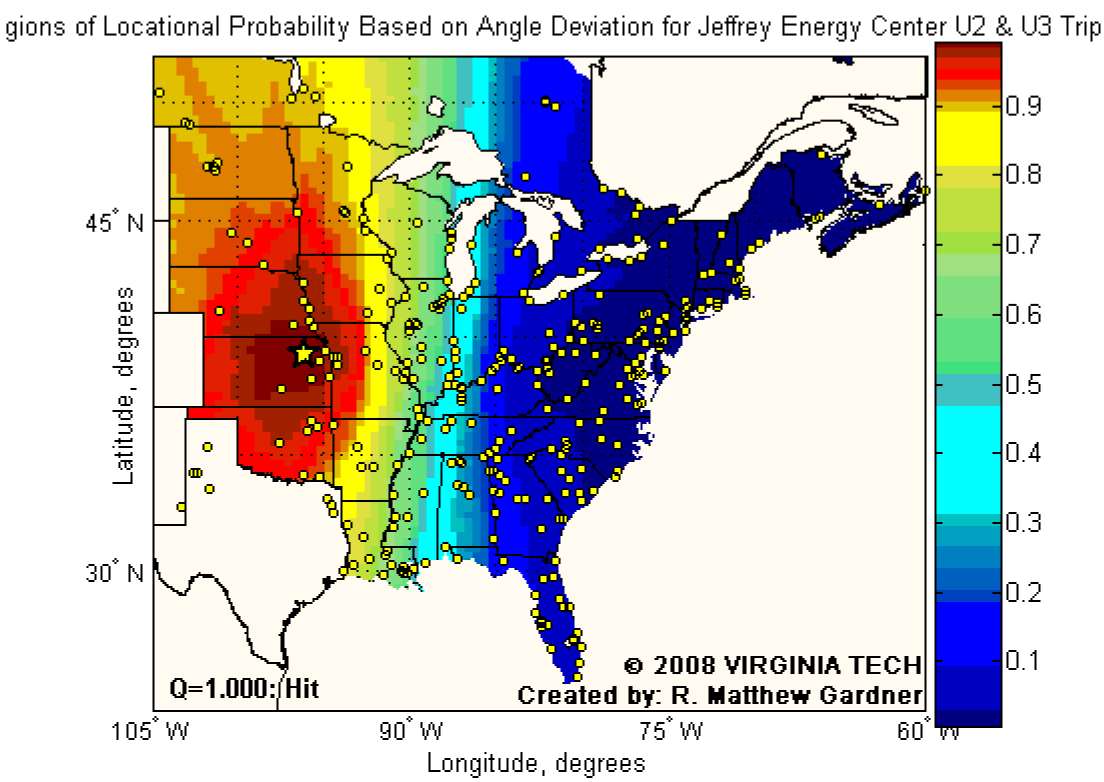
gions of Locational Probability Based on Angle Deviation for Jeffrey Energy Center U2 & U3 Trip
45° N
30° N
Latitude, degrees
105° W
90° W
75° W
60° W
Longitude, degrees
Q=1.000:/Hit
© 2008 VIRGINIA TECH
Created by: R. Matthew Gardner
0.9
0.8
0.7
0.6
0.5
0.4
0.3
0.2
0.1

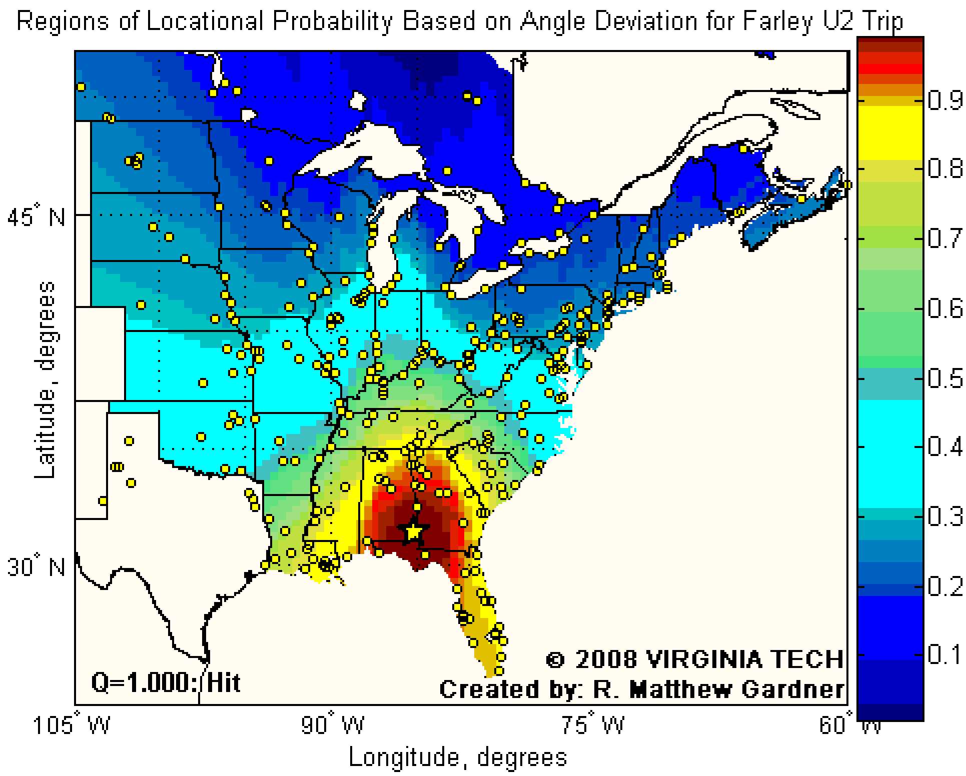
Regions of Locational Probability Based on Angle Deviation for Farley U2 Trip
45° N
30° N
Latitude, degrees
105° W
90° W
75° W
60° W
Longitude, degrees
Q=1.000:/Hit
© 2008 VIRGINIA TECH
Created by: R. Matthew Gardner
0.9
0.8
0.7
0.6
0.5
0.4
0.3
0.2
0.1

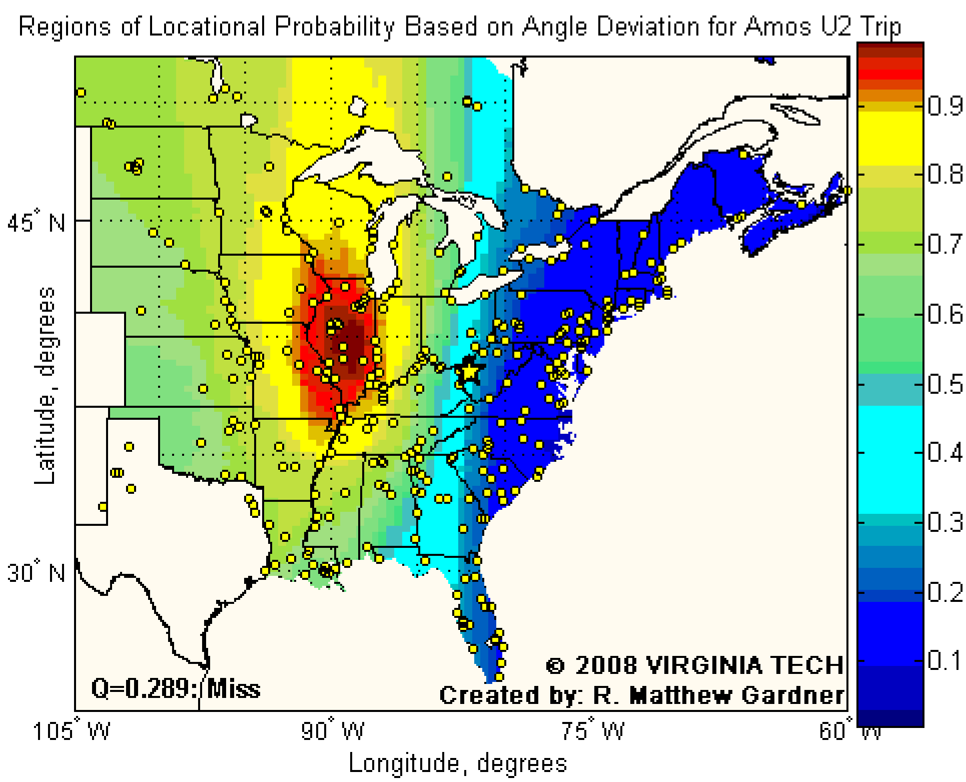
Regions of Locational Probability Based on Angle Deviation for Amos U2 Trip
45° N
30° N
Latitude, degrees
105° W
90° W
75° W
60° W
Longitude, degrees
Q=0.289:/Miss
© 2008 VIRGINIA TECH
Created by: R. Matthew Gardner
0.9
0.8
0.7
0.6
0.5
0.4
0.3
0.2
0.1

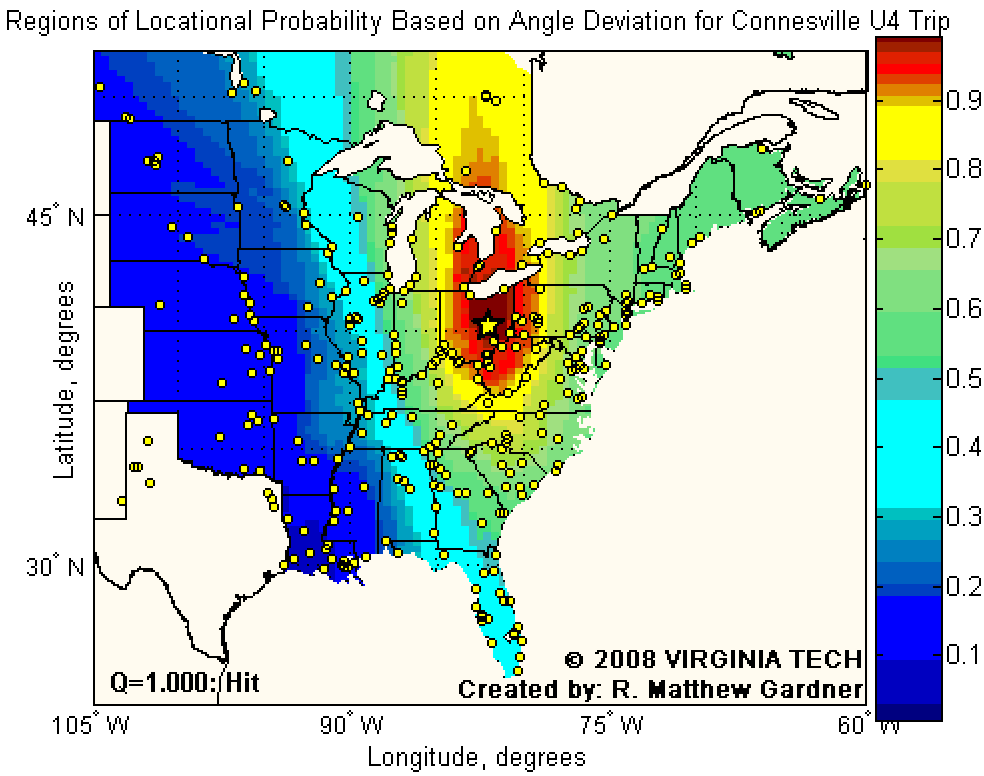
Regions of Locational Probability Based on Angle Deviation for Connesville U4 Trip
45° N
30° N
Latitude, degrees
105° W
90° W
75° W
60° W
Longitude, degrees
Q=1.000:/Hit
© 2008 VIRGINIA TECH
Created by: R. Matthew Gardner
0.9
0.8
0.7
0.6
0.5
0.4
0.3
0.2
0.1

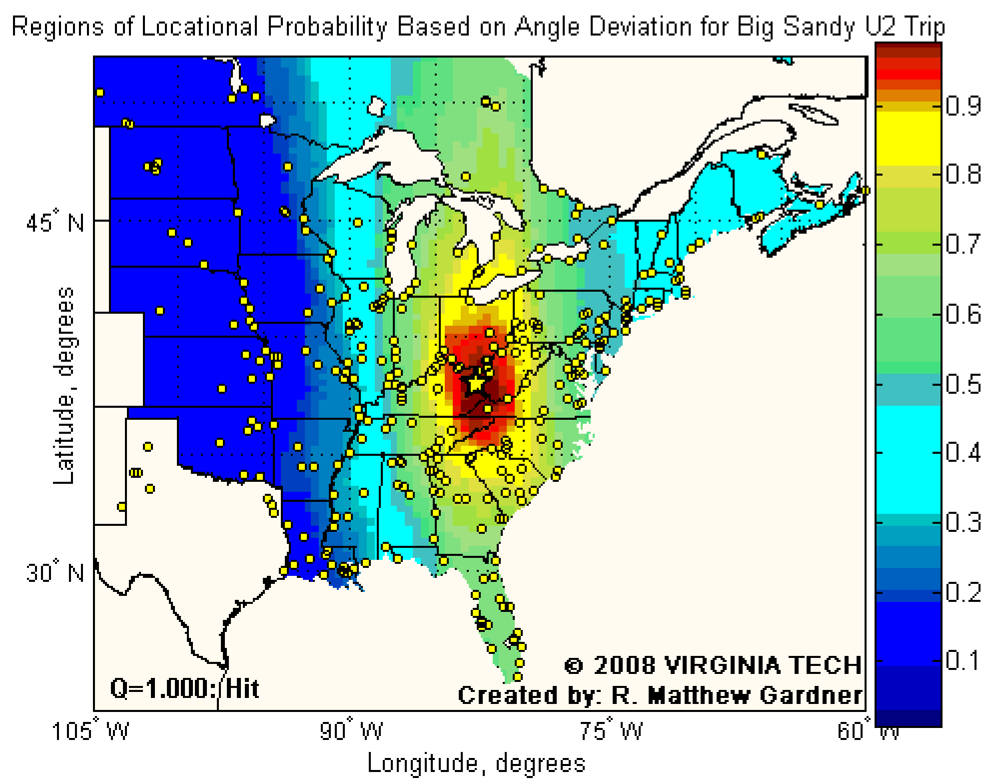
Regions of Locational Probability Based on Angle Deviation for Big Sandy U2 Trip
45° N
30° N
Latitude, degrees
105° W
90° W
75° W
60° W
Longitude, degrees
Q=1.000:/Hit
© 2008 VIRGINIA TECH
Created by: R. Matthew Gardner
0.9
0.8
0.7
0.6
0.5
0.4
0.3
0.2
0.1

Appendix XVII: Full Half-Plane Event Location Based Upon Measurement of EI Frequency

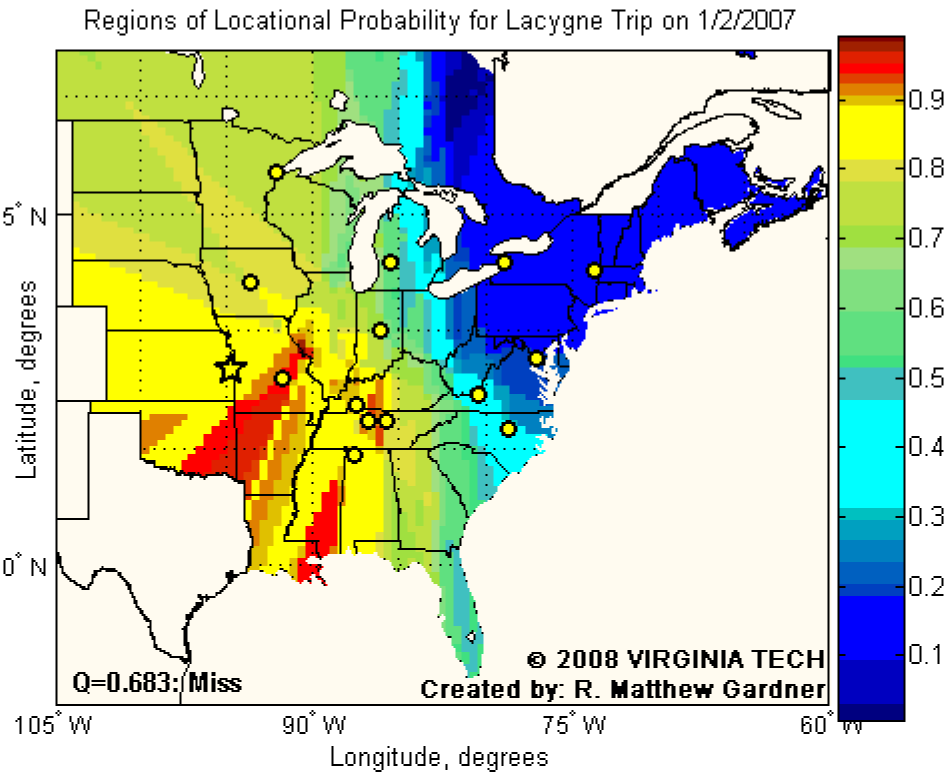

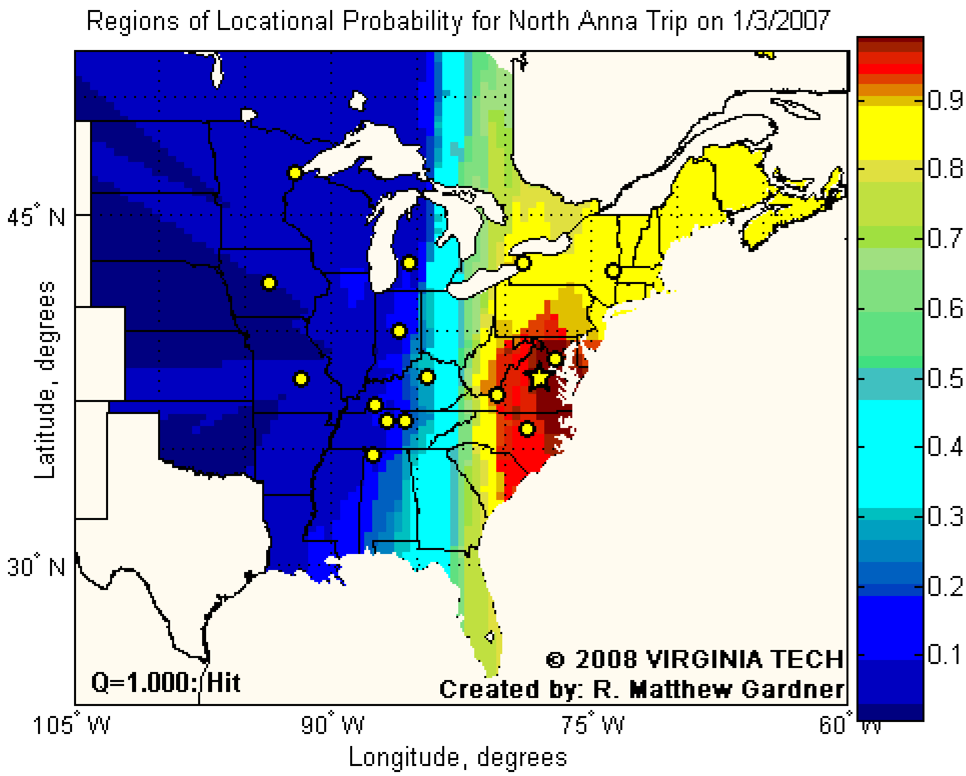
Regions of Locational Probability for North Anna Trip on 1/3/2007
45° N
30° N
Latitude, degrees
105° W
90° W
75° W
60° W
Longitude, degrees
Q=1.000:/Hit
© 2008 VIRGINIA TECH
Created by: R. Matthew Gardner
0.9
0.8
0.7
0.6
0.5
0.4
0.3
0.2
0.1

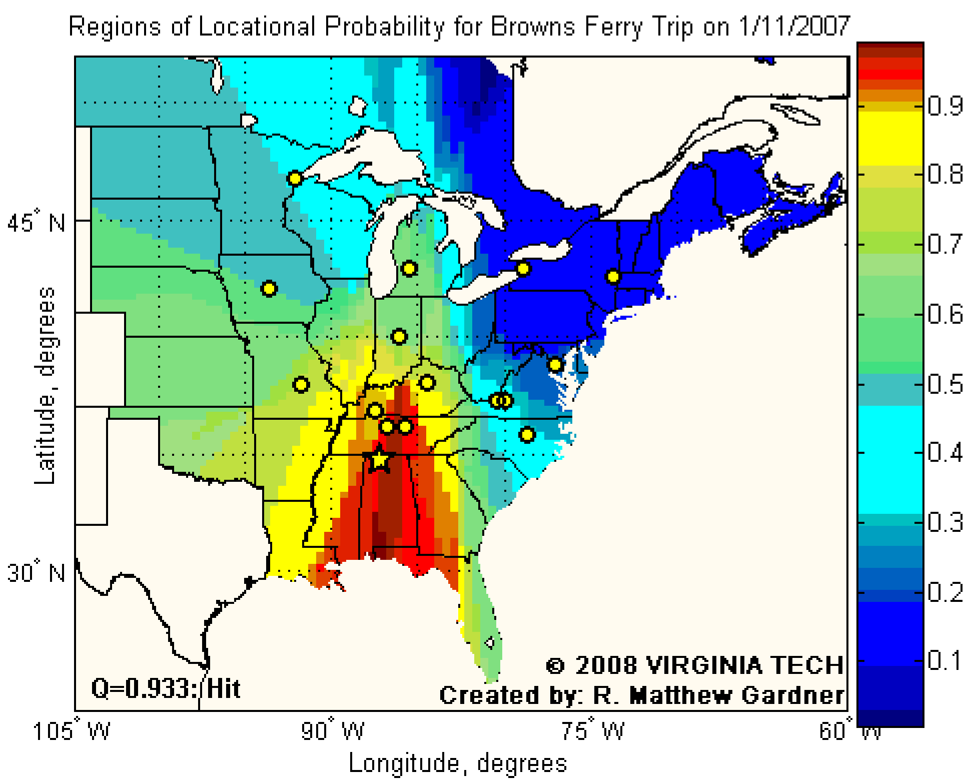
Regions of Locational Probability for Browns Ferry Trip on 1/11/2007
45° N
30° N
Latitude, degrees
105° W
90° W
75° W
60° W
Longitude, degrees
Q=0.933:/Hit
© 2008 VIRGINIA TECH
Created by: R. Matthew Gardner
0.9
0.8
0.7
0.6
0.5
0.4
0.3
0.2
0.1

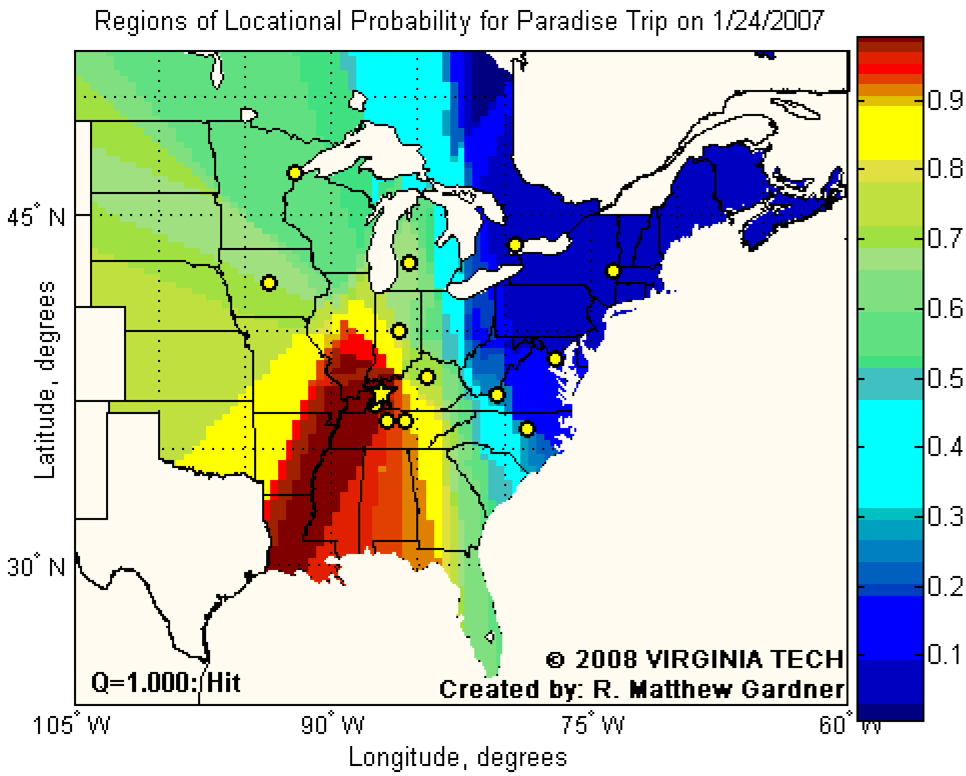
Regions of Locational Probability for Paradise Trip on 1/24/2007
45° N
30° N
Latitude, degrees
105° W
90° W
75° W
60° W
Longitude, degrees
Q=1.000:/Hit
© 2008 VIRGINIA TECH
Created by: R. Matthew Gardner
0.9
0.8
0.7
0.6
0.5
0.4
0.3
0.2
0.1

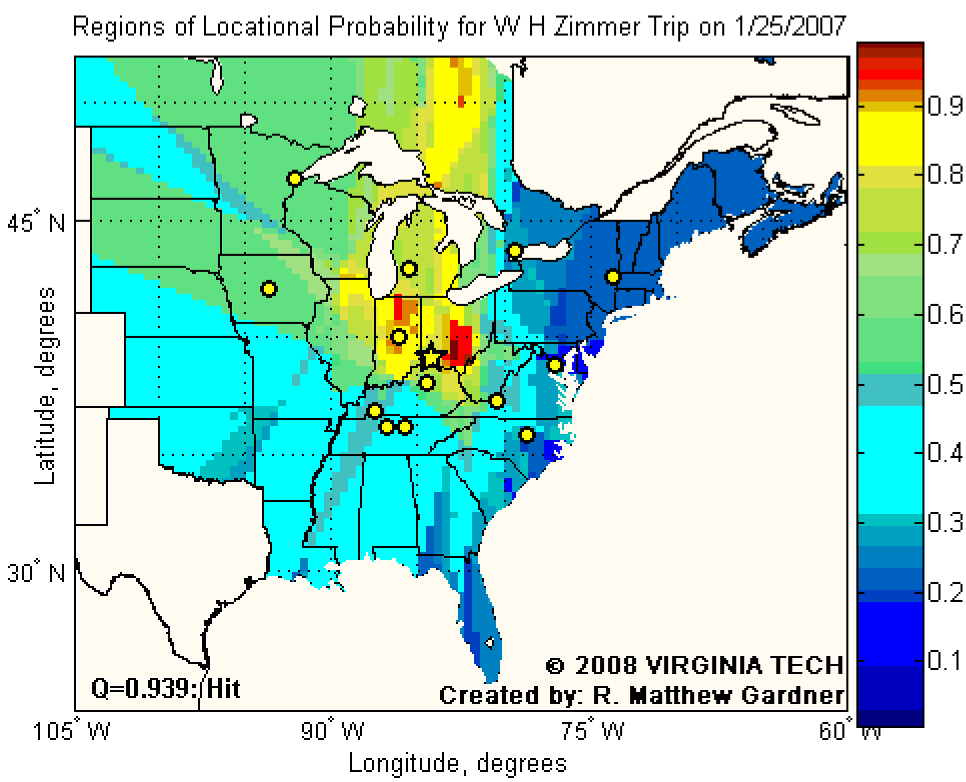
Regions of Locational Probability for W H Zimmer Trip on 1/25/2007
45° N
30° N
Latitude, degrees
105° W
90° W
75° W
60° W
Longitude, degrees
Q=0.939:/Hit
© 2008 VIRGINIA TECH
Created by: R. Matthew Gardner
0.9
0.8
0.7
0.6
0.5
0.4
0.3
0.2
0.1

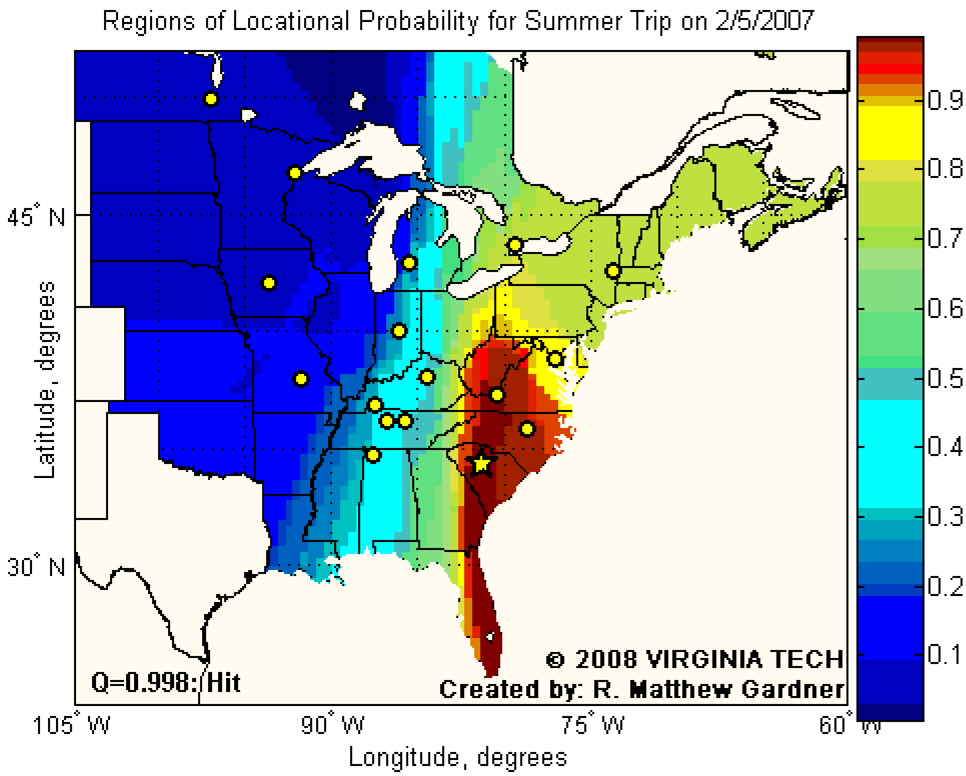
Regions of Locational Probability for Summer Trip on 2/5/2007
45° N
30° N
Latitude, degrees
105° W
90° W
75° W
60° W
Longitude, degrees
Q=0.998: Hit
© 2008 VIRGINIA TECH
Created by: R. Matthew Gardner
0.9
0.8
0.7
0.6
0.5
0.4
0.3
0.2
0.1

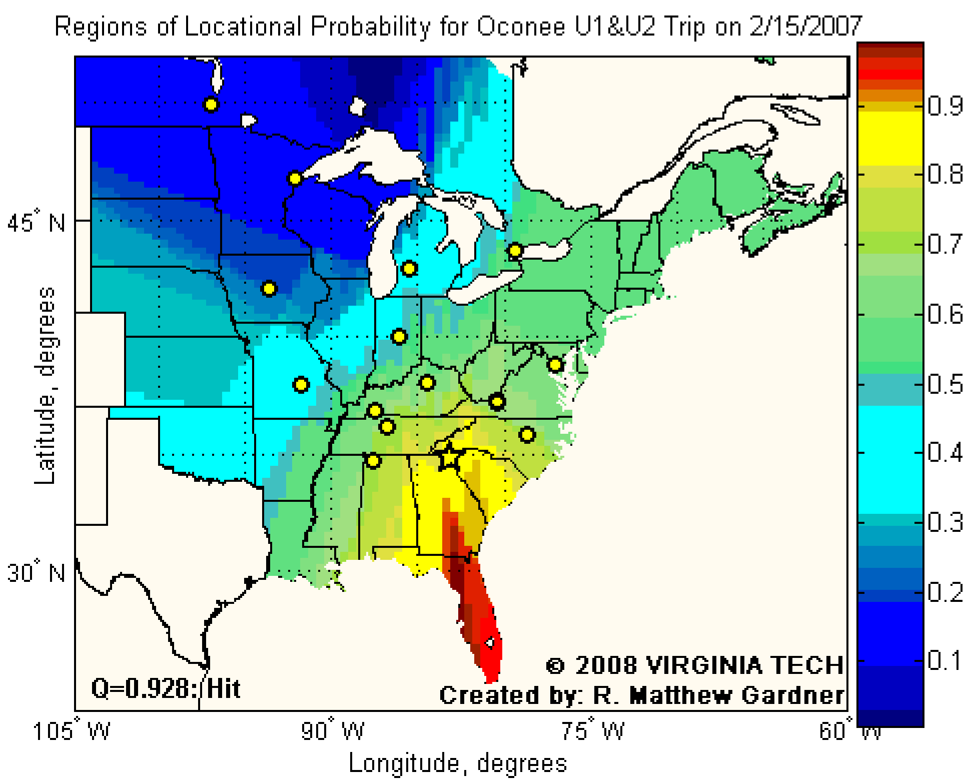
Regions of Locational Probability for Oconee U1&U2 Trip on 2/15/2007
45° N
30° N
Latitude, degrees
105° W
90° W
75° W
60° W
Longitude, degrees
Q=0.928: Hit
© 2008 VIRGINIA TECH
Created by: R. Matthew Gardner
0.9
0.8
0.7
0.6
0.5
0.4
0.3
0.2
0.1

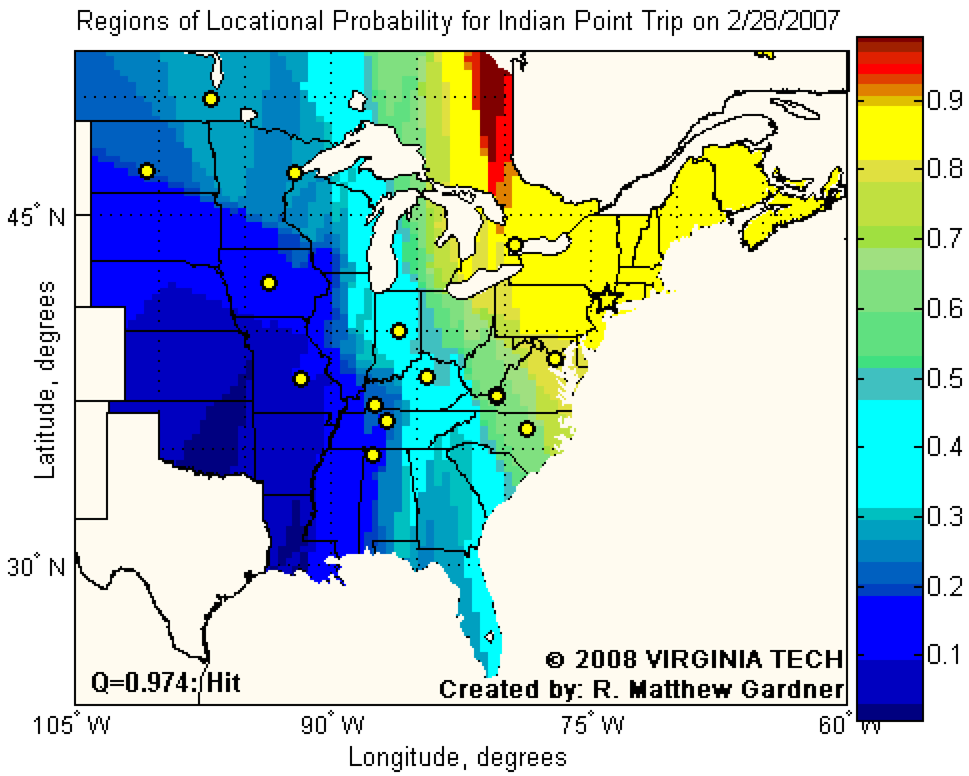
Regions of Locational Probability for Indian Point Trip on 2/28/2007
0.9
0.8
0.7
0.6
0.5
0.4
0.3
0.2
0.1
45° N
30° N
Latitude, degrees
Q=0.974: Hit
© 2008 VIRGINIA TECH
Created by: R. Matthew Gardner
105° W
90° W
75° W
60° W
Longitude, degrees

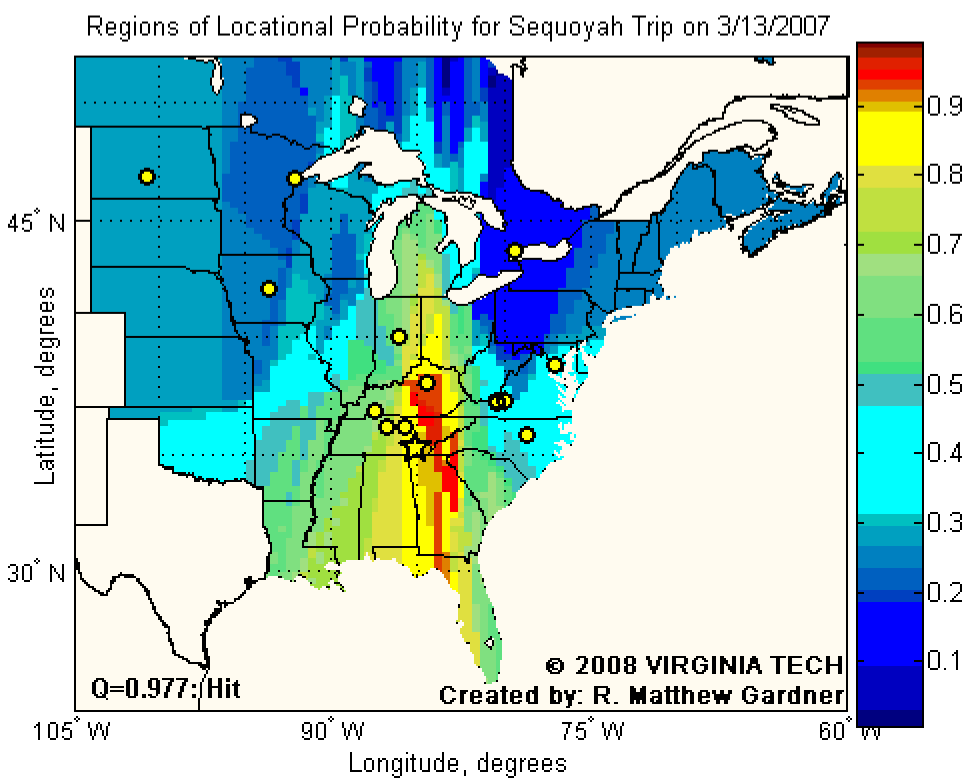
Regions of Locational Probability for Sequoyah Trip on 3/13/2007
0.9
0.8
0.7
0.6
0.5
0.4
0.3
0.2
0.1
45° N
30° N
Latitude, degrees
Q=0.977: Hit
© 2008 VIRGINIA TECH
Created by: R. Matthew Gardner
105° W
90° W
75° W
60° W
Longitude, degrees

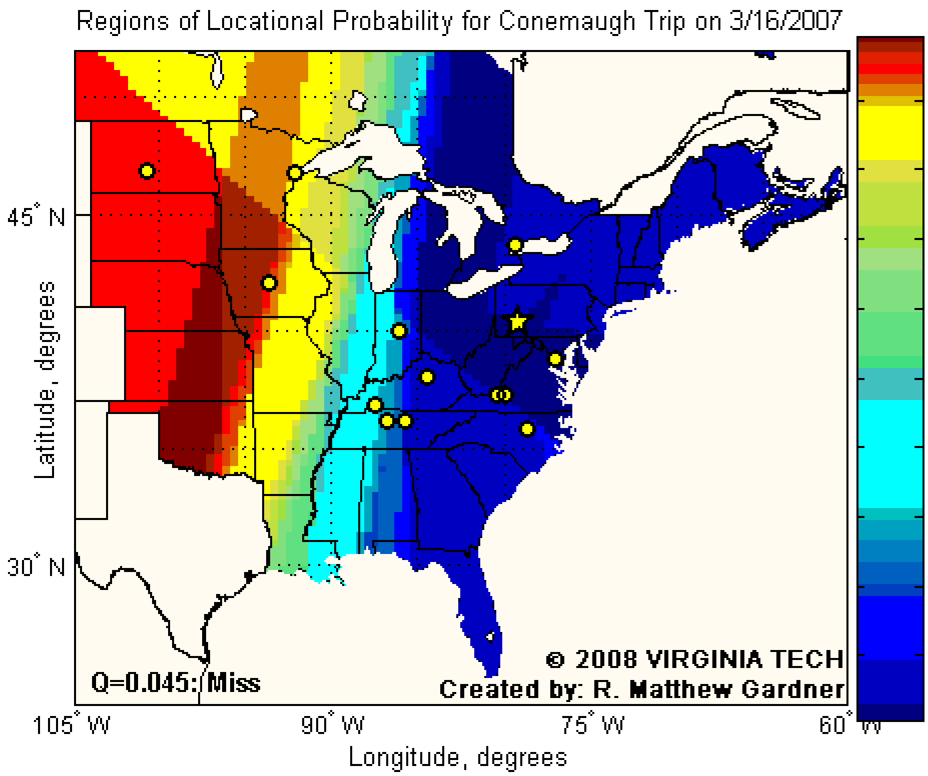
Regions of Locational Probability for Conemaugh Trip on 3/16/2007
45° N
30° N
Latitude, degrees
105° W
90° W
75° W
60° W
Longitude, degrees
Q=0.045: Miss
© 2008 VIRGINIA TECH
Created by: R. Matthew Gardner
0.9
0.8
0.7
0.6
0.5
0.4
0.3
0.2
0.1

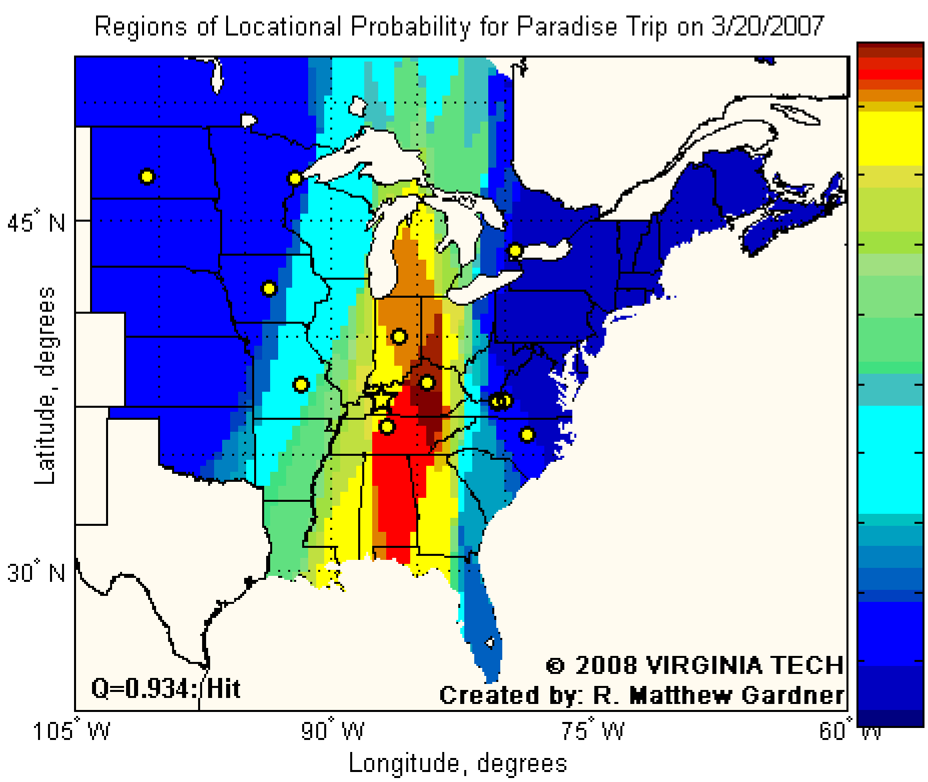
Regions of Locational Probability for Paradise Trip on 3/20/2007
45° N
30° N
Latitude, degrees
105° W
90° W
75° W
60° W
Longitude, degrees
Q=0.934: Hit
© 2008 VIRGINIA TECH
Created by: R. Matthew Gardner
0.9
0.8
0.7
0.6
0.5
0.4
0.3
0.2
0.1

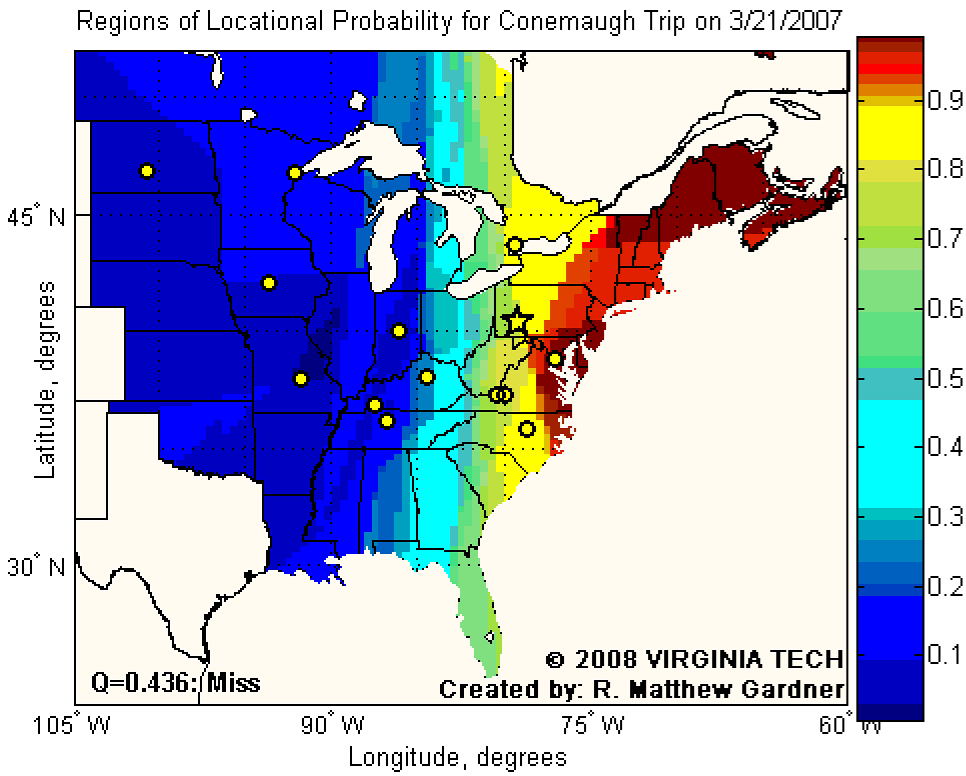
Regions of Locational Probability for Conemaugh Trip on 3/21/2007
45° N
30° N
Latitude, degrees
105° W
90° W
75° W
60° W
Longitude, degrees
Q=0.436: Miss
© 2008 VIRGINIA TECH
Created by: R. Matthew Gardner
0.9
0.8
0.7
0.6
0.5
0.4
0.3
0.2
0.1

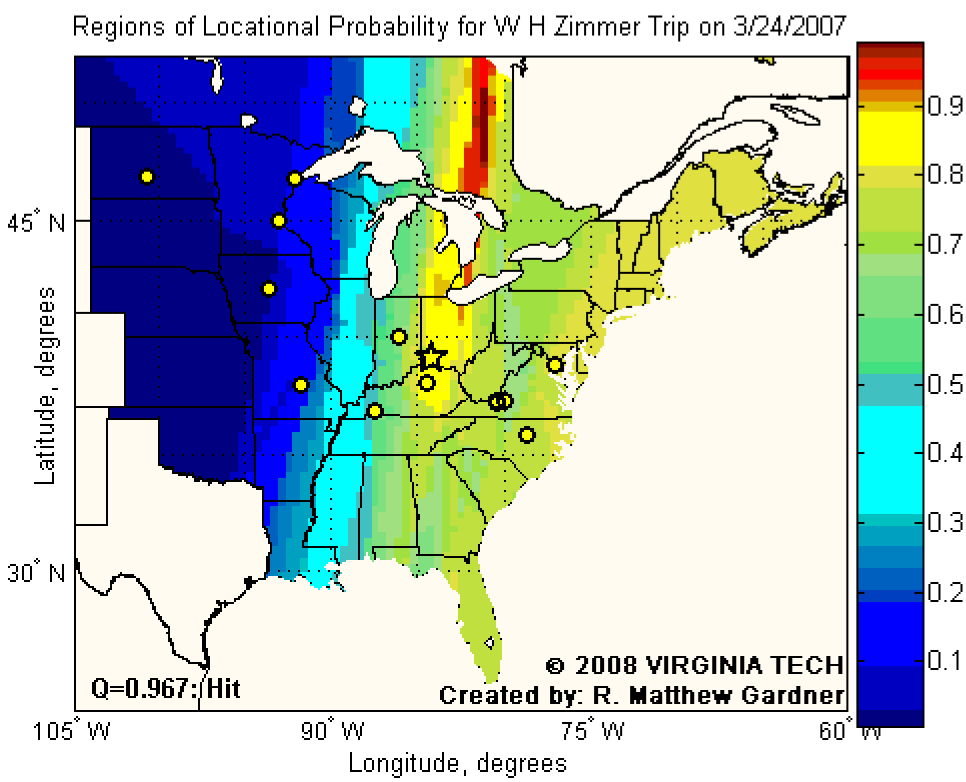
Regions of Locational Probability for W H Zimmer Trip on 3/24/2007
45° N
30° N
Latitude, degrees
105° W
90° W
75° W
60° W
Longitude, degrees
Q=0.967: Hit
© 2008 VIRGINIA TECH
Created by: R. Matthew Gardner
0.9
0.8
0.7
0.6
0.5
0.4
0.3
0.2
0.1

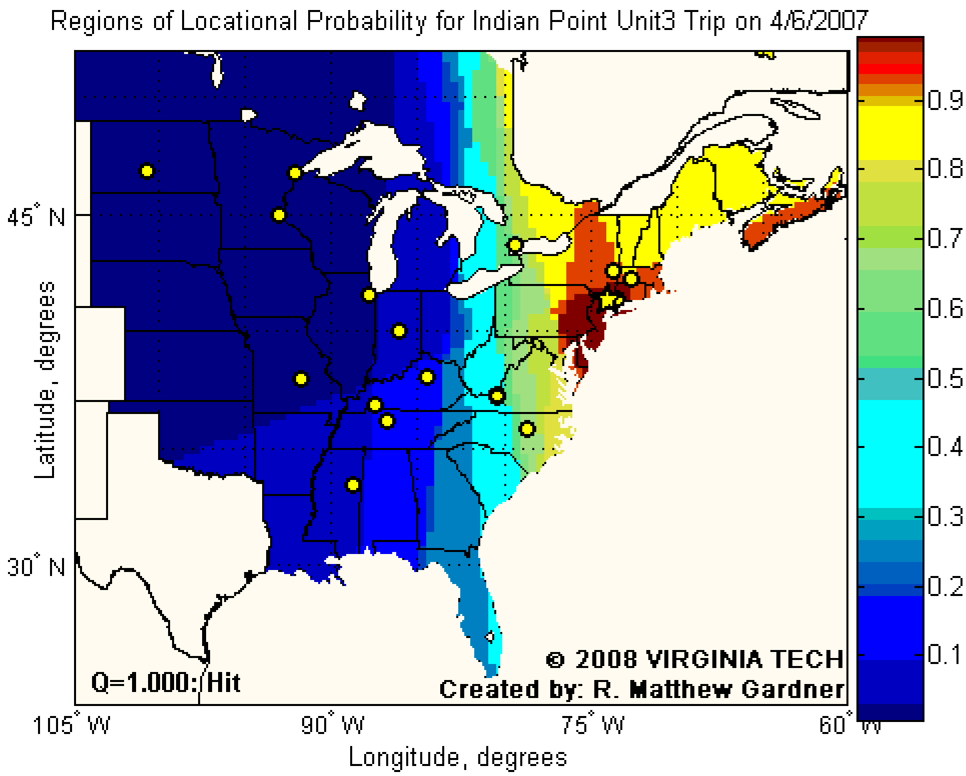
Regions of Locational Probability for Indian Point Unit3 Trip on 4/6/2007
Q=1.000:/Hit
© 2008 VIRGINIA TECH
Created by: R. Matthew Gardner
45° N
30° N
Latitude, degrees
105° W
90° W
75° W
60° W
Longitude, degrees
0.9
0.8
0.7
0.6
0.5
0.4
0.3
0.2
0.1

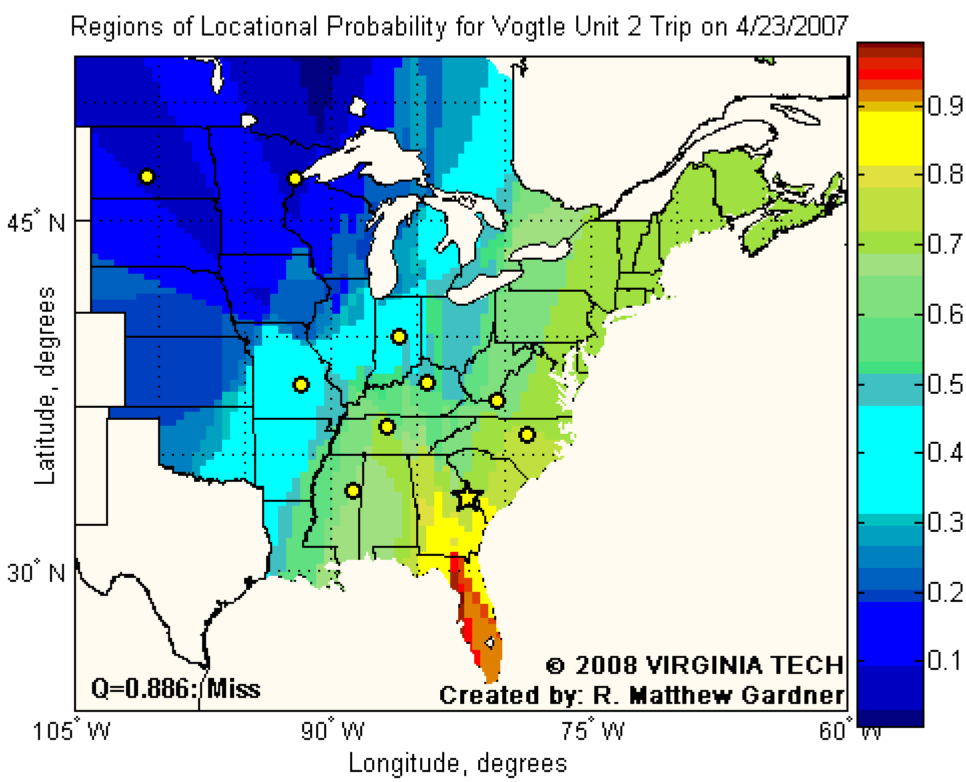
Regions of Locational Probability for Vogtle Unit 2 Trip on 4/23/2007
Q=0.886:/Miss
© 2008 VIRGINIA TECH
Created by: R. Matthew Gardner
45° N
30° N
Latitude, degrees
105° W
90° W
75° W
60° W
Longitude, degrees
0.9
0.8
0.7
0.6
0.5
0.4
0.3
0.2
0.1

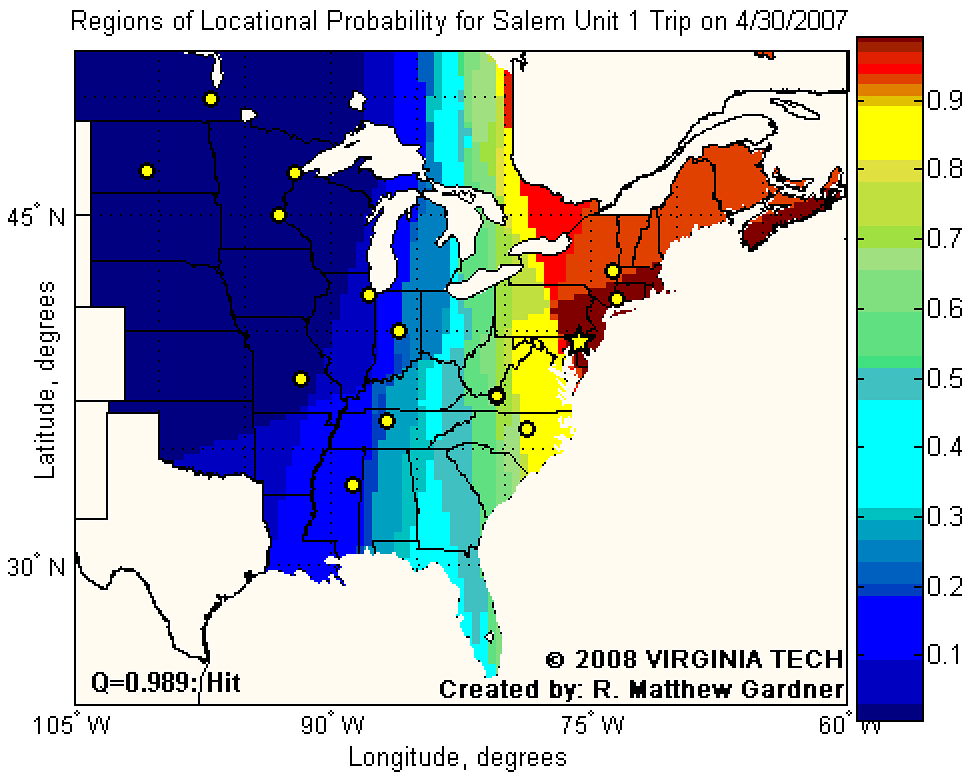
Regions of Locational Probability for Salem Unit 1 Trip on 4/30/2007
45° N
30° N
Latitude, degrees
105° W
90° W
75° W
60° W
Longitude, degrees
0.9
0.8
0.7
0.6
0.5
0.4
0.3
0.2
0.1
Q=0.989: Hit
© 2008 VIRGINIA TECH
Created by: R. Matthew Gardner

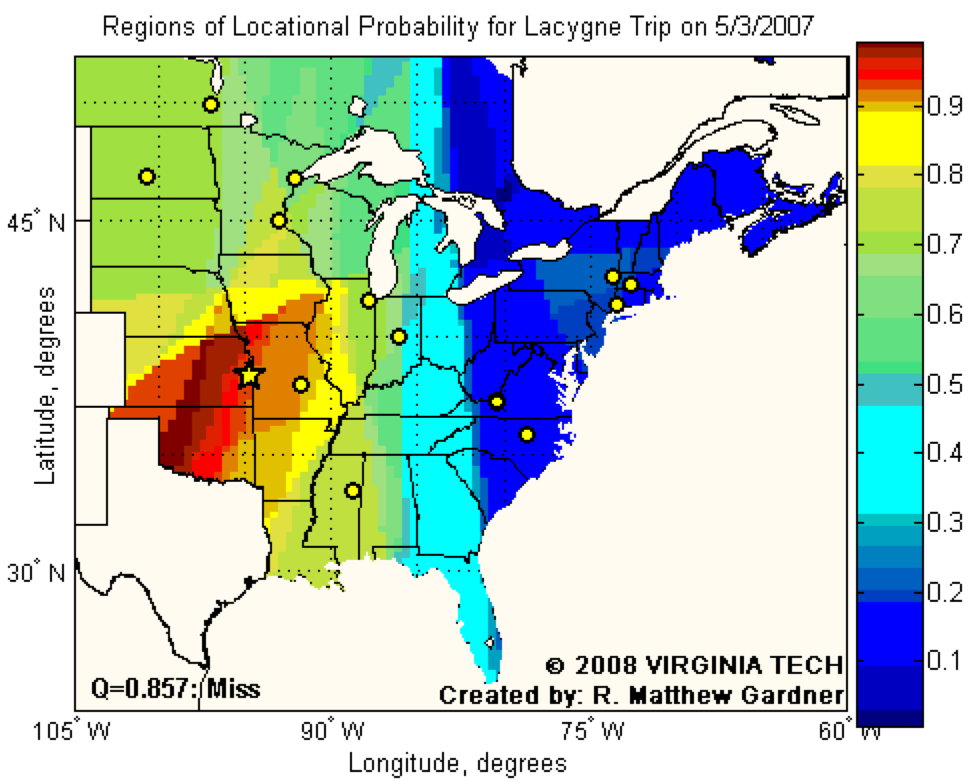
Regions of Locational Probability for Lacygne Trip on 5/3/2007
45° N
30° N
Latitude, degrees
105° W
90° W
75° W
60° W
Longitude, degrees
0.9
0.8
0.7
0.6
0.5
0.4
0.3
0.2
0.1
Q=0.857: Miss
© 2008 VIRGINIA TECH
Created by: R. Matthew Gardner

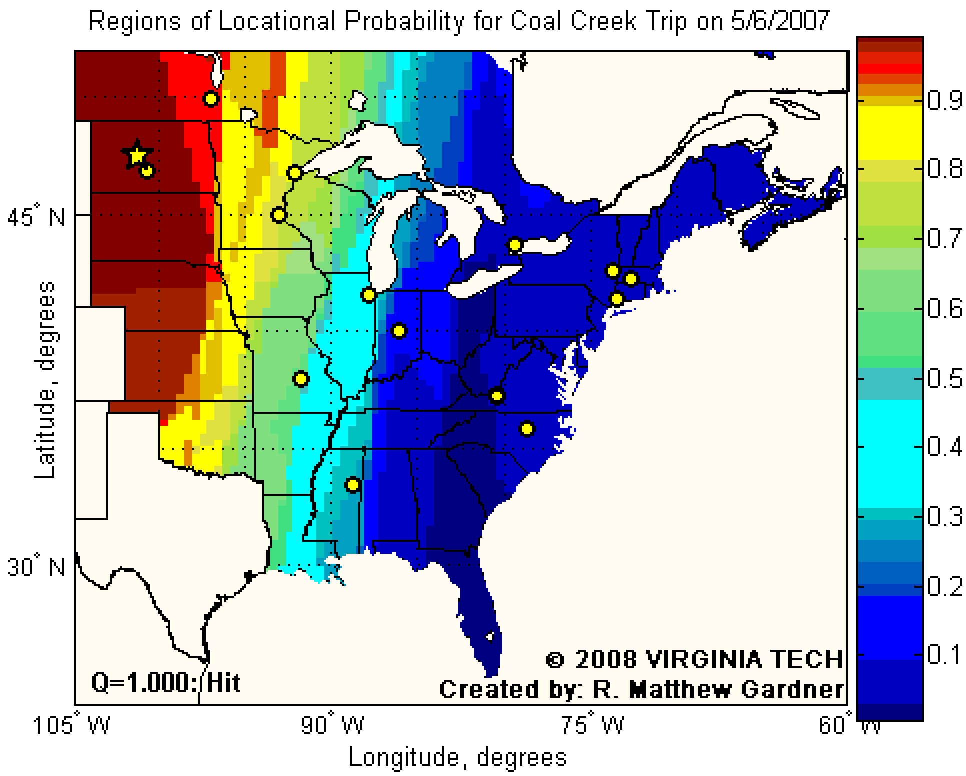
Regions of Locational Probability for Coal Creek Trip on 5/6/2007
45° N
30° N
Latitude, degrees
105° W
90° W
75° W
60° W
Longitude, degrees
Q=1.000: Hit
© 2008 VIRGINIA TECH
Created by: R. Matthew Gardner
0.9
0.8
0.7
0.6
0.5
0.4
0.3
0.2
0.1

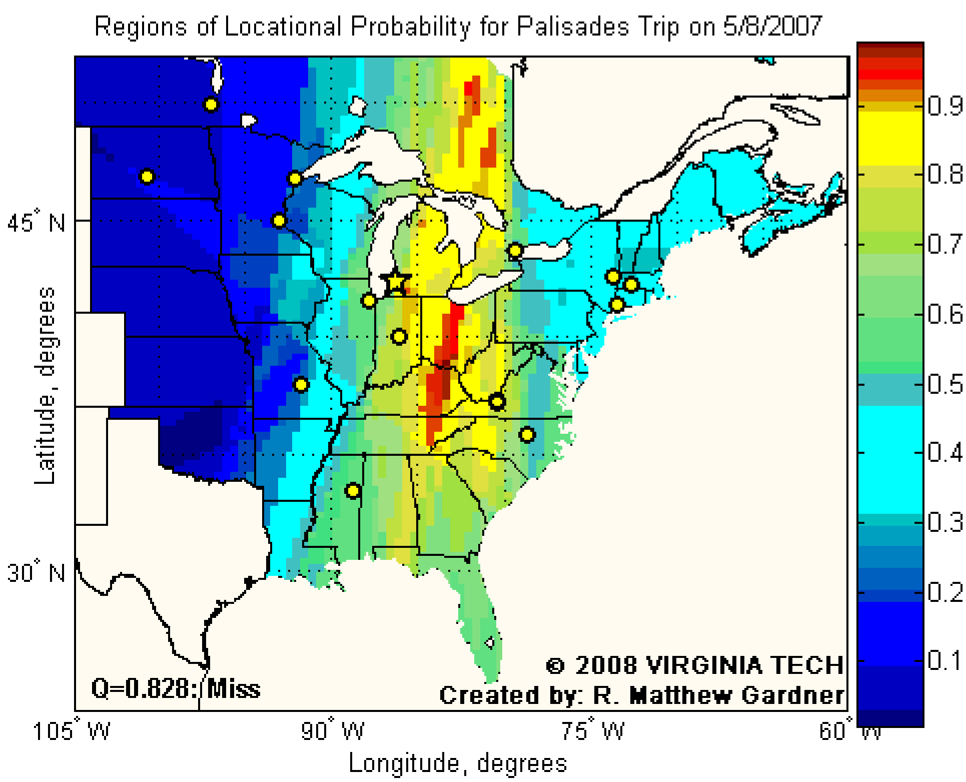
Regions of Locational Probability for Palisades Trip on 5/8/2007
45° N
30° N
Latitude, degrees
105° W
90° W
75° W
60° W
Longitude, degrees
Q=0.828: Miss
© 2008 VIRGINIA TECH
Created by: R. Matthew Gardner
0.9
0.8
0.7
0.6
0.5
0.4
0.3
0.2
0.1

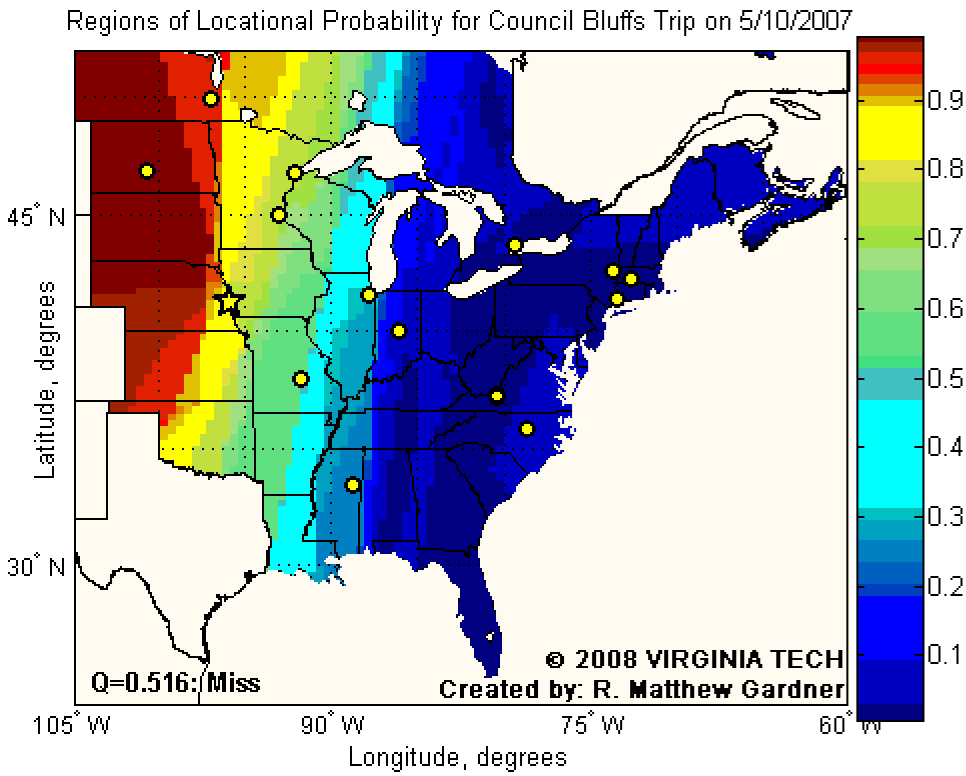
Regions of Locational Probability for Council Bluffs Trip on 5/10/2007
Latitude, degrees
45° N
30° N
105° W
90° W
75° W
60° W
Longitude, degrees
Q=0.516: Miss
© 2008 VIRGINIA TECH
Created by: R. Matthew Gardner
0.9
0.8
0.7
0.6
0.5
0.4
0.3
0.2
0.1

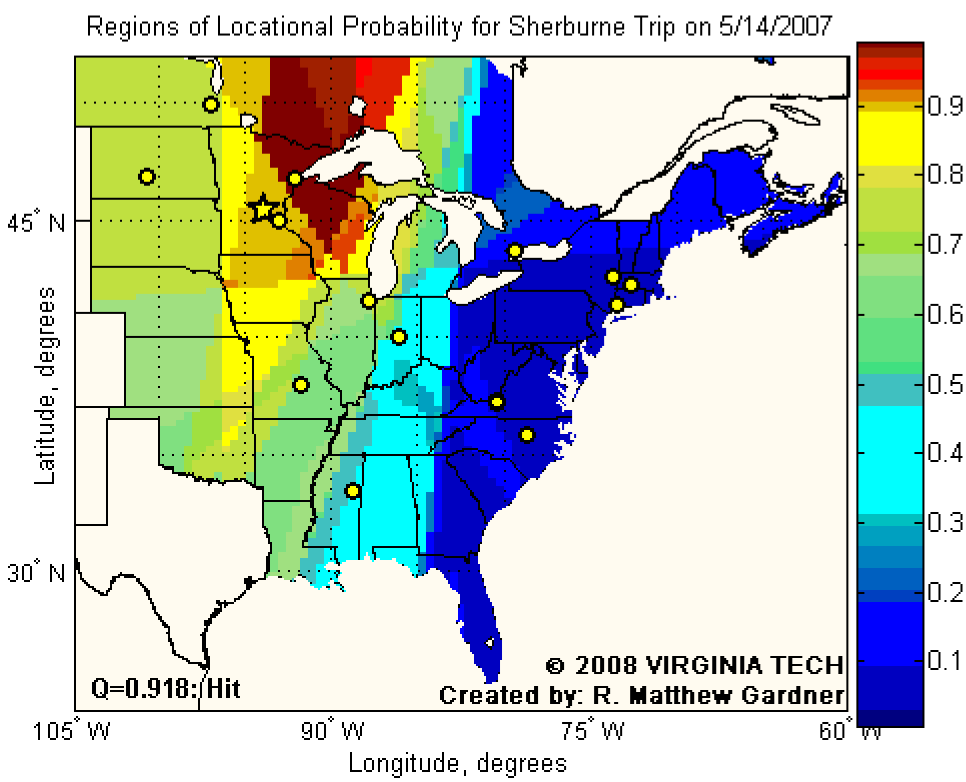
Regions of Locational Probability for Sherburne Trip on 5/14/2007
Latitude, degrees
45° N
30° N
105° W
90° W
75° W
60° W
Longitude, degrees
Q=0.918: Hit
© 2008 VIRGINIA TECH
Created by: R. Matthew Gardner
0.9
0.8
0.7
0.6
0.5
0.4
0.3
0.2
0.1

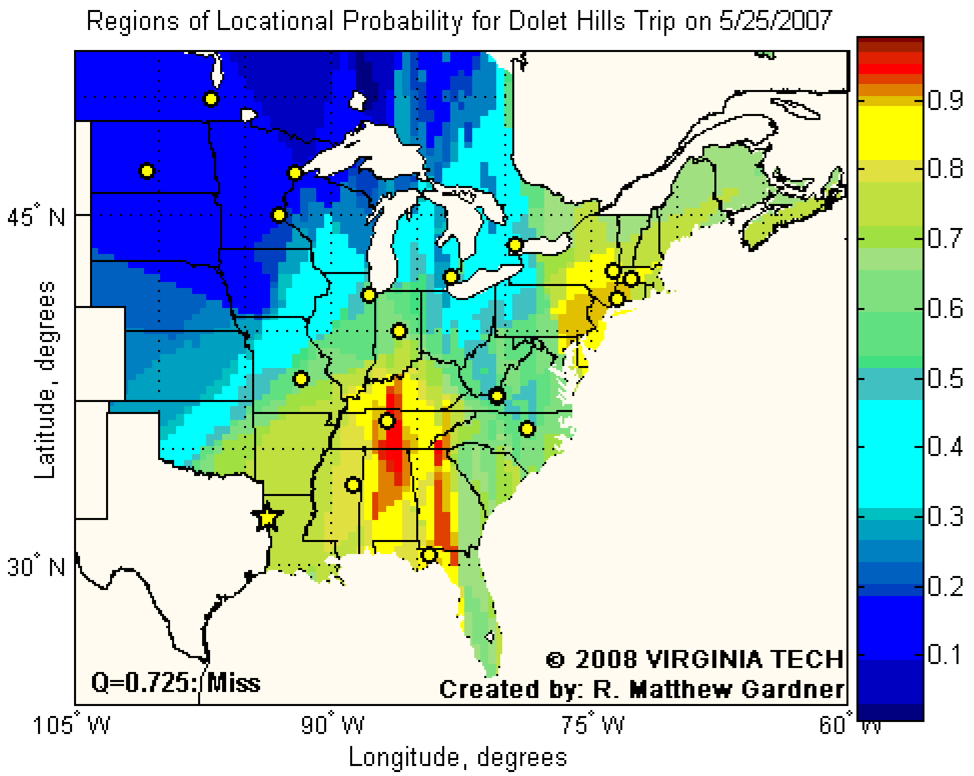
Regions of Locational Probability for Dolet Hills Trip on 5/25/2007
Latitude, degrees
45° N
30° N
105° W
90° W
75° W
60° W
Longitude, degrees
0.9
0.8
0.7
0.6
0.5
0.4
0.3
0.2
0.1
Q=0.725: Miss
© 2008 VIRGINIA TECH
Created by: R. Matthew Gardner

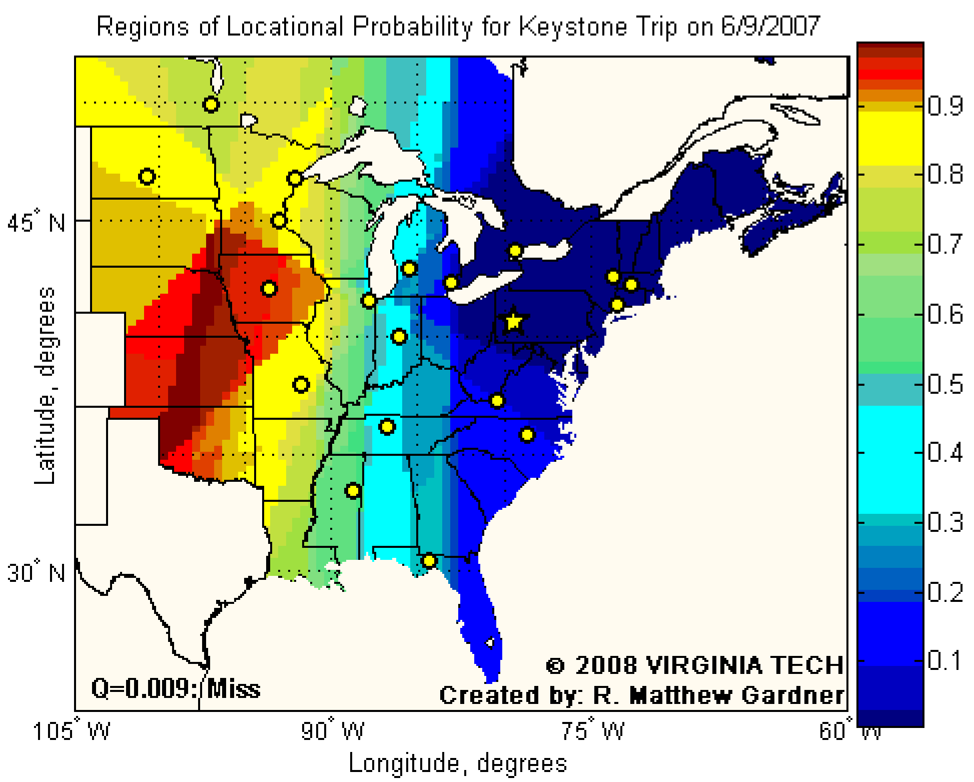
Regions of Locational Probability for Keystone Trip on 6/9/2007
Latitude, degrees
45° N
30° N
105° W
90° W
75° W
60° W
Longitude, degrees
0.9
0.8
0.7
0.6
0.5
0.4
0.3
0.2
0.1
Q=0.009: Miss
© 2008 VIRGINIA TECH
Created by: R. Matthew Gardner

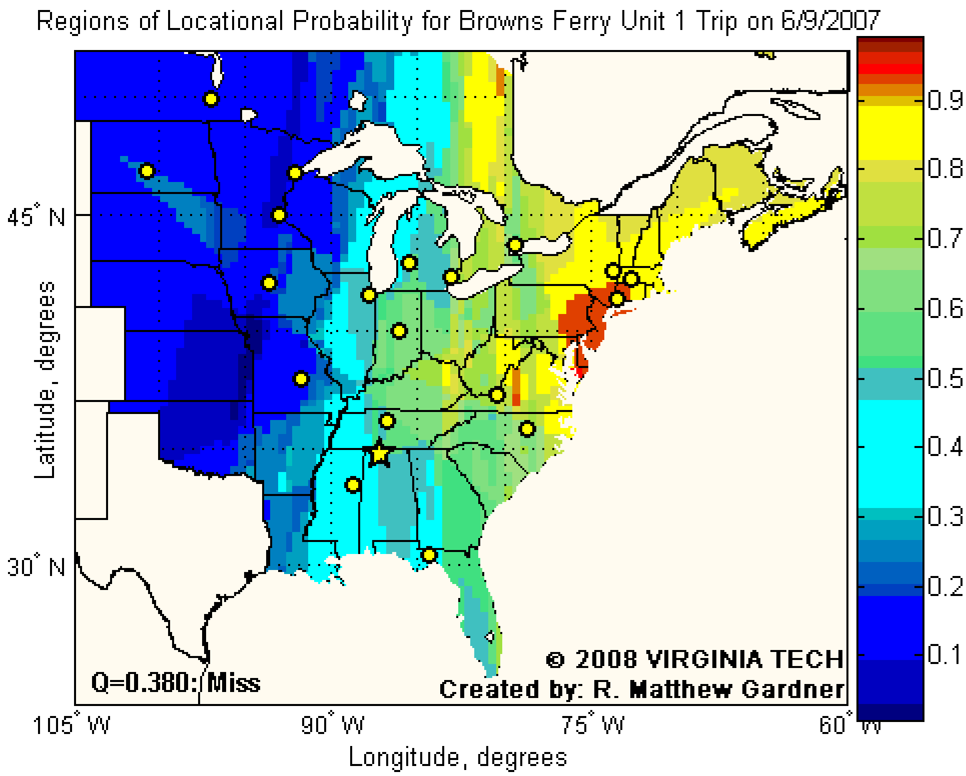
Regions of Locational Probability for Browns Ferry Unit 1 Trip on 6/9/2007
45° N
30° N
Latitude, degrees
105° W
90° W
75° W
60° W
Longitude, degrees
0.9
0.8
0.7
0.6
0.5
0.4
0.3
0.2
0.1
Q=0.380:/Miss
© 2008 VIRGINIA TECH
Created by: R. Matthew Gardner

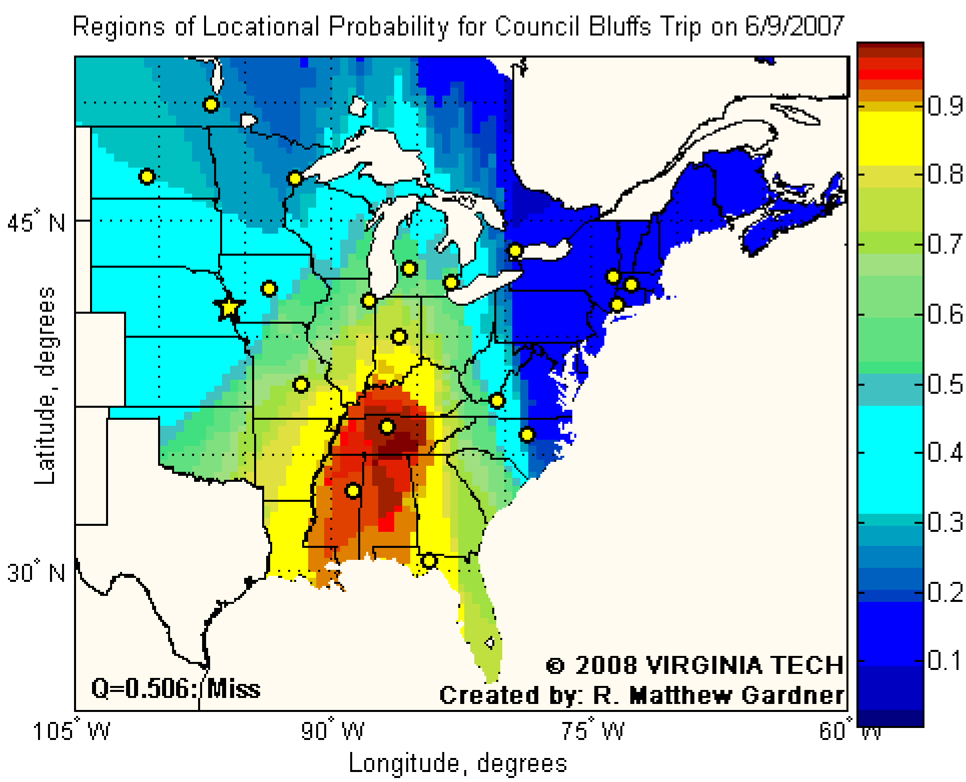
Regions of Locational Probability for Council Bluffs Trip on 6/9/2007
45° N
30° N
Latitude, degrees
105° W
90° W
75° W
60° W
Longitude, degrees
0.9
0.8
0.7
0.6
0.5
0.4
0.3
0.2
0.1
Q=0.506:/Miss
© 2008 VIRGINIA TECH
Created by: R. Matthew Gardner

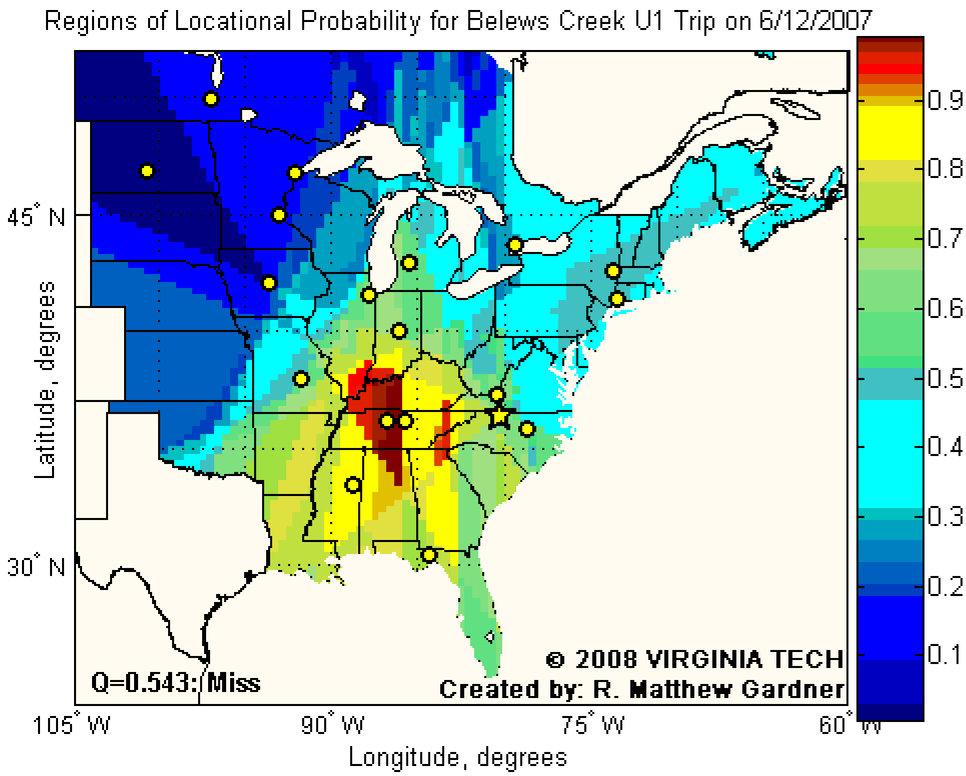
Regions of Locational Probability for Belews Creek U1 Trip on 6/12/2007
45° N
30° N
Latitude, degrees
105° W
90° W
75° W
60° W
Longitude, degrees
0.9
0.8
0.7
0.6
0.5
0.4
0.3
0.2
0.1
Q=0.543:/Miss
© 2008 VIRGINIA TECH
Created by: R. Matthew Gardner

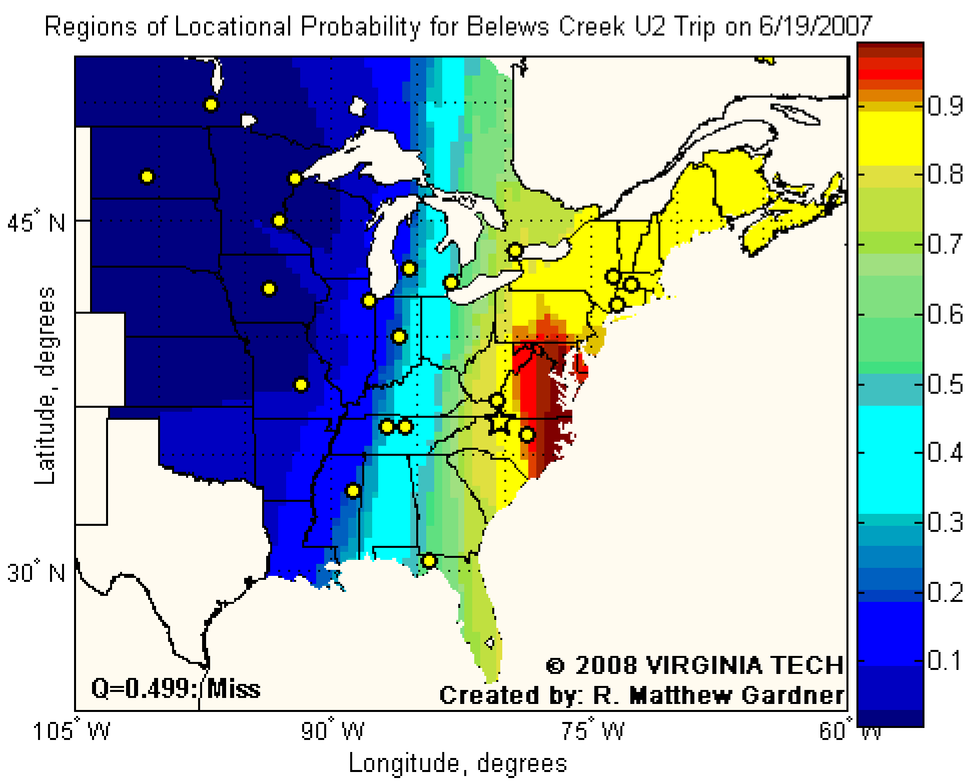
Regions of Locational Probability for Belews Creek U2 Trip on 6/19/2007
45° N
30° N
Latitude, degrees
105° W
90° W
75° W
60° W
Longitude, degrees
0.9
0.8
0.7
0.6
0.5
0.4
0.3
0.2
0.1
Q=0.499:/Miss
© 2008 VIRGINIA TECH
Created by: R. Matthew Gardner

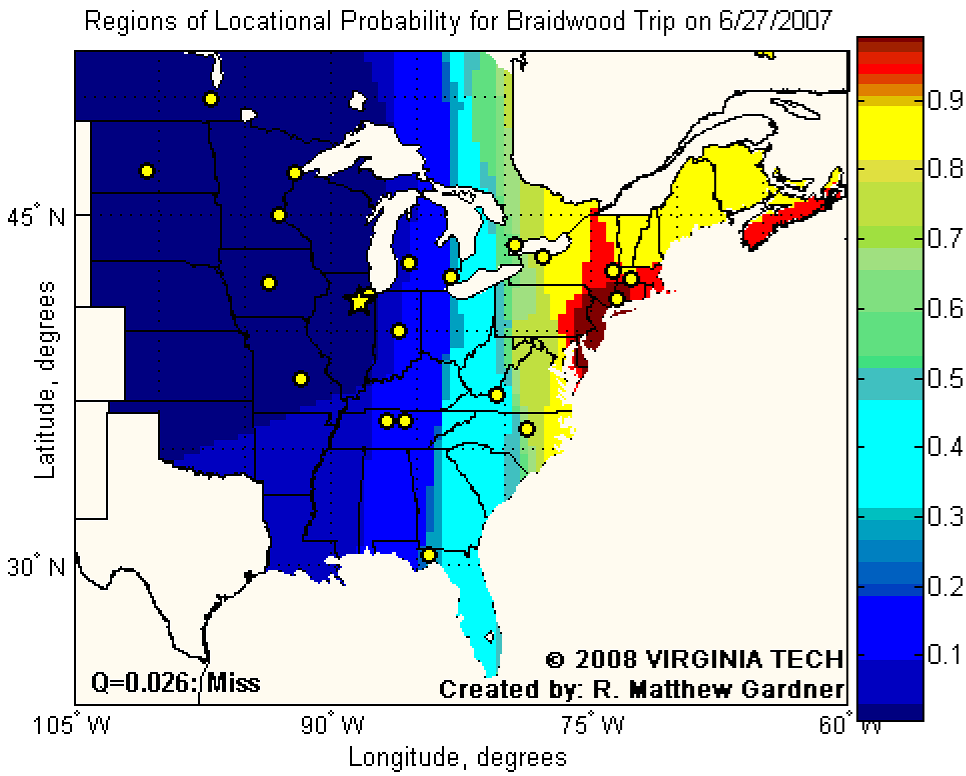
Regions of Locational Probability for Braidwood Trip on 6/27/2007
45° N
30° N
Latitude, degrees
105° W
90° W
75° W
60° W
Longitude, degrees
Q=0.026: Miss
© 2008 VIRGINIA TECH
Created by: R. Matthew Gardner
0.9
0.8
0.7
0.6
0.5
0.4
0.3
0.2
0.1

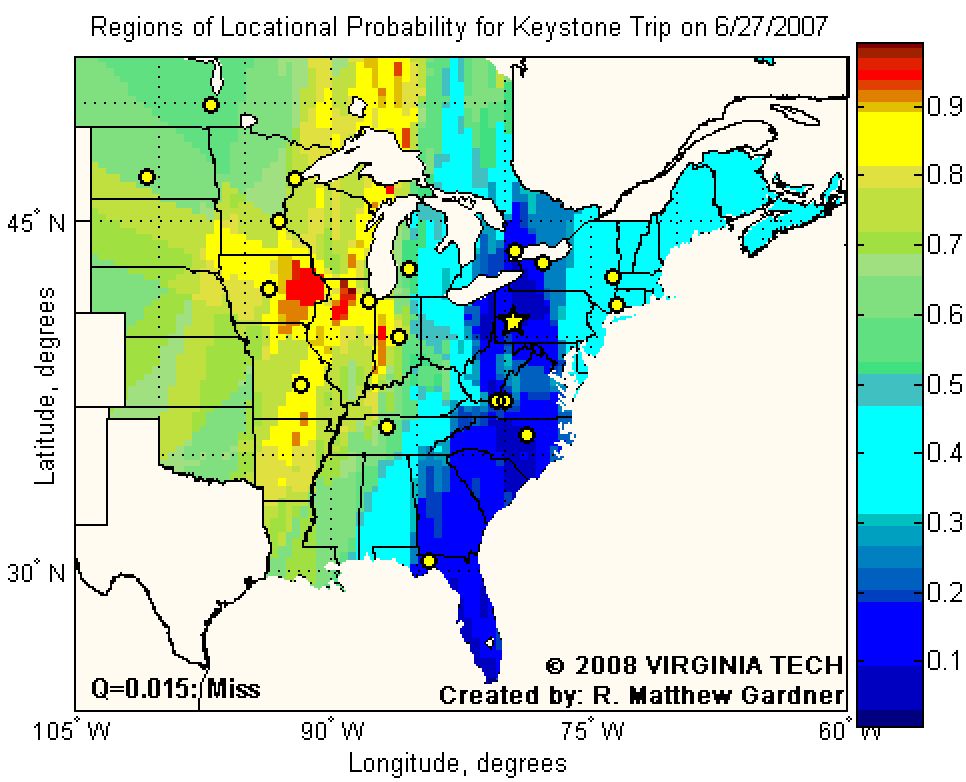
Regions of Locational Probability for Keystone Trip on 6/27/2007
45° N
30° N
Latitude, degrees
105° W
90° W
75° W
60° W
Longitude, degrees
Q=0.015: Miss
© 2008 VIRGINIA TECH
Created by: R. Matthew Gardner
0.9
0.8
0.7
0.6
0.5
0.4
0.3
0.2
0.1

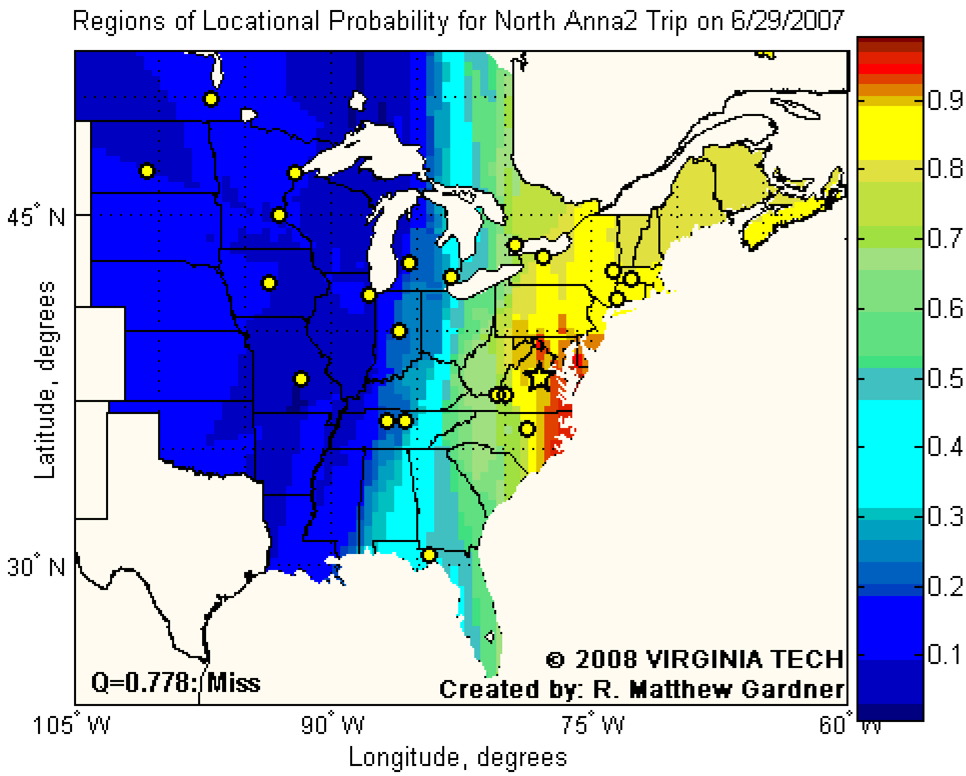

Regions of Locational Probability for North Anna2 Trip on 6/29/2007
45° N
30° N
Latitude, degrees
105° W
90° W
75° W
60° W
Longitude, degrees
Q=0.778: Miss
© 2008 VIRGINIA TECH
Created by: R. Matthew Gardner
0.9
0.8
0.7
0.6
0.5
0.4
0.3
0.2
0.1

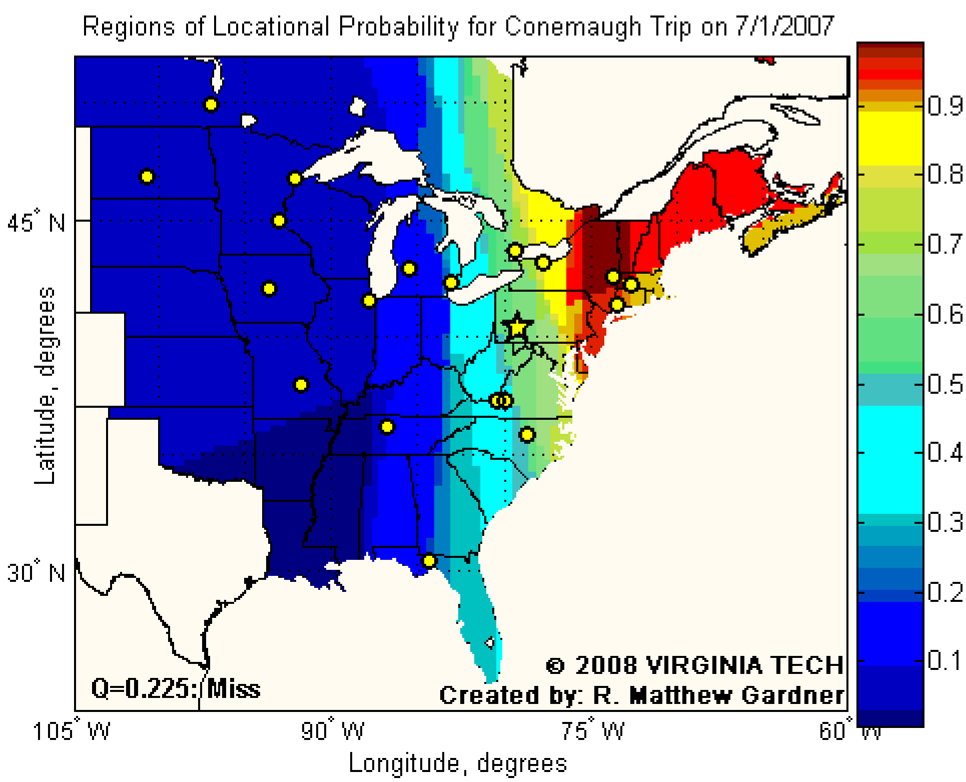

Regions of Locational Probability for Conemaugh Trip on 7/1/2007
45° N
30° N
Latitude, degrees
105° W
90° W
75° W
60° W
Longitude, degrees
Q=0.225: Miss
© 2008 VIRGINIA TECH
Created by: R. Matthew Gardner
0.9
0.8
0.7
0.6
0.5
0.4
0.3
0.2
0.1

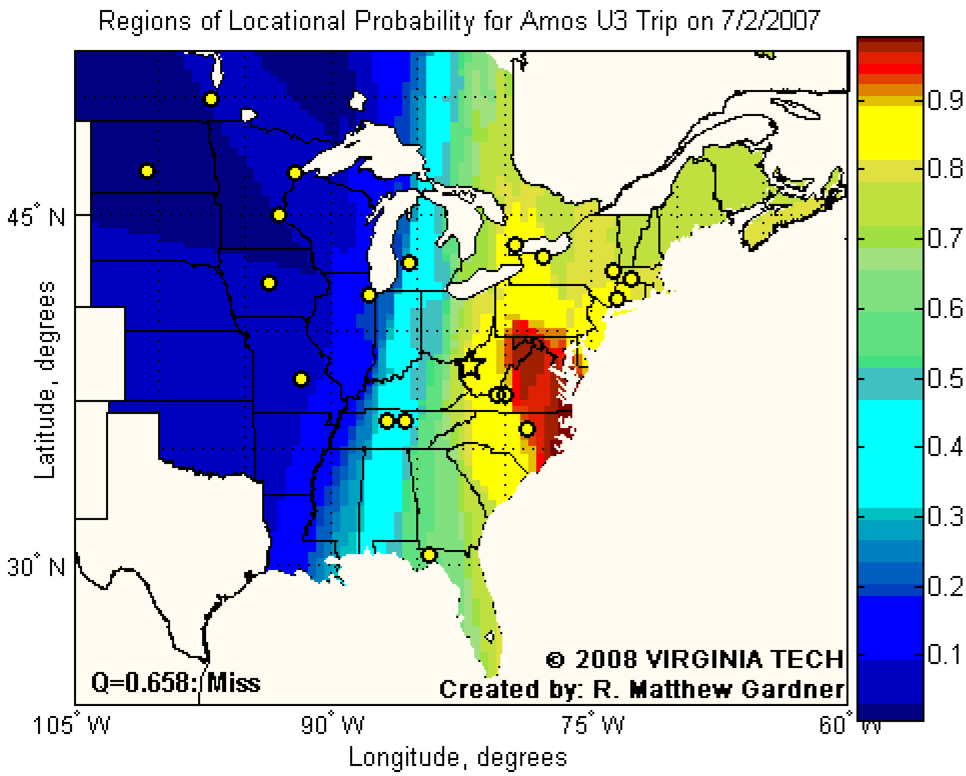
Regions of Locational Probability for Amos U3 Trip on 7/2/2007
45° N
30° N
Latitude, degrees
105° W
90° W
75° W
60° W
Longitude, degrees
Q=0.658: Miss
© 2008 VIRGINIA TECH
Created by: R. Matthew Gardner
0.9
0.8
0.7
0.6
0.5
0.4
0.3
0.2
0.1

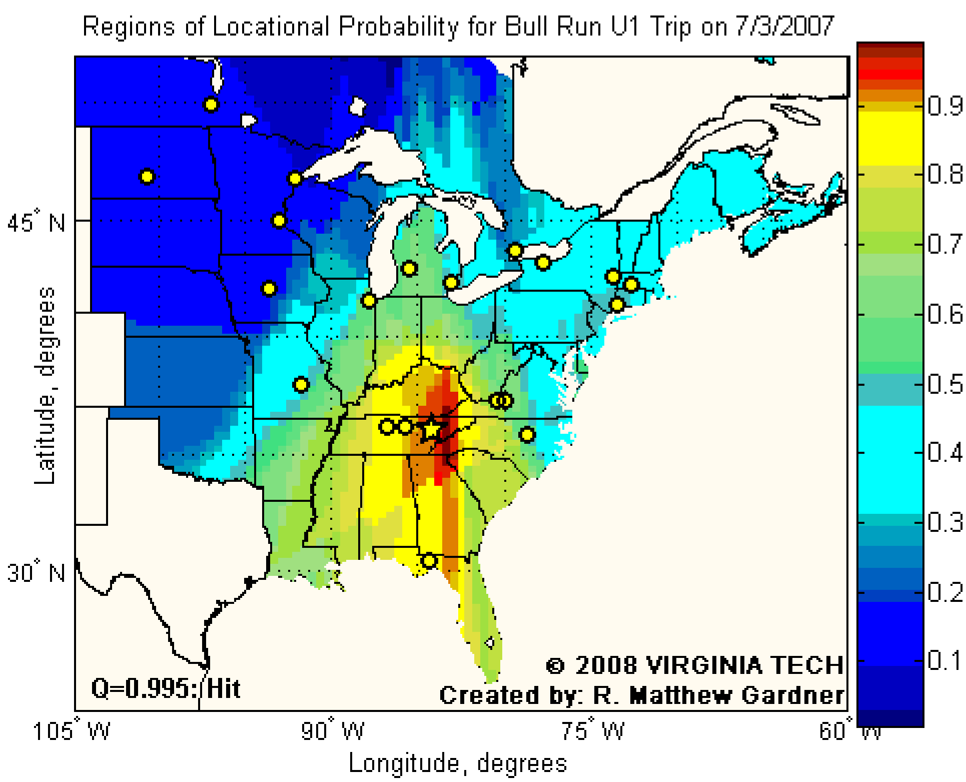
Regions of Locational Probability for Bull Run U1 Trip on 7/3/2007
45° N
30° N
Latitude, degrees
105° W
90° W
75° W
60° W
Longitude, degrees
Q=0.995: Hit
© 2008 VIRGINIA TECH
Created by: R. Matthew Gardner
0.9
0.8
0.7
0.6
0.5
0.4
0.3
0.2
0.1

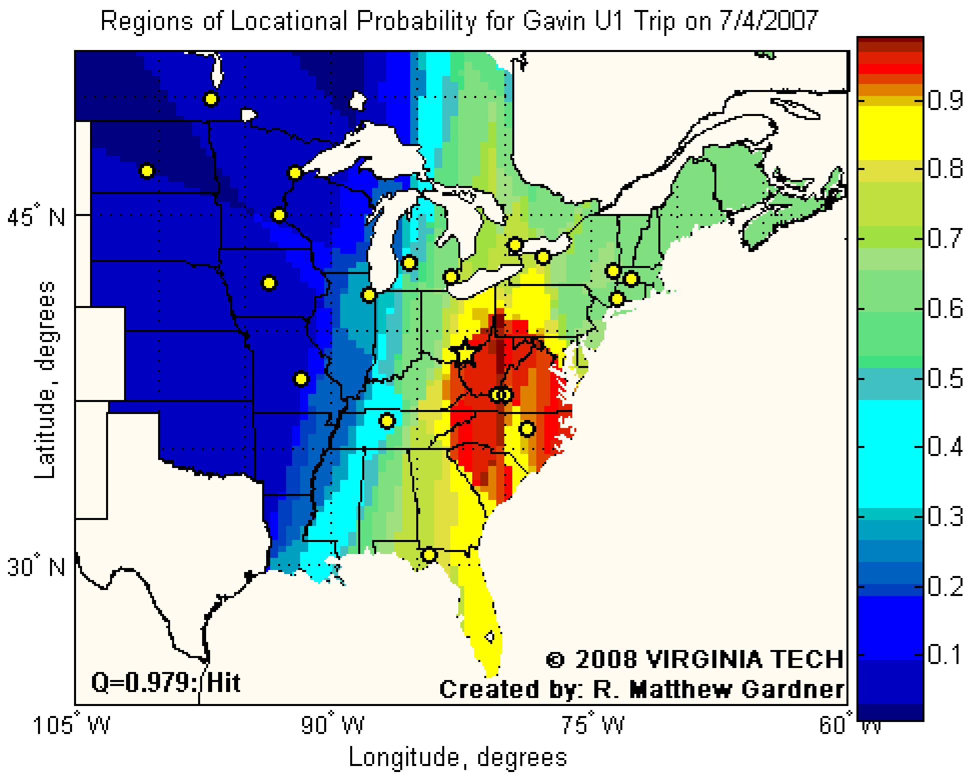
Regions of Locational Probability for Gavin U1 Trip on 7/4/2007
45° N
30° N
Latitude, degrees
105° W
90° W
75° W
60° W
Longitude, degrees
Q=0.979: Hit
© 2008 VIRGINIA TECH
Created by: R. Matthew Gardner
0.1
0.2
0.3
0.4
0.5
0.6
0.7
0.8
0.9

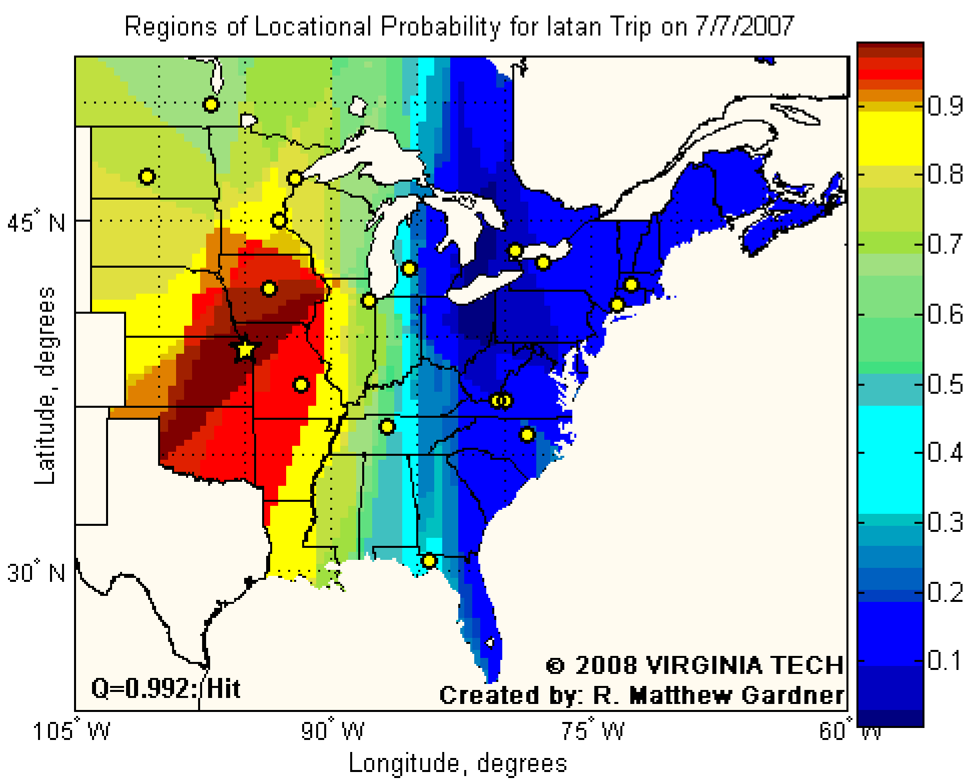
Regions of Locational Probability for Iatan Trip on 7/7/2007
45° N
30° N
Latitude, degrees
105° W
90° W
75° W
60° W
Longitude, degrees
Q=0.992: Hit
© 2008 VIRGINIA TECH
Created by: R. Matthew Gardner
0.1
0.2
0.3
0.4
0.5
0.6
0.7
0.8
0.9

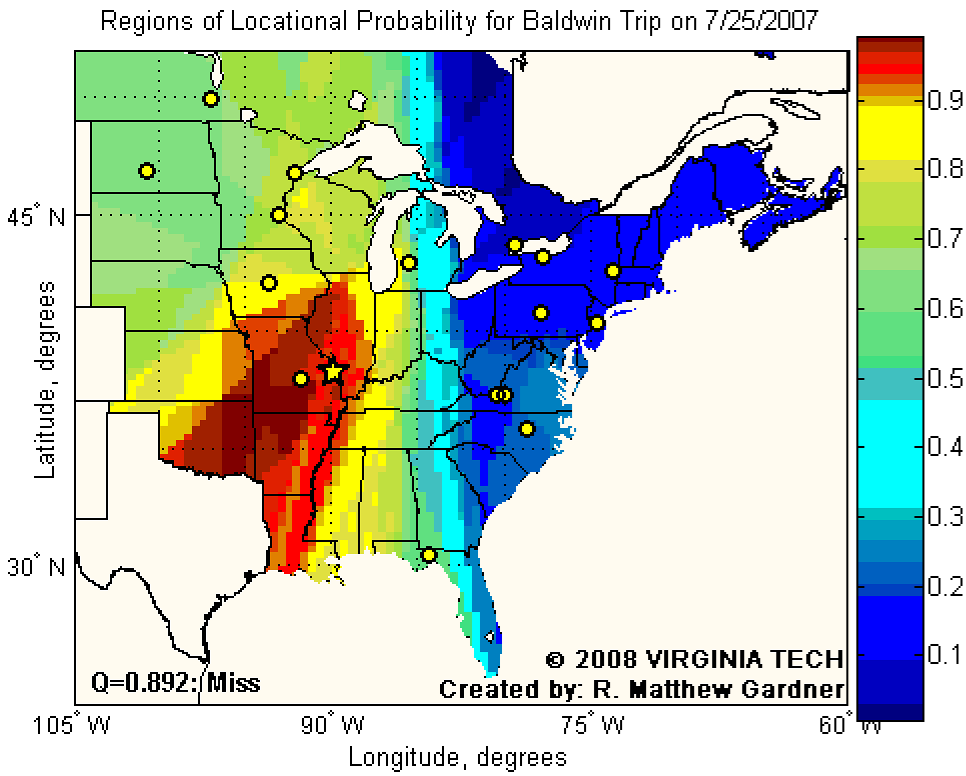
Regions of Locational Probability for Baldwin Trip on 7/25/2007
45° N
30° N
Latitude, degrees
105° W
90° W
75° W
60° W
Longitude, degrees
Q=0.892: Miss
© 2008 VIRGINIA TECH
Created by: R. Matthew Gardner
0.9
0.8
0.7
0.6
0.5
0.4
0.3
0.2
0.1

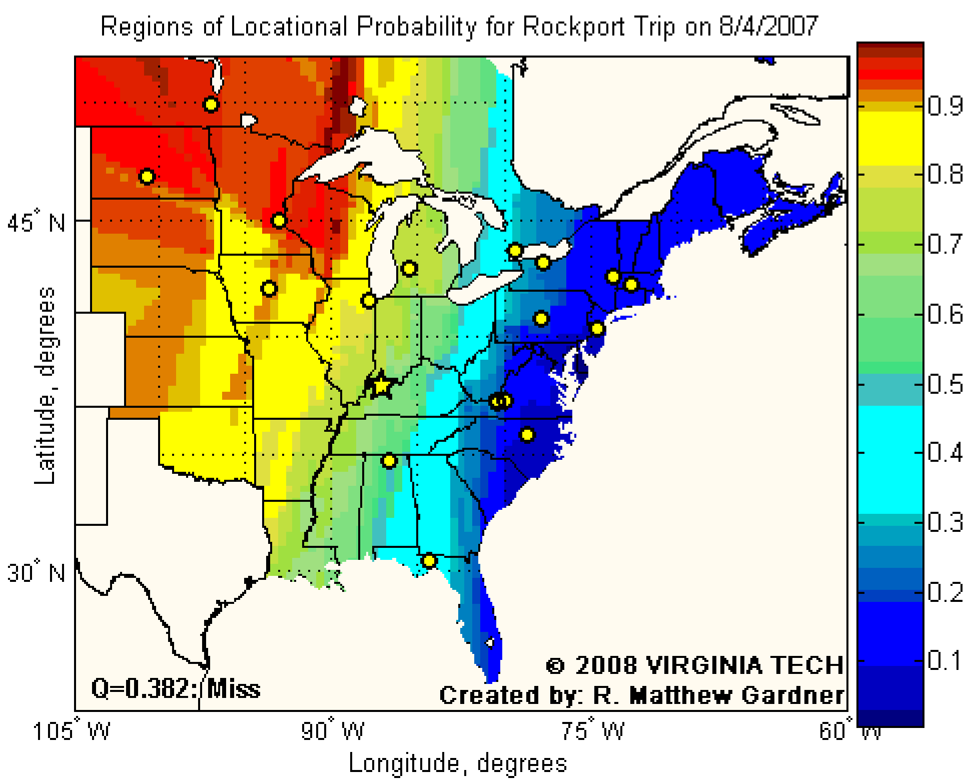
Regions of Locational Probability for Rockport Trip on 8/4/2007
45° N
30° N
Latitude, degrees
105° W
90° W
75° W
60° W
Longitude, degrees
Q=0.382: Miss
© 2008 VIRGINIA TECH
Created by: R. Matthew Gardner
0.9
0.8
0.7
0.6
0.5
0.4
0.3
0.2
0.1

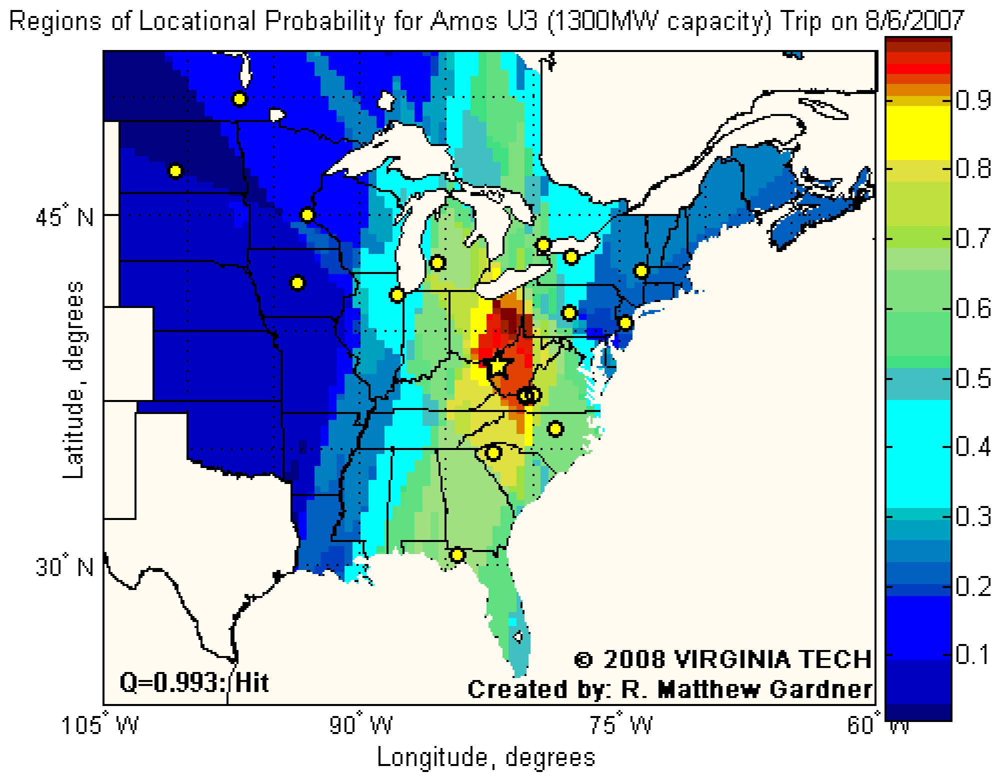
Regions of Locational Probability for Amos U3 (1300MW capacity) Trip on 8/6/2007
45° N
30° N
Latitude, degrees
105° W
90° W
75° W
60° W
Longitude, degrees
0.9
0.8
0.7
0.6
0.5
0.4
0.3
0.2
0.1
Q=0.993: Hit
© 2008 VIRGINIA TECH
Created by: R. Matthew Gardner

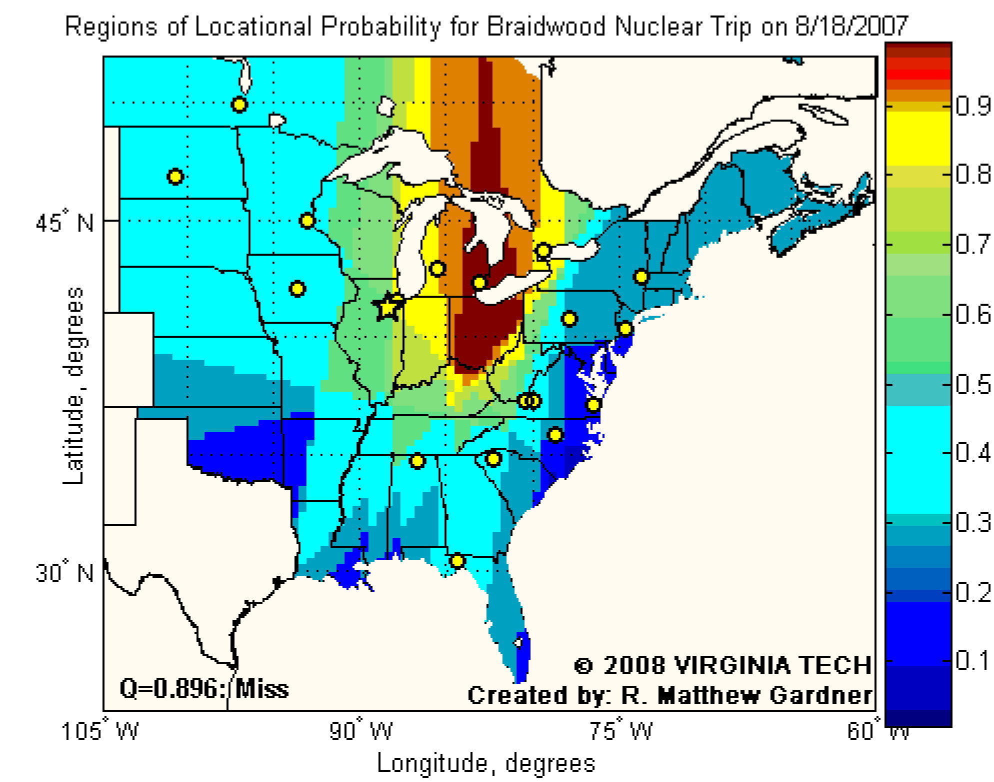
Regions of Locational Probability for Braidwood Nuclear Trip on 8/18/2007
45° N
30° N
Latitude, degrees
105° W
90° W
75° W
60° W
Longitude, degrees
0.9
0.8
0.7
0.6
0.5
0.4
0.3
0.2
0.1
Q=0.896: Miss
© 2008 VIRGINIA TECH
Created by: R. Matthew Gardner

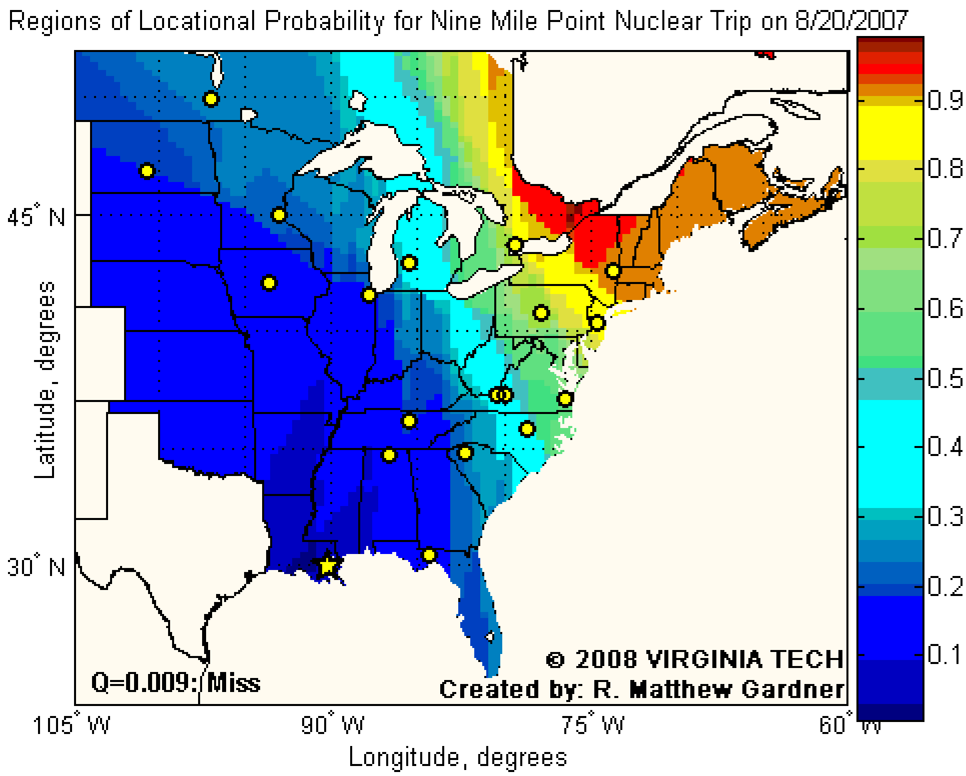
Regions of Locational Probability for Nine Mile Point Nuclear Trip on 8/20/2007
45° N
30° N
Latitude, degrees
105° W
90° W
75° W
60° W
Longitude, degrees
0.9
0.8
0.7
0.6
0.5
0.4
0.3
0.2
0.1
Q=0.009: Miss
© 2008 VIRGINIA TECH
Created by: R. Matthew Gardner

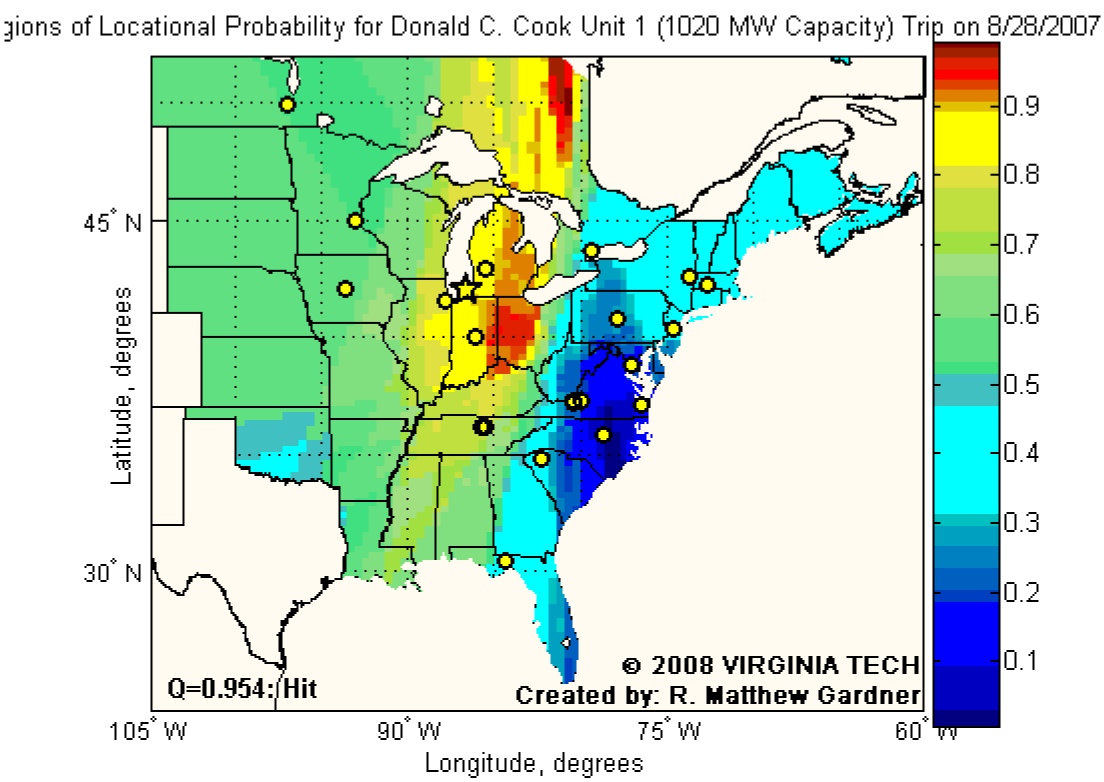
gions of Locational Probability for Donald C. Cook Unit 1 (1020 MW Capacity) Trip on 8/28/2007
45° N
30° N
Latitude, degrees
105° W
90° W
75° W
60° W
Longitude, degrees
0.9
0.8
0.7
0.6
0.5
0.4
0.3
0.2
0.1
Q=0.954: Hit
© 2008 VIRGINIA TECH
Created by: R. Matthew Gardner

Regions of Locational Probability for Mountaineer U1 (1300 MW Capacity) Trip on 9/1/2007

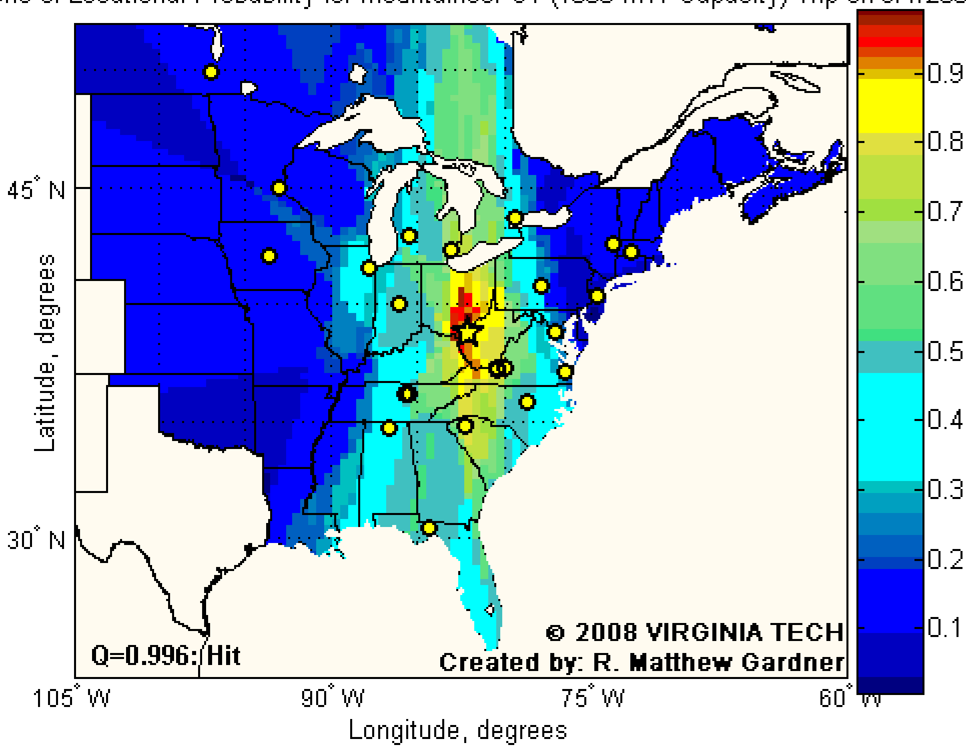

Regions of Locational Probability for Rockport Unit2 (1300 MW Capacity) Trip on 9/4/2007

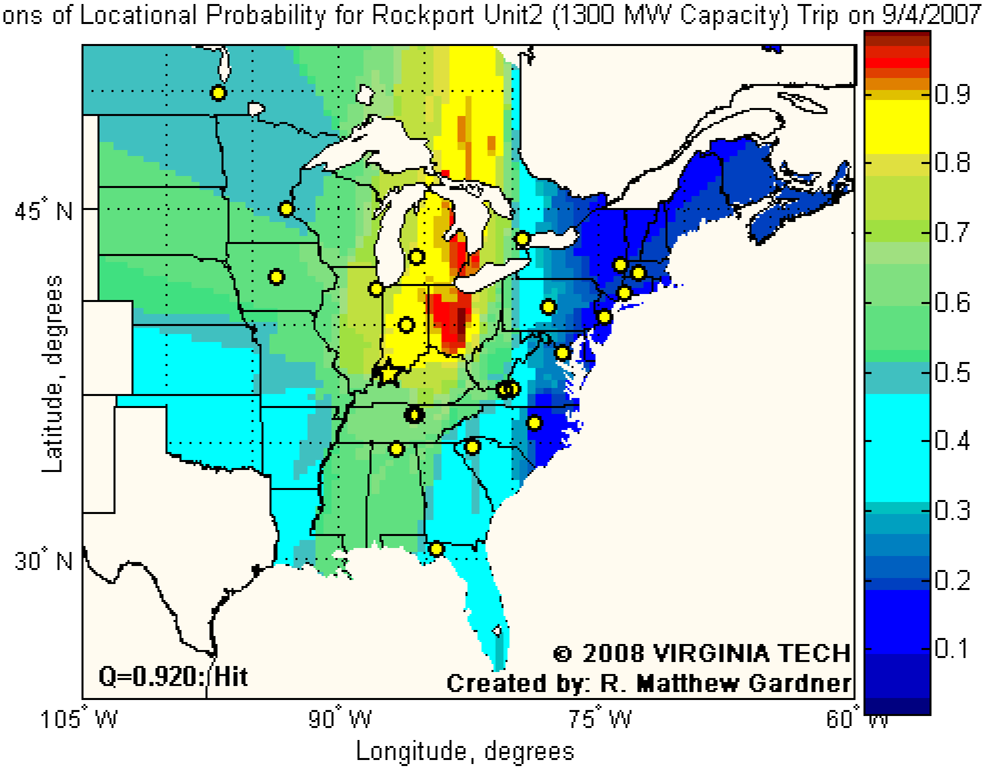

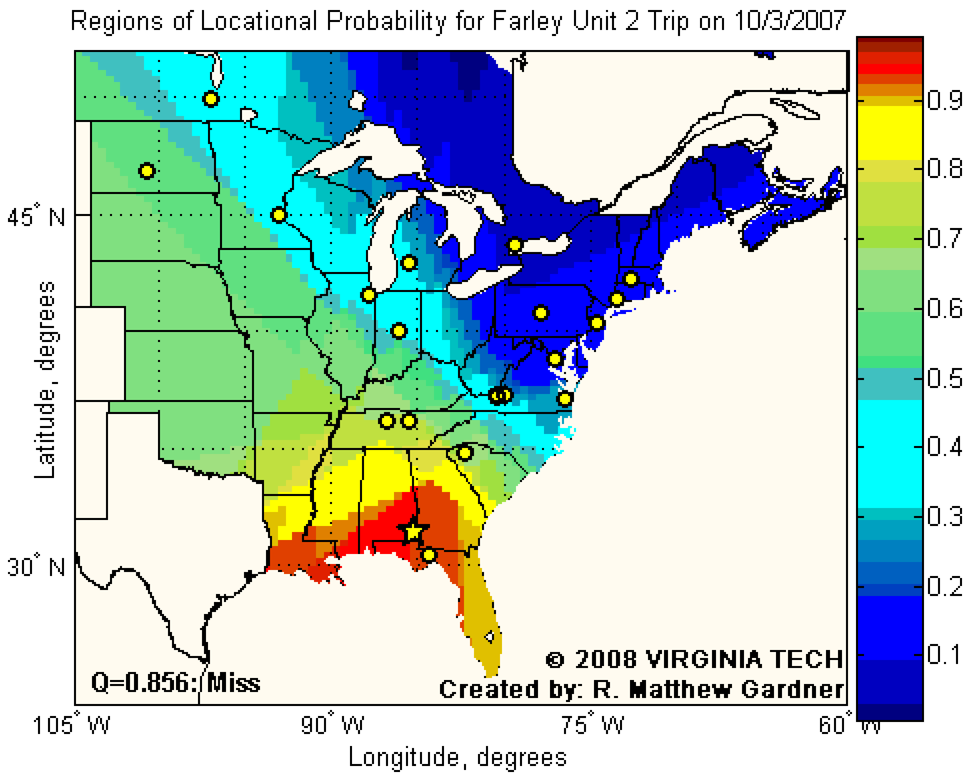
Regions of Locational Probability for Farley Unit 2 Trip on 10/3/2007
45° N
30° N
Latitude, degrees
105° W
90° W
75° W
60° W
Longitude, degrees
Q=0.856:/Miss
© 2008 VIRGINIA TECH
Created by: R. Matthew Gardner
0.9
0.8
0.7
0.6
0.5
0.4
0.3
0.2
0.1

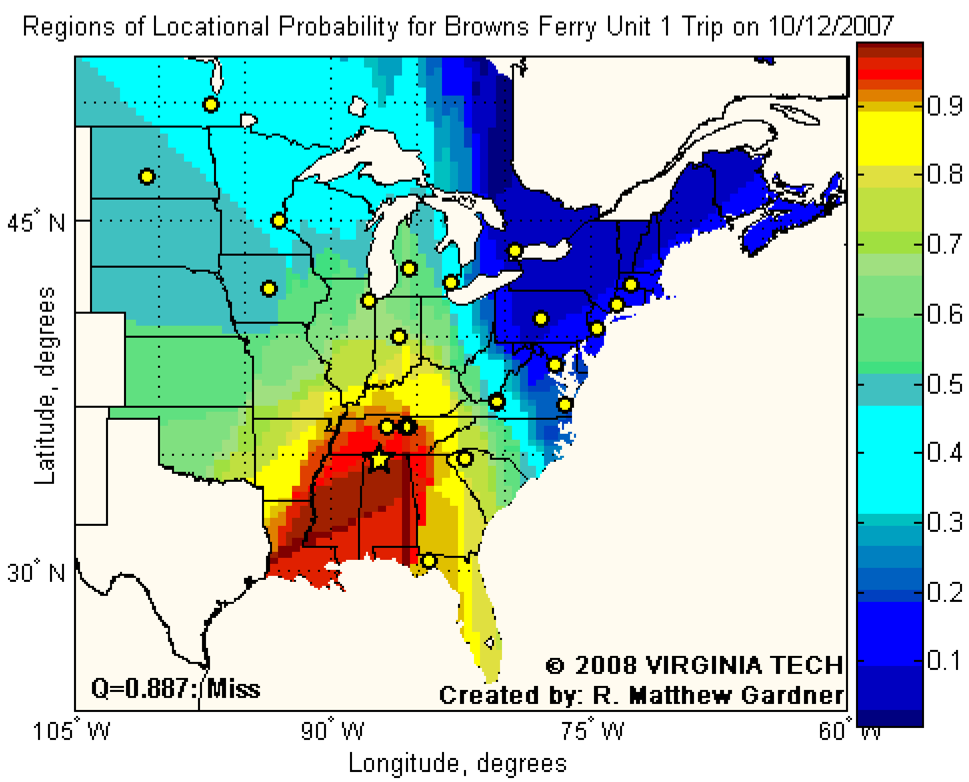
Regions of Locational Probability for Browns Ferry Unit 1 Trip on 10/12/2007
45° N
30° N
Latitude, degrees
105° W
90° W
75° W
60° W
Longitude, degrees
Q=0.887:/Miss
© 2008 VIRGINIA TECH
Created by: R. Matthew Gardner
0.9
0.8
0.7
0.6
0.5
0.4
0.3
0.2
0.1

Regions of Locational Probability for Connesville U4 (780 MW Capacity) Trip on 11/4/2007

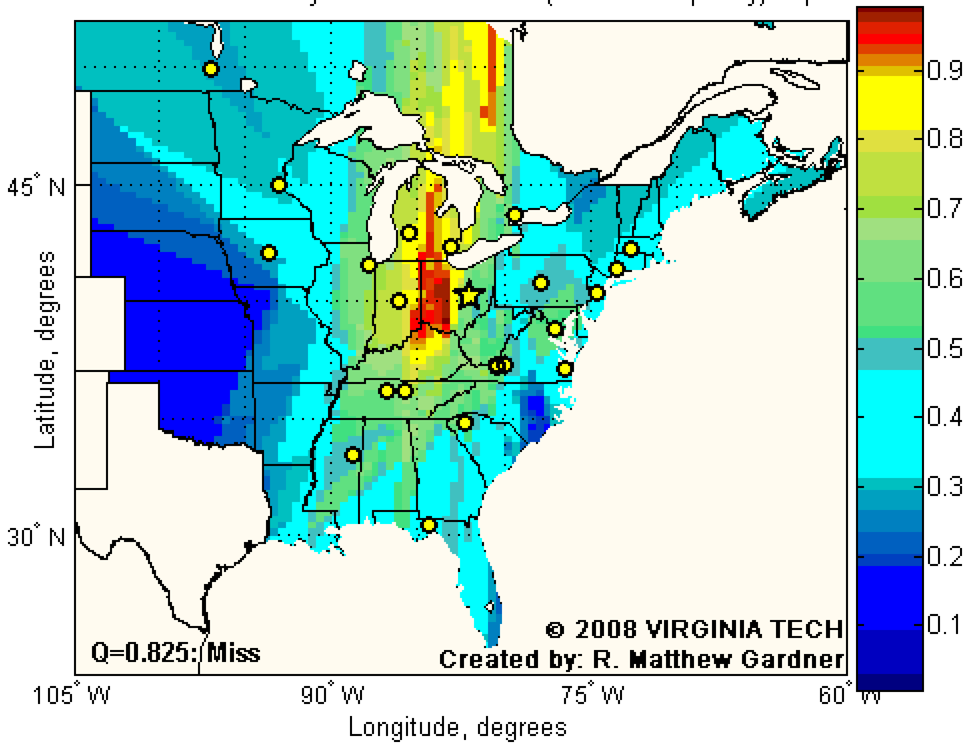

Regions of Locational Probability for Mitchell U2 (800 MW Capacity) Trip on 11/4/2007

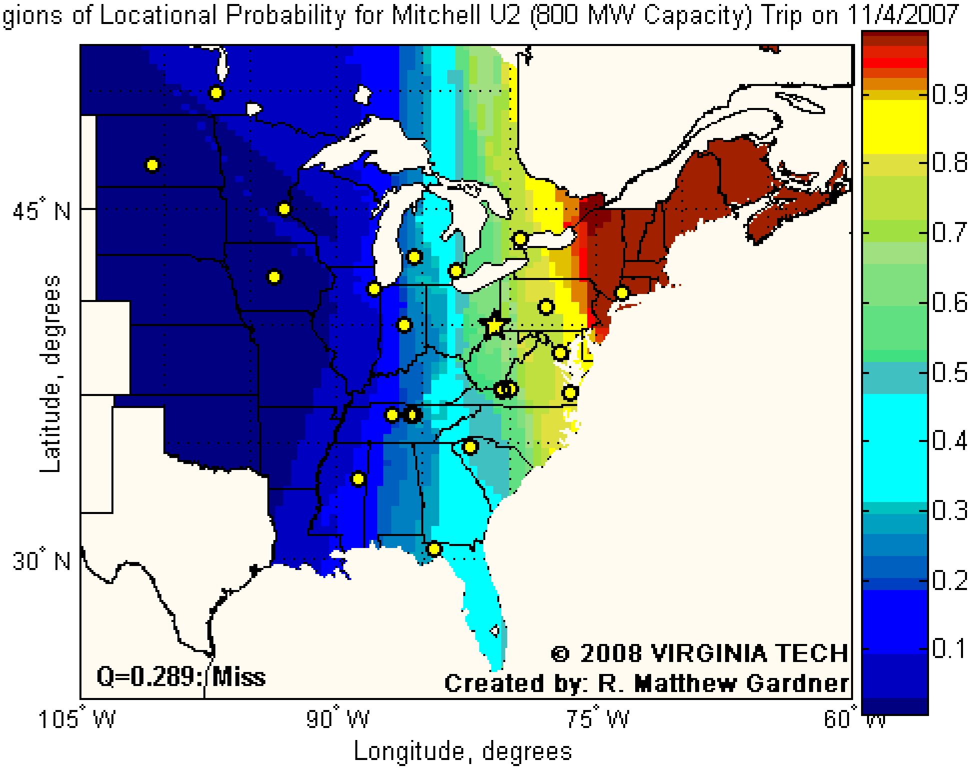

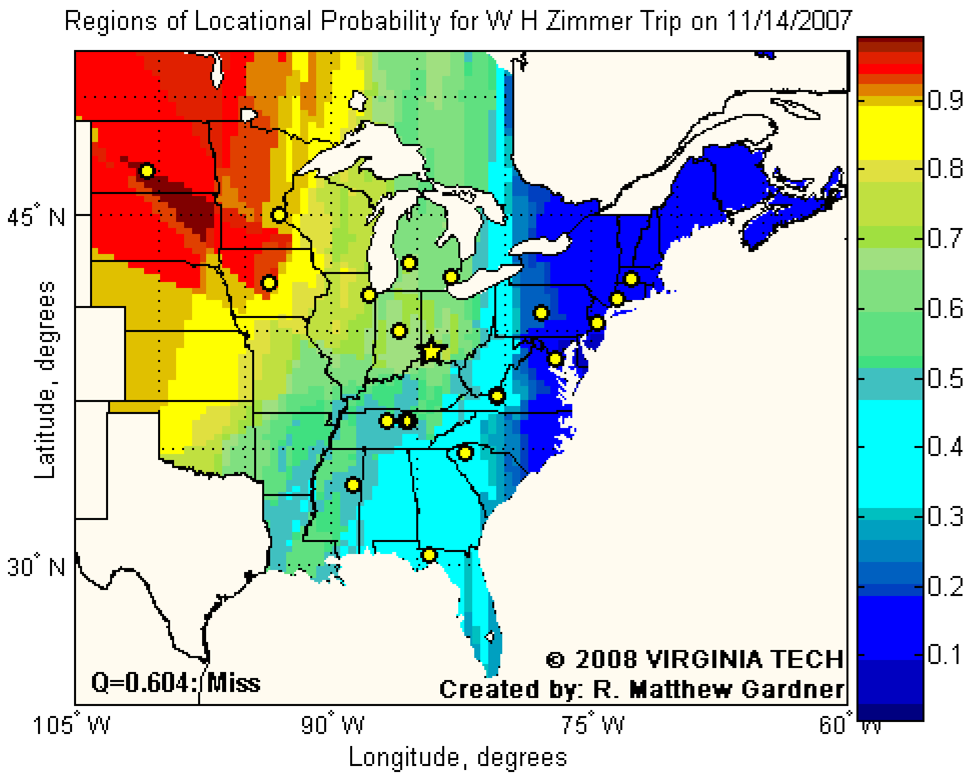
Regions of Locational Probability for W H Zimmer Trip on 11/14/2007
45° N
30° N
Latitude, degrees
105° W
90° W
75° W
60° W
Longitude, degrees
Q=0.604: Miss
© 2008 VIRGINIA TECH
Created by: R. Matthew Gardner
0.9
0.8
0.7
0.6
0.5
0.4
0.3
0.2
0.1

Appendix XVIII: Half-Plane Event Location Based Upon Simulation of EI Frequency at Random Points

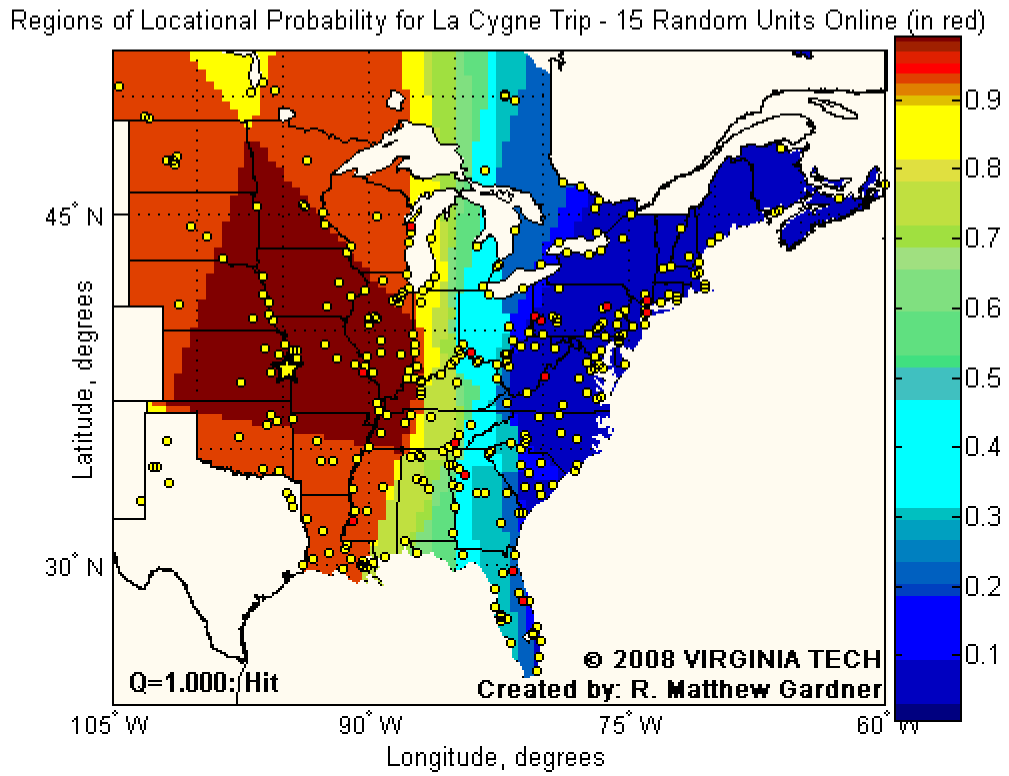

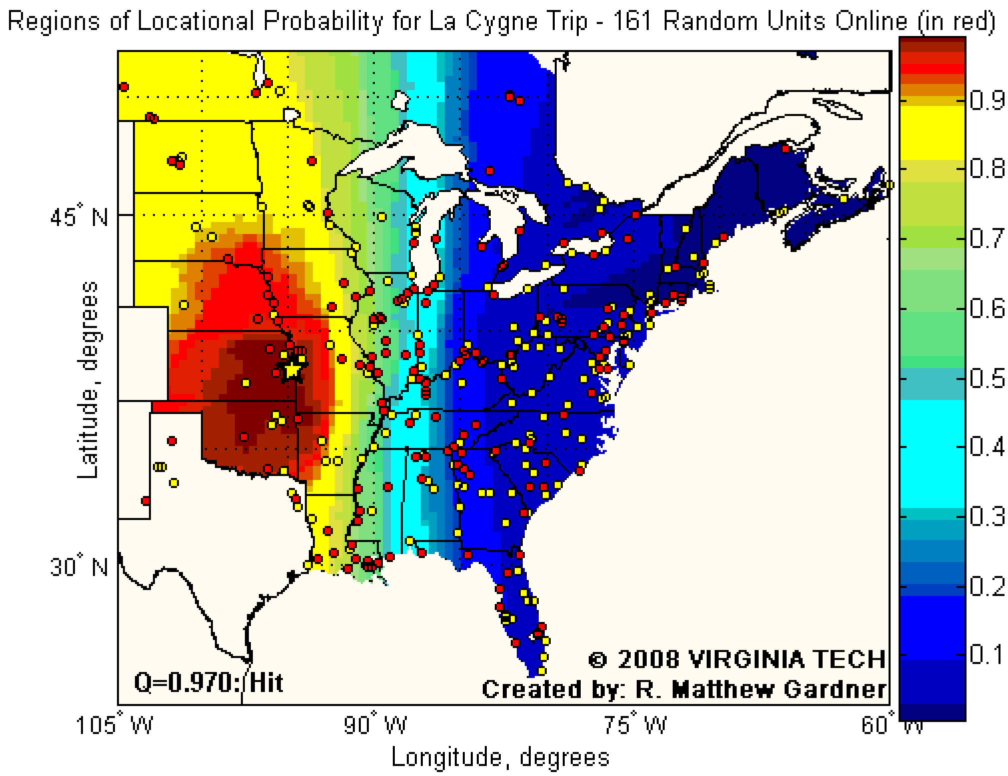
Regions of Locational Probability for La Cygne Trip - 161 Random Units Online (in red)
45° N
30° N
Latitude, degrees
105° W
90° W
75° W
60° W
Longitude, degrees
Q=0.970:/Hit
© 2008 VIRGINIA TECH
Created by: R. Matthew Gardner
0.9
0.8
0.7
0.6
0.5
0.4
0.3
0.2
0.1

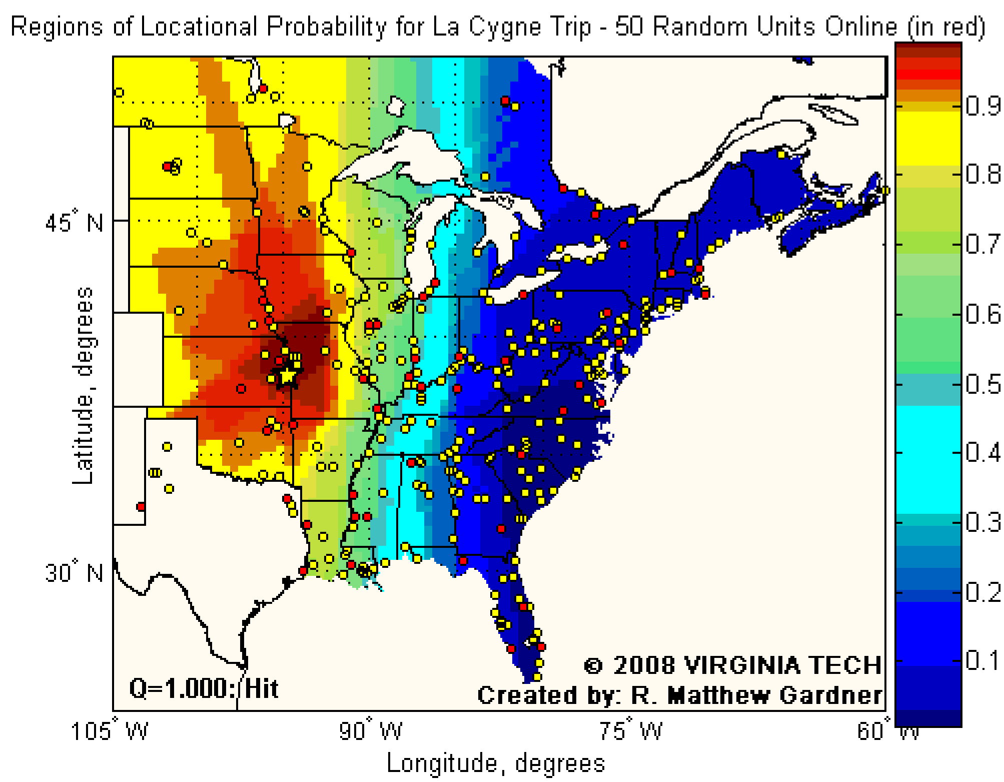
Regions of Locational Probability for La Cygne Trip - 50 Random Units Online (in red)
45° N
30° N
Latitude, degrees
105° W
90° W
75° W
60° W
Longitude, degrees
Q=1.000:/Hit
© 2008 VIRGINIA TECH
Created by: R. Matthew Gardner
0.9
0.8
0.7
0.6
0.5
0.4
0.3
0.2
0.1

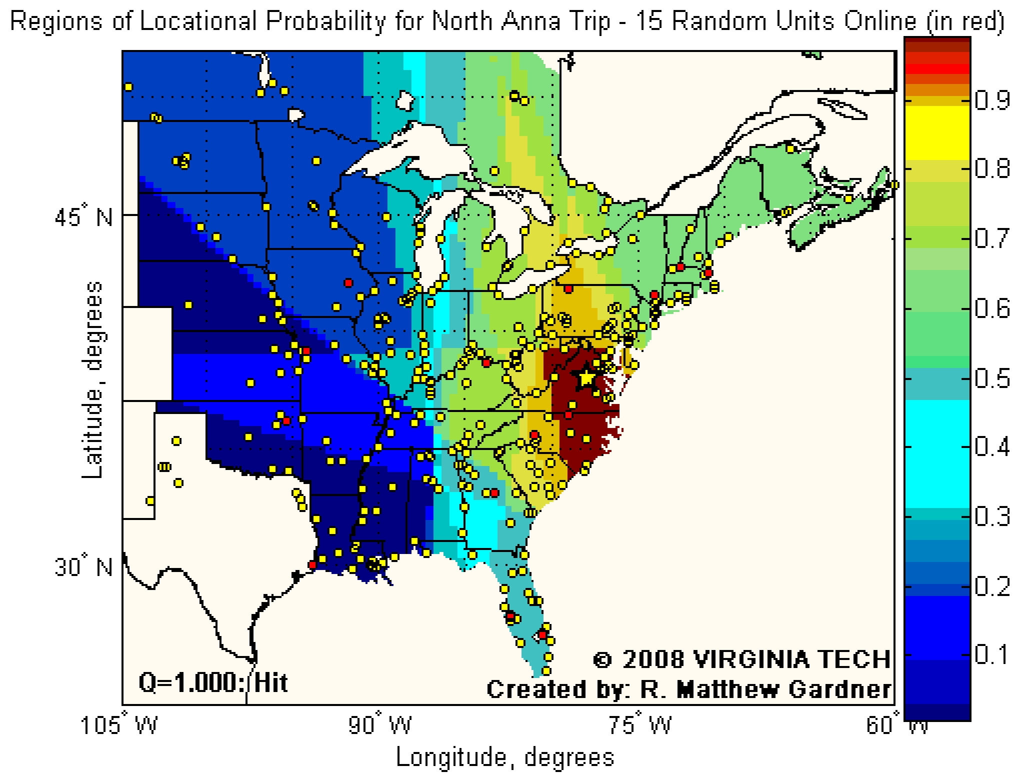
Regions of Locational Probability for North Anna Trip - 15 Random Units Online (in red)
Q=1.000: Hit
© 2008 VIRGINIA TECH
Created by: R. Matthew Gardner
45° N
30° N
Latitude, degrees
105° W
90° W
75° W
60° W
Longitude, degrees
0.9
0.8
0.7
0.6
0.5
0.4
0.3
0.2
0.1

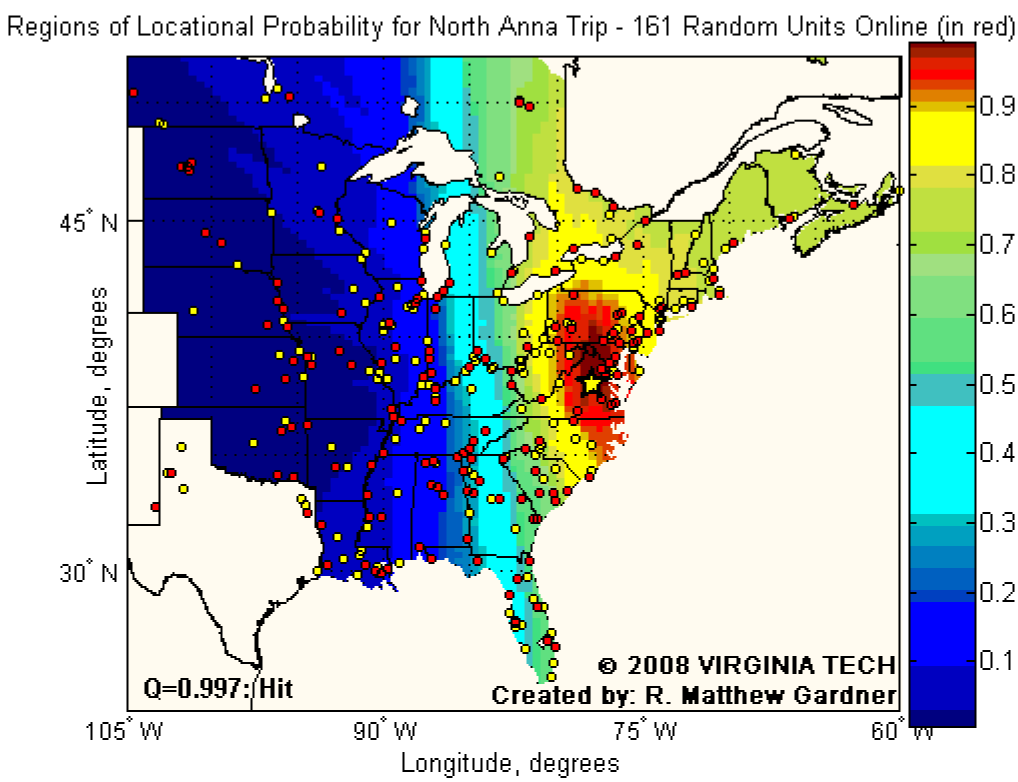
Regions of Locational Probability for North Anna Trip - 161 Random Units Online (in red)
Q=0.997: Hit
© 2008 VIRGINIA TECH
Created by: R. Matthew Gardner
45° N
30° N
Latitude, degrees
105° W
90° W
75° W
60° W
Longitude, degrees
0.9
0.8
0.7
0.6
0.5
0.4
0.3
0.2
0.1

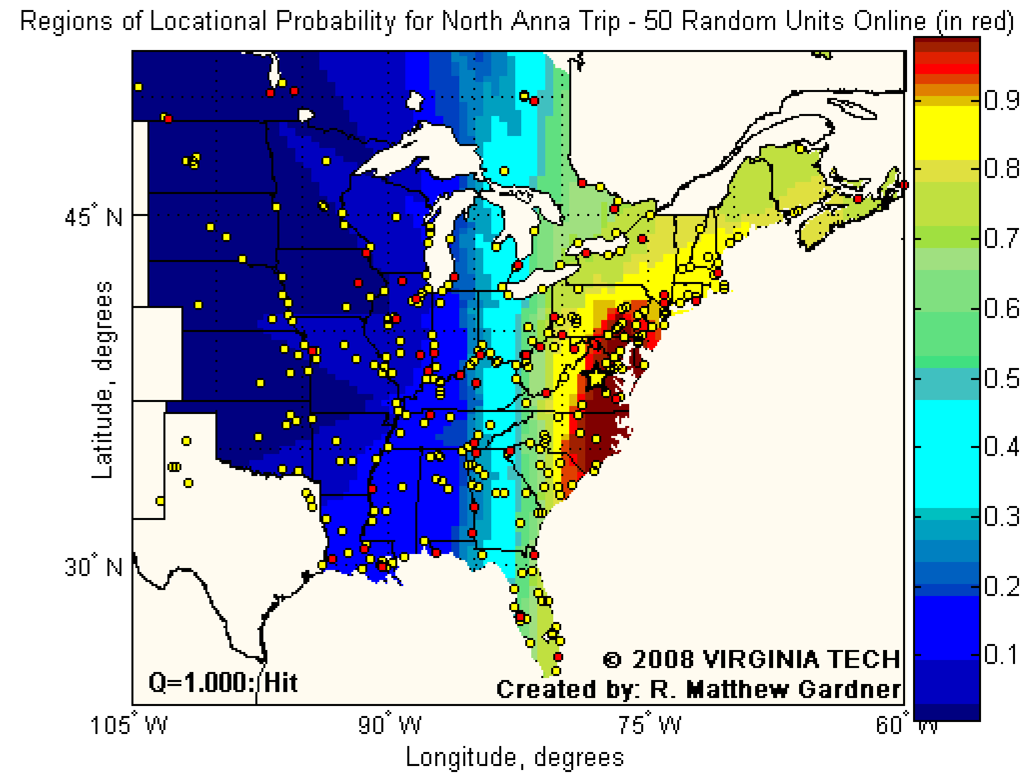
Regions of Locational Probability for North Anna Trip - 50 Random Units Online (in red)
Latitude, degrees
45° N
30° N
105° W
90° W
75° W
60° W
Longitude, degrees
Q=1.000: Hit
© 2008 VIRGINIA TECH
Created by: R. Matthew Gardner
0.9
0.8
0.7
0.6
0.5
0.4
0.3
0.2
0.1

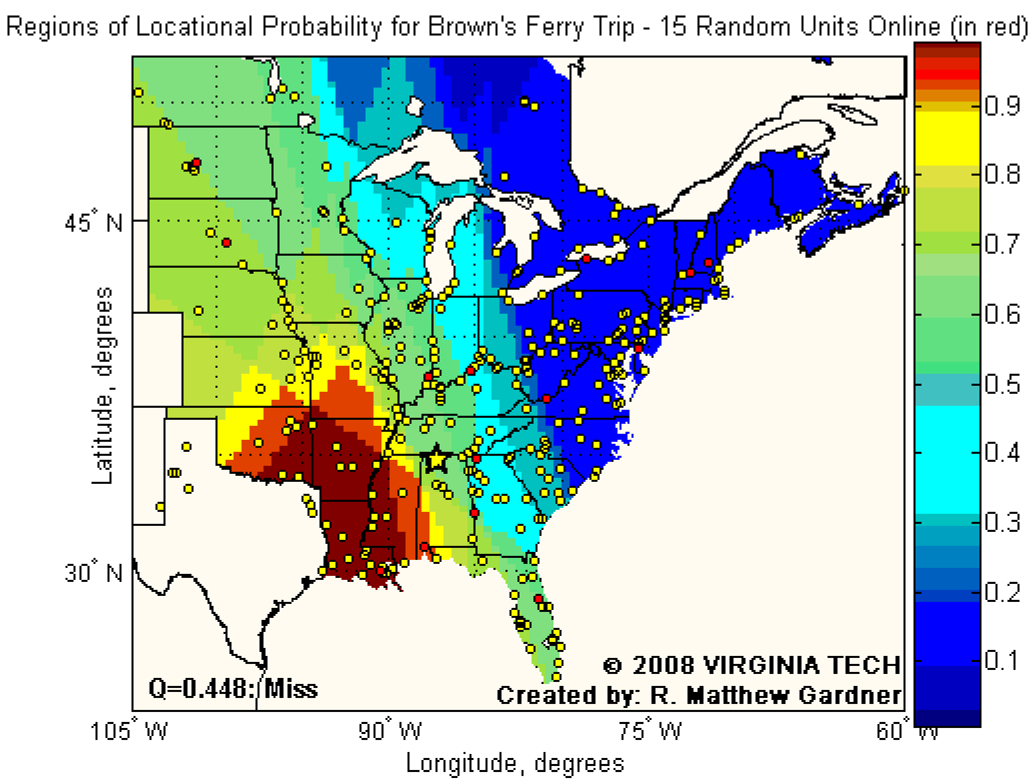
Regions of Locational Probability for Brown's Ferry Trip - 15 Random Units Online (in red)
Latitude, degrees
45° N
30° N
105° W
90° W
75° W
60° W
Longitude, degrees
Q=0.448: Miss
© 2008 VIRGINIA TECH
Created by: R. Matthew Gardner
0.9
0.8
0.7
0.6
0.5
0.4
0.3
0.2
0.1

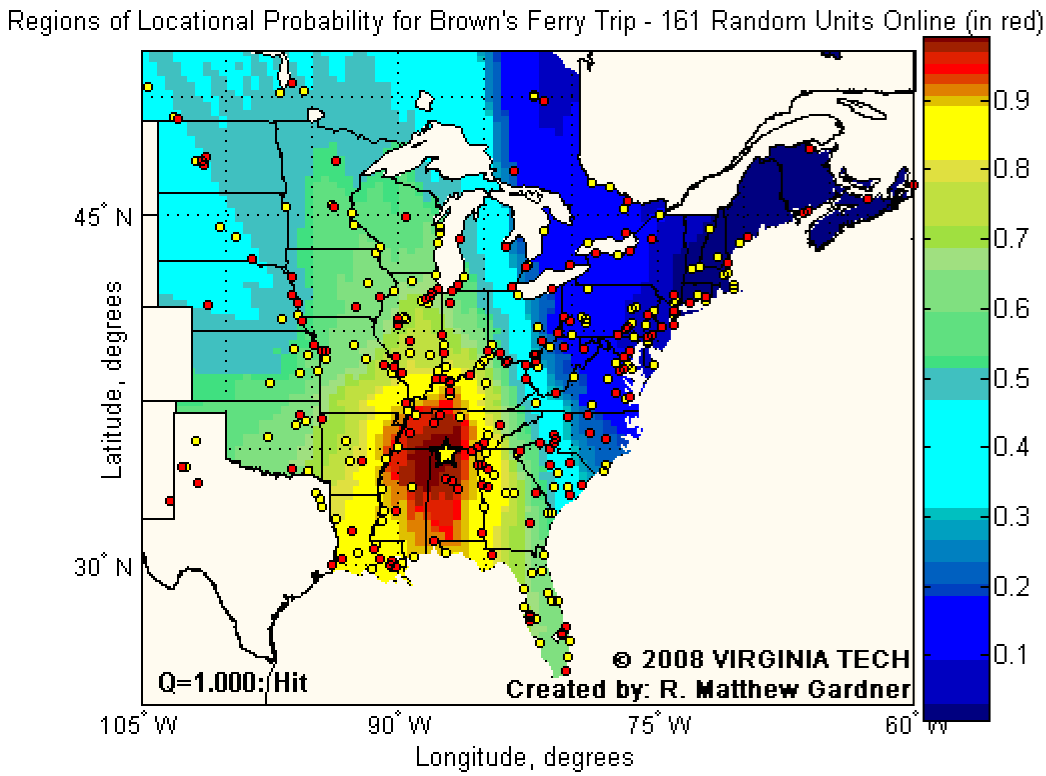
Regions of Locational Probability for Brown's Ferry Trip - 161 Random Units Online (in red)
45° N
30° N
Latitude, degrees
105° W
90° W
75° W
60° W
Longitude, degrees
Q=1.000: Hit
© 2008 VIRGINIA TECH
Created by: R. Matthew Gardner
0.9
0.8
0.7
0.6
0.5
0.4
0.3
0.2
0.1

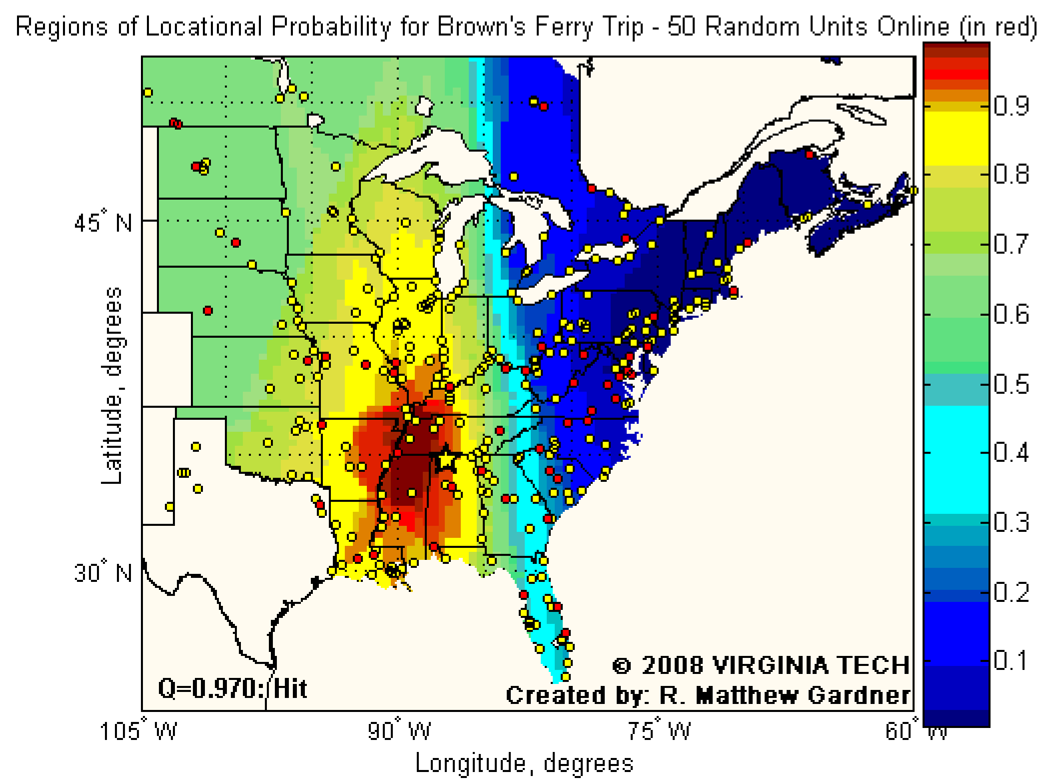
Regions of Locational Probability for Brown's Ferry Trip - 50 Random Units Online (in red)
45° N
30° N
Latitude, degrees
105° W
90° W
75° W
60° W
Longitude, degrees
Q=0.970: Hit
© 2008 VIRGINIA TECH
Created by: R. Matthew Gardner
0.9
0.8
0.7
0.6
0.5
0.4
0.3
0.2
0.1

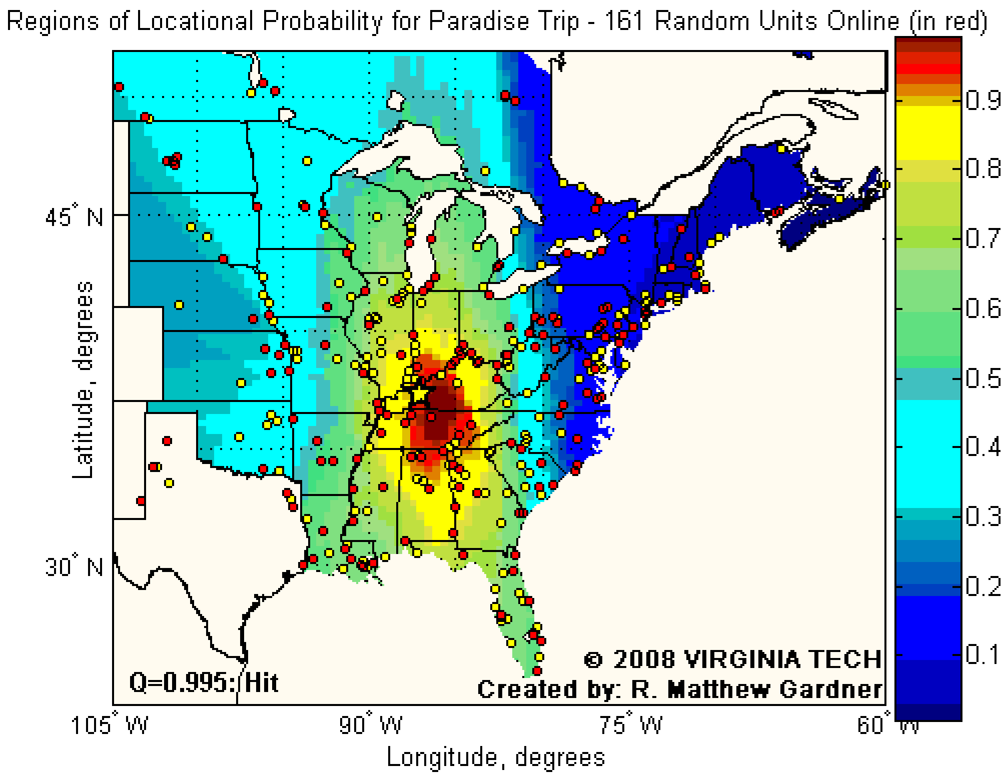
Regions of Locational Probability for Paradise Trip - 161 Random Units Online (in red)
45° N
30° N
Latitude, degrees
105° W
90° W
75° W
60° W
Longitude, degrees
Q=0.995: Hit
© 2008 VIRGINIA TECH
Created by: R. Matthew Gardner
0.9
0.8
0.7
0.6
0.5
0.4
0.3
0.2
0.1

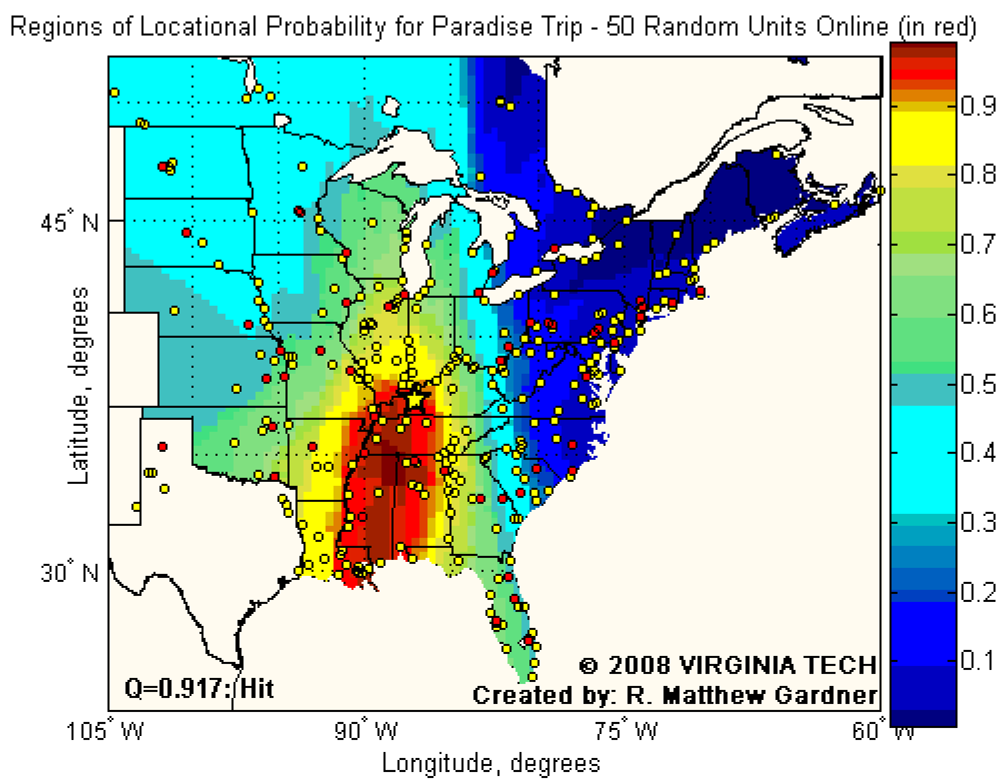
Regions of Locational Probability for Paradise Trip - 50 Random Units Online (in red)
45° N
30° N
Latitude, degrees
105° W
90° W
75° W
60° W
Longitude, degrees
Q=0.917: Hit
© 2008 VIRGINIA TECH
Created by: R. Matthew Gardner
0.9
0.8
0.7
0.6
0.5
0.4
0.3
0.2
0.1

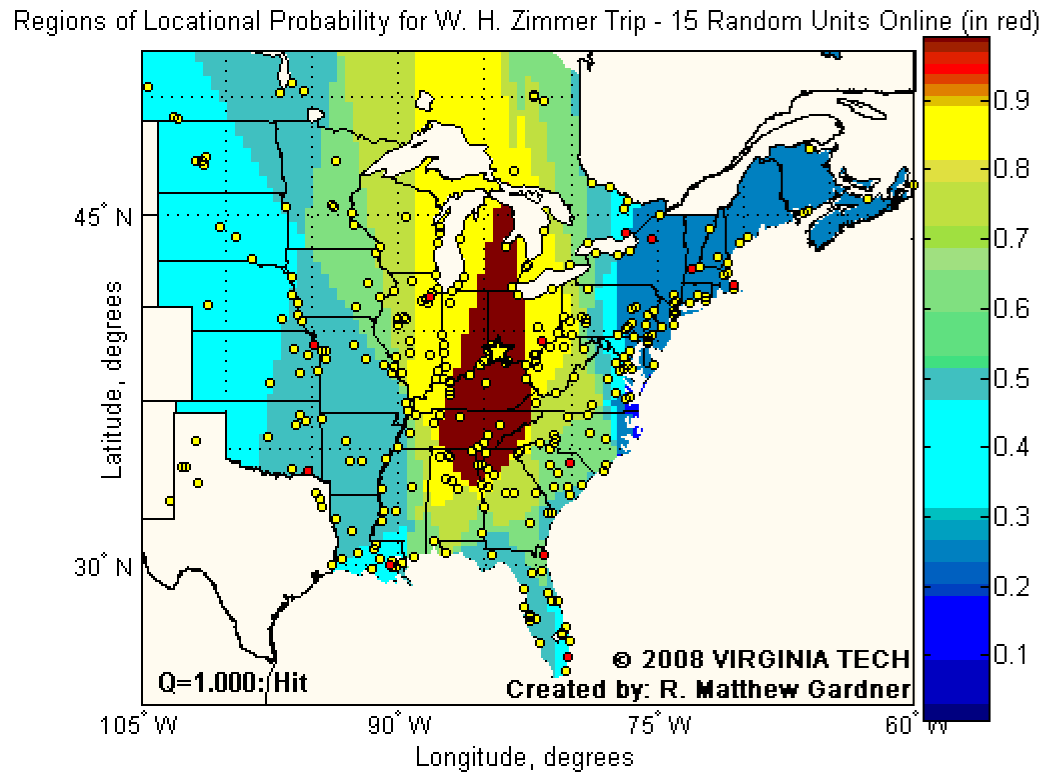
Regions of Locational Probability for W. H. Zimmer Trip - 15 Random Units Online (in red)
Latitude, degrees
45° N
30° N
105° W
90° W
75° W
60° W
Longitude, degrees
Q=1.000:/Hit
© 2008 VIRGINIA TECH
Created by: R. Matthew Gardner
0.9
0.8
0.7
0.6
0.5
0.4
0.3
0.2
0.1

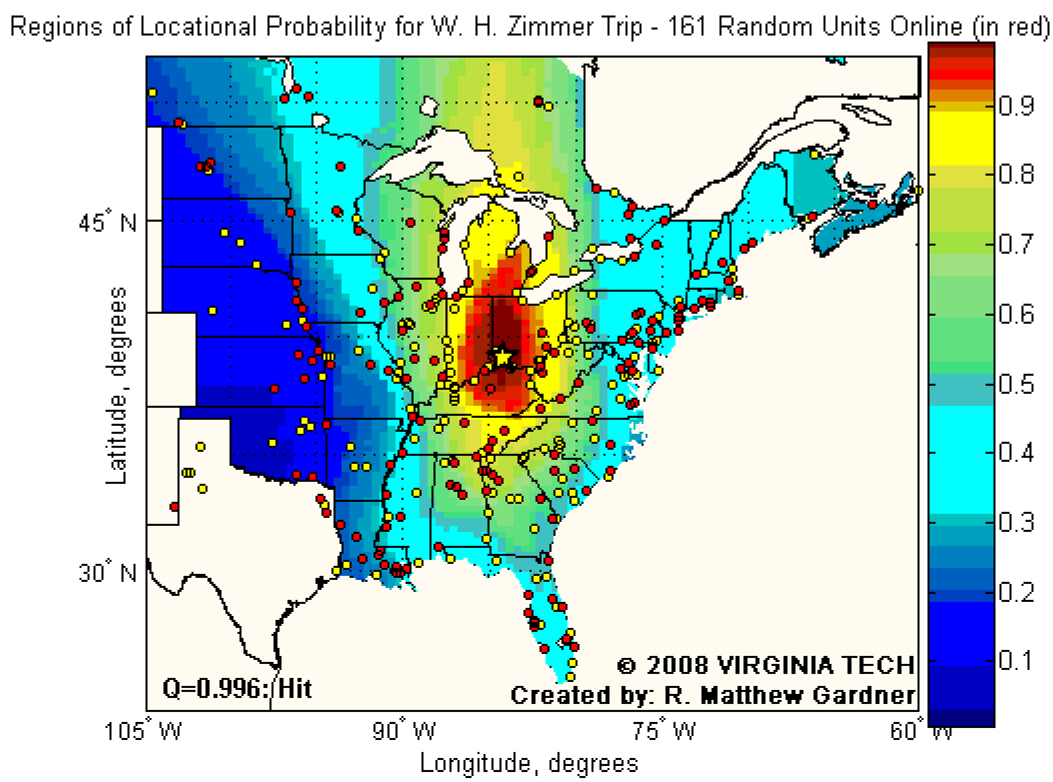
Regions of Locational Probability for W. H. Zimmer Trip - 161 Random Units Online (in red)
Latitude, degrees
45° N
30° N
105° W
90° W
75° W
60° W
Longitude, degrees
Q=0.996:/Hit
© 2008 VIRGINIA TECH
Created by: R. Matthew Gardner
0.9
0.8
0.7
0.6
0.5
0.4
0.3
0.2
0.1

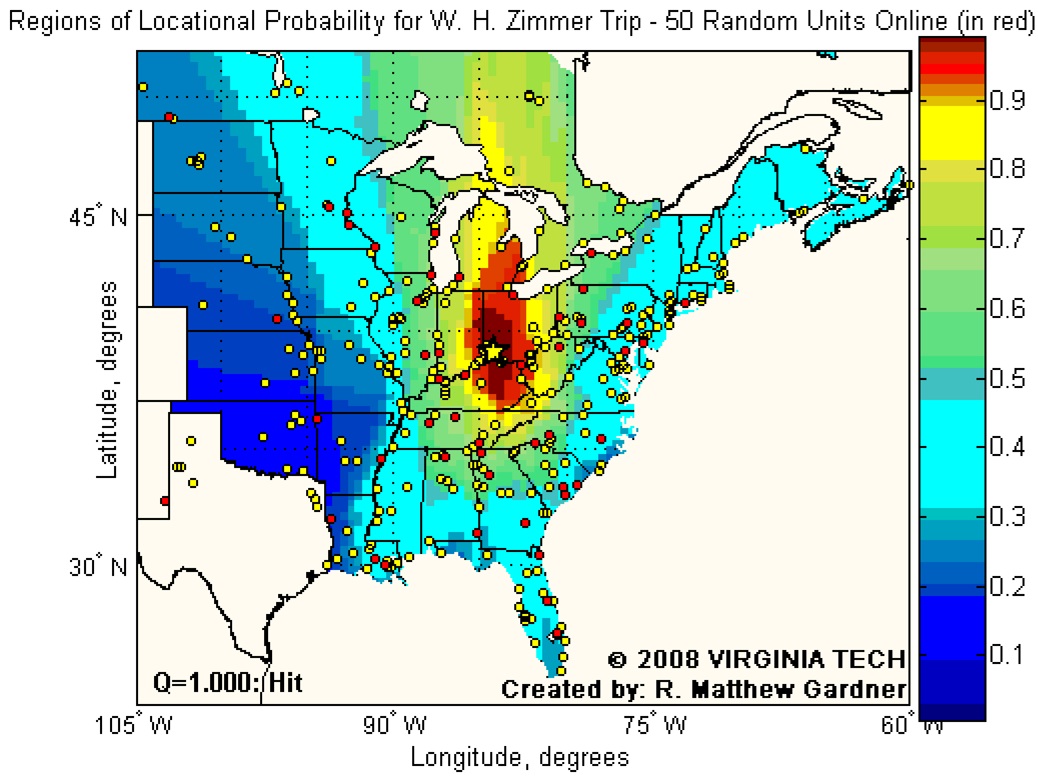
Regions of Locational Probability for W. H. Zimmer Trip - 50 Random Units Online (in red)
45° N
30° N
Latitude, degrees
105° W
90° W
75° W
60° W
Longitude, degrees
Q=1.000:/Hit
© 2008 VIRGINIA TECH
Created by: R. Matthew Gardner
0.9
0.8
0.7
0.6
0.5
0.4
0.3
0.2
0.1

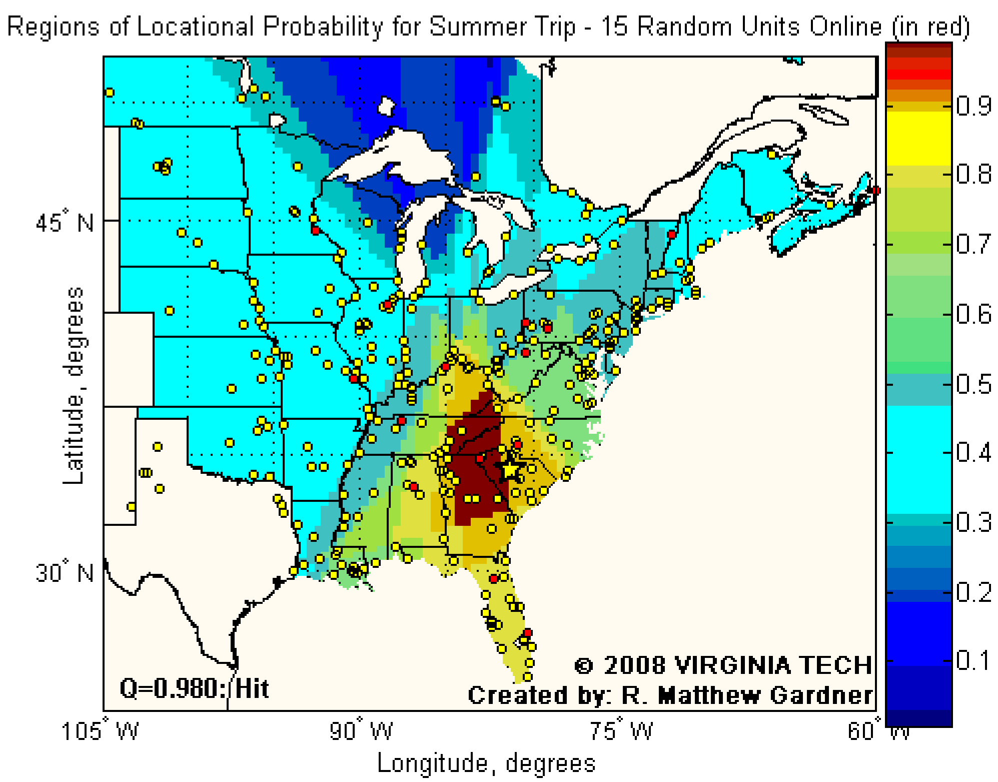
Regions of Locational Probability for Summer Trip - 15 Random Units Online (in red)
45° N
30° N
Latitude, degrees
105° W
90° W
75° W
60° W
Longitude, degrees
Q=0.980:/Hit
© 2008 VIRGINIA TECH
Created by: R. Matthew Gardner
0.9
0.8
0.7
0.6
0.5
0.4
0.3
0.2
0.1

Regions of Locational Probability for Summer Trip - 161 Random Units Online (in red)

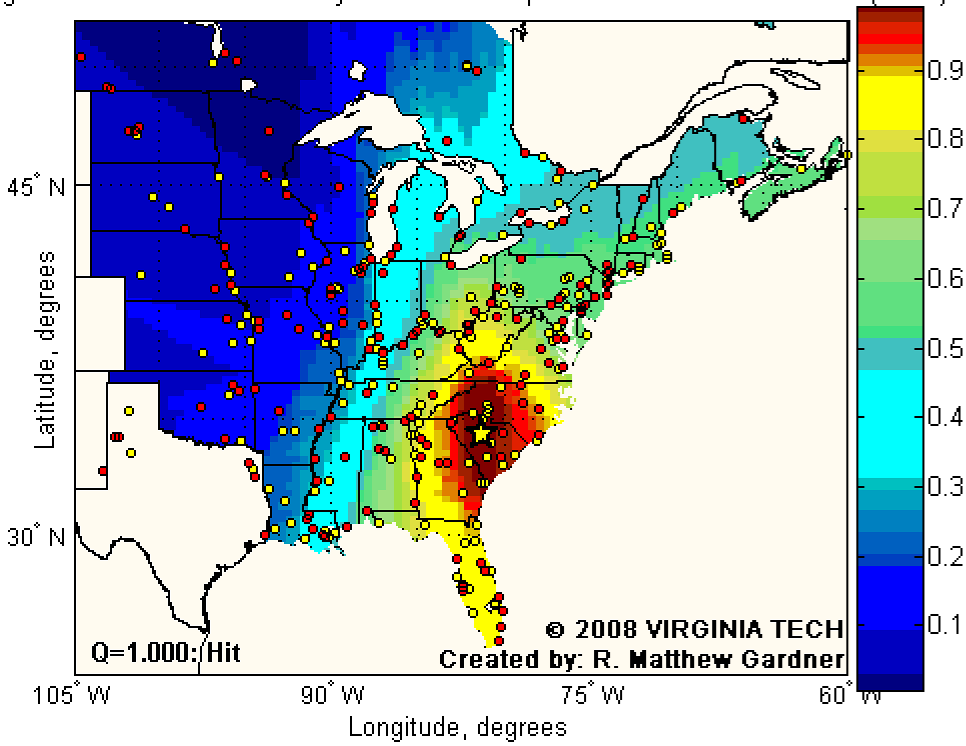

Regions of Locational Probability for Summer Trip - 50 Random Units Online (in red)

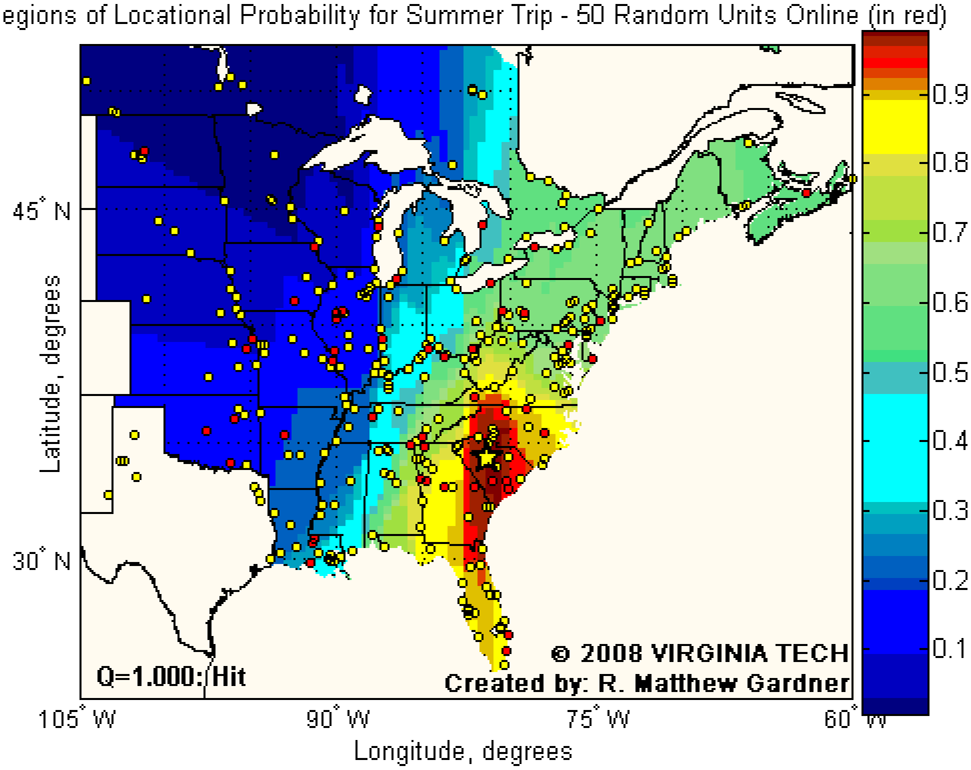

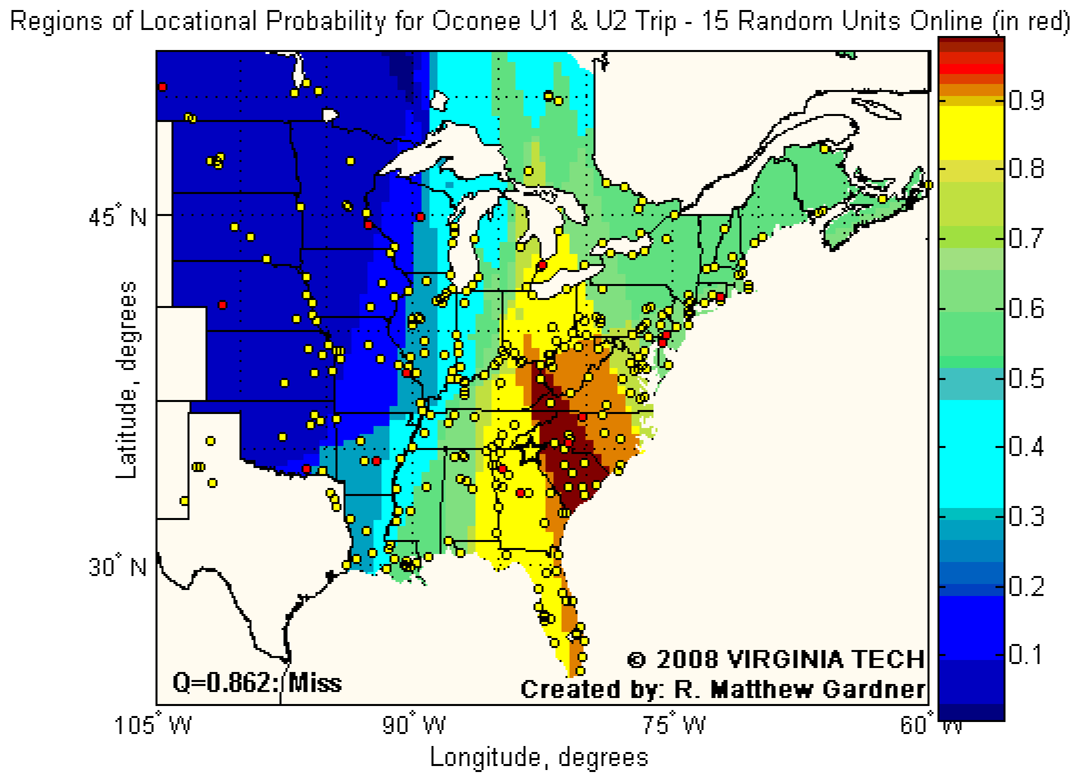
Regions of Locational Probability for Oconee U1 & U2 Trip - 15 Random Units Online (in red)
45° N
30° N
Latitude, degrees
105° W
90° W
75° W
60° W
Longitude, degrees
0.9
0.8
0.7
0.6
0.5
0.4
0.3
0.2
0.1
Q=0.862: Miss
© 2008 VIRGINIA TECH
Created by: R. Matthew Gardner

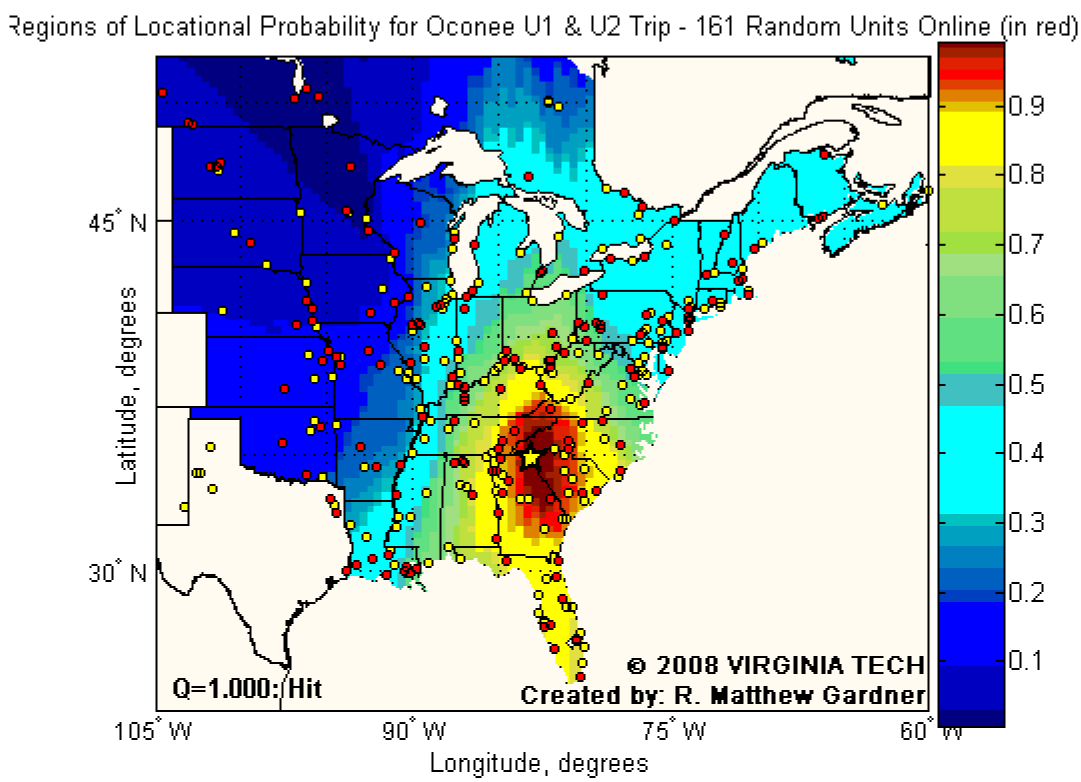
Regions of Locational Probability for Oconee U1 & U2 Trip - 161 Random Units Online (in red)
45° N
30° N
Latitude, degrees
105° W
90° W
75° W
60° W
Longitude, degrees
0.9
0.8
0.7
0.6
0.5
0.4
0.3
0.2
0.1
Q=1.000: Hit
© 2008 VIRGINIA TECH
Created by: R. Matthew Gardner

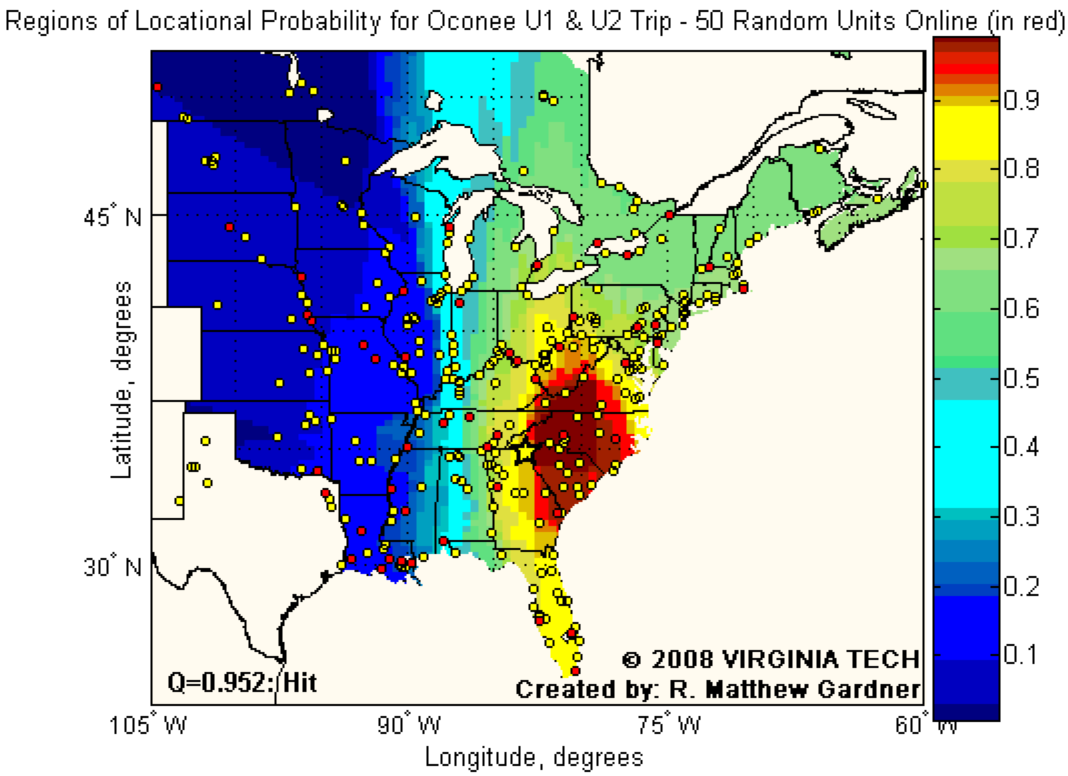
Regions of Locational Probability for Oconee U1 & U2 Trip - 50 Random Units Online (in red)
45° N
30° N
Latitude, degrees
105° W
90° W
75° W
60° W
Longitude, degrees
Q=0.952: Hit
© 2008 VIRGINIA TECH
Created by: R. Matthew Gardner
0.9
0.8
0.7
0.6
0.5
0.4
0.3
0.2
0.1

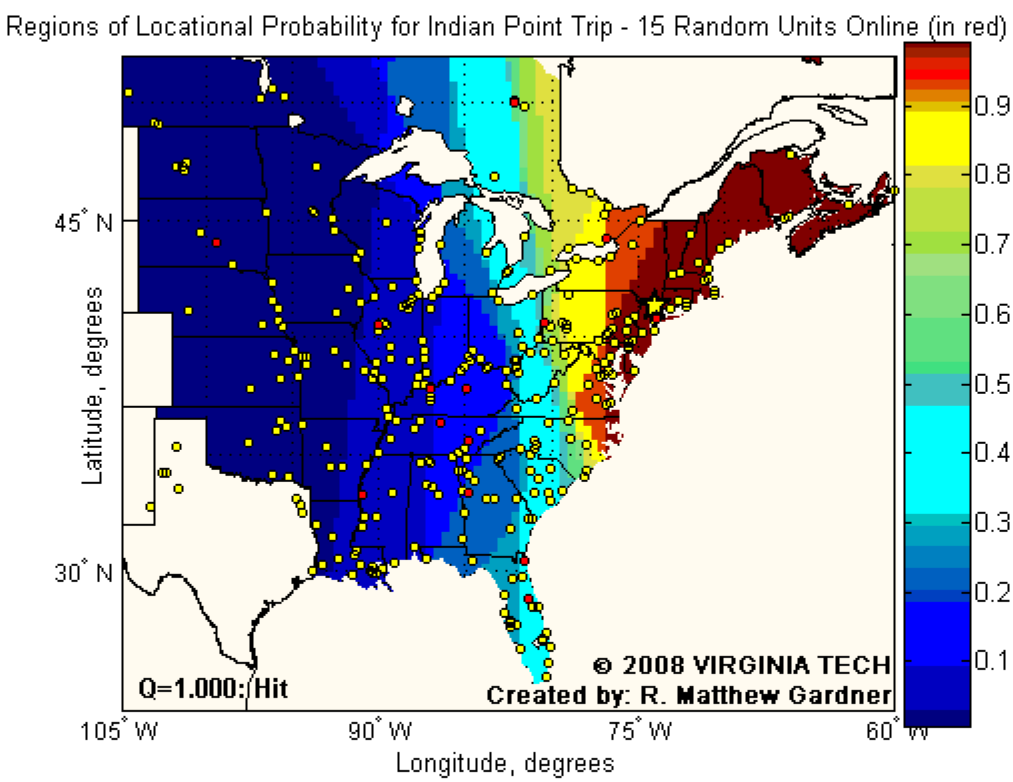
Regions of Locational Probability for Indian Point Trip - 15 Random Units Online (in red)
45° N
30° N
Latitude, degrees
105° W
90° W
75° W
60° W
Longitude, degrees
Q=1.000: Hit
© 2008 VIRGINIA TECH
Created by: R. Matthew Gardner
0.9
0.8
0.7
0.6
0.5
0.4
0.3
0.2
0.1

Regions of Locational Probability for Indian Point Trip - 161 Random Units Online (in red)

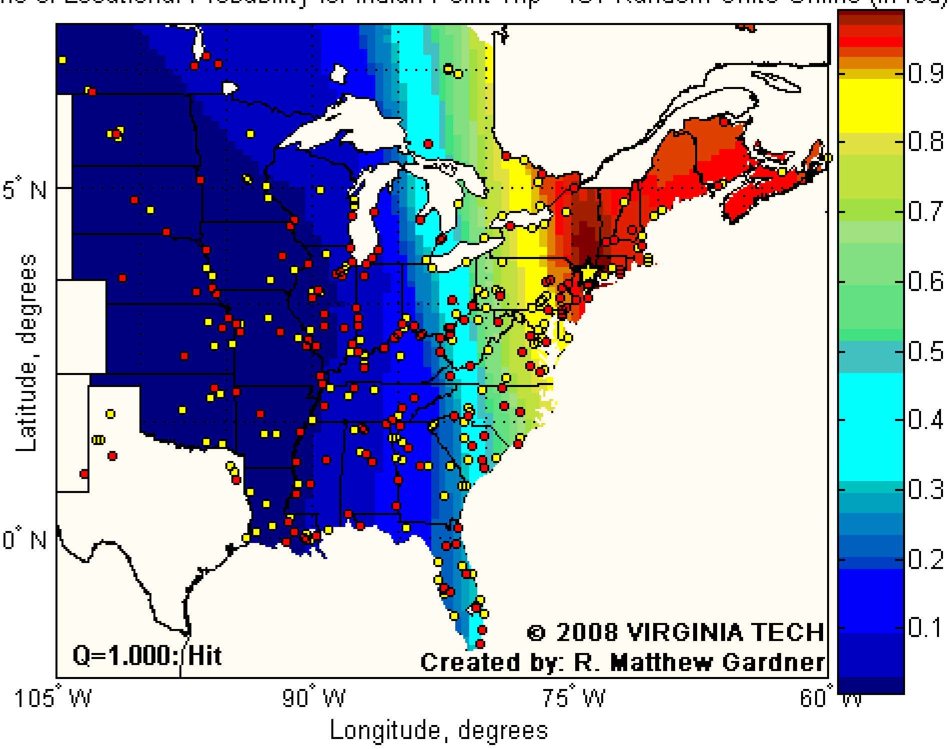

Regions of Locational Probability for Indian Point Trip - 50 Random Units Online (in red)

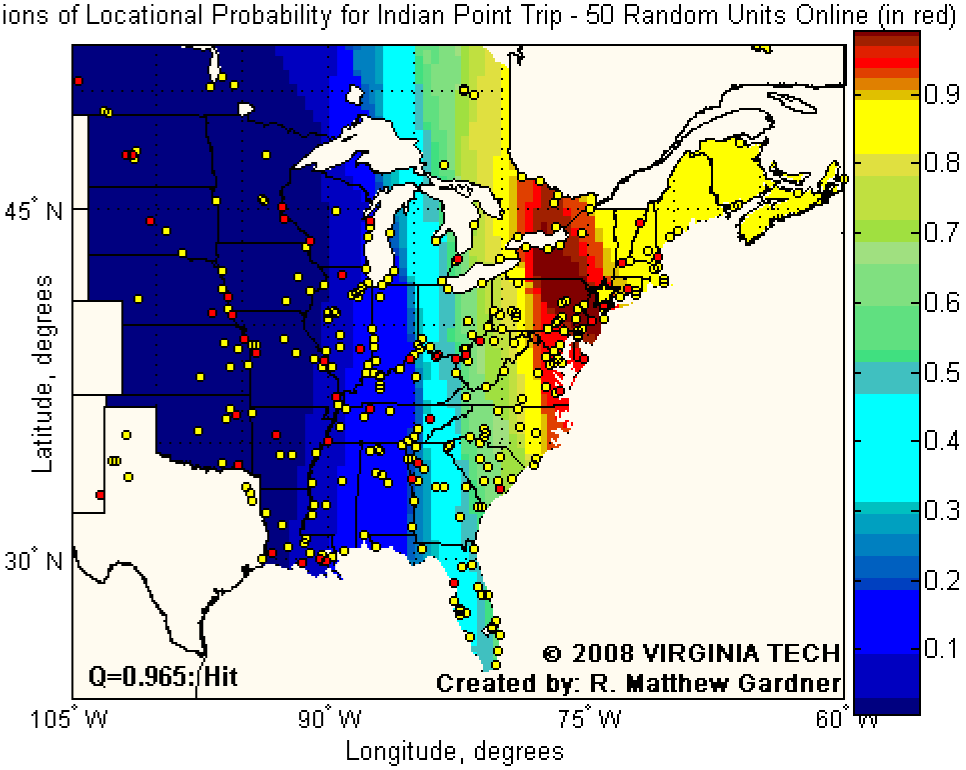

Regions of Locational Probability for Sequoyah Trip - 15 Random Units Online (in red)

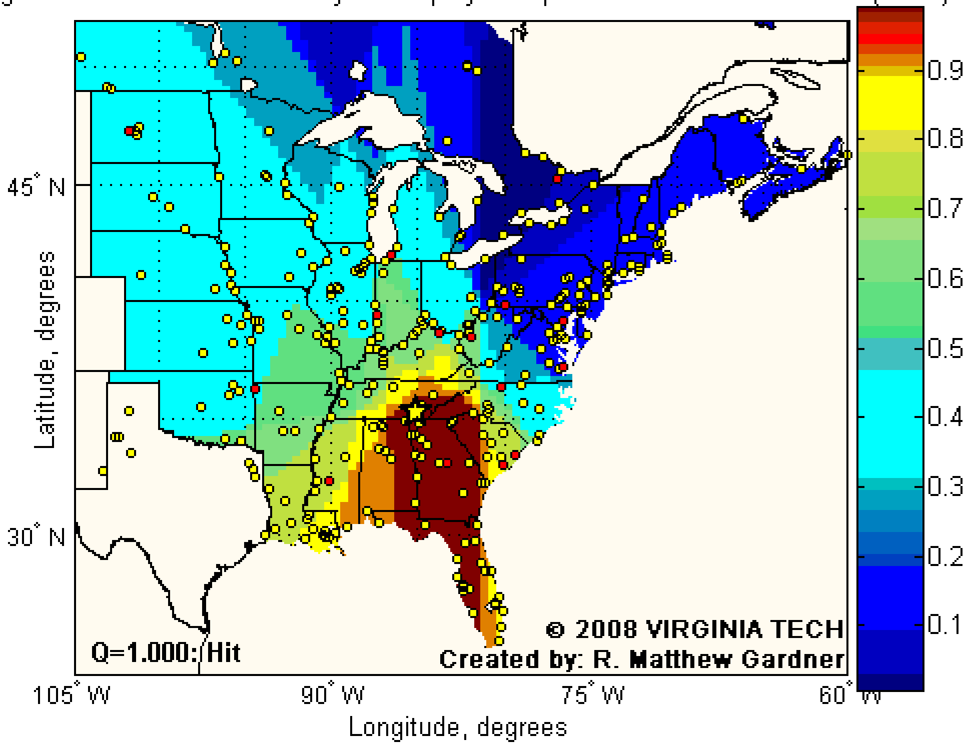

Regions of Locational Probability for Sequoyah Trip - 161 Random Units Online (in red)

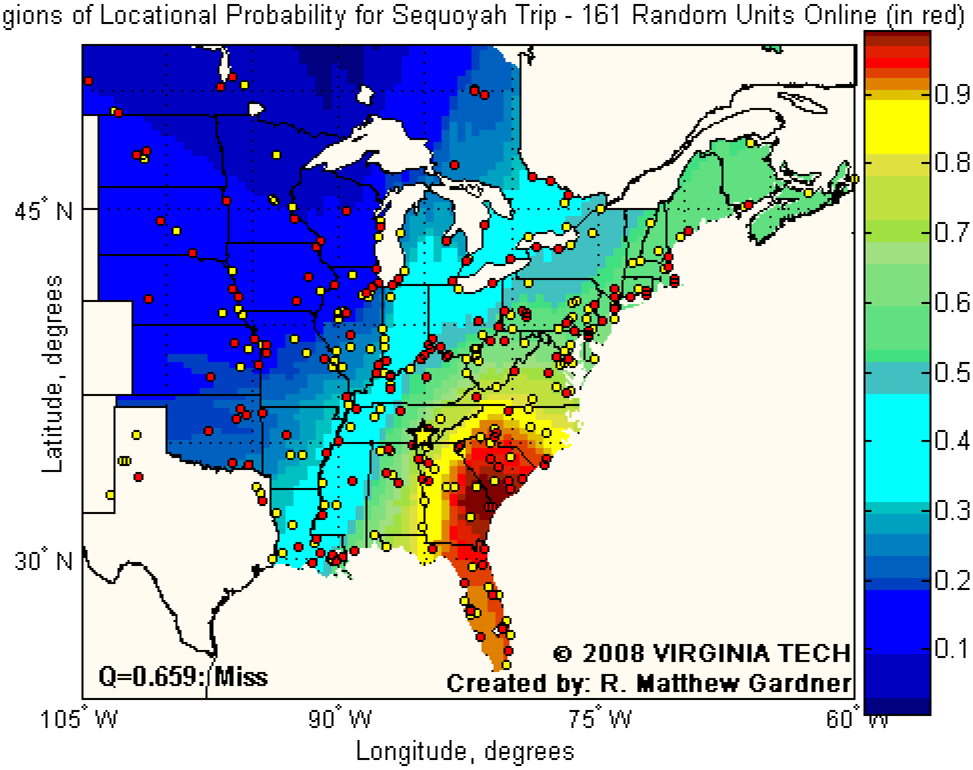

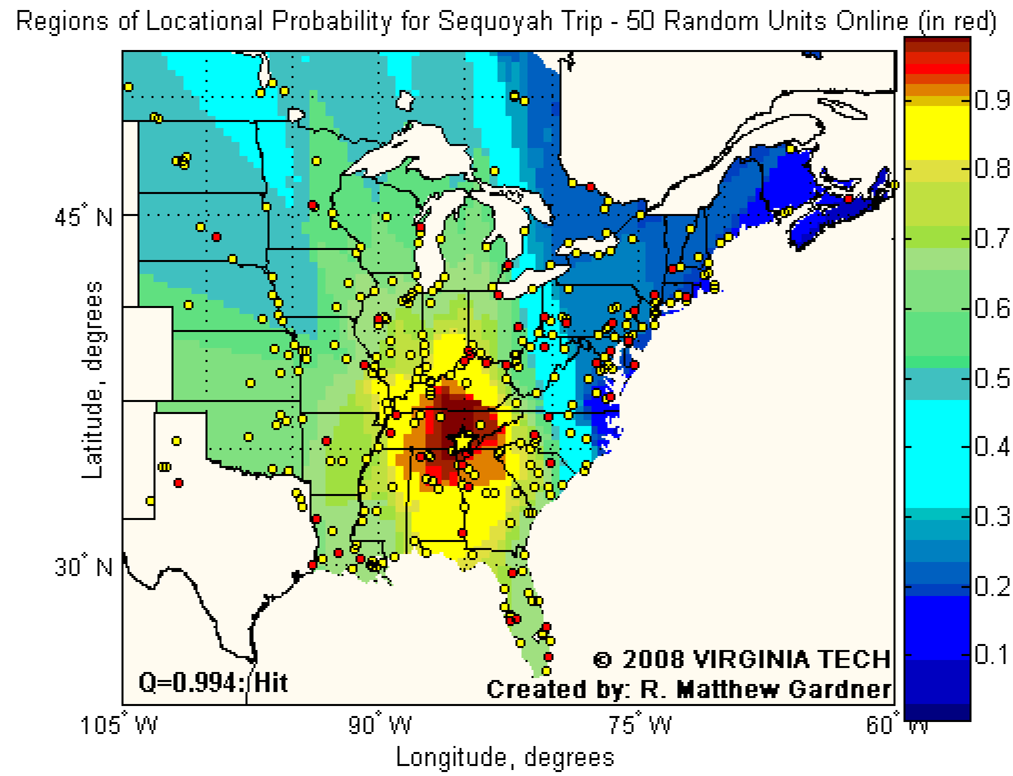
Regions of Locational Probability for Sequoyah Trip - 50 Random Units Online (in red)
45° N
30° N
Latitude, degrees
105° W
90° W
75° W
60° W
Longitude, degrees
Q=0.994: Hit
© 2008 VIRGINIA TECH
Created by: R. Matthew Gardner
0.9
0.8
0.7
0.6
0.5
0.4
0.3
0.2
0.1

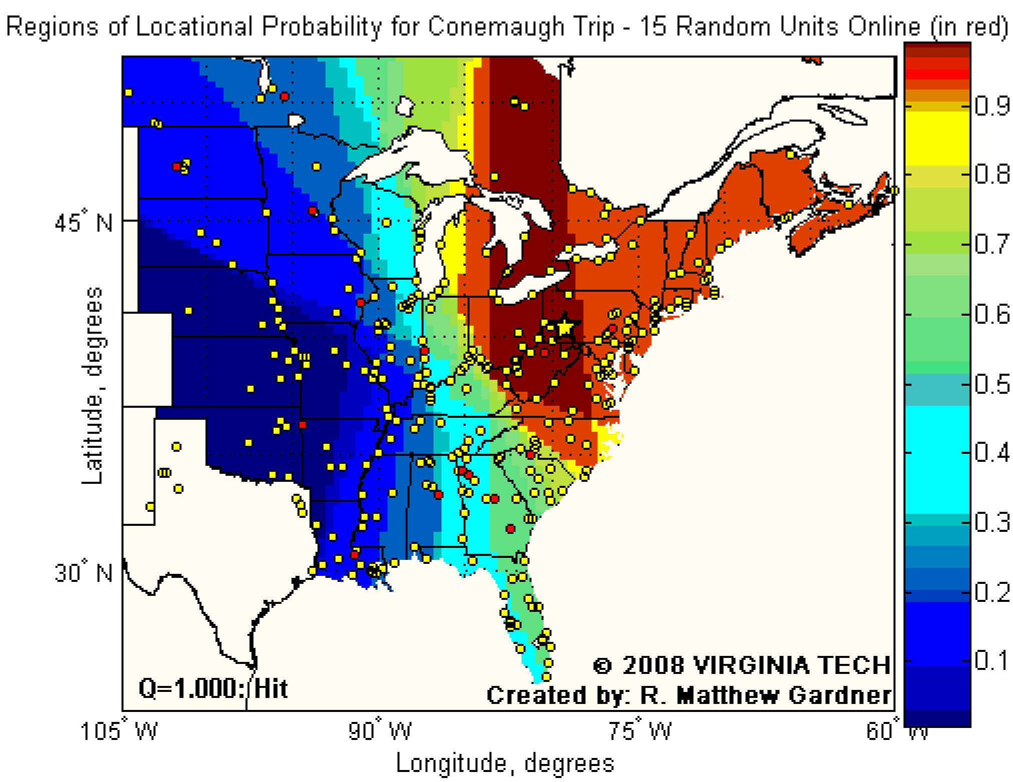
Regions of Locational Probability for Conemaugh Trip - 15 Random Units Online (in red)
45° N
30° N
Latitude, degrees
105° W
90° W
75° W
60° W
Longitude, degrees
Q=1.000: Hit
© 2008 VIRGINIA TECH
Created by: R. Matthew Gardner
0.9
0.8
0.7
0.6
0.5
0.4
0.3
0.2
0.1

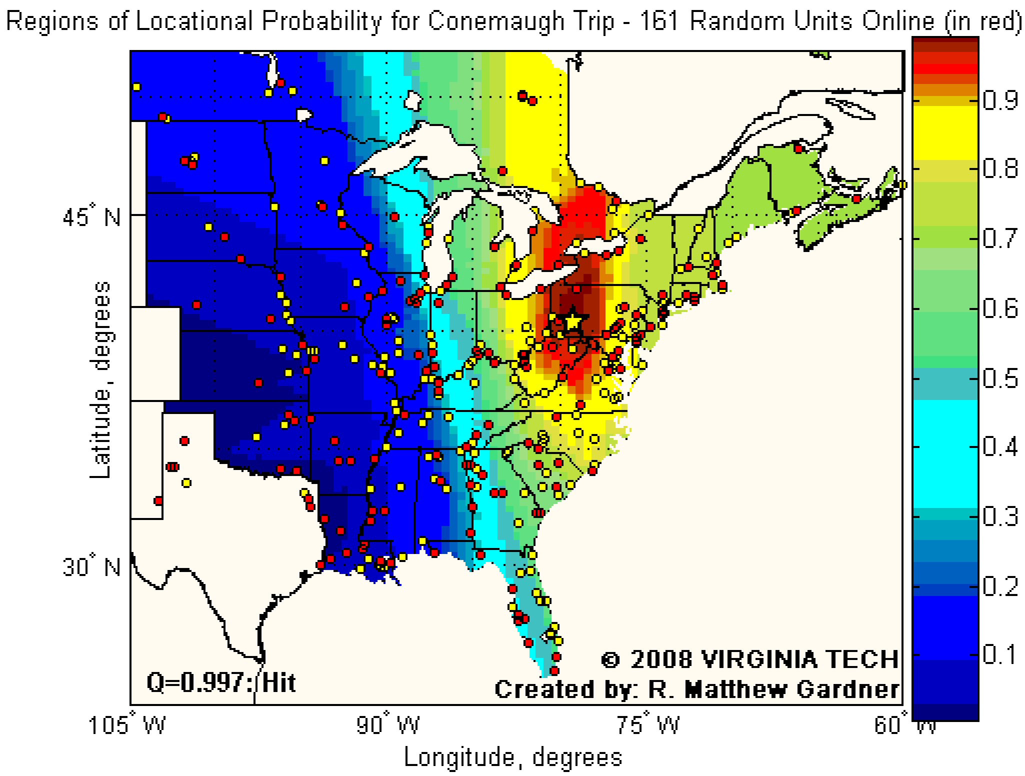
Regions of Locational Probability for Conemaugh Trip - 161 Random Units Online (in red)
45° N
30° N
Latitude, degrees
105° W
90° W
75° W
60° W
Longitude, degrees
Q=0.997: Hit
© 2008 VIRGINIA TECH
Created by: R. Matthew Gardner
0.9
0.8
0.7
0.6
0.5
0.4
0.3
0.2
0.1

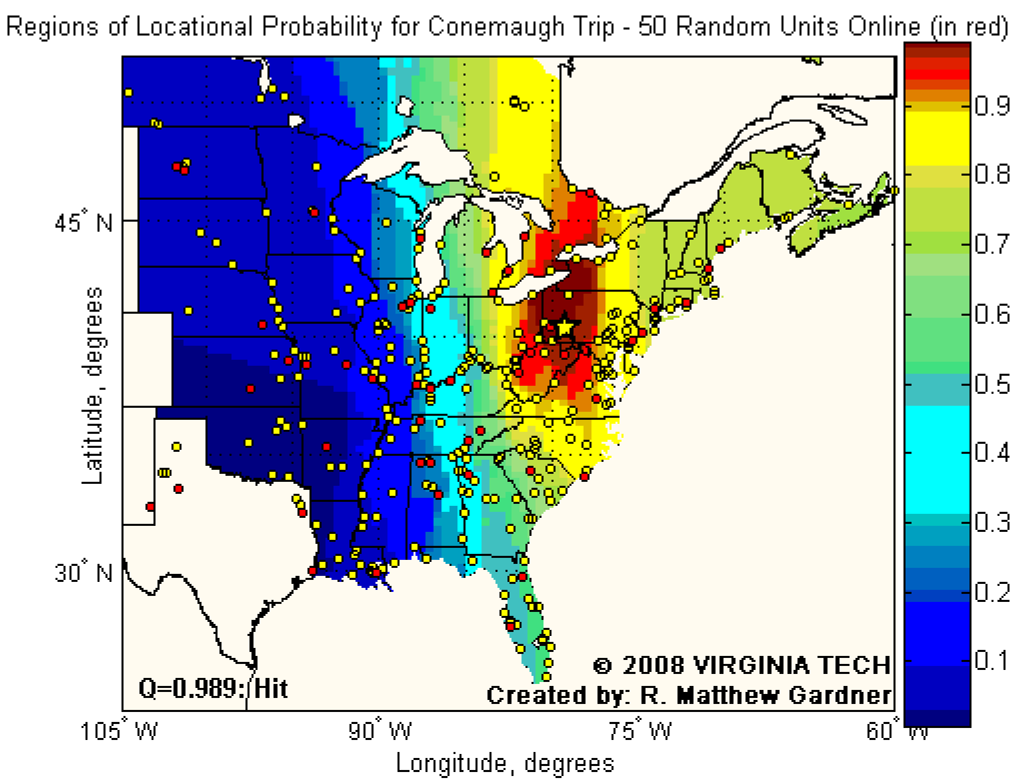
Regions of Locational Probability for Conemaugh Trip - 50 Random Units Online (in red)
45° N
30° N
Latitude, degrees
105° W
90° W
75° W
60° W
Longitude, degrees
Q=0.989: Hit
© 2008 VIRGINIA TECH
Created by: R. Matthew Gardner
0.9
0.8
0.7
0.6
0.5
0.4
0.3
0.2
0.1

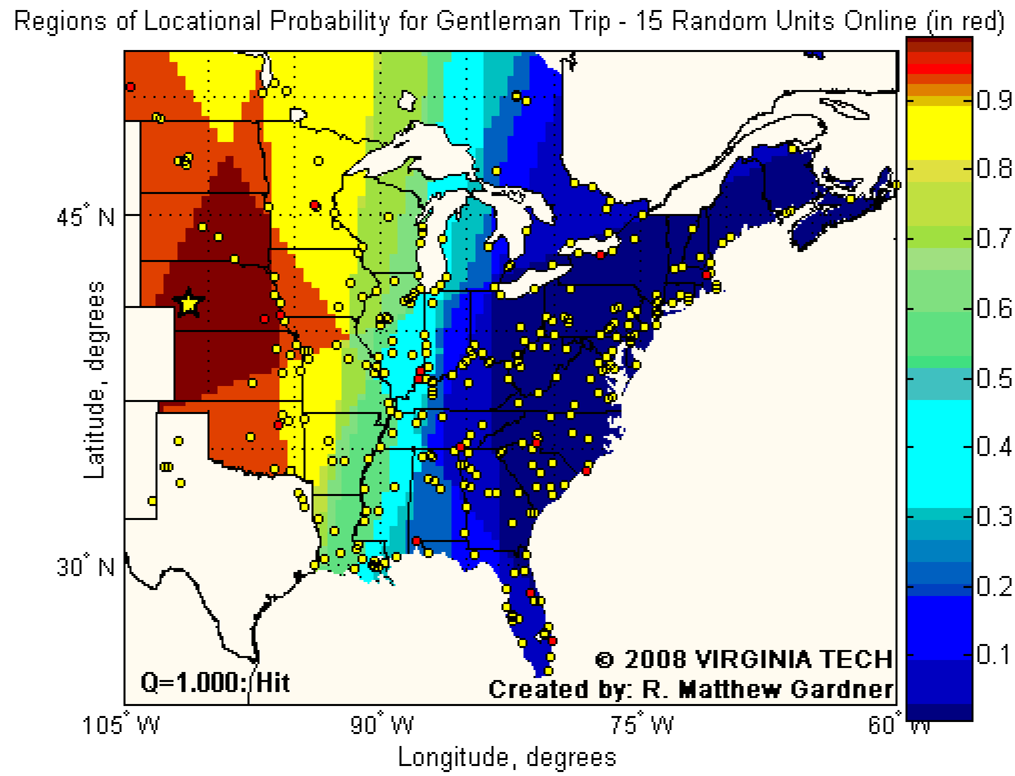
Regions of Locational Probability for Gentleman Trip - 15 Random Units Online (in red)
45° N
30° N
Latitude, degrees
105° W
90° W
75° W
60° W
Longitude, degrees
Q=1.000:/Hit
© 2008 VIRGINIA TECH
Created by: R. Matthew Gardner
0.9
0.8
0.7
0.6
0.5
0.4
0.3
0.2
0.1

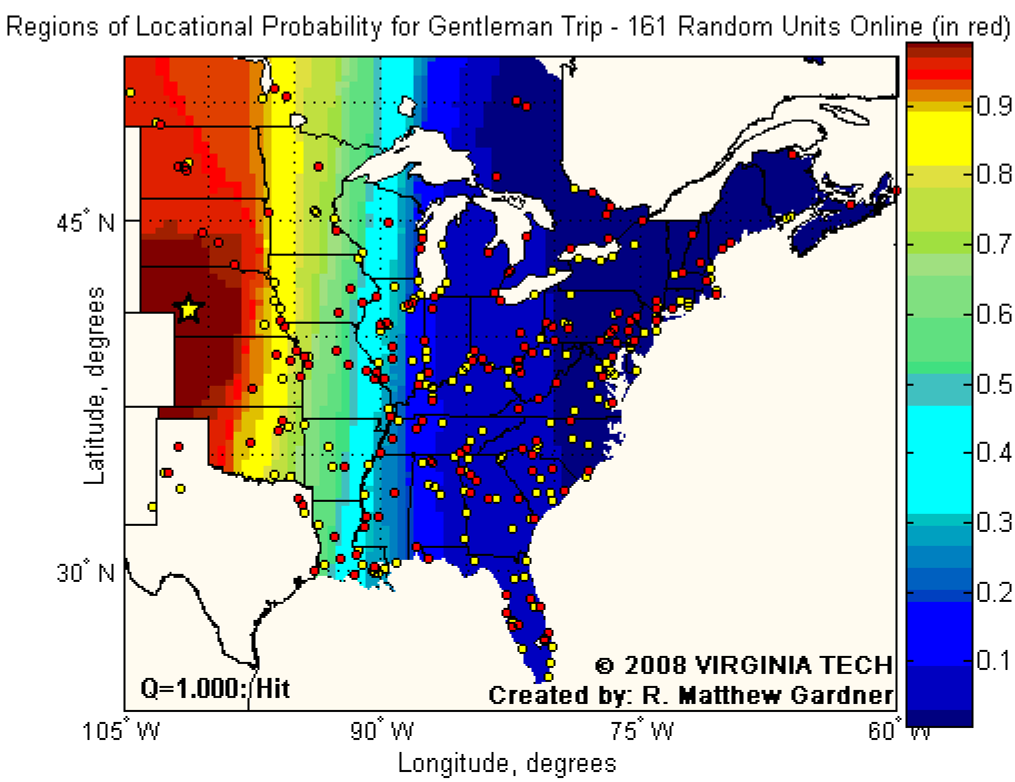
Regions of Locational Probability for Gentleman Trip - 161 Random Units Online (in red)
45° N
30° N
Latitude, degrees
105° W
90° W
75° W
60° W
Longitude, degrees
Q=1.000:/Hit
© 2008 VIRGINIA TECH
Created by: R. Matthew Gardner
0.9
0.8
0.7
0.6
0.5
0.4
0.3
0.2
0.1

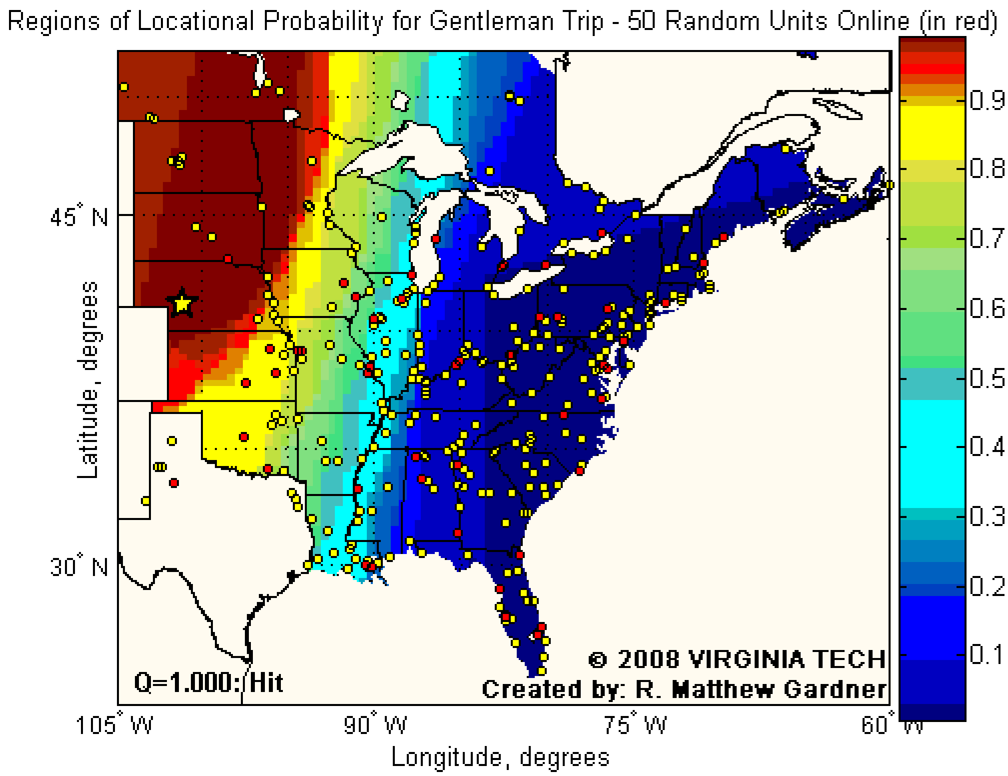
Regions of Locational Probability for Gentleman Trip - 50 Random Units Online (in red)
45° N
30° N
Latitude, degrees
105° W
90° W
75° W
60° W
Longitude, degrees
Q=1.000:/Hit
© 2008 VIRGINIA TECH
Created by: R. Matthew Gardner
0.9
0.8
0.7
0.6
0.5
0.4
0.3
0.2
0.1

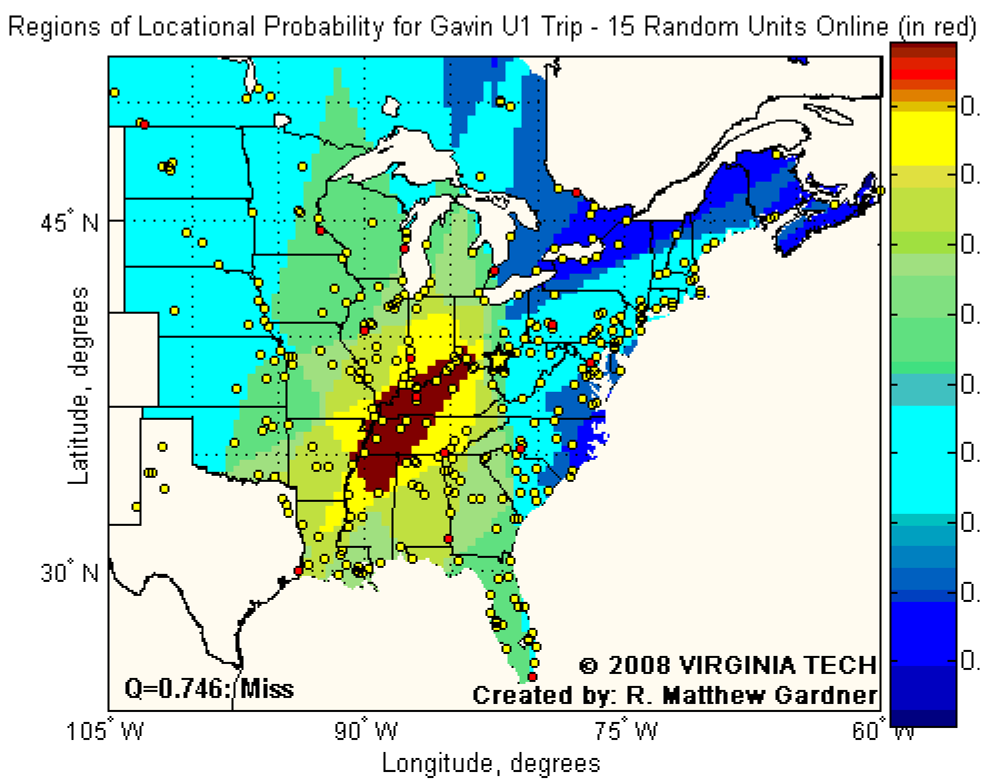
Regions of Locational Probability for Gavin U1 Trip - 15 Random Units Online (in red)
45° N
30° N
Latitude, degrees
105° W
90° W
75° W
60° W
Longitude, degrees
Q=0.746:/Miss
© 2008 VIRGINIA TECH
Created by: R. Matthew Gardner
0.9
0.8
0.7
0.6
0.5
0.4
0.3
0.2
0.1

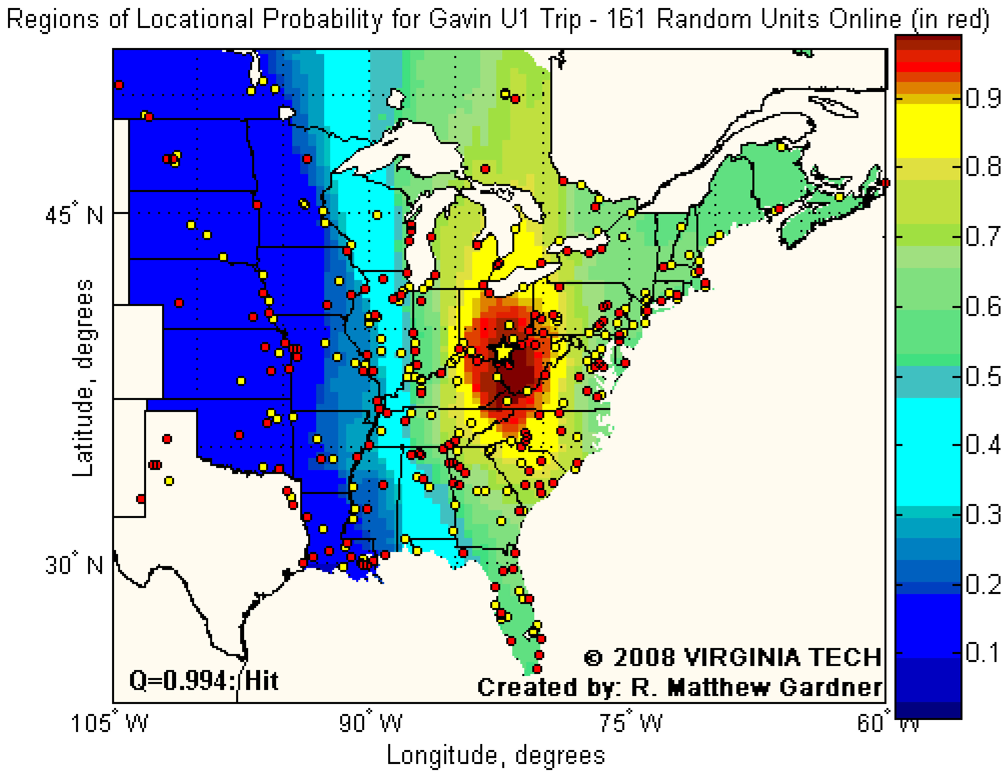
Regions of Locational Probability for Gavin U1 Trip - 161 Random Units Online (in red)
45° N
30° N
Latitude, degrees
105° W
90° W
75° W
60° W
Longitude, degrees
Q=0.994: Hit
© 2008 VIRGINIA TECH
Created by: R. Matthew Gardner
0.9
0.8
0.7
0.6
0.5
0.4
0.3
0.2
0.1

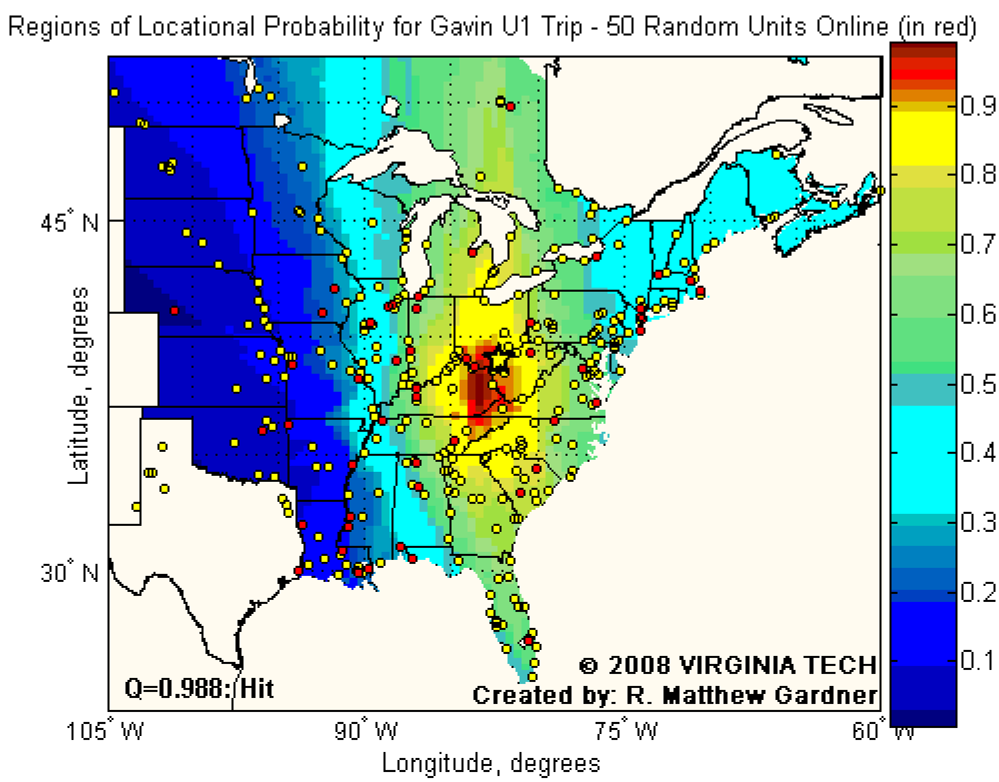
Regions of Locational Probability for Gavin U1 Trip - 50 Random Units Online (in red)
45° N
30° N
Latitude, degrees
105° W
90° W
75° W
60° W
Longitude, degrees
Q=0.988: Hit
© 2008 VIRGINIA TECH
Created by: R. Matthew Gardner
0.9
0.8
0.7
0.6
0.5
0.4
0.3
0.2
0.1

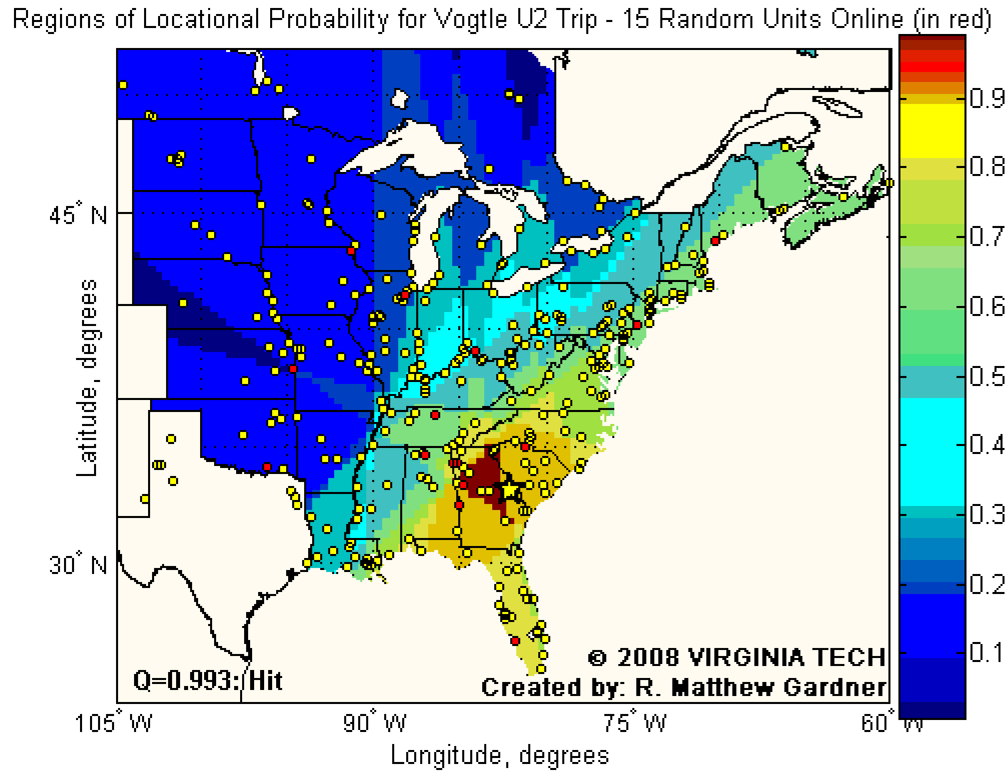
Regions of Locational Probability for Vogtle U2 Trip - 15 Random Units Online (in red)
Latitude, degrees
Longitude, degrees
45° N
30° N
105° W
90° W
75° W
60° W
0.9
0.8
0.7
0.6
0.5
0.4
0.3
0.2
0.1
Q=0.993: Hit
© 2008 VIRGINIA TECH
Created by: R. Matthew Gardner

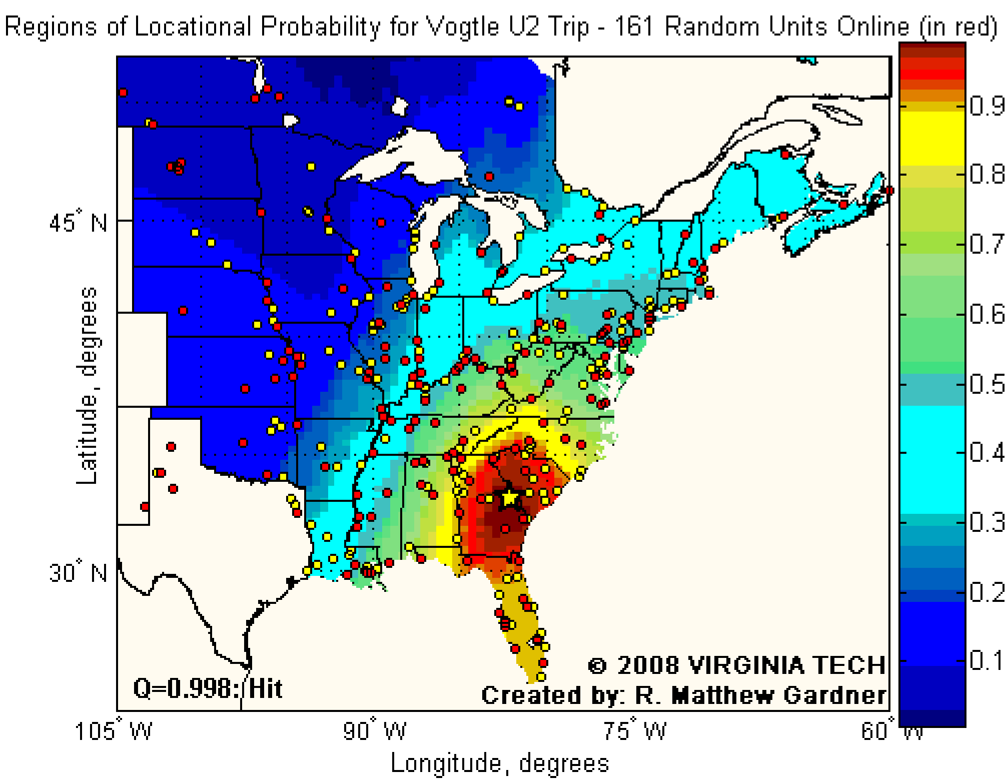
Regions of Locational Probability for Vogtle U2 Trip - 161 Random Units Online (in red)
Latitude, degrees
Longitude, degrees
45° N
30° N
105° W
90° W
75° W
60° W
0.9
0.8
0.7
0.6
0.5
0.4
0.3
0.2
0.1
Q=0.998: Hit
© 2008 VIRGINIA TECH
Created by: R. Matthew Gardner

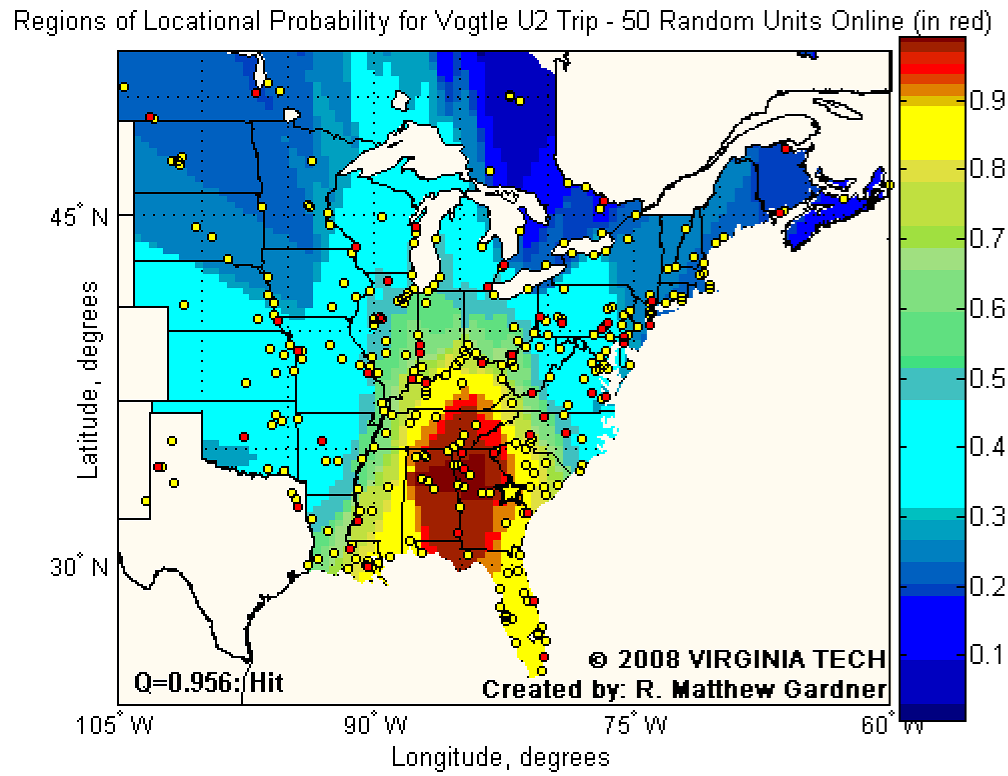
Regions of Locational Probability for Vogtle U2 Trip - 50 Random Units Online (in red)
45° N
30° N
Latitude, degrees
105° W
90° W
75° W
60° W
Longitude, degrees
Q=0.956: Hit
© 2008 VIRGINIA TECH
Created by: R. Matthew Gardner
0.9
0.8
0.7
0.6
0.5
0.4
0.3
0.2
0.1

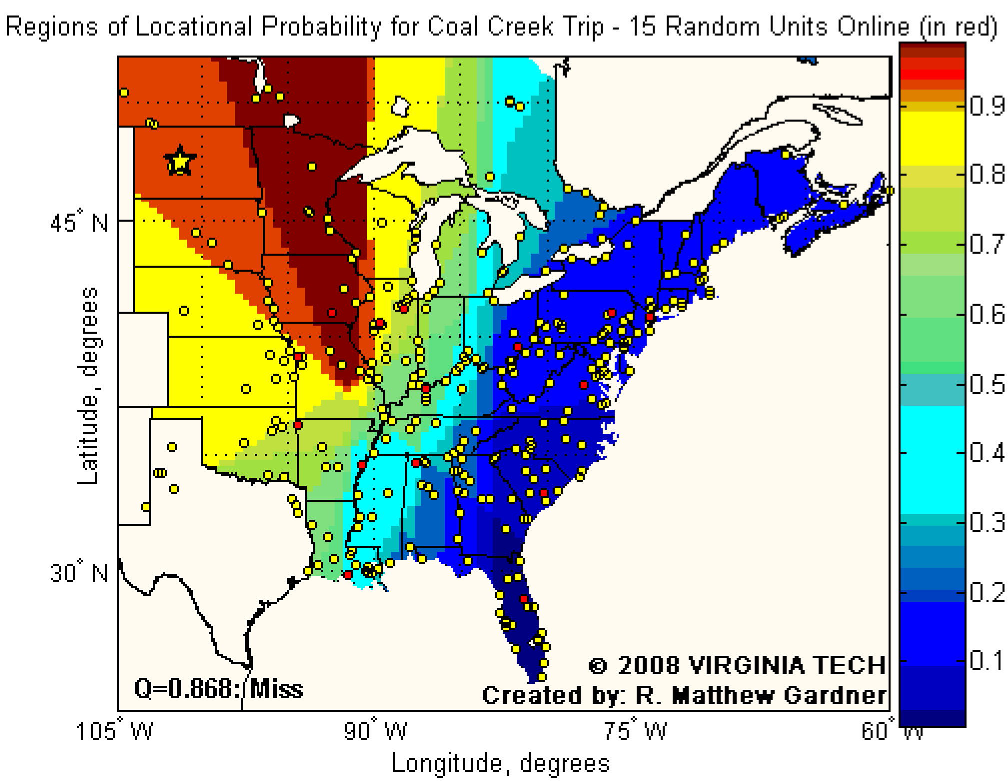
Regions of Locational Probability for Coal Creek Trip - 15 Random Units Online (in red)
45° N
30° N
Latitude, degrees
105° W
90° W
75° W
60° W
Longitude, degrees
Q=0.868: Miss
© 2008 VIRGINIA TECH
Created by: R. Matthew Gardner
0.9
0.8
0.7
0.6
0.5
0.4
0.3
0.2
0.1

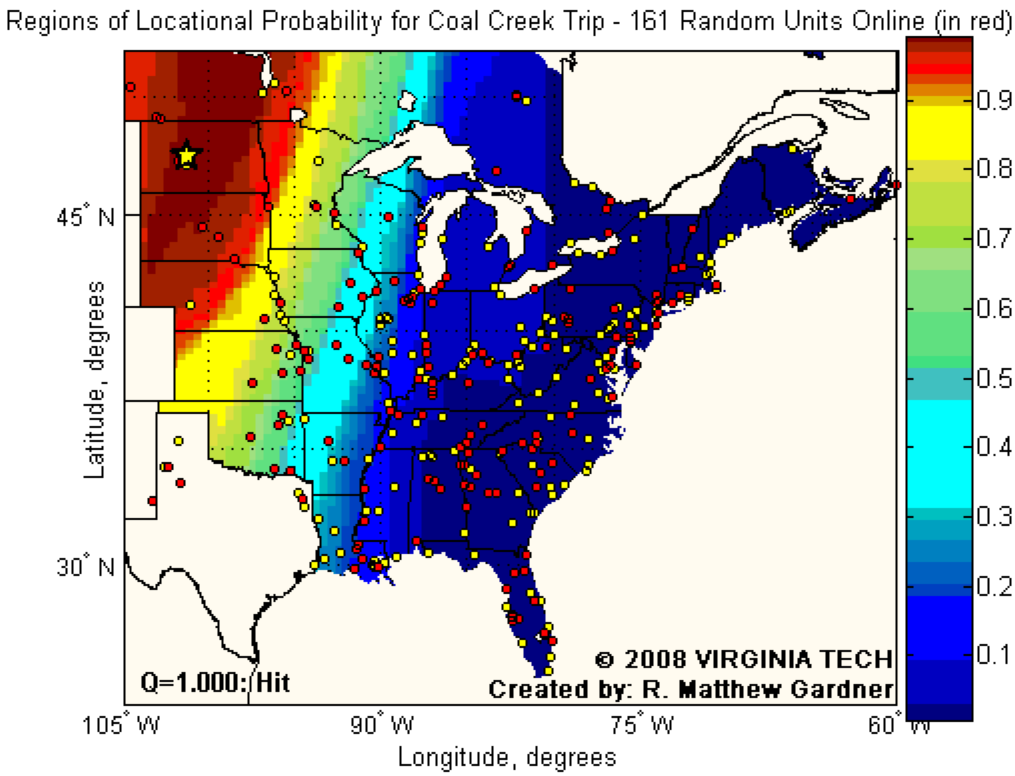
Regions of Locational Probability for Coal Creek Trip - 161 Random Units Online (in red)
45° N
30° N
Latitude, degrees
105° W
90° W
75° W
60° W
Longitude, degrees
Q=1.000:/Hit
© 2008 VIRGINIA TECH
Created by: R. Matthew Gardner
0.9
0.8
0.7
0.6
0.5
0.4
0.3
0.2
0.1

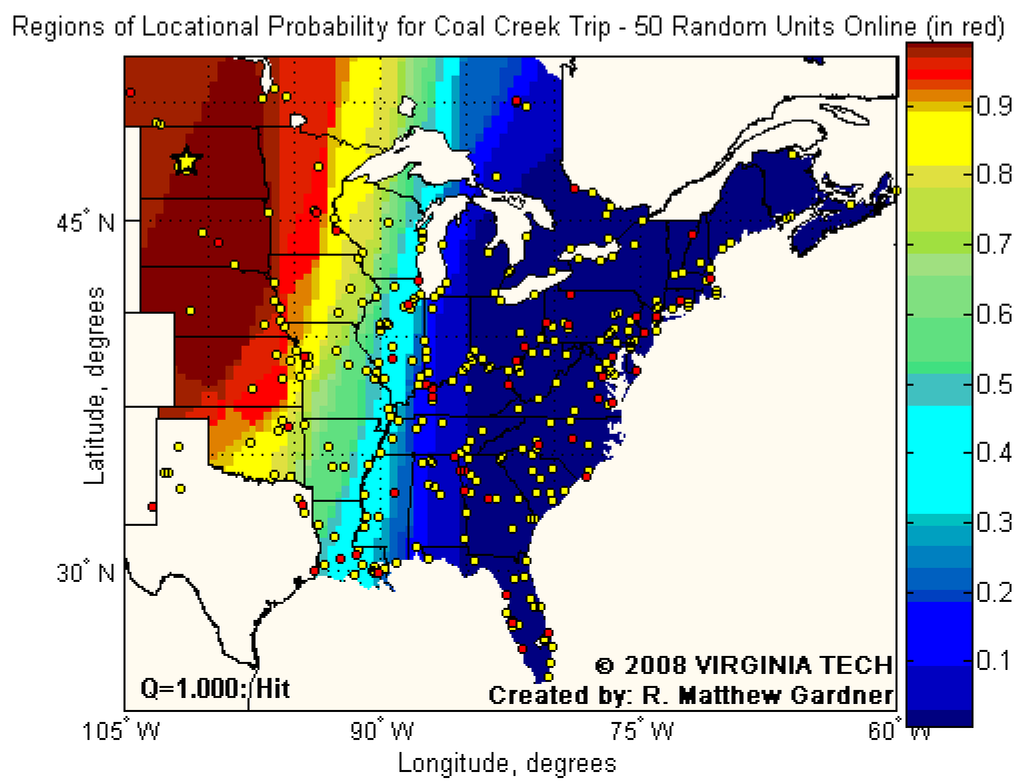
Regions of Locational Probability for Coal Creek Trip - 50 Random Units Online (in red)
45° N
30° N
Latitude, degrees
105° W
90° W
75° W
60° W
Longitude, degrees
Q=1.000:/Hit
© 2008 VIRGINIA TECH
Created by: R. Matthew Gardner
0.9
0.8
0.7
0.6
0.5
0.4
0.3
0.2
0.1

Regions of Locational Probability for Palisades Trip - 15 Random Units Online (in red)

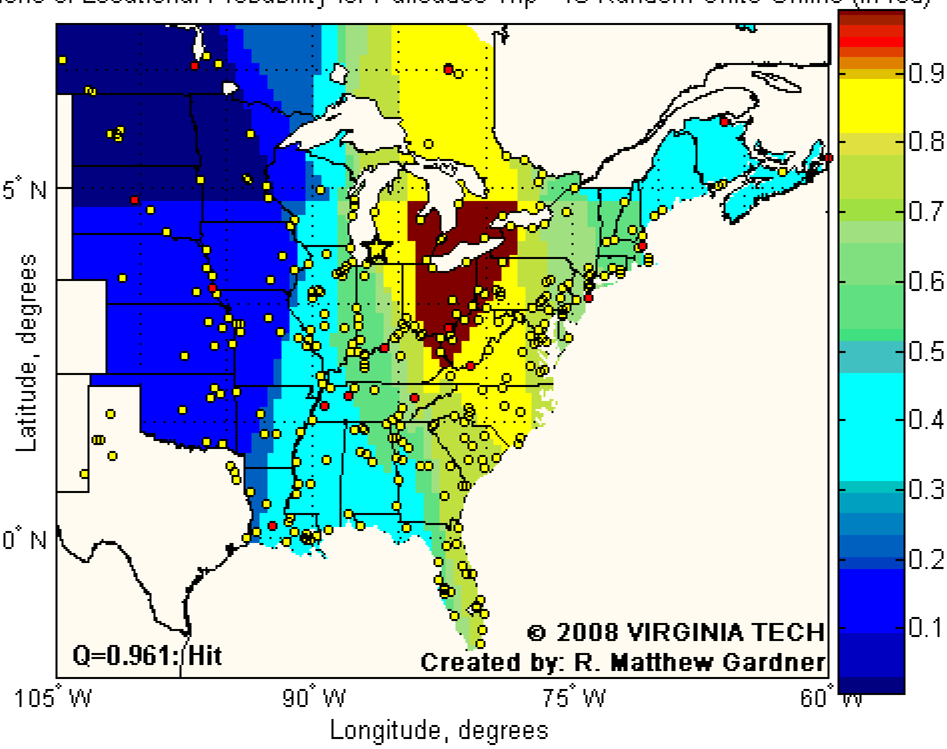

Regions of Locational Probability for Palisades Trip - 161 Random Units Online (in red)

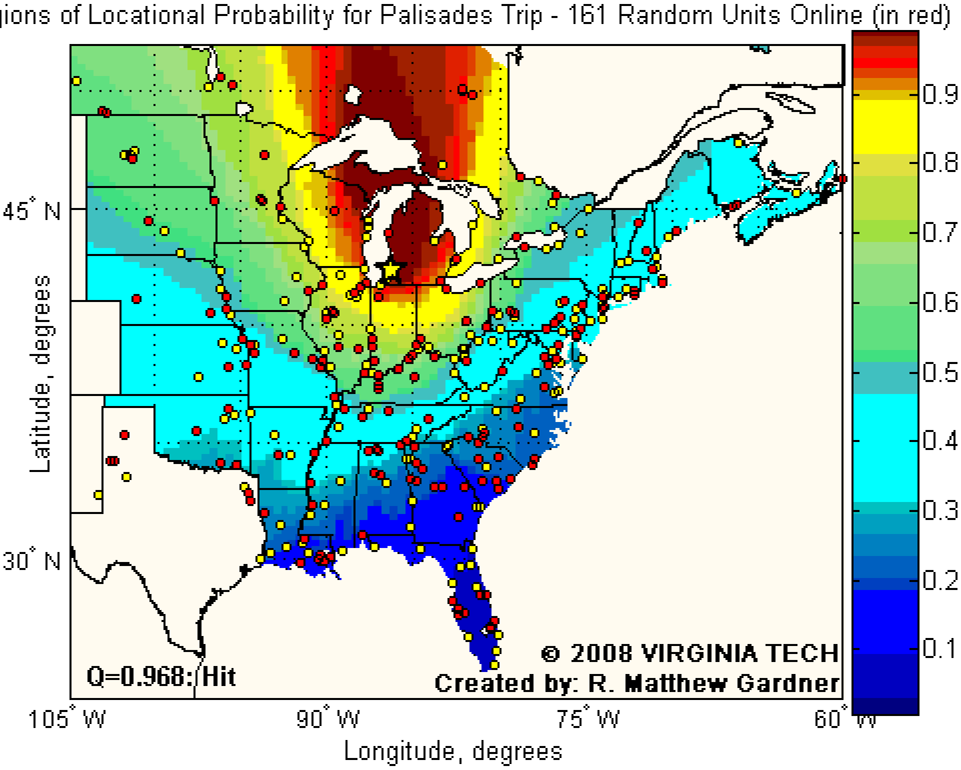

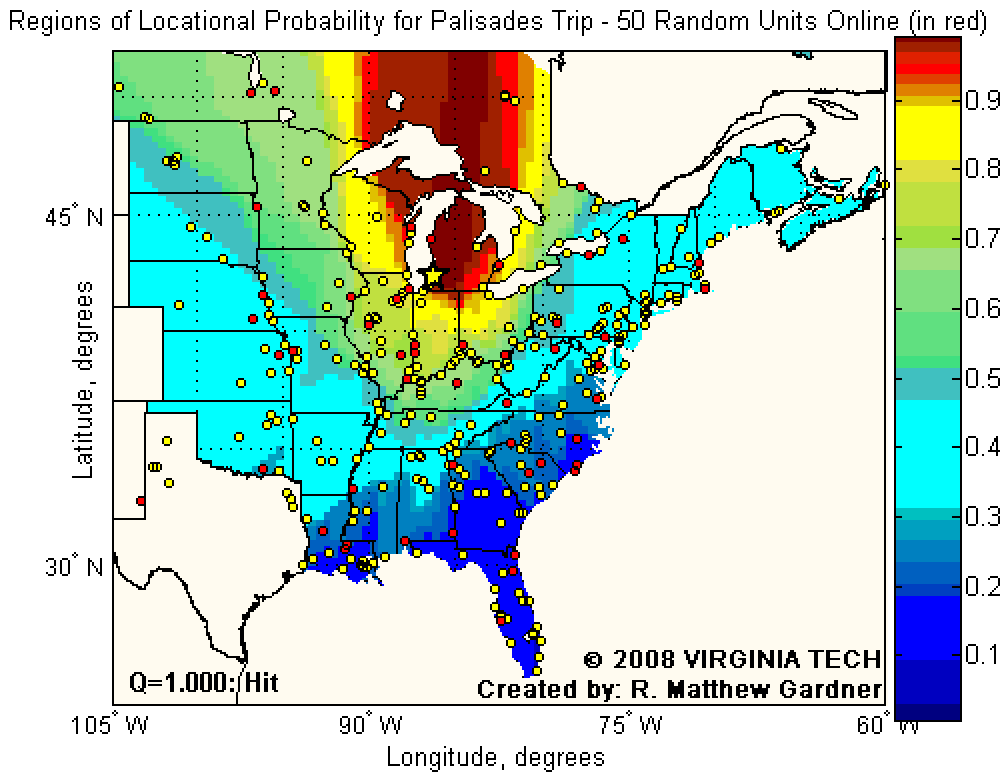
Regions of Locational Probability for Palisades Trip - 50 Random Units Online (in red)
45° N
30° N
Latitude, degrees
105° W
90° W
75° W
60° W
Longitude, degrees
Q=1.000: Hit
© 2008 VIRGINIA TECH
Created by: R. Matthew Gardner
0.9
0.8
0.7
0.6
0.5
0.4
0.3
0.2
0.1

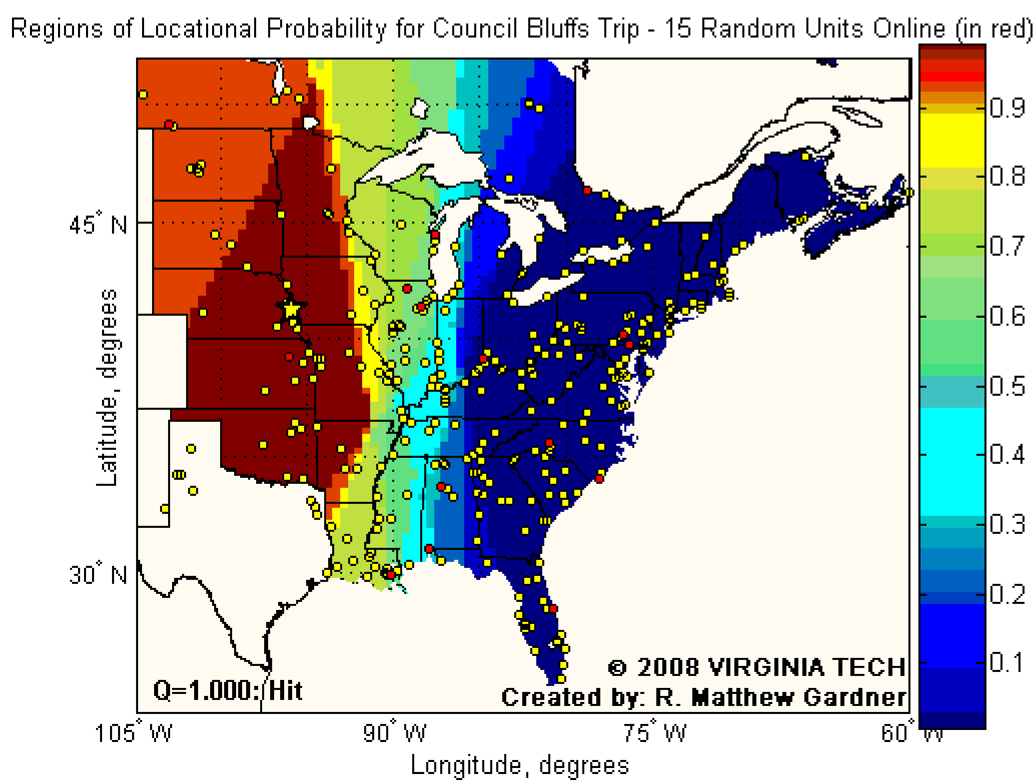
Regions of Locational Probability for Council Bluffs Trip - 15 Random Units Online (in red)
45° N
30° N
Latitude, degrees
105° W
90° W
75° W
60° W
Longitude, degrees
Q=1.000: Hit
© 2008 VIRGINIA TECH
Created by: R. Matthew Gardner
0.9
0.8
0.7
0.6
0.5
0.4
0.3
0.2
0.1

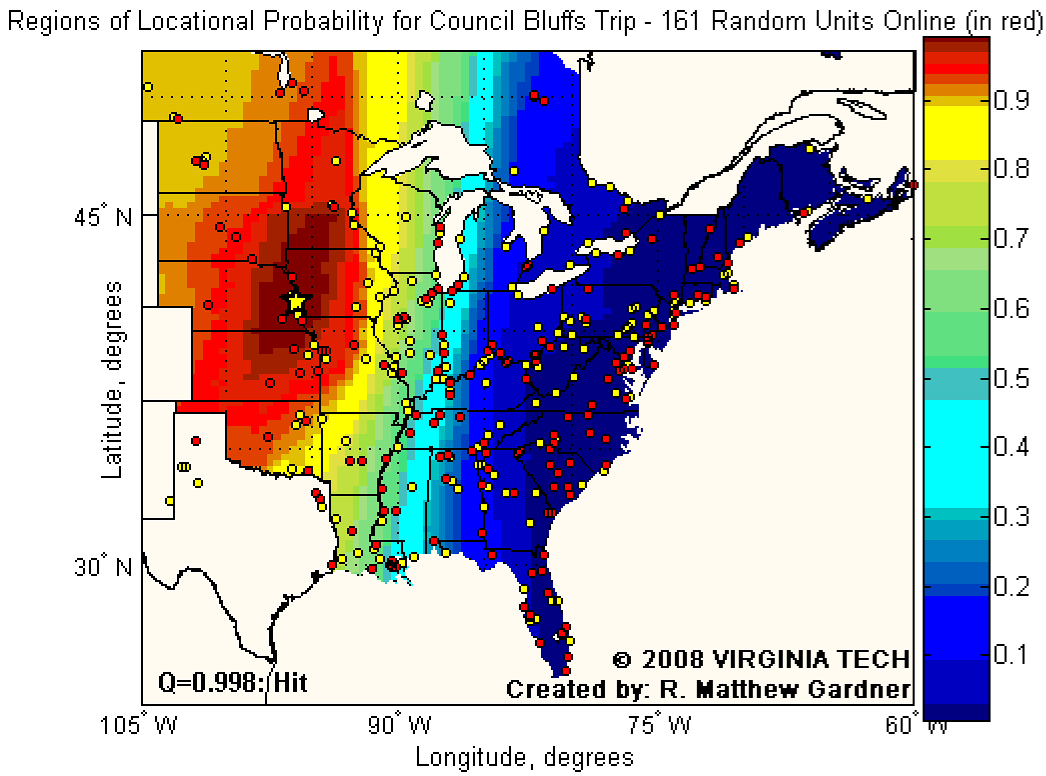
Regions of Locational Probability for Council Bluffs Trip - 161 Random Units Online (in red)
45° N
30° N
Latitude, degrees
105° W
90° W
75° W
60° W
Longitude, degrees
Q=0.998: Hit
© 2008 VIRGINIA TECH
Created by: R. Matthew Gardner
0.9
0.8
0.7
0.6
0.5
0.4
0.3
0.2
0.1

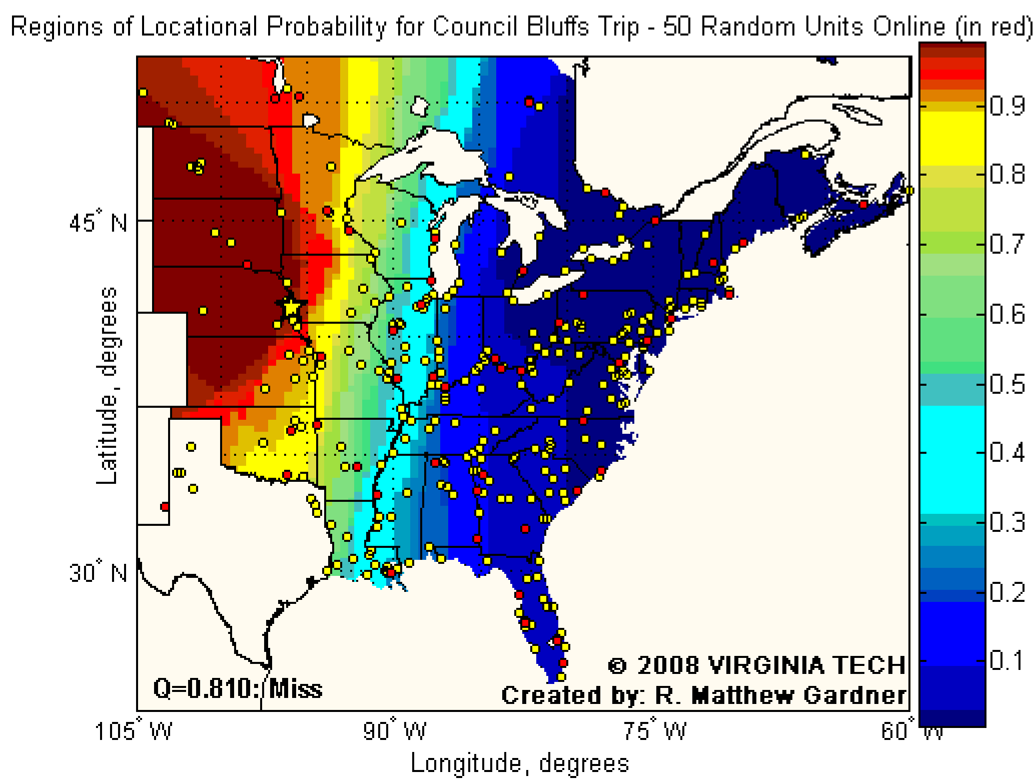
Regions of Locational Probability for Council Bluffs Trip - 50 Random Units Online (in red)
45° N
30° N
Latitude, degrees
105° W
90° W
75° W
60° W
Longitude, degrees
Q=0.810: Miss
© 2008 VIRGINIA TECH
Created by: R. Matthew Gardner
0.9
0.8
0.7
0.6
0.5
0.4
0.3
0.2
0.1

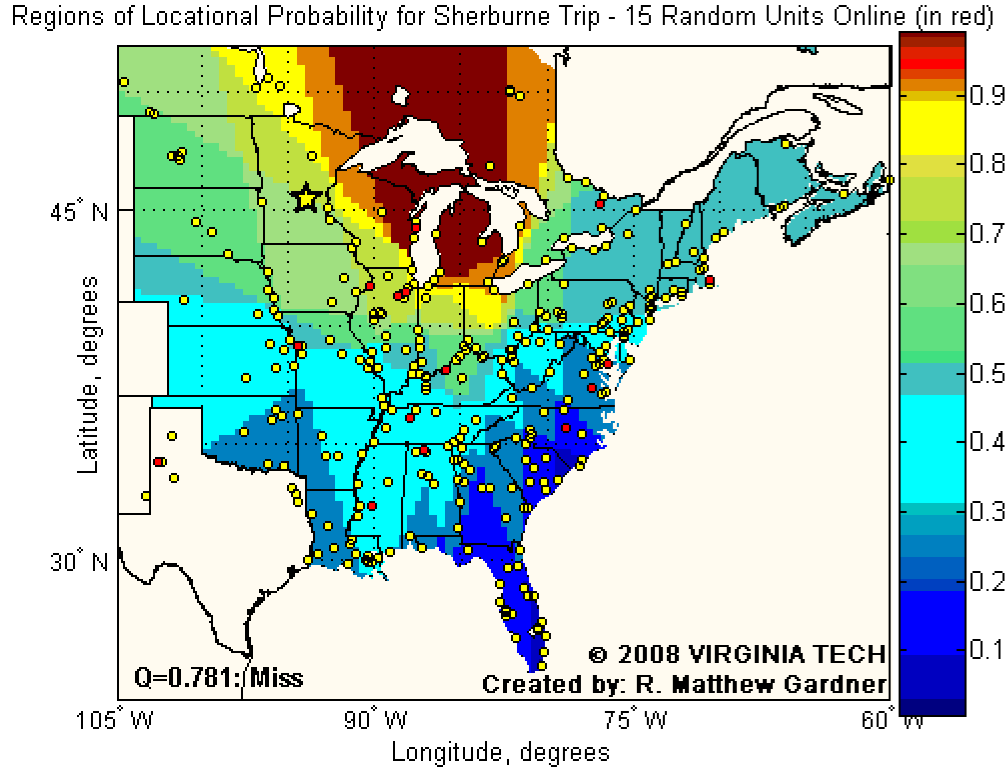
Regions of Locational Probability for Sherburne Trip - 15 Random Units Online (in red)
45° N
30° N
Latitude, degrees
105° W
90° W
75° W
60° W
Longitude, degrees
Q=0.781: Miss
© 2008 VIRGINIA TECH
Created by: R. Matthew Gardner
0.9
0.8
0.7
0.6
0.5
0.4
0.3
0.2
0.1

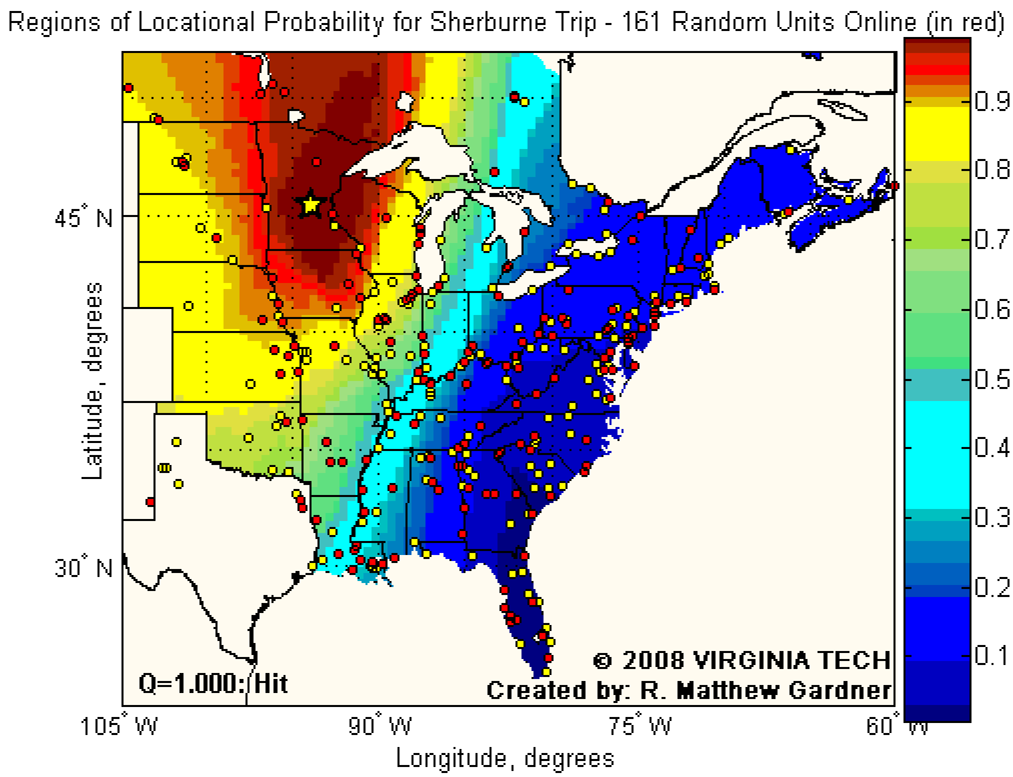
Regions of Locational Probability for Sherburne Trip - 161 Random Units Online (in red)
45° N
30° N
Latitude, degrees
105° W
90° W
75° W
60° W
Longitude, degrees
Q=1.000: Hit
© 2008 VIRGINIA TECH
Created by: R. Matthew Gardner
0.9
0.8
0.7
0.6
0.5
0.4
0.3
0.2
0.1

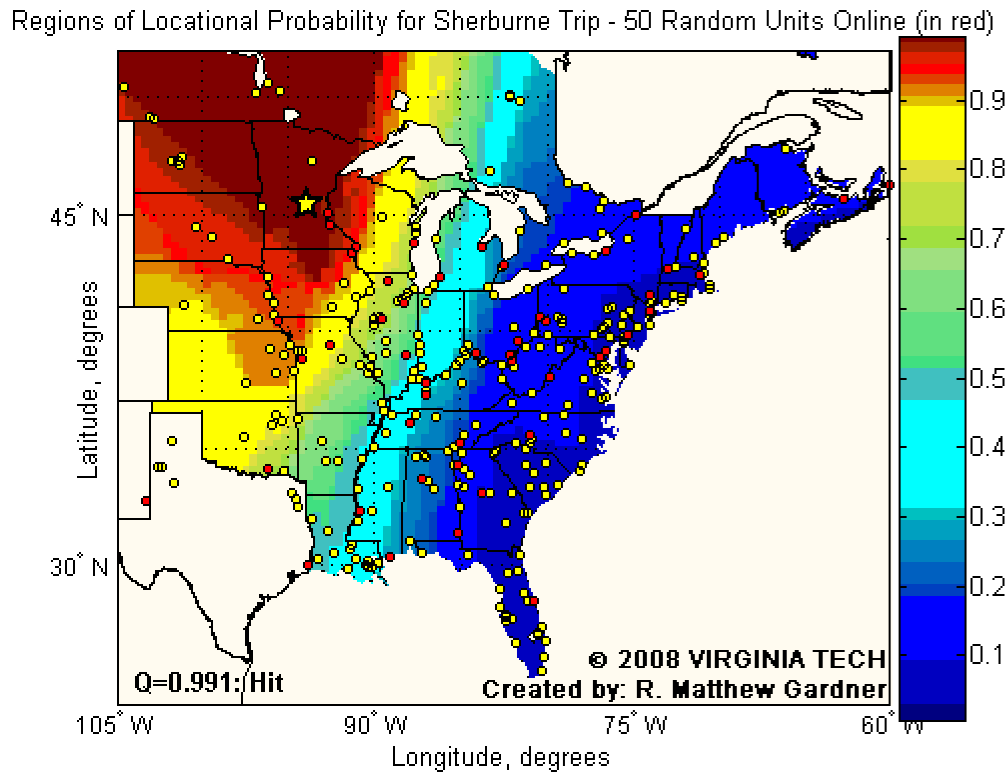
Regions of Locational Probability for Sherburne Trip - 50 Random Units Online (in red)
Latitude, degrees
45° N
30° N
Longitude, degrees
105° W
90° W
75° W
60° W
Q=0.991: Hit
© 2008 VIRGINIA TECH
Created by: R. Matthew Gardner
0.9
0.8
0.7
0.6
0.5
0.4
0.3
0.2
0.1

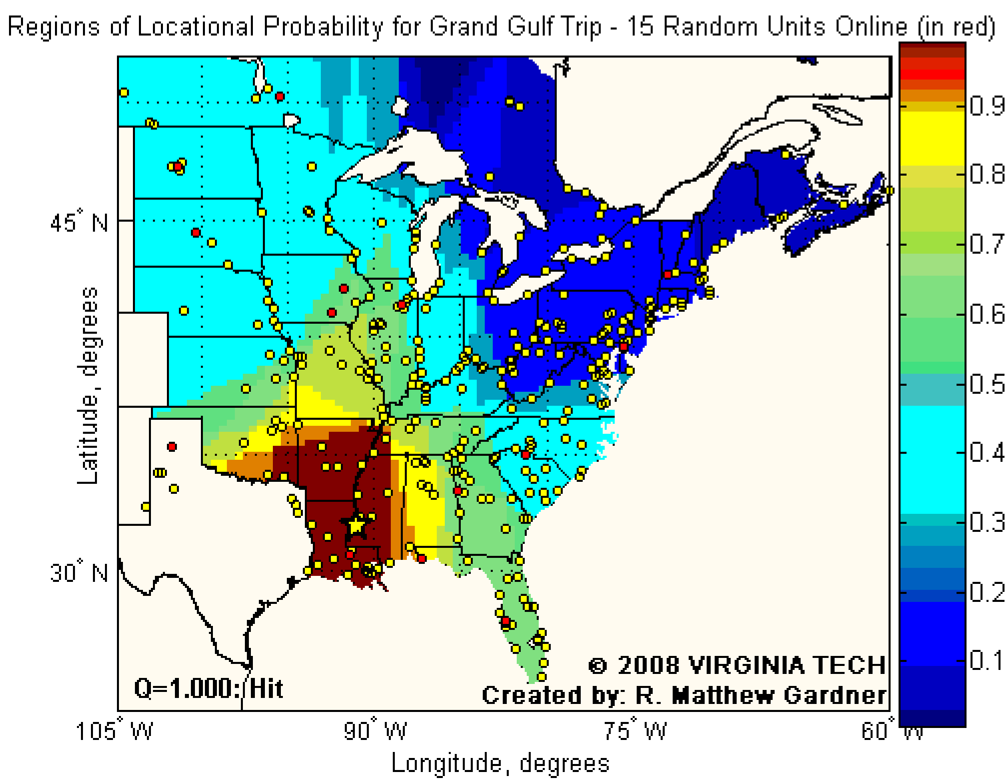
Regions of Locational Probability for Grand Gulf Trip - 15 Random Units Online (in red)
Latitude, degrees
45° N
30° N
Longitude, degrees
105° W
90° W
75° W
60° W
Q=1.000: Hit
© 2008 VIRGINIA TECH
Created by: R. Matthew Gardner
0.9
0.8
0.7
0.6
0.5
0.4
0.3
0.2
0.1

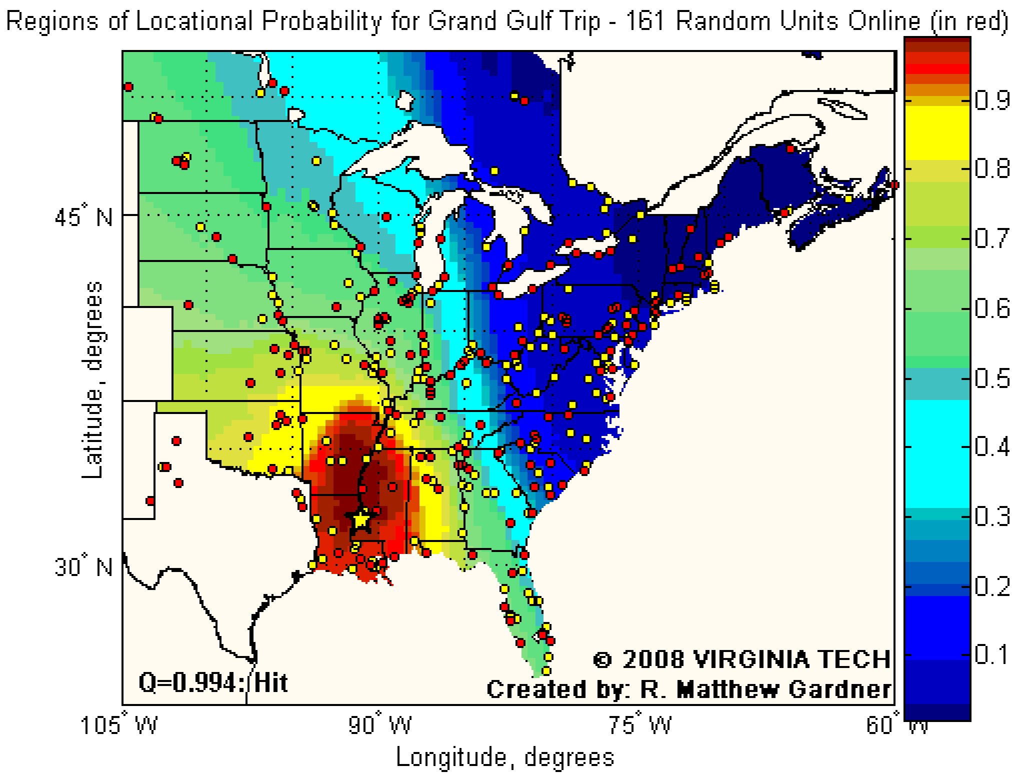
Regions of Locational Probability for Grand Gulf Trip - 161 Random Units Online (in red)
45° N
30° N
Latitude, degrees
105° W
90° W
75° W
60° W
Longitude, degrees
Q=0.994: Hit
© 2008 VIRGINIA TECH
Created by: R. Matthew Gardner
0.9
0.8
0.7
0.6
0.5
0.4
0.3
0.2
0.1

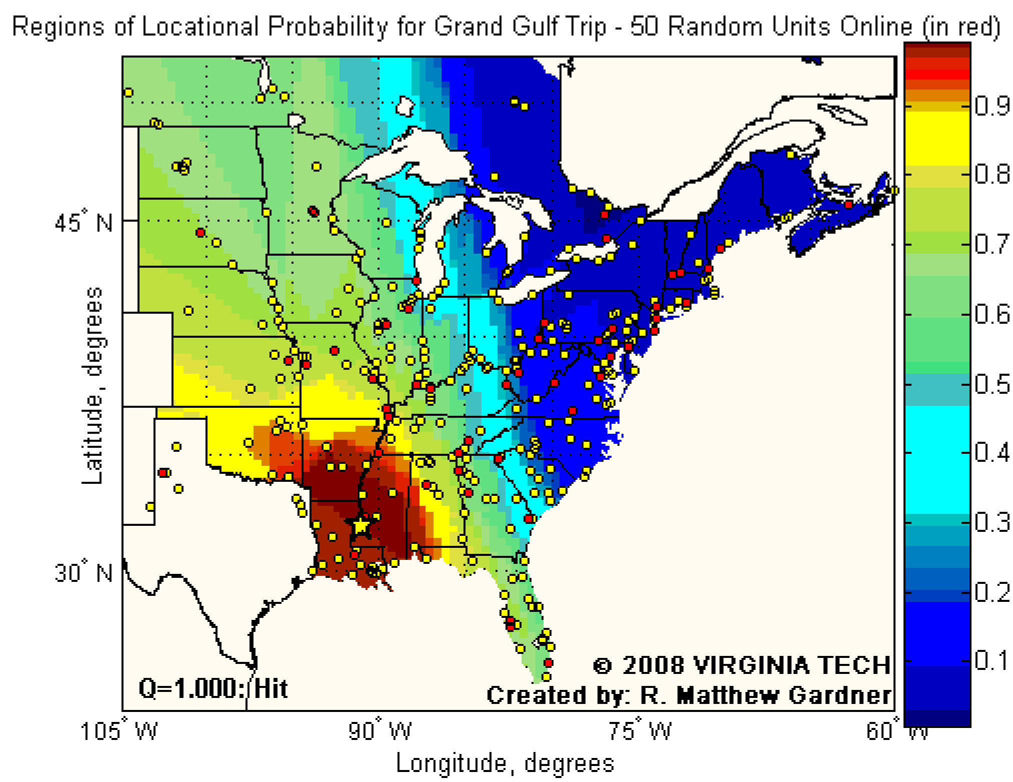
Regions of Locational Probability for Grand Gulf Trip - 50 Random Units Online (in red)
45° N
30° N
Latitude, degrees
105° W
90° W
75° W
60° W
Longitude, degrees
Q=1.000: Hit
© 2008 VIRGINIA TECH
Created by: R. Matthew Gardner
0.9
0.8
0.7
0.6
0.5
0.4
0.3
0.2
0.1

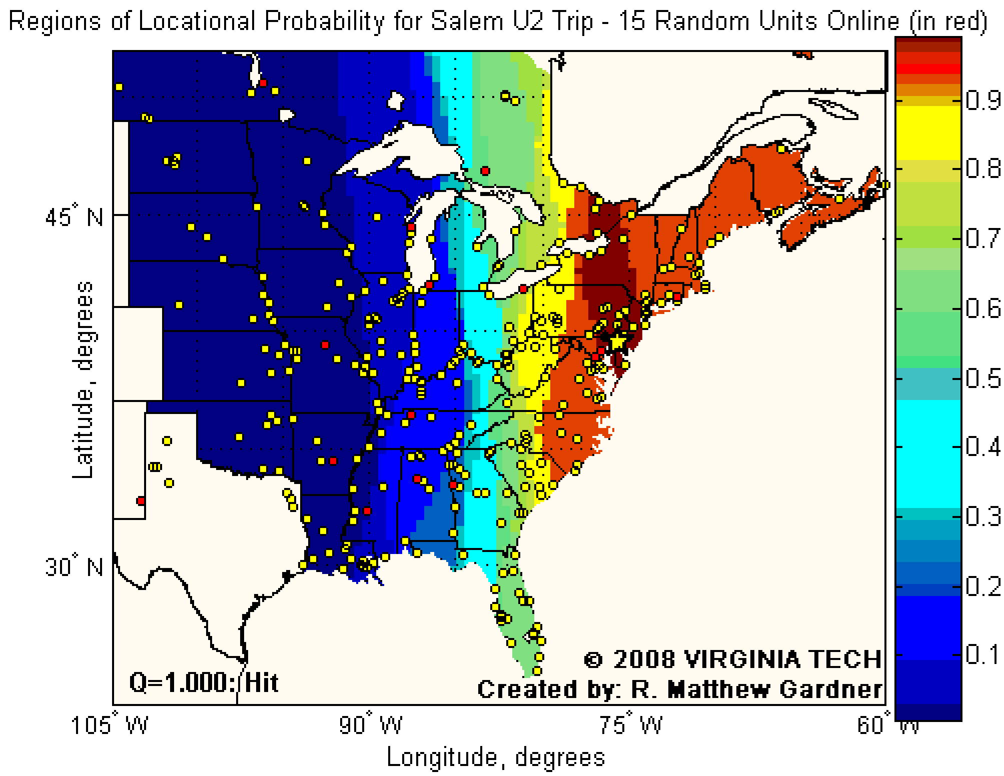
Regions of Locational Probability for Salem U2 Trip - 15 Random Units Online (in red)
45° N
30° N
Latitude, degrees
105° W
90° W
75° W
60° W
Longitude, degrees
Q=1.000: Hit
© 2008 VIRGINIA TECH
Created by: R. Matthew Gardner
0.9
0.8
0.7
0.6
0.5
0.4
0.3
0.2
0.1

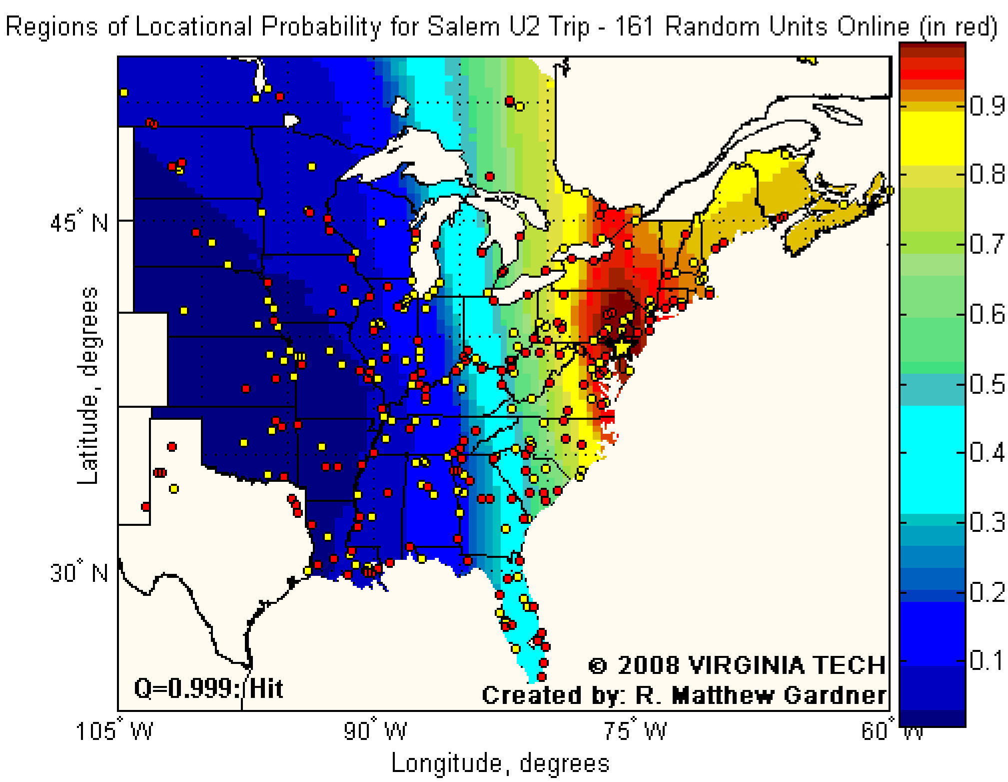
Regions of Locational Probability for Salem U2 Trip - 161 Random Units Online (in red)
45° N
30° N
Latitude, degrees
105° W
90° W
75° W
60° W
Longitude, degrees
Q=0.999: Hit
© 2008 VIRGINIA TECH
Created by: R. Matthew Gardner
0.9
0.8
0.7
0.6
0.5
0.4
0.3
0.2
0.1

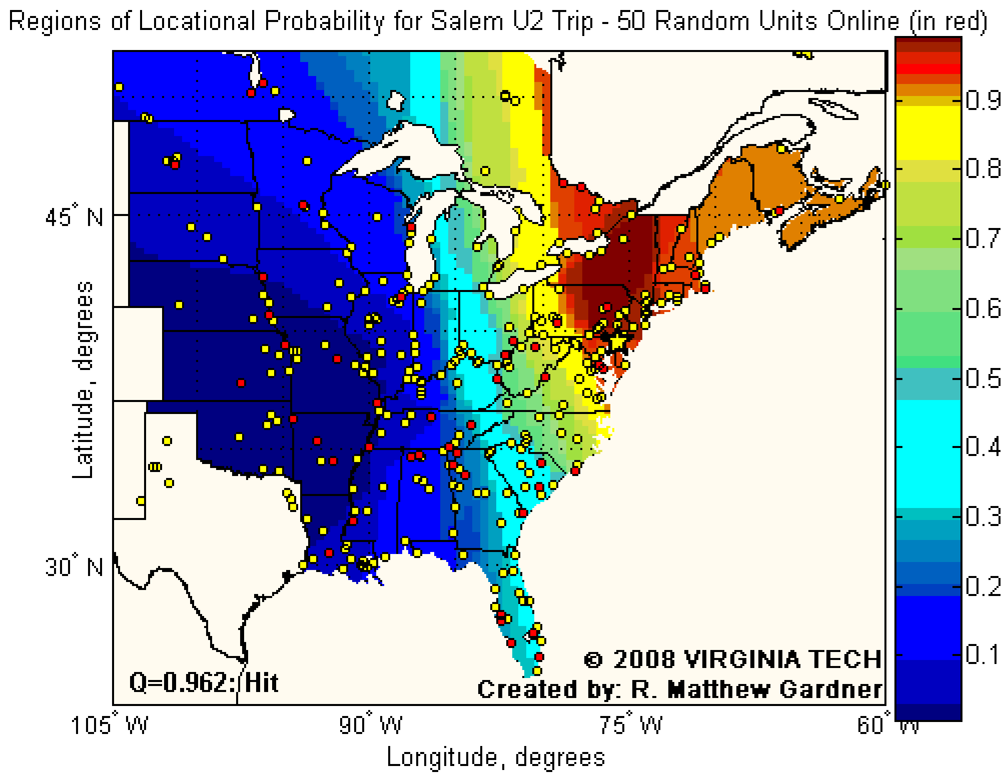
Regions of Locational Probability for Salem U2 Trip - 50 Random Units Online (in red)
45° N
30° N
Latitude, degrees
105° W
90° W
75° W
60° W
Longitude, degrees
Q=0.962: Hit
© 2008 VIRGINIA TECH
Created by: R. Matthew Gardner
0.9
0.8
0.7
0.6
0.5
0.4
0.3
0.2
0.1

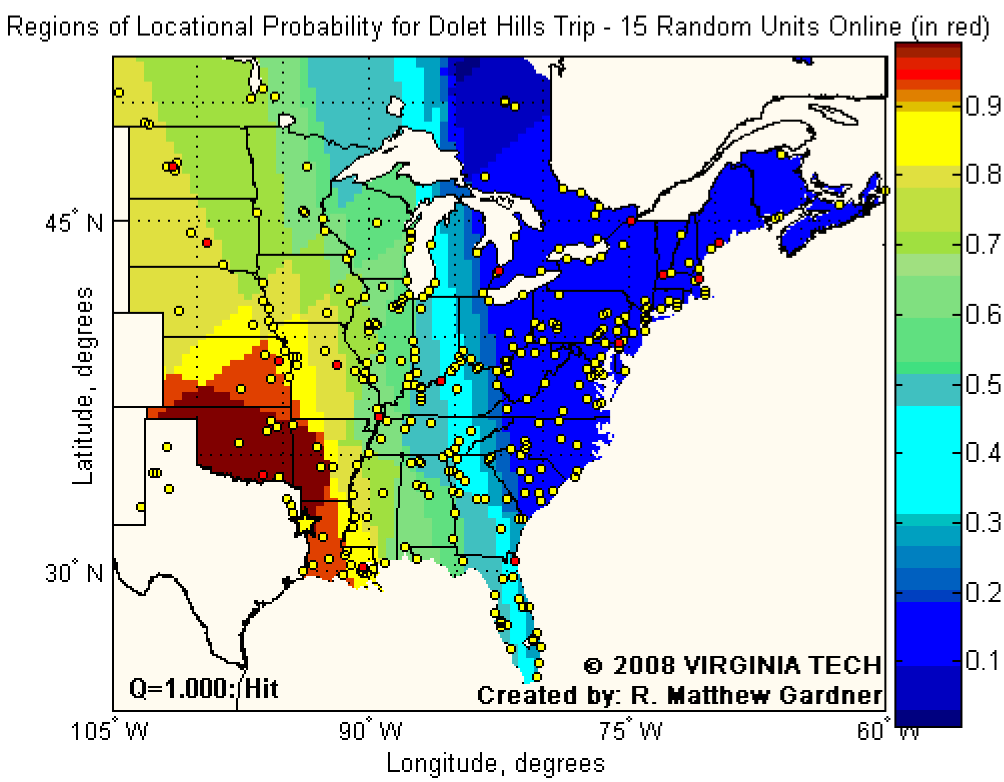
Regions of Locational Probability for Dolet Hills Trip - 15 Random Units Online (in red)
45° N
30° N
Latitude, degrees
105° W
90° W
75° W
60° W
Longitude, degrees
Q=1.000: Hit
© 2008 VIRGINIA TECH
Created by: R. Matthew Gardner
0.9
0.8
0.7
0.6
0.5
0.4
0.3
0.2
0.1

Regions of Locational Probability for Dolet Hills Trip - 161 Random Units Online (in red)

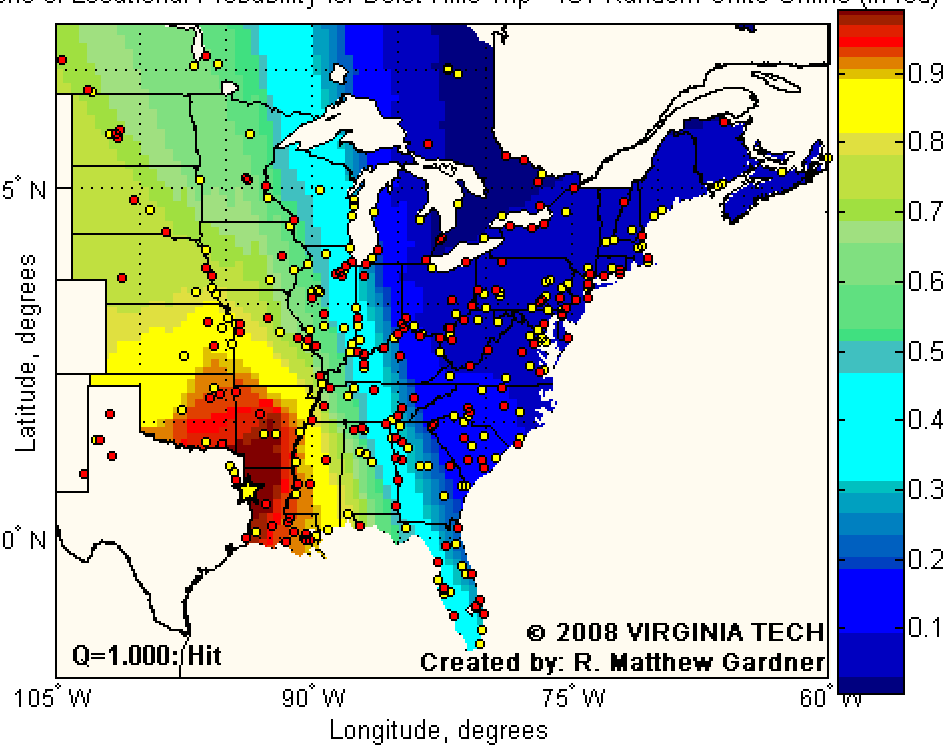

Regions of Locational Probability for Dolet Hills Trip - 50 Random Units Online (in red)

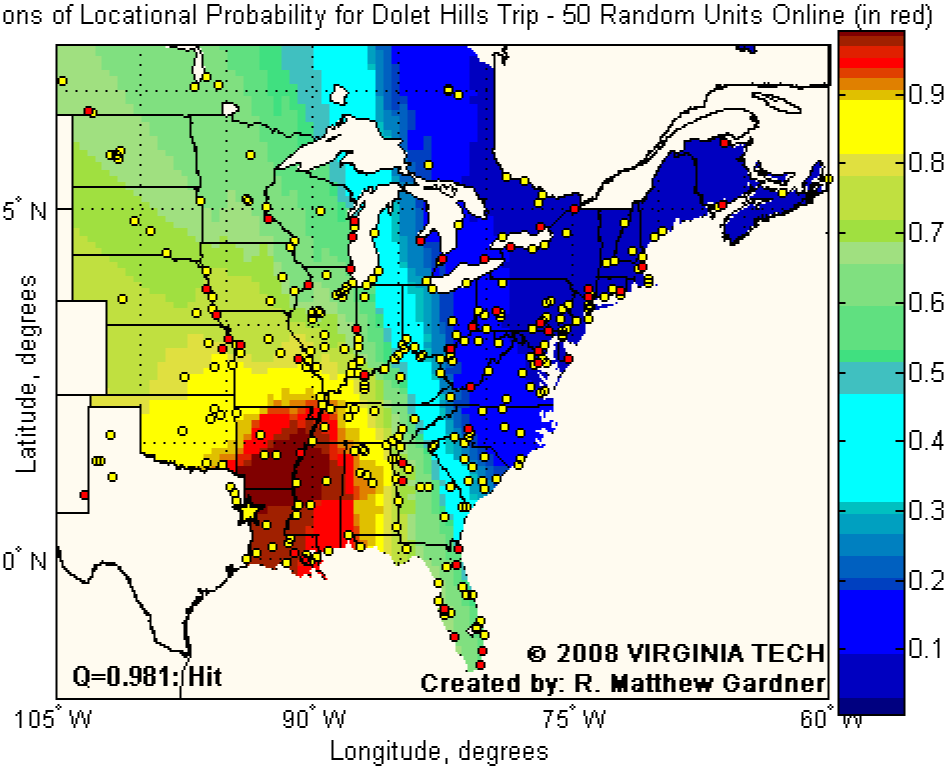

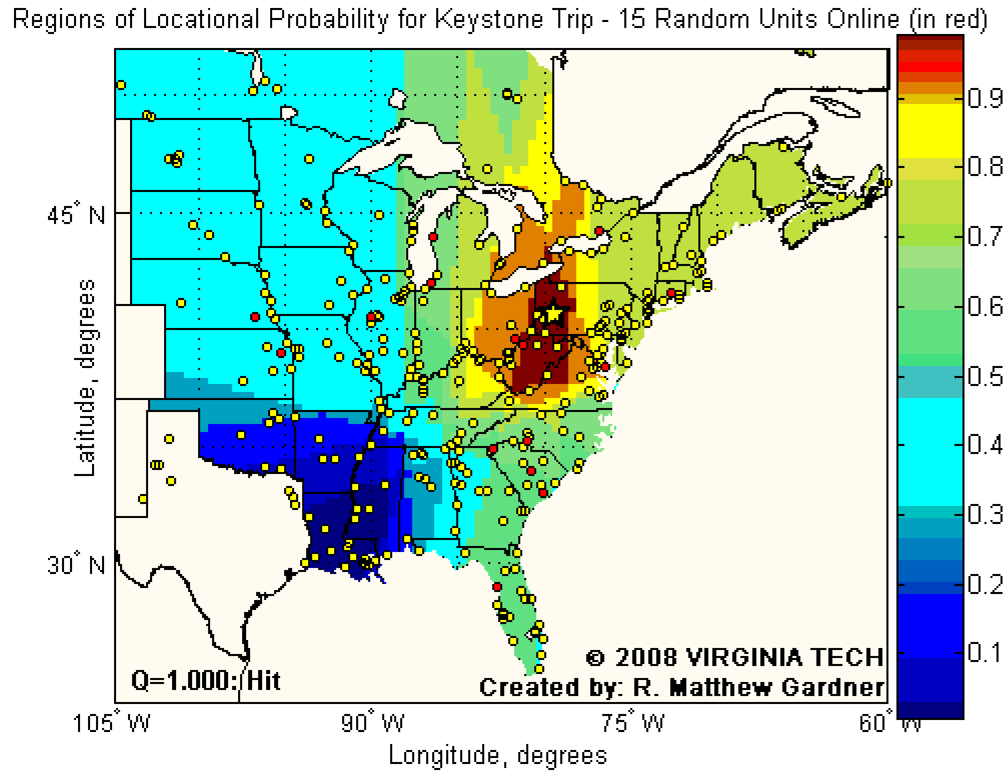
Regions of Locational Probability for Keystone Trip - 15 Random Units Online (in red)
45° N
30° N
Latitude, degrees
105° W
90° W
75° W
60° W
Longitude, degrees
Q=1.000: Hit
© 2008 VIRGINIA TECH
Created by: R. Matthew Gardner
0.9
0.8
0.7
0.6
0.5
0.4
0.3
0.2
0.1

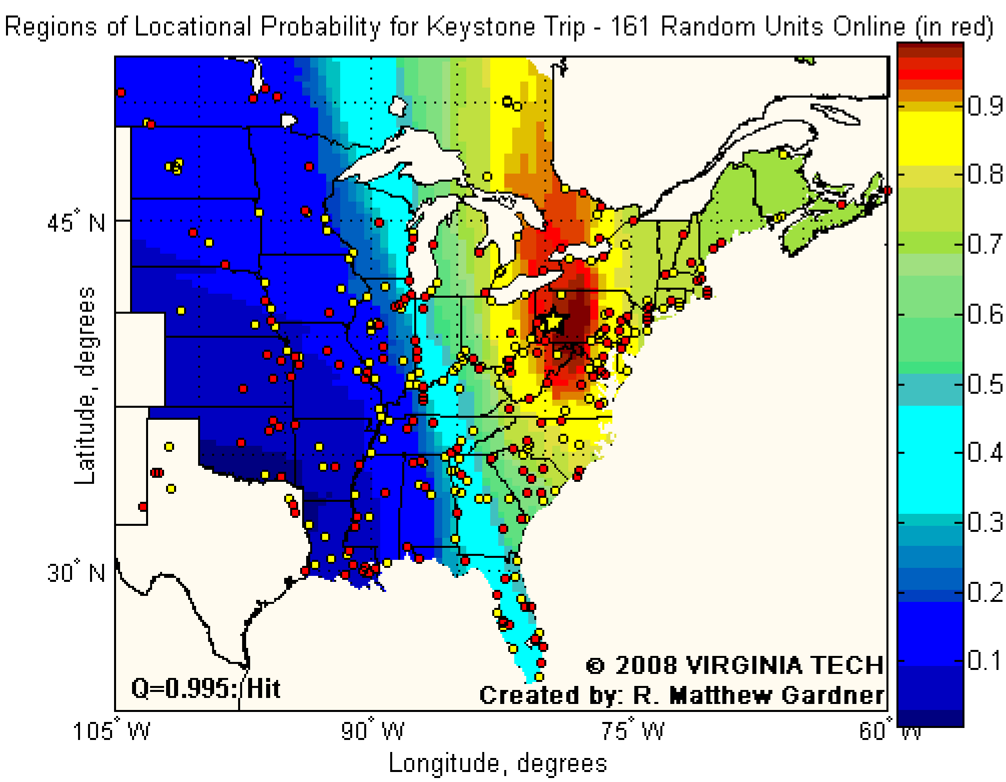
Regions of Locational Probability for Keystone Trip - 161 Random Units Online (in red)
45° N
30° N
Latitude, degrees
105° W
90° W
75° W
60° W
Longitude, degrees
Q=0.995: Hit
© 2008 VIRGINIA TECH
Created by: R. Matthew Gardner
0.9
0.8
0.7
0.6
0.5
0.4
0.3
0.2
0.1

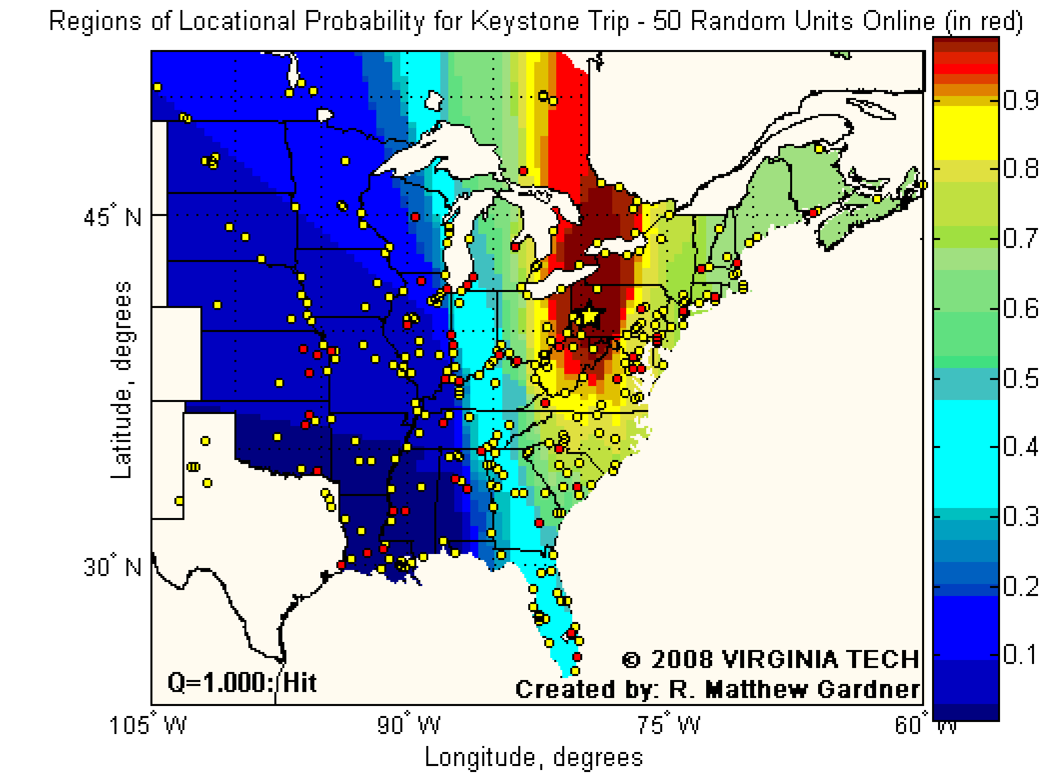
Regions of Locational Probability for Keystone Trip - 50 Random Units Online (in red)
45° N
30° N
Latitude, degrees
105° W
90° W
75° W
60° W
Longitude, degrees
Q=1.000:/Hit
© 2008 VIRGINIA TECH
Created by: R. Matthew Gardner
0.9
0.8
0.7
0.6
0.5
0.4
0.3
0.2
0.1

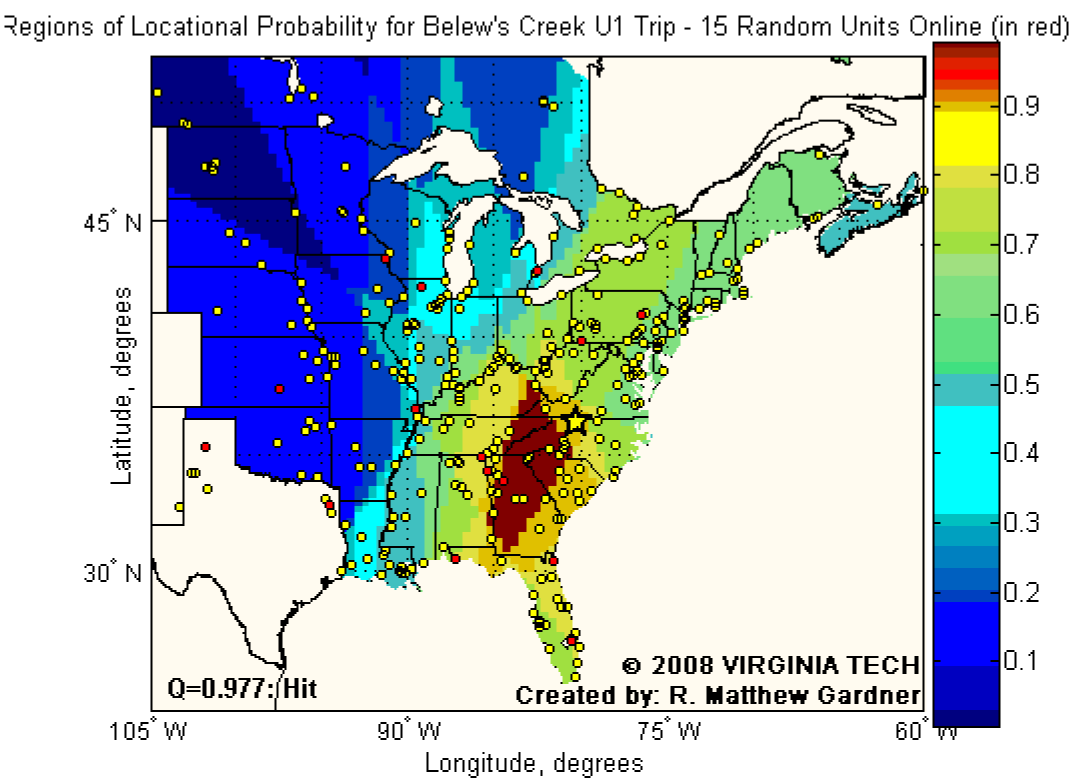
Regions of Locational Probability for Belew's Creek U1 Trip - 15 Random Units Online (in red)
45° N
30° N
Latitude, degrees
105° W
90° W
75° W
60° W
Longitude, degrees
Q=0.977:/Hit
© 2008 VIRGINIA TECH
Created by: R. Matthew Gardner
0.9
0.8
0.7
0.6
0.5
0.4
0.3
0.2
0.1

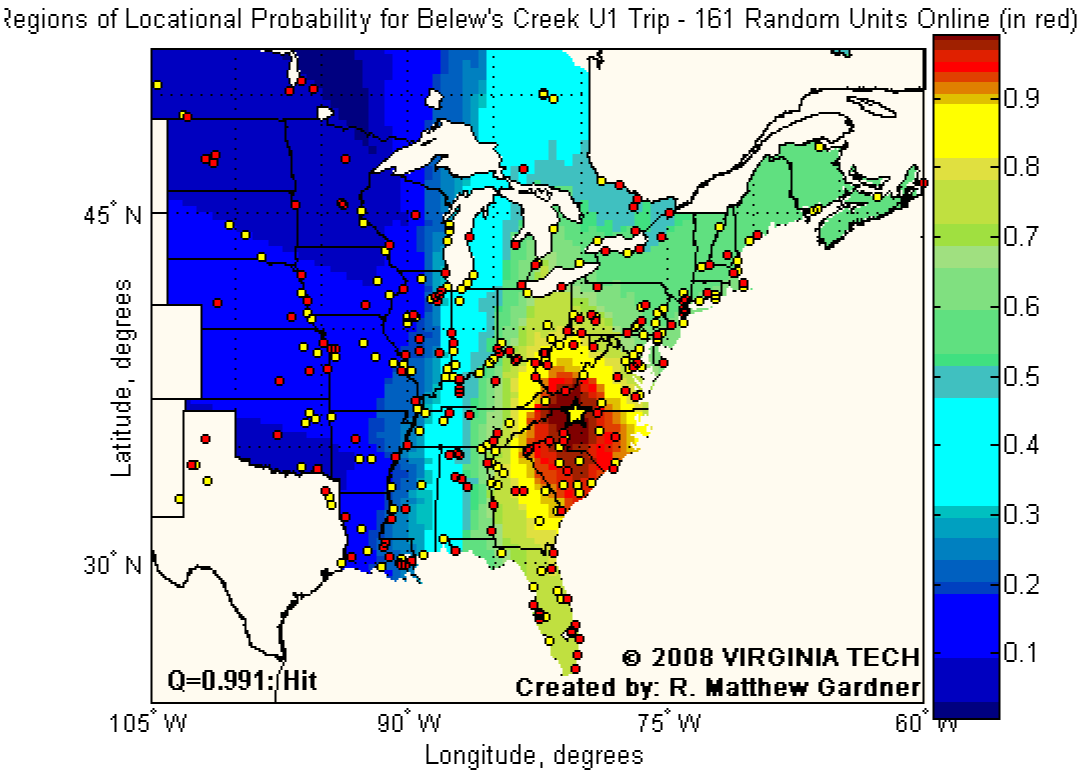
Regions of Locational Probability for Belew's Creek U1 Trip - 161 Random Units Online (in red)
45° N
30° N
Latitude, degrees
105° W
90° W
75° W
60° W
Longitude, degrees
Q=0.991: Hit
© 2008 VIRGINIA TECH
Created by: R. Matthew Gardner
0.9
0.8
0.7
0.6
0.5
0.4
0.3
0.2
0.1

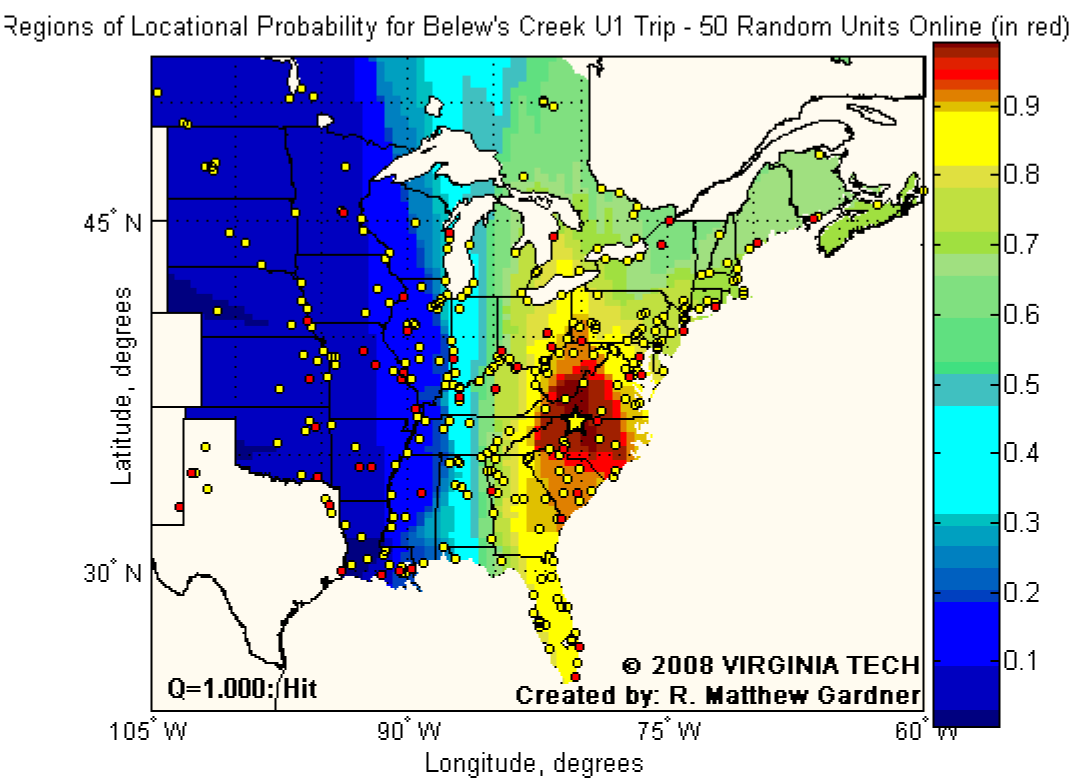
Regions of Locational Probability for Belew's Creek U1 Trip - 50 Random Units Online (in red)
45° N
30° N
Latitude, degrees
105° W
90° W
75° W
60° W
Longitude, degrees
Q=1.000: Hit
© 2008 VIRGINIA TECH
Created by: R. Matthew Gardner
0.9
0.8
0.7
0.6
0.5
0.4
0.3
0.2
0.1

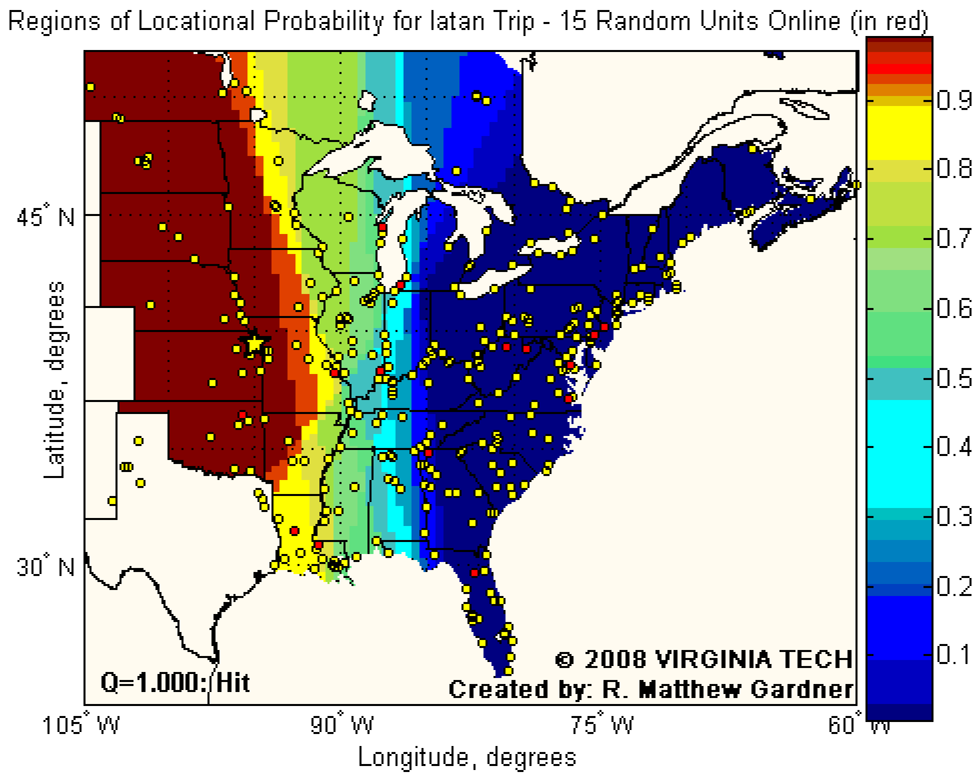
Regions of Locational Probability for Iatan Trip - 15 Random Units Online (in red)
45° N
30° N
Latitude, degrees
105° W
90° W
75° W
60° W
Longitude, degrees
Q=1.000: Hit
© 2008 VIRGINIA TECH
Created by: R. Matthew Gardner
0.9
0.8
0.7
0.6
0.5
0.4
0.3
0.2
0.1

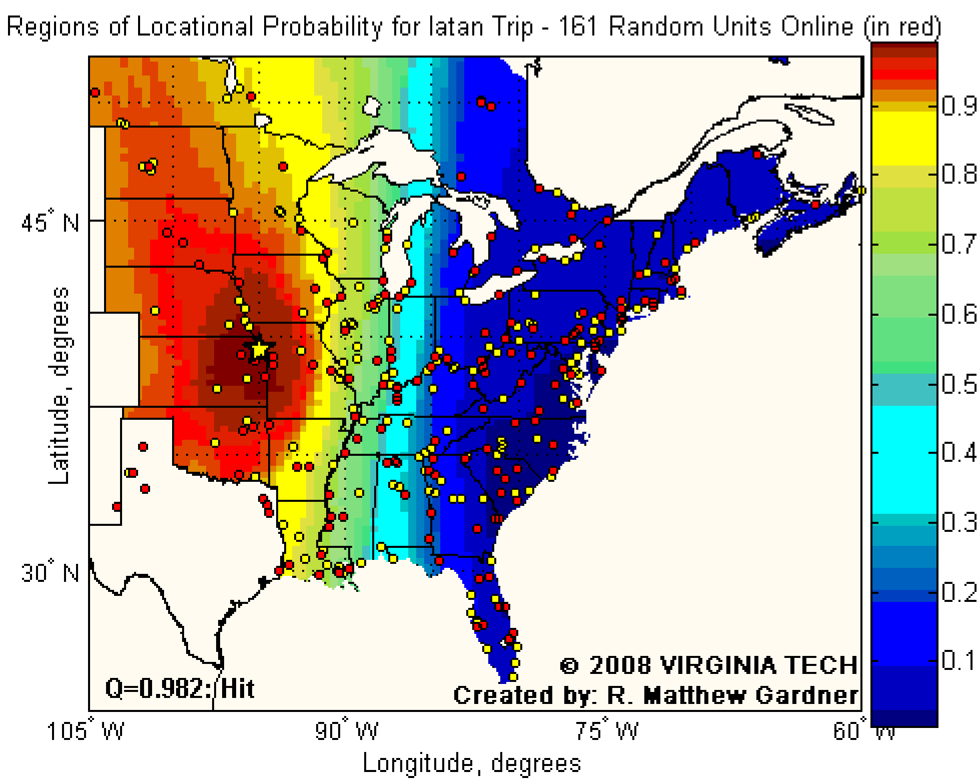
Regions of Locational Probability for Iatan Trip - 161 Random Units Online (in red)
45° N
30° N
Latitude, degrees
105° W
90° W
75° W
60° W
Longitude, degrees
Q=0.982: Hit
© 2008 VIRGINIA TECH
Created by: R. Matthew Gardner
0.9
0.8
0.7
0.6
0.5
0.4
0.3
0.2
0.1

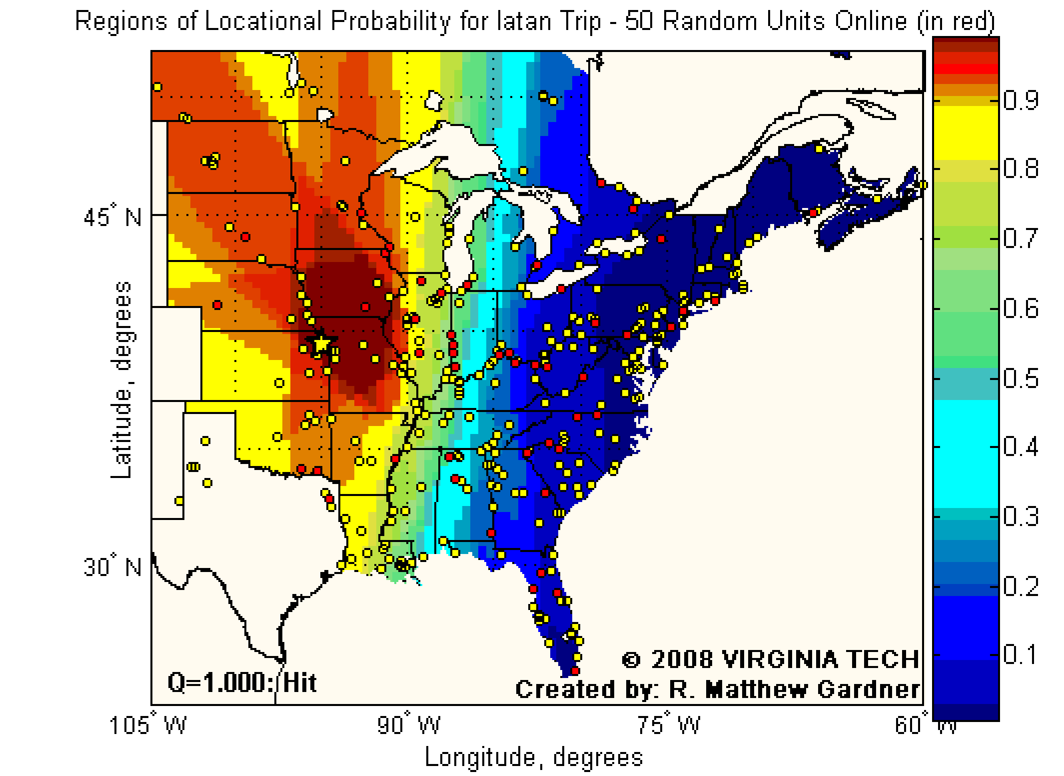
Regions of Locational Probability for Iatan Trip - 50 Random Units Online (in red)
Q=1.000:/Hit
© 2008 VIRGINIA TECH
Created by: R. Matthew Gardner
45° N
30° N
Latitude, degrees
105° W
90° W
75° W
60° W
Longitude, degrees
0.9
0.8
0.7
0.6
0.5
0.4
0.3
0.2
0.1

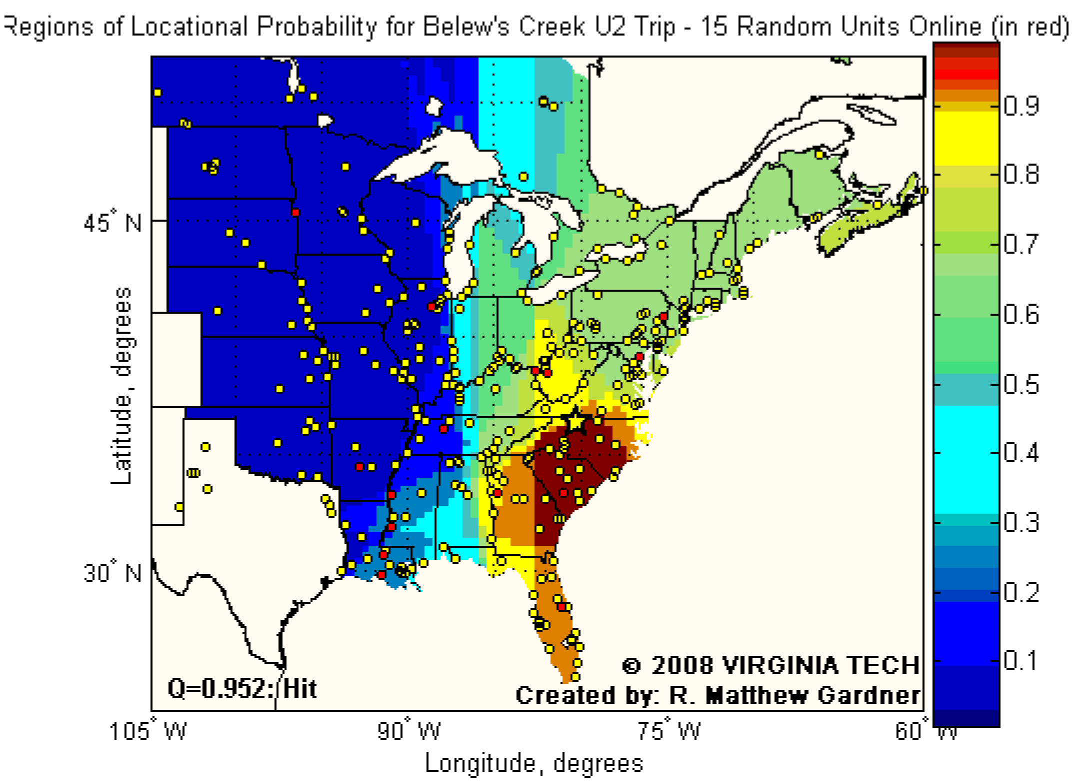
Regions of Locational Probability for Belew's Creek U2 Trip - 15 Random Units Online (in red)
Q=0.952:/Hit
© 2008 VIRGINIA TECH
Created by: R. Matthew Gardner
45° N
30° N
Latitude, degrees
105° W
90° W
75° W
60° W
Longitude, degrees
0.9
0.8
0.7
0.6
0.5
0.4
0.3
0.2
0.1

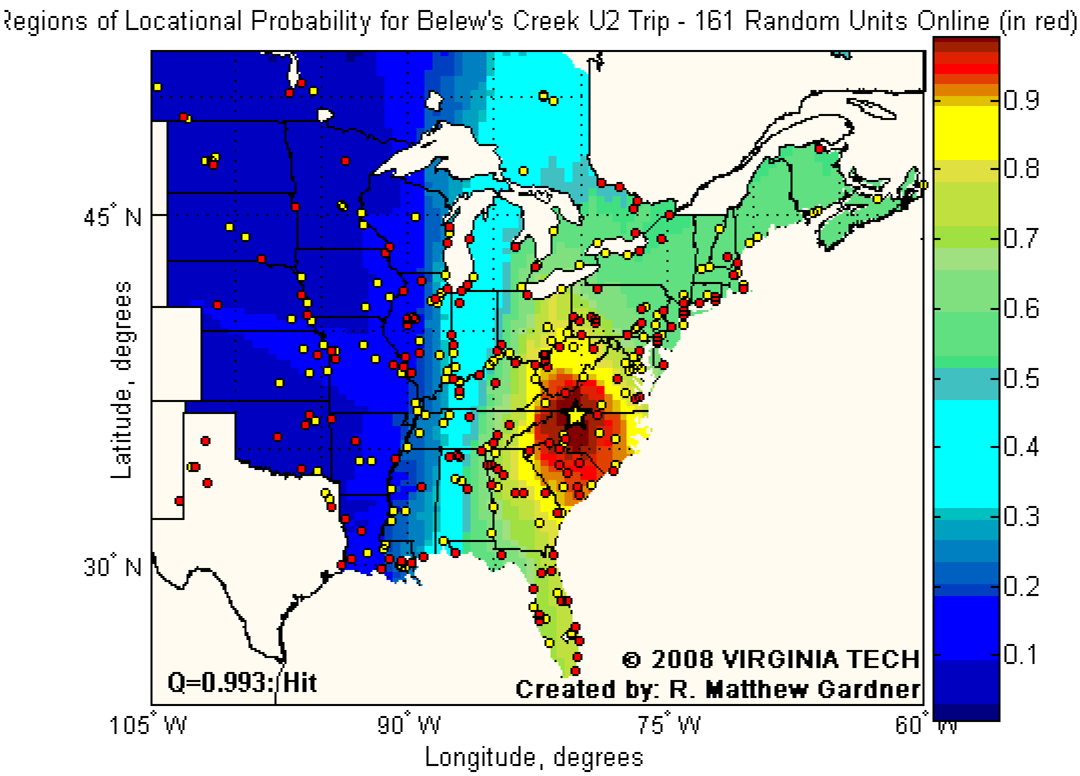
Regions of Locational Probability for Belew's Creek U2 Trip - 161 Random Units Online (in red)
45° N
30° N
Latitude, degrees
105° W
90° W
75° W
60° W
Longitude, degrees
Q=0.993: Hit
© 2008 VIRGINIA TECH
Created by: R. Matthew Gardner
0.9
0.8
0.7
0.6
0.5
0.4
0.3
0.2
0.1

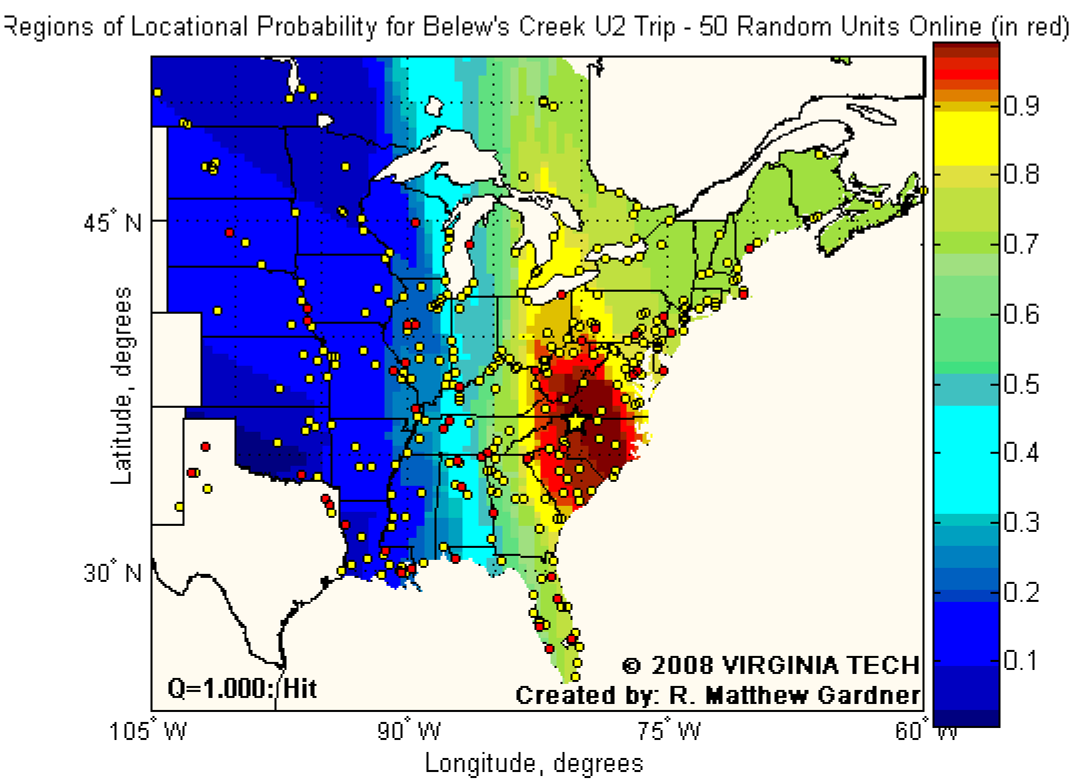
Regions of Locational Probability for Belew's Creek U2 Trip - 50 Random Units Online (in red)
45° N
30° N
Latitude, degrees
105° W
90° W
75° W
60° W
Longitude, degrees
Q=1.000: Hit
© 2008 VIRGINIA TECH
Created by: R. Matthew Gardner
0.9
0.8
0.7
0.6
0.5
0.4
0.3
0.2
0.1

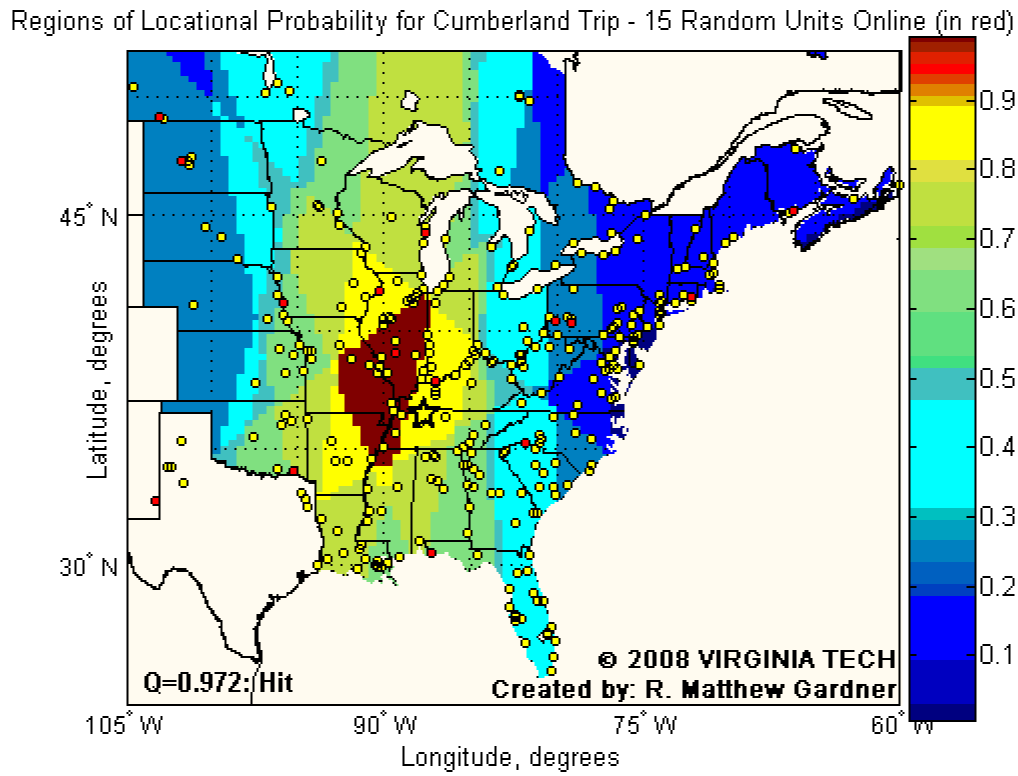
Regions of Locational Probability for Cumberland Trip - 15 Random Units Online (in red)
45° N
30° N
Latitude, degrees
105° W
90° W
75° W
60° W
Longitude, degrees
Q=0.972: Hit
© 2008 VIRGINIA TECH
Created by: R. Matthew Gardner
0.9
0.8
0.7
0.6
0.5
0.4
0.3
0.2
0.1

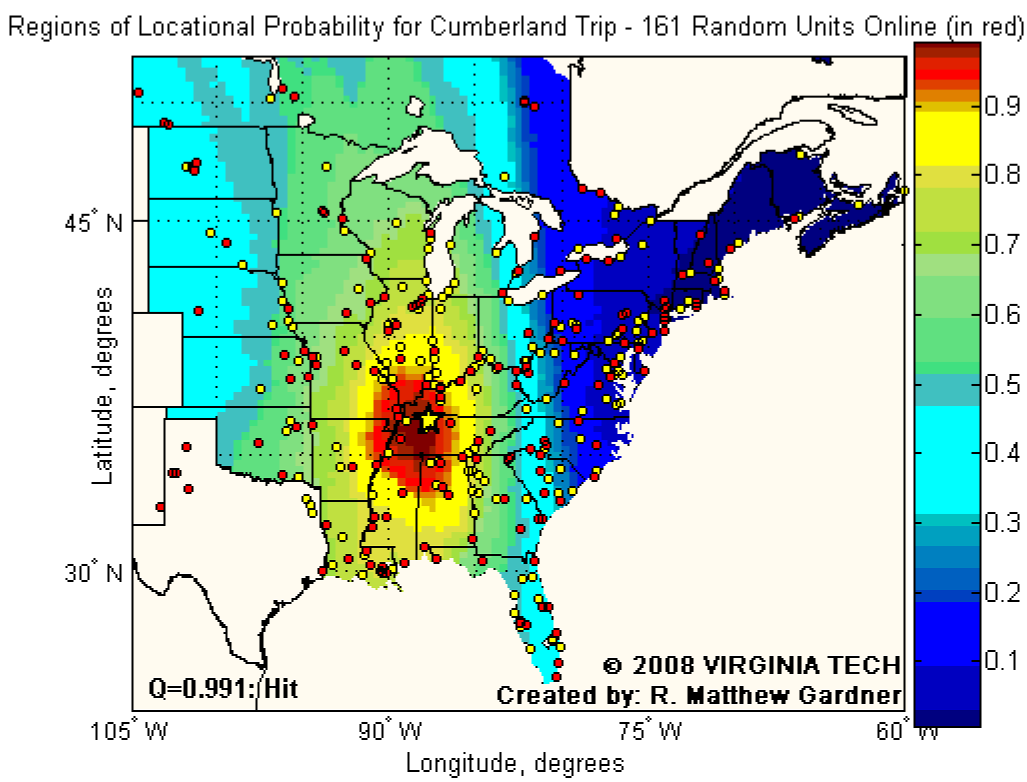
Regions of Locational Probability for Cumberland Trip - 161 Random Units Online (in red)
45° N
30° N
Latitude, degrees
105° W
90° W
75° W
60° W
Longitude, degrees
Q=0.991: Hit
© 2008 VIRGINIA TECH
Created by: R. Matthew Gardner
0.9
0.8
0.7
0.6
0.5
0.4
0.3
0.2
0.1

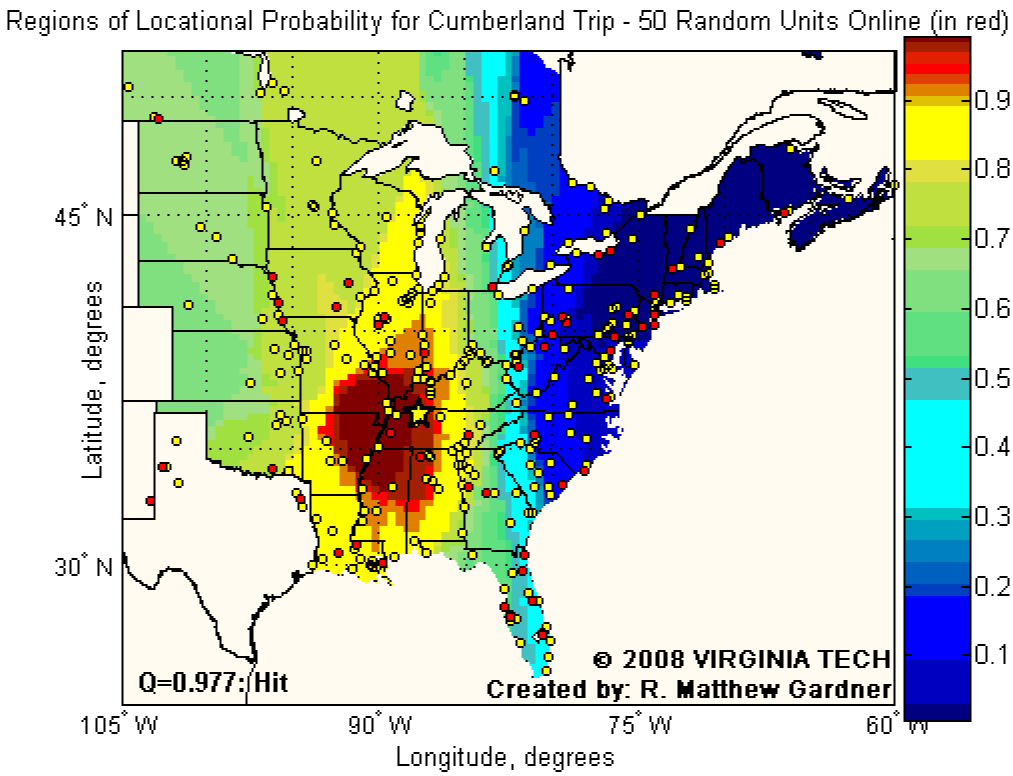

Regions of Locational Probability for Cumberland Trip - 50 Random Units Online (in red)
45° N
30° N
Latitude, degrees
105° W
90° W
75° W
60° W
Longitude, degrees
Q=0.977: Hit
© 2008 VIRGINIA TECH
Created by: R. Matthew Gardner
0.9
0.8
0.7
0.6
0.5
0.4
0.3
0.2
0.1

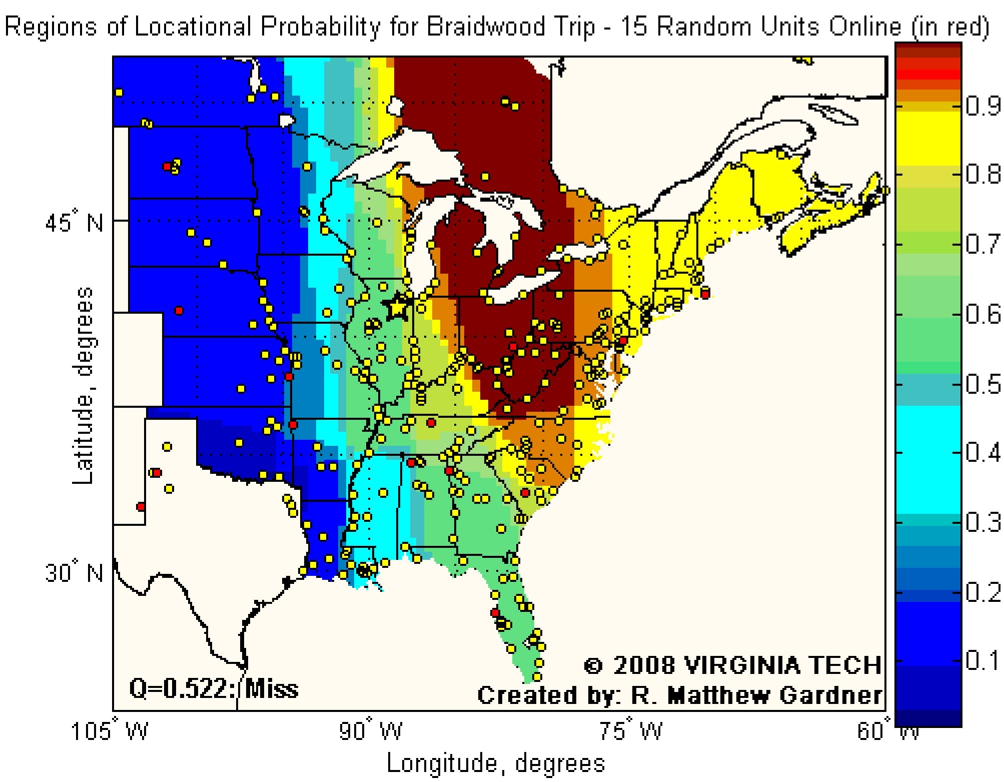

Regions of Locational Probability for Braidwood Trip - 15 Random Units Online (in red)
45° N
30° N
Latitude, degrees
105° W
90° W
75° W
60° W
Longitude, degrees
Q=0.522: Miss
© 2008 VIRGINIA TECH
Created by: R. Matthew Gardner
0.9
0.8
0.7
0.6
0.5
0.4
0.3
0.2
0.1

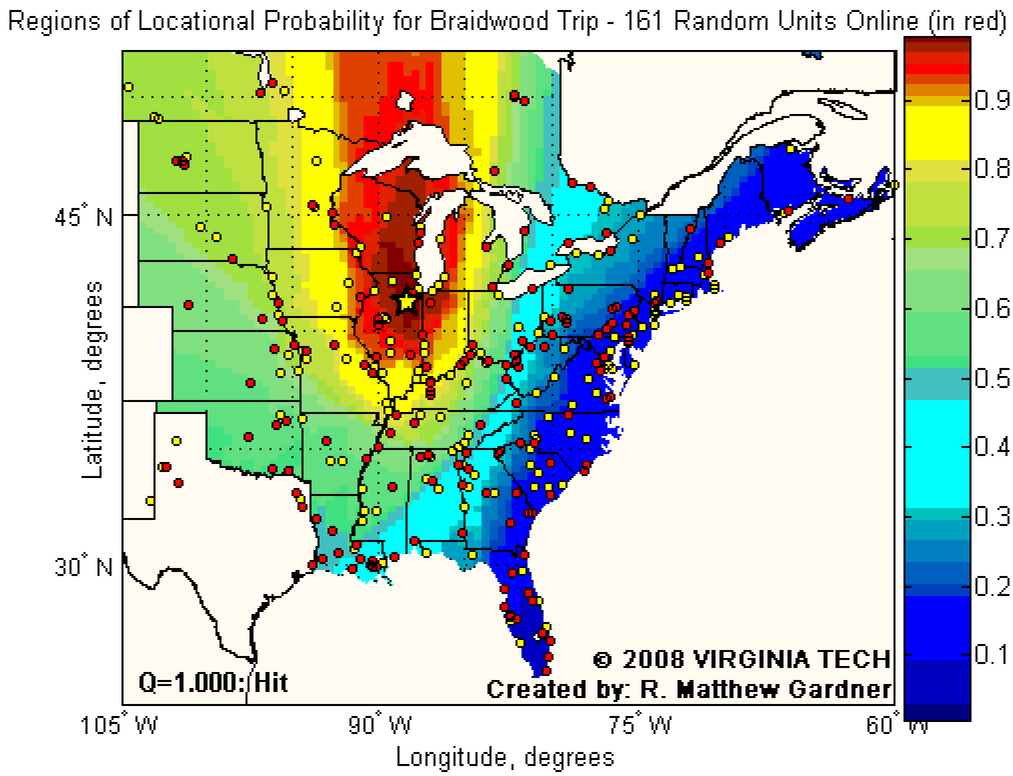
Regions of Locational Probability for Braidwood Trip - 161 Random Units Online (in red)
45° N
30° N
Latitude, degrees
105° W
90° W
75° W
60° W
Longitude, degrees
Q=1.000: Hit
© 2008 VIRGINIA TECH
Created by: R. Matthew Gardner
0.9
0.8
0.7
0.6
0.5
0.4
0.3
0.2
0.1

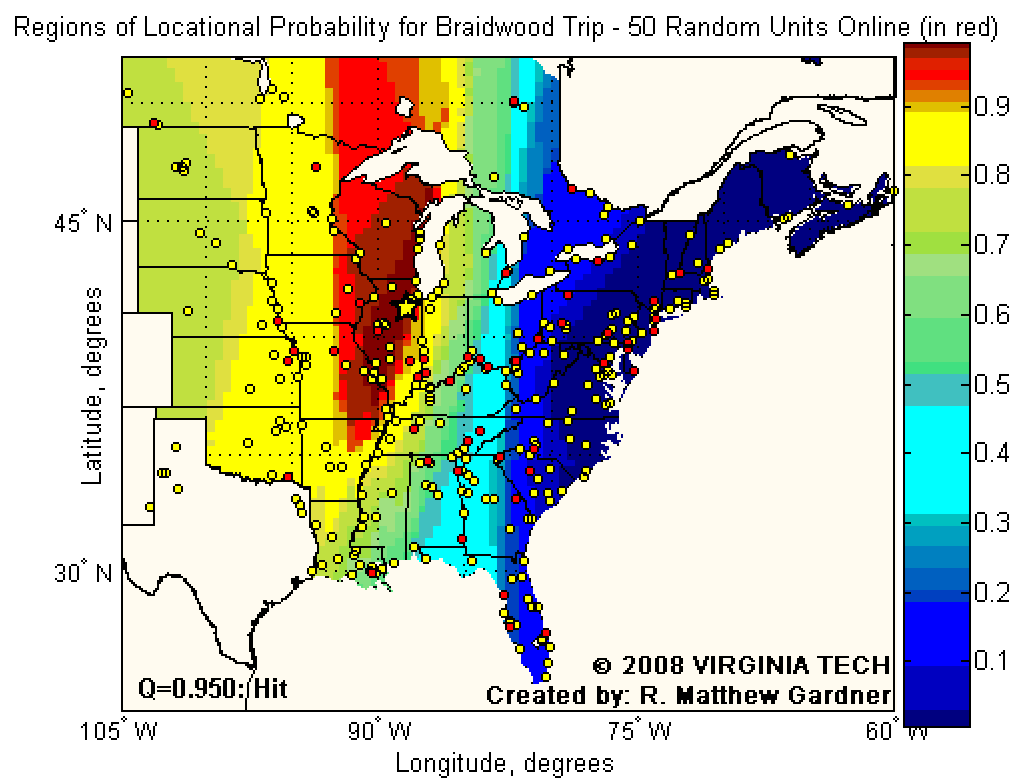
Regions of Locational Probability for Braidwood Trip - 50 Random Units Online (in red)
45° N
30° N
Latitude, degrees
105° W
90° W
75° W
60° W
Longitude, degrees
Q=0.950: Hit
© 2008 VIRGINIA TECH
Created by: R. Matthew Gardner
0.9
0.8
0.7
0.6
0.5
0.4
0.3
0.2
0.1

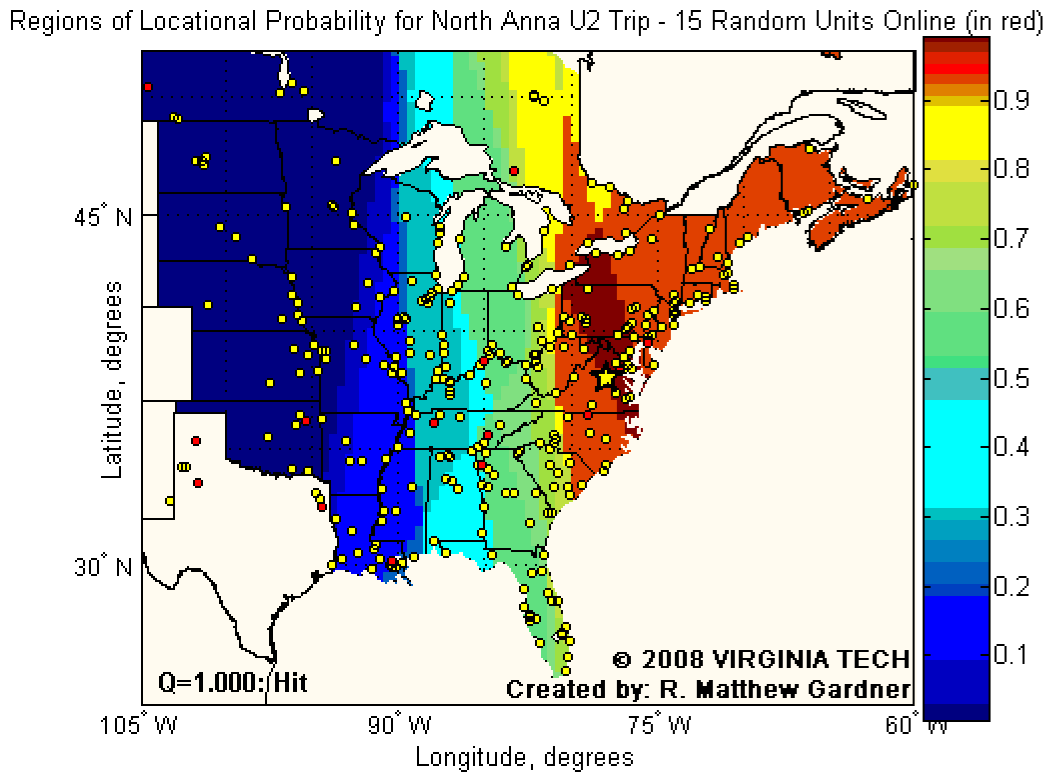
Regions of Locational Probability for North Anna U2 Trip - 15 Random Units Online (in red)
45° N
30° N
Latitude, degrees
105° W
90° W
75° W
60° W
Longitude, degrees
Q=1.000:/Hit
© 2008 VIRGINIA TECH
Created by: R. Matthew Gardner
0.9
0.8
0.7
0.6
0.5
0.4
0.3
0.2
0.1

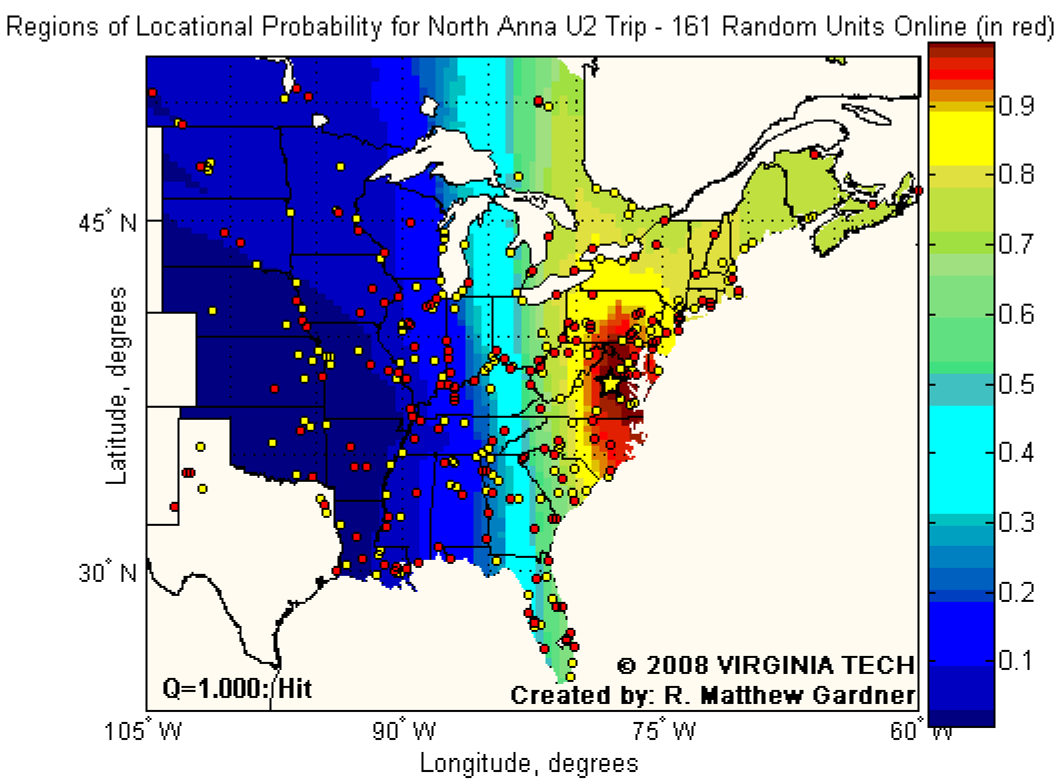
Regions of Locational Probability for North Anna U2 Trip - 161 Random Units Online (in red)
45° N
30° N
Latitude, degrees
105° W
90° W
75° W
60° W
Longitude, degrees
Q=1.000:/Hit
© 2008 VIRGINIA TECH
Created by: R. Matthew Gardner
0.9
0.8
0.7
0.6
0.5
0.4
0.3
0.2
0.1

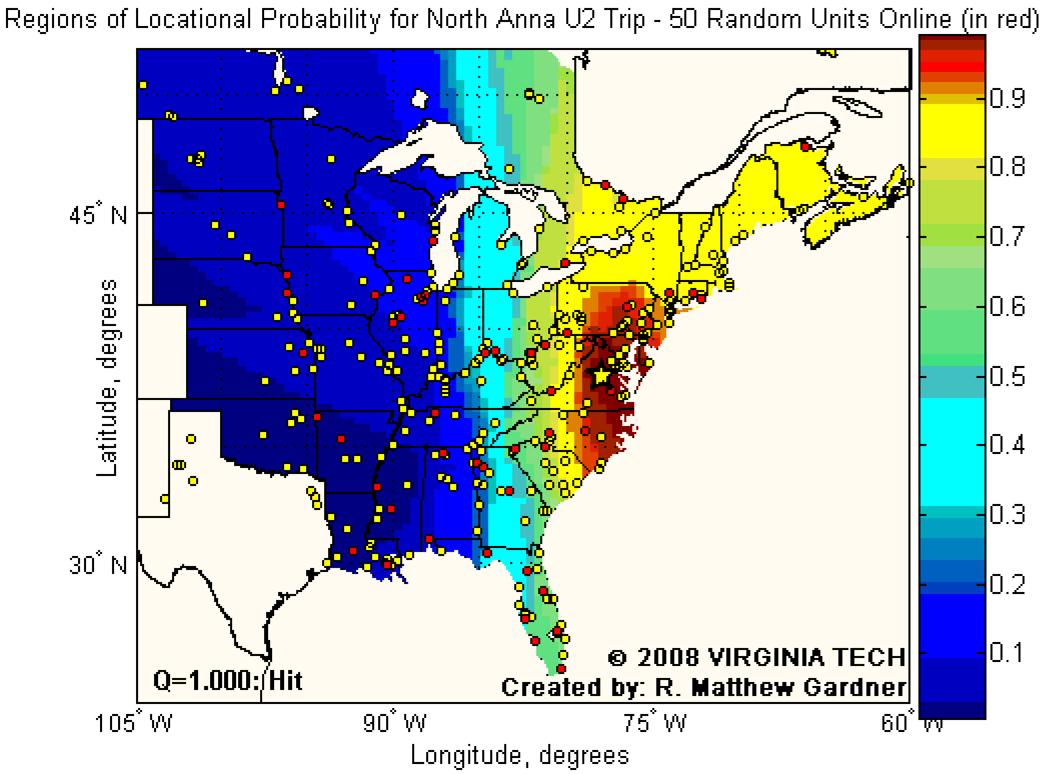
Regions of Locational Probability for North Anna U2 Trip - 50 Random Units Online (in red)
45° N
30° N
Latitude, degrees
105° W
90° W
75° W
60° W
Longitude, degrees
0.9
0.8
0.7
0.6
0.5
0.4
0.3
0.2
0.1
Q=1.000:/Hit
© 2008 VIRGINIA TECH
Created by: R. Matthew Gardner

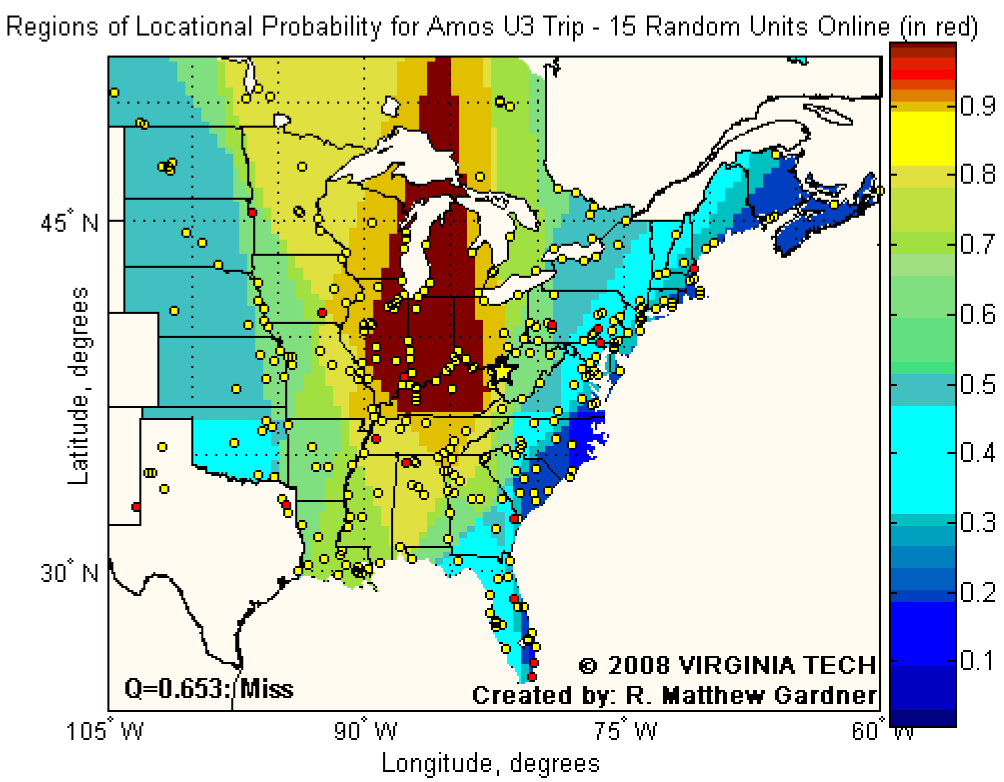
Regions of Locational Probability for Amos U3 Trip - 15 Random Units Online (in red)
45° N
30° N
Latitude, degrees
105° W
90° W
75° W
60° W
Longitude, degrees
0.9
0.8
0.7
0.6
0.5
0.4
0.3
0.2
0.1
Q=0.653:/Miss
© 2008 VIRGINIA TECH
Created by: R. Matthew Gardner

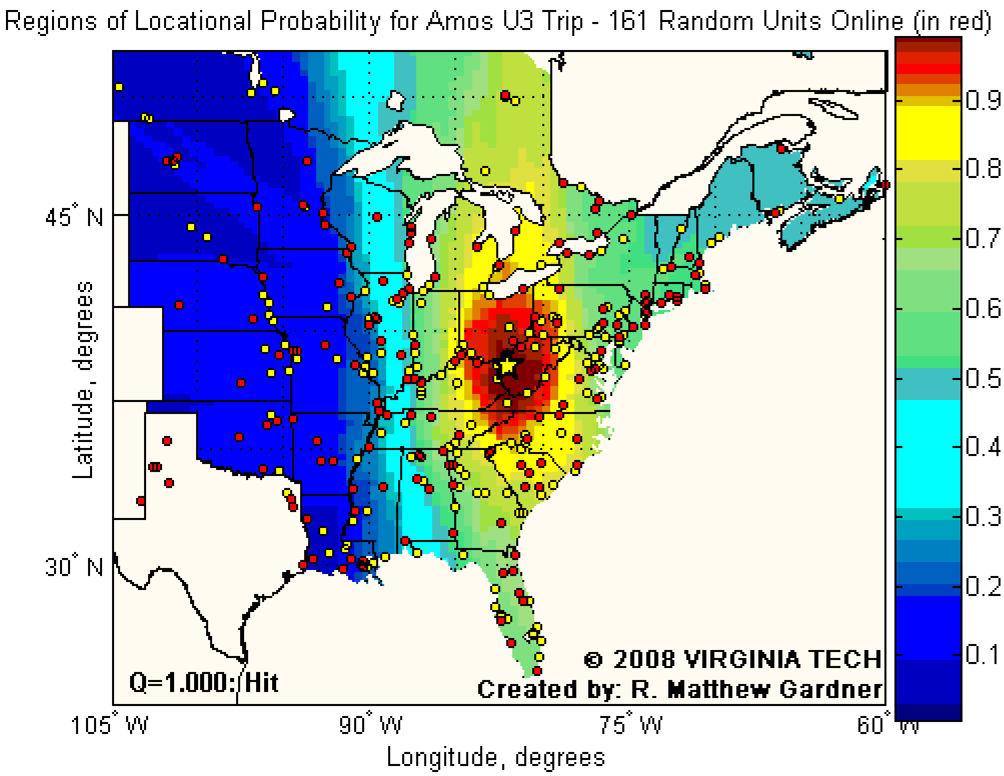
Regions of Locational Probability for Amos U3 Trip - 161 Random Units Online (in red)
45° N
30° N
Latitude, degrees
105° W
90° W
75° W
60° W
Longitude, degrees
Q=1.000:/Hit
© 2008 VIRGINIA TECH
Created by: R. Matthew Gardner
0.9
0.8
0.7
0.6
0.5
0.4
0.3
0.2
0.1

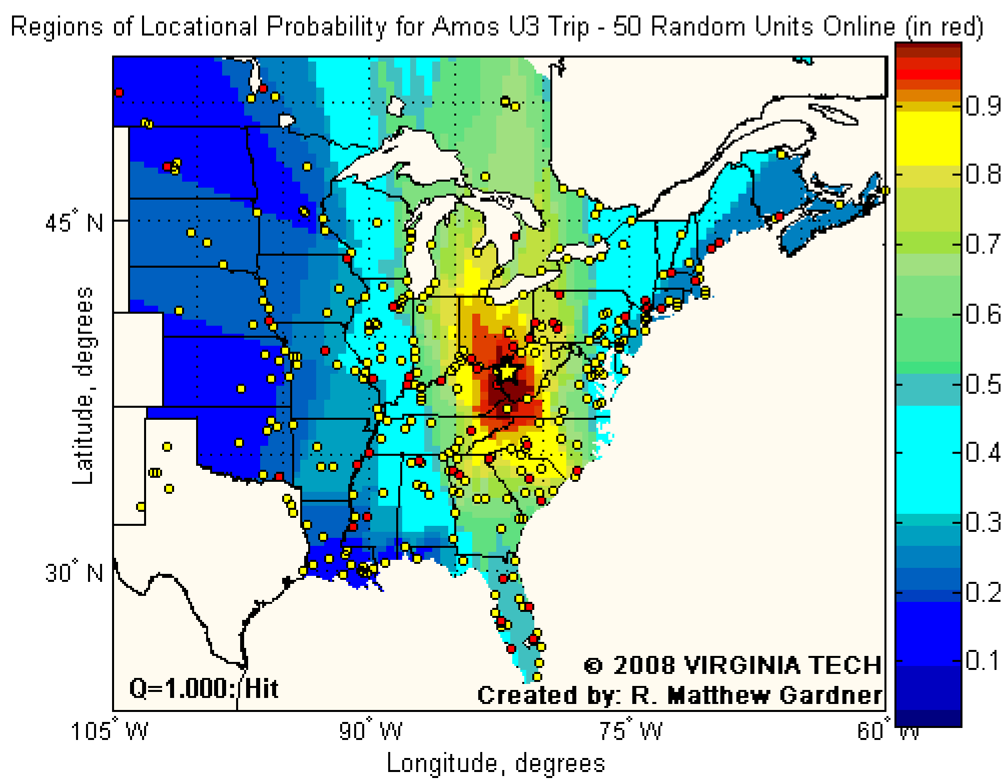
Regions of Locational Probability for Amos U3 Trip - 50 Random Units Online (in red)
45° N
30° N
Latitude, degrees
105° W
90° W
75° W
60° W
Longitude, degrees
Q=1.000:/Hit
© 2008 VIRGINIA TECH
Created by: R. Matthew Gardner
0.9
0.8
0.7
0.6
0.5
0.4
0.3
0.2
0.1

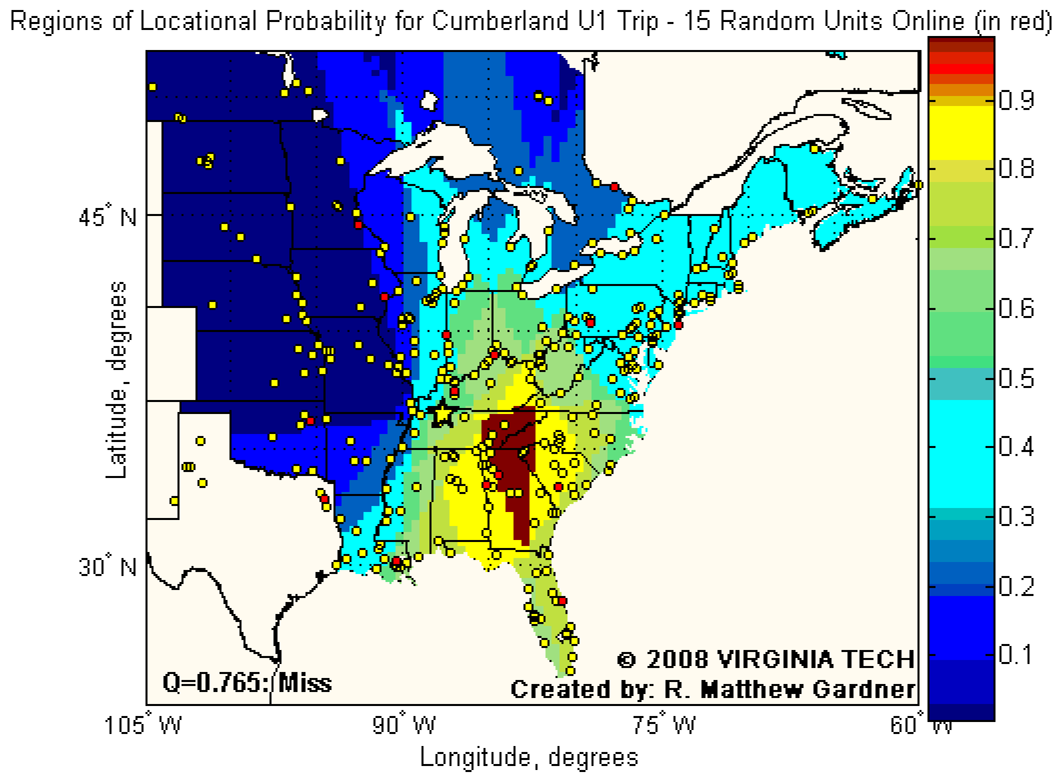
Regions of Locational Probability for Cumberland U1 Trip - 15 Random Units Online (in red)
45° N
30° N
Latitude, degrees
105° W
90° W
75° W
60° W
Longitude, degrees
Q=0.765: Miss
© 2008 VIRGINIA TECH
Created by: R. Matthew Gardner
0.9
0.8
0.7
0.6
0.5
0.4
0.3
0.2
0.1

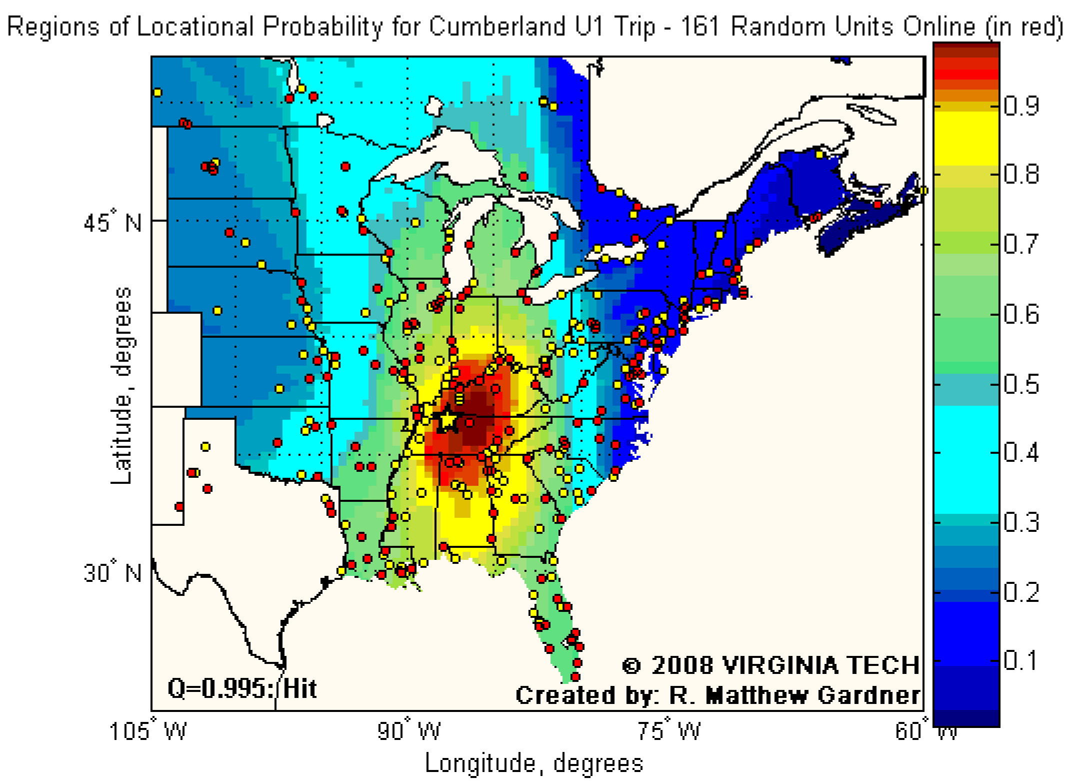
Regions of Locational Probability for Cumberland U1 Trip - 161 Random Units Online (in red)
45° N
30° N
Latitude, degrees
105° W
90° W
75° W
60° W
Longitude, degrees
Q=0.995: Hit
© 2008 VIRGINIA TECH
Created by: R. Matthew Gardner
0.9
0.8
0.7
0.6
0.5
0.4
0.3
0.2
0.1

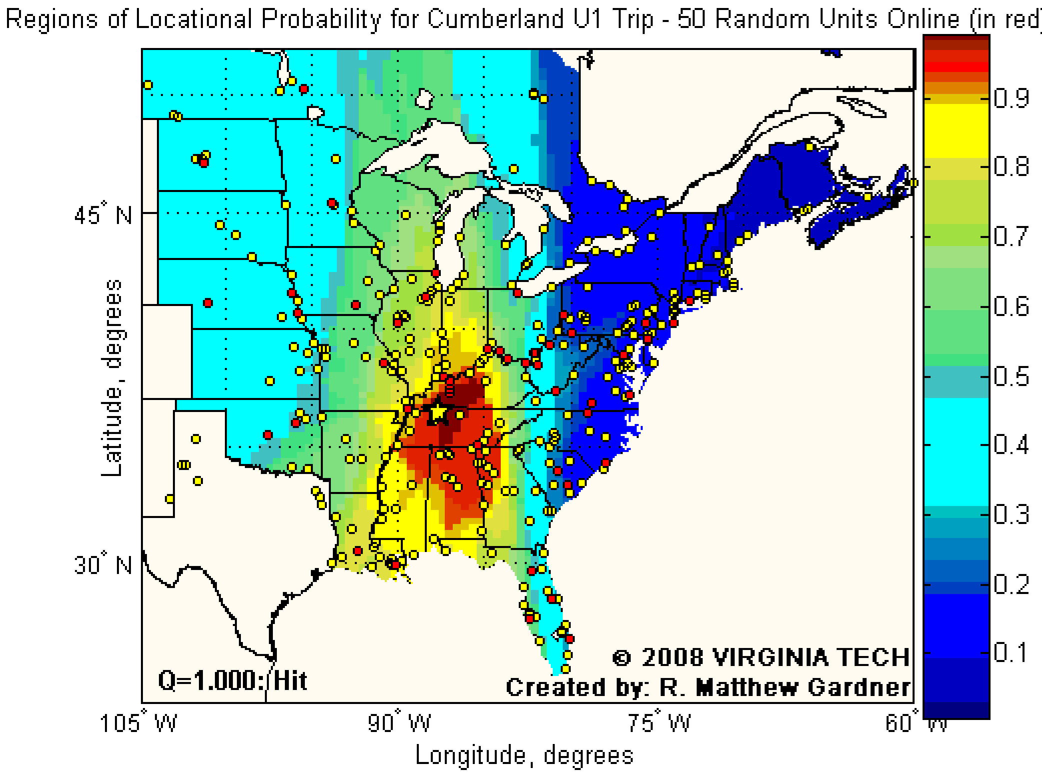
Regions of Locational Probability for Cumberland U1 Trip - 50 Random Units Online (in red)
45° N
30° N
Latitude, degrees
105° W
90° W
75° W
60° W
Longitude, degrees
Q=1.000:/Hit
© 2008 VIRGINIA TECH
Created by: R. Matthew Gardner
0.9
0.8
0.7
0.6
0.5
0.4
0.3
0.2
0.1

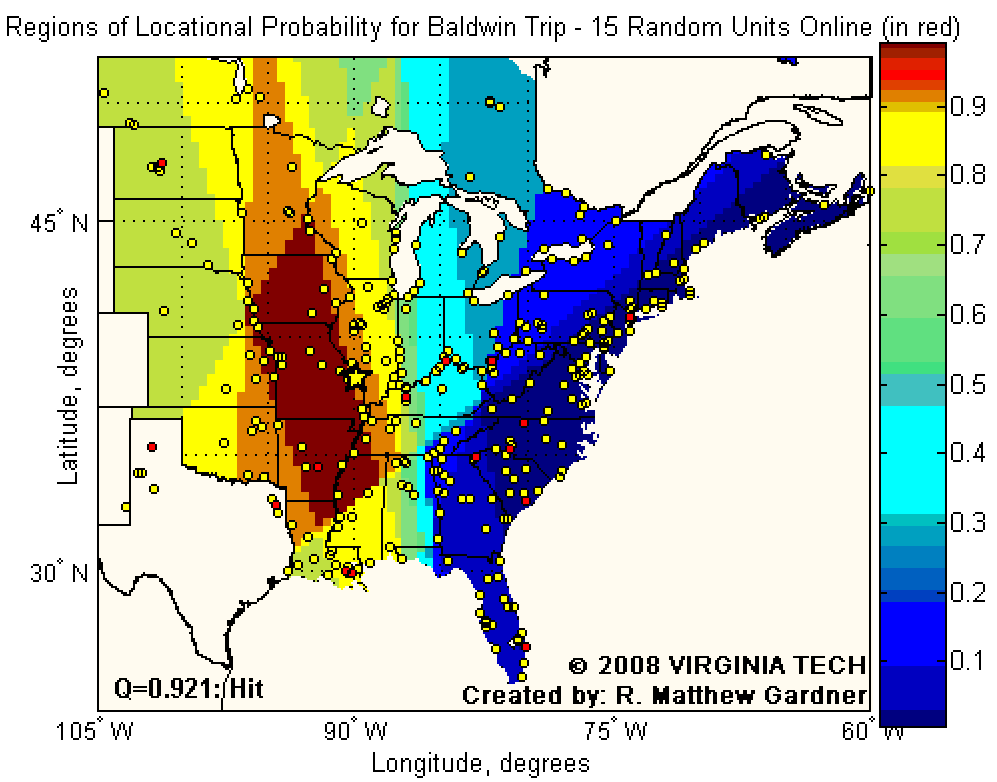
Regions of Locational Probability for Baldwin Trip - 15 Random Units Online (in red)
45° N
30° N
Latitude, degrees
105° W
90° W
75° W
60° W
Longitude, degrees
Q=0.921:/Hit
© 2008 VIRGINIA TECH
Created by: R. Matthew Gardner
0.9
0.8
0.7
0.6
0.5
0.4
0.3
0.2
0.1

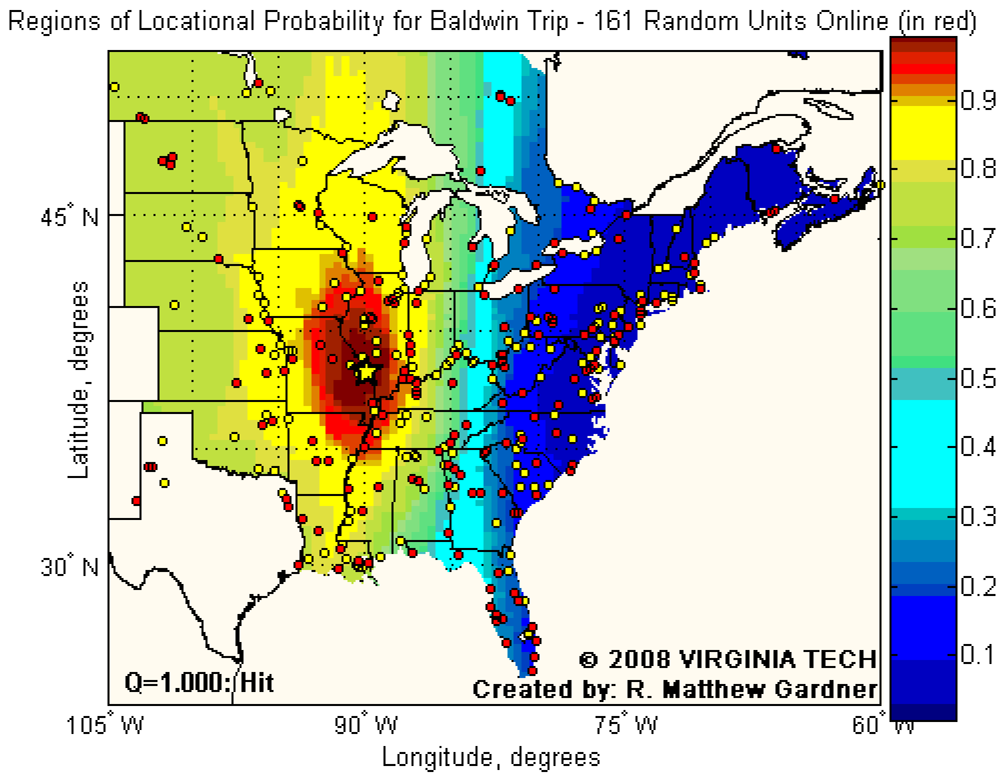
Regions of Locational Probability for Baldwin Trip - 161 Random Units Online (in red)
45° N
30° N
Latitude, degrees
105° W
90° W
75° W
60° W
Longitude, degrees
Q=1.000: Hit
© 2008 VIRGINIA TECH
Created by: R. Matthew Gardner
0.9
0.8
0.7
0.6
0.5
0.4
0.3
0.2
0.1

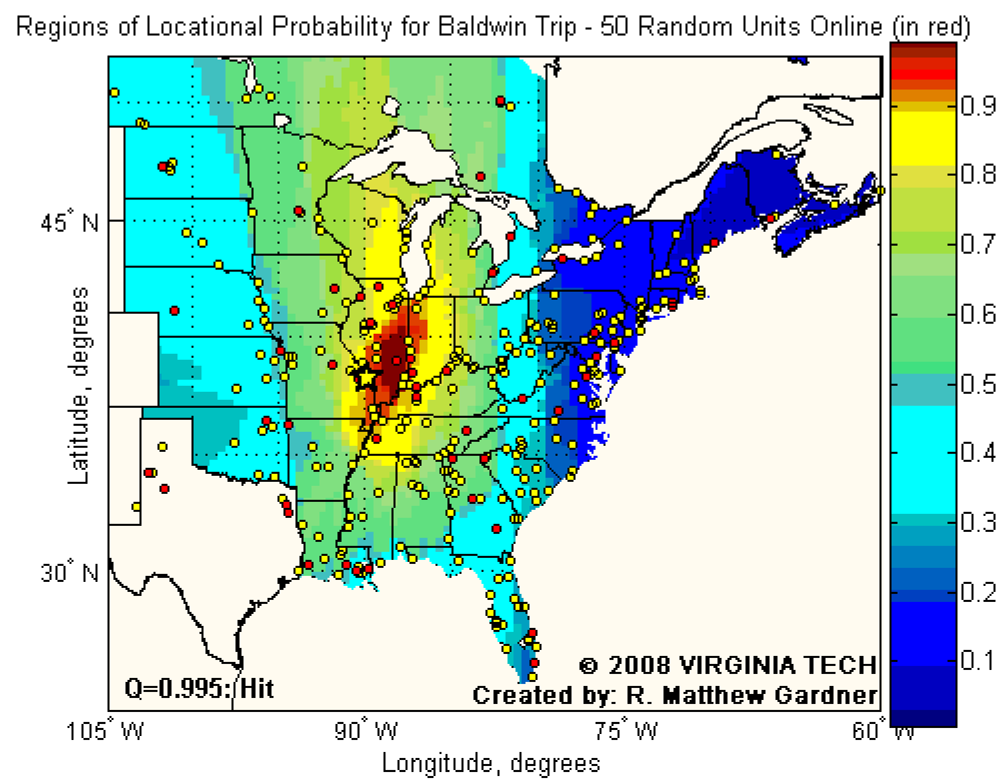
Regions of Locational Probability for Baldwin Trip - 50 Random Units Online (in red)
45° N
30° N
Latitude, degrees
105° W
90° W
75° W
60° W
Longitude, degrees
Q=0.995: Hit
© 2008 VIRGINIA TECH
Created by: R. Matthew Gardner
0.9
0.8
0.7
0.6
0.5
0.4
0.3
0.2
0.1

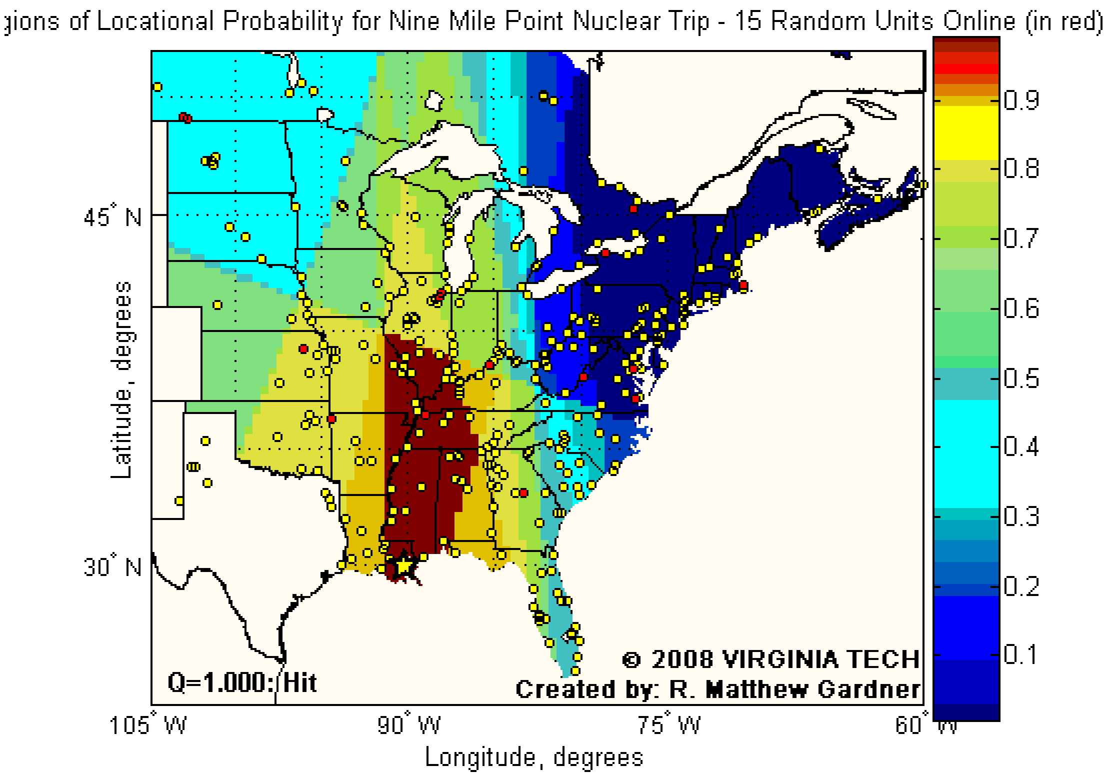
gions of Locational Probability for Nine Mile Point Nuclear Trip - 15 Random Units Online (in red)
45° N
30° N
Latitude, degrees
105° W
90° W
75° W
60° W
Longitude, degrees
Q=1.000:/Hit
© 2008 VIRGINIA TECH
Created by: R. Matthew Gardner
0.9
0.8
0.7
0.6
0.5
0.4
0.3
0.2
0.1

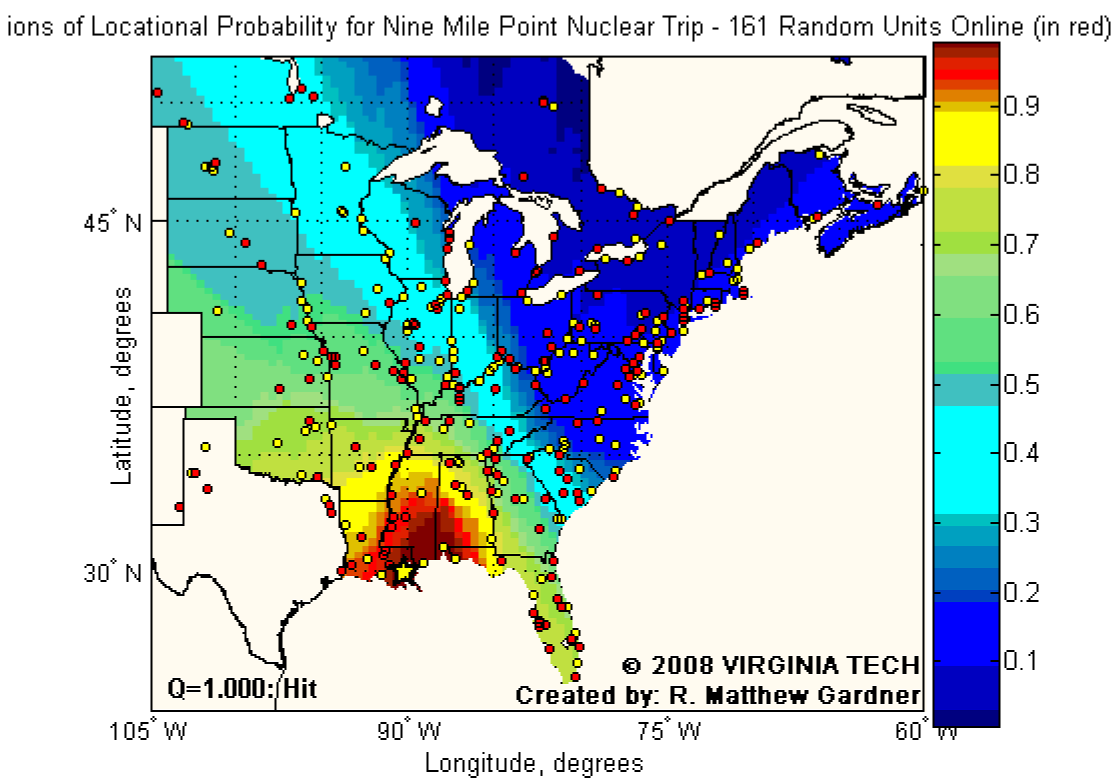
ions of Locational Probability for Nine Mile Point Nuclear Trip - 161 Random Units Online (in red)
45° N
30° N
Latitude, degrees
105° W
90° W
75° W
60° W
Longitude, degrees
Q=1.000:/Hit
© 2008 VIRGINIA TECH
Created by: R. Matthew Gardner
0.9
0.8
0.7
0.6
0.5
0.4
0.3
0.2
0.1

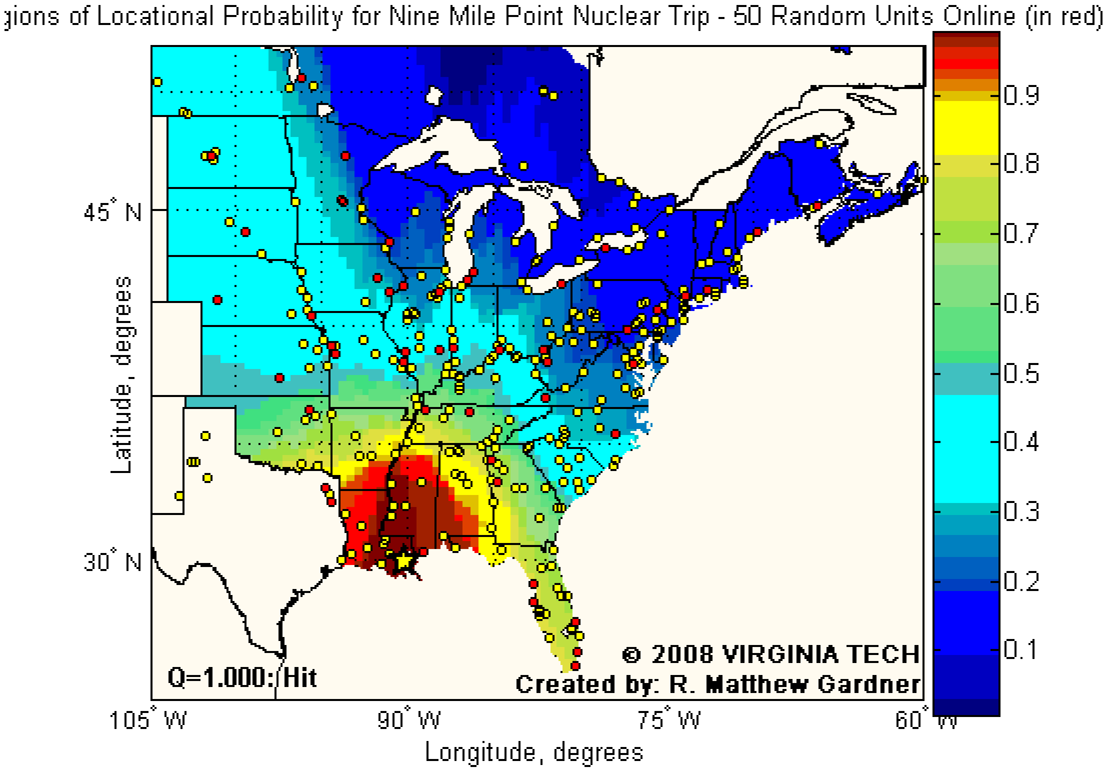
jions of Locational Probability for Nine Mile Point Nuclear Trip - 50 Random Units Online (in red)
45° N
30° N
Latitude, degrees
105° W
90° W
75° W
60° W
Longitude, degrees
0.9
0.8
0.7
0.6
0.5
0.4
0.3
0.2
0.1
Q=1.000:/Hit
© 2008 VIRGINIA TECH
Created by: R. Matthew Gardner

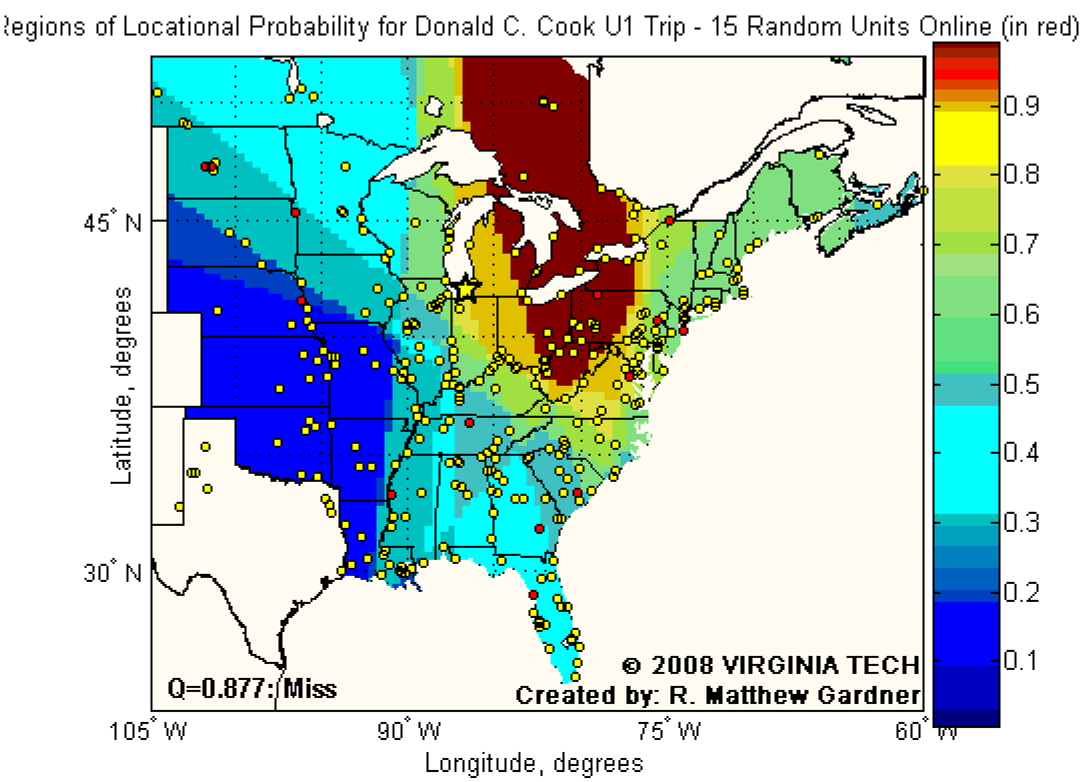
Regions of Locational Probability for Donald C. Cook U1 Trip - 15 Random Units Online (in red)
45° N
30° N
Latitude, degrees
105° W
90° W
75° W
60° W
Longitude, degrees
0.9
0.8
0.7
0.6
0.5
0.4
0.3
0.2
0.1
Q=0.877:/Miss
© 2008 VIRGINIA TECH
Created by: R. Matthew Gardner

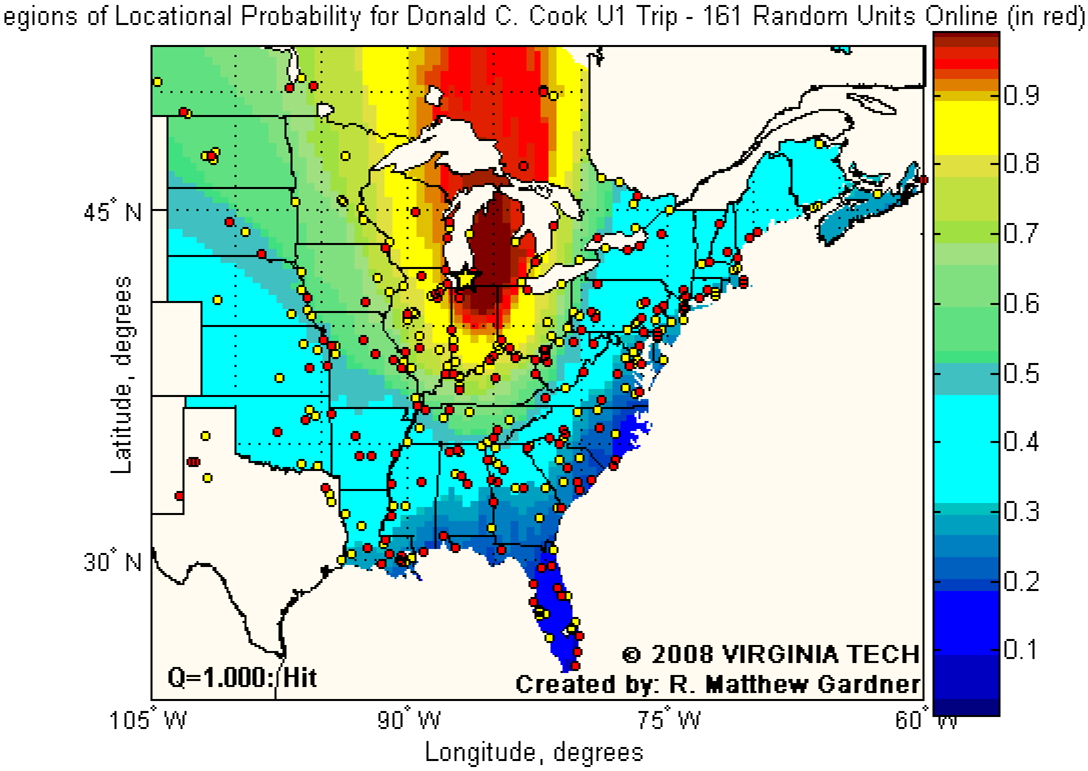
egions of Locational Probability for Donald C. Cook U1 Trip - 161 Random Units Online (in red)
45° N
30° N
Latitude, degrees
105° W
90° W
75° W
60° W
Longitude, degrees
Q=1.000:/Hit
© 2008 VIRGINIA TECH
Created by: R. Matthew Gardner
0.9
0.8
0.7
0.6
0.5
0.4
0.3
0.2
0.1

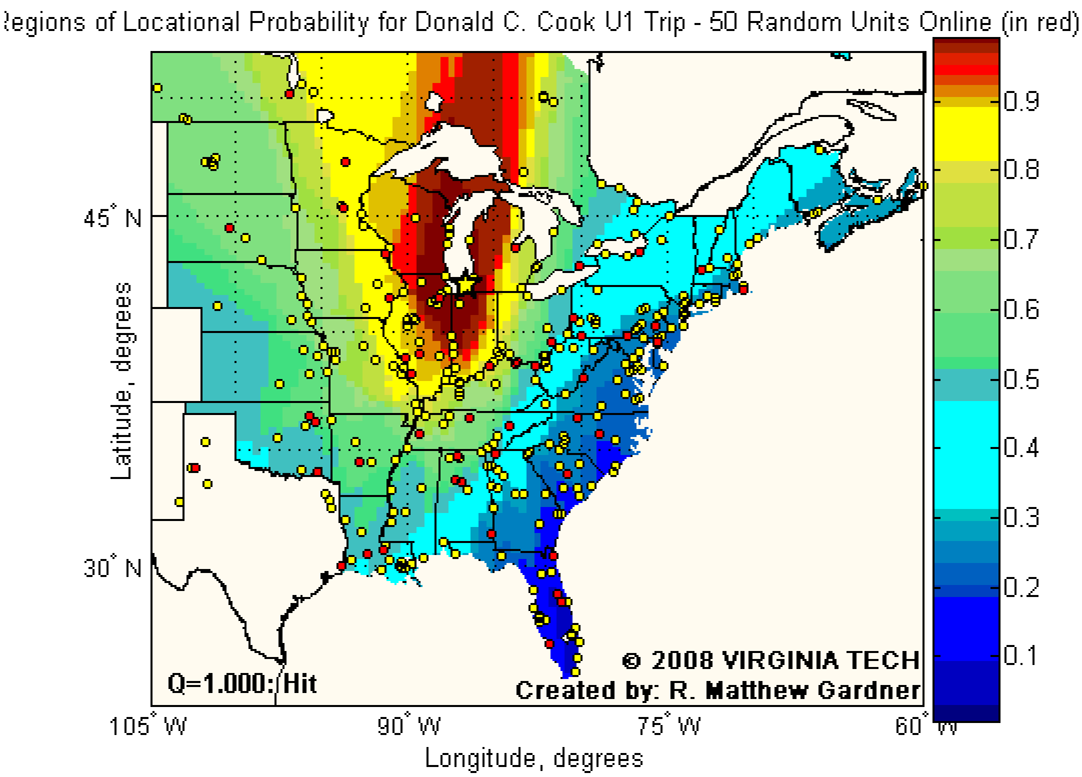
Regions of Locational Probability for Donald C. Cook U1 Trip - 50 Random Units Online (in red)
45° N
30° N
Latitude, degrees
105° W
90° W
75° W
60° W
Longitude, degrees
Q=1.000:/Hit
© 2008 VIRGINIA TECH
Created by: R. Matthew Gardner
0.9
0.8
0.7
0.6
0.5
0.4
0.3
0.2
0.1

Regions of Locational Probability for Mountaineer U1 Trip - 15 Random Units Online (in red)

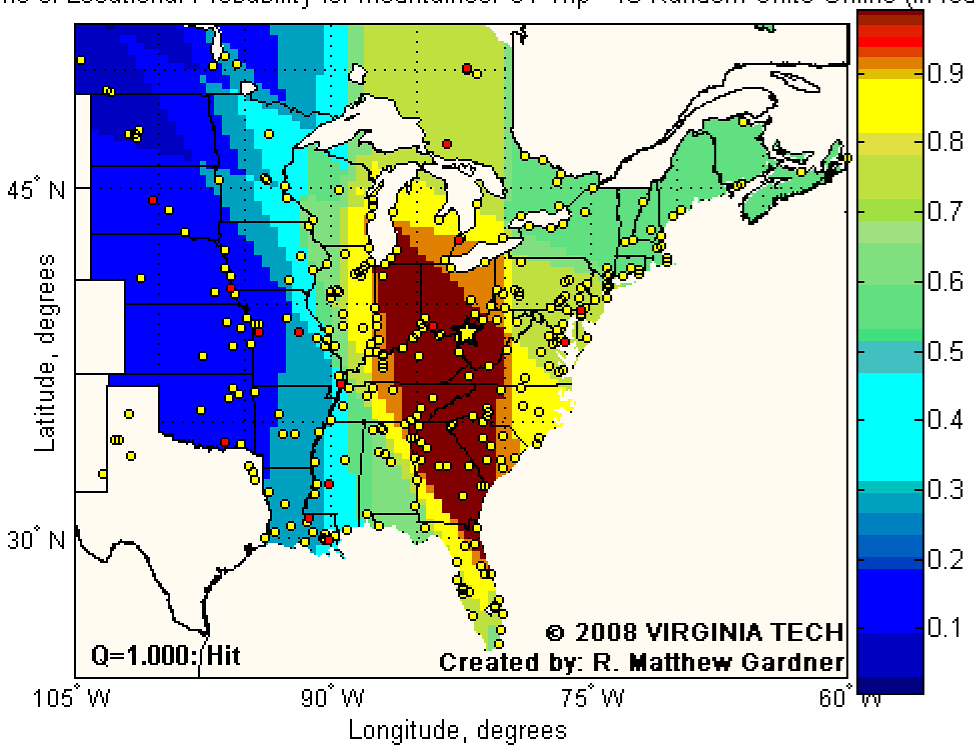

Regions of Locational Probability for Mountaineer U1 Trip - 161 Random Units Online (in red)

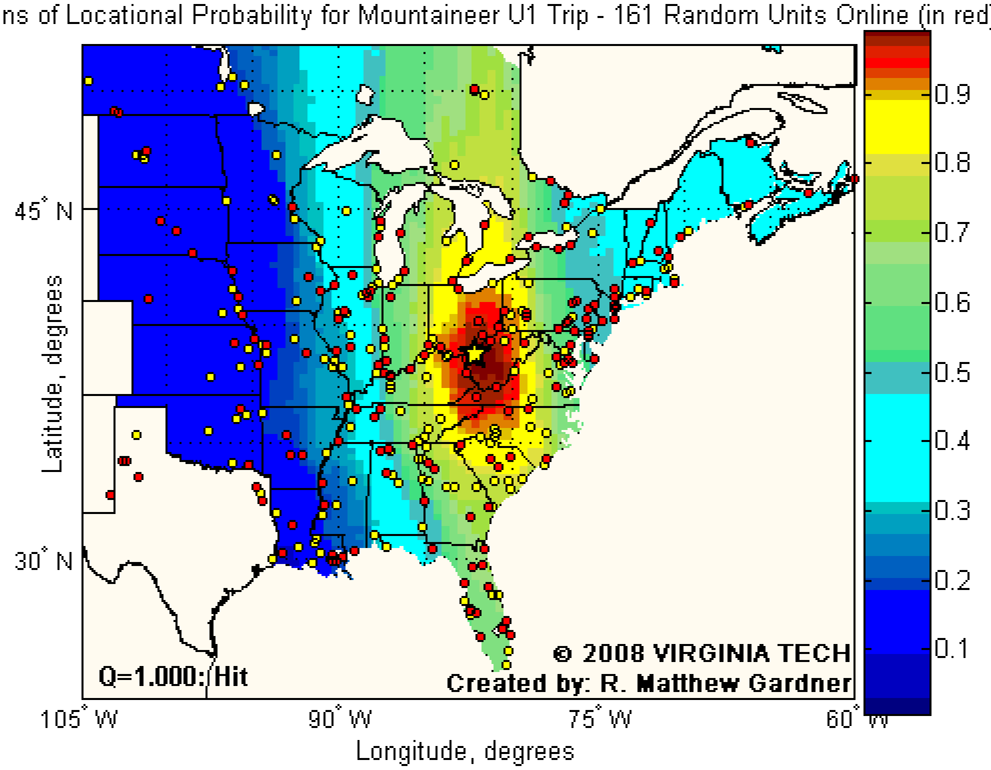

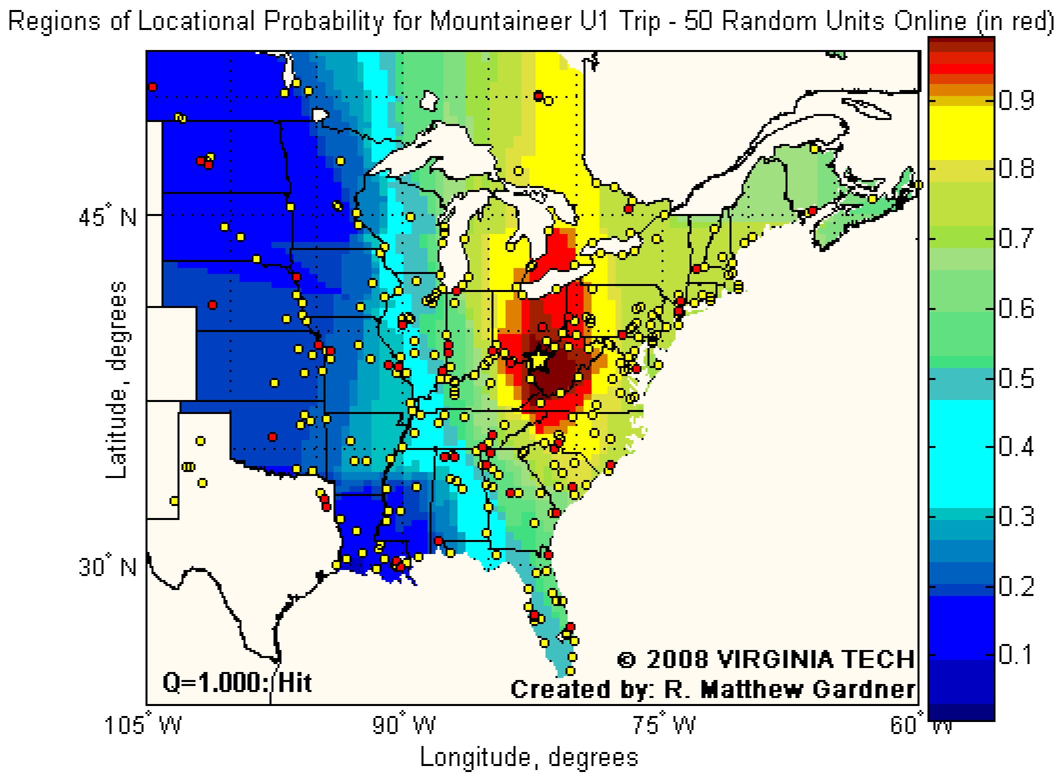
Regions of Locational Probability for Mountaineer U1 Trip - 50 Random Units Online (in red)
45° N
30° N
Latitude, degrees
105° W
90° W
75° W
60° W
Longitude, degrees
Q=1.000:/Hit
© 2008 VIRGINIA TECH
Created by: R. Matthew Gardner
0.9
0.8
0.7
0.6
0.5
0.4
0.3
0.2
0.1

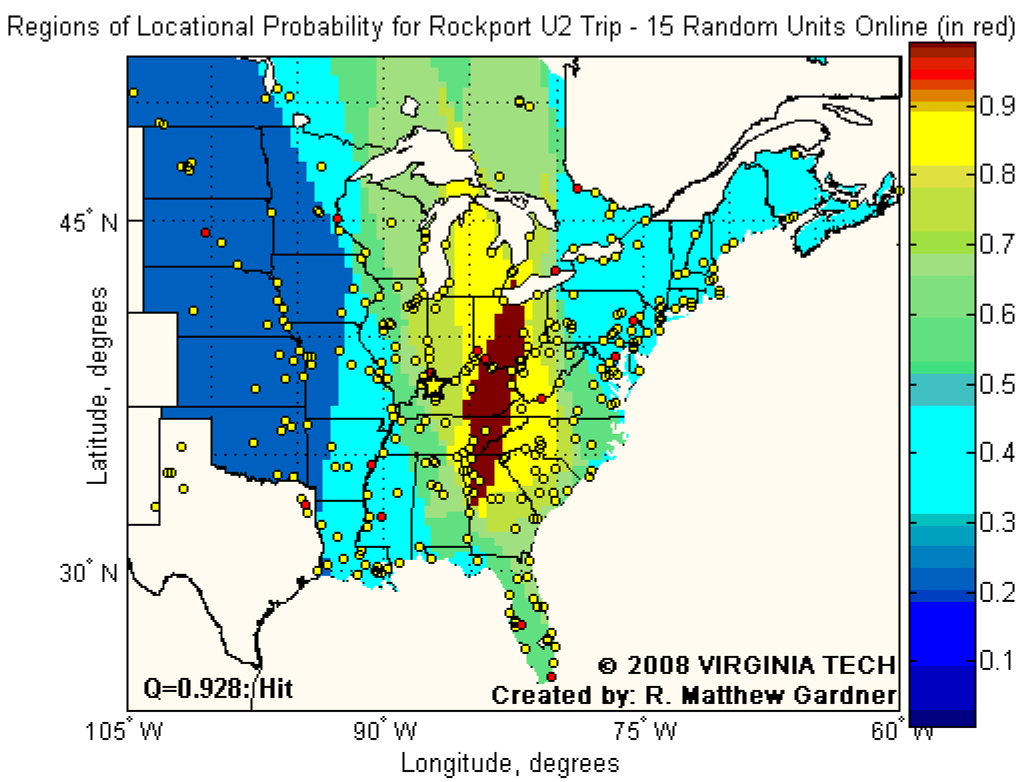
Regions of Locational Probability for Rockport U2 Trip - 15 Random Units Online (in red)
45° N
30° N
Latitude, degrees
105° W
90° W
75° W
60° W
Longitude, degrees
Q=0.928:/Hit
© 2008 VIRGINIA TECH
Created by: R. Matthew Gardner
0.9
0.8
0.7
0.6
0.5
0.4
0.3
0.2
0.1

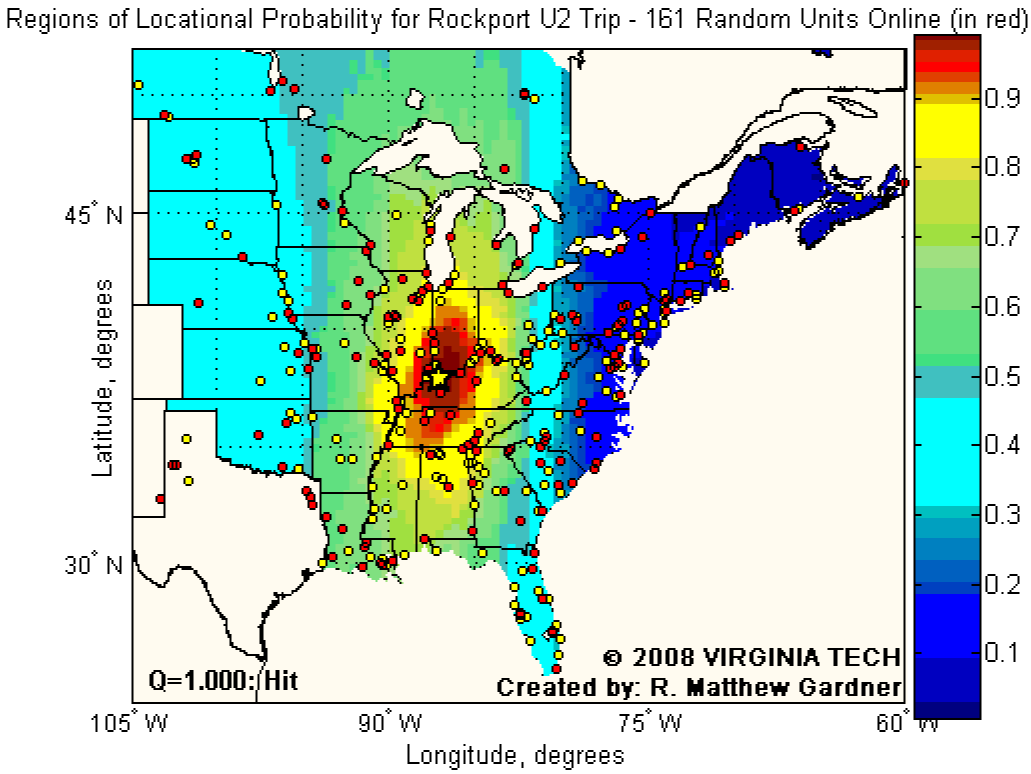
Regions of Locational Probability for Rockport U2 Trip - 161 Random Units Online (in red)
45° N
30° N
Latitude, degrees
105° W
90° W
75° W
60° W
Longitude, degrees
Q=1.000:/Hit
© 2008 VIRGINIA TECH
Created by: R. Matthew Gardner
0.9
0.8
0.7
0.6
0.5
0.4
0.3
0.2
0.1

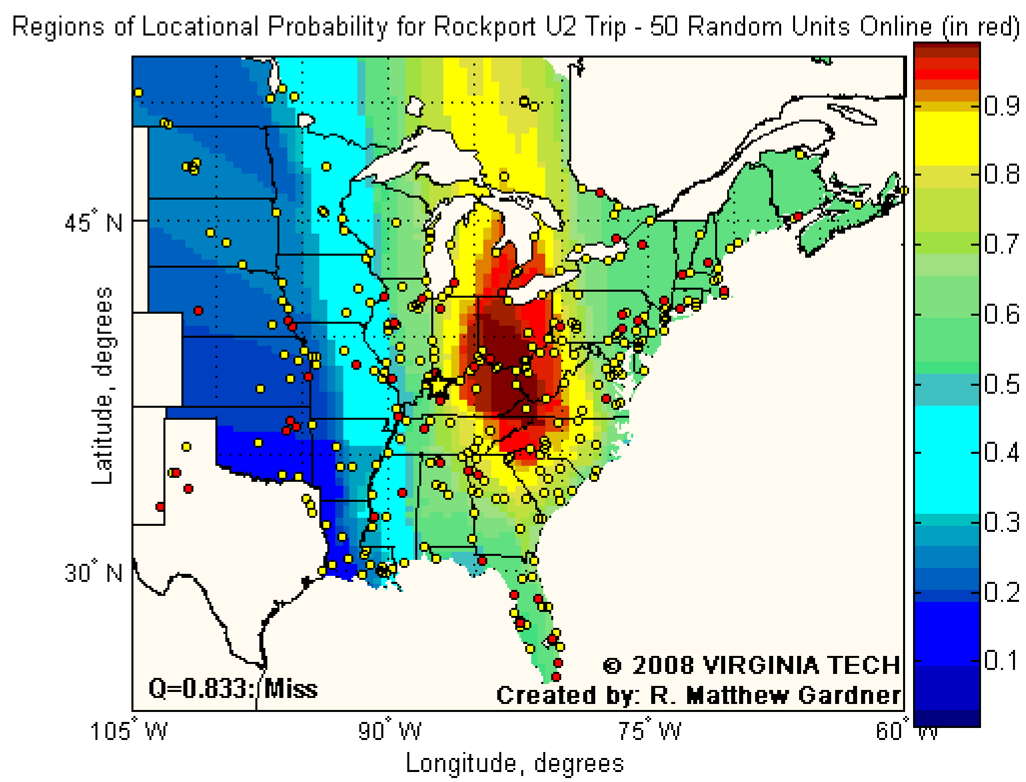
Regions of Locational Probability for Rockport U2 Trip - 50 Random Units Online (in red)
45° N
30° N
Latitude, degrees
105° W
90° W
75° W
60° W
Longitude, degrees
Q=0.833:/Miss
© 2008 VIRGINIA TECH
Created by: R. Matthew Gardner
0.9
0.8
0.7
0.6
0.5
0.4
0.3
0.2
0.1

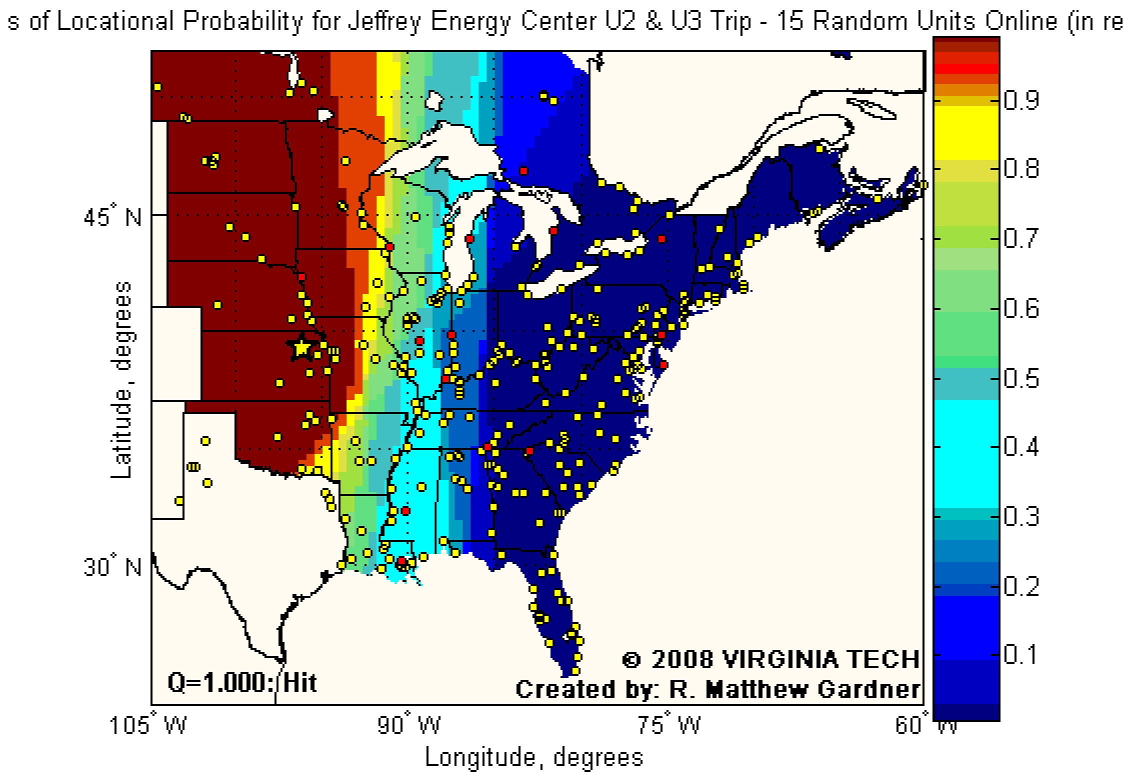
s of Locational Probability for Jeffrey Energy Center U2 & U3 Trip - 15 Random Units Online (in re
45° N
30° N
Latitude, degrees
105° W
90° W
75° W
60° W
Longitude, degrees
Q=1.000:/Hit
© 2008 VIRGINIA TECH
Created by: R. Matthew Gardner
0.9
0.8
0.7
0.6
0.5
0.4
0.3
0.2
0.1

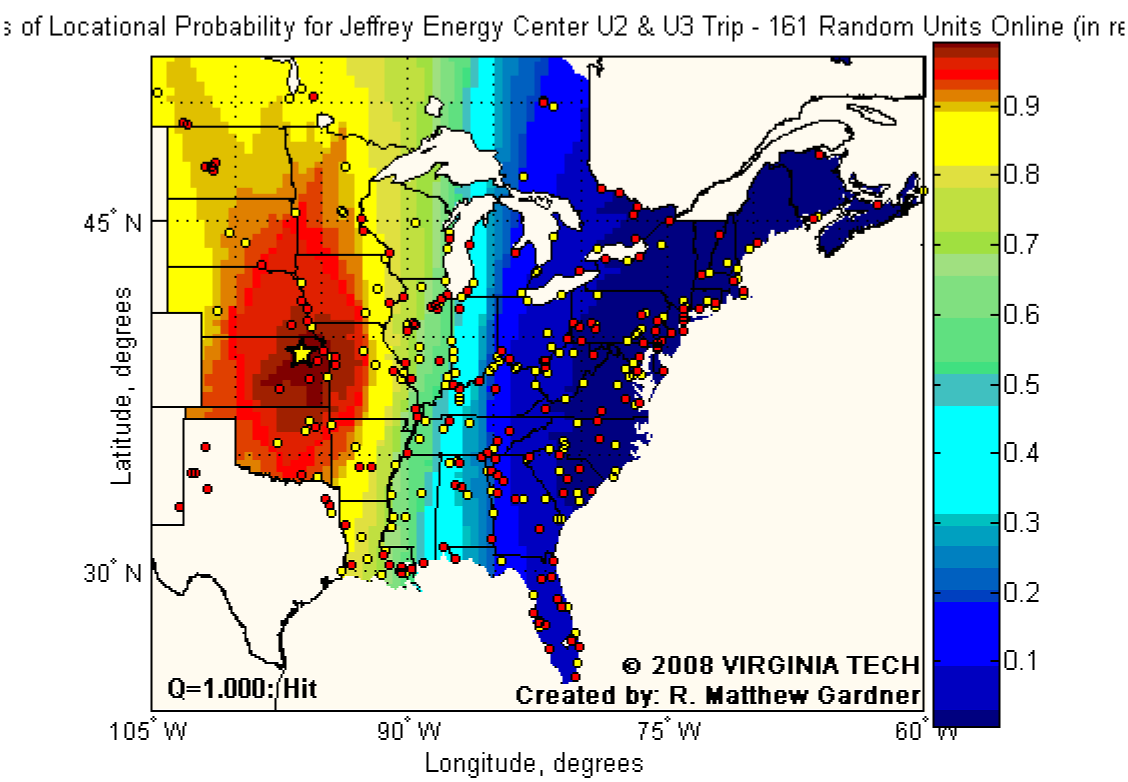
s of Locational Probability for Jeffrey Energy Center U2 & U3 Trip - 161 Random Units Online (in re
45° N
30° N
Latitude, degrees
105° W
90° W
75° W
60° W
Longitude, degrees
Q=1.000:/Hit
© 2008 VIRGINIA TECH
Created by: R. Matthew Gardner
0.9
0.8
0.7
0.6
0.5
0.4
0.3
0.2
0.1

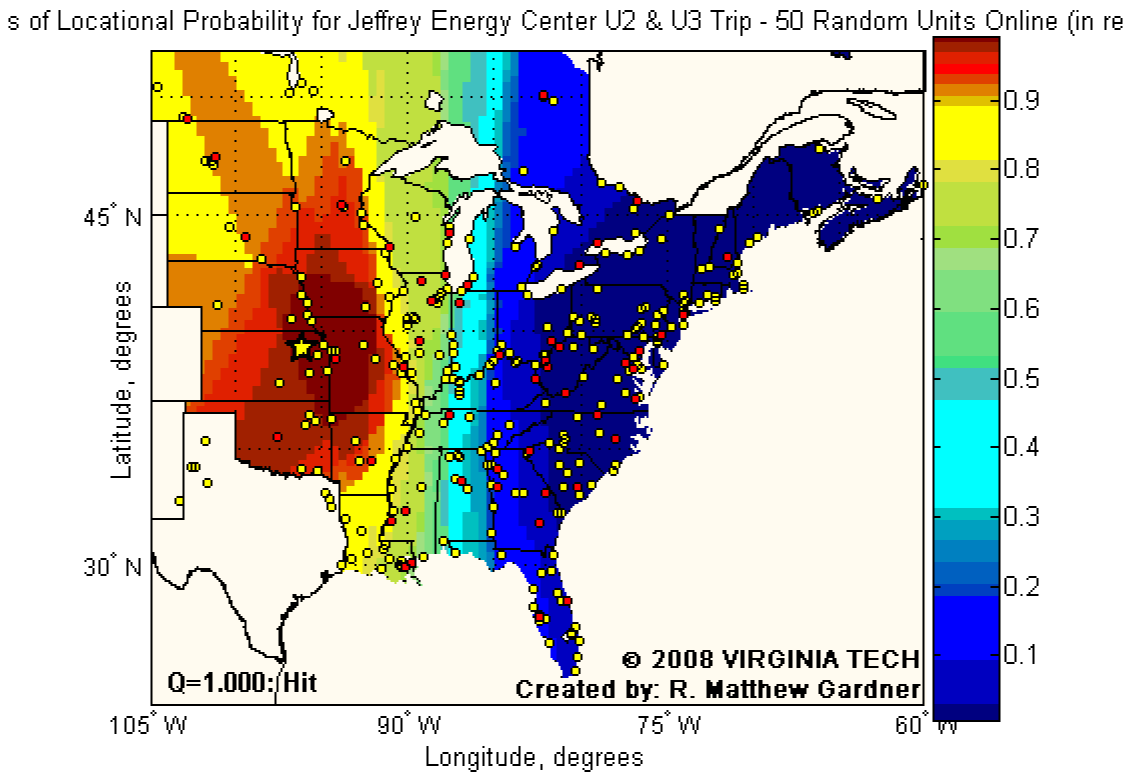
s of Locational Probability for Jeffrey Energy Center U2 & U3 Trip - 50 Random Units Online (in re
45° N
30° N
Latitude, degrees
105° W
90° W
75° W
60° W
Longitude, degrees
Q=1.000:/Hit
© 2008 VIRGINIA TECH
Created by: R. Matthew Gardner
0.9
0.8
0.7
0.6
0.5
0.4
0.3
0.2
0.1

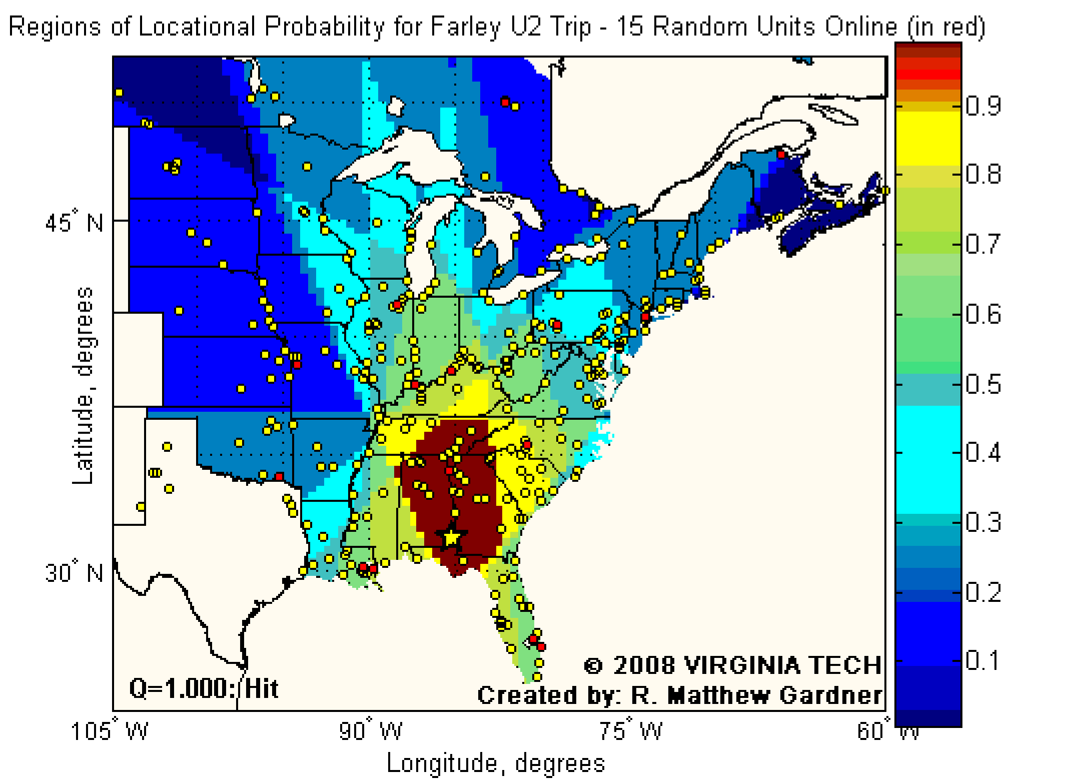
Regions of Locational Probability for Farley U2 Trip - 15 Random Units Online (in red)
45° N
30° N
Latitude, degrees
105° W
90° W
75° W
60° W
Longitude, degrees
Q=1.000:/Hit
© 2008 VIRGINIA TECH
Created by: R. Matthew Gardner
0.9
0.8
0.7
0.6
0.5
0.4
0.3
0.2
0.1

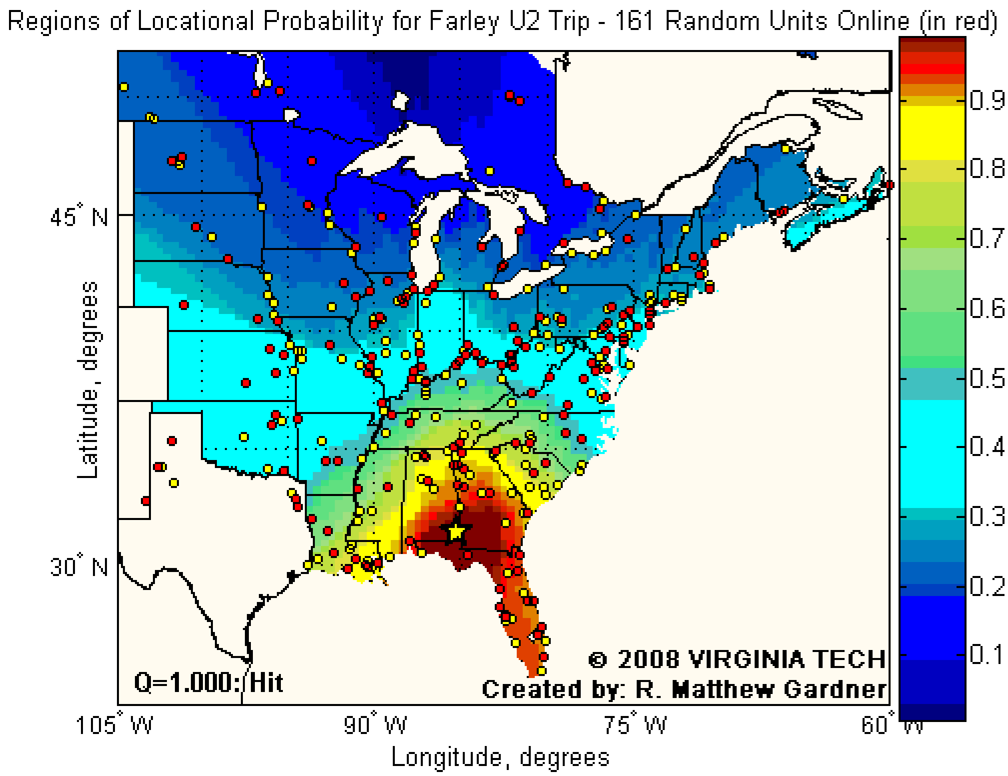
Regions of Locational Probability for Farley U2 Trip - 161 Random Units Online (in red)
45° N
30° N
Latitude, degrees
105° W
90° W
75° W
60° W
Longitude, degrees
0.9
0.8
0.7
0.6
0.5
0.4
0.3
0.2
0.1
Q=1.000:/Hit
© 2008 VIRGINIA TECH
Created by: R. Matthew Gardner

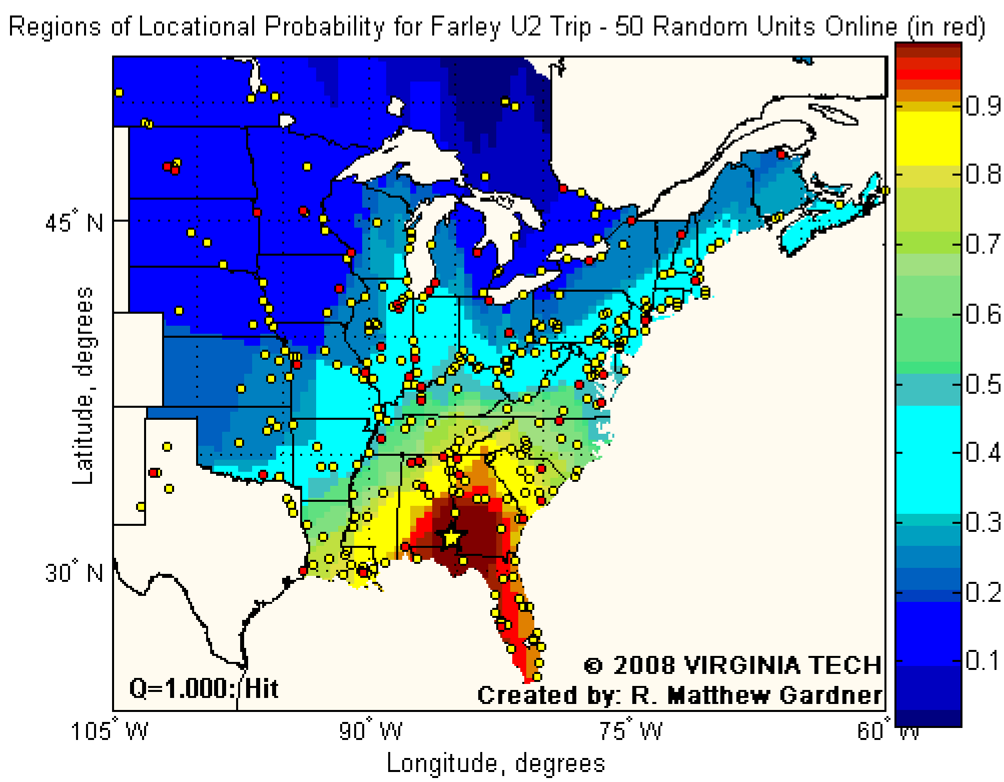
Regions of Locational Probability for Farley U2 Trip - 50 Random Units Online (in red)
45° N
30° N
Latitude, degrees
105° W
90° W
75° W
60° W
Longitude, degrees
0.9
0.8
0.7
0.6
0.5
0.4
0.3
0.2
0.1
Q=1.000:/Hit
© 2008 VIRGINIA TECH
Created by: R. Matthew Gardner

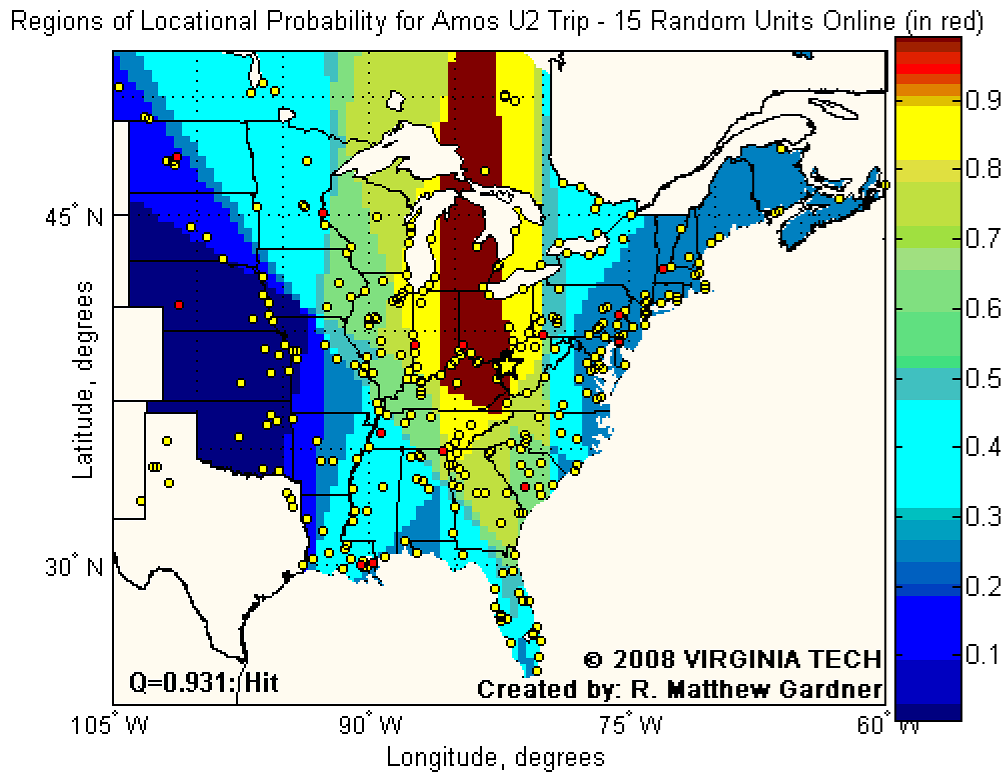
Regions of Locational Probability for Amos U2 Trip - 15 Random Units Online (in red)
45° N
30° N
Latitude, degrees
105° W
90° W
75° W
60° W
Longitude, degrees
0.9
0.8
0.7
0.6
0.5
0.4
0.3
0.2
0.1
Q=0.931: Hit
© 2008 VIRGINIA TECH
Created by: R. Matthew Gardner

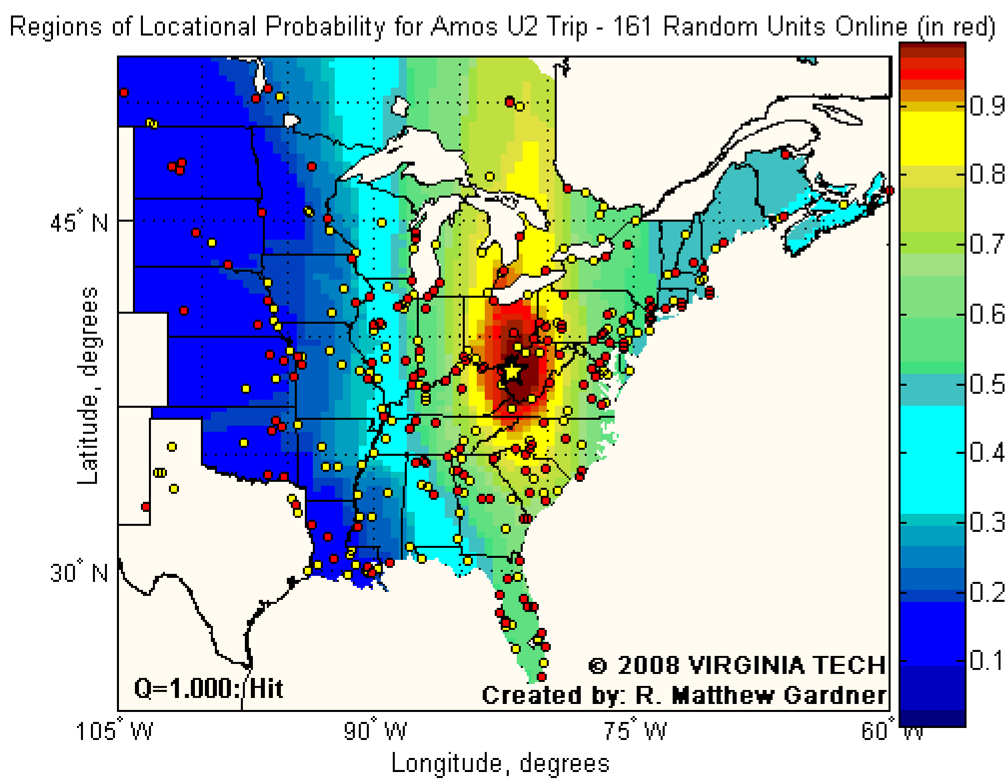
Regions of Locational Probability for Amos U2 Trip - 161 Random Units Online (in red)
45° N
30° N
Latitude, degrees
105° W
90° W
75° W
60° W
Longitude, degrees
0.9
0.8
0.7
0.6
0.5
0.4
0.3
0.2
0.1
Q=1.000: Hit
© 2008 VIRGINIA TECH
Created by: R. Matthew Gardner

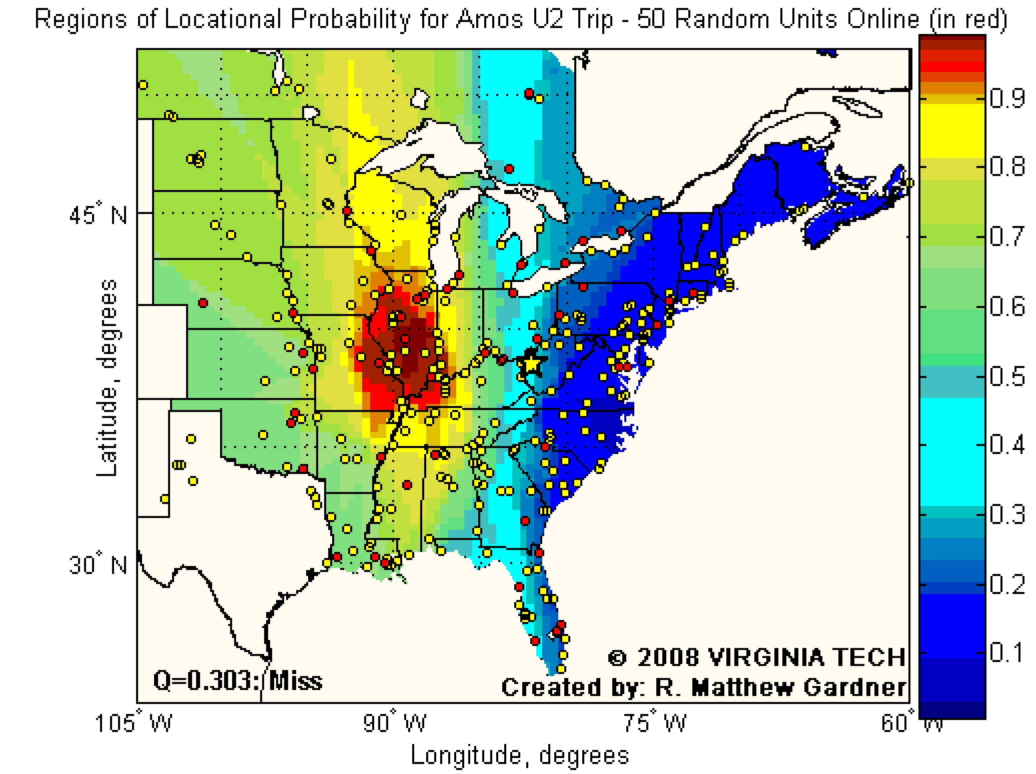
Regions of Locational Probability for Amos U2 Trip - 50 Random Units Online (in red)
45° N
30° N
Latitude, degrees
105° W
90° W
75° W
60° W
Longitude, degrees
Q=0.303: Miss
© 2008 VIRGINIA TECH
Created by: R. Matthew Gardner
0.9
0.8
0.7
0.6
0.5
0.4
0.3
0.2
0.1

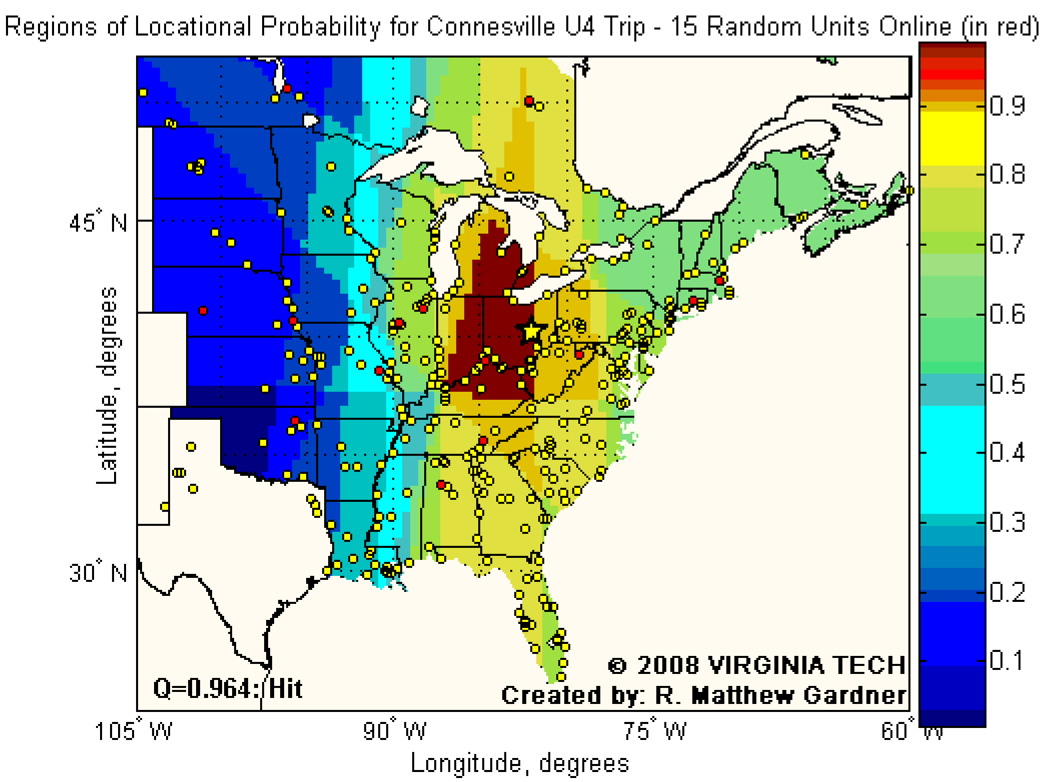
Regions of Locational Probability for Connesville U4 Trip - 15 Random Units Online (in red)
45° N
30° N
Latitude, degrees
105° W
90° W
75° W
60° W
Longitude, degrees
Q=0.964: Hit
© 2008 VIRGINIA TECH
Created by: R. Matthew Gardner
0.9
0.8
0.7
0.6
0.5
0.4
0.3
0.2
0.1

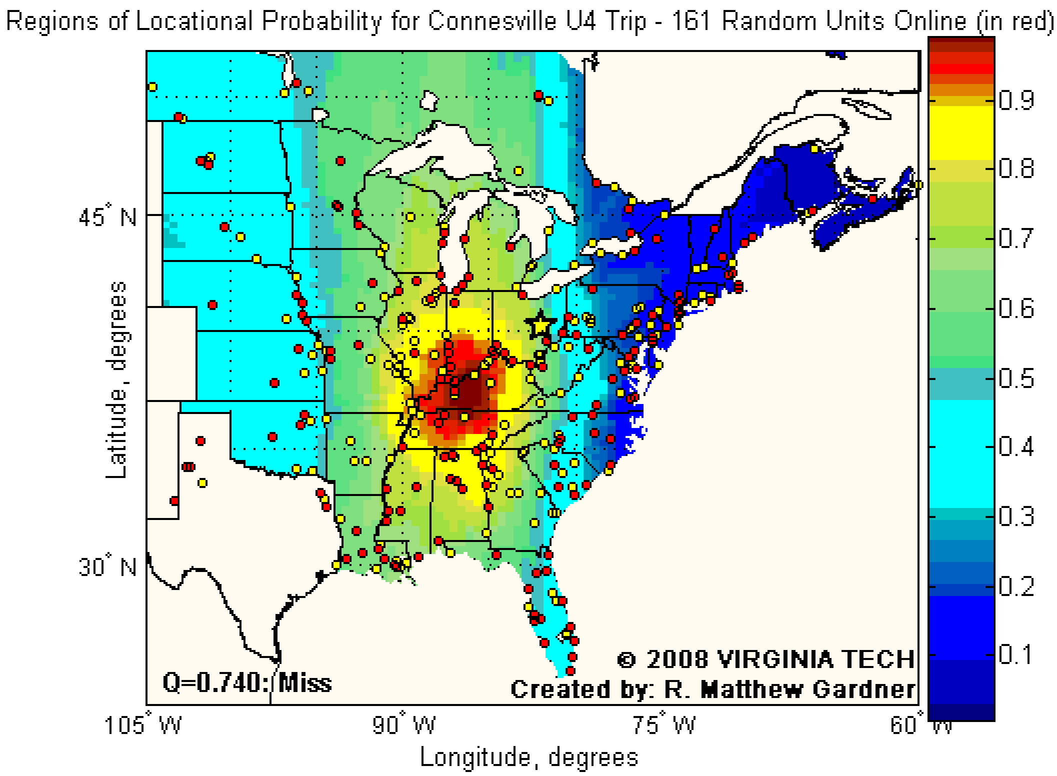
Regions of Locational Probability for Connesville U4 Trip - 161 Random Units Online (in red)
Latitude, degrees
Longitude, degrees
45° N
30° N
105° W
90° W
75° W
60° W
0.9
0.8
0.7
0.6
0.5
0.4
0.3
0.2
0.1
Q=0.740: Miss
© 2008 VIRGINIA TECH
Created by: R. Matthew Gardner

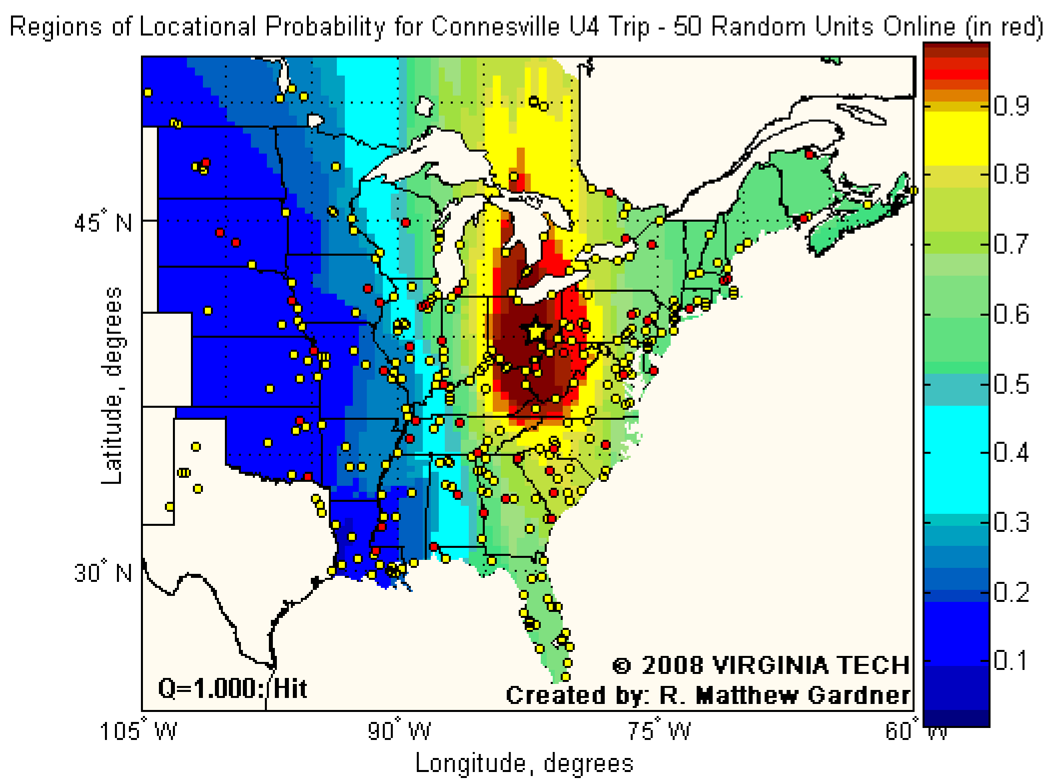
Regions of Locational Probability for Connesville U4 Trip - 50 Random Units Online (in red)
Latitude, degrees
Longitude, degrees
45° N
30° N
105° W
90° W
75° W
60° W
0.9
0.8
0.7
0.6
0.5
0.4
0.3
0.2
0.1
Q=1.000: Hit
© 2008 VIRGINIA TECH
Created by: R. Matthew Gardner

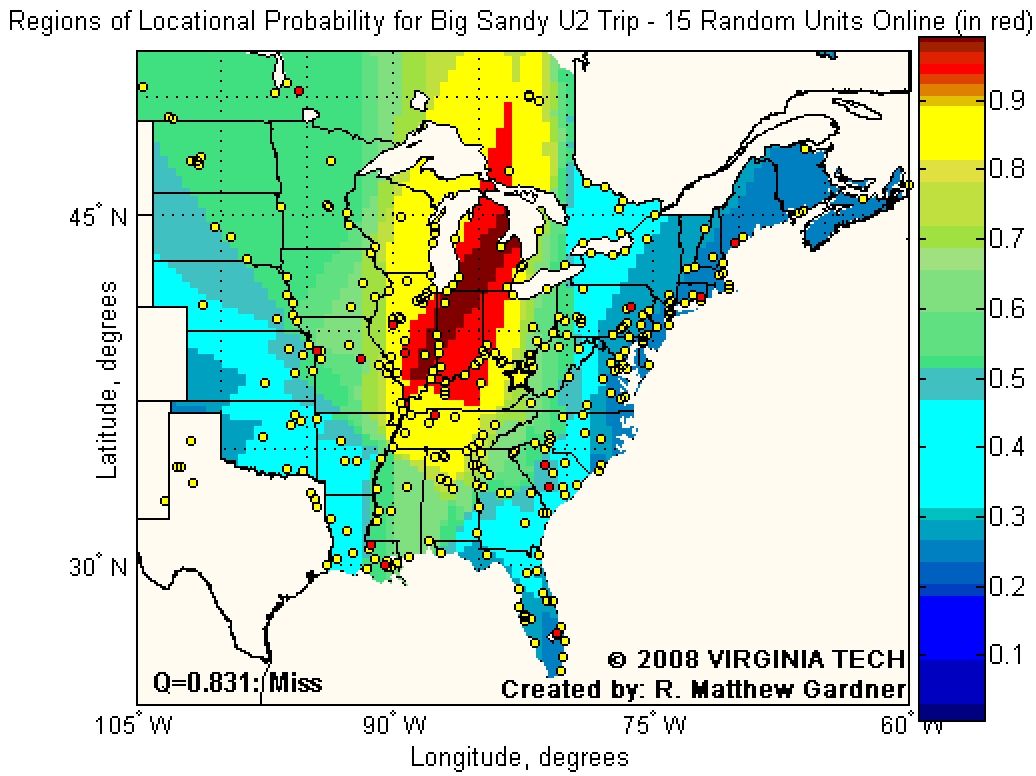
Regions of Locational Probability for Big Sandy U2 Trip - 15 Random Units Online (in red)
45° N
30° N
Latitude, degrees
105° W
90° W
75° W
60° W
Longitude, degrees
Q=0.831: Miss
© 2008 VIRGINIA TECH
Created by: R. Matthew Gardner
0.9
0.8
0.7
0.6
0.5
0.4
0.3
0.2
0.1

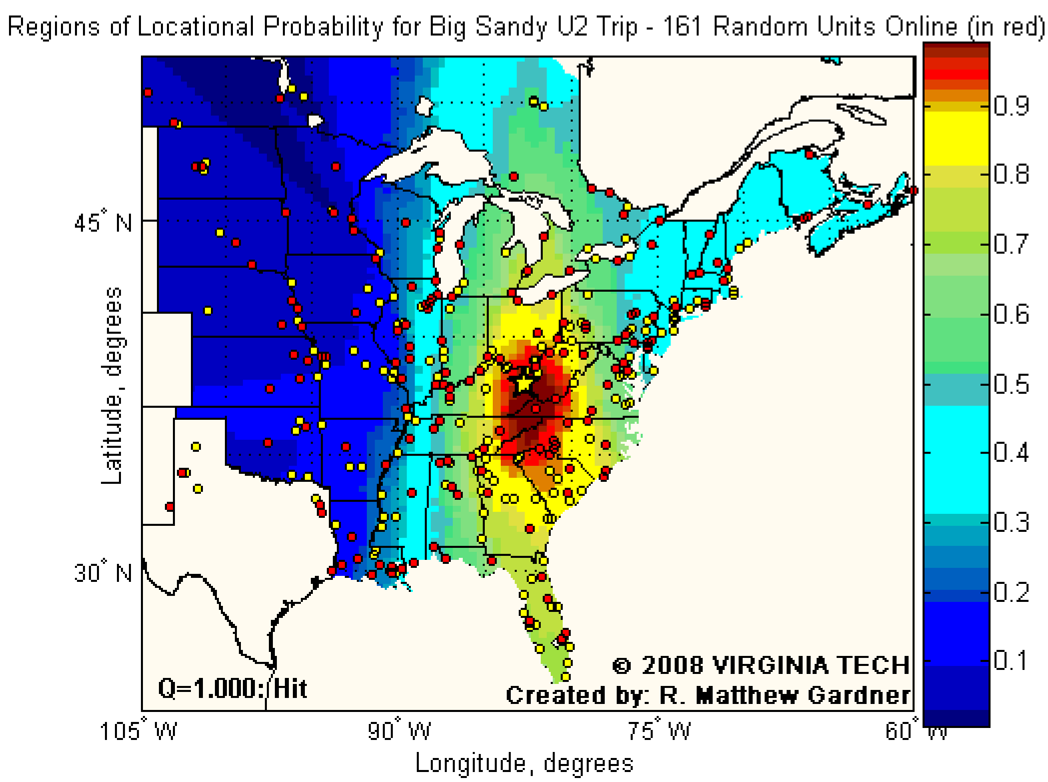
Regions of Locational Probability for Big Sandy U2 Trip - 161 Random Units Online (in red)
45° N
30° N
Latitude, degrees
105° W
90° W
75° W
60° W
Longitude, degrees
Q=1.000: Hit
© 2008 VIRGINIA TECH
Created by: R. Matthew Gardner
0.9
0.8
0.7
0.6
0.5
0.4
0.3
0.2
0.1

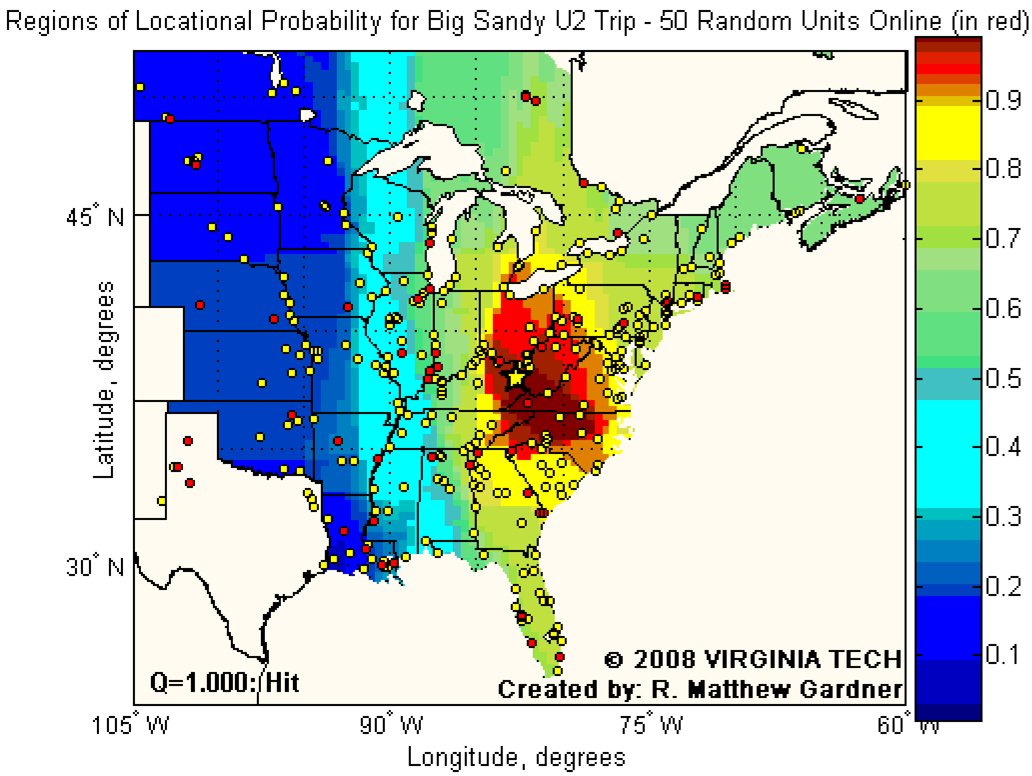
Regions of Locational Probability for Big Sandy U2 Trip - 50 Random Units Online (in red)
45° N
30° N
Latitude, degrees
105° W
90° W
75° W
60° W
Longitude, degrees
Q=1.000: Hit
© 2008 VIRGINIA TECH
Created by: R. Matthew Gardner
0.9
0.8
0.7
0.6
0.5
0.4
0.3
0.2
0.1

Appendix XIX: Half-Plane Event Location Based Upon Simulation of EI Angles at Random Points

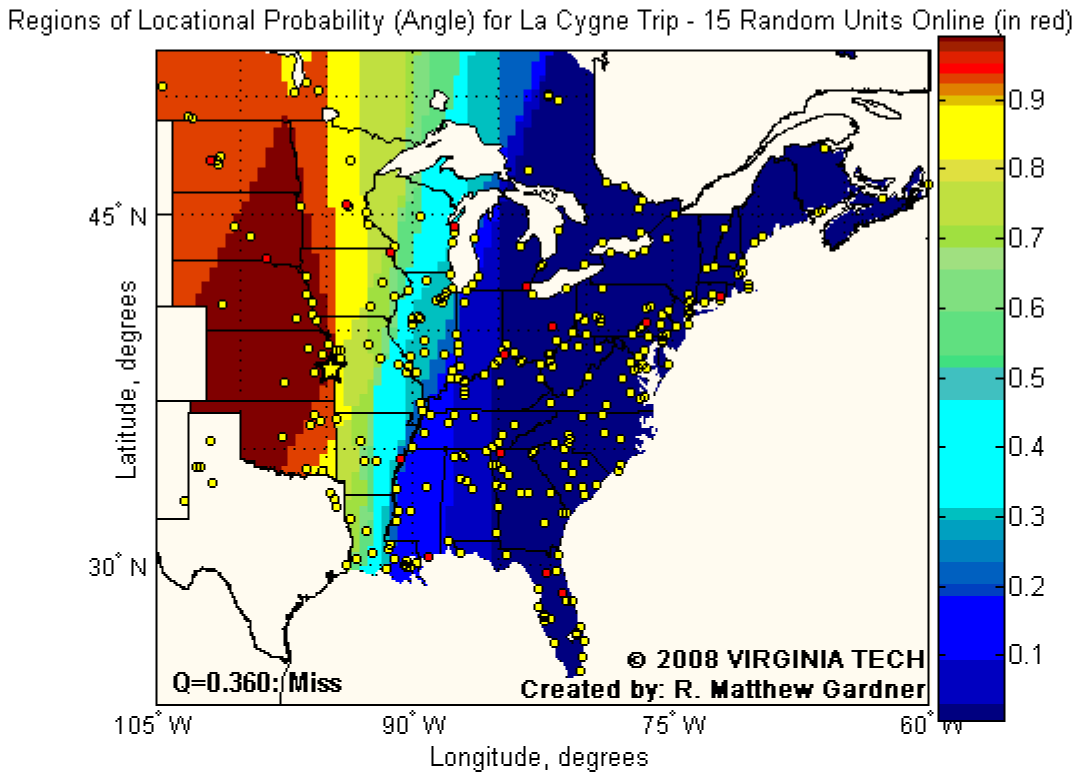

Regions of Locational Probability (Angle) for La Cygne Trip - 161 Random Units Online (in red)

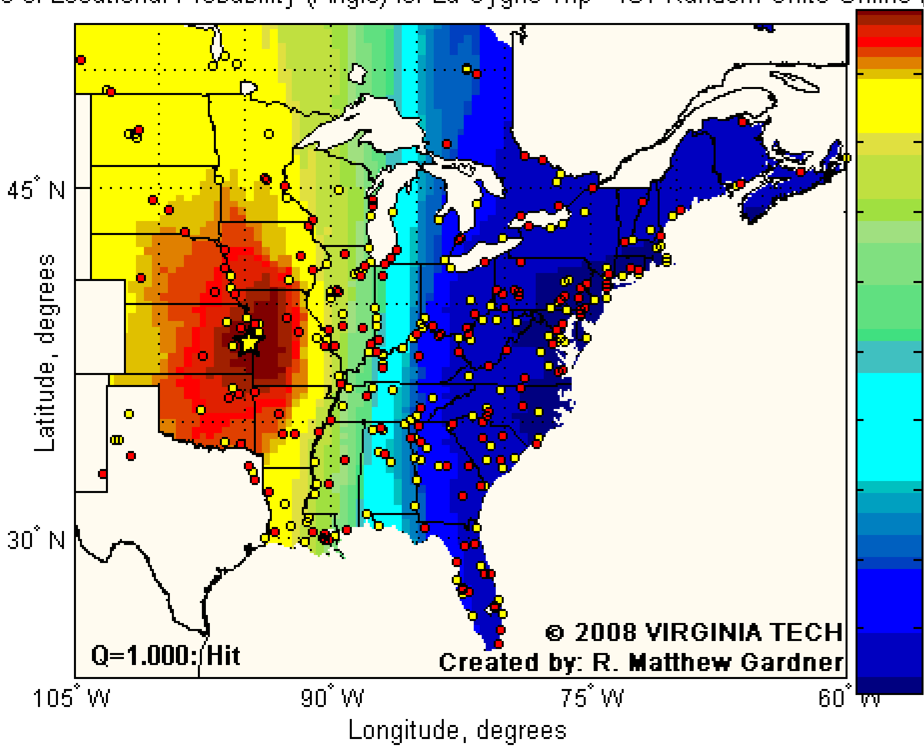

Regions of Locational Probability (Angle) for La Cygne Trip - 50 Random Units Online (in red)

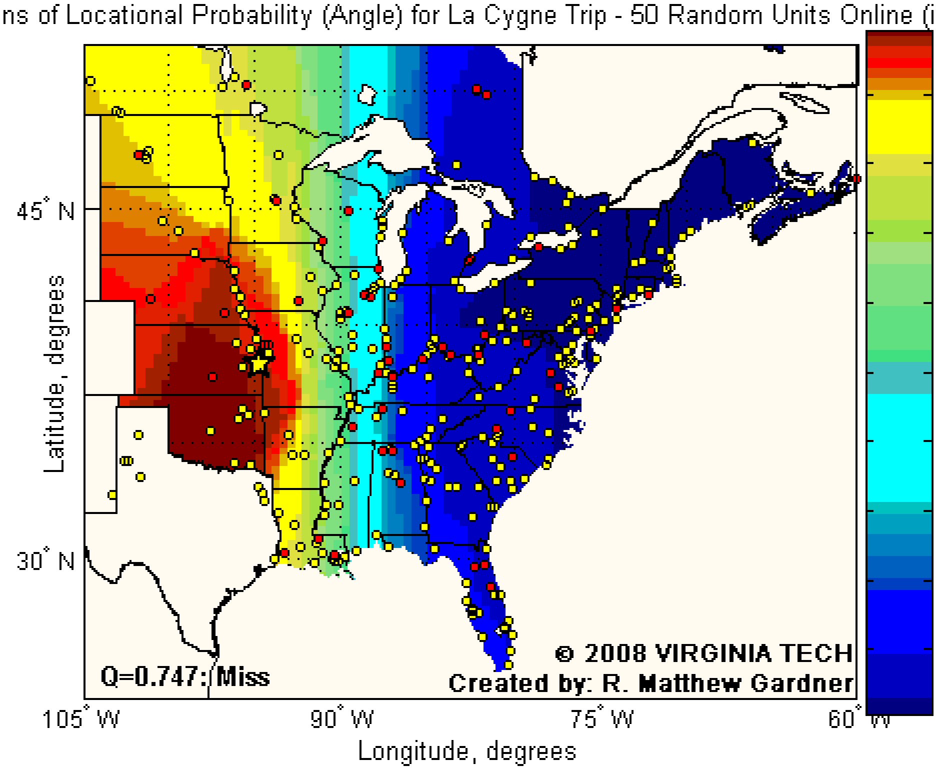

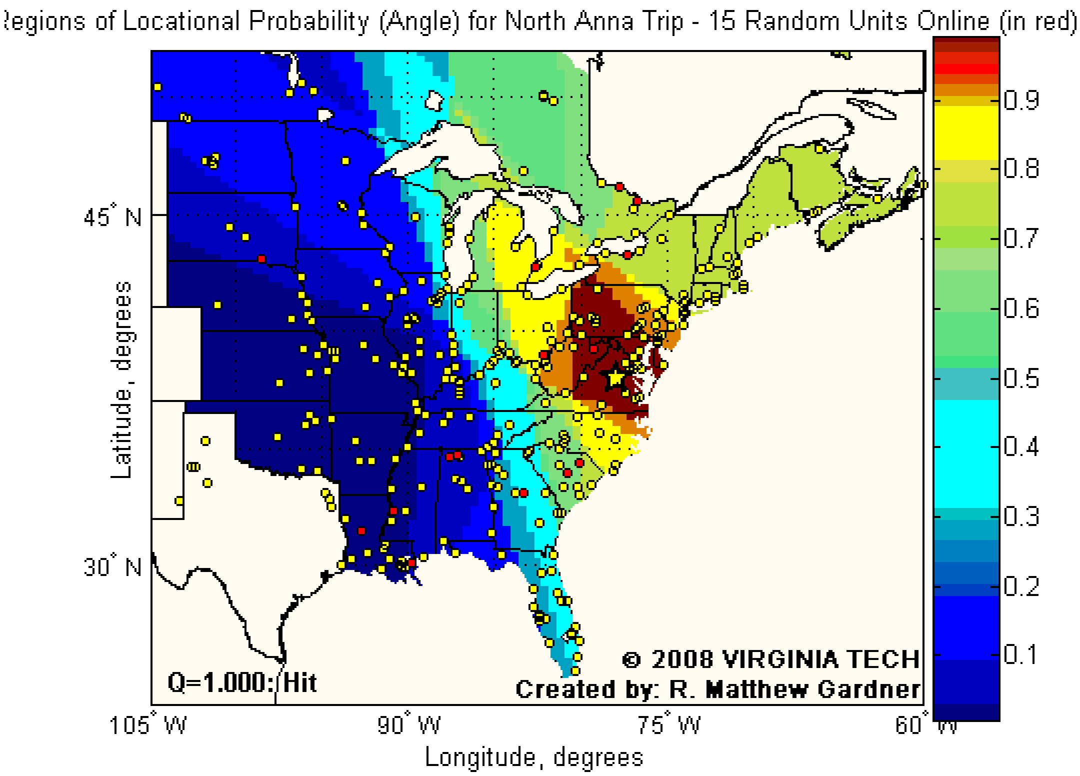

Regions of Locational Probability (Angle) for North Anna Trip - 15 Random Units Online (in red)
Latitude, degrees
45° N
30° N
105° W
90° W
75° W
60° W
Longitude, degrees
Q=1.000:/Hit
© 2008 VIRGINIA TECH
Created by: R. Matthew Gardner
0.9
0.8
0.7
0.6
0.5
0.4
0.3
0.2
0.1

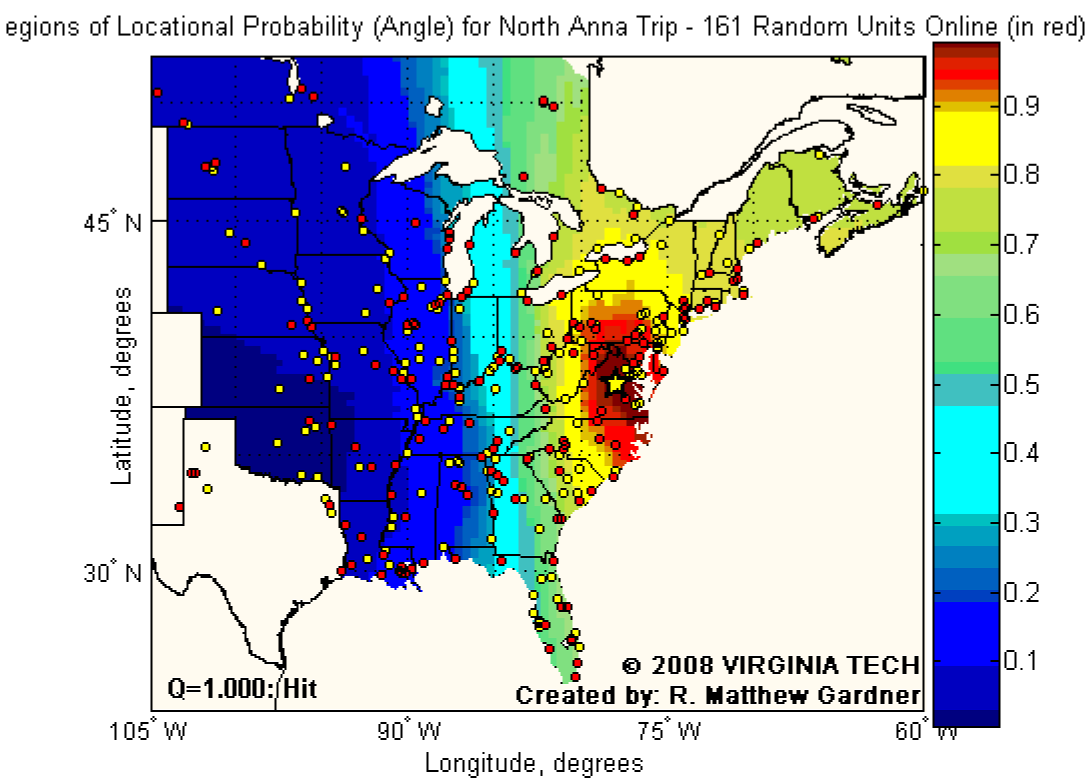

egions of Locational Probability (Angle) for North Anna Trip - 161 Random Units Online (in red)
Latitude, degrees
45° N
30° N
105° W
90° W
75° W
60° W
Longitude, degrees
Q=1.000:/Hit
© 2008 VIRGINIA TECH
Created by: R. Matthew Gardner
0.9
0.8
0.7
0.6
0.5
0.4
0.3
0.2
0.1

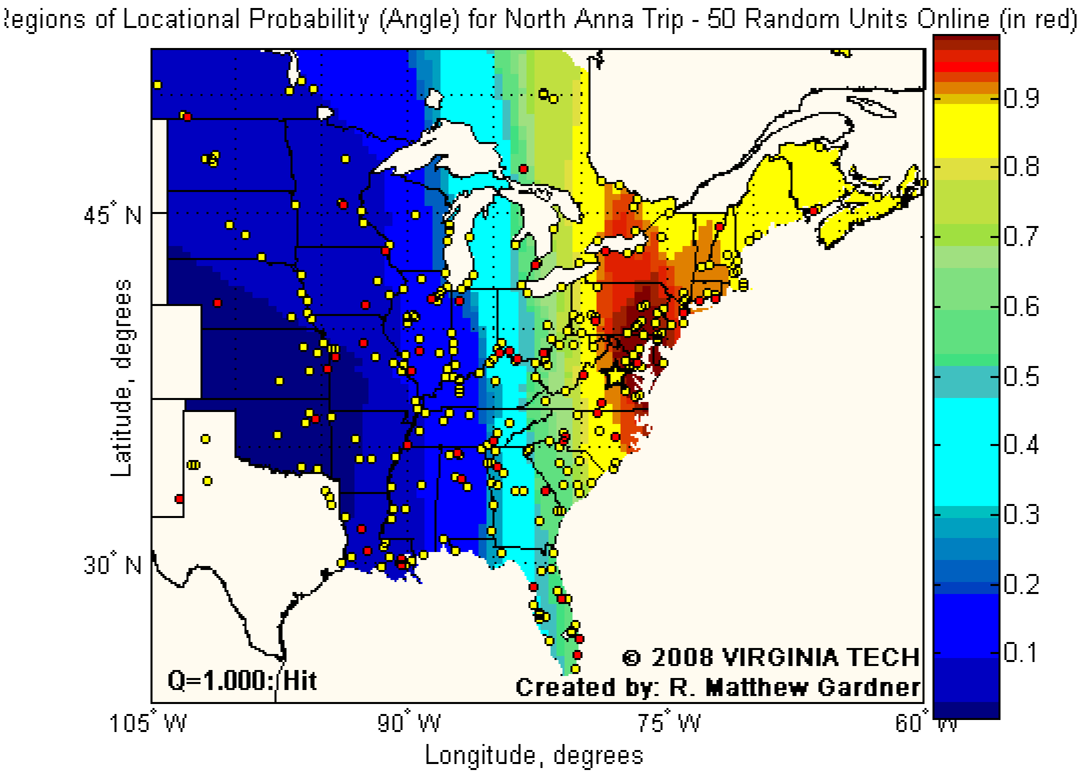
Regions of Locational Probability (Angle) for North Anna Trip - 50 Random Units Online (in red)
45° N
30° N
Latitude, degrees
105° W
90° W
75° W
60° W
Longitude, degrees
Q=1.000:/Hit
© 2008 VIRGINIA TECH
Created by: R. Matthew Gardner
0.9
0.8
0.7
0.6
0.5
0.4
0.3
0.2
0.1

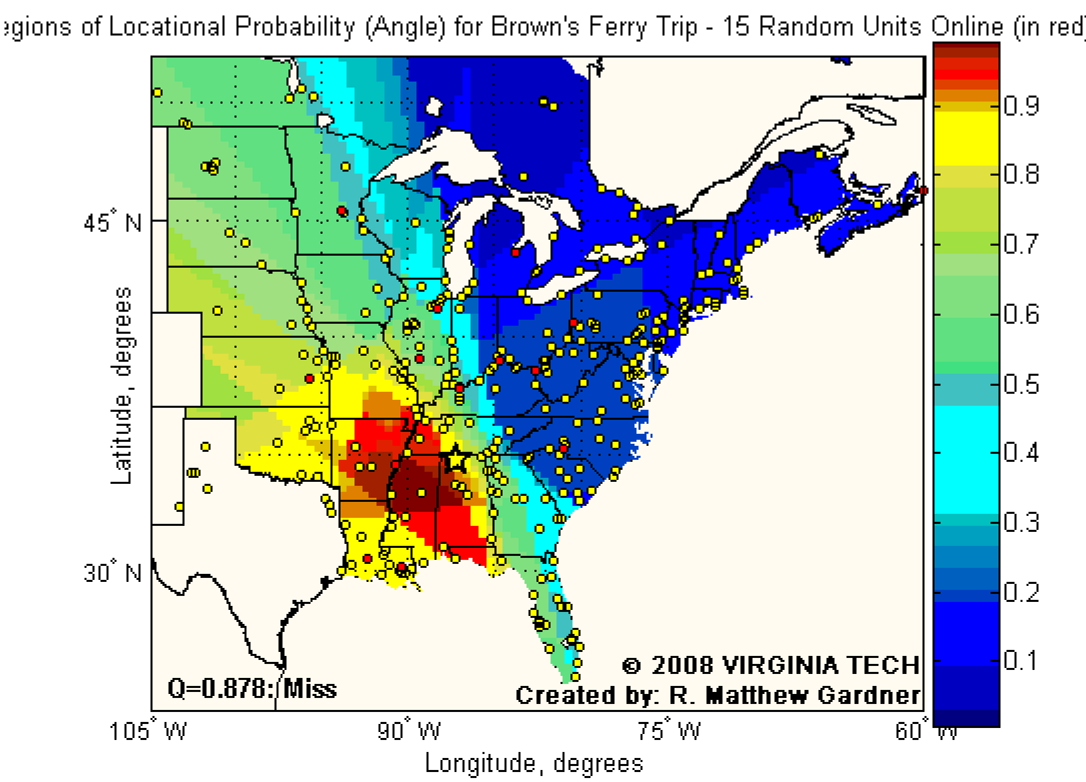
Regions of Locational Probability (Angle) for Brown's Ferry Trip - 15 Random Units Online (in red)
45° N
30° N
Latitude, degrees
105° W
90° W
75° W
60° W
Longitude, degrees
Q=0.878:/Miss
© 2008 VIRGINIA TECH
Created by: R. Matthew Gardner
0.9
0.8
0.7
0.6
0.5
0.4
0.3
0.2
0.1

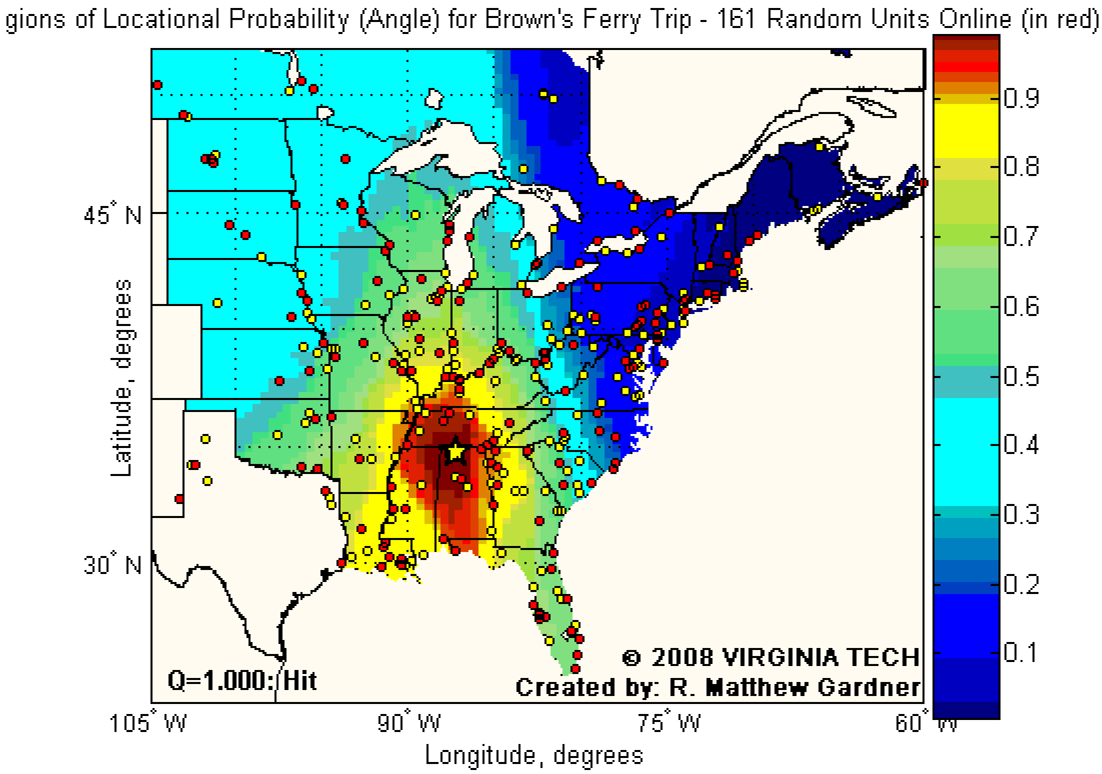
gions of Locational Probability (Angle) for Brown's Ferry Trip - 161 Random Units Online (in red)
45° N
30° N
Latitude, degrees
105° W
90° W
75° W
60° W
Longitude, degrees
Q=1.000:/Hit
© 2008 VIRGINIA TECH
Created by: R. Matthew Gardner
0.9
0.8
0.7
0.6
0.5
0.4
0.3
0.2
0.1

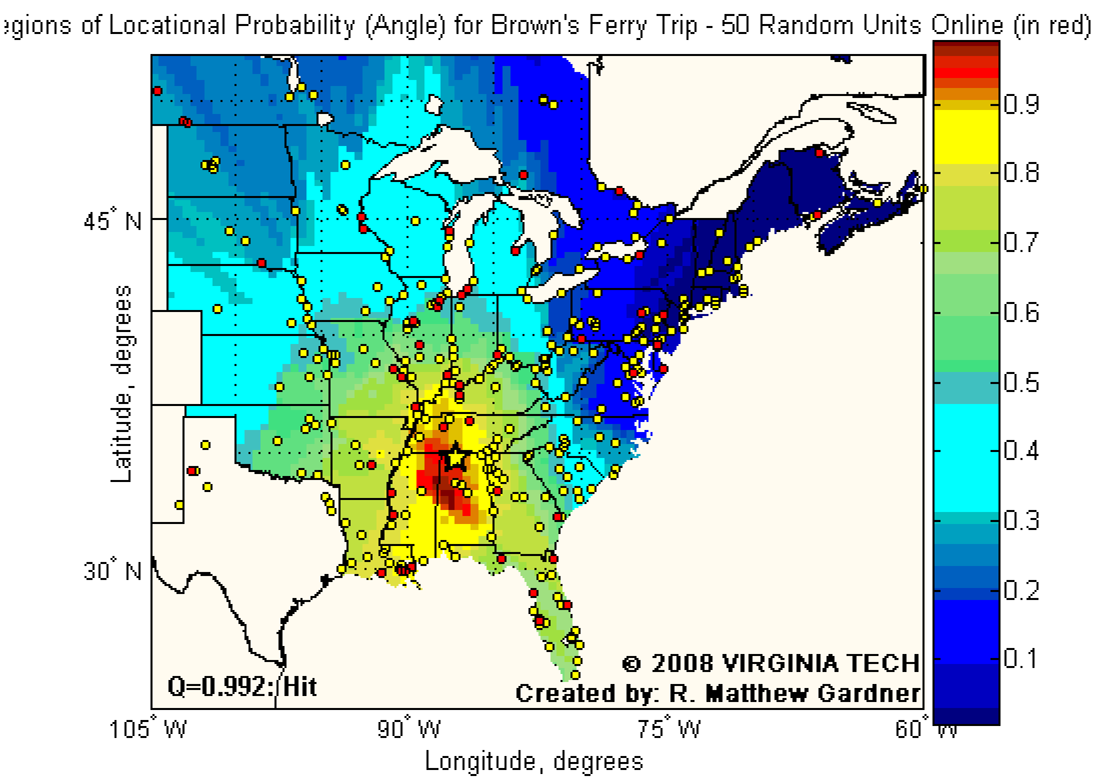
egions of Locational Probability (Angle) for Brown's Ferry Trip - 50 Random Units Online (in red)
45° N
30° N
Latitude, degrees
105° W
90° W
75° W
60° W
Longitude, degrees
Q=0.992:/Hit
© 2008 VIRGINIA TECH
Created by: R. Matthew Gardner
0.9
0.8
0.7
0.6
0.5
0.4
0.3
0.2
0.1

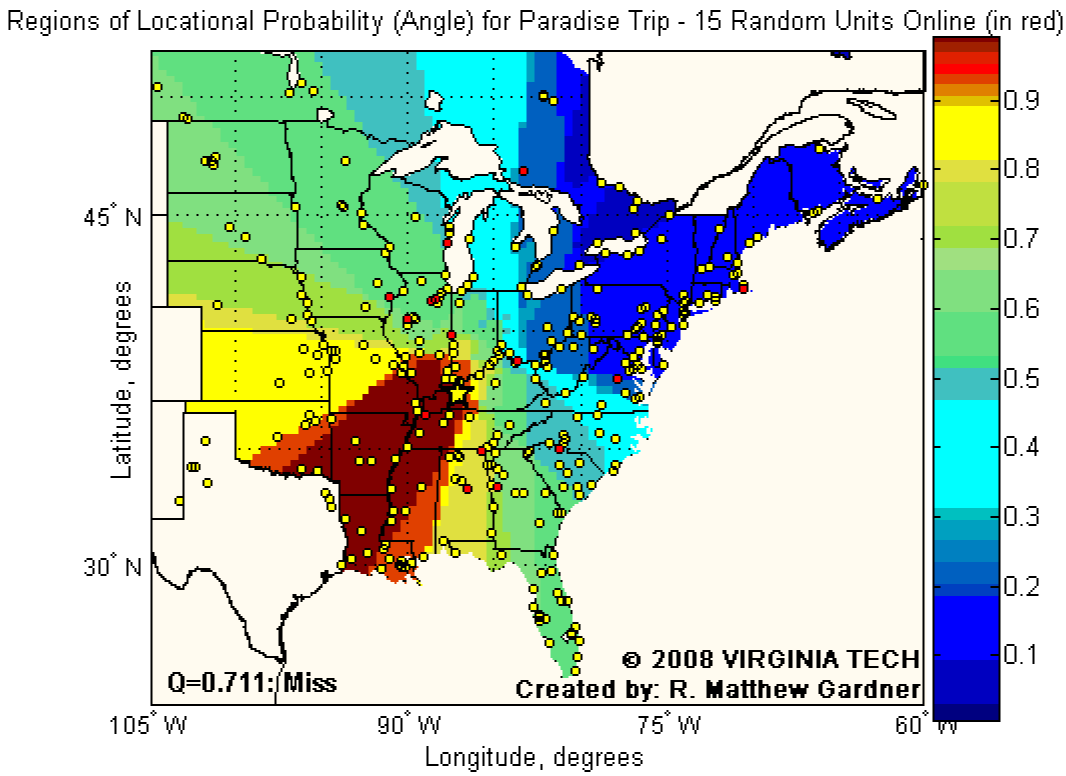
Regions of Locational Probability (Angle) for Paradise Trip - 15 Random Units Online (in red)
45° N
30° N
Latitude, degrees
105° W
90° W
75° W
60° W
Longitude, degrees
Q=0.711: Miss
© 2008 VIRGINIA TECH
Created by: R. Matthew Gardner
0.9
0.8
0.7
0.6
0.5
0.4
0.3
0.2
0.1

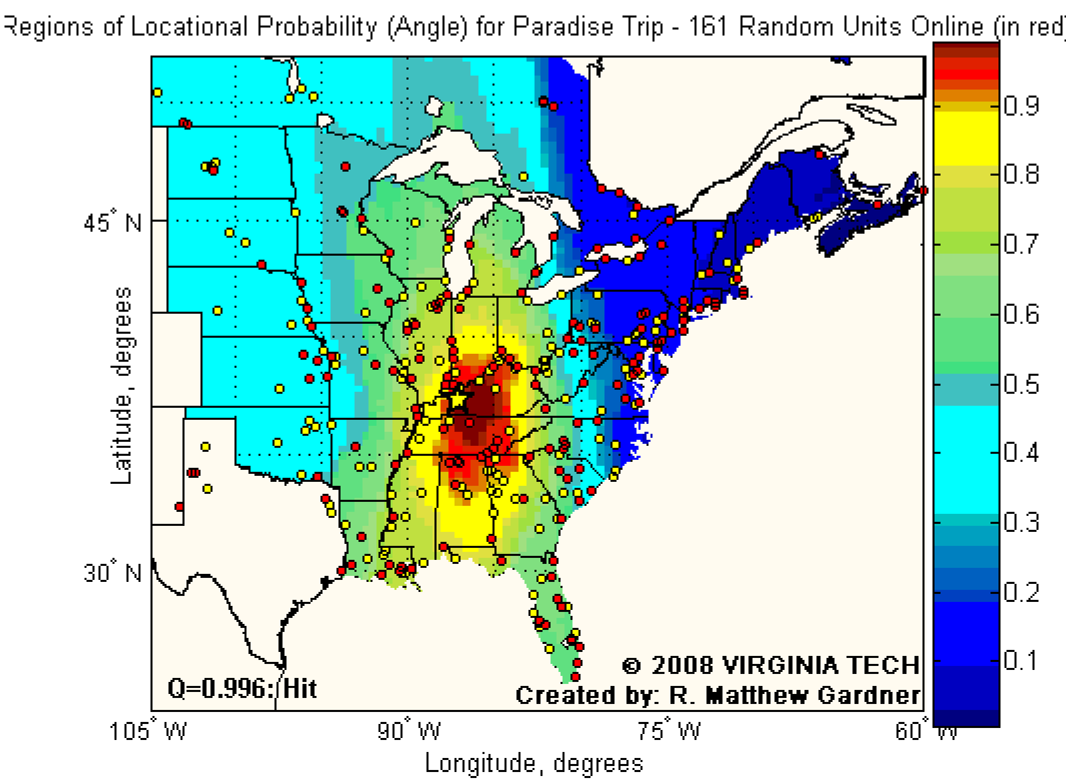
Regions of Locational Probability (Angle) for Paradise Trip - 161 Random Units Online (in red)
45° N
30° N
Latitude, degrees
105° W
90° W
75° W
60° W
Longitude, degrees
Q=0.996: Hit
© 2008 VIRGINIA TECH
Created by: R. Matthew Gardner
0.9
0.8
0.7
0.6
0.5
0.4
0.3
0.2
0.1

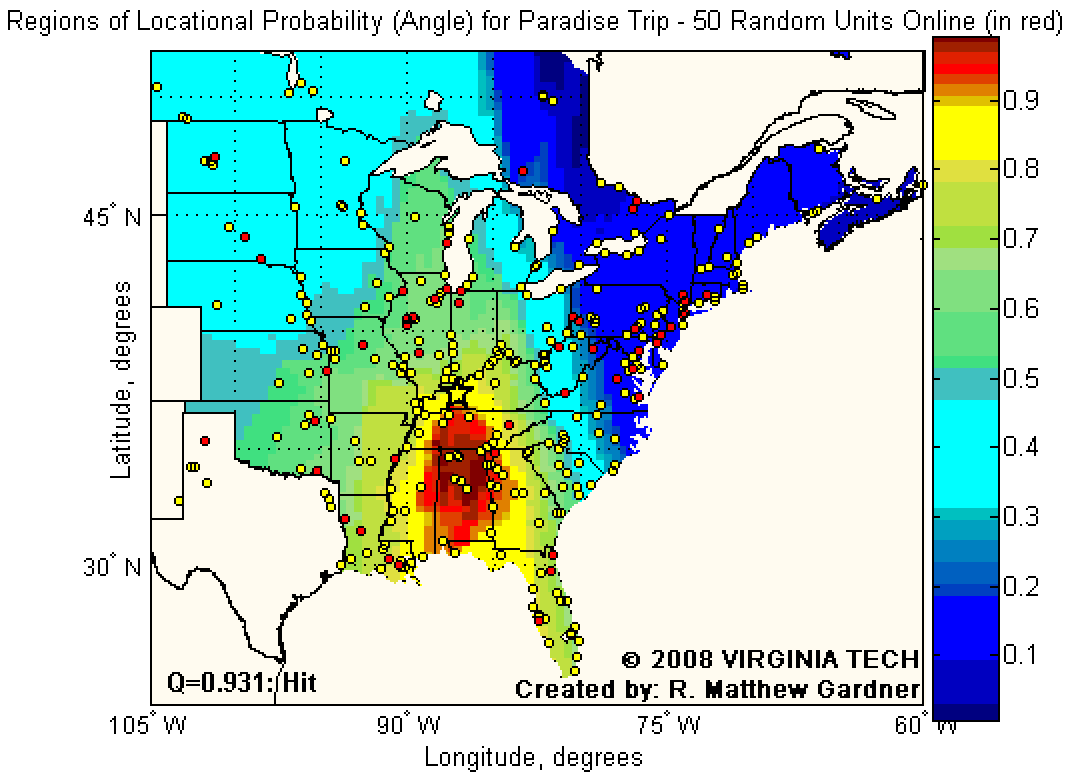
Regions of Locational Probability (Angle) for Paradise Trip - 50 Random Units Online (in red)
45° N
30° N
Latitude, degrees
105° W
90° W
75° W
60° W
Longitude, degrees
Q=0.931: Hit
© 2008 VIRGINIA TECH
Created by: R. Matthew Gardner
0.9
0.8
0.7
0.6
0.5
0.4
0.3
0.2
0.1

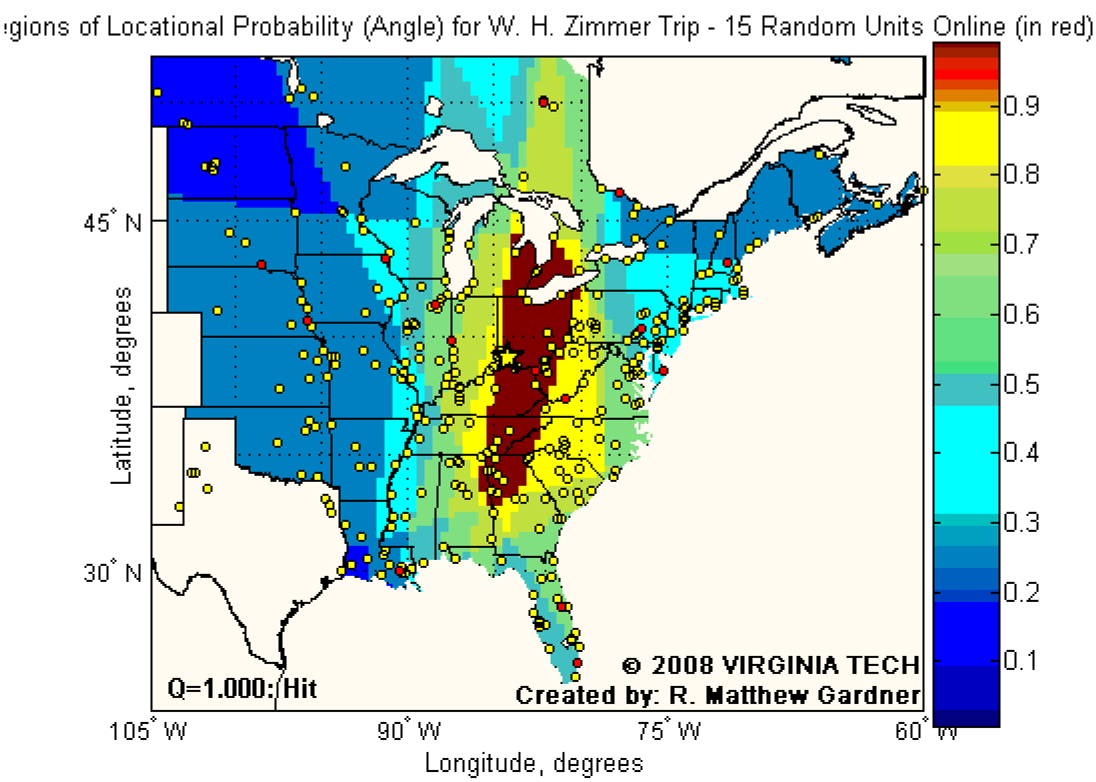
egions of Locational Probability (Angle) for W. H. Zimmer Trip - 15 Random Units Online (in red)
45° N
30° N
Latitude, degrees
105° W
90° W
75° W
60° W
Longitude, degrees
Q=1.000: Hit
© 2008 VIRGINIA TECH
Created by: R. Matthew Gardner
0.9
0.8
0.7
0.6
0.5
0.4
0.3
0.2
0.1

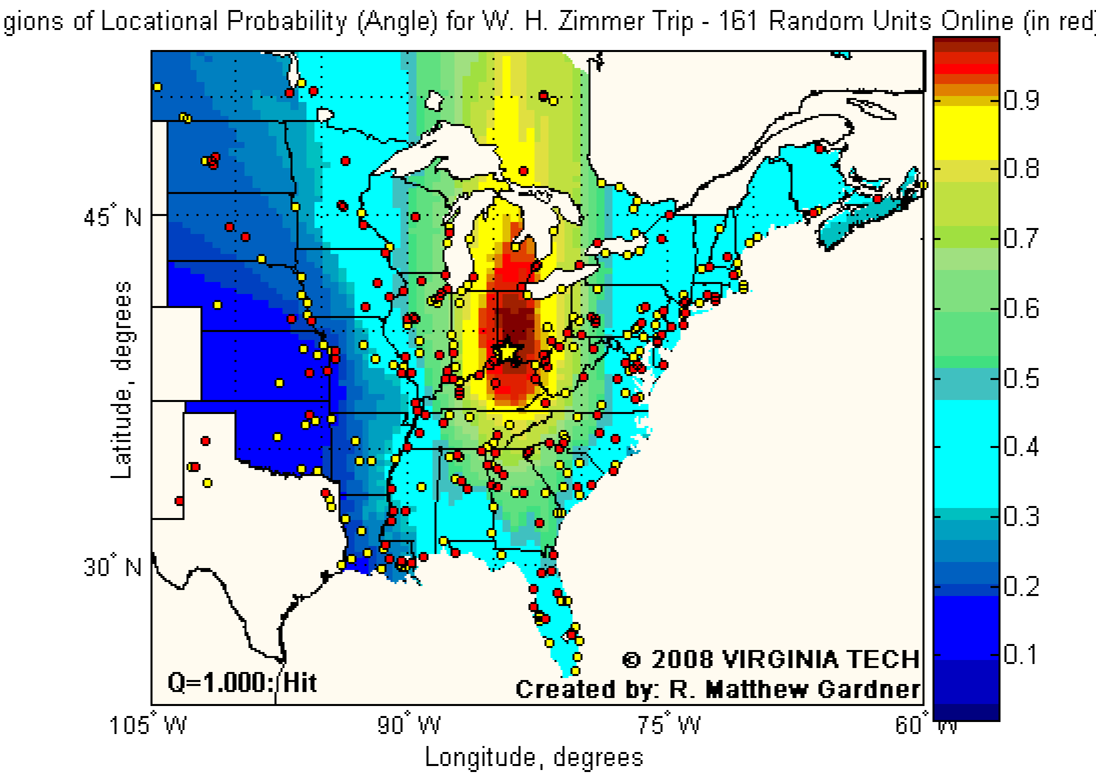
gions of Locational Probability (Angle) for W. H. Zimmer Trip - 161 Random Units Online (in red)
45° N
30° N
Latitude, degrees
105° W
90° W
75° W
60° W
Longitude, degrees
0.9
0.8
0.7
0.6
0.5
0.4
0.3
0.2
0.1
Q=1.000:/Hit
© 2008 VIRGINIA TECH
Created by: R. Matthew Gardner

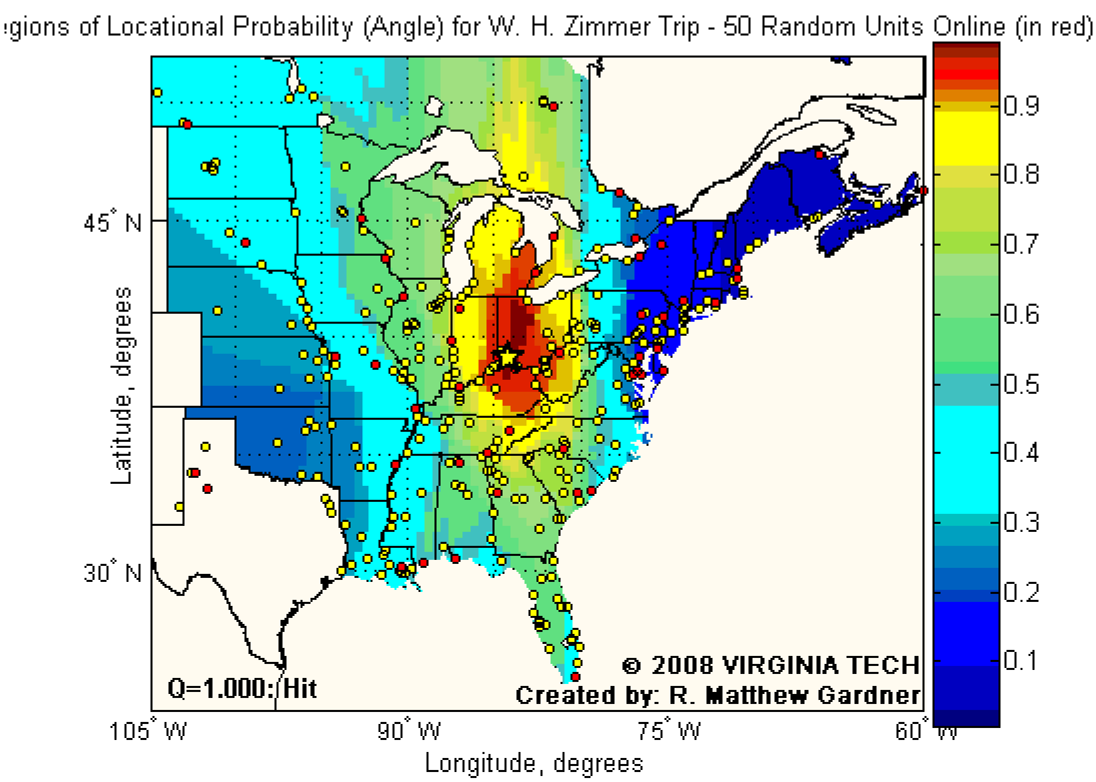
gions of Locational Probability (Angle) for W. H. Zimmer Trip - 50 Random Units Online (in red)
45° N
30° N
Latitude, degrees
105° W
90° W
75° W
60° W
Longitude, degrees
0.9
0.8
0.7
0.6
0.5
0.4
0.3
0.2
0.1
Q=1.000:/Hit
© 2008 VIRGINIA TECH
Created by: R. Matthew Gardner

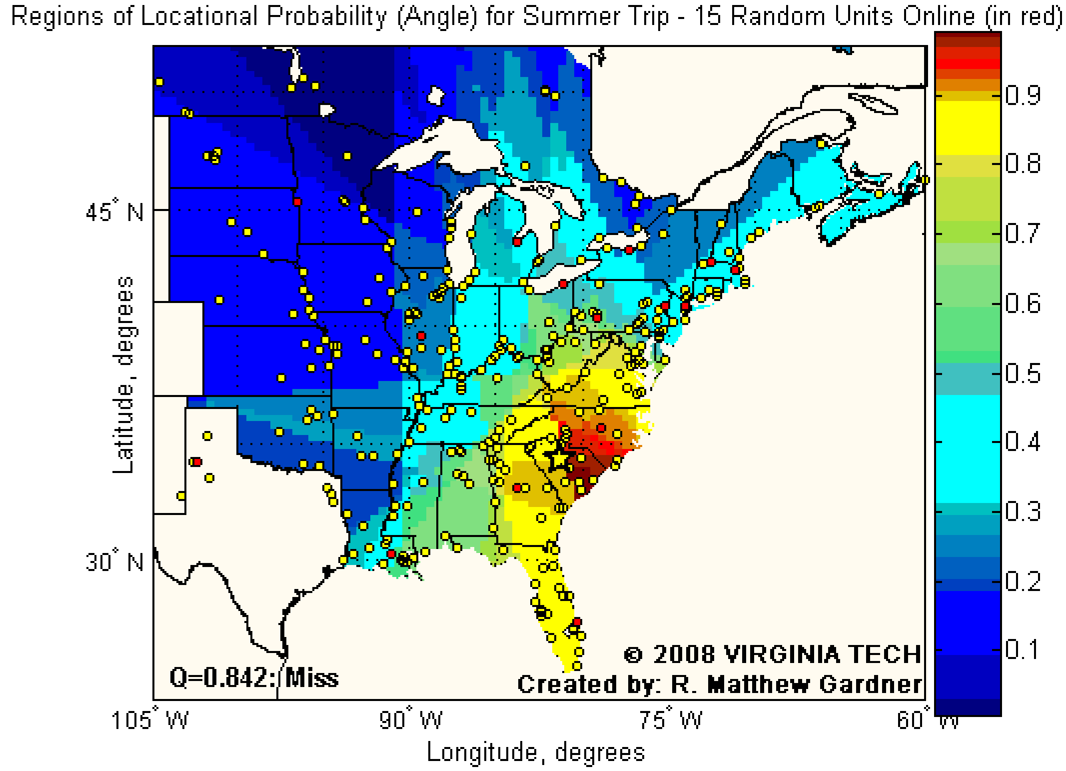

Regions of Locational Probability (Angle) for Summer Trip - 15 Random Units Online (in red)
Latitude, degrees
45° N
30° N
105° W
90° W
75° W
60° W
Longitude, degrees
Q=0.842: Miss
© 2008 VIRGINIA TECH
Created by: R. Matthew Gardner
0.9
0.8
0.7
0.6
0.5
0.4
0.3
0.2
0.1

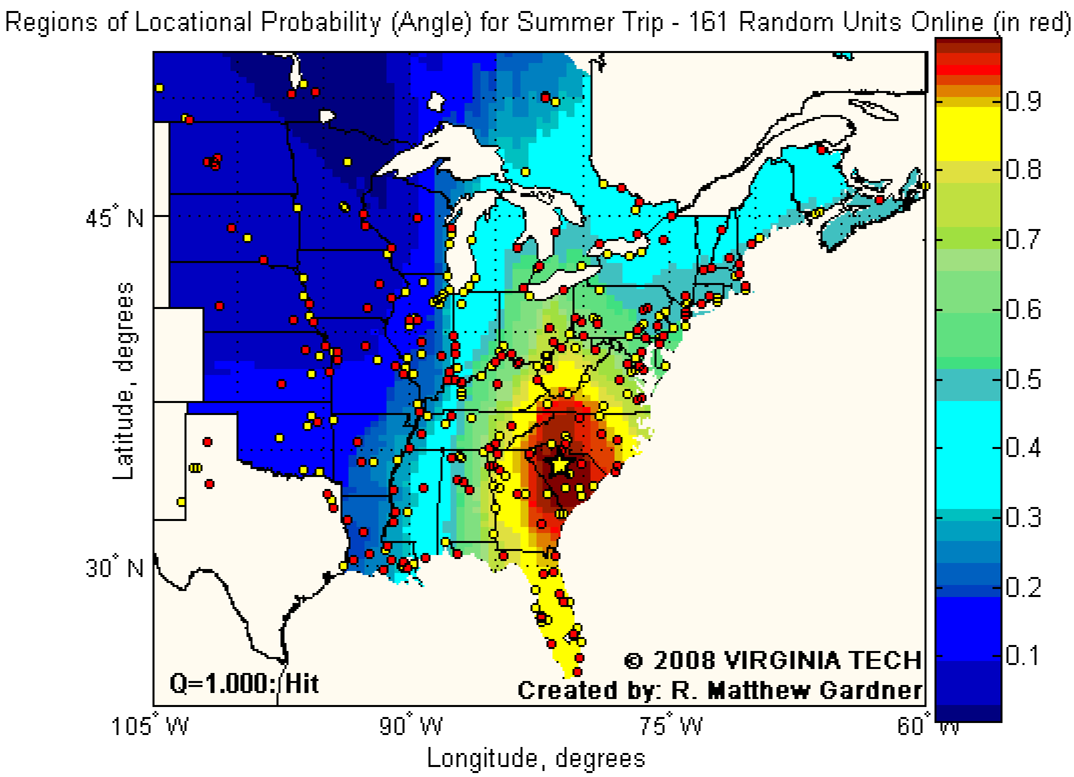

Regions of Locational Probability (Angle) for Summer Trip - 161 Random Units Online (in red)
Latitude, degrees
45° N
30° N
105° W
90° W
75° W
60° W
Longitude, degrees
Q=1.000: Hit
© 2008 VIRGINIA TECH
Created by: R. Matthew Gardner
0.9
0.8
0.7
0.6
0.5
0.4
0.3
0.2
0.1

Regions of Locational Probability (Angle) for Summer Trip - 50 Random Units Online (in red)

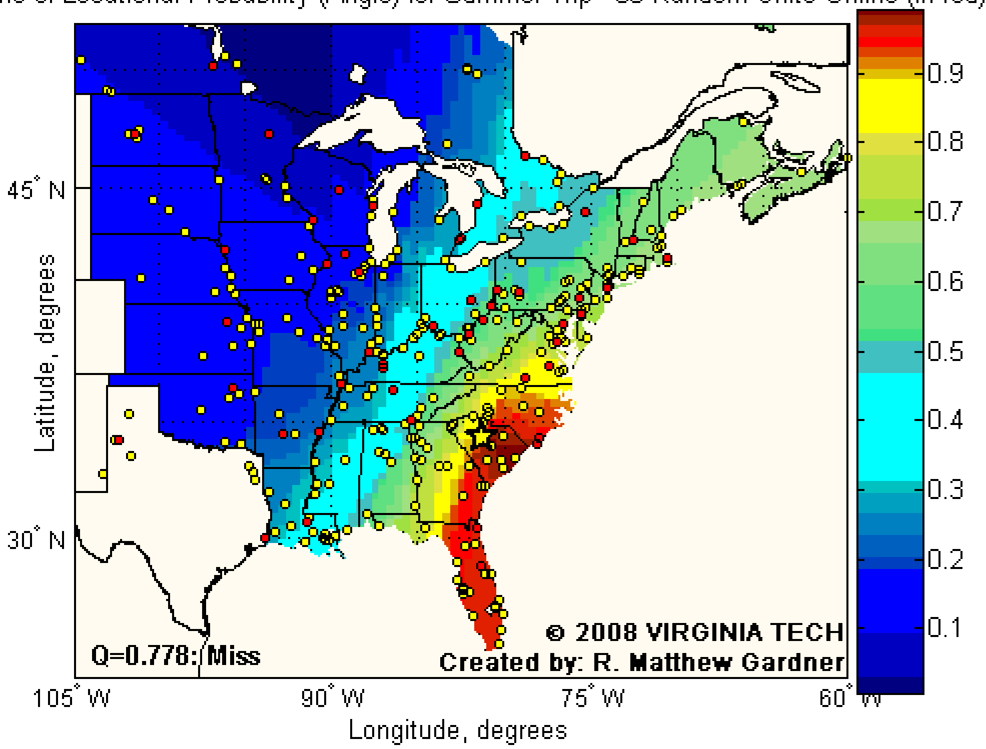

ions of Locational Probability (Angle) for Oconee U1 & U2 Trip - 15 Random Units Online (in red)

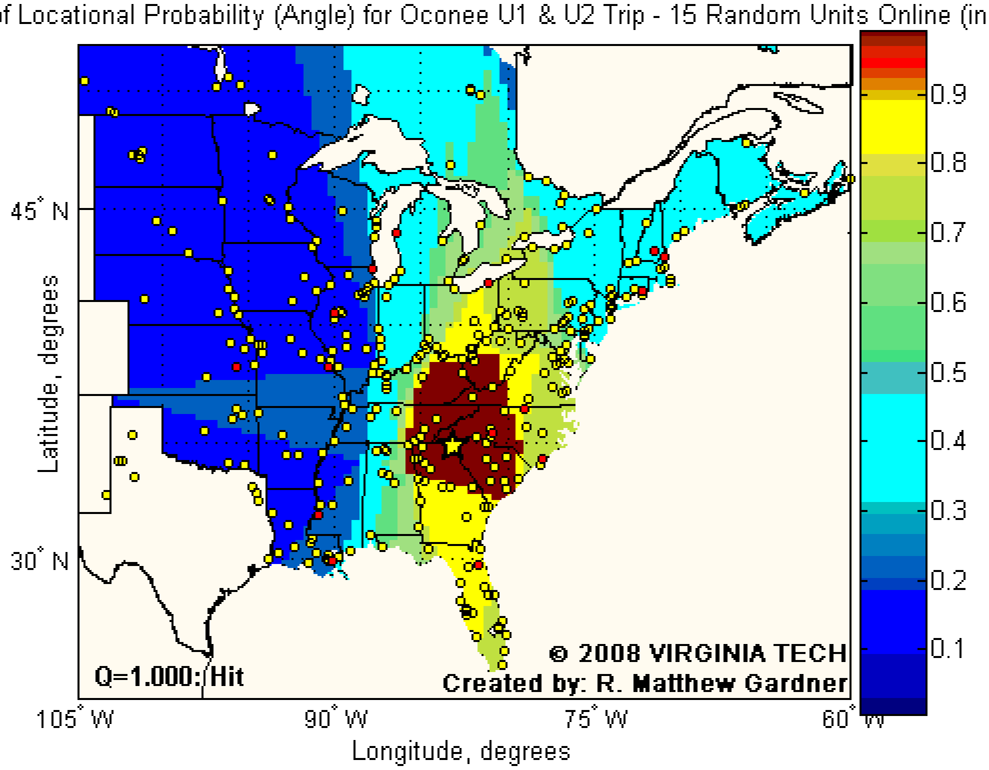

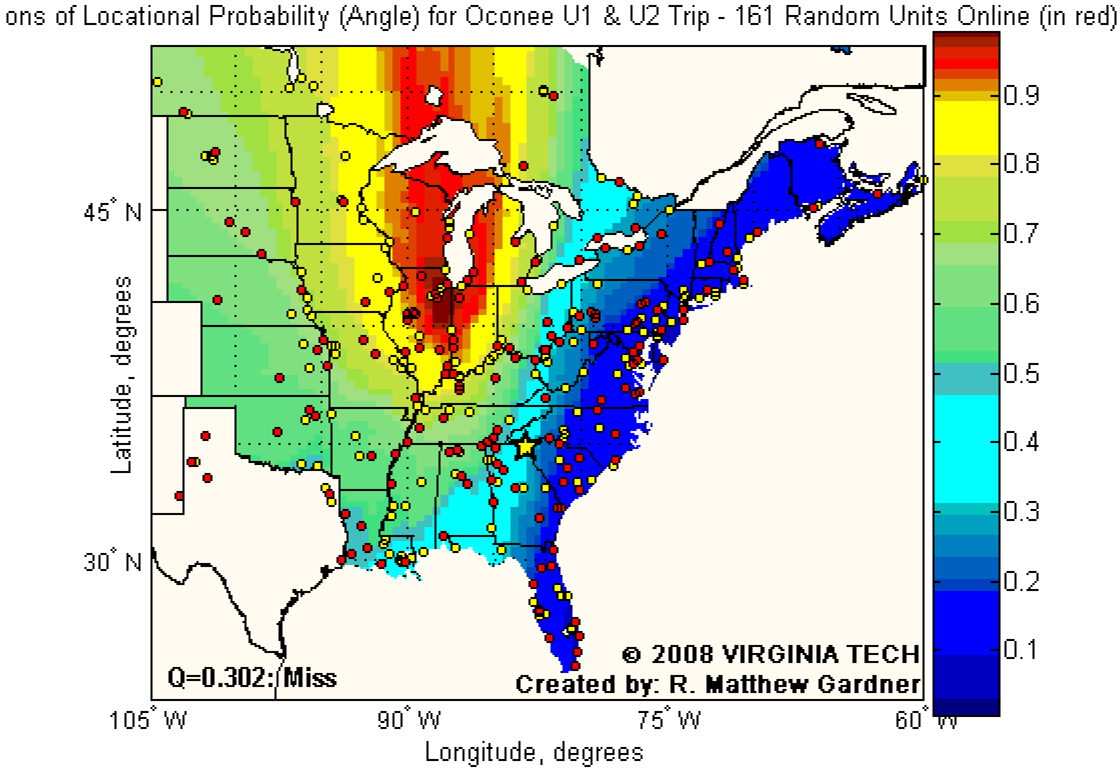
ons of Locational Probability (Angle) for Oconee U1 & U2 Trip - 161 Random Units Online (in red)
45° N
30° N
Latitude, degrees
105° W
90° W
75° W
60° W
Longitude, degrees
Q=0.302: Miss
© 2008 VIRGINIA TECH
Created by: R. Matthew Gardner
0.9
0.8
0.7
0.6
0.5
0.4
0.3
0.2
0.1

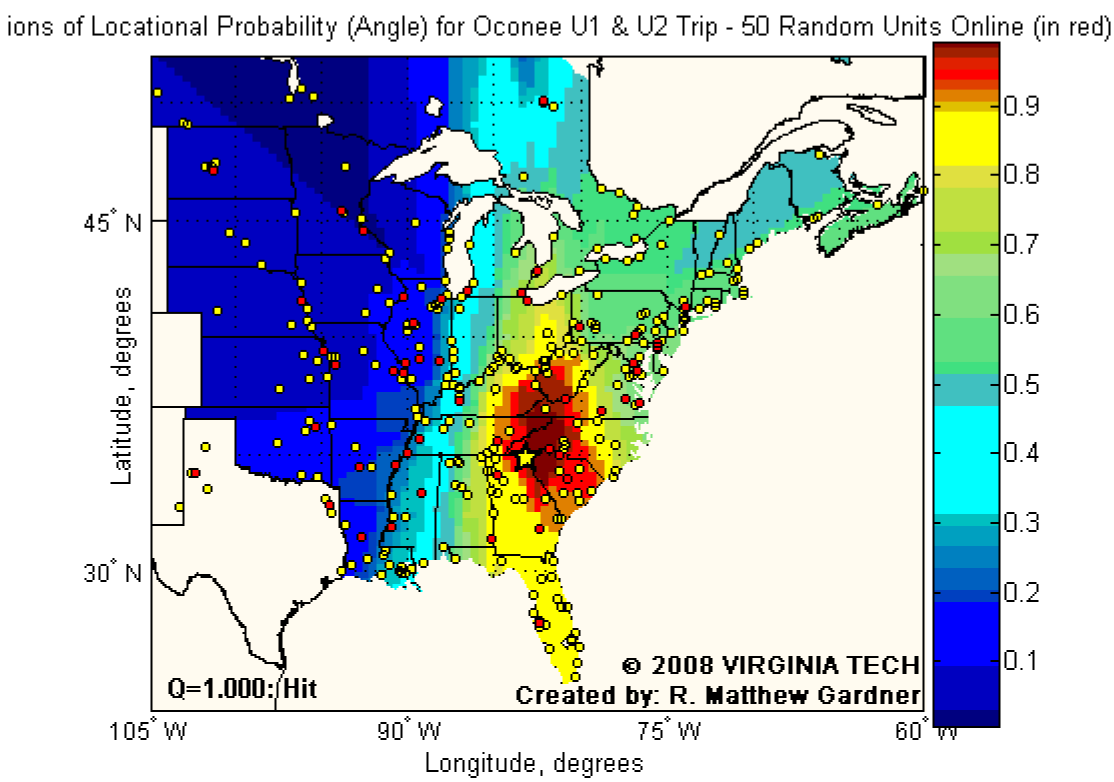
ions of Locational Probability (Angle) for Oconee U1 & U2 Trip - 50 Random Units Online (in red)
45° N
30° N
Latitude, degrees
105° W
90° W
75° W
60° W
Longitude, degrees
Q=1.000: Hit
© 2008 VIRGINIA TECH
Created by: R. Matthew Gardner
0.9
0.8
0.7
0.6
0.5
0.4
0.3
0.2
0.1

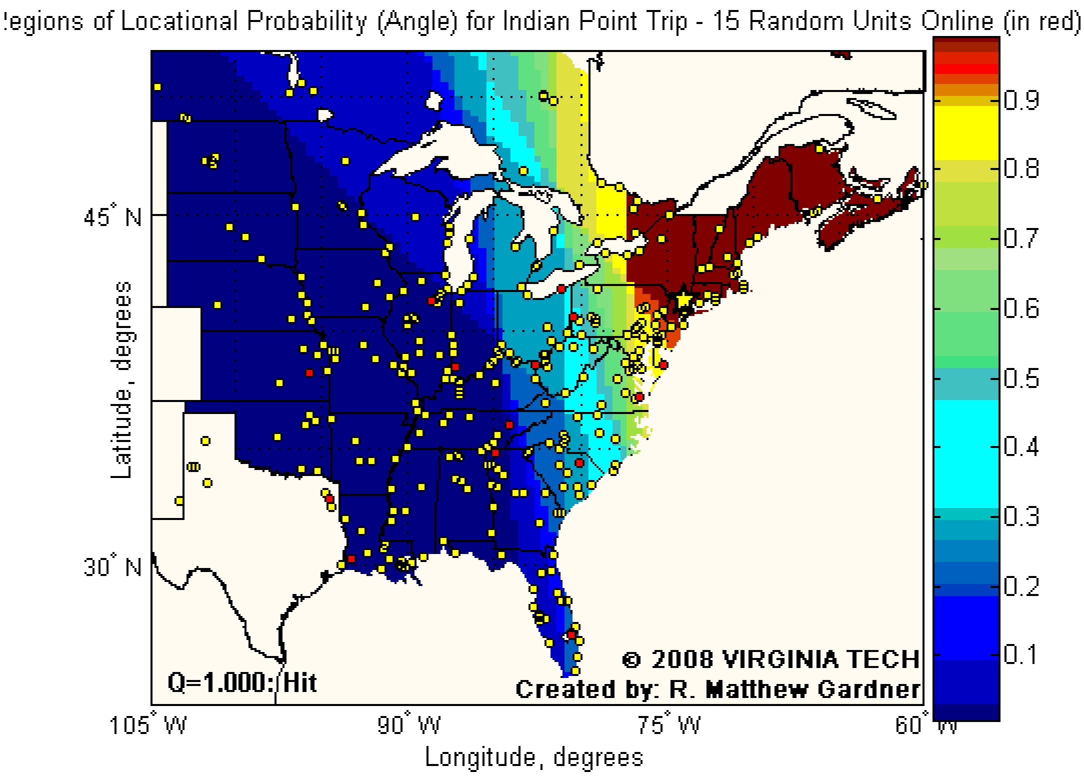
Regions of Locational Probability (Angle) for Indian Point Trip - 15 Random Units Online (in red)
Latitude, degrees
Longitude, degrees
45° N
30° N
105° W
90° W
75° W
60° W
0.9
0.8
0.7
0.6
0.5
0.4
0.3
0.2
0.1
Q=1.000:/Hit
© 2008 VIRGINIA TECH
Created by: R. Matthew Gardner

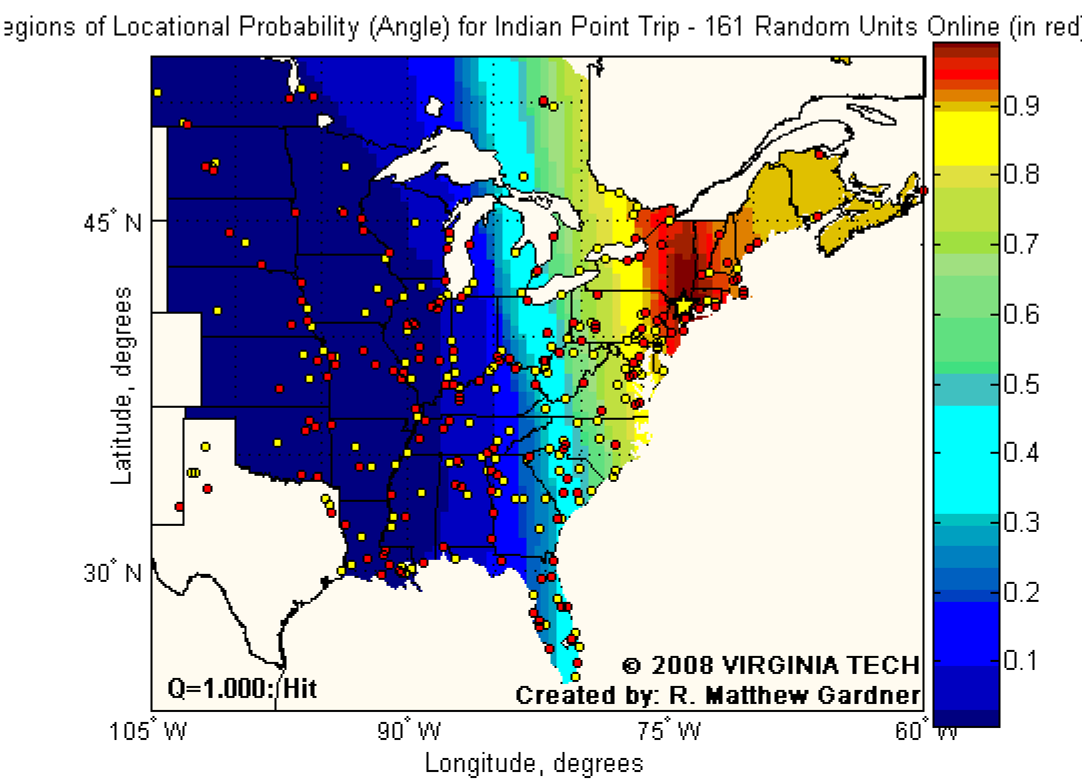
Regions of Locational Probability (Angle) for Indian Point Trip - 161 Random Units Online (in red)
Latitude, degrees
Longitude, degrees
45° N
30° N
105° W
90° W
75° W
60° W
0.9
0.8
0.7
0.6
0.5
0.4
0.3
0.2
0.1
Q=1.000:/Hit
© 2008 VIRGINIA TECH
Created by: R. Matthew Gardner

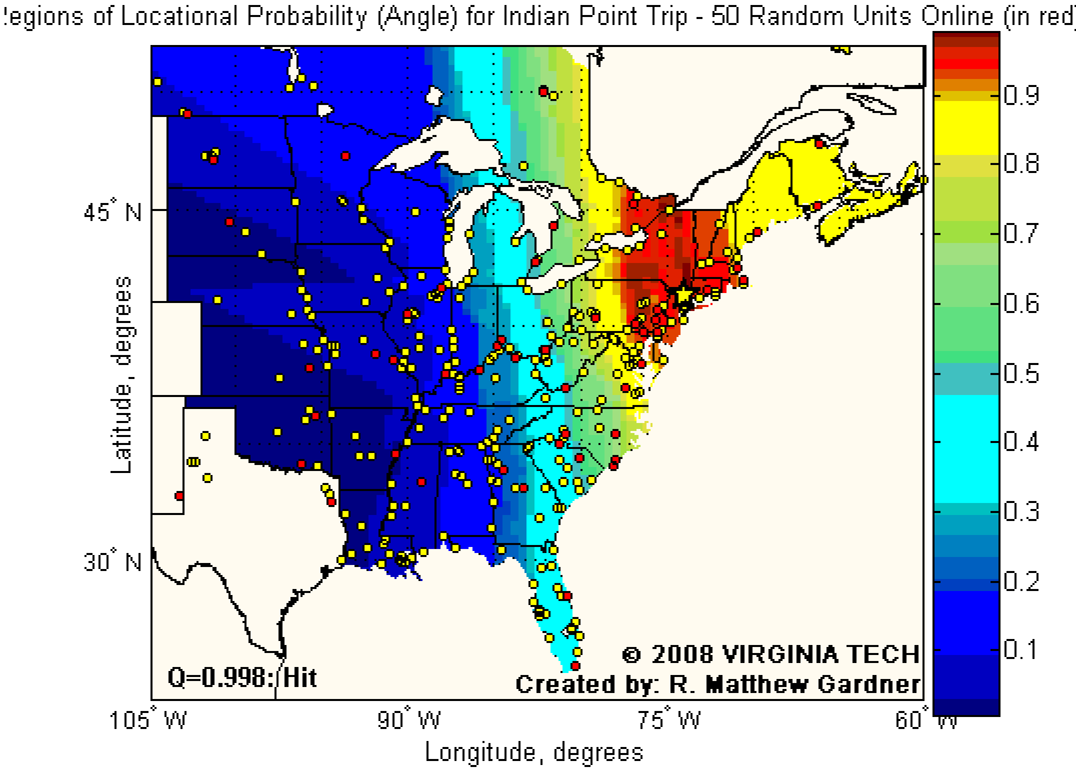

Regions of Locational Probability (Angle) for Indian Point Trip - 50 Random Units Online (in red)
45° N
30° N
Latitude, degrees
105° W
90° W
75° W
60° W
Longitude, degrees
Q=0.998: Hit
© 2008 VIRGINIA TECH
Created by: R. Matthew Gardner
0.9
0.8
0.7
0.6
0.5
0.4
0.3
0.2
0.1

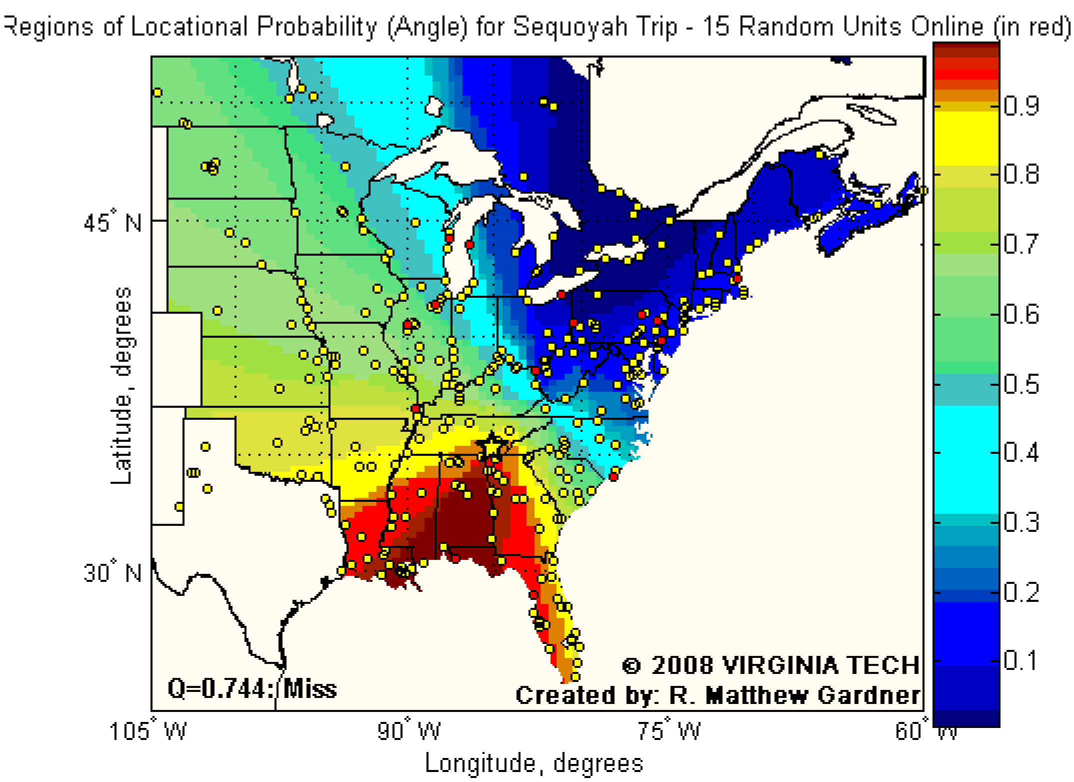

Regions of Locational Probability (Angle) for Sequoyah Trip - 15 Random Units Online (in red)
45° N
30° N
Latitude, degrees
105° W
90° W
75° W
60° W
Longitude, degrees
Q=0.744: Miss
© 2008 VIRGINIA TECH
Created by: R. Matthew Gardner
0.9
0.8
0.7
0.6
0.5
0.4
0.3
0.2
0.1

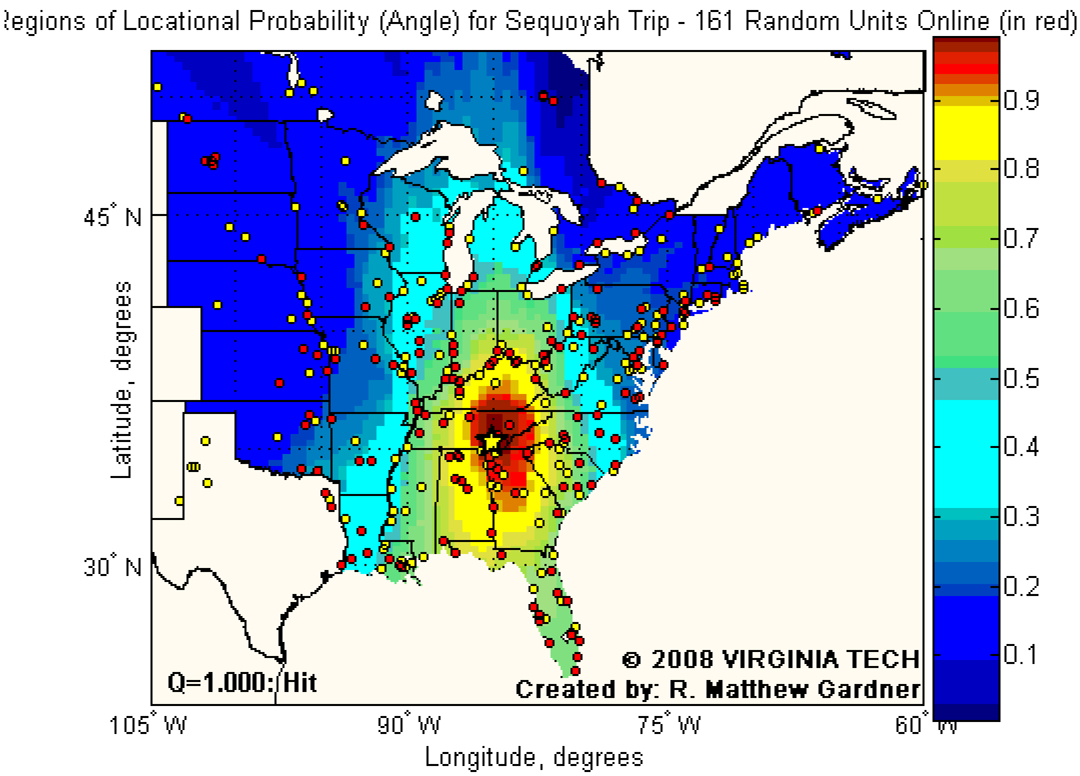
Regions of Locational Probability (Angle) for Sequoyah Trip - 161 Random Units Online (in red)
45° N
30° N
Latitude, degrees
105° W
90° W
75° W
60° W
Longitude, degrees
0.9
0.8
0.7
0.6
0.5
0.4
0.3
0.2
0.1
Q=1.000: Hit
© 2008 VIRGINIA TECH
Created by: R. Matthew Gardner

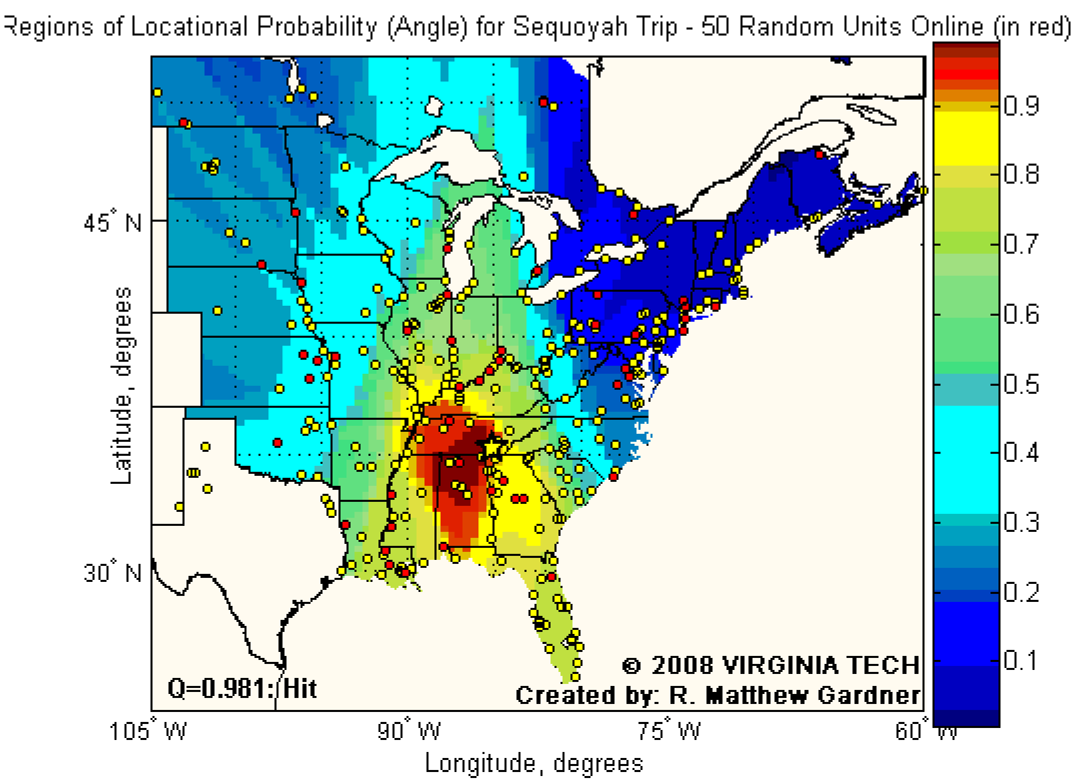
Regions of Locational Probability (Angle) for Sequoyah Trip - 50 Random Units Online (in red)
45° N
30° N
Latitude, degrees
105° W
90° W
75° W
60° W
Longitude, degrees
0.9
0.8
0.7
0.6
0.5
0.4
0.3
0.2
0.1
Q=0.981: Hit
© 2008 VIRGINIA TECH
Created by: R. Matthew Gardner

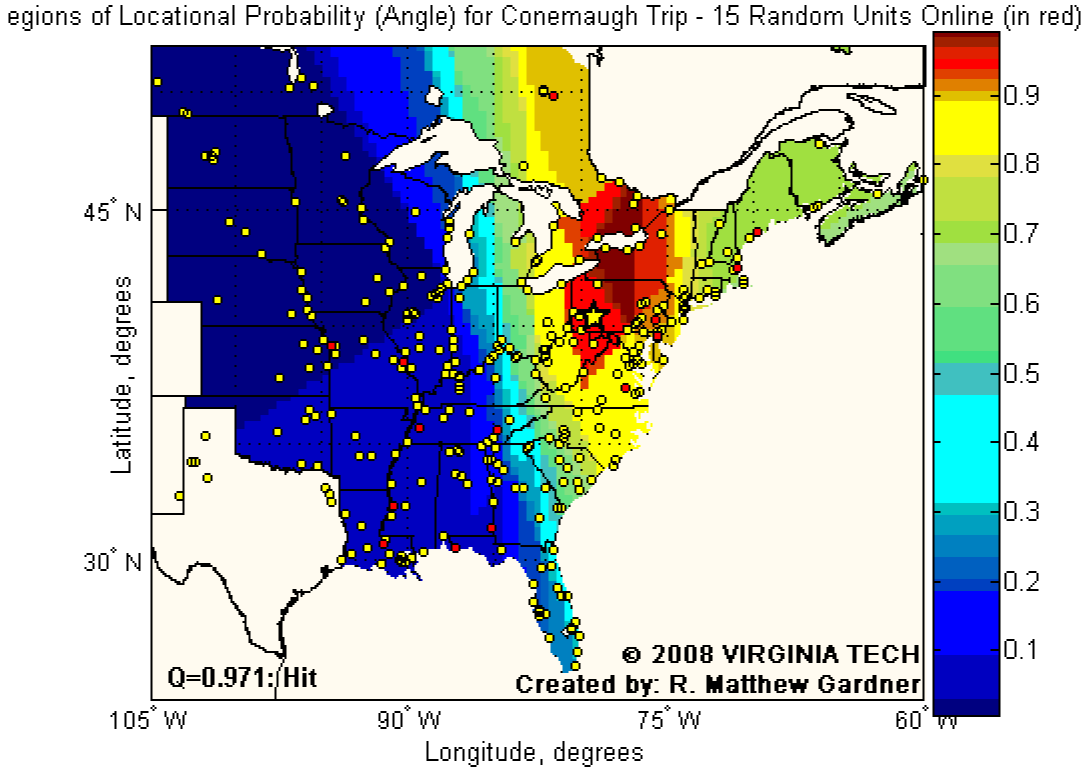
egions of Locational Probability (Angle) for Conemaugh Trip - 15 Random Units Online (in red)
45° N
30° N
Latitude, degrees
105° W
90° W
75° W
60° W
Longitude, degrees
Q=0.971: Hit
© 2008 VIRGINIA TECH
Created by: R. Matthew Gardner
0.9
0.8
0.7
0.6
0.5
0.4
0.3
0.2
0.1

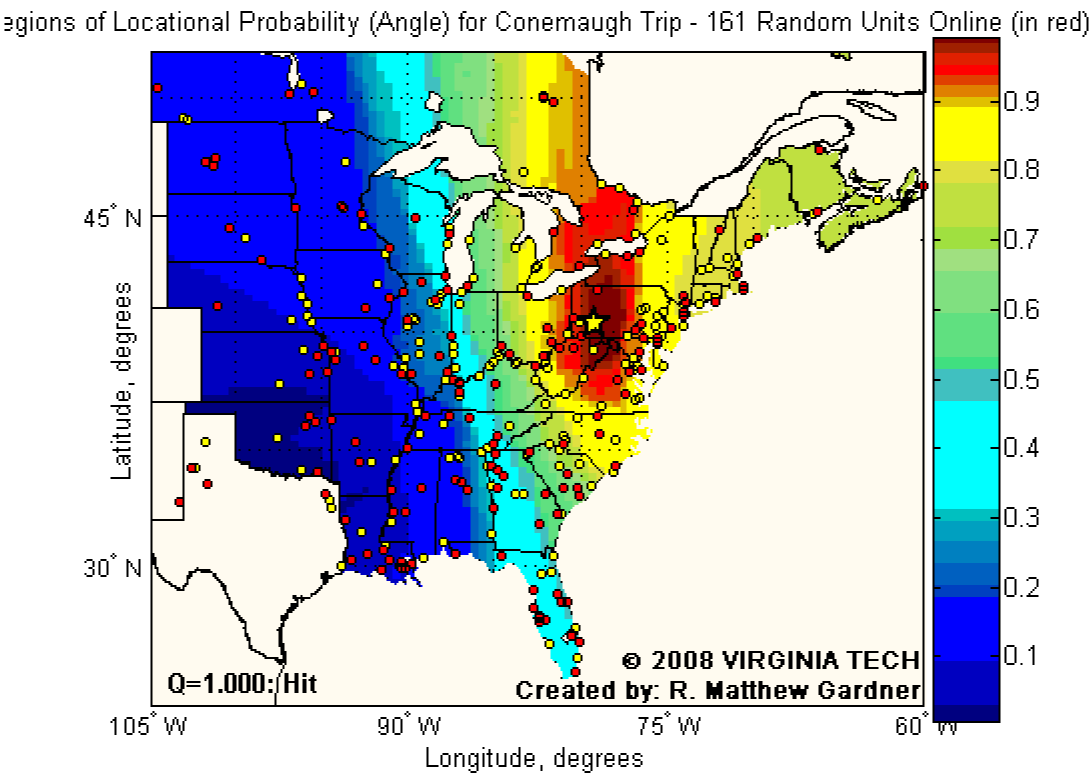
egions of Locational Probability (Angle) for Conemaugh Trip - 161 Random Units Online (in red)
45° N
30° N
Latitude, degrees
105° W
90° W
75° W
60° W
Longitude, degrees
Q=1.000: Hit
© 2008 VIRGINIA TECH
Created by: R. Matthew Gardner
0.9
0.8
0.7
0.6
0.5
0.4
0.3
0.2
0.1

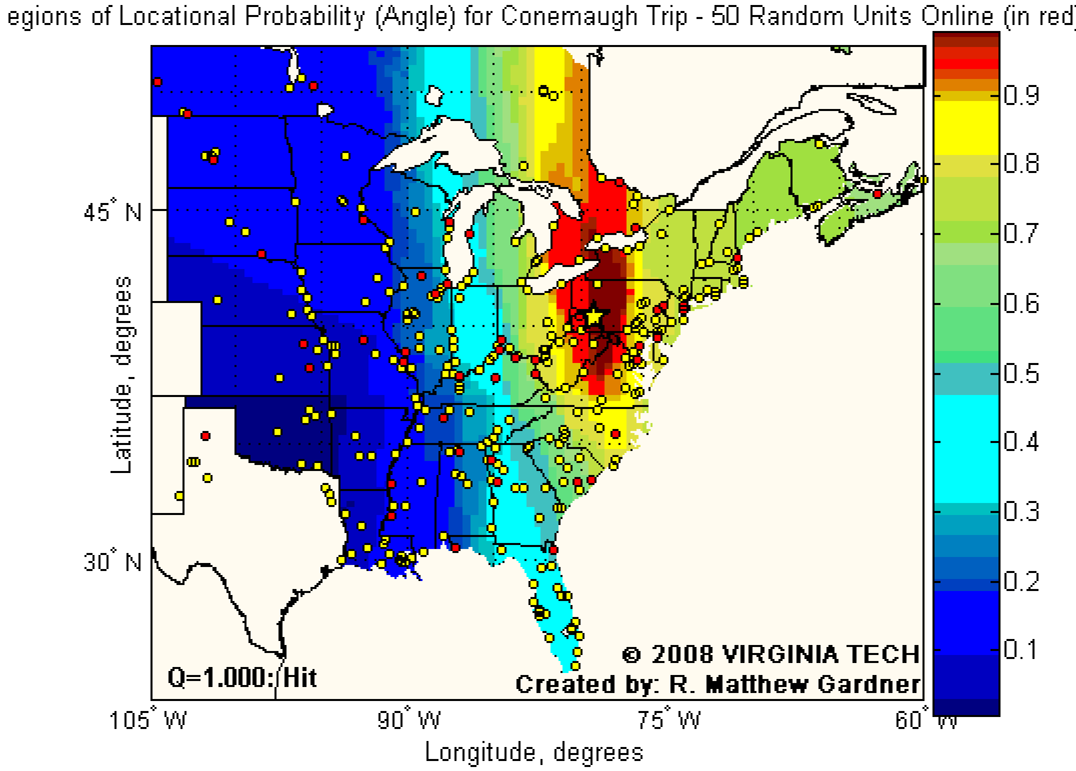
egions of Locational Probability (Angle) for Conemaugh Trip - 50 Random Units Online (in red)
Latitude, degrees
Longitude, degrees
45° N
30° N
105° W
90° W
75° W
60° W
0.9
0.8
0.7
0.6
0.5
0.4
0.3
0.2
0.1
Q=1.000:/Hit
© 2008 VIRGINIA TECH
Created by: R. Matthew Gardner

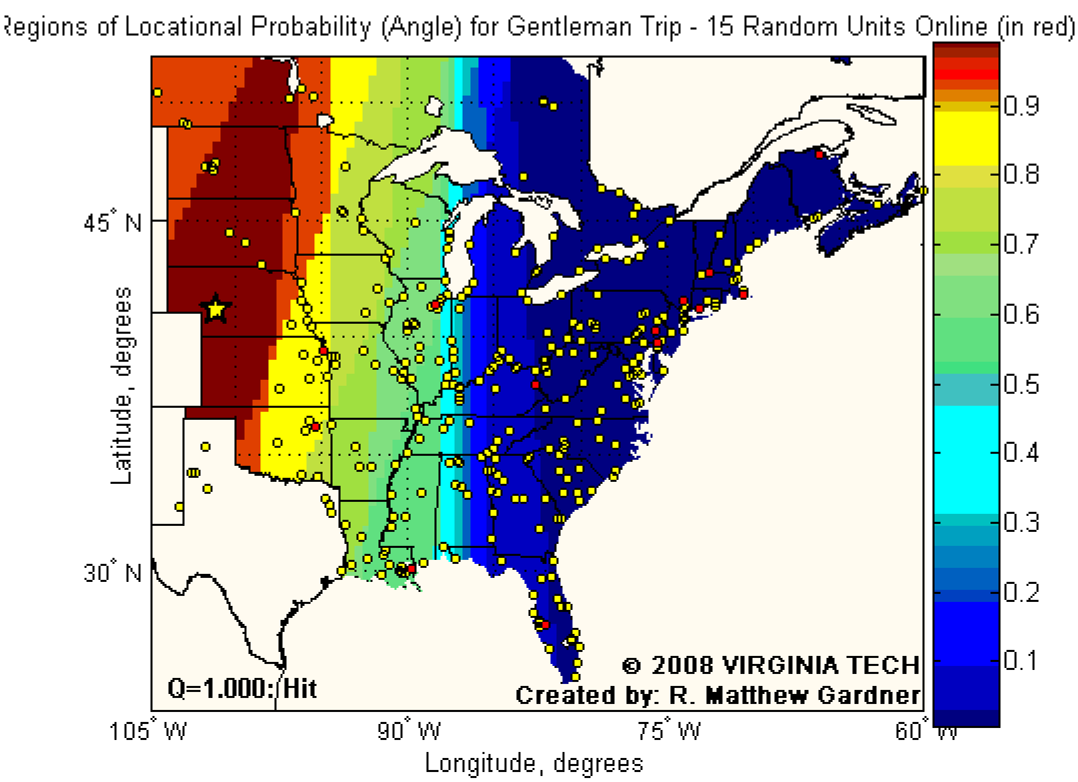
Regions of Locational Probability (Angle) for Gentleman Trip - 15 Random Units Online (in red)
Latitude, degrees
Longitude, degrees
45° N
30° N
105° W
90° W
75° W
60° W
0.9
0.8
0.7
0.6
0.5
0.4
0.3
0.2
0.1
Q=1.000:/Hit
© 2008 VIRGINIA TECH
Created by: R. Matthew Gardner

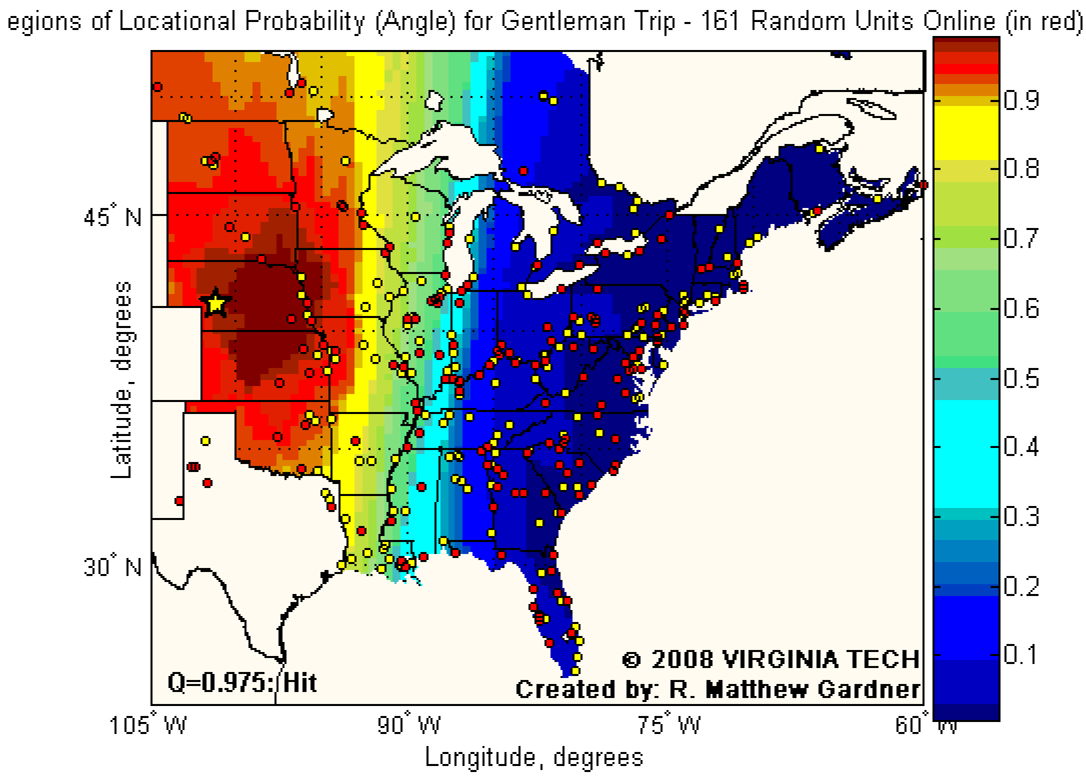
egions of Locational Probability (Angle) for Gentleman Trip - 161 Random Units Online (in red)
45° N
30° N
Latitude, degrees
105° W
90° W
75° W
60° W
Longitude, degrees
0.9
0.8
0.7
0.6
0.5
0.4
0.3
0.2
0.1
Q=0.975: Hit
© 2008 VIRGINIA TECH
Created by: R. Matthew Gardner

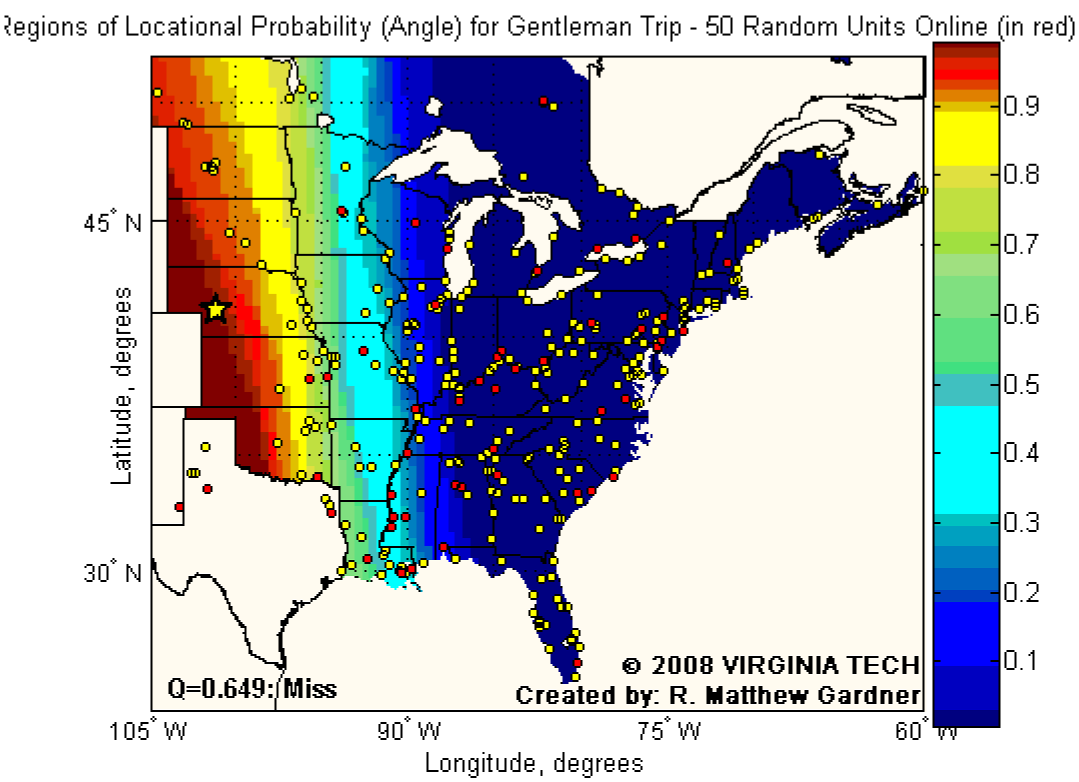
Regions of Locational Probability (Angle) for Gentleman Trip - 50 Random Units Online (in red)
45° N
30° N
Latitude, degrees
105° W
90° W
75° W
60° W
Longitude, degrees
0.9
0.8
0.7
0.6
0.5
0.4
0.3
0.2
0.1
Q=0.649: Miss
© 2008 VIRGINIA TECH
Created by: R. Matthew Gardner

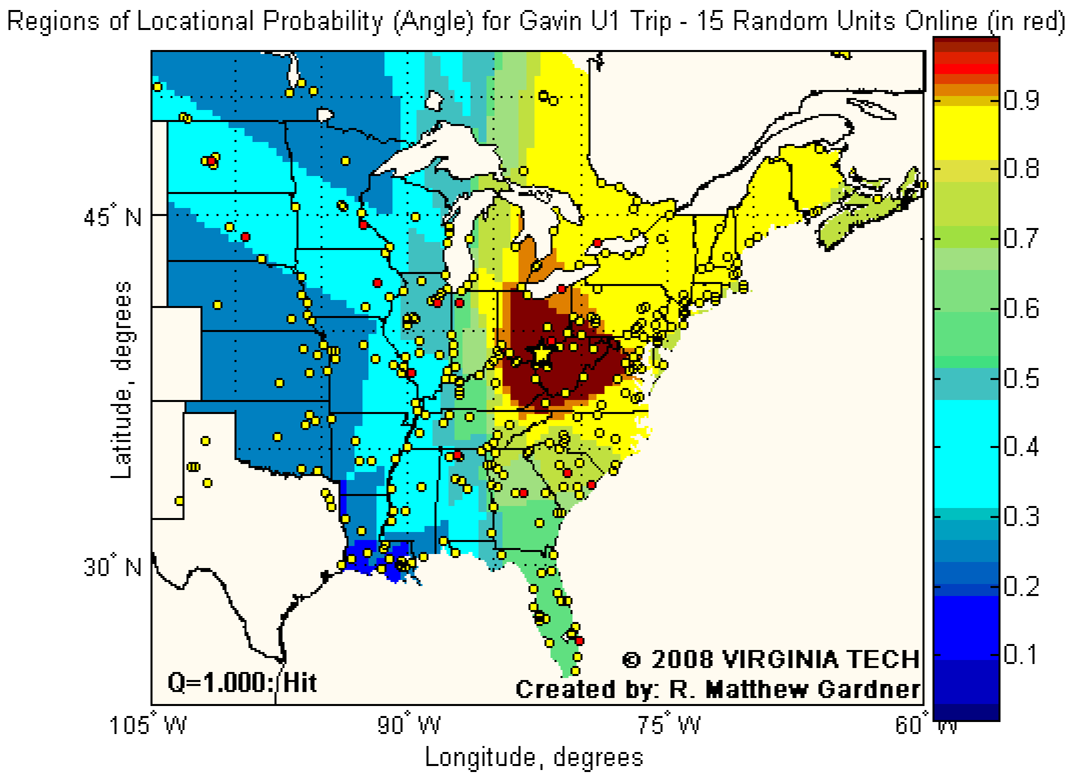
Regions of Locational Probability (Angle) for Gavin U1 Trip - 15 Random Units Online (in red)
45° N
30° N
Latitude, degrees
105° W
90° W
75° W
60° W
Longitude, degrees
0.9
0.8
0.7
0.6
0.5
0.4
0.3
0.2
0.1
Q=1.000: Hit
© 2008 VIRGINIA TECH
Created by: R. Matthew Gardner

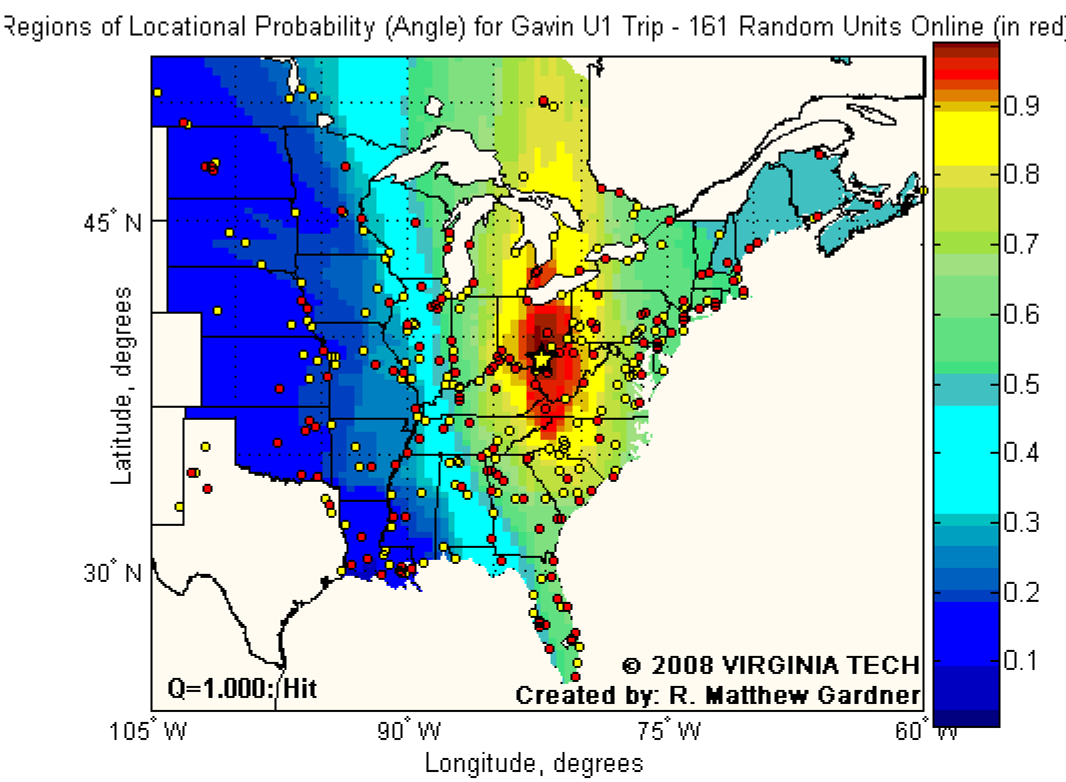
Regions of Locational Probability (Angle) for Gavin U1 Trip - 161 Random Units Online (in red)
45° N
30° N
Latitude, degrees
105° W
90° W
75° W
60° W
Longitude, degrees
0.9
0.8
0.7
0.6
0.5
0.4
0.3
0.2
0.1
Q=1.000: Hit
© 2008 VIRGINIA TECH
Created by: R. Matthew Gardner

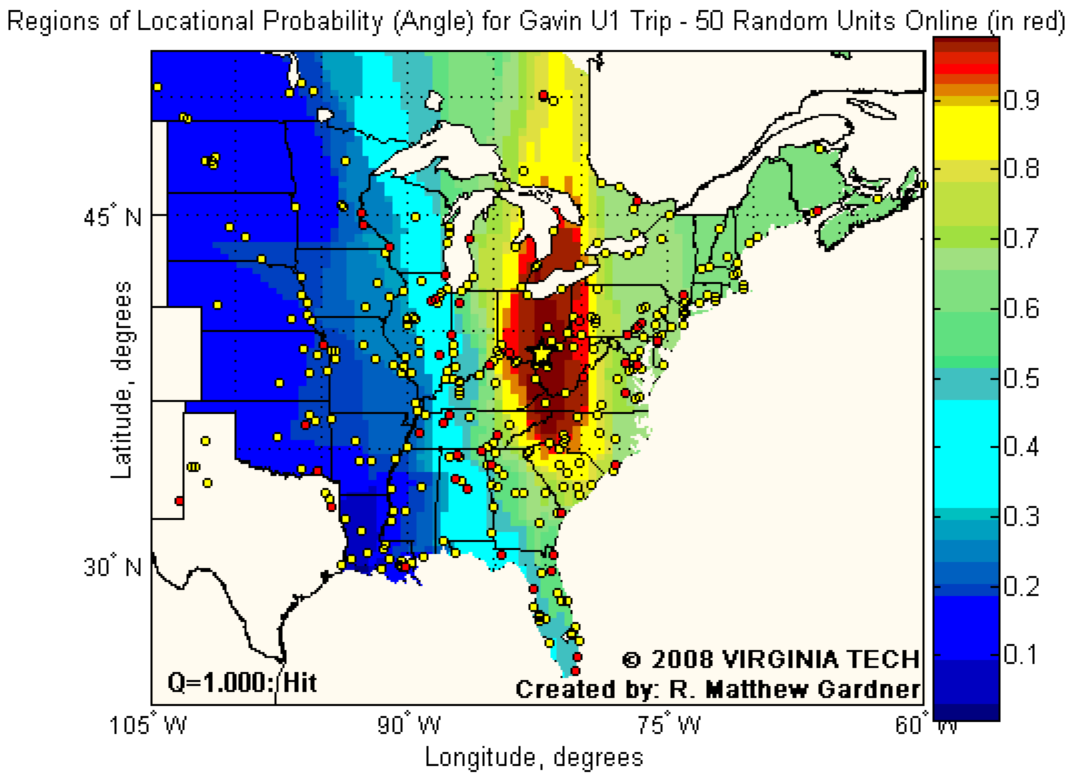
Regions of Locational Probability (Angle) for Gavin U1 Trip - 50 Random Units Online (in red)
45° N
30° N
Latitude, degrees
105° W
90° W
75° W
60° W
Longitude, degrees
Q=1.000:/Hit
© 2008 VIRGINIA TECH
Created by: R. Matthew Gardner
0.9
0.8
0.7
0.6
0.5
0.4
0.3
0.2
0.1

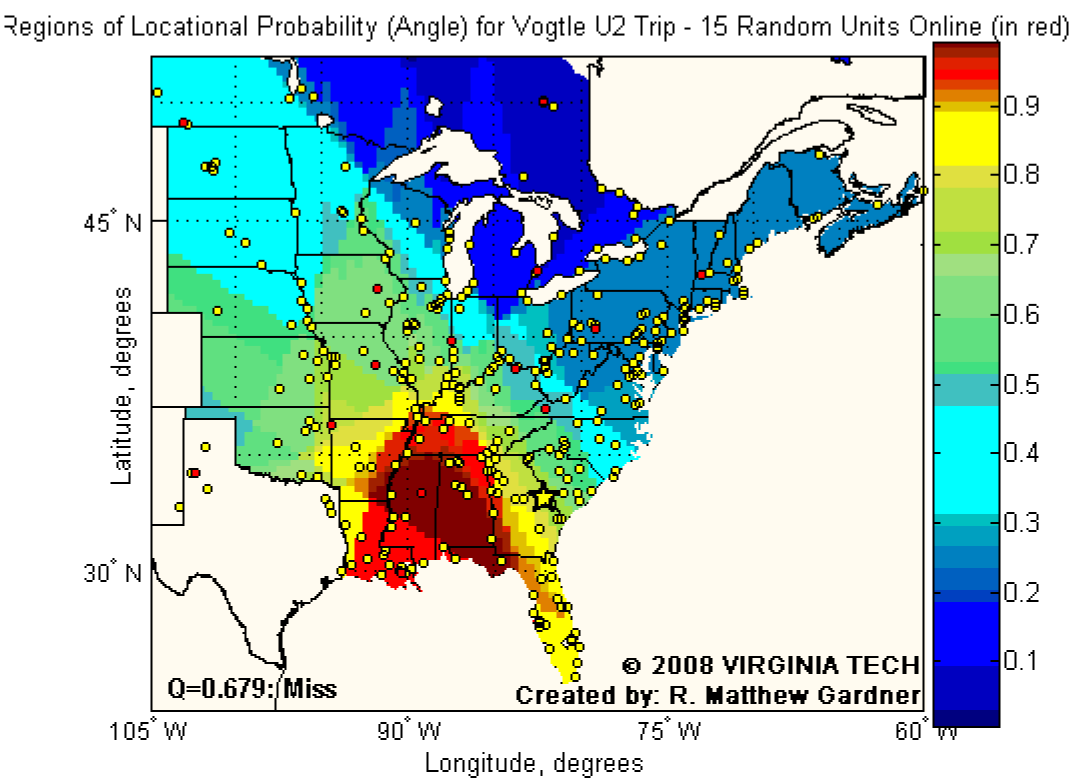
Regions of Locational Probability (Angle) for Vogtle U2 Trip - 15 Random Units Online (in red)
45° N
30° N
Latitude, degrees
105° W
90° W
75° W
60° W
Longitude, degrees
Q=0.679:/Miss
© 2008 VIRGINIA TECH
Created by: R. Matthew Gardner
0.9
0.8
0.7
0.6
0.5
0.4
0.3
0.2
0.1

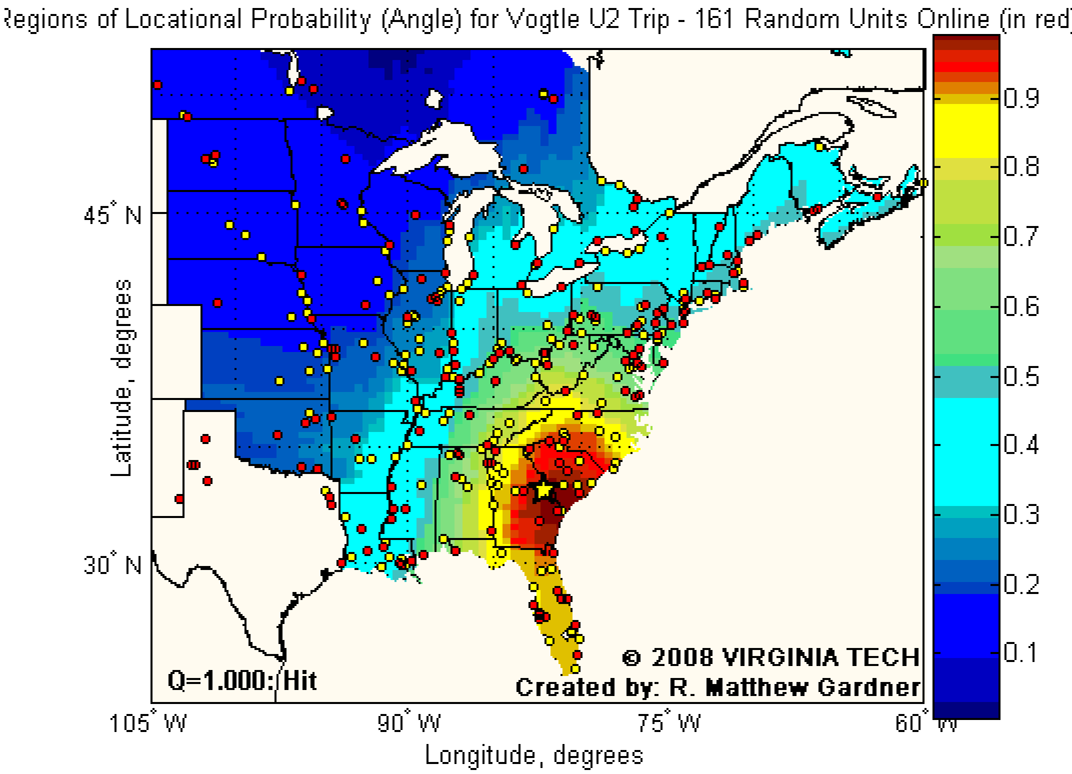
Regions of Locational Probability (Angle) for Vogtle U2 Trip - 161 Random Units Online (in red)
45° N
30° N
Latitude, degrees
105° W
90° W
75° W
60° W
Longitude, degrees
0.9
0.8
0.7
0.6
0.5
0.4
0.3
0.2
0.1
Q=1.000:/Hit
© 2008 VIRGINIA TECH
Created by: R. Matthew Gardner

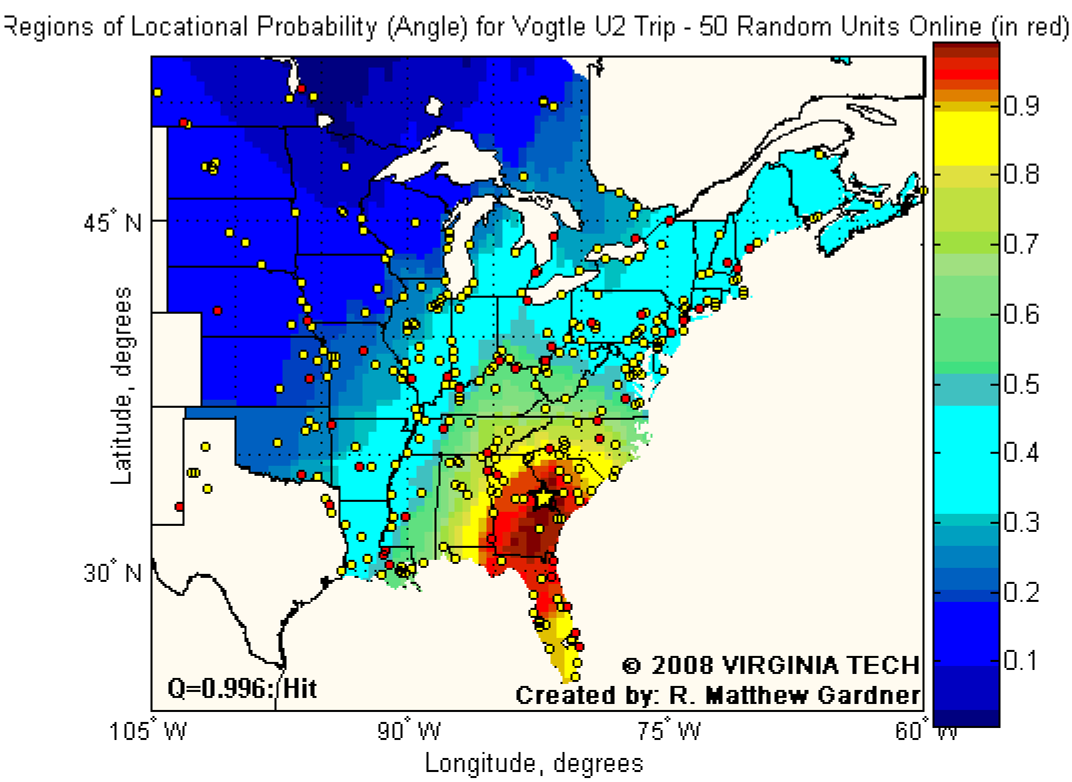
Regions of Locational Probability (Angle) for Vogtle U2 Trip - 50 Random Units Online (in red)
45° N
30° N
Latitude, degrees
105° W
90° W
75° W
60° W
Longitude, degrees
0.9
0.8
0.7
0.6
0.5
0.4
0.3
0.2
0.1
Q=0.996:/Hit
© 2008 VIRGINIA TECH
Created by: R. Matthew Gardner

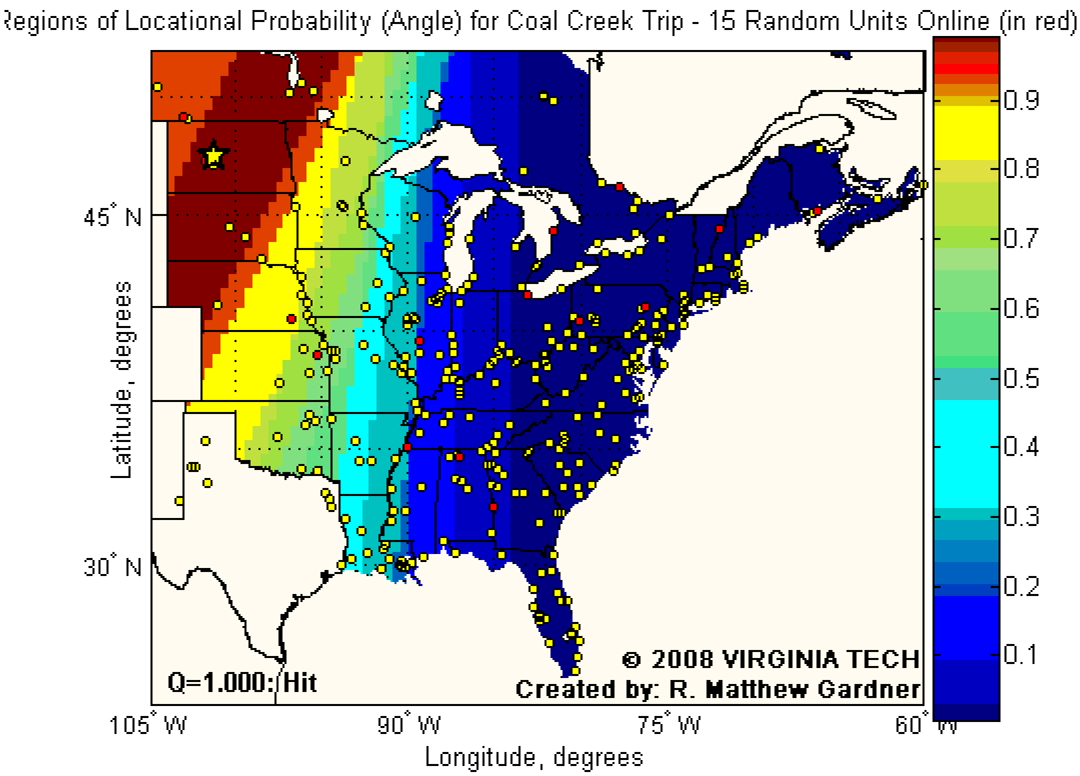
Regions of Locational Probability (Angle) for Coal Creek Trip - 15 Random Units Online (in red)
0.9
0.8
0.7
0.6
0.5
0.4
0.3
0.2
0.1
45° N
30° N
Latitude, degrees
Q=1.000: Hit
© 2008 VIRGINIA TECH
Created by: R. Matthew Gardner
105° W
90° W
75° W
60° W
Longitude, degrees

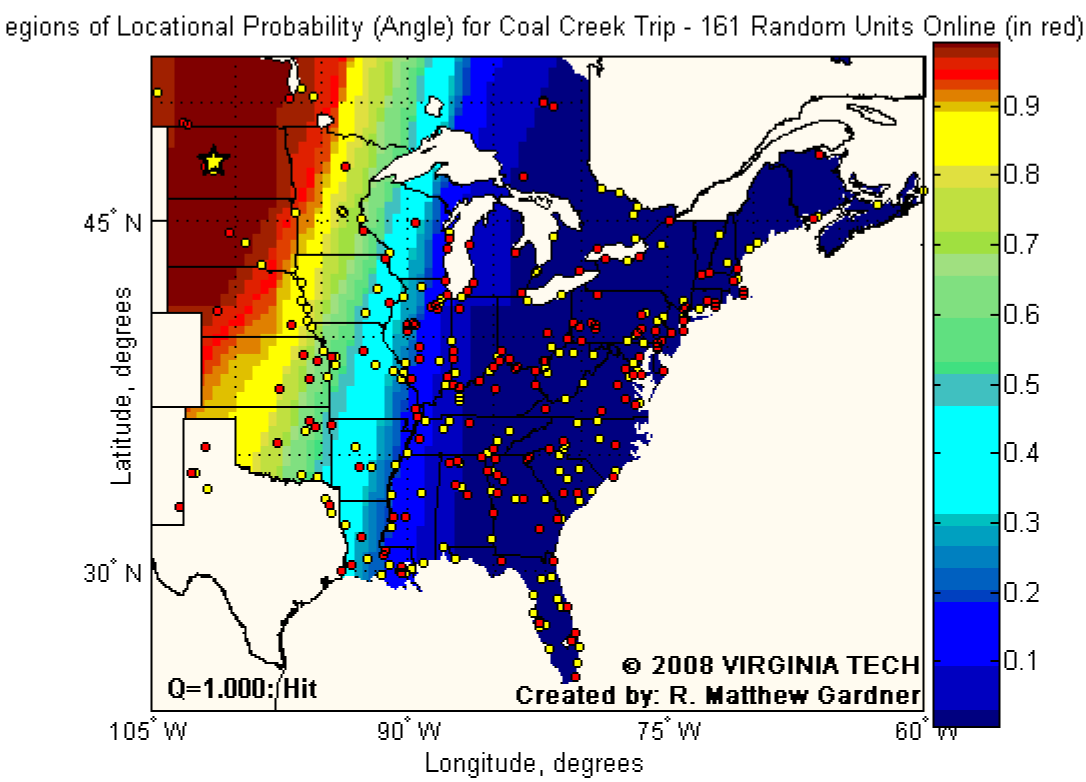
Regions of Locational Probability (Angle) for Coal Creek Trip - 161 Random Units Online (in red)
0.9
0.8
0.7
0.6
0.5
0.4
0.3
0.2
0.1
45° N
30° N
Latitude, degrees
Q=1.000: Hit
© 2008 VIRGINIA TECH
Created by: R. Matthew Gardner
105° W
90° W
75° W
60° W
Longitude, degrees

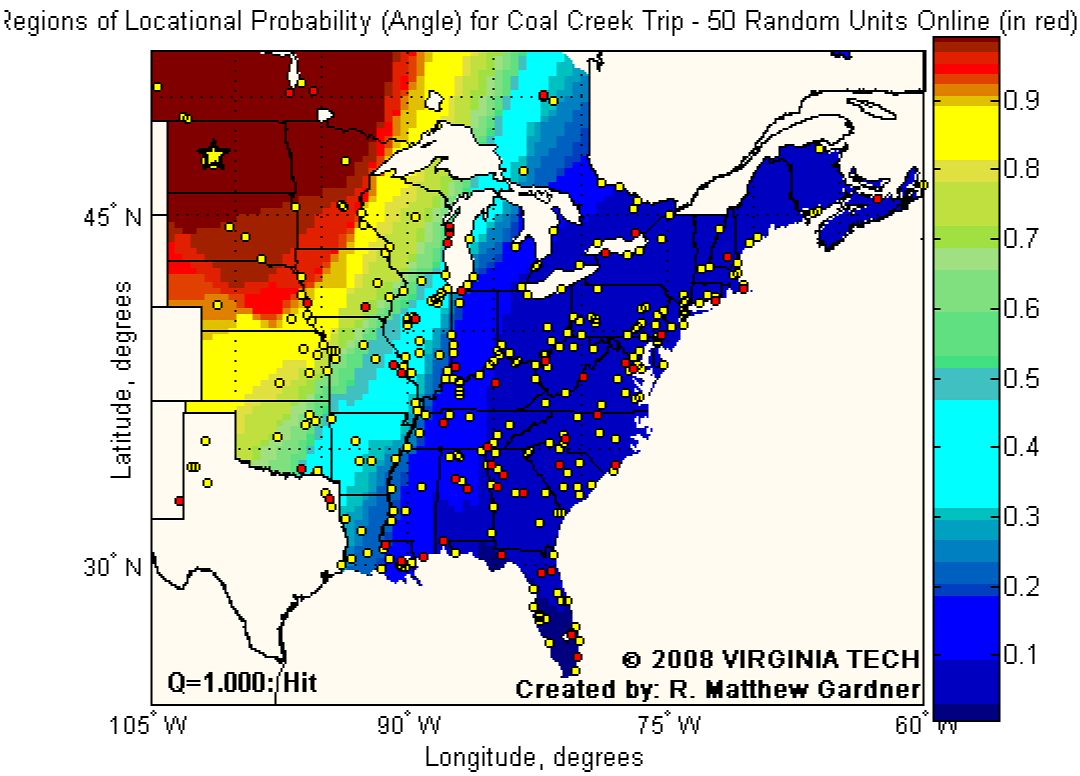
Regions of Locational Probability (Angle) for Coal Creek Trip - 50 Random Units Online (in red)
45° N
30° N
Latitude, degrees
105° W
90° W
75° W
60° W
Longitude, degrees
Q=1.000:/Hit
© 2008 VIRGINIA TECH
Created by: R. Matthew Gardner
0.9
0.8
0.7
0.6
0.5
0.4
0.3
0.2
0.1

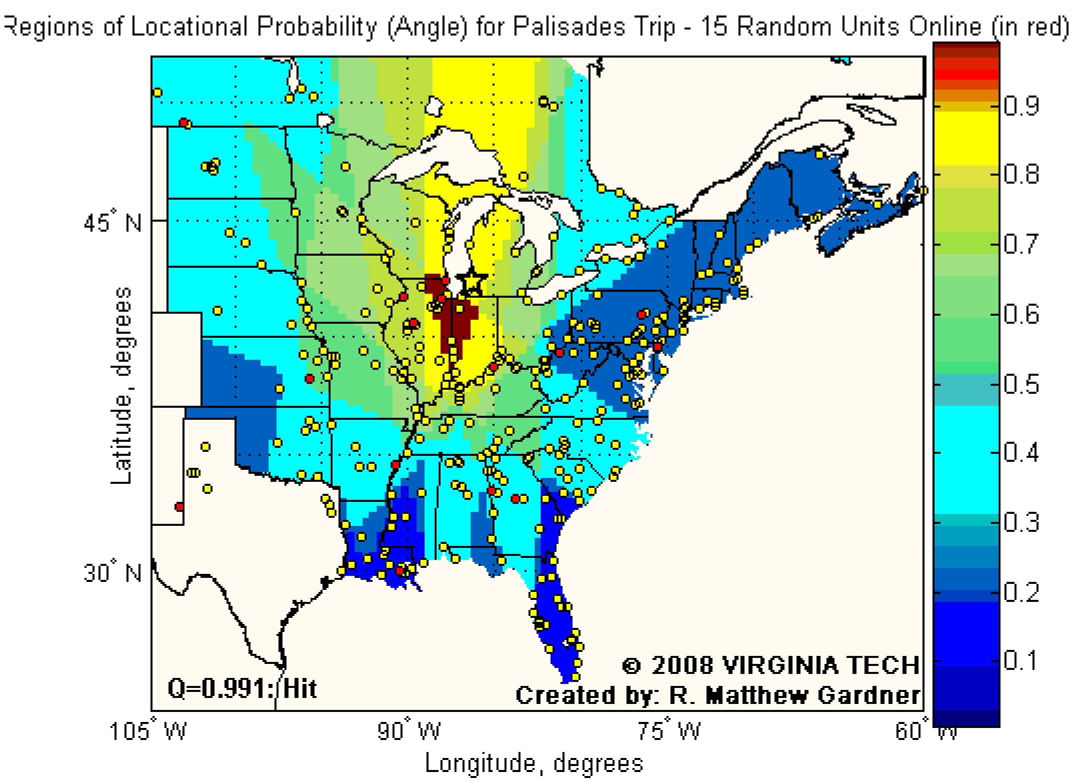
Regions of Locational Probability (Angle) for Palisades Trip - 15 Random Units Online (in red)
45° N
30° N
Latitude, degrees
105° W
90° W
75° W
60° W
Longitude, degrees
Q=0.991:/Hit
© 2008 VIRGINIA TECH
Created by: R. Matthew Gardner
0.9
0.8
0.7
0.6
0.5
0.4
0.3
0.2
0.1

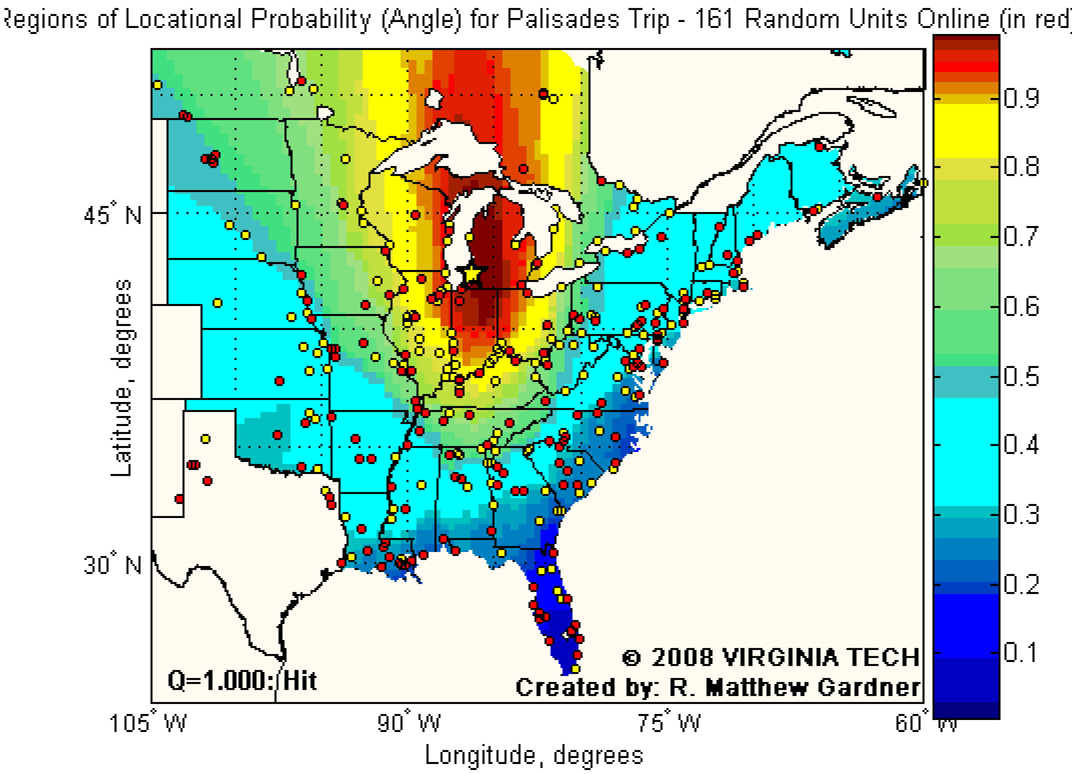
Regions of Locational Probability (Angle) for Palisades Trip - 161 Random Units Online (in red)
Latitude, degrees
Longitude, degrees
45° N
30° N
105° W
90° W
75° W
60° W
Q=1.000: Hit
© 2008 VIRGINIA TECH
Created by: R. Matthew Gardner
0.9
0.8
0.7
0.6
0.5
0.4
0.3
0.2
0.1

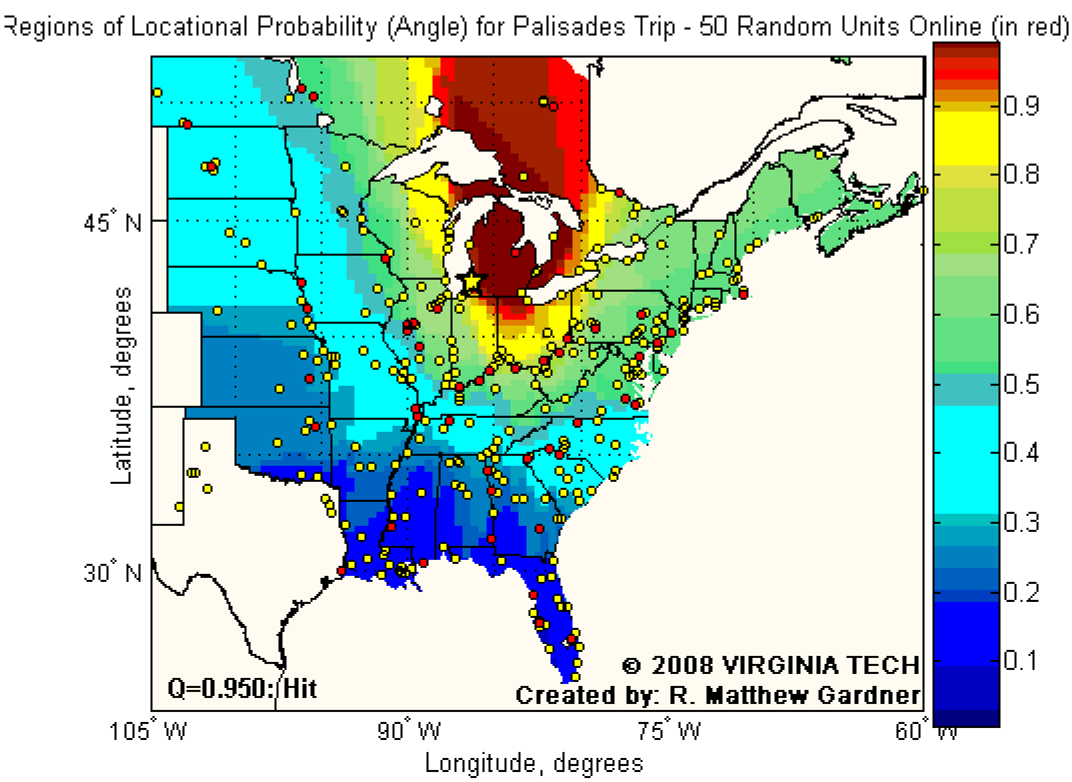
Regions of Locational Probability (Angle) for Palisades Trip - 50 Random Units Online (in red)
Latitude, degrees
Longitude, degrees
45° N
30° N
105° W
90° W
75° W
60° W
Q=0.950: Hit
© 2008 VIRGINIA TECH
Created by: R. Matthew Gardner
0.9
0.8
0.7
0.6
0.5
0.4
0.3
0.2
0.1

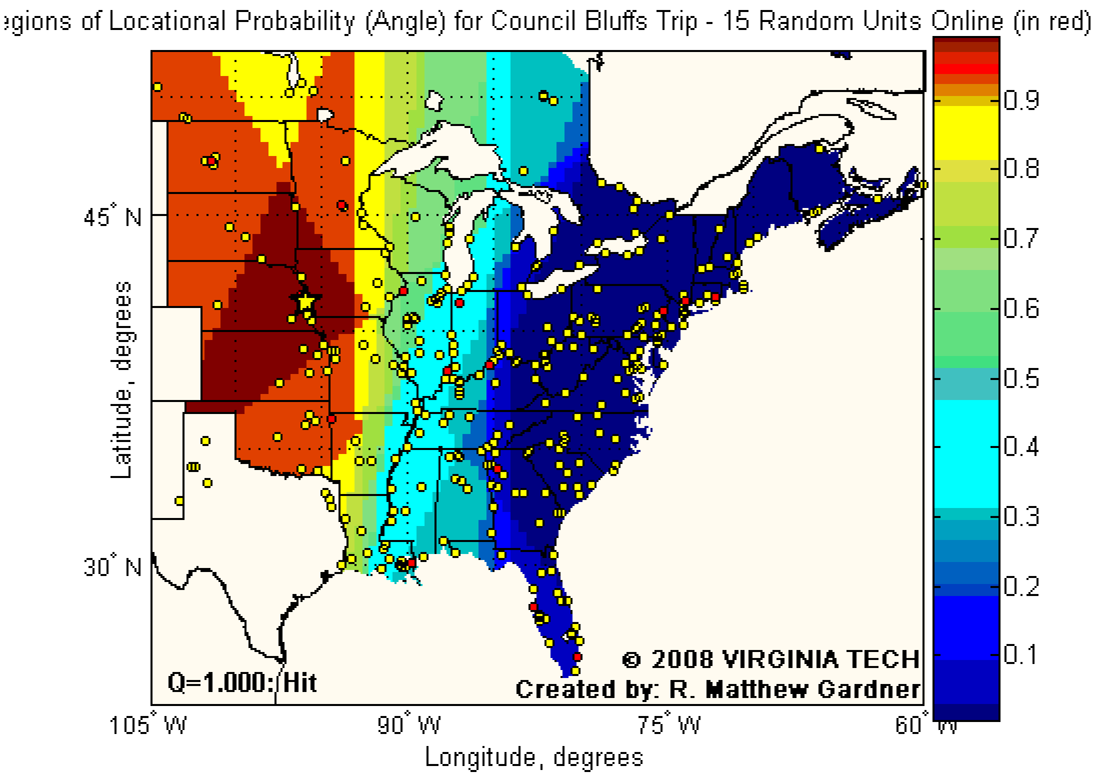
egions of Locational Probability (Angle) for Council Bluffs Trip - 15 Random Units Online (in red)
Latitude, degrees
Longitude, degrees
45° N
30° N
105° W
90° W
75° W
60° W
0.9
0.8
0.7
0.6
0.5
0.4
0.3
0.2
0.1
Q=1.000:/Hit
© 2008 VIRGINIA TECH
Created by: R. Matthew Gardner

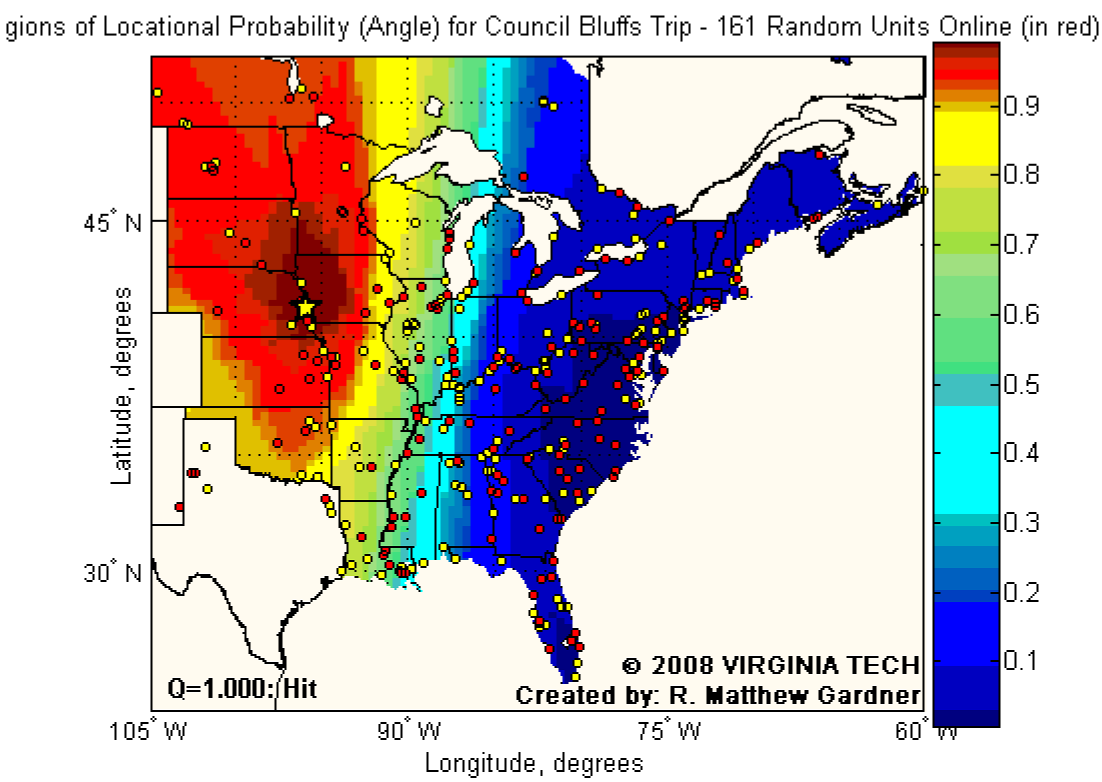
gions of Locational Probability (Angle) for Council Bluffs Trip - 161 Random Units Online (in red)
Latitude, degrees
Longitude, degrees
45° N
30° N
105° W
90° W
75° W
60° W
0.9
0.8
0.7
0.6
0.5
0.4
0.3
0.2
0.1
Q=1.000:/Hit
© 2008 VIRGINIA TECH
Created by: R. Matthew Gardner

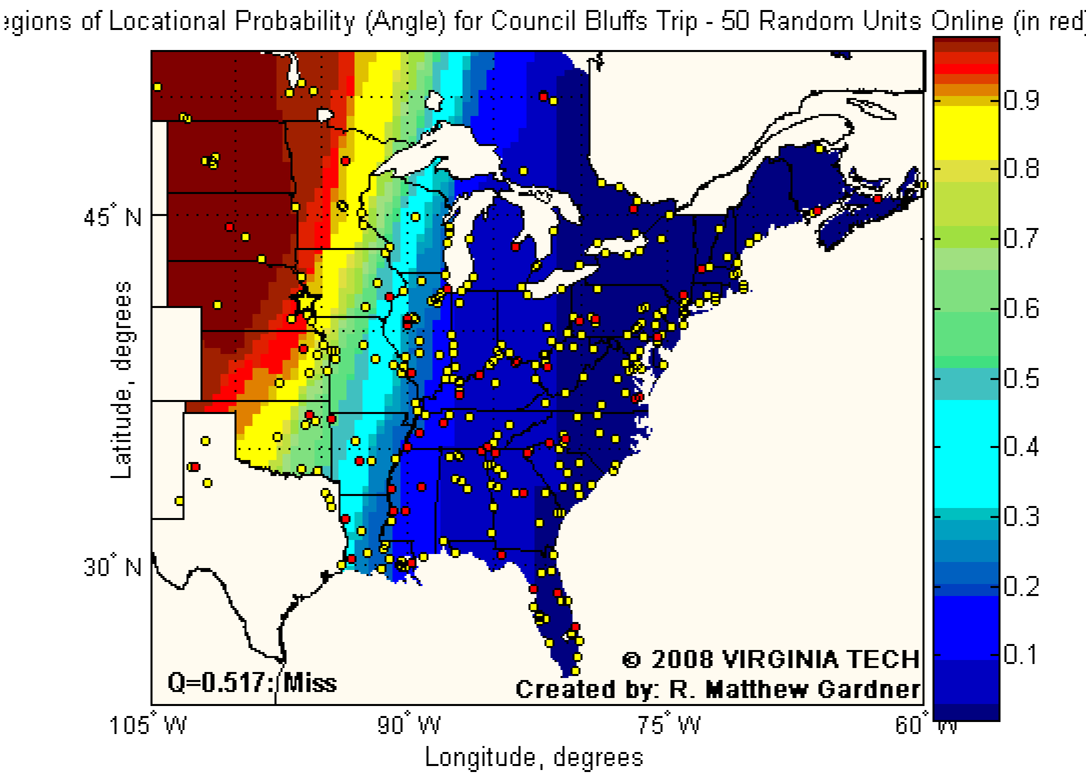
egions of Locational Probability (Angle) for Council Bluffs Trip - 50 Random Units Online (in red)
45° N
30° N
Latitude, degrees
105° W
90° W
75° W
60° W
Longitude, degrees
Q=0.517:/Miss
© 2008 VIRGINIA TECH
Created by: R. Matthew Gardner
0.9
0.8
0.7
0.6
0.5
0.4
0.3
0.2
0.1

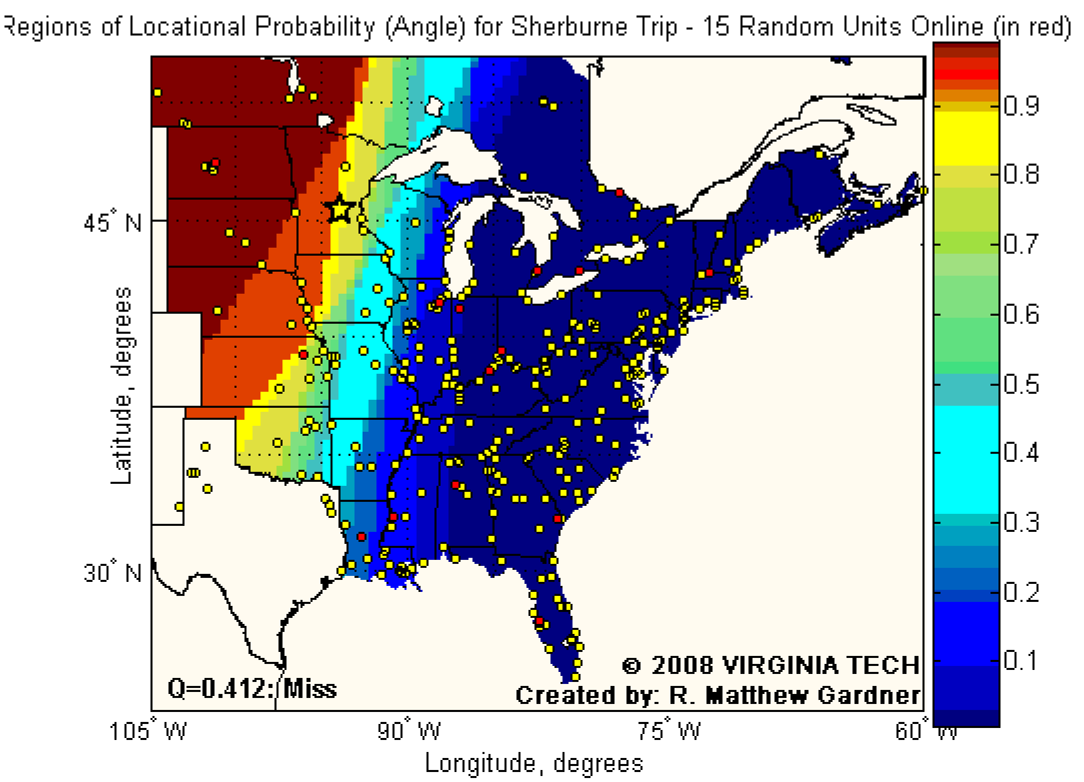
Regions of Locational Probability (Angle) for Sherburne Trip - 15 Random Units Online (in red)
45° N
30° N
Latitude, degrees
105° W
90° W
75° W
60° W
Longitude, degrees
Q=0.412:/Miss
© 2008 VIRGINIA TECH
Created by: R. Matthew Gardner
0.9
0.8
0.7
0.6
0.5
0.4
0.3
0.2
0.1

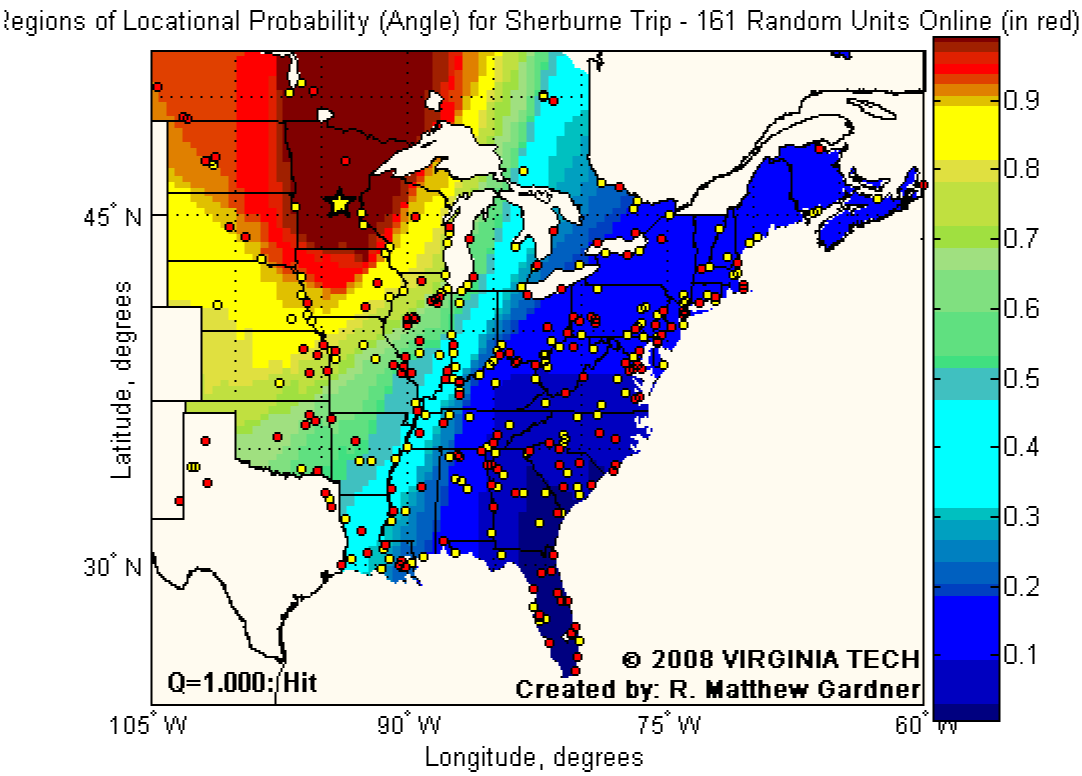
Regions of Locational Probability (Angle) for Sherburne Trip - 161 Random Units Online (in red)
45° N
30° N
Latitude, degrees
105° W
90° W
75° W
60° W
Longitude, degrees
Q=1.000:/Hit
© 2008 VIRGINIA TECH
Created by: R. Matthew Gardner
0.9
0.8
0.7
0.6
0.5
0.4
0.3
0.2
0.1

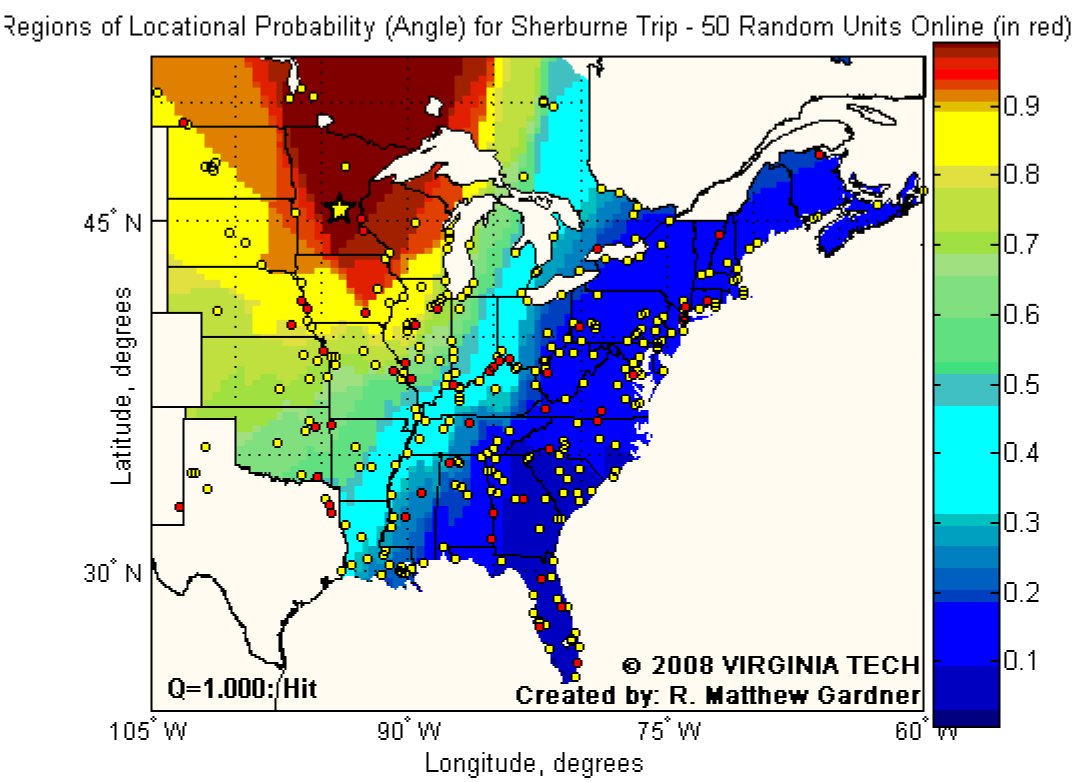
Regions of Locational Probability (Angle) for Sherburne Trip - 50 Random Units Online (in red)
45° N
30° N
Latitude, degrees
105° W
90° W
75° W
60° W
Longitude, degrees
Q=1.000:/Hit
© 2008 VIRGINIA TECH
Created by: R. Matthew Gardner
0.9
0.8
0.7
0.6
0.5
0.4
0.3
0.2
0.1

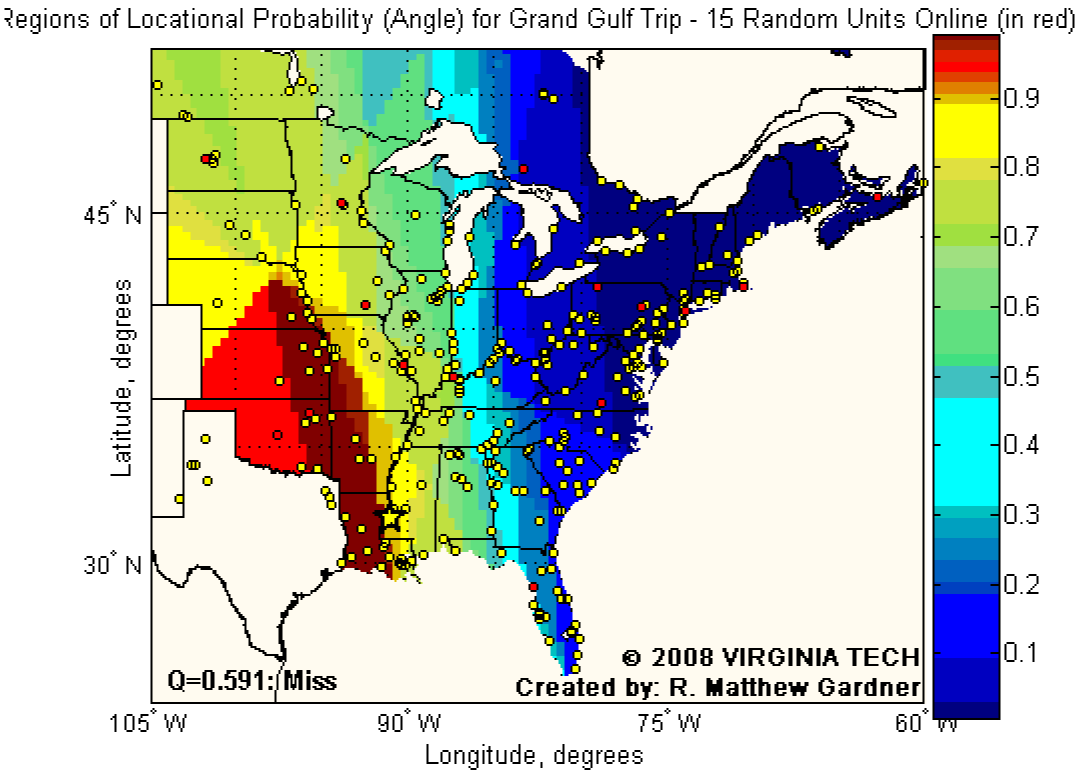
Regions of Locational Probability (Angle) for Grand Gulf Trip - 15 Random Units Online (in red)
45° N
30° N
Latitude, degrees
105° W
90° W
75° W
60° W
Longitude, degrees
Q=0.591: Miss
© 2008 VIRGINIA TECH
Created by: R. Matthew Gardner
0.9
0.8
0.7
0.6
0.5
0.4
0.3
0.2
0.1

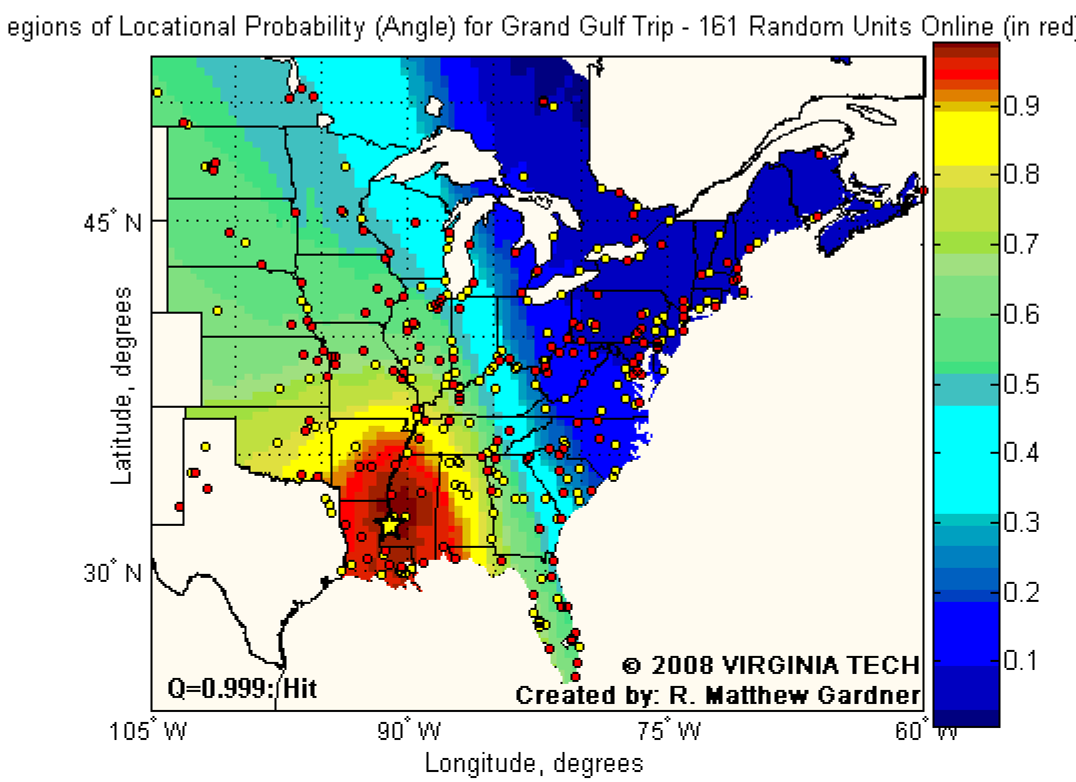
egions of Locational Probability (Angle) for Grand Gulf Trip - 161 Random Units Online (in red)
45° N
30° N
Latitude, degrees
105° W
90° W
75° W
60° W
Longitude, degrees
Q=0.999: Hit
© 2008 VIRGINIA TECH
Created by: R. Matthew Gardner
0.9
0.8
0.7
0.6
0.5
0.4
0.3
0.2
0.1

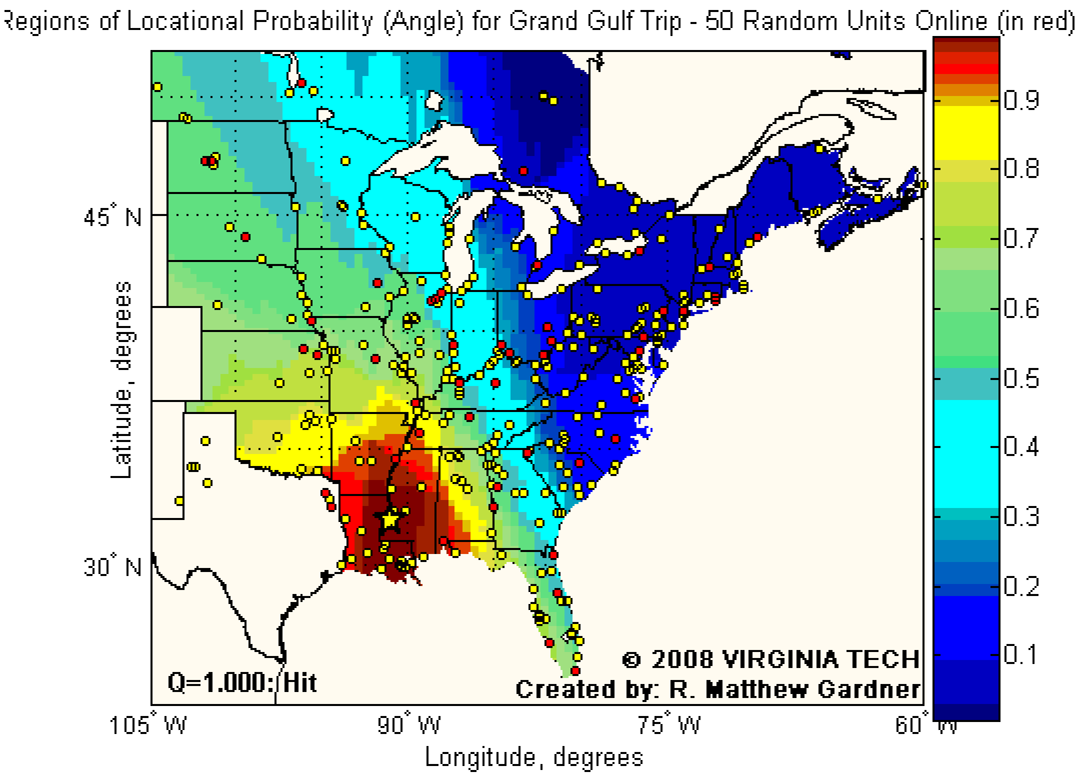
Regions of Locational Probability (Angle) for Grand Gulf Trip - 50 Random Units Online (in red)
45° N
30° N
Latitude, degrees
105° W
90° W
75° W
60° W
Longitude, degrees
Q=1.000: Hit
© 2008 VIRGINIA TECH
Created by: R. Matthew Gardner
0.9
0.8
0.7
0.6
0.5
0.4
0.3
0.2
0.1

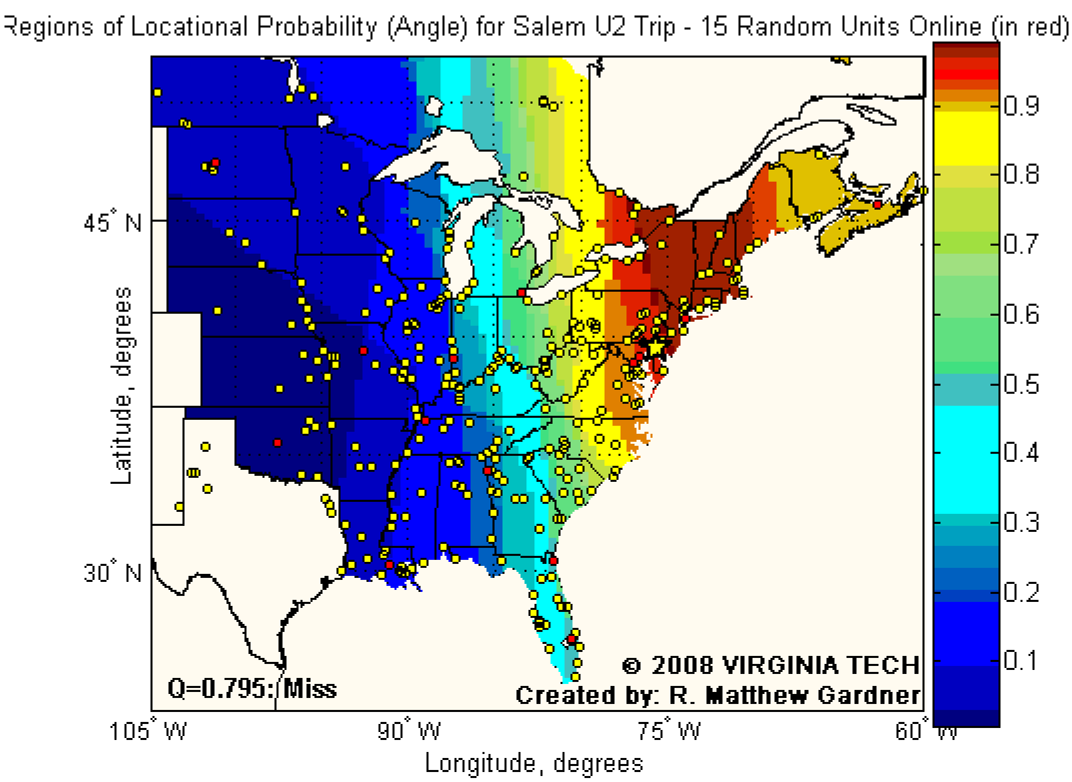
Regions of Locational Probability (Angle) for Salem U2 Trip - 15 Random Units Online (in red)
45° N
30° N
Latitude, degrees
105° W
90° W
75° W
60° W
Longitude, degrees
Q=0.795: Miss
© 2008 VIRGINIA TECH
Created by: R. Matthew Gardner
0.9
0.8
0.7
0.6
0.5
0.4
0.3
0.2
0.1

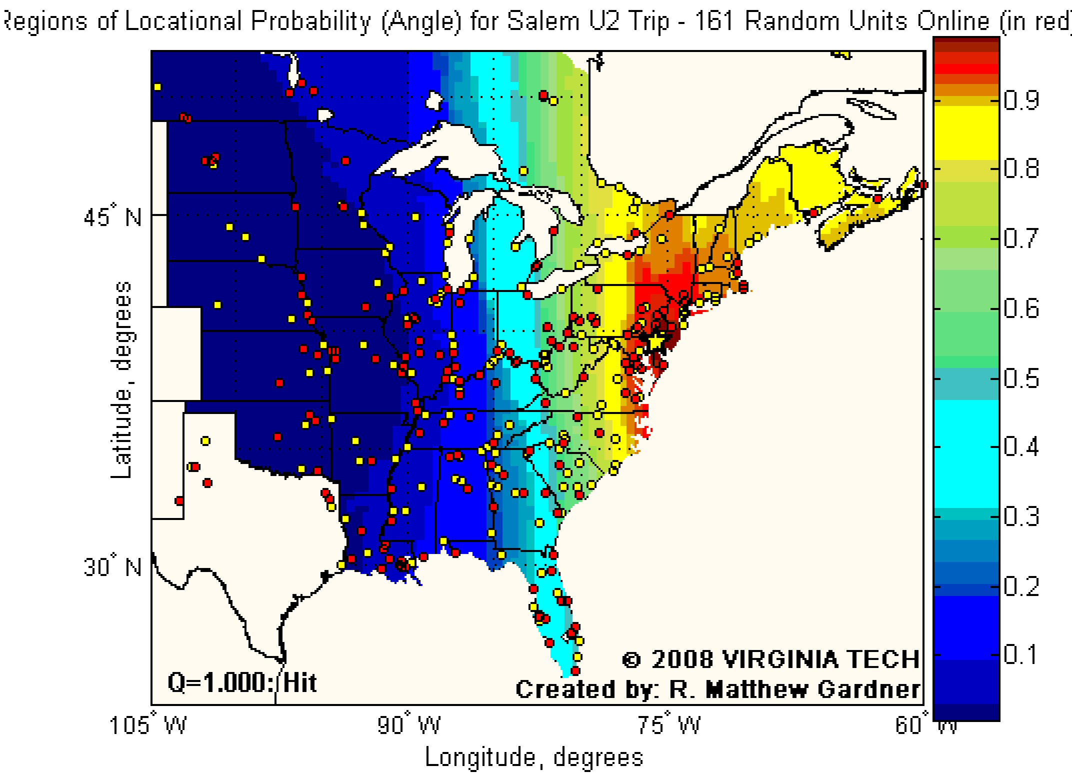
Regions of Locational Probability (Angle) for Salem U2 Trip - 161 Random Units Online (in red)
Latitude, degrees
Longitude, degrees
45° N
30° N
105° W
90° W
75° W
60° W
0.9
0.8
0.7
0.6
0.5
0.4
0.3
0.2
0.1
Q=1.000:/Hit
© 2008 VIRGINIA TECH
Created by: R. Matthew Gardner

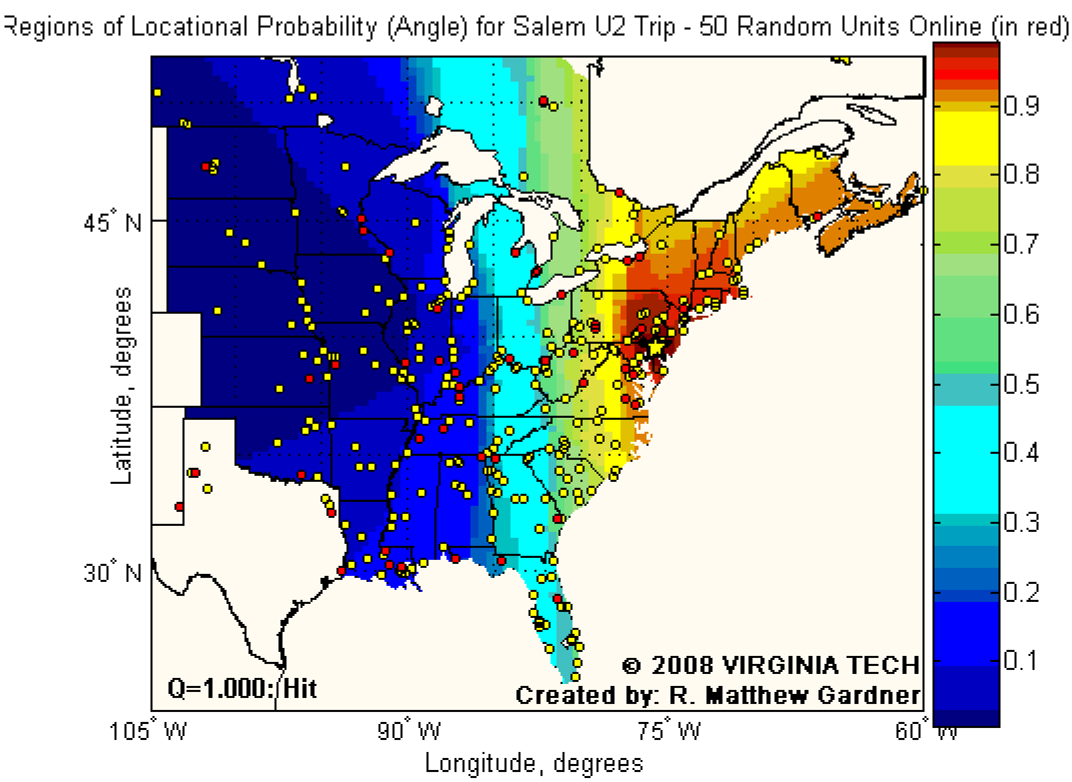
Regions of Locational Probability (Angle) for Salem U2 Trip - 50 Random Units Online (in red)
Latitude, degrees
Longitude, degrees
45° N
30° N
105° W
90° W
75° W
60° W
0.9
0.8
0.7
0.6
0.5
0.4
0.3
0.2
0.1
Q=1.000:/Hit
© 2008 VIRGINIA TECH
Created by: R. Matthew Gardner

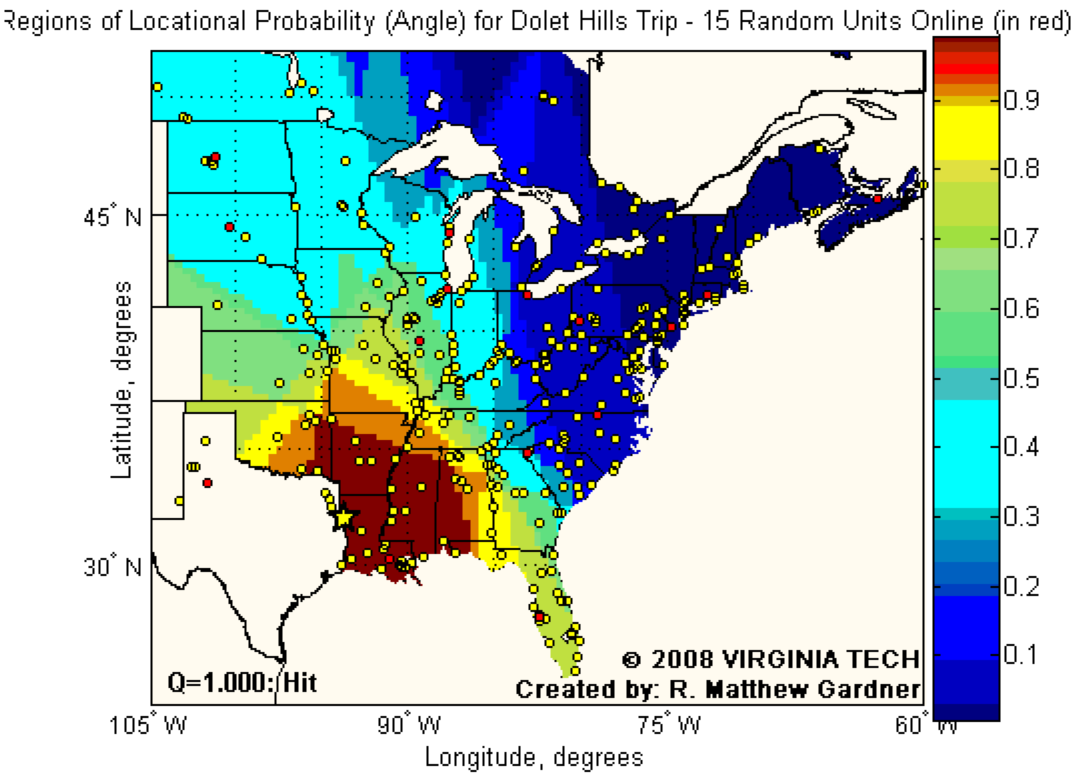
Regions of Locational Probability (Angle) for Dolet Hills Trip - 15 Random Units Online (in red)
45° N
30° N
Latitude, degrees
105° W
90° W
75° W
60° W
Longitude, degrees
Q=1.000:/Hit
© 2008 VIRGINIA TECH
Created by: R. Matthew Gardner
0.9
0.8
0.7
0.6
0.5
0.4
0.3
0.2
0.1

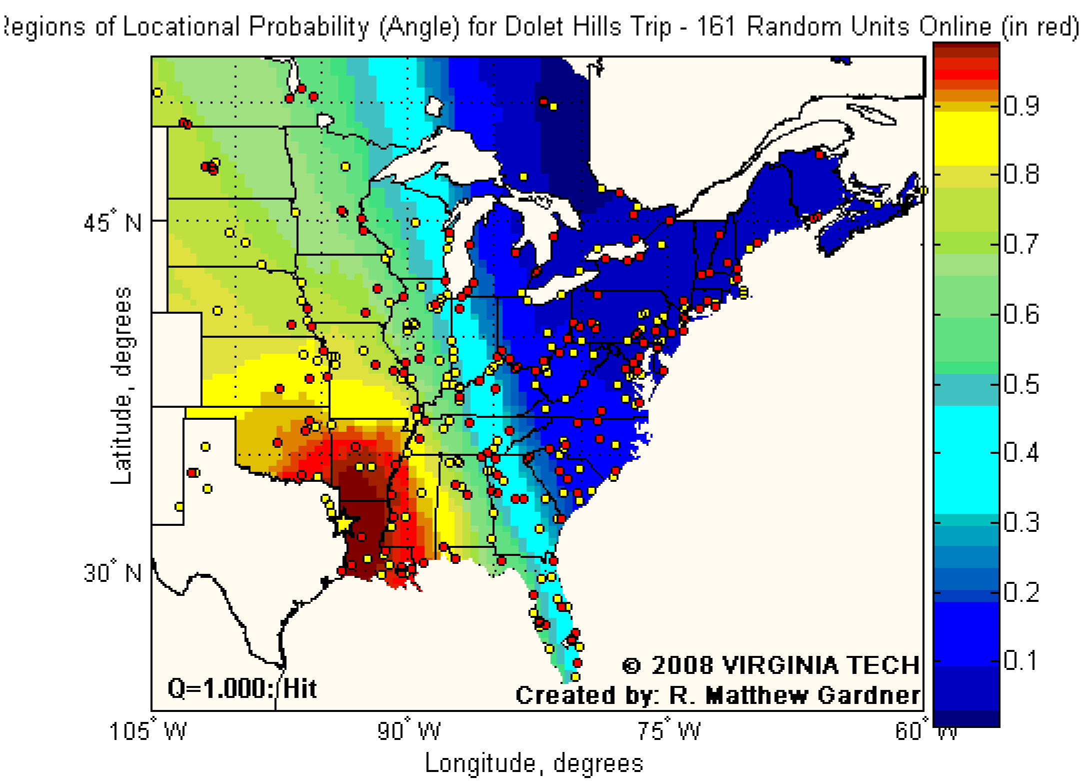
Regions of Locational Probability (Angle) for Dolet Hills Trip - 161 Random Units Online (in red)
45° N
30° N
Latitude, degrees
105° W
90° W
75° W
60° W
Longitude, degrees
Q=1.000:/Hit
© 2008 VIRGINIA TECH
Created by: R. Matthew Gardner
0.9
0.8
0.7
0.6
0.5
0.4
0.3
0.2
0.1

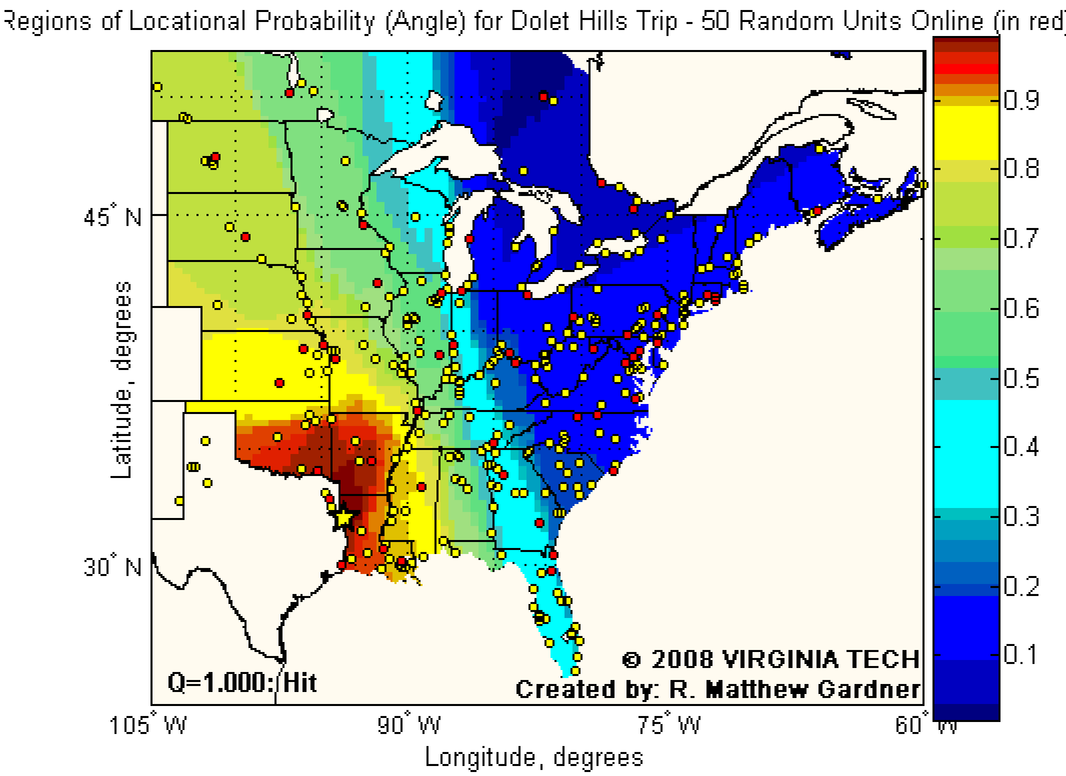
Regions of Locational Probability (Angle) for Dolet Hills Trip - 50 Random Units Online (in red)
45° N
30° N
Latitude, degrees
105° W
90° W
75° W
60° W
Longitude, degrees
Q=1.000: Hit
© 2008 VIRGINIA TECH
Created by: R. Matthew Gardner
0.9
0.8
0.7
0.6
0.5
0.4
0.3
0.2
0.1

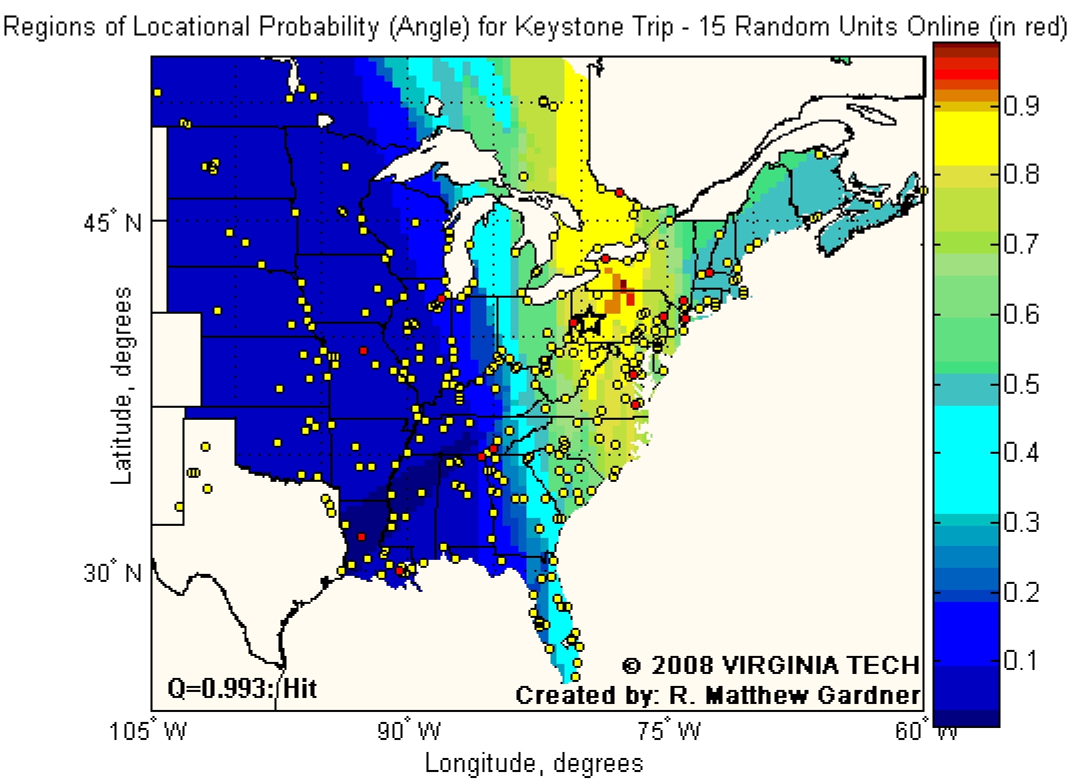
Regions of Locational Probability (Angle) for Keystone Trip - 15 Random Units Online (in red)
45° N
30° N
Latitude, degrees
105° W
90° W
75° W
60° W
Longitude, degrees
Q=0.993: Hit
© 2008 VIRGINIA TECH
Created by: R. Matthew Gardner
0.9
0.8
0.7
0.6
0.5
0.4
0.3
0.2
0.1

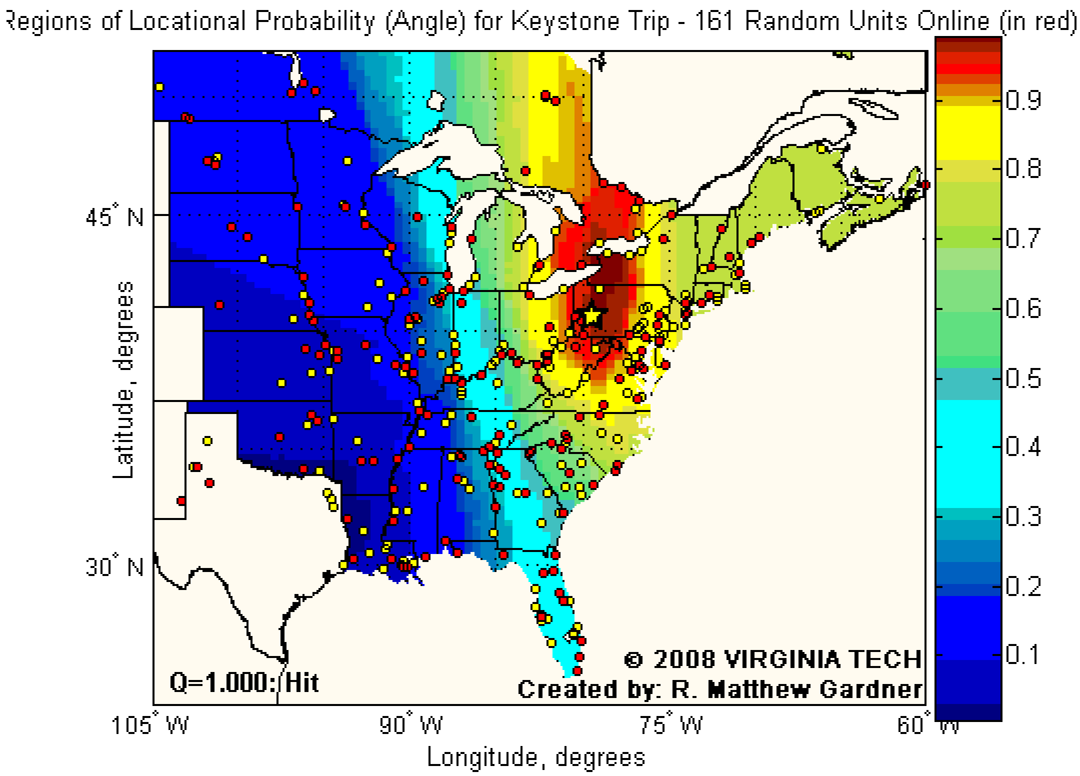
Regions of Locational Probability (Angle) for Keystone Trip - 161 Random Units Online (in red)
Latitude, degrees
45° N
30° N
105° W
90° W
75° W
60° W
Longitude, degrees
Q=1.000: Hit
© 2008 VIRGINIA TECH
Created by: R. Matthew Gardner
0.9
0.8
0.7
0.6
0.5
0.4
0.3
0.2
0.1

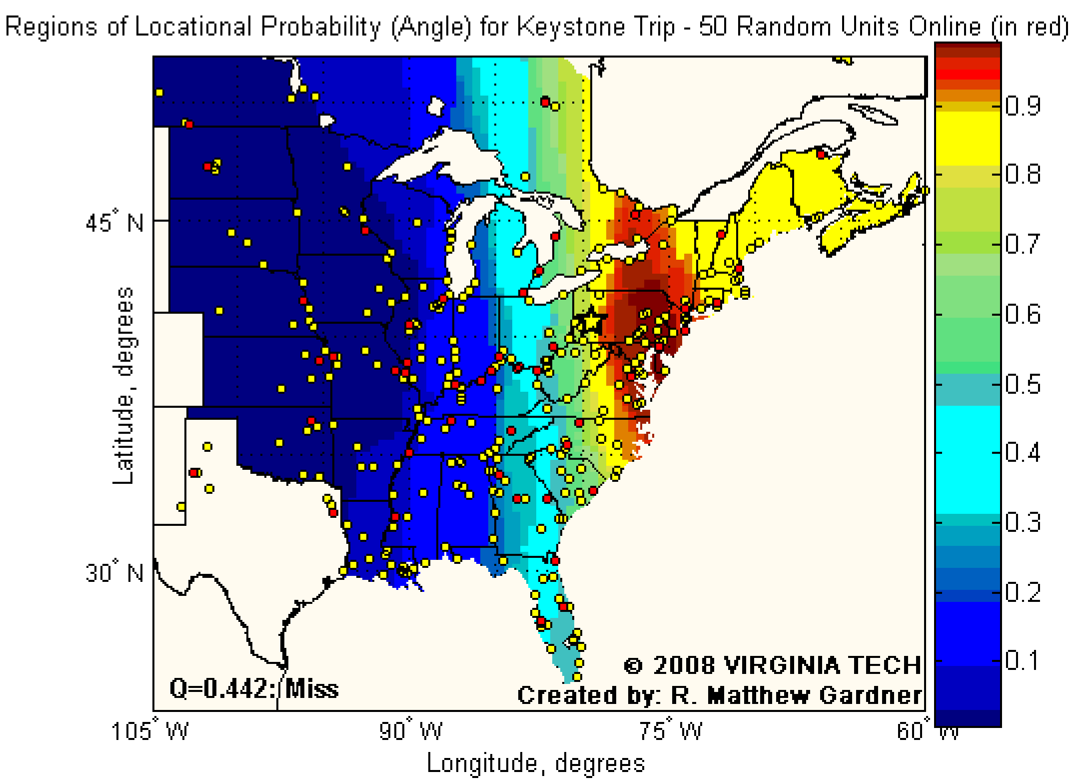
Regions of Locational Probability (Angle) for Keystone Trip - 50 Random Units Online (in red)
Latitude, degrees
45° N
30° N
105° W
90° W
75° W
60° W
Longitude, degrees
Q=0.442: Miss
© 2008 VIRGINIA TECH
Created by: R. Matthew Gardner
0.9
0.8
0.7
0.6
0.5
0.4
0.3
0.2
0.1

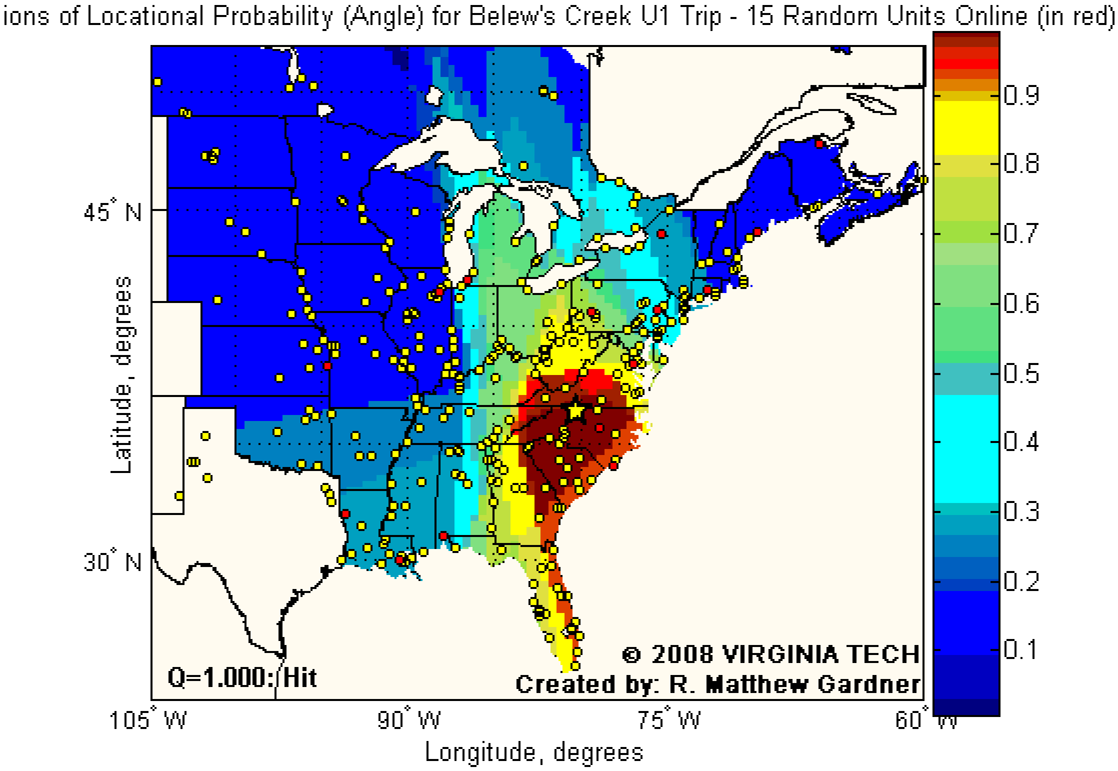
ions of Locational Probability (Angle) for Belew's Creek U1 Trip - 15 Random Units Online (in red)
45° N
30° N
Latitude, degrees
105° W
90° W
75° W
60° W
Longitude, degrees
Q=1.000:/Hit
© 2008 VIRGINIA TECH
Created by: R. Matthew Gardner
0.9
0.8
0.7
0.6
0.5
0.4
0.3
0.2
0.1

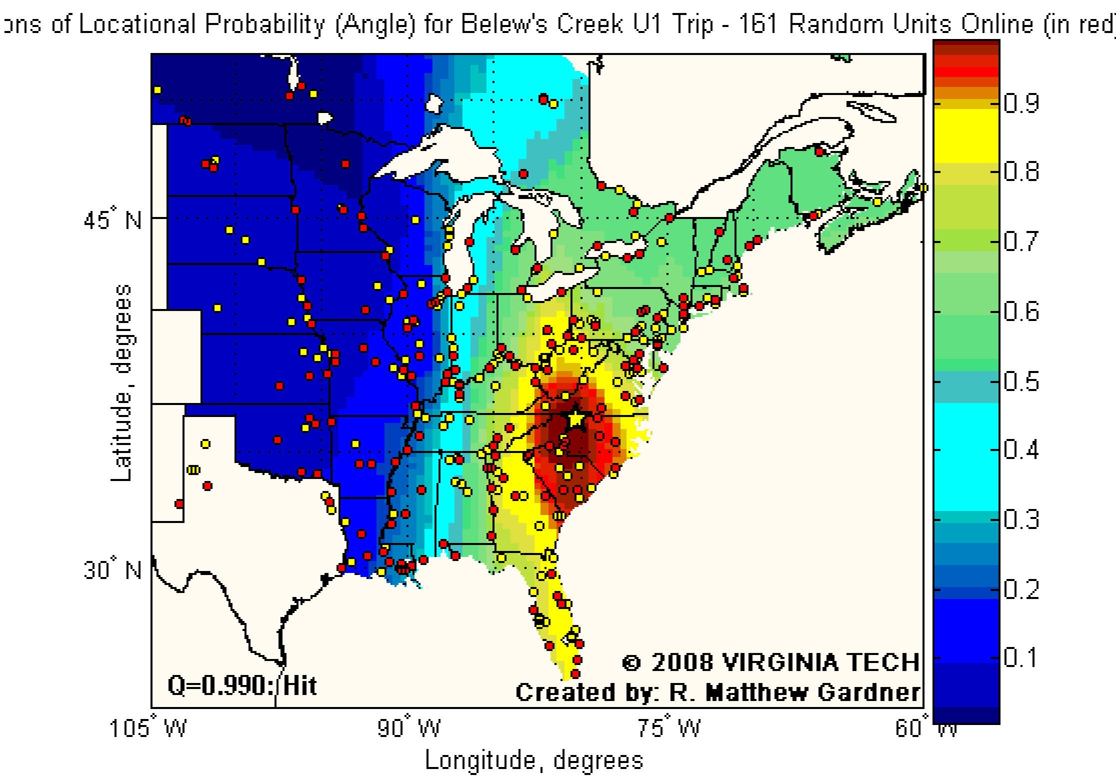
ons of Locational Probability (Angle) for Belew's Creek U1 Trip - 161 Random Units Online (in red)
45° N
30° N
Latitude, degrees
105° W
90° W
75° W
60° W
Longitude, degrees
Q=0.990:/Hit
© 2008 VIRGINIA TECH
Created by: R. Matthew Gardner
0.9
0.8
0.7
0.6
0.5
0.4
0.3
0.2
0.1

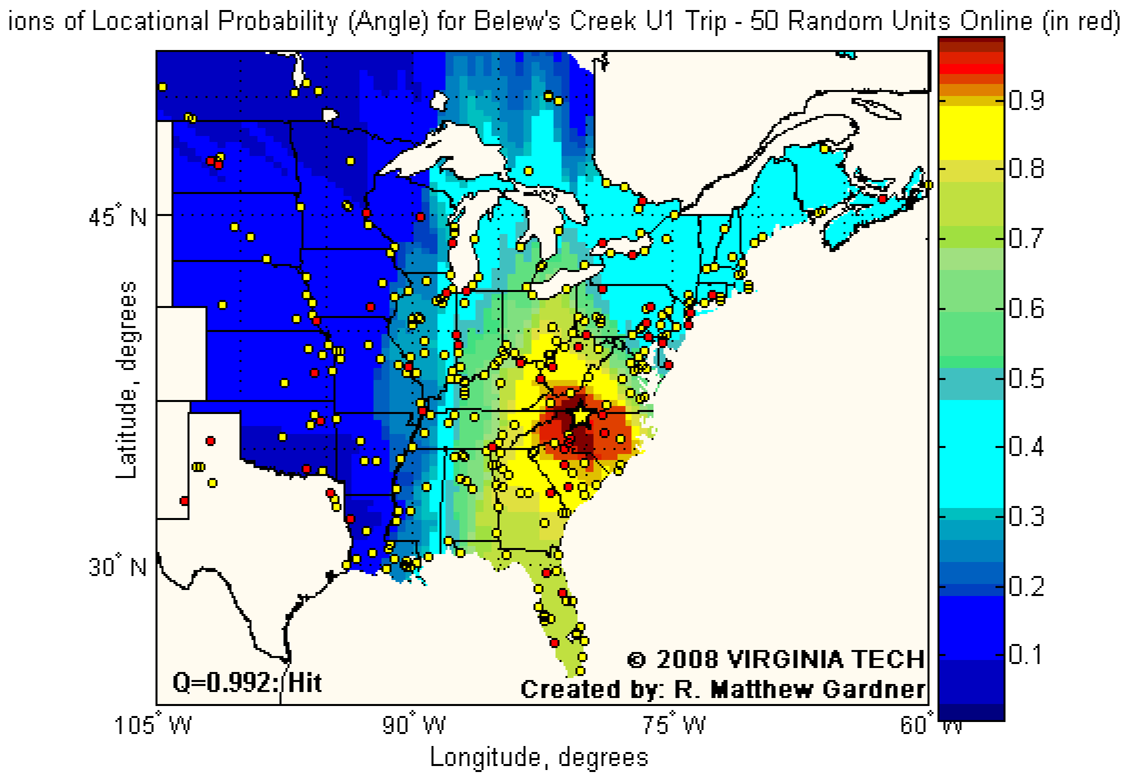
ions of Locational Probability (Angle) for Belew's Creek U1 Trip - 50 Random Units Online (in red)
Latitude, degrees
45° N
30° N
105° W
90° W
75° W
60° W
Longitude, degrees
0.9
0.8
0.7
0.6
0.5
0.4
0.3
0.2
0.1
Q=0.992: Hit
© 2008 VIRGINIA TECH
Created by: R. Matthew Gardner

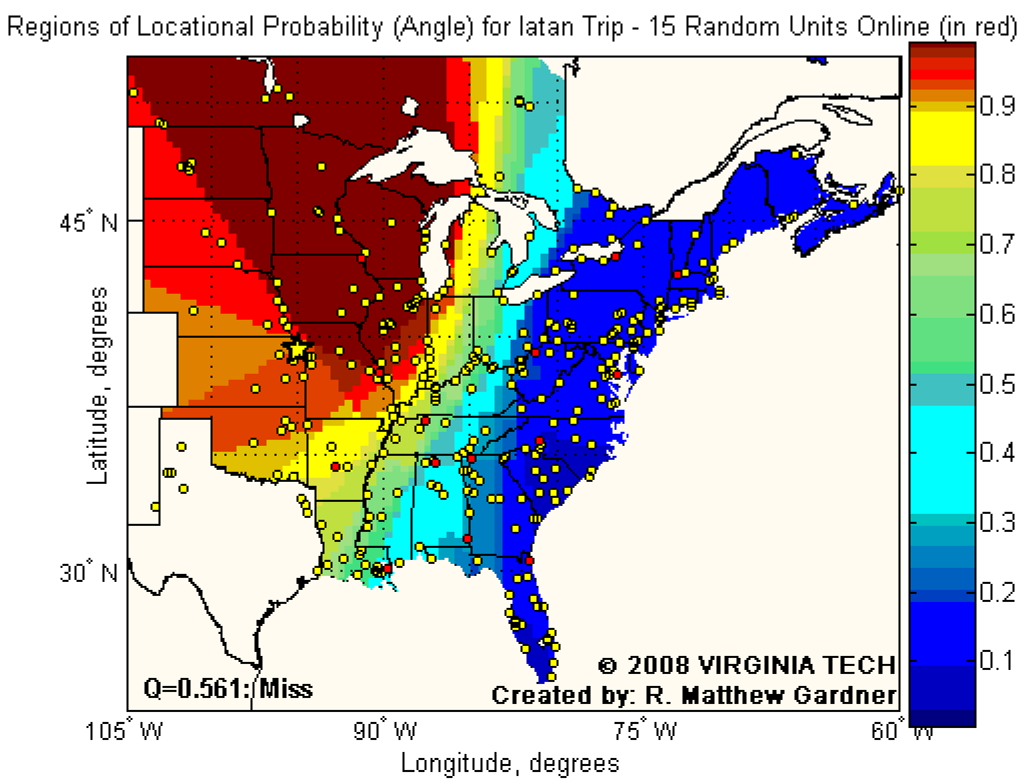
Regions of Locational Probability (Angle) for Iatan Trip - 15 Random Units Online (in red)
Latitude, degrees
45° N
30° N
105° W
90° W
75° W
60° W
Longitude, degrees
0.9
0.8
0.7
0.6
0.5
0.4
0.3
0.2
0.1
Q=0.561: Miss
© 2008 VIRGINIA TECH
Created by: R. Matthew Gardner

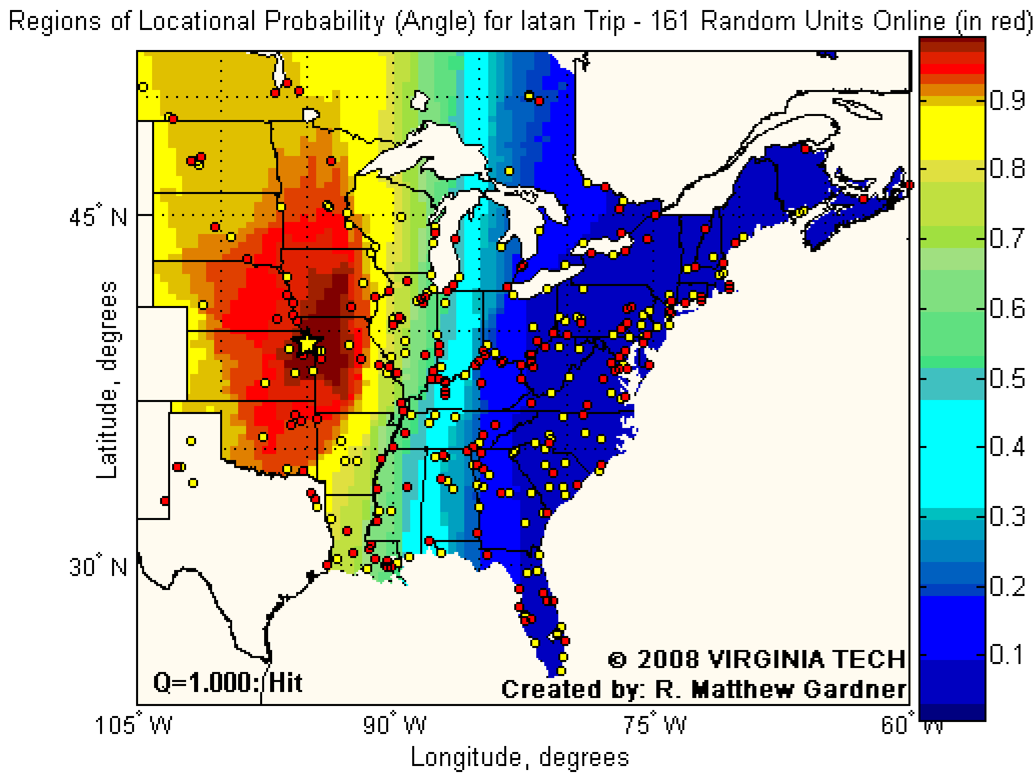

Regions of Locational Probability (Angle) for Iatan Trip - 161 Random Units Online (in red)
45° N
30° N
Latitude, degrees
105° W
90° W
75° W
60° W
Longitude, degrees
Q=1.000:/Hit
© 2008 VIRGINIA TECH
Created by: R. Matthew Gardner
0.9
0.8
0.7
0.6
0.5
0.4
0.3
0.2
0.1

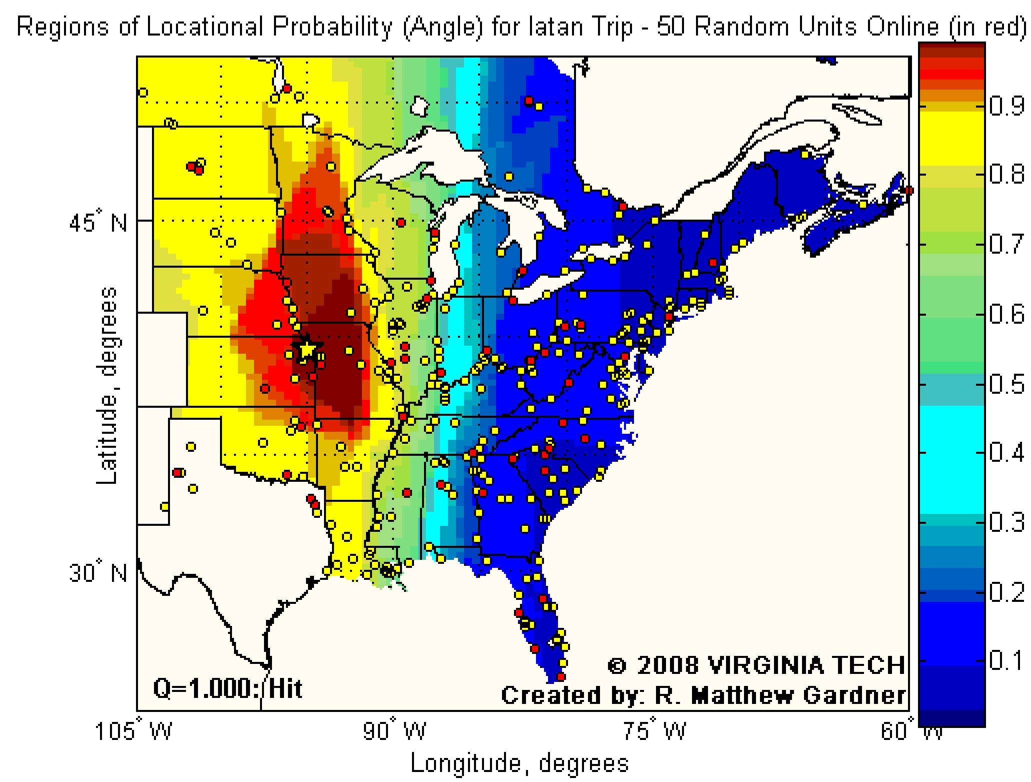

Regions of Locational Probability (Angle) for Iatan Trip - 50 Random Units Online (in red)
45° N
30° N
Latitude, degrees
105° W
90° W
75° W
60° W
Longitude, degrees
Q=1.000:/Hit
© 2008 VIRGINIA TECH
Created by: R. Matthew Gardner
0.9
0.8
0.7
0.6
0.5
0.4
0.3
0.2
0.1

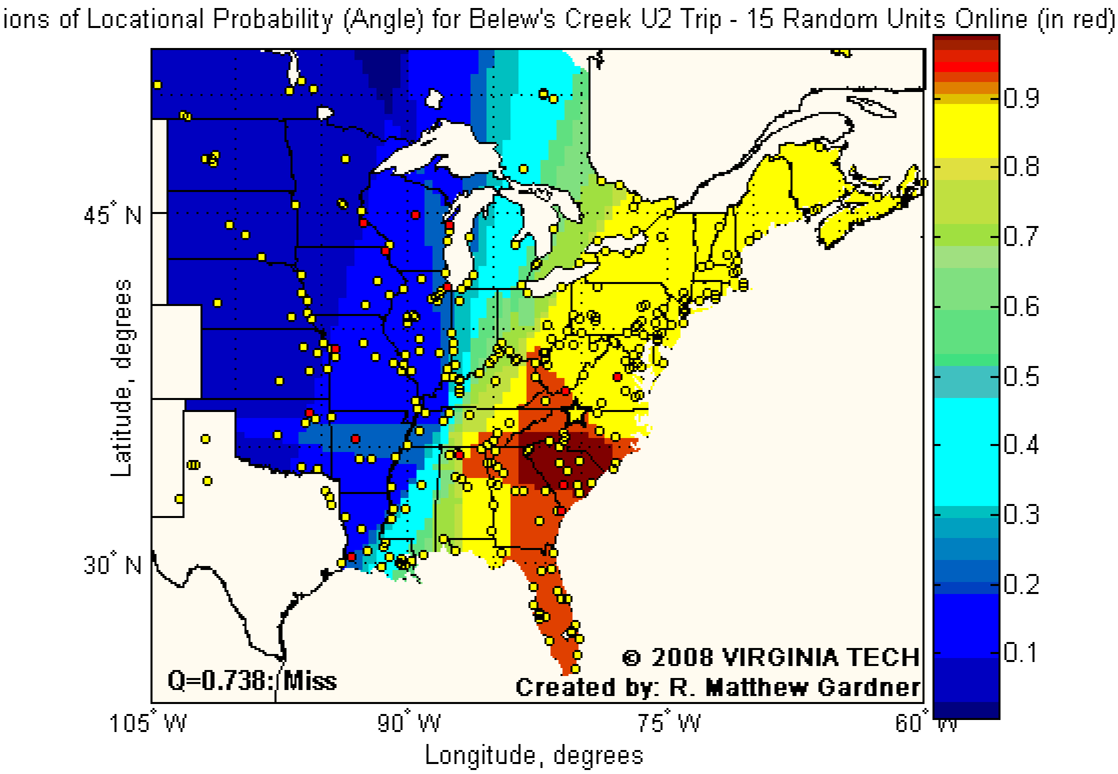
ions of Locational Probability (Angle) for Belew's Creek U2 Trip - 15 Random Units Online (in red)
45° N
30° N
Latitude, degrees
105° W
90° W
75° W
60° W
Longitude, degrees
Q=0.738: Miss
© 2008 VIRGINIA TECH
Created by: R. Matthew Gardner
0.9
0.8
0.7
0.6
0.5
0.4
0.3
0.2
0.1

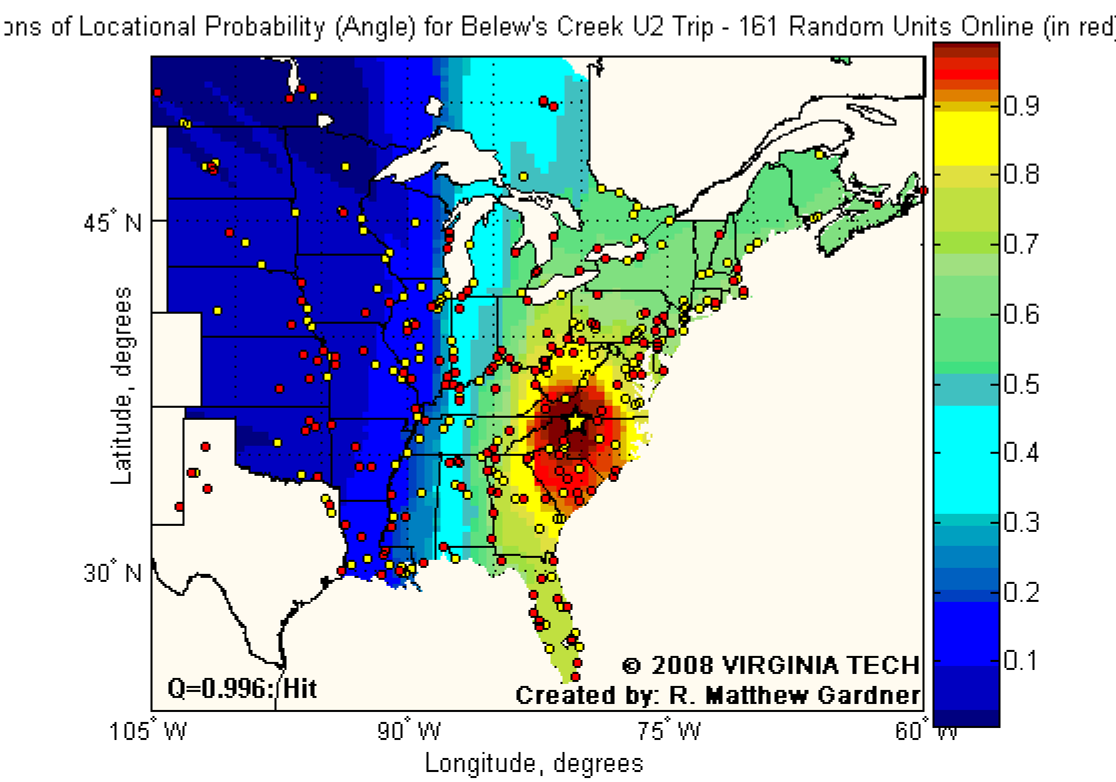
ons of Locational Probability (Angle) for Belew's Creek U2 Trip - 161 Random Units Online (in red)
45° N
30° N
Latitude, degrees
105° W
90° W
75° W
60° W
Longitude, degrees
Q=0.996: Hit
© 2008 VIRGINIA TECH
Created by: R. Matthew Gardner
0.9
0.8
0.7
0.6
0.5
0.4
0.3
0.2
0.1

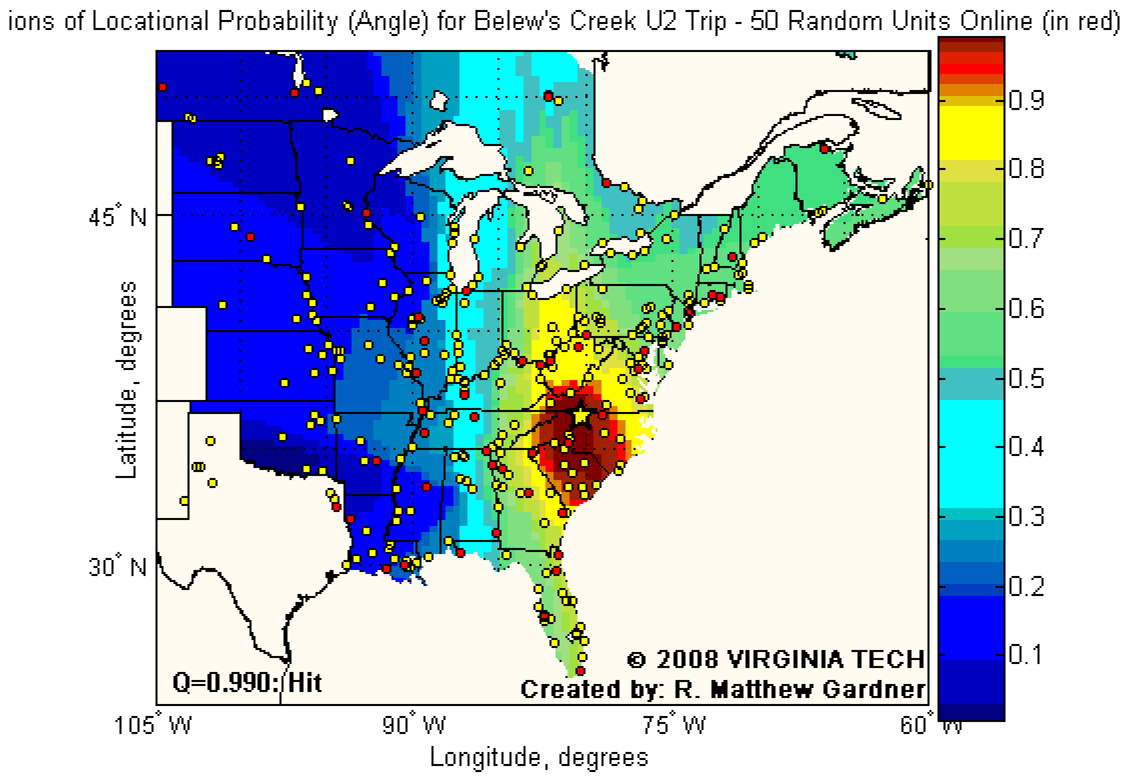
ions of Locational Probability (Angle) for Belew's Creek U2 Trip - 50 Random Units Online (in red)
45° N
30° N
Latitude, degrees
105° W
90° W
75° W
60° W
Longitude, degrees
Q=0.990:/Hit
© 2008 VIRGINIA TECH
Created by: R. Matthew Gardner
0.9
0.8
0.7
0.6
0.5
0.4
0.3
0.2
0.1

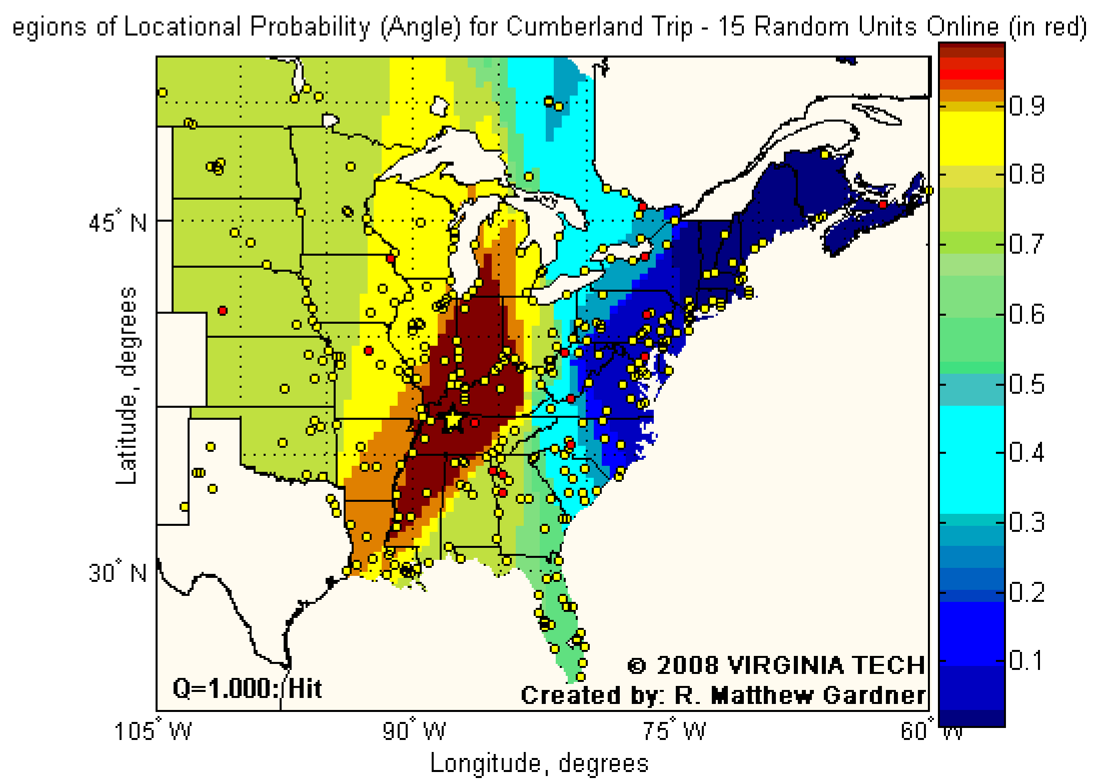
egions of Locational Probability (Angle) for Cumberland Trip - 15 Random Units Online (in red)
45° N
30° N
Latitude, degrees
105° W
90° W
75° W
60° W
Longitude, degrees
Q=1.000:/Hit
© 2008 VIRGINIA TECH
Created by: R. Matthew Gardner
0.9
0.8
0.7
0.6
0.5
0.4
0.3
0.2
0.1

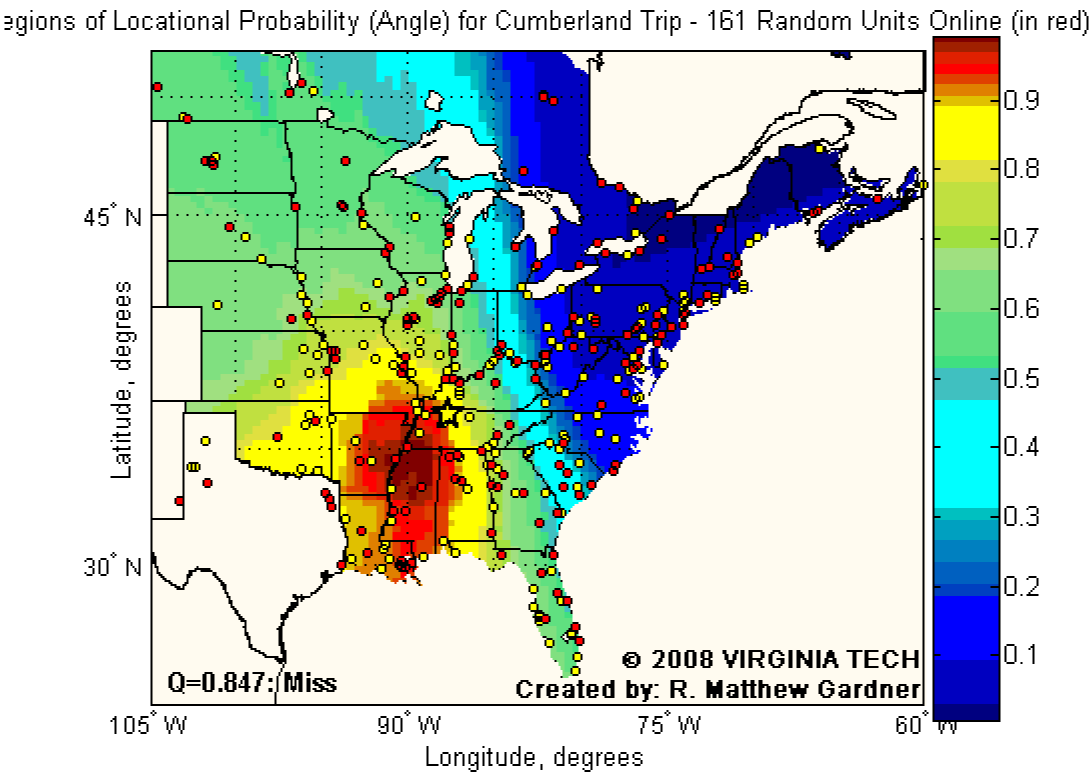
egions of Locational Probability (Angle) for Cumberland Trip - 161 Random Units Online (in red)
45° N
30° N
Latitude, degrees
105° W
90° W
75° W
60° W
Longitude, degrees
Q=0.847: Miss
© 2008 VIRGINIA TECH
Created by: R. Matthew Gardner
0.9
0.8
0.7
0.6
0.5
0.4
0.3
0.2
0.1

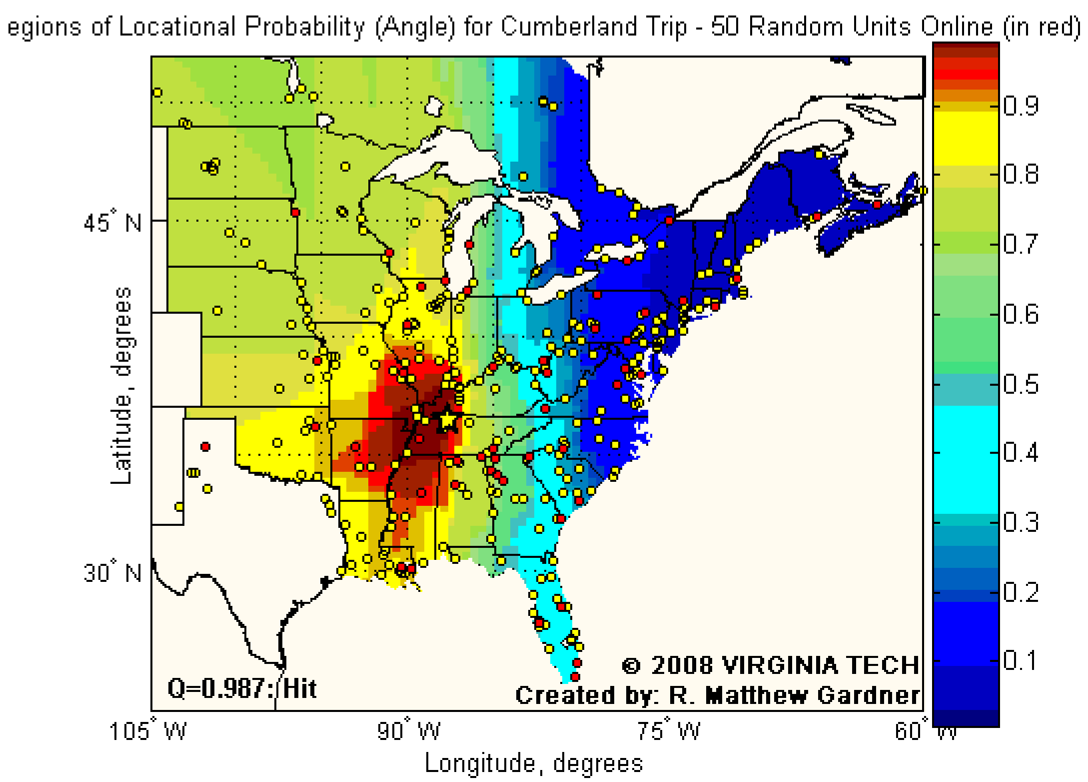
egions of Locational Probability (Angle) for Cumberland Trip - 50 Random Units Online (in red)
45° N
30° N
Latitude, degrees
105° W
90° W
75° W
60° W
Longitude, degrees
Q=0.987: Hit
© 2008 VIRGINIA TECH
Created by: R. Matthew Gardner
0.9
0.8
0.7
0.6
0.5
0.4
0.3
0.2
0.1

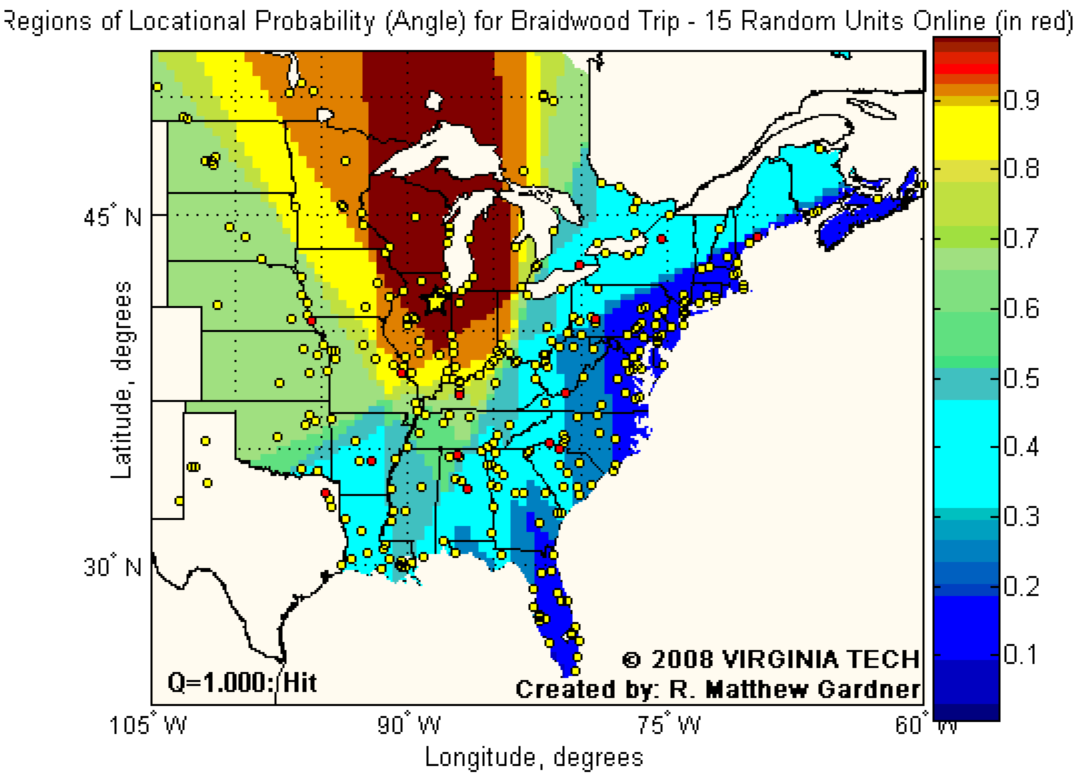
Regions of Locational Probability (Angle) for Braidwood Trip - 15 Random Units Online (in red)
45° N
30° N
Latitude, degrees
105° W
90° W
75° W
60° W
Longitude, degrees
Q=1.000: Hit
© 2008 VIRGINIA TECH
Created by: R. Matthew Gardner
0.9
0.8
0.7
0.6
0.5
0.4
0.3
0.2
0.1

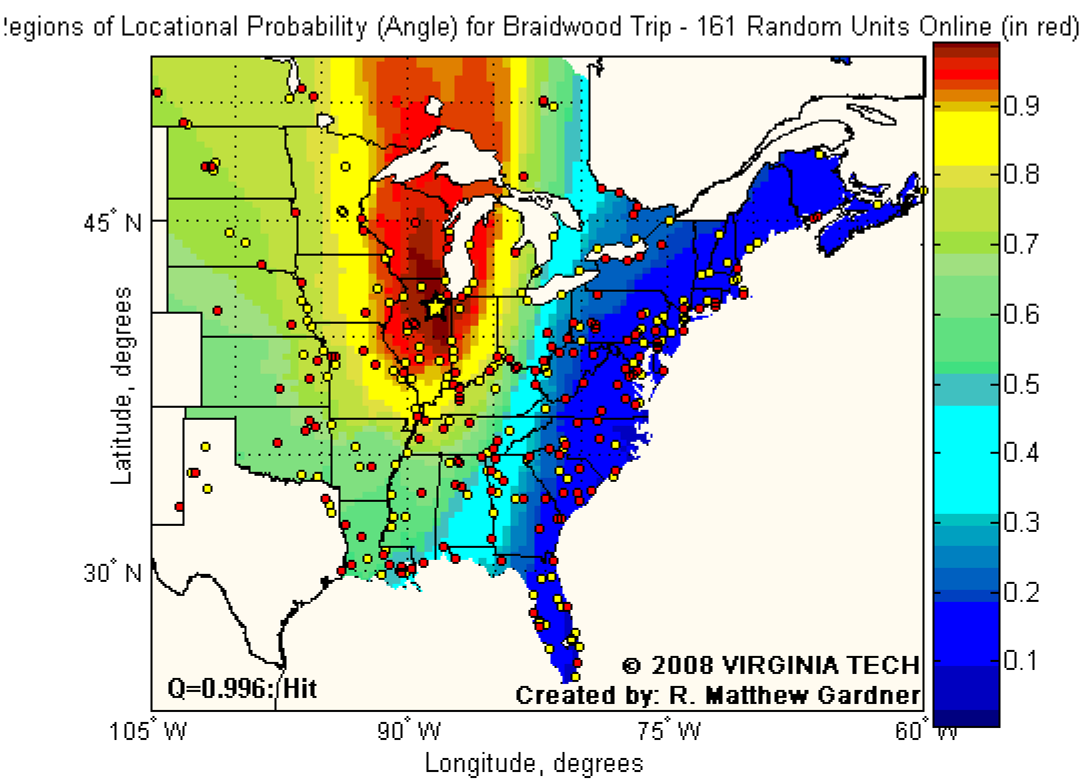
Regions of Locational Probability (Angle) for Braidwood Trip - 161 Random Units Online (in red)
45° N
30° N
Latitude, degrees
105° W
90° W
75° W
60° W
Longitude, degrees
Q=0.996: Hit
© 2008 VIRGINIA TECH
Created by: R. Matthew Gardner
0.9
0.8
0.7
0.6
0.5
0.4
0.3
0.2
0.1

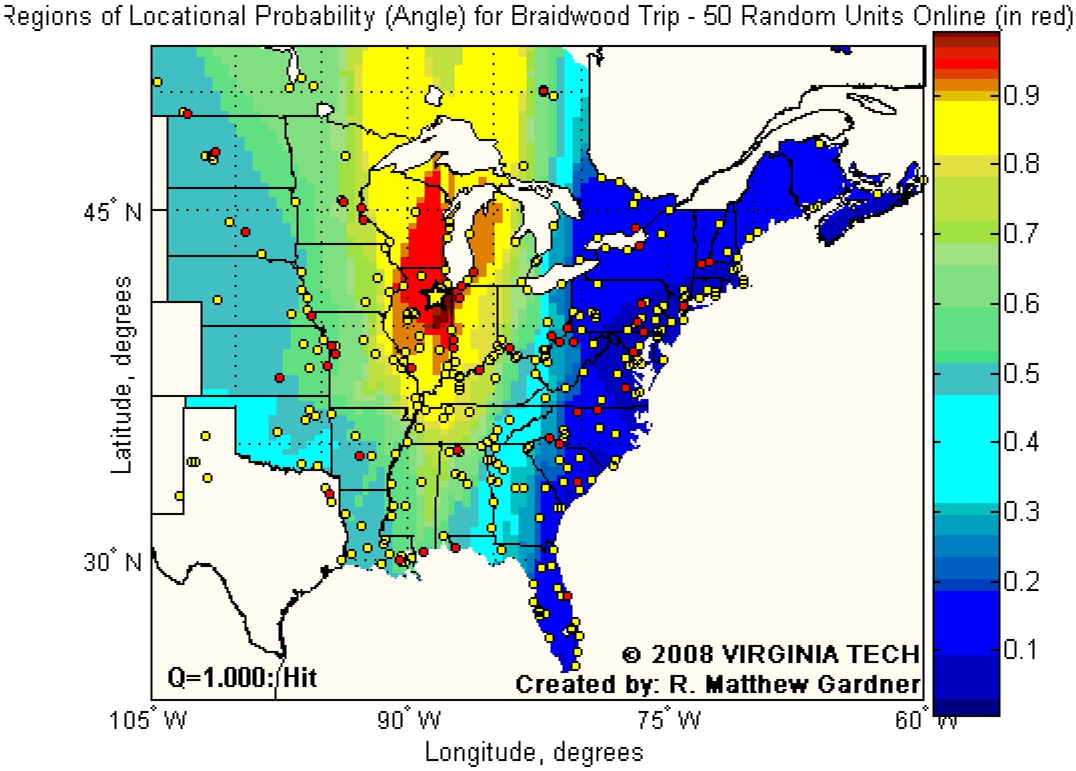
Regions of Locational Probability (Angle) for Braidwood Trip - 50 Random Units Online (in red)
Latitude, degrees
Longitude, degrees
45° N
30° N
105° W
90° W
75° W
60° W
0.9
0.8
0.7
0.6
0.5
0.4
0.3
0.2
0.1
Q=1.000: Hit
© 2008 VIRGINIA TECH
Created by: R. Matthew Gardner

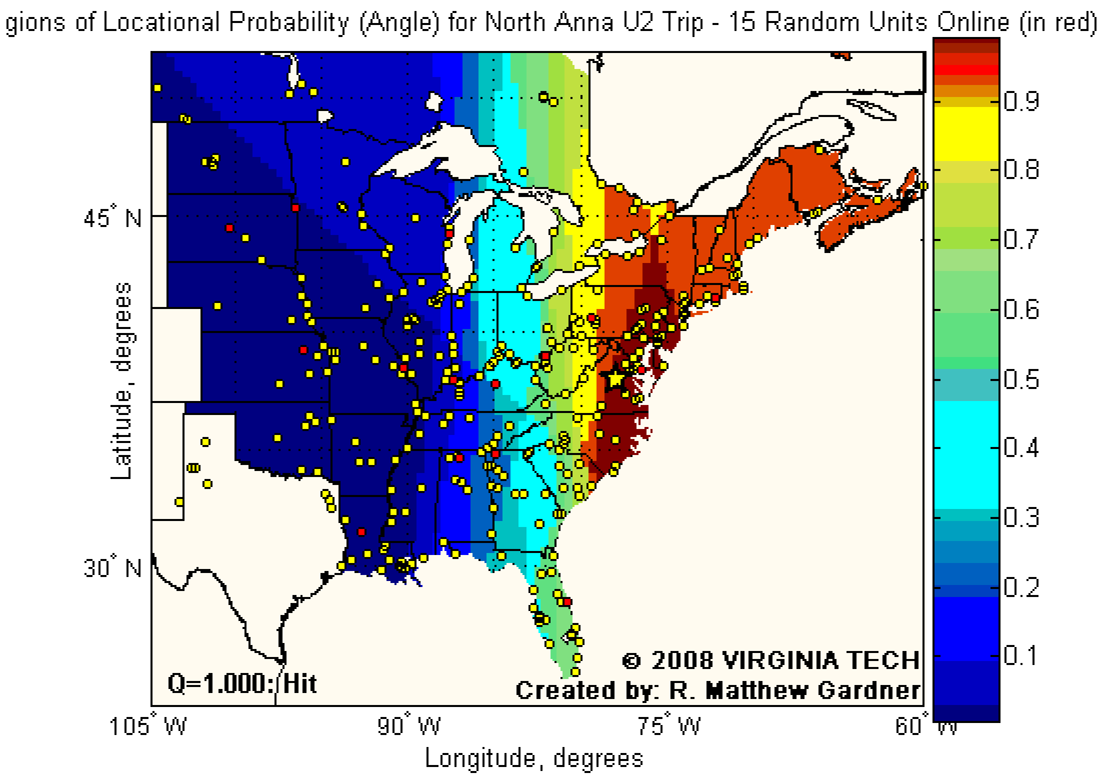
gions of Locational Probability (Angle) for North Anna U2 Trip - 15 Random Units Online (in red)
Latitude, degrees
Longitude, degrees
45° N
30° N
105° W
90° W
75° W
60° W
0.9
0.8
0.7
0.6
0.5
0.4
0.3
0.2
0.1
Q=1.000: Hit
© 2008 VIRGINIA TECH
Created by: R. Matthew Gardner

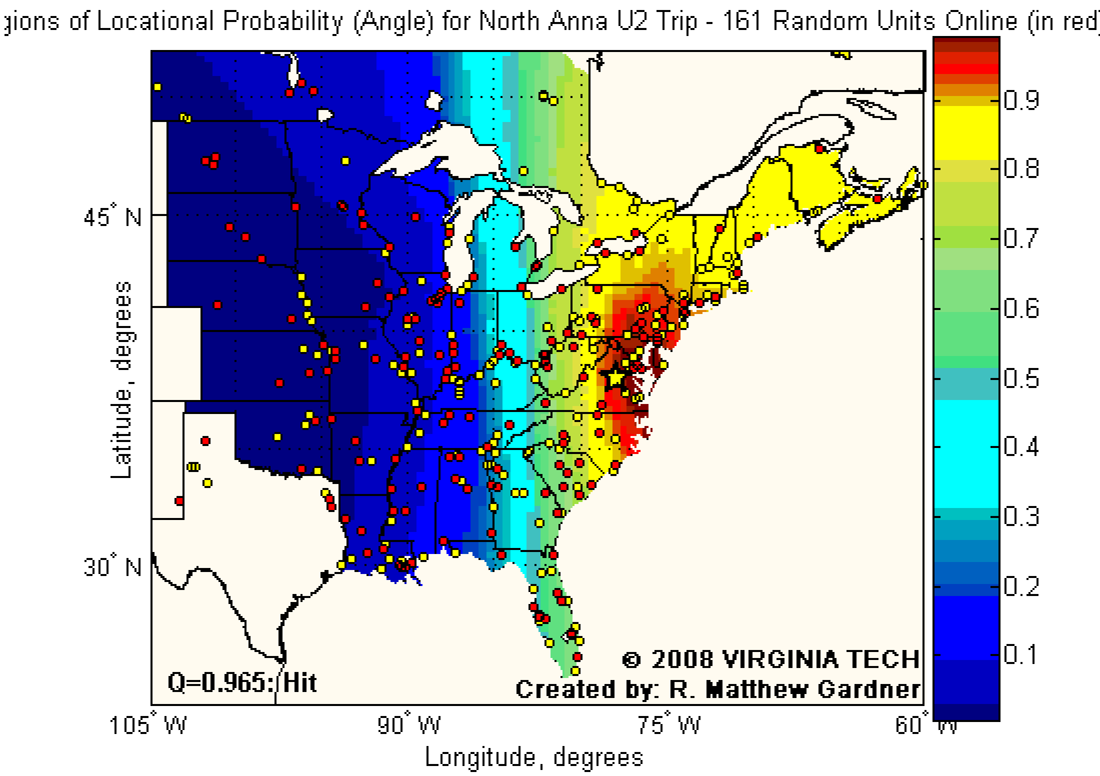
gions of Locational Probability (Angle) for North Anna U2 Trip - 161 Random Units Online (in red)
Latitude, degrees
Longitude, degrees
45° N
30° N
105° W
90° W
75° W
60° W
0.9
0.8
0.7
0.6
0.5
0.4
0.3
0.2
0.1
Q=0.965: Hit
© 2008 VIRGINIA TECH
Created by: R. Matthew Gardner

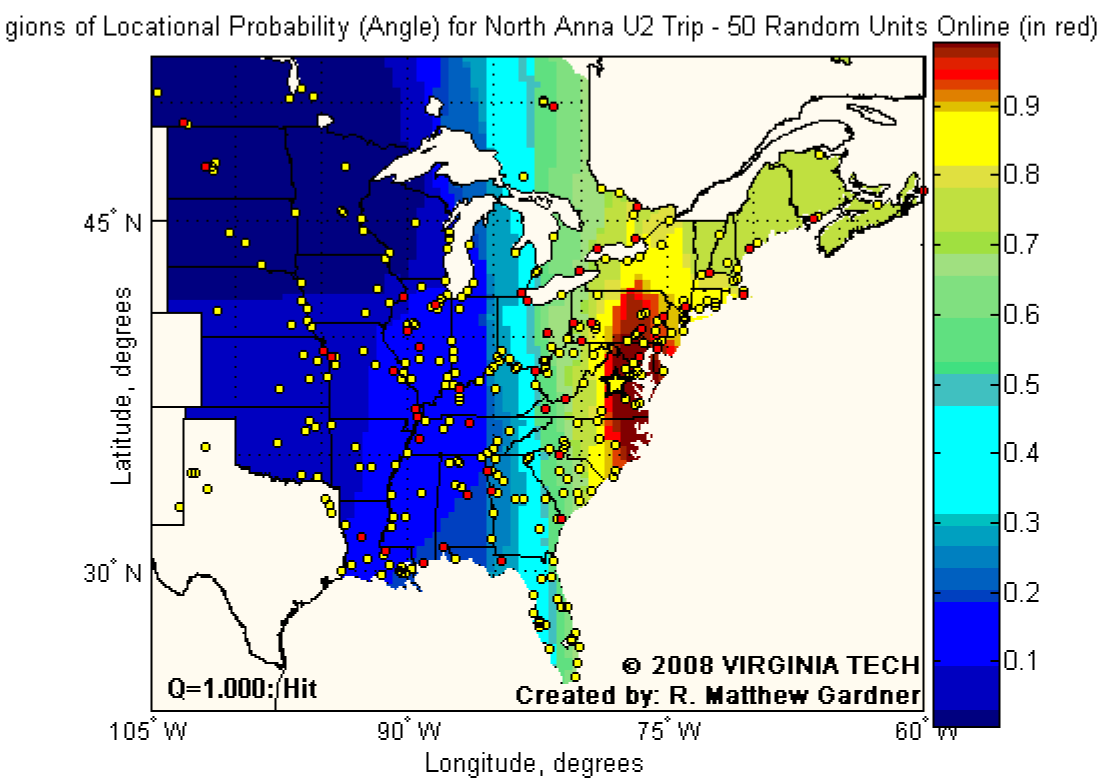
gions of Locational Probability (Angle) for North Anna U2 Trip - 50 Random Units Online (in red)
Latitude, degrees
Longitude, degrees
45° N
30° N
105° W
90° W
75° W
60° W
0.9
0.8
0.7
0.6
0.5
0.4
0.3
0.2
0.1
Q=1.000: Hit
© 2008 VIRGINIA TECH
Created by: R. Matthew Gardner

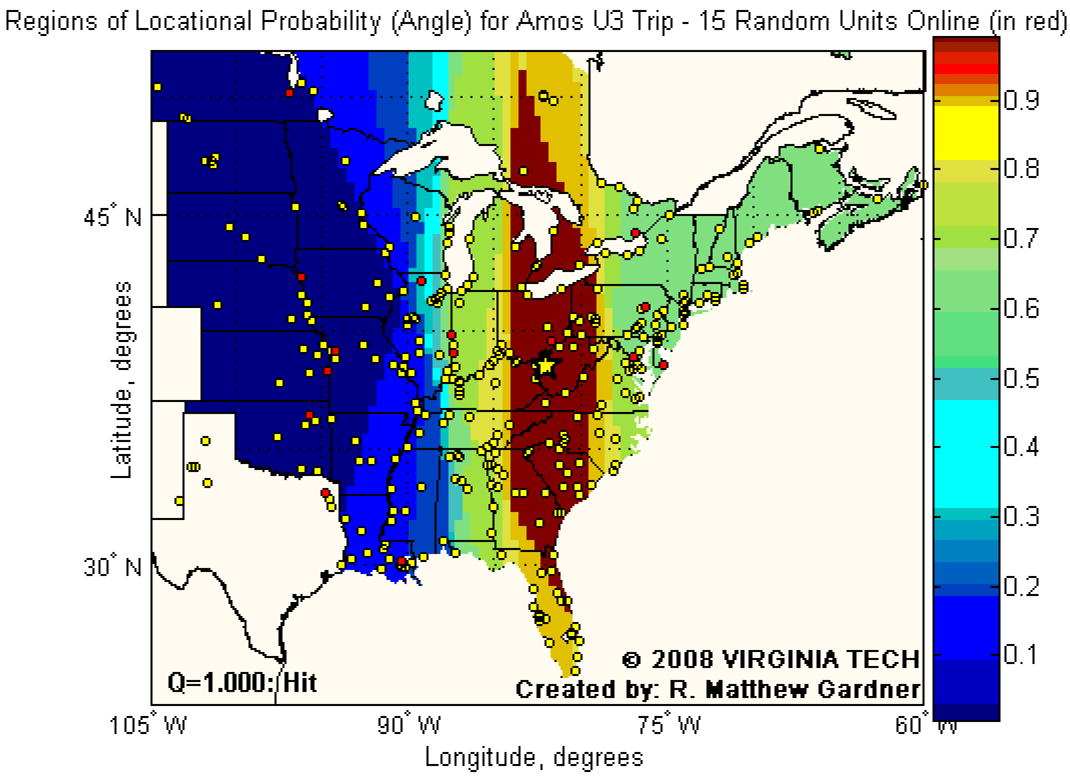
Regions of Locational Probability (Angle) for Amos U3 Trip - 15 Random Units Online (in red)
45° N
30° N
Latitude, degrees
105° W
90° W
75° W
60° W
Longitude, degrees
Q=1.000:/Hit
© 2008 VIRGINIA TECH
Created by: R. Matthew Gardner
0.9
0.8
0.7
0.6
0.5
0.4
0.3
0.2
0.1

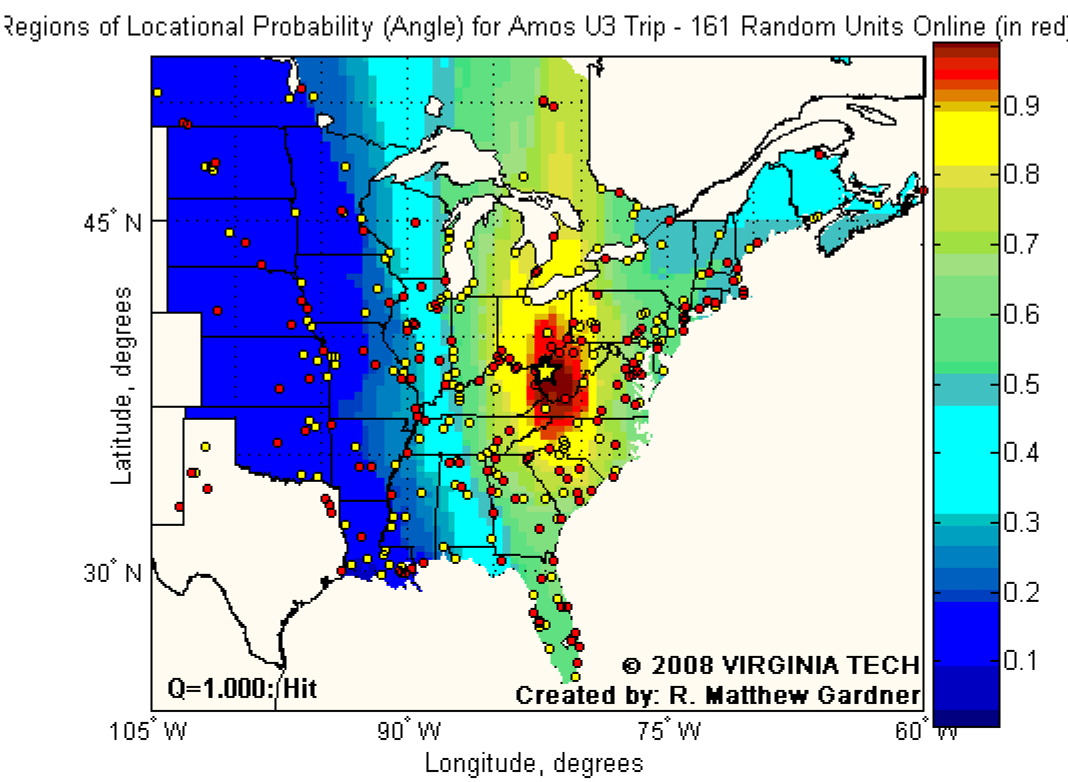
Regions of Locational Probability (Angle) for Amos U3 Trip - 161 Random Units Online (in red)
45° N
30° N
Latitude, degrees
105° W
90° W
75° W
60° W
Longitude, degrees
Q=1.000:/Hit
© 2008 VIRGINIA TECH
Created by: R. Matthew Gardner
0.9
0.8
0.7
0.6
0.5
0.4
0.3
0.2
0.1

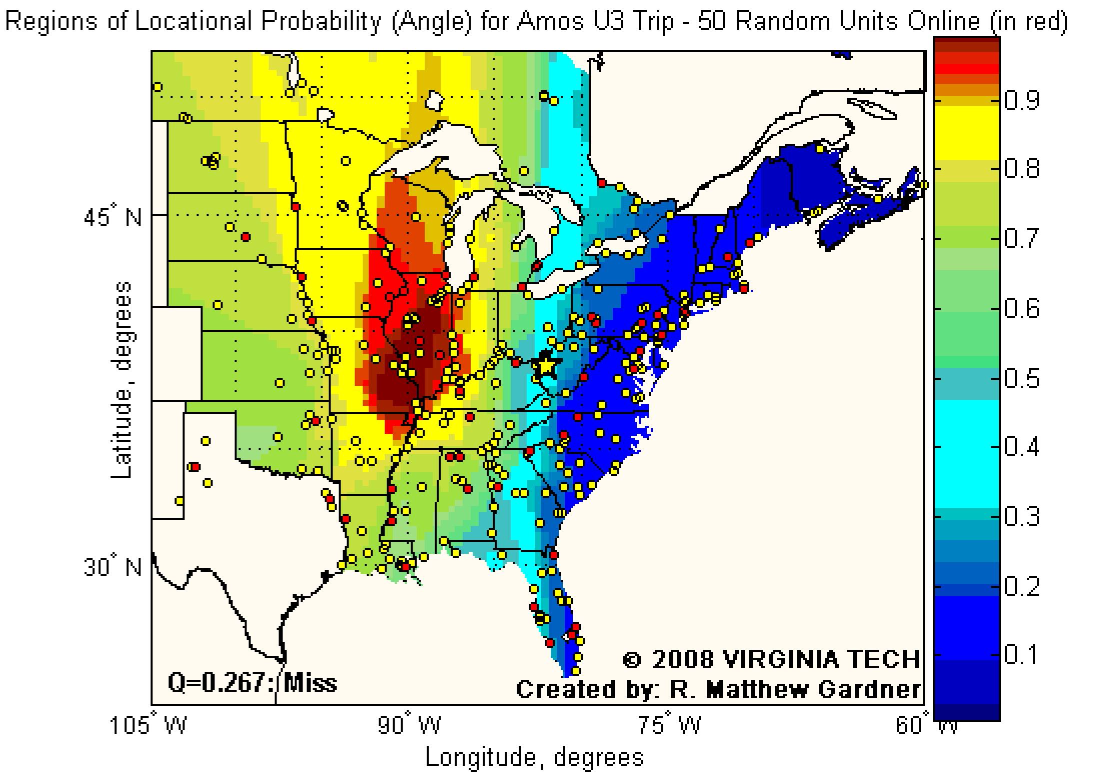
Regions of Locational Probability (Angle) for Amos U3 Trip - 50 Random Units Online (in red)
45° N
30° N
Latitude, degrees
105° W
90° W
75° W
60° W
Longitude, degrees
Q=0.267: Miss
© 2008 VIRGINIA TECH
Created by: R. Matthew Gardner
0.9
0.8
0.7
0.6
0.5
0.4
0.3
0.2
0.1

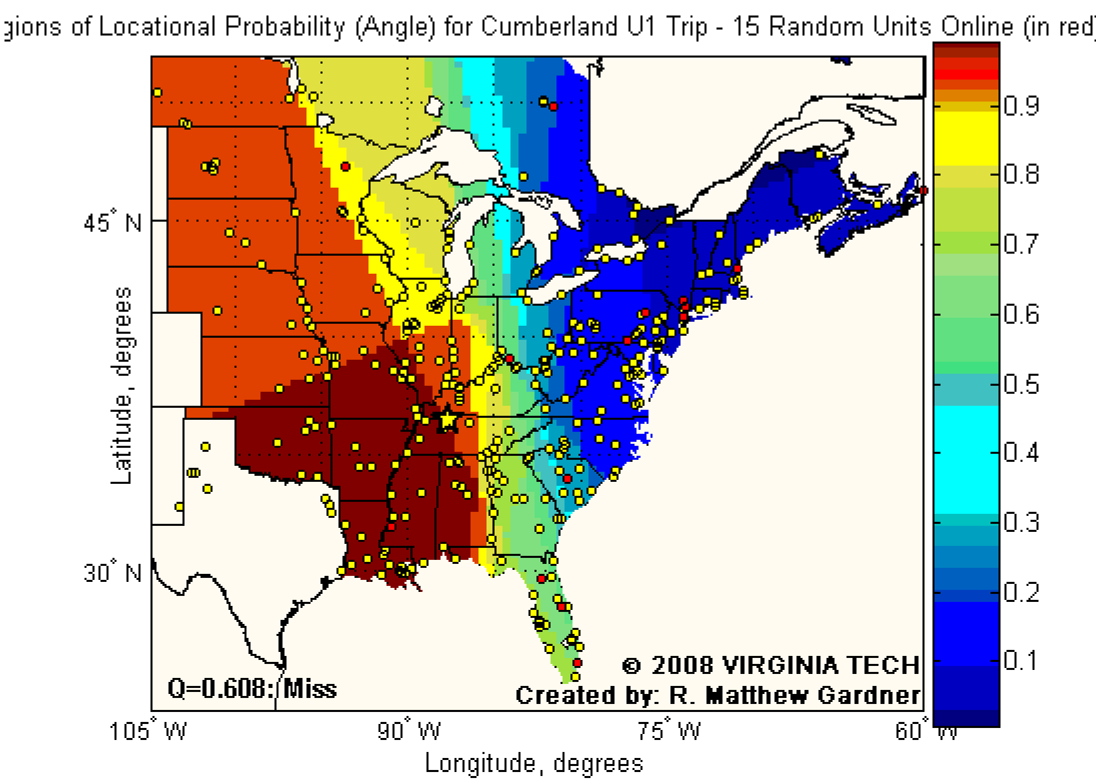
gions of Locational Probability (Angle) for Cumberland U1 Trip - 15 Random Units Online (in red)
45° N
30° N
Latitude, degrees
105° W
90° W
75° W
60° W
Longitude, degrees
Q=0.608: Miss
© 2008 VIRGINIA TECH
Created by: R. Matthew Gardner
0.9
0.8
0.7
0.6
0.5
0.4
0.3
0.2
0.1

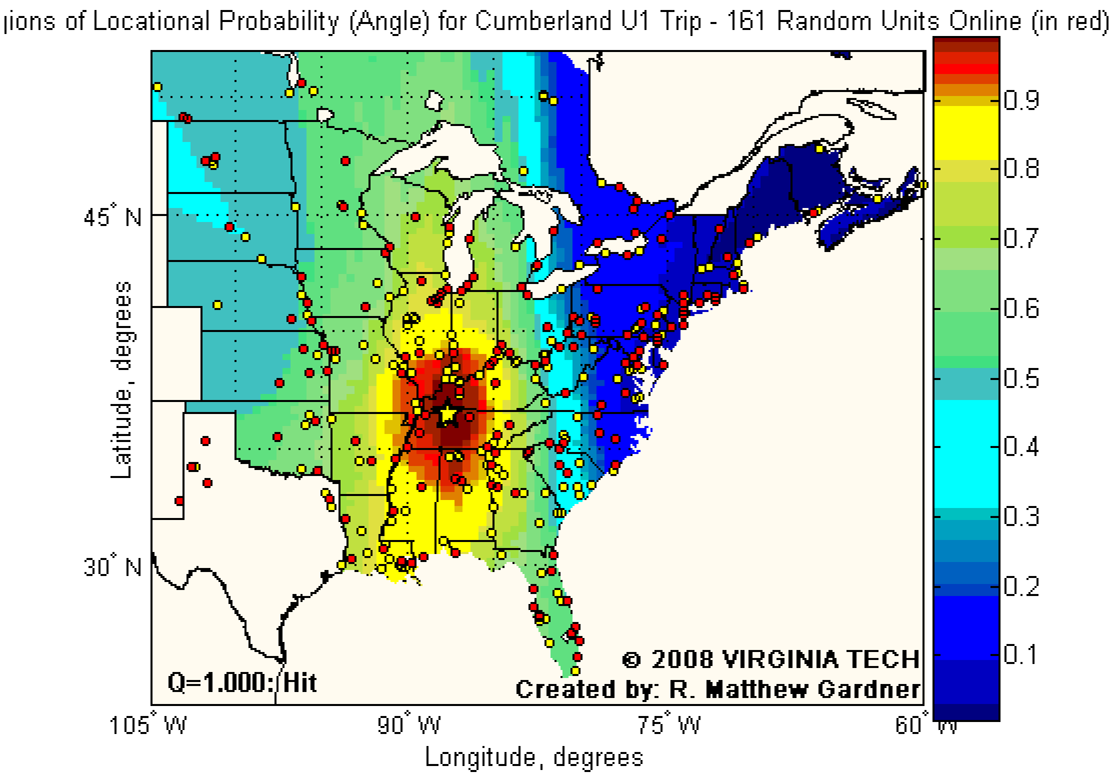
jions of Locational Probability (Angle) for Cumberland U1 Trip - 161 Random Units Online (in red)
45° N
30° N
Latitude, degrees
105° W
90° W
75° W
60° W
Longitude, degrees
Q=1.000: Hit
© 2008 VIRGINIA TECH
Created by: R. Matthew Gardner
0.9
0.8
0.7
0.6
0.5
0.4
0.3
0.2
0.1

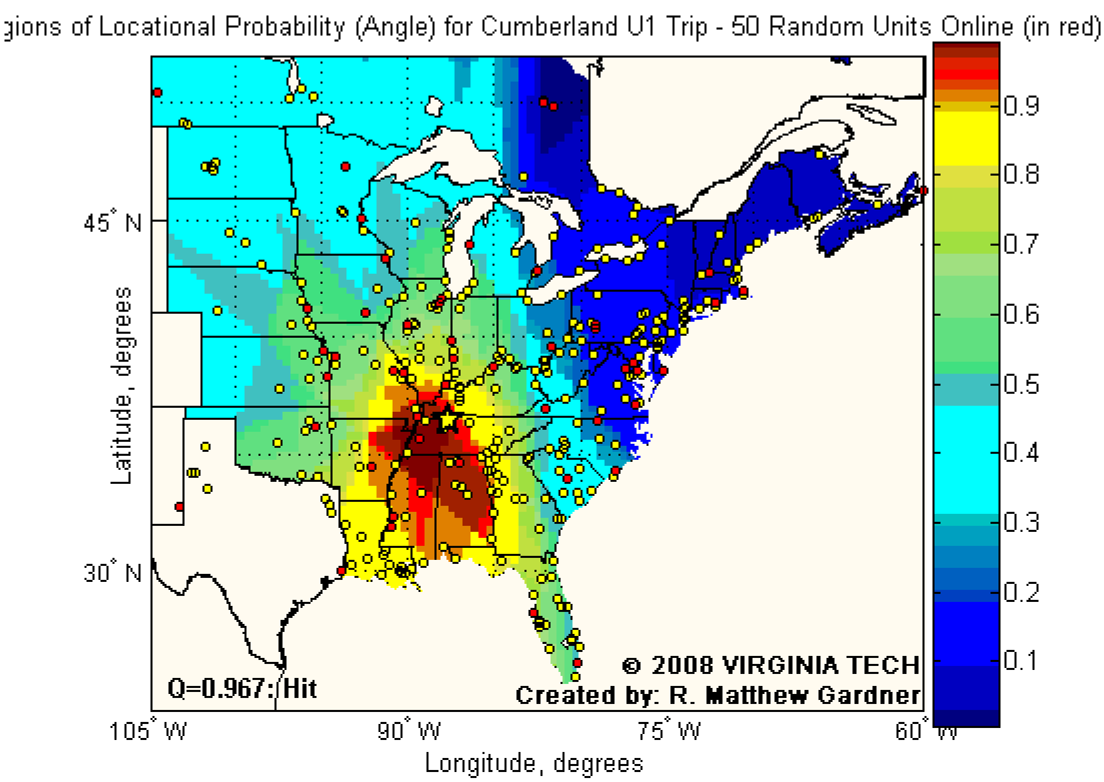
gions of Locational Probability (Angle) for Cumberland U1 Trip - 50 Random Units Online (in red)
45° N
30° N
Latitude, degrees
105° W
90° W
75° W
60° W
Longitude, degrees
Q=0.967: Hit
© 2008 VIRGINIA TECH
Created by: R. Matthew Gardner
0.9
0.8
0.7
0.6
0.5
0.4
0.3
0.2
0.1

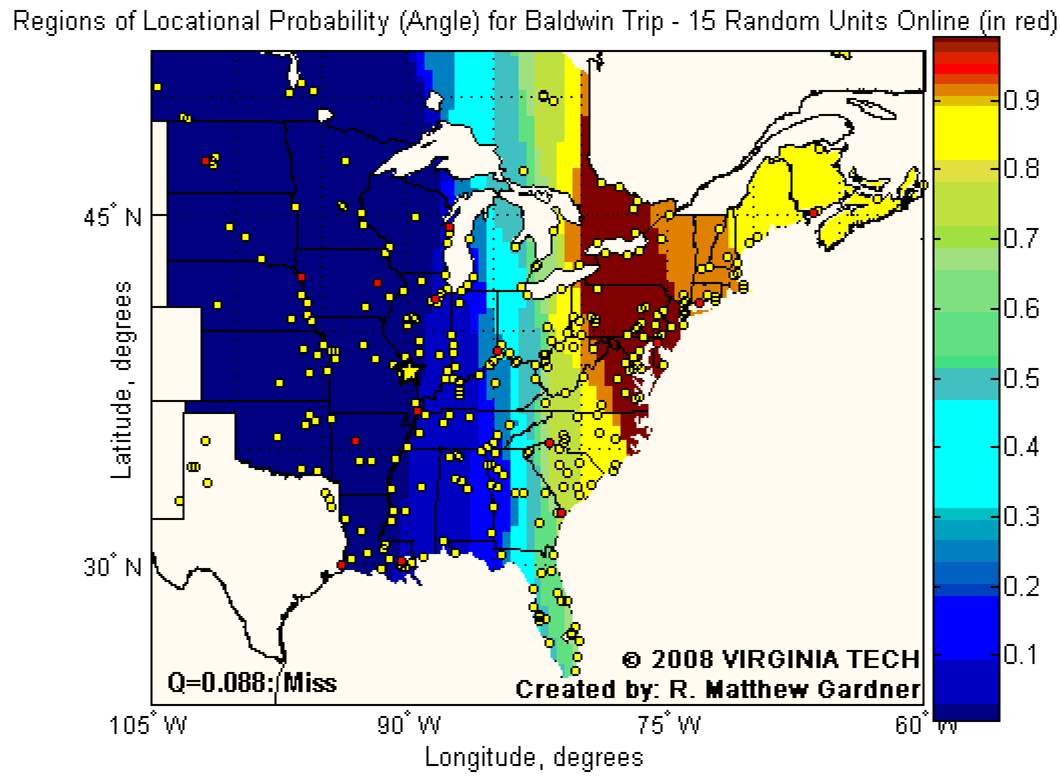
Regions of Locational Probability (Angle) for Baldwin Trip - 15 Random Units Online (in red)
45° N
30° N
Latitude, degrees
105° W
90° W
75° W
60° W
Longitude, degrees
Q=0.088: Miss
© 2008 VIRGINIA TECH
Created by: R. Matthew Gardner
0.9
0.8
0.7
0.6
0.5
0.4
0.3
0.2
0.1

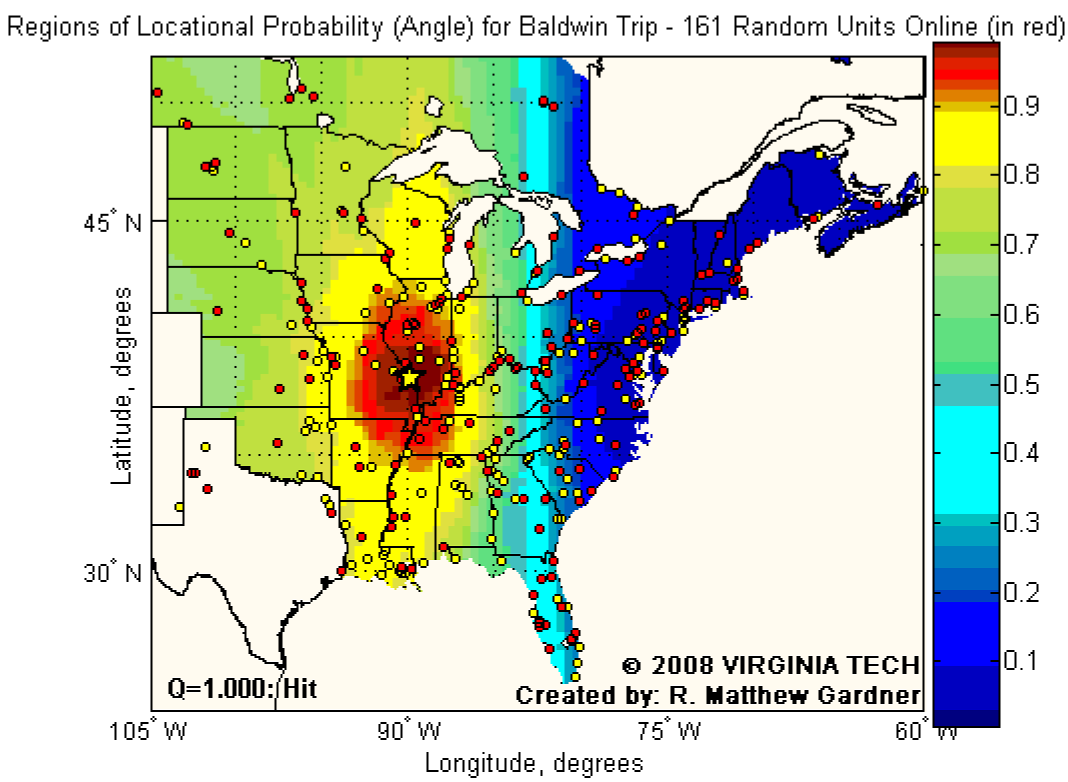
Regions of Locational Probability (Angle) for Baldwin Trip - 161 Random Units Online (in red)
45° N
30° N
Latitude, degrees
105° W
90° W
75° W
60° W
Longitude, degrees
Q=1.000: Hit
© 2008 VIRGINIA TECH
Created by: R. Matthew Gardner
0.9
0.8
0.7
0.6
0.5
0.4
0.3
0.2
0.1

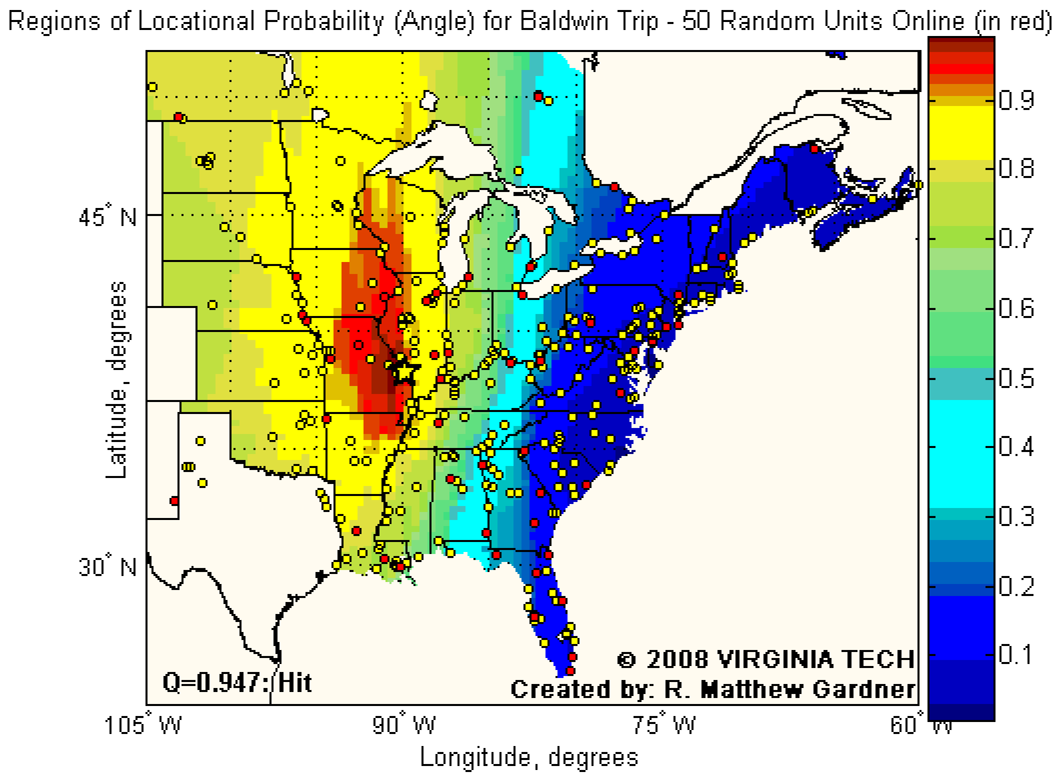
Regions of Locational Probability (Angle) for Baldwin Trip - 50 Random Units Online (in red)
45° N
30° N
Latitude, degrees
105° W
90° W
75° W
60° W
Longitude, degrees
Q=0.947: Hit
© 2008 VIRGINIA TECH
Created by: R. Matthew Gardner
0.9
0.8
0.7
0.6
0.5
0.4
0.3
0.2
0.1

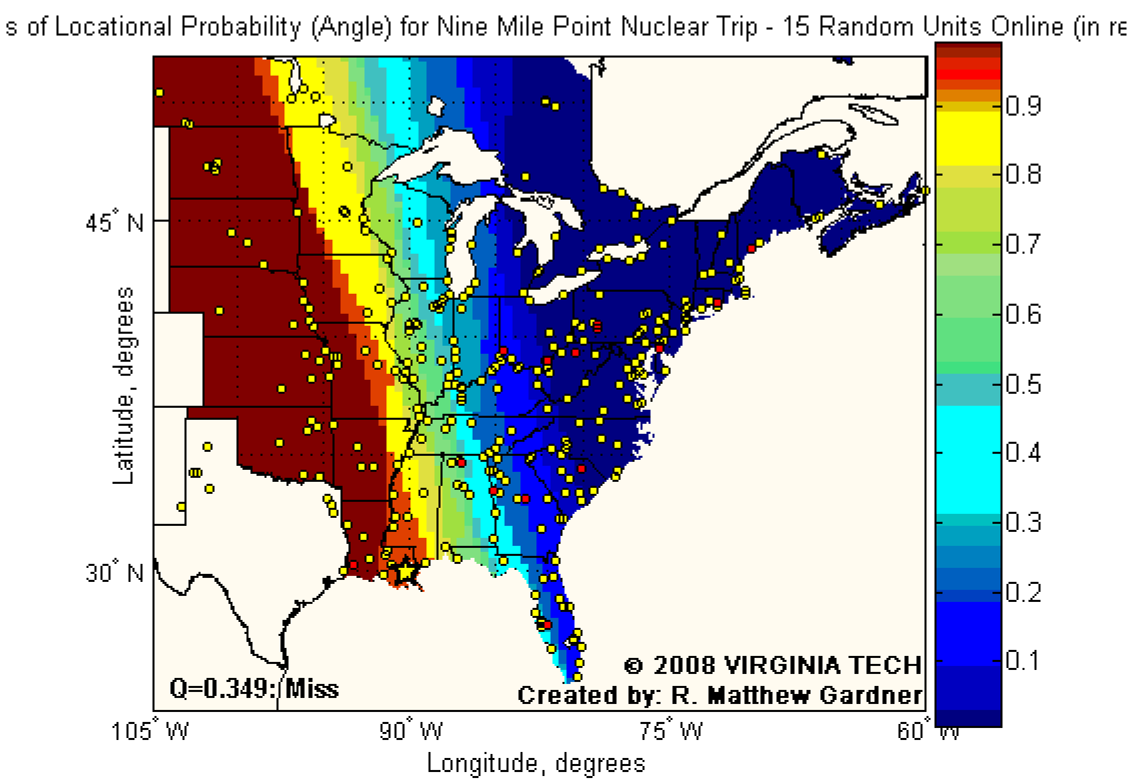
s of Locational Probability (Angle) for Nine Mile Point Nuclear Trip - 15 Random Units Online (in re
45° N
30° N
Latitude, degrees
105° W
90° W
75° W
60° W
Longitude, degrees
Q=0.349: Miss
© 2008 VIRGINIA TECH
Created by: R. Matthew Gardner
0.9
0.8
0.7
0.6
0.5
0.4
0.3
0.2
0.1

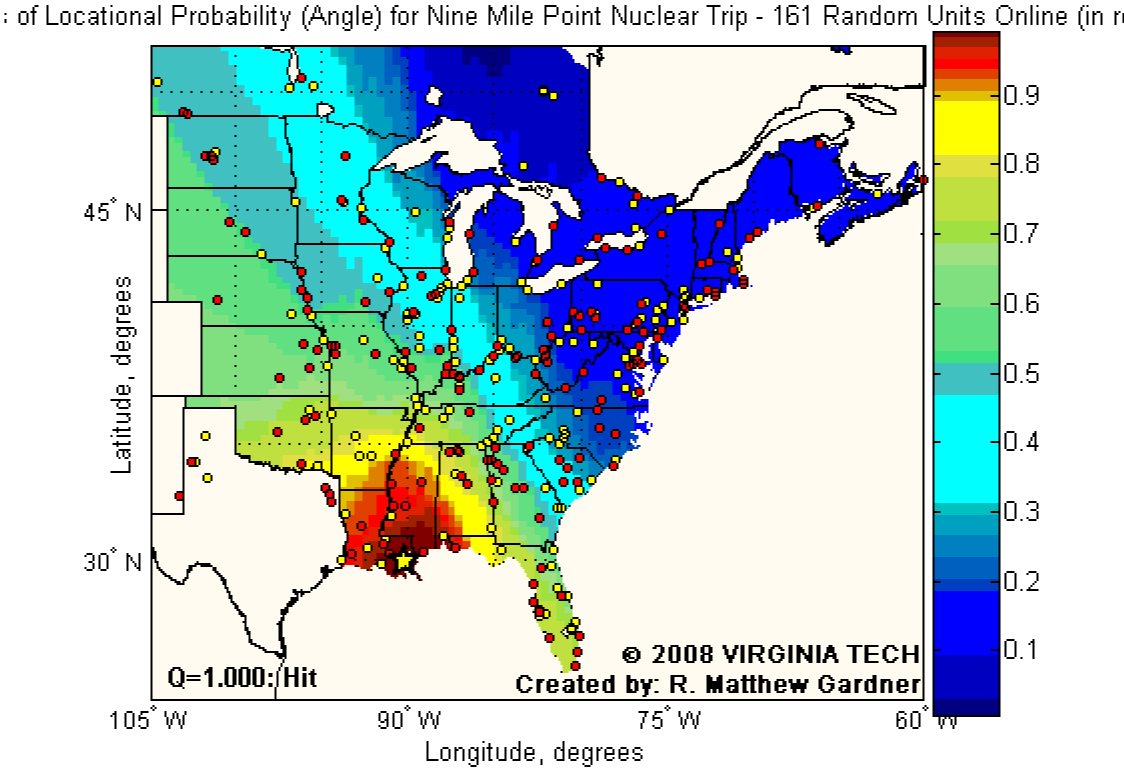
: of Locational Probability (Angle) for Nine Mile Point Nuclear Trip - 161 Random Units Online (in r
45° N
30° N
Latitude, degrees
105° W
90° W
75° W
60° W
Longitude, degrees
Q=1.000:/Hit
© 2008 VIRGINIA TECH
Created by: R. Matthew Gardner
0.9
0.8
0.7
0.6
0.5
0.4
0.3
0.2
0.1

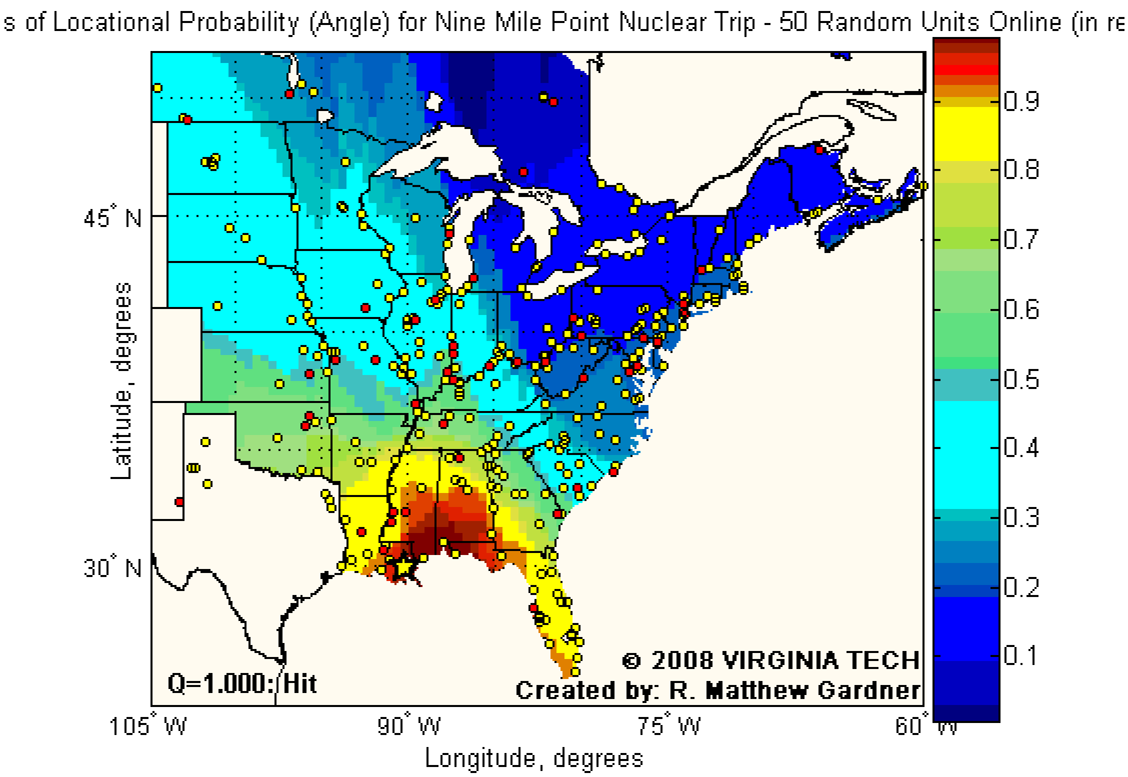
s of Locational Probability (Angle) for Nine Mile Point Nuclear Trip - 50 Random Units Online (in re
45° N
30° N
Latitude, degrees
105° W
90° W
75° W
60° W
Longitude, degrees
Q=1.000:/Hit
© 2008 VIRGINIA TECH
Created by: R. Matthew Gardner
0.9
0.8
0.7
0.6
0.5
0.4
0.3
0.2
0.1

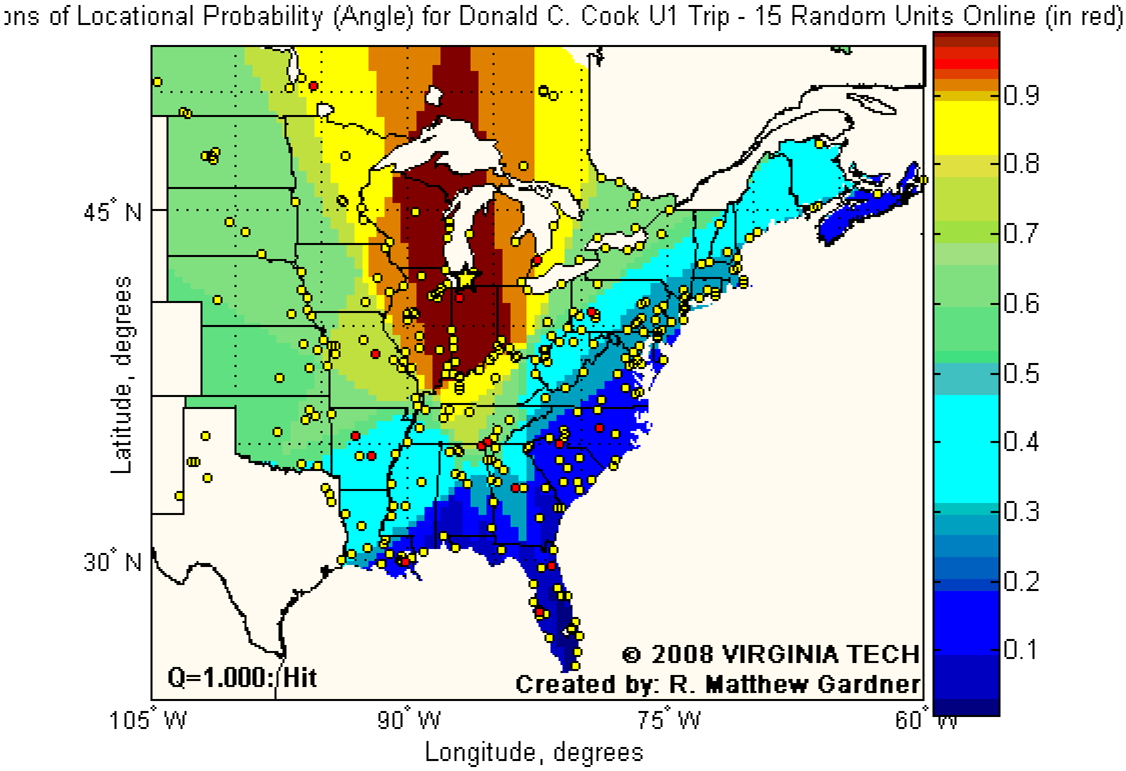
ons of Locational Probability (Angle) for Donald C. Cook U1 Trip - 15 Random Units Online (in red)
45° N
30° N
Latitude, degrees
105° W
90° W
75° W
60° W
Longitude, degrees
0.9
0.8
0.7
0.6
0.5
0.4
0.3
0.2
0.1
Q=1.000:/Hit
© 2008 VIRGINIA TECH
Created by: R. Matthew Gardner

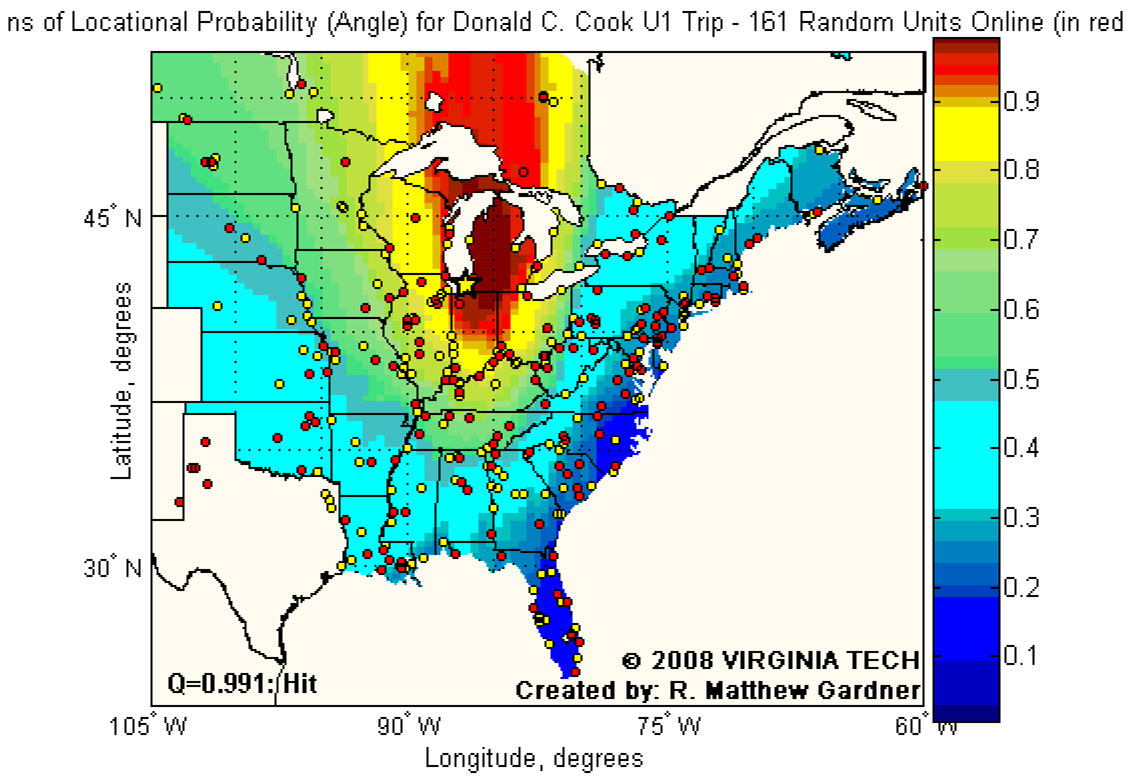
ns of Locational Probability (Angle) for Donald C. Cook U1 Trip - 161 Random Units Online (in red
45° N
30° N
Latitude, degrees
105° W
90° W
75° W
60° W
Longitude, degrees
0.9
0.8
0.7
0.6
0.5
0.4
0.3
0.2
0.1
Q=0.991:/Hit
© 2008 VIRGINIA TECH
Created by: R. Matthew Gardner

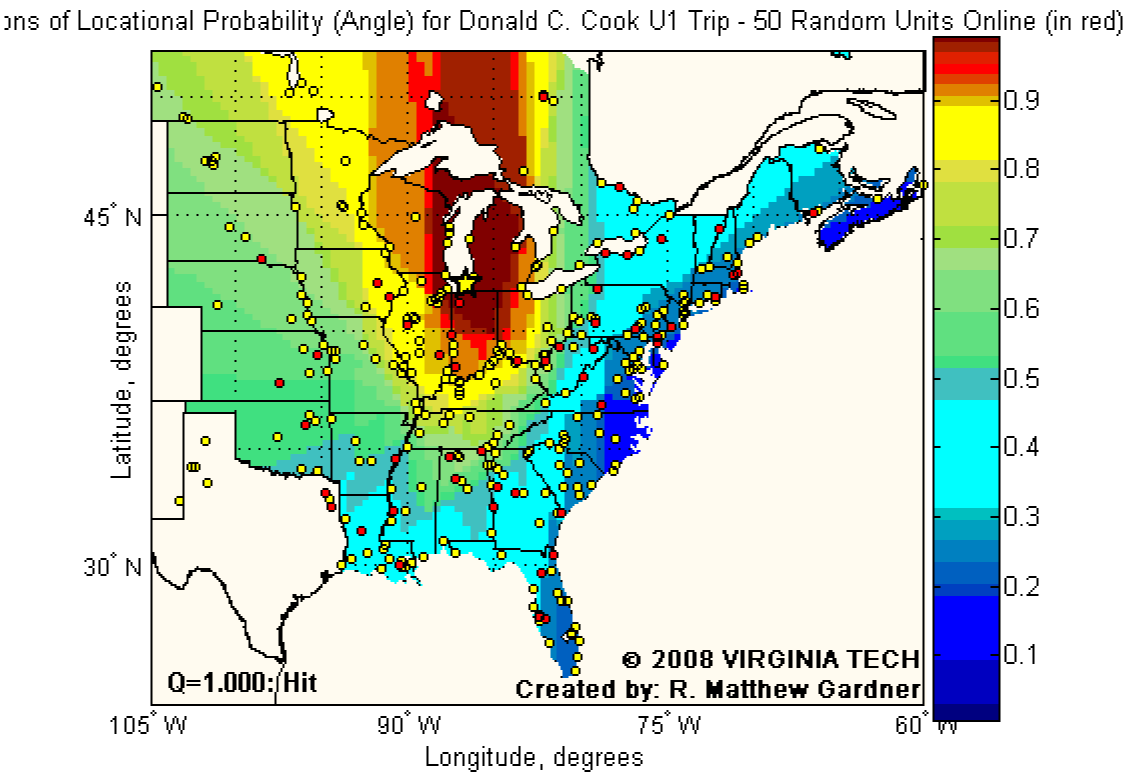

ons of Locational Probability (Angle) for Donald C. Cook U1 Trip - 50 Random Units Online (in red)
45° N
30° N
Latitude, degrees
105° W
90° W
75° W
60° W
Longitude, degrees
Q=1.000: Hit
© 2008 VIRGINIA TECH
Created by: R. Matthew Gardner
0.9
0.8
0.7
0.6
0.5
0.4
0.3
0.2
0.1

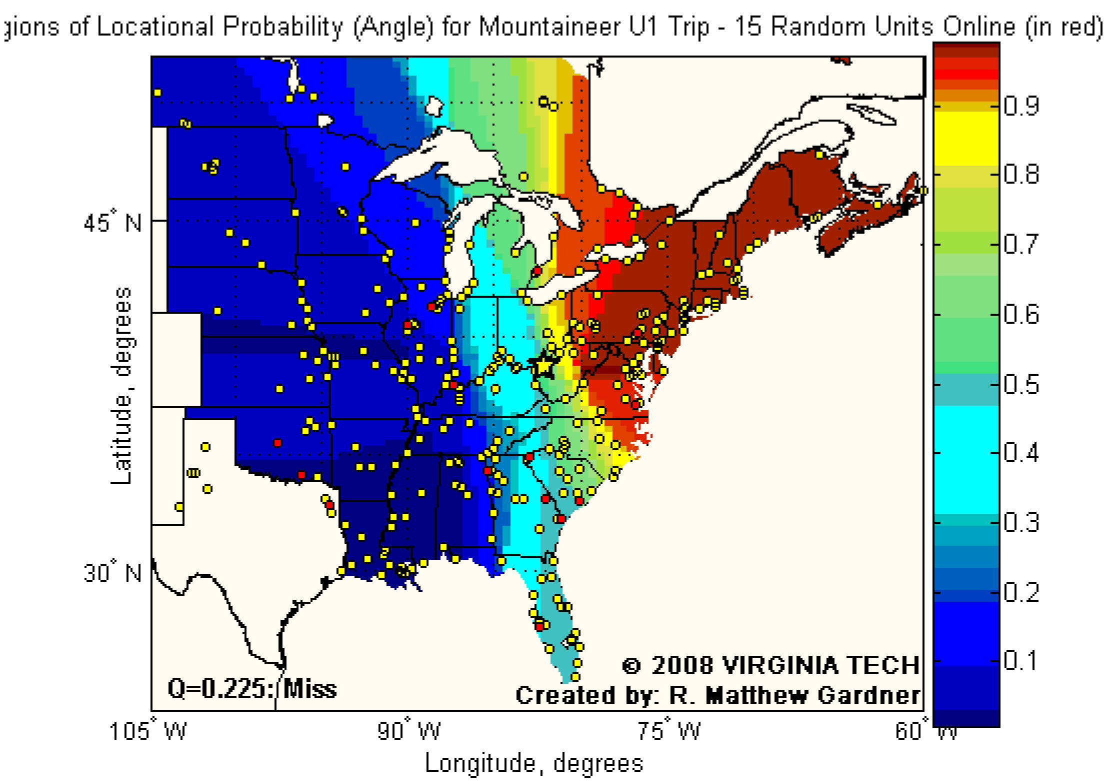

gions of Locational Probability (Angle) for Mountaineer U1 Trip - 15 Random Units Online (in red)
45° N
30° N
Latitude, degrees
105° W
90° W
75° W
60° W
Longitude, degrees
Q=0.225: Miss
© 2008 VIRGINIA TECH
Created by: R. Matthew Gardner
0.9
0.8
0.7
0.6
0.5
0.4
0.3
0.2
0.1

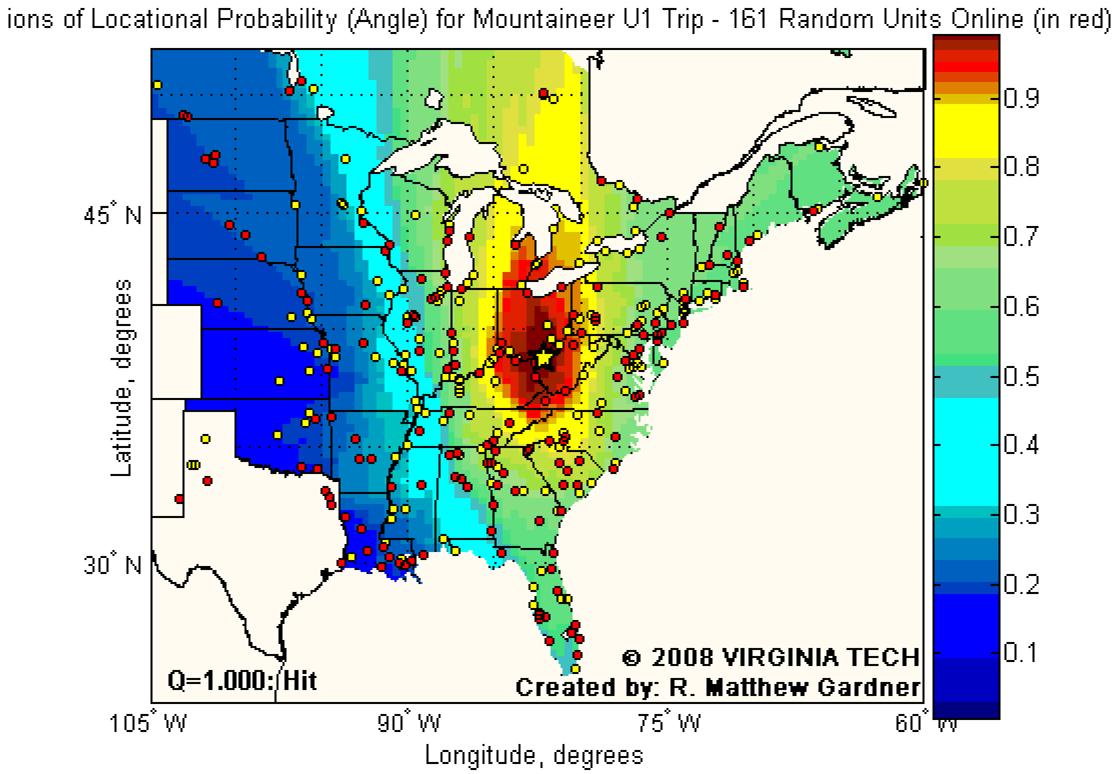
ions of Locational Probability (Angle) for Mountaineer U1 Trip - 161 Random Units Online (in red)
45° N
30° N
Latitude, degrees
105° W
90° W
75° W
60° W
Longitude, degrees
0.9
0.8
0.7
0.6
0.5
0.4
0.3
0.2
0.1
Q=1.000:/Hit
© 2008 VIRGINIA TECH
Created by: R. Matthew Gardner

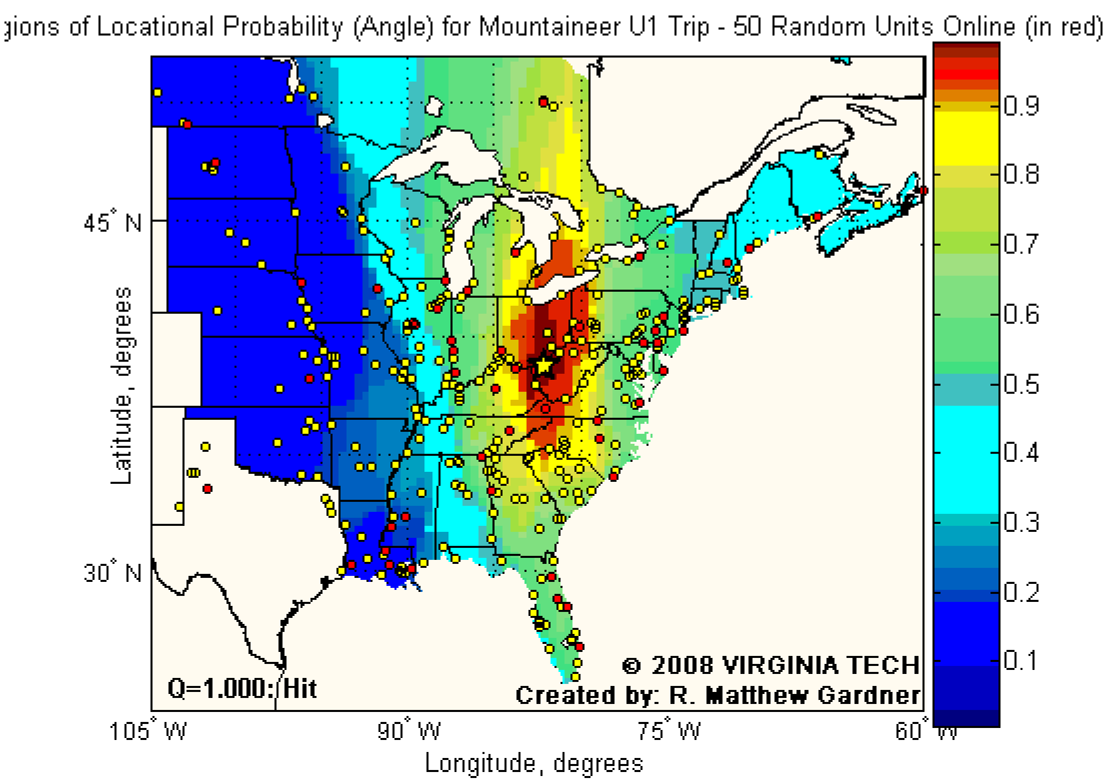
gions of Locational Probability (Angle) for Mountaineer U1 Trip - 50 Random Units Online (in red)
45° N
30° N
Latitude, degrees
105° W
90° W
75° W
60° W
Longitude, degrees
0.9
0.8
0.7
0.6
0.5
0.4
0.3
0.2
0.1
Q=1.000:/Hit
© 2008 VIRGINIA TECH
Created by: R. Matthew Gardner

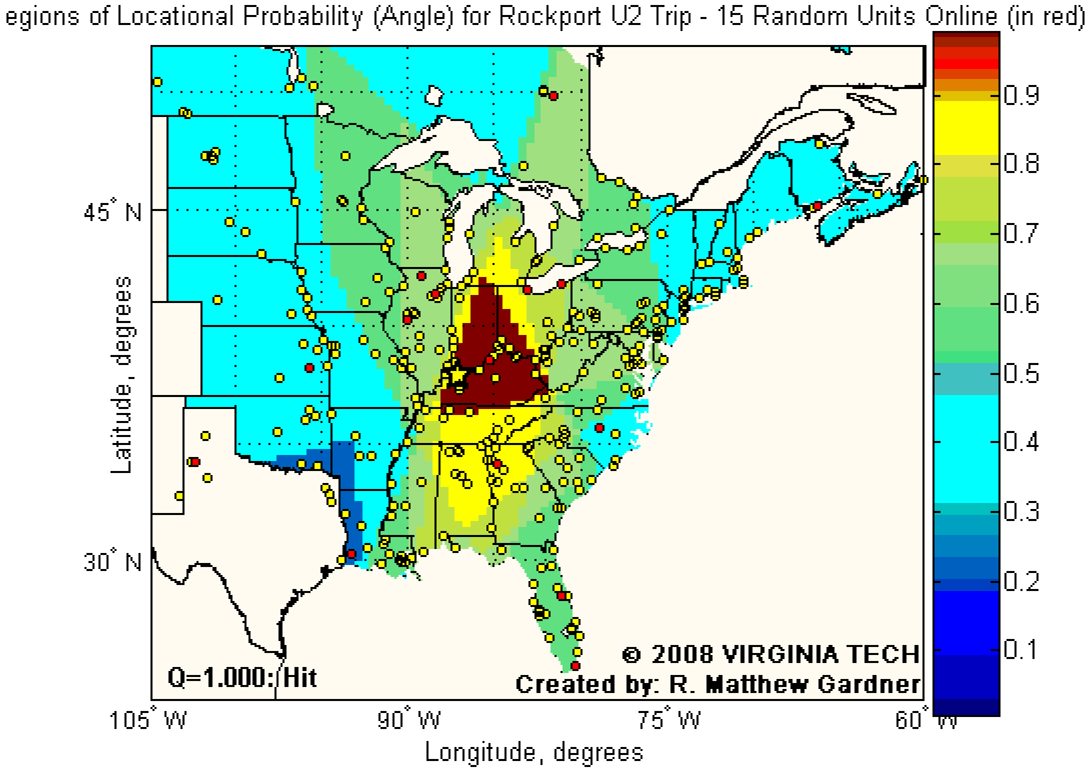
egions of Locational Probability (Angle) for Rockport U2 Trip - 15 Random Units Online (in red)
45° N
30° N
Latitude, degrees
105° W
90° W
75° W
60° W
Longitude, degrees
Q=1.000:/Hit
© 2008 VIRGINIA TECH
Created by: R. Matthew Gardner
0.9
0.8
0.7
0.6
0.5
0.4
0.3
0.2
0.1

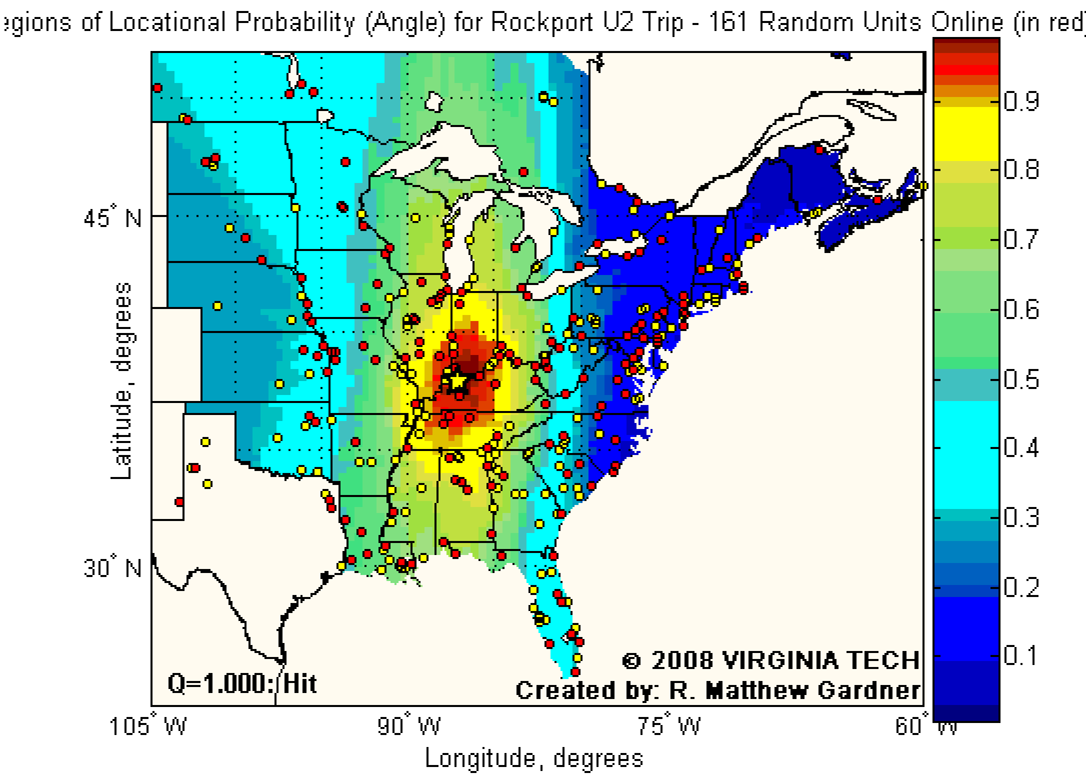
egions of Locational Probability (Angle) for Rockport U2 Trip - 161 Random Units Online (in red)
45° N
30° N
Latitude, degrees
105° W
90° W
75° W
60° W
Longitude, degrees
Q=1.000:/Hit
© 2008 VIRGINIA TECH
Created by: R. Matthew Gardner
0.9
0.8
0.7
0.6
0.5
0.4
0.3
0.2
0.1

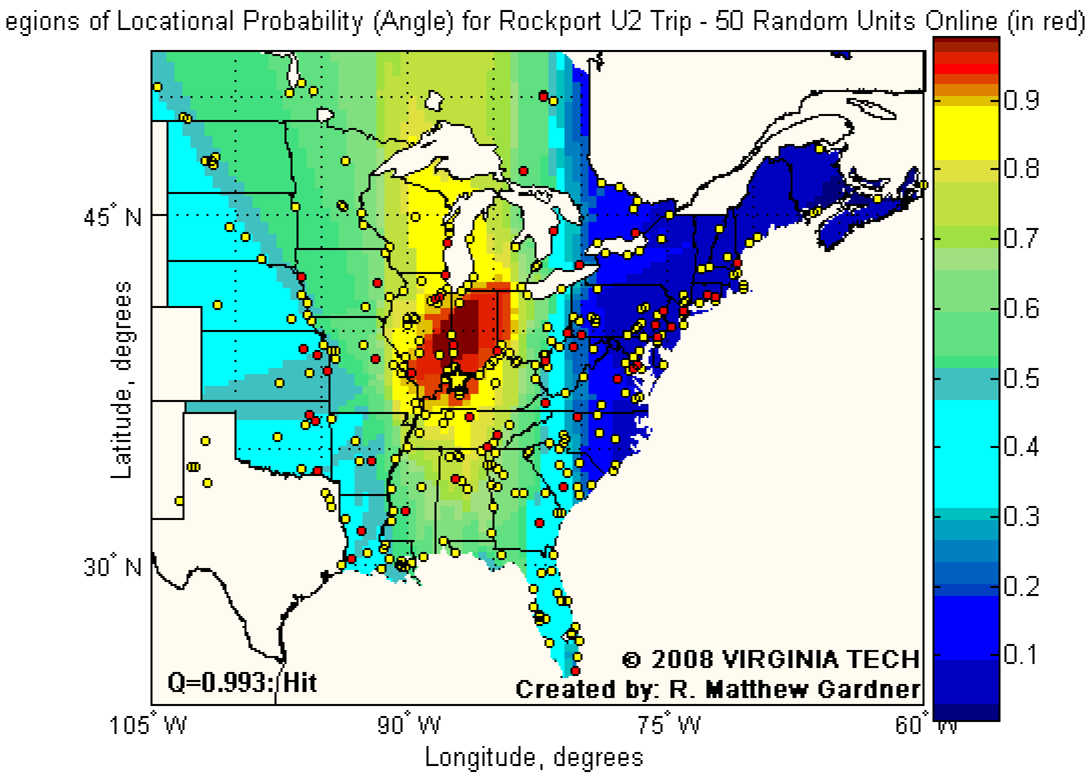
egions of Locational Probability (Angle) for Rockport U2 Trip - 50 Random Units Online (in red)
45° N
30° N
Latitude, degrees
105° W
90° W
75° W
60° W
Longitude, degrees
Q=0.993: Hit
© 2008 VIRGINIA TECH
Created by: R. Matthew Gardner
0.9
0.8
0.7
0.6
0.5
0.4
0.3
0.2
0.1

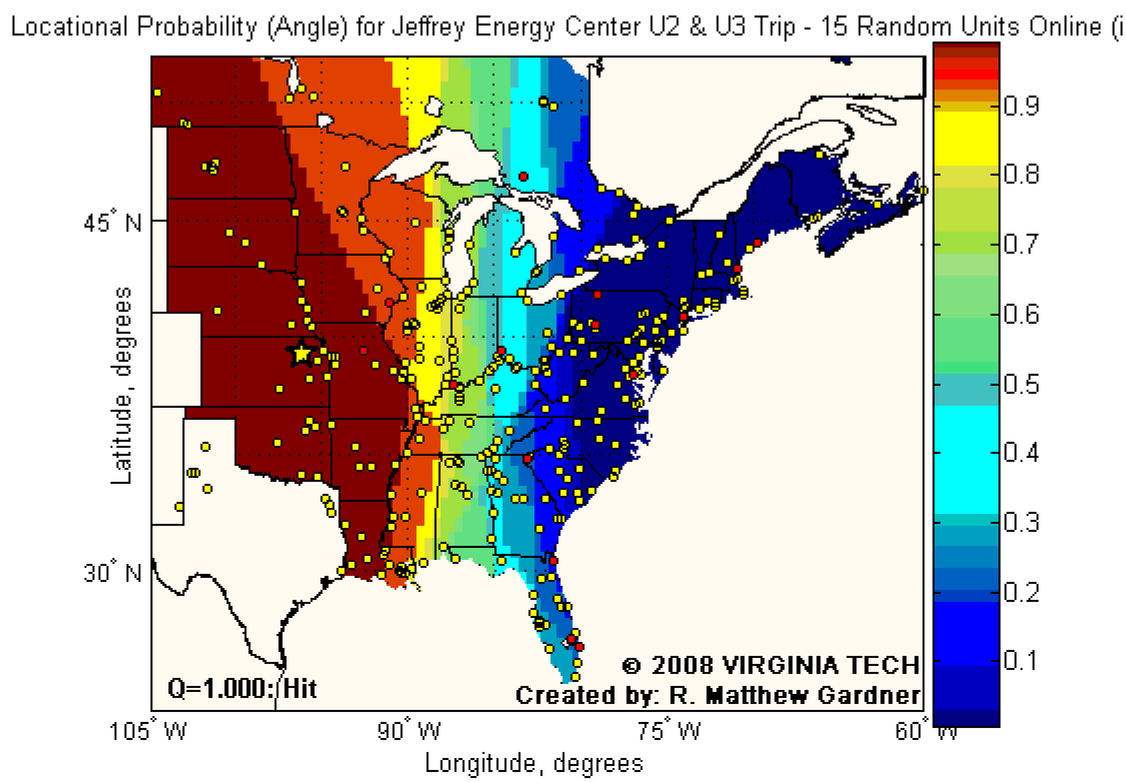
Locational Probability (Angle) for Jeffrey Energy Center U2 & U3 Trip - 15 Random Units Online (i
45° N
30° N
Latitude, degrees
105° W
90° W
75° W
60° W
Longitude, degrees
Q=1.000: Hit
© 2008 VIRGINIA TECH
Created by: R. Matthew Gardner
0.9
0.8
0.7
0.6
0.5
0.4
0.3
0.2
0.1

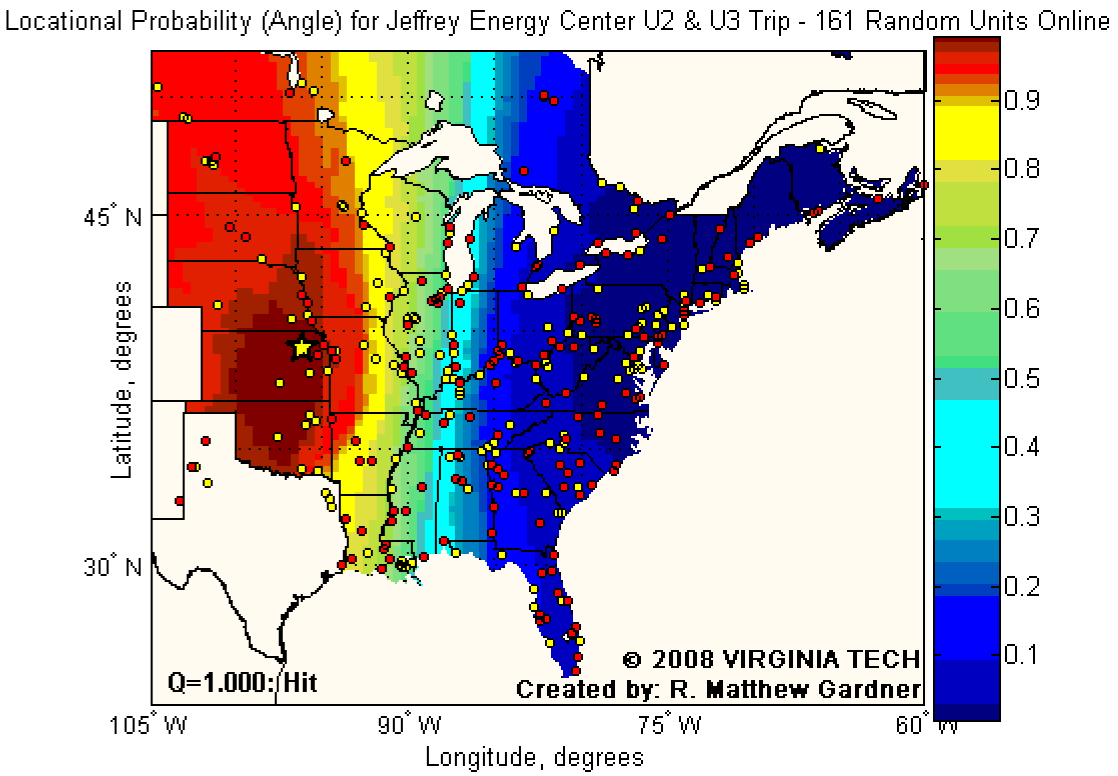
Locational Probability (Angle) for Jeffrey Energy Center U2 & U3 Trip - 161 Random Units Online (
Q=1.000: Hit
© 2008 VIRGINIA TECH
Created by: R. Matthew Gardner
45° N
30° N
Latitude, degrees
105° W
90° W
75° W
60° W
Longitude, degrees
0.9
0.8
0.7
0.6
0.5
0.4
0.3
0.2
0.1

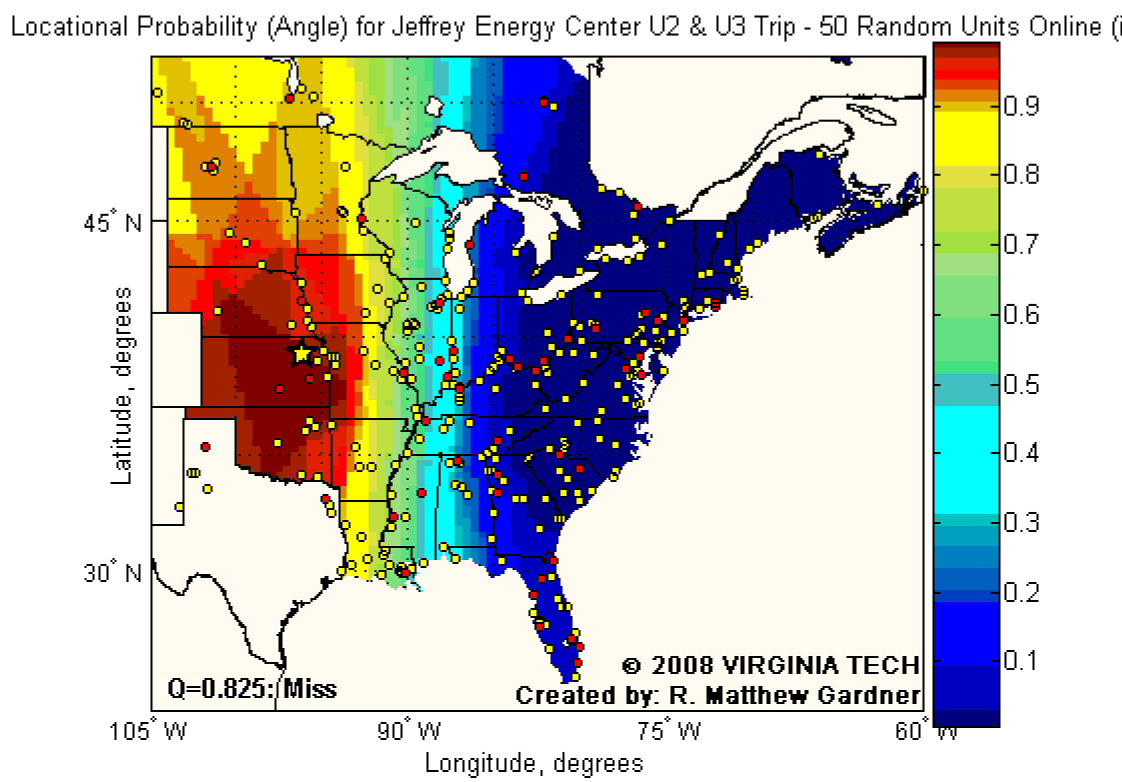
Locational Probability (Angle) for Jeffrey Energy Center U2 & U3 Trip - 50 Random Units Online (i
Q=0.825: Miss
© 2008 VIRGINIA TECH
Created by: R. Matthew Gardner
45° N
30° N
Latitude, degrees
105° W
90° W
75° W
60° W
Longitude, degrees
0.9
0.8
0.7
0.6
0.5
0.4
0.3
0.2
0.1

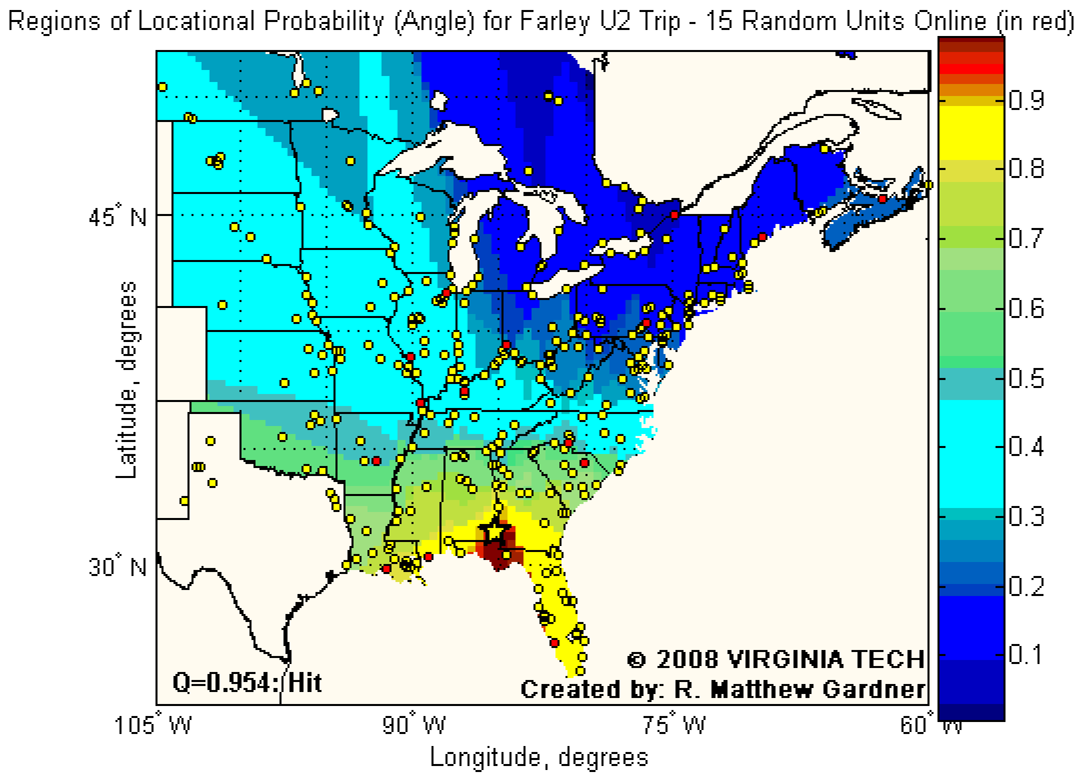
Regions of Locational Probability (Angle) for Farley U2 Trip - 15 Random Units Online (in red)
45° N
30° N
Latitude, degrees
105° W
90° W
75° W
60° W
Longitude, degrees
Q=0.954: Hit
© 2008 VIRGINIA TECH
Created by: R. Matthew Gardner
0.9
0.8
0.7
0.6
0.5
0.4
0.3
0.2
0.1

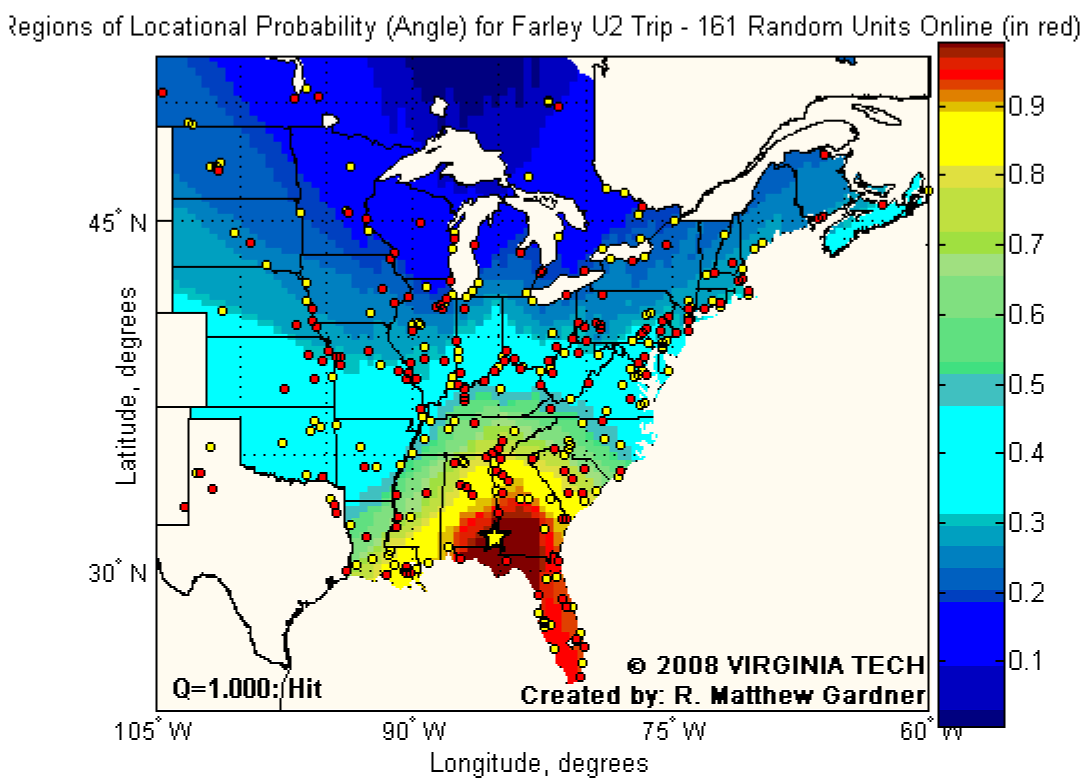
Regions of Locational Probability (Angle) for Farley U2 Trip - 161 Random Units Online (in red)
45° N
30° N
Latitude, degrees
105° W
90° W
75° W
60° W
Longitude, degrees
Q=1.000: Hit
© 2008 VIRGINIA TECH
Created by: R. Matthew Gardner
0.9
0.8
0.7
0.6
0.5
0.4
0.3
0.2
0.1

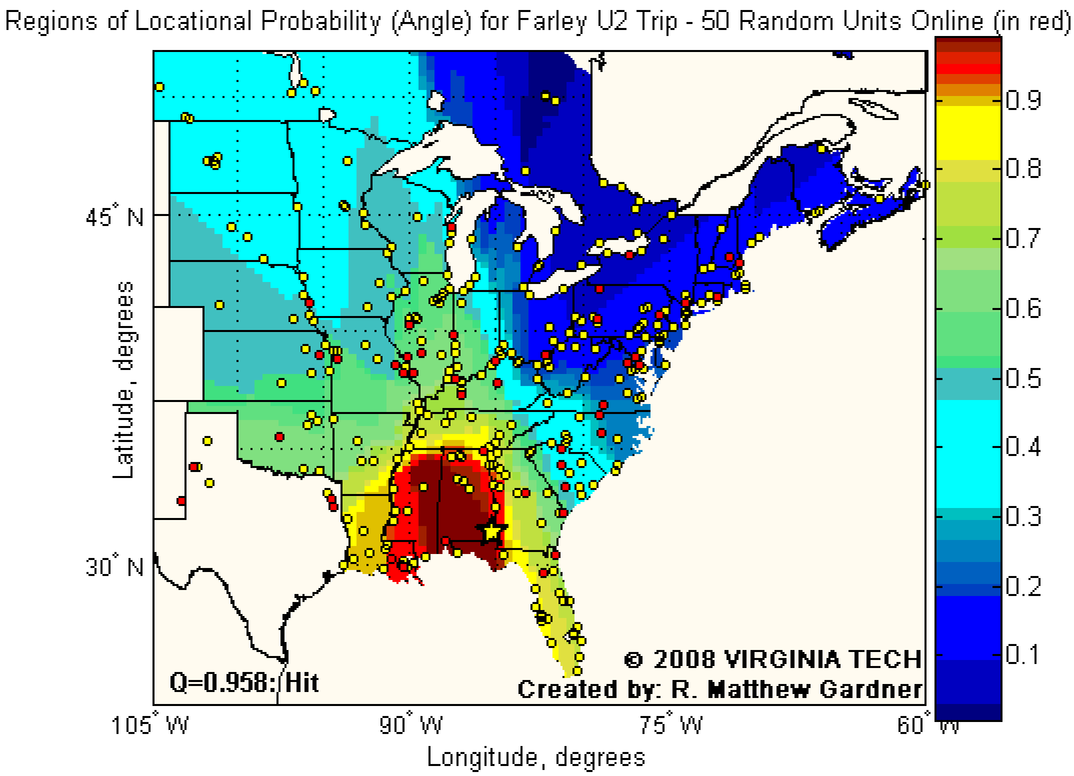
Regions of Locational Probability (Angle) for Farley U2 Trip - 50 Random Units Online (in red)
45° N
30° N
Latitude, degrees
105° W
90° W
75° W
60° W
Longitude, degrees
Q=0.958: Hit
© 2008 VIRGINIA TECH
Created by: R. Matthew Gardner
0.9
0.8
0.7
0.6
0.5
0.4
0.3
0.2
0.1

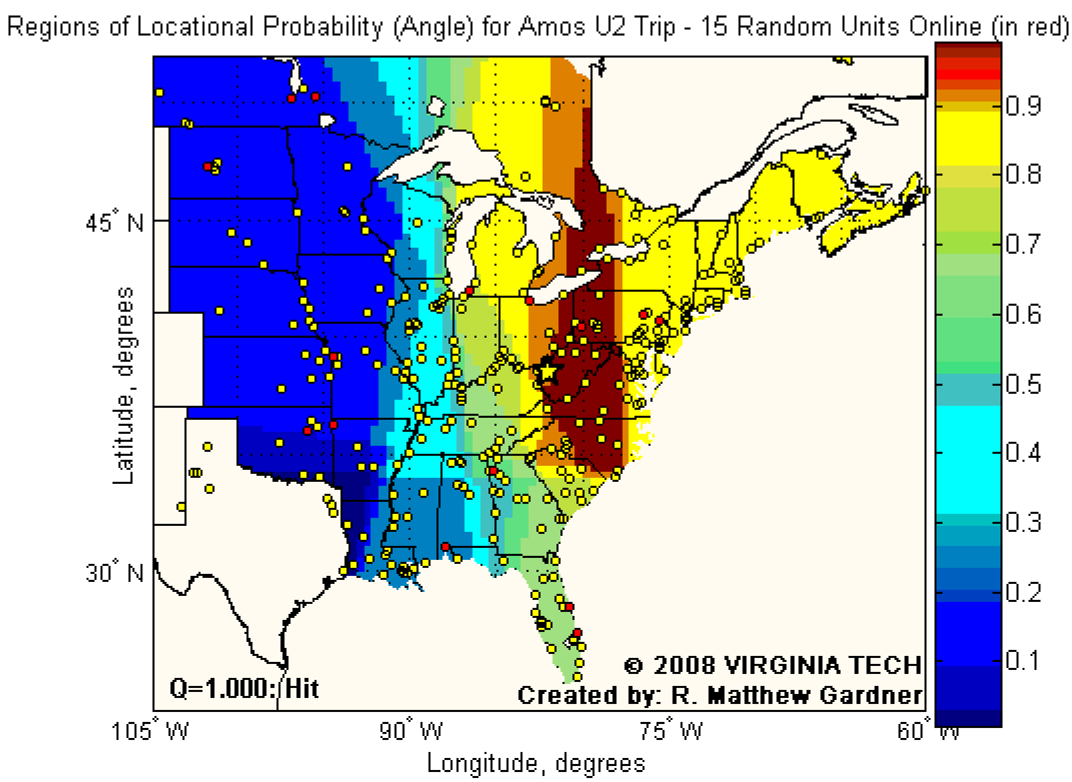
Regions of Locational Probability (Angle) for Amos U2 Trip - 15 Random Units Online (in red)
45° N
30° N
Latitude, degrees
105° W
90° W
75° W
60° W
Longitude, degrees
Q=1.000: Hit
© 2008 VIRGINIA TECH
Created by: R. Matthew Gardner
0.9
0.8
0.7
0.6
0.5
0.4
0.3
0.2
0.1

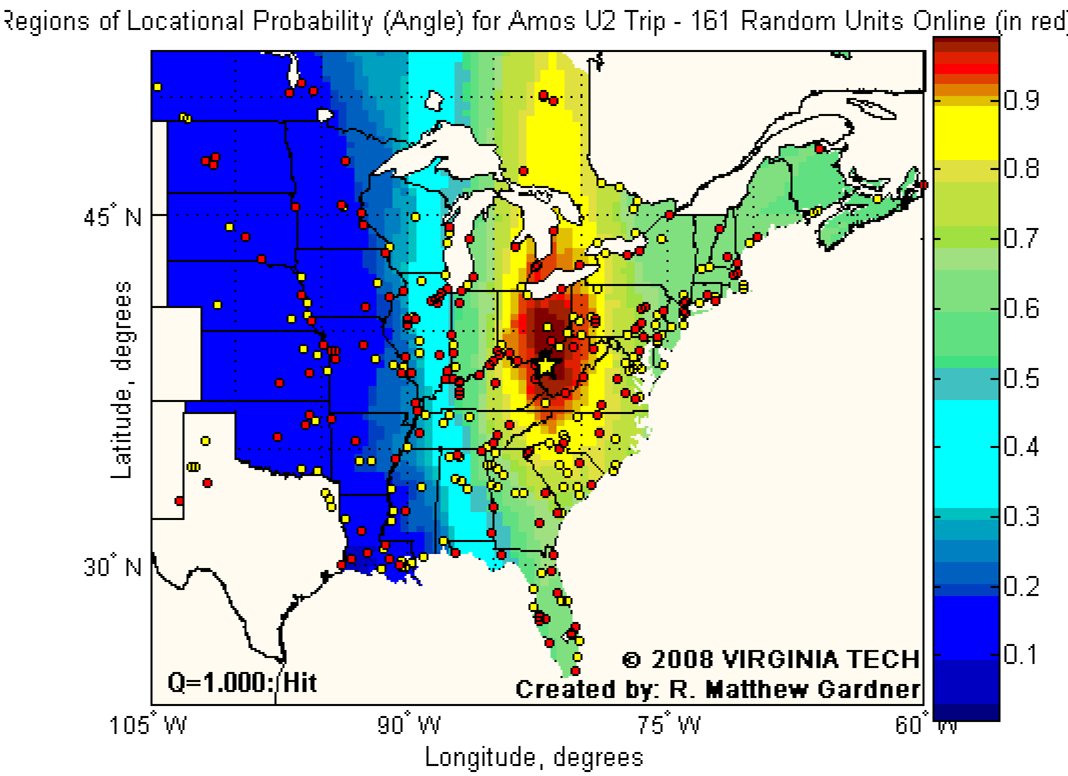
Regions of Locational Probability (Angle) for Amos U2 Trip - 161 Random Units Online (in red)
45° N
30° N
Latitude, degrees
105° W
90° W
75° W
60° W
Longitude, degrees
Q=1.000: Hit
© 2008 VIRGINIA TECH
Created by: R. Matthew Gardner
0.9
0.8
0.7
0.6
0.5
0.4
0.3
0.2
0.1

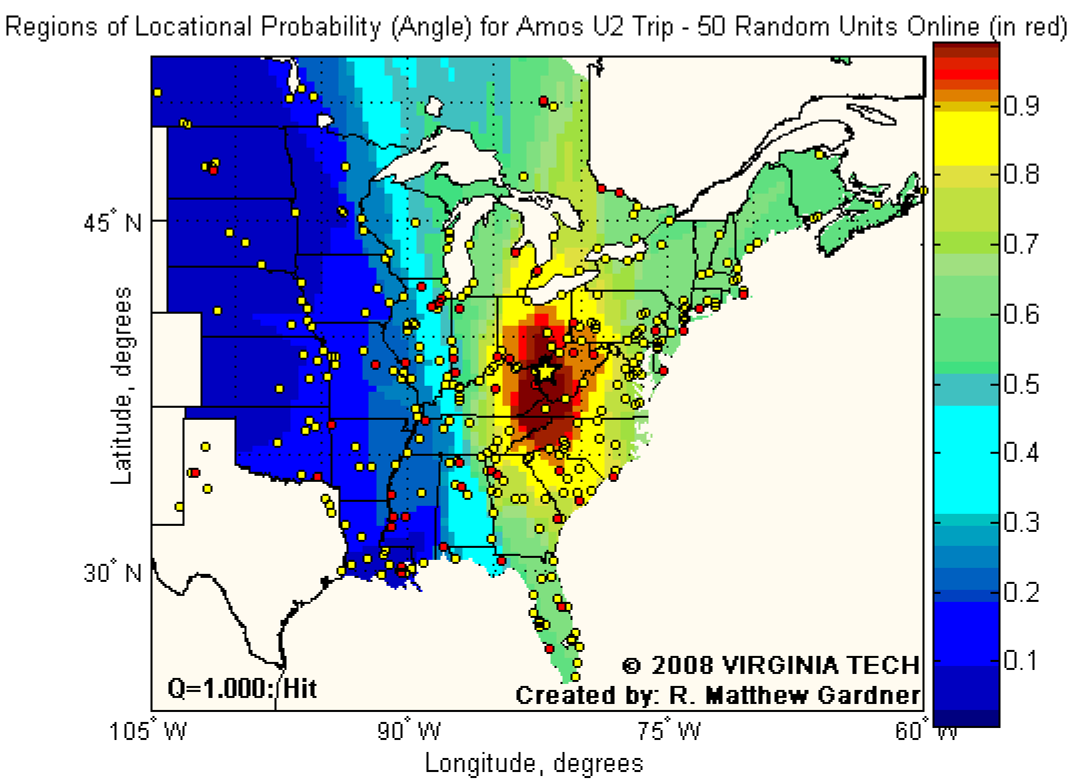
Regions of Locational Probability (Angle) for Amos U2 Trip - 50 Random Units Online (in red)
45° N
30° N
Latitude, degrees
105° W
90° W
75° W
60° W
Longitude, degrees
Q=1.000: Hit
© 2008 VIRGINIA TECH
Created by: R. Matthew Gardner
0.9
0.8
0.7
0.6
0.5
0.4
0.3
0.2
0.1

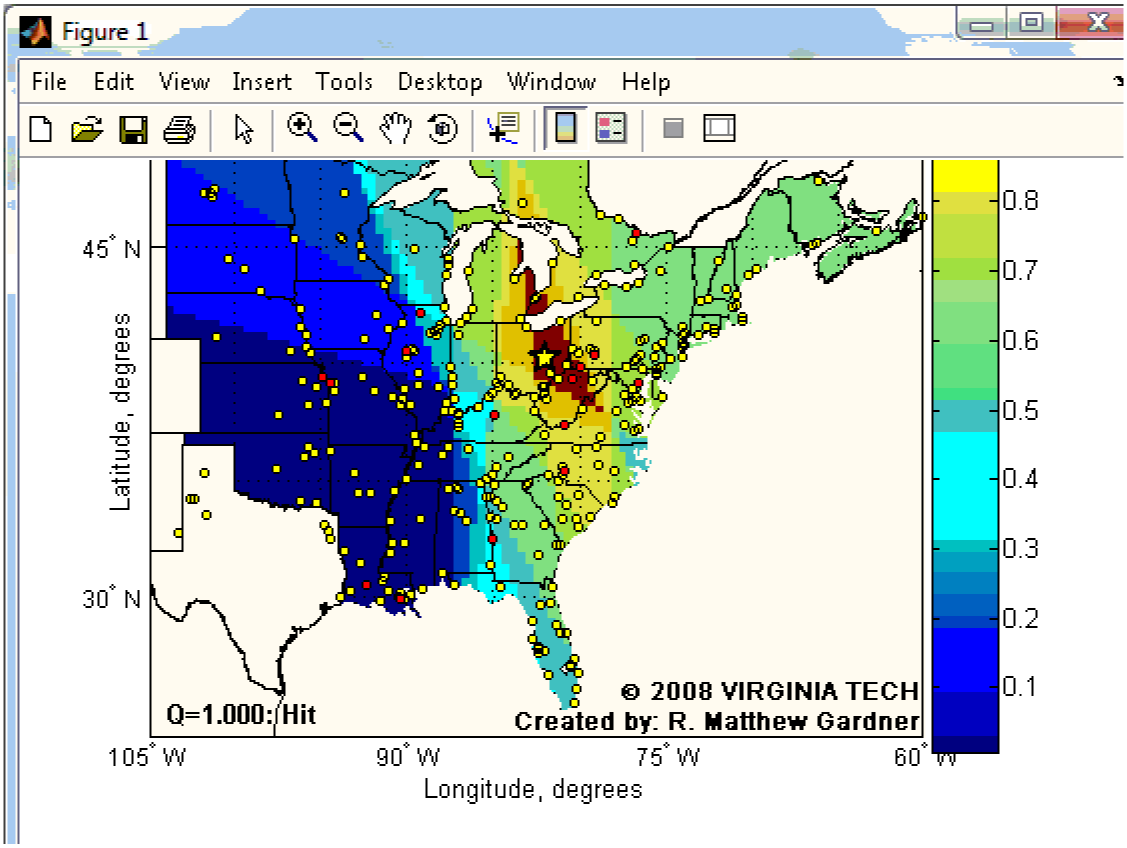
Figure 1
File Edit View Insert Tools Desktop Window Help
45° N
30° N
Latitude, degrees
105° W
90° W
75° W
60° W
Longitude, degrees
Q=1.000:/Hit
© 2008 VIRGINIA TECH
Created by: R. Matthew Gardner
0.8
0.7
0.6
0.5
0.4
0.3
0.2
0.1

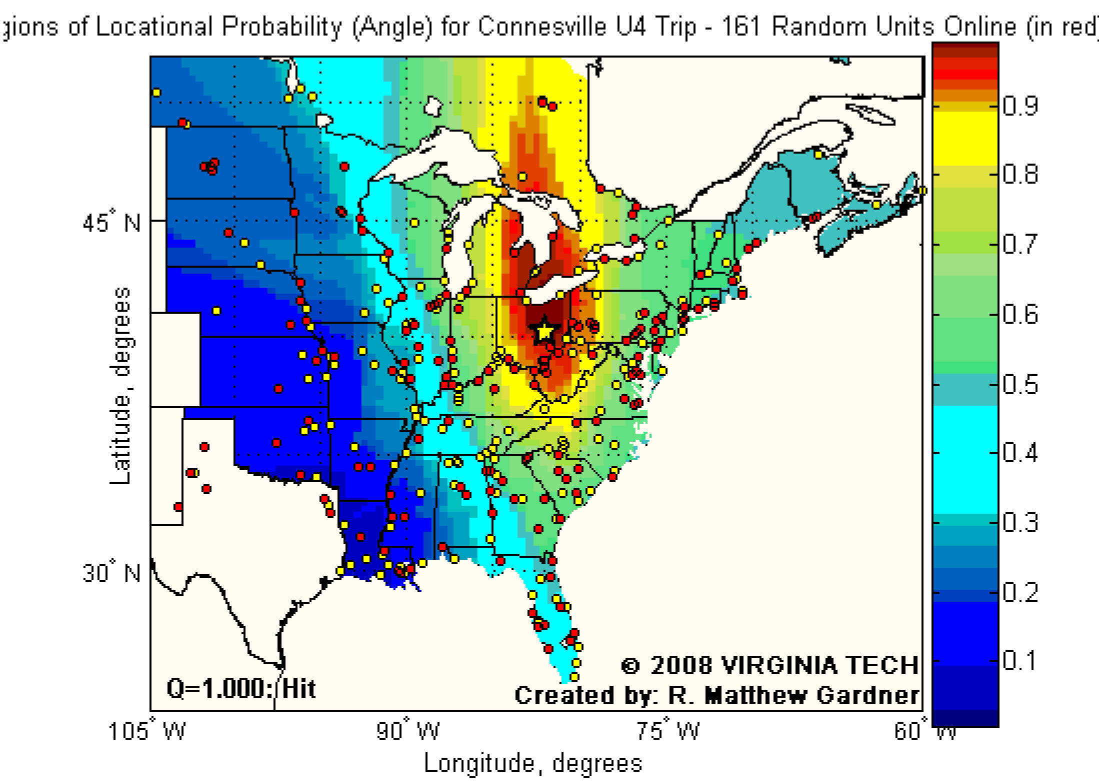
gions of Locational Probability (Angle) for Connesville U4 Trip - 161 Random Units Online (in red)
45° N
30° N
Latitude, degrees
105° W
90° W
75° W
60° W
Longitude, degrees
Q=1.000:/Hit
© 2008 VIRGINIA TECH
Created by: R. Matthew Gardner
0.9
0.8
0.7
0.6
0.5
0.4
0.3
0.2
0.1

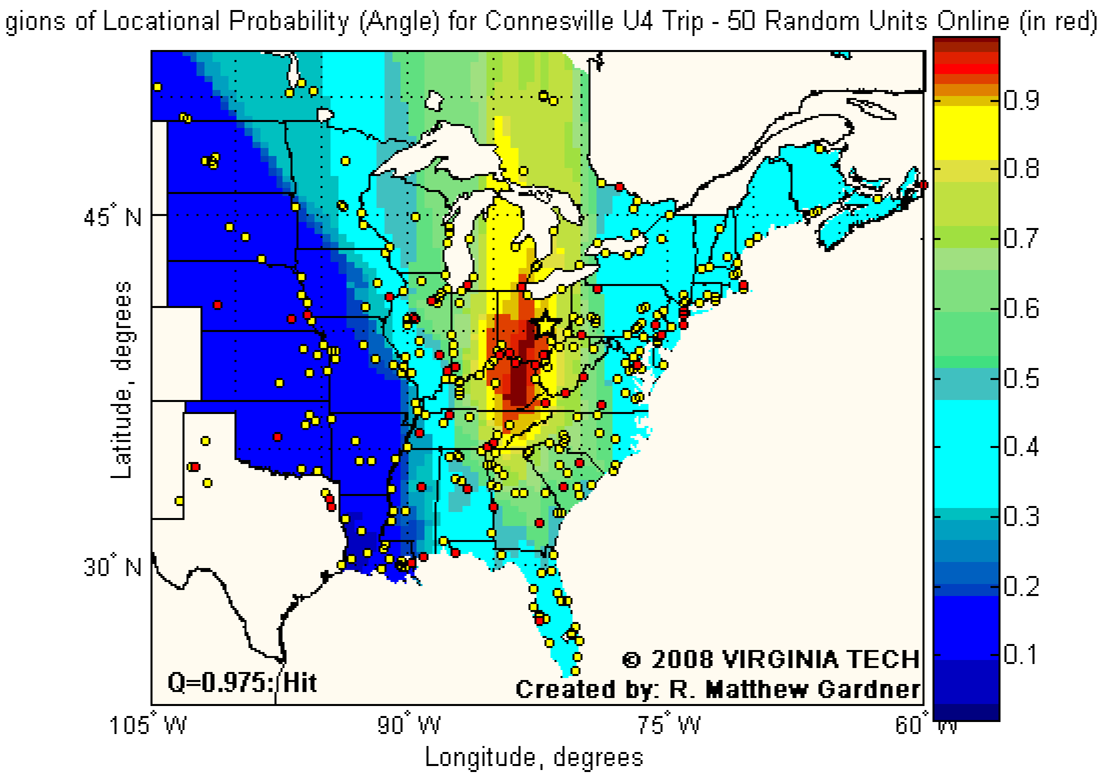
gions of Locational Probability (Angle) for Connesville U4 Trip - 50 Random Units Online (in red)
45° N
30° N
Latitude, degrees
105° W
90° W
75° W
60° W
Longitude, degrees
Q=0.975: Hit
© 2008 VIRGINIA TECH
Created by: R. Matthew Gardner
0.9
0.8
0.7
0.6
0.5
0.4
0.3
0.2
0.1

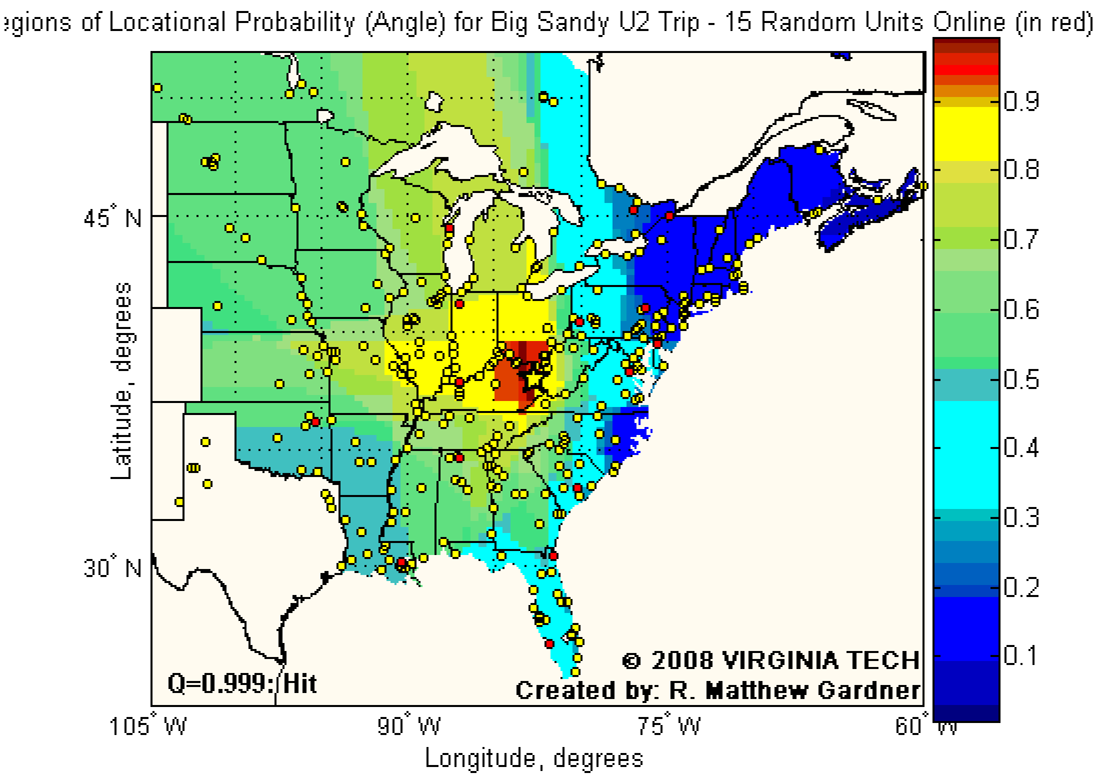
egions of Locational Probability (Angle) for Big Sandy U2 Trip - 15 Random Units Online (in red)
45° N
30° N
Latitude, degrees
105° W
90° W
75° W
60° W
Longitude, degrees
Q=0.999: Hit
© 2008 VIRGINIA TECH
Created by: R. Matthew Gardner
0.9
0.8
0.7
0.6
0.5
0.4
0.3
0.2
0.1

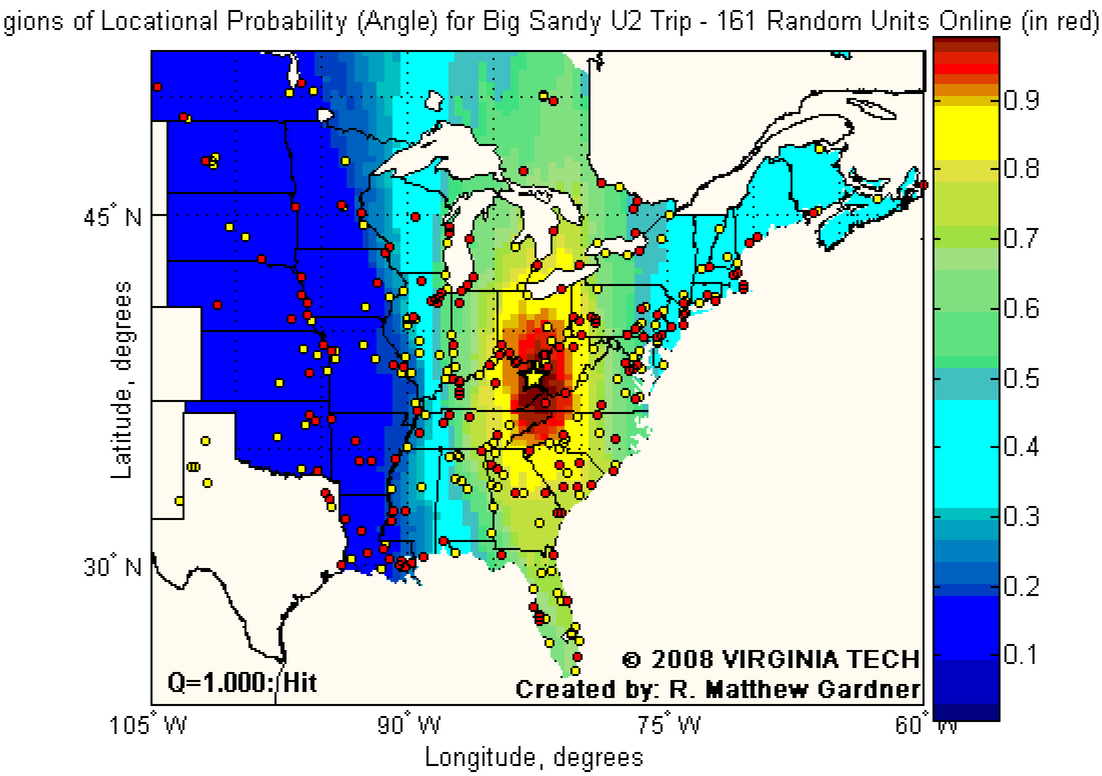
gions of Locational Probability (Angle) for Big Sandy U2 Trip - 161 Random Units Online (in red)
45° N
30° N
Latitude, degrees
105° W
90° W
75° W
60° W
Longitude, degrees
Q=1.000:/Hit
© 2008 VIRGINIA TECH
Created by: R. Matthew Gardner
0.9
0.8
0.7
0.6
0.5
0.4
0.3
0.2
0.1

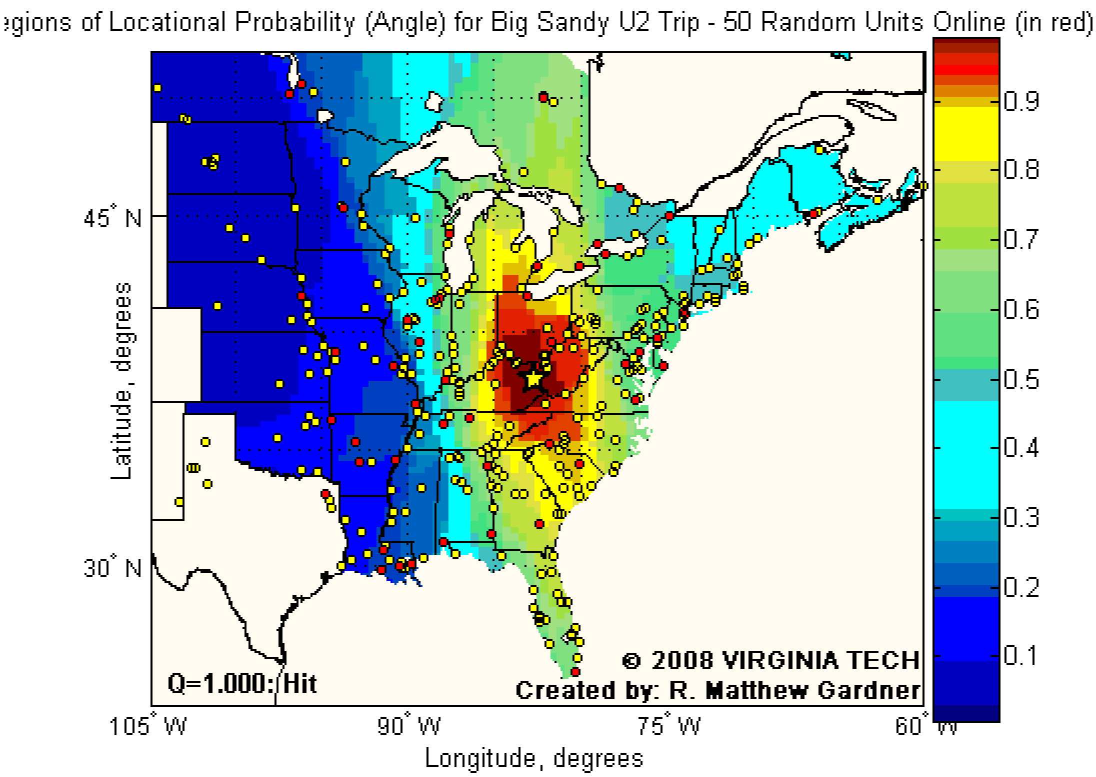
egions of Locational Probability (Angle) for Big Sandy U2 Trip - 50 Random Units Online (in red)
45° N
30° N
Latitude, degrees
105° W
90° W
75° W
60° W
Longitude, degrees
Q=1.000:/Hit
© 2008 VIRGINIA TECH
Created by: R. Matthew Gardner
0.9
0.8
0.7
0.6
0.5
0.4
0.3
0.2
0.1

Appendix XX: Variance-Weighted Frequency-Based Event Location (Full Simulation)

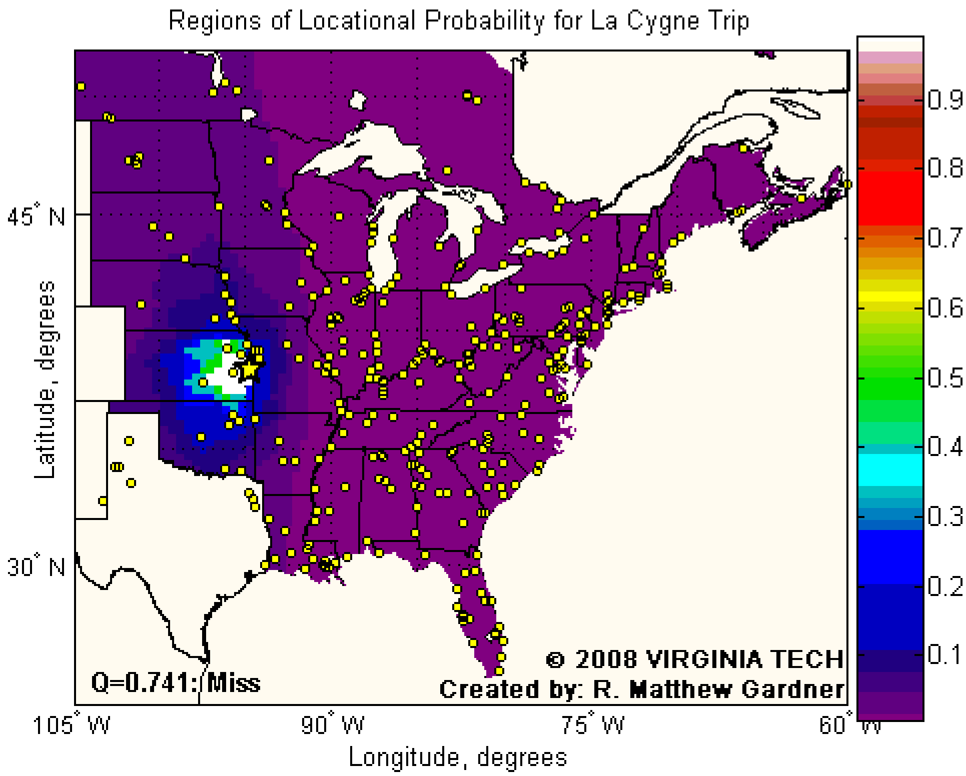

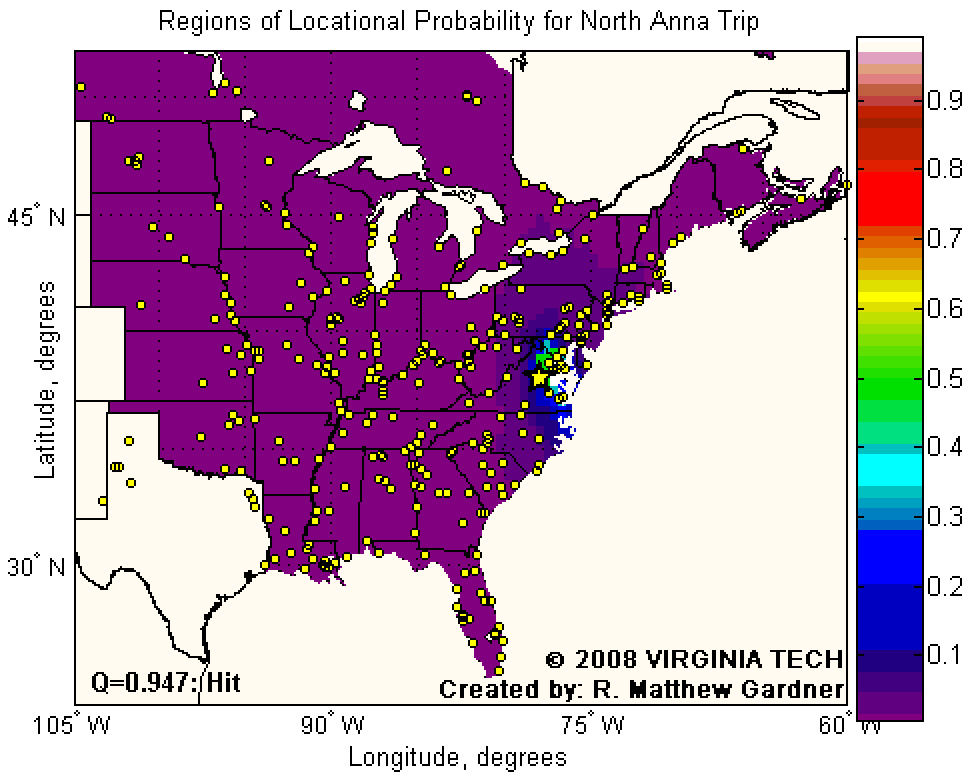
Regions of Locational Probability for North Anna Trip
45° N
30° N
Latitude, degrees
105° W
90° W
75° W
60° W
Longitude, degrees
Q=0.947: Hit
© 2008 VIRGINIA TECH
Created by: R. Matthew Gardner
0.9
0.8
0.7
0.6
0.5
0.4
0.3
0.2
0.1

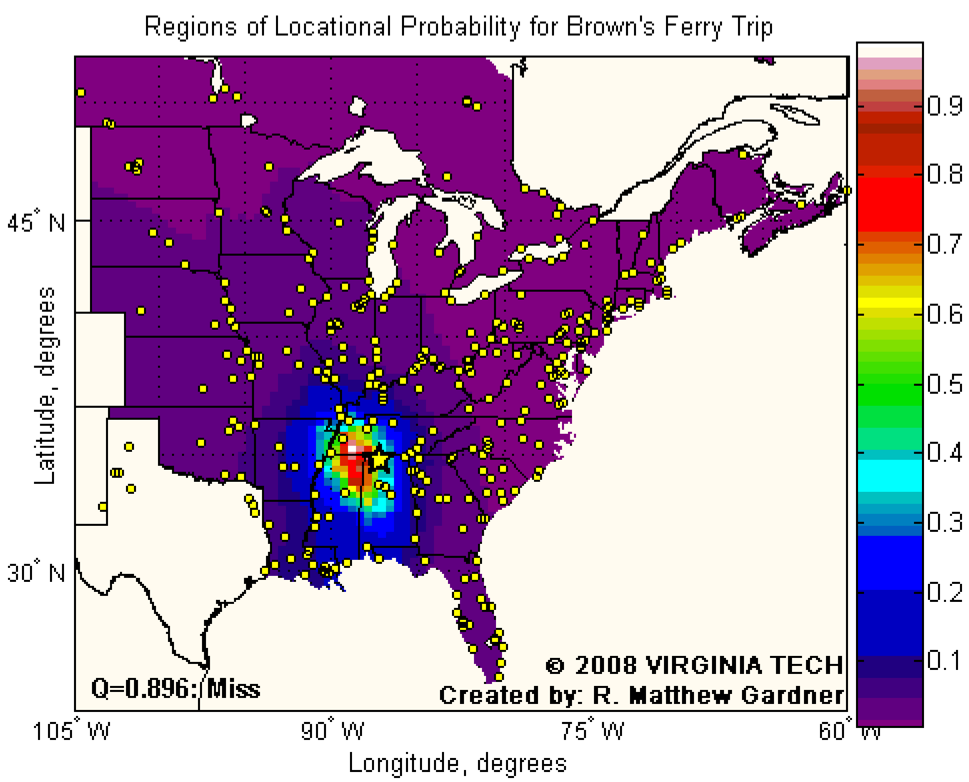
Regions of Locational Probability for Brown's Ferry Trip
45° N
30° N
Latitude, degrees
105° W
90° W
75° W
60° W
Longitude, degrees
Q=0.896: Miss
© 2008 VIRGINIA TECH
Created by: R. Matthew Gardner
0.9
0.8
0.7
0.6
0.5
0.4
0.3
0.2
0.1

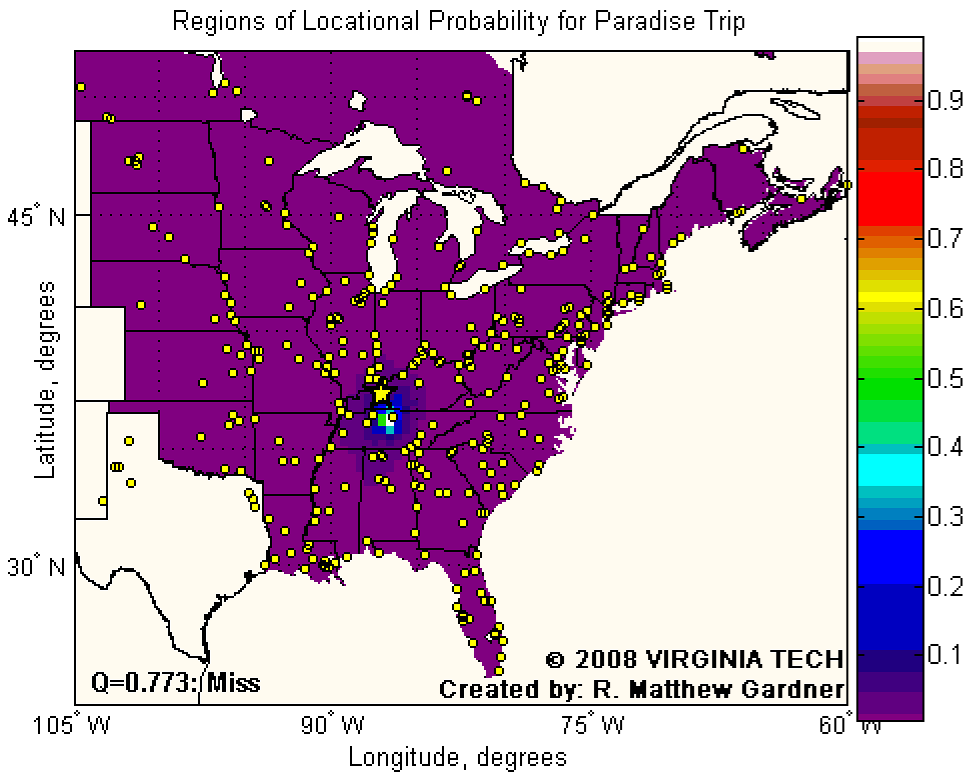
Regions of Locational Probability for Paradise Trip
45° N
30° N
Latitude, degrees
105° W
90° W
75° W
60° W
Longitude, degrees
Q=0.773: Miss
© 2008 VIRGINIA TECH
Created by: R. Matthew Gardner
0.9
0.8
0.7
0.6
0.5
0.4
0.3
0.2
0.1

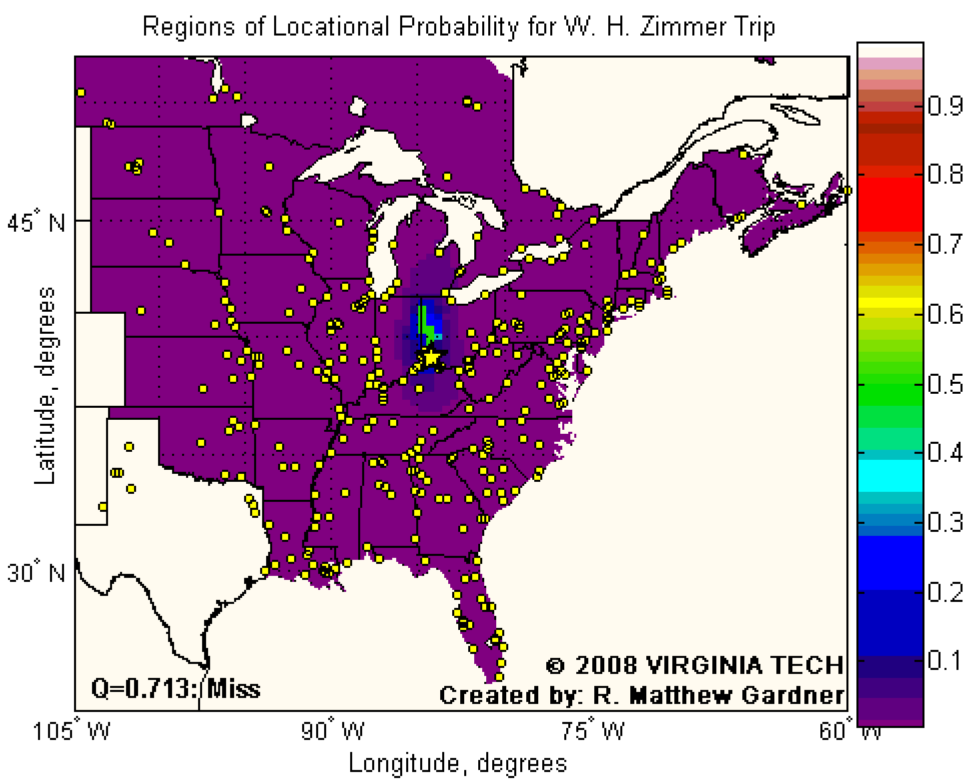
Regions of Locational Probability for W. H. Zimmer Trip
45° N
30° N
Latitude, degrees
105° W
90° W
75° W
60° W
Longitude, degrees
Q=0.713: Miss
© 2008 VIRGINIA TECH
Created by: R. Matthew Gardner
0.9
0.8
0.7
0.6
0.5
0.4
0.3
0.2
0.1

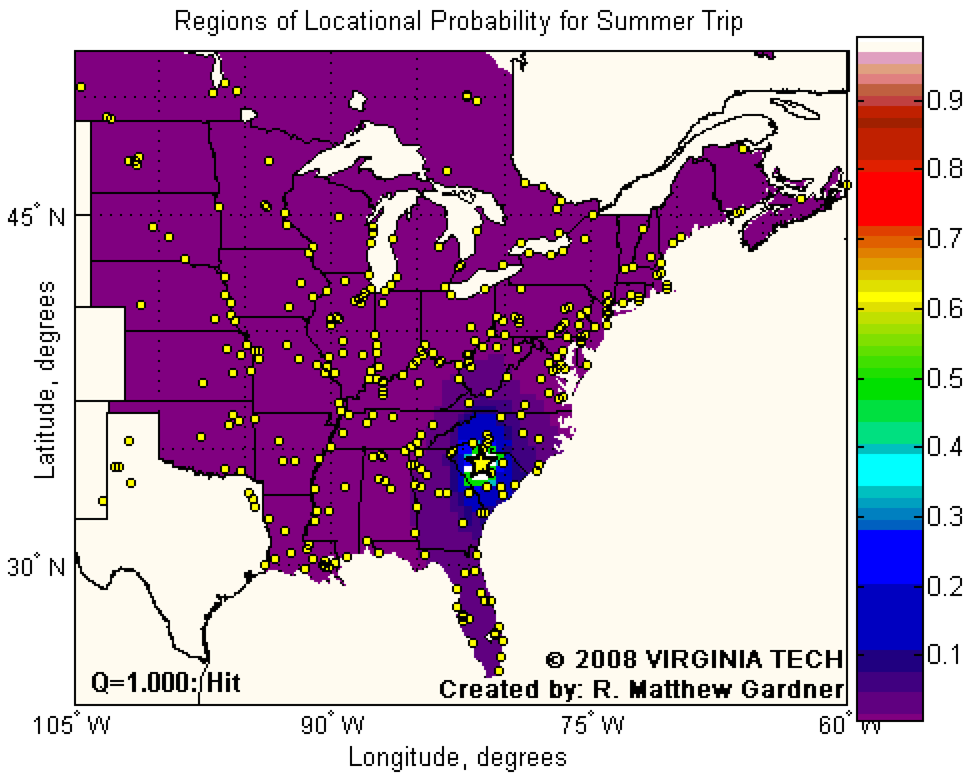
Regions of Locational Probability for Summer Trip
45° N
30° N
Latitude, degrees
105° W
90° W
75° W
60° W
Longitude, degrees
Q=1.000: Hit
© 2008 VIRGINIA TECH
Created by: R. Matthew Gardner
0.9
0.8
0.7
0.6
0.5
0.4
0.3
0.2
0.1

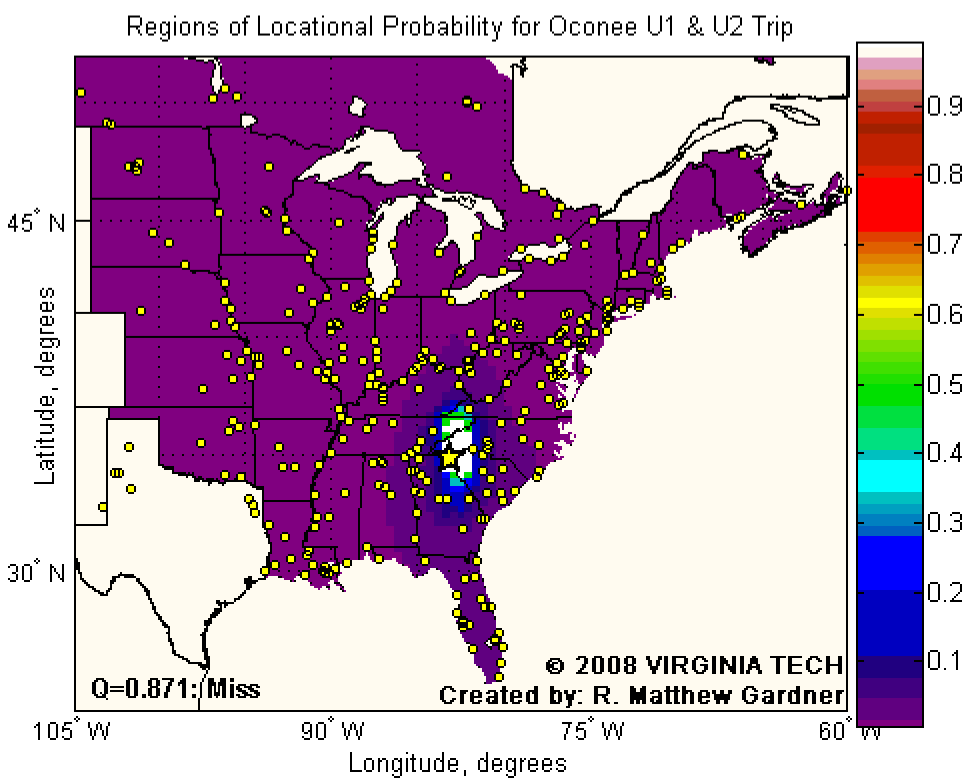
Regions of Locational Probability for Oconee U1 & U2 Trip
45° N
30° N
Latitude, degrees
105° W
90° W
75° W
60° W
Longitude, degrees
Q=0.871: Miss
© 2008 VIRGINIA TECH
Created by: R. Matthew Gardner
0.9
0.8
0.7
0.6
0.5
0.4
0.3
0.2
0.1

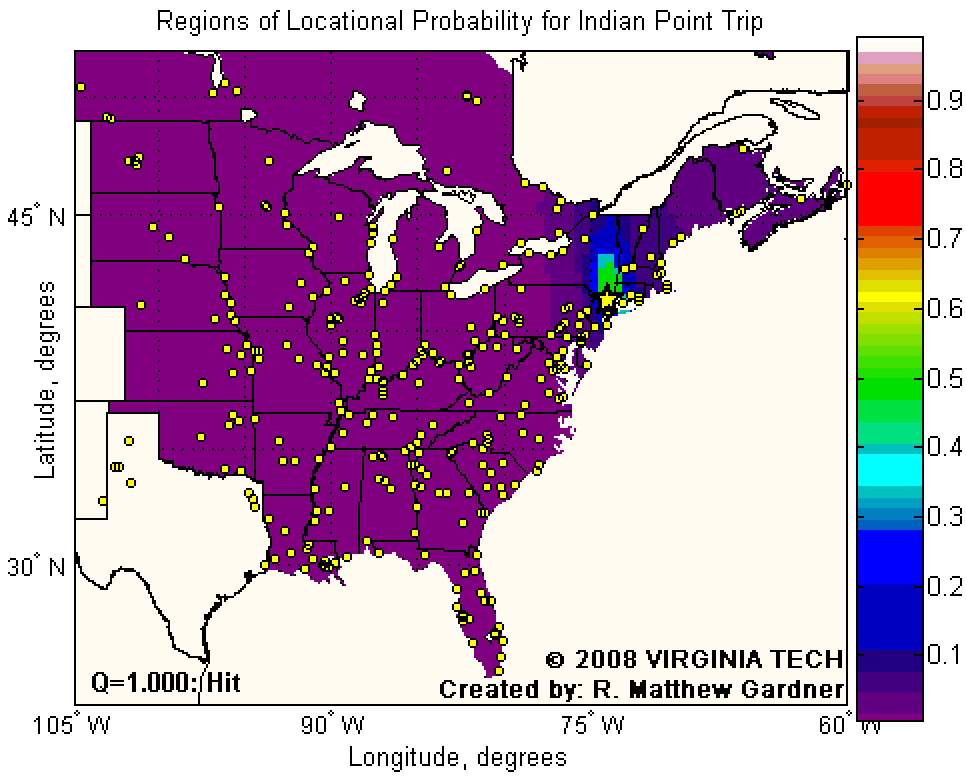
Regions of Locational Probability for Indian Point Trip
45° N
30° N
Latitude, degrees
105° W
90° W
75° W
60° W
Longitude, degrees
Q=1.000: Hit
© 2008 VIRGINIA TECH
Created by: R. Matthew Gardner
0.9
0.8
0.7
0.6
0.5
0.4
0.3
0.2
0.1

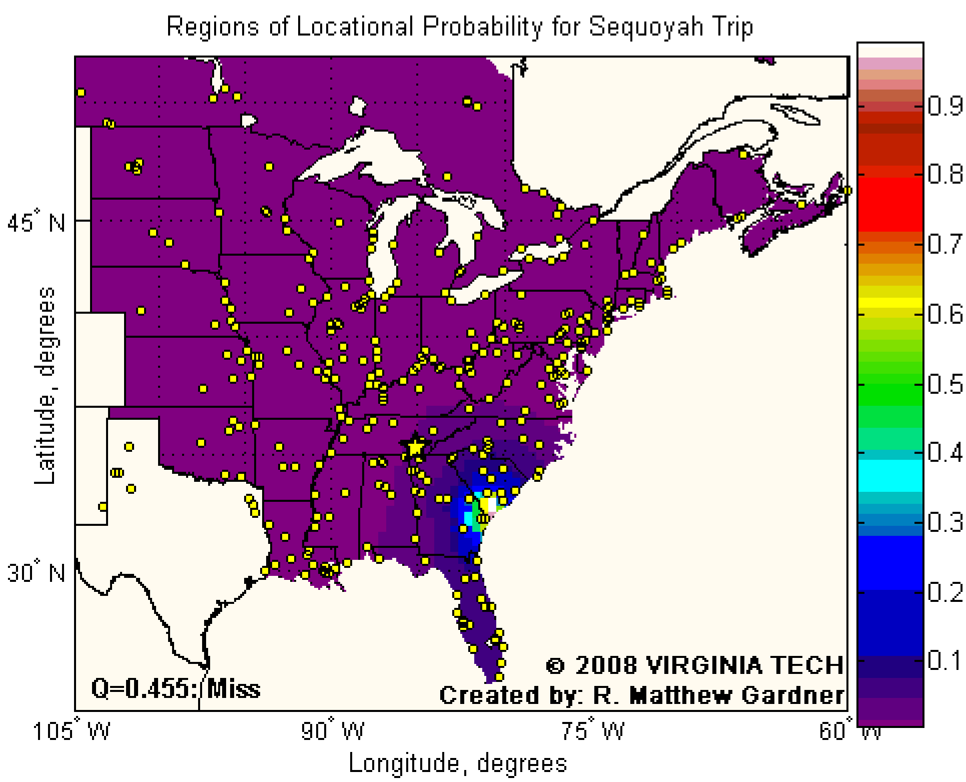
Regions of Locational Probability for Sequoyah Trip
45° N
30° N
Latitude, degrees
105° W
90° W
75° W
60° W
Longitude, degrees
Q=0.455: Miss
© 2008 VIRGINIA TECH
Created by: R. Matthew Gardner
0.9
0.8
0.7
0.6
0.5
0.4
0.3
0.2
0.1

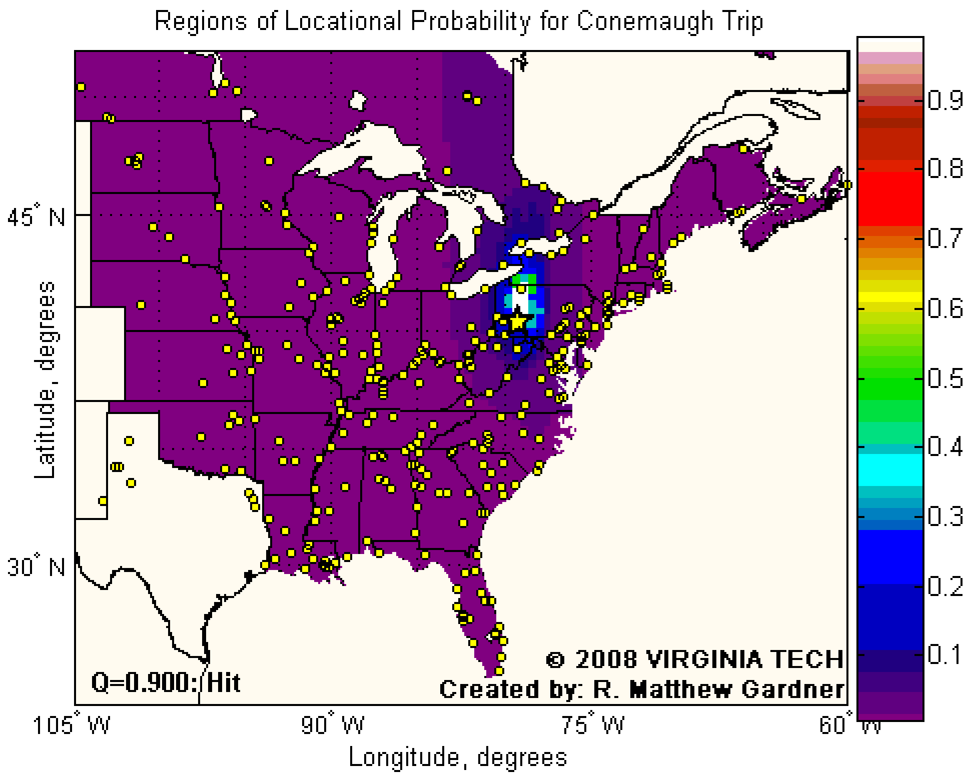
Regions of Locational Probability for Conemaugh Trip
45° N
30° N
Latitude, degrees
105° W
90° W
75° W
60° W
Longitude, degrees
Q=0.900: Hit
© 2008 VIRGINIA TECH
Created by: R. Matthew Gardner
0.9
0.8
0.7
0.6
0.5
0.4
0.3
0.2
0.1

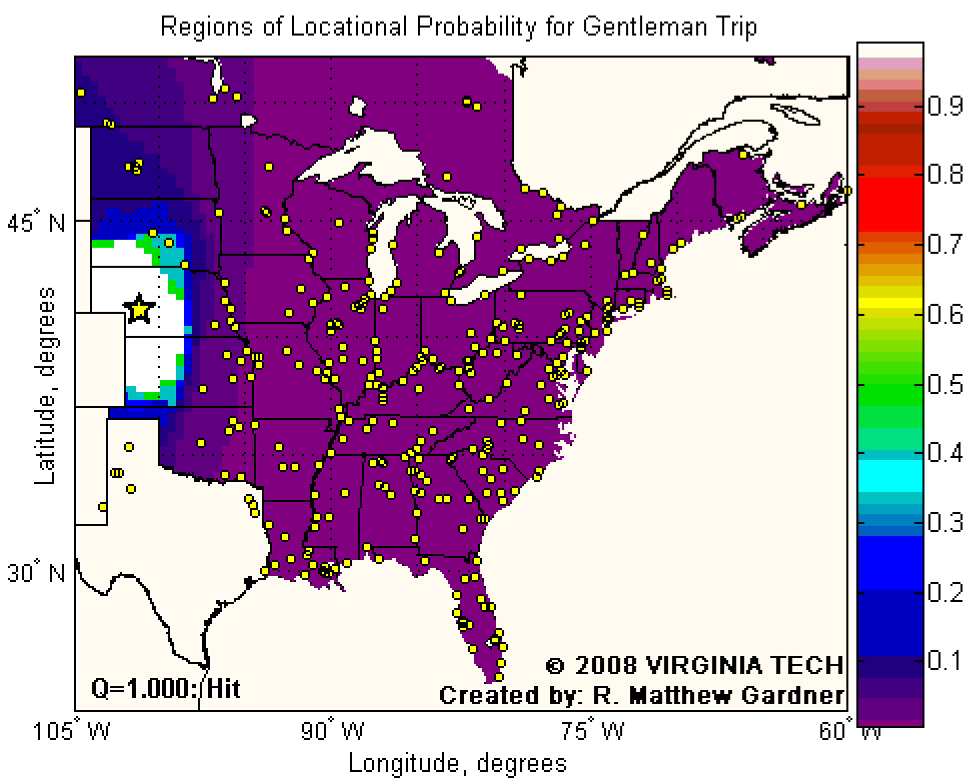
Regions of Locational Probability for Gentleman Trip
45° N
30° N
Latitude, degrees
105° W
90° W
75° W
60° W
Longitude, degrees
Q=1.000: Hit
© 2008 VIRGINIA TECH
Created by: R. Matthew Gardner
0.9
0.8
0.7
0.6
0.5
0.4
0.3
0.2
0.1

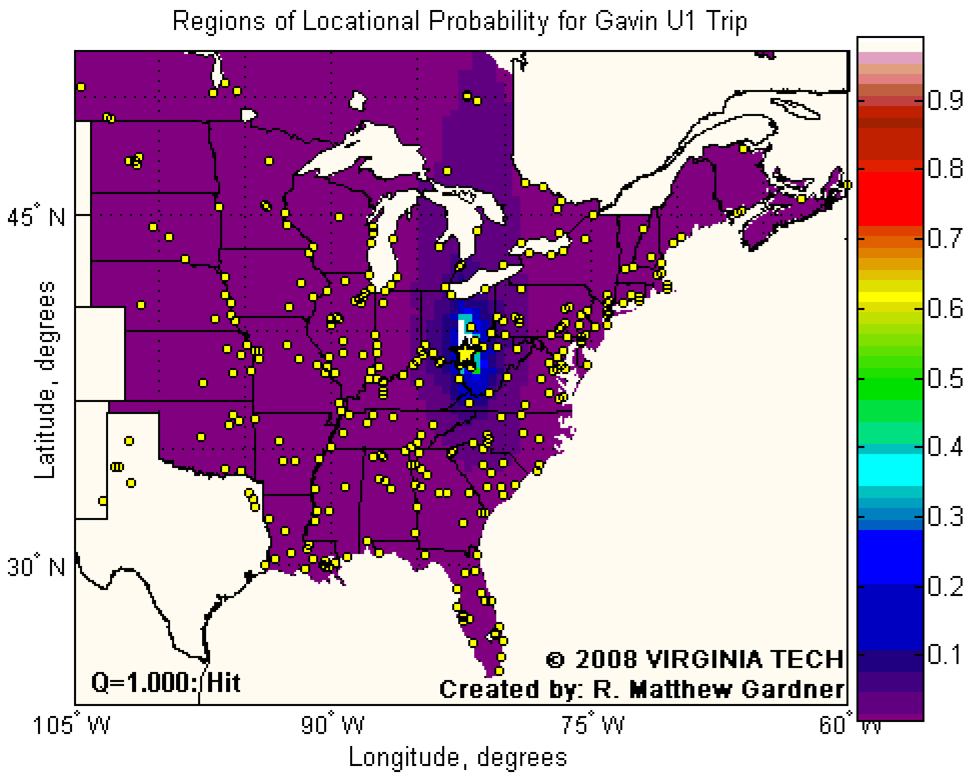
Regions of Locational Probability for Gavin U1 Trip
45° N
30° N
Latitude, degrees
105° W
90° W
75° W
60° W
Longitude, degrees
Q=1.000: Hit
© 2008 VIRGINIA TECH
Created by: R. Matthew Gardner
0.9
0.8
0.7
0.6
0.5
0.4
0.3
0.2
0.1

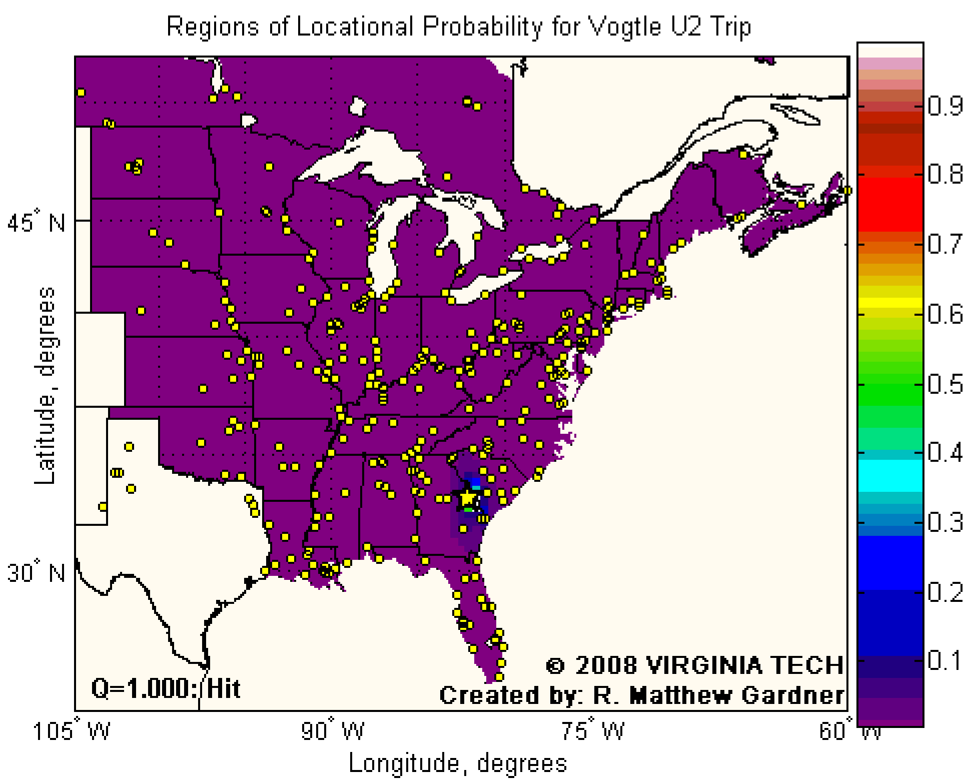
Regions of Locational Probability for Vogtle U2 Trip
45° N
30° N
Latitude, degrees
105° W
90° W
75° W
60° W
Longitude, degrees
Q=1.000: Hit
© 2008 VIRGINIA TECH
Created by: R. Matthew Gardner
0.9
0.8
0.7
0.6
0.5
0.4
0.3
0.2
0.1

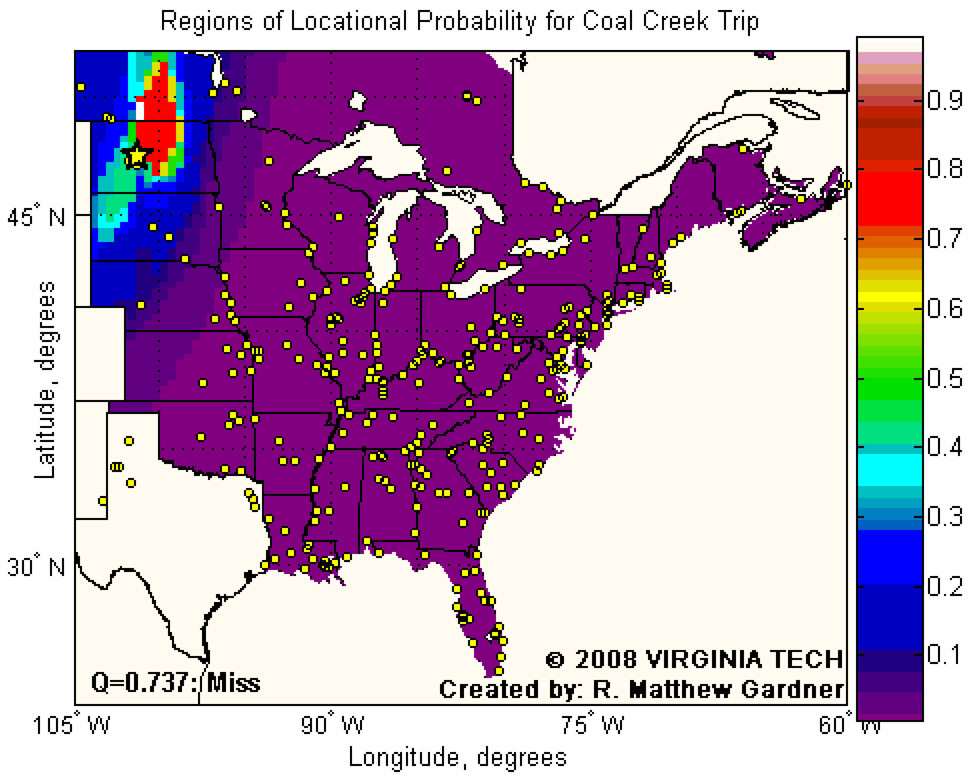
Regions of Locational Probability for Coal Creek Trip
45° N
30° N
Latitude, degrees
105° W
90° W
75° W
60° W
Longitude, degrees
Q=0.737: Miss
© 2008 VIRGINIA TECH
Created by: R. Matthew Gardner
0.9
0.8
0.7
0.6
0.5
0.4
0.3
0.2
0.1

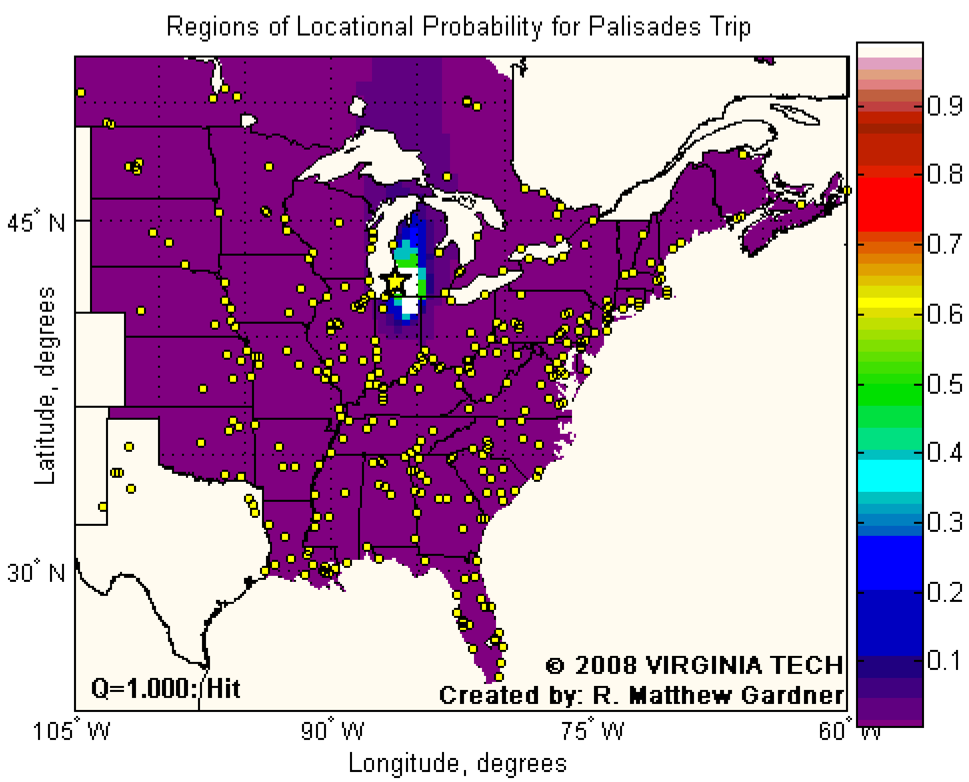
Regions of Locational Probability for Palisades Trip
45° N
30° N
Latitude, degrees
105° W
90° W
75° W
60° W
Longitude, degrees
Q=1.000: Hit
© 2008 VIRGINIA TECH
Created by: R. Matthew Gardner
0.9
0.8
0.7
0.6
0.5
0.4
0.3
0.2
0.1

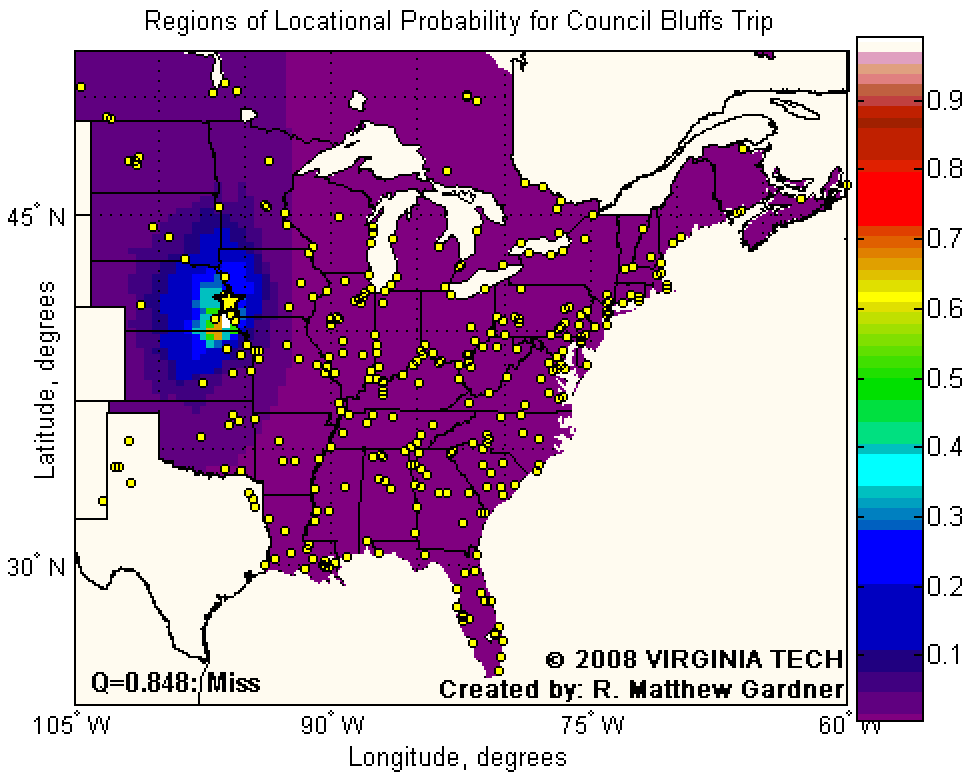
Regions of Locational Probability for Council Bluffs Trip
45° N
30° N
Latitude, degrees
105° W
90° W
75° W
60° W
Longitude, degrees
Q=0.848: Miss
© 2008 VIRGINIA TECH
Created by: R. Matthew Gardner
0.9
0.8
0.7
0.6
0.5
0.4
0.3
0.2
0.1

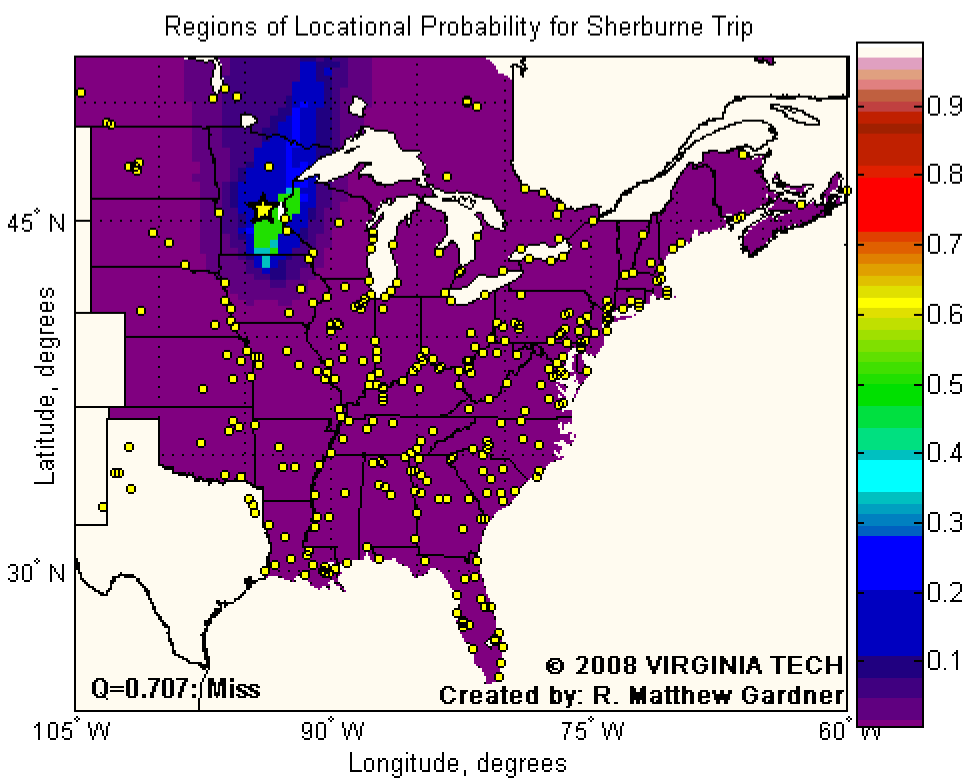
Regions of Locational Probability for Sherburne Trip
45° N
30° N
Latitude, degrees
105° W
90° W
75° W
60° W
Longitude, degrees
Q=0.707: Miss
© 2008 VIRGINIA TECH
Created by: R. Matthew Gardner
0.9
0.8
0.7
0.6
0.5
0.4
0.3
0.2
0.1

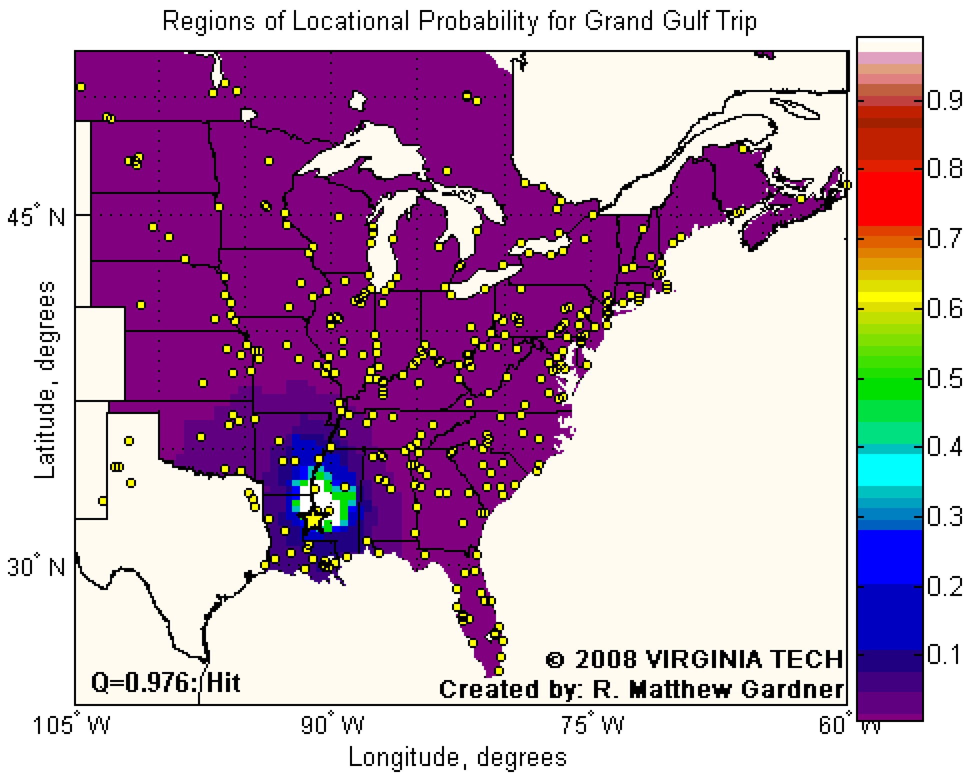
Regions of Locational Probability for Grand Gulf Trip
Latitude, degrees
45° N
30° N
105° W
90° W
75° W
60° W
Longitude, degrees
Q=0.976: Hit
© 2008 VIRGINIA TECH
Created by: R. Matthew Gardner
0.9
0.8
0.7
0.6
0.5
0.4
0.3
0.2
0.1

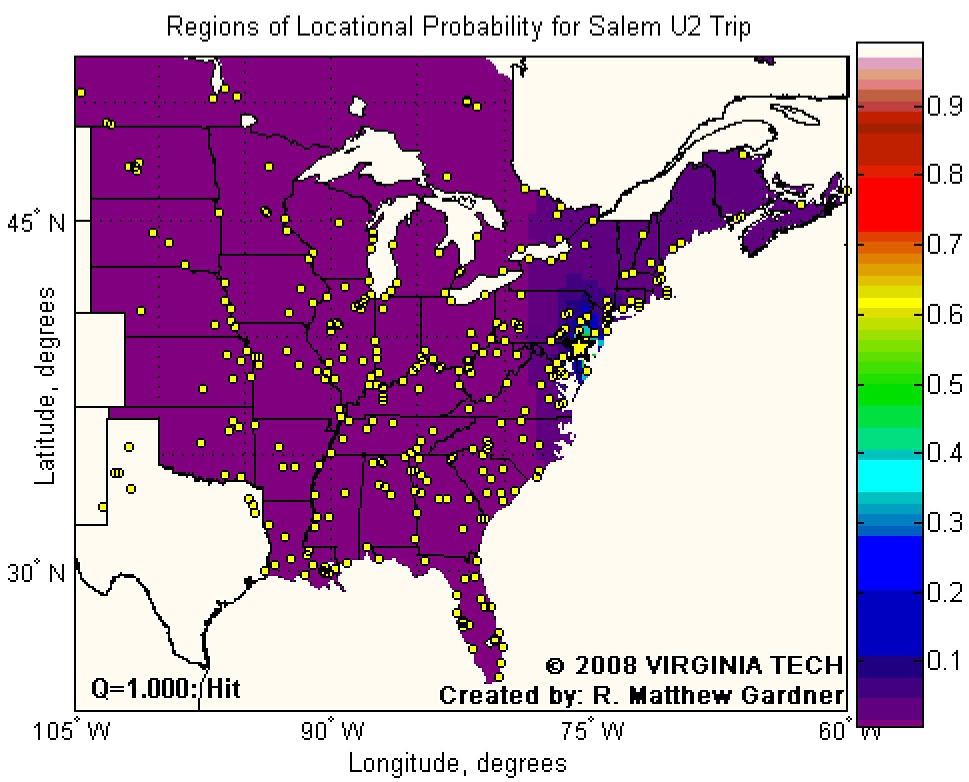
Regions of Locational Probability for Salem U2 Trip
Latitude, degrees
45° N
30° N
105° W
90° W
75° W
60° W
Longitude, degrees
Q=1.000: Hit
© 2008 VIRGINIA TECH
Created by: R. Matthew Gardner
0.9
0.8
0.7
0.6
0.5
0.4
0.3
0.2
0.1

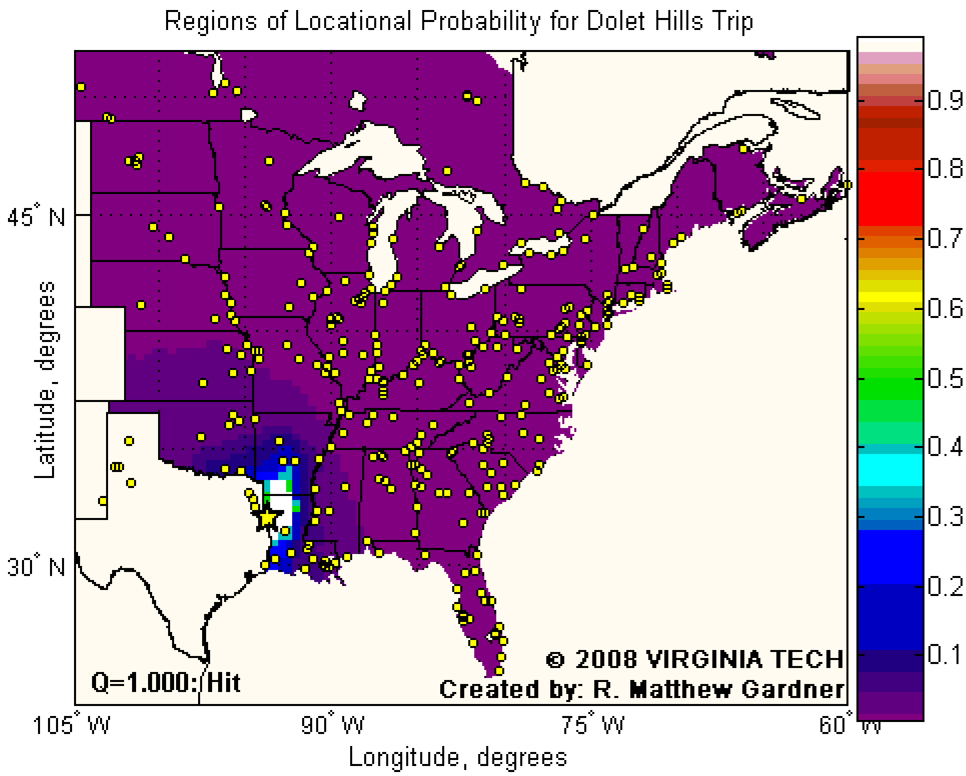

Regions of Locational Probability for Dolet Hills Trip
45° N
30° N
Latitude, degrees
105° W
90° W
75° W
60° W
Longitude, degrees
Q=1.000: Hit
© 2008 VIRGINIA TECH
Created by: R. Matthew Gardner
0.9
0.8
0.7
0.6
0.5
0.4
0.3
0.2
0.1

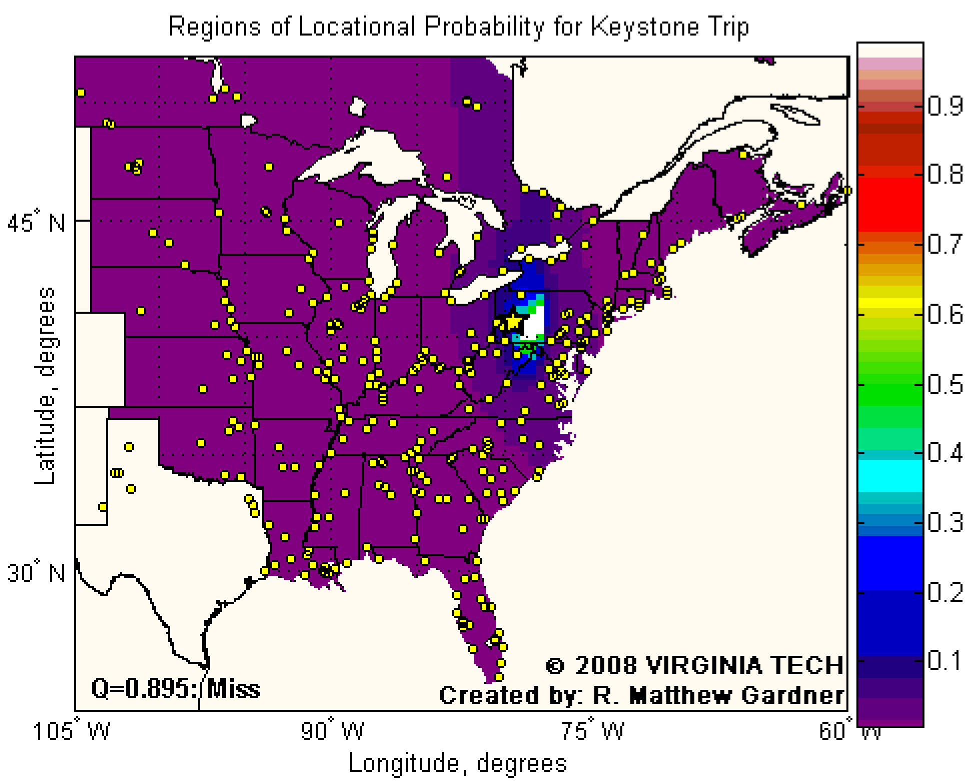

Regions of Locational Probability for Keystone Trip
45° N
30° N
Latitude, degrees
105° W
90° W
75° W
60° W
Longitude, degrees
Q=0.895: Miss
© 2008 VIRGINIA TECH
Created by: R. Matthew Gardner
0.9
0.8
0.7
0.6
0.5
0.4
0.3
0.2
0.1

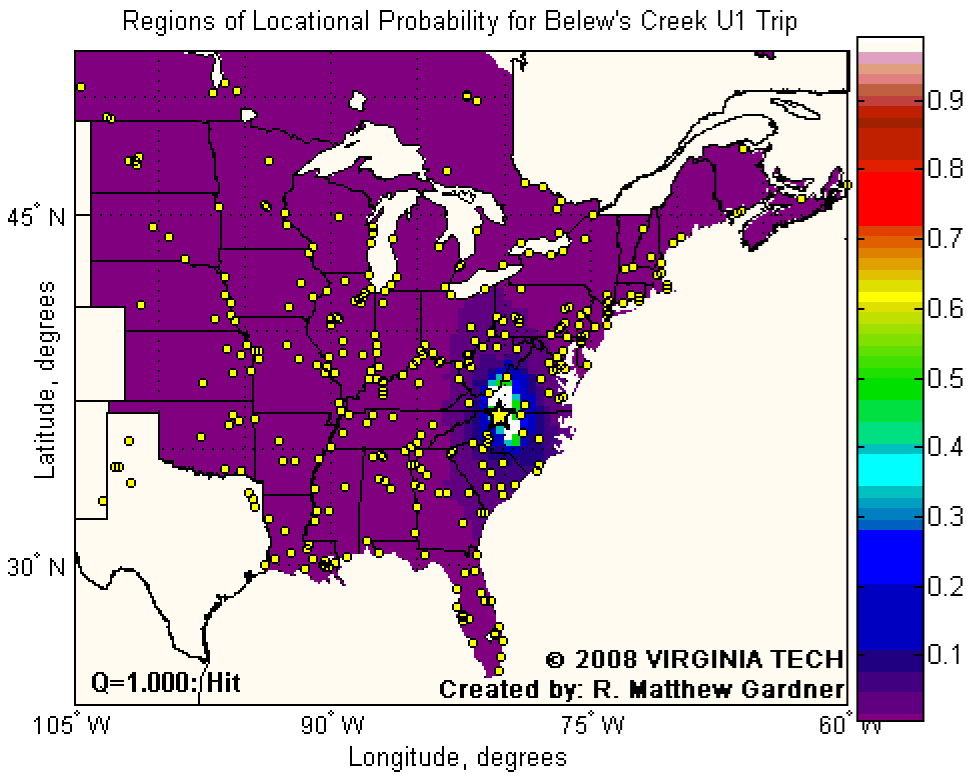
Regions of Locational Probability for Belew's Creek U1 Trip
45° N
30° N
Latitude, degrees
105° W
90° W
75° W
60° W
Longitude, degrees
Q=1.000:/Hit
© 2008 VIRGINIA TECH
Created by: R. Matthew Gardner
0.9
0.8
0.7
0.6
0.5
0.4
0.3
0.2
0.1

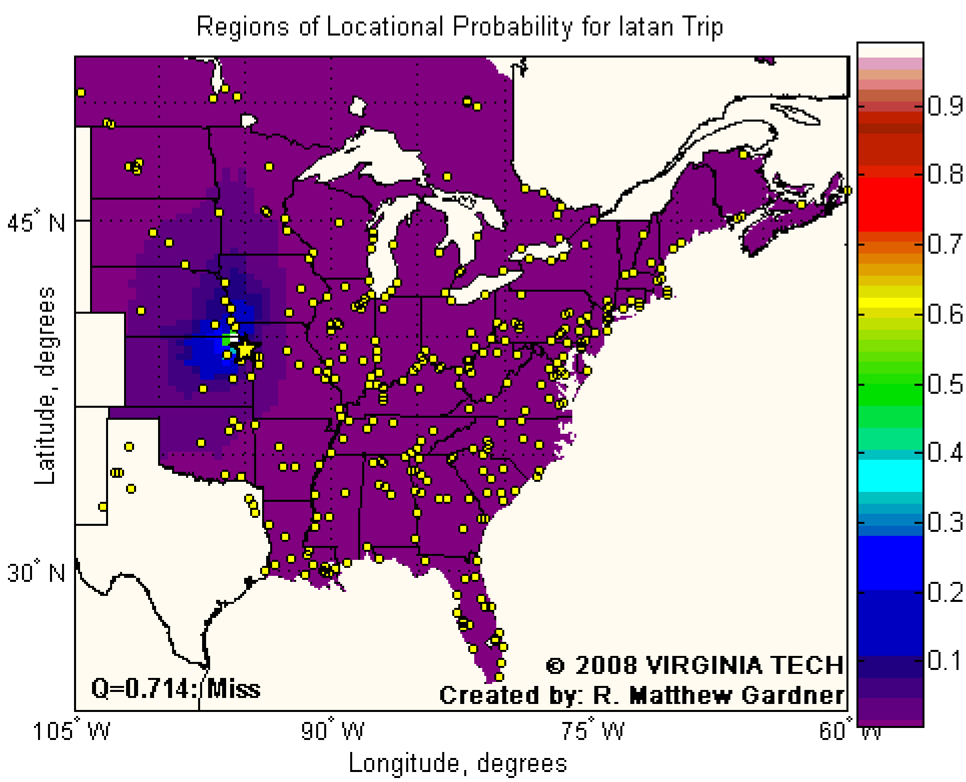
Regions of Locational Probability for Iatan Trip
45° N
30° N
Latitude, degrees
105° W
90° W
75° W
60° W
Longitude, degrees
Q=0.714:/Miss
© 2008 VIRGINIA TECH
Created by: R. Matthew Gardner
0.9
0.8
0.7
0.6
0.5
0.4
0.3
0.2
0.1

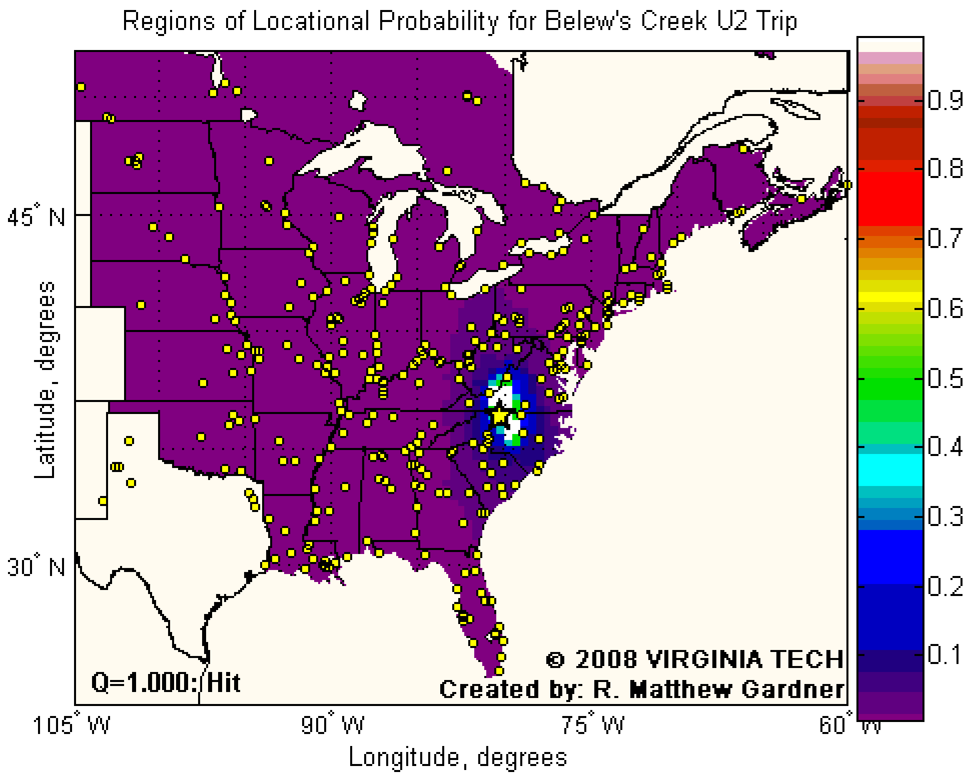
Regions of Locational Probability for Belew's Creek U2 Trip
45° N
30° N
Latitude, degrees
105° W
90° W
75° W
60° W
Longitude, degrees
Q=1.000:/Hit
© 2008 VIRGINIA TECH
Created by: R. Matthew Gardner
0.9
0.8
0.7
0.6
0.5
0.4
0.3
0.2
0.1

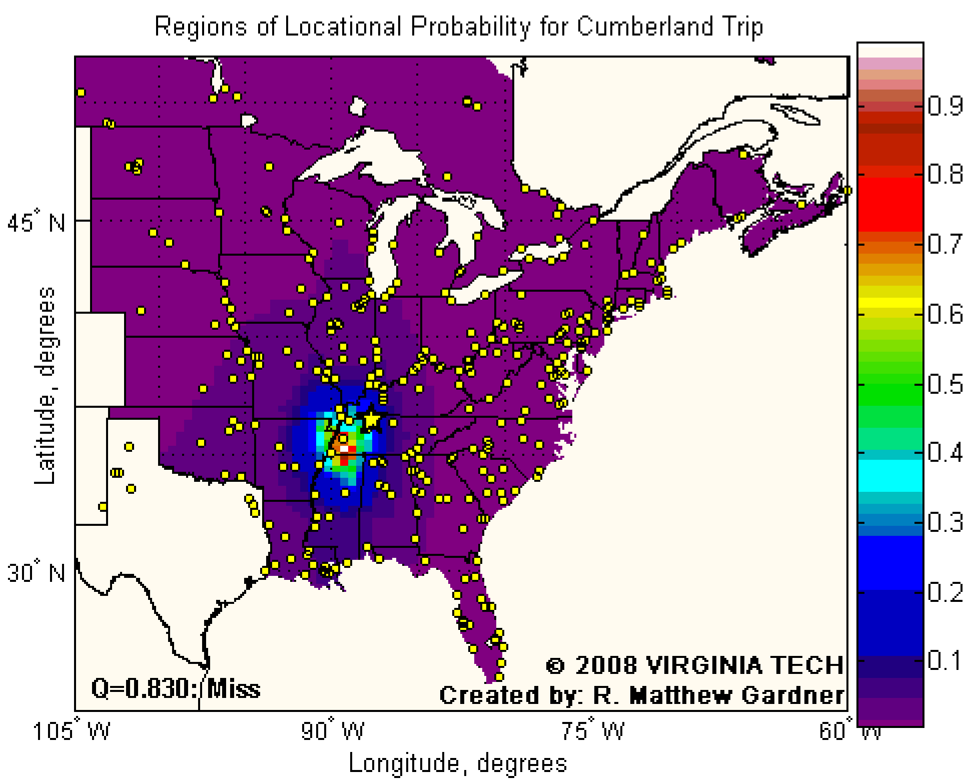
Regions of Locational Probability for Cumberland Trip
45° N
30° N
Latitude, degrees
105° W
90° W
75° W
60° W
Longitude, degrees
Q=0.830:/Miss
© 2008 VIRGINIA TECH
Created by: R. Matthew Gardner
0.9
0.8
0.7
0.6
0.5
0.4
0.3
0.2
0.1

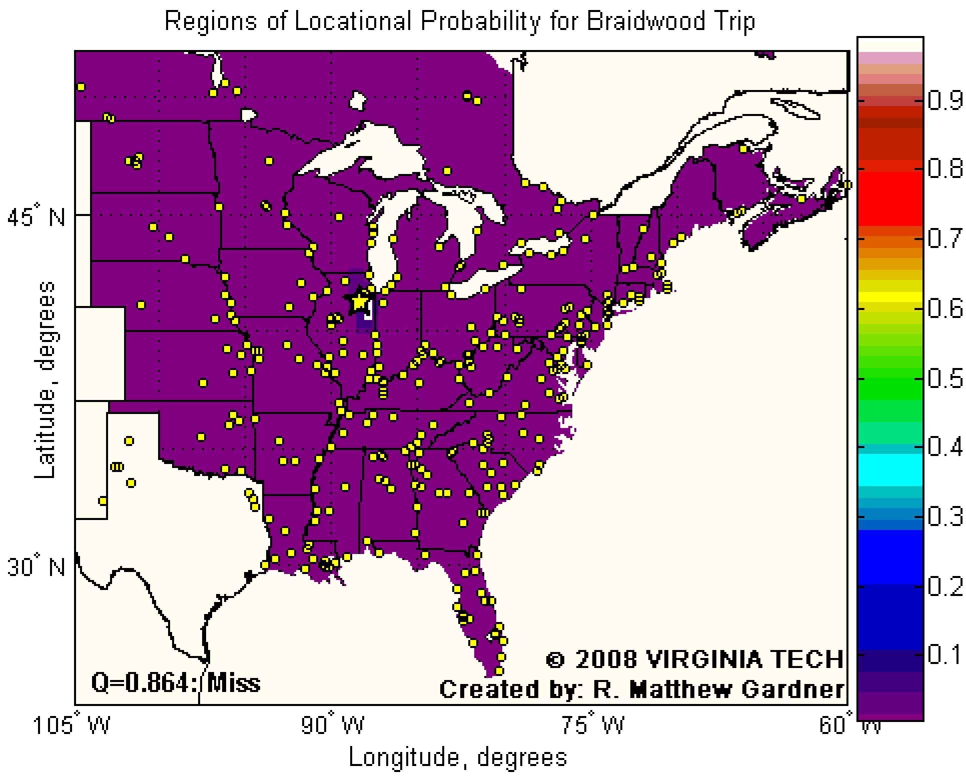
Regions of Locational Probability for Braidwood Trip
Latitude, degrees
45° N
30° N
105° W
90° W
75° W
60° W
Longitude, degrees
Q=0.864: Miss
© 2008 VIRGINIA TECH
Created by: R. Matthew Gardner
0.9
0.8
0.7
0.6
0.5
0.4
0.3
0.2
0.1

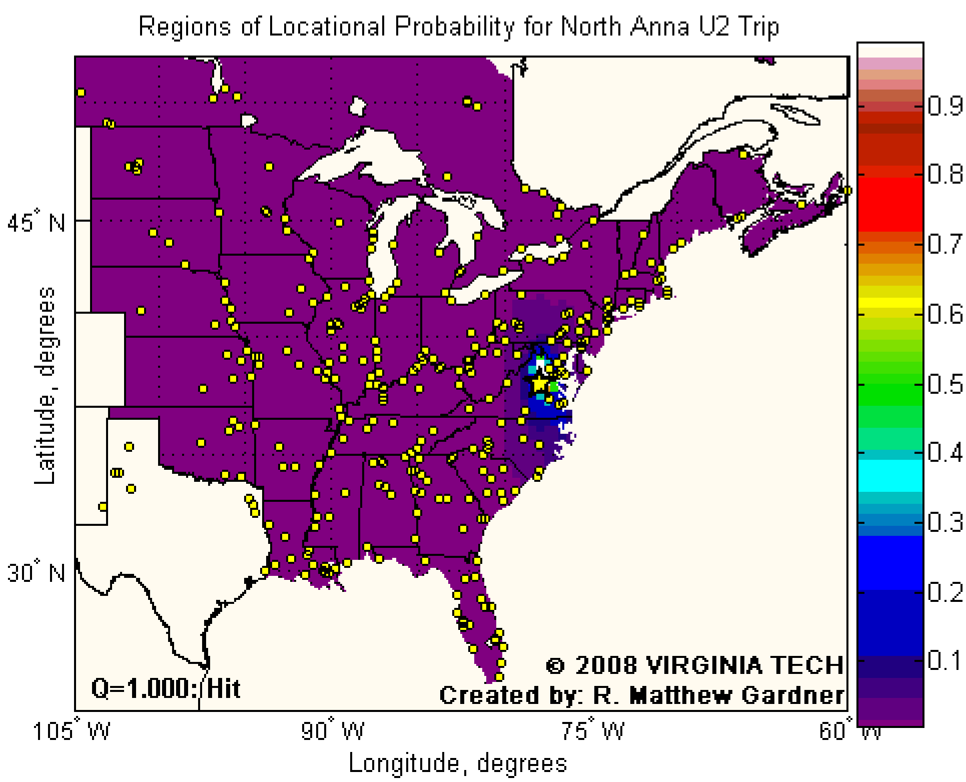
Regions of Locational Probability for North Anna U2 Trip
Latitude, degrees
45° N
30° N
105° W
90° W
75° W
60° W
Longitude, degrees
Q=1.000: Hit
© 2008 VIRGINIA TECH
Created by: R. Matthew Gardner
0.9
0.8
0.7
0.6
0.5
0.4
0.3
0.2
0.1

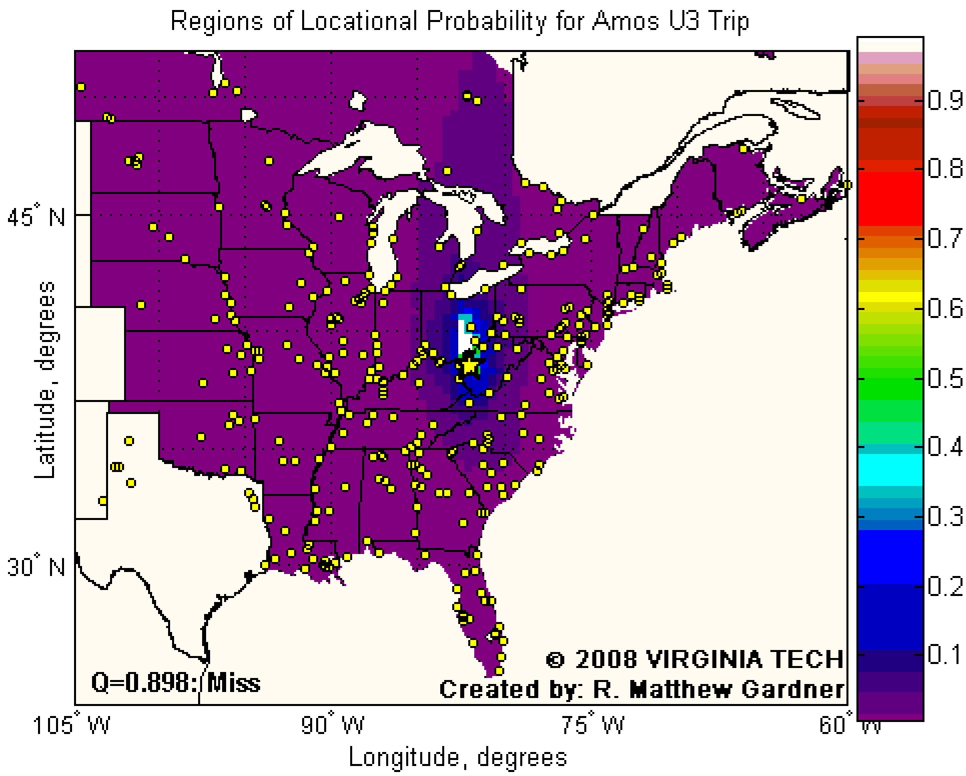
Regions of Locational Probability for Amos U3 Trip
45° N
30° N
Latitude, degrees
105° W
90° W
75° W
60° W
Longitude, degrees
Q=0.898: Miss
© 2008 VIRGINIA TECH
Created by: R. Matthew Gardner
0.9
0.8
0.7
0.6
0.5
0.4
0.3
0.2
0.1

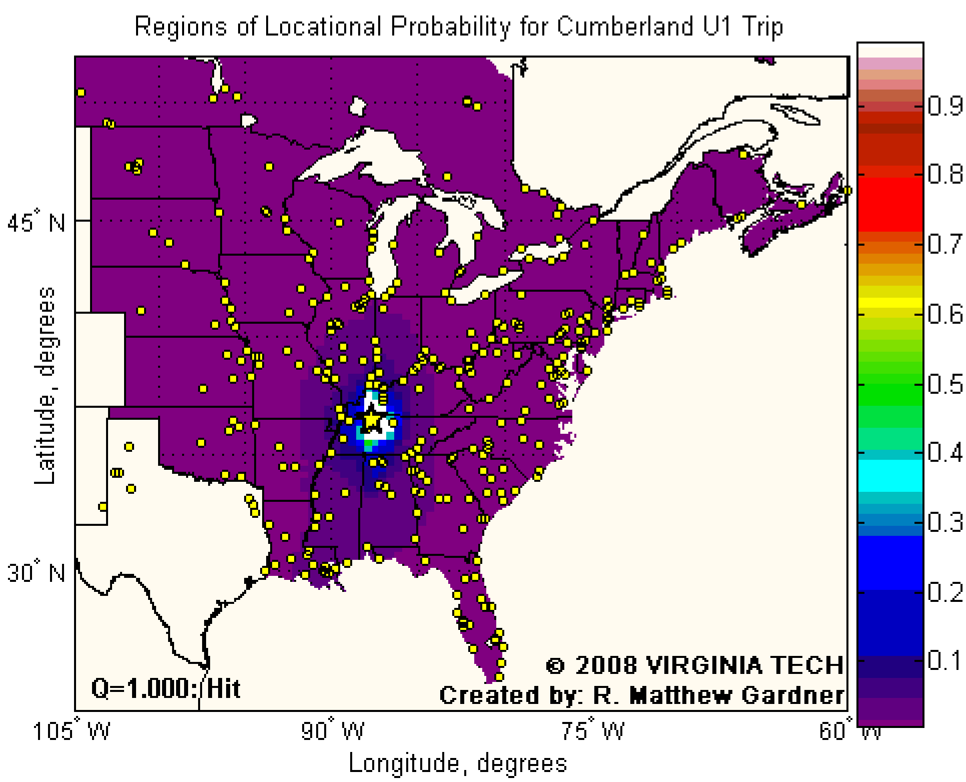
Regions of Locational Probability for Cumberland U1 Trip
45° N
30° N
Latitude, degrees
105° W
90° W
75° W
60° W
Longitude, degrees
Q=1.000: Hit
© 2008 VIRGINIA TECH
Created by: R. Matthew Gardner
0.9
0.8
0.7
0.6
0.5
0.4
0.3
0.2
0.1

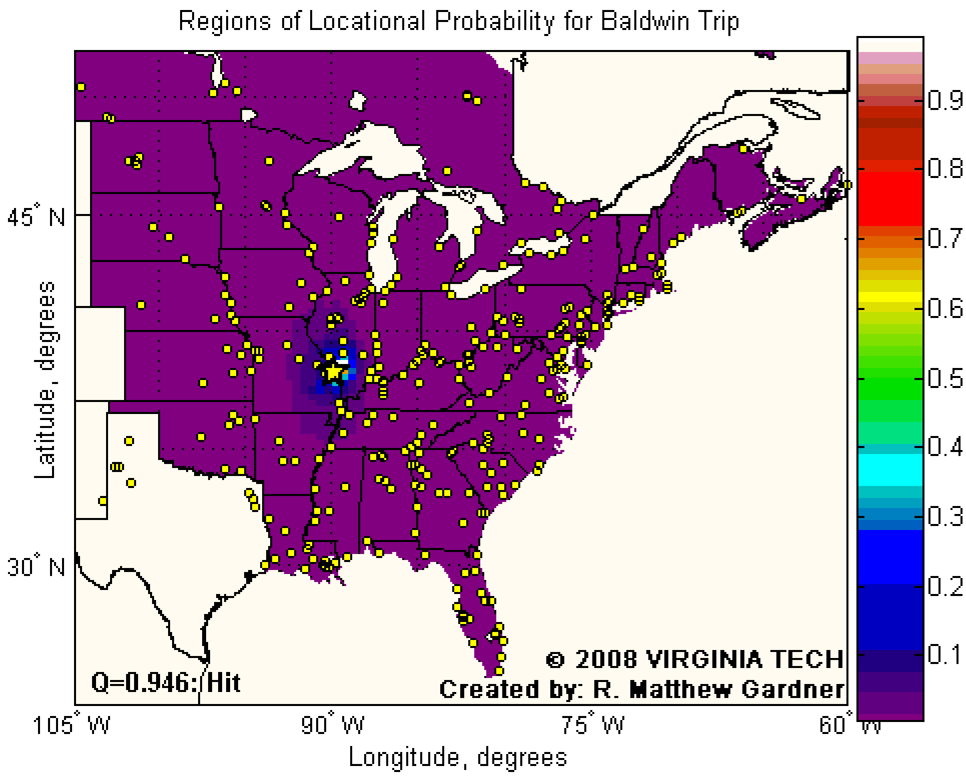
Regions of Locational Probability for Baldwin Trip
Latitude, degrees
45° N
30° N
105° W
90° W
75° W
60° W
Longitude, degrees
Q=0.946: Hit
© 2008 VIRGINIA TECH
Created by: R. Matthew Gardner
0.9
0.8
0.7
0.6
0.5
0.4
0.3
0.2
0.1

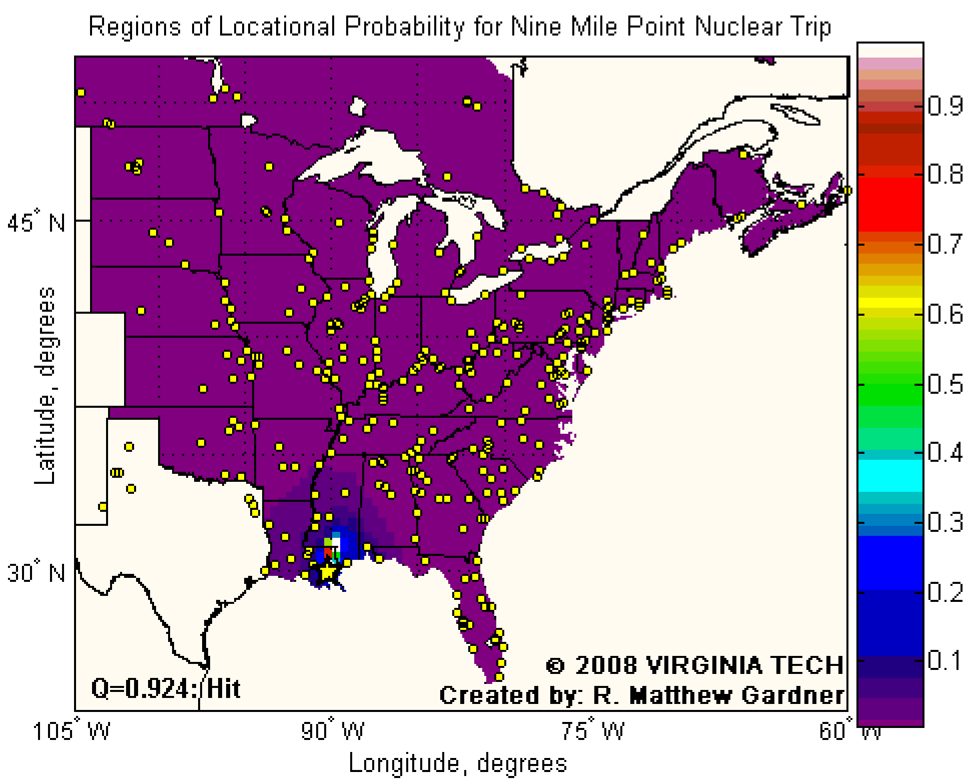
Regions of Locational Probability for Nine Mile Point Nuclear Trip
Latitude, degrees
45° N
30° N
105° W
90° W
75° W
60° W
Longitude, degrees
Q=0.924: Hit
© 2008 VIRGINIA TECH
Created by: R. Matthew Gardner
0.9
0.8
0.7
0.6
0.5
0.4
0.3
0.2
0.1

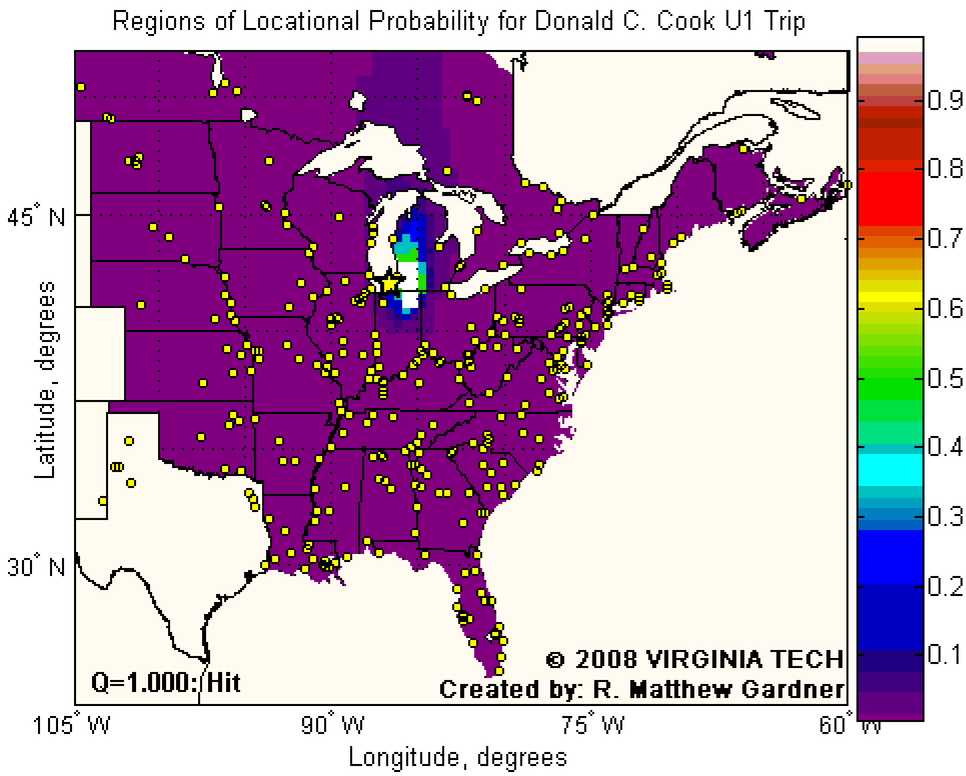
Regions of Locational Probability for Donald C. Cook U1 Trip
45° N
30° N
Latitude, degrees
105° W
90° W
75° W
60° W
Longitude, degrees
Q=1.000: Hit
© 2008 VIRGINIA TECH
Created by: R. Matthew Gardner
0.9
0.8
0.7
0.6
0.5
0.4
0.3
0.2
0.1

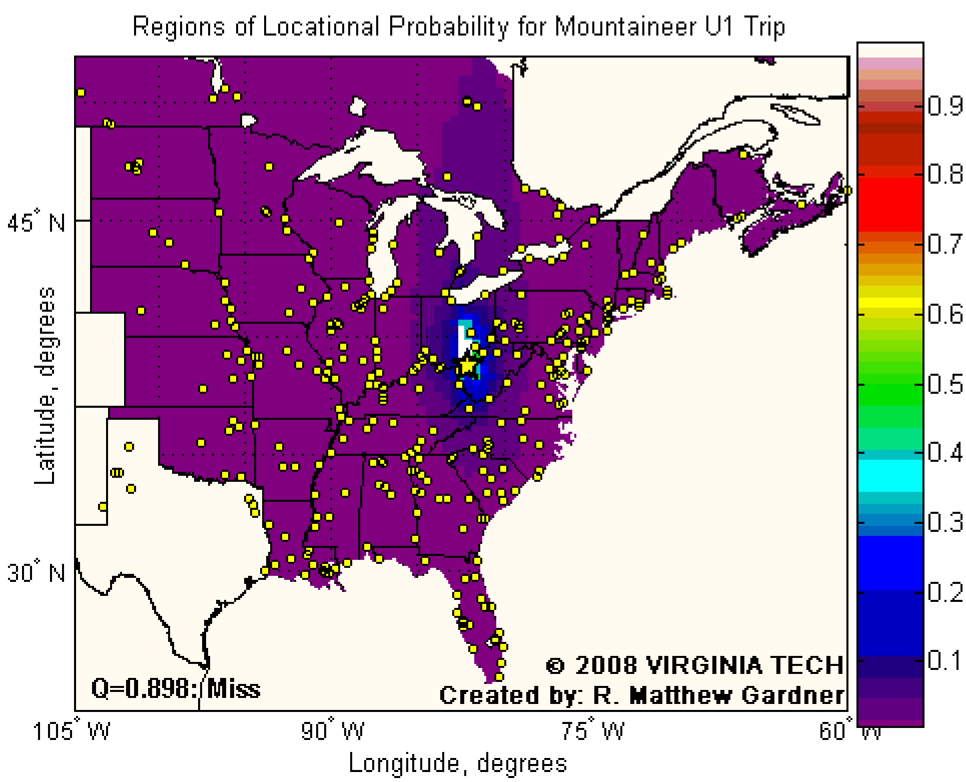
Regions of Locational Probability for Mountaineer U1 Trip
45° N
30° N
Latitude, degrees
105° W
90° W
75° W
60° W
Longitude, degrees
Q=0.898: Miss
© 2008 VIRGINIA TECH
Created by: R. Matthew Gardner
0.9
0.8
0.7
0.6
0.5
0.4
0.3
0.2
0.1

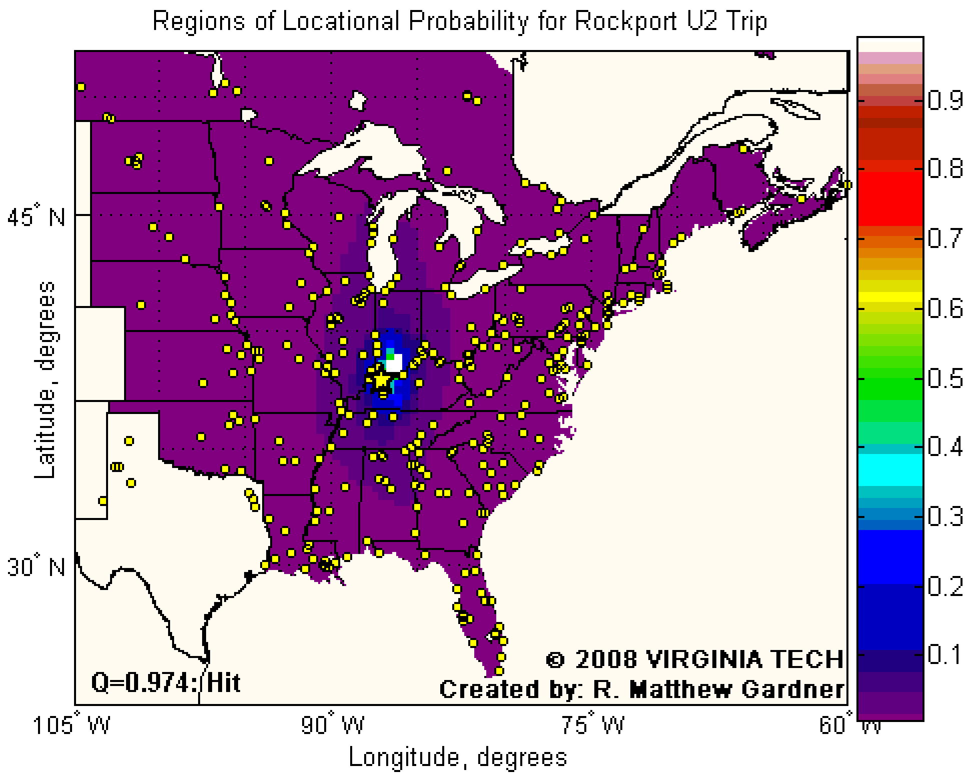
Regions of Locational Probability for Rockport U2 Trip
45° N
30° N
Latitude, degrees
105° W
90° W
75° W
60° W
Longitude, degrees
Q=0.974: Hit
© 2008 VIRGINIA TECH
Created by: R. Matthew Gardner
0.9
0.8
0.7
0.6
0.5
0.4
0.3
0.2
0.1

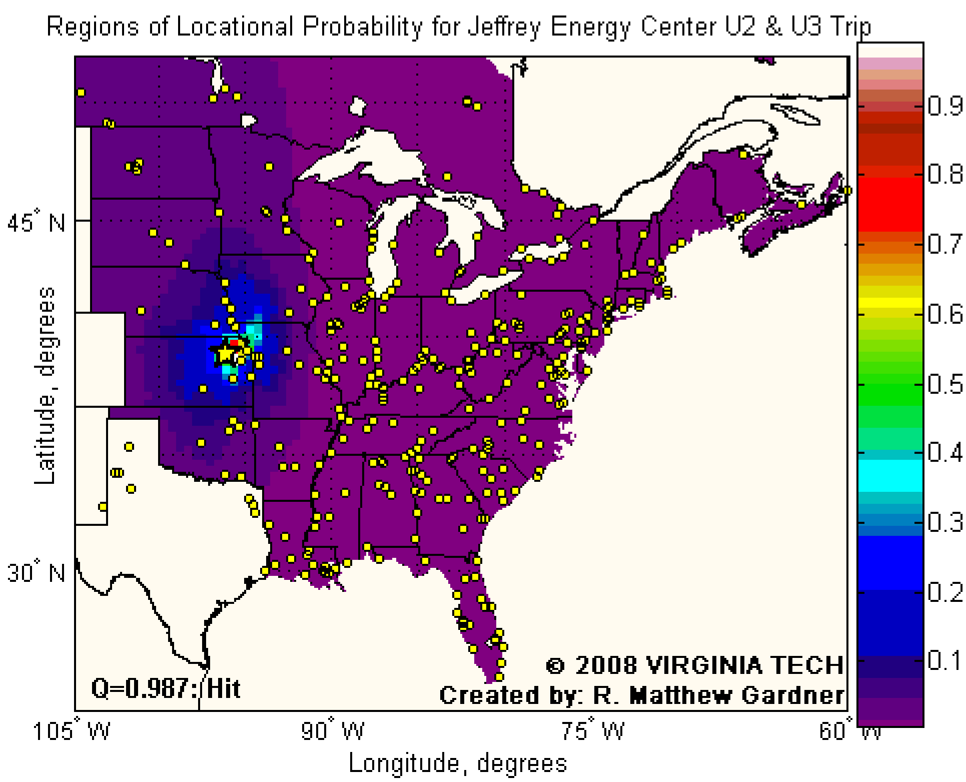
Regions of Locational Probability for Jeffrey Energy Center U2 & U3 Trip
45° N
30° N
Latitude, degrees
105° W
90° W
75° W
60° W
Longitude, degrees
Q=0.987: Hit
© 2008 VIRGINIA TECH
Created by: R. Matthew Gardner
0.9
0.8
0.7
0.6
0.5
0.4
0.3
0.2
0.1

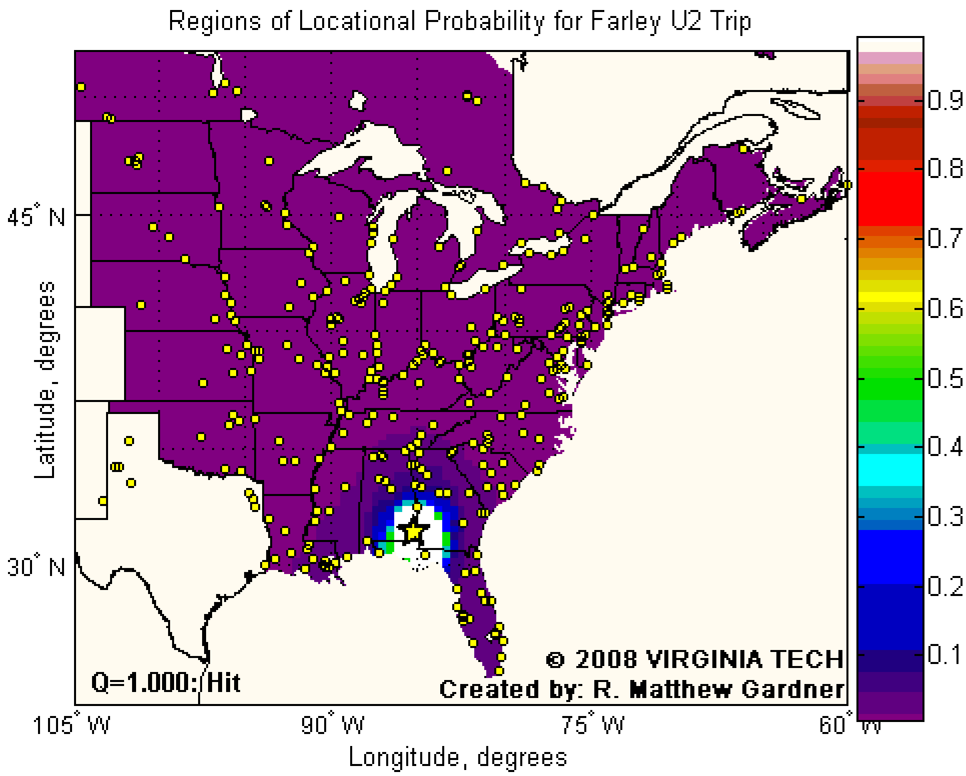
Regions of Locational Probability for Farley U2 Trip
45° N
30° N
Latitude, degrees
105° W
90° W
75° W
60° W
Longitude, degrees
Q=1.000: Hit
© 2008 VIRGINIA TECH
Created by: R. Matthew Gardner
0.9
0.8
0.7
0.6
0.5
0.4
0.3
0.2
0.1

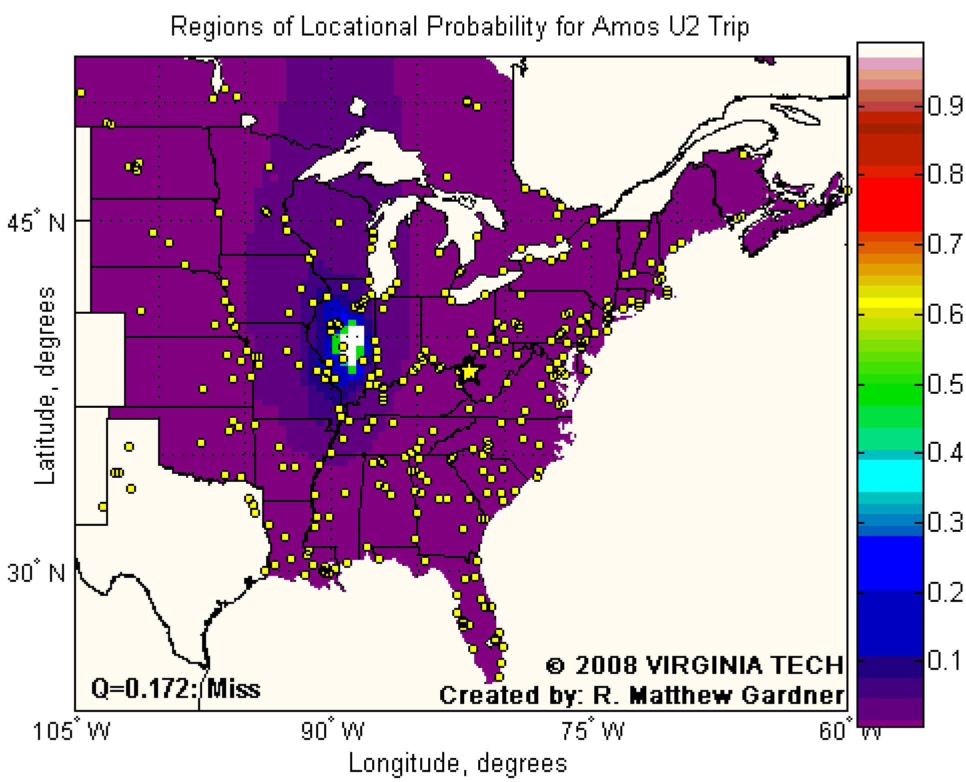
Regions of Locational Probability for Amos U2 Trip
45° N
30° N
Latitude, degrees
105° W
90° W
75° W
60° W
Longitude, degrees
Q=0.172: Miss
© 2008 VIRGINIA TECH
Created by: R. Matthew Gardner
0.9
0.8
0.7
0.6
0.5
0.4
0.3
0.2
0.1

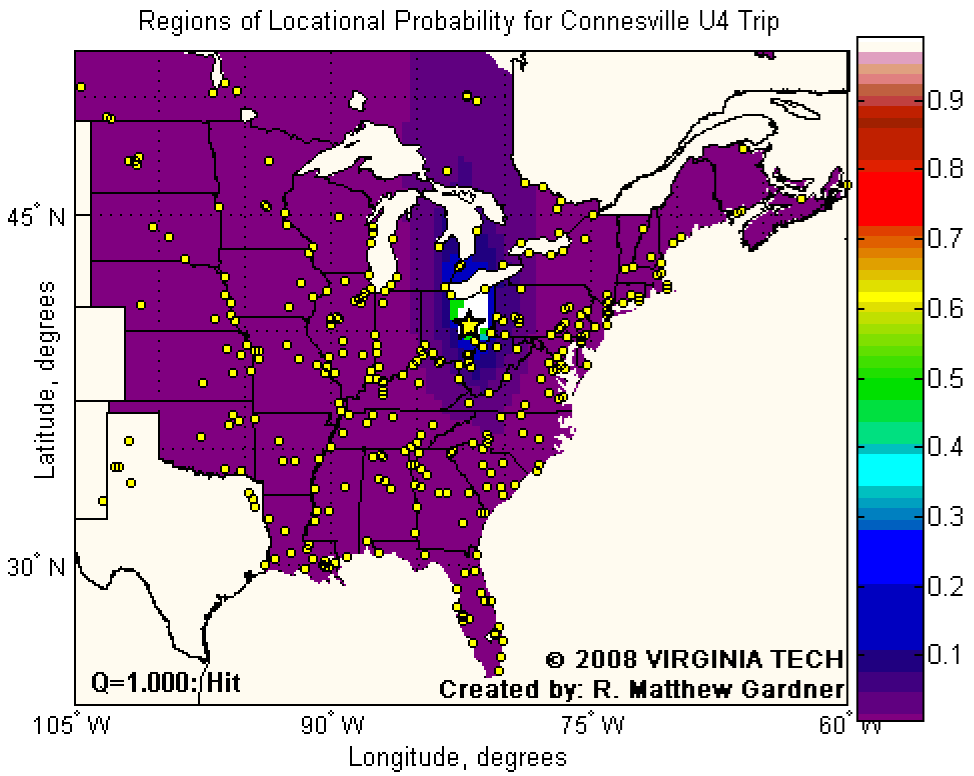
Regions of Locational Probability for Connesville U4 Trip
45° N
30° N
Latitude, degrees
105° W
90° W
75° W
60° W
Longitude, degrees
Q=1.000: Hit
© 2008 VIRGINIA TECH
Created by: R. Matthew Gardner
0.9
0.8
0.7
0.6
0.5
0.4
0.3
0.2
0.1

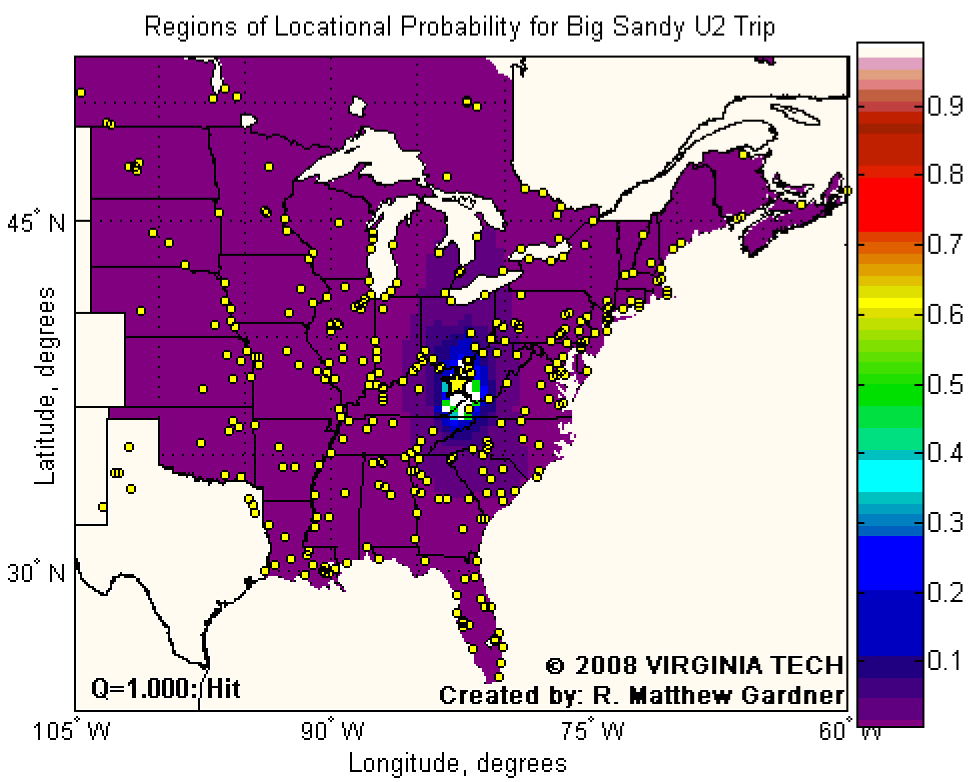
Regions of Locational Probability for Big Sandy U2 Trip
45° N
30° N
Latitude, degrees
105° W
90° W
75° W
60° W
Longitude, degrees
Q=1.000: Hit
© 2008 VIRGINIA TECH
Created by: R. Matthew Gardner
0.9
0.8
0.7
0.6
0.5
0.4
0.3
0.2
0.1

Appendix XXI: Variance-Weighted Frequency-Based Event Location (2007 Event Observations)

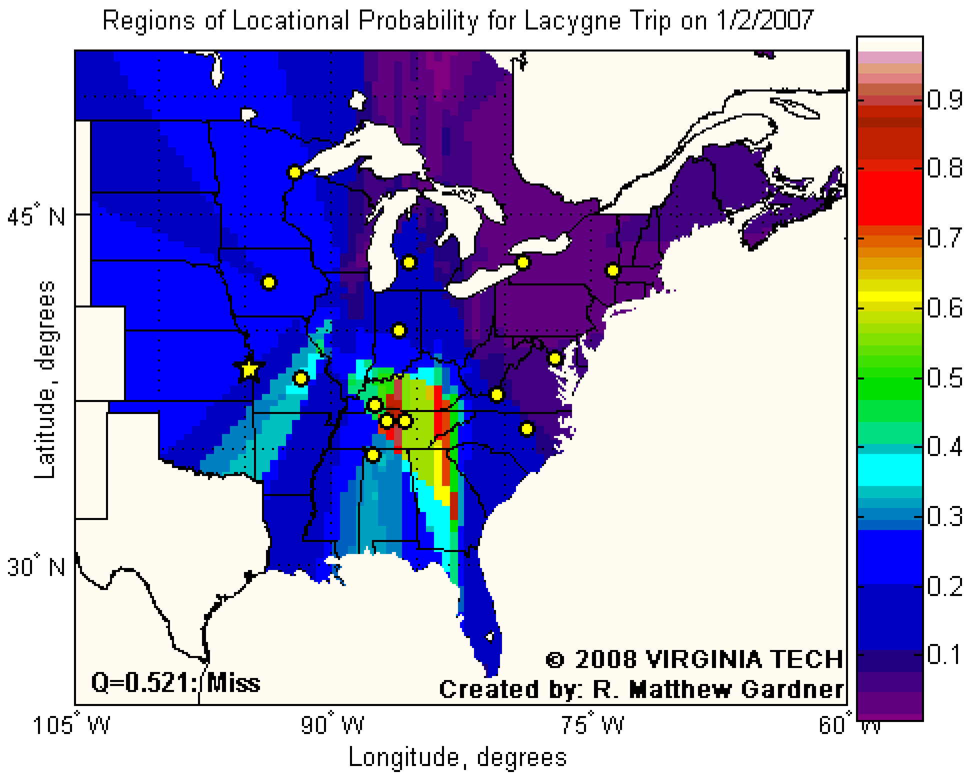

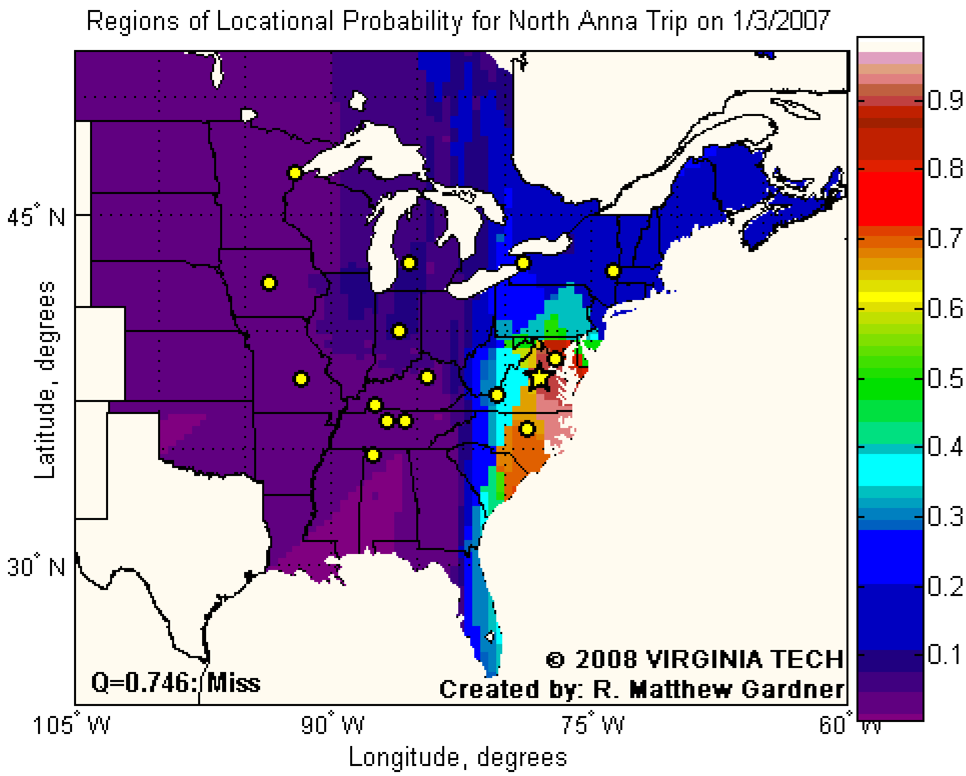
Regions of Locational Probability for North Anna Trip on 1/3/2007
45° N
30° N
Latitude, degrees
105° W
90° W
75° W
60° W
Longitude, degrees
Q=0.746: Miss
© 2008 VIRGINIA TECH
Created by: R. Matthew Gardner
0.9
0.8
0.7
0.6
0.5
0.4
0.3
0.2
0.1

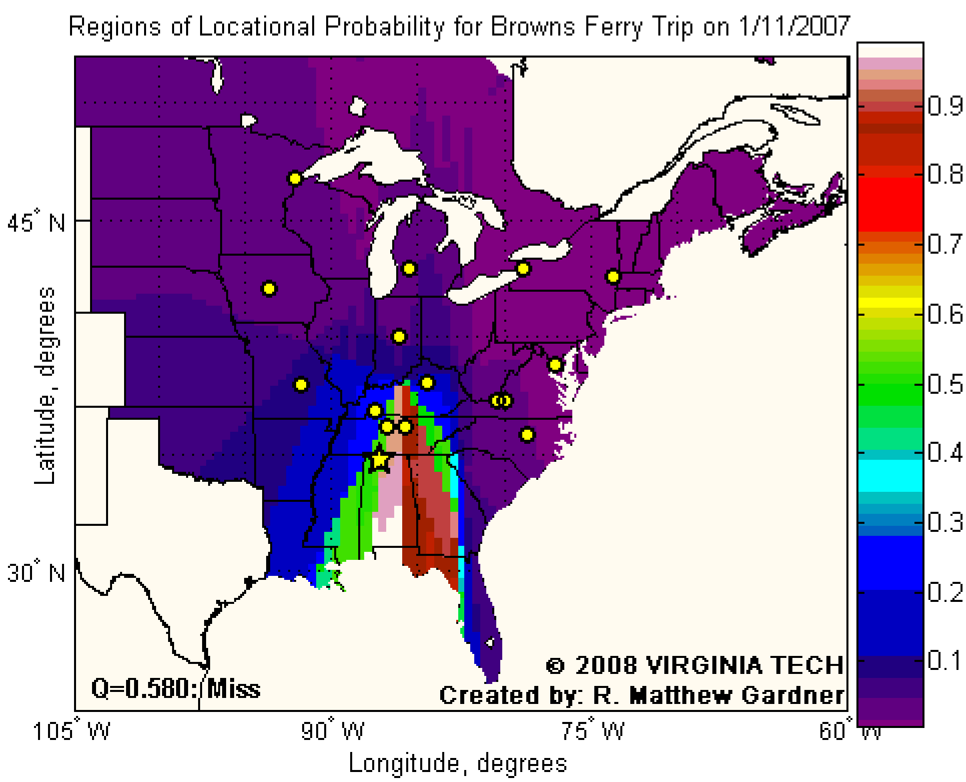
Regions of Locational Probability for Browns Ferry Trip on 1/11/2007
45° N
30° N
Latitude, degrees
105° W
90° W
75° W
60° W
Longitude, degrees
Q=0.580: Miss
© 2008 VIRGINIA TECH
Created by: R. Matthew Gardner
0.9
0.8
0.7
0.6
0.5
0.4
0.3
0.2
0.1

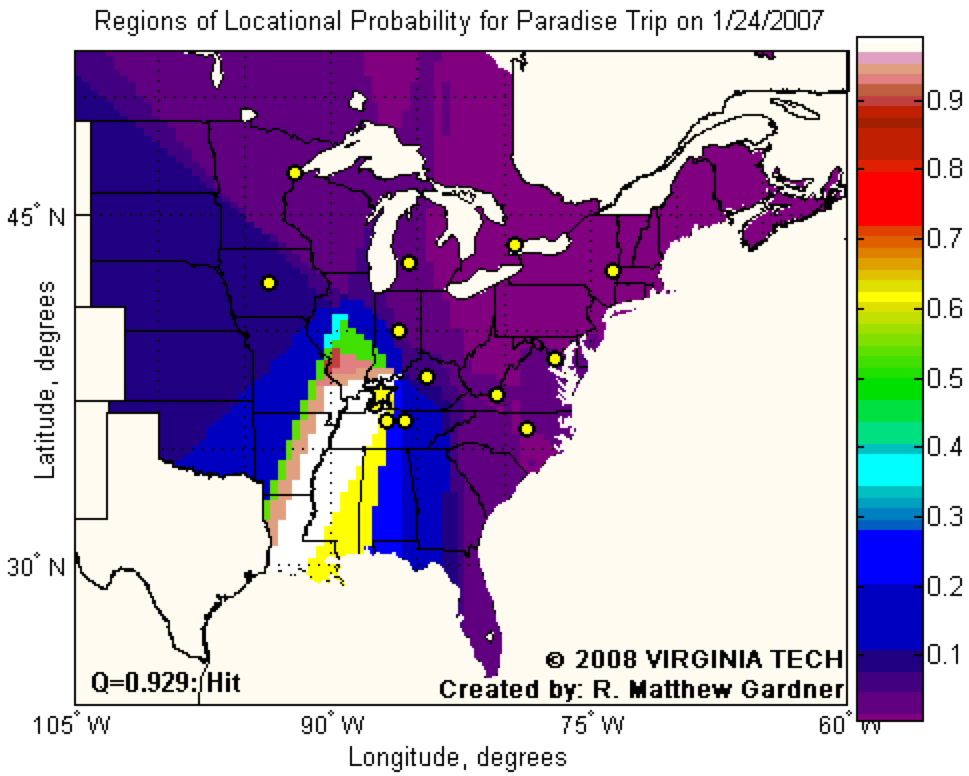
Regions of Locational Probability for Paradise Trip on 1/24/2007
45° N
30° N
Latitude, degrees
105° W
90° W
75° W
60° W
Longitude, degrees
Q=0.929: Hit
© 2008 VIRGINIA TECH
Created by: R. Matthew Gardner
0.9
0.8
0.7
0.6
0.5
0.4
0.3
0.2
0.1

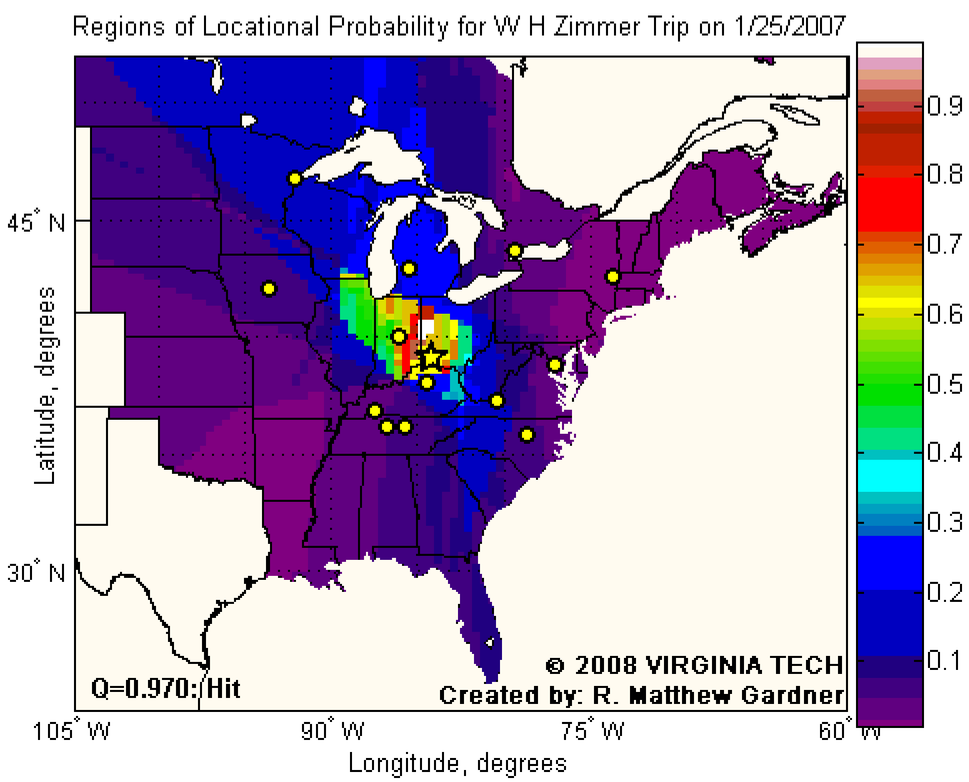
Regions of Locational Probability for W H Zimmer Trip on 1/25/2007
45° N
30° N
Latitude, degrees
105° W
90° W
75° W
60° W
Longitude, degrees
Q=0.970: Hit
© 2008 VIRGINIA TECH
Created by: R. Matthew Gardner
0.9
0.8
0.7
0.6
0.5
0.4
0.3
0.2
0.1

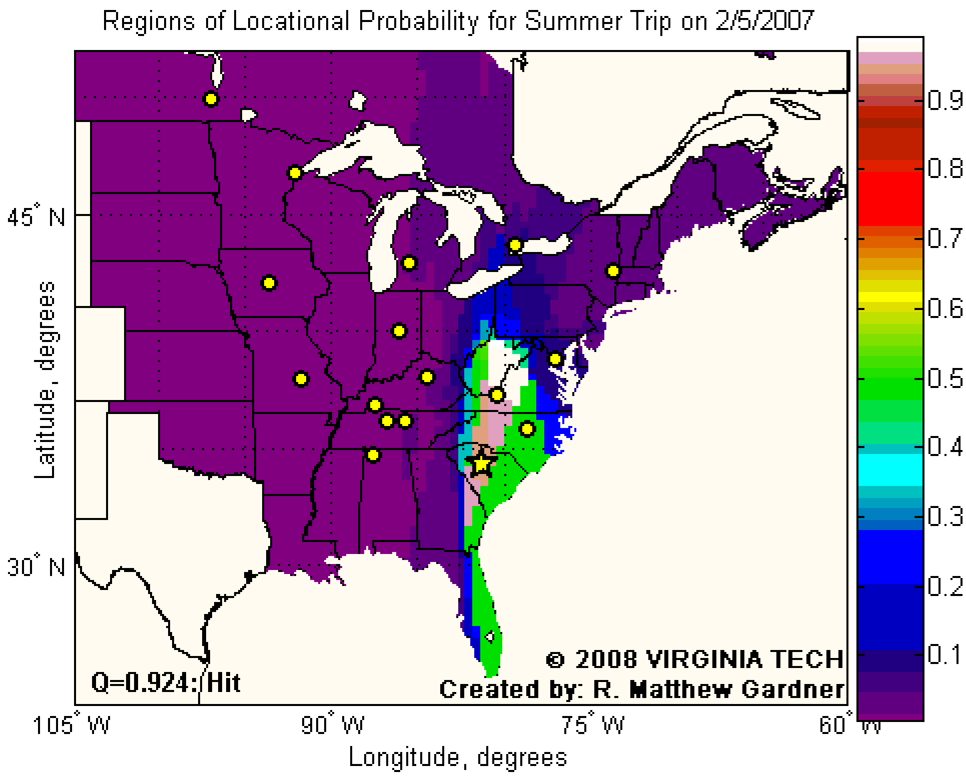
Regions of Locational Probability for Summer Trip on 2/5/2007
45° N
30° N
Latitude, degrees
105° W
90° W
75° W
60° W
Longitude, degrees
Q=0.924: Hit
© 2008 VIRGINIA TECH
Created by: R. Matthew Gardner
0.9
0.8
0.7
0.6
0.5
0.4
0.3
0.2
0.1

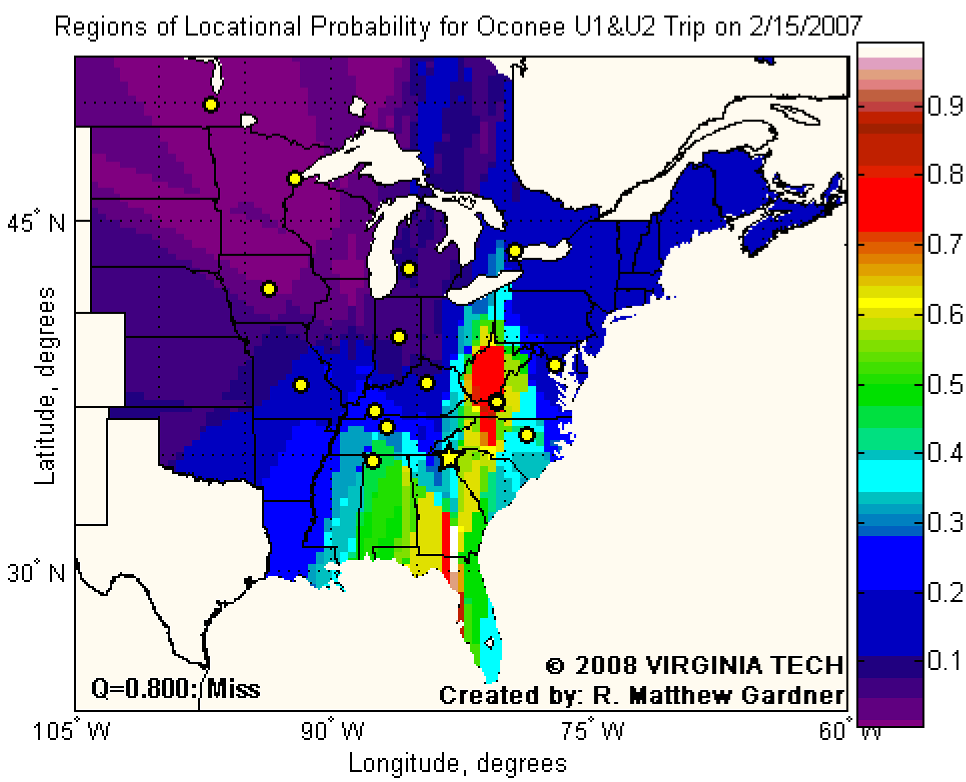
Regions of Locational Probability for Oconee U1&U2 Trip on 2/15/2007
45° N
30° N
Latitude, degrees
105° W
90° W
75° W
60° W
Longitude, degrees
Q=0.800: Miss
© 2008 VIRGINIA TECH
Created by: R. Matthew Gardner
0.9
0.8
0.7
0.6
0.5
0.4
0.3
0.2
0.1

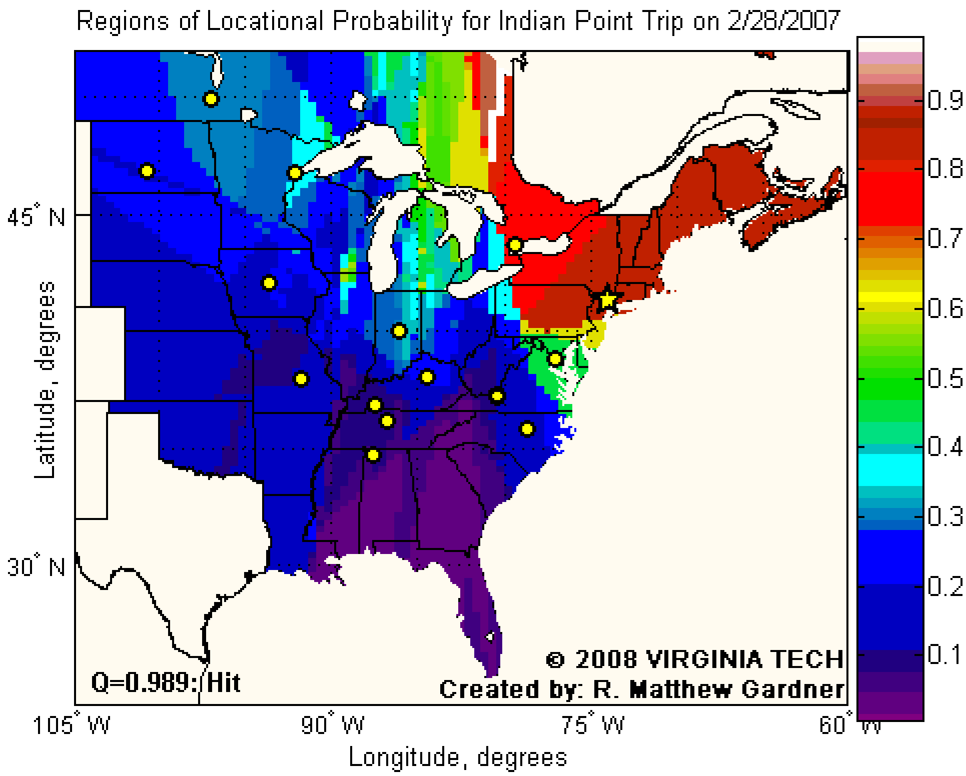
Regions of Locational Probability for Indian Point Trip on 2/28/2007
45° N
30° N
Latitude, degrees
105° W
90° W
75° W
60° W
Longitude, degrees
Q=0.989: Hit
© 2008 VIRGINIA TECH
Created by: R. Matthew Gardner
0.9
0.8
0.7
0.6
0.5
0.4
0.3
0.2
0.1

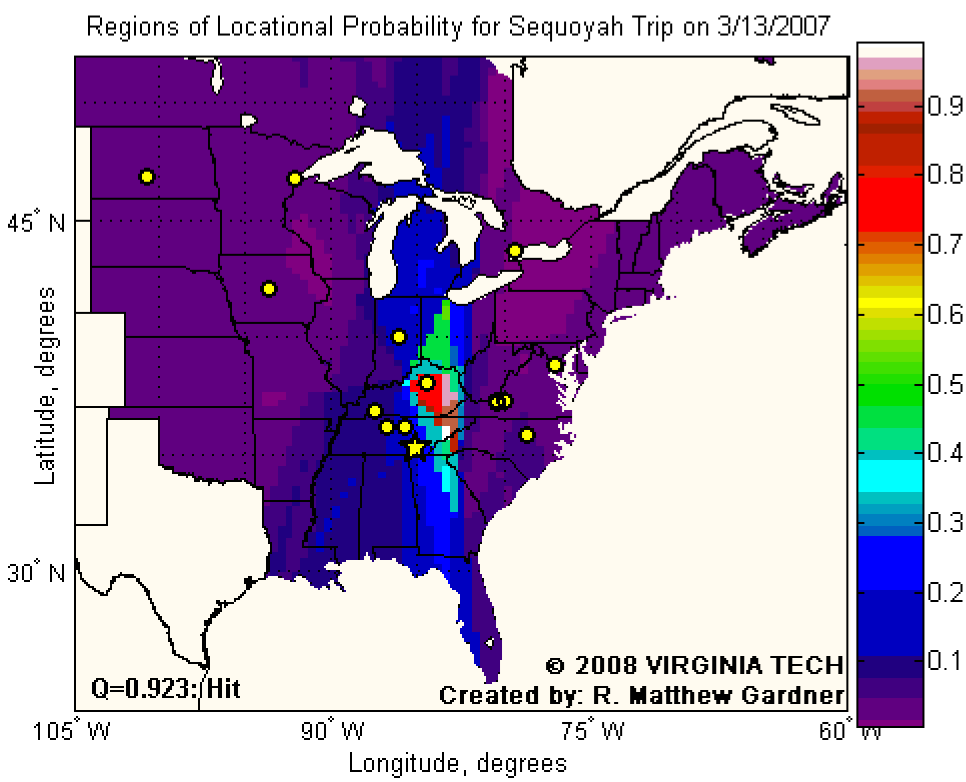
Regions of Locational Probability for Sequoyah Trip on 3/13/2007
45° N
30° N
Latitude, degrees
105° W
90° W
75° W
60° W
Longitude, degrees
Q=0.923: Hit
© 2008 VIRGINIA TECH
Created by: R. Matthew Gardner
0.9
0.8
0.7
0.6
0.5
0.4
0.3
0.2
0.1

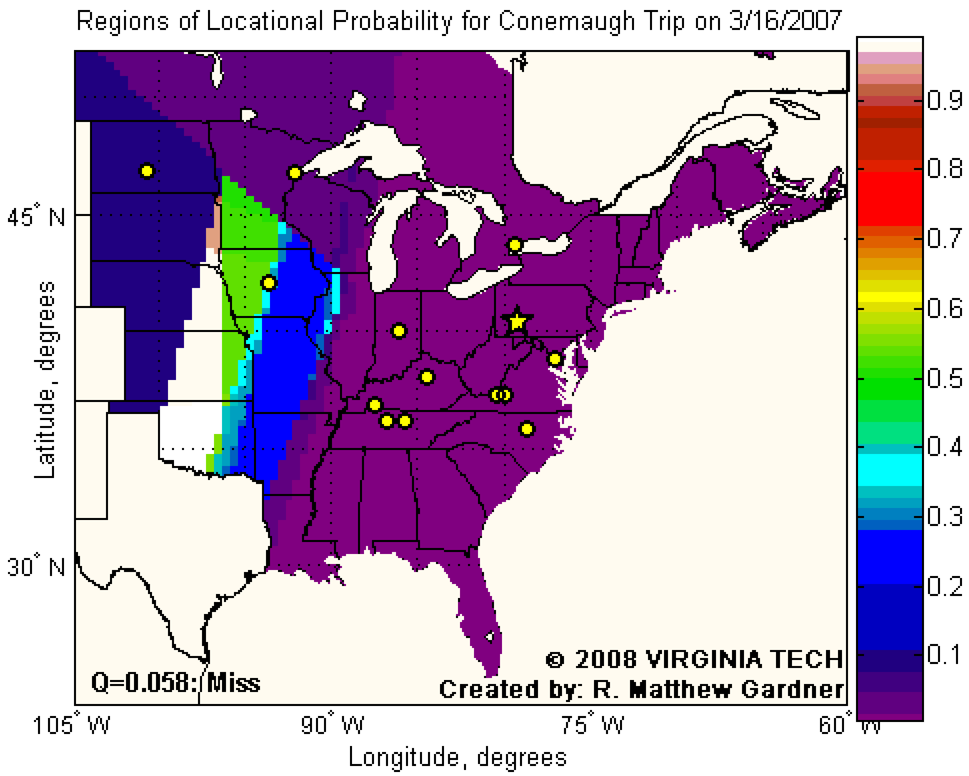
Regions of Locational Probability for Conemaugh Trip on 3/16/2007
45° N
30° N
Latitude, degrees
105° W
90° W
75° W
60° W
Longitude, degrees
Q=0.058:/Miss
© 2008 VIRGINIA TECH
Created by: R. Matthew Gardner
0.9
0.8
0.7
0.6
0.5
0.4
0.3
0.2
0.1

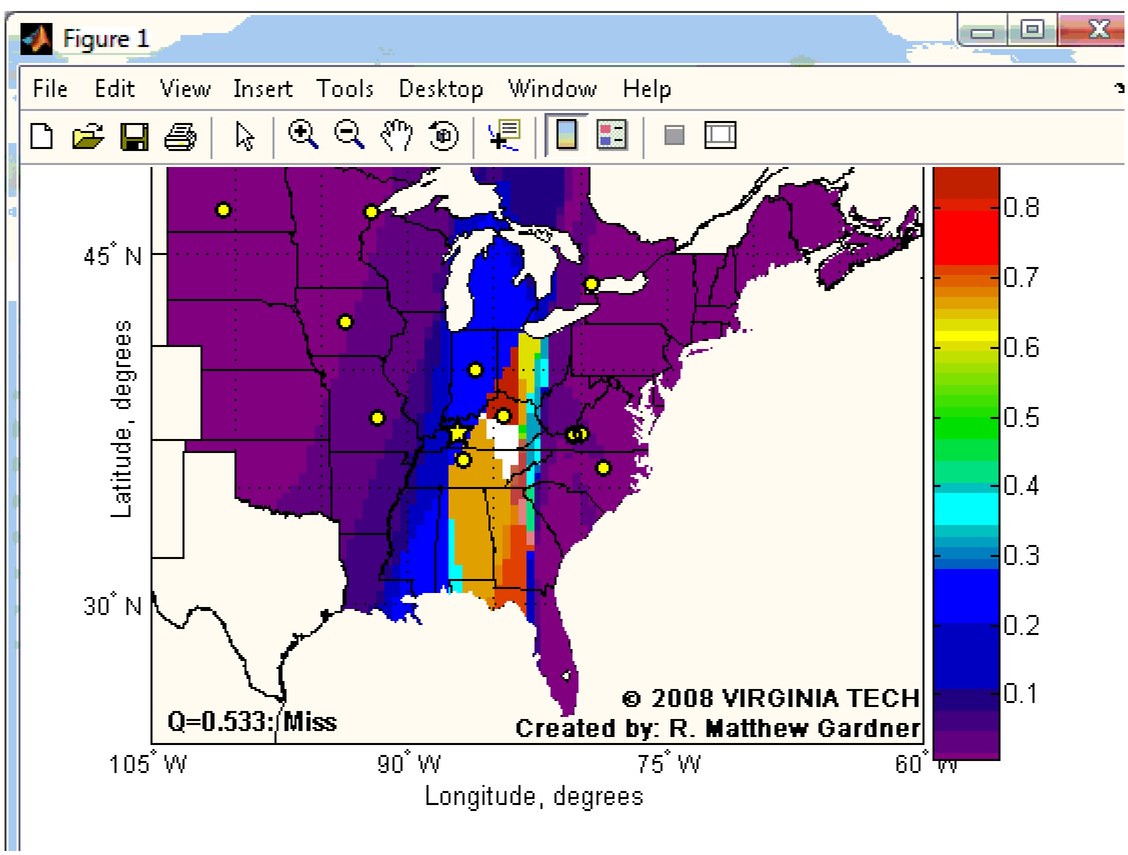
Figure 1
File Edit View Insert Tools Desktop Window Help
45° N
30° N
Latitude, degrees
105° W
90° W
75° W
60° W
Longitude, degrees
Q=0.533:/Miss
© 2008 VIRGINIA TECH
Created by: R. Matthew Gardner
0.8
0.7
0.6
0.5
0.4
0.3
0.2
0.1

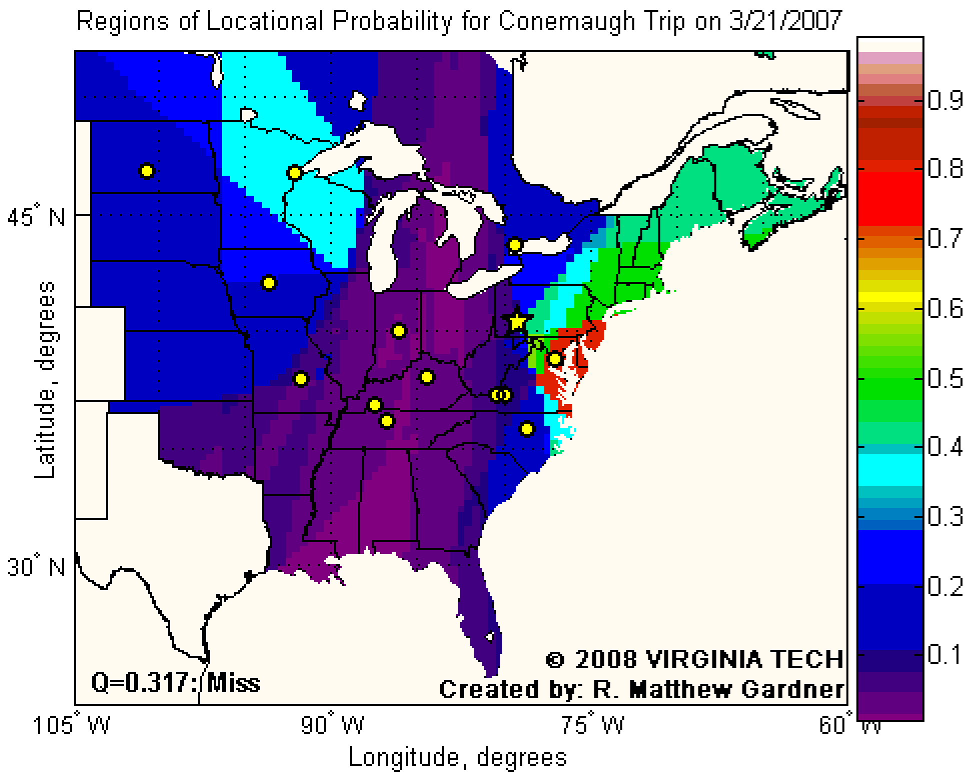
Regions of Locational Probability for Conemaugh Trip on 3/21/2007
45° N
30° N
Latitude, degrees
105° W
90° W
75° W
60° W
Longitude, degrees
Q=0.317: Miss
© 2008 VIRGINIA TECH
Created by: R. Matthew Gardner
0.9
0.8
0.7
0.6
0.5
0.4
0.3
0.2
0.1

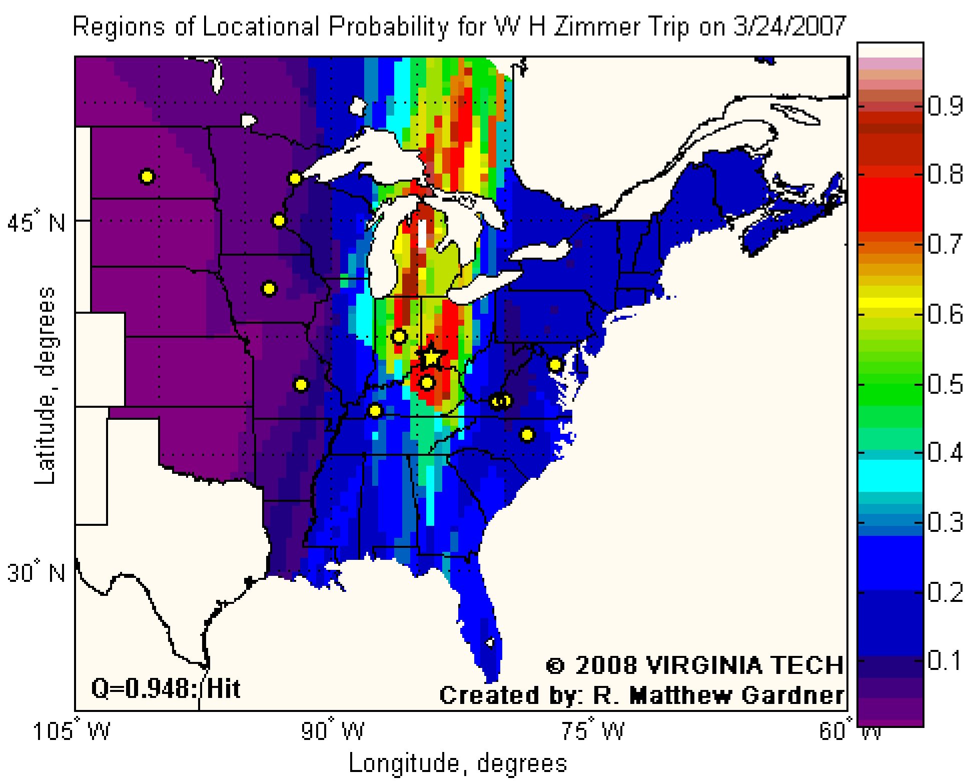
Regions of Locational Probability for W H Zimmer Trip on 3/24/2007
45° N
30° N
Latitude, degrees
105° W
90° W
75° W
60° W
Longitude, degrees
Q=0.948: Hit
© 2008 VIRGINIA TECH
Created by: R. Matthew Gardner
0.9
0.8
0.7
0.6
0.5
0.4
0.3
0.2
0.1

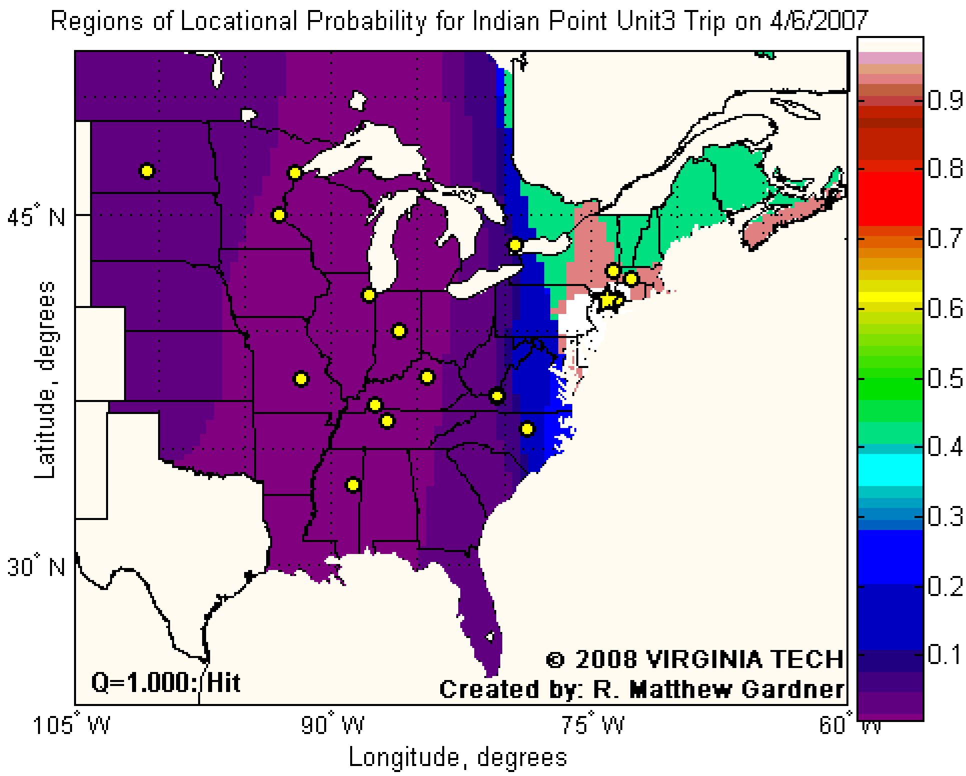
Regions of Locational Probability for Indian Point Unit3 Trip on 4/6/2007
45° N
30° N
Latitude, degrees
105° W
90° W
75° W
60° W
Longitude, degrees
Q=1.000: Hit
© 2008 VIRGINIA TECH
Created by: R. Matthew Gardner
0.9
0.8
0.7
0.6
0.5
0.4
0.3
0.2
0.1

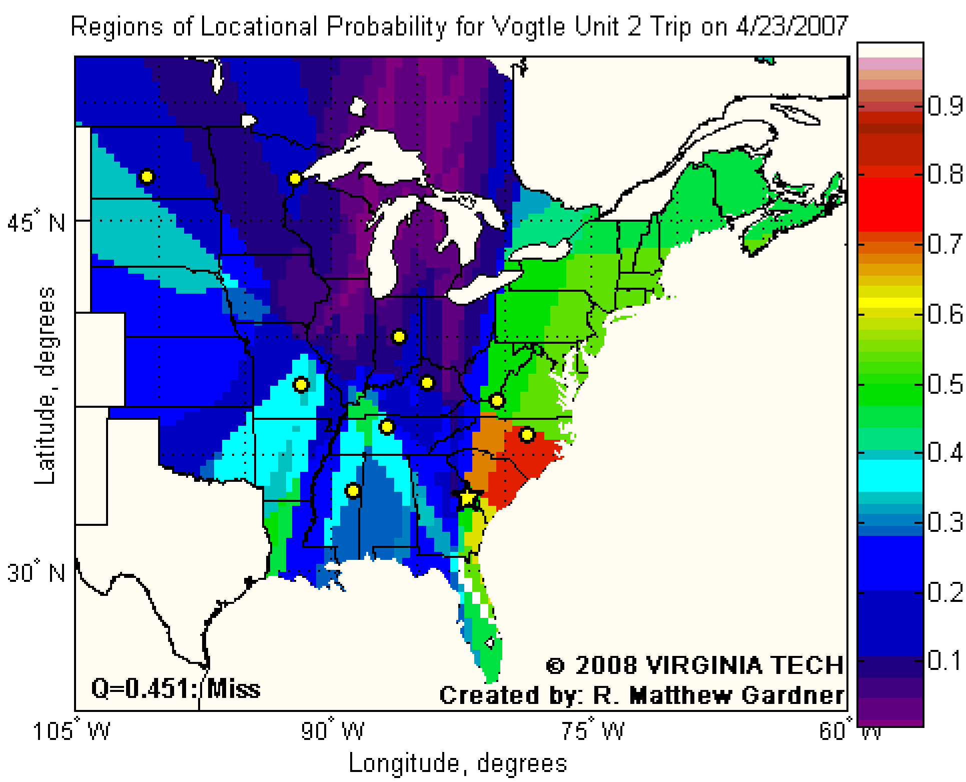
Regions of Locational Probability for Vogtle Unit 2 Trip on 4/23/2007
45° N
30° N
Latitude, degrees
105° W
90° W
75° W
60° W
Longitude, degrees
Q=0.451: Miss
© 2008 VIRGINIA TECH
Created by: R. Matthew Gardner
0.9
0.8
0.7
0.6
0.5
0.4
0.3
0.2
0.1

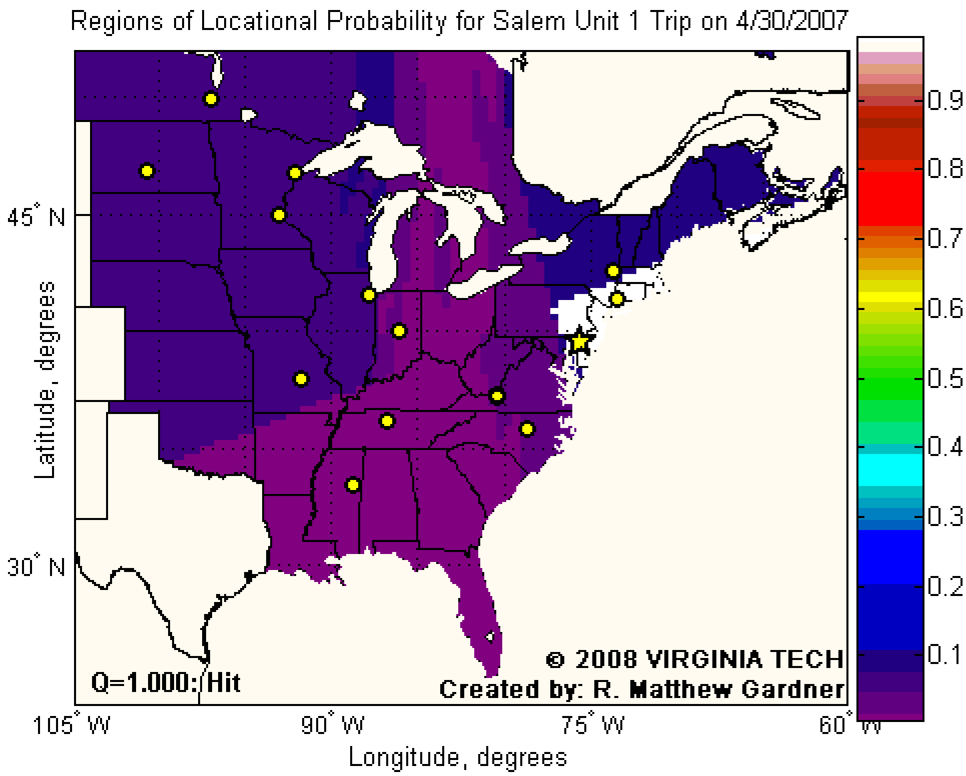
Regions of Locational Probability for Salem Unit 1 Trip on 4/30/2007
45° N
30° N
Latitude, degrees
105° W
90° W
75° W
60° W
Longitude, degrees
Q=1.000:/Hit
© 2008 VIRGINIA TECH
Created by: R. Matthew Gardner
0.9
0.8
0.7
0.6
0.5
0.4
0.3
0.2
0.1

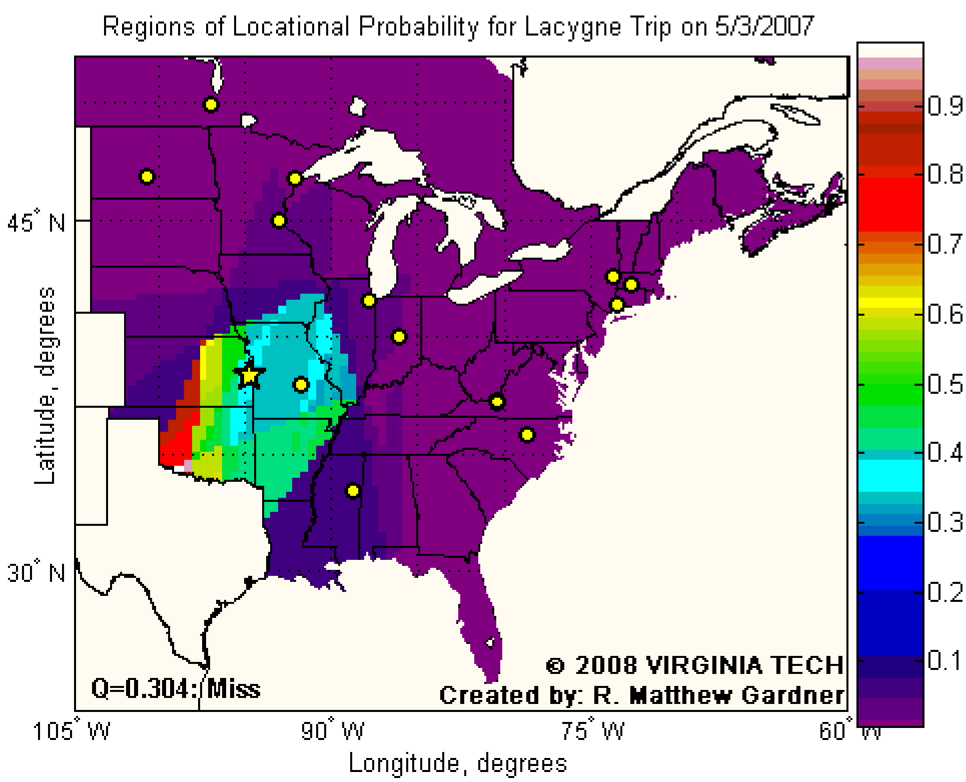
Regions of Locational Probability for Lacygne Trip on 5/3/2007
45° N
30° N
Latitude, degrees
105° W
90° W
75° W
60° W
Longitude, degrees
Q=0.304:/Miss
© 2008 VIRGINIA TECH
Created by: R. Matthew Gardner
0.9
0.8
0.7
0.6
0.5
0.4
0.3
0.2
0.1

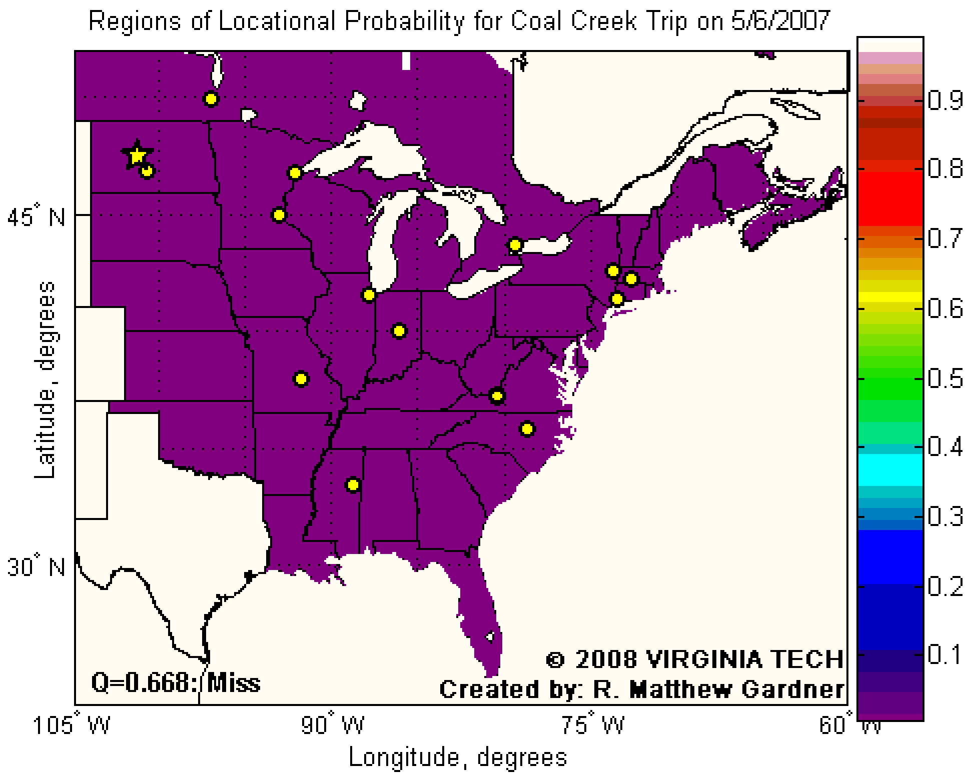
Regions of Locational Probability for Coal Creek Trip on 5/6/2007
45° N
30° N
Latitude, degrees
105° W
90° W
75° W
60° W
Longitude, degrees
Q=0.668:/Miss
© 2008 VIRGINIA TECH
Created by: R. Matthew Gardner
0.9
0.8
0.7
0.6
0.5
0.4
0.3
0.2
0.1

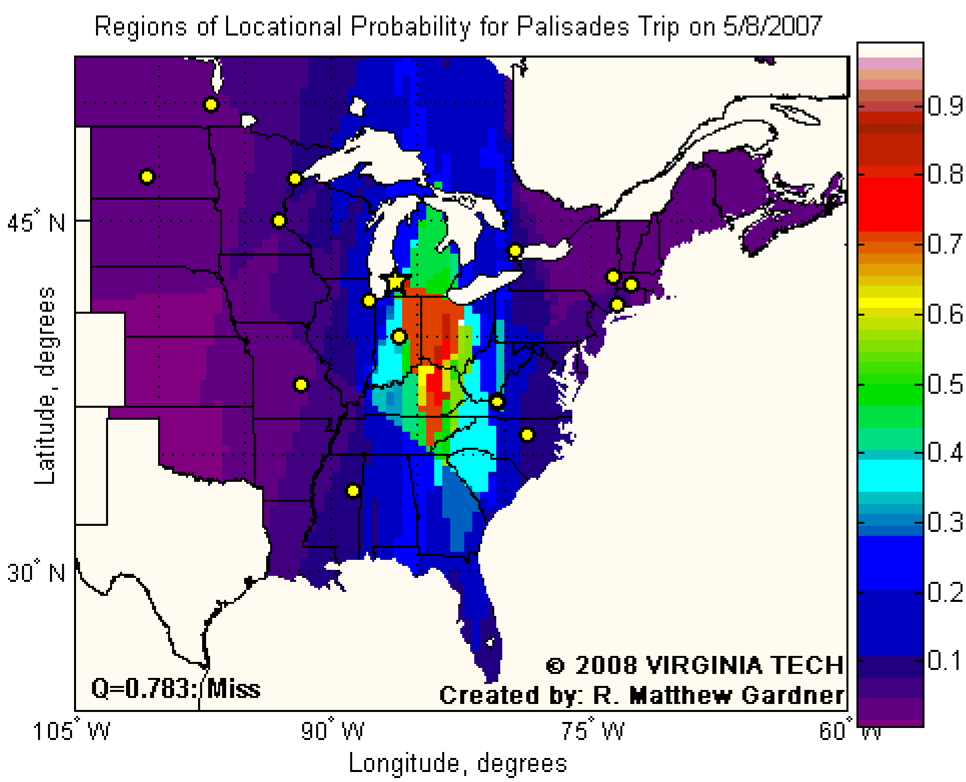
Regions of Locational Probability for Palisades Trip on 5/8/2007
45° N
30° N
Latitude, degrees
105° W
90° W
75° W
60° W
Longitude, degrees
Q=0.783:/Miss
© 2008 VIRGINIA TECH
Created by: R. Matthew Gardner
0.9
0.8
0.7
0.6
0.5
0.4
0.3
0.2
0.1

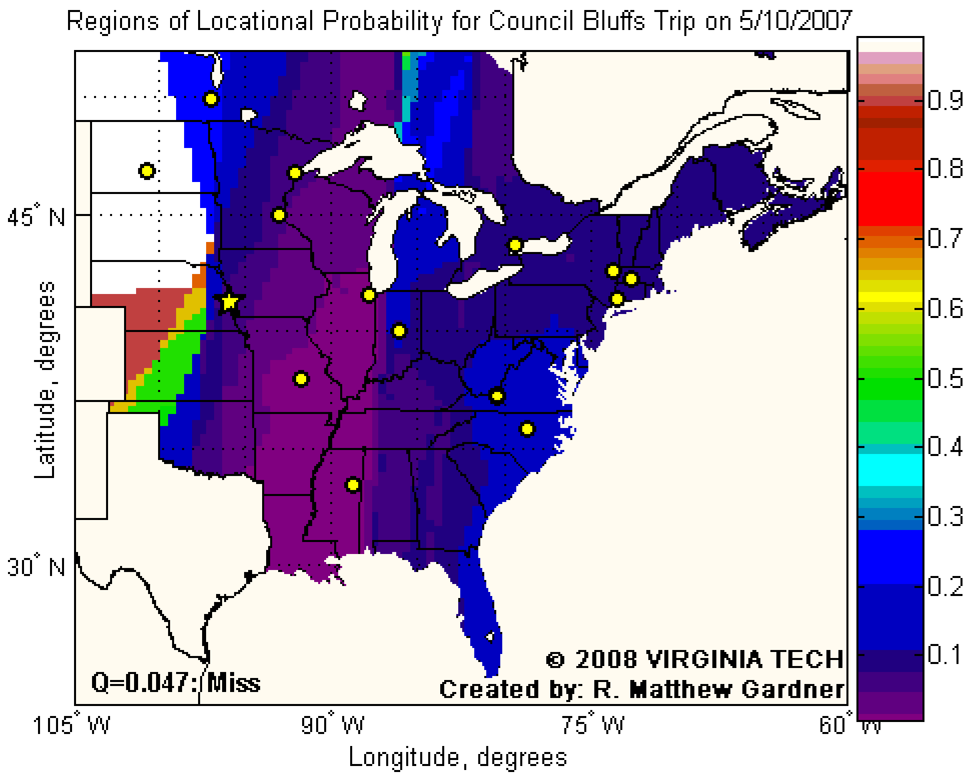
Regions of Locational Probability for Council Bluffs Trip on 5/10/2007
45° N
30° N
Latitude, degrees
105° W
90° W
75° W
60° W
Longitude, degrees
Q=0.047: Miss
© 2008 VIRGINIA TECH
Created by: R. Matthew Gardner
0.9
0.8
0.7
0.6
0.5
0.4
0.3
0.2
0.1

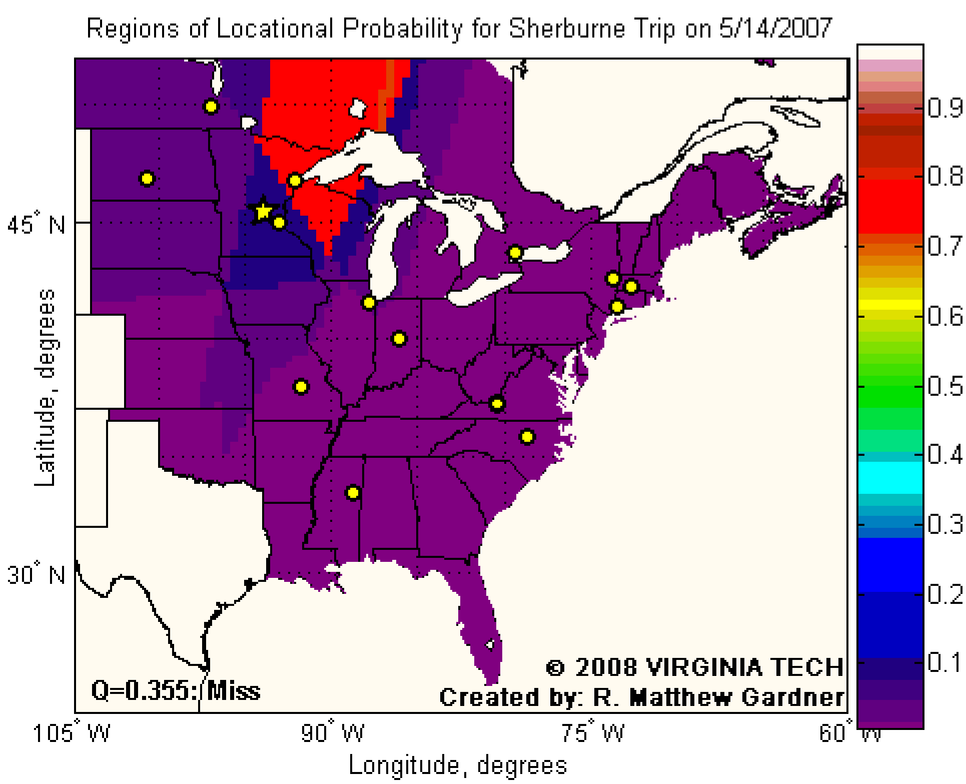
Regions of Locational Probability for Sherburne Trip on 5/14/2007
45° N
30° N
Latitude, degrees
105° W
90° W
75° W
60° W
Longitude, degrees
Q=0.355: Miss
© 2008 VIRGINIA TECH
Created by: R. Matthew Gardner
0.9
0.8
0.7
0.6
0.5
0.4
0.3
0.2
0.1

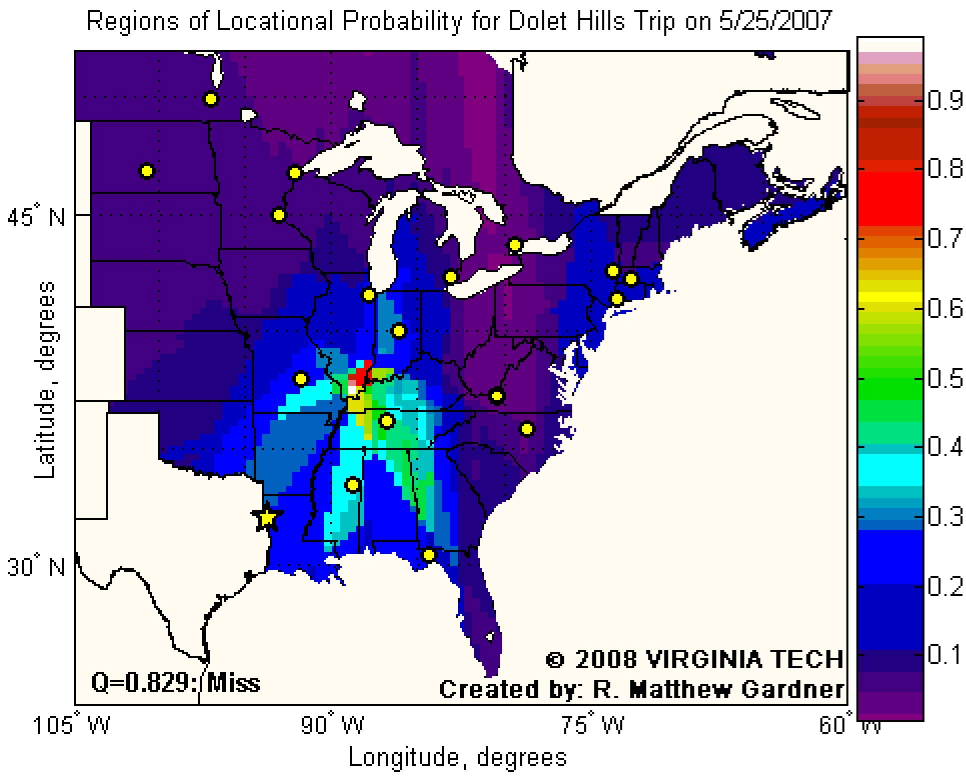
Regions of Locational Probability for Dolet Hills Trip on 5/25/2007
45° N
30° N
Latitude, degrees
105° W
90° W
75° W
60° W
Longitude, degrees
Q=0.829: Miss
© 2008 VIRGINIA TECH
Created by: R. Matthew Gardner
0.9
0.8
0.7
0.6
0.5
0.4
0.3
0.2
0.1

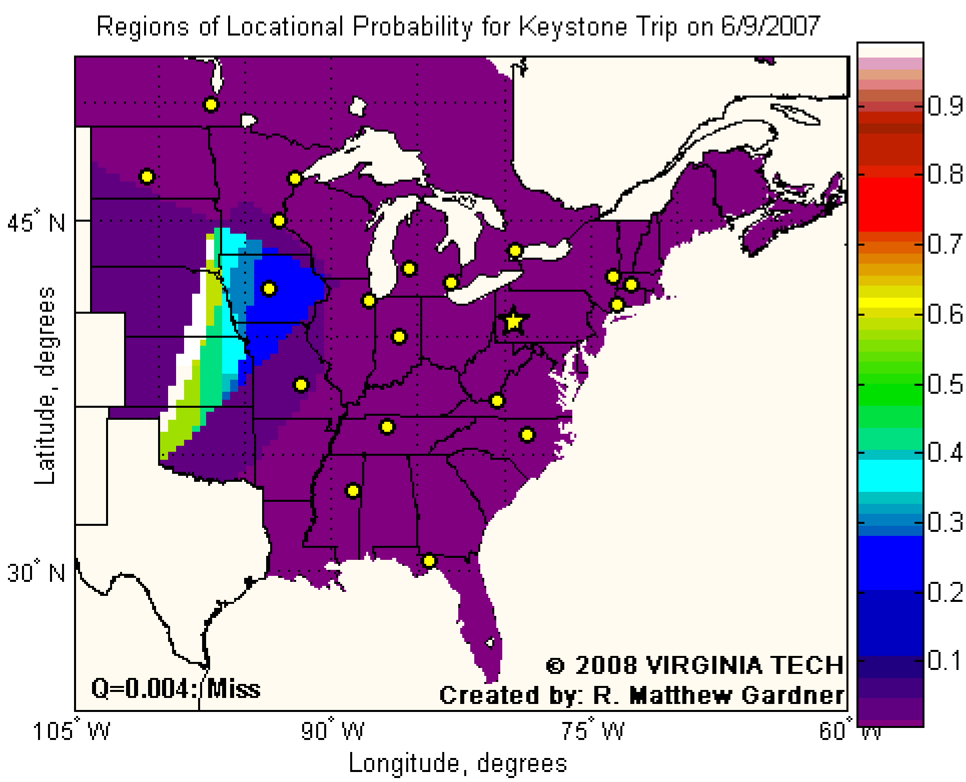
Regions of Locational Probability for Keystone Trip on 6/9/2007
45° N
30° N
Latitude, degrees
105° W
90° W
75° W
60° W
Longitude, degrees
Q=0.004: Miss
© 2008 VIRGINIA TECH
Created by: R. Matthew Gardner
0.9
0.8
0.7
0.6
0.5
0.4
0.3
0.2
0.1

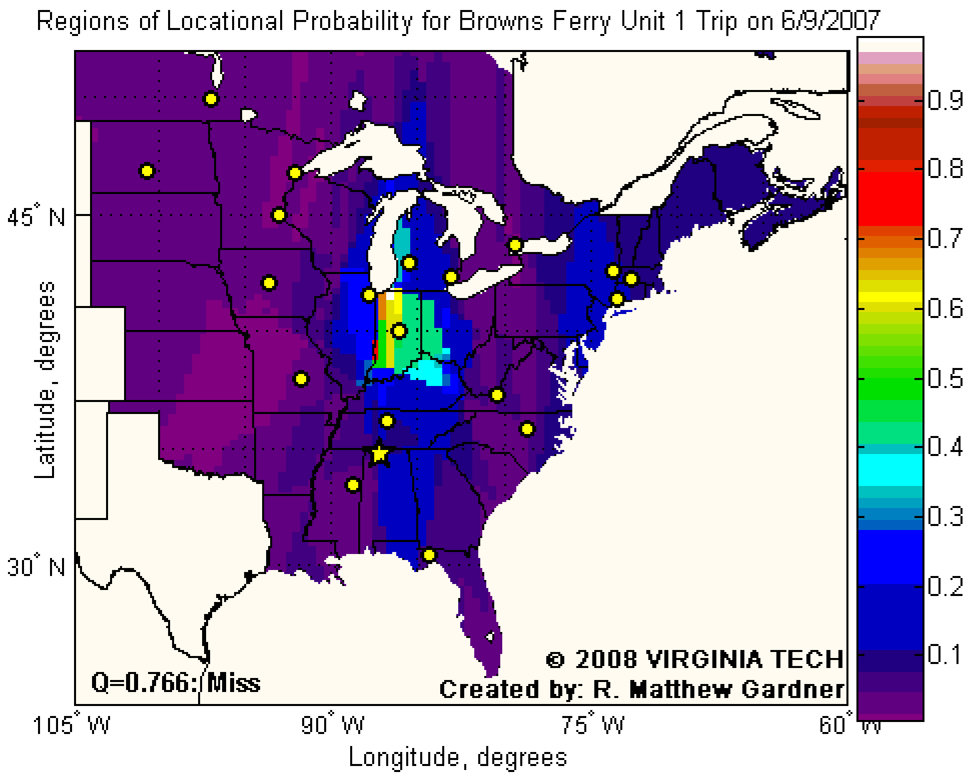
Regions of Locational Probability for Browns Ferry Unit 1 Trip on 6/9/2007
45° N
30° N
Latitude, degrees
105° W
90° W
75° W
60° W
Longitude, degrees
Q=0.766: Miss
© 2008 VIRGINIA TECH
Created by: R. Matthew Gardner
0.9
0.8
0.7
0.6
0.5
0.4
0.3
0.2
0.1

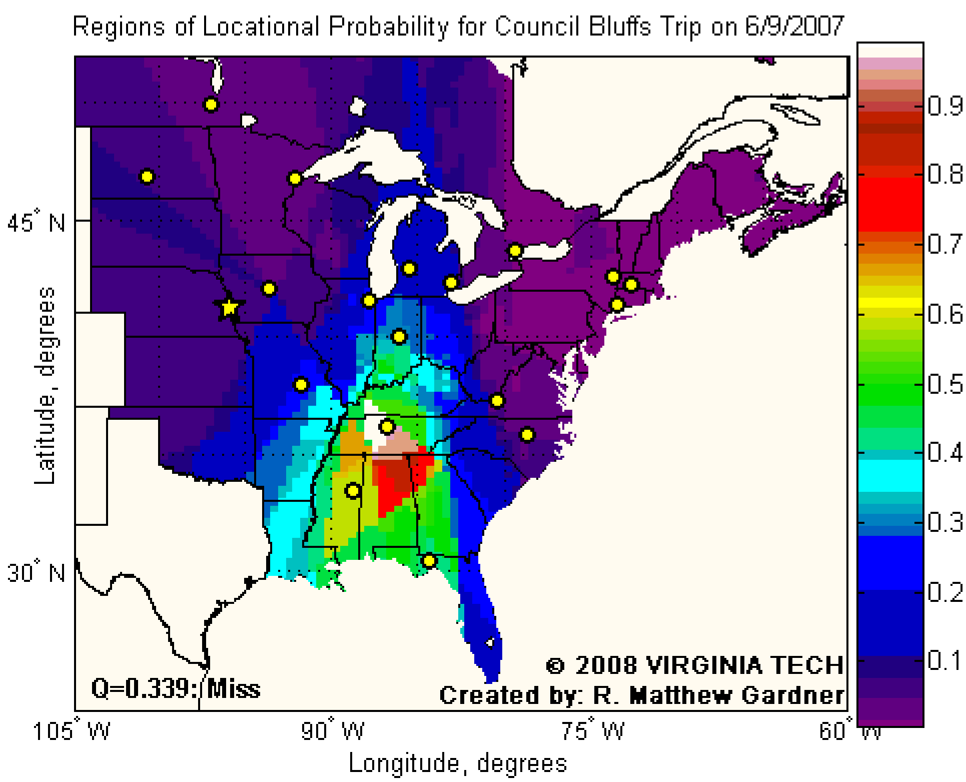
Regions of Locational Probability for Council Bluffs Trip on 6/9/2007
45° N
30° N
Latitude, degrees
105° W
90° W
75° W
60° W
Longitude, degrees
Q=0.339: Miss
© 2008 VIRGINIA TECH
Created by: R. Matthew Gardner
0.9
0.8
0.7
0.6
0.5
0.4
0.3
0.2
0.1

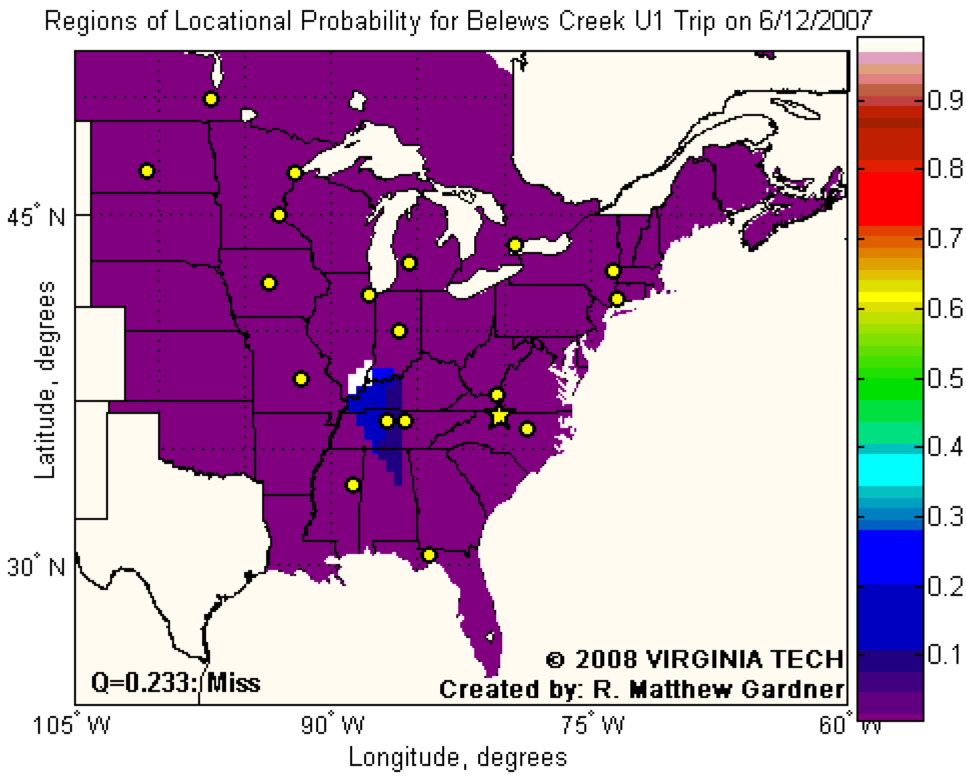
Regions of Locational Probability for Belews Creek U1 Trip on 6/12/2007
45° N
30° N
Latitude, degrees
105° W
90° W
75° W
60° W
Longitude, degrees
0.9
0.8
0.7
0.6
0.5
0.4
0.3
0.2
0.1
Q=0.233:/Miss
© 2008 VIRGINIA TECH
Created by: R. Matthew Gardner

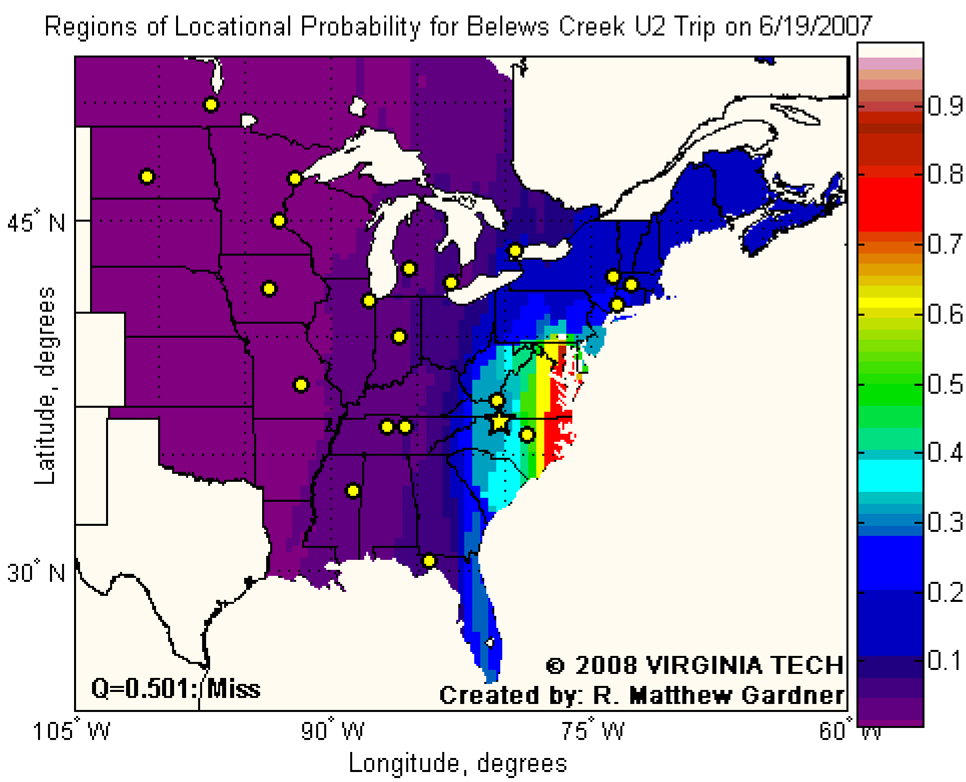
Regions of Locational Probability for Belews Creek U2 Trip on 6/19/2007
45° N
30° N
Latitude, degrees
105° W
90° W
75° W
60° W
Longitude, degrees
0.9
0.8
0.7
0.6
0.5
0.4
0.3
0.2
0.1
Q=0.501:/Miss
© 2008 VIRGINIA TECH
Created by: R. Matthew Gardner

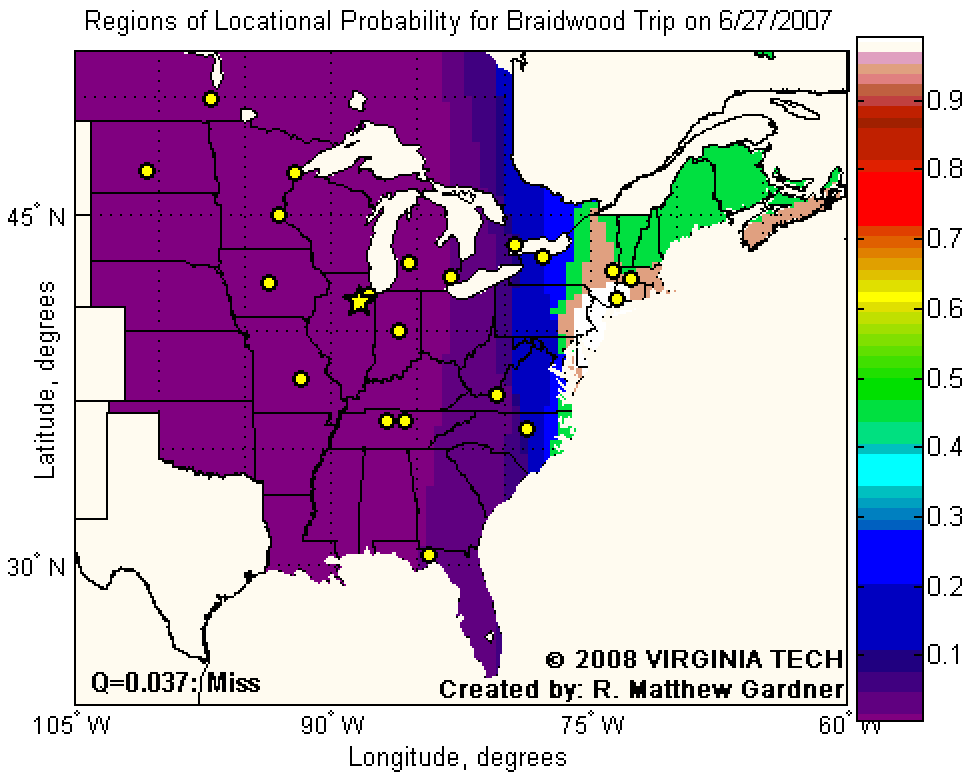
Regions of Locational Probability for Braidwood Trip on 6/27/2007
45° N
30° N
Latitude, degrees
105° W
90° W
75° W
60° W
Longitude, degrees
Q=0.037: Miss
© 2008 VIRGINIA TECH
Created by: R. Matthew Gardner
0.9
0.8
0.7
0.6
0.5
0.4
0.3
0.2
0.1

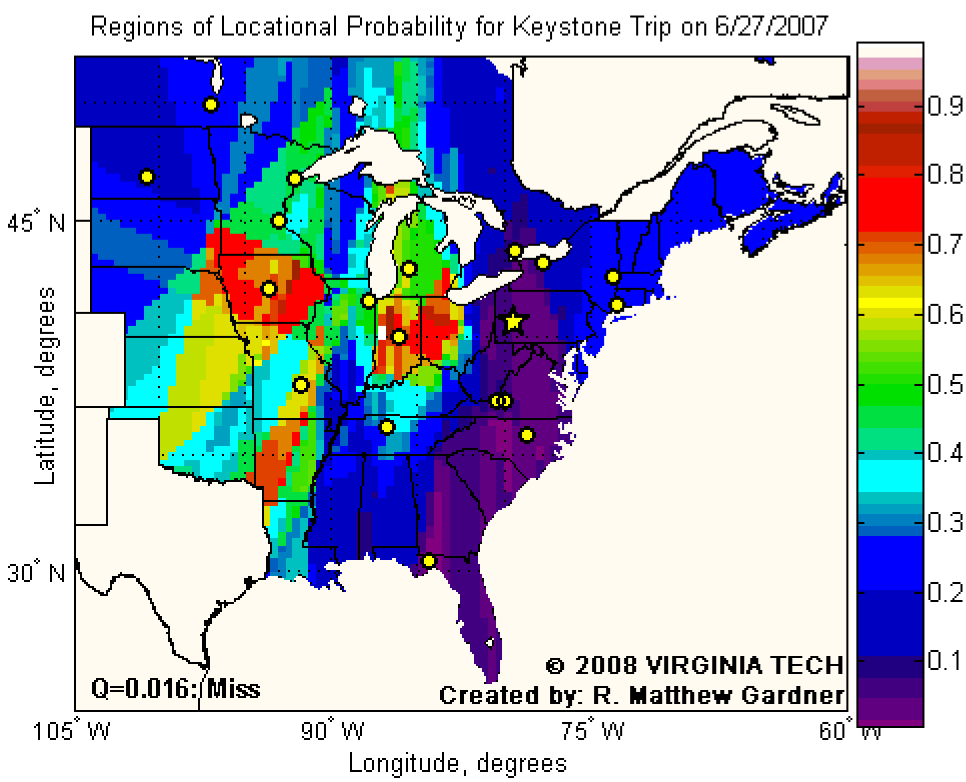
Regions of Locational Probability for Keystone Trip on 6/27/2007
45° N
30° N
Latitude, degrees
105° W
90° W
75° W
60° W
Longitude, degrees
Q=0.016: Miss
© 2008 VIRGINIA TECH
Created by: R. Matthew Gardner
0.9
0.8
0.7
0.6
0.5
0.4
0.3
0.2
0.1

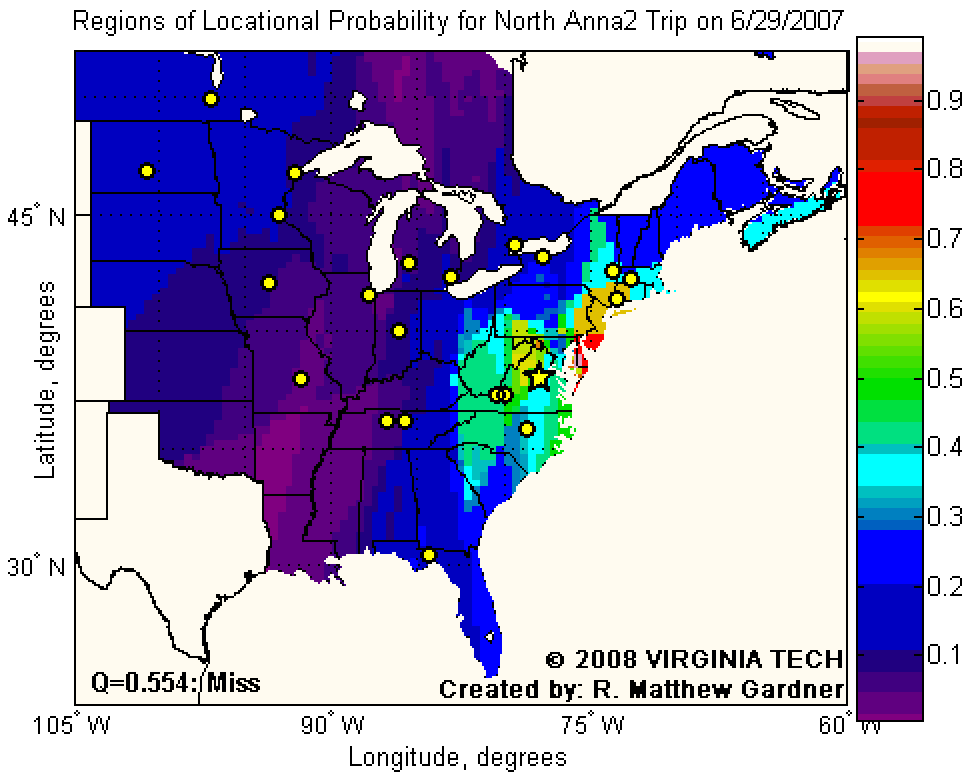
Regions of Locational Probability for North Anna2 Trip on 6/29/2007
45° N
30° N
Latitude, degrees
105° W
90° W
75° W
60° W
Longitude, degrees
Q=0.554: Miss
© 2008 VIRGINIA TECH
Created by: R. Matthew Gardner
0.9
0.8
0.7
0.6
0.5
0.4
0.3
0.2
0.1

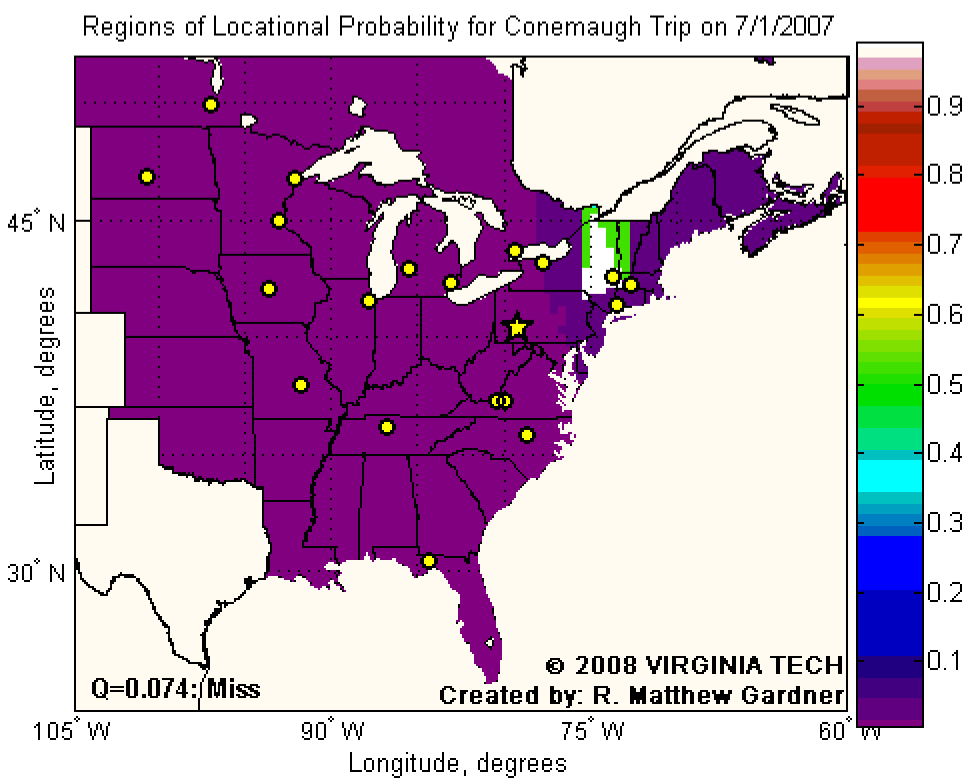
Regions of Locational Probability for Conemaugh Trip on 7/1/2007
45° N
30° N
Latitude, degrees
105° W
90° W
75° W
60° W
Longitude, degrees
Q=0.074: Miss
© 2008 VIRGINIA TECH
Created by: R. Matthew Gardner
0.9
0.8
0.7
0.6
0.5
0.4
0.3
0.2
0.1

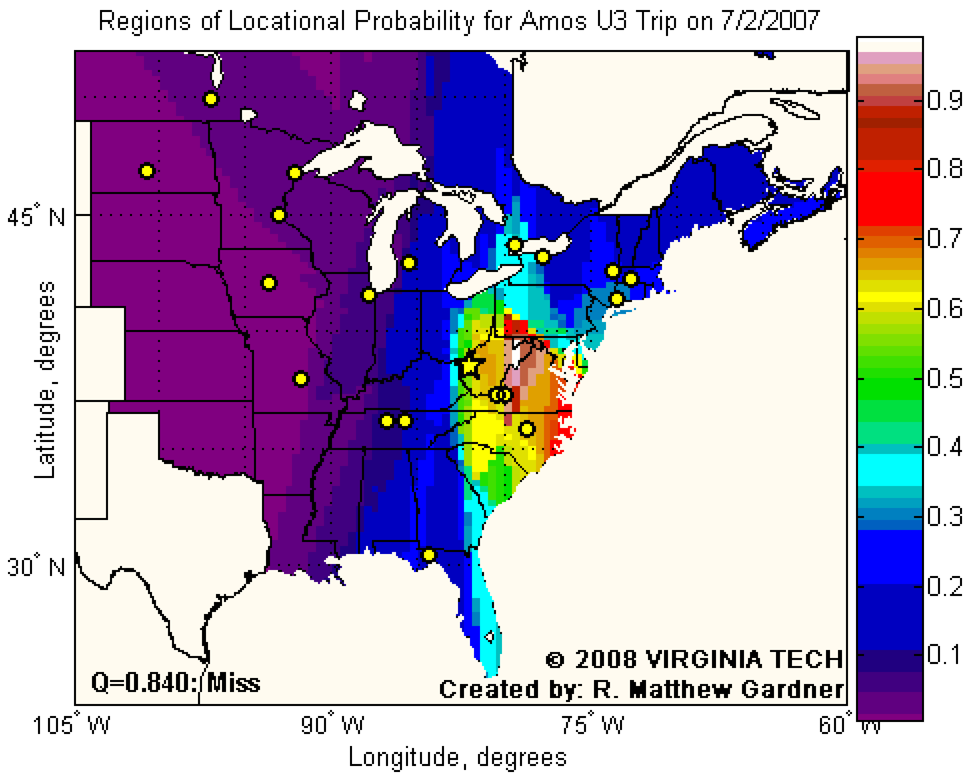
Regions of Locational Probability for Amos U3 Trip on 7/2/2007
45° N
30° N
Latitude, degrees
105° W
90° W
75° W
60° W
Longitude, degrees
Q=0.840: Miss
© 2008 VIRGINIA TECH
Created by: R. Matthew Gardner
0.9
0.8
0.7
0.6
0.5
0.4
0.3
0.2
0.1

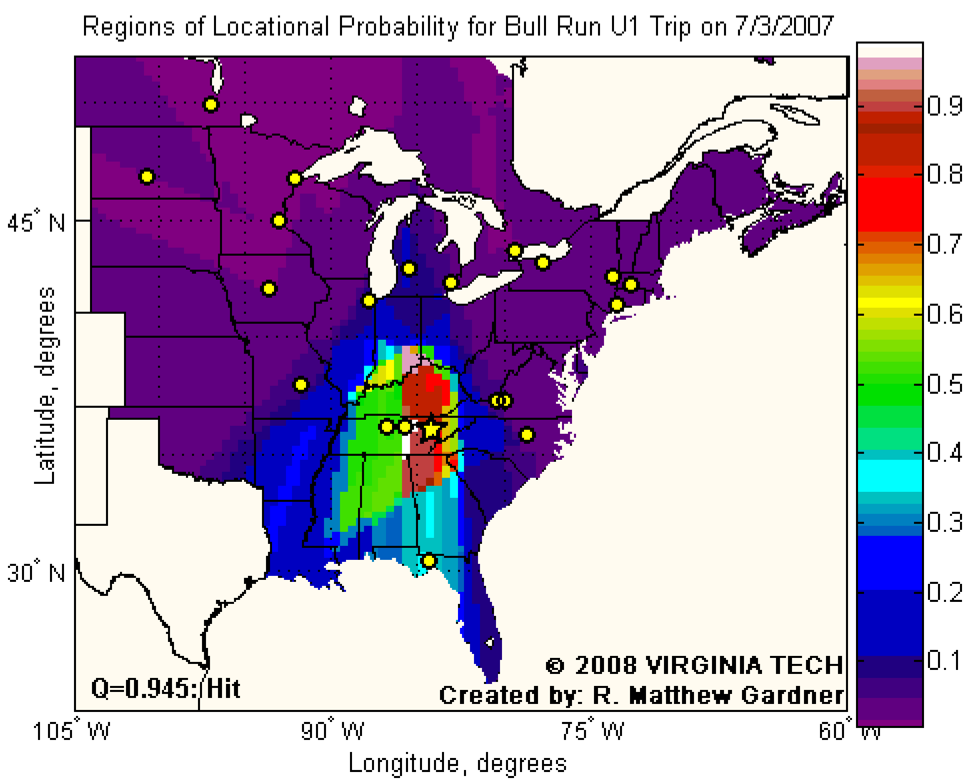
Regions of Locational Probability for Bull Run U1 Trip on 7/3/2007
45° N
30° N
Latitude, degrees
105° W
90° W
75° W
60° W
Longitude, degrees
Q=0.945: Hit
© 2008 VIRGINIA TECH
Created by: R. Matthew Gardner
0.9
0.8
0.7
0.6
0.5
0.4
0.3
0.2
0.1

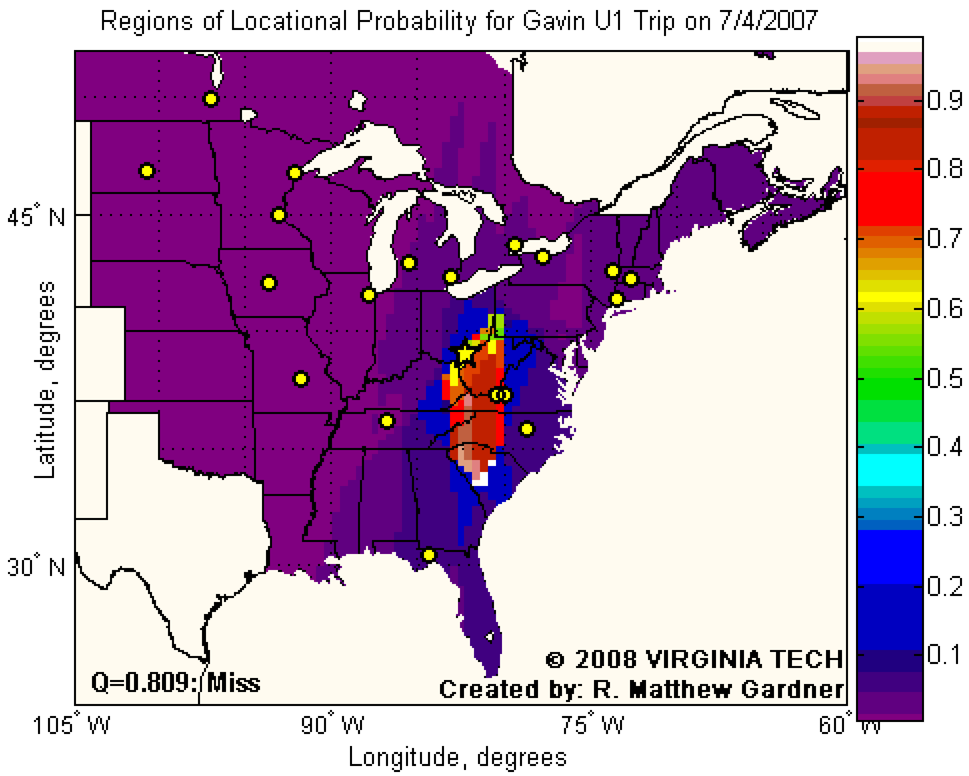
Regions of Locational Probability for Gavin U1 Trip on 7/4/2007
45° N
30° N
Latitude, degrees
105° W
90° W
75° W
60° W
Longitude, degrees
Q=0.809: Miss
© 2008 VIRGINIA TECH
Created by: R. Matthew Gardner
0.9
0.8
0.7
0.6
0.5
0.4
0.3
0.2
0.1

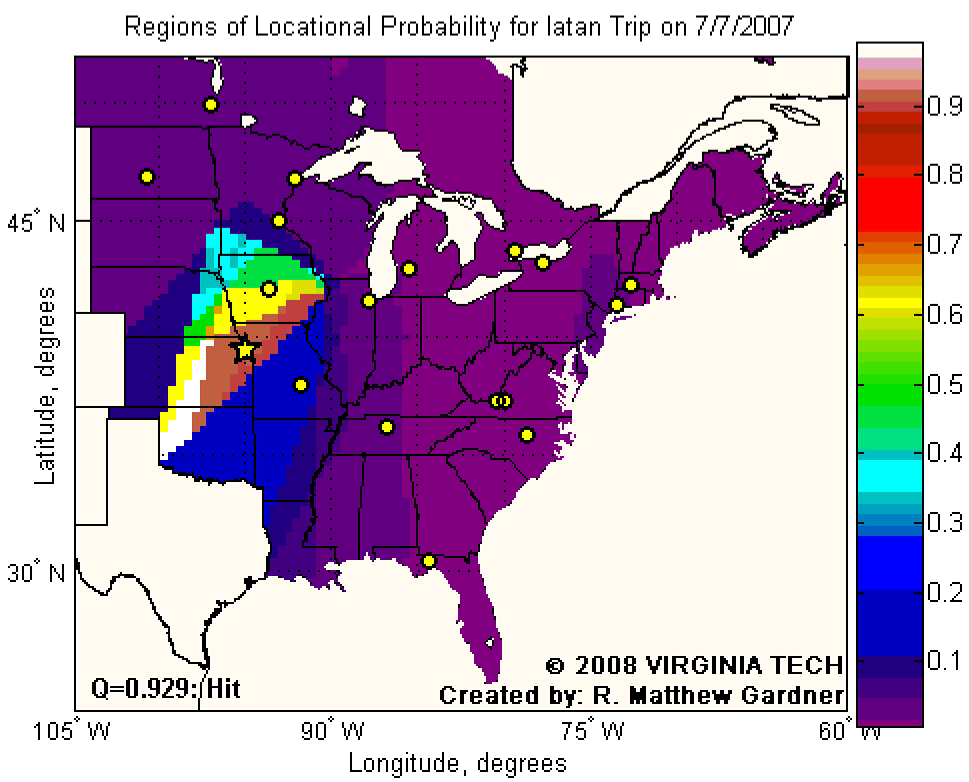
Regions of Locational Probability for Iatan Trip on 7/7/2007
45° N
30° N
Latitude, degrees
105° W
90° W
75° W
60° W
Longitude, degrees
Q=0.929: Hit
© 2008 VIRGINIA TECH
Created by: R. Matthew Gardner
0.9
0.8
0.7
0.6
0.5
0.4
0.3
0.2
0.1

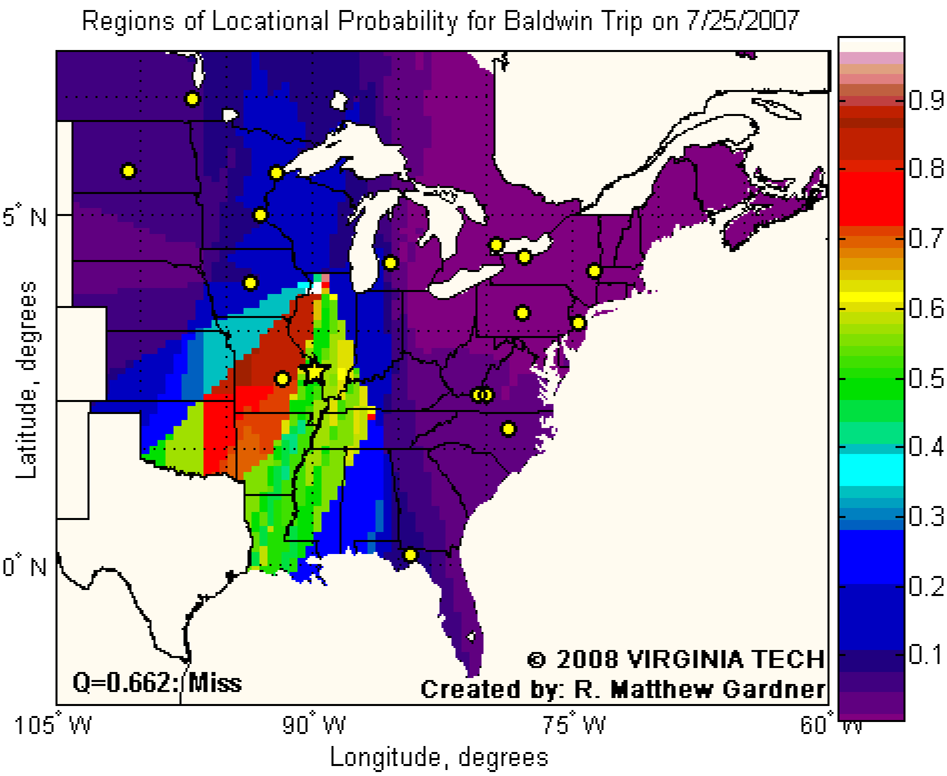
Regions of Locational Probability for Baldwin Trip on 7/25/2007
45° N
30° N
Latitude, degrees
105° W
90° W
75° W
60° W
Longitude, degrees
Q=0.662: Miss
© 2008 VIRGINIA TECH
Created by: R. Matthew Gardner
0.9
0.8
0.7
0.6
0.5
0.4
0.3
0.2
0.1

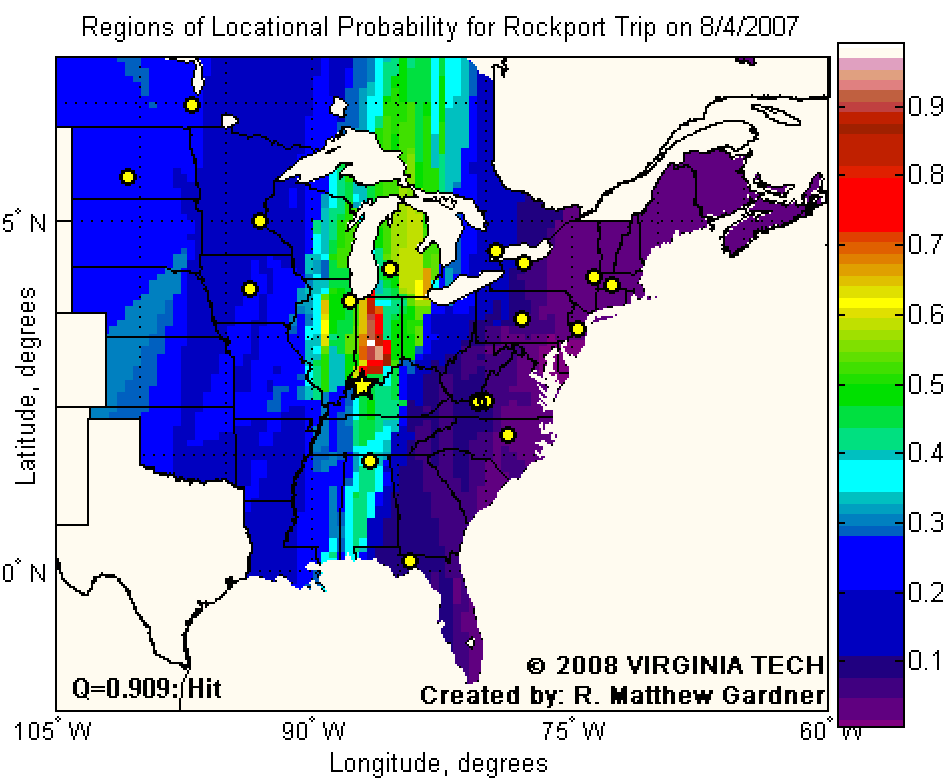
Regions of Locational Probability for Rockport Trip on 8/4/2007
45° N
30° N
Latitude, degrees
105° W
90° W
75° W
60° W
Longitude, degrees
Q=0.909: Hit
© 2008 VIRGINIA TECH
Created by: R. Matthew Gardner
0.9
0.8
0.7
0.6
0.5
0.4
0.3
0.2
0.1

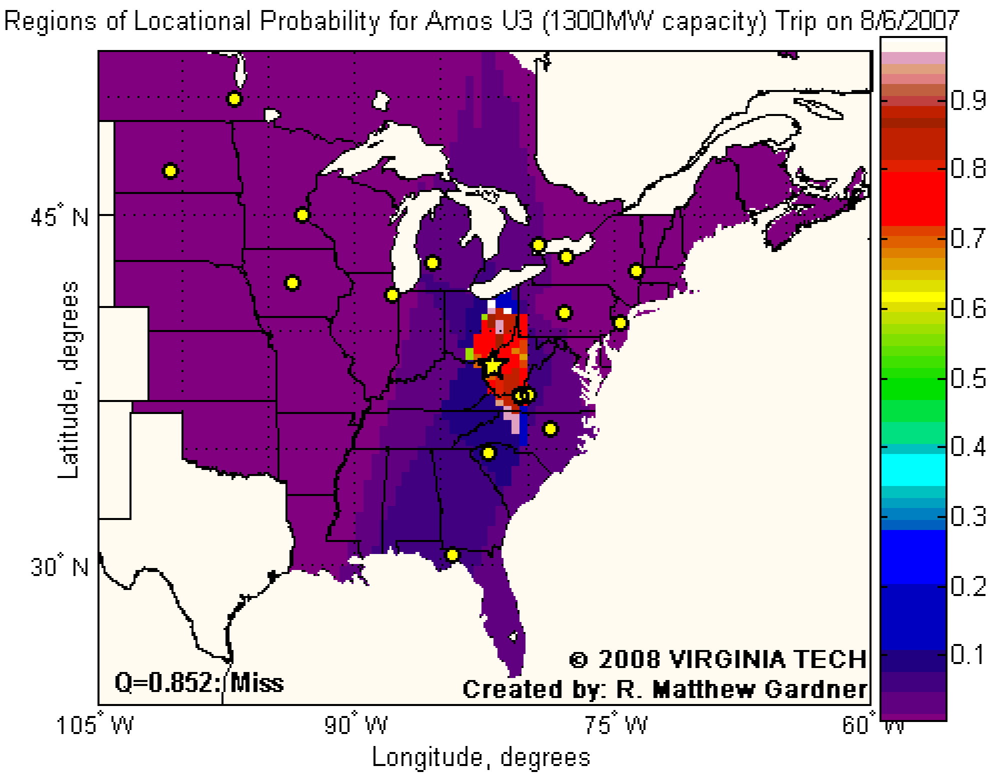
Regions of Locational Probability for Amos U3 (1300MW capacity) Trip on 8/6/2007
45° N
30° N
Latitude, degrees
105° W
90° W
75° W
60° W
Longitude, degrees
Q=0.852: Miss
© 2008 VIRGINIA TECH
Created by: R. Matthew Gardner
0.9
0.8
0.7
0.6
0.5
0.4
0.3
0.2
0.1

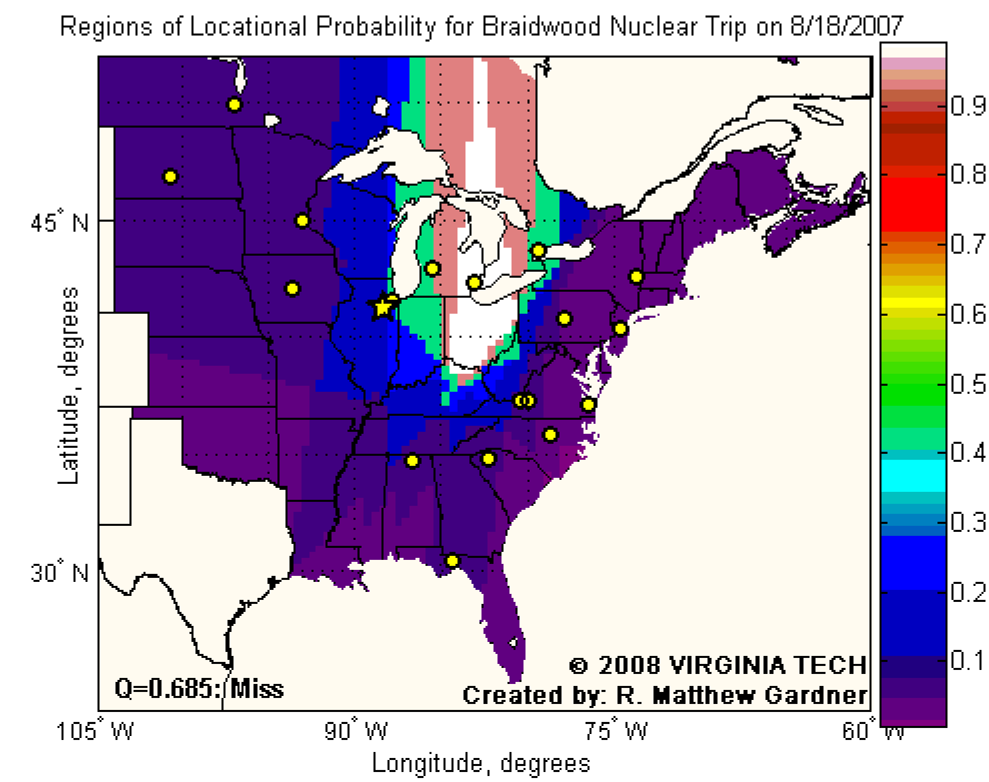
Regions of Locational Probability for Braidwood Nuclear Trip on 8/18/2007
45° N
30° N
Latitude, degrees
105° W
90° W
75° W
60° W
Longitude, degrees
Q=0.685: Miss
© 2008 VIRGINIA TECH
Created by: R. Matthew Gardner
0.9
0.8
0.7
0.6
0.5
0.4
0.3
0.2
0.1

Regions of Locational Probability for Nine Mile Point Nuclear Trip on 8/20/2007

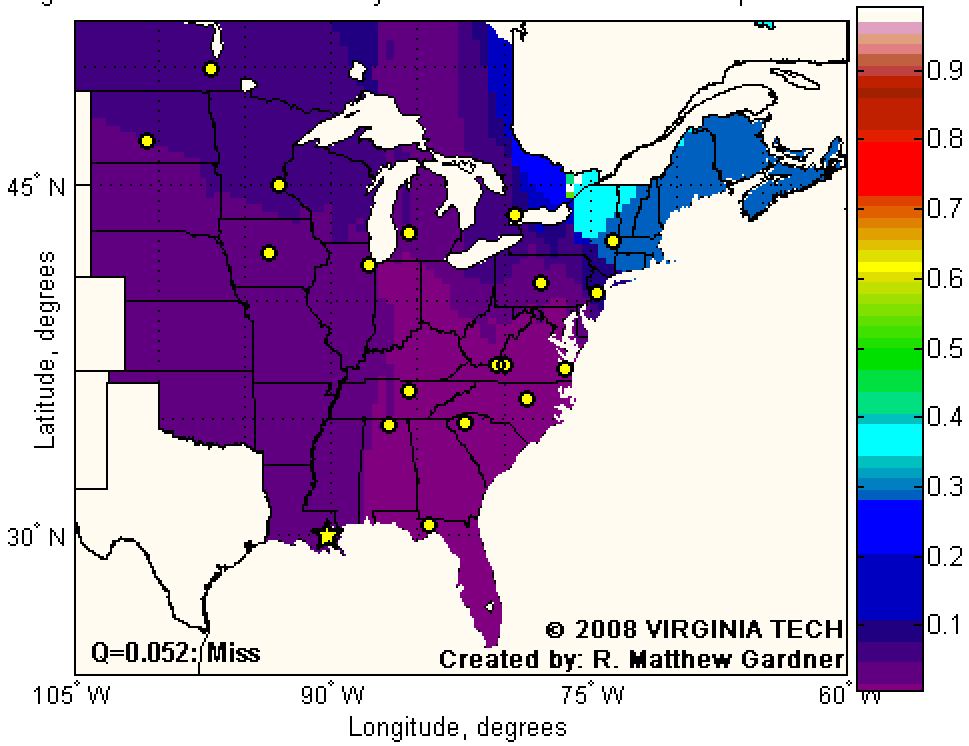

gions of Locational Probability for Donald C. Cook Unit 1 (1020 MW Capacity) Trip on 8/28/2007

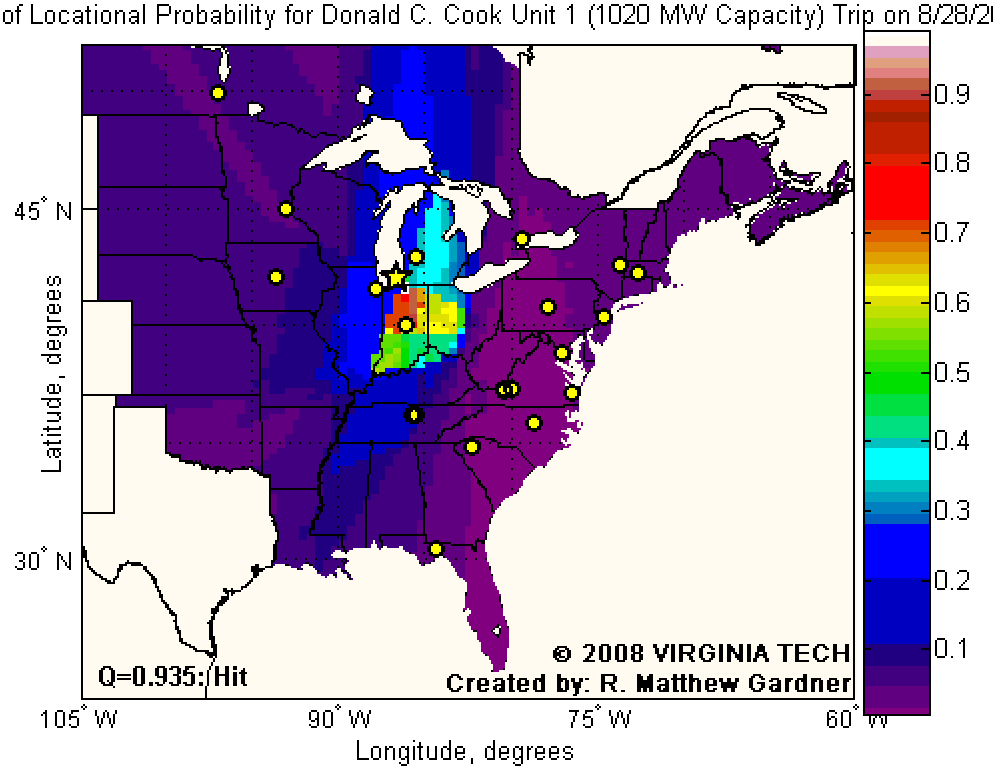

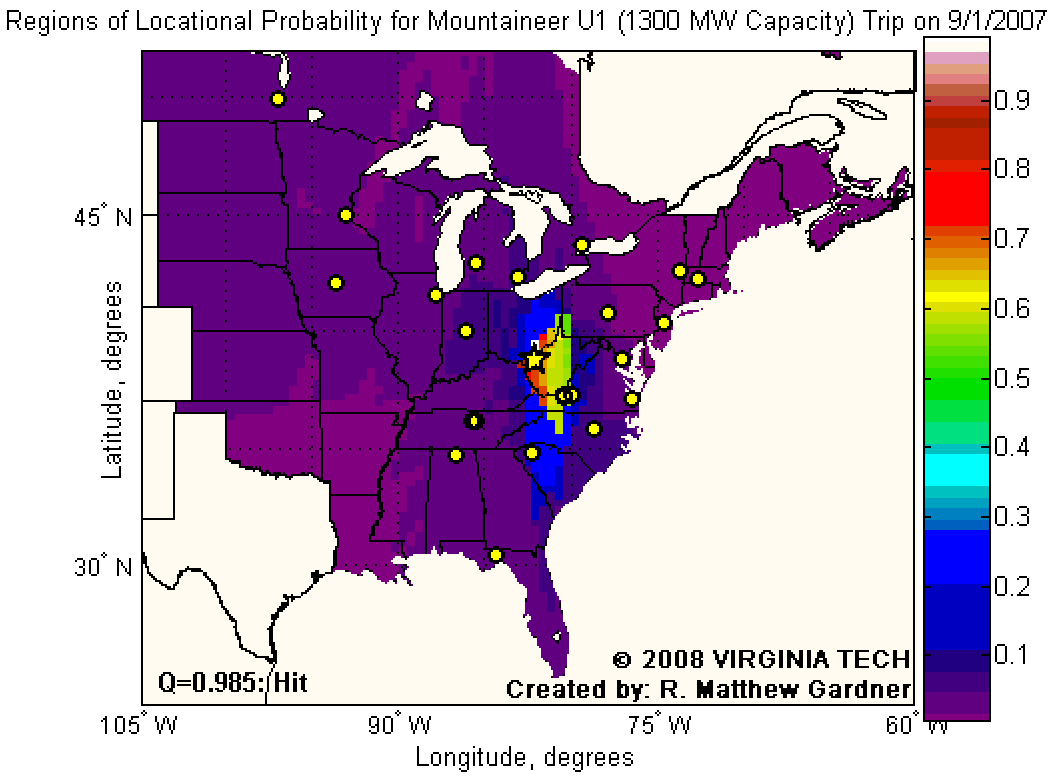
Regions of Locational Probability for Mountaineer U1 (1300 MW Capacity) Trip on 9/1/2007
45° N
30° N
Latitude, degrees
105° W
90° W
75° W
60° W
Longitude, degrees
Q=0.985: Hit
© 2008 VIRGINIA TECH
Created by: R. Matthew Gardner
0.9
0.8
0.7
0.6
0.5
0.4
0.3
0.2
0.1

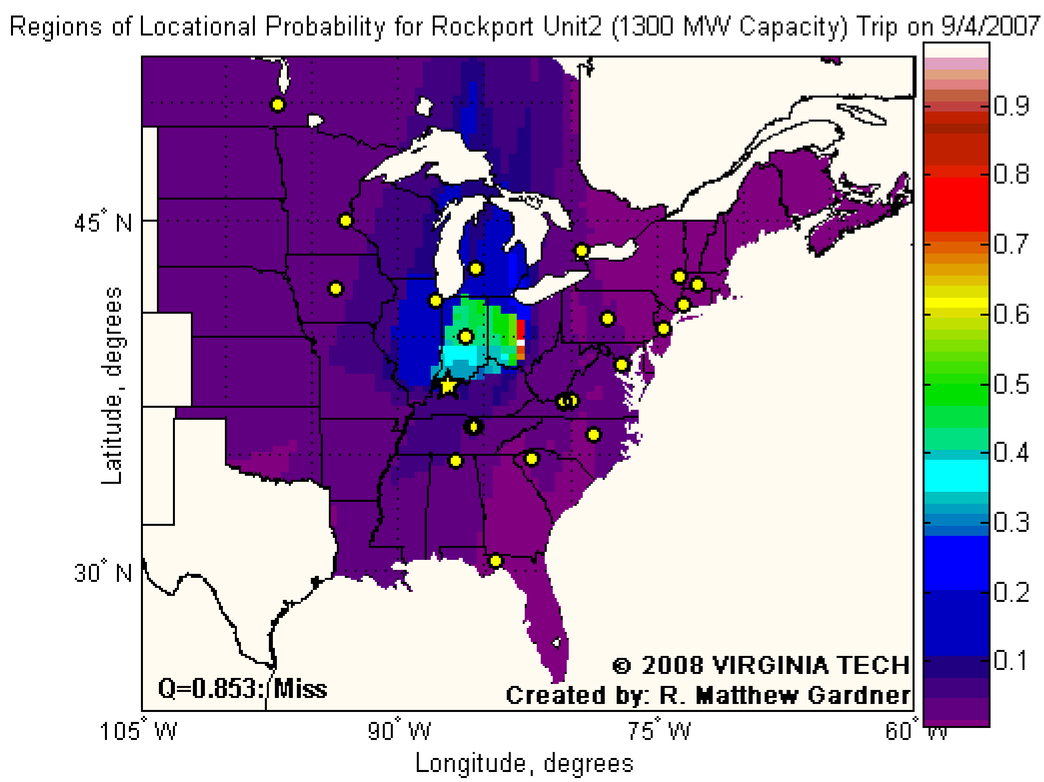
Regions of Locational Probability for Rockport Unit2 (1300 MW Capacity) Trip on 9/4/2007
45° N
30° N
Latitude, degrees
105° W
90° W
75° W
60° W
Longitude, degrees
Q=0.853: Miss
© 2008 VIRGINIA TECH
Created by: R. Matthew Gardner
0.9
0.8
0.7
0.6
0.5
0.4
0.3
0.2
0.1

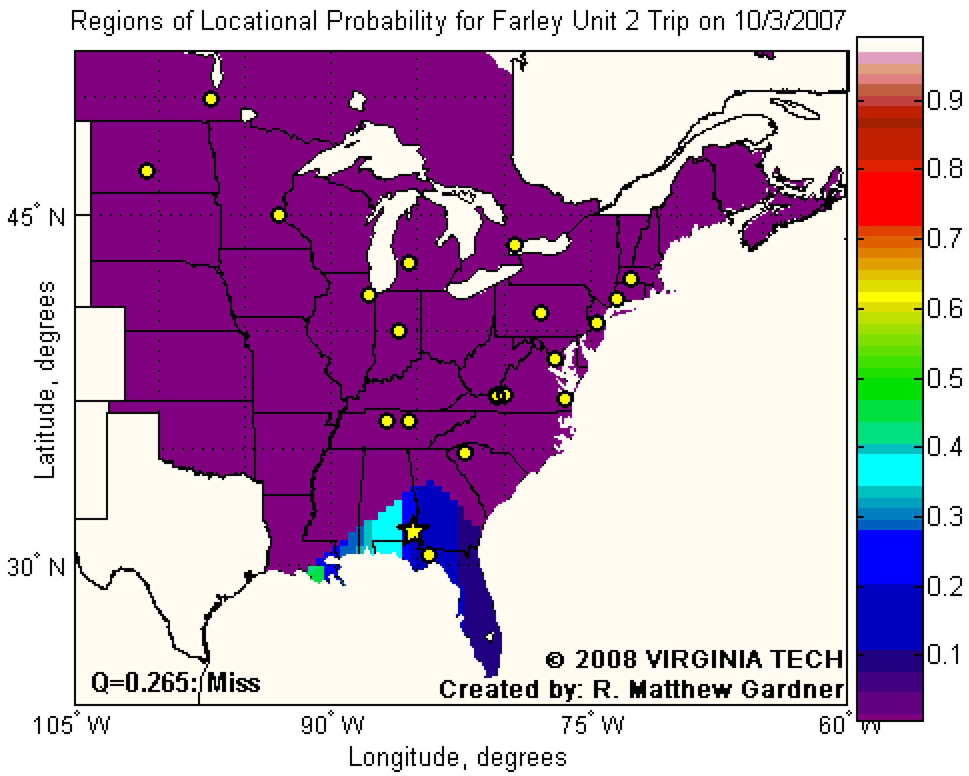
Regions of Locational Probability for Farley Unit 2 Trip on 10/3/2007
Latitude, degrees
45° N
30° N
105° W
90° W
75° W
60° W
Longitude, degrees
Q=0.265:/Miss
© 2008 VIRGINIA TECH
Created by: R. Matthew Gardner
0.9
0.8
0.7
0.6
0.5
0.4
0.3
0.2
0.1

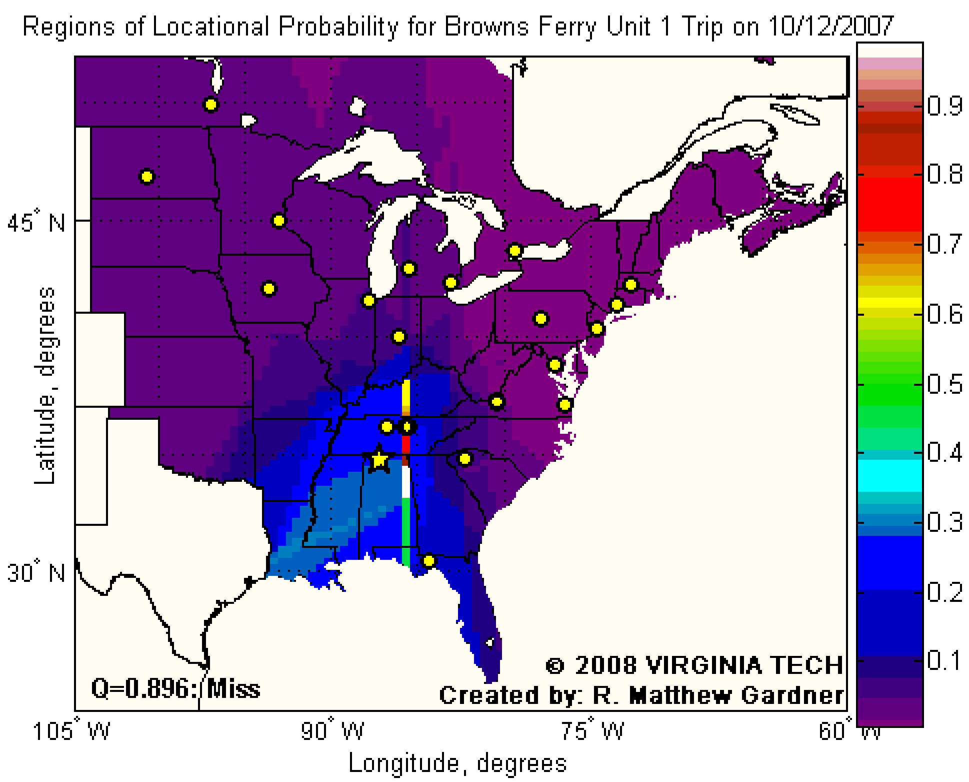
Regions of Locational Probability for Browns Ferry Unit 1 Trip on 10/12/2007
Latitude, degrees
45° N
30° N
105° W
90° W
75° W
60° W
Longitude, degrees
Q=0.896:/Miss
© 2008 VIRGINIA TECH
Created by: R. Matthew Gardner
0.9
0.8
0.7
0.6
0.5
0.4
0.3
0.2
0.1

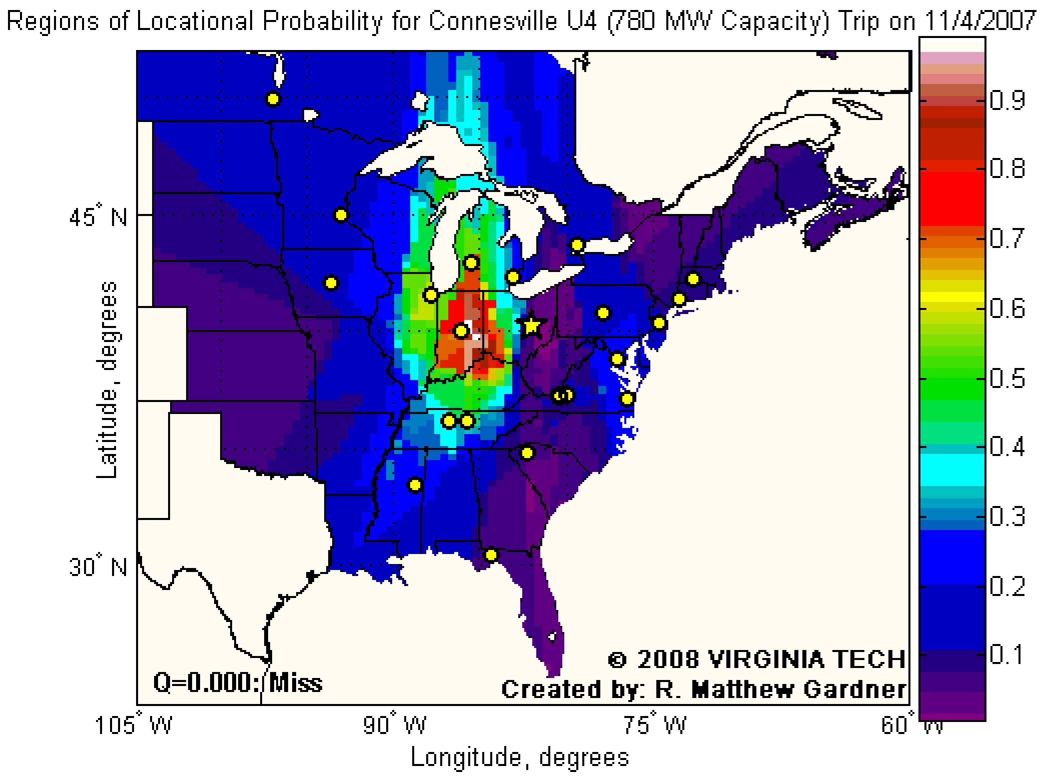
Regions of Locational Probability for Connesville U4 (780 MW Capacity) Trip on 11/4/2007
45° N
30° N
Latitude, degrees
105° W
90° W
75° W
60° W
Longitude, degrees
0.9
0.8
0.7
0.6
0.5
0.4
0.3
0.2
0.1
Q=0.000:/Miss
© 2008 VIRGINIA TECH
Created by: R. Matthew Gardner

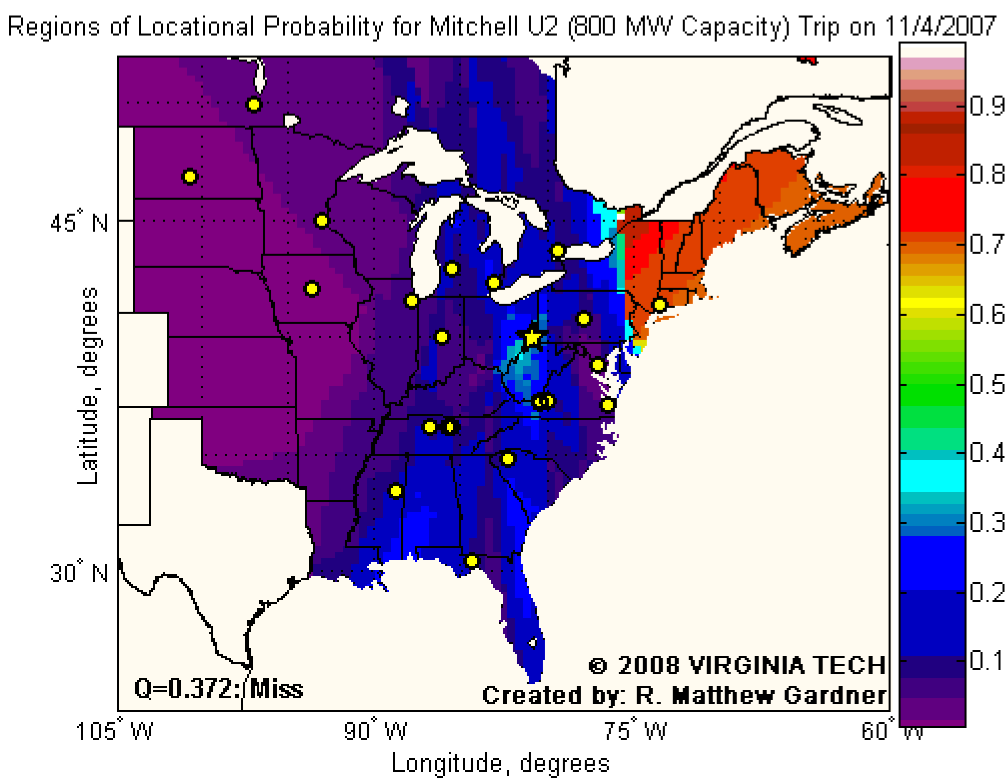
Regions of Locational Probability for Mitchell U2 (800 MW Capacity) Trip on 11/4/2007
45° N
30° N
Latitude, degrees
105° W
90° W
75° W
60° W
Longitude, degrees
0.9
0.8
0.7
0.6
0.5
0.4
0.3
0.2
0.1
Q=0.372:/Miss
© 2008 VIRGINIA TECH
Created by: R. Matthew Gardner

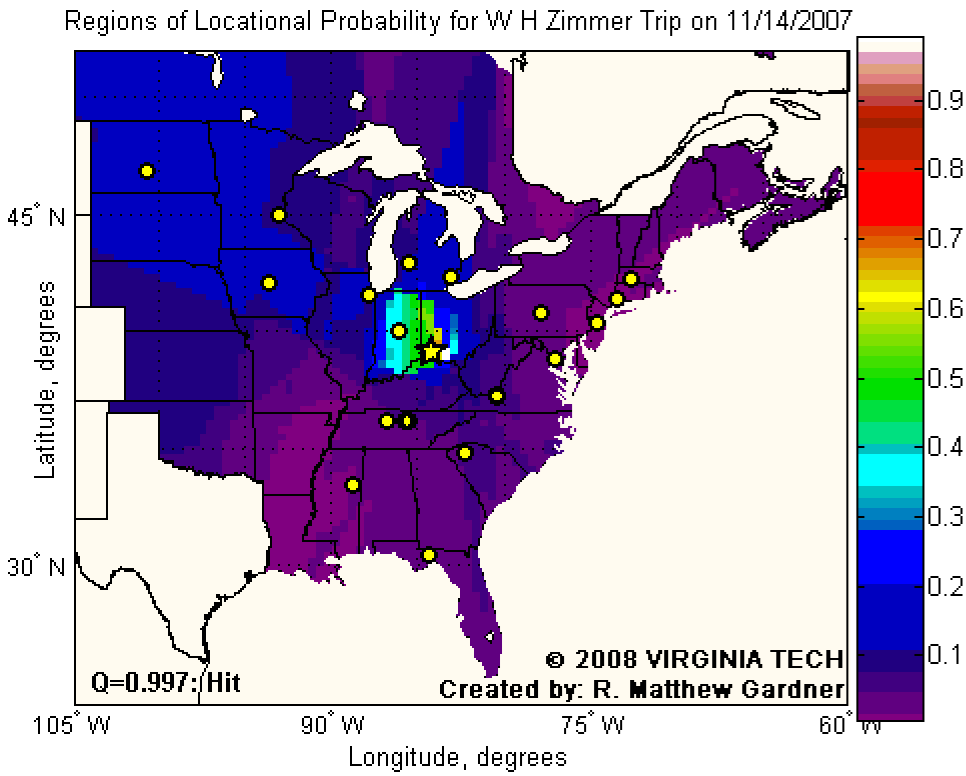
Regions of Locational Probability for W H Zimmer Trip on 11/14/2007
45° N
30° N
Latitude, degrees
105° W
90° W
75° W
60° W
Longitude, degrees
Q=0.997: Hit
© 2008 VIRGINIA TECH
Created by: R. Matthew Gardner
0.9
0.8
0.7
0.6
0.5
0.4
0.3
0.2
0.1

Appendix XXII: Performance of Event Location Methods

Measured Frequency Data

Unweighted Method

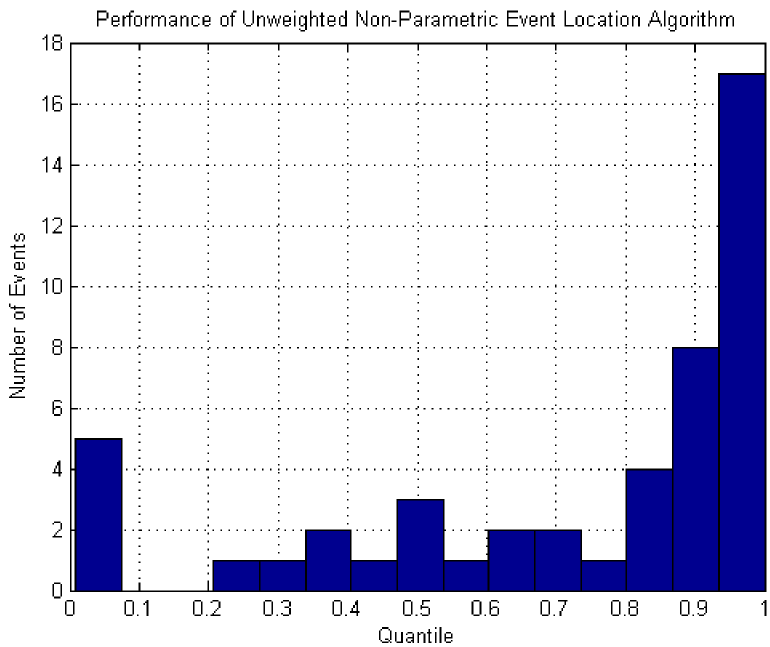

Weighted Method

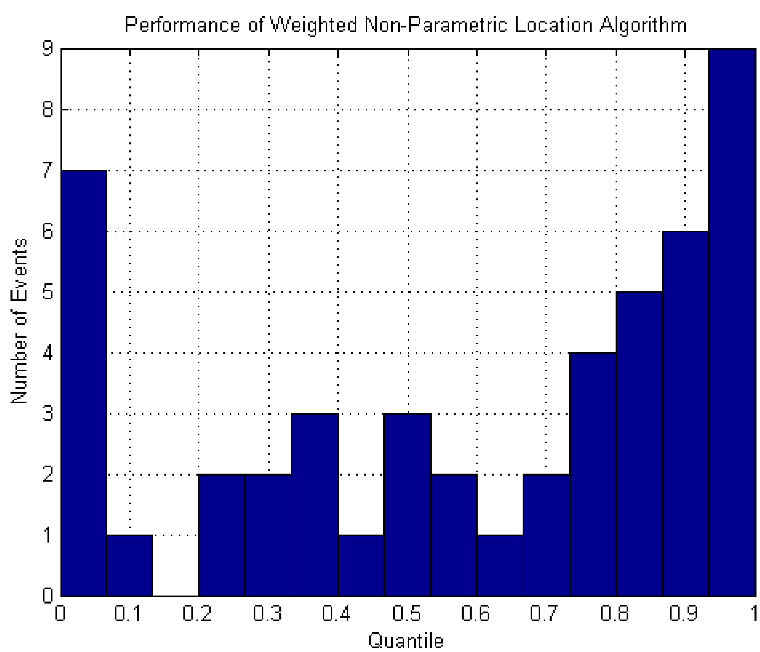

Simulated Frequency Data

Unweighted Method

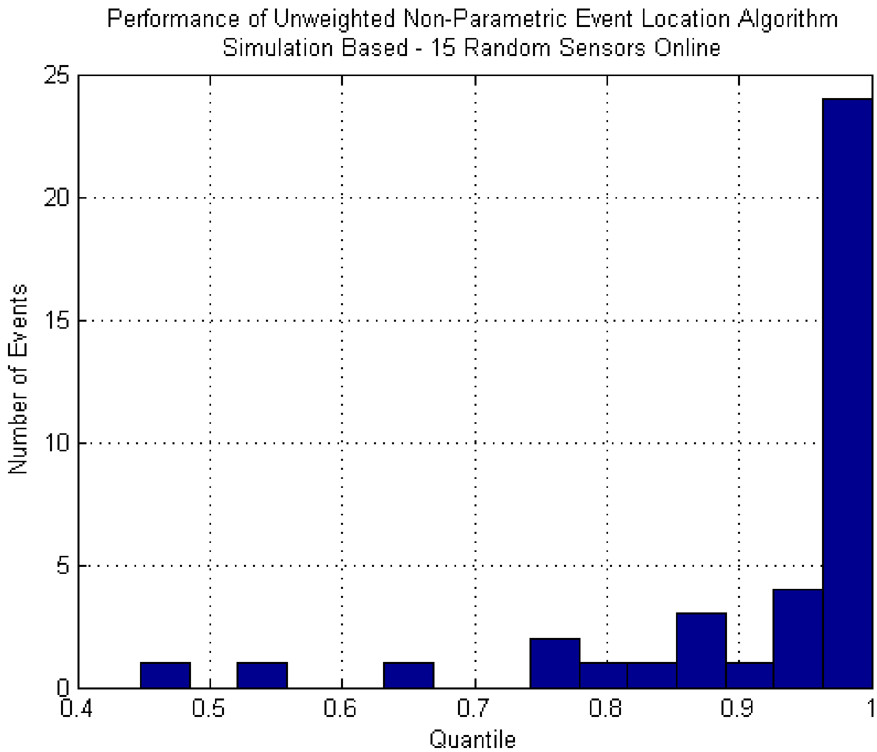

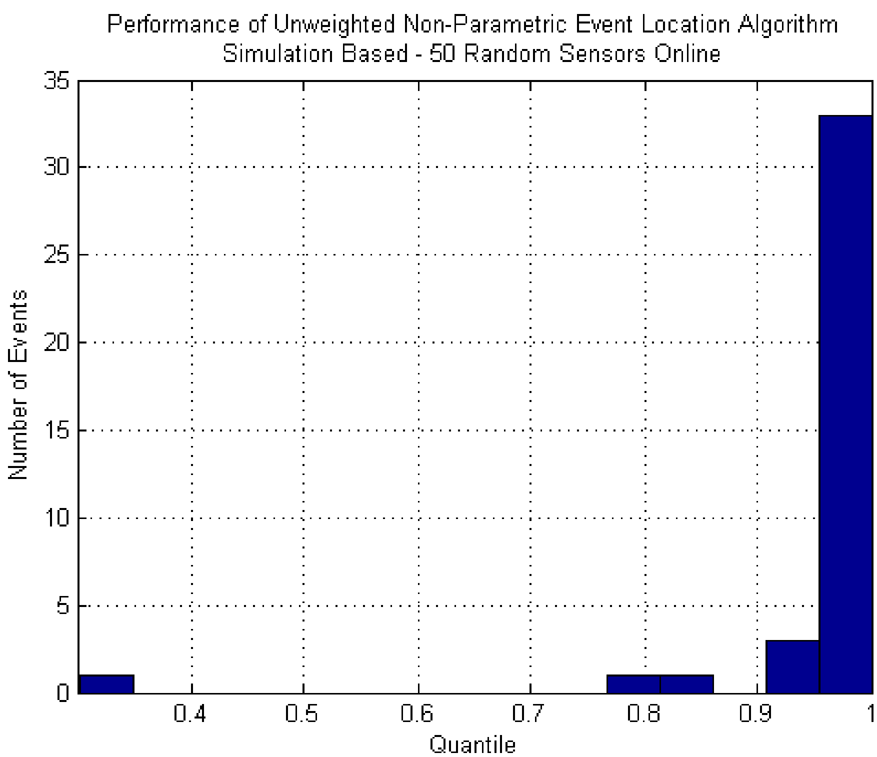

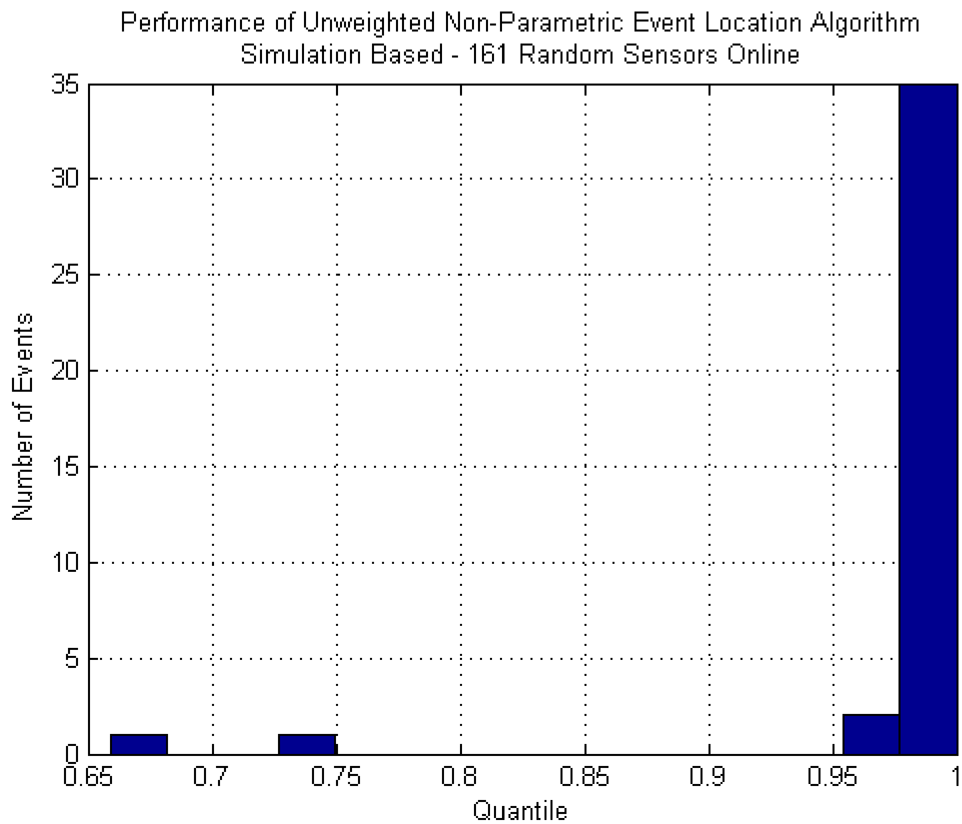
Performance of Unweighted Non-Parametric Event Location Algorithm
Simulation Based - 161 Random Sensors Online
Number of Events
Quantile
0
5
10
15
20
25
30
35
0.65
0.7
0.75
0.8
0.85
0.9
0.95
1

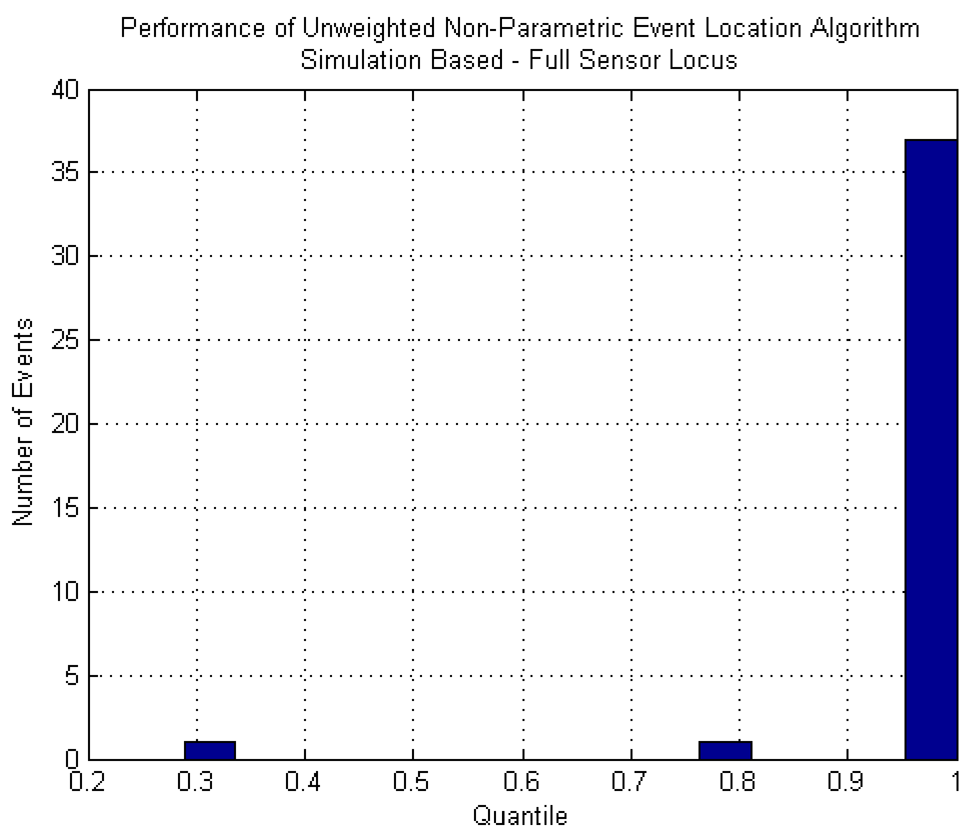
Performance of Unweighted Non-Parametric Event Location Algorithm
Simulation Based - Full Sensor Locus
Number of Events
Quantile
0
5
10
15
20
25
30
35
40
0.2
0.3
0.4
0.5
0.6
0.7
0.8
0.9
1

Weighted Method

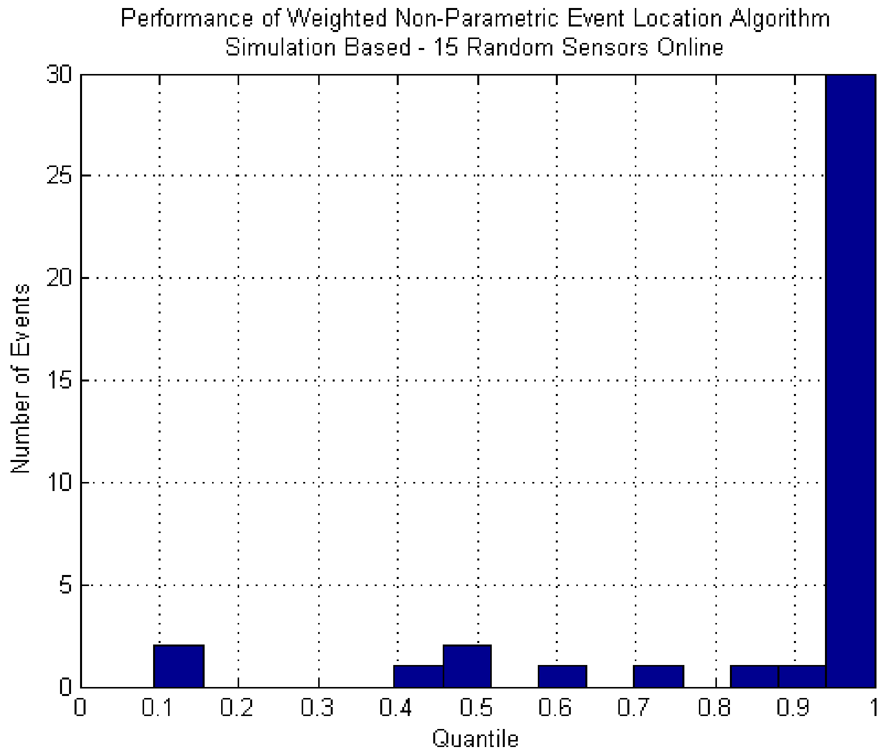

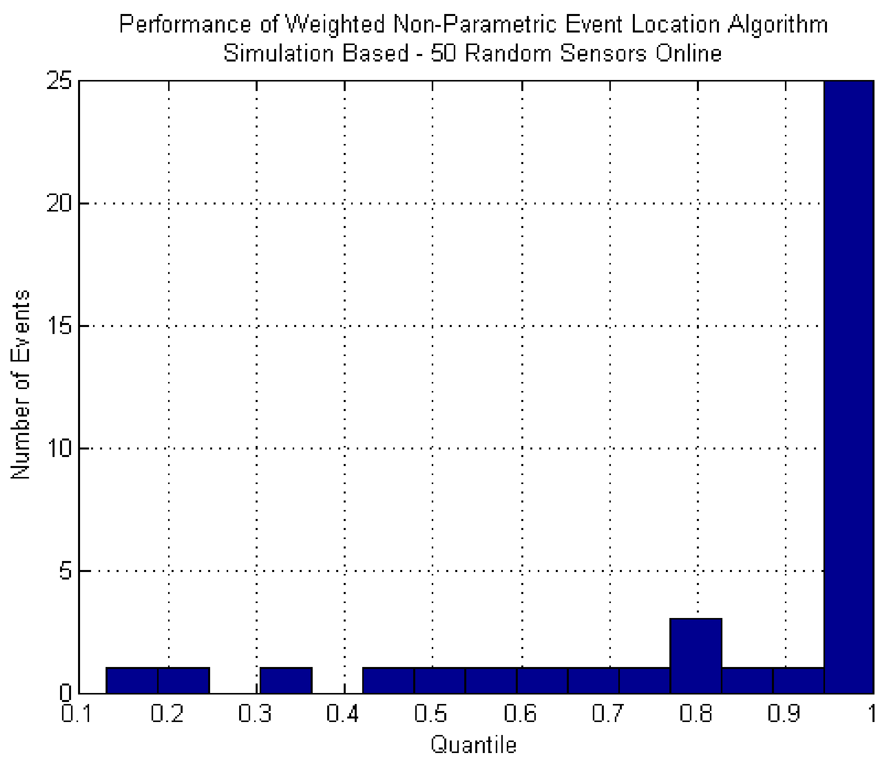

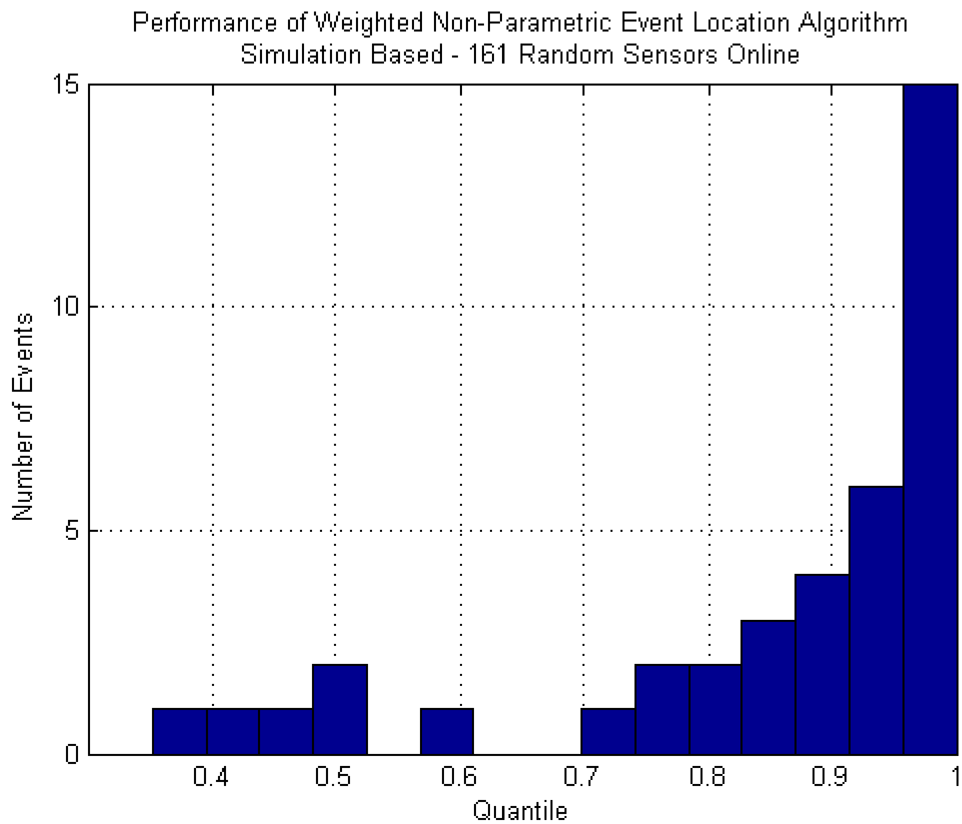
Performance of Weighted Non-Parametric Event Location Algorithm
Simulation Based - 161 Random Sensors Online
Number of Events
Quantile
0
5
10
15
0.4
0.5
0.6
0.7
0.8
0.9
1

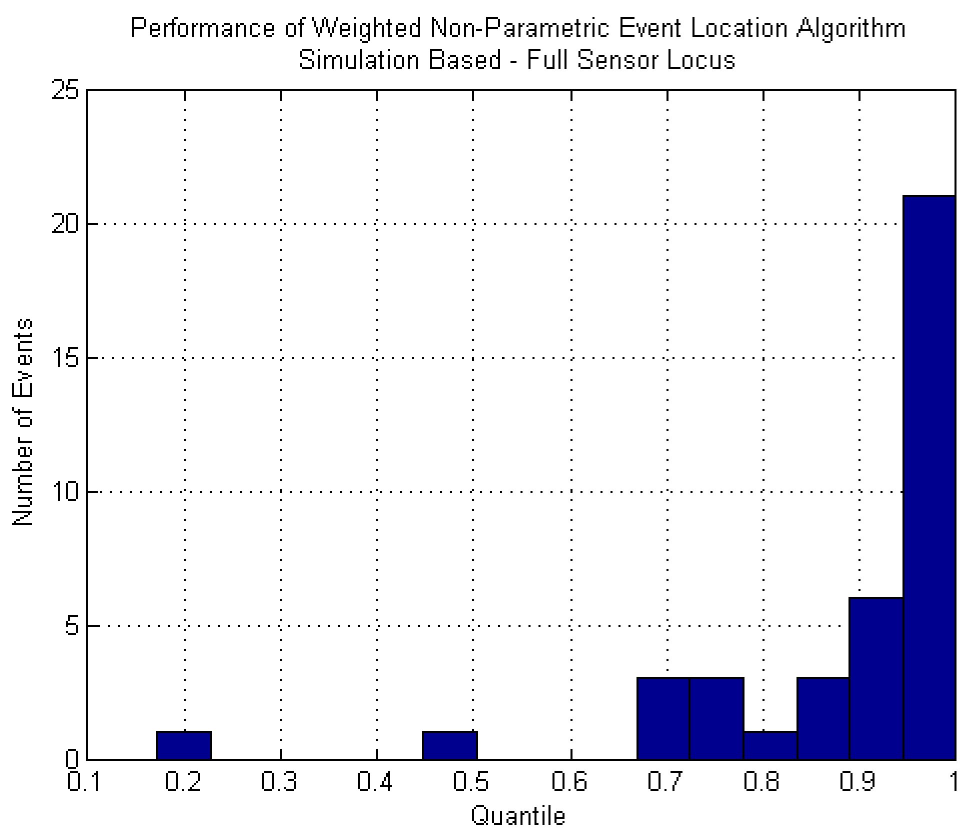
Performance of Weighted Non-Parametric Event Location Algorithm
Simulation Based - Full Sensor Locus
Number of Events
Quantile
0
5
10
15
20
25
0.1
0.2
0.3
0.4
0.5
0.6
0.7
0.8
0.9
1

Simulated Phase Angle Data

Unweighted Method

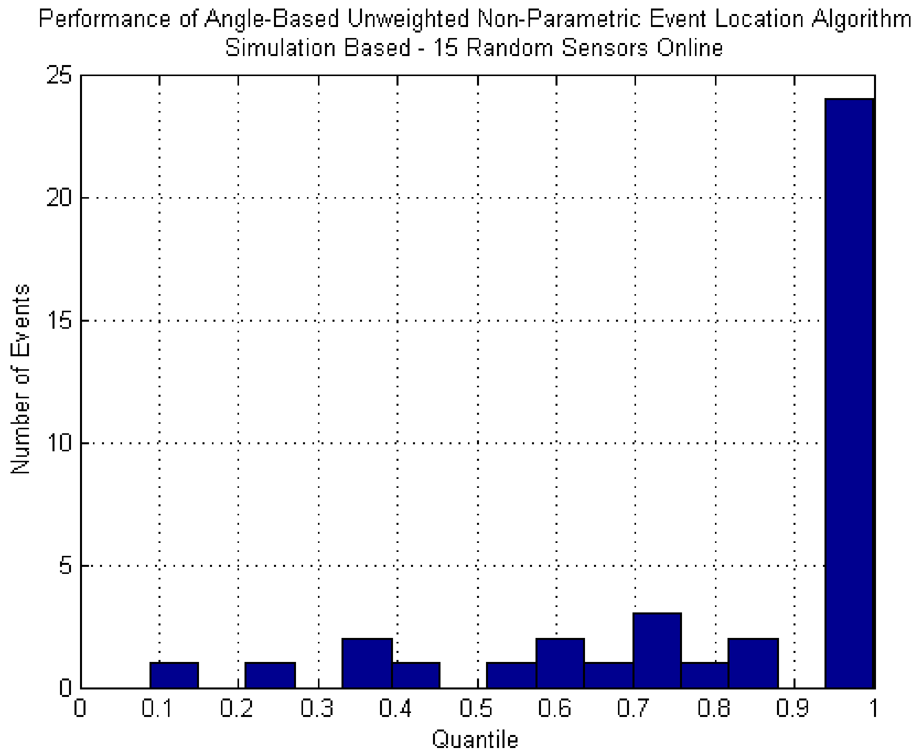

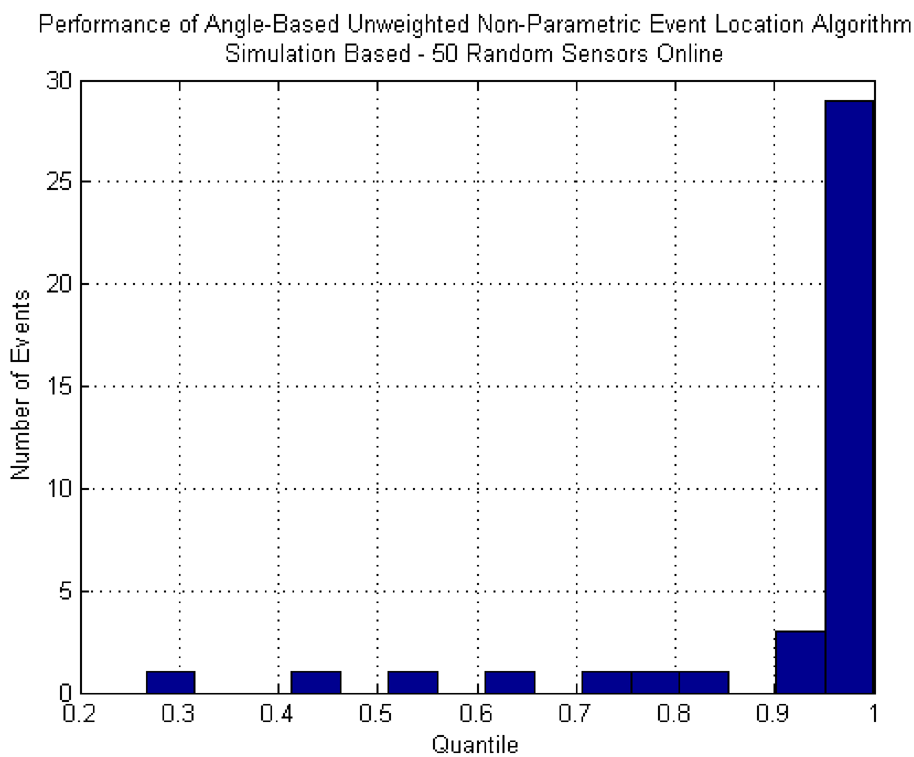

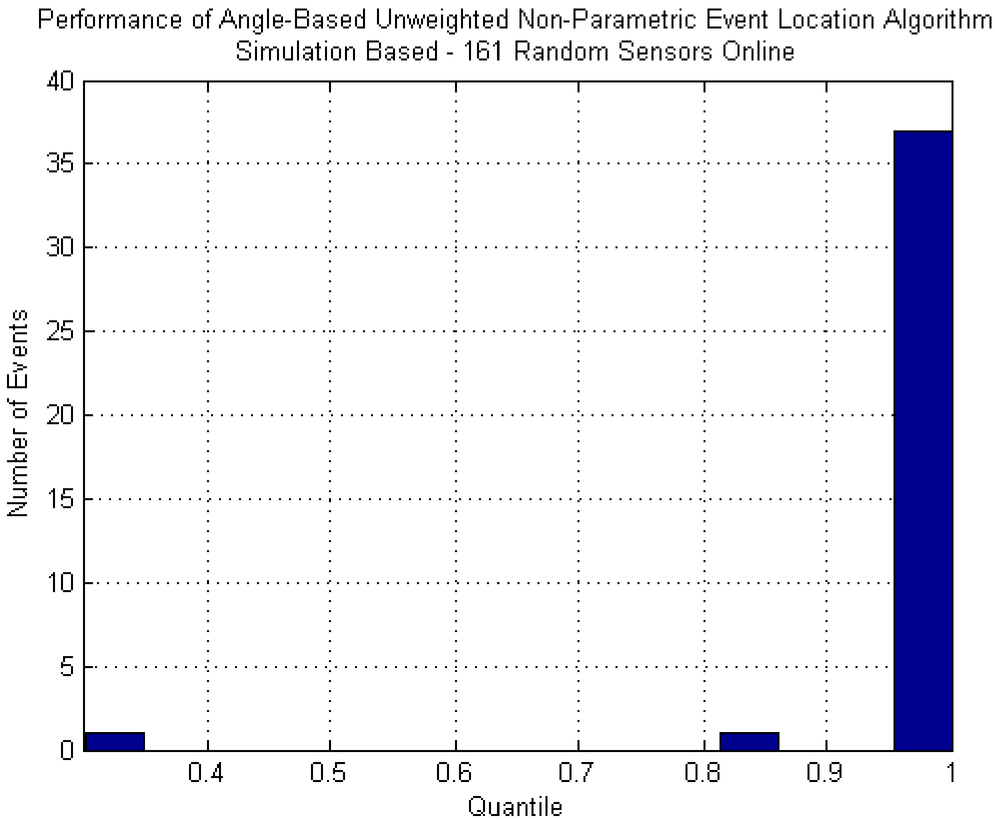
Performance of Angle-Based Unweighted Non-Parametric Event Location Algorithm
Simulation Based - 161 Random Sensors Online
Number of Events
Quantile
0
5
10
15
20
25
30
35
40
0.4
0.5
0.6
0.7
0.8
0.9
1

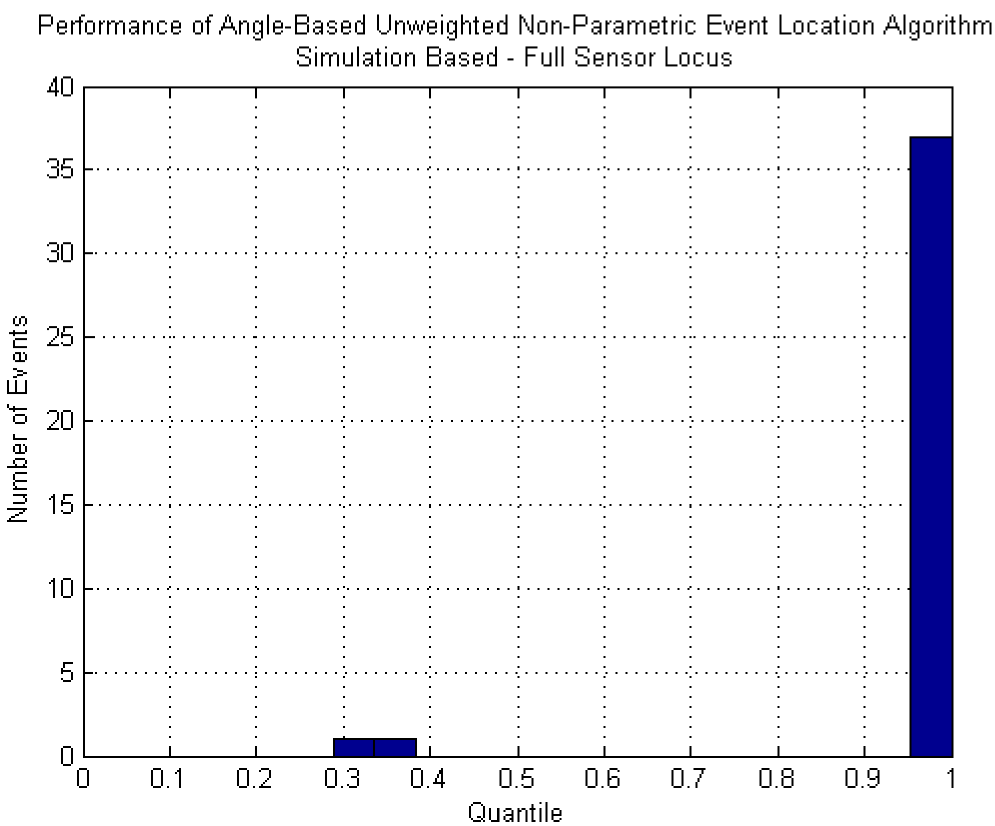
Performance of Angle-Based Unweighted Non-Parametric Event Location Algorithm
Simulation Based - Full Sensor Locus
Number of Events
Quantile
0
5
10
15
20
25
30
35
40
0
0.1
0.2
0.3
0.4
0.5
0.6
0.7
0.8
0.9
1

Weighted Method

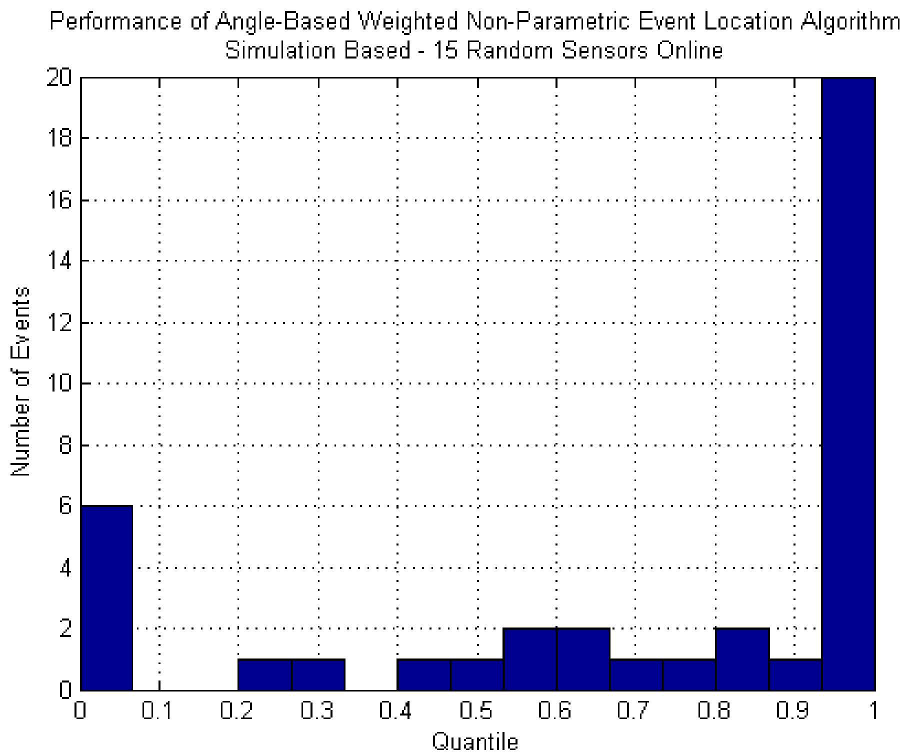

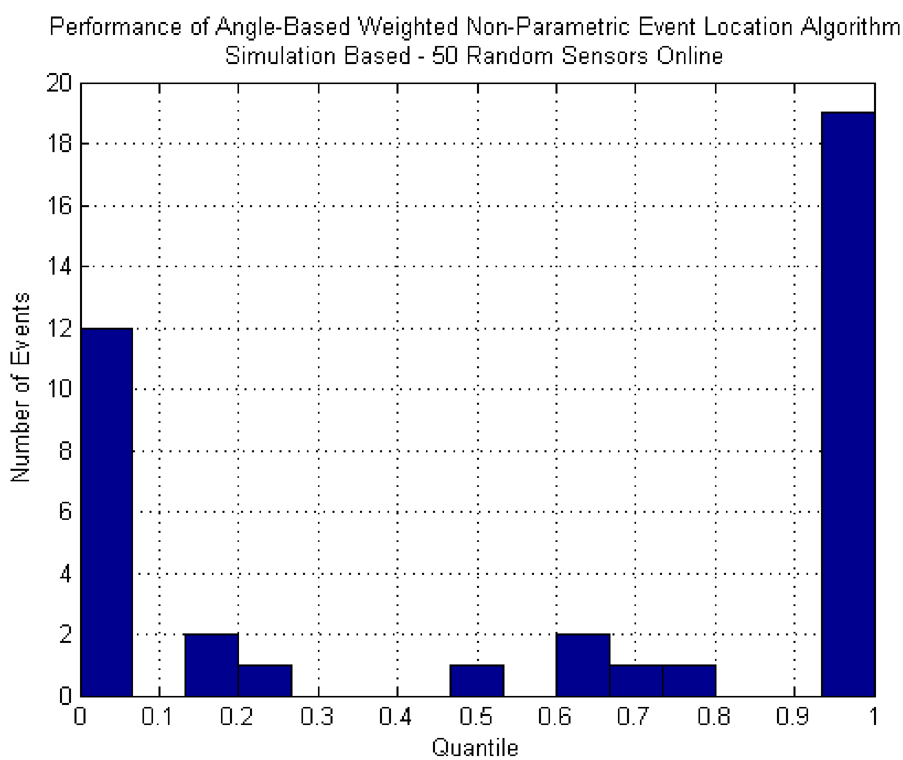

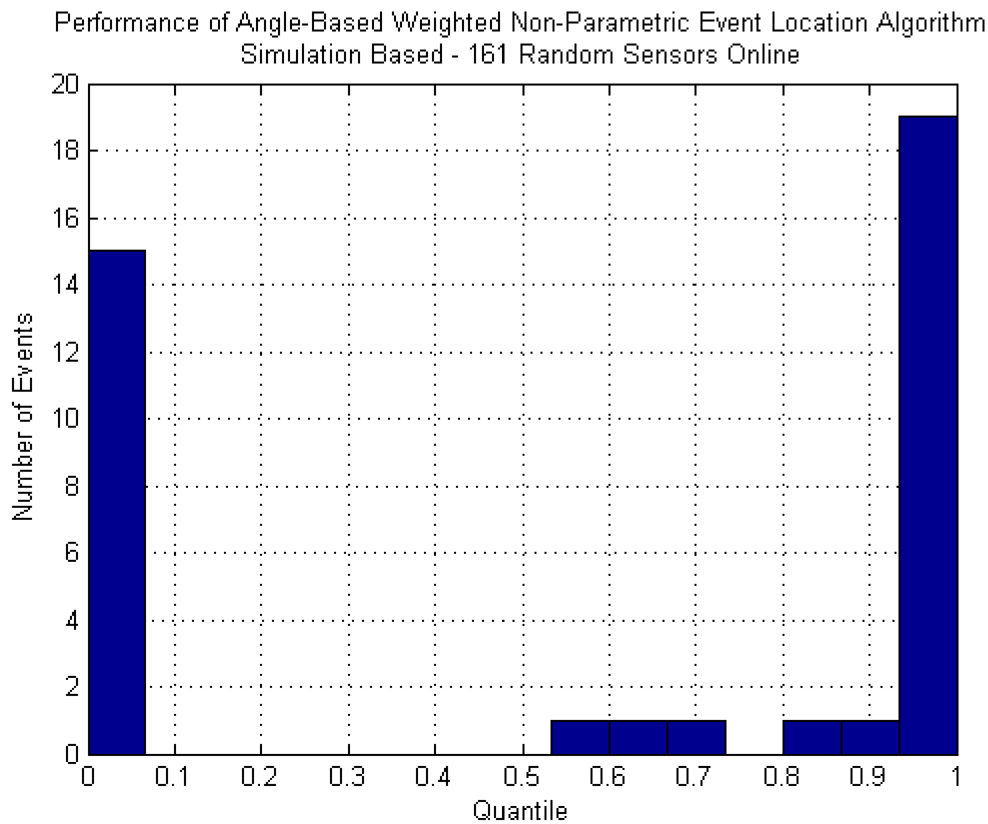
Performance of Angle-Based Weighted Non-Parametric Event Location Algorithm
Simulation Based - 161 Random Sensors Online
Number of Events
Quantile
0
2
4
6
8
10
12
14
16
18
20
0
0.1
0.2
0.3
0.4
0.5
0.6
0.7
0.8
0.9
1

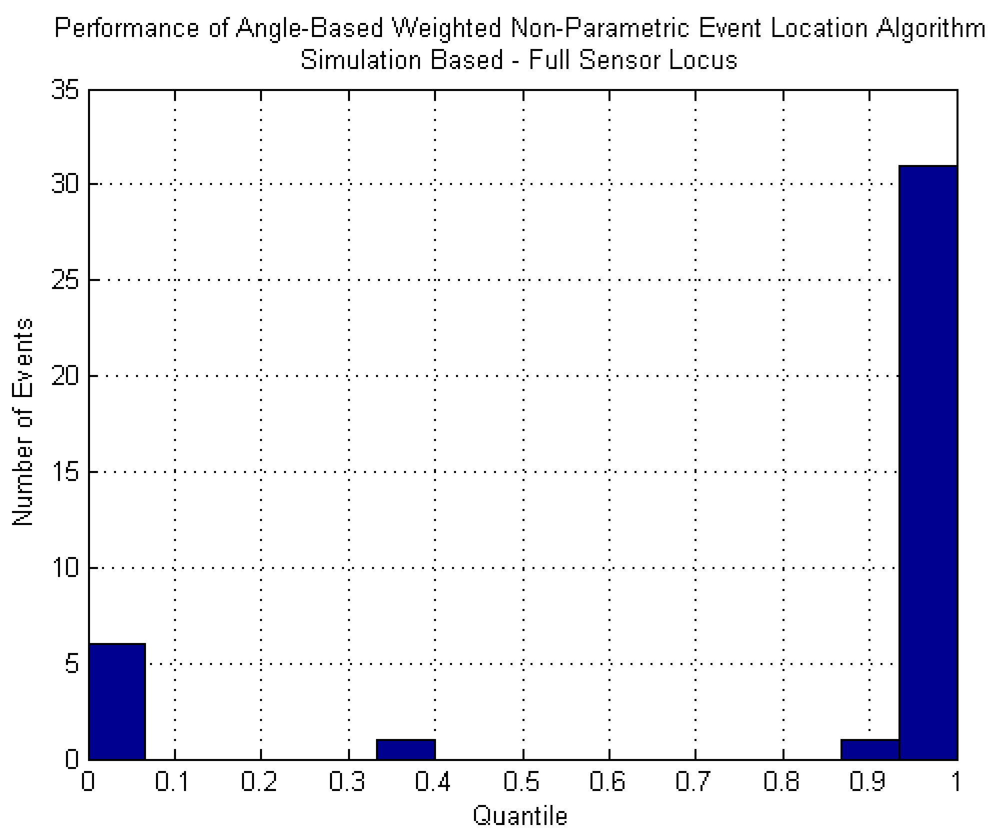
Performance of Angle-Based Weighted Non-Parametric Event Location Algorithm
Simulation Based - Full Sensor Locus
Number of Events
Quantile
0
5
10
15
20
25
30
35
0
0.1
0.2
0.3
0.4
0.5
0.6
0.7
0.8
0.9
1